BIOTECHNOLOGY: PHARMACEUTICAL ASPECTS

Nanotechnology in Drug Delivery

Edited by
Melgardt M. de Villiers
Pornanong Aramwit
Glen S. Kwon

Springer

AAPS PRESS

Nanotechnology in Drug Delivery

Biotechnology: Pharmaceutical Aspects

Volume I: *Pharmaceutical Profiling in Drug Discovery for Lead Selection*
R.T. Borchardt, E.H. Kerns, C.A. Lipinski, D.R. Thakker, B. Wang

Volume II: *Lypophilization of Biopharmaceuticals*
H.R. Constantino, M.J. Pikal

Volume III: *Methods for Structural Analysis of Protein Pharmaceuticals*
W. Jiskoot, D.J.A. Crommelin

Volume IV: *Optimizing the "Drug-Like" Properties of Leads in Drug Discovery*
R.T. Borchardt, E.H. Kerns, M.J. Hageman, D.R. Thakker, J.L. Stevens

Volume V: *Prodrugs: Challenges and Rewards, Parts 1 and 2*
V.J. Stella, R.T. Borchardt, M.J. Hageman, R. Oliyai, H. Maag, J.W. Tilley

Volume VI: *Solvent Systems and Their Selection in Pharmaceutics and Biopharmaceutics*
P. Augustijns, M.E. Brewster

Volume VII: *Drug Absorption Studies: In Situ, In Vitro and In Silico Models*
C. Ehrhardt, K.J. Kim

Volume VIII: *Immunogenicity of Biopharmaceuticals*
M. van de Weert, E.H. Møller

Volume IX: *Advances in Bioactivation Research*
A. Elfarra

Volume X: *Nanotechnology in Drug Delivery*
M.M. de Villiers, P. Aramwit, G.S. Kwon

Nanotechnology in Drug Delivery

Melgardt M. de Villiers
University of Wisconsin, Madison, WI, USA

Pornanong Aramwit
Chulalongkorn University, Bangkok, Thailand

Glen S. Kwon
University of Wisconsin, Madison, WI, USA

Springer

AAPS PRESS

Editors
Melgardt M. de Villiers
University of Wisconsin
Madison, WI, USA
mmdevilliers@pharmacy.wisc.edu

Pornanong Aramwit
Chulalongkorn University
Bangkok, Thailand

Glen S. Kwon
University of Wisconsin
Madison, WI, USA
gskwon@pharmacy.wisc.edu

ISBN: 978-0-387-77667-5 e-ISBN: 978-0-387-77668-2
DOI: 10.1007/978-0-387-77667-5

Library of Congress Control Number: 2008935894

Printed on acid-free paper

springer.com

Preface

Nanotechnology, a multidisciplinary scientific undertaking, involves creation and utilization of materials, devices, or systems on the nanometer scale and is currently undergoing explosive development on many fronts. It is expected to spark innovation and play a critical role in various biomedical applications, especially in drug delivery, as is shown by the wealth of information presented in this book particular, advances in nanotechnology that enable drugs to preserve their efficacy while being delivered to precise therapeutic targets are creating a host of opportunities for drug developers. In addition, by combining nanotechnology-based target-specific drug therapy with methods for early diagnosis of pathologies, we are getting closer to creating the ultimate functional drug carrier.

This book is primarily designed to be a reference textbook on the application of nanotechnology in the development of drug delivery systems and to highlight some of the most exciting developments in this field. For this purpose, the reader is introduced to various aspects of the fundamentals of nanotechnology-based drug delivery systems and the application of these systems for the delivery of small molecules, proteins, peptides, oligonucleotides, and genes. How these systems overcome challenges offered by biological barriers to drug absorption and drug targeting is also highlighted. To best do this the text is divided into the following sections: Fundamentals of Nanotechnology in Drug Delivery; Biopharmaceutical, Physiological and Clinical Considerations for Nanotechnology in Drug Delivery; Nanotechnology for the Delivery of Small Molecules, Peptides, Proteins, and Nucleic Acids; and A Look to the Future of Nanotechnology in Drug Delivery.

The reason for putting the book together this way can be found in the purpose of any drug delivery system, which is to enhance or facilitate the action of any active moiety by using sound scientific and therapeutic principles. Most current methods of drug delivery are direct descendents of ancient practices that have changed little over the last few centuries. However, advances in the fields of drug discovery, biotechnology, and molecular biology have resulted in the discovery of large numbers of novel molecules with the potential to revolutionize the treatment of disease if severe delivery and targeting obstacles can be overcome. This means that using these new armaments in the war against disease must stimulate the development of new strategies for drug and vaccine administration. One such development is the explosion in nanotechnology research geared toward improving drug delivery and targeting.

As shown in this text, a variety of nanostructures are being investigated as functional drug carriers for treating a wide range of therapies, most notably cardiovascular defects, autoimmune diseases, and cancer. While the concept of nanoparticles in drug delivery is not new, the number of research programs and active drug development projects in this field has escalated as funding for nanotechnology has increased. The result is the emergence of a host of novel nanotechnologies tailored to meet the physicochemical and therapeutic requirements of drug developers. With all this potential for advanced drug delivery and targeted therapy, with reduced side effects, nanotechnology-based drug delivery systems hold the promise of significantly improving quality of life through "nanomedicine".

We hope that this book will help to bring these technologies and the underlying fundamental science together in one text for the reader. One or more distinguished authors from each relevant field wrote each chapter, and ample use of figures and tables has been included to help demonstrate the most important aspects.

The successful completion of this text was made possible by the assistance of a large number of people to whom we are very grateful. We extend special thanks to the individual chapter contributors. We also want to thank the publisher and in particular Melanie Wilichinsky for her support.

Melgardt M. de Villiers
Pornanong Aramwit
Glen S. Kwon

Contents

Contributors

Christine Allen
Department of Pharmaceutical Sciences, University of Toronto,
144 College St., Toronto, Ontario, Canada, M5S 3M2,
e-mail: cj.allen@utoronto.ca

Aws Alshamsan
Faculty of Pharmacy and Pharmaceutical Sciences, 3133 Dentistry/
Pharmacy Centre, University of Alberta, Edmonton, Alberta, Canada,
T6G 2N8, e-mail: aalshmsan@pharmacy.ualberta.ca

Tania Betancourt
Department of Biomedical Engineering, The University of Texas at
Austin, Austin, TX 78712, USA,
e-mail: tania.betancourt@mail.utexas.edu

Lisa Brannon-Peppas
Appian Labs LLC, 11412 Bee Caves Road, Suite 300, Austin
TX 78738, USA, e-mail: lpeppas@etibio.com

Melgardt M. de Villiers
School of Pharmacy, University of Wisconsin-Madison, Madison,
WI 53705, USA,
e-mail: mmdevilliers@pharmacy.wisc.edu

Amber Doiron
Department of Biomedical Engineering, The University of Texas at
Austin, Austin, TX 78712, USA,
e-mail: adoiron@mail.utexas.edu

Michael Dunne
Department of Pharmaceutical Sciences, University of Toronto,
144 College St., Toronto, Ontario, Canada, M5S 3M2

Jonathan P. Fast
Department of Chemistry, University of Wisconsin-Madison, Madison,
WI, 53706, USA

Hamidreza Ghandehari
University of Utah, Department of Pharmaceutics and Pharmaceutical Chemistry and Bioengineering, Salt Lake City, Utah, 84108, USA, e-mail: hamid.ghandehari@pharm.utah.edu

Islam Hamad
The Molecular Targeting and Polymer Toxicology Group, School of Pharmacy, University of Brighton, Brighton BN2 4GJ, UK

Samar Hamdy
Faculty of Pharmacy and Pharmaceutical Sciences, 3133 Dentistry/Pharmacy Centre, University of Alberta, Edmonton, Alberta, Canada, T6G 2N8, e-mail: shamdy@pharmacy.ualberta.ca

Kimberly A. Homan
Department of Biomedical Engineering, The University of Texas at Austin, Austin, TX USA, 78712, e-mail: kim@usdsg.com

Anja Judefeind
School of Pharmacy, University of Wisconsin-Madison, Madison, WI 53705, USA

Weiyuan John Kao
Department of Biomedical Engineering, School of Pharmacy, University of Wisconsin-Madison, Madison, WI 53705 USA, e-mail: wjkao@pharmacy.wisc.edu

Mansoor A. Khan
Division of Product Quality Research, Office of Testing and Research, Office of Pharmaceutical Sciences, Center for Drug Evaluation and Research, Food and Drug Administration, Silver Spring, MD 20993 USA, e-mail: Mansoor.khan@fda.hhs.gov

Sungwon Kim
Department of Industrial and Physical Pharmacy, Purdue University, West Lafayette, Indiana 47907, USA, e-mail: kim27@purdue.edu

Kelly M. Kitchens
Alba Therapeutics Corporation, Discovery and Preclinical Development, Baltimore, MD, USA, MD 21201

Oliver Kreft
Max-Planck-Institute of Colloids and Interfaces, Research Campus Golm, 14424 Potsdam-Golm, Germany

Ick Chan Kwon
Biomedical Research Center, Korea Institute of Science and Technology, Seoul 136-791, Korea, e-mail: ikwon@kist.re.kr

Il Keun Kwon
School of Dentistry, Kyung Hee University, Seoul 130-701, Korea, e-mail: kwoni@khu.ac.kr

Afsaneh Lavasanifar
Faculty of Pharmacy and Pharmaceutical Sciences, University of Alberta, Edmonton, AB, Canada T6G 2NB,
e-mail: alavasanifar@pharmacy.ualberta.ca

Jubo Liu
Department of Pharmaceutical Sciences, University of Toronto, 144 College St., Toronto, Ontario, Canada, M5S 3M2

Shingai Majuru
Department of Pharmaceutics Research and Development, Emisphere Technologies, Inc., 765 Old Saw Mill River Road, Tarrytown, NY, 10591, USA, e-mail: smajuru@emisphere.com

Sandro Mecozzi
Department of Chemistry and School of Pharmacy, University of Wisconsin, Madison, WI 53705, USA, e-mail: smecozzi@wisc.edu

Jessica B. Melanko
Department of Chemical and Biochemical Engineering, Division of Pharmaceutics, College of Pharmacy, University of Iowa, Iowa City, IA 52242, USA

Mohammed J. Meziani
Department of Chemistry and Laboratory for Emerging Materials and Technology, Clemson University, Clemson, SC 29634-0973, USA,
e-mail: mmezian@clemson.edu

S. Moein Moghimi
Department of Pharmaceutics and Analytical Chemistry, Faculty of Pharmaceutical Sciences, University of Copenhagen, DK-2100 Copenhagenϕ, Denmark, e-mail: s.m.moghimi@brighton.ac.uk

Yukio Nagasaki
Tsukuba Research Center for Interdisciplinary Materials Science (TIMS) and Graduate School of Pure and Applied Sciences, University of Tsukuba, 1-1-1 Ten-noudai, Tsukuba, Ibaraki 305-8573, Japan,
e-mail: nagasaki@nagalabo.jp

Motoi Oishi
Tsukuba Research Center for Interdisciplinary Materials Science (TIMS) and Graduate School of Pure and Applied Sciences, University of Tsukuba, 1-1-1 Ten-noudai, Tsukuba, Ibaraki 305-8573, Japan.

Daniel P. Otto
School of Pharmacy, University of Wisconsin-Madison, Madison, WI 53705, USA

Moses O. Oyewumi
Department of Pharmaceutics Research and Development, Emisphere Technologies, Inc., 765 Old Saw Mill River Road, Tarrytown, NY 10591, USA

Kinam Park
Department of Industrial and Physical Pharmacy, Weldon School of Biomedical Engineering, Purdue University, West Lafayette, Indiana 47907, USA e-mail: kpark@purdue.edu

Pankaj Pathak
Department of Chemistry and Laboratory for Emerging Materials and Technology, Clemson University, Clemson, SC 29634-0973, USA, e-mail: ppalthak@clemson.edu

Megan E. Pearce
Department of Biomedical Engineering, Division of Pharmaceutics, College of Pharmacy, University of Iowa, Iowa City, IA 52242, USA

Michael V. Pishko
Department of Materials Science and Engineering, The Pennsylvania State University, University Park, PA 16802, USA. Department of Chemistry, University Park, PA 16802, USA, e-mail: mpishko@engr.psu.edu

Aliasger K. Salem
Division of Pharmaceutics, College of Pharmacy, University of Iowa, Iowa City, IA 52242, USA, e-mail: aliasger-salem@uiowa.edu

John Samuel
Faculty of Pharmacy and Pharmaceutical Sciences, 3133 Dentistry/ Pharmacy Centre, University of Alberta, Edmonton, Alberta, Canada, T6G 2N8, e-mail: jsamuel@pharmacy.ualberta.ca

Rakhi B. Shah
Division of Product Quality Research, Office of Testing and Research, Office of Pharmaceutical Sciences, Center for Drug Evaluation and Research, Food and Drug Administration, Silver Spring, MD 20993 USA, e-mail: rakhi.shah@fda.hhs.gov

Andre G. Skirtach
Max-Planck-Institute of Colloids and Interfaces, Research Campus Golm, 14424 Potsdam-Golm, Germany, e-mail: skirtach@mpikg.mpg.de

Patrick Lim Soo
Department of Pharmaceutical Sciences, University of Toronto, 144 College St., Toronto, Ontario, Canada, M5S 3M2

Ya-Ping Sun
Department of Chemistry and Laboratory for Emerging Materials and Technology, Clemson University, Clemson, SC 29634-0973, USA

Vladimir P. Torchilin
Department of Pharmaceutical Sciences and Center for Pharmaceutical Biotechnology and Nanomedicine, Northeastern University, Boston, MA 02115, USA, e-mail: v.torchilin@neu.edu

Hasan Uludağ
Faculty of Pharmacy and Pharmaceutical Sciences, Department of Chemical & Materials Engineering, Faculty of Engineering, University of Alberta, Edmonton, Alberta, Canada T6G 2G6,
e-mail: huludag@ualberta.ca

Xiao-Bing Xiong
Faculty of Pharmacy and Pharmaceutical Sciences, University of Alberta, Edmonton, Alberta, Canada T6G 2N8,
e-mail: xxiong@pharmacy.ualberta.ca

Alisar S. Zahr
Department of Chemical Engineering, The Pennsylvania State University, University Park, PA 16802

Guigen Zhang
Faculty of Engineering, The University of Georgia, Anthens, GA 30602, USA

Sean T. Zuckerman
Department of Biomedical Engineering, School of Pharmacy, University of Wisconsin-Madison, Madison, WI 53705 USA

Part I

Fundamentals of Nanotechnology in Drug Delivery

1

Physicochemical Principles of Nanosized Drug Delivery Systems

Daniel P. Otto and Melgardt M. de Villiers

Introduction to Nanoscience and Nanotechnology

Today, nanotechnology is a commonly used buzzword in numerous fields of science and everyday life, and fairly recently in drug delivery (Dosch, 2001; Navrotsky, 2007). Numerous definitions have been coined to describe nanotechnology and nanoscience and these are often used interchangeably. Nanoscience could be defined as the activity aimed at the understanding of natural laws at a nanoscale level and nanotechnology as the novel and practical applications of this scientific knowledge to change the world we live in (Balzani, 2005).

Several restrictions have been placed on what exactly nanotechnology is. It has been described as the exploitation of materials with structural features at the intermediate range between atoms and the molecular scale with the important prerequisite that at least one dimension is in the nanometer length scale (Rao & Cheetham, 2001; Rao, Kulkarni, Thomas & Edwards, 2002; Jortner & Rao, 2002). The most common consensus, however, is that nanotechnology investigates and manipulates materials and phenomena where at least one length scale is below 100 nm (NNI, 2007).

Some early studies reported the potential of nanoscale drug delivery systems and since then a myriad of these delivery systems have been documented (Khanna & Speiser, 1969; Brasseur, Couvreur, Kante, Deckers-Passau, Roland, Deckers & Speisers, 1980; El-Egakey, Bentele & Kreuter, 1983; Krause, Schwarz & Rohdewald, 1985).

The scale of some nanoparticulate drug delivery systems is compared to some other easily recognizable objects in Figure 1.1.

The applications described in this chapter focus on the pharmaceutical aspect of nanotechnology by elucidating applications of nanotechnology in drug delivery systems. Some fundamental properties make these nanoscaled systems special, and a physicochemical perspective is required to explain this. The next sections will focus on the unique characteristics that make nanosized delivery systems different from conventional or traditional dosage forms.

M.M. de Villiers et al. (eds.), *Nanotechnology in Drug Delivery*, DOI: 10.1007/978-0-387-77667-5_1,

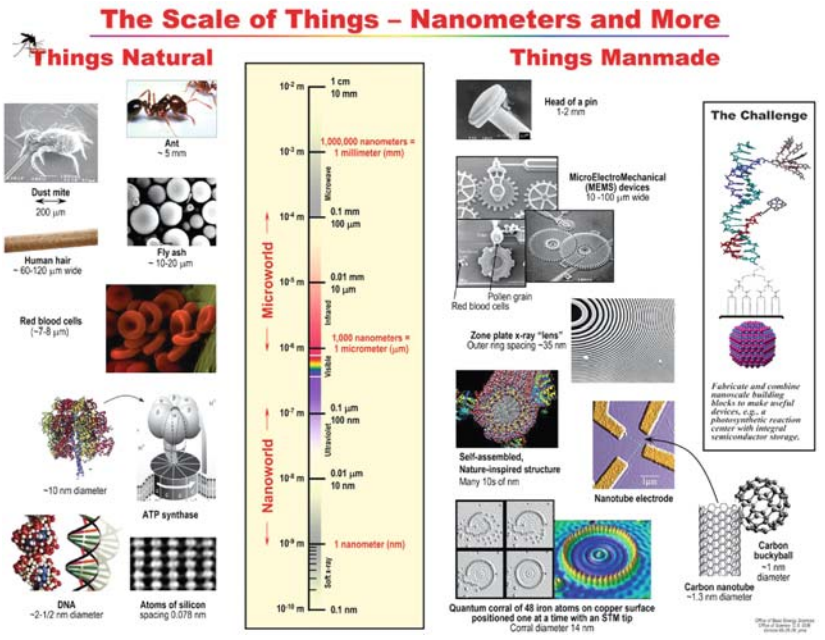

Figure 1.1 Relative size of nanoparticles compared to familiar items (courtesy of the Office of Basic Energy Sciences, Office of Science, U.S. Department of Energy, http://www.sc.doe.gov/bes/scale_of_things.html). (*See* Color Plate 1)

The Fundamental Properties of Nanomaterials

Two aspects of nanomaterials render them fundamentally different in their behavior compared to bulk systems. These aspects can be delineated as surface-related properties and quantum properties (Roduner, 2006).

Surface-to-Volume Ratio

The surface-to-volume ratio of nanomaterials is significantly larger than that of their bulky counterparts. If a sphere was taken, it would be seen that its surface is scaled with its radius, r; however its volume scales with r^3. The fraction of atoms at the surface is known as the dispersion, F, and the dispersion scales with the ratio of surface area to volume and therefore the inverse radius (Roduner, 2006).

The dependence of the surface dispersion is illustrated for a cube of n atoms along an edge, with the total number of atoms in the cube described as $N = n^3$. A cube would therefore expose 6 surfaces and 12 edges, with the total number of surface atoms equal to $6n$ that has been corrected to eliminate double counting of corner atoms. For large numbers of atoms in a cube, these corrections become negligible and the dispersion could be scaled as follows:

$$F = \frac{6n^2 - 12n + 8}{n^3} = \frac{6}{N^{1/3}}\left(1 - \frac{2}{N^{1/3}} + \frac{8}{6N^{2/3}}\right) \approx \frac{6}{N^{1/3}} \qquad (1)$$

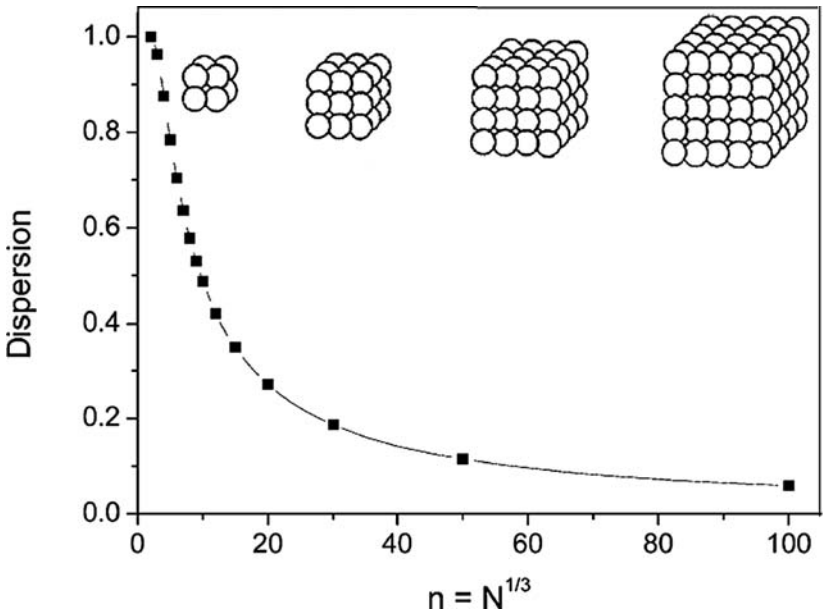

Figure 1.2 Evolution of the dispersion F as a function of n for cubic clusters up to $n = 100$ ($N = 106$). The structure of the first four clusters is displayed. (Reprinted with permission from the PCCP Owner Societies.)

The conclusion from this equation is that all properties that are related to the dispersion of surface groups will result in a dependence on the inverse radius of the particle and also on the number of the atoms by $N^{-1/3}$ (Roduner, 2006) as depicted in Figure 1.2.

The dispersion of surface atoms is also known as the coordination number, $<NN>$, and describes the number of nearest neighboring atoms. For particles with significant fractions of surface atoms, a low coordination number is found. For infinitely large clusters, the coordination number extrapolates to 12 and resembles the bulk of the material. A typical property of materials that scales with $N^{1/3}$ is the cohesive energy of particles. Typically, corner and edge atoms are missing due to their low stability and tendency to form bonds. Typically, these nanosystems also show lower melting points with a liquid-like surface property. The surface-related properties of nanoparticles will be discussed in this chapter.

Quantum Effects

It has been found that the electronic structure of small particles is generally very discrete and not overlapping as is the case with bulk material phases. This is due to confinement of the electron wavefunctions of certain physical dimensions of the nanoparticles (Rao et al., 2002).

As with most orbital systems, electrons can be found at different (higher and lower) energy levels, and the average spacing of this energy level is known as the Kubo gap, δ. By considering the lowest unoccupied energy

state of the electronic system of a bulk material, the Fermi energy, E_f, could be incorporated to describe the Kubo gap:

$$\delta = 4E_f/3n \tag{2}$$

where n is representing the number of valence electrons in the nanosystems. In the case where the thermal energy of systems exceeds the Kubo gap, they will behave metallically, and if the thermal energy does not exceed this value, they will behave non-metallically. This change is especially prevalent in small systems at the nanoscale and explains why certain materials become magnetic or electrically conductive at the nanometer scale. Differences in optical properties are also noted for nanosystems that are observed as luminescence and size-dependent color changes of certain metallic nanoparticles. Before we discuss the thermal and optical properties of nanosystems, some more definitions are needed.

The thermal and optical properties of materials arise from the vibration of adjacent molecules, atoms or ions that are arranged in the lattice and these vibrations are known as phonons. The order in the lattice is momentarily disturbed as phonons vibrate like waves from one point to the next. These phonons are quantized and therefore only certain vibration frequencies are allowed. This term is analogous to the term photon referring to the emission of electrons in the form of light energy, also in discrete units of energy or quanta. Phonons are responsible for heat transfer, optical effects and the acoustic properties observed in all materials. As we already established, nanosystems are very confined compared to macrosystems, and therefore the phonon transport under confined conditions imparts different properties to nanomaterials compared to their bulk counterparts (Balandin, 2005; Cahill, Ford, Goodson, Mahan, Majumdar, Maris, Merlin & Phillpot, 2003; Shakouri, 2006).

Optical Properties of Nanoparticles

Gold nanoparticles have received a lot of attention over the years, and the peculiar optical behavior at the nanoscale has seen marked interest. The differences in particle colors are a direct consequence of the interaction of phonons and photons and result in size-dependent color emissions. The Raman effect is one of the most widely known phenomena that arise from this interaction. As seen previously, decreasing size will increase the Kubo gap and therefore the energy emitted by the photons will change frequency and hence their color. (Sun & Xia, 2003; Nobile, Kudera, Fiore, Carbone, Chilla, Kipp, Heitmann, Cingolani, Manna & Kranhe, 2007; Xu & Cortie, 2006; He, Liu, Kong & Liu, 2005; Hu, Chen, Li, Au, Hartland, Li, Marquez & Xia, 2006; Hirsch, Gobon, Lowery, Tam, Drezek, Halas & West, 2006; Aizpurua, Hanarp, Sutherland, Käll, Bryant & de Abajo, 2003).

Multiple sensing applications are made possible by the color changes associated with gold and other metal nanoparticles as they change in size

or due to interactions with target biomolecules that alter their size. Therefore, one can perform quantitative and qualitative analyses of particle size and distributions and particle concentration and the effect of particle shape as consequence of optical spectrum shifts. A typical example includes detection of cholera toxin which if agglomerated with gold particles changes the gold nanoparticle color from red to purple (Schofield, Field & Russell, 2007).

Assembly and disassembly of nanoparticles can also be monitored as aptly illustrated for gold nanoparticles that are functionalized with DNA. Upon assembly of a DNA-gold complex, the gold nanoparticles display a blue color due to the size change of the DNA complex. As these complexes hydrolyze in the presence of lead, they release the individual, red gold nanoparticles (Liu & Lu, 2004).

Obviously, these examples indicate the sensing capabilities of these particles. Various chemical and biochemical binding events could be envisioned based on various silver and gold nanoparticles in different environments. Additionally, it has also been shown that gold nanoshells (with hollow interiors) are significantly more sensitive to environmental changes than solid colloids (Figure 1.3) (Sun & Xia, 2003; Hutter & Fendler, 2004).

By adjusting the composition of the particles from pure silver or gold to alloys of the two metals, the UV–visible extinction spectrum of these particles could be tuned, and therefore their activity could be changed. Figure 1.4 illustrates these effects.

The effect of swelling and temperature was also shown for various metals incorporated into polymer gels. The authors speculate that these effects could have application in the biomedical and electronic fields. Gold and silver nanoparticles were synthesized in an acrylic polymer matrix containing charged amino groups in the polymer chains. Subsequently, the gold nanoparticles were in proximity to each other if the polymer matrices were cooled down and moved away from each other once heat

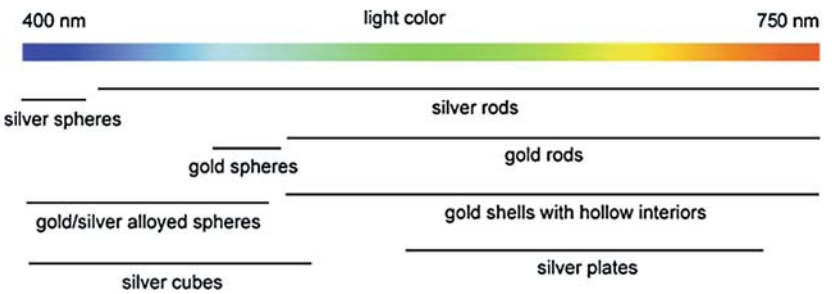

Figure 1.3 A list of silver and gold nanoparticles having various morphologies, compositions and structures, together with their typical locations of surface plasmon resonance bands in the visible regime (Sun & Xia, 2003). (Reprinted with permission from The Royal Society of Chemistry.) (*See* Color Plate 2)

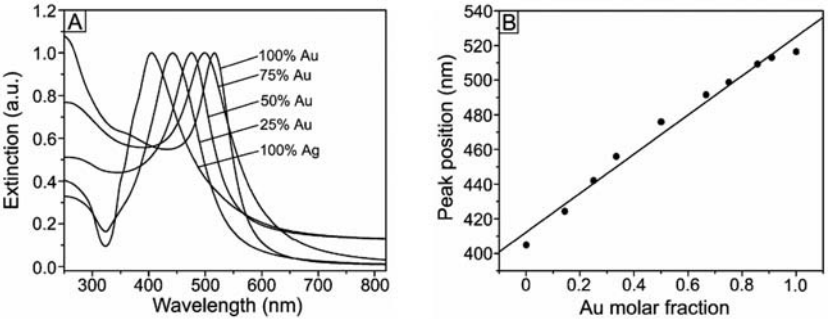

Figure 1.4 (**A**) UV–visible extinction spectra of solid colloids made of pure silver, pure gold, and silver/gold alloys with various molar fractions of gold. All spectra were normalized against their peak extinctions. (**B**) A plot showing the linear dependence between the extinction peak position (λ_{max}) and the molar fraction of gold (χ_{Au}) in the nanoparticles (Sun & Xia, 2003). (Reprinted with permission from the Royal Society of Chemistry.)

was applied to swell the polymer matrix. The color changes are observed in Figure 1.5 (Suzuki & Kawaguchi, 2006).

One could typically speculate about the application of the temperature-dependent extinction maxima of the nanoparticles. It could be stated that these polymer–gold nanoparticle complexes could be stored at some predetermined temperature for stability purposes and therefore exhibit some distinct color or color change once the temperature is changed. If the polymer matrix was synthesized such that a color change was irreversible, it should prove a valuable visual indicator of stability.

An in vivo effect of this type of polymer–nanoparticle complex could arise once these nanosensors are absorbed in the body. The polymer matrix would heat up and show a spectral shift in terms of the absorption maximum for the gold particle as the polymer swells. Some lesions in the body could show different temperatures compared to unaffected parts due to localized inflammation or localized concentration of nanoparticles. Applications could be tuned toward this absorption maximum, such as seen later, for cancer treatment and diagnosis, and for potentially other inflammatory responses such as arthritis. Figure 1.5 illustrates the swelling and temperature effect on the colorimetric properties of copolymer nanoparticles with various metallic compositions.

We can speculate that it will not be long before the size- and aspect-dependent optical effects are employed in the pharmaceutical field. The sensing capabilities of these particles could prove invaluable in applications such as monitoring stability. Pharmaceutical substances could agglomerate at any stage during manufacturing and storage; and these sensors could give visual inspection of particle size and distribution. Furthermore, these sensors do not show the characteristic photobleaching of currently employed fluorescent probes. These metallic type probes could probably render in vitro and vivo studies even more effective in terms of detection efficiency (Gobin, O'Neal, Watkins, Halas, Drezek & West, 2006; Burns, Ow & Wiesner, 2006).

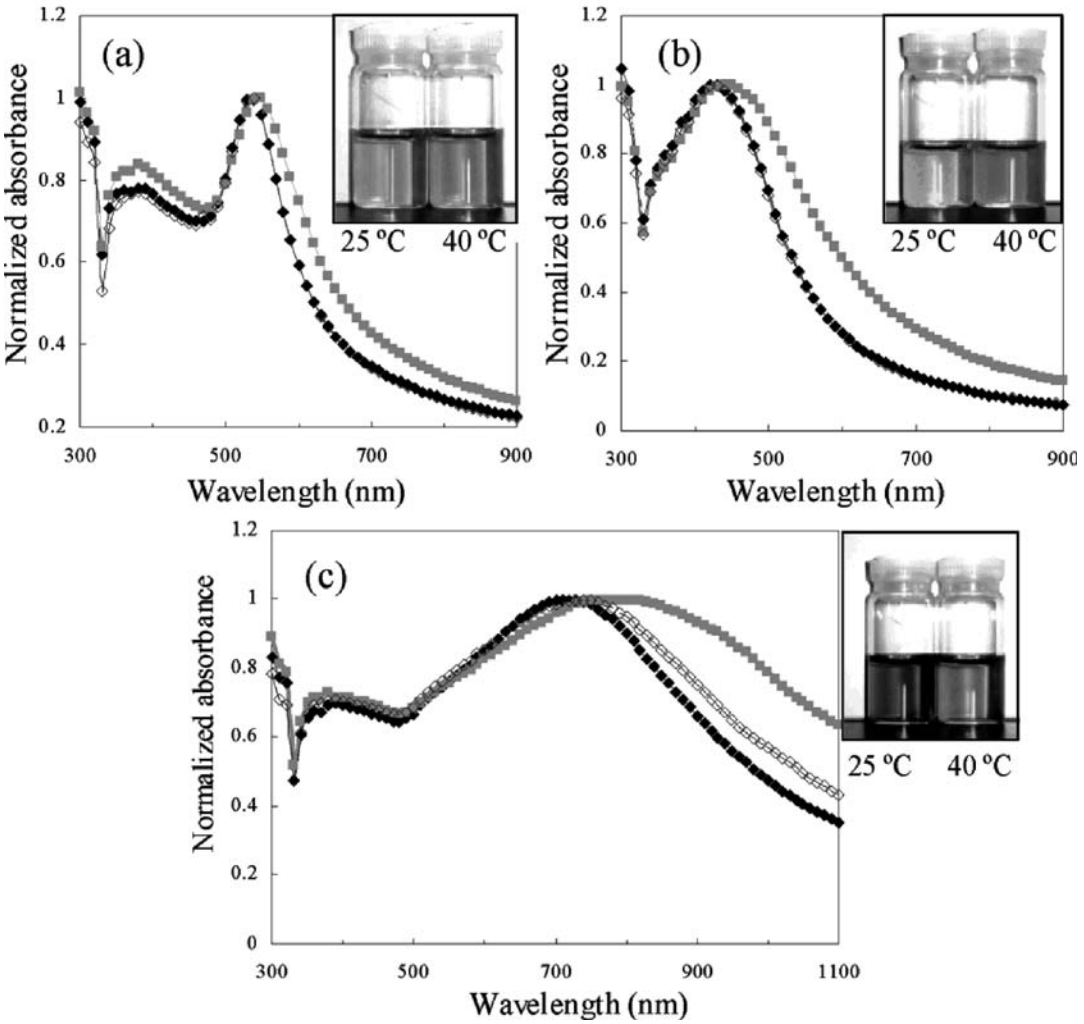

Figure 1.5 (**a**) UV–visible spectra of NG-NH_2-Au/Au2, (**b**) NG-NH_2-Au/Ag/Au microgels (NG is the copolymer gel), (**c**) measured at 25°C (*black diamonds*), 40°C (*gray squares*) and 25°C after 10 heating–cooling cycles (*open diamonds*). All spectra presented here were normalized by taking the temperature effects into account (Suzuki & Kawaguchi, 2006). (Reprinted with permission from ACS publications.) (*See* Color Plate 3)

The interaction of phonons and electrons has already provided very useful effects, and since these optical resonances could be tuned to scatter or absorb light in the UV and NIR regions, they could also be employed as UV shields. Photosensitive drugs including nifedipine have been shown to benefit from a nanocoating composed of titanium dioxide particles to shield it from UV radiation (Li, Kommireddy, Lvov, Liebenberg, Tiedt & De Villiers, 2006).

Nanoencapsulation of a sunscreen agent in PLGA nanoparticles also curbed the photodegradation of the agent. The polymer most probably filtered the UV radiation due to a photon–phonon interaction, although, it has not been stated directly by the authors. The two examples of

photostability should, however, provide enough motivation to investigate the effects on other photosensitive drugs.

Finally, cancer therapy and diagnostics could be optimized when nanometallic particles are used as augmentation to chemotherapeutic agents. Not only could the particles serve as heat absorbents, but the particles could be tuned to absorb the maximum quantity of light energy from a laser source at a very discreet wavelength due to a tunable surface plasmon resonance which could also enhance the target-specific thermolysis of tumors (Loo, Lowery, Halas, West & Drezek, 2005; Gobin et al., 2006; Lin, Lewinski, West, Halas & Drezek, 2005; Liao, Nehl & Hafner, 2006).

Thermodynamic Properties of Nanoparticles

Heat Transfer

One can generally validate thermodynamics when the number of atoms in a particular system is large and again consider the coordination number of a certain atom. However, the coordination number is small in nanosystems and some deviations are evident. A primary problem is how to define a local temperature in a small system, something that could easily be observed in a bulk system. An oversimplification could be made stating that one might not have abrupt variations in temperature between two successive rows of atoms in a nanosystem as would be the case in bulk transitions (Guisbiers, Shirinyan & Wautelet, 2005).

We already saw that phonons can play a vital role in the optical properties of nanoparticles (as a consequence of surface plasmon resonance effects), and these vibrations are also the mechanism for heat transport in the nanosystems. Phonons fluctuate over a specified length scale, the mean free path, since they are quantized in the nanoscale range. If different regions showed different local temperatures, then the distributions of their phonons are also different. Phonons can scatter its energy along its mean free path, resulting in local temperature differences. The phonon scattering is highly dependent on the frequency of the solid, and the mean free path of the phonon can therefore not be readily predicted as found for silica nanofilms (Ju & Goodson, 2000) which showed a mean free path of 250–300 nm instead of the predicted 40 nm (Chen, 2000). This perspective implies that temperature could not be defined for an atom or atom plane and will need to be investigated in the future.

A troublesome issue in nanosystems is therefore that the particles are too small to show deviations in temperature in different regions of the material. Additionally, the effect of phonon vibrations (that are quantitized along a specified pathlength) on the heat dispersion in nanopartciles, is still not fully understood. A local nanosized region with a defined local temperature would only be possible if it is larger than the mean free path of the phonon. This definition is compounded by the fact that different phonons have different mean free path lengths, i.e., low-frequency phonons have long mean free path lengths and high-frequency phonons short mean free path lengths (Cahill et al., 2003; Hatta, 2002).

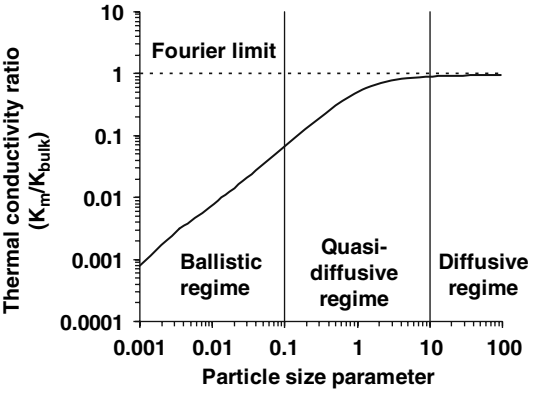

Figure 1.6 Effective thermal conductivity as a function of the particle size parameter (particle radius normalized by the phonon free path in the surrounding medium) for heat conduction in the vicinity of a nanoparticle embedded in a host material. As the particle size becomes smaller than the phonon mean free path in the host material, the effective thermal conductivity that the particle feels about the surrounding medium is reduced to a rarefied gas effect. The particle size parameter is the ratio of the particle radius to the mean free path of the phonon. (Reproduced from the original data) (Chen, 2000).

Closely related to the definition of temperature is that of heat transfer for which bulk materials follow Fourier's law (Chen, 2000; Michel, Gemmer & Mahler, 2006; Lepri, Livi & Politi, 2003):

$$q = -k\nabla T \tag{3}$$

The local heat flux is defined by the term q and the temperature gradient is denoted by ∇T, and finally the thermal conductivity is noted as the term k.

The heat flux is proportional to the temperature gradient between the material extremities and also to the thermal conductance of the material. However, this is invalid for nanoparticles since the phonon free length path is larger than the distance between adjacent heat sources and the Fourier law fails to describe heat transfer, and the heat transport between nanoparticles is therefore said to be ballistic rather than diffusive (Tien & Chen, 1994; Cenian & Gabriel, 2001; Chen, 2000; Chen, 1996).

The ballistic nature of heat transfer arises from boundaries between nanoparticles and the contribution of these boundaries to phonon scattering at the boundaries by in and out of plain lattice vibrations rather than diffusive transfer to the next particles (Chen, 2002; Gomes, Madrid, Goicochea, Amon, 2006). Figure 1.6 depicts the Fourier limit to heat transfer.

The difference between the heat transfer mechanism in nano- and macroscale materials also results in different thermal properties as will be discussed in the following sections.

Basic Treatment of Classic Nucleation Theory

Classic treatment of nucleation states that a multicomponent system exists as a single phase, and following a change in boundary conditions by events such as a change in temperature and pressure or by mixing with a further homogenous phase the free energy changes as well and favors phase separation. This approach assumes that the particles of one component would tend to coalesce and form nuclei. Equation (4) describes the change in energy as the Gibbs-free energy (Rieger & Horn, 2001):

$$\Delta G = \Delta G_S + \Delta G_V = 4\pi r^2\gamma + 4/3\pi r^3 \Delta g_v \tag{4}$$

where the subscripts S and V refers to the surface and bulk volume, respectively. Clearly, the equation is derived to accommodate geometrical parameters of the surface and bulk and, the nucleus radius is given by r, the surface tension between the two phases by γ and very importantly, the difference in free energy per unit volume between the two phases by Δg_v. At a radius exceeding the critical radius r^*(Equation 5) particles start to grow whilst those below this value redissolve (the Ostwald-ripening effect). The effect of the critical radius on the Ostwald ripening is discussed elsewhere (Finsy, 2004):

$$r^* = -2\gamma/\Delta g_v \tag{5}$$

If an equilibrium approach is followed, the rate of nucleation can be described as function of time and volume by the Arrhenius relation (Equation 6):

$$J = A\exp(-\Delta G^*/kT) \tag{6}$$

where A is determined by the molecular process frequency, k is the reaction tempo constant and T is the absolute temperature of the reaction environment.

Thus, the nucleation rate J expressed in terms of supersaturation and particle radius is given by Equation (7):

$$J = A\exp(-(16\pi\gamma^3 v^2)/(3k^3T^3[\ln S]^2)) \tag{7}$$

where the supersaturation is presented by $S = c(r)/c^*$, with $c^*$the equilibrium solubility and if coupled to molecular volume assumes the form in Equation (8):

$$kT\ln(S) = 2\sigma v/r \tag{8}$$

Figure 1.7 depicts the energy changes and also illustrates the classic colloid effect where a substance will dissolve or react to produce an

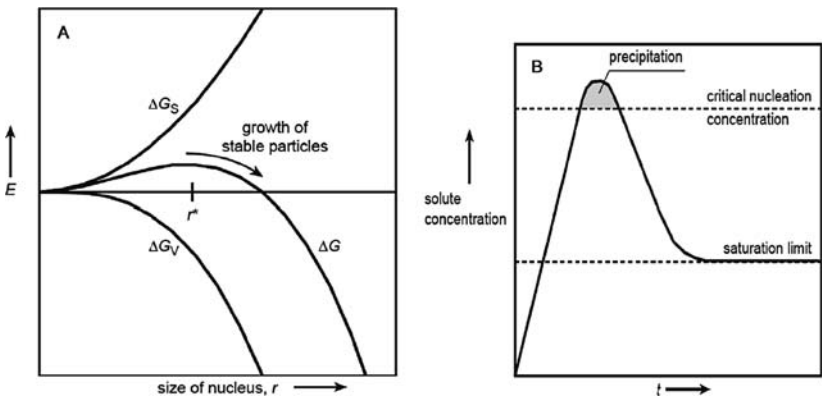

Figure 1.7 (**A**) Energy diagram to explain the nucleation process ($\Delta G$is the free energy of a particle of radius$r$, $\Delta G_S$and ΔG_V is the surface and bulk energies, respectively, $r^*$is the critical nucleus radius of a particle. (**B**) The concentration relationship in controlled particle formation (Rieger & Horn, 2001). (Reprinted with permission from John Wiley.)

increasing concentration until a critical concentration is attained. At the critical concentration a multitude of nuclei forms can grow. With precipitation of these grown particles, the concentration of the solute momentarily drops below the critical level and no new nuclei forms. The nuclei that did form, however, grows until the concentration of the solute approximates the equilibrium concentration.

Various manipulations of these surface energies have been documented and particularly dedicated to the nanoscale regime. The following sections will explain some of these findings in, glass transition, melting point and solubility.

Glass Transition Temperature

A multitude of materials can solidify as glasses rather than crystals and it has been found that finite size effects exist in the glass transition state that affects the stability of low-dimensional materials (Zhang, Zhao & Jiang, 2001; Jiang, Shi & Li, 1999).

Since the 1990 s, significant interest has been focused on the glass transition temperature (T_g) for nanomaterials for which both depressions and increases of the values were found compared to bulk material transitions. The T_g provides a very practical guide to the maximum processing temperature of the material for many applications (Koh, Mckenna & Simon, 2006). This development was most probably the offspring of a study by Bares (1975) that found that the T_g of styrene–butadiene–styrene triblock copolymers decreased as surface-to-volume ratio increased. Bares (1975) expanded the dependence of the T_g on the molecular weight as follows from the original form (Equation 9) (Fox & Flory, 1950) to the form (Equation 10) (Bares, 1975):

$$T_g = T_{g\infty} - K_M/M \tag{9}$$

$$T_g = T_{g\infty} - K_M/M - K_S(S/V) \tag{10}$$

where T_g is the glass transition temperature of the material, $T_{g\infty}$ is a constant glass transition temperature of the material where the molecular weight of the material is infinite (therefore constant). K_M is a constant describing the change in glass transition temperature for a specific material with a molecular mass of M. K_S is a constant that describes the change in glass transition temperature as a function of the surface-to-volume ratio, (S/V), of particles in the nanomaterial. Illustrations of Equation (10) are seen in Figure 1.8.

From Figure 1.7, one can see that a strong dependence is noted for T_g on molecular weight for this specific polymer fraction and most materials will show at least some dependence on weight. In addition, in the work of Bares (1975), some depression in T_g could also be expected as function of the surface-to-volume ratio of small particles. It was found that the depression of T_g was linear in the range that was evaluated for styrene–butadiene–styrene triblock copolymers as well as for styrene–isoprene–styrene triblock copolymers.

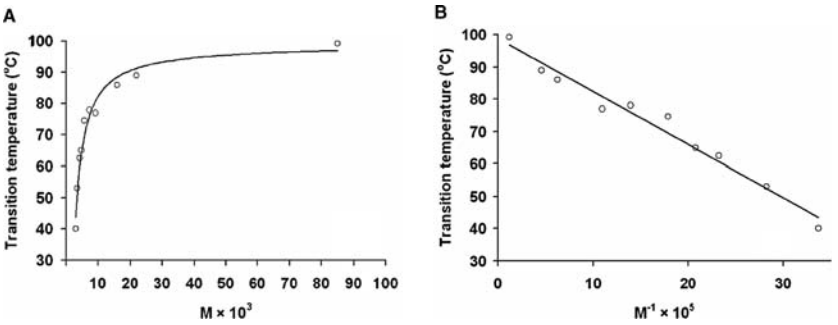

Figure 1.8 Transition temperatures of polystyrene fractions versus (**A**) molecular weight and (**B**) inverse molecular weight (Reproduced from the original data) (Fox & Flory, 1950).

A number of studies have shown that T_g is depressed for ultrathin polymer films of nanoscale proportions compared to the bulk (Koh et al., 2006) and that the depression is proportional to the thickness of the films. These depressions could probably tie in with the decrease in the associated $<NN>$ of the films as they become thinner (Jiang et al., 1999). Consequently, lower cohesive energies are apparent, resulting in depression of T_g of the film. Figure 1.9 illustrates the change in T_g for ultrathin polystyrene films as function of thickness. The films were collected as free-standing films or on support and this also influenced their glass transition depression.

It is not just nanofilms of polymers that could show depression of glass transition temperature of the material compared to the bulk. If organic

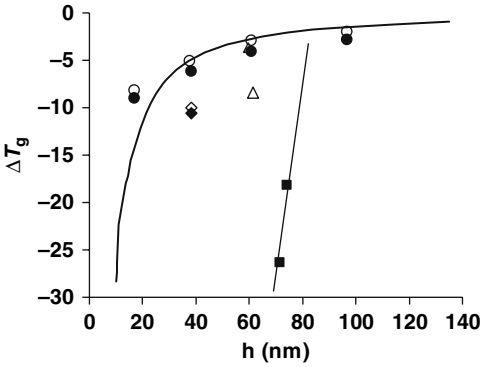

Figure 1.9 T_g of PS ultrathin films as a function of the film thickness (h): (•) first DSC heating scan for films spin coated from toluene and collected with tweezers; (○) subsequent heating scan for films spin coated from toluene and collected with tweezers; (♦) DSC heating scan for films spin coated from toluene and collected on Teflon; (◇) DSC cooling scan for films spin coated from toluene and collected on Teflon; and (△) DSC second heating scan for films spin coated from a cosolvent and collected on Teflon. The *thick line* is the best fit found (Keddie & Jones, 1995) for supported PS thin films. The *thin line* and *squares* for freely standing PS thin films (Dalnoki-Veress, Forrest, Murray, Cigault, & Dutcher, 2001) that have a molecular weight similar to that of this sample (Koh et al., 2006). (Reprinted with permission from John Wiley.)

liquids are confined in nanoscale pores of a certain substrate, the nucleation of the liquid could be markedly affected. It is known that a critical nucleus size must be exceeded for the liquid to start crystallizing. This nucleation is affected by the surface-to-volume ratio of the small crystals and subsequently the wetting properties of the specific crystallization material in a specific liquid. The confinement can often be induced by small pore matrices composed of polymer films and gels, porous glass, silica gels and zeolites (Jackson & McKenna, 1996). Ultimately, this confinement should retain the liquid in a supercooled state and thereby facilitate crystallographers to prepare and study the glass phase of the material in question (MacFarlane & Angell, 1982; Alba, Busse, List & Angell, 1990).

The melting point of nanocrystals has been studied and based on this the argument was expanded to the glass transition of these materials. The finite size effects or confinement of nanoparticles could be studied for the glass transition as derived from the melting point model in Equation (7) and predicted by modification of the model to Equation (11):

$$\frac{T_{\mathrm{m}}(D)}{T_{\mathrm{m}}(\infty)} = \frac{\sigma_{\mathrm{cb}}^2[T_{\mathrm{m}}(\infty)]}{\sigma_{\mathrm{c}}^2[T_{\mathrm{m}}(D)]} = \exp\left(-\frac{2S_{\mathrm{m}}(\infty)}{3RD/D_0 - 1}\right) \tag{11}$$

where $\sigma_{\mathrm{c}}^2[T_{\mathrm{m}}(D)]$ is the averaged mean-squares displacement of atoms of a crystal at the melting point of the crystal, $T_{\mathrm{m}}(D)$. $T_{\mathrm{m}}(\infty)$ and $\sigma_{\mathrm{cb}}^2[T_{\mathrm{m}}(\infty)]$ are the corresponding bulk values of $T_{\mathrm{m}}(D)$ and $\sigma_{\mathrm{c}}^2[T_{\mathrm{m}}(D)]$ respectively. $S_{\mathrm{m}}(\infty)$ indicates the melting entropy of the bulk crystal. R is the ideal gas constant and D_0 represents a critical diameter at which all atoms of a low-dimensional particle are located at the surface (Zhang, Zhao & Jiang, 2001).

The critical diameter, D_0, is further related to certain shape dimensions of the crystal (Zhang et al., 2001; Jiang et al., 1999; Jiang, Aya & Shi, 1997) by Equation (12):

$$D_0 = 2(3 - d)h \tag{12}$$

where $d = 0$ for particles, $d = 1$ denotes nanowires and $d = 2$ is used for thin films and the molecular diameter of the crystals is denoted by h. Therefore, if $d = 2$ it represents the thickness of a thin film layer.

Mott's equation and Equation (13) are used to derive the size-dependent melting entropy of a nanosized particle:

$$S_m(D)/S_m(\infty) = 1 - 1(D/D_0 - 1) \tag{13}$$

where (D) and (∞) are again representative of specific small particle diameter and of the bulk particle diameter, respectively. Theoretical and experimental analyses have shown that (Zhang, et al., 2001; Novikov, Rössler, Malinovsky & Surovtsev, 1996)

$$\sigma_{\mathrm{gb}}^2(T_{\mathrm{g}}) \cong \sigma_{\mathrm{cb}}^2(T_m) \tag{14}$$

where the mean square displacement of molecules of the bulk glass at the glass transition temperature of the bulk, $T_g(\infty)$, is assigned the term, σ^2_{gb}. This implies that as the mean displacement of atoms or ions reach a critical fraction of the interatomic distance, a crystal or glass will melt owing to a common feature: a sharp decrease in viscosity.

By substitution of the bulk heat capacity difference between the glass and liquid, $\Delta C_p(\infty)$, at $T_g(\infty)$ for the entropy term $S_m(\infty)$ and changing notation of the various terms to account for glass transition instead of melting, Equation (15) is derived:

$$\frac{T_g(D)}{T_g(\infty)} = \frac{\sigma^2_{gb}[T_g(\infty)]}{\sigma^2_g[T_g(D)]} = \exp\left(-\frac{2\Delta C_p(\infty)}{3RD/D_0 - 1}\right) \tag{15}$$

where $T_g(D)$ is the size-dependent glass transition temperature with D the diameter of the particle. $\sigma^2_g[T_g(D)]$ is the averaged mean-squared displacement of atoms of a crystal at $T_g(D)$ and the corresponding values for the bulk is given by $T_g(\infty)$and $\sigma^2_{gb}[T_g(\infty)]$, respectively.

Correspondingly, the critical diameter is also now modified (Jiang et al., 1999) in Equation (16):

$$D'_0 = 2(3 - d)h' \tag{16}$$

where h'now represents the smallest distance unit in glasses, i.e., the average chemical bond length between nuclei. A comparison of the size-dependent depression of both melting and glass transition is shown in Figure 1.10 as determined from the derived model in (Equations 11 and 15).

The question could now be raised on the importance of the above-mentioned equations. It seems very complex and inapplicable to a pharmaceutical delivery system. In fact, it could be very important to exploit these properties and explain some observations studied during the processing and analysis of nanoparticulate delivery systems. Clearly, there is a departure in the glass transition behavior of nanomaterials from the bulk.

A recent study on the effect of nanocoating on the stability of amorphous indomethacin material might be interpreted from the effect of confinement of the surface molecules as imparted by the polymer nanofilm. The molecular mobility of the surface molecules is numerous orders

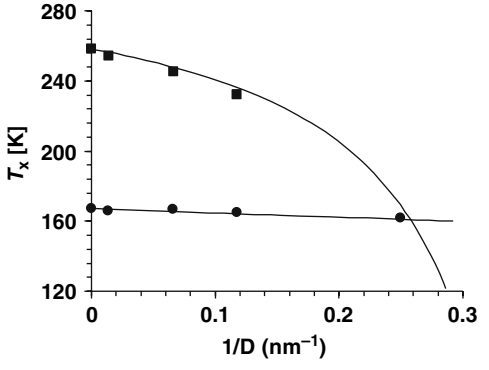

Figure 1.10 $T_m(D)$ and $T_g(D)$ versus $1/D$ for benzyl alcohol. The *solid lines* are the modeled predictions of $T_m(D)$ and $T_g(D)$. The calculation of $T_m(D)$ employed a value of $h = 0.707$ nm, the maximum calculated size of a molecule from bonding lengths for benzyl alcohol. $D_0 = 4h = 2.828$ nm. The symbols (■) and (•) represent experimental data obtained for $T_m(D)$ and $T_g(D)$ respectively (Zhang et al., 2001). (Reprinted with permission from Elsevier.)

higher than in the interior bulk of the crystals. The surface coating employed successfully arrested the molecular surface mobility and therefore precluded crystallization of the surface and subsequently that of the interior bulk (Wu, Sun, Li, De Villiers & Yu, 2007).

Regarding this study of Wu et al. (2007), one might speculate that studies of the nanocoated surface layer should show a lower T_g compared to the bulk indomethacin or interior of the amorphous solid. This would potentially affirm the decrease in cohesive energy of surface molecules and hence their lack of clustering to reach the kinetic critical radius for nucleation. Furthermore, it could confirm findings for the polymer films on substrates or without supports as already discussed earlier. AFM studies could evaluate this hypothesis if coupled to DSC. In addition, it is probable that the surface coating arrests the scattering of the phonon, subsequently stunting energy and heat transfer, and therefore limits lattice mobility and crystallization of the surface layer. It is not yet known whether this nanocoating would also result in optical phonon effects.

The nanocoating approach holds promise to result in a dual action imparted by the polymer nanofilms as both crystallization and photostabilizing agents. The nanocoating could manipulate phonon properties to tailor particles to exhibit specific properties. This development will result in numerous pharmaceutical applications in the years to follow. In fact, phonon filtering or insulation was already suggested to be a major development in the near future of thermal management systems (Kim, Wang & Majumdar, 2007).

Melting Point

As was seen for glass transition temperature, the melting points of nanomaterials also differ from their corresponding bulk materials as a consequence of their free surface and size. Several examples could be found to illustrate the melting point depression as function of the particle size and the reader is referred to these studies (Jiang, Yang & Li, 2002; Liang, Zhao & Jiang, 2002; Shrivastava, 2002; Xue, Zhao & Luan, 2001). The melting temperature is linear to the reciprocal of crystal size and can be expressed (Qi, 2005) in Equation (17):

$$T_m = T_{\mathrm{mb}}(1 - C/D) \tag{17}$$

The terms in Equation (17) are assigned as follows: T_{m} is the melting temperature of the nanosolid, $T_{\mathrm{m\,b}}$ is the bulk melting temperature corresponding to the material of the nanosolid, D is the crystal size of the nanosolid and $C$is a material constant.

Qi (2005) further developed Equation (17) by stating that the number of total atoms of a nanosolid is equated to $n$and the number of surface atoms as N. The number of interior atoms in the solid is therefore $n - N$, and this interior structure could be compared closely to that of the bulk material. If the cohesive energy of a single atom in the bulk is set as E_0, then the total contribution of the interior atoms in the nanosolid is $E_0(n - N)$. Furthermore, half of the total bonds of each surface atom do not contribute to the cohesive energy, and therefore the contribution of the surface bonds to

cohesive energy is expressed as $E_0/2$ and the total contribution of the surface atoms to cohesive energy therefore assumes the form $NE_0/2$. The cohesive energy could therefore be expressed as in Equation (18):

$$E_{\text{tot}} = E_0(n - N) + \frac{1}{2}E_0N \tag{18}$$

Equation (18) is further elaborated by consideration of the Avogadro number, A, to account for the energy per mole of nanosolid, E_{p} (Equation 19):

$$E_{\text{p}} = E_{\text{b}}\left(1 - \frac{N}{2n}\right) \tag{19}$$

where $E_{\text{b}} = AE_0$. In turn it has also been reported that the cohesive energy and melting temperatures of material are indicative of the bond strength between nuclei of the material, and in fact the cohesive energy is linearly proportional to the melting temperature of the material (Guinea, Rose, Smith & Ferrante, 1984).

As is to be expected, the cohesive energy of the nanosolid is therefore a function of the ratio, N/n, and the melting temperature relation can be derived from (Qi, 2005) Equation (20):

$$T_{\text{m}} = T_{\text{mb}}\left(1 - \frac{N}{2n}\right) \tag{20}$$

Considering all arguments stated to this point we can easily deduce, as was predicted by W. Thomson in as early as 1871, that the ratio N/n is dependent on the particle size (Buffat & Borel, 1976) as well as the shape of the particles in question (Guisbiers & Wautelet, 2006; Wang, Fei, Zheng, Jin & Zhang, 2006; Zhang, Li & Jiang, 2000; Wautelet, Dauchot & Hecq, 2003).

Several permutations of the ratio are allowed according to shape, and it was apparent that the variation in $T_{\text{m}}$for particles of equivalent size but for geometries of nanospheres, nanowires and nanofilms is in the relation 3:2:1 (Wautelet, 1998). The reader is referred to the study of Qi (2005). Figure 1.11 depicts the findings of this study.

The effect of size and shape was additionally studied (Wautelet et al., 2003) and some conclusions became apparent. Non-spherical particles of the same volume as that of the spherical ones will solidify at a lower temperature. Nanodisks and nanorods melt at a lower temperature than nanospheres. Under certain conditions the liquid nanoparticles could act as an adhesive between solid particles. It is expected that the shape of the nanoparticle would play a significant effect in the nucleation and reactivity of the particle.

The studies discussed to this point focused primarily on metallic or inorganic materials; however, organic nanocrystals of benzene, chlorobenzene and heptane and naphthalene have also shown Figure 1.12, the identical dependency of melting temperature on particle size as was found for their inorganic and metallic counterparts (Jiang, Shi & Zhao,

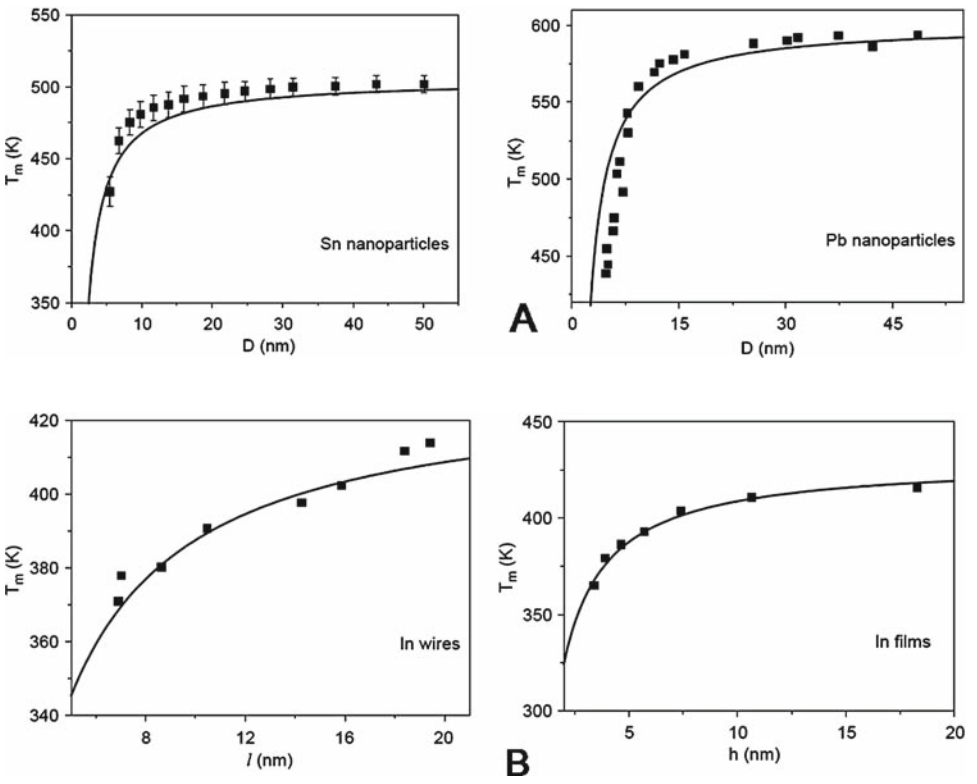

Figure 1.11 (**A**) The dependence of melting temperature on particle size for tin and lead nanoparticles and (**B**) on the geometry of the particles, i.e., nanowires and thin films (Qi, 2005). (Reprinted with permission from Elsevier.)

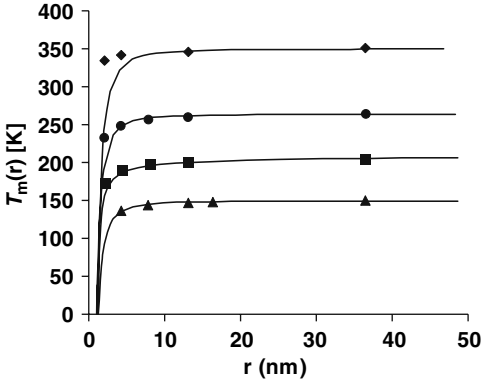

Figure 1.12 Size-dependent melting temperatures of benzene, chlorobenzene, heptane and naphthalene. The *solid lines* are the theoretical predictions of the values and the *symbols* indicate the experimental data (Reproduced from the original artwork) (Jiang, Shi & Zhao, 1999). (Reprinted with permission from the American Institute of Physics.)

1999). This illustrates again that nanoscience deals with the fundamental building blocks of materials and that certain universal laws apply to this field.

One should realize that as was observed with glass transition temperature, the melting point temperature could also oscillate under and above the melting point of the bulk material. This phenomenon is also attributed

to size and the modification of the cohesive energy in a particular system. This cohesive energy change is explained in terms of the bond-order length strength that fluctuates in lower-coordinated systems and is determined by geometry, phonon and surface lattice instability (Sun, Li, Bai & Jiang, 2005).

An application of the oscillation of the melting temperature could be illustrated by introducing single impurity effects on the melting of nanoclusters of materials. By introduction of a single impurity atom, such as Ni or Cu (smaller than the atoms in the nanocluster) that tends to be incorporated inside the cluster, the melting point of a silver cluster could be increased. Though the study was modeled, experimental proof should become apparent in the near future illustrating the selective tuning of the melting temperature of nanomaterials (Mottet, Rossi, Baletto & Ferrando, 2005).

We now focus again on the potential effect of a polymer matrix as a medium for confining the crystallization of organic crystals. Upon achieving a critical size, crystal nuclei will become stable resulting in the growth of mature crystals. The sum of the surface free energy (dominating the precritical size stage) and volume free energy (dominating the stage beyond the critical nucleus size) determines this growth process. Structures that mimic the crystal packing of mature crystal forms could be exploited to manipulate polymorphism, crystal habit and size (Oxtoby, 1998).

Since the dimensions of the near critical size are in the nano-dimensional range, it is thought that modification of a matrix to provide crystallization chambers of a specific dimension and shape could be exploited to regulate crystal properties as illustrated for crystallization in nanoscopic pores of glass and polymer matrices (Ha, Wolf, Hillmyer & Ward, 2004).

Expanding these findings, it was found that interaction of the melt with the polymer matrix walls also affected the total depression of melting temperature of the nanocrystals and is not explained purely from the Gibbs–Thomson equation (Jackson & McKenna, 1990) in Equation (21):

$$\Delta T_{\mathrm{m}} = T_{\mathrm{m}} - T_{\mathrm{m}}(d) = \frac{4\gamma_{\text{solid-melt}} T_{\mathrm{m}}}{d\Delta H^{\mathrm{fus}} \rho_{\text{solid}}} \tag{21}$$

where the bulk melting temperature of the bulk is T_{m}, $T_{\mathrm{m}}(d)$is the melting temperature of a small cylindrical solid with diameter d. ΔH^{fus} is the molar enthalpy of fusion, ρ_{solid} is the molar density of the solid and $\gamma_{\text{solid-melt}}$ is the specific free energy of the interface between the solid and melt. From this (Equation 20), the familiar inverse relationship between the depression of the melting point and crystal size, which would be equal to the pore diameter that poses a physical constraint on crystal size, is observed again. However, it negates the contribution of other interfaces to specific free energy such as the solid-pore and liquid-wall interfaces and also the effect of the characteristics of the material on the interface properties. This was proven by virtue of a polystyrene matrix that had a more pronounced depression on T_{m} than a silica-based matrix and prompts further investigation possibly modification of the equation for these situations (Ha et al.,

2005). Clearly, the validity of Equation (21) could be questioned and should be investigated in future studies.

At this point, we emphasize again that the majority of work done to this point arises from an array of sciences outside that of pharmaceutical sciences. However, the principles that were revealed by these studies could be applied in biomedical research. One example that could be found to illustrate the application of these principles was for a drug-polymer matrix intended for oral drug delivery. It is a well-established fact that the oral route of drug administration is the most popular considering patient compliance. However, poor bioavailability of drugs administered orally often limits the successful exploitation of the route.

Numerous drugs have demonstrated poor dissolution properties and this might hamper the absorption of drugs tremendously. If the drug could be forced to assume a nanoscale periodicity, the dissolution could be significantly enhanced and, for some drugs at least, improve their oral bioavailability. Induction of this nanoscale periodicity is characterized by profound increases in interface boundaries and changes in melting temperature and enthalpy. As illustrations of this, the melting temperature of nanostructured griseofulvin and nifedipine in cross-linked PVP showed significant depression if compared to the bulk and could find application in the improvement of bioavailability of these drugs (Beregese, Colombo, Gervasoni & Depero, 2004).

The technological advances arising from studying the melting point and glass transition temperature of nanomaterials and how these differ from the bulk could find various applications such as drug crystallization, dissolution and bioavailability of drugs prone to problematic behavior.

Pharmaceutical scientists should familiarize themselves with the developments concerning the thermodynamics of nanosystems since it is apparent from trends in research and industry that nanotechnology will have a profound impact on both sectors. Additional studies should be consulted for more comprehensive analysis of the thermodynamics of nanosystems compared to the bulk phases (Shirinyan & Wautelet, 2004; Shirinyan, Gusaka & Wautelet, 2005).

Solubility

Solubility of solids in liquids is a fundamental property of materials. Many models are used to predict the solubility of materials based on cohesive energy density (Hildebrandt, 1929), melting point and oil–water partitioning coefficient (Yalkowsky & Valvani, 1980) and the molecular surface area (Amidon, Yalkowsky, & Leung, 1974); and the results of these all vary. One of the latest models considers the fractal surface dimensions (Mihranyan & Strømme, 2007). This model considers that rough nanoparticles are much more soluble than that predicted by the Ostwald–Freundlich equation. First we will discuss the theory before considering the factors that might influence the solubility of nanoparticles.

Two general descriptors of solubility that should be considered are the molecular descriptors that elaborate the bulk properties of the solute

material and the particulate descriptors that describe the interfacial properties between the solvent and solute. In macrosystems, the surface-to-volume ratio is significantly smaller and molecular descriptors dominate the solubility. As we have become familiar with by now, the ratio increases as we move into the micro range and becomes very significant in the nano regime. Therefore, in these small systems, the particulate descriptors overshadow the solubility properties of the material under investigation (Mihranyan & Strømme, 2007).

One of the earliest descriptions of the dependence of solubility on particle size is given by the Kelvin equation in Equation (22) (Galvin, 2005; Nanda, Maisels, Kruis, Fissan & Stappert, 2003) that considers vapor pressure for a liquid droplet in equilibrium with its vapor pressure, and was extended to the Ostwald–Freundlich relationship to consider solubility terms (Smolen & Kildsig, 1967) in Equation (23):

$$\frac{RT}{V_{\mathrm{m}}}\ln\frac{P}{P_0}=\frac{2\gamma}{r} \tag{22}$$

where R is the universal gas constant, T is the absolute temperature, P is the measured vapor pressure on the vapor side of the liquid–vapor interface for a droplet of radius r (nanoparticle) and P_0 is the saturated vapor pressure of the surrounding medium or a flat surface. V_{m} is the molecular volume of the solute particle and the surface tension is represented by the term γ:

$$\frac{RT}{V_{\mathrm{m}}}\ln\frac{S}{S_0}=\frac{2\gamma}{r} \tag{23}$$

where S is the solubility of small particle and S_0 is the solubility at equilibrium.

Numerous arguments have been conducted that dispute the validity of the Ostwald–Freundlich equation (Equation 23) to predict the solubility of small particles and is still being debated. However, some correlations could be found for spherical particles. The surface tension for small particles is however not constant and interferes with the prediction of the Ostwald–Freundlich relation. Corrections have been suggested for both surface charge (by W.C.M. Lewis) and opposing effects of surface tension (inward pressure on the particle) and electric tension (outward pressure) (by L.F. Knapp) (Mihranyan & Strømme, 2007). The limitations of the Kelvin equation is that it describes macrosystems and as we have seen by now the definitions of density, surface tension and radius of curvature may not be applicable in nanosystems.

Knapp's correction for surface charge is given by Equation (24) ((Mihranyan & Strømme, 2007):

$$\frac{RT}{V_{\mathrm{m}}}\ln\frac{S}{S_0}=\frac{2\gamma}{r}=\frac{q^2}{8\pi Kr^4} \tag{24}$$

where q is the electric charge and k is the permittivity of the particle dispersion medium, with the other parameters as previously described.

The Ostwald–Freundlich–Knapp equation implies an exponential increase in solubility that is not infinite; in fact a maximum is seen at the Lewis critical radius, r^*, whereafter the solubility again approximates the equilibrium solubility.

The authors would like to make an interjection at this point and point to the fact that the melting point of nanomaterials also fluctuates as seen in the section discussing the melting point of nanoparticles that showed an initial decrease to a certain minimum and then an increase to attain the bulk melting point. Therefore, the arguments of Lewis and Knapp could most probably apply to the melting point as well.

The effect of the critical radius of particles was seen for the solubility of alloying metal particles that showed a threshold limit for particle size and the exponential increase in solubility. Therefore, particle size should decrease below a certain critical size before an exponential increase in solubility was observed. The study did, however, not investigate whether a certain critical Lewis radius existed for these systems; however, the significant drop in solubility of the nanoparticles below the critical radius alludes to this (Ouyang, Tan, Wang & Yang, 2006). Kipp (2004) also reviewed the increased solubility of poorly water-soluble drugs as function of particle size to exploit nanosuspensions for prolonged release of these substances. From this drug-related study it is also unclear whether the Lewis critical radius would in fact hamper solubility. The implication of the Knapp correction is seen in Figure 1.13, and the reader is referred to the study of Mihranyan and Strømme (2007) for additional discussions on the topic of surface geometry and solubility of nanoparticles.

The solubility of nanoparticles clearly differs from their corresponding bulk materials, and the effects of surface tension, which is related to particle size, will be a subject of intense research in the near future. The fluctuations in solubility is also an interesting subject, and solubility should again not be investigated without consideration of other properties at the nanolevel, including cohesive and free surface energy and melting point, all of which are related to particle size and geometry at some level.

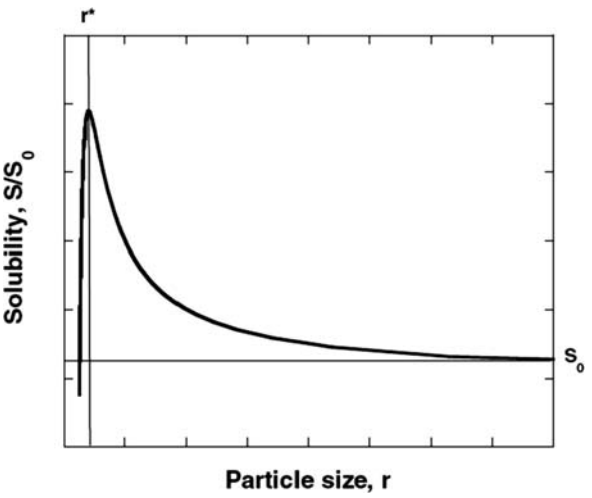

Figure 1.13 The effect of particle size on solubility according to Knapp. S_0 is the equilibrium solubility of the particle and r^* is the particle size at which the maximum solubility is obtained (Mihranyan & Strømme, 2007). (Reprinted with permission from Elsevier.)

Rheology

The success of liquid and semi-solid dosage forms is often dependent on their rheology or flow properties. Good knowledge of the mixing, pumping, filling and packing behavior is often required to determine optimum conditions for the manufacturing of these dosage forms and other products (Barnes, 1994).

This section will not elucidate all the classic descriptions of rheology, but try to add the observations made on nanoscale systems. The readers should familiarize themselves with the classic descriptions for coarse systems and subsequently realize that the behavior of nanosystems are once again different compared to the coarse systems. Therefore, one should consider that this section will be biased to some extent as to illustrate the effect of particle size and especially nanoparticle size on the flow properties. The classic approaches will only be discussed briefly.

The Newtonian definition of viscosity, η, relates the rate of flow to the applied stress (Marriott, 1988) and is expressed in Equation (25):

$$\eta = \tau / D \tag{25}$$

where rate of flow is denoted by D and applied stress by τ.

Various derivations of the Newtonian law of viscosity followed to determine relative viscosity (Marriott, 1988) as in Equation (26):

$$\eta_{\mathrm{r}} = \frac{\eta}{\eta_0} \tag{26}$$

where η_{r} is the relative viscosity, η is the solution viscosity and pure solvent viscosity η_0.

Equation (26) can take the form of the Krieger–Dougherty equation (Equation 26). This condition considers the expected viscosity for suspensions of weakly attractive particles coated with long-tail dispersants, taking into account the suspension-effective solids content (Studart et al., 2006) as shown in Equation (27):

$$\eta_{\mathrm{r}} = \frac{\eta}{\eta_0} = \left(1 - \frac{\phi_{\mathrm{eff}}}{\phi_{\max}}\right)^{-k_{\mathrm{v}}\phi_{\max}} \tag{27}$$

where the unknown terms in Equation (27) are $\phi_{\max}$ representing the suspension maximum solid content, k_{v} is a constant equal to 2.5 for spherical particles.

Finally, the Einstein equation (Marriott, 1988) (Equation 28) could be derived that related the volume fraction of the dispersed phase to the viscosity of the dispersion and the solvent:

$$\frac{\eta}{\eta_0} = 1 + 2.5\phi \tag{28}$$

where the volume fraction of the colloidal phase ϕ is the ratio of the dispersed phase to the total dispersion volume.

The specific viscosity is defined by $\eta_s = \eta_r - 1$ and Equation (28) can be expressed as follows (Mariott, 1988) in Equation (29):

$$\frac{\eta_s}{C} = k \tag{29}$$

where concentration of the particles in the dispersion is denoted by C.

If k is determined (Equation 29) for a series of concentrations of the polymer, the linear plot could be extrapolated to zero concentration to obtain the limiting viscosity number or intrinsic viscosity of the dispersion. The intrinsic viscosity is related to polymer molecular mass and shape by the Mark-Houwink equation (Marriott, 1988) expressed in Equation (30):

$$[\eta] = KM^{\alpha} \tag{30}$$

where the exponent, α, indicates the shape of the particle and $[\eta]$ is the intrinsic viscosity.

The slope of the plot of k versus C is equal to the Huggins constant that illustrates the interaction of the polymer with the solvent. The power series form of Equation (27) is derived (Marriott, 1988) and shown in Equation (31):

$$\frac{\eta_s}{C} = k_1 + k_2 C + k_3 C^2 \tag{31}$$

where the solvent interaction constant is denoted by k_2.

These equations illustrate the influence of particle concentration on viscosity; however, the effect of particle size on the rheology of dispersions is very complex. It has been established that dispersions with micrometer dimensions to that of approximately 100 nm undergo a transition to a shear-thickened state at high shear stresses. This is of course a problematic occurrence in the processing of these particles. The lower limit of reversible shear thickening has not been established and studies have reported shear thickening for particles of 75 nm. However, this would indicate that the thickening is caused by short-range lubrication forces. The shear thickening is marked by an increase in the viscosity as a function of an increase in shear stress or shear rate (Lee, Norman, Wagner, 2006).

One of the key challenges in the preparation of nanoparticle suspensions is the limit placed on solid contents due to the size effects of nanoparticles on the viscosity of nanodispersions. The preliminary limit for the concentration of suspended nanosolids is approximately 40 vol % for particles of less than 70 nm diameter. The limit to this solid content is attributed to the excluded volume that is formed around each particle to prevent agglomeration. Typically, a layer of dispersion medium molecules that sterically stabilizes the particle or electric bilayer prevents particle attraction. By now the reader should immediately realize that surface will have an effect on this stabilization. In the event of adsorption of dispersion medium molecules, the adlayer thickness defines the excluded volume and in the instance of electric double layers, the Debye length describes this volume (Studart, Amstad, Antoni & Gauckler, 2006).

The effective solid content of a suspension is therefore determined by the excluded volume and can be described (Studart et al., 2006) in Equation (32):

$$\phi_{\text{eff}} = \phi + \phi_{\text{excl}} = \phi\left[1 + \left(\frac{\delta}{a}\right)\right]^3 \tag{32}$$

where the particle solid content is ϕ, the excluded volume fraction is ϕ_{excl}, A is the particle radius and δ is the adlayer thickness or the Debye length. Clearly, the ratio δ/a increases as particles become smaller and the excluded volume fraction increase dramatically as particle size decreases. Subsequently, the viscosity of nanoparticle suspensions is significantly higher than that of the conventional suspensions with a comparatively low solid content (Studart, Amstad, Antoni & Gauckler, 2006). Figure 1.14 indicates the effects of effective volume fraction and adlayer thickness on the relative viscosity of alumina nanopowders.

However, Studart et al. (2006) also considers one important aspect which is that the attractive forces between nanoparticles are smaller than that between larger particles as seen from their van der Waals potential energy that is dependent on the distance between surfaces and the size of the spheres. The estimation made from this potential energy is that for a fixed interparticle distance of 10 nm, 500 nm particles show a 30 times higher energy than experienced by 50 nm particles. From this estimation it was reasoned that a lower adlayer thickness would be required to prevent agglomeration of particles. Very importantly, this statement indicates that the use of standard polyelectrolytes provides adlayer thicknesses far

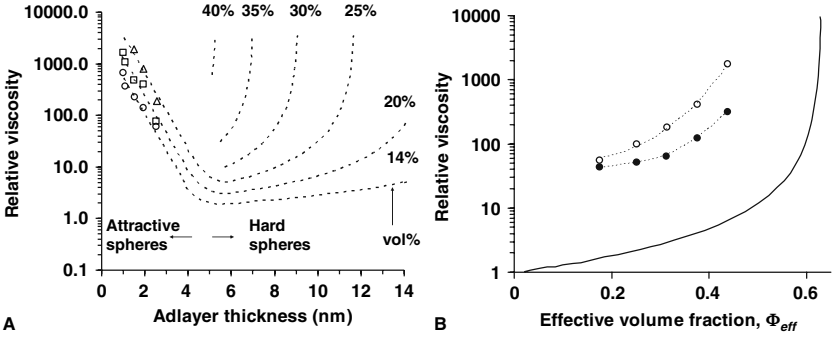

Figure 1.14 (**A**) Relative viscosity predicted for suspensions containing 65 nm alumina particles as a function of the dispersant adlayer thickness. The *dashed curves* were obtained from the extrapolation of the apparent viscosity at $100\,s^{-1}$of suspensions at various solid contents (○, 14 vol%; □, 20 vol%; △, 25 vol%. The *short dotted lines* at the right of the curves were calculated with the Krieger–Dougherty equation for model non-attractive hard spheres with a maximum solids fraction of 0.63. (**B**) Viscosity of suspensions containing nanoparticles dispersed with octadecyla gallate in toluene as a function of the effective solids volume fraction. The apparent viscosity at $100\,s^{-1}$ is represented by (○) and the Casson viscosity as expected for high shearing conditions by (•). The *solid line curve* was obtained from the Krieger–Dougherty equation for non-attractive hard spheres with $\phi_{\max} = 0.63$ for $k_v = 2.5$ (Studart, Amstad, Antoni & Gauckler, 2006). (Reprinted with permission from the American Ceramic Association.)

exceeding the value actually required to stabilize these suspensions and in fact contributed to excluded volume and subsequently resulted in significant increases in the viscosity.

This effect of excluded volume and adlayer thickness was illustrated for aqueous kaolinite suspensions upon addition of nanoparticles. This study illustrated that upon exceeding a critical concentration of added nanoparticles or electrolyte, an increase in yield stress and viscosity was observed (Baird & Walz, 2007). The effect of coating the alumina powder nanoparticles was also investigated and resulted in complex rheology behavior. The effect of coating on ϕ was investigated, and it was concluded that particle– particle interaction and maximum volume fraction should be investigated further (Mary, Dubois, Carreau & Brousseau, 2006).

Rhodes and Lewis (2006) did in fact investigate particle–particle interaction to determine the structure and influence on rheology and illustrated that nanoparticles at a certain concentration provide the beneficial adlayer to stabilize suspended microparticles; however, higher concentrations resulted in flocculation. The relative van der Waals potential proved to be very important in this behavior as was the particle size of interacting particles.

In addition to solid dispersions, nanoemulsions also demonstrated fascinating rheology that was related to the ϕ of the emulsified droplet. If the volume fraction of emulsions increased, the liquid changed from a viscous dispersion to an elastic solid with a significantly shear modulus at high volume fractions. The elasticity is a consequence of an increase in droplet surface arising from droplet deformation under the influence of shear. Therefore, the rheological properties of an emulsion are dependent on the concentration and particle size of the droplets of the dispersed phase. Figure 1.15 is a depiction of these occurrences.

The rheology behavior of nanosystems is also in its infancy and several studies are emerging to study its behavior. The technological impact will become clear as we gain further understanding of nanosystems rheology,

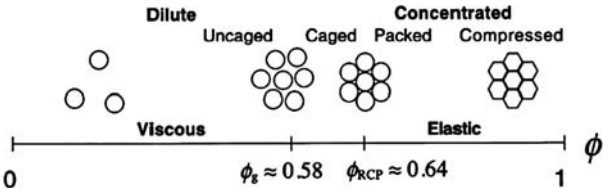

Figure 1.15 Diagram of droplet positional structure and interfacial morphology for disordered monodisperse emulsions of repulsive droplets as a function of the volume fraction,ϕ, of the dispersed phase. In the dilute regime at lowϕ, the droplets are spherical in the absence of shear. As ϕ is raised near the hard sphere glass transition volume fraction, $\phi_g = 0.58$, the droplets become transiently caged by their neighbors. As ϕ is further increased into the concentrated regime, the droplets start to randomly close pack at $\phi_{RCP} \approx 0.64$ and become compressed with deformed interfaces for larger ϕ. As $\phi \rightarrow 1$, the droplets become nearly polyhedral in shape and form a biliquid foam. Dilute emulsions behave as viscous liquids, whereas concentrated emulsions exhibit solid-like elasticity (Mason, 1999). (Reprinted with permission from Elsevier.)

and the application could be numerous and advantageous compared with macrosystems.

Additional elaborations on rheology will not be made here and the reader is referred to additional text in the literature expanding the rheology of nanoscale systems (Hoekstra, Vermant, Mewis, Narayanan, 2002; Lee, Norman, Wagner, 2006; Sarvestani & Jabbari, 2006; Probstein, Sengun & Tseng, 1994 and Tuteja & MacKay, 2005).

Conclusion

Numerous fields of science are converging to study science at a very fundamental level or building block level, namely nanoscience. The applications that have spawned under the collective of nanotechnology are emerging and some major breakthroughs have been made. The majority of studies have focused on materials sciences, ceramics and electronics, with some applications emerging in the biomedical field.

It is virtually impossible to imagine that such marked differences in the physical behavior of nanosystems could be seen compared to what is considered bulk systems. The two main effects that arise at the nanolevel are the surface-to-volume ratio that becomes very significant at this level and the lesser discussed in this text, quantum effects. Hopefully, the focus of research in the following years will investigate nanoscale phenomena and give answers to fundamental questions and the beneficial application to developing new drug delivery technology.

Very few fundamental studies have been performed in the pharmaceutical field discussing the fundamentally different properties of pharmaceuticals at the nanolevel. The application is clear and promising; however, the basics of nanoscience in drug delivery are poorly understood. To perplex these studies, the biological component is included in this field and might pose challenges that are significantly different than those encountered in the non-living world. Some aspects of thermodynamics have been elaborated here; however, the challenge is to extrapolate it to biological systems. With sound investigation of these basic properties, the scope of pharmaceutical sciences within the invisible nanoworld seems poised to result in a revolution in our world as we experience it in our everyday lives.

References

Aizpurua, J., Hanarp, P., Sutherland, D.S., Käll, M., Bryant, G.W. & De Abajo, F.J.G. (2003). Optical properties of gold nanorings. *Physical Review Letters*, *90*, 057401-1–057401-5.

Alba, C., Busse, L.E., List, D.J. & Angell, C.A. (1990). Thermodynamic aspects of the vitrification of toluene, and xylene isomers, and the fragility of liquid hydrocarbons. *Journal of Chemical Physics*, *92*, 617–624.

Amidon, G.L., Yalkowsky, S.H. & Leung, S. (1974). Solubility of nonelectrolytes in polar solvents II: solubility of aliphatic alcohols in water. *Journal of Pharmaceutical Sciences*, *63*, 1858–1866.

Baird, J.C. & Walz, J.Y. (2007). The effects of added nanoparticles on aqueous kaolinite suspensions II. Rheological effects. *Journal of Colloid and Interface Science*, *306*, 411–420.

Balandin, A.A. (2005). Nanophononics: Phonon engineering in nanostructures and nanodevices. *Journal of Nanoscience and Nanotechnology*, *5*, 1015–1022.

Balzani, V. (2005). Nanoscience and nanotechnology: a personal view of a chemist. *Small*, *1*, 278–283.

Bares, J. (1975). Glass transition of the polymer microphase. *Macromolecules*, *8*, 244–246.

Barnes, H.A. (1994). Rheology of emulsions – a review. *Colloids and Surfaces A: Physicochemical and Engineering Aspects*, *91*, 89–95.

Beregese, P., Colombo, I., Gervasoni, D & Depero, L.E. (2004). Melting of nanostructured drugs embedded into a polymeric matrix. *Journal of Physical Chemistry B*, *108*, 15488–15493.

Brasseur, F., Couvreur, Kante, B., Deckers-Passau, L., Roland, M., Deckers, C. & Speisers, P. (1980). Actinomycin D adsorbed on polymethylcyanoacrylate nanoparticles: increased efficiency against an experimental tumor. *European Journal of Cancer*, *16*, 1441–1445.

Buffat, Ph. & Borel, J.-P. (1976). Size effect on the melting temperature of gold particles. *Physical Review A*, *13*, 2287–2298.

Burns, A, Ow, H. & Wiesner, U. (2006). Fluorescent core-shell nanoparticles: towards "Lab on a Particle" architectures for nanobiotechnology. *Chemical Society Reviews*, *35*, 1028–1042.

Cahill, D.G., Ford, W.K., Goodson, K.E., Mahan, G.D., Majumdar, A., Maris, H.J., Merlin, R & Phillpot, S.R. (2003). Nanoscale thermal transport. *Journal of Applied Physics*, *93*, 793–818.

Cenian, A. & Gabriel, H. (2001). Ballistic energy transfer in dielectric Ar crystals. *Journal of Physics: Condensed Matter*, *13*, 4323–4339.

Chen, G. (2002). Ballistic-diffusive equations for transient heat conduction from nano to macroscales. *Journal of Heat Transfer*, *124*, 320–328.

Chen, G. (1996). Nonclonal and nonequiilibrium heat conduction in the vicinity of nanoparticles. *Journal of Heat Transfer*, *118*, 539–545.

Chen, G. (2000). Particularities of heat conduction in nanostructures. *Journal of Nanoparticle Research*, *2*, 199–204.

Dalnoki-Veress, K., Forrest, J.A., Murray, C., Cigault, C. & Dutcher, J.R. (2001). Molecular weight dependence of of reductions in the glass transition temperature of thin, freely standing polymer films. *Physical Review E: Statistical, Nonlinear, and Soft Matter Physics*, *63*, 031801-1–031801-10.

Dosch, H. (2001). Some general aspects of confinement in nanomaterials. *Applied Surface Science*, *82*, 192–195.

El-Egakey, M.A., Bentele, V. & Kreuter, J. (1983). Molecular weights of polycyanoacrylate nanoparticles. *International Journal of Pharmaceutics*, *13*, 349–352.

Finsy, R. (2004). On the critical radius in Ostwald ripening. *Langmuir*, *20*, 2975–2976.

Fox, T.G. Jr. & Flory, P.J. (1950). Second-order transition temperatures and related properties of polystyrene. I. Influence of the molecular weight. *Journal of Applied Physics*, *21*, 581–591.

Galvin, K.P. (2005). A conceptually simple derivation of the Kelvin equation. *Chemical Engineering Science*, *60*, 4659–4660.

Gobin, A.M., O'Neal, D.P., Watkins, D.M., Halas, N.J., Drezek, R.A. & West, J.L. (2006). Near infrared laser-tissue welding using nanoshells as exogenous absorber. *Lasers in Surgery and Medicine*, *37*, 123–129.

Gomes, C.J., Madrid, M., Goicochea, J.V., Amon, C.H. (2006). In-plane and out-of-plane thermal conductivity of silicon thin films predicted by molecular dynamics. *Journal of Heat Transfer*, *128*, 1114–1121.

Guinea, F., Rose, J.R., Smith, J.R. & Ferrante, J. (1984). Scaling relations in the equation of state, thermal expansion, and melting of metals. *Applied Physics Letters*, *44*, 53–55.

Guisbiers, G. & Wautelet, M. (2006). Size, shape and stress effects on the melting temperature of nano-polyhedral grains on a substrate. *Nanotechnology*, *17*, 2008–2011.

Guisbiers, G., Shirinyan, A.S. & Wautelet, M. (2005). The physics of macro-, micro- and nanomaterials. *Physicalia Magazine*, *27*, 131–141.

Ha, J.-M., Hillmyer, M.A. & Ward, M.D. (2005). Properties of organic nanocrystals embedded in ultrasmall crystallization chambers. *Journal of Physical Chemistry B*, *109*, 1392–1399.

Ha, J.-M., Wolf, J.H., Hillmyer & Ward, M.A. (2004). Polymorph selection under nanoscopic confinement. *Journal of the American Chemical Society*, *126*, 3382–3383.

Hatta, I. (2002). Thermal characteristics in a nanometer scale. *Journal of Thermal Analysis and Calorimetry*, *69*, 717–725.

He, Y.Q., Liu, S.P., Kong, L. & Liu, Z.F. (2005). A study on the sizes and concentrations of gold nanoparticles by spectra of absorption, resonance Rayleigh scattering and resonance non-linear scattering. *Spectrochimica Acta Part A: Molecular and Biomolecular Spectroscopy*, *61*, 2861–2866.

Hildebrandt, J.H. (1929). Solubility. XII. Regular solutions. *Journal of the American Chemical Society*, *51*, 66–80.

Hirsch, L.R., Gobon, A.M., Lowery, A.R., Tam, F., Drezek, R.A., Halas, N.J. & West, J.L. (2006). Metal nanoshells. *Annals of Biomedical Engineering*, *34*, 15–22.

Hoekstra, H., Vermant, J., Mewis, J. & Narayanan. (2002). Rheology and structure of suspensions in liquid crystalline solutions. *Langmuir*, *18*, 5695–5703.

Hu, M., Chen, J., Li, Z.-Y., Au, L., Hartland, G.V., Li, X., Marquez, M. & Xia, Y. (2006). Gold nanostructures: engineering their plasmonic properties for biomedical applications. *Chemical Society Reviews*, *35*, 1084–1094.

Hutter, E. & Fendler, J.H. (2004). Exploitation of localized surface plasmon resonance. *Advanced Materials*, *16*, 1685–1706.

Jackson, C.L. & McKenna, G.B. (1990). The melting behavior of organic materials confined in porous solids. *Journal of Chemical Physics,). 93*, 9002–9011.

Jackson, C.L. & McKenna, G.B. (1996). Vitrification and crystallization of organic liquids confined to nanoscale pores. *Chemistry of Materials*, *8*, 2128–2137.

Jiang, Q., Aya, N & Shi, F.G. (1997). Nanotube size-dependent melting of single crystals in carbon nanotubes. *Applied Physics A*, *64*, 627–629.

Jiang, Q., Shi, H.X. & Li, J.C. (1999). Finite size effect on glass transition temperatures. *Thin Solid Films*, *354*, 283–286.

Jiang, Q., Shi, H.X. & Zhao, M. (1999). Melting thermodynamics of organic nanocrystals. *Journal of Chemical Physics*, *111*, 2176–2180.

Jiang, Q., Yang, C.C. & Li, J.C. (2002). Melting enthalpy depression of nanocrystals. *Materials Letters*, *56*, 1019–1021.

Jortner, J. & Rao, C.N.R. (2002). Nanostructured advanced materials. Perspectives and directions. *Pure and Applied Chemistry*, *74*, 1491–1506.

Ju, Y.S. & Goodson, K.E. (1999). Phonon scattering in silicon films with thickness of order 100 nm. *Applied Physics Letters*, *74*, 3005–3007.

Keddie, J,L. & Jones, R.A. (1995). Glass transition behavior in ultrathin polystyrene films. *Israel Journal of Chemistry*, *35*, 21–26.

Khanna, S.C. & Speiser, P. (1969). Epoxy resin beads as pharmaceutical dosage form I: methods of preparation. *Journal of Pharmaceutical Science*, *58*, 1114–1117.

Kim, W., Wang, R. & Majumdar, A. (2007). Nanostructuring expands thermal limits. *NanoToday*, *2*, 40–47.

Kipp, J.E. (2004). The role of solid nanoparticle technology in the parenteral delivery of poorly water-slouble drugs. *International Journal of Pharmaceutics*, *284*, 109–122.

Koh, Y.P., McKenna, G.B. & Simon, S.L. (2006). Calorimetric glass transition temperature and absolute heat capacity of polystyrene ultrathin films. *Journal of Polymer Science: Part B: Polymer Physics,* 44, 3518–3527.

Krause, H.-J., Schwarz, A. & Rohdewald, P. (1985). Polylactic acid nanoparticles, a colloidal delivery system for lipophilic drugs. *International Journal of Pharmaceutics*, *27*, 145–155.

Lee, Y.S. & Wagner, N.J. (2006). Rheological properties and small-angle neutron scattering of shear thickening, nanoparticle dispersion at high shear rates. *Industrial and Engineering Chemistry Research*, *45*, 715–7024.

Lepri, S., Livi, R. & Politi, A. (2003). Thermal conduction in classical low-dimensional lattices. *Physics Reports*, *377*, 1–80.

Li, N., Kommireddy, D.S., Lvov, Y., Liebenberg, W., Tiedt, L. & De Villiers, M.M. (2006). Nanoparticle multilayers: surface modification of photosensitive drug microparticles for increased stability and in vitro bioavailability. *Journal of Nanoscience and Nanotechnology*, *6*, 3252–3260.

Liang, L.H., Zhao, M. & Jiang, Q. (2002). Melting enthalpy depression of nanocrystals based on surface effect. *Journal of Materials Science Letters*, *21*, 1843–1845.

Liao, H., Nehl, C.L. & Hafner, J.H. (2006). Biomedical applications of plasmon resonant metal nanoparticles. *Nanomedicine*, *1*, 201–208.

Lin, A.W.H., Lewinski, N.A., West, J.L., Halas, N. & Drezek, R.A. (2005). Optically tunable nanoparticle contrast agents for early cancer detection: model-based analysis of gold nanoshells. *Journal of Biomedical Optics*, *10*, 064035-1–064035-10.

Liu, J. & Lu, Y. (2004). Colorimetric biosensors based on DNAzyme-assembled gold nanoparticles. *Journal of Fluoresence*, *14*, 343–354.

Loo, C., Lowery, A., Halas, West, J. & Drezek, R. (2005). Immunotargeted nanoshells for integrated caner imaging and therapy. *Nano Letters, 5*, 709–711.

MacFarlane, D.R. & Angell, C.A. (1982). An emulsion technique for the study of marginal glass formation in molecular liquids. *Journal of Physical Chemistry*, *86*, 1927–1930.

Marriott, C. (1988). Rheology and the flow of liquids. In M.E. Aulton (Ed.), *Pharmaceutics – The science of dosage form design* (pp. 17–37). New York: Churchill Livingstone.

Mason, T.G. (1999). New fundamental concepts in emulsion rheology. *Current Opinion in Colloid & Interfcae Science*, *4*,23–238.

Mary, B., Dubois, C., Carreau, P.J. & Brousseau, P. (2006).Rheological properties of suspensions of polyethylene-coated aluminum nanoparticles. *Rheologica Acta*, *45*, 561–573.

McNeil. S.E. (2005). Nanotechnology for the biologist. *Journal of Leukocyte Biology*, *78*, 585–594.

Michel, M., Gemmer, J. & Mahler, G. (2006). Microscopic quantum mechanical foundation of Fouriers's Law. *International Journal of Modern Physics B*, *1*, 1–30.

Mihranyan, A. & Strømme, M. (2007). Solubility of fractal nanoparticles. *Surface Science*, *601*, 315–319.

Mottet, C., Rossi, G., Baletto, F. & Ferrando, R. (2005). Single impurity effect on the melting of nanoclusters. *Physical Review Letters*, *95*, 035501-1–035501-4.

Nanda. K.K., Maisels, A., Kruis, F.E., Fissan, H. & Stappert, S. (2003). Higher surface energy of free nanoparticles. *Physical Review Letters*, *91*, 106102-1–106102-4.

Navrotsky, A. (2007). Calorimetry of nanoparticles, surfaces, interfaces, thin films, and multilayers. *Journal of Chemical Thermodynamics*, *39*, 2–9.

NNI. National Nanotechnology Initiative. 2007. (February 6, 2007); http://www.nano.gov.

Nobile, C., Kudera, S., Fiore, A., Carbone, L., Chilla, G., Kipp, T., Heitmann, D., Cingolani, R., Manna, L. & Krahne, R. (2007). Confinement effects on optical phonons in spherical, rod-, and tetrapod-shaped nanocrystals detected by Raman spectroscopy. *Physica Status Solidi A: Applications and Materials Science*, *204*, 483–486.

Novikov, V.N., Rössler, E., Malinovsky, V.K. & Surovtsev, N.V. (1996). Strong and fragile liquids in percolation approach to the glass transition. *Europhysics Letters*, *35*, 289–294.

Ouyang, G, Tan, X., Wang, C.X. & Yang, G.W. (2006). Solid solubility limit in alloying nanoparticles. *Nanotechnology*, *17*, 4257–4262.

Oxtoby, D.W. (1998). Nucleation of first-order phase transitions. *Accounts of Chemical Research*, *31*, 91–97.

Perugini, P., Simeoni, S., Scalia, S., Genta, I., Modena, T., Conti, B. & Pavanetto, F. (2002). Effect of nanoparticle encapsulation on the photostability of the sunscreen agent, 2-ethylhexyl-*p*-methoxycinnamate. *International Journal of Pharmaceutics*, *246*, 37–45.

Probstein, R.F., Sengun, M.Z. & Tseng, T.-C. (1994). Bimodal of concentrated suspension viscosity for distributed particle sizes. *Journal of Rheology*, *38*, 811–829.

Qi, W.H. (2005). Size effect on melting temperature of nanosolids. *Physica B*, *368*, 46–50.

Rao, C.N.R. & Cheetham, A.K. (2001). Science and technology of nanomaterials: current status and features. *Journal of Materials Chemistry*, *11*, 2887–2894.

Rao, C.N.R., Kulkarni, G.U., Thomas, P.J. & Edwards, P.P. (2002). Size-dependent chemistry: properties of nanocrystals. *Chemistry – A European Journal*, *8*, 28–35.

Rhodes, S.K. & Lewis, J.A. (2006). Phase behavior, 3-D structure, amd rheology of colloidal microsphere-nanoparticle suspension. *Journal of the American Ceramic Society*, *89*, 1840–1846.

Rieger, J. & Horn, D. Organic nanoparticles in the aqueous phase – theory, experiment, and use. *Angewandte Chemie, International Edition (Weinheim, Germany)*, *40*, 4330–4361.

Roduner, E. (2006). Size matters: why nanomaterials are different. *Chemical Society Reviews*, *35*, 583–592.

Sarvestani, A.S. & Jabbari, E. (2006). Modeling and experimental investigation of rheological properties of injectable poly(lactide ethylene oxide fumarate)/hydroxyapatite nanocomposites. *Biomacromolecules*, *7*, 1573–1580.

Schofield, C.L., Field, R.A. & Russell, D.A. (2007). Glyconanoparticles for the colorimetric detection of cholera toxin. *Analytical Chemistry*, *79*, 1356–1361.

Shakouri, A. (2006). Nanoscale thermal transport and microrefrigerators on a chip. *Proceedings of The IEEE*, *94*, 1613–1638.

Shirinyna, A.S., Gusak, A.M. & Wautelet, M. (2005). Phase diagram versus diagram of solubility: What is the difference for nanosystems. *Acta Materialia*, *53*, 5025–5032.

Shirinyan, A.S. & Wautelet, M. (2004). Phase separation in nanoparticles. *Nanotechnology*, *15*, 1720–1731.

Shrivastava, K.N. (2002). Melting temperature, Brillouin shift, and density of states of states of nanocrystals. *Nano Letters*, *2*, 519–523.

Smolen, V.F. & Kildsig, D.O. (1967). Vapor pressure and solubility of small particles. *American Journal of Pharmaceutical Education, 31*, 512–514.

Studart, A.R., Amstad, E., Antoni, M. & Gauckler, L.J. (2006). Rheology of concentrated suspension containing weakly attractive alumina nanoparticles. *Journal of the American Ceramic Society*, *89*, 2418–2425.

Sun, C.Q., Li, C.M., Bai, H.L. & Jiang, E.Y. (2005). Melting point oscillation of a solid over the whole range of sizes. *Nanotechnology*, *16*, 1290–1293.

Sun, Y. & Xia, Y. (2003). Gold and silver nanoparticles: A class of chromophores with colors tunable in the range form 400 to 750 nm. *Analyst*, *128*, 686–691.

Suzuki, D. & Kawaguchi, H. (2006). Hybrid microgels with reversibly changeable multiple brilliant color. *Langmuir*, *22*, 3818–3822.

Tien, C.L. & Chen, G. (1994). Challenges in microscale conductive and radiative heat transfer. *Journal of Heat Transfer*, *116*, 799–807.

Tuteja, A. & MacKay, M.E. (2005). Effects of ideal, organic nanoparticles on the flow properties of linear polymers: non-Einstein-like behavior. *Macromolecules*, *38*, 8000–8011.

Wang, X.W., Fei, G.T., Zheng, K., Jin, Z. & Zhang, L.D. (2006). Size-dependent melting behavior of Zn nanowire arrays. *Applied Physics Letters*, *88*, 173114-1–173114-3.

Wautelet, M. (1998). On the shape dependence of the melting temperature of small particles. *Physics Letters A*, *246*, 341–342.

Wautelet, M., Dauchot, J.P. & Hecq, M. (2003). Size effects on the phase diagrams of nanoparticles of various shapes. *Materials Science and Engineering C*, *23*, 187–190.

Wu, T., Sun, Y., Li, N., De Villiers, M.M. & Yu, L. (2007). Inhibiting surface crystallization of amorphous indomethacin by nanocoating. *Langmuir*, *23*, 5148–5153..

Xu, X. & Cortie, M.B. (2006). Shape change and color gamut in gold nanorods, dumbbells, and dog bones. *Advanced Functional Materials*, *16*, 2170–2176.

Xue, Y., Zhao, Q. & Luan, C. (2001). The thermodynamic relations between the melting point and the size of crystals. *Journal of Colloid and Interface Science*, *243*, 388–390.

Yalkowsky, S.H. & Valvani, S.C. (1980). Solubility and partitioning I: solubility of nonelectrolytes in water. *Journal of Pharmaceutical Sciences*, *69*, 912–922.

Zhang, Z., Li, J.C. & Jiang, Q. (2000). Modelling for size-dependent and dimension-dependent melting of nanocrystals. *Journal of Physics D: Applied Physics*, *33*, 2653–2656.

Zhang, Z., Zhao, M. & Jiang, Q. (2001). Glass transition thermodynamics of organic nanoparticles. *Physica B*, *293*, 232–236.

2

Block Copolymer Synthesis for Nanoscale Drug and Gene Delivery

Motoi Oishi and Yukio Nagasaki

Introduction

One of the fascinating subjects in areas such as materials science, nanochemistry, and biomimetic chemistry is concerned with the creation of supramolecular architectures with well-defined shapes and functions. Self-assembly of block polymers through non-covalent forces including hydrophobic and hydrophilic effects, electrostatic interactions, hydrogen bonding, and metal complication has great potential for creating such supramolecular structures. In particular, polymeric micelles formed in aqueous media through the self-assembly of block copolymers containing poly(ethylene glycol) (PEG) as the corona-forming segment have attracted considerable attention in the field of drug and gene delivery systems due to their excellent biocompatibility, long blood circulation time, and nontoxicity (Otsuka, Nagasaki & Kataoka, 2003). As can be seen in Figure 2.1, the number of publications on drug and gene delivery systems using block copolymer and PEG-based block copolymer is increasing significantly every year. Thus, the merits of PEG-based block copolymer have been becoming clearer to the research community every year.

The PEG corona of the PEGylated polymeric micelles is believed to prevent recognition by a group of scavenger cells, viz., the reticuloendothelial system (RES) that is located mainly at the liver, the spleen, and the lungs. In addition, the increase in the apparent molecular mass by self-assembly of the block copolymers reduces clearance by renal excretion, resulting in prolonged blood circulation. Thus, the stealth effect of the PEG corona of the polymeric micelles is fairly effective in vivo. Indeed, a variety of nano-sized (< 100 nm) PEGylated polymeric micelles have been developed to precisely and safely deliver the appropriate concentrations of the anticancer drugs to tumor tissue, and some of these carriers have been approved for clinical use (Maeda, Sawa, & Konno, 2001) or are being studied currently in clinical trials, since they showed preferentially tumor accumulation caused by the enhanced permeability and retention (EPR) effect (Matsumura & Maeda, 1986). Furthermore, the installation of specific ligand molecules on the surface of PEGylated polymeric micelles

M.M. de Villiers et al. (eds.), *Nanotechnology in Drug Delivery*, DOI: 10.1007/978-0-387-77667-5_2,

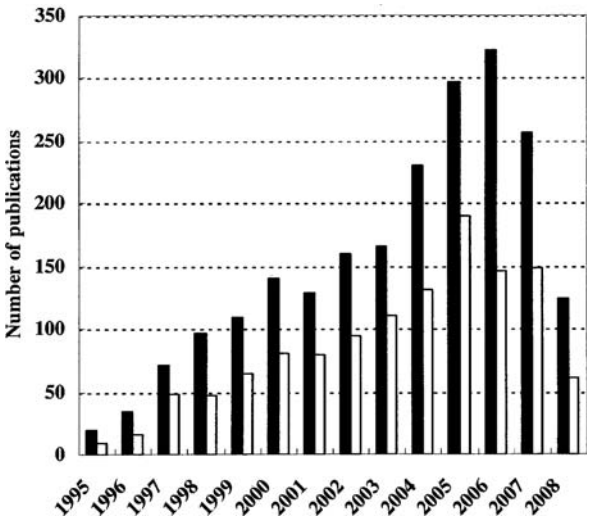

Figure 2.1 Number of publications on drug and gene delivery systems using block copolymer (*black bar*) and PEG-based block copolymer (*white bar*) cited in SCI Finder from 1995 to 2008.

is indispensable to the achievement of specific and enhanced cellular uptake at the target tissue, allowing the effective dose and side effects of the drugs to be reduced. Thus, ligand-installed and PEGylated polymeric micelles are a promising approach to constructing targetable drug and gene carriers. Nevertheless, end group of the PEG-based block copolymer, usually the methoxy-group, should be inert, viz., it is not possible to use the PEG end group for further linking to ligand molecules.

A major key to the successful development of targetable drug and gene carriers is considered to be the preparation of an end-functionalized PEG-based block copolymer that allows easy installation of ligand molecules in the reactive group located at the PEG chain end. We have been focusing on the synthesis of end-functionalized PEG-based block copolymer which denotes PEG possessing a functional group at the PEG chain end, selectively and quantitatively. Several types of end-functionalized PEG-based block copolymers have been prepared so far using heterobifunctional PEGs as the macroinitiator. In this chapter, the synthesis, characteristics, and application of these compounds are described.

Synthesis of Heterobifunctional Poly(ethylene glycol)s

A major key to the success of the preparation of the end-functionalized PEG-based block copolymers is believed to be the development of the efficient synthetic approach to the heterobifunctional PEGs. Although there are several reports on the preparation of heterobifunctional PEGs (Zalipsky, 1995; Kaiser, Marek, Haselgrubler, Schindler, & Gruber, 1997; Bettinger, Remy, Erbacher, & Behr, 1998), most of them started from commercially available PEGs possessing hydroxyl groups at both ends. In particular, one of the hydroxyl groups at the PEG ends was converted to another functional group first; then, the other hydroxyl group was converted to one of the other functional groups. These complex consecutive

steps not only make the overall process troublesome but also cause several problems. Because the reactivity of hydroxyl groups at both PEG ends is the same, the resulting PEG must be a mixture of three types of PEG homologues at most in the first step (HO-PEG-OH: 25%, R-PEG-OH: 50%, R-PEG-R: 25%).In this case, the mono-reacted PEG should be separated from the mixture. It is well known that the separation of polymeric compounds is very difficult and, thus, leads to low yield and low purity.

In order to obtain heterobifunctional PEGs that give rise to both high yield and high purity, we have applied a functional initiator to a living anionic ring-opening polymerization of ethylene oxide to design new routes (Kim, Nagasaki, Kataoka, Kato, Yokoyama, Okano, & Sakurai, 1994; Cammas, Nagasaki, & Kataoka, 1995; Nagasaki et al., 1995a). In this case, the initiator was introduced to one of the ends of the obtained PEG quantitatively as shown in Scheme 2.1. Several types of initiators were examined for the effective polymerization of ethylene oxide (Oishi, Nagasaki, & Kataoka, 2005). One of the most important and convenient compounds we prepared so far is an acetal-ended PEG. The acetal group at the PEG chain end can be easily converted to an aldehyde group by the acid treatment (Greene, 1991). The aldehyde group is known to rapidly react with primary amine, generating a Schiff base intermediate (-CH = N-), which can be converted to a secondary amino group ($-CH_2$-NH-) by the addition of a reducing agent. Also, the aldehyde group is stable under the neutral media. Thus, the aldehyde-ended heterobifunctional PEG can be utilized as the ligand installation via the reductive amination reaction.

As the typical example (Scheme 2.2), a synthesis of α-acetal-ω-hydroxyl-PEG (acetal-PEG-OH) was carried out as follows (Nagasaki, Kutsuna, Iijima, Kato, Kataoka, Kitano, & Kadoma, 1995b): To 1 mmol of potassium 3,3-diethoxypropanolate in dry THF under argon atmosphere, 130 mmol of ethylene oxide was added via a cooled syringe. The mixture was stirred magnetically and allowed to react for 48 h at room temperature. The resulting polymer was precipitated into ether, and the precipitate was filtered. Finally, the collected sample was freeze-dried with benzene.

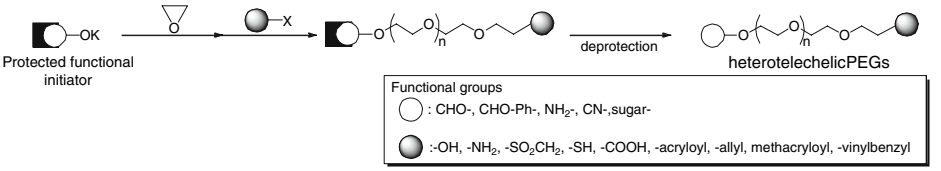

Scheme 2.1 Novel synthetic approach to heterobifunctional PEGs using the functional initiators.

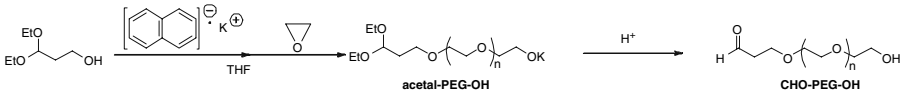

Scheme 2.2 Synthesis of heterobifunctional PEG possessing an aldehyde group at the α-end and hydroxyl group at the ω-end (CHO-PEG-OH).

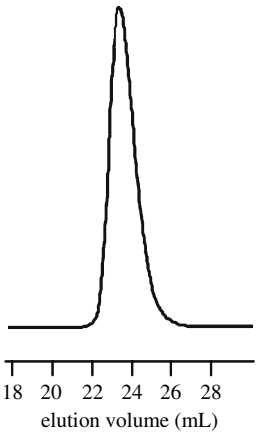

Figure 2.2 SEC chromatogram of acetal-PEG-OH.

Figure 2.2 shows the size exclusion chromatogram (SEC) of the obtained polymer. The molecular weight could be controlled by the monomer/initiator ratio, retaining a low molecular weight distribution factor (obsd. M_n = 3200, M_w/M_n = 1.05, calcd. M_n = 3230, $[EO]_0/[initiator]_0$ = 70). Figure 2.3 shows the ^{13}C NMR spectra of the obtained polymer before and after the acid treatment. The signals based on the end acetal group can be observed at 15, 34, 62, and 101 ppm before the acid treatment. On the contrary, the acetal signals disappeared completely after the acid treatment. Instead of them, a new signal based on the carbonyl carbon at 202 ppm appeared after the acid treatment, indicating that the acetal group at the PEG chain end can be converted completely to the aldehyde group. Thus, α-acetal-ω-potassium alcholate-PEG (acetal-PEG-OK) acts

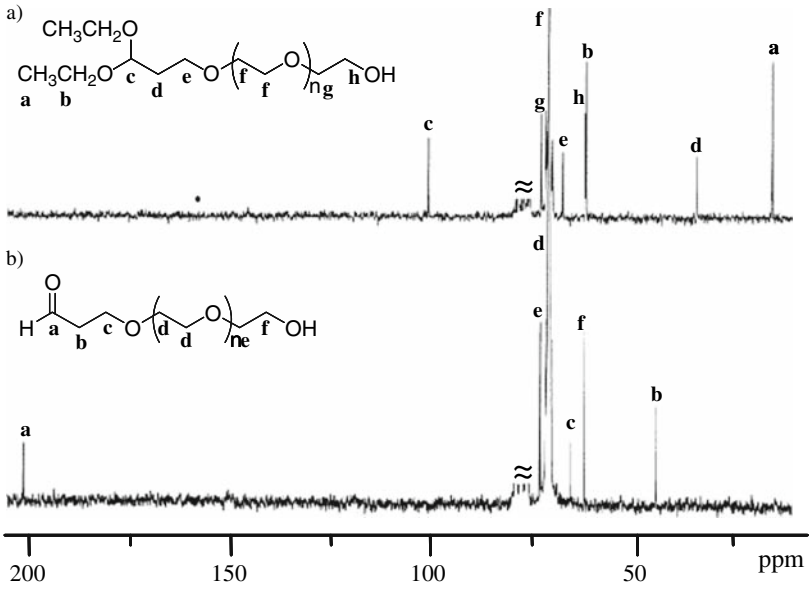

Figure 2.3 ^{13}C NMR spectra of (**a**) acetal-PEG-OH and (**b**) CHO-PEG-OH.

as a key intermediate to precisely synthesize the end-functionalized PEG-based block copolymers.

PEG-Hydrophobic Block Copolymer Synthesis for Drug Delivery Systems

Block copolymers composed of PEG and hydrophobic segments have become attractive in the field of drug delivery systems, because they form core–shell type polymeric micelles in aqueous media with a 10–100 nanometer particle size, viz., they can be utilized as a nanoscaled drug carrier (Scheme 2.3). Diverse drugs with a hydrophobic nature can be loaded with high efficacy into the core of polymeric micelles, allowing drugs to be solubilized in aqueous media. Indeed, polymeric micelles loaded with the anticancer drug, doxorubicin, were shown to stably circulate in the blood stream for a prolonged time period, eventually accumulating in the solid tumor by the EPR effect (Tsukioka, Matsumura, Hamaguchi, Koike, Moriyasu, & Kakizone, 2002).

Synthesis and Micellization of End-Functionalized PEG-poly(D,L-lactide) Block Copolymer

In the field of drug delivery systems, PEG-poly(D,L-lactide) (PEG-PLA) block copolymers (Scholz, Iijima, Nagasaki, & Kataoka, 1995) have been extensively studied because of the following reasons: (i) the potassium alcholate species of the PEG chain end can initiate the ring-opening polymerization of the D,L-lactide (LA) monomer without any side reactions (Inoue, & Aida, 1989) and (ii) PLA is biodegradable and nontoxic (Kimura, 1993). After the preparation of acetal-PEG-OK in THF, a certain amount of LA was added to obtain the acetal-PEG-PLA block copolymer, as shown in Scheme 2.4 (Nagasaki, Okada, Scholz, Iijima, Kato, & Kataoka, 1998; Iijima, Nagasaki, Okada, Kato, Kataoka, 1999). Figure 2.4 shows the SEC chromatograms and ^{1}H NMR spectrum of the obtained block copolymer. As can be seen in the SEC chromatograms, the molecular weight of the block copolymer increased, retaining narrow molecular weight distribution (MWD) as well as no remaining prepolymer peak, indicating the high efficiency of block copolymerization. In addition to the signals based on both PEG and PLA segments on the ^{1}H

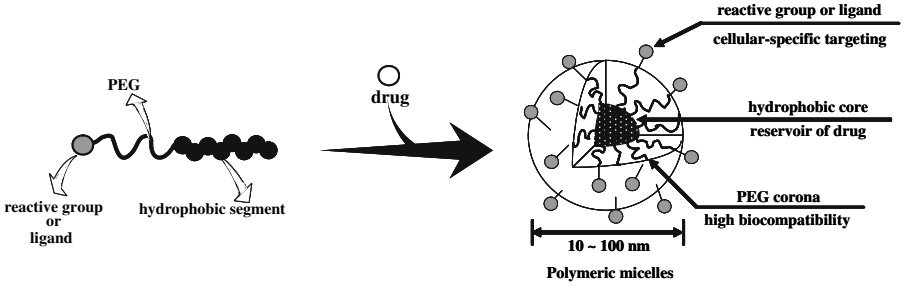

Scheme 2.3 Schematic illustration of polymeric micelle as a drug carrier.

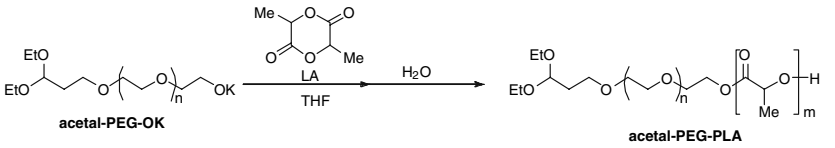

Scheme 2.4 Synthesis of acetal-PEG-PLA block copolymer.

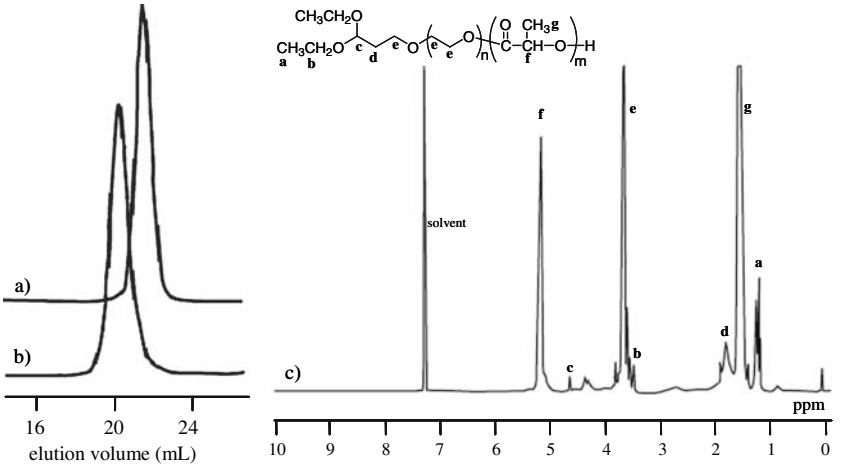

Figure 2.4 SEC chromatograms of (**a**) acetal-PEG-OH, (**b**) acetal-PEG-PLA block copolymer, and (**c**) ^{1}H NMR spectrum of acetal-PEG-PLA block copolymer.

NMR spectrum, the end acetal protons were clearly observed at 4.7 ppm. Thus, the PEG-PLA (hydrophilic–hydrophobic) block copolymer possessing an acetal group at the PEG chain end was quantitatively obtained. It is known that, when exposed to aqueous media, amphiphilic block copolymers with a suitable hydrophilic–hydrophobic balance form micelle structures. In our case, after the block polymer was dissolved in *N,N*-dimethylacetamide (DMAc), the solution was dialyzed against water. Dynamic light scattering (DLS) measurements made possible an angular-dependent analysis, from which it was found that the acetal-PEG-PLA ($DP_{PEG} = 52$, $DP_{PLA} = 56$) micelle has a spherical shape and a size of ca. 30 nm with a unimodal distribution.

The conversion of the acetal end group into an aldehyde end group was conducted after the micelle formation. Hydrochloric acid was used to adjust the acetal-PEG-PLA (52/56) micelle solution to pH = 2. After a predicted period, the reaction was quenched by neutralization with $NaOH_{aq.}$ and the polymeric micelle was purified by dialysis. The conversion reaction of the acetal group into the aldehyde group was monitored by means of ^{1}H NMR spectroscopy. Figure 2.5 shows the ^{1}H NMR spectra of CHO-PEG-PLA (52/56) in $CDCl_3$ and D_2O after the hydrolysis reaction. As can be seen in both of the figures, the end-aldehyde proton appeared at 9.8 ppm, whereas the acetal methine proton disappeared at about 4.6 ppm. Protons based on the PLA segment

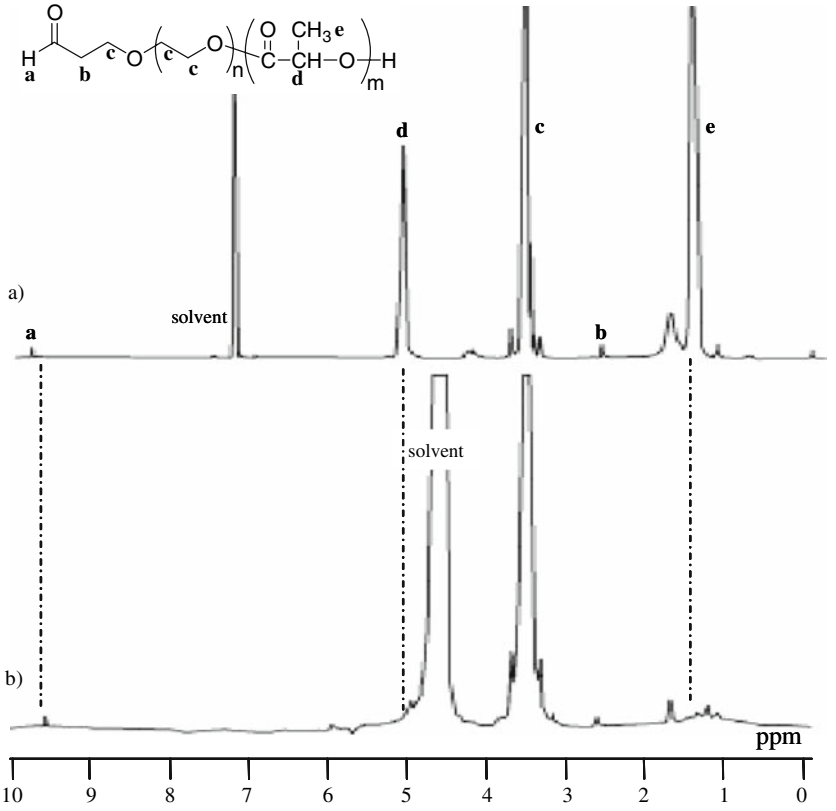

Figure 2.5 ^{1}H NMR spectra of CHO-PEG-PLA block copolymer (52/26) in (**a**) $CDCl_3$ and (**b**) D_2O after the acidic treatment of acetal-PEG-PLA block copolymer.

almost disappeared when the spectrum was monitored in D_2O. This disappearance indicates that the PLA segments form a solid core in aqueous media, the solidity, in turn, causing a broadening effect due to the restricted mobility in NMR spectroscopy. Therefore, it is reasonable to consider that the CHO-PEG-PLA micelle possesses a core–shell structure having aldehyde groups on its surface. The extent of the conversion from the acetal group to the aldehyde group was determined by the ^{1}H NMR spectrum. More than 80% of the acetal group was converted to the aldehyde group by the 4 h reaction. This reactive polymeric micelle will be utilized as the precursor for the targetable drug carrier.

Enzyme-Catalyzed Selective Synthesis and Micellization of End-Functionalized PEG-poly(D,L-lactide) Block Copolymer

One of the extensive studies done in the fields of DDS is related to polymeric micelles composed of poly(ethylene glycol)-*block*–poly(ε-caprolactone) copolymers (PEG-PCL), since the PEG-PCL block copolymer micelles bearing FDA-approved polymer components (Bei, Li, Wang, Le, & Wang, 1997)

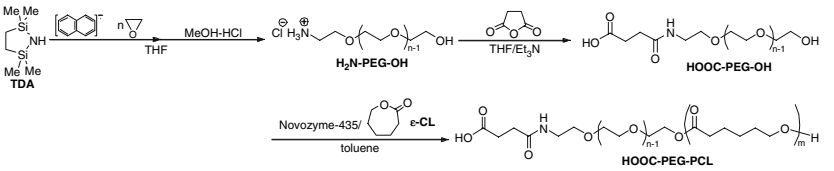

Scheme 2.5 Synthetic route to carboxylic acid-ended PEG-PCL block copolymer.

showed excellent biocompatibility, nontoxicity, high drug-loading capacity, long circulation time in the bloodstream, and high biodegradability (Allen, Yu, Maysinger, & Eisenberg, 1998). We recently reported a novel synthetic approach to carboxylic acid end-functionalized PEG-PCL block copolymer by means of the one-pot lipase-catalyzed polymerization of ε-CL using an α-carboxylic acid-ω-hydroxy-PEG as a macroinitiator (Oishi, Ikeo, & Nagasaki, 2007). The benefit of using a heterobifunctional PEG and lipase as a macroinitiator and catalyst, respectively, is that tedious production steps, such as end-functional group changes and protection–deprotection, are unnecessary.

A synthetic route to the carboxylic acid end-functionalized PEG-*b*-PCL copolymer is shown in Scheme 2.5. A heterobifunctional PEG possessing a carboxylic acid group at the α-end and a hydroxyl group at the ω-end (HOOC-PEG-OH) was successfully prepared, and thus the anionic ring-opening polymerization of ethylene oxide with the 2,2,5,5-tetramethyl-2,5-disila-1-azacyclopentane (TDA)/potassium-naphthalene system quantitatively afforded H_2N-PEG-OH (Yokoyama, Okano, Sakurai, Kikuchi, Ohsako, Nagasaki, & Kataoka, 1992), which was in turn converted into the HOOC-PEG-OH by treatment with 1.2 equivalents of succinic anhydride. According to the SEC analysis (Figure 2.6a), the molecular weight and polydispersity of the HOOC-PEG-OH were found to be $M_n = 6300$ and $M_w/M_n = 1.3$, respectively, which agrees fairly well with the calculated value (calcd. $M_n = 5200$). A ^{1}H NMR spectrum of HOOC-PEG-OH is shown in Figure 2.6c with assignments, where ethylene protons between the two carbonyl groups were observed at around 2.5 ppm (HOOC-C***H*****$_2$**C***H*****$_2$**-CONH-), along with a markedly diminished methylene peak at 2.86 ppm (H_2N-C***H*****$_2$**-CH_2-O-) attributed to the H_2N-PEG-OH. In addition, ethylene protons corresponding to the succinate ester group at around 2.3 ppm (-OCO-C***H*****$_2$**C***H*****$_2$**-COOH) formed through the reaction with succinic anhydride and hydroxyl group at the PEG ω-end were not observed, indicating that succinic anhydride was selectively reacted with the amino group of the H_2N-PEG-OH. The degree of functionality of the carboxylic acid was determined to be > 94.5% based on the integral ratio between the PEG-backbone protons (3.7 ppm –OC***H*****$_2$**C***H*****$_2$**-) and the ethylene protons of the succinate carbonyl moiety (2.52 and 2.64 ppm, HOOC-C***H*****$_2$**C***H*****$_2$**-CONH-).

The ring-opening lipase-catalyzed (Novozyme-435: immobilized lipase B from *Candida antarctica*) polymerization of ε-CL in the presence of the HOOC-PEG-OH macroinitiator was carried out at 60°C in toluene for 24 h with an ε-CL to HOOC-PEG-OH molar ratio of 128

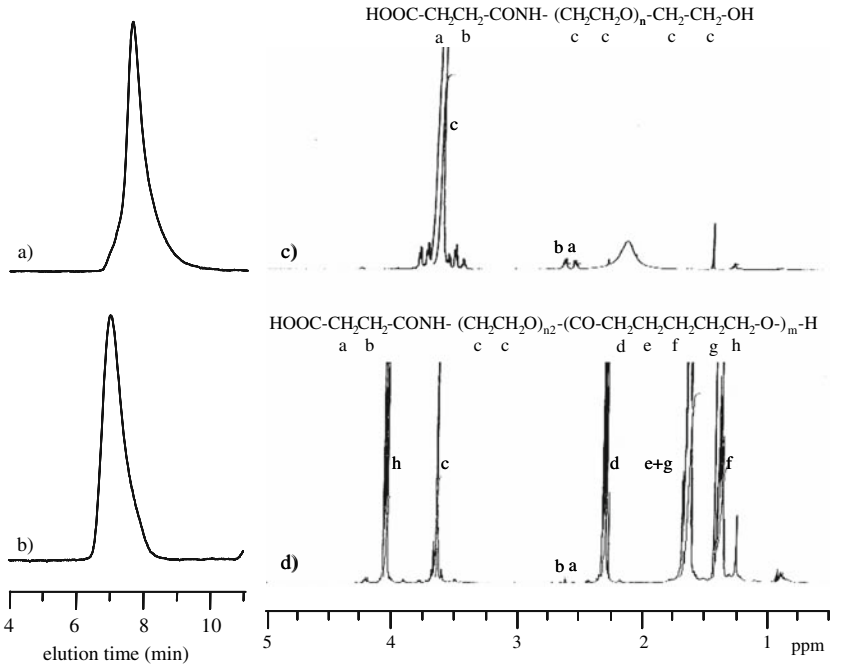

Figure 2.6 SEC chromatograms of (**a**) HOOC-PEG-OH and (**b**) HOOC-PEG-PCL block copolymer, and ^{1}H NMR spectra of (**c**) HOOC-PEG-OH and (**d**) HOOC-PEG-PCL block copolymer.

([ε-CL]/[HOOC-PEG-OH] = 128). The polymerization smoothly proceeded with complete consumption of the ε-CL within 6 h (100% conversion), but a large amount of the HOOC-PEG-OH macroinitiator (< 30% conversion) still remained due to the formation of homo-oligoCL initiated by trace amounts of water in the polymerization system (Hedfors, Ostmark, Malmstrom, Hult, & Martinelle, 2005). Figure 2.6b and 6d shows the SEC chromatogram and ^{1}H NMR spectrum of the purified PEG-PCL block copolymer with assignments, respectively. As seen in the SEC chromatograms (Figure 2.6b), the PEG-*b*-PCL copolymer ($M_n = 16000$, $M_w/M_n = 1.6$) gave a unimodal peak at a higher-molecular-weight position (i.e., shorter elution time) compared to the HOOC-PEG-OH ($M_n = 6300$, $M_w/M_n = 1.3$, Figure 2.6a). Note that the unreacted HOOC-PEG-OH and homo-oligoCL were not observed in the SEC chromatogram of the PEG-PCL block copolymer. In the ^{1}H NMR spectrum (Figure 2.6d), the peaks corresponding to both of the PEG and the PCL segments were clearly observed, which is consistent with the formation of a block copolymer. Based on the integral ratio between the PEG-backbone protons (3.7 ppm –OC***H*****$_2$**C***H*****$_2$**-) and the methylene protons of the PCL segment (4.17 ppm, -CO-$CH_2CH_2CH_2CH_2C$***H*****$_2$**-O-), the DP of the PCL segment and the molecular weight of the block copolymer were calculated to be 260 and 32300, respectively. Although the molecular weight calculated from ^{1}H NMR spectrum in Figure 2.6d does not agree with the molecular weight

calculated from the SEC analysis (Figure 2.6b), the PEG-PCL block copolymer tends to appear on the lower-molecular-weight position in the SEC analysis, presumably due to adsorption of the block copolymer on the gel in SEC column. Furthermore, it is difficult to estimate the degree of functionality of the carboxylic acid in the PEG-PCL block copolymer from the peaks corresponding to the two terminal methylene moieties at δ 2.52 and 2.64 ppm in the ^{1}H NMR spectrum.

To clarify the presence of the carboxylic acid at the PEG chain end of the block copolymer, the surface charge of the PEG-PCL block copolymer micelles was evaluated by means of zeta potential (ζ) measurement under various pH conditions. The size and polydispersity index of the PEG-PCL block copolymer micelles thus prepared were estimated by means of DLS measurement at pH 7.4. The PEG-PCL block copolymer micelle had an average hydrodynamic diameter of 35.3 nm with a relatively narrow polydispersity index (μ_2/Γ^2) of 0.150, showing a unimodal distribution, as shown in Figure 2.7a. As can be seen in Figure 2.7b, the PEG-PCL block copolymer micelles had a negative value of the zeta potential, $\zeta = -14$ mV, at pH 7.2. Note that the existence of carboxylic acid groups on the surface of the PEG-PCL block copolymer micelles obviously contributed to this negative value, since most of the carboxylic acid groups should be in dissociated form (-COO$^-$) at pH 7.2. Concomitantly, as the pH decreased, the zeta potential of the PEG-PCL block copolymer micelles shifted from negative values ($\zeta < 0$) to zero ($\zeta \sim 0$) due to the protonation of the carboxylic acid groups (-COOH) on the surface of PEG-PCL block copolymer micelles. It should also be observed that these zeta potential values for the changes in pH are indeed close to the pK_a value of carboxylic acid (~ 5), strongly suggesting the formation of a carboxylic acid end-functionalized PEG-PCL block copolymer. PEG-PCL block copolymer micelles had a negative zeta potential, indicating that reactive carboxylic acid groups were located on the surface of the PEG-PCL block copolymer micelles. Therefore, this reactive PEG-PCL block copolymer micelle may have potential uses in the field of drug delivery systems as a targetable drug carrier.

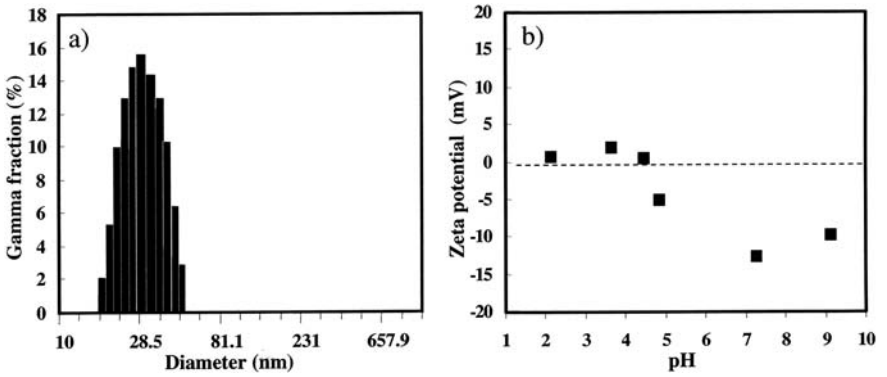

Figure 2.7 (**a**) DLS and (**b**) zeta potential measurements for the PEG-*b*-PCL micelles. DLS measurement was carried out in aqueous solution at pH 7.4 at 37°C (detection angle, 90°). Zeta potential measurement was carried out at various pH (2.1, 3.6, 4.4, 4.8, 7.2, and 9.1).

PEG-polyelectrolyte Block Copolymers Synthesis for Gene and OligoDNA/RNA Delivery Systems

Recently, Kataoka, Togawa, Harada, Yasugi, Matsumoto, & Katayose (1996) reported that PEG/polyelectrolyte block copolymers were found to form polyion complex (PIC) micelles with oppositely charged polyelectrolytes through electrostatic interaction. In particular, the PIC micelles composed of the PEG-block-polyamine copolymer and negatively charged DNA have attracted much attention in the field of gene and oligoDNA/RNA delivery systems (Katayose, & Kataoka, 1997; Harada, Togawa, & Kataoka, 2001; Harada-Shiba, Yamauchi, Harada, Takamisawa, Shimokado, & Kataoka, 2002), because the PIC micelles exhibited excellent solubility in aqueous media, tolerance against enzymatic degradation, and minimal interaction with the cell membrane and the serum compartment due to the steric stabilization of the high-density PEG corona surrounding the PIC core (Scheme 2.6). Most of the polymeric micelles including PIC micelles, however, prepared so far possess no reactive group on the surface. If reactive groups can be introduced on the surface, any kind of ligand molecule can be installed on the surface of the micelle. For the preparation of reactive polymeric micelle, it is important to synthesize block copolymers possessing a functional group at the PEG chain end. By using heterobifunctional PEGs thus prepared, new types of block copolymers possessing a functional group at the PEG chain end can be designed. In this section, the new molecular design of the three types of PEG end-functionalized block copolymers for the gene and oligoDNA/RNA delivery systems is described.

Synthesis and Micellization of Lactosylated-PEG-poly [2-(N, N-dimethylamino) ethyl methacrylate)] Block Copolymer

Recently, we have found that methacrylic ester possessing an amino group at the β-position of the ester moiety can be polymerized by a simple alkoxide species such as potassium ethoxide (Nagasaki, Sato, & Kato, 1997). We proposed the increased reactivity of an alkoxide initiator that was generated by a chelation that was located between the monomer molecule and the initiator. This polymerization system can be applicable to a new block copolymer synthesis. In the same way as mentioned above,

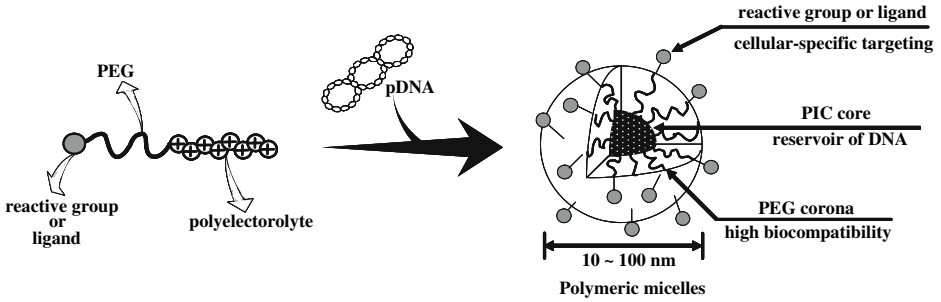

Scheme 2.6 Schematic illustration of polymeric micelle as gene carrier.

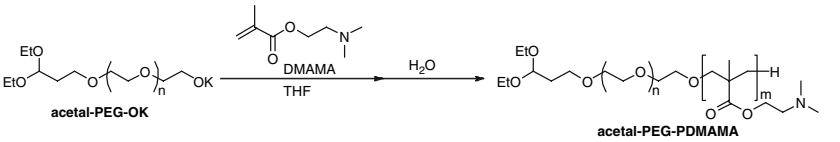

Scheme 2.7 Synthesis of acetal-PEG-PDMAMA block copolymer.

the acetal-PEG-OK was prepared in THF, followed by the addition of a certain amount of 2-*N,N*-(dimethylamino)ethyl methacrylate (DMAMA) to the reaction mixture, which was stirred for several minutes (Scheme 2.7) (Kataoka, Harada, Wakebayashi, Nagasaki, 1999). Figure 2.8 shows the SEC chromatograms and the ^{1}H NMR spectrum of the obtained block copolymer. By the addition of a DMAMA monomer to the polymerization system after all of the ethylene oxide was consumed, block polymerization proceeded, although a small amount of the prepolymer remained, as shown in Figure 2.8a and b. It should be noted that the MWD of the obtained block copolymer was still low, indicating that the possible ester exchange reaction was negligible. After the treatment with ion exchange resin, the remaining prepolymer was removed completely, as shown in Figure 2.8c. Along with the signals based on both PEG and PDMAMA segments, the end acetal protons were observed on the ^{1}H NMR spectrum (Figure 2.8d), indicating that, although the heterobifunctional PEG is used as a macroinitiator, a new end-functionalized PEG/polyamine block copolymer can be synthesized. Furthermore, lactose-ended PEG-PDMAMA block copolymer was obtained from the reductive amination reaction of the aldehyde-PEG-PDMAMA block copolymer with *p*-aminophenyl-β-D-lactopyranoside,

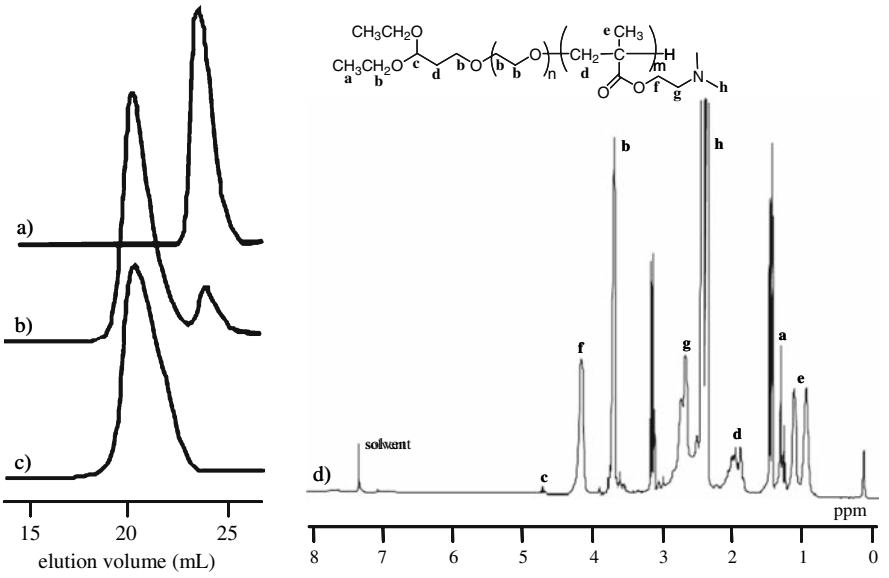

Figure 2.8 SEC chromatograms of (**a**) acetal-PEG-OH, (**b**) crude acetal-PEG-PDMAMA block copolymer, (**c**) acetal-PEG-PDMAMA block copolymer purified ion exchange resin, and (**d**) ^{1}H NMR spectrum of purified acetal-PEG-PDMAMA block copolymer.

and this step, in turn, initiated the introduction of the lactose group (ligand) to the acetal-PEG-PDMAMA block copolymer (Wakebayashi, Nishiyama, Yamasaki, Itaka, Kanayama, Harada, Nagasaki, & Kataoka, 2004). From the ^{1}H NMR spectrum of the lactose-PEG-PDMAMA block copolymer, the degree of the functionality of the lactose moiety was determined to be 28.5%.

Lactose-installed PIC micelles were prepared by simple and direct mixing of pDNA (pGL3 plasmid DNA encoding firefly luciferase) with lactose-PEG-PDMAMA block copolymer solutions at various charge ratios (cationic charge/anionic charge; N/P ratio). All the PIC micelles prepared at various N/P ratios had a unimodal distribution (μ_2/Γ^2 = 0.16–0.22) with an average diameter of ca. 100 nm, as revealed by DLS measurements. The small size of the PIC micelles compared to the dimension of free pDNA strongly suggests the compaction of complexed pDNA, which forms the collapsed core of the micelles. In addition, the PIC micelles exhibited not only lower absolute values of zeta potential compared to the reported zeta potential values of the polyplex that was composed of both simple polycations (without a PEG segment) (Cherng, Wetering, Talam, Crommelin,& Hennink, 1996) and pDNA but also stability against deoxyribonuclease (DNase I) digestion. This is reasonably assumed to be due to the formation of a corona surrounding the PIC core of the micelles.

To estimate the transfection ability of the lactose-installed PIC micelles against cultured HepG2 cells (human hepatoma cells) possessing an abundance of ASGP receptors on the cell surface (Schwartz, Fridovich, Knowles, & Lodish, 1981), a transfection study was carried out in the presence of 100 μM hydroxychloroquine (HCQ) as an endosomolytic agent. PIC micelles without the lactose moiety (acetal-PIC micelle) and Lipofectamine/pDNA complexes (lipoplex) were used as controls. HepG2 cells were co-incubated with lactose-installed PIC micelles (N/P = 6.25), acetal-PIC micelles (N/P = 6.25), or lipoplex (N/P = 5.0) for varying periods of time so that the time-dependent gene transfection could be observed, as shown in Figure 2.9. After approximately 1 h of an induction period, both

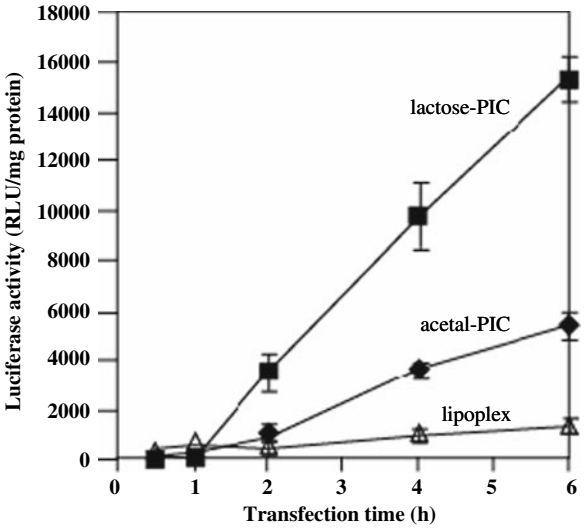

Figure 2.9 Effect of transfection time on gene expression. HepG2 cells were transfected with lactose- and acetal-PIC micelles at N/P = 6.25 in a medium containing 100 μM of hydroxychloroquine (HCQ). Transfection with lipoplex was done in the same conditions except in the absence of HCQ. Data are the mean ± SEM (n = 4).

the lactose-installed and the acetal-PIC micelles exhibited a time-dependent increase in transfection efficiency that was greater than that of the lipoplex. Interestingly, the lactose-installed PIC micelles achieved significantly higher transfection efficiency than the acetal-PIC micelles, suggesting that interaction between the lactose moieties of the PIC micelles and the ASGP receptors on the HepG2 cells (ASGP receptor-mediated endocytosis) may play a role in this phenomenon. In order to confirm the ASGP receptor-mediated endocytosis mechanism, a competitive assay using asialofetuin (ASF) was performed for both the lactose-installed and the acetal-PIC micelles. ASF, which is a natural ligand for the ASGP receptor, should serve as the inhibitor of the lactose-installed PIC micelle, unless the ASGP receptor-mediated mechanism does not play a substantial role, therein. The presence of excess ASF (4 mg/mL) resulted in a significant decrease in transfection efficiency of the lactose-installed PIC micelles, whereas the transfection efficiency of the acetal-PIC micelles was not affected by the presence of ASF up to 4 mg/mL, indicating that ASF in the medium has a negligible effect on the cellular uptake of the acetal-PIC micelle. Thus, it can be concluded that an appreciable fraction of the lactose-installed PIC micelles is taken up into HepG2 cells through an ASGP receptor-mediated endocytosis process, although a fluid-phase endocytosis pathway may concomitantly take part in the transfection efficiency to some extent. Thus, the installation of lactose (ligand) moieties increases the gene transfer efficiency of the PIC micelles composed of PEG-PDMAMA block copolymers and pDNA against HepG2 cells through the contribution of the receptor-mediated endocytosis mechanism, all of which indicates that the polymeric micelles are a promising contribution to cellular targetable gene delivery systems.

Synthesis and Micellization of pH-Responsive and Ligand-Installed Triblock Copolymer: Lactosylated-PEG-poly(silamine)-poly[2-(N, N-dimethylamino) ethyl methacrylate)]

Ligand-installed PIC micelles prepared from lactose-PEG-PDMAMA block copolymer and pDNA showed an increase in the cellular uptake through a receptor-mediated endocytosis process compared to those without lactose (ligand) moieties, as mentioned above. To observe an appreciable effect of the ligand molecules on gene expression, however, the presence of hydroxychloroquine (100 μM) as an endosomolytic agent has so far been required. This indicates that endosomal escape should be the most critical barrier to intracellular gene delivery by PIC micelles (Lloyd, 2000). Therefore, approaches are needed to devise PIC micelles with a function to escape from the endosome where the pH is 1.4–2.4 units lower than the physiological pH of 7.4 (Mukherjee, Ghosh, & Maxfield, 1997; Clague, 1998; Gruenberg, 2001). Worth noting in this regard is that a polyamine segment with a high pK_a as the C block preferentially forms a polyion complex with phosphate groups in pDNA (DNA-condensation segment), whereas the pH-responsive polyamine segment (B block) with a comparatively low pK_a, located between the PEG segment (A block) and the pDNA-condensation segment (C block), is expected to retain a substantial fraction of unprotonated amino groups (free-base) even in the PIC

due to the low protonation ability. As a consequence, the polyion complexation between such an ABC triblock copolymer and pDNA may lead to the formation of a three-layered PIC micelle possessing an unprotonated pH-responsive polyamine segment as an intermediate layer to function as a buffering moiety for facilitated endosomal escape (Fukushima, Miyata, Nishiyama, Kanayama, Yamasaki, & Kataoka, 2005). This section was devoted to the design and preparation of a novel ABC triblock copolymer for constructing a pH-responsive and targetable nonviral gene vector. The copolymer, lactosylated poly(ethylene glycol)-*block*-poly(silamine)-*block*-poly[2-(*N,N*-dimethylamino)ethyl methacrylate] (lactose-PEG-PSAO-PDMAMA), consists of lactosylated poly(ethylene glycol) (A-segment), a pH-responsive polyamine segment (B-segment), and a DNA-condensing polyamine segment (C-segment) (Oishi, Kataoka, & Nagasaki, 2006; Figure 2.10). Here, PSAO was selected as the pH-responsive polyamine segment showing two-step protonation (Figure 2.11, $pK_{a1} = 8.6$ and $pK_{a2} = 5.8$) along with a unique conformational transition at the critical pH (Nagasaki, Honzawa, Kato, & Kataoka, 1994). The unprotonated PSAO is insoluble in water, assuming a globular conformation with high flexibility, whereas fully protonated PSAO is soluble in water, assuming a rod-like conformation with rigid and expanded polymer strands. Such a unique conformational transition (rod-globule transition) can be explained by the rotational hindrance around the polymer chain due to the protonation of the amino groups along with the counter anion binding to the Si atoms (Figure 2.11).

A synthetic route to lactosylated poly(ethylene glycol)-*block*-poly (silamine)–*block*-poly[2-(*N,N*-dimethlyamino)ethyl methacrylate] (lactose-PEG-PSAO-PDMAMA) triblock copolymer is shown in Scheme 2.8. A heterobifunctional PEG possessing an allyl group at the α-end and an orthoester group at the ω-end (allyl-PEG-orthoester) was synthesized via the anionic ring-opening polymerization of ethylene oxide using the allyl alcohol /potassium-naphthalene initiator system, followed by termination with trimethyl 4-bromoorthobutyrate in the presence of 18-Crown-6. The radical addition of 2-aminoethanethiol hydrochloride to the allyl-PEG-orthoester quantitatively afforded an amine-PEG-methoxycarbonyl (H_2N-PEG-COOMe). Conversion of the orthoester group into a methoxycarbonyl group (COOMe) occurred due to the hydrolysis of the orthoester group during the purification (dialysis) process. The H_2N-PEG-COOMe was

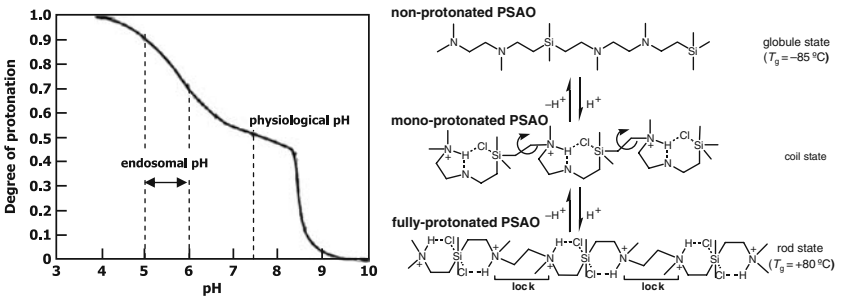

Figure 2.10 Change in the protonation degree of poly(silamine) (PSAO) with pH accompanying the conformation transition (globule-coil-rod).

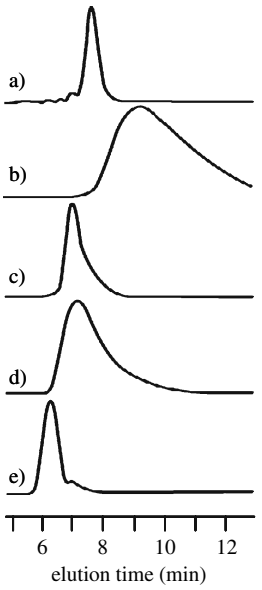

Figure 2.11 SEC chromatograms of (**a**) lac-PEG-COOH, (**b**) bis(amino)-PSAO, (**c**) lac-PEG-PSAO block copolymer, (**d**) HOOC-PDMAMA, and (**e**) lac-PEG-PSAO-PDMAMA triblock copolymer.

then converted into an amine-PEG-carboxylic acid (H_2N-PEG-COOH) by hydrolysis with 10% NaOHaq. The SEC, ^1H NMR, and MALDI-TOF MS analyses revealed that the determined molecular weight of the H_2N-PEG-COOH (SEC:$M_n = 6200$, $M_w/M_n = 1.04$, TOF-MS:$M_n = 6190$, $M_w/M_n = 1.03$) agrees well with the calculated value (calcd. $M_n = 6130$), and an amino group and carboxylic acid group were quantitatively introduced into the α-end and ω-end of PEG, respectively, to confirm the successful synthesis of allyl-PEG-orthoester and H_2N-PEG-COOMe. The introduction of a lactose group to the amine end of H_2N-PEG-COOH was performed by reaction with an excess amount of lactose-lactone (Kitano, Shoda, Kosaka, 1995). In the ^1H NMR spectrum of lactose-PEG-COOH, the degree of lactose functionality was determined to be 72%.To obtain the lactose-ended PEG-PSAO block copolymer, bis(amino)-PSAO ($M_n = 1550$, degree of polymerization (DP) = 6) was prepared as reported previously by the anionic polyaddition of dimethyldivinylsilane with *N,N'*-diethylethylenediamine in the presence of a catalytic amount of *n*-BuLi in THF at 60°C. The conjugation of the lactose-PEG-COOH with bis(amino)-PSAO was performed by activating the terminal carboxylic acid of lactose-PEG-COOH using dicyclohexylcarbodiimide (DCC) and *N*-hydroxysuccinimide (NHS). A large excess (50 eq.) of the bis(amino)-PSAO was used to suppress the formation of triblock copolymer, viz., lactose-PEG-PSAO-PEG-lactose. After the conjugation reaction, unconjugated bis(amino)-PSAO and other chemicals were removed by precipitation into Et_2O. Figure 2.11c and 2.12a, respectively, shows the SEC chromatogram and ^1H NMR spectrum of the lactose-PEG-PSAO block copolymer with assignments. As seen in the SEC chromatograms (Figure 2.11), lactose-PEG-PSAO (Figure 2.11c) gave a unimodal peak at a high molecular weight position (i.e., shorter elution time) compared to the lactose-PEG-COOH ($M_n = 6300$, $M_w/M_n = 1.05$, Figure 2.11a) and bis(amino)-PSAO ($M_n = 1550$, $M_w/M_n = 2.01$, Figure 2.11b).

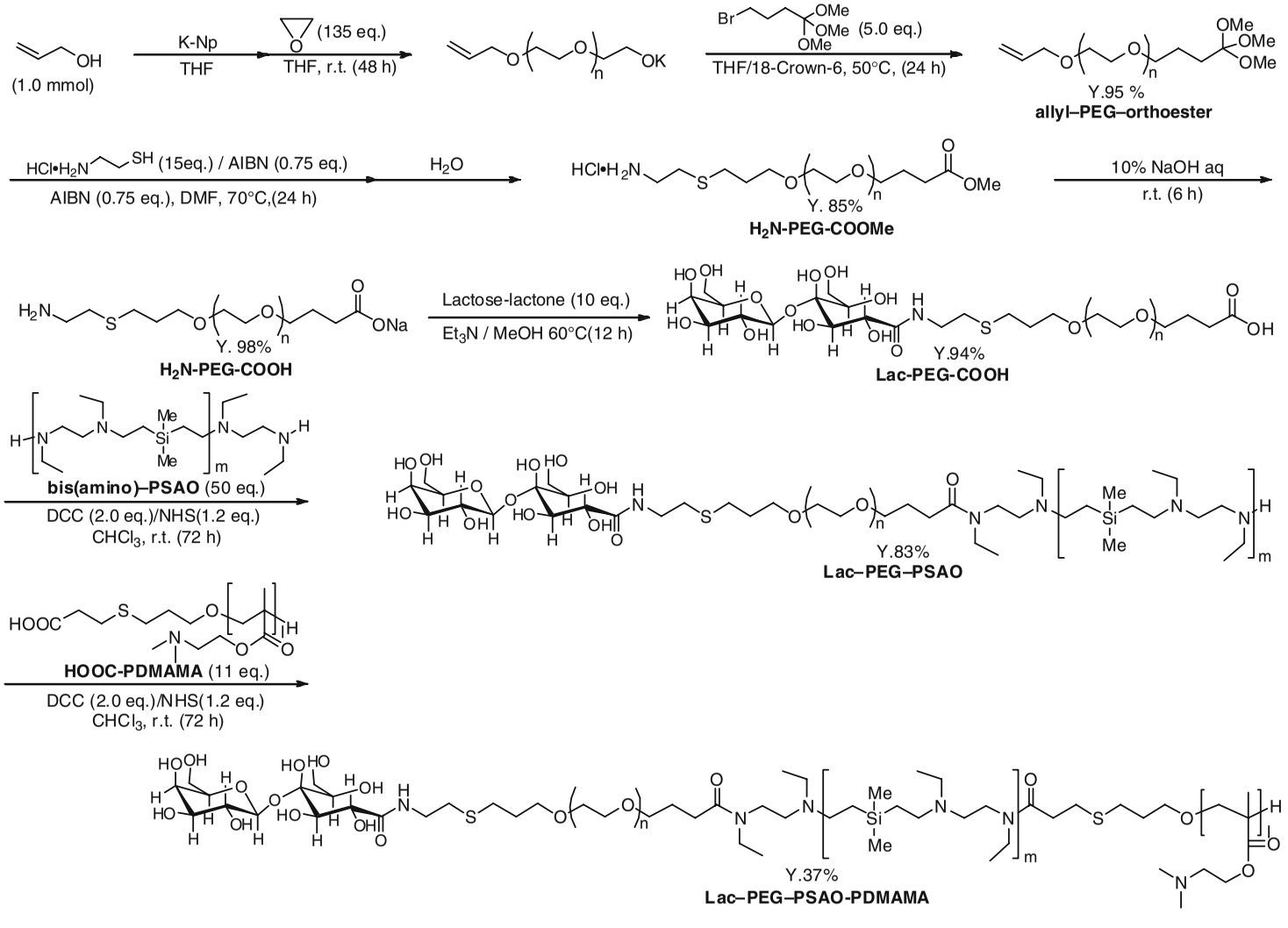

Scheme 2.8 Synthetic route to lactose-ended PEG-PSAO-PDMAMA triblock copolymer.

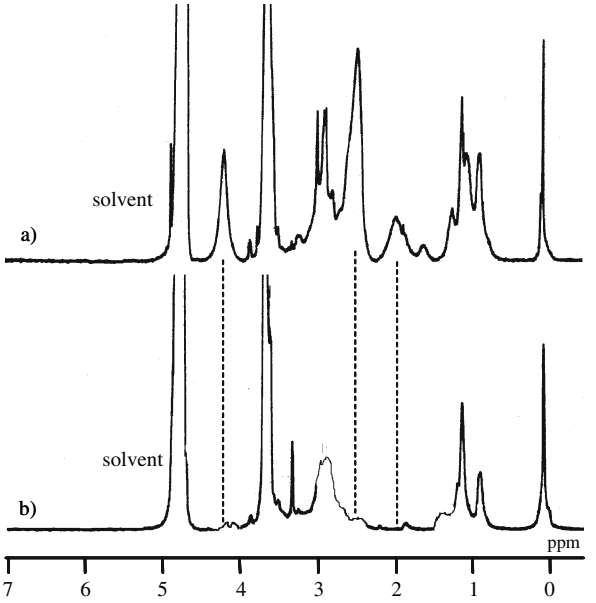

Figure 2.12 ^{1}H NMR spectra of (**a**) lac-PEG-PSAO block copolymer and (**b**) lac-PEG-PSAO-PAMA triblock copolymer.

Note that the unreacted lactose-PEG-COOH and bis(amino)-PSAO were not observed in the SEC chromatogram (Figure 2.11c) of the lactose-PEG-PSAO (obsd. $M_n = 7150$, $M_w/M_n = 1.15$, calcd. $M_n = 7850$). In the ^{1}H NMR spectrum (Figure 2.12a), the peaks corresponding to both of the PEG and PSAO segments were clearly observed, consistent with the formation of a diblock copolymer. Note that the peaks corresponding to the terminal lactose moiety were also observed at δ 4.0–5.3 ppm in the ^{1}H NMR spectrum in DMSO-d_6. From the integral ratio between the PEG-backbone protons (3.7 ppm –OCH_2CH_2-) and the methyl protons of PSAO segment (0.1 ppm, $SiMe_2$), the DP of the PSAO segment in the block copolymer was calculated to be 5.67, which is in good accordance with that of the starting bis(amino)-PSAO (DP = 6). To obtain the lactose-PEG-PSAO-PDMAMA triblock copolymer, the conjugation of the lactose-PEG-PSAO diblock copolymer and HOOC-PDMAMA was performed in a manner similar to the conjugation of lactose-PEG-COOH and bis(amino)-PSAO. After the conjugation reaction, unconjugated HOOC-PAMA and other chemicals were removed by precipitation into cold 2-propanol, followed by centrifugation. Figure 2.11e and 11b, respectively, shows the SEC chromatogram and ^{1}H NMR spectrum of the lactose-PEG-PSAO-PDMAMA triblock copolymer with assignments. The lactose-PEG-PSAO-PDMAMA (Figure 2.11e, $M_n = 10850$, $M_w/M_n = 1.29$, calcd. $M_n = 13450$) had a shorter elution time compared to the lactose-PEG-PSAO ($M_n = 7170$, $M_w/M_n = 1.15$, Figure 2.11c) and HOOC-PDMAMA ($M_n = 5670$, $M_w/M_n = 1.50$, DP = 35, Figure 2.11d), indicating an increased molecular weight due to the formation of the triblock polymer. Nevertheless, a slight portion of unreacted lactose-PEG-PSAO and/or HOOC-PDMAMA seems to still remain (about 10%) in the sample as indicated by the small accompanying peak appearing after the main fraction (Figure 2.11e). In the ^{1}H NMR spectrum (Figure 2.12b), the peaks corresponding to the PEG, PSAO, and PDMAMA segments were clearly observed, suggesting the

formation of a triblock copolymer. From the integral ratio between the PEG-backbone protons (3.7 ppm –OCH_2CH_2-) and methylene protons of the PDMAMA segment (4.08 ppm, –COOCH_2CH$_2$N(CH$_3$)$_2$), the DP of the PDMAMA segment was calculated to be 31.3 (DP of starting PDMAMA = 35). This result indicates that the purity of the triblock copolymer was 89%.

The PIC micelle prepared from lactose-PEG-PSAO-PDMAMA and pDNA was characterized by ^{1}H NMR spectroscopy in D_2O containing 0.15 M NaCl at pD = 7.4. Figure 2.13b shows the ^{1}H NMR spectrum of the polyplex micelle prepared at N/P = 3, where the residual molar ratio of the protonated PDMAMA segment in the block copolymer, calculated from the pK_a value, to the phosphate groups in pDNA is estimated to be unity at physiological pH (= 7.4). Obviously, the peaks from the PDMAMA segment, which were clearly observed in the spectrum of the free polymers (Figure 2.13a), nearly disappeared upon complexation with pDNA

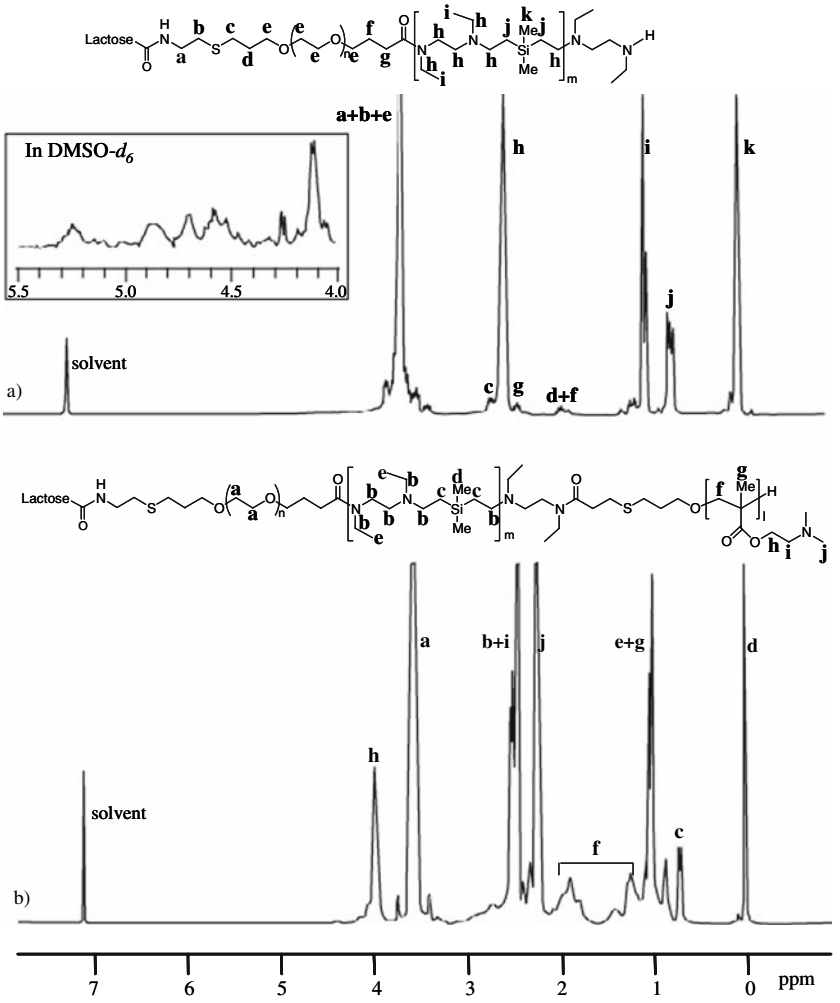

Figure 2.13 ^{1}H NMR spectra of (**a**) lac-PEG-PSAO-PDMAMA triblock copolymer and (**b**) lac-PEG-PSAO-PDMAMA/pDNA PIC micelle at pD = 7.4 in D_2O containing 0.15 M NaCl at 37°C.

(Figure 2.13b), whereas the peaks from the PSAO segment were still clearly observed in the spectrum. The selective disappearance of PDMAMA peaks upon complexation strongly suggests that the PDMAMA segment predominantly forms a PIC with pDNA to cause significant peak broadening. On the other hand, observation of the peaks from the PSAO segment even in the spectrum of the PIC micelle suggests the presence of the uncomplexed PSAO fraction. Eventually, these results are consistent with the formation of the three-layered structure of the PIC micelle with a PAMA/pDNA PIC core, a free PSAO inner shell, and a lactosylated PEG outer shell. To estimate the effect of the environmental pH on the hydrodynamic diameter of the PIC micelles, the lactose-PEG-PSAO-PDMAMA/pDNA, lactose-PEG-PSAO/pDNA, and lactose-PEG-PDMAMA/pDNA PIC micelles were prepared in 0.15 M NaClaq (pH 7.4) at N/P = 3. By decreasing the pH from 7.4 to 4.0, the diameter of the lactose-PEG-PSAO-PDMAMA/pDNA and lactose-PEG-PSAO/pDNA PIC micelles proportionally increases with a unimodal distribution ($\mu_2/\Gamma^2 < 0.25$), reaching a 2.7-times larger hydrodynamic volume at pH 4.0 compared to that at pH 7.4, as shown in Figure 2.14. On the contrary, there was negligible change in the hydrodynamic diameter of the lactose-PEG-PDMAMA/pDNA PIC micelle with decreasing pH from 7.4 to 4.0. This pH-induced size variation observed for the system containing the PSAO segment is most likely to be related to the conformational changes in the PSAO chain due to progressive protonation with decreasing pH. Apparently, the high rigidity of the protonated PSAO chain in the lower pH region should be unfavorable for triggering the DNA condensation upon complexation. As a consequence, a loose complex may form between pDNA and the PSAO segment without condensation in the lower pH region, showing an appreciable size increase. To estimate the transfection ability of the lactose-PEG-PSAO-PDMAMA/pDNA, lactose-PEG-PDMAMA/pDNA, and lactose-PEG-PSAO/pDNA PIC micelles with various N/P ratios, a transfection study using HuH-7 cells containing asialoglycoprotein receptors on their surface (Stockert, 1995; Hashida, Takemura, Nishikawa, & Takakura, 1998) was carried out in the presence of 10% FBS. A pGL-3 control plasmid DNA encoding firefly luciferase was used as a reporter gene. In addition, the

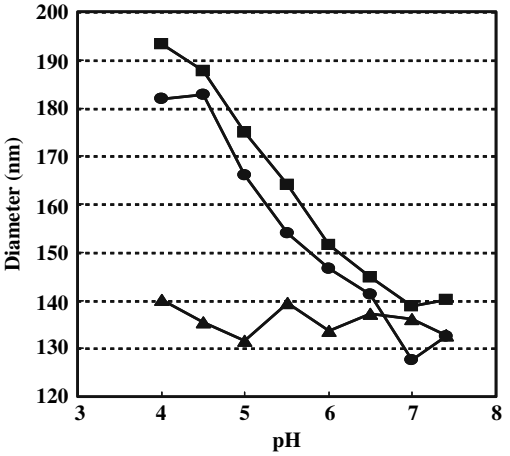

Figure 2.14 pH vs. diameter of lac-PEG-PSAO-PDMAMA/pDNA (*circle*), lac-PEG-PDMAMA/pDNA (*triangle*), and lac-PEG-PSAO/pDNA (*square*) PIC micelles at N/P = 3 (angle, 90°; solvent, distilled water including 0.15 M NaCl; temperature, 37°C).

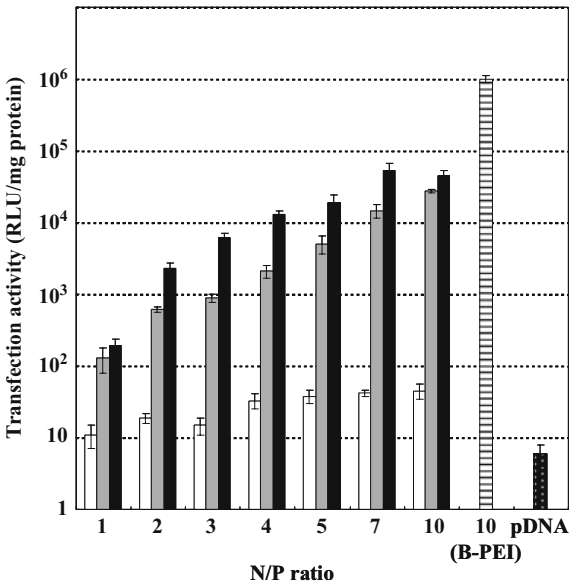

Figure 2.15 Transfection efficiency to HuH-7 cells of the lac-PEG-PSAO-PDMAMA/pDNA (*black bar*), Lac-PEG-PDMAMA/pDNA (*gray bar*), and lac-PEG-PSAO/pDNA (*white bar*) PIC micelles prepared at various N/P ratios with a fixed pDNA amount. Data are the mean ± SD ($n = 3$).

B-PEI/pDNA polyplex was used as a control vector at the optimal N/P ratio of 10 to show the highest transfection efficacy. As shown in Figure 2.15, the transfection efficiency of the lactose-PEG-PSAO-PDMAMA/pDNA and lactose-PEG-PDMAMA/pDNA PIC micelles was substantially improved with an increasing N/P ratio. In particular, one order of magnitude increase in transfection efficiency was achieved by increasing the N/P ratio from 1 to 2 ($P<0.05$), corresponding to the formation of a stable micelle structure judging from the agarose gel retardation assay. Alternatively, the lactose-PEG-PSAO/pDNA PIC micelles exhibited only limited transfection efficiency, presumably due to the low DNA-condensing capacity of the PSAO chain as indicated from the results of the EtBr exclusion assay. Thus, PIC micelles formed from lactose-PEG-PSAO may not be stable enough to be tolerated in the culture medium containing a substantial amount of serum proteins. Of interest, the transfection efficiency of the lactose-PEG-PSAO-PDMAMA/pDNA PIC micelles always revealed a higher transfection efficiency than the lactose-PEG-PDMAMA/pDNA PIC micelles in the range of N/P ratios between 2 and 10 ($P<0.05$). To = determine whether the difference in the transfection efficiency between the lactose-PEG-PSAO-PDMAMA/pDNA and lactose-PEG-PDMAMA/pDNA PIC micelles is related to the endosomal escape function, confocal microscope experiments were performed on the HuH-7 cells treated with the PIC micelles containing FITC-labeled pDNA. Cells were co-incubated with LysoTracker Red DND-99 probe, which specifically stains acidic organelles such as endosomes and lysosomes. Thus, the colocalization of the polyplex micelles and the LysoTracker Red probe in an acidic compartment (endosome and lysosome) should be detected as yellow (or orange) fluorescence due to the merging of green and red colors. In the case of the lactose-PEG-PDMAMA/pDNA PIC micelles (Figures 2.16a and b), the yellow and red fluorescences were observed without isolated green fluorescence even after 120 min incubation, indicating that

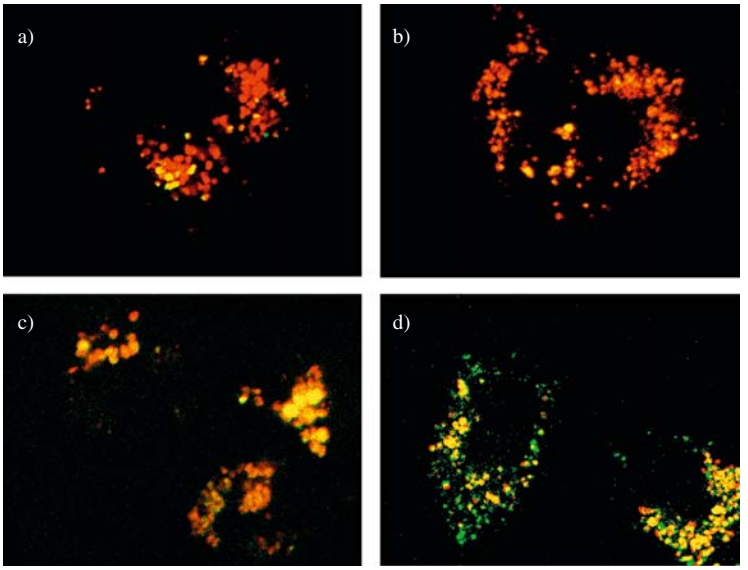

Figure 2.16 Confocal fluorescent microscope images of the HuH-7 cells in the presence of LysoTracker Red DND-99 and PIC micelles prepared at N/P = 3 with FITC-labeled pDNA. (**a**) lac-PEG-PDMAMA/pDNA PIC micelles (incubation time: 30 min), (**b**) lac-PEG-PDMAMA/pDNA PIC micelles (incubation time: 120 min), (**c**) lac-PEG-PSAO-PDMAMA/pDNA PIC micelles, (incubation time: 30 min), (**d**) lac-PEG-PSAO-PDMAMA/pDNA PIC micelles (incubation time: 120 min). These images are the typical image of triplicate experiments. (*See* Color Plate 4)

the PIC micelles localized in the endosomes and/or lysosomes with the LysoTracker Red probe. The lactose-PEG-PSAO-PDMAMA/pDNA PIC micelles localized in the endosomes and/or the lysosomes with the LysoTracker Red probe after 30 min incubation (Figure 2.16c), as suggested by the partially yellow fluorescence. At 120 min of incubation, diffused green fluorescence was observed in the cytoplasm (Figure 2.16d), indicating that the lactose-PEG-PSAO-PDMAMA/pDNA PIC micelles gradually escaped from the endosomes and/or lysomes into the cytoplasm in a time-dependent manner. These results suggest that both the PDMAMA segment as a DNA-condensing polycation and the PSAO segment as the buffering moiety (buffer effect) (Boussif, Lezoualc, Zanta, Mergny, Scherman, Demeneix, & Behr, 1995) may synergistically contribute to enhance the transfection efficiency of the lactose-PEG-PSAO-PDMAMA/pDNA PIC micelles. Although the lactose-PEG-PSAO-PDMAMA/pDNA PIC micelles showed one order of magnitude lower transfection efficiency than the B-PEI/pDNA polyplex at N/P = 10 ($P<0.05$), this value may still be appreciable considering that the polyplex micelles have hydrophilic and neutral PEG palisades on their surface to shield the cationic character.

Synthesis and Micellization of PEG-asDNA/siRNA Block Copolymer

Nucleic acid medicines such as antisense DNAs (asDNAs) and small interfering RNAs (siRNAs) have attracted much attention as a new class

of therapeutic agents (Uhlman, & Peyman, 1990; Elbashir, Harborth, Lendeckel, Yalcin, Weber, & Tuschl, 2001). Nevertheless, the therapeutic value of nucleic acid medicines under in vivo conditions is still controversial due to their low stability against enzymatic degradation, low permeability across cell membrane, and preferential liver and renal clearance (Braasch, Paroo, Constantiescu, Ren, Öz, Mason, & Corey, 2004). We have recently reported the synthesis of PEG-asDNA/siRNA block copolymers possessing a smart linkage such as acid-labile linkage (β-thiopropionate linkage) (Oishi, Sasaki, Nagasaki, & Kataoka, 2003) and glutathione-sensitive linkage (disulfide linkage) (Oishi, Hayama. Akiyama, Takae, Harada, Yamasaki, Nagatsugi, Sasaki, Nagasaki, & Kataoka, 2005), as shown in Scheme 2.9. The key issue of the introduction of smart linkage between PEG and asDNA/siRNA segments is to release the active (free) asDNA/siRNA in response to the endosomal pH (6.0–5.0) and glutathione concentration (1–10 mM), leading to efficient interaction of nucleic acid medicines with the target mRNA in the cytoplasm. Furthermore, it is expected that PEG-asDNA/siRNA block copolymer will mix with the appropriate polycation to form a PIC micelle, since the PEG-asDNA/siRNA block copolymer (PEG-polyanion block polymer) is one of the homologues of PEG-polyanion block copolymers.

As a typical example for the formulation of pH-sensitive and targetable PIC micelles of siRNA (Oishi, Nagasaki, Itaka, Nishiyama, & Kataoka, 2005), Michael addition of the 5′-thiol-modified sense RNA (firefly luciferase, pGL3-control sense sequence) toward ω-acrylate group of α-lactosyl-ω-acryl-PEG gave a conjugate of lactose-PEG with single-stranded RNA (lactose-PEG-ssRNA), which revealed a retarded migration in gel electrophoretic assay (Figure 2.17a, lane 3) compared to free-sense RNA (lane 1) in line with PEGylation. Then, the lactose-PEG-ssRNA was annealed with antisense RNA to undergo hybridization, preparing the lactose-PEG-siRNA block copolymer. The lactose-PEG-siRNA thus prepared gave a single band in gel electrophoresis (lane 4), and had further retarded migration compared to lactose-PEG-ssRNA (lane 3) and free siRNA (lane 2). All of these results are consistent with the successful preparation of the lactose-PEG-siRNA with negligible contamination with unreacted and intermediate compounds. The PIC micelles from the lactose-PEG-siRNA conjugate and PLL (degree of polymerization = 40) were then prepared at the charge ratio of 1 (N/P = 1), where no free lactose-PEG-siRNA conjugate and almost complete retardation were observed in a polyacrylamide gel electrophoresis (Figure 2.17a, lane 5), suggesting that polyion complexation between the siRNA segment and the PLL quantitatively took

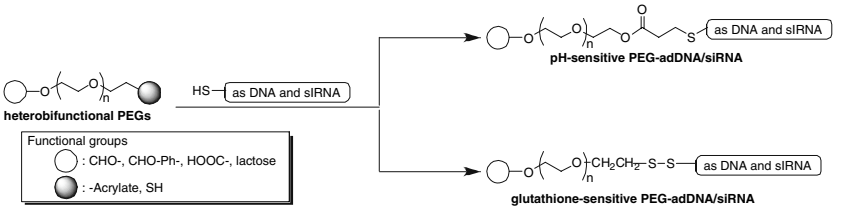

Scheme 2.9 Synthesis of end-functionalized PEG-asDNA/siRNA block copolymer.

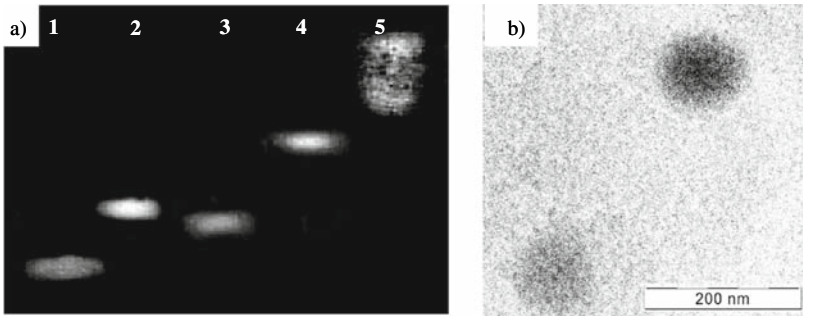

Figure 2.17 (**a**) Polyacrylamide gel retardation assay: lane 1, sense RNA; lane 2, siRNA; lane 3, lac-PEG-ssRNA; lane 4, lac-PEG-siRNA; and lane 5, PIC micelle; and (**b**) transmission electron micrograph of the disulfide cross-linked PIC micelle.

place. The PIC micelle with disulfide cross-linked core was also prepared by using thiolated PLL tolerable for the transmission electron microscopy (TEM) observation. The disulfide cross-linked PIC micelles have spherical shape with average size ($n = 36$) of 117 ± 26 nm, consistent with the formation of multi-molecular micellization of the Lac-PEG-siRNA with PLL, as shown in Figure 2.17b.

Dual luciferase reporter assay was done in HuH-7 cells (human hepatoma cells) possessing asialoglycoprotein (ASGP) receptors, which recognize compounds bearing terminal galactose moieties, to evaluate the gene-silencing ability of the conjugate and the PIC micelle system (Figure 2.18). Both the lactose-PEG-siRNA conjugate and the PIC micelle (N/P = 1) revealed RNAi activities with dose-dependent manner even in the presence of 10% FBS and, in particular, the PIC micelles achieved far more effective RNAi activity than the lactose-PEG-siRNA conjugate alone, viz., 50%

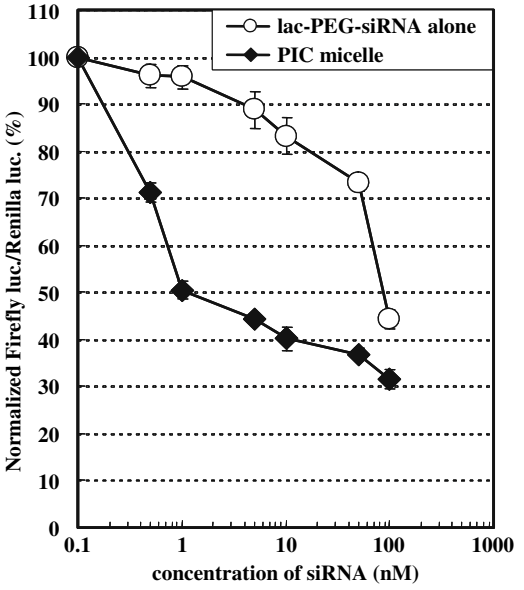

Figure 2.18 RNAi activities of lac-PEG-siRNA alone and PIC micelle against the firefly luciferase gene generated in cultured HuH-7 cells. Normalized ratios between the firefly luciferase activity (firefly luc.) and the renilla luciferase activity (renilla luc.) are shown on the ordinate. Data are the mean ± SD ($n = 3$).

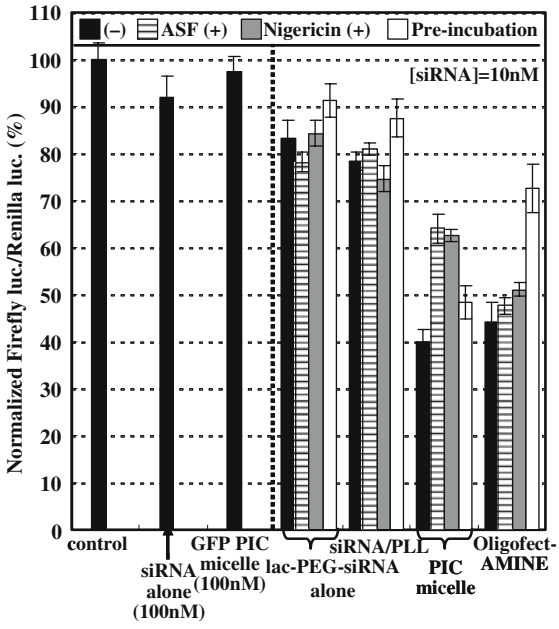

Figure 2.19 RNAi activities of PIC micelle, lac-PEG-siRNA alone, siRNA alone, siRNA/PLL, and OligofectAMINE against the firefly luciferase gene generated in cultured HuH-7 cells under various conditions. Normalized ratios between the firefly luciferase activity (firefly luc.) and the renilla luciferase activity (renilla luc.) are shown on the ordinate. Data are the mean ± SD ($n = 3$).

inhibitory concentration (IC_{50}) was found to be 1.3 and 91.4 nM for the PIC micelle and Lac-PEG-siRNA conjugate, respectively. This increase of almost 100 times in RNAi activity by PIC micelle is remarkable. On the other hand, no RNAi activity was observed for free siRNA even at 100nM of siRNA concentration, as shown in Figure 2.19. The lack of RNAi activity for free siRNA may be ascribed to the low tolerability against enzymatic attack and/or the restricted uptake into cellular interior due to the electrostatic repulsion with the negatively charged plasma membranes. Note that the PIC micelle including a GFP sequence induced no RNAi, strongly suggesting that an inhibition of firefly luciferase expression observed here indeed occurred through the sequence-specific RNAi effect. In addition, siRNA/PLL (polyplex) showed significantly lower RNAi activity compared to the PIC micelle probably owing to the aggregation at charge neutralized condition (N/P = 1) and non-specific interaction with serum proteins. Although the RNAi activity for the PIC micelle at 10 nM of conjugate concentrations was the same level compared to the commercially available oligofectAMINE (cationic liposome), the RNAi activity for the oligofectAMINE after pre-incubation with 50% serum for 30 min was significantly reduced (56 → 27% inhibition, $P<0.05$) due to the non-specifically interacting nature of the cationic carriers with negatively charged serum proteins. In sharp contrast, the PIC micelle still retained the RNAi activity even after pre-incubation for 30 min with 50% serum due to the segregation of the siRNA into the PEG environment. In order to confirm the cellular uptake pathway, asialofetuin (ASF) as the inhibitor for the ASGP receptor-mediated endocytosis was added to the culture medium (4 mg/mL). As a consequence, RNAi activities were reduced significantly for the PIC micelles (60 → 36% inhibition, $P<0.05$), whereas there was negligible effect of ASF on RNAi activities for lactose-PEG-siRNA

conjugate, siRNA/PLL, and oligofectAMINE in HuH-7 cells (Figure 2.19). Obviously, these results indicate that the lactose moieties clustering on the surface of PIC micelle appreciably facilitates ASGP receptor-mediated endocytosis to direct a remarkable RNAi efficacy. Then, nigericin as the inhibitor for the endosomal acidification was added to the culture medium (5 μM) to confirm that the acid-labile linkage in the conjugate contributes to RNAi activity. Consequently, the RNAi activity was significantly reduced for the PIC micelle (60 → 37% inhibition, $P<0.05$), whereas no effect was observed for the lactose-PEG-siRNA conjugate, siRNA/PLL, and oligofectAMINE. This result suggests that after the endocytotic internalization the cleavage of the acid-labile linkage of the micelles occurred in the manner synchronized with the pH decrease in endosomal compartment, releasing hundreds of free PEG strands to increase the colloidal osmotic pressure (Goh, Murthy, Xu, & Fréchet, 2004). This may induce the swelling and disruption of the endosome, facilitating the transport of free siRNA into cytoplasm. Several important factors are likely to be synergistically involved in the pronounced RNAi activity of the PIC micelles, such as the improvement of the stability against enzymatic degradation, minimal interaction with serum proteins, enhancement of the cellular uptake through the ASGP receptor-mediated endocytosis, and the effective transport of free siRNA from endosome into cytoplasm. It should be noted that the PIC micelles entrapping the lactose-PEG-siRNA conjugate reported here showed about 5800 times higher gene-silencing effect as compared to that of entrapping the lactose-PEG-asDNA conjugate targeting the same gene sequence ($IC_{50} = 7.6$ μM) (Oishi, Nagatsugi, Sasaki, Nagasaki, & Kataoka, 2005).

PEGylated Gold Nanoparticle Based on the Self-Assembling of Block Copolymers for siRNA Delivery System

Gold nanoparticles (AuNPs) have attracted much attention in the field of drug and gene delivery systems, because they have the advantages of easy preparation, no cytotoxicity, and the possibility of chemical modification of the surface. We recently reported the PEGylated AuNPs constructed through the self-assembly of heterobifunctional poly(ethylene glycol) possessing a thiol group at the ω-end and a reactive acetal group (ligand installation moiety) at the α-end (Otsuka, Akiyama, Nagasaki, & Kataoka, 2001). Ligand-installed, PEGylated AuNPs have been found to exhibit excellent stability under physiological conditions, minimal interaction with biomacromolecules, and specific molecular recognition due to the steric stabilization of tethered PEG chains surrounding the AuNPs through the thiol interactions. Furthermore, the thiol–Au interaction often causes an exchange reaction between R-SH/Au and thiol-containing compounds such as dithiothreitol (DTT) and glutathione, leading to the efficient dissociation of R-SH from the gold surface (Verma, Simard, Worrall, & Rotello, 2004). The concentrations of glutathione, which is an abundant thiol-containing compound in most cells, are in a millimolar range (1–10 mM) in cytoplasm, whereas those in the blood are in the micromolar range (2 μM) (Meister, & Anderson, 1983), indicating that R-SH/AuNPs might be stable in the blood stream but show the glutathione-mediated release of R-SH in the cytoplasm.

More recently, there has emerged a new class of promising approaches to the PEGylated AuNPs based on the self-assembly of poly(ethylene glycol)-*block*-poly(2-(*N*,*N*-dimethylamino)ethyl methacrylate) copolymer (PEG-PDMAMA) possessing a reactive acetal group (ligand installation moiety) at the α-end. The PEGylated GNPs formed from PEG-PDMAMA block copolymer showed excellent stability under physiological conditions even in the presence of high concentrations of thiol compounds, due to the multivalent coordination between the gold surface and the tertiary amino groups of the PDMAMA segment (Ishii, Otsuka, Kataoka, & Nagasaki, 2004). In this section, we describe the enhancement of RNAi activity in cultured hepatoma cells by glutathione-sensitive PEGylated AuNPs composed of PEG-PDMAMA block copolymer and siRNA bearing a thiol group at 5′-end of the sense chain (SH-siRNA). Note that the smart PEGylated AuNPs composed of PEG-PDMAMA and SH-siRNA facilitate the specific glutathione-mediated release of siRNA in the cytoplasm (Scheme 2.10) (Oishi, Nakaogami, Ishii, & Nagasaki, 2006).

Our strategy of constructing glutathione-sensitive PEGylated AuNPs is based on the complexation between PEG-PDMAMA (PEG: M_n = 5000, PDMAMA: M_n = 7500, DP_{PDMAMA} = 48, M_w/M_n = 1.6) and commercially available AuNPa with a size of 15 nm, followed by the immobilization of SH-siRNA. To estimate the average number of siRNA molecules per PEGylated AuNP, various concentrations of SH-dsDNA were added to the PEGylated AuNPs. The average number of SH-dsDNA molecules per PEGylated AuNP was estimated as almost 45 molecules per PEGylated GNP (0.06 molecules/nm^2). It should be noted that the use of the SH-dsDNA enabled a far more effective immobilization of dsDNA onto the

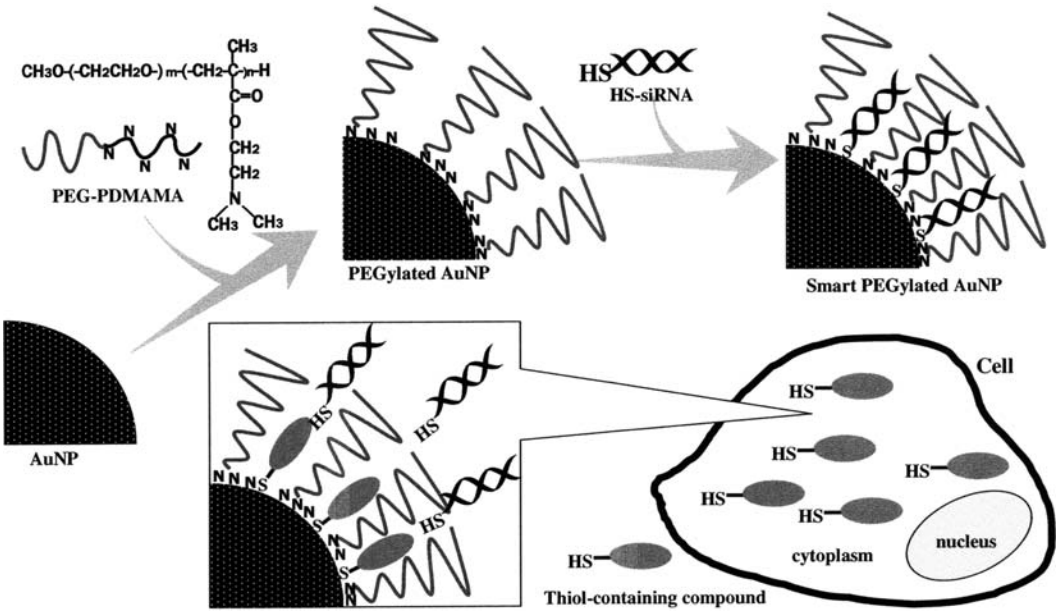

Scheme 2.10 Schematic illustration of gluthatione-sensitive PEGylated AuNPs as a siRNA carrier.

PEGylated AuNPs than the dsDNA without the thiol group (ca. 23 molecules per PEGylated AuNP). It is most likely that the immobilization of dsDNA molecules onto PEGylated AuNPs occurs mainly through an electrostatic interaction between the negatively charged dsDNA and the cationic surface of the AuNPs, leading to the lying orientation of dsDNA on the surface of the AuNPs. On the contrary, the SH-dsDNA molecules were immobilized onto the PEGylated AuNPs predominantly through the thiol–Au interaction, leading to the mainly standing and partially lying orientations of the SH-dsDNA on the surface of the AuNPs. To confirm the glutathione sensitivity of the PEGylated AuNPs containing SH-dsDNA, the PEGylated AuNPs solution was incubated under physiological environment or in a cytoplasmic environment for 20 h at 37°C. As can be seen in Figure 2.20, only a 25% release of the SH-dsDNA was observed under physiological environment. Furthermore, a slight increase in the amount of released SH-dsDNA (10%) was observed even under physiological environment in the presence of an excess amount of the polyanions, suggesting that the SH-dsDNA molecules were obviously immobilized through the thiol–Au interaction. On the other hand, a 60% release of the SH-dsDNA was observed in the cytoplasmic environment, where an abundance of glutathione and polyanions (RNA and anionic carbohydrates) exists, indicating that the effective release of the SH-dsDNA from the PEGylated glutathione is due to two exchange reactions, one with DTT and other with the counter polyanion.

To evaluate the RNAi activity (gene inhibition effect) of the smart PEGylated AuNPs containing SH-siRNA, we carried out a dual luciferase reporter assay in HuH-7 cells (human hepatoma cells) in the presence of 10% fetal bovine serum, as shown in Figure 2.21. Almost no RNAi activity was observed for the free siRNA even at a siRNA concentration of 100 nM. The lack of RNAi activity for the free siRNA may be ascribed to the low tolerance against enzymatic attack. Both the PEGylated AuNPs

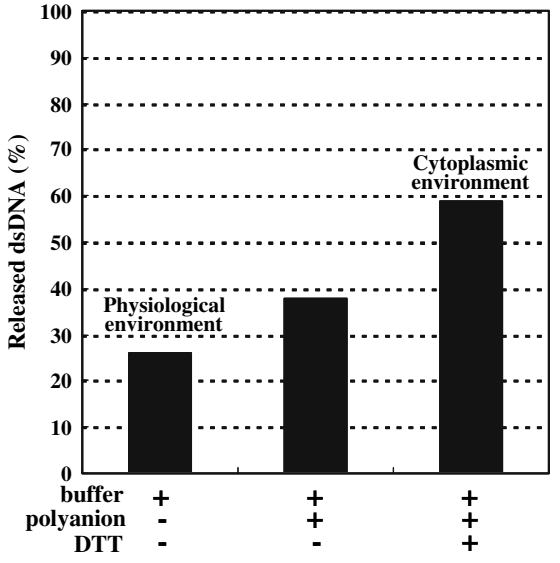

Figure 2.20 Release of the SH-dsDNA from the PEGylated AuNPs. Samples in 10 mM Tris–HCl buffer, pH 7.4, with 0.15 M NaCl (physiological environment), in buffer with an excess amount of polyanions (sodium dextran sulfate), and in buffer with an excess amount of polyanions and DTT (10 mM) were incubated at 37°C for 20 h.

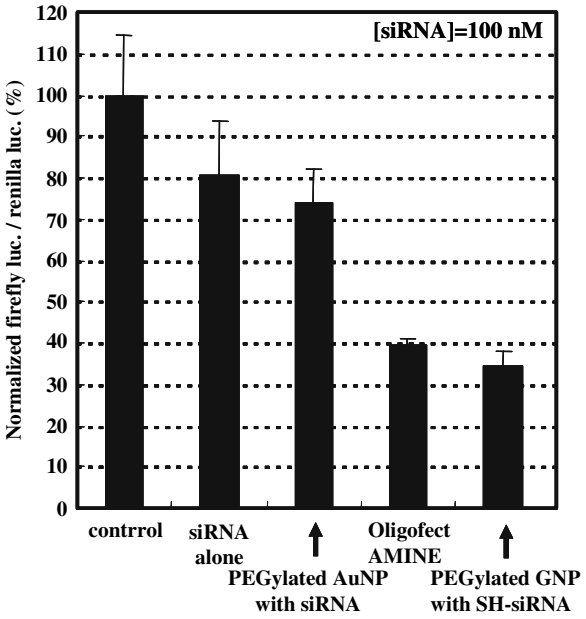

Figure 2.21 RNAi activity against the firefly luciferase gene expression in cultured HuH-7 cells. The normalized ratios between the firefly luciferase activity (firefly luc.) and the renilla luciferase activity (renilla luc.) are shown along the vertical axis of the figure. The indicated siRNA concentrations are as the feed concentrations of siRNA (not immobilized siRNA concentration). Data are the mean ± SD ($n = 3$).

containing siRNA (without the thiol group) and the SH-siRNA revealed RNAi activity and, in particular, the PEGylated AuNPs containing SH-siRNA achieved a far more effective RNAi activity (65% inhibition) than the PEGylated GNPs containing siRNA (25% inhibition). Thus, the PEGylated AuNPs containing SH-siRNA engage in the thiol–Au interaction, which exchanges SH-siRNA with glutathione in the cytoplasm; in other words, the efficient release of siRNA from the PEGylated AuNPs occurred synchronously with the increase in the glutathione concentrations, leading to the enhancement of RNAi activity. On the other hand, the PEGylated AuNPs containing siRNA, engaging only in electrostatic interaction, which is a weak form of interaction under extremely diluted conditions, led to the dissociation of the siRNA in the medium. Note that the RNAi activity of PEGylated AuNPs containing SH-siRNA is remarkably similar to that of OligofectAMINE (cationic liposome) (60% inhibition). Cytotoxicity and the inhibition of the renilla luciferase expression were not observed at all, suggesting that the inhibition of firefly luciferase expression observed here indeed occurred through a sequence-specific RNAi effect.

Conclusions

We described here a novel approach to both the precise synthesis of the end-functionalized block copolymer based on the heterotelechelic PEGs and their application to drug gene delivery systems. In particular, use of potassium 3,3-diethoxy-1-propananolate as an initiator of the polymerization of ethylene oxide not only produced various heterotelechelic PEGs but also end-functionalized PEG block copolymers such as acetal-PEG-PLA and acetal-PEG-PDMAMA with well-defined structure, high yield,

and high purity. In addition to the preparation of the end-functionalized PEG block copolymers, heterotelechelic PEGs were found to be useful for the conjugation of nucleic acid medicines so that both the lactosylated PEG-asDNA block copolymer and the lactosylated PEG-siRNA block copolymer could be obtained. The end-functionalized block copolymers, thus prepared, formed functionalized polymeric micelles and PEGylated AuNPs that exhibited cellular-specific uptake, that tolerated enzymatic degradation, and that interacted minimally with serum components owing to the steric stabilization of the highly dense end-functionalized PEG corona surrounding the micelle core and AuNP. Therefore, the synthesis of block polymers using the bifunctional PEGs offers researchers in the field a promising approach to targetable drugs, proteins, and gene delivery systems.

References

Allen, C., Yu, Y., Maysinger, D., & Eisenberg, A. (1998). Polycaprolactone-*b*-poly(ethylene Oxide) block copolymer micelles as a novel drug delivery vehicle for neurotrophic agents FK506 and L-685,818. *Bioconjug Chem*, *9*, 564–572.

Bei, J. Z., Li, J. M., Wang, Z. F., Le, J. C., & Wang, S. G. (1997). Polycaprolactone-poly(ethylene-glycol) block copolymer. IV: Biodegradation behavior *in vitro* and *in vivo*. *Polym Adv Technol*, *8*, 693–696.

Bettinger, T., Remy, J. S., Erbacher, P., & Behr, J. P. (1998). Convenient polymer-supported synthetic route to heterobifunctional polyethylene glycols *Bioconjug Chem*, *9*, 842–846.

Boussif, O., Lezoualc, F., Zanta, M. A., Mergny, M. D., Scherman, D., Demeneix, B., & Behr, J. P. (1995). A versatile vector for gene and oligonucleotide transfer into cells in culture and in vivo: polyethylenimine. *Proc Natl Acad Sci USA 92*, 7297–7301.

Braasch, D., Paroo, Z., Constantiescu, A., Ren, G., Öz, O. K., Mason, R. P., & Corey, D. R. (2004). Biodistribution of phosphodiester and phosphorothioate siRNA. *Bioorg Med Chem Lett, 14*, 1139–1143.

Cammas, S., Nagasaki, Y., & Kataoka, K. (1995). Heterobifunctional poly(ethylene oxide): synthesis of alpha-methoxy-omega-amino and alpha-hydroxy-omega-amino PEOs with the same molecular weights. *Bioconjug Chem*, *6*, 226–230.

Cherng, J. Y., Wetering, P. van de., Talsma, H., Crommelin, D. J. A., & Hennink, W. E. (1996). Effect of size and serum proteins on transfection efficiency of poly ((2-dimethylamino)ethyl methacrylate)-plasmid nanoparticles. *Pharm Res*, *13*, 1038–1042.

Clague, M. J. (1998). Molecular aspects of the endocytic pathway. *Biochem J, 336*, 271–282.

Elbashir, S. M., Harborth, J., Lendeckel, W., Yalcin, A., Weber, K., & Tuschl, T. (2001). Duplexes of 21-nucleotide RNAs mediate RNA interference in cultured mammalian cells. *Nature 411*, 494–498.

Fukushima, S., Miyata, K., Nishiyama, N., Kanayama, N., Yamasaki, Y., & Kataoka, K. (2005) PEGylated polyplex micelles from triblock catiomers with spatially ordered layering of condensed pDNA and buffering units for enhanced intracellular gene delivery. *J Am Chem Soc*, *127*, 2810–2811.

Goh, S. L., Murthy, N., Xu, M., & Fréchet, J. M. J. (2004), Cross-linked microparticles as carriers for the delivery of plasmid DNA for vaccine development**.** *Bioconjug Chem, 15*, 467–474.

Greene, T. W. (1991). *Protecting groups in organic synthesis*. Wiley-Interscience.
Gruenberg, J. (2001). The endocytic pathway: A mosaic of domains. *Nat Rev Mol Cell Biol, 2*, 721–730.
Harada, A., Togawa, H., & Kataoka, K. (2001). Physicochemical properties and nuclease resistance of antisense-oligodeoxynucleotides entrapped in the core of polyion complex micelles composed of poly(ethylene glycol)–poly(-Lysine) block copolymers. *Eur J Pharm Sci*, *13*, 35–42.
Harada-Shiba, M., Yamauchi, K., Harada, A., Takamisawa, I., Shimokado, K., & Kataoka, K. (2002). Polyion complex micelles as vectors in gene therapy pharmacokinetics and *in vivo* gene transfer. *Gene Ther*, *9*, 407–414.
Hashida, M., Takemura, S., Nishikawa, M., & Takakura, Y. (1998). Targeted delivery of plasmid DNA complexed with galactosylated poly(L-lysine) *J Control Release, 53*, 301–310.
Hedfors, C., Ostmark, E., Malmstrom, E., Hult, K., & Martinelle, M. (2005). Thiol end-functionalization of poly(ε-caprolactone), catalyzed by *Candida antarctica* lipase B *Macromoloecules*, *38,* 647–649.
Iijima, M., Nagasaki, Y., Okada, T., Kato, M., & Kataoka, K. (1999). Core-polymerized reactive micelles from heterotelechelic amphiphilic block copolymers *Macromolecules, 32*, 1140–1146.
Inoue, S., & Aida, T. (1989). Anionic ring opening polymerization: copolymerization. In S. G. Allen & J. C. Bevington (Eds.), *Comprehensive polymer science: The synthesis, characterization, reactions and applications of polymers* (pp. 553–570). New York: Pergamon Press.
Ishii, T., Otsuka, H., Kataoka, K., & Nagasaki, Y. (2004). Preparation of functionally PEGylated gold nanoparticles with narrow distribution through autoreduction of auric cation by α-biotinyl-PEG-*block*-[poly(2-(*N,N*-dimethylamino)ethyl methacrylate)]. *Langmuir*, *20*, 561–564.
Kaiser, K., Marek, M., Haselgrubler, T., Schindler, H., & Gruber H. J. (1997). Basic studies on heterobifunctional biotin-PEG conjugates with a 3-(4-pyridyldithio)-propionyl marker on the second terminus**.** *Bioconjug Chem*, *8*, 545–551.
Kataoka, K., Harada, A., Wakebayashi, D., & Nagasaki, Y. (1999). Polyion complex micelles with reactive aldehyde groups on their surface from plasmid DNA and end-functionalized charged block copolymer. *Macromolecules, 32*, 6892–6894.
Kataoka, K., Togawa, H., Harada, A., Yasugi, K., Matsumoto, T., & Katayose, S. (1996). Spontaneous formation of polyion complex micelles with narrow distribution from antisense oligonucleotide and cationic block copolymer in physiological saline *Macromolecules*, *29*, 8556–8557.
Katayose, S., & Kataoka, K. (1997). Water-soluble polyion complex associates of DNA and poly(ethylene glycol)-poly(L-lysine) block copolymer. *Bioconjug Chem*, *8*, 702–707.
Kim, Y. J., Nagasaki, Y., Kataoka, K., Kato, M., Yokoyama, M., Okano, T., & Sakurai, Y. (1994). Heterobifunctional poly(ethylene oxide). *Polym Bull*, *33*, 1–6.
Kimura, Y. (1993). Biocompatible polymer. In T. Tsuruta, T. Hayashi, K. Katoka, K. Ishihara, & Y. Kimura (Eds.), *Biomedical applications of polymeric materials* (pp. 164–189). Boca Raton, FL: CRC Press.
Kitano, H., Shoda, K., & Kosaka, A. (1995). Galactose-containing amphiphiles prepared with a lipophilic radical initiator. *Bioconjug Chem*, *6*, 131–134.
Lloyd, J. B. (2000). Lysosome membrane permeability: implications for drug delivery. *Adv Drug Deliv Rev, 41*, 189–200.
Maeda, H., Sawa, T., & Konno, T. (2001). Mechanism of tumor-targeted delivery of macromolecular drugs, including the EPR effect in solid tumor and clinical overview of the prototype polymeric drug SMANCS. *J Control Release*, *74*, 47–61.

Matsumura, Y., & Maeda, H. (1986). A new concept for macromolecular therapeutics in cancer chemotherapy:mechanism of tumoritropic accumulation of proteins and the antitumor agent Smancs. *Cancer Res*, *46*, 6387–6392.

Meister, A., & Anderson, M. E. (1983). Glutathione. *Annu Rev Biochem*, *52*, 711–760.

Mukherjee, S., Ghosh, R. N., & Maxfield, F. R. (1997). Endocytosis. *Physiol Rev, 77*, 759–803.

Nagasaki, Y., Honzawa, E., Kato, M., & Kataoka, K. (1994). Novel stimuli-sensitive telechelic oligomers. pH and temperature sensitivities of poly(silamine) oligomers. *Macromolecules*, *27*, 4848–4850.

Nagasaki, Y., Kutsuna, T., Iijima, M., Kato, M., & Kataoka, K. (1995a). Primary amino-terminal heterobifunctional poly(ethylene oxide). Facile synthesis of poly(ethylene oxide) with a primary amino group at one end and a hydroxyl group at the other end. *Bioconjug Chem*, *6*, 702–704.

Nagasaki, Y., Kutsuna, T., Iijima, M., Kato, M., Kataoka, K., Kitano, S., & Kadoma. Y. (1995b). Formyl-ended heterobifunctional poly(ethylene oxide): synthesis of poly(ethylene oxide) with a formyl group at one end and a hydroxyl group at the other end. *Bioconjug Chem*, *6*, 231–233.

Nagasaki, Y., Okada, T, Scholz, C., Iijima, M., Kato, M., & Kataoka, K. (1998). The reactive polymeric micelle based on an aldehyde-ended poly(ethylene glycol)/poly(lactide) block copolymer. *Macromolecules, 31*, 1473–1479.

Nagasaki, Y., Sato, Y., & Kato, M. (1997). A novel synthesis of semitelechelic functional poly(methacrylate)s through an alcoholate initiated polymerization. Synthesis of poly[2-(*N*,*N*-diethylaminoethyl) methacrylate] macromonomer**.** *Macromol Rapid Commun*, *18*, 827–835.

Oishi, M., Hayama, T., Akiyama, Y., Harada, A., Yamasaki, Y., Nagatsugi, F., Sasaki, S., Nagasaki, Y., & Kataoka, K. (2005). Supramolecular assemblies for the cytoplasmic delivery of antisense oligodeoxynucleotide: polyion complex (PIC) micelles based on poly(ethylene glycol)-SS-oligodeoxynucleotide conjugate. *Biomacromolecules*, *6*, 2449–2454.

Oishi, M., Ikeo, S., & Nagasaki, Y. (2007). Lipase-Catalyzed Selective Synthesis and Micellization of Poly(ethylene glycol)-*block*-Poly(ε-caprolactone) Copolymer Possessing a Carboxylic Acid Group at the PEG Chain End. *Polym J, 39*, 239–244.

Oishi, M., Kataoka, K., & Nagasaki, Y. (2006). pH-Responsive Three-layered PEGylated polyplex micelle based on a lactosylated ABC triblock copolymer as a targetable and endosome-disruptive nonviral gene vector. *Bioconjug Chem*, *17*, 677–688.

Oishi, M., Nagasaki, Y., & Kataoka, K. (2005). Functional PEG for drug delivery. In G, S. Kwon (Ed.), *Polymeric Drug Delivery Systems* (pp. 93–127). New York: Taylor & Francis.

Oishi, M., Nagastugi, F., Sasaki, S., Nagasaki, Y., & Kataoka, K. (2005). Smart polyion complex micelles for targeted intracellular delivery of PEGylated antisense oligonucleotides containing acid-labile linkages. *Chem Bio Chem*, *6*, 718–725.

Oishi, M., Nagasaki, Y., Itaka, K., Nishiyama, N., & Kataoka, K. (2005). Lactosylated poly(ethylene glycol)-siRNA conjugate through acid-labile β-thiopropionate linkage to construct pH-sensitive polyion complex micelles achieving enhanced gene silencing in hepatoma cells. *J Am Chem Soc*, *127*, 1624–1625.

Oishi, M., Nakaogami, J., Ishii, T., & Nagasaki, Y. (2006). Smart PEGylated gold nanoparticles for the cytoplasmic delivery of siRNA to induce enhanced gene silencing. *Chem Lett*, *35*, 1046–1047.

Oishi, M., Sasaki, S., Nagasaki, Y., & Kataoka, K. (2003). pH-Responsive oligodeoxynucleotide (ODN)-poly(ethylene glycol) conjugate through acid-labile

β-thiopropionate linkage: preparation and polyion complex micelle formation. *Biomacromolecules*, *4*, 1426–1432.

Otsuka, H., Akiyama, Y., Nagasaki, Y., & Kataoka, K. (2001). Quantitative and reversible lectin-induced association of gold nanoparticles modified with α-lactosyl-ω-mercapto-poly(ethylene glycol) . *J Am Chem Soc*, *123*, 8226–8230.

Otsuka, H., Nagasaki, Y., & Kataoka, K. (2003). PEGylated nanoparticles for biological and pharmaceutical applications. *Adv Drug Deliv Rev*, *55*, 403–419.

Scholz, C., Iijima, M., Nagasaki, Y., & Kataoka, K. (1995). A novel reactive polymeric micelle with aldehyde groups on its surface. *Macromolecules*, *28*, 7295–7297.

Schwartz, A. L., Fridovich, S. E., Knowles, B. B., & Lodish, H. F. (1981). Characterization of the asialoglycoprotein receptor in a continuous hepatoma line. *J Bio Chem*, *256*, 8878–8881.

Stockert, R. J. (1995). The asialoglycoprotein receptor: Relationships between structure, function, and expression. *Physiol Rev, 75*, 591–609.

Tsukioka, Y., Matsumura, Y., Hamaguchi, T., Koike, H., Moriyasu, F., & Kakizone, T. (2002). Pharmaceutical and biomedical differences between miceller doxorubicin (NK911) and liposomal doxorubicin (Doxil). *Japan J Cancer Res*, *93*, 1145–1153.

Uhlman, E., & Peyman, A. (1990). Antisense oligonucleotides: a new therapeutic principle *Chem Rev*, *90*, 543–584.

Verma, A., Simard, J. M., Worrall, J. W., & Rotello, V. M. (2004). Tunable reactivation of nanoparticle-inhibited β-galactosidase by glutathione at intracellular concentrations**.** *J Am Chem Soc*, *126*, 13987–13991.

Wakebayashi, D., Nishiyama, N., Yamasaki, Y., Itaka, K., Kanayama, N., Harada, A., Nagasaki, Y., & Kataoka, K. (2004). Lactose-conjugated polyion complex micelles incorporating plasmid DNA as a targetable gene vector system: their preparation and gene transfecting efficiency against cultured HepG2 cells. *J Control Release, 95*, 653–664.

Yokoyama, M., Okano, T., Sakurai, Y., Kikuchi, A., Ohsako, N., Nagasaki, Y., & Kataoka. K. (1992). Synthesis of poly(ethylene oxide) with heterobifunctional reactive groups at its terminals by an anionic initiator. *Bioconjug Chem*, *3*, 275–276.

Zalipsky, S. (1995). Functionalized poly(ethylene glycols) for preparation of biologically relevant conjugates. *Bioconjug Chem, 6*, 150–165.

3

Supercritical Fluid Technology for Nanotechnology in Drug Delivery

Mohammed J. Meziani, Pankaj Pathak, and Ya-Ping Sun

Introduction

In the past few decades, supercritical fluid technology has attracted the attention of both scientists and engineers (McHugh and Krukonis, 1994; Taylor, 1996; Brennecke, 1993; Hutchenson and Foster, 1995; Levelt Sengers, 1991; Kendall et al., 1999). Early studies on the application of supercritical fluid technology were primarily in extraction and chromatography. Extensive experimental and theoretical investigations have been aimed toward an understanding of the properties of supercritical fluid systems, particularly intermolecular interactions (solute–solvent, solvent–solvent, and solute–solute) in supercritical fluid solutions (Tucker, 1999; Jessop and Leitner, 1999; Sun, 2002). Much progress has also been made in the use of supercritical fluids and mixtures as reaction media for chemical synthesis and as alternative solvent systems for materials processing (Sun, 2002; Poliakoff et al., 1996; Kajimoto, 1999; Savage, 1999; Musie et al., 2001). Recently, several supercritical fluid processing techniques have found significant applications in the nanotechnology development for drug formulation and delivery, especially the production of nanosized drugs and pharmaceuticals. In fact, drug formulation and delivery-related applications have emerged as a new frontier in the development of supercritical fluid technology.

In this chapter, we provide background information on the supercritical fluid processing techniques relevant to drug formulation and delivery, highlight the recent advances and novel applications, and discuss the successful development of a new supercritical fluid rapid expansion technique for producing exclusively nanoscale drug particles.

Supercritical Fluid Processing Techniques

A supercritical fluid is defined as a solvent at temperature and pressure above the critical temperature and pressure, respectively, where the fluid remains a single phase. Among the most important properties of a supercritical fluid are the low and tunable densities, which can be easily varied

M.M. de Villiers et al. (eds.), *Nanotechnology in Drug Delivery*, DOI: 10.1007/978-0-387-77667-5_3,

from gas-like to liquid-like via a simple change in pressure at constant temperature or vice versa, and the unusual solvation effects at densities near the critical density. Generally, solute–solvent interactions in supercritical fluids are understood in terms of a three-density region solvation model (Sun and Bunker, 1995). In the low-density gas-like region, the solvation increases almost linearly with density at constant temperature. This behavior is probably dictated by short-range interactions in the inner solvation shell. Before the inner shell is saturated, the microscopic consequence of increasing density is the addition of solvent molecules to the solvation shell, which causes large incremental effects. In the near-critical density region, the solvation is nearly independent of changes in density. A supercritical fluid in the near-critical region may be considered as being macroscopically homogeneous but microscopically inhomogeneous (a mixture of solvent molecules and "free volumes"). Thus, changes in the bulk density primarily correspond to decreases in the free volumes, with little effect on the solute molecules. A further increase in the fluid density to reach the point where the free volumes are largely gone affects the microscopic solvation environment of the solute molecules in a way similar to that in a liquid solution (Sun and Bunker, 1995).

Commonly used supercritical solvents include CO_2, ethylene, ethane, fluoroform, and ammonia, although the flammability and toxicity of some of these may limit their uses for specific applications in pharmaceutical processing. Supercritical CO_2 is obviously a favored choice for its near-ambient critical temperature ($\sim 31^{\circ}C$) and relatively low critical pressure (73.8 bar), and for its nontoxic, nonflammable, abundant, and inexpensive characteristics. Since CO_2 is nonpolar, a polar modifier such as a cosolvent or a surfactant may be added to improve the solubility of some solute molecules (Sauceau et al., 2004; Ting et al., 1993).

Supercritical fluid technology has shown great promise in addressing many of the challenges facing the pharmaceutical industry in drug delivery systems, including particle generation and processing techniques; and issues such as controllable particle size and shape, clean, environmentally responsible, and scalable (Rogers et al., 2001; York, 1999; Kompella and Koushik, 2001; Subramaniam et al., 1997a; Jung and Perrut, 2001; Stanton et al., 2002; Fages et al., 2004; Young et al., 2000; Tan and Borsadia, 2001; Del Valle and Galan, 2005; York, 2004; Date and Patravale, 2004; Hu et al., 2004). Several supercritical fluid methods have been successfully developed, leading to the production of micron-sized particles of different shape, size, and morphology (McHugh and Krukonis, 1994; Taylor, 1996; Brennecke, 1993; Hutchenson and Foster, 1995; Levelt Sengers, 1991; Eckert et al., 1996; Johnston and Penninger, 1989; Squires and Paulaitis, 1987; Bright and McNally, 1992; Von Rohr and Treep, 1996). These particle design and formation processes offer many drug formulation options such as dry powders, nanoparticle suspensions, microspheres or microcapsules as drug carriers, and drug-impregnated excipients (Rogers et al., 2001; York, 1999; Kompella and Koushik, 2001; Subramaniam et al., 1997a; Jung and Perrut, 2001; Stanton et al., 2002; Fages et al., 2004; Young et al., 2000; Tan and Borsadia, 2001; Del Valle and Galan, 2005; York, 2004; Date and Patravale, 2004; Hu et al., 2004). Among widely investigated and most relevant techniques are SAS (*s*upercritical

*a*nti-*s*olvent), RESS (*r*apid *e*xpansion of *s*upercritical *s*olutions), and more recently the RESOLV (*r*apid *e*xpansion of a supercritical solution into a liquid *solv*ent) (Sauceau et al., 2004; Ting et al., 1993; Rogers et al., 2001; York, 1999; Kompella and Koushik, 2001; Subramaniam et al., 1997a; Jung and Perrut, 2001; Stanton et al., 2002; Fages et al., 2004; Young et al., 2000).

Supercritical Anti-solvent (SAS) Process

SAS generally refers to the precipitation for particle formation in a compressed fluid at supercritical as well as subcritical conditions. The process is also called PCA (*p*recipitation with *c*ompressed *a*nti-solvent) or GAS (*g*as *a*nti-*s*olvent) in some literature. As with any precipitation process, the anti-solvent can be added to the solution (normal-addition precipitation) or the solution can be added to the anti-solvent (reverse-addition precipitation). The SAS method requires that the supercritical anti-solvent be miscible with the solution solvent and that the solute be insoluble in the supercritical anti-solvent. In the normal-addition SAS, a solute is dissolved in a liquid solvent, and then a supercritical anti-solvent is added to the solution in a partially filled closed container that is initially at ambient pressure. With the addition of the supercritical anti-solvent, both the volume of the solution/anti-solvent mixture and the pressure of the closed container increase. The decrease in solubility of the solute with increasing anti-solvent fraction in the mixture results in the precipitation of the solute. The precipitate is then washed with the anti-solvent to yield the desired particles. The size and size distribution of the particles depend on the selection of the solution/anti-solvent system, the solution concentration, the relative solution and anti-solvent quantities, the rate of the anti-solvent addition, and the degree of mixing (Reverchon, 1999). In the reverse-addition SAS, a liquid solution is sprayed through a nozzle into a supercritical anti-solvent. The rapid diffusion of the solvent from the solution droplets sprayed into the bulk supercritical fluid results in the precipitation of the solute. The precipitate is then washed with the anti-solvent and filtered to obtain the desired particles.

Supercritical anti-solvent methods have been used for preparing a variety of micron and submicron particles and fine powders from inorganics, polymers, pigments, proteins, pharmaceuticals, and even explosives (Reverchon, 1999; Debenedetti et al., 1993a; Reverchon and De Marco, 2004; Wang et al., 2005; Winters et al., 1996; Del Valle and Galan, 2005; Jovanovic et al., 2004; Chattopadhyay and Gupta, 2002). For example, fine particles of trypsin, lysozyme, and insulin proteins with diameters ranging from 1 to 5 μm were produced by a continuous flow supercritical anti-solvent process (Winters et al., 1996). In the preparation, a solution of the protein in DMSO was sprayed through a small orifice into concurrently flowing supercritical CO_2. The particle sizes could be varied via changing processing conditions; for example, larger particles were obtained by decreasing the pressure or increasing the temperature of the supercritical anti-solvent or by using a larger-diameter expansion nozzle. The biological activity of the micron-sized powders compared to the starting materials was hardly affected by the processing.

Supercritical anti-solvent processing has also been used in the preparation of pharmaceutically important compounds, including salmetrol xinafoate (York and Hanna, 1996), sulfathiazole (Kitamura et al., 1997), methylprednisolone (Schmitt et al., 1995), and hydrocortisone acetate (Schmitt et al., 1995). In a modification to the typical supercritical anti-solvent process, step-wise addition of supercritical anti-solvent to ethanol solutions of sulfathiazole was used to control the nucleation and control processes (Kitamura et al., 1997). Sulfathiazole crystals with sizes ranging from tens to hundreds of microns, up to 2–6 mm, can be prepared by varying the timing and amount of supercritical anti-solvent added. The particle size was also found to be dependent on the operating pressure: smaller particles were formed due to the increase in the pressure of the initially added anti-solvent. The formation of smaller particles was attributed to faster nucleation during the process. In another modification to the SAS process, compressed gas was used as an anti-solvent to precipitate and prepare particles of several commercial pigments (Gao et al., 1998). Particles of $\sim$1 μm were obtained by using acetone as a solvent and compressed CO_2 as anti-solvent. Addition of anti-solvent as a compressed gas or a supercritical fluid did not significantly change the particle properties. However, a decrease in the pressure or an increase in the temperature of the anti-solvent (compressed gas) or an increase in the nozzle size resulted in the formation of larger particles. Antibiotic tetracycline was also successfully processed by SAS by using *N*-methyl-2-pyrrolidone (NMP) as the solvent. The mean particle size of precipitated particles was $\sim$150 nm (Reverchon and Della Porta, 1999).

Chattopadhyay et al. developed a batch supercritical anti-solvent micronization process enhanced by the addition of a vibrating surface in the precipitation vessel, named supercritical anti-solvent with enhanced mass transfer (SAS-EM) (Chattopadhyay and Gupta, 2001a,b). They produced griseofulvin (antifungal, antibiotic) particles as small as 130 nm and lysozyme (enzyme) particles of about 190 nm. Nanometric lysozyme particles with a minimum mean diameter of 180 nm were also produced by Muhrer et al. using the GAS process (Muhrer and Mazzotti, 2003). Snavely et al. produced insulin (antidiabetic) nanoparticles by SAS with the aid of an ultrasonic nozzle (Snavely et al., 2002).

Mechanistically, the particles are formed from the solution droplets, which collide into the fluid phase. Either the addition of anti-solvent into solution or vice versa, the knowledge on the phase diagram is crucial to the understanding of the mass transfer and nucleation phenomena in SAS. The precipitation of the solute occurs either by the dissolution of the anti-solvent into the solution, leading to swelling of solution droplets, or by evaporation of the solvent into anti-solvent, causing shrinkage of the droplets (Fages et al., 2004). Shekunov et al. studied ethanol–CO_2 SAS system using optical methods (image analysis, laser interferometry, and particle-image velocimetry) to determine if the anti-solvent swells or shrinks during precipitation. According to their results, nucleation occurred within the shrinking ethanol-rich droplets, and no swelling was observed under any operating conditions (Shekunov et al., 2000). Rantakylä et al. studied the influence of several parameters on the size of poly-lactic acid particles formed in SAS process (Rantakylä et al., 2002).

The mean particle size was found to depend slightly on the temperature and pressure, but independent of nozzle exit velocity and nozzle diameter. The initial droplet sizes formed at the nozzle had no effect on the particle size (Rantakylä et al., 2002). Another study with the toluene–CO_2 system (without a third component to be crystallized) showed the dependence of droplet fate on the respective densities of the solvent and anti-solvent (Werling and Debenedetti, 2000). To optimize particle production from the droplets, it is generally advantageous to work in the single-phase zone at high pressures, where higher mass transfer and higher supersaturation ratios are achieved.

A major disadvantage of the SAS method is that particle formation is followed by a lengthy drying period, which often leads to particle agglomeration and aggregation (Dixon et al., 1993; Falk et al., 1997; Debenedetti, 1994; Vemavarapu et al., 2005). However, the problem may be minimized by intensive mixing of the solution with the supercritical anti-solvent, which leads to more efficient mass transfer and smaller droplet size. One way to achieve the intensive mixing in a slightly modified SAS is the use of an ultrasonic nozzle, a process in which the increased mass transfer rate due to sonic waves in an energizing gas stream leads to the formation of discrete submicron drug particles (Subramaniam et al., 1997a,b). With sound waves rather than inertial and frictional forces for droplet formation, large-diameter nozzles (instead of capillary or micro-orifice nozzles) could be used in the process for fine particle production (Subramaniam et al., 1997b). Another conceptually similar modification to the traditional SAS, the solution-enhanced dispersion by supercritical fluids (SEDS) technique (York, 1999; Hanna and York, 1998; Sloan et al., 1998), uses the supercritical fluid as both an anti-solvent and a "spray enhancer", where a nozzle with two coaxial passages allows the simultaneous introduction of the drug solution and supercritical anti-solvent into the particle formation vessel with controlled temperature and pressure. This modified SAS process has been used to formulate a variety of drug particles, including nicotinic acid, paracetamol, salmeterol xinafoate, fluticasone propionate, and water-soluble proteins (York, 1999). The process has also allowed manipulation of particle size, shape, and morphology by changing the process working conditions. For example, polymorphs of salmeterol xinafoate and fluticasone propionate were obtained from the SEDS by processing in different regions of the supercritical phase with the same organic solvent (Hanna and York, 1998). The same process was also applied to prepare microfine particles of lysozyme from an aqueous solution of the protein (Sloan et al., 1998).

In addition to SEDS, other variations of SAS including precipitation with compressed anti-solvent (PCA) and aerosol supercritical extraction system (ASES) have been developed (Rogers et al., 2001; York, 1999; Kompella and Koushik, 2001; Subramaniam et al., 1997a; Jung and Perrut, 2001; Helfgen et al., 2000; Rogers et al., 2003). For example, Johnston and coworkers used the PCA method to prepare polymer particles and fibers (Dixon et al., 1993; Mawson et al., 1997a,b; Dixon et al., 1994; Yates et al., 1999). Microparticles and fibers of polystyrene were formed by spraying a toluene solution into liquid CO_2 (Yates et al., 1999). Increasing CO_2 density and decreasing temperature resulted in the

formation of smaller particles ranging from 0.1 to 1 μm. An increase in the polymer concentration from 1 to 5 wt% resulted in formation of fibers with diameters of 20–60 μm under certain conditions.

The other variation of the SAS technique, ASES process, involves spraying fine solution droplets through an atomization nozzle into compressed CO_2. The dissolution of the supercritical fluid into the liquid droplets is accompanied by a large volume expansion and, consequently, the supersaturation and formation of small uniform particles (Dehghani and Foster, 2003; Tu et al., 2002). Foster et al. used the ASES technique to micronize and microencapsulate parahydroxybenzoic acid (*p*-HBA) and lysozyme with poly(L-lactic acid) (L-PLA) from various organic solutions (Tu et al., 2002). In these studies, the effects of various parameters, such as pressure, temperature, solution concentration, solvent system, and spraying velocity on the nature of the particles were determined. Effective size reduction of the particles was achieved at low-to-moderate temperatures in an essentially one-step process. In general, it was found that the high-molecular-weight compounds, L-PLA and lysozyme, precipitated as microspheres and nanospheres, whereas the lighter-weight compound, *p*-HBA, precipitated as crystalline particles resembling platelets (averaging 3 μm in length). The maximum encapsulation efficiencies obtained for *p*-HBA and lysozyme with L-PLA particles were 9.2 and 15.6%, respectively. The ASES technique has also been applied to the micronization of poorly water-soluble drugs to improve their dissolution rates, and for re-engineering of proteins, steroids, and antibiotics so that they can be administered via the respiratory tract or other routes (Reverchon, 1999; Foster et al., 2003; Reverchon, 2003; Reverchon and De Marco, 2006; Kikic and Sist, 2000). Proteins such as insulin, rhDNase, lysozyme, and albumin were precipitated by the ASES process from aqueous solutions with a uniform primary particle size of less than 500 nm (Bustami et al., 2000). The structure and biochemical integrity of the proteins could be retained, but these were dependent on the operating conditions and the modified anti-solvent used. There have also been many investigations on the feasibility of utilizing the ASES process for the processing of fragile and heat-labile molecules, such as proteins which are difficult to process by conventional techniques (Snavely et al., 2002; Foster et al., 2003; Bustami et al., 2003; Bustami et al., 2001).

SAS and related supercritical fluid processing methods are advantageous over a liquid solution-based technique for the ability to prepare dry powders in a single step (Gallagher et al., 1992). In addition, several new techniques have evolved in which the primary use of supercritical fluid is to assist the nebulization of the solution while also acting as an anti-solvent to precipitate the solute. In these techniques that closely resemble classic micronization by spray drying, the supercritical fluid and solution are intimately mixed and sprayed in a drying atmosphere. For example, carbon dioxide-assisted nebulization with a bubble dryer (CAN-BD) (Sellers et al., 2001; Sievers et al., 2003) and supercritical fluid-assisted atomization (SAA) (Reverchon and Della Porta, 2003a,b) have been used to prepare drug particles and process water-soluble proteins and vaccines. The preparation of dry powders at low temperature is particularly important for pharmaceuticals, protein samples, and other materials that are thermally

labile or shock sensitive. Because many compounds of interest have higher solubility in liquid solvents than in low-temperature supercritical fluids, the SAS method generally allows higher throughputs than the RESS method discussed below.

Rapid Expansion of Supercritical Solutions (RESS)

RESS process has been widely studied as an effective technique for particle formation (McHugh and Krukonis, 1994; Rogers et al., 2001; York, 1999; Kompella and Koushik, 2001; Subramaniam et al., 1997a; Jung and Perrut, 2001; Stanton et al., 2002; Fages et al., 2004; Krukonis, 1984; Lele and Shine, 1994; Matson et al., 1986a, 1987a,b; Teja and Eckert, 2000; Blasig et al., 2002; Yeo and Kiran, 2005; Mohamed et al., 1989b; Domingo et al., 1997; Petersen et al., 1986, 1987; Mawson et al., 1995; Weber and Thies, 2002; Ginosar et al., 2000; Rollins, 1999; Leuner and Dressman, 2000; Matson et al., 1986b, 1987c,d; Smith et al., 1986; Matson et al., 1989; Matson and Smith, 1989; Burukhin et al., 1998; Williams et al., 1998; Yeo et al., 1994; Lele and Shine, 1992; Mishima et al., 2000; Krober et al., 2000; Aniedobe and Thies, 1997). It differs from the SAS process in that in RESS the solute is dissolved in a supercritical fluid to form a solution, and then the solution is rapidly expanded through a small nozzle or orifice into a region of lower pressure or ambient air (Eckert et al., 1996; Teja and Eckert, 2000; Blasig et al., 2002; Yeo and Kiran, 2005; Mohamed et al., 1989b). The rapid reduction in pressure and thus density results in the precipitation of the solute. Experimentally, the supercritical solution can be generated either by heating and pressurizing a solution from room temperature or by continuously extracting the solute using an extraction column. The preparation of the solution at room temperature allows expansion to be performed at a known constant concentration, whereas the use of an extraction column is useful for solutes that are insoluble or sparingly soluble in the solvents. The temperature of the solvent can be the same as or different from the temperature at which the expansion is carried out. The extraction temperature and flow rate may be used to control the solute concentration. The expansion is driven by the drop in pressure, which can propagate at speeds up to the speed of sound in the expansion nozzle. Because solubilities in supercritical fluids can be up to 10^6 times higher than those under ideal gas conditions, the rapid expansion from supercritical pressure to ambient pressure leads to extreme supersaturation. The rapid decrease in pressure results in homogeneous nucleation of the solute, leading to narrow size distributions in the processed materials. This technique can be used for the preparation of particles and films of inorganic, organic, and polymeric materials. Fibers of polymeric materials can also be prepared under the appropriate expansion conditions. Thus, variations in expansion conditions allow modifications in the product morphology (Rollins, 1999).

The first report on RESS processing was published by Krukonis in 1984 (Krukonis, 1984). The preparation of small particles or fibers of aluminium isopropoxide, dodecanolactam, polypropylene, β-estradiol, ferrocen, navy blue dye, and soybean lecithin using RESS was reported (Mohamed et al., 1989b). CO_2 was used as a supercritical solvent for all

the samples except polypropylene, which was processed with propylene. Primary products for most of the samples were micron-size particles, with a few exceptions like dodecanolactam and polypropylene, for which needles ~30 μm long and 1 μm diameter and fiber-like particles were obtained. Smith and coworkers carried out a series of RESS experiments aimed at evaluating the effects of processing conditions on product morphology from particles to films, size, and distribution (Matson et al., 1986b, 1987c,d; Smith et al., 1986).

Besides inorganic particles and films, several polymers have also been processed into particles and fibers via RESS. For example Matson, Smith, Peterson et al. used supercritical pentane for the RESS processing of polystyrene, polypropylene, poly(carbosilane), and cellulose acetate (Matson et al., 1987a; Petersen et al., 1986, 1987; Matson et al., 1986b, 1987d; Mishima et al., 2000). In these investigations, pre-expansion temperatures significantly higher or lower than the melting point of the polymer led to the formation of particles, while pre-expansion temperatures close to the polymer melting point resulted in fiber morphology. Lele and Shine reported preparation of fibers and particles of polycaprolactone, poly(methyl methacrylate), and a styrene/methyl methacrylate block copolymer using chlorodifluoromethane (Lele and Shine, 1992, 1994). The group found that the formation of particles was favored over fibers at a low polymer concentration, low pre-expansion temperature, high pre-expansion pressure, and small length/diameter ratio for the nozzle. The results were explained on the basis of the location of phase separation in the nozzle: particles if the precipitation of polymer-rich phase occurs late in the nozzle and fibers if the precipitation occurs upstream in the nozzle. Thies and coworkers (Aniedobe and Thies, 1997) also reported the impact of polymer concentration on product size and morphology for cellulose acetate in supercritical methanol and fluoroacrylate in supercritical CO_2. They found a transition from continuous fibers to particles as the polymer concentration decreased from more than 5 wt% to less than 1 wt% (Aniedobe and Thies, 1997).

In addition to production of inorganic and polymeric materials, RESS has been used for processing organic materials and pharmaceuticals. Naphthalene was initially used as a model compound to study the effects of RESS processing conditions on product size and morphology (Mohamed et al., 1989a; Liu and Nagahama, 1996; Tai and Cheng, 1997). CO_2 was used as a supercritical solvent, and the effects of pre- and post-expansion temperatures and pressures and naphthalene concentration were evaluated. The particle size increased from 2–35 μm to 4–51 μm with the increase in the pre-expansion temperature from 110 to 170°C. This dependence was more pronounced at higher solute concentrations, and both particle size and size distribution decreased with the decrease in the post-expansion temperature. The effect of particle morphology as a function of particle composition was also studied for naphthalene and phenanthrene particles. These particles exhibited a systematic change from plate-like particles for pure naphthalene to needle-like particles for pure phenanthrene. Similar studies on the effects of RESS processing conditions on product morphology of salicylic acid were evaluated by Reverchon et al. (Reverchon et al., 1993). The primary product morphology of salicylic acid was needles with diameters in the 1–10 μm range and lengths of 5–170 μm. The needle diameter

and length both increased with the increase in the pre-expansion temperature from 100 to 140°C. A decrease in the post-expansion chamber temperature from 30 to –10°C resulted in a transition from needle-like to particle-like products. Concentration effects were also seen in the case of salicylic acid: an increase in the concentration by a factor of 4 for a decrease in needle diameter from 1 to less than 1 μm and a corresponding decrease in needle length from 5–15 to 3–6 μm. The results were in good agreement with those in the formation of naphthalene particles.

Ohgaki et al. also observed the formation of crystalline whiskers or needles when processing sigmasterol in supercritical CO_2 at pre-expansion pressures between 13 and 15 MPa, which changed to amorphous agglomerates at lower pre-expansion pressures (Ohgaki et al., 1990). The formation of agglomerates and needles was attributed to the subsequent growth of the primary particles (~10 nm in diameter) on the substrate, and the difference in the growth mechanisms was thought to be due to differences in the surface properties of the crystals. Needles that collected on the substrate after 10 min exposure time using a pre-expansion pressure of 15 MPa had a diameter of 0.2 μm and lengths of 2–3 μm.

In another report, an antimicotic compound griseofulvin was processed using trifluoromethane as a supercritical solvent in RESS (Reverchon et al., 1995; Donsi and Reverchon, 1991). As in previous studies, the product morphology changed from needles to particles with increases in pre-expansion temperature. For example, lower pre-expansion temperature of 60°C resulted in the formation of griseofulvin needles with 1.1 μm diameter and lengths of 13–36 μm; but at the higher pre-expansion temperature of 150°C, only particles with a diameter of 1.1 μm were formed.

The effects of RESS processing conditions on the particle formation of steroid drugs progesterone and medroxyprogesterone acetate were also studied by using supercritical CO_2 (Alessi et al., 1996). For progesterone, the particle diameter decreased from 7.4 to 4.1 μm with the use of a smaller diameter nozzle of 30 μm instead of 100 μm. The increase in progesterone concentration from 4.55×10^{-5} to 1.35×10^{-4} mole fraction resulted in a decrease in particle size from 7.5 to 6.0 μm, and an increase in the post-expansion temperature from 40 to 60°C resulted in a slight increase in particle size. The authors also found that a decrease in the post-expansion pressure from 50 to 1 bar resulted in a change of particle morphology from needle-like with a dendritic structure to more particle-like, and only a slight decrease in size, from 9.1 to 7.5 μm, with little effect on size distribution. Similarly, for *n*-octacosane processed using CO_2, an increase in pre-expansion temperature resulted in decreases in particle size and distribution (Griscik et al., 1995).

Foster et al. employed RESS processing for the micronization of ibuprofen, an anti-inflammatory drug (Charoenchaitrakool et al., 2000). They studied the effect of spraying distance, pre-expansion pressure, and nozzle length on particle size. The median particle size of ibuprofen precipitated by RESS was less than 2.5 μm. Although the particles obtained were aggregated, they were easily dispersed by ultrasonication in water. The pre-expansion pressure and nozzle length had no effect on particle size and morphology within the range of operating conditions studied. An increase in spraying distance resulted in a slight decrease in particle size and degree of aggregation. The degree of crystallinity of the processed

ibuprofen was slightly decreased; as a result, the micronized product exhibited a higher disk intrinsic dissolution rate. The RESS process was also successful in processing ultrafine spherical particles (0.1–0.3 μm) of aspirin, as demonstrated by Huang et al. (Huang et al., 2005). Their results showed that extraction pressure and extraction temperature could significantly affect the morphology and size of the precipitated particles, whereas the nozzle diameter and pre-expansion temperature did not influence the RESS-produced particles.

One of the major limitations of the RESS process with supercritical CO_2 is the low solubility of polar drugs. To overcome this limitation, a modified process of rapid expansion of supercritical solution with solid cosolvent (RESS-SC) was proposed by Gupta (Thakur and Gupta, 2005, 2006a,b). The solid cosolvent (SC) enhances the solubility, provides a barrier for coagulation in the expansion chamber, and can be removed from the solute particles later by lyophilization (sublimation). For example, with the use of menthol as cosolvent, griseofulvin (an antifungal drug) solubility in supercritical CO_2 was increased by about 28-fold. Griseofulvin particles in the range of 50–250 nm were obtained by using RESS-SC, which is a 10-fold reduction in size compared with those from the conventional RESS processing (Thakur and Gupta, 2005). The same process was also applied to phenytoin drug using menthol solid cosolvent, resulting in a 400-fold increase in the phenytoin solubility (Thakur and Gupta, 2006b).

Similarly, Johnston et al. modified the RESS process by rapid expansion from supercritical to aqueous solution (RESAS), which produced nanosuspensions of water-insoluble drugs (Young et al., 2000; Hu et al., 2004; Chen et al., 2002). Phospholipids and other suitable surfactants were integrated into the process to increase the solute solubility and enhance the dispersion of the particles. The Johnston group reported the formation of cyclosporine nanoparticles by spraying the drug–CO_2 solution into a Tween-80 solution to prevent nanoparticle agglomeration. Cyclosporine particles formed by RESAS had a size of 500–700 nm and could be stabilized for drug concentrations as high as 6.2 and 37.5 mg/ml in 1 and 5 wt% Tween-80 solutions, respectively.

Besides CO_2, several other supercritical solvents, like ethane and ethylene, have been used in RESS processing. Supercritical ethane, ethylene, and ethylene/1.5% toluene cosolvent systems were used for the RESS processing of β-carotene particles with diameters of less than 1 μm (Chang and Randolph, 1989). β-Carotene was dissolved in supercritical ethylene and then expanded into air under pre-expansion conditions of 316 bar and 70°C to produce particles with an average size of 1.0 μm and size distribution of 36%. Under similar pre-expansion conditions, when the expansion was expanded into a 10 wt% aqueous gelatin solution, small particles of 0.3 μm size and 34% size distribution were obtained.

Domingo and coworkers investigated the effect of nozzle characteristics on the particle properties of benzoic acid, salicylic acid, aspirin, and phenanthrene with supercritical CO_2 (Domingo et al., 1996, 1997). The authors used porous frits as alternatives to capillary nozzles and evaluated the particle morphologies as a function of processing conditions (Domingo et al., 1996, 1997). Although porous frit nozzles resulted in smaller particles with particle size of 0.1 μm, clogging of frits was one of the main

problems encountered. The clogging was prominent in the case of aspirin, which could not be processed using frit nozzles. On the other hand, the use of capillary nozzles resulted in more needle-like particles with an average particle size of 2–8 μm.

RESS technique has also been applied to the production of multi-component particles for various applications, particularly for the controlled release of pharmaceuticals, medical devices, etc. (Reverchon and Adami, 2006). The method allows preparation of intimately mixed samples of components with very different properties. The most promising area of application for these composite materials is in the controlled release of drugs using polymer particles. For example, RESS processing of several polyhydroxy acids for controlled release was reported by Tom and Debenedetti (Tom and Debenedetti, 1991). Polymer microparticles of bioerodible polymers poly(L-lactic acid), poly(D,L-lactic acid), and poly(glycolic acid) with diameters ranging from 2 to 25 μm were successfully prepared via RESS processing with neat CO_2, CO_2 with 1 wt% acetone cosolvent, and chlorotrifluoromethane. Benedetti et al. also did a comparative study of RESS and SAS methods for the preparation of micron-size particles of the biocompatible polymer hyaluronic acid benzylic ester (Benedetti et al., 1997).

The ideal targeted morphology for controlled release applications is uniform spherical drug particles homogeneously distributed throughout the polymer particles. RESS process was applied for the preparation of uniformly distributed pyrene within the poly(L-lactic acid) microparticles (Tom et al., 1994; Knutson et al., 1996). Pyrene was chosen as a model organic solute because the pyrene distribution in poly(L-lactic acid) could be easily determined using fluorescence microscopy. Poly(D,L-lactic acid) was extracted using CO_2-$CHClF_2$ (60 wt% CO_2) at 200 bar and 55°C in one column, and pyrene was extracted with neat CO_2 at 200 bar and 65°C in the other column. The pyrene concentration was adjusted by diluting the extract to the desired concentration using CO_2. Both extraction columns were used in parallel and the two solutions were mixed and brought to the pre-expansion temperature and expanded through a 50 μm capillary nozzle. The uniform distribution of pyrene inside poly(D,L-lactic acid) microspheres was evident from the results.

Lovastatin, an anti-cholesterol drug, was successfully encapsulated in poly(D,L-lactic acid) microparticles by Debenedetti et al. (Debenedetti et al., 1993b). Two separate extraction columns for the solutes were used to prepare encapsulated particles. Simultaneous extraction of the polymer and drug solutes using supercritical CO_2 at 200 bar and 55°C followed by expansion at 75–80°C produced a range of polymer particles from spherical to oblong, containing lovastatin needles. A single extraction column packed with a mixture of both solutes was also used for the processing. However, the use of separate extraction columns for individual solutes was preferred because separate columns allow better control over the solute extraction parameters and final product properties.

Naproxen (6-methoxy-methyl-2-naphthaleneacetic acid), an anti-inflammatory drug, was used with poly(L-lactic acid) to prepare encapsulated microparticles (Kim et al., 1996). Simultaneous extraction of both naproxen and poly(L-lactic acid) solutes was accomplished by using a single extraction column with supercritical CO_2. The solution containing

both the solutes was co-precipitated at pre-expansion conditions of 190 bar and 114°C using a 50 μm diameter capillary nozzle. Naproxen microparticles ranging from size 2 to 5 μm were found to be embedded inside poly(L-lactic acid) spheres with 10–90 μm diameter.

The RESS techniques have been applied to processing of other pharmaceutical compounds, such as salicylic acid, aspirin, lecithin, nifedepin, lovastatin, paracetamol, ketoprofen, nicotinic acid, and drug–polymer systems (York, 1999; Kompella and Koushik, 2001; Subramaniam et al., 1997a; Jung and Perrut, 2001; Vemavarapu et al., 2005; Subramaniam et al., 1997b; Hanna and York, 1998; Sloan et al., 1998; Helfgen et al., 2000; Rogers et al., 2003). The morphology of the prepared materials was found to be dependent on the different processing conditions, which allows some control over the materials properties. Although particles of a few microns are generally obtained as primary products, smaller particles (100–300 nm) have been produced in RESS with the use of appropriate nozzles (Jung and Perrut, 2001). To better understand the relationships between processing conditions and materials properties, numerous efforts have been made to model and simulate the supercritical fluid processing technique. The results from these studies suggest that traditional RESS process generally produces micron-size particles with only few exceptions (Lele and Shine, 1992, 1994; Matson et al., 1987a; Petersen et al., 1986; Matson et al., 1986b, 1987c,d; Smith et al., 1986; Matson et al., 1989; Matson and Smith, 1989; Burukhin et al., 1998; Williams et al., 1998; Yeo et al., 1994). Mechanistically, several theoretical studies suggest that the traditional RESS should facilitate the formation of primarily nanoscale particles and that agglomerations during the rapid expansion process are responsible for the growth of the initially formed particles beyond the nanoscale and thus for the observation of micron-size particles as major products (Helfgen et al., 2000; Weber and Thies, 2002). Ginosar and coworkers have shown experimentally that both nanosize and micron-size particles are present in the expansion jet and that the particle sizes increase with the distance from the expansion nozzle, consistent with the theoretically predicted agglomeration mechanism (Ginosar et al., 2000). For example, they found that the nanosize particles increased in size from an average diameter of 10 to 22 nm as the distance from the expansion nozzle increased from 0.26 to 5 mm, while micron-size particles maintained a relatively constant average diameter of $\sim$ 0.7 μm (Ginosar et al., 2000). These theoretical and experimental results suggest that nanoscale particles could be obtained from the RESS process if the nanoparticles could be effectively "captured".

RESOLV and Nanotechnology

Sun and coworkers made a procedure-wise simple modification, but mechanistically significant, to the classical RESS processing by rapidly expanding a supercritical solution into a liquid instead of air or gas phase, namely the *r*apid *e*xpansion of a supercritical solution into a liquid *solv*ent (RESOLV), as illustrated in Scheme 1 (Sun and Rollins, 1998; Sun et al., 1999a,b). Alternatively in some cases, a reacting system has been used,

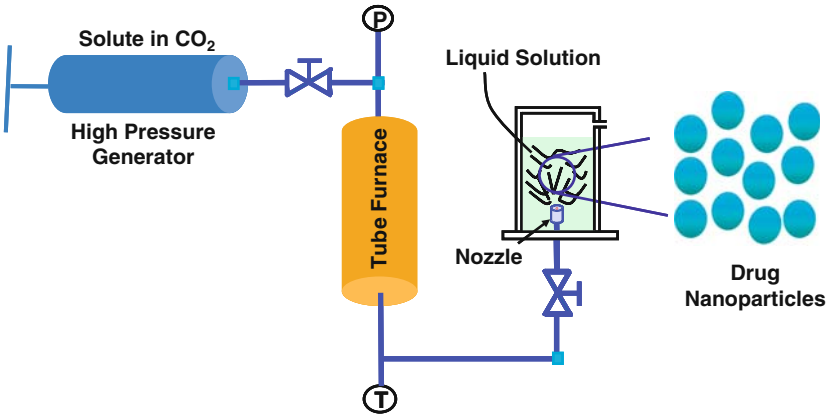

RESOLV for processing drug nanoparticles

Scheme 3.1 RESOLV for processing drug nanoparticles. (*See* Color Plate 5)

in which one reactant is dissolved in the supercritical solution and one in the liquid receiving solution. However, these variations of RESOLV all involve expansion into a liquid to produce exclusively nanoscale particles, and the nanoparticles thus produced are generally of narrow size distributions (Pathak et al., 2004, 2005, 2006, 2007a,b; Sun et al., 2000, 2001, 2005; Meziani and Sun, 2002; Meziani and Sun, 2002, 2003; Sane and Thies, 2005; Meziani et al., 2003, 2005a,b, 2002, 2006).

RESOLV for Nanoscale Semiconductor and Metal Particles

Semiconductor and metal nanoparticles were prepared by using RESOLV with a reacting system. While not necessarily applicable to the processing of drug nanoparticles, the results are highlighted to demonstrate the feasibility and potentials of the technique. A simple example is the preparation of cadmium sulfide (CdS) nanoparticles. In the experiment, a supercritical ammonia solution of $Cd(NO_3)_2$ was prepared for rapid expansion into a room-temperature ethanol solution of Na_2S. The reaction of Cd^{2+} ions contained in the sprayed supercritical ammonia solution with S^{2-} in the receiving liquid ethanol solution resulted in the formation of CdS nanoparticles (Sun and Rollins, 1998). The same method has been applied to the preparation of other semiconductor (PbS, Ag_2S, ZnS), metal (Cu, Ni, Co, Fe), and metal oxide (Fe_2O_3) nanoparticles (Sun et al., 1999a,b, 2000).

An important feature of the RESOLV method is that it requires no nanoscale templates (such as nanoscale cavities in micelles) for the formation of nanoparticles. The supercritical fluid rapid expansion itself provides the templating effect, creating nanoscale droplets of the expanding supercritical fluid solution in the receiving solution (Sun et al., 1999a,b, 2000). Thus, the method offers a "clean" way to produce nanoscale materials that are conjugated directly with biological species (Meziani et al., 2002, 2005b; Meziani and Sun, 2003). For example, it was demonstrated that the semiconductor and metal nanoparticles coated directly with

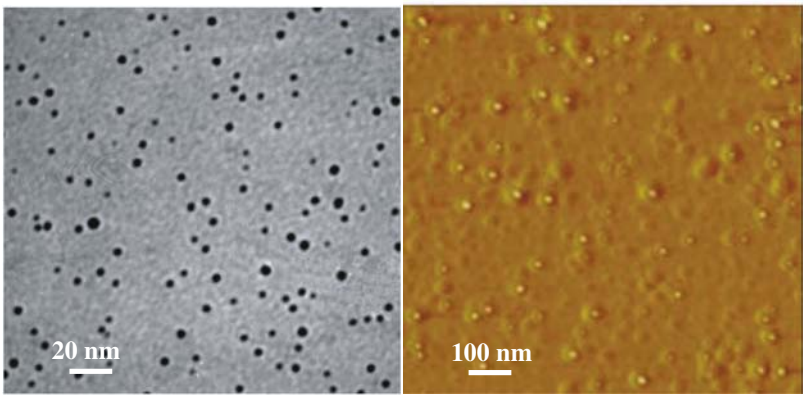

Figure 3.1 TEM (*left*) and AFM (*right*) images of BSA-conjugated Ag_2S nanoparticles prepared via RESOLV. (From Meziani and Sun, 2003.) (*See* Color Plate 6)

natural protein species could be prepared via RESOLV process (Meziani et al., 2002, 2005b; Meziani and Sun, 2003). Shown in Figure 3.1 is a TEM image of the BSA-conjugated Ag_2S nanoparticles, corresponding to an average particle size of 6.3 nm and a size distribution standard deviation of 1.6 nm. The result from atomic force microscopy (AFM) analysis is also shown in Figure 3.1.

Supercritical CO_2 with its favorable properties is obviously the preferred clean solvent in RESOLV. However, the limitation of neat supercritical CO_2 is that it mostly dissolves only nonpolar solutes. Sun and coworkers have investigated the use of other CO_2-based supercritical solvent systems with RESOLV, including the stabilized CO_2 microemulsions (Sun et al., 2001; Meziani and Sun, 2002; Meziani et al., 2003, 2005a). For example, in an evaluation of the feasibility as supercritical solvent systems in the preparation of nanoparticles via RESOLV, the supercritical CO_2-based microemulsions stabilized by perfluoropolyether ammonium carboxylate (PFPE-NH_4) have been used to dissolve silver and copper salts in RESOLV for the preparation of pure nanoscale silver and copper nanoparticles (Sun et al., 2001; Meziani and Sun, 2002; Meziani et al., 2003, 2005a). These metal nanoparticles, as well as nanoscale metal sulfides (Ag_2S, CdS, and PbS), have been considered as model systems for the evaluation of the microemulsion-for-RESOLV approach.

There have also been systematic investigations on the experimental conditions and parameters required or suitable for the dissolution of different metal salts in water-in-CO_2 microemulsions (Meziani and Sun, 2002). In a RESOLV experiment for pure silver nanoparticles, as an example, $AgNO_3$ was dissolved in the water cores of the PFPE-NH_4-protected reverse micelles in supercritical CO_2. The microemulsion containing the aqueous $AgNO_3$ was rapidly expanded into an ambient solution with a reductant in the classical RESOLV arrangement for the nanoparticle formation. The results from this approach are more complicated than those from the use of neat supercritical solvent discussed in previous sections. The particle size distributions are generally broader with the rapid expansion of the microemulsion when the receiving liquid solution is close to neutral pH (Meziani et al.,

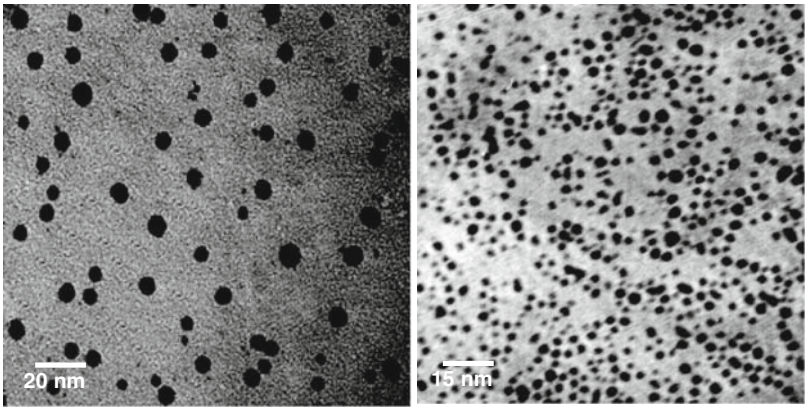

Figure 3.2 TEM images of the two sets of Ag nanoparticles. (From Meziani et al., 2005a.)

2005a). However, in an optimization of the process, it was found that the use of basic liquid receiving solution resulted in two sets of silver particles, each of which with a reasonably narrow size distribution. Shown in Figure 3.2 are TEM images of the two sets of silver nanoparticles obtained from the basic receiving solution conditions (pH $\sim$ 11). The separation of the two sets of nanoparticles was accomplished via simple centrifuging. The set of a smaller average particle size represents the initially formed nanoparticles, and the other set of a larger average particle size probably represents those that grow from the initially formed nanoparticles. Such an assignment is supported by the fact that the average size of the set of smaller nanoparticles is dependent on the water-to-surfactant ratio (or the Wo value) of the pre-expansion microemulsion. A higher Wo value corresponds to a larger average size of the initially produced silver nanoparticles (Figure 3.3). This nice size correlation suggests that the reverse micelles in supercritical CO_2 before the rapid expansion still play a role in the post-expansion formation of nanoparticles, which may have significant implications to the effort on controlling particle sizes. Although the use of supercritical CO_2-based microemulsions in RESOLV complicates the overall technical platform, it does offer important flexibility in the nanoparticle production.

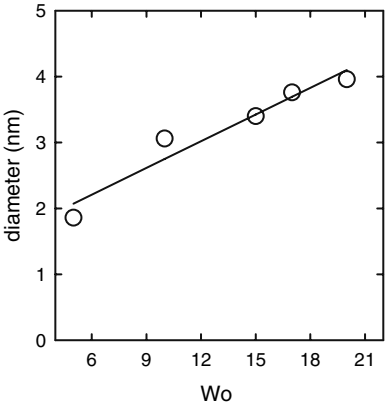

Figure 3.3 Variation of Ag nanoparticle sizes with the pre-expansion Wo values. (From Meziani et al., 2005a.)

RESOLV for Nanoscale Polymeric and Organic Particles

Polymeric nanoparticles (100 nm or less), especially those that are biocompatible and/or biodegradable, have attracted much attention for their various applications. In the field of drug delivery, as an example, these nanoparticles may be used to carry a wide range of drugs, proteins, vaccines, or other biological species and for the purpose of controlled release of drugs. Available methods for preparing polymeric nanoparticles include solvent-in-emulsion evaporation, phase separation, and spray drying. These methods are limited by issues such as excessive use of surfactant and solvent, unwanted impurities, and insufficient colloidal stability. Thus, it remains an ongoing challenge to find reliable and versatile techniques for clean and nontoxic production of well-dispersed organic and polymeric nanoparticles. RESOLV has been demonstrated as such a technique with the CO_2-soluble fluoropolymer poly(heptadecafluorodecyl acrylate) (PHDFDA) as model polymeric solute (Meziani et al., 2004; Sun et al., 2005). Experimentally, the fluoropolymer PHDFDA was dissolved in supercritical CO_2. The supercritical solution was rapidly expanded into ambient pure water to yield nanoscale PHDFDA particles. In order to prevent the particles from agglomeration, polymeric and surfactant stabilization agents were used in the aqueous suspension. For example, when an anionic surfactant sodium dodecyl sulfate (SDS) was presented, even at a relatively low concentration (20 mM), the aqueous-suspended PHDFDA nanoparticles could be protected to remain exclusively nanoscale, about 40 nm in average diameter according to scanning electron microscopy (SEM) analysis (Figure 3.4). Similarly, water-soluble polymers can be effective stabilization agents for the initially formed aqueous suspension of polymeric nanoparticles in RESOLV. In the presence of poly(vinyl alcohol) (PVA) in the aqueous receiving solution, as an example, the PHDFDA nanoparticles from RESOLV remained homogeneous without any significant precipitation (Sun et al., 2005). An SEM image of the PVA-protected PHDFDA nanoparticles is also shown in Figure 3.4.

The same RESOLV processing was applied to produce nanoparticles from biodegradable and biocompatible polymers, including poly(L-lactic acid) (PLA) (Figure 3.5a) and poly(methyl methacrylate) (PMMA) (Figure 3.5b), for stable aqueous suspensions of the nanosized particles (Meziani et al., 2006). For organic materials, the feasibility of RESOLV

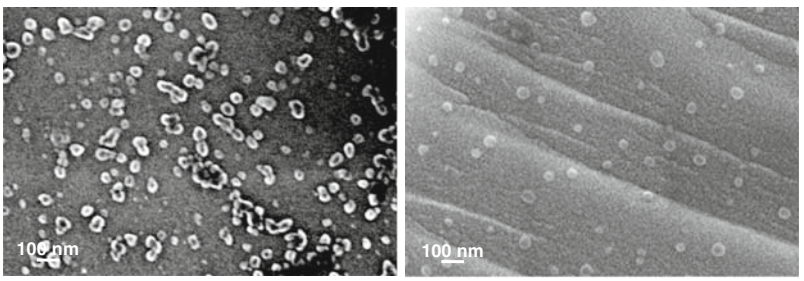

Figure 3.4 SEM images of poly(HDFDA) nanoparticles from RESOLV with aqueous SDS solution (*left*) and aqueous PVA solution (*right*) at the receiving end of rapid expansion. (From Meziani et al., 2004.)

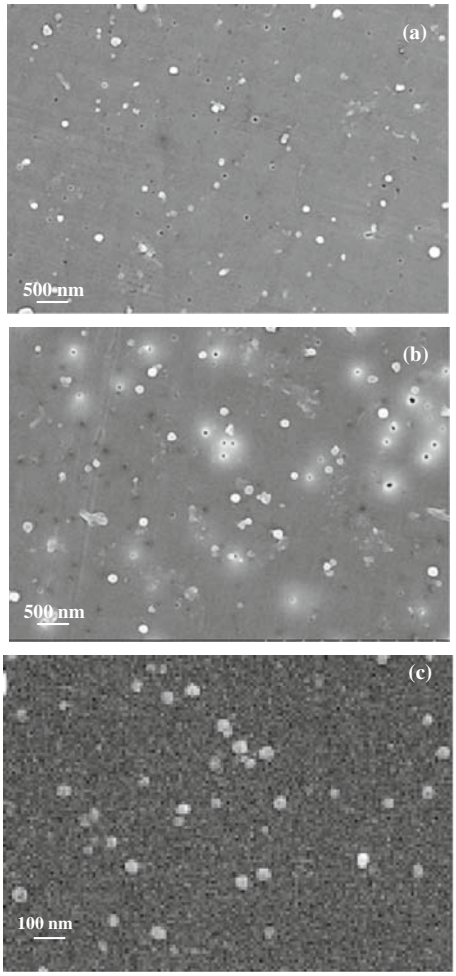

Figure 3.5 SEM images of the SDS-protected PLA nanoparticles (**a**), SDS-protected PMMA nanoparticles (**b**), and pluronic-protected TBTPP nanoparticles (**c**). (From Sane and Thies, 2005; Meziani et al., 2006.)

for the production of nanoscale particles has been demonstrated with 5,10,15,20-tetrakis(3,5-bis(trifluoromethyl) phenyl) porphyrin (TBTPP) as a model compound (Figure 3.5c) (Sane and Thies, 2005).

RESOLV for Nanosizing Drug Particles

For the formulation and delivery of drugs that are insoluble or poorly soluble in water, particle size reduction has emerged as a promising strategy. Particulate drug delivery systems are useful for administering drugs by various routes, including aqueous suspensions for oral, parenteral, or topical applications and dry powders for inhalation and other uses. The purpose of these delivery systems can be either immediate release or sustained release of the therapeutic agent conjugated with a polymer excipient. Since the particle size and morphology of a drug may directly affect its pharmacokinetics, it is important to tailor the drug particle size in a dosage to the route of administration. The RESOLV technique has demonstrated great potential in the production of exclusively nanoscale

drug particles (Pathak et al., 2004, 2005, 2006, 2007a,b). Various anti-inflammatory (ibuprofen and naproxen), antifungal (amphotericin B), and anti-cancer (paclitaxel) drugs were selected for demonstration, for which CO_2 and CO_2–cosolvent systems were used. The experimental procedure of RESOLV for the production of drug nanoparticles was similar to that for polymeric nanoparticles. The drug particles produced in the RESOLV process are exclusively nanoscale (less than 100 nm), but without protection, these suspended nanoscale particles can form larger aggregates and precipitate. In the case of ibuprofen, naproxen, and paclitaxel nanoparticles, the water-soluble polymer poly(*N*-vinyl-2-pyrrolidone) (PVP) was found to be an effective stabilization agent. Figure 3.6 shows homogeneously distributed ibuprofen (40 nm in average diameter) and naproxen (64 nm in average size) nanoparticles obtained from RESOLV with aqueous PVP solution at the receiving end of the rapid expansion. The average particle size and size distribution were both found to be dependent on the PVP concentration in the aqueous receiving solution and PVP average molecular weight.

Various other water-soluble polymers, surfactants, and food emulsifiers can also be used to protect the drug nanoparticles produced in RESOLV and stabilize the aqueous suspensions for formulation and other purposes (Pathak et al., 2006). The investigated stabilization agents, such as PVP, sodium dodecyl sulfate (SDS), poly(ethylene glycol) (PEG), and bovine serum albumin (BSA) protein are all biocompatible and/or biodegradable additives, with an accepted GRAS (*g*enerally *r*eferred as *s*afe) status. In fact, these polymers have already found other biological and biomedical applications, such as drug-encapsulated polymeric particles and drug–polymer composites. The particle properties were found to be dependent on the type and properties of the stabilization agent used (Table 3.1). Figure 3.7 shows ibuprofen particles of various sizes obtained by using various stabilization agents. The difference in particle sizes might be due to the further growth of the initially formed drug particles, for which the less effective protection by the stabilizer might be responsible. Conjugation of drug nanoparticles with different stabilization agents (thus different surface properties) can have important implications in the delivery and targeting of these nanoparticles. For example, PEG-protected drug nanoparticles are often referred to as "stealth nanoparticles", because they can prevent recognition and clearance from the blood stream to achieve longer

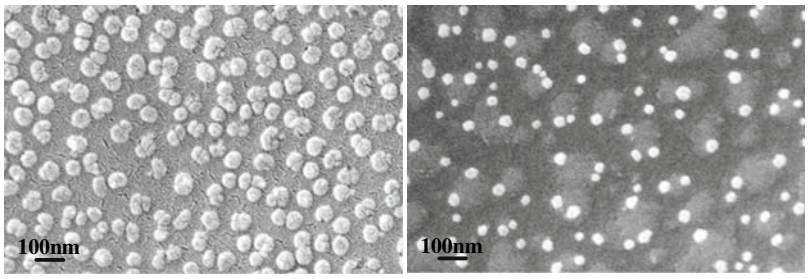

Figure 3.6 SEM images of the naproxen (*left*) and ibuprofen (*right*) nanoparticle samples obtained from RESOLV with the expansion into aqueous PVP solution. (From Pathak et al., 2004.)

Table 3.1 Parameters of ibuprofen nanoparticles with different stabilization agents.

Stabilization agent	Concentration (mg/mL)	Average size (nm)	Deviation (nm)
PVP ($M_W \sim 40{,}000$)	0.5	40	8.2
PVP ($M_W \sim 40{,}000$)	2	39	8.4
PVP ($M_W \sim 360{,}000$)	0.5	30	6.2
PEG ($M_W \sim 6{,}000$)	2	276	58
PEG ($M_W \sim 35{,}000$)	2	44	7.8
PVA	2	~50	
BSA protein	2	82	15
SDS	3.3	25	5

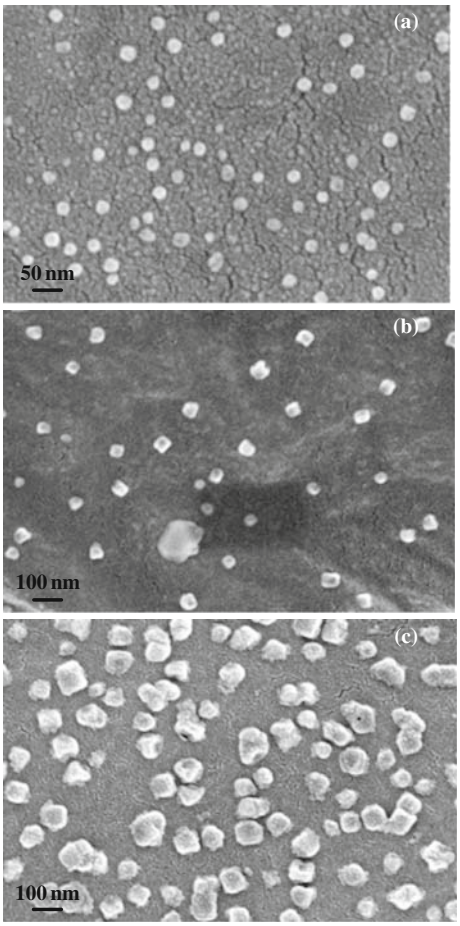

Figure 3.7 SEM images of the ibuprofen nanoparticles obtained with SDS (**a**), PEG (**b**), and BSA (**c**) as stabilization agents in RESOLV. (From Pathak et al., 2006.)

circulation. Beyond the use of different stabilization agents, the properties of the drug nanoparticles could also be altered by other RESOLV experimental conditions (such as temperature, pressure, drug concentration, cosolvent amount). For example, while a higher pre-expansion pressure had only marginal effect, an increase in the pre-expansion temperature

resulted in larger particle sizes (Pathak et al., 2004). Similarly, an increase in the dissolved drug concentration in supercritical CO_2 resulted in larger nanoparticles with different particle morphology (Pathak et al., 2006).

Nanosizing Amphotericin B Particles

Amphotericin B (AmB), an amphipathic polyene macrolide, is practically insoluble in water but soluble in CO_2 with DMSO or methanol as a cosolvent (less than 4 vol%). These cosolvents make homogeneous mixtures with CO_2 at moderate temperature and pressure and are miscible with water, and they belong to class 3 (nontoxic) in the pharmaceutical guidelines. The solubility of AmB in the CO_2–cosolvent systems was evaluated spectroscopically under various temperature and pressure conditions by using a high-pressure optical cell with quartz windows (Meziani and Sun, 2002). In a typical RESOLV experiment, a solution of AmB in DMSO (3 mg in 0.57 mL) was added to the syringe pump, followed by filling the pump with liquid CO_2 to a pressure of 310 bar (total volume 50 mL, DMSO volume fraction 1%). The solution was pushed through the heating unit to reach the desired supercritical temperature of 40°C before the expansion nozzle. The rapid expansion was carried out at pre-expansion pressure of 310 bar through a 50-μm orifice into ambient water. The as-produced aqueous suspension of AmB nanoparticles appeared homogeneous (Figure 3.8) and it remained stable for an extended period of time. The suspension was used to prepare specimen for SEM analyses. The SEM images suggest that the RESOLV process produced nanoscale AmB particles (Figure 3.9), with an average particle size of 38 nm diameter (particles treated as spheres) and a size distribution standard deviation of 7 nm.

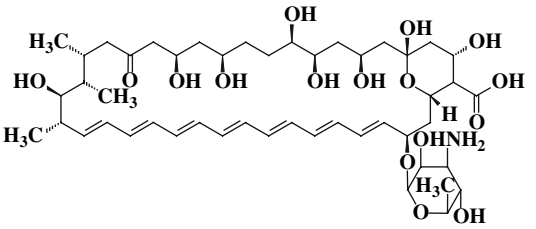

Amphotericin B

The use of methanol as a cosolvent with supercritical CO_2 in the RESOLV processing of AmB yielded similar nanoscale particles. The solution for rapid expansion contained 2 vol% methanol with an AmB concentration of 0.05 mg/mL, and the expansion was at 40°C and 310 bar into ambient water. The as-produced aqueous suspension, appearing homogeneous initially, was used to prepare specimen for SEM analyses. The average particle size of 39 nm and the size distribution standard deviation of 8.5 nm from the SEM images (Figure 3.10) are comparable with those of the AmB nanoparticles obtained with DMSO as cosolvent. However, a significant difference is that the aqueous suspension from methanol as cosolvent was not stable, exhibiting precipitation soon after its formation. The precipitate was aggregates of AmB nanoparticles, as suggested by the SEM results. The different stabilities in the aqueous suspensions of the nanoparticles

Figure 3.8 AmB nanoparticles from RESOLV in a stable and optically transparent aqueous suspension. (From Pathak et al., 2007a.) (*See* Color Plate 7)

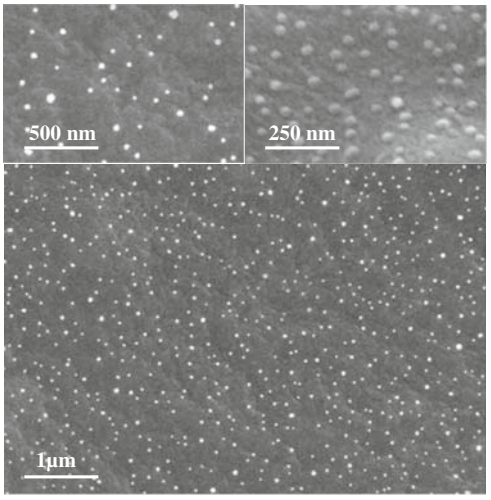

Figure 3.9 SEM images (different resolutions) of the AmB nanoparticles from RESOLV with DMSO as cosolvent into neat water. (From Pathak et al., 2007a.)

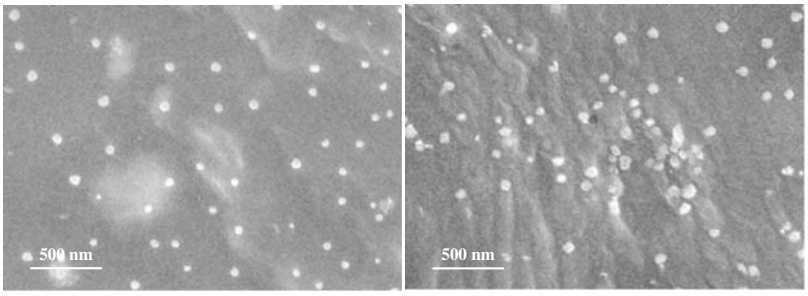

Figure 3.10 SEM images of the AmB nanoparticles from RESOLV with methanol as cosolvent: aqueous suspension right after the expansion (*left*), and with PVA as a stabilizer (*right*). (From Pathak et al., 2007a.).

associated with the use of different cosolvents is an interesting topic for further investigations.

The initially formed drug nanoparticles in RESOLV could be protected from agglomeration by using a stabilization agent in the aqueous suspension. For example, when an aqueous solution of PVA polymer (50 mg/mL) instead of neat water was used at the receiving end of the rapid expansion, the aqueous suspension of AmB nanoparticles from the same RESOLV process remained stable without precipitation. As shown in Figure 3.10, the AmB nanoparticles from the PVA-stabilized suspension are larger (average size of 64 nm diameter and size distribution standard deviation of 12 nm), but distributed homogeneously. PVA is an effective stabilizer commonly used in drug formulation. Various other polymeric and oligomeric stabilizers may also be used with RESOLV to protect the drug nanoparticles from agglomeration (Pathak et al., 2004, 2005, 2006, 2007a,b).

The amount of cosolvent in the supercritical solution for rapid expansion was found to have significant effects on the properties of the produced AmB nanoparticles. For example, an increase of DMSO from 1 to 2 vol% led to increases in the average particle size and crystallinity. As shown in Figure 3.11, the AmB particles thus produced were faceted and square in shape, indicating a higher crystallinity. This was confirmed by the melting results from differential scanning calorimetry (DSC). The nanoparticles obtained with less cosolvent showed a 7.2°C decrease in melting point from that of the bulk AmB, but those obtained with more cosolvent had only a 5.2°C decrease (consistent with larger particles and higher crystallinity). The particle sizes as measured diagonally are on average 225 nm with a size distribution standard deviation of 49 nm. Similar changes in AmB particle sizes and crystallinity were observed with an increase in the amount of cosolvent methanol from 2 to 4 vol% in the supercritical solution for rapid expansion. The particles were also faceted (Figure 3.11) and larger (on average 143 nm diagonally with a distribution standard deviation of 40 nm). The higher crystallinity was also confirmed by DSC analysis. Mechanistically, the formation of more crystalline structures could simply be due to the significant increase in particle sizes, namely that only very small AmB particles could be made into largely amorphous under the

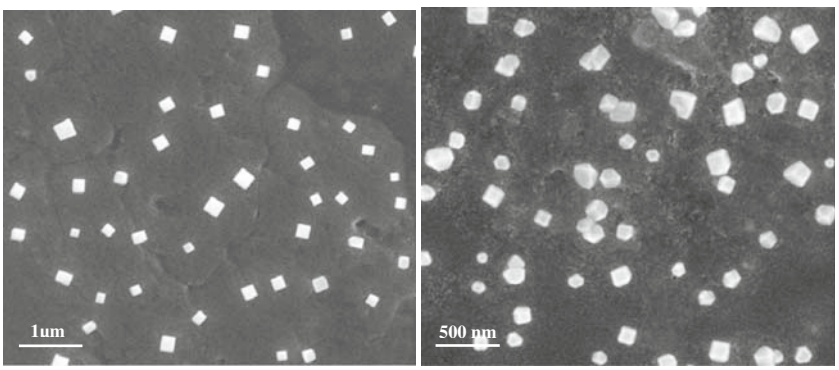

Figure 3.11 SEM images of the AmB nanoparticles from RESOLV with higher cosolvent concentrations, DMSO (*left*) and methanol (*right*). (From Pathak et al., 2007a.)

RESOLV processing conditions. However, probably the higher cosolvent content also alters the rate of crystallization, thus producing more faceted particles (York, 1999; Jaarmo et al., 1997). The effect of solvent or solvent mixture on the formation of stable and unstable polymorphs is well recognized in the literature (Shekunov and York, 2000).

The variation in the morphology or crystallinity of the different AmB nanoparticles is an interesting feature in the nanosizing of drug particles via RESOLV. AmB is known to exhibit nonlinear concentration dependence in its pharmacodynamic characteristics, and thus higher doses are typically not recommended for toxicity considerations (Klepser et al., 1997; Bekersky et al., 2002; Andes, 2003). Because of the unusual biopharmaceutical property of AmB, its protein binding in plasma increases with increasing drug concentration and continuous infusion or less frequent administration of higher doses is generally preferred (Imhof et al., 2003; Lewis and Wiederhold, 2003).

Nanosizing Paclitaxel Particles

Paclitaxel, as one of the best antineoplastic drugs, is found to be effective or highly effective against a wide spectrum of cancers including ovarian cancer, breast cancer, lung cancer, colon cancer, head and neck cancer, etc. (Rowinsky et al., 1990; Lopes et al., 1993). Like many other anti-cancer drugs, it has difficulties in clinical administration due to its poor solubility in water and most pharmaceutical reagents. In its current clinical application, an adjuvant called Cremophor EL has to be employed, which has been found to be responsible for many serious side effects. Nanoparticle encapsulation of the drug has been considered as an alternative to realize a controlled and targeted delivery of the drug with better efficacy and less side effects.

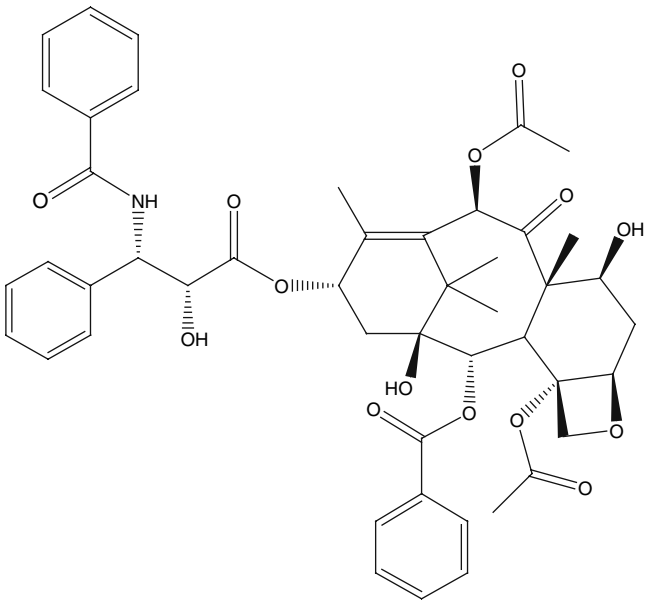

Paclitaxel

The RESOLV processing technique was applied to produce paclitaxel nanoparticles suspended in aqueous buffer (Pathak et al., 2007b). The drug has some solubility in supercritical CO_2, with experimentally estimated solubility of 1.1×10^{-6} to 6.3×10^{-6} mole fraction at pressure and temperature ranges of 140–340 bar and 311–330 K, respectively. In a typical experiment, a solution of paclitaxel (2 mg) was added to the syringe pump, followed by CO_2 filling to a pressure of 310 bar. The solution was pushed through the heating unit to reach the desired supercritical temperature of 40°C before the expansion nozzle. The rapid expansion was carried out at a pre-expansion pressure of 310 bar through a 50-μm orifice into ambient water solution. In the case of neat water at the receiving end of the rapid expansion, the nanoscale drug particles agglomerated over time to form larger aggregates and precipitated from the suspension. In the presence of a stabilization agent in the aqueous suspension, however, the initially formed paclitaxel nanoparticles in RESOLV could be protected from the agglomeration. For example, when an aqueous solution of PVP polymer (average molecular weight $\sim$ 40,000, 1 mg/mL) was used at the receiving end of the rapid expansion, no agglomeration and precipitation were observed following the RESOLV process. The suspended nanoparticles were used to prepare specimens for SEM characterization, which shows well-dispersed nanoparticles (Figure 3.12a). According to a statistical analysis of the SEM images, the paclitaxel nanoparticles are of an average size of $\sim$ 40 nm in diameter.

The particle sizes and size distribution were found to be dependent on the concentration of the stabilization agent PVP, which allowed the variation/manipulation of these particle parameters. For example, the use of PVP at a somewhat lower concentration of 0.33 mg/mL under otherwise similar conditions resulted in larger paclitaxel nanoparticles (Figure 3.12b), with an average particle size of about 500 nm. In both cases the RESOLV processing yielded stable aqueous suspensions (solution-like) with homogeneously dispersed paclitaxel nanoparticles. There have been reports (Vandana and Teja, 1997; Nalesnik et al., 1998; Suleiman et al., 2005) that the use of a cosolvent such as ethanol or ethyl acetate with supercritical CO_2 increases the solubility of paclitaxel under comparable pressure and temperature conditions. These reported findings were confirmed in our experiments, though their application to the RESOLV processing of paclitaxel nanoparticles requires detailed investigation.

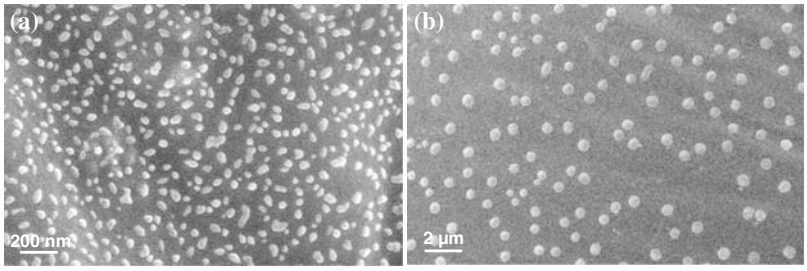

Figure 3.12 (**a**) Paclitaxel nanoparticles (average size $\sim$ 40 nm) from RESOLV with expansion into a somewhat higher concentration PVP solution. (**b**) Paclitaxel nanoparticles (average size $\sim$ 500 nm) from RESOLV with expansion into a somewhat lower concentration PVP solution. (From Pathak et al., 2007b.)

The nanosized drug particles from the RESOLV processing are in aqueous suspensions, readily compatible with established in vitro assays and in vivo tests (Pathak et al., 2007b; Bharadwaj and Prasad, 2002). For the in vitro cytotoxicity assay, actively growing MDA-MB-231 cells (10,000–20,000) were plated in 12-well cluster dishes in regular growth media and allowed to adhere overnight. For paclitaxel nanoparticles of 38 or 530 nm in average size, the particle suspension was sonicated in a water-bath, diluted directly into cell growth medium, and added to the cells at a desired paclitaxel concentration. The same procedures were used with a paclitaxel solution in ethanol at equimolar concentration. In assays for all three samples, cells were harvested at various time points from 4 h of plating to 72 h in culture. Cells treated without any additions were used as controls. At the time of harvest, the growth medium was replaced and rinsed with PBS. Cells were fixed and stained in 0.5% crystal violet in 50% ethanol at room temperature for 15 min, washed to remove excess dye, and allowed to dry. The dye was extracted with 50% ethanol for 15 min, and the absorbance was recorded at 540 nm.

The evaluation was based on the anti-proliferation effects on the human malignant breast cell line MDA-MB-231 (Pathak et al., 2007b; Mahadev et al., 2002). Treatment of cells with small (38 nm) and larger (530 nm) paclitaxel nanoparticles resulted in marked inhibition of cell proliferation. The estimated IC_{50} values (based on the results after 48 h exposure) are 100 nM (paclitaxel equivalent concentration in the nanoparticle samples), comparable with what is reported in the literature for paclitaxel dissolved in DMSO against the same cancer cell line. The use of paclitaxel ethanol solution under the same experimental conditions yielded similar results (Figure 3.13). However, the control experiments on PVP only (0.33 and 1.0 mg/mL) showed no toxicity to the cells, consistent with the known conclusion that the polymer is generally nontoxic.

A known function of paclitaxel is to stabilize microtubules, thus interfering with the formation of mitotic spindle and inhibiting cell division and inducing apoptosis (Pathak et al., 2007b; Bharadwaj et al., 2005) as observed

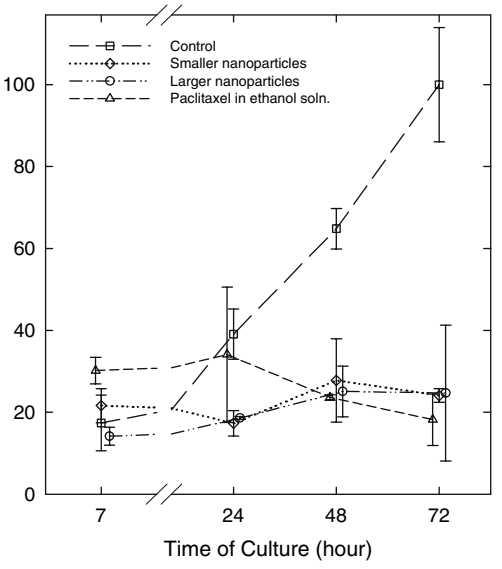

Figure 3.13 Cytotoxicity assays of the paclitaxel nanoparticles (smaller 38 nm and larger 530 nm average sizes) and the paclitaxel ethanol solution at equimolar concentration (0.5 μM) against MDA-MB-231 cells (normalized to the cell growth of the control after 72 h culture), with significant inhibition in comparison with the controls (p values <0.05). Error bars indicate standard deviation, and the data points are offset slightly on purpose for easier viewing. (From Pathak et al., 2007b.)

in the cytotoxicity assay above. For MDA-MB-231 cells treated with the paclitaxel nanoparticles of small or larger sizes (10 μM drug concentration) for 24 h, there was marked disruption of microtubule architecture and nuclear morphology according to confocal microscopy images (Figure 3.14)

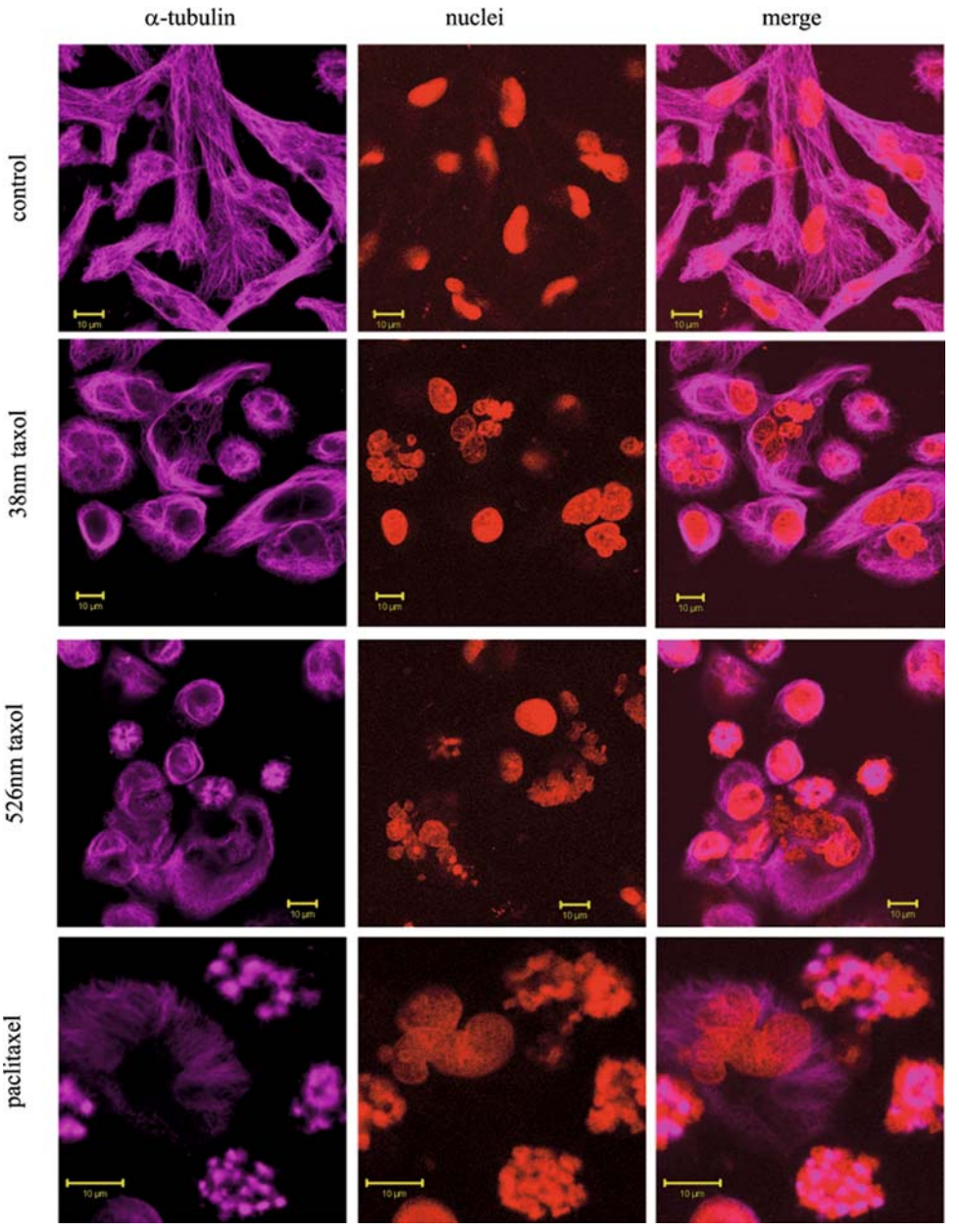

Figure 3.14 The cellular organization of microtubule network in MDA-MB-231 cells with and without paclitaxel treatment (10 μm for all scale bars). Experimentally, the cells were plated in Nunc chamber slides and allowed to attach overnight. After the treatment with the drug (10 μM concentration for all) in the different forms for 6–24 h, or no treatment as control, the cells were fixed with paraformaldehyde and stained for microfilaments with anti-actin antibody followed by rhodamine-conjugated antibody, and then reacted with DAPI to stain nuclei (DNA). Samples were mounted using Prolong Antifade kit (Molecular Probes) for imaging on a Zeiss LSM 510 confocal microscope. (From Pathak et al., 2007b.) (*See* Color Plate 8)

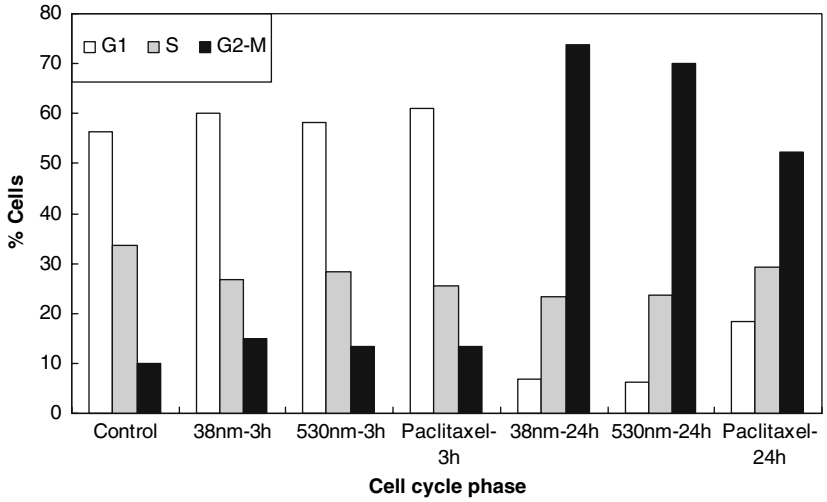

Figure 3.15 Flow cytometry analysis of MDA-MB-231 cells after 3 and 24 h incubation with different paclitaxel formulations (nanoparticles of sizes averaging 38 and 530 nm, and the paclitaxel ethanol solution) at equimolar concentrations and the control (without paclitaxel). A graphical interpretation of the percentage of cells in each cell cycle phases G1, S, and G2-M is shown for different paclitaxel formulations. (From Pathak et al., 2007b.)

(Pathak et al., 2007b; Bharadwaj et al., 2005; Hartsel and Bolard, 1996). The disruption of microtubule architecture and the accumulation of alpha-tubulin around the nucleus were evident in drug-treated cells. Furthermore, nuclear examination revealed the presence of fragmented, diffusely stained, and multinucleated nuclei, which are consistent with apoptosis (Figure 3.14). Colocalization of microtubules with fragmented DNA was also detected.

The interference of paclitaxel nanoparticles with the cell cycle progression was probed in terms of flow cytometry. For MDA-MB-231 cells treated 24 h with the nanoparticles of a small (38 nm) or larger (530 nm) average size, there was a marked increase (about sixfold) in G_2-M phase and a concomitant decrease in G_0–G_1 populations (Figure 3.15). This is consistent with the blockade of mitosis. In a comparison with paclitaxel dissolved in ethanol, the nanoparticles appeared to be more effective, with a higher population of cells accumulated in the G_2-M phase (about 70 vs about 50% for the paclitaxel ethanol solution).

Summary and Perspective

There has obviously been exciting progress over the past few years in the use of supercritical fluid processing techniques as alternative or unique solutions to many problems in drug formulation, especially with respect to the production of micron-sized and nanoscale drug particles and related systems. These techniques outperform conventional ones in many areas, including moderate operation conditions, low levels of residual solvents, products with targeted properties, etc. As demonstrated primarily at the laboratory scale, the SAS method is often preferred in the processing of drugs and polymers with limited solubilities in supercritical CO_2, while the

RESS method is more advantageous as a single-step process and with much reduced organic solvent usage. The potential of the RESS method could be enhanced by a better drug solubility in supercritical CO_2 through the use of cosolvent. The RESOLV process has demonstrated great potential in producing exclusively nanoscale drug particles, especially those drugs with little or no solubility in water. The produced drug particles are not only protected from agglomeration but also offer the much needed flexibility in their further processing such as coupling with biological species and for specific formulation and delivery requirements.

Despite the progress, there are still enormous challenges in the supercritical fluid processing of drug particles and related materials and systems. For example, the manipulation or even control of particle morphology, size, dispersion, crystallinity, and the drug distribution within polymeric particles is still in need of major improvement and optimization. The modeling and mechanistic understanding of the particle formation in the supercritical fluid processes, and also the influence of processing parameters and conditions on the product properties are generally considered as being only at the early stage. Equally important is the issue on the use of the technology at the industrial scale, for which a likely solution is through collaborations between industry and academia. In any case, the future is bright for the application of supercritical fluid technology in drug formulation and for enhanced drug delivery and other related applications.

Acknowledgment. Financial support from NSF and the Center for Advanced Engineering Fibers and Films (NSF-ERC at Clemson University) is gratefully acknowledged.

References

Alessi P, Cortesi A, Kikic I, Foster NR, Macnaughton SJ, Colombo I (1996) Particle production of steroid drugs using supercritical fluid processing, Ind Eng Chem Res 35:4718

Andes D (2003) In vivo pharmacodynamics of antifungal drugs in treatment of candidiasis, Antimicrob Agents Chemother 47:1179

Aniedobe NE, Thies MC (1997) Formation of cellulose acetate fibers by the rapid expansion of supercritical methanol solutions, Macromolecules 30:2792

Bekersky I, Fielding RM, Dressler DE, Lee JW, Buell DN, Walsh TJ (2002) Plasma protein binding of Amphotericin B and pharmacokinetics of bound versus unbound Amphotericin B after administration of intravenous liposomal Amphotericin B (AmBisome) and Amphotericin B Deoxycholate, Antimicrob Agents Chemother 46:834

Benedetti L, Bertucco A, Pallado P (1997) Production of micronic particles of biocompatible polymer using supercritical carbon dioxide, Biotechnol Bioeng 53:232

Bharadwaj S, Prasad GL (2002) Tropomyosin-1 a novel suppressor of cellular transformation is down regulated by promoter methylation in cancer cells, Cancer Lett 183:205

Bharadwaj S, Thanawala R, Bon G, Falcioni R, Prasad GL (2005) Resensitization of breast cancer cells to anoikis by Tropomyosin-1: role of rho kinase-dependent cytoskeleton and adhesion, Oncogene 56:8291

Blasig A, Shi CM, Enick RM, Thies MC (2002) Effect of concentration and degree of saturation on RESS of a CO_2-soluble fluoropolymer, Ind Eng Chem Res 41:4976–4983

Bright FV, McNally MEP (1992) Supercritical fluid technology: theoretical and applied approaches to analytical chemistry, American Chemical Society, Washington DC

Brennecke JF (1993) Supercritical fluid engineering science: fundamentals and applications, In: Kiran E, Brennecke JF, (eds) vol 11, American Chemical Society, Washington, DC

Burukhin AA, Churagulov BR, Oleynikov NN, Kolen'ko YV (1998) Nanostructured powders and their industrial applications, Mater Res Soc Symp Proc 520:171

Bustami RT, Chan HK, Dehghani F, Foster NR (2000) Generation of microparticles of proteins for aerosol delivery using high pressure modified carbon dioxide, Pharm Res 17:1360

Bustami RT, Chan HK, Dehghani F, Foster NR (2001) Recent applications of supercritical fluid technology to pharmaceutical powder systems, Kona 19:57

Bustami RT, Chan HK, Sweeney T, Dehghani F, Foster NR (2003) Generation of fine powders of recombinant human deoxyribonuclease using the aerosol solvent extraction system, Pharm Res 20:2028–2035

Chang CJ, Randolph AD (1989) Precipitation of microsize organic particles from supercritical fluids, AICHE J 35:1876

Charoenchaitrakool M, Deghani F, Foster NR, Chan HK (2000) Micronization by rapid expansion of supercritical solutions to enhance the dissolution rates of poorly water-soluble pharmaceuticals, Ind Eng Chem Res 39:4794

Chattopadhyay P, Gupta RB (2001a) Production of griseofulvin nanoparticles using supercritical CO_2 antisolvent with enhanced mass transfer, Int J Pharm 228:19

Chattopadhyay P, Gupta RB (2001b) Production of antibiotic nanoparticles using supercritical CO_2 as antisolvent with enhanced mass transfer, Ind Eng Chem Res 40:3530–3539

Chattopadhyay P, Gupta RB (2002) Protein nanoparticles formation by supercritical antisolvent with enhanced mass transfer AIChE J 48:235

Chen XX, Young TJ, Sarkari M, Williams RO, Johnston KP (2002) Preparation of cyclosporine A nanoparticles by evaporative precipitation into aqueous solution, Int J Pharm 242:3–14

Date AA, Patravale VB (2004) Current strategies for engineering drug nanoparticles, Curr Opin Colloid Interface Sci 9:222

Debenedetti PG (1994) Supercritical fluids: fundamentals for application, Kluwer Academic Publishers, Boston MA, pp. 273:719

Debenedetti PG, Tom JW, Kwauk X, Yeo SD (1993a) Rapid expansion of supercritical solutions (RESS)- Fundamentals and applications, Fluid Phase Equilib 82:311

Debenedetti PG, Tom JW, Yeo SD, Lim GB (1993b) Application of supercritical fluids for the production of sustained delivery devices, J Controlled Release 24:27

Del Valle EMM, Galan MA (2005) Supercritical fluid technique for particle engineering: Drug delivery applications, Rev Chem Eng 21:33

Dehghani F, Foster NR (2003) Dense gas anti-solvent processes for pharmaceutical formulation, Cur Opin Solid State Mater Sci 7:363

Dixon DJ, Johnston KP, Brodemier RA (1993) Polymeric materials formed by precipitation with a compressed fluid antisolvent, AIChE J 39:127

Dixon DJ, Lunabarcenas G, Johnston KP (1994) Microcellular microspheres and microballoons by precipitation with a vapor-liquid compressed fluid antisolvent, Polymer 35:3998

Domingo C, Berends EM, Vanrosmalen GM (1996) Precipitation of ultrafine benzoic acid by expansion of a supercritical carbon dioxide solution through a porous plate nozzle, J Cryst Growth 166:989

Domingo CE, Berends CE, Vanrosmalen GM (1997) Precipitation of ultrafine organic crystals from the rapid expansion of supercritical solutions over a capillary and a frit nozzle, J Supercrit Fluids 10:39

Donsi G, Reverchon E (1991) Micronization by means of supercritical fluids – possibility of application to pharmaceutical field, Pharma Acta Helv 66:170

Eckert CA, Knutson BL, Debenedetti PG (1996) Supercritical fluids as solvents for chemical and materials processing, Nature 383:313

Fages J, Lochard H, Letourneau JJ, Sauceau M, Rodier E (2004) Particle generation for pharmaceutical applications using supercritical fluid technology, Powder Technol 141:219

Falk R, Randoloh TW, Meyer JD, Kelley RM, Manning MC (1997) Controlled release of ionic compounds from poly (L-lactide) microspheres produced by precipitation with a compressed antisolvent, J Control Release 44:77

Foster NR, Mammucari R, Dehghani F, Barrett A, Bezanehtak K, Coen E, Combes G, Meure L, Ng A, Regtop HL, Tandya A (2003) Processing pharmaceutical compounds using dense gas technology, Ind Eng Chem Res 42:6476

Gao Y, Mulenda TK, Shi Y-F, Yuan W-K (1998) Fine particles preparation of Red Lake C Pigment by supercritical fluid, J Supercrit Fluids 13:369

Gallagher PM, Coffey MP, Krukonis VJ, Hillstrom WW (1992) Gas Antisolvent recrystallization of RDX – formation of ultra-fine particles of a difficult-to-comminute explosive, J Supercrit Fluids 5:130

Ginosar DM, Swank WD, Mcmurtery RD, Carmack WJ, (2000) Flow-Field studies of the RESS process, Proc 5th Int Symp Supercrit fluids, April 8–12, Atlanta

Griscik GJ, Rousseau RW, Teja AS (1995) Crystallization of N-Octacosane by the rapid expansion of supercritical solutions, J Cryst Growth 155:112

Hanna MH, York P (1998) Method and apparatus for the formation of particles, US5851453

Hartsel S, Bolard J (1996) Amphotericin B: new life for an old drug, Trends Pharmacol Sci 17:445

Helfgen B, Turk M, Schaber K (2000) Theoretical and experimental investigations of the micronization of organic solids by rapid expansion of supercritical solutions, Powder Technol 110:22

Huang Z, Sun GB, Chiew YC, Kawi S (2005) Formation of ultrafine aspirin particles through rapid expansion of supercritical solutions (RESS), Powder Tech 160:127

Hutchenson KW, Foster NR (1995) Innovations in supercritical fluids: science and technology, In: Hutchenson KW, Foster NR (eds), American Chemical Society, Washington, DC

Hu J, Johnston KP, Williams III RO (2004) Nanoparticle engineering processes for enhancing the dissolution rates of poorly water soluble drugs, Drug Dev Ind Pharm 30:233

Imhof A, Walter RB, Schaffner A (2003) Continuous infusion of escalated doses of Amphotericin B Deoxycholate: an open-label observational study, Clin Infect Dis 36:943–951

Jaarmo S, Rantakylä M, Aaltonen O, (1997) Particle tailoring with supercritical fluids: production of amorphous pharmaceutical particles, In: Saito S, Arai K (eds) Proceedings of 4th International Symposium on Supercritical Fluids, Sendai, vol A, pp. 263–266

Jessop PG, Leitner W (1999) Chemical synthesis using supercritical fluids, Wiley-VCH, Weinheim

Johnston KP, Penninger JML (1989) Supercritical fluid science and technology, American Chemical Society, Washington DC

Jovanovic N, Bouchard A, Hofland GW, Witkamp GJ, Crommelin DJA, Jiskoot W (2004) Stabilization of proteins in dry powder formulations using supercritical fluid technology, Pharm Res 21:1955

Jung J, Perrut MJ (2001) Particle design using supercritical fluids: Literature and patent survey, J Supercrit Fluids 20:179

Kajimoto O (1999) Solvation in supercritical fluids: Its effects on energy transfer and chemical reactions, Chem Rev 99:355

Kendall JL, Canelas DA, Young JL, DeSimone JM (1999) Polymerizations in supercritical carbon dioxide, Chem Rev 99:543

Kikic S, Sist P (2000) Applications of supercritical fluids to pharmaceuticals: Controlled drug release systems, In: Kiran E, Debenedetti PG, Peters CJ (eds) NATO Sci Ser, Kluwer Academic Publishers, Boston MA, p 291

Kim JH, Paxton TE, Tomasko DL (1996) Microencapsulation of naproxen using rapid expansion of supercritical solutions, Biotech Prog 12:650

Kitamura M, Yamamoto M, Yoshinaga Y, Masuoka H (1997) Crystal size control of sulfathiazole using high pressure carbon dioxide, J Cryst Growth 178:378

Klepser ME, Wolfe EJ, Jones RN, Nightingale CH, Pfaller MA (1997) Antifungal pharmacodynamic characteristics of Fluconazole and Amphotericin B tested against *Candida albicans*, Antimicrob Agents Chemother 41:1392

Knutson BL, Debenedetti PG, Tom JW (1996) Preparation of microparticulates using supercritical fluids, Drugs Pharm Sci 77 In: Microparticulate Systems for the Delivery of Proteins and Vaccines, Cohen S, Bernstein, H (eds), Marcel Dekker, New York, p 89

Kompella UB, Koushik K (2001) Preparation of drug delivery systems using supercritical fluid, Crit Rev Ther Drug Carrier Syst 18:173

Krukonis VJ (1984) Supercritical fluid nucleation of difficult-to-comminute solids, Annual Meeting AIChE, San Francisco

Krober H, Teipal U, Krause H (2000) Manufacture of submicron particles via expansion of supercritical fluids, Chem Eng Technol 23(9):763–765

Lele AK, Shine AD (1992) Morphology of polymers precipitated from a supercritical solvent, AICHE J 38:742

Lele AK, SHINE AD (1994) Effect of RESS dynamics on polymer morphology, Ind Eng Chem Res 33:1476

Leuner C, Dressman J (2000) Improving drug solubility for oral delivery using solid dispersions, Eur J Pharm Biopharm 50:47–60

Levelt Sengers JMH (1991) Supercritical fluid technology: reviews in modern theory and applications, In: Bruno TJ, Ely JF (eds), CRC Press, Boca Raton

Lewis RE, Wiederhold NP (2003) The solubility ceiling: a rationale for continuous infusion Amphotericin B therapy? Clin Infect Dis 37:871–872 and the references therein

Liu GT, Nagahama K (1996) Application of rapid expansion of supercritical solutions in the crystallization separation, Ind Eng Chem Res 35:4626

Lopes NM, Adams EG, Pitts TW, Bhuyan BK (1993) Cell kill kinetics and cell-cycle effects of Taxol on human and hamster ovarian cell-lines, Cancer Chemother Pharmacol 32:235

Mahadev K, Raval G, Bharadwaj S, Willingham MC, Lange EM, Vonderhaar B, Salomon D, Prasad GL (2002) Suppression of the transformed phenotype of breast cancer by tropomyosin-1, Exp Cell Res 279:40

Matson DW, Petersen RC, Smith RD (1986a) Psychopathology of sensory-impaired children, Adv Ceramic Mat 1:242

Matson DW, Petersen RC, Smith RD (1986b) The preparation of polycarbosilane powders and fibers during rapid expansion of supercritical fluid solutions, Mater Lett 4:429

Matson DW, Fulton JL, Petersen RC, Smith RD (1987a) Rapid expansion of supercritical fluid solutions – solute formation of powders, thin-films, and fibers, Ind Eng Chem Res 26:2298

Matson DW, Petersen RC, Smith RD (1987b) Production of powders and films by the rapid expansion of supercritical solutions, J Mater Sci 22:1919

Matson DW, Fulton JL, Smith RD, (1987c) Formation of fine particles in supercritical fluid micelle systems, Mater Lett 6:31

Matson DW, Petersen RC, Smith RD (1987d) Production of fine powders from the rapid expansion of supercritical solutions, Adv Ceram 21:109

Matson DW, Smith RD (1989) Supercritical fluid technologies for ceramic-processing applications, J Am Ceram Soc 72:871

Matson DW, Norton KA, Smith RD (1989) Making powder and film from supercritical fluid solutions, Chem Tech 19:480–486

Mawson S, Johnston KP, Combes JR, Desimone JM (1995) Formation of poly(1,1,2,2-tetrahydroperfluorodecyl acrylate) submicron fibers and particles from supercritical carbon-dioxide, Macromolecules 28:3182

Mawson S, Kanakia S, Johnston KP (1997a) Metastable polymer blends by precipitation with a compressed fluid antisolvent, Polymer 38:2957

Mawson S, Yates MZ, Oneill ML, Johnston KP (1997b) Stabilized polymer microparticles by precipitation with a compressed fluid antisolvent. 2. Poly(propylene oxide)- and poly(butylene oxide)-based copolymers, Langmuir 13:1519

McHugh M, Krukonis VJ (1994) Supercritical fluid extraction: principles and practice, 2nd Ed. Butterworth-Heinemann, Boston, MA

Meziani MJ, Sun Y-P (2002) Spectrophotometry study of aqueous salt solution in carbon dioxide microemulsions, Langmuir 18:3787

Meziani MJ, Rollins HW, Allard LF, Sun Y-P (2002) Protein-protected nanoparticles from rapid expansion of supercritical solution into aqueous solution, J Phys Chem B 106:11178

Meziani MJ, Sun Y-P (2003) Protein-conjugated nanoparticles from rapid expansion of supercritical fluid solution into aqueous solution, J Am Chem Soc 125:8015

Meziani MJ, Pathak P, Allard LF, Sun Y-P (2003) Nanoparticle formation in rapid expansion of water-in-carbon dioxide microemulsion into liquid solvent, Am Chem Soc Symp Ser 860:309

Meziani MJ, Pathak P, Hurezeanu R, Thies MC, Enick RM, Sun Y-P (2004) Supercritical-fluid processing technique for nanoscale polymer particles, Angew Chem Int Ed 43:704 HIGHLIGHTED by Lavine M (2004) Capturing polymer nanoparticles, Science 303:927

Meziani MJ, Pathak P, Beacham F, Allard LF, Sun Y-P (2005a) Nanoparticle formation in rapid expansion of water-in-supercritical carbon dioxide microemulsion into liquid solution, J Supercrit Fluids 34:91

Meziani MJ, Pathak P, Harruff BA, Hurezeanu R, Sun YP (2005b) Direct conjugation of semiconductor nanoparticles with Proteins, Langmuir 21:2008

Meziani MJ, Pathak P, Desai T, Sun Y-P (2006) Supercritical fluid processing of nanoscale particles from biodegradable and biocompatible polymers, Ind Eng Chem Res 45:3420

Mishima K, Matsuyama K, Tanabe D, Yamauchi S, Young TJ, Johnston KP (2000) Microencapsulation of proteins by rapid expansion of supercritical solution with a nonsolvent, AICHE J 46(4):857–865

Mohamed RS, Debenedetti PG, Prudhomme RK (1989a) Effects of process conditions on crystals obtained from supercritical mixtures, AICHE J 35:325

Mohamed RS, Halverson DS, Debenedetti PG, Prud'homme RK (1989b) Supercritical fluid science and technology ACS symposium Series 406, Washington DC, p. 355

Muhrer G, Mazzotti M (2003) Precipitation of lysozyme nanoparticles from dimethyl sulfoxide using carbon dioxide as antisolvent, Biotechnol Prog 19:549
Musie G, Wei M, Subramaniam B, Busch DH (2001) Catalytic oxidations in carbon dioxide-based reaction media, including novel CO_2-expanded phases, Coord Chem Rev 219:789
Nalesnik CA, Hansen BN, Hsu JT (1998) Solubility of pure taxol in supercritical carbon dioxide, Fluid Phase Equilibria 146:315
Ohgaki K, Kobayashi H, Katayama T, Hirokawa N (1990) Whisker formation from jet of supercritical fluid solution, J Supercrit Fluids 3:103
Pathak P, Meziani MJ, Desai T, Sun Y-P (2004) Nanosizing drug particles in supercritical fluid processing, J Am Chem Soc 126:10842
Pathak P, Meziani MJ, Sun Y-P (2005) Supercritical fluid technology for enhanced drug delivery, Expert Opin Drug Deliv 2:747
Pathak P, Meziani MJ, Desai T, Sun Y-P (2006) Formation and stabilization of Ibuprofen nanoparticles in supercritical fluid processing, J Supercrit Fluids 37:279
Pathak P, Meziani MJ, Desai T, Foster C, Sun Y-P (2007a) Supercritical fluid processing of drug nanoparticles in stable suspension, J Nanosci Nanotech 7:2542
Pathak P, Prasad GL, Meziani MJ, Joudeh AA, Sun Y-P (2007b) Nanosized Paclitaxel particles from supercritical carbon dioxide processing and their biological evaluation, Langmuir 23:2674
Petersen RC, Matson DW, Smith RD (1986) Rapid precipitation of low vapor-pressure solids from supercritical fluid solutions – the formation of thin-films and powders, J Am Chem Soc 108:2100
Petersen RC, Matson DW, Smith RD (1987) The formation of polymer fibers from the rapid expansion of supercritical fluid solutions, Polym Eng Sci 27:1693
Poliakoff M, George MW, Howdle SM (1996) Chemistry under extreme and non-classical conditions, In: van Eldik R, Hubbard CD (eds) John Wiley & Sons Inc., New York, p. 189
Rantakylä M, Jäntti M, Aaltonen O, Hurme M (2002) The effect of initial drop size on particle size in the supercritical antisolvent precipitation (SAS) technique, J Supercrit Fluids 24:251
Reverchon E (1999) Supercritical antisolvent precipitation of micro- and nano-particles, J Supercrit Fluids 15:1
Reverchon E (2003) Process for production of micro and/or nanoparticles, WO 03004142
Reverchon E, Adami R (2006) Nanomaterials and supercritical fluids, J Supercrit Fluids 37:1
Reverchon E, Della Porta G (1999) Production of antibiotic micro- and nano-particles by supercritical antisolvent precipitation, Powder Technol 106:23
Reverchon E, Della Porta G (2003a) Particle design using supercritical fluids, Chem Eng Tech 26:840
Reverchon E, Della Porta G (2003b) Micronization of antibiotics by supercritical assisted atomization, J Supercritic Fluids 26:243
Reverchon E, De Marco I (2004) Supercritical antisolvent micronization of cefonicid: thermodynamic interpretation of results, J Supercrit Fluids 31:207
Reverchon E, De Marco I (2006) Supercritical antisolvent precipitation of Cephalosporins, Powder Tech 164:139–146
Reverchon E, Dellaporta G, Taddeo R, Pallado P, Stassi A (1995) Solubility and micronization of griseofulvin in supercritical CHF_3, Ind Eng Chem Res 34:4087
Reverchon E, Donsi G, Gorgoglione D (1993) Salicylic-acid solubilization in supercritical CO_2 and its micronization by RESS, J Supercrit Fluids 6:241

Rogers TL, Johnston KP, Williams III RO (2001) Solution-based particle formation of pharmaceutical powders by supercritical or compressed fluid CO_2 and cryogenic spray-freezing technologies, Drug Dev Ind Pharm 27:1003

Rogers TL, Johnston KP, Williams III RO (2003) Physical stability of micronized powders produced by spray-freezing into liquid (SFL) to enhance the dissolution of an insoluble drug, Pharm Develop Tech 8:187–197

Rollins H (1999) Preparation and characterization of nanoscale materials, Dissertation, Clemson University

Rowinsky EK, Cazenave LA, Donehower RC (1990) Taxol – a novel investigational antimicrotubule agent, J Nat Cancer Inst 82:1247

Sane A, Thies MC (2005) The formation of fluorinated tetraphenylporphyrin nanoparticles via rapid expansion processes: RESS vs RESOLV, J Phys Chem B 109:19688

Sauceau M, Letourneau JJ, Freiss B, Richon D, Fages J (2004) Solubility of eflucimibe in supercritical carbon dioxide with or without a co-solvent, J Supercrit Fluids 31:133

Savage PE (1999) Organic chemical reactions in supercritical water, Chem Rev 99:603

Schmitt WJ, Salada MC, Shook GG, Speaker SMI (1995) Finely-divided powders by carrier solution injection into a near or supercritical-fluid, AIChE J 41:2476

Sellers SP, Clark GS, Sievers RE, Carpenter JF (2001) Dry powders of stable protein formulations from aqueous solutions prepared using supercritical CO_2-assisted aerosolization, J Pharm Sc 90:785

Shekunov B, Sun Y, Astracharchik E, York P, Baldyga J (2000) Optical characterisation and mechanism of antisolvent precipitation in turbulent flow, Proc. 7th Meeting on Supercritical Fluids, vol. 1, ISASF International Society for the Advancement of Supercritical Fluids, Nancy, France, pp. 65–70

Shekunov BY, York P (2000) Crystallization processes in pharmaceutical technology and drug delivery design, J Crystal Growth 211:122

Sievers RE, Huang ETS, Villa JA, Engling G, Brauer PR (2003) Micronization of water-soluble or alcohol-soluble pharmaceuticals and model compounds with a low-temperature Bubble Dryer (R), J Supercrit Fluids 26:9

Sloan R, Hollowood ME, Humpreys GO, Ashraf W, York P (1998) Preparation of stable protein particles. Proceedings of the 5th meeting on Supercritical fluids, In: Perrut M, Subra P (eds), 23–25 March, Nice, 301

Smith RD, Fulton JL, Petersen RC, Kopriva AJ, Wright BW (1986) Performance of capillary Restrictors in supercritical fluid chromatography, Anal Chem 58:2057

Snavely WK, Subramaniam B, Rajewski RA, Defelippis MR (2002) Micronization of insulin from halogenated alcohol solution using supercritical carbon dioxide as an antisolvent, J Pharm Sci 91:2026

Squires TG, Paulaitis ME (1987) Supercritical fluids: chemical and engineering principals, American Chemical Society, Washington DC

Stanton LA, Dehghani F, Foster NR (2002) Improving drug delivery using polymers and supercritical fluid technology, Aust J Chem 55:443

Subramaniam B, Rajewski RA, Snavely K (1997a) Pharmaceutical processing with supercritical carbon dioxide, J Pharm Sci 86:885

Subramaniam B, Saim S, Rajewski RA, Stella V (1997b) Method of particle precipitation and coating using nearcritical and supercritical antisolvents, US5833891

Suleiman D, Estevez LA, Pulido JC, Garcia JE, Mojica C (2005) Solubility of anti-inflammatory anti-cancer and anti-HIV drugs in supercritical carbon dioxide, J Chem Eng Data 50:1234

Sun Y-P (2002) Supercritical fluid technology in materials science and engineering: synthesis, properties, and applications, Marcel Dekker, New York

Sun Y-P, Atorngitjawat P, Meziani MJ (2001) Preparation of silver nanoparticles via rapid expansion of water in carbon dioxide microemulsion into reductant solution, Langmuir 17:5707

Sun Y-P, Bunker CE (1995) Solute and solvent dependencies of intermolecular interactions in different density regions in supercritical fluids – A generalization of the 3-density-region salvation mechanism, Ber Bunseges Phys Chem 99:976

Sun Y-P, Guduru R, Lin F, Whiteside T (2000) Preparation of nanoscale semiconductors through the rapid expansion of supercritical solution (RESS) into liquid solution, Ind Eng Chem Res 39:4663

Sun Y-P, Meziani MJ, Pathak P, Qu L (2005) Polymeric nanoparticles from rapid expansion of supercritical-fluid solution, Chem Eur J 11:1366

Sun Y-P, Rollins HW (1998) Preparation of polymer-protected semiconductor nanoparticles through the rapid expansion of supercritical fluid solution, Chem Phys Lett 288:585

Sun Y-P, Riggs JE, Rollins HW, Guduru R (1999a) Strong optical limiting of silver-containing nanocrystalline particles in stable suspensions, J Phys Chem B 103:77

Sun Y-P, Rollins HW, Guduru R (1999b) Preparations of nickel, cobalt, and iron nanoparticles through the rapid expansion of supercritical fluid solutions (RESS) and chemical reduction, Chem Mater 11:7

Tai CY, Cheng CS (1997) Crystal morphology and growth rate of naphthalene in various processes involving supercritical carbon dioxide, Chem Eng Res Des 75:228

Tan HS, Borsadia S (2001) Particle formation using supercritical fluids: Pharmaceutical applications, Expert Opin Ther Pat 11:861

Taylor LT (1996) Supercritical fluid extraction, JohnWiley & Sons, Inc., NewYork

Teja AS, Eckert CA (2000) Commentary on supercritical fluids: Research and applications, Ind Eng Chem Res 39:4442–4444

Ting SST, Macaughton SJ, Tomasko DL, Foster NR (1993) Solubility of naproxen in supercritical carbon-dioxide with and without cosolvents, Ind Eng Chem Res 32:1471

Thakur R, Gupta RB (2005) Rapid expansion of supercritical solution with solid cosolvent (RESS-SC) process: Formation of griseofulvin nanoparticles, Ind Eng Chem Res 44:7380

Thakur R, Gupta RB (2006a) Rapid expansion of supercritical solution with solid cosolvent (RESS-SC) process: Formation of 2-aminobenzoic acid nanoparticle, J Supercrit Fluids 37:307

Thakur R, Gupta RB (2006b) Formation of phenytoin nanoparticles using rapid expansion of supercritical solution with solid cosolvent (RESS-SC) process, Int J Pharm Sci 308:190

Tom JW, Debenedetti PG (1991) Formation of bioerodible polymeric microspheres and microparticles by rapid expansion of supercritical solutions, Biotech Prog 7:403

Tom JW, Debenedetti PG, Jerome R (1994) Precipitation of poly(L-LACTIC acid) and composite poly(L-LACTIC acid) – pyrene particles by rapid expansion of supercritical solutions, J Supercrit Fluids 7:9

Tucker SC (1999) Solvent density inhomogeneities in supercritical fluids, Chem Rev 99:391

Tu SL, Dehghani F, Foster NR (2002) Micronisation and micro encapsulation of pharmaceuticals using a carbon dioxide antisolvent, Powder Tech 126:134

Vandana V, Teja AS (1997) The solubility of paclitaxel in supercritical CO_2 and N_2O, Fluid Phase Equilibria 135:83

Vemavarapu C, Mollan MJ, Lodaya M, Needham TE (2005) Design and process aspects of laboratory scale SCF particle formation systems, Int J Pharm 292:1

Von Rohr PR, Treep C (1996) High pressure chemical engineering, Elsevier, Amsterdam

Wang Y, Pfeffer R, Dave R, Enick R (2005) Polymer encapsulation of fine particles by a supercritical antisolvent process, AICHE J 51:440

Weber M, Thies MC (2002) Supercritical fluid technology in materials science and engineering: Synthesis properties and applications, In: Sun YP (ed), Marcel Dekker, New York, pp. 387–437

Werling JO, Debenedetti PG (2000) Numerical modeling of mass transfer in the supercritical antisolvent process: miscible conditions, J Supercrit Fluids 18:11

Williams JR, Clifford AA, Bartle KD, Kee TP (1998) The production of fine particles of metal complexes using supercritical fluids, Powder Technol 96:158

Winters MA, Knutson BL, Debenedetti PG, Sparks HG, Przybycien TM, Stevenson CL, Prestreslki SJ (1996) Precipitation of proteins in supercritical carbon dioxide, J Pharm Sci 85:586

Yates MZ, Li G, Shim JJ, Maniar S, Johnston KP, Lim KT, Webber S (1999) Ambidextrous surfactants for water-dispersible polymer powders from dispersion polymerization in supercritical CO_2, Macromolecules 32:1018–1026

Yeo SD, Debenedetti PG, Patro SY, Przybycien TM (1994) Secondary structure characterization of microparticulate insulin powders, J Pharm Sci 83:1651

Yeo SD, Kiran E (2005) Formation of polymer particles with supercritical fluids: A review, J Supercrit Fluids 34:287

York P (1999) Strategies for particle design using supercritical fluid technologies, Pharm Sci Tech Today 2:430

York P, Hanna M (1996) Particle engineering by supercritical technologies for powder inhalation drug delivery, Respir Drug Delivery V, Program Proc, Pheonix AZ, pp. 231–239

York P, Kompella UB, Shekunov BY (2004) Supercritical fluid technology for drug product development, Marcel Dekker, New York

Young TJ, Mawson S, Johnston KP, Henriksen I B, Pace GW, Mishra AK (2000) Rapid expansion from supercritical to aqueous solution to produce submicron suspensions of water-insoluble drugs, Biotech Progress 16:402

4

Nanotubes, Nanorods, Nanofibers, and Fullerenes for Nanoscale Drug Delivery

Jessica B. Melanko, Megan E. Pearce, and Aliasger K. Salem

Introduction

A drug's delivery vehicle can have a significant impact on its efficacy. Nanoscale manipulation of drug delivery vehicles can substantially improve pharmacokinetics, pharmacodynamics, non-specific toxicity, immunogenicity, and biorecognition properties (Dillon et al. 1999; Kopecek 2003; Couvreur 2006). As a result, applying these technologies to pharmaceutical development has the potential to revolutionize the delivery of biologically active compounds.

The ideal drug delivery system needs to protect drugs from degradation via enzymatic, mechanical, or chemical pathways. It should also have enhanced diffusion through the epithelium, targeted tissue distribution, or increased penetration into its target cell depending on the application (Couvreur 2006). Therefore, drug delivery vehicles need to be rationally designed to overcome many of these physical barriers. Of the inorganic delivery systems currently in development, nanotubes, nanorods, fullerenes, and nanofibers show some of the greatest promise in physical manipulation and synthesis for optimal drug conjugation and transport.

Nanotubes

Carbon nanotubes (CNT) have shown substantial potential in a variety of biological applications including use as DNA and protein biosensors, ion channel blockers, bioseparators, and biocatalysts (Bianco et al. 2005a). This potential stems from their specific surface or adaptable size-dependent properties in combination with their anisotropic character. Their anisotropy is of consequence since it influences their electronic, photonic, mechanical, and chemical properties (Ajima et al. 2005).

The first successful multi-walled carbon nanotube synthesis was demonstrated in 1991, and the first single-walled carbon nanotube synthesis followed in 1993 (Iijima 1991; Martin Steinhart et al. 2003). Multiple methods of synthesis have subsequently been reported. These include self-assembly of precursor compounds (Iijima and Ichihashi 1993), vapor

M.M. de Villiers et al. (eds.), *Nanotechnology in Drug Delivery*, DOI: 10.1007/978-0-387-77667-5_4,

deposition (Lam et al. 2004), and template synthesis (Whitesides et al. 1991; Schmidt and Eberl 2001; Martin Steinhart et al. 2003). The method of synthesis determines its innate physicochemical properties.

Physical–Chemical Properties

The chemical composition of a nanotube can have significant impact on its structure. Polymeric nanotubes are hollow, molecular scale versions of nanowires (Shim et al. 2002). Carbon nanotubes are cylindrical macromolecules with variable radii starting at a few nanometers with maximum lengths up to 20 cm (Martin Steinhart et al. 2003). CNTs have an allotropic crystalline carbonic form that is consistent with fullerenes (Zhu et al. 2002). There are two main types of carbon nanotubes. The first of these is the single-wall carbon nanotube (SWCNT), which is composed of a hexagonal lattice of carbon atoms equivalent to atomic planes of graphite (Figure 4.1) ranging in diameter from 7 to 16 Å (Dresselhaus M et al. 1996a). The second is the multi-wall nanotube (MWCNT), consisting of a concentric arrangement of similar graphene sheets that are spaced by a distance of approximately 3.4 Å. This is comparable to the distance found between planes of graphite (Dresselhaus M et al. 1996a; Bianco et al. 2005a; Klumpp et al. 2006). These MWCNTs can reach diameters of up to 100 nm (Lu 1997). Both single- and multi-walled tubes are capped at their ends by one half of a fullerene-like molecule (Balasubramanian and Burghard 2005; Bianco et al. 2005a; Bianco et al. 2005b; Klumpp et al. 2006). However, open-ended tubules have also been reported (Dresselhaus M et al. 1996a). In addition, nanotubes are able, due to strong Van der Waals forces, to self-organize into hexagonal-ordered rope-like structures consisting of 50–100 tubes that range in lengths up to several microns (Lu 1997).

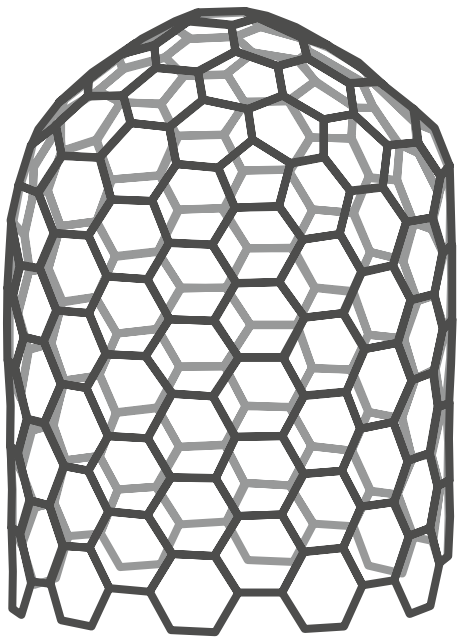

Figure 4.1 A representation of a single-wall carbon nanotube structure with a fullerene-like cap.

CNTs produced at lower temperatures have increased surface defects in both the walls and caps than those formed at higher temperatures. As a result, several shapes of nanotubes have been produced, such as straight, corkscrew, and bamboo structured (Sinnott and Andrews 2001).

Carbon nanotubes are generally acknowledged as the ultimate carbon fiber with a high strength and superior thermal conductivity (Iijima 1991; Yu et al. 2000; Klumpp et al. 2006). A CNT can behave as a metal or a semiconductor, depending on its chiral vector (J.G. Wen et al. 2001b; Haddon 2002). According to molecular dynamics simulations, CNTs have a Young's modulus several times greater than that of diamond (Hone et al. 2000). They also possess enhanced field emission properties (Lu 1997).

The chemical modification and solubilization of carbon nanotubes is essential to their successful application in drug delivery. Atomically ordered, carbon nanotubes demonstrate low chemical reactivity (Sinnott and Andrews 2001). However, many researchers have reported successful functionalization of both the ends and side-walls of SWCNTs and MWCNTs (Yao et al. 1998). In addition, nanotubes have the advantage of facile DNA, peptide, or other molecular incorporation into their hollow space (Sun et al. 2002; Bianco et al. 2005a).

Ideal SWCNTs contain two separate regions, each with a unique reactivity toward covalent chemical modification. The intermittent five-membered rings on the caps increase reactivity at these points to levels similar to fullerenes (Balasubramanian and Burghard 2005). The functionalization of carbon nanotubes can broadly be divided into two categories: (a) direct attachment of functional groups to the graphitic surface and (b) the use of the nanotube-bound carboxylic acids (Bianco et al. 2005b). For example, functionalization of CNTs using polyethylene-oxide chains has been achieved by using carboxylic acid end groups (Jain 2005). This imparts the nanotubes with enhanced water solubility and non-specific protein-resistant properties. Surface functionalization in this manner enables adsorption or attachment of various molecules or antigens. This provides a mechanism for specific recognition and cell targeting (Shim et al. 2002; Ajima et al. 2005). Nanotubes, therefore, have significant potential for targeted drug delivery.

Nanotubes in Drug Delivery

Toxicity

The ideal drug delivery vehicle must also display low toxicity. Nanotubes have displayed low toxicity but this is dependent on the route of administration and surface functionalization.

The high aspect ratio of carbon nanotubes gives them unique toxicological profiles (Vasir et al. 2005).

For example, exposure of human epidermal keratinocytes (HaCaT) to unrefined and unfunctionalized SWCNT has been shown to result in increased oxidative stress resulting in accelerated free radical generation, accumulation of peroxidative products, a decrease of intracellular levels of glutathione, oxidation of protein SH groups, and depletion of total antioxidant reserve and vitamin E 18 hours after exposure. Ultrastructure

and morphological changes were also observed in the cells (Shvedova et al. 2003). Culture of SWCNT with human embryonic kidney (HEK293) cells resulted in a downregulation of genes related to signal transduction, cellular arrest in the G_1/S phase, marked decrease in translation of adhesive proteins (laminin, fibronectin, FAK, and cadherin), and formation of nodular structures (Cui et al. 2005). Similar results have also been noted within rat cardiac muscle cells (H9c2) (Garibaldi et al. 2006). These observations have also been seen with in vivo rat pulmonary experiments (Lam et al. 2004).

Cellular toxicity has been attributed to the insolubility of non-functionalized carbon nanotubes and the associated traces of catalyst materials such as nickel, iron, or cobalt (Dillon et al. 1999; Donaldson et al. 2004). To overcome this, nanotubes can be purified via oxidation with strong acid treatments that allow for the removal of the metallic impurities (Figure 4.2) (Dillon et al. 1999; J.G. Wen et al. 2001; Bianco et al. 2005b). Nevertheless, unfunctionalized nanotubes, whether purified or unrefined, are toxic.

In contrast to unfunctionalized CNTs, chemically functionalized CNTs are soluble in aqueous biological media (Bianco et al. 2005b). Experimental results have consistently demonstrated that functionalized SWCNT themselves exhibit low toxicity (Malik et al. 2000; Shvedova et al. 2003; Lam et al. 2004; Cui et al. 2005; Carrero-Sanchez et al. 2006; Garibaldi et al. 2006; Panessa-Warren et al. 2006; Warheit 2006). Moreover, it has been shown that peptide-functionalized CNTs are able to enhance an antibody-mediated response against the peptide with no discernable cross-reactivity to the nanotubes themselves, thus demonstrating a lack of immunogenicity (Salvador-Morales et al. 2006).

Cellular Behavior and Uptake

Carbon nanotubes enhance uptake of both small molecules, large proteins, and amino acids that have previously demonstrated low cellular penetration (Klumpp et al. 2006). This cell-penetrating ability can be enhanced further by conjugation of cell-penetrating peptides onto the carbon nanotubes.

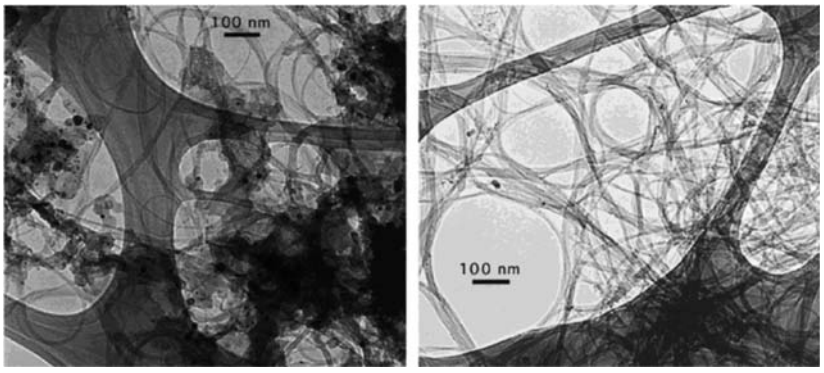

Figure 4.2 Transmission electron microscopy images of as-produced ~20 W/cm^2 laser-generated SWNT soot (left) and purified SWNTs produced by (1) refluxing in 60 mL 3 M HNO_3 for 16 hours at 120°C followed by (2) oxidizing for 30 min in air at 550°C (A. C. Dillon 1999).

Because carbon nanotubes have a high loading capacity for cargo molecules due to their innately high aspect ratios, they have the potential to be ideal shuttles for peptide antigens. Carbon nanotubes with attached protein conjugates have been found to possess antibody recognition equal to that of free peptides, indicating that the integrity and functionality of a nanotube-linked peptide is maintained (Ajima et al. 2005).

The mechanism for cellular uptake of nanotubes is not yet entirely understood. However, two routes of internalization have been proposed. In the first, functionalized nanotubes have been shown to penetrate a cell via passive diffusion across the lipid bilayer in a needle-like manner. The second mechanism stems from the observation that cellular endocytosis serves as the route for internalization of CNTs with adsorbed surface proteins (Klumpp et al. 2006).

An advantage to delivering non-solution-based therapies for cancer treatment is the ubiquitous leaky vasculature serving the cancerous tissues. The rampant vascular structure, created due to the rapid vascularization necessary to feed fast-growing cancers, couples inadequate lymphatic drainage and allows an enhanced permeation and retention effect (EPR effect) (Brannon-Peppas and Blanchette 2004). Large clusters of SWCNTs, known as single-wall carbon nanohorns (SWCNH), have an ideal morphology for utilizing the EPR effect (Maeda et al. 2001). For example, cisplatin, an anticancer agent, can easily be incorporated into SWCNH structures (Figure 4.3 d, e, f). This delivery system increased anticancer activity within human lung cancer cells (NCl-H460). Furthermore, it was demonstrated that single-wall carbon nanohorns alone produced no such effect (Figure 4.3 a–c) (Ajima et al. 2005).

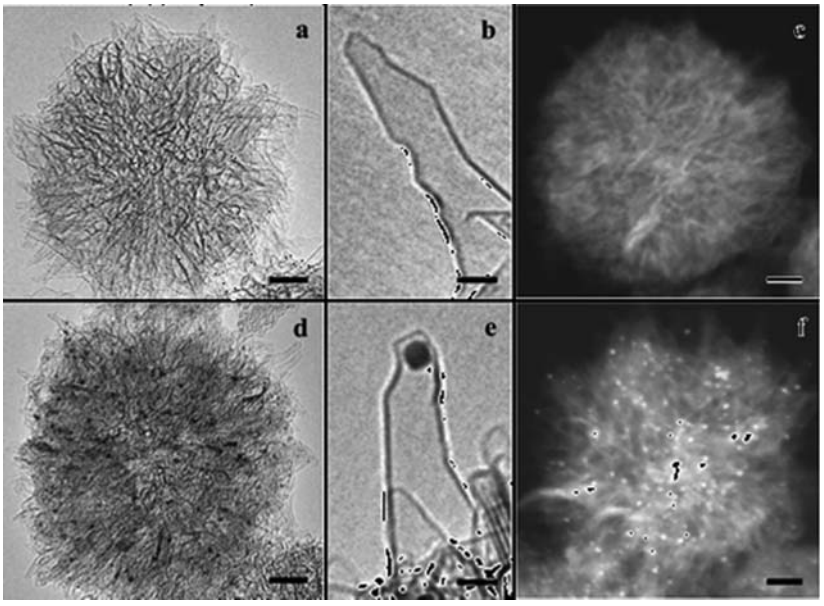

Figure 4.3 (**a,b**) HRTEM images of oxidized SWCNH with scale bars at 10 and 2 nm, respectively. (**c**) Z-contrast image of oxidized SWCNH aggregate (10 nm). (**d,e**) HRTEM images of cisplatin-loaded oxidized SWCNH (10 and 2 nm) in which the black spots of the cisplatin clusters can be found. (**f**) Z-contrast image of cisplatin-loaded SWCNH; the bright spots are the drug aggregates (Ajima et al. 2005).

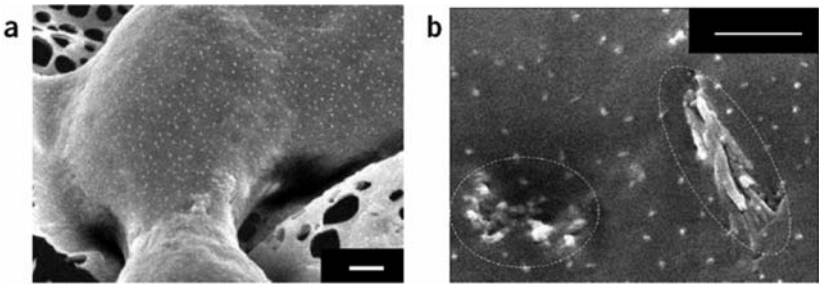

Figure 4.4 Nanotube spearing in MCF-7 cells. (**a**) Cell membrane without spearing at 1 μm scale. (**b**) Cell membrane following spearing. The scale is 500 nm with the dashed ovals showing imbedded nanoparticles. The microvilli in the membranes have the same site density: 15 microvilli/μm^2 (Cai D 2005).

The cell-penetrating properties of carbon nanotubes in combination with the magnetic properties of nickel have also been used to drive nickel-embedded nanotubes into cell membranes. The momentum achieved with the magnetic field is of sufficient strength to ferry adjoined macromolecules and proteins immobilized on the carbon nanotubes into the cell. The process involves utilizing vertically aligned carbon nanotubes that have nickel particles encased within their tips, which provide controlled response to magnetic manipulation. Images of cellular membranes prior to and after nanotube spearing can be seen in Figure 4.4.

Carbon nanotubes represent one of the few materials with as much potential accompanied with as many challenges. Considerations for success of the use of nanotubes in drug delivery include:

- Preparation of carbon nanotubes
- Purification from catalyst residues, carbon nanoparticles, and amorphous carbon
- Separation according to length, diameter, chirality
- Division of semi-conducting and metallic nanotubes
- Thorough control and comprehension of their formation and chemistry (Steinle et al. 2002)

In drug delivery, it is widely agreed that key progress will be made through functionalization. Since there are a variety of cellular receptors and mechanisms for internalization, nanotube uptake will also be dependent on the nature of functionalization. With successful surface modifications, carbon nanotubes have potential to be a vehicle used for compartment-specific targeting (Balasubramanian and Burghard 2005).

Nanorods

Nanorods have unique innate chemical, electrical, magnetic, and optical anisotropy, thus allowing them to interact with cells, tissues, and biomolecules in fundamentally novel ways (Bauer et al. 2004). The two most frequently used methods of manufacturing nanorods involve template

synthesis (Bianco et al. 2005a) and chemical synthesis (Jana N 2001; Salem et al. 2003; Gole and Murphy 2004). Template synthesis involves electrochemical deposition into a non-conducting membrane that has an array of cylindrical pores (Whitney et al. 1993; Martin 1994). Subsequent removal of the membrane by etching yields metallic nanorods of controlled dimensions. Template synthesis is advantageous because it is easily adapted for the deposition of multiple submicrometer segments. Furthermore, template synthesis can produce large quantities of monodisperse nanorods, and properties such as aspect ratio can be controlled in a systematic way (Salem et al. 2003).

Metallic nanorods for bioapplications are most frequently synthesized from gold, copper, platinum, or silver (Bauer et al. 2004; Salem et al. 2004; Salem et al. 2005). Inorganic metallic nanorods are obtainable on a micron to Ångstrom scale (Glomm 2005), and possess physical and chemical characteristics completely unique of their bulk properties. Gold is the most widely used inorganic material in diagnostic and delivery nanoparticulate research, and the following section will be devoted to illustrating its properties and bioapplications.

Gold nanoproperties are different from bulk properties because of a change in the quantum confinement of electron motion (Huang 2006). As particles become smaller, their surface:interior atomic ratio increases until the surface properties become a primary behavioral factor. The coherent collective oscillation of electrons in noble metals within the conduction band induces large surface electric fields. This greatly enhances the radiative properties of nanoparticles when they associate with resonant electromagnetic radiation as shown in Figure 4.5 (Huang 2006). Gold nanoparticles have been used to demonstrate multiphoton absorption-induced luminescence (MAIL), where particular tissues or cells are fluorescently labeled. Gold nanoparticles emit light that is so intense that it is easily possible to observe a single nanoparticle at laser intensities lower than those commonly used for MAIL (Farrer et al. 2005). Gold nanoparticles will maintain emission intensity, regardless of the duration of their excitation. These

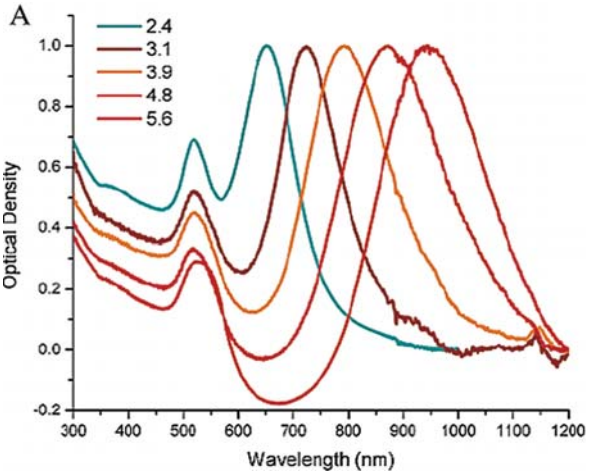

Figure 4.5 Surface plasmon absorption spectra of gold nanorods with varying aspect ratios; this demonstrates the sensitivity of the strong longitudinal band to the aspect ratios of the nanorods (Huang 2006). (*See* Color Plate 9)

observations promote the concept of metal nanoparticles as a workable alternative to fluorophores or semiconductor nanoparticles for biological labeling and imaging (Jain 2005). In addition, they are excellent contrast agents and are able to convert radiation to heat in picoseconds, also giving them potential in photothermal cancer therapy (El-Sayed 2005).

Gold nanorods have many other uses as well. For instance, they are used as a linking molecule to assemble biosensors for DNA detection. Gold nanoparticles can replace fluorescent molecules for attachment of antibodies and other molecules, such as DNA. Multi-component nanorods can even act as bar codes (Nicewarner-Pena, Freeman et al. 2001). Because many copies of an antibody or DNA can be attached to a single nanoparticle, this approach proves to be much more sensitive and accurate than the fluorescent molecule tests (Jain 2005).

Nanorods in Drug Delivery

Cellular Behavior and Uptake

Gold nanorods allow for a simple bottom-up approach to the development of nanoscale delivery systems. In comparison to spherical particles, asymmetric particles offer additional degrees of freedom in self-assembly due to their inherent shape anisotropy (Sun et al. 2002; Chen, Sun et al. 2003). Furthermore, the ability to synthesize nanoparticles with different segments provides the opportunity to introduce multiple chemical functionalities by exploiting the selective binding of different ligands to the different segments (Benjamin R. Martin 1999; Nicewarner-Pena 2001; Salem et al. 2003; Salem et al. 2004).

This ability to engineer nanorods with multiple functionalities in spatially defined regions offers the potential for increased efficacy for drug and gene delivery systems over alternative single-component inorganic non-viral vectors (Salem et al. 2005). For example, we have assembled a non-viral gene delivery system based on multisegment bimetallic nanorods that can simultaneously bind compacted DNA plasmids and targeting ligands in a spatially defined manner (Figure 4.6). This approach allows precise control of composition, size, and multi-functionality of the gene delivery system. Transfection experiments performed in vitro and in vivo provided promising results that have subsequently shown potential in genetic vaccination applications. The goal in immunotherapeutic vaccinations is to target antigens to macrophages or dendritic cells (key antigen-presenting cells or APCs). APCs process these antigens via class I or class II pathways where they bind to major histocompatibility complexes that present the antigen on the surface of the APCs. These APCs then traffic themselves to the lymphoid organs where T lymphocytes that scavenge the surfaces of the APCs become stimulated to respond against the antigen presented (Raychaudhuri 1998). When the encoded antigen is tumor specific, for example, a strong CD8+ T-cell and antibody response can be generated for protection and prevention against that tumor (Cheng, Hung et al. 2001; Hung CF. 2003). We have developed an inorganic nickel–gold nanorod vector that can generate transient transgene expression when

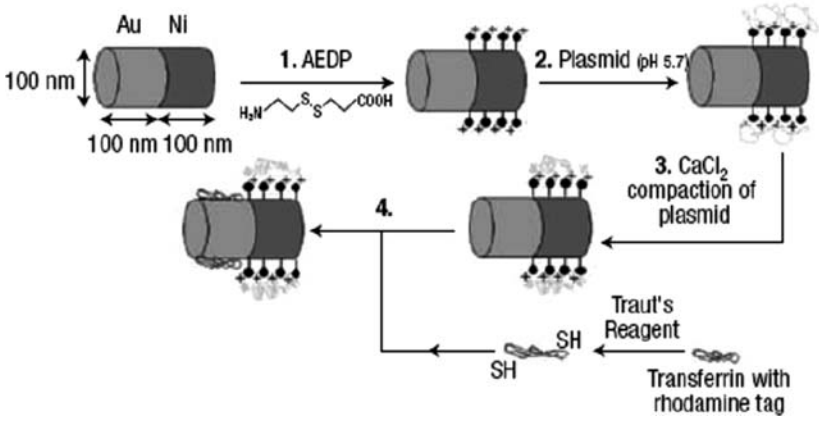

Figure 4.6 A brief illustration of nanorod functionalization. Nanorods are incubated with the 3-[(2-aminoethyl) dithio] propionic acid (AEDP) linker. The carboxylate end-group binds to the Ni segment. The disulphide linkage acts as a cleavable point within the spacer to promote DNA release within the reducing environment of the cell (Salem et al. 2003).

bombarded into skin, which has a natural abundance of antigen-presenting cells (Salem et al. 2005). These nanorods therefore have potential for a variety of vaccination applications.

In addition to active targeting with ligand functionalization, nanorods can be easily manufactured at various aspect ratios or readily surface engineered for passive targeting. The physicochemical properties of nanorods are major factors in the characteristic biodistribution and residence times of these particles in vivo (Nishikawa 1998; Takakura 2002). For example, particle size is a significant determinant of extravasation rate, and surface charge can impact non-specific uptake and degradation by macrophages (Bergen 2006). Additionally, particles with engineered hydrophobic surfaces are preferentially taken up by the liver, followed by the spleen and lungs (Gaur et al. 2000; Brannon-Peppas and Blanchette 2004). Similar to nanotubes, nanorods offer significant potential in the formation of cell-penetrating complexes for drug or probe molecule delivery (J. K. N. Mbindyo et al. 2001).

Toxicity

Elemental gold is known as one of the most biocompatible materials for use in drug delivery due to its chemical inertness (Qin 2006). In a sample of gold nanoparticles tested for uptake and acute toxicity in human leukemia cells, the results indicated that although some precursors of nanoparticles may be toxic, the nanoparticles themselves are not necessarily detrimental to cellular morphology, proliferation, or function (Ellen E. Connor et al. 2005). Furthermore, cellular transfection studies have been carried out demonstrating the biocompatibility of nanorods for delivery function (Salem et al. 2003).

Aside from high stability and low toxicity, other advantages of the gold nanorods are that the particles can be prepared easily and they can be

attached readily to molecules of biological interest. In addition, the laser light that is now being used for visualization and cancer treatment is at a wavelength that causes only minimal damage to most biological tissues. Eventually, nanorod technology could enable the tracking of a single drug molecule in a cell or in other biological samples (Jain 2005).

Nanofibers

In the areas of tissue engineering and drug delivery, nanofibers have emerged as biocompatible, biodegradable scaffolds, and delivery vehicles (Figure 4.7). They are used for the replacement of tissues with structural or physiological deficiencies. The use of nanofibers in tissue restoration can potentially produce an efficient, compact organ with a rapid recovery process. This is because of the large surface area that polymer and protein-based nanofibers possess. Additionally, the large surface area helps to support cell growth on the scaffold materials. These characteristics are also advantageous for wound healing, the construction of biocompatible prostheses and bone substitutes, implant epithelialization, and drug delivery applications. Nanofibrous scaffolds designed to elicit specific cellular responses through the incorporation of signaling ligands, such as growth factors or DNA fragments, show particular promise for future treatment strategies (Venugopal and Ramakrishna 2005).

Nanofibers of different chemistries and structures can be formed by self-assembly at the molecular level. These nanofibers have potential applications in the promotion of cell adhesion and growth, targeted drug delivery, tissue engineering, and filtration systems for toxic chemicals (Thandavamoorthy et al. 2006). For example, the pentapeptide epitope IKVAV is an amino acid sequence of laminin that promotes neurite adhesion. Amphiphiles that present this sequence can self-assemble in aqueous media, or at the site of injection in tissues, and fibers with a diameter of 5–10 nm are formed (Moghimi et al. 2005). These scaffolds discourage astrocyte development while inducing prompt differentiation to neurons. These findings suggest that synthetic materials such as these self-assembling nanofibers may have the ability to modulate selective gene expression. In another instance, self-assembling nanofibers have been

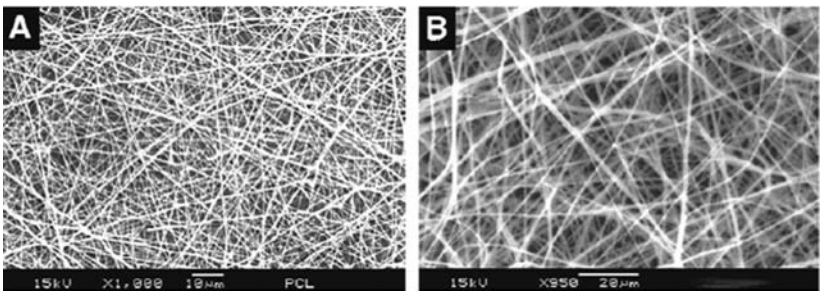

Figure 4.7 **A**. Polycaprolactone (PCL) nanofibers. Polycaprolactone (9%). 724 nm; **B**. Collagen (0.85%) nanofibers. 261 nm (Venugopal and Ramakrishna, 2005).

developed that promote angiogenesis both in vitro and in vivo. The nanofibers contain multiple binding sites for heparin and other compounds necessary for new blood vessel growth. The release of these proteins as nanofibers break down can stimulate neighboring cells for continued growth (Service 2005; Rajangam et al. 2006). An alternative approach to natural collagen is the use of synthetic collagen substitutes that self-assemble into nanocylindrical structures. The nanofiber is made up of a long hydrophobic alkyl group on one end and a hydrophilic peptide on the other end. These nanocylinders can direct the formation of hydroxyapatite crystallites with dimensions and orientations similar to those in natural bone (Moghimi et al. 2005). Therefore, self-assembled nanofibers have unique properties with significant potential for drug delivery applications.

Physical–Chemical Properties

The electrospinning process was first developed in the 1930 s and 1940 s to form fine fibers using electrostatic forces (Figure 4.8). A polymer solution or melt is charged with an electric field of high voltage. This produces charge carriers with the same polarity as the electric field that was applied. Electrostatic repulsion because of this accumulation of similar charges pulls the polymer solution or melt forward in a cone-like shape. When the electric field voltage is high enough to overcome the surface tension of the polymer, a fiber jet formation occurs at the cone tip. A collector screen of opposite charge collects these nanofibers. The potential for nanofiber production for use in tissue engineering and as filters for toxic chemicals has generated increased interest in the electrospinning process (Thandavamoorthy et al. 2006).

Nanofibers can be created from synthetic polymers, such as polylactides or polyamides, as well as natural polymers, such as collagen, silk, and celluloses. The polymers are spun into nanofibers using organic solvents like chloroform, ethanol, or formic acid, and water is used in the spinning solution. The spinning parameters of solution concentration, viscosity, electrical conductivity, surface free energy, and solvent permeability affect the diameter of the nanofibers and their resulting surface topology, which may be smooth or porous. Nanofibers may be produced with diameters ranging from a few nanometers to a few micrometers. However, the length can theoretically be infinitely long (Greiner et al. 2006).

Self-assembled nanofibers will align themselves into distinctive 3D patterns such as honeycomb meshes on a collector substrate (Figure 4.8).

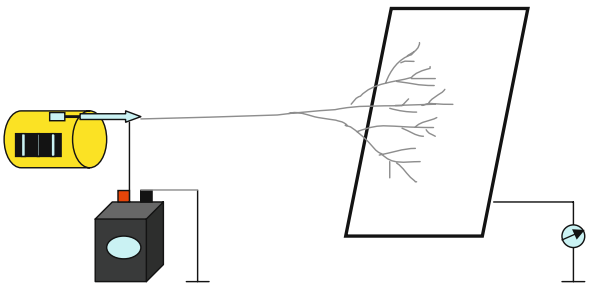

Figure 4.8 Diagram of the electrospinning process (Adapted from Thandavamoorthy et al. 2006). (*See* Color Plate 10)

These "nanowebs" give increased trapping and filtering mechanisms that have potential for use in chemical defense masks and protective clothing (Thandavamoorthy et al. 2006). Additionally, the polymer nanofiber-based filtration devices are now commercially developed for industrial air filtrations, as filters for gas turbine generators and filters for heavy-duty engines. Due to the very small diameter of the polymer fibers obtained by electrospinning, the surface area to volume ratio of the fibers is quite high. The non-woven mats formed from nanofibers have very small pore sizes; however, the total porosity of the mats is still very high (Ma et al. 2005).

The conversion of polymer to nanofiber is mediated by several parameters. The solution viscosity will play a role in the electrospinning process, as well as other solution parameters such as surface tension, conductivity, and polarity. Additionally, the physical parameters of the processing equipment will enhance development, such as applied electric potential, the distance between the needle tip and the collecting screen, size of the needle tip, feed rate, and the hydrostatic pressure applied to the polymer solution. Ambient parameters such as the temperature, air velocity, and humidity of the electrospinning chamber will also modulate nanofiber formation (Huang Z.M. et al. 2003). Besides offering an opportunity to generate ultra-thin diameters, small size porosity, and suitable surface morphology, the electrospinning process can provide fiber carriers for drug delivery with attractive features on multiple levels. For example, drugs can be conveniently incorporated into the carrier polymers without structural and bioactive alteration. The small diameter of the nanofibers can provide a short diffusion passage length, and the high surface area facilitates mass transfer and efficient drug release (He et al. 2006).

The properties of nanofibers such as fiber diameter, diameter distribution, and surface morphology can be characterized using scanning electron microscopy (SEM) Other methods of fiber characterization include transmission electron microscopy (TEM) and atomic force microscopy (AFM). The surface chemistry of the electrospun nanofibers can be determined by techniques such as X-ray photoelectron spectroscopy (XPS), contact angle measurements, and by attenuated total reflectance Fourier transform infra red spectroscopy (FTIR-ATR). The structures of the polymer molecules within the nanofibers can be characterized by Fourier transform infra red spectroscopy (FTIR) and nuclear magnetic resonance (NMR). The formation of thin polymer fibers from polymer solution usually changes the orientation of polymer chains. The configuration of the polymer chains in the nanofiber is usually determined by differential scanning calorimetry (DSC), wide angle X-ray diffraction (WAXD), and optical birefringence (Huang Z.M. et al. 2003).

Nanofibers in Drug Delivery

Cellular Behavior and Uptake

For effective cell interactions, polymer nanofibers often need to be functionalized to yield increased bioactivity and fiber–cell interaction

properties. The addition of other molecules such as genes, drugs, growth factors, and other ligands directly to the polymer solution or melt prior to electrospinning will produce functionalized, bioactive nanofibers. For example, plasmid DNA has been added directly to solutions of PLA–PEG and PLGA in dimethylformamide (DMF) prior to electrospinning for nanofiber production. Over a 20-day study period, there was a sustained release of plasmid DNA from the scaffold, with maximum release occurring at 2 hours after implantation (Luu et al. 2003). An optical sensor for the detection of the Fe^{3+} and Hg^{2+} ions was prepared by adding a fluorescent polymer to a polyurethane latex solution. The polymer solution was then electrospun into a nanofibrous membrane that gives a high response in optical sensing (Wang et al. 2002). Polyurethane nanofibers have been prepared for use in drug delivery applications by the addition of a solvent to the polymer solution. The drugs itraconazole and ketanserin, with the addition of DMF and dimethylacetamide (DMAc), respectively, showed linear release profiles over time (Verreck et al. 2003; Ma et al. 2005).

Surface modification can also be used to functionalize polymeric nanofibers. With degradable polymer nanofibers, special care must be taken to protect the nanofibers from rapid degradation and destruction. Strong reaction conditions such as exposure to plasma, ultraviolet, or gamma-radiation, high temperatures, and acidic or basic environments can easily degrade the nanofibers. Additionally, the high surface area of biodegradable nanofibers such as PLA and PGA tends to degrade much faster compared with bulk materials. Polyethylene terephthalate (PET) nanofibers showed significant degradation in acidic or basic solutions (Ma et al. 2005). Alternative surface modification methods that focus on coating or layering using electrostatic interactions might be more suited to immobilization of biomolecules onto polymer surfaces. Studies have shown that the ECM proteins collagen, fibronectin, and laminin can be coated on silk fibroin nanofiber surfaces to promote cell adhesion (Min et al. 2004; Ma et al. 2005).

One drug delivery application for polymeric nanofibers that shows great promise is the use of nanofibers as ECM-mimetic biomaterials. The extracellular matrix is composed of proteins that have similar structure and dimensions when compared to polymeric nanofibers that have been electrospun. ECM-mimetic fiber matrices have shown good cell attachment, cytocompatibility, and maintenance of cell phenotypes. Nanofibers can be produced with specialized functions by modifying the electrospinning technique. For example, aligned nanofibers allow the matrix to dictate cell orientation, while core–shell-structured nanofibers provide the ability for drug release from the nanofiber matrix (Ma et al. 2005).

Toxicity

The effects of shape, size, and surface properties of carbon nanomaterials can directly impact cellular toxicity. Health and growth of human lung tumor cells can be correlated with increasing concentrations of nanotubes, nanofibers, and nanoparticles. Within 24 hours, all the materials exhibited some levels of toxicity. Carbon nanoparticles are the most toxic, and

carbon nanotubes the least. It has been hypothesized that the difference in toxicity might be due to the "dangling bonds" present in nanoparticles that are not as prevalent in nanofibers or nanotubes. These dangling bonds are from carbon atoms which remain unbound to three other carbon atoms – making them highly reactive with other biomolecules (Arnaud Magrez et al. 2006).

Polymer nanofibers have shown good compatibility with other tissues when used as scaffolds and matrices. Fibers made of natural materials show the most promising compatibility. When human bone marrow stromal cells are grown on fibroin-based nanofibers, these electrospun silk matrices are able to support cell attachment and growth in culture over a 2-week period (Jin et al. 2004). Human keratinocytes and fibroblasts have also been reported to attach and proliferate on these fibroin-based nanofibers (Wan-Ju 2002; Min et al. 2004; Ma et al. 2005).

Fullerenes

Fullerenes are a recently discovered class of carbon allotropes, found in hollow spherical ellipse or tube shapes. The entire class of these closed-caged carbon molecules is called fullerenes (Figure 4.9). The C_{60} fullerene is commonly referred to as a buckyball, in honor of Buckminster Fuller (Dresselhaus et al. 1996b). Fullerenes have potential applications in the treatment of diseases where oxidative stress plays a role in the pathogenesis, such as neurodegenerative diseases. Another possible application of fullerenes is in nuclear medicine, as an alternative to chelating compounds that prevent the direct binding of toxic metal ions to serum components. This could increase the therapeutic potency of radiation treatments and decrease their adverse effects because fullerenes are resistant to biochemical degradation within the body (Jain 2005). The hydrophobic C_{60} molecule can be modified to include covalently bonded hydrophilic molecules, which increase the solubility and potential use in biological applications. Water-soluble fullerenes are able to cross the cell membrane, strengthening

Figure 4.9 Representation of the C_{60} "buckyball".

the proposed use of fullerenes in drug delivery systems and targeting of specific tissues and cell types (Foley et al. 2002).

Metallofullerenes are all-carbon fullerenes that enclose metal ions to deliver radioactive atoms directly to diseased tissues, such as cancer. This has the potential to decrease the side effects of non-targeted radiation treatments, since the radioactive atoms will not damage healthy surrounding tissue. This is one example of the potential drug delivery applications of the fullerene family (Vogelson 2001).

Physical–Chemical Properties

Within the past 10 years, the physical and chemical properties of fullerenes have gained increasing interest as scientists try to understand how these properties can be exploited to yield new treatments and applications. Fullerenes can be produced through combustion and oxidation of benzene and argon gas mixtures, by resistive heating of carbon rods in vacuum, or through laser vaporization. The most commonly used and most efficient method involves running a large current between two nearby graphite electrodes in an inert atmosphere, such as helium, at a pressure of 200 Torr. A carbon plasma arc will be formed between the electrodes, and the cooled carbon soot contains fullerenes that must be extracted and then purified (Dresselhaus et al. 1996).

While fullerenes are stable, they are not completely unreactive. The sp^2-hybridized carbon atoms exist at an energy minimum in planar graphite. To form a spherical or tube shape, they must be bent, which will cause angle strain. To alleviate this strain, fullerenes tend to undergo an electrophilic addition at 6,6-double bonds to reduce angle strain by converting the sp^2-hybridized orbitals into sp^3-hybridized orbitals. This hybridization change allows the bond angles to decrease from about 120 degrees in the sp^2 orbitals to about 109.5 degrees in the sp^3 orbitals. Molecular stability increases because the atoms undergo less bending when forming their spherical shape (Diederich Francois and Thilge). Endohedral fullerenes are fullerenes with additional atoms trapped inside them. Endohedral metallofullerenes formed using the rhonditic steel process were one of the first commercially viable uses of buckyballs (Bethune et al. 1993). Fullerene-binding molecules have potential in drug delivery applications. For example, they could facilitate specific antibiotics targeting resistant bacteria or drugs targeting cancer cells such as melanoma. Other examples include the use of fullerenes as light-activated antimicrobial agents (Tegos et al. 2005).

Fullerenes are the only known carbon allotrope that can be dissolved in common solvents at room temperature, and are moderately soluble in nonpolar and weakly polar solvents. At the same time, the fact that they are nanosized means that they can be treated as colloidal particles. This is observed when the solid phase of fullerenes is added to a liquid, and a molecular solution is first formed. Subsequently, dispersion forces will cause the fullerenes to cluster into a colloidal solution (Tropin et al. 2006). While no single parameter can be used to predict the solubility of a fullerene in a solvent, several general trends have been found to govern their behavior in a particular solvent. The solubility in a solvent generally

increases with increasing molecular weight of the solvent. An increase in the polarizability parameter generates higher solubilities (Dresselhaus et al. 1996b). The solubility of a selected solvent will be important in its successful use in the further extraction and purification of fullerenes.

On their own, fullerenes are not readily soluble in water, so a solubilization method is necessary for the fullerene acting in biological systems. A fairly quick method involves solubilization by tetrahydrofuran (THF), mixing with water, and then evaporation to eliminate the THF. The water stirred method is simply weeks of water stirring. This method is more environmentally friendly than the previous method, but takes a considerable amount of time. However, studies have shown that fullerenes produced by the THF method exhibit higher toxicities in vivo, possible because of residual solvent trapped within the fullerene (Shiqian Zhu and Mary L. Haasch 2006).

Fullerenes in Drug Delivery

Cellular Behavior and Uptake

Because fullerenes have numerous points of attachment, they have the ability to give control to the 3D positioning of chemical groups onto their structure. This improves their ability to target specific cells and molecules. The 60 carbons in the buckyball formation, for example, give 60 points of attachment for forming a more complex delivery assembly (Leary et al. 2006). This, along with their nanosize dimensions, redox potential, and ability to encapsulate other molecules, makes fullerenes an attractive candidate for drug delivery applications. Water-soluble derivatives of C_{60} fullerenes have shown uptake and localization primarily in the mitochondria. Additionally, researchers have found that fullerenes react with damaging oxygen free radicals through their C–C double bonds. This binding occurs so quickly that only diffusion controls the reaction. This means that the fullerene will bind the radical each time it encounters one. By binding and inactivating these free radicals that circulate throughout the body, fullerenes could be used to treat diseases caused by excessive free radical production. Fullerene antioxidants could provide more effective therapies for CNS-degenerative diseases such as Parkinson's disease, which is currently only marginally treated by natural and synthetic antioxidants (Dugan LL et al. 1997). Fullerenes have also demonstrated antiprotease activity which has the potential for use in treatment of human immunodeficiency virus and acquired immunodeficiency syndrome (Zhu et al. 2003).

Toxicity

There is conflicting evidence on whether fullerenes are relatively inert or potentially harmful to the body. When fullerenes were dispersed in water at concentrations of 0.5 parts per million and evaluated in largemouth bass, it was found that the fish suffered a 17-fold increase in cellular damage in the brain tissue after 48 hours. Fullerenes induced lipid peroxidation, which has been shown to impair the functioning of cell membranes

and lead to cellular damage. Inflammatory changes also occurred in the liver and genes that are related to the making of repair enzymes. The damage to lipid-rich tissues likely occurred because the fullerenes are redox active. To overcome this limitation further research into biocompatible coatings that eliminate the redox-reactive surface while still allowing for drug delivery is necessary (Oberdörster 2004).

To better understand how cells process these fullerenes, high-resolution 3D electron microscopy was used to track where buckyballs travel within cells. With non-toxic doses, buckyballs concentrated in intracellular lysosomes along the cell membrane, the nuclear membrane, and within the nucleus. The localization of fullerenes in and around the nucleus (Figure 4.10) raises concern that DNA damage could occur if interaction with the buckyballs disrupts DNA's helical structure (Porter AE et al. 2006). In aqueous solution, buckyballs were found to prefer to bind to DNA rather than each other because of strong hydrophobic interactions. These associations can cause the DNA to deform, which would potentially interfere with its biological functions. However, additional studies are necessary to see if in vitro results translate to in vivo (Zhao et al. 2005).

Fullerene uptake in rats has been evaluated by oral administration and intravenous routes of delivery. Oral administration of water-soluble buckyballs in rats showed that the compounds were not efficiently absorbed, while intravenous distribution showed uptake in multiple organs and the ability to penetrate the blood brain barrier. The acute

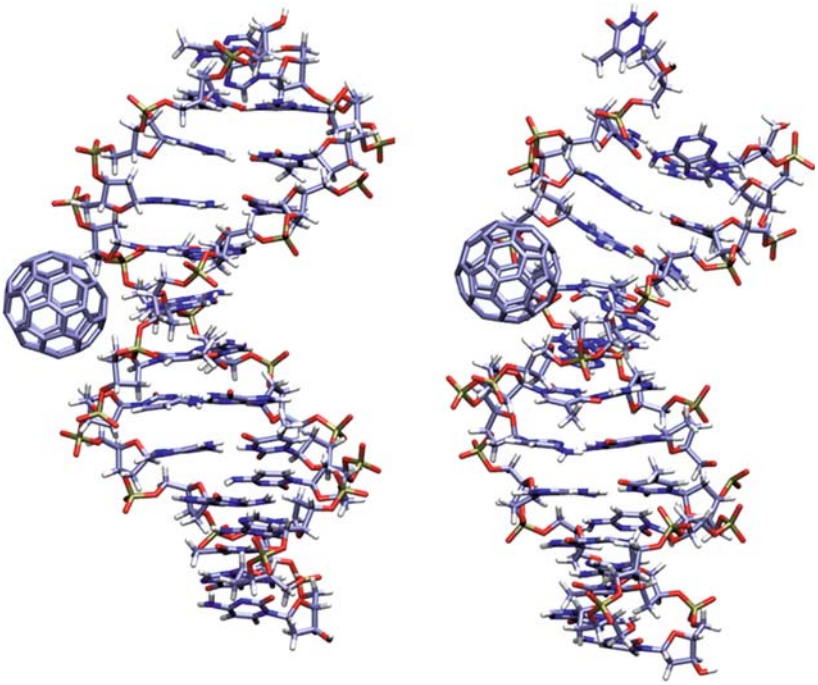

Figure 4.10 Complexes of C_{60} in the minor groove, starting from the B-DNA (***a***) and A-DNA (***b***) conformations. C_{60} has more contact with DNA starting from A-form than that from B-form, resulting in a slightly greater (more negative) binding energy (Zhao 2005). (*See* Color Plate 11)

toxicity was low, but further investigation is needed to determine how chronic exposure would affect cytotoxicity since the materials were still present after 1 week (Yamago et al. 1995). C_{60} fullerenes did not cause human leukocytes to secrete inflammatory molecules in vitro (Moussa et al. 1995). In addition, buckyballs that transfected into macrophage cell lines were not cytotoxic and had negligible effects on the formation of reactive oxygen species (Baierl and Seidel 1996).

As with nanotubes, functionalization of the surface of fullerenes can change their behavior to induce targeting or other cell interactions. Moreover, these modifications can also cause them to become cytotoxic. When modified fullerenes are irradiated with UVA or UVB light, they cause cell membrane damage leading to cell death, in a dose-dependent fashion (Rancan et al. 2002). Functionalization of fullerenes to make them water soluble also then results in aggregating the fullerenes in human liver carcinoma cells, dermal fibroblasts, and neuronal astrocytes. Based on these findings for functionalized and non-functionalized fullerenes, it appears that it is surface modifications of fullerenes that result in their cytotoxicity (Sayes et al. 2004; Fiorito et al. 2006).

Conclusion

Nanorods, nanotubes, nanofibers, and fullerenes have potential in drug delivery applications. Development of these materials requires an approach that is interdisciplinary, combining expertise in chemistry, biology, engineering, and materials science (Silva 2006). These nanomaterials have unique structural and functional properties that are not found in the individual molecules or bulk solids (Sinha et al. 2006). Before the potential of these nanomaterials can be realized, there are challenges that must be overcome. While nanoparticles are heralded for their unique properties, these characteristics can result in cytotoxicity. Long-term studies of the chronic implications of nanomaterial exposure are necessary to determine whether these particles can safely be used as drug delivery vehicles in humans. Targeted drug delivery using these materials may minimize harmful side effects, while increasing the efficiency of treatment, leading to better patient compliance and greater efficacy of the therapy (Emerich and Thanos 2006). The addition of a coating or functionalization of the nanomaterial surface might eliminate toxicity in the laboratory environment, but it is unclear whether this will still be the case in the human body (Fiorito et al. 2006). However, the application of nanorods, nanotubes, nanofibers, and fullerenes in drug delivery has also opened doors for exploration in the areas of biosensing, bioimaging, tissue engineering, and chemical defense.

References

A. C. Dillon, T. Gennett, K. M. Jones, J. L. Alleman, P. A. Parilla, and M. J. Heben (1999). “A simple and complete purification of single-walled carbon nanotube.” Materials. **11:** 1354–1358.

Ajima, K., M. Yudasaka, et al. (2005). “Carbon nanohorns as anticancer drug carriers.” *Molecular Pharmacology* **2**(6): 475–80.

Arnaud Magrez, S. K., Valérie Salicio, Nathalie Pasquier, Jin Won Seo, Marco Celio, Stefan Catsicas, Beat Schwaller, and László Forro (2006). "Cellular Toxicity of Carbon-Based Nanomaterials." *Nano letters* **6**(6): 1121.

Baierl, T. and A. Seidel (1996). "In vitro effects of fullerene C-60 and fullerene black on immunofunctions of macrophages." *Fullerene Science and Technology* **4**(5): 1073–1085.

Balasubramanian, K. and M. Burghard (2005). "Chemically functionalized carbon nanotubes." *Small* **1**(2): 180–192.

Bauer, L. A., N. S. Birenbaum, et al. (2004). "Biological applications of high aspect ratio nanoparticles." *Journal of Materials Chemistry* **14**(4): 517–526.

Bergen, J. M., et al. (2006). "Gold nanoparticles as a versatile platform for optimizing physicochemical parameters for targeted drug delivery." 506–516.

Bethune, D. S., R. D. Johnson, et al. (1993). "Atoms in carbon cages: the structure and properties of endohedral fullerenes." *Nature* **366**(6451): 123–128.

Bianco, A., J. Hoebeke, et al. (2005a). "Carbon nanotubes: on the road to deliver." *Current Drug Delivery* **2**(3): 253–9.

Bianco, A., K. Kostarelos, et al. (2005b). "Biomedical applications of functionalised carbon nanotubes." *Chemical Communications*(5): 571–577.

Brannon-Peppas, L. and J. O. Blanchette (2004). "Nanoparticle and targeted systems for cancer therapy." *Advanced Drug Delivery Reviews* **56**(11): 1649–1659.

Carrero-Sanchez, J. C., A. L. Elias, et al. (2006). "Biocompatibility and toxicological studies of carbon nanotubes doped with nitrogen." *Nano Letters* **6**(8): 1609–1616.

Chen, M., et al. (2003). "Gold-coated iron nanoparticles for biomedical applications." *Journal of Applied Physics* **93**(10): 7551–7553.

Cheng, W. F., Hung, C. F., Chai, C. Y., Hsu, K. F., He, L., Ling, M., and Wu, T. C. (2001) "Tumor-specific immunity and antiangiogenesis generated by a DNA vaccine encoding calreticulin linked to a tumor antigen." *Journal of Clinical Invest* **108**(5): 669–678.

Couvreur, P. a. V., C (2006). "Nanotechnology: Intelligent Design to Treat Complex Disease." g*Pharmaceutical Research* **23**(7): 1417–1450.

Cui, D. X., F. R. Tian, et al. (2005). "Effect of single wall carbon nanotubes on human HEK293 cells." *Toxicology Letters* **155**(1): 73–85.

Diederich Francois and Thilge, C (1996). "Covalent Fullerene Chemistry." *Science* **271**(5247): 317–323.

Donaldson, K., V. Stone, et al. (2004). Nanotoxicology. **61:** 727–728.

Dresselhaus M, D. G., Eklund PC (1996a). *Science of Fullerenes and Carbon Nanotubes*. San Diego, Academic Press, Inc.

Dresselhaus, M. S., Dresselhaus, G., Eklund, P.C. (1996b). *Science of Fullerenes and Carbon Nanotubes*. San Diego, CA, Academic Press, Inc.

Dugan LL, T. D., Du C, Lobner D, Wheeler M, Almli CR, Shen CK-F, Luh T-Y Choi DW, and Lin T-S (1997). "Carboxyfullerenes as neuroprotective agents." *Proceedings of the National Academy of Sciences USA* **94**: 9434–9439.

Ellen E. Connor, J. M. A. G. Catherine J. M. and Michael D. W. (2005). Gold nanoparticles are taken up by human cells but do not cause acute cytotoxicity. *Small* **1:** 325–327.

El-Sayed, M. E. H., Hoffman, A. S., and Stayton, P. S. (2005). "Smart polymeric carriers for enhanced intracellular delivery of therapeutic macromolecules." *Expert Opinion on Biological Therapy* **5**(1): 23–32.

Emerich, D. F. and C. G. Thanos (2006). "The pinpoint promise of nanoparticle-based drug delivery and molecular diagnosis." *Biomolecular Engineering* **23**(4): 171–184.

Farrer, R. A., F. L. Butterfield, et al. (2005). "Highly efficient multiphoton-absorption-induced luminescence from gold nanoparticles." *Nano Letters* **5:** 1139–1142.

Fiorito, S., A. Serafino, et al. (2006). "Toxicity and biocompatibility of carbon nanoparticles." *Journal of Nanoscience and Nanotechnology* **6**(3): 591–599.

Foley, S., C. Crowley, et al. (2002). "Cellular localisation of a water-soluble fullerene derivative." *Biochemical and Biophysical Research Communications* **294**(1): 116–119.

Garibaldi, S., C. Brunelli, et al. (2006). "Carbon nanotube biocompatibility with cardiac muscle cells." *Nanotechnology* **17**(2): 391–397.

Gaur, U., S. K. Sahoo, et al. (2000). "Biodistribution of fluoresceinated dextran using novel nanoparticles evading reticuloendothelial system." *International Journal of Pharmaceutics* **202**(1–2): 1–10.

Glomm, W. R. (2005). "Functionalized gold nanoparticles for applications in bionanotechnology." *Journal of Dispersion Science and Technology* **26**(3): 389–414.

Gole, A. and C. J. Murphy (2004). "Seed-mediated synthesis of gold nanorods: Role of the size and nature of the seed." *Chemistry of Materials* **16**(19): 3633–3640.

Greiner, A., J. H. Wendorff, et al. (2006). "Biohybrid nanosystems with polymer nanofibers and nanotubes." *Applied Microbiology and Biotechnology* **71**(4): 387–393.

Haddon, R. C. (2002). "Carbon Nanotubes." *Acc. Chem. Res.* **35**(12).

He, C. L., Z. M. Huang, et al. (2006). "Coaxial electrospun poly(L-lactic acid) ultrafine fibers for sustained drug delivery." *Journal of Macromolecular Science Part B-Physics* **45**(4): 515–524.

Hone, J., B. Batlogg, et al. (2000). Quantized Phonon Spectrum of Single-Wall Carbon Nanotubes. **289:** 1730–1733.

Huang Z.M., Z. Y. Z., Kotaki M., and Ramakrishna S. (2003). "A review on polymer nanofibers by electrospinning and their applications in nanocomposites." *Composites Science and Technology***63**: 2223–53.

Huang, K., et al. (2006). Preparation of highly conductive, self-assembled gold/polyaniline nanocables and polyaniline nanotubes. *Chemistry-a European Journal* **12**(20): 5314–5319.

Hung, C. F. and Wu T. C. (2003). "Improving DNA vaccine potency via modification of professional antigen presenting cells." *Current Opinion in Molecular Therapeutics* **5**(1): 20–24.

Iijima, S. (1991). "Helical microtubules of graphitic carbon." *Nature* **354**(6348): 56–58.

Iijima, S. and T. Ichihashi (1993). "Single-shell carbon nanotubes of 1-nm diameter." *Nature* **363**(6430): 603–605.

J. K. N. Mbindyo, B. R. Reiss, B. R. Martin, C. D. Keating, M. J. Natan, and T. E. Mallouk (2001). "DNA-Directed Assembly of Gold Nanowires on Complementary Surfaces." *Advanced Materials* **13:** 249–254.

J.G. Wen, Z. P. H., D.Z. Wang, J.H. Chen, S.X. Yang, and Z.F. Ren, J.H. Wang, L.E. Calvet, J. Chen, J.F. Klemic, and M.A. Reed (2001). "Growth and characterization of aligned carbon nanotubes from patterned nickel nanodots and uniform thin films." *Journals of Materials Research* **16**(11): 8.

Jain, K. K. (2005). "The role of nanobiotechnology in drug discovery." *Drug Discovery Today* **10**(21–24): 1435–1442.

Jana, N. R., Gearheart, L., and Murphy, C. J. (2001). "Wet chemical synthesis of high aspect ratio cylindrical gold nanorods." *Journal of Physical Chemistry B* **105**(19): 4065–4067.

Jin, H. J., Chen, J.S., Karageorgiou, V., Altman, G.H., and D. L. Kaplan (2004). "Human bone marrow stromal cell responses on electrospun silk fibroin mats." *Biomaterials* **25**: 1039.

Klumpp, C., K. Kostarelos, et al. (2006). "Functionalized carbon nanotubes as emerging nanovectors for the delivery of therapeutics." *Biochimica et Biophysica Acta-Biomembranes* **1758**(3): 404–412.

Kopecek, J. (2003). "Smart and genetically engineered biomaterials and drug delivery systems." *European Journal of Pharmaceutical Sciences* **20**(1): 1–16.

Lam, C.-W., J. T. James, et al. (2004). Pulmonary Toxicity of Single-Wall Carbon Nanotubes in Mice 7 and 90 Days After Intratracheal Instillation. **77:** 126–134.

Leary, S. P., C. Y. Liu, et al. (2006). "Toward the emergence of nanoneurosurgeryPart III – Nanomedicine: Targeted nanotherapy, nanosurgery, and progress toward the realization of nanoneurosurgery." *Neurosurgery* **58**(6): 1009–1025.

Li, W.-J., et al. (2002). "Electrospun nanofibrous structure: A novel scaffold for tissue engineering." *Journal of Biomedical Materials Research* **60**(4): 613–621.

Lu, J. P. (1997). "Elastic Properties of Carbon Nanotubes and Nanoropes." *Physical Review Letters* **79**(7): 1297.

Luu, Y. K., Kim, K., Hsiao, B.S., Chu, B., and Hadjiargyrou, and M. (2003). "Development of a nanostructured DNA delivery scaffold via electrospinning of PLGA and PLA–PEG block copolymers." *Journal of Controlled Release***89**(341).

Ma, Z. W., M. Kotaki, et al. (2005). "Potential of nanofiber matrix as tissue-engineering scaffolds." *Tissue Engineering* **11**(1–2): 101–109.

Maeda, H., T. Sawa, et al. (2001). "Mechanism of tumor-targeted delivery of macromolecular drugs, including the EPR effect in solid tumor and clinical overview of the prototype polymeric drug SMANCS." *Journal of Controlled Release* **74**(1–3): 47–61.

Malik, N., R. Wiwattanapatapee, et al. (2000). "Dendrimers:: Relationship between structure and biocompatibility in vitro, and preliminary studies on the biodistribution of 125I-labelled polyamidoamine dendrimers in vivo." *Journal of Controlled Release* **65**(1–2): 133–148.

Martin, C. R. (1994). "Nanomaterials: A Membrane-Based Synthetic Approach." *Science* **266**(5193): 1961–1966.

Martin, B. R., et al. (1999). "Orthogonal self-assembly on colloidal gold-platinum nanorods." 1021–1025.

Min, B. M., Lee, G., Kim, S.H., Nam, Y.S., Lee, T.S., and W. H. Park (2004). "Electrospinning of silk fibroin nanofibers and its effect on the adhesion and spreading of normal human keratinocytes and fibroblasts in vitro." *Biomaterials* **25**: 1289.

Moghimi, S. M., A. C. Hunter, et al. (2005). "Nanomedicine: current status and future prospects." *Faseb Journal* **19**(3): 311–330.

Moussa, F., P. Chretien, et al. (1995). "The Influence of C-60 Powders on Cultured Human-Leukocytes." *Fullerene Science and Technology* **3**(3): 333–342.

Nicewarner-Pena, S. R., et al. (2001). "Submicrometer metallic barcodes." *Science* **294**(5540): 137–141.

Nishikawa, M., et al. (1998). "Targeted delivery of plasmid DNA to hepatocytes in vivo: Optimization of the pharmacokinetics of plasmid DNA galactosylated poly(L-lysine) complexes by controlling their physicochemical properties." *Journal of Pharmacology and Experimental Therapeutics* **287**(1): 408–415.

Oberdörster, E. (2004). "Manufactured Nanomaterials (Fullerenes, C60) Induce Oxidative Stress in the Brain of Juvenile Largemouth Bass." *Environmental Health Perspectives* **112**(10): 1058.

Panessa-Warren, B. J., J. B. Warren, et al. (2006). "Biological cellular response to carbon nanoparticle toxicity." *Journal of Physics-Condensed Matter* **18**(33): S2185–S2201.

Porter AE, M. K., Skepper J, Midgley P, and Welland M. (2006). "Uptake of C60 by human monocyte macrophages, its localization and implications for toxicity: studied by high resolution electron microscopy and electron tomography." *Acta Biomaterialia* **2**(4): 409–19.

Qin, D. H., et al. (2006). "Surfactant-assisted synthesis of size-controlled trigonal Se/Te alloy nanowires." *Nanotechnology* **17**(3): 674–679.

Rajangam, K., Behanna, Heather A., Hui, Michael J., Han, Xiaoqiang, Hulvat, James F., Lomasney, Jon W., and Stupp, Samuel I. (2006). "Heparin Binding Nanostructures to Promote Growth of Blood Vessels." *Nano Letters* **6**(9): 2086–2090.

Rancan, F., S. Rosan, et al. (2002). "Cytotoxicity and photocytotoxicity of a dendritic C-60 mono-adduct and a malonic acid C-60 tris-adduct on Jurkat cells." *Journal of Photochemistry and Photobiology B-Biology* **67**(3): 157–162.

Raychaudhuri, S. and Rock, K. L. (1998). "Fully mobilizing host defense: Building better vaccines." *Nature Biotechnology* **16**(11): 1025–1031.

Salem, A. K., C. F. Hung, et al. (2005). "Multi-component nanorods for vaccination applications." *Nanotechnology* **16**(4): 484–487.

Salem, A. K., P. C. Searson, et al. (2003). "Multifunctional nanorods for gene delivery." *Nature Materials* **2**(10): 668–671.

Salem, A. K., et al. (2004). "Receptor-mediated self-assembly of multi-component magnetic nanowires." *Advanced Materials* **16**(3): 268–271.

Salem, A. K., et al. (2004). "Directed assembly of multisegment Au/Pt/Au nanowires." *Nano Letters* **4**(6): 1163–1165.

Salvador-Morales, C., E. Flahaut, et al. (2006). "Complement activation and protein adsorption by carbon nanotubes." *Molecular Immunology* **43**(3): 193–201.

Sayes, C. M., J. D. Fortner, et al. (2004). "The differential cytotoxicity of water-soluble fullerenes." *Nano Letters* **4**(10): 1881–1887.

Schmidt, O. G. and K. Eberl (2001). "Nanotechnology: Thin solid films roll up into nanotubes." *Nature* **410**(6825): 168–168.

Service, R. F. (2005). Nanofibers seed blood vessels. *Science*. **308:** 44–45.

Shim, M., N. W. S. Kam, et al. (2002). "Functionalization of carbon nanotubes for biocompatibility and biomolecular recognition." *Nano Letters* **2**(4): 285–288.

Shiqian Zhu, E. O. and Mary L. Haasch (2006). "Toxicity of an engineered nanoparticle (fullerene, C60) in two aquatic species, Daphnia and fathead minnow." *Marine Environmental Research* **62**: S5–S9.

Shvedova, A., V. Castranova, et al. (2003). "Exposure to Carbon Nanotube Material: Assessment of Nanotube Cytotoxicity using Human Keratinocyte Cells." *Journal of Toxicology and Environmental Health Part A* **66**(20): 1909–1926.

Silva, G. A. (2006). "Neuroscience nanotechnology: Progress, opportunities and challenges." *Nature Reviews Neuroscience* **7**(1): 65–74.

Sinha, R., G. J. Kim, et al. (2006). Nanotechnology in cancer therapeutics: bioconjugated nanoparticles for drug delivery. *Molecular Cancer Therapeutics* **5:** 1909–1917.

Sinnott, S. B. and R. Andrews (2001). "Carbon Nanotubes: Synthesis, Properties, and Applications." *Critical Reviews in Solid State and Material Sciences* **26**(3): 145–249.

Steinhart, M., J. H. Wendorff, R. B. Wehrspohn (2003). Nanotubes à la Carte: Wetting of Porous Templates. *ChemPhysChem* **4:** 1171–1176.

Steinle, E. D., D. T. Mitchell, et al. (2002). Ion Channel Mimetic Micropore and Nanotube Membrane Sensors. *Analytical Chemistry* **74:** 2416–2422.

Sun, Y. P., K. Fu, et al. (2002). Functionalized Carbon Nanotubes: Properties and Applications. *Accounts of Chemical Research* **35:** 1096–1104.

Takakura, Y., et al. (2002). "Influence of physicochemical properties on pharmacokinetics of non-viral vectors for gene delivery." *Journal of Drug Targeting* **10**(2): 99–104.

Tegos, G. P., T. N. Demidova, et al. (2005). "Cationic Fullerenes Are Effective and Selective Antimicrobial Photosensitizers." *Chemistry & Biology* **12**(10): 1127–1135.

Thandavamoorthy, S., N. Gopinath, et al. (2006). "Self-assembled honeycomb polyurethane nanofibers." *Journal of Applied Polymer Science* **101**(5): 3121–3124.

Tropin, T. V., M. V. Avdeev, et al. (2006). "Nonmonotonic behavior of the concentration in the kinetics of dissolution of fullerenes." *Jetp Letters* **83**(9): 399–404.

Vasir, J. K., M. K. Reddy, et al. (2005). "Nanosystems in drug targeting: Opportunities and challenges." *Current Nanoscience* **1**(1): 47–64.

Venugopal, J. and S. Ramakrishna (2005). "Applications of polymer nanofibers in biomedicine and biotechnology." *Applied Biochemistry and Biotechnology* **125**(3): 147–157.

Verreck, G., Chun, I., Rosenblatt, J., Peeters, J., Dijck, and M. A.V., J., Noppe M., and Brewster, M.E. (2003). "Incorporation of drugs in an amorphous state into electrospun nanofibers composed of a water-insoluble, nonbiodegradable polymer " *Journal of Controlled Release* **92**: 349.

Vogelson, C. T. (2001). Advances in drug delivery systems. *Modern Drug Discovery*. **4:** 49–52.

Wang, X. Y., Drew, C., Lee, S.H., Senecal, K.J., Kumar, J., and L. A. and Samuelson (2002). "Electrospun nanofibrous membranes for highly sensitive optical sensors." *Nano Letters* **2**: 1273.

Warheit, D. B. (2006). "What is currently known about the health risks related to carbon nanotube exposures?" *Carbon* **44**(6): 1064–1069.

Whitesides, G. M., J. P. Mathias, et al. (1991). Molecular self-assembly and nanochemistry: a chemical strategy for the synthesis of nanostructures. *Science* **254:** 1312–1319.

Whitney, T. M., J. S. Jiang, et al. (1993). "Fabrication and Magnetic Properties of Arrays of Metallic Nanowires." *Science* **261**(5126): 1316–1319.

Yamago, S., H. Tokuyama, et al. (1995). "In vivo biological behavior of a water-miscible fullerene: 14C labeling, absorption, distribution, excretion and acute toxicity." *Chemistry & Biology* **2**(6): 385–389.

Yao, N., V. Lordi, et al. (1998). "Structure and Oxidation Patterns of Carbon Nanotubes." *Journal of Materials Research* **13**.

Yu, M.-F., B. S. Files, et al. (2000). "Tensile Loading of Ropes of Single Wall Carbon Nanotubes and their Mechanical Properties." *Physical Review Letters* **84**(24): 5552.

Zhao X, S. A., Cummings PT. (2005). "C60 binds to and deforms nucleotides." *Biophys J*. **89**(6): 3856–62.

Zhu, H. W., C. L. Xu, et al. (2002). Direct Synthesis of Long Single-Walled Carbon Nanotube Strands. **296:** 884–886.

Zhu Z, S. D. andTuckerman ME (2003)."Molecular dynamics study of the connection between flap closing and binding of fullerene-based inhibitors of the HIV-1 protease." *Biochemistry* **42**: 1326–1333.

5

Drug Loading into and In Vitro Release from Nanosized Drug Delivery Systems

Anja Judefeind and Melgardt M. de Villiers

Introduction

Drug loading during preparation and subsequent release after administration are two important properties that have to be built into a drug delivery system during their development as they largely determine the efficiency of such systems. Drug loading is the process of incorporation of the drug into a polymer matrix or capsule. Drug release is the reverse process by which the drug molecules are liberated from the solid phase and become available for absorption and pharmacological action. Therefore, in addition, in vitro drug release can be a quality control of the drug delivery system, provide information about the internal structure of the carrier, the interaction between the drug and carrier, and can be used to predict in vivo behavior (Chorny, Fishbein, Danenberg, & Golomb, 2002; Washington, 1990a). Drug loading and release are related to each other because both depend on the physicochemical properties of the matrix, the physicochemical properties of the drug and the interaction between the matrix, drug and the environment. This chapter describes the various processes involved with drug loading into nanosized drug delivery systems and how it influences the subsequent release of the drug from these systems.

Drug Loading

Definitions and Mechanisms of Drug Loading

Drug loading is the process of incorporation of drug into a carrier system. Two common terms are utilized in literature. These are drug loading (DL) (or drug content) and entrapment efficiency (EE) and they are defined as

$$\text{Drug loading}\ (\%) = \frac{\text{mass of drug in nanoparticles}}{\text{mass of nanoparticles}} \times 100 \qquad (1)$$

$$\text{Entrapment efficiency}\ (\%) = \frac{\text{experimental drug loading}}{\text{nominal drug loading}} \times 100 \qquad (2)$$

M.M. de Villiers et al. (eds.), *Nanotechnology in Drug Delivery*, DOI: 10.1007/978-0-387-77667-5_5,

During comparison of various drug delivery systems, one should consider both drug loading and entrapment efficiency. Entrapment efficiency describes the efficiency of the preparation method to incorporate drug into the carrier system. Ideally, a high drug loading with a minimum nominal drug loading is aimed for because this improves the entrapment efficiency. In addition, the amount of drug entrapped also determines the performance of the drug delivery system since it influences the rate and extent of drug release from the system. Both drug loading and entrapment efficiency depend on the physicochemical properties and the interactions between the drug, the carrier matrix and the surrounding medium.

The drug can either be incorporated into nanoparticles by hydrogen bonding, ionic interaction, dipole interaction, physical entrapment (or encapsulation), precipitation, covalent bonding or be adsorbed to the surface. In most drug delivery systems, more than one loading mechanism is involved. Different techniques are utilized to investigate the mechanism of loading. These include UV, NMR, FTIR, X-ray and DSC to test for interaction and electron spectroscopy for chemical analysis (ESCA) as well as X-ray photoelectron spectroscopy (XPS) for investigating the surface chemistry.

Drug Loading of Various Nanocarriers

Drug loading depends on the type of nanoparticles (e.g., nanospheres, nanocapsules, solid lipid nanoparticles, dendrimers, polymeric micelles, nanoemulsions) and the preparation method (Huo, Liu, Wang, Jiang, Lambert, & Fang, 2006; Zhang, Li, Qiu, Li, Yan, Jin, & Zhu, 2006a). Various types of nanoparticles, techniques to produce them and their advantages and disadvantages have been extensively described in literature: nanospheres (Bala, Hariharan, & Kumar, 2004; Bilati, Allémann, & Doelker, 2005; Peppas & Robinson, 2007; Reis, Neufeld, Ribeiro, & Veiga, 2006; Soppimath, Aminabhavi, Kulkarni, & Rudzinski, 2001), dendrimers (Amir & Shabat, 2006; D'Emanuele & Attwood, 2005; Gupta, Agashe, Asthana, & Jain, 2006; Yang & Kao, 2006), solid lipid nanoparticles and nanostructured lipid carriers (Müller, Mäder, & Gohla, 2000; Müller, Radtke, & Wissing, 2002; Üner, 2006), polymeric micelles (Aliabadi & Lavasanifar, 2006; Liu, Lee, & Allen, 2006a), nanocapsules (Couvreur, Barratt, Fattal, Legrand, & Vauthier, 2002; Mayer, 2005) and nanoemulsions (Solans, Izquierdo, Nolla, Azemar, & Garcia-Celma, 2005).

Tables 5.1–5.5 show some examples of drug loading of various nanoparticles (Table 5.1: nanospheres, Table 5.2: dendrimers, Table 5.3: solid lipid nanoparticles and nanostructured lipid carriers, Table 5.4: polymeric micelles and Table 5.5: nanoemulsions and nanocapsules). The various examples were chosen to illustrate the effect of drug, loading method (with modification in pH, temperature, sequence of adding excipients), type of polymer/copolymer, copolymer ratios, functional groups on polymers, molecular weights (MW) of polymers/copolymers, nominal drug loading, etc., on drug loading and entrapment efficiency.

In general, two ways of drug loading can be distinguished: drug loading during nanoparticle formation and loading after the preparation of nanoparticles (Allemann, Gurny, & Doelker, 1993). If preformed nanoparticles

Table 5.1 Examples of drug loading of nanospheres.

Drug	Loading method	Time of loading	Entrapment efficiency (EE) and drug loading (DL)	Ref.
Clotrimazol Econazole	• Double emulsion/solvent evaporation for PLG NP[1] • Cation-induced controlled gelification for alginate NP	During	PLG NP: 48% clotrimazol, 52% econazole (EE) Alginate NP: 90% clotrimazol, 95% econazole (EE)	[1]
Gentamicin	• Double emulsion/solvent evaporation different PLGA copolymers and nominal drug loading	During	NP: 1.5–13% (EE), 0.7–6 μg/mg particle (DL) MP[2]: 4–19% (EE), 2–9 μg/mg particle (DL)	[2]
CPA[3] BSA[4]	• Nanoprecipitation or • Single and double emulsion/evaporation or • Novel method with thermosensitive Pluronic F-127 gel PLA or PLGA polymer, different nominal drug loading	During	CPA: 0.7–35% (EE), 0.01–0.46% (DL) BSA: 58–74% (EE), 6.8–8.7% (DL)	[3]
BSA	• Incubation in PBS (pH 7.4) for 24 h chitosan and lactic acid-grafted chitosan	After	Chitosan: 92% (EE) Lactic acid-grafted chitosan: 96% (EE)	[4]
Plasmid DNA	• Double emulsion/solvent evaporation Various poly(ester-anhydride) copolymer ratios	During	Up to 40% EE Decreased EE with increased polyanhydride content	[5]
Dexa-methasone phosphate	• Instantaneous precipitation using supercritical CO_2 and encapsulation of drug NP in PLGA matrix by anhydrous solid-oil-oil-oil technique	During	90% EE vs. 80% EE for unprocessed drug	[6]
Ibuprofen	• Co-precipitation of drug and DEAE dextran Different drug/dextran ratios Different pH of preparation solution	During	EE: 70% (pH 6), 57% (pH 9) DL: 10–31% (pH 6), 7–23% (pH 9)	[7]
Retinoic acid	• Nanoprecipitation or • Melting-sonication PCL-PEO amphiphilic block copolymers with triblock or star-diblock architecture	During	Nanoprecipitation: 2.3–6.3% (EE), 0.2–0.6% (DL) Melting-sonication: 6.4–9.5% (EE), 0.6–0.9% (DL)	[8]
Procaine HCl/ procaine dihydrate	• Nanoprecipitation Effect of aqueous phase pH, additional formulation excipients and changing to base form of drug	During	Procaine HCl: pH 5.8: 6.3–14.5% (EE), 0.2–4.6% (DL) pH 9.3: 28.3–62.0% (EE), 0.7–3.2% (DL) Procaine dehydrate: pH 5.8: 34.8–44.1% (EE), 0.4–4.1% (DL)	[9]
L-Asparaginase	• Double emulsion/solvent evaporation PLG copolymer with different MW and carboxyl groups	During	EE: 15–40%, DL 1.8–4.9% Increased DL and EE with increased MW and existence of carboxyl groups	[10]

(*Continued*)

Table 5.1 (*Continued*).

Drug	Loading method	Time of loading	Entrapment efficiency (EE) and drug loading (DL)	Ref.
Cyclosporine A	• Emulsion/solvent evaporation PLA-PEG copolymer vs. PLA polymer nanoparticles vs. microparticles	During	PLA-PEG: 86–96% (EE), 14.4–16.2% (DL) PLA: 83–96% (EE), 14.7–16.7% (DL)	[11]
Doxorubicin	• Polymerization with drug added before or after completion of polymerization	During vs. after	During: 50–70% (EE), 80 μg/mg particle (DL) After: 25–35% (EE), 40 μg/mg particle (DL)	[12]

[1]Nanoparticle, [2]microparticle, [3]N^6-cyclopentyladenosine, [4]bovine serum albumin

[1] Pandey, Ahmad, Sharma, & Khuller (2005)
[2] Lecaroz, Gamazo, Renedo, & Blanco-Prieto (2006)
[3] Leo, Scatturin, Vighi, & Dalpiaz (2006)
[4] Bhattarai, Ramay, Chou, & Zhang (2006)
[5] Pfeifer, Burdick, Little, & Langer (2005)
[6] Thote & Gupta (2005)
[7] Jiang, Hu, Gao, & Shen (2005)
[8] Quaglia, Ostacolo, De Rosa, La Rotonda, Ammendola, Nese, Maglio, Palumbo, & Vauthier (2006)
[9] Govender, Stolnik, Garnett, Illum, & Davis (1999)
[10] Gaspar, Blanco, Cruz, & Alonso (1998)
[11] Gref, Quellec, Sanchez, Calvo, Dellacherie, & Alonso (2001)
[12] Bapat & Boroujerdi (1992)

Table 5.2 Examples of drug loading of dendrimers.

Drug	Loading method	Time of loading	Entrapment efficiency (EE) and drug loading (DL)	Ref.
Chloroquine phosphate	• Equilibrium dialysis method PEGylated peptide dendrimers with PEG of various MW different generations, coated vs. uncoated	After	DL: 3–27 mol/mol dendrimer (≡ 0.2–1%)	[13]
Adriamycin methotrexate	• Incubation for 24 h, separation: adding non-solvent for drug PAMAM-PEG dendrimers with PEG of various MW different generations	After	DL: adriamycin: 1–7 mol/mol dendrimer Methotrexate: 10–26 mol/mol dendrimer	[14]
Flurbiprofen	• Incubation for 24 h in drug solution with different pH separation: filtration	After	Increased drug loading with increased pH	[15]
Rhodamine β-Carotine	• Incubation, separation: dialysis Novel polyester-*co*-polyether dendrimers with hydrophilic core Effect of different nominal drug loading and drugs with different polarities	After	Rhodamine (hydrophilic): 63.3–64.5% (EE), 10.8–15.8% (DL) β-Carotine (hydrophobic): 33.5–33.7% (EE), 5.9–6.5% (DL)	[16]
5-Fluorouracil	• Incubation for 24 h, separation: dialysis Effect of different solvents, pH and ionic strength PAMAM dendrimer grafts with phospholipids coating	After	DL for dendrimer grafts with phospholipid coating: 53%	[17]
Efavirenz	• Equilibrium dialysis method PPI dendrimers conjugated with t-Boc-glycine or mannose	After	EE: 32% (PPI), 47% (mannose PPI), 23% (t-Boc-PPI)	[18]
Ibuprofen	• Incubation for 24 h, separation: adding non-solvent for drug PAMAM-NH_2 (G3 and G4), hyperbranched Polyol-OH	After	DL: 32 mol/mol G3, 78 mol/mol G4, 24 mol/mol polyol	[19]

(*Continued*)

Table 5.2 (*Continued*).

Drug	Loading method	Time of loading	Entrapment efficiency (EE) and drug loading (DL)	Ref.
Ibuprofen	• Conjugation of drug to end group of dendrimers	After	DL: 58 mol/mol dendrimer (≡ 47%)	[20]
5-Amino-salicylic acid	• Conjugation of drug to surface end group of PAMAM dendrimers with different spacers (PABA or PAH)	After	DL: 6.6% (PABA), 14.6% (PAH)	[21]
Indomethacin	• Incubation for 24 h, separation: centrifugation PAMAM and folate-conjugated PAMAM dendrimers	After	DL: 18–61 mol/mol dendrimers (≡ 31–48%), increased DL with increased folate content	[22]
Salicylic acid L-Dopa	Drug chemically incorporated into dendrimer structure	During	DL in G3: salicylic acid: 60 mol and L-dopa: 30 mol/mol dendrimer	[23]

[13] Bhadra, Bhadra, & Jain (2006)
[14] Kojima, Kono, Maruyama, & Takagishi (2000)
[15] Asthana, Chauhan, Diwan, & Jain (2005)
[16] Dhanikula & Hildgen (2006)
[17] Tripathi, Khopade, Nagaich, Shrivastava, Jain, & Jain (2002)
[18] Dutta, Agashe, Garg, Balasubramanium, Kabra, & Jain (2007)
[19] Kolhe, Misra, Kannan, Kannan, & Lieh-Lai (2003)
[20] Kolhe, Khandare, Pillai, Kannan, Lieh-Lai, & Kannan (2006)
[21] Wiwattanapatapee, Lomlim, & Saramunee (2003)
[22] Chandrasekar, Sistla, Ahmad, Khar, & Diwan (2007)
[23] Tang, June, Howell, & Chai (2006a); Tang, Martinez, Sharma, & Chai (2006b)

Table 5.3 Examples of drug loading of solid lipid nanoparticles and nanostructured lipid carriers.

Drug	Loading method	Time of loading	Entrapment efficiency (EE) and drug loading (DL)	Ref.
Prednisolone	• Cold and hot homogenization at different temperature and surfactant concentration	During	EE: 85% (cold homogenization), 50–56% (hot homogenization)	[24]
Tetracaine Etomidate Prednisolone	• Cold homogenization (prednisolone) • Hot homogenization (tetracaine, etomidate) with different types of surfactant	During	Tetracaine, etomidate: 85–99% (EE), 1–10% (DL) prednisolone: 71–80% (EE), 2–4% (DL)	[25]
Isotretinoin	• Hot homogenization with different surfactant concentration	During	EE: 80–100%	[26]
Insulin	• Three different modifications of precipitation method WGA-*N*-glut-PE-modified SLN	During	EE: 26–67% (SLN) EE: 17–40% (WGA-*N*-glut-PE-modified SLN)	[27]
Methotrexate	• Microemulsion technique Different lipid concentration	During	DL: 37–52%	[28]
Retinol	• Hot homogenization SLN vs. NLC	During	DL: 0.3% (SLN), 3.8% (NLC)	[29]
Clobetasol	• Precipitation method at different temperatures SLN vs. NLC with different amount of liquid lipid	During	EE: 45–53% (SLN), 67–70% (NLC); DL: 2.3–2.6% (SLN), 3.4–3.5% (NLC)	[30]

[24] zur Mühlen & Mehnert (1998a)
[25] zur Mühlen, Schwarz, & Mehnert (1998b)
[26] Liu, Hu, Chen, Ni, Xu, & Yang (2007)
[27] Zhang, Ping, Huang, Xu, Cheng, & Han (2006b)
[28] Ruckmani, Sivakumar, & Ganeshkumar (2006)
[29] Jenning, Thünemann, & Gohla (2000)
[30] Hu, Jiang, Du, Yuan, Ye, & Zeng (2006)

are incubated in a drug solution for drug loading, drug can be extensively adsorbed to the large surface area of nanoparticles which in turn can result in initial burst release, which is more pronounced the smaller the article. (Chorny et al., 2002; Lecaroz, Gamazo, Renedo, & Blanco-Prieto, 2006; Pohlmann, Soares, Cruz, Da Silveira, & Guterres, 2004). Furthermore, this method in general results in lower drug loading (Bapat & Boroujerdi, 1992; Illum, Khan, Mak, & Davis, 1986; Lopes, Pohlmann, Bassani, & Guterres, 2000; Soppimath et al., 2001). Additionally, the time of incubation can also influence the drug loading, and the incubation time has to be sufficient to reach equilibrium for maximum loading (Lopes et al., 2000).

An important factor when loading drugs is the interaction between drug and carrier system because with increasing interaction the drug loading as well as entrapment efficiency increases; however, the release rate declines (Bhattarai, Ramay, Chou, & Zhang, 2006; Gaspar, Blanco, Cruz, & Alonso, 1998; Govender, Riley, Ehtezazi, Garnett, Stolnik, Illum, & Davis, 2000; Huo et al., 2006; Jiang, Hu, Gao, & Shen, 2005; Lee, Cho, & Cho, 2004;

Table 5.4 Examples of drug loading of polymeric micelles.

Drug	Loading method	Time of loading	Entrapment efficiency (EE) and drug loading (DL)	Ref.
Camptothecin	• Dialysis method with different solvents Different nominal drug loading	During	EE: 30–90%	[31]
Cyclosporine A	• Co-solvent evaporation method with different co-solvent compositions and sequences of adding MePEO-*b*-PCL micelles with various MePEO and PCL molecular weights	During	Co-solvent composition EE: 36–76%, DL: 0.11–0.23 (w/w) MePEO and PCL molecular weights EE: 12–76%, DL: 0.04–0.23 (w/w)	[32]
Beclomethasone dipropionate	• Solvent evaporation method Different nominal drug loadings and drug/polymer ratios	During	EE: 4–100%	[33]
Fenofibrate	• Evaporation of a negative acetonitrile-water azeotrope PEG-*b*-PCL micelles with various MW of PCL	During	EE: 29–95%	[34]
Indomethacin	• Dialysis method Micelles with different lactone monomers, feed molar ratios of lactone/PEG and MW of PEG	During	EE: 5–100%	[35]
DMS[1] MPG[2] PNS[3] IBU[4] KET[5] IND[6]	• Dialysis method Effect of copolymer composition (polyphosphazenes), drug structure and nominal drug loading	During	DMS: 1.1–4.2% (EE), 0.2–0.7% (DL) MPG: 3.0–7.8% (EE), 0.5–1.3% (DL) PNS: 2.2–7.2% (EE), 0.4–1.2% (DL) IBU: 21.8–42.8% (EE), 3.6–7.1% (DL) KET: 5.5–10.7% (EE), 0.9–1.8% (DL) IND: 42.7–78.2% (EE), 7.1–13% (DL)	[36]
Papaverine	• Dialysis method PEO-PLA block copolymers with different content of carboxylic acid in PLA block	During	DL: 4–15% DL increased with increased number of carboxylic groups in copolymer	[37]
Adriamycin	• Dialysis method Polymeric mixed micelle with various ratios of polyHis/PEG and PLLA/PEG	During	EE: 75–85%, DL: 15–17%	[38]

[1]Dxamethasone, [2]medroxyprogesterone acetate, [3]prednisone acetate, [4]ibuprofen, [5]ketoprofen, [6]indomethacin

[31] Opanasopit, Ngawhirunpat, Chaidedgumjorn, Rojanarata, Apirakaramwong, Phongying, Choochottiros, & Chirachanchai (2006)
[32] Aliabadi, Elhasi, Mahmud, Gulamhusein, Mahdipoor, & Lavasanifar (2007)
[33] Gaber, Darwis, Peh, & Tan (2006)
[34] Jette, Law, Schmitt, & Kwon (2004)
[35] Lin, Juang, & Lin (2003)
[36] Zhang, Li, Qiu, Li, Yan, Jin, & Zhu (2006a)
[37] Lee, Cho, & Cho (2004)
[38] Lee, Na, & Bae (2003)

Table 5.5 Examples of drug loading of nanoemulsions (NE) and nanocapsules (NC).

Drug	Loading method	Time of loading	Entrapment efficiency (EE) and drug loading (DL)	Ref.
Triclosan	• Solvent displacement method (NE) + chitosan (NC) Various oil amounts and chitosan at two different viscosity degrees	During	Emulsion: 86–99% (EE), 2–13% (DL) Capsules: 93–98% (EE), 2–14% (DL)	[39]
Ethionamide	• During: interfacial deposition (NC), nanoprecipitation (NS), spontaneous emulsification (NE) • After: incubation for different time periods	During vs. after	During: EE: 62.4% (NC), 53.0% (NS), 38.5% (NE) After (24 h): 56.2% (NC), 43.4% (NS)	[40]
Indomethacin	• Interfacial deposition (NC), nanoprecipitation (NS), spontaneous emulsification (NE)	During	EE: 94.5% (NC), 95.4% (NS), 90.0% (NE)	[41]
Metipranolol	• Interfacial polymerization (IP) vs. • Interfacial deposition (ID) with various polymer and oil types	During	EE: oil type: 34.6–49.9% (Migliol 840), 48.6–62.2% (Labrafil 1944 CS) Preparation: 40.7–62.2% (IP), 34.6–60.2% (ID)	[42]

[39] Maestrelli, Mura, & Alonso (2004)
[40] Lopes, Pohlmann, Bassani, & Guterres (2000)
[41] Calvo, Vila-Jato, & Alonso (1996)
[42] Losa, Marchal-Heussler, Orallo, Vila Jato, & Alonso (1993)

Pandey, Ahmad, Sharma, & Khuller, 2005; Zhang et al., 2006a). For high entrapment efficiency, it is necessary that the drug interacts preferentially with the carrier system (polymer, lipid) rather than with the surrounding medium (Opanasopit, Ngawhirunpat, Chaidedgumjorn, Rojanarata, Apirakaramwong, Phongying, Choochottiros, & Chirachanchai, 2006).

Another factor influencing drug loading as well as entrapment efficiency is the nominal drug loading. Several studies showed that the drug loading can be enhanced by increased nominal drug loading (Govender, Stolnik, Garnett, Illum, & Davis, 1999; Kolhe, Misra, Kannan, Kannan, & Lieh-Lai, 2003). However, the entrapment efficiency does not necessarily increase with higher initial drug loading (Figure 5.1). If the maximum loading capacity of the nanocarrier is reached, further increase in nominal drug loading can even decrease the efficiency (Gaber, Darwis, Peh, & Tan, 2006; Lecaroz et al., 2006).

The examples of drug loading of nanospheres (Table 5.1) demonstrate that the drugs are predominantly incorporated during nanoparticle formation. However, a high serum bovine albumin entrapment was also achieved by incubation of the pre-formulated nanoparticles in the protein solution. Another approach to load polymeric particles was performed by Zhu & McShane (2005) who loaded hydrophobic compounds by adsorbing surfactants onto the surfaces of the polymeric particles with subsequent swelling in organic solvents. In general, it can be seen that the preparation method as well as the modification of the methods such as changing the pH affects the drug loading and entrapment efficiency (Bapat & Boroujerdi, 1992; Govender et al., 1999; Jiang et al., 2005; Leo, Scatturin, Vighi, & Dalpiaz,

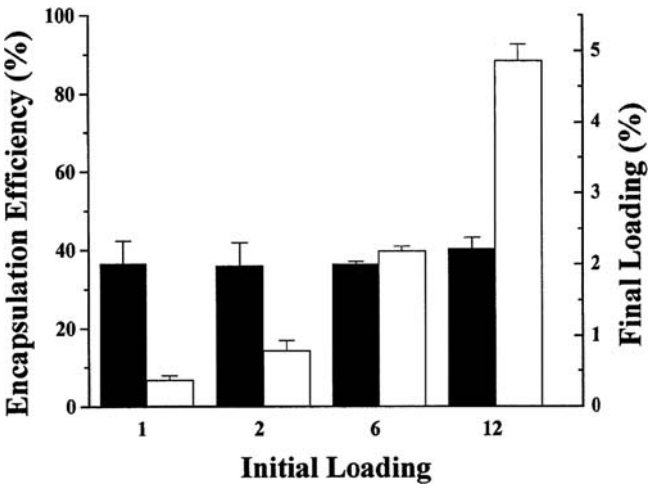

Figure 5.1 Encapsulation parameters of nanoparticles made of PLG with carboxylic-end groups (Resomer RG 503H): encapsulation efficiency (*black bars*) and final loading (*white bars*). Reprinted from Gaspar, Blanco, Cruz, & Alonso (1998) with permission from Elsevier.

2006; Quaglia, Ostacolo, De Rosa, La Rotonda, Ammendola, Nese, Maglio, Palumbo, & Vauthier, 2006). Moreover, for polymeric nanosystems, the right selection of polymer, copolymer (molecular weight, existence of functional groups, charge) and copolymer ratio is crucial for optimizing the entrapment of drugs (Gaspar et al., 1998; Pandey et al., 2005; Pfeifer, Burdick, Little, & Langer, 2005). The type of drug, e.g., base vs. salt form, also influences the drug entrapment (Govender et al., 1999).

Loading of drugs into dendrimers (Table 5.2) is usually achieved after the synthesis of the dendrimers by either incubation of the dendrimers in the drug solution or conjugation of the drug molecules to the functional end groups of the dendrimers. In general, the drug entrapment increases with higher generations (Kojima, Kono, Maruyama, & Takagishi, 2000; Kolhe et al., 2003). Furthermore, the drug loading varies with different types of dendrimers (Kolhe et al., 2003), surface modification (Bhadra, Bhadra, & Jain, 2006; Dutta, Agashe, Garg, Balasubramanium, Kabra, & Jain, 2007; Kojima et al., 2000; Tripathi, Khopade, Nagaich, Shrivastava, Jain, & Jain, 2002), different spacers used for the conjugation of the drug to the surface end group of the dendrimer (Wiwattanapatapee, Lomlim, & Saramunee, 2003) and polarity of the drug (Dhanikula & Hildgen, 2006). The drug entrapment is additionally influenced by the pH of the incubation solution, and therefore, by adjusting the pH the drug loading can be controlled (Asthana, Chauhan, Diwan, & Jain, 2005; Tripathi et al., 2002). Another new approach is the synthesis of dendrimers consisting of drug molecules (Tang, June, Howell, & Chai, 2006a; Tang, Martinez, Sharma, & Chai, 2006b) resulting in high entrapment efficiency.

From Table 5.3 it can be seen that loading of solid lipid nanoparticles (SLN) and nanostructured lipid carriers (NLC) occurs predominantly during particle formation. We could only find one example where cationic SLN was loaded with RNA after the preparation of SLN (Montana, Bondi, Carrotta, Picone, Craparo, San Biagio, Giammona, & Di Carlo, 2007). However, neither entrapment efficiency nor RNA loading was

given. The drug loading of SLN and NLC differs due to various preparation methods. In general, cold homogenization results in higher drug incorporation than hot homogenization (Üner, 2006; zur Mühlen & Mehnert, 1998a). The type of surfactant, surfactant concentration as well as production temperature also affect drug loading during the hot homogenization process (Liu, Hu, Chen, Ni, Xu, & Yang, 2007; zur Mühlen & Mehnert, 1998a; zur Mühlen, Schwarz, & Mehnert, 1998b). The introduction of liquid lipid into the solid lipid matrix (forming nanostructured lipid carriers) is another approach to increase the drug entrapment in lipid nanoparticles (Hu, Jiang, Du, Yuan, Ye, & Zeng, 2006; Jenning, Thünemann, & Gohla, 2000). As the drug must be soluble in the lipid matrix, lipophilic drugs can be entrapped into SLN and NLC with higher efficiencies.

As seen with lipid nanoparticles, polymeric micelle formation and drug incorporation also occur simultaneously (Table 5.4). Lipophilic drugs especially are favorably incorporated into polymeric micellar carrier systems. Drug loading can be improved by increasing the polymer concentration (Figure 5.2), employing polymers with higher molecular weights (MW) (Aliabadi, Elhasi, Mahmud, Gulamhusein, Mahdipoor, & Lavasanifar, 2007; Jette, Law, Schmitt, & Kwon, 2004) or using grafted copolymers with functional end groups (Lee et al., 2004). However, the micelle production procedure can be optimized to obtain higher entrapment of drugs by careful selection of solvent, cosolvent and experimental setup (Aliabadi et al., 2007; Opanasopit et al., 2006).

Table 5.5 shows examples of drug loading in nanoemulsions and nanocapsules, as well as the comparison between them and nanospheres. In general, higher drug loading is obtained for nanocapsules (prepared by interfacial deposition) compared to nanospheres (formed by nanoprecipitation) as the relative mass of the polymer used for capsules is reduced (Couvreur et al., 2002; Lopes et al., 2000). The entrapment of drugs into nanoemulsions is reduced compared to nanospheres and nanocapsules (Calvo, Vila-Jato, & Alonso, 1996; Lopes et al., 2000). Moreover, the higher the solubility of the drug in the oil phase, the higher the drug entrapment in nanocapsules and nanoemulsions (Losa, Marchal-Heussler, Orallo, Vila Jato, & Alonso, 1993).

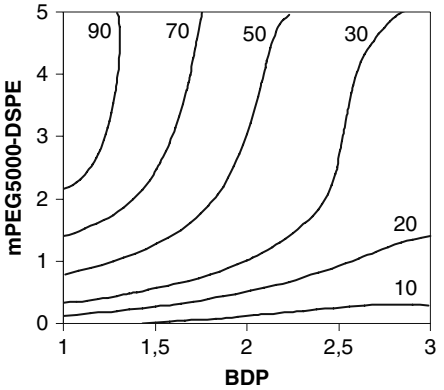

Figure 5.2 Contour plot showing the entrapment efficiency (%) at various concentrations of beclomethasone dipropionate, BDP ($\times 10^{-1}$ μmol/ml) and poly-(ethylene oxide)-*block*-distearoyl phosphatidyl-ethanolamine, mPEG5000-DSPE ($\times 10^{-1}$ μmol/ml). Reproduced from Gaber, Darwis, Peh, & Tan (2006) with permission from ACS Publications.

In summary, no overall guideline can be given for drug loading as it depends on the drug that should be incorporated into the nanocarrier system, the intended administration route, the target as well as the release profile (burst release at a specific target, sustained release, etc.). Based on the choice of the drug, the administration route, drug target and release profile, a nanocarrier system as well as loading technique can be selected using some general rules as outlined in this chapter. By doing this, the optimum drug loading and entrapment efficiency can be achieved.

Drug Release

Mechanisms of Release from Nanosystems

Dissolution

Dissolution is a kinetic, usually diffusion-controlled process, and the rate of dissolution is defined as the mass of drug dissolved at a given time. The basic principle of dissolution rate was given by Noyes & Whitney (1897) and is described by the well-known equation:

$$\frac{\mathrm{d}M}{\mathrm{d}t} = \frac{DA}{h}(C_S - C) \tag{3}$$

where $\mathrm{d}M/\mathrm{d}t$ is the mass rate of dissolution, D is the diffusion coefficient of the drug in solution, A is the surface area of solid in contact with dissolution medium, C_S is the solubility of the drug, C is the concentration of the drug at time t and h is the thickness of the diffusion boundary layer at the solid's surface. In Eq. 3 it is assumed that the surface area A of the solid is constant during dissolution. However, if a particle dissolves, its surface area and volume change with time. Therefore, Hixson & Crowell (1931) derived an equation for the dissolution rate that was normalized for the decrease in surface area as the particle dissolves assuming that the shape of the particle is not changing during dissolution:

$$M^{1/3} = M_0^{1/3} - \kappa t \tag{4}$$

Equation 4 is known as the Hixson–Crowell cube-root equation and M_0 is the mass of the drug particles prior to dissolution, M is the mass of undissolved drug particles at time t and κ is the cube-root dissolution constant defined as

$$\kappa = [N\rho(\pi/6)]^{1/3}\,\frac{2DC_S}{h\rho} = \frac{M_0^{1/3}}{d}\frac{2DC_S}{h\rho} \tag{5}$$

where N is the number of particles and ρ is the drug's density. If drug particles with different sizes are present, a new correlation model between particle size distribution and dissolution can be used to predict the in vitro dissolution rate of a drug formulation with different particle sizes (Tinke, Vanhoutte, De Maesschalck, Verheyen, & De Winter, 2005).

It can be seen from Eqs. 3 and 5 that the dissolution rate is directly proportional to the surface area A of the particle and the saturated solubility C_S of the drug. In contrast, the particle size (described by the diameter d) and the thickness of the diffusion boundary layer h are inversely related to the dissolution rate. These parameters change and affect the dissolution rate of drugs when a system is moved from microsized particles to nanosized particles. It is a well-known effect that the specific surface area is increased by decreased particle size, yielding a higher dissolution rate (Figure 5.3). Anderberg, Bisrat, & Nyström (1988) showed in a study, investigating the dissolution of felodipine, that the dissolution was enhanced for smaller particles. However, a plot of the surface-specific dissolution rate vs. particle size revealed that the increase in dissolution rate with decreasing particle size was stronger than what can be explained from an increase in surface area alone.

This effect was explained by a decrease in diffusion boundary layer thickness with decreasing drug particle radius. Bisrat & Nyström (1988) investigated the effect of particle size on the thickness of the diffusion boundary layer and found that for particles smaller than 5 μm the agitation intensity did not significantly change the surface-specific dissolution rate, whereas the dissolution rate was significantly increased at higher agitation intensities for particles in the range of 15 and 25 μm. They concluded that the increase in dissolution rate for smaller particles might also be explained by a reduced boundary diffusion layer thickness in addition to an increased surface area and explained it with the Prandtl boundary layer equation:

$$h_H = k \cdot L^{1/2} / V^{1/2} \tag{6}$$

where h_H is the hydrodynamic boundary layer thickness, L is the length of the surface in the direction of flow, k is a constant and V is the relative velocity of the flowing liquid vs. the flat surface. The higher curvature of smaller particles results in a reduced surface in the direction of flow (L) and therefore in a thinner diffusion boundary layer.

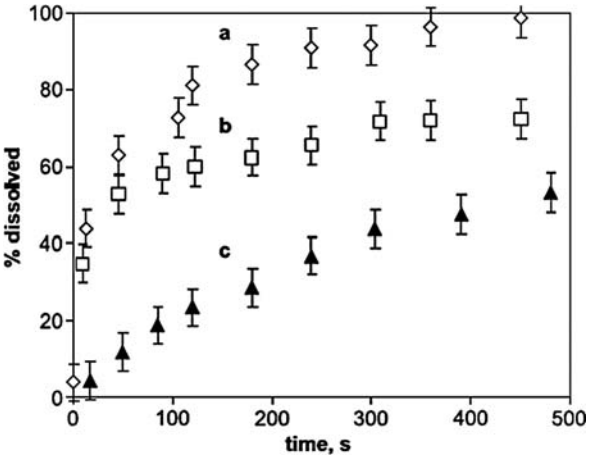

Figure 5.3 Dissolution profiles of two griseofulvin suspensions with (**a**) VMD = 760 nm and NMD = 224 nm, and (**b**) VMD = 978 nm and NMD = 784 nm compared with a micronized material with (**c**) VMD = 5.9 μm and NMD = 2.3 μm. Reprinted from Shekunov, Chattopadhyay, Seitzinger, & Huff (2006) with permission from Springer.

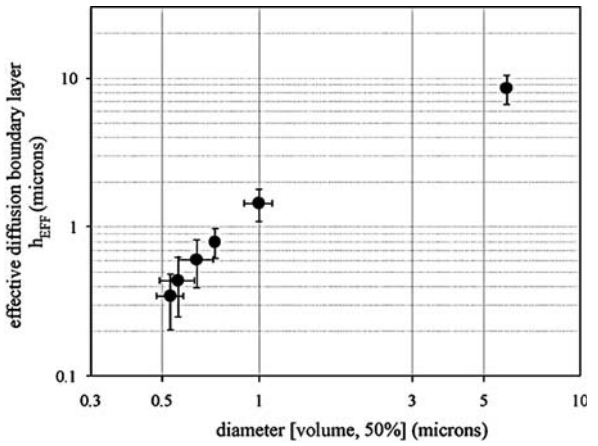

Figure 5.4 Experimentally determined values for the effective hydrodynamic diffusion layer h_{EFF}. Reprinted from Galli (2006) with permission from Elsevier.

Galli (2006) confirmed by indirect experimental determination of the diffusion boundary layer thickness of particles in the range of 0.53–5.9 μm that the effective diffusion boundary layer h_{EFF} is directly proportional to the particle diameter for smaller particles (Figure 5.4). Moreover, the dissolution rate is indirectly proportional to the square of the particle diameter.

However, smaller particles do not always result in higher surface-specific dissolution rates. By using the Heywood's shape factor (Heywood, 1954), Mosharraf & Nyström (1995) suggested a combined effect of particle size and shape on dissolution rate (Figure 5.5) and found that small spherical particles (with shape factor of approximately 6) dissolved faster than large, irregular particles (with shape factors > 6) due to a change in the diffusion boundary layer (increase in L with enhanced degree of irregularity yielding a broader diffusion boundary layer). Mihranyan & Strømme (2007) also described in their work that the surface properties, and therefore the surface dimension, become more important for smaller particles. They derived a relationship between fractal surface dimension

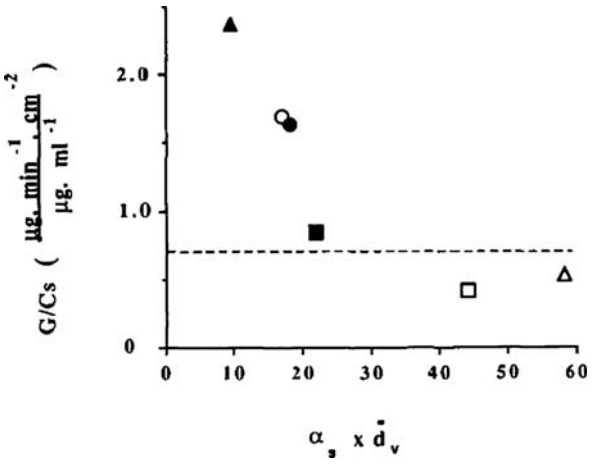

Figure 5.5 Combined effect of particle size and shape on the surface-specific dissolution rate (G) corrected for the effect of solubility (C_S). (○) Griseofulvin, (▲) glibenclamide, (●) barium sulphate quality I, (△) barium sulphate quality II, (■) barium sulphate quality III, (□) oxazepam. Reprinted from Mosharraf & Nyström (1995) with permission from Elsevier.

and solubility and predicted a higher solubility for particles with a rough surface compared to particles with a smooth surface. Additionally, the surface properties can alter due to changes in the surface environment. Zhang, Gilbert, Huang, & Banfield (2003) observed a structural modification to a more crystalline structure of ZnS nanoparticles when they were in contact with water compared to methanol. The addition of water resulted in strong interactions between the surface of the nanoparticles and water and hence in a reduction of the interfacial energy. This structural modification due to surface environment can also have an influence on the dissolution rate of nanoparticles.

Another important property of the drug to consider is the solubility. A decreased particle size causes a higher curvature resulting in higher surface free energy and therefore higher solubility. The Ostwald-Freundlich equation derives the inverse relationship of particle size and solubility as the solubility increases with decreasing radius r of spherical particles:

$$\ln \frac{S}{S_0} = \frac{2\gamma_{SL} M}{rRT\rho} \tag{7}$$

S and S_0 are the solubilities of the spherical particle and the flat surface, respectively, M is the molecular weight, ρ is the density of the drug and γ_{SL} is the interfacial tension between the solid and the liquid phase surrounding the particles. This equation has been corrected by Knapp (1922) who introduced the effect of surface charge on solubility. It was found that the solubility is increased by decreased particle size up to a certain particle radius r^* below which the solubility is decreasing again (Figure 5.6) (Mihranyan & Strømme, 2007).

It should also be mentioned that with an increase in free surface energy (smaller particles) the particles tend to agglomerate and grow (Ostwald ripening) which in turn can decrease the surface area. Therefore, one has to keep in mind that with a higher degree of agglomeration and growth, the surface area, taking part in the dissolution process, can be overestimated (Bisrat & Nyström, 1988).

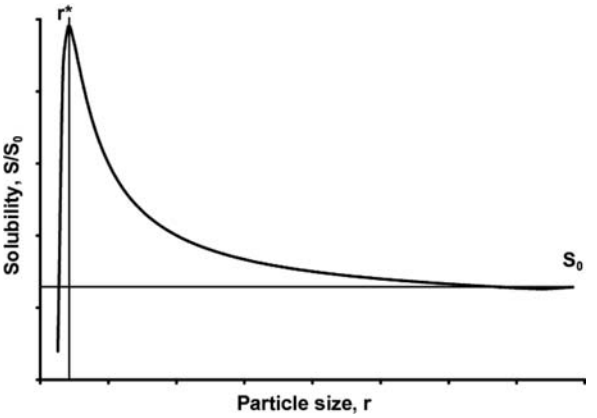

Figure 5.6 The effect of the particle size on solubility according to Knapp (1922). S_0 is the equilibrium solubility and r^* is the particle size at which maximum solubility is obtained. Reprinted from Mihranyan & Strømme (2007) with permission from Elsevier.

Contrary to the known theory, the smaller the particles, the higher the dissolution rate, Tang, Wang, Orme, Bonstein, Bush, & Nancollas (2004) observed an unusual dissolution behavior for small crystallites approaching a critical value. They obtained higher dissolution rates for the larger crystallites (500–600 nm) of synthetic apatite than for the smaller crystallites (150–250 nm) and found that the dissolution may be self-inhibited. This behavior was attributed to a kinetic phenomenon, and a dissolution model was given.

Limited attention has been focused on the effect of surface tension and wettability of nanoparticles employed in pharmaceutical sciences. However, a study performed by Sdobnyakov & Samsonov (2005) investigating the size dependence of surface tension for Lennard-Jones, polymeric and metallic nanosized droplets revealed that for very small droplets (2–10 nm in radius) the surface tension decreases with size, whereas above this critical radius (R_c) the surface tension approaches the one of the macroscopic planar interface (Figure 5.7).

In another study (Powell, Fenwick, Bresme, & Quirke, 2002), it was found that the wettability of nanoparticles (> 1 nm) can be described by the Young's equation for high surface tension interfaces. This may be one example where a model utilized for the description of macroscopic systems can also be used for the nanoscale systems. The wettability of aligned carbon nanotubes was successfully manipulated by changes in surface structure and chemical modification, and could be adjusted from hydrophilic to hydrophobic and even to superhydrophobic (Liu, Zhai, & Jiang, 2006b).

In summary, the dissolution of a drug from small particles occurs in two steps (Figure 5.8) (Crisp, Tucker, Rogers, Williams, & Johnston, 2007; Mosharraf & Nyström, 1995): first, the interaction between the solute and solvent resulting in dissociation of drug molecules from the solid (solvation step) and the second step which is the diffusion of the drug molecule into the bulk dissolution media.

Usually, the diffusion is the rate-limiting step (Bisrat, Anderberg, Barnett, & Nyström, 1992), and mathematical models describing the dissolution process are based on Fickian diffusion laws. As already

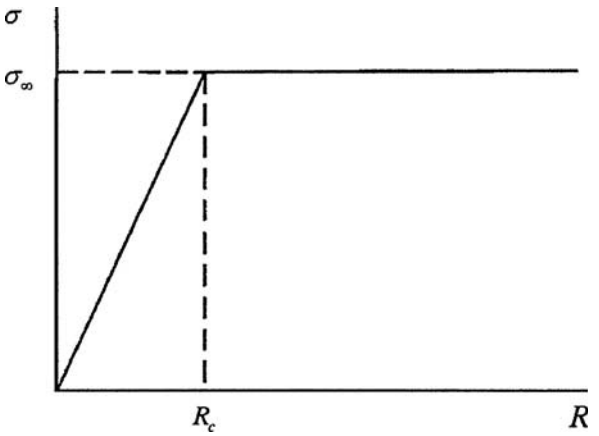

Figure 5.7 A first approximation for the surface tension (σ (R)) dependence adequate for nanodroplets of different types (molecular fluids, water, metal melts). Reprinted from Sdobnyakov & Samsonov (2005) with permission from Versita.

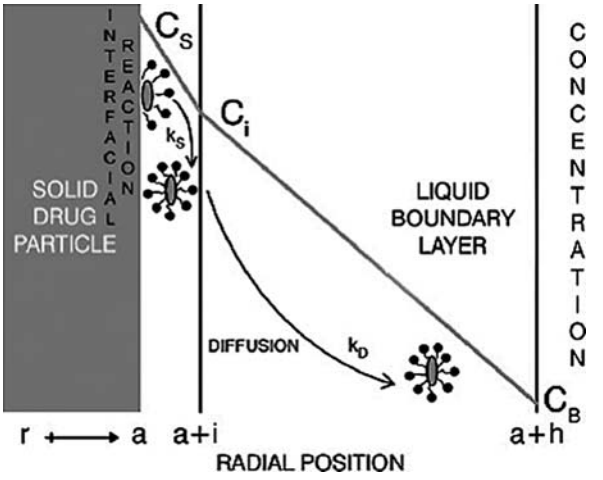

Figure 5.8 Interfacial reaction and diffusion resistances in two-step dissolution model. C_B is the bulk concentration, $r = a + h$ is the boundary layer, $r = a$ is the solid–liquid interface and $r = a + i$ is the distance where interfacial reaction takes place. Reprinted from Crisp, Tucker, Rogers, Williams, & Johnston (2007) with permission from Elsevier.

mentioned, the dissolution rate described as a diffusional process is directly proportional to surface area, drug solubility and indirectly proportional to the diffusion boundary layer. For very small particles, the surface area as well as solubility is increased and the diffusion boundary layer is decreased. Therefore, the question arises if the dissolution is still diffusion controlled when the obtained results are extrapolated to nanosized particles, does the diffusion boundary layer still exist for infinitely small particles? Or is the interaction between solvent and solute becoming the rate-limiting step? An attempt to distinguish between these two steps during dissolution was carried out by Shekunov, Chattopadhyay, Seitzinger, & Huff (2006), and it was found that for particles in the range of 100–1000 nm the solvation step (surface kinetic, k_S) controls the dissolution rather than the diffusion of the drug molecules into the bulk medium. Similar conclusions were drawn by Crisp et al. (2007) as they stated that the solvation step becomes the dominant factor in the dissolution rate of nanoparticles. Additionally, they found that the interfacial reaction rate constant, k_S (solvation step), is independent of particle size and suggested that the dissolution rate of nanosized drug particles can be predicted from the dissolution rate of micron-sized drug particles. However, k_S differed due to the type of drug and release media. Figure 5.9 shows that for increasing particle size the rate of solvation (k_S) becomes less dominant in the process of dissolution relative to the rate of diffusion (k_D). The increase in dissolution rate (k_{Eff}) by reducing the particle size will be more pronounced for drugs with higher values of k_S because the rate of diffusion becomes more important.

The process of dissolution not only is important for drug delivery systems but can also be used to evaluate the nanomaterials (Borm, Klaessig, Landry, Moudgil, Pauluhn, Thomas, Trottier, & Wood, 2006).

Drug Release from Homogeneous and Granular Matrices

If a drug is uniformly dispersed in a polymer matrix system (nanospheres) which is non-biodegradable or the degradation of the polymer only occurs

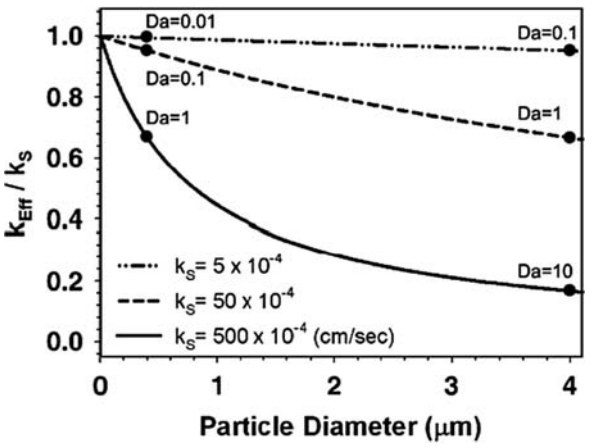

Figure 5.9 Ratio of effective dissolution rate constant, k_{Eff} to interfacial rate constant, k_S, as a function of particle size for various values of k_S. $D = 1\times10^{-6}$ cm^2/s and $h = a$. The diffusion resistance is zero when $k_{Eff}/k_S = 1$. Reprinted from Crisp et al. (2007) with permission from Elsevier.

much later than the release of the drug (drug is not released by erosion of the polymer matrix), the drug has to dissolve and diffuse in the polymer matrix to reach the surface and to partition into the surrounding medium. In this case of diffusion-controlled release, the well-known Higuchi equation (Higuchi, 1963) describes the release transport and indicates that the release rate is proportional to the square root of time:

$$Q = [D(2C_T - C_S)\, C_S t]^{1/2} \tag{8}$$

Q is the amount of drug released at time t and per unit area of exposed matrix surface, D is the diffusion coefficient of the drug in the polymer matrix, C_T is the total concentration and C_S the solubility of the drug in the polymer matrix. In case of a porous matrix, the Higuchi equation is extended by the porosity (ε) of the matrix and the tortuosity (τ) of the capillary system and is expressed as

$$Q = \left[\frac{D\varepsilon}{\tau}(2C_T - \varepsilon\, C_S)C_S t\right]^{1/2} \tag{9}$$

Despite the porosity, the Higuchi equations indicate that the release rate is directly proportional to the surface area, the total amount of drug incorporated in the matrix (drug loading), the solubility of the drug in the polymer matrix and the diffusion coefficient of the drug in the polymer matrix. A very important factor in release is the interaction between drug and polymer that is expressed by an alteration of the diffusion coefficient: the higher the interaction between matrix and drug, the lower the diffusion coefficient (Chorny et al., 2002). Examples where the release kinetic from nanoparticles followed the Higuchi model are the release of beclomethasone dipropionate and indomethacin, respectively, from polymeric micelles (Gaber et al., 2006; Zhang et al., 2006a).

Guy, Hadgraft, Kellaway, & Taylor (1982) derived equations to describe the release rate from spherical particles and pointed out that for particles with a radius smaller than 1 mm the effect of the interfacial transfer kinetics becomes rate limiting. Two expressions were given, one for a short time period (Eq. 10) and another one for a long time period (Eq. 11):

$$M_t = Ac_0 r\kappa\tau \tag{10}$$

$$M_t = \frac{1}{3} Ac_0 r(1 - e^{-3\kappa\tau}) \tag{11}$$

where M_t is the released amount of drug at time t, A is the surface area, τ is a normalized parameter, c_0 is the initial drug concentration in the particle, r is the radial distance from the center of the sphere and κ describes the interfacial transfer process.

A simple, empirical equation to describe the first 60% of the release curve was derived by Ritger & Peppas (1987a) where the diffusional exponent n characterizes the release mechanism:

$$\frac{M_t}{M_\infty} = kt^n \tag{12}$$

M_t/M_∞ is the fractional solute release, t is the release time and k is constant describing characteristics of the polymer matrix and the drug. Release transport can be classified according to the diffusional exponent that has different values for the various swellable as well as non-swellable carrier systems (Ritger & Peppas, 1987 a,b). This empirical equation was, for example, employed to determine the mechanism of the release of bovine serum albumin from nanospheres (Leo et al., 2006).

Another mechanism of drug release from a polymer matrix is the liberation of drug by erosion of the polymer. The degradation kinetic of polymers is complex and influenced by a variety of factors. The erosion kinetic is not covered by this chapter and the reader is referred to other literature (Siepmann & Göpferich, 2001; Siepmann, Faisant, & Benoit, 2002; von Burkersroda, Schedl, & Göpferich, 2002). However, the size of the particles might also have an influence on the degradation rate as Panyam, Dali, Sahoo, Ma, Chakravarthi, Amidon, Levy, & Labhasetwar (2003) found that the degradation rate of poly(D,L-lactide-*co*-glycolide) during the initial phase was higher for 100 nm particles than for 1 or 10 μm particles. Another study confirmed that the hydrolytic degradation rate of nano-fibrous poly(L-lactic acid) foams was accelerated by the larger surface area compared to the solid-walled foams (Chen & Ma, 2006). It should also be emphasized that for these systems different release mechanisms can occur simultaneously and that it is difficult to separate these mechanisms when evaluating experimental data.

Many mathematical models for release kinetic are described in the literature, most of them for macroscopic and microscopic systems. Some attempts of modeling the release pattern from nanoparticles have been carried out (Cruz, Soares, Costa, Mezzalira, da Silveira, Guterres, &

Pohlmann, 2006; Jo, Kim, Kim, Kim, Jeong, Kim, & Muhammed, 2004; Polakovič, Görner, Gref, & Dellacherie, 1999). Jo et al. and Polakovič et al. used a diffusion model and dissolution model to fit experimental data. Polakovič et al. (1999) found that the diffusion model could be used to describe the release from nanoparticles with a low drug loading where the drug was molecularly dispersed. On the contrary, if the drug was in the crystallized form at higher drug loading, the release rate was dissolution controlled. Cruz et al. (2006) investigated the kinetic release behavior of indomethacin and indomethacin ethyl ester, respectively, from different nanocarriers: nanocapsules, nanoemulsions and nanospheres. They discovered no difference in the release pattern of the various nanocarriers when the drug (indomethacin) is adsorbed on the nanoparticles (Figure 5.10A). However, if the drug (indomethacin ethyl ester) is entrapped into the nanocarrier, the various delivery systems exhibit different release kinetics (Figure 5.10B).

Referring to the examples given for drug loading (Tables 5.1–5.5), for most of these systems their release properties are also reported. Only few samples will be mentioned here as another chapter 10 in this book deals in more detail with controlled release. In general, the release from nanocarriers follows a biphasic pattern with an initial burst release of adsorbed and weakly bound drug from the surface followed by a slower release rate attributed to the diffusion of entrapped drug through the matrix. This fact implies that the drug distribution within the nanoparticles influences the release pattern because with a higher amount of drug close to the surface or adsorbed to the surface, the initial burst effect is increased. In contrast, if the drug is more uniformly distributed or a higher amount is entrapped inside the nanoparticles compared to the amount close to the surface, the initial rapid release rate is reduced. The burst release is an important issue that has to be taken into account for drug delivery systems on nanoscale because of the high surface to volume ratio. Furthermore, the release profile depends on the method of drug loading because the particle production method influences the drug distribution (Quaglia et al., 2006; Zhang et al., 2006a). An example of the influence of drug loading is the

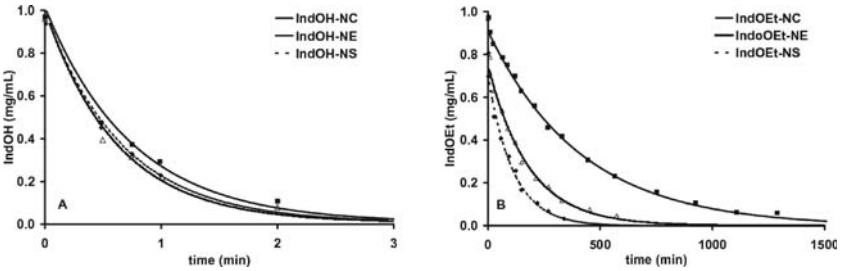

Figure 5.10 (**A**) Indomethacin (IndOH) and (**B**) indomethacin ethyl ester (IndOEt) consumption from probe-loaded nanocapsules (NC), probe-loaded nanoemulsion (NE) and probe-loaded nanospheres (NS). Reprinted from Cruz, Soares, Costa, Mezzalira, da Silveira, Guterres, & Pohlmann (2006) with permission from Elsevier.

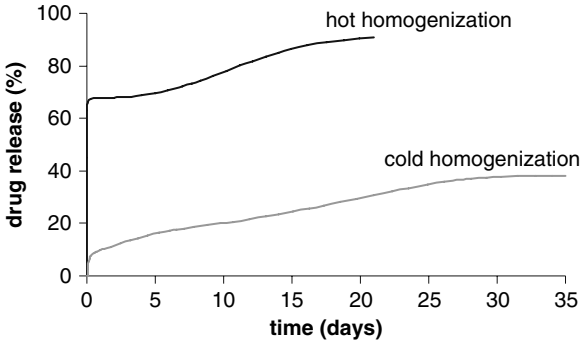

Figure 5.11 Release profiles of prednisolone (1% calculated on the particle mass) from compritol SLN produced by hot (90°C) and cold homogenization. The systems were stabilized with 2.5% poloxamer 188. Reproduced from zur Mühlen & Mehnert (1998a) with permission from Govi Verlag.

effect of hot and cold homogenization on the release profile of prednisolone (zur Mühlen & Mehnert, 1998a). The burst release was more pronounced for solid lipid nanoparticles prepared at a higher production temperature (Figure 5.11), because it was found that the hot homogenization procedure resulted in a drug enrichment of the outer layers of the solid lipid nanoparticles.

Different loading techniques were also used by Leo et al. (2006) to load bovine serum albumin (BSA) into nano- and microspheres. The release experiments demonstrated the differences in release pattern due to the various methods used for particle formation. The nanospheres prepared by the double emulsion method showed an elevated burst release compared to the particles prepared by a novel method employing thermosensitive Pluronic F-127 gel (Figure 5.12). Confocal laser scanning

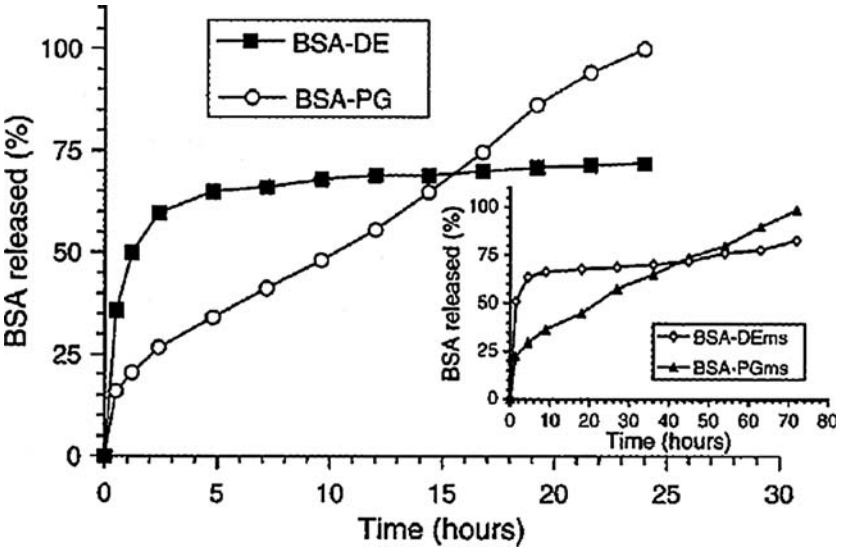

Figure 5.12 In vitro release in 20 mM phosphate buffer at 37°C of bovine serum albumin (BSA) from nanospheres and microspheres (ms, inset) obtained by the double emulsion method (DE) or the novel encapsulation method (PG). Results are the means of three independent experiments (SD less than 10%). Reprinted from Leo, Scatturin, Vighi, & Dalpiaz (2006) with permission from ACS Publications.

microscopy revealed that the particles prepared by the double emulsion method yielded a higher amount of BSA at the particles' surface compared to the particles formed by the other preparation method where the drug could be entrapped in the core of the nanospheres.

As mentioned before, the interaction between drug and carrier matrix not only affects the drug loading but also influences the release rate as well as the extent of release. Sometimes, the interaction between drug and matrix has to be neutralized by, e.g., introducing ions (buffer solutions) to enable the release from the carrier. The dendrimer-methotrexate inclusion complex released methotrexate in PBS buffer, while no methotrexate was released when water was used (Patri, Kukowska-Latallo, & Baker, Jr., 2005). Similar results were obtained with ibuprofen (Kolhe et al., 2003).

More fundamental investigations are required to fully elaborate and understand the release mechanism of drugs from nanocarriers. The effect of nanopore size on water and drug permeation is one aspect. Pores below 1 nm are found in carbon nanotubes, zeolites and ion channel proteins, all of which could be used for nanoparticle drug delivery. Beckstein, Tai, & Sansom (2004b) have simulated the movement of ion permeation through nanopores and found that ions were still excluded from pores even though these pores had radii larger than the ionic radius. They attributed the resistance of ion permeation through pores (larger than the ionic radius) as a consequence of the hydration shell of the ions. Therefore, the pores are too small to accommodate ions with their surrounding solvent layer. The effect is estimated to be applicable to pores that are ten times as wide as the bare ions. Since many drugs are larger than mere ions, one can expect resistance to their movement out of pores into the surrounding environment or that a suitable pore size should be present to facilitate drug delivery. Furthermore, the geometry of the pore (radius, shape and length), the chemical character of the pore wall as well as the wall's surface roughness have an effect on the permeation of ions and water (Beckstein & Sansom, 2004a). For example, hydrophobic pores smaller than 0.45 nm inhibit the permeation of water, whereas pore walls of higher polarity can shift this transition radius to smaller values. This fact can be very important in the choice of the matrix, as water permeation into the matrix can be a prerequisite for the drug release (e.g., swelling of the matrix to enable drug diffusion or dissolving the drug in the matrix prior to diffusion).

Drug Release Through Polymer Shells

If a drug is encapsulated into nanocapsules, the drug has to traverse the capsule shell prior to reaching the surrounding medium. Release can occur by permeation through the capsule wall, erosion of the shell or diffusion through pores (if existing). The mass rate of permeation $\mathrm{d}M/\mathrm{d}t$ of a drug through the capsule shell can be written according to the first law of Fick under sink condition:

$$\frac{\mathrm{d}M}{\mathrm{d}t} = \frac{DKAC_{\mathrm{D}}}{h} \tag{13}$$

where D is the diffusion coefficient of the drug in the capsule shell, A is the surface area, K is the partitioning coefficient of the drug between capsule interior and shell, C_D is the solubility (solid) or concentration (dissolved) of the drug in the interior of the capsule and h is the thickness of the capsule shell. To compare various systems with different capsule shells with each other, the permeability coefficient is used as it is independent of the surface area and the concentration of the drug on the donor side C_D. The permeability coefficient, also known as the permeability P, of a polymer shell is described as follows:

$$P = \frac{DK}{h} \tag{14}$$

In practice, the two transport mechanisms, pore diffusion and permeation through the capsule shell, cannot always be distinguished. Therefore, the decrease in permeability is sometimes explained by the formation of pores in the polymer shell where the drug rather diffuses through the pores than permeates through the polymer shell (Sukhorukov, Fery, Brumen, & Möhwald, 2004).

Particular interest has been focused on polyelectrolyte capsules as a drug delivery system. Loading of and release from polyelectrolyte capsules are not part of this chapter, and interested readers are referred to reviews in literature (De Geest, Sanders, Sukhorukov, Demeester, & De Smedt, 2007; Johnston, Cortez, Angelatos, & Caruso, 2006). They describe the different techniques for loading polyelectrolyte capsules and the various triggers for drug release.

Comparison of Nanosized with Micro-sized Drug Carrier System

Only few studies have been performed to compare the release from microparticles and nanoparticles though not all of the parameters were kept constant except of the size as to enable the determination of the effect of different sizes on drug release. It is well known that the surface to volume ratio is increased for nanoparticles and therefore higher drug amount is located at the surface compared to the core (Redhead, Davis, & Illum, 2001). Additionally, the diffusion distance is reduced. Gref, Quellec, Sanchez, Calvo, Dellacherie, & Alonso (2001) prepared cyclosporine A (CyA) loaded poly(lactic acid)-poly(ethylene glycol) (PLA-PEG) micro- and nanoparticles and compared them to conventional PLA particles. The determination of the surface chemical composition revealed a higher amount of CyA at the surface of nanoparticles than at the surface of microparticles which resulted in a higher initial burst release from nanoparticles than from microparticles. It is interesting to note that the two different carriers (PLA-PEG vs. PLA) exhibited different release rates at micro-scale but not at nano-scale (Figure 5.13). Unfortunately, no explanation for this finding was given.

Lecaroz et al. (2006) found that the drug loading as well as entrapment efficiency was higher for microparticles compared to nanoparticles. Furthermore, they assumed a higher amount of drug on the particle

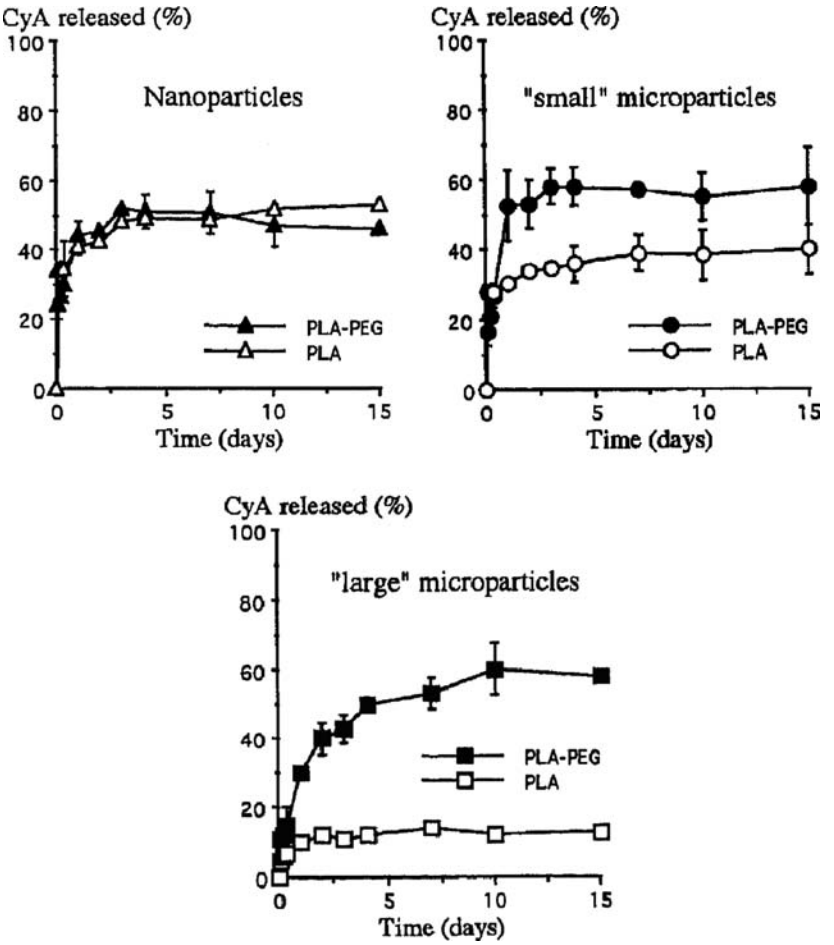

Figure 5.13 Release profiles of cyclosporine A (CyA) from poly(lactic acid) (PLA) and poly(lactic acid)-poly(ethylene glycol) (PLA-PEG) micro- and nanoparticles. Reprinted from Gref, Quellec, Sanchez, Calvo, Dellacherie, & Alonso (2001) with permission from Elsevier.

surface based on zeta potential analysis, and the initial burst release was higher for nanoparticles than for microparticles.

Methods to Measure Drug Release from Nanosystems

In studying release, an important issue to consider is the method that can be used to measure drug release. No standardized in vitro release method exists (Kostanski & DeLuca, 2000), and there are different opinions about the suitability of the various methods for the assessment of release from nanocarriers (Chorny et al., 2002). Several methods are utilized and described by D'Souza & DeLuca (2006) and Washington (1990a). They include the membrane diffusion technique (e.g., dialyze and reverse dialyze), the sample and separate technique with various separation methods

(e.g., centrifugation, filtration or centrifugal ultracentrifugation), the in situ technique and the continuous flow method.

As seen from Table 5.6, the most commonly used methods for the determination of drug release from nanocarriers are the dialysis method and the sample and separate technique. In the membrane diffusion technique, the drug-loaded nanoparticles are physically separated from the release media by a dialysis membrane (with a defined molecular weight cut-off) which is permeable for the drug but not for the carrier system. The drug-loaded particles can be loaded in a dialysis bag or tube and samples are withdrawn from the agitated outer release media. In contrast, in reverse dialysis, the drug-loaded carriers are placed in the outer release medium and samples are taken from inside the dialysis bags. This method has the

Table 5.6 Methods to measure drug release.

Release method	Drug	Ref.
Membrane diffusion		
Dialysis bag/tube	N^6-cyclopentyladenosine	[3]
	Ibuprofen	[7]
	Retinoic acid	[8]
	Camptothecin	[31]
	Papaverine	[37]
	Adriamycin	[38]
	Beclomethasone dipropionate	[33]
	Efavirenz	[18]
	Indomethacin	[22]
	Rifampicin	[43]
	Chloroquine phosphate	[13]
	Methotrexate, adriamycin	[14]
	Flurbiprofen	[15]
	5-Fluorouracil	[17]
	Metipranolol	[42]
Reverse dialysis	Triclosan	[39]
	3′,5′-Dioctanoyl-5-fluoro-2′-deoxyuridine	[44]
	3'-Azido-3'-deoxythimidine	[45]
	Indomethacin	[41]
Diffusion cell	Paclitaxel	[46]
	Nitrendipine	[47]
	Methotrexate	[28]
	Retinol	[29]
	Rhodamine, β-carotene	[16]
Sample and separate		
Centrifugation	Plasmid DNA	[5]
	Gentamicin	[2]
	Salicylic acid	[48]
	Bovine serum albumin	[3]
	Ampicillin	[49]
	Ampicillin, dexamethasone	[50]
Filtration	Cholesterol acetate, griseofulvin, megestrol	[51]
	5-Fluorouracil	[52]
	Prednisolone	[24]
	Clobetasol propionate	[30]

(*Continued*)

Table 5.6 (*Continued*).

Release method	Drug	Ref.
Centrifugal ultrafiltration	Ethionamide	[40]
In situ measurement		
Fluorescence-spectrometry	Tyrphostin AG-1295	[53]
UV-spectrometry	Ibuprofen	[54]
Differential pulse polarography	Pyroxicam	[55]

[2] Lecaroz, Gamazo, Renedo, & Blanco-Prieto (2006)
[3] Leo, Scatturin, Vighi, & Dalpiaz (2006)
[5] Pfeifer, Burdick, Little, & Langer (2005)
[7] Jiang, Hu, Gao, & Shen (2005)
[8] Quaglia, Ostacolo, De Rosa, La Rotonda, Ammendola, Nese, Maglio, Palumbo, & Vauthier (2006)
[13] Bhadra, Bhadra, & Jain (2006)
[14] Kojima, Kono, Maruyama, & Takagishi (2000)
[15] Asthana, Chauhan, Diwan, & Jain (2005)
[16] Dhanikula & Hildgen (2006)
[17] Tripathi, Khopade, Nagaich, Shrivastava, Jain, & Jain (2002)
[18] Dutta, Agashe, Garg, Balasubramanium, Kabra, & Jain (2007)
[22] Chandrasekar, Sistla, Ahmad, Khar, & Diwan (2007)
[24] zur Mühlen & Mehnert (1998a)
[28] Ruckmani, Sivakumar, & Ganeshkumar (2006)
[29] Jenning, Thünemann, & Gohla (2000)
[30] Hu, Jiang, Du, Yuan, Ye, & Zeng (2006)
[31] Opanasopit, Ngawhirunpat, Chaidedgumjorn, Rojanarata, Apirakaramwong, Phongying, Choochottiros, & Chirachanchai (2006)
[33] Gaber, Darwis, Peh, & Tan (2006)
[37] Lee, Cho, & Cho (2004)
[38] Lee, Na, & Bae (2003)
[39] Maestrelli, Mura, & Alonso (2004)
[40] Lopes, Pohlmann, Bassani, & Guterres (2000)
[41] Calvo, Vila-Jato, & Alonso (1996)
[42] Losa, Marchal-Heussler, Orallo, Vila Jato, & Alonso (1993)
[43] Kumar, Asthana, Dutta, & Jain (2006)
[44] Wang, Sun, & Zhang (2002)
[45] Heiati, Tawashi, Shivers, & Phillips (1997)
[46] Lee, Lim, & Kim (2007)
[47] Manjunath & Venkateswarlu (2006)
[48] Boonsongrit, Mitrevej, & Müller (2006)
[49] Fontana, Pitarresi, Tomarchio, Carlisi, & San Biagio (1998)
[50] Seijo, Fattal, Roblot-Treupel, & Couvreur (1990)
[51] Shekunov, Chattopadhyay, Seitzinger, & Huff (2006)
[52] Lo, Lin, & Hsiue (2005)
[53] Chorny, Fishbein, Danenberg, & Golomb (2002)
[54] Qiu, Leporatti, Donath, & Möhwald (2001)
[55] Charalampopoulos, Avgoustakis, & Kontoyannis (2003)

advantage that it minimizes the effect of membrane clogging. Another experimental setup of the membrane diffusion technique is the diffusion cell consisting of two chambers separated by the dialysis membrane. In the sample and separate technique, the drug-loaded nanoparticles are incubated in the release media and agitated throughout the release study. At specified time intervals, samples are withdrawn and the particles are separated from the bulk media with the dissolved drug by centrifugation or filtration.

Several technical problems occur when using these release methods to determine the drug release from nanocarriers, e.g., in the dialysis technique the transport across the membrane can be rate limiting, and therefore, the true release rate is not measured. The disadvantages of the sample and separate technique are the high sample frequency needed for nanoparticles and the physical separation of the released drug from the nanocarriers. The time-consuming separation procedures can give erroneous release profiles. Another limiting factor in determining the initial burst release as well as the fast dissolution rate of nanoparticles is the time resolution of the analytical procedure (Washington & Koosha, 1990b). Because of the technical limitations (sample frequency, physical separation), in situ methods become interesting because the drug-loaded nanoparticles are incubated in the release medium and the released drug is analyzed in this medium without separation from the carrier (avoiding the complications with sampling and separation).

However, only a limited number of compounds are applicable to the in situ technique as the compounds need spectral properties which are different for the free and entrapped compound. Chorny et al. (2002) studied the in vitro release of tyrphostin AG-1295 from nanospheres in situ based on the difference in fluorescence intensity between released and encapsulated compound. The same principle was used by Landry, Bazile, Spenlehauer, Veillard, & Kreuter (1997) to determine the release of a fluorescent marker. UV-spectroscopy was utilized to monitor the release of ibuprofen from microcapsules in quartz cuvettes (Qiu, Leporatti, Donath, & Möhwald, 2001). A wavelength was used for monitoring where the dissolved ibuprofen showed absorbance but the mircro-sized ibuprofen did not absorb. Another example of in situ methodology is the employment of differential pulse polarography (Charalampopoulos, Avgoustakis, & Kontoyannis, 2003).

The experimental setup for drug release has to be studied carefully if good in vitro–in vivo correlation is the goal, because for nanosystems the in vitro release is sometimes severely affected by setup and sample techniques (D'Souza & DeLuca, 2006). A main issue is the maintenance of sink condition particularly for poorly water soluble drugs in aqueous media (Washington, 1990a). The detection limit of the analytical method gives a limitation on the maximum volume of the release medium to be used as a high dilution might result in concentrations of the drug below the detection limit. In some cases, the release medium can be changed so that it is a good solvent for the drug but a non-solvent for the carrier (Chorny et al., 2002). Another novel release technique was introduced by Pohlmann et al. (2004) where they maintained sink conditions throughout the release study and without using a separation step. To achieve this, entrapped indomethacin ethyl ester was hydrolyzed at the particle/water interface, and therefore, the concentration gradient of the ethyl ester in the nanocarriers was maintained.

Summary

Drug loading and release are two important properties for the performance of drug delivery systems. Different methods for drug loading of nanosized delivery systems and release methods have been described in this

chapter. The various examples showed that both properties are influenced by many factors, e.g., physicochemical properties of the drug, physicochemical properties of the carrier matrix, interaction between drug, matrix and environment, type of nanoparticles, method of loading and nanoparticle preparation, release medium, and it could be demonstrated that drug loading and release are related to each other. Therefore, with a careful selection of the carrier system, particle preparation method and loading technique, it is possible to optimize drug loading and entrapment efficiency as well as to achieve the desired release pattern.

However, more fundamental investigations are required to gain more knowledge about the release mechanism from nanocarriers and the effect of changes in physicochemical properties of nanoparticles compared to micro- and macroparticles on drug release. Examples are the wettability of nanoparticles and its effect on the solid–liquid interaction (solvation step of dissolution) or the effect of nanopore size and flow behavior through these nanopores on water and drug permeation and therefore on drug release.

References

Aliabadi, H.M., & Lavasanifar, A. (2006). Polymeric micelles for drug delivery. *Expert Opin. Drug Deliv.*, *3*, 139–162.

Aliabadi, H.M., Elhasi, S., Mahmud, A., Gulamhusein, R., Mahdipoor, P., & Lavasanifar, A. (2007). Encapsulation of hydrophobic drugs in polymeric micelles through co-solvent evaporation: the effect of solvent composition on micellar properties and drug loading. *Int. J. Pharm.*, *329*, 158–165.

Allemann, E., Gurny, R., & Doelker, E. (1993). Drug-loaded nanoparticles. Preparation methods and drug targeting issues. *Eur. J. Pharm. Biopharm.*, *39*, 173–191.

Amir, R.J., & Shabat, D. (2006). Domino dendrimers. *Adv. Polym. Sci.*, *192*, 59–94.

Anderberg, E.K., Bisrat, M., & Nyström, C. (1988). Physicochemical aspects of drug release. VII. The effect of surfactant concentration and drug particle size on solubility and dissolution rate of felodipine, a sparingly soluble drug. *Int. J. Pharm.*, *47*, 67–77.

Asthana, A., Chauhan, A.S., Diwan, P.V., & Jain, N.K. (2005). Poly(amidoamine) (PAMAM) dendritic nanostructures for controlled site-specific delivery of acidic anti-inflammatory active ingredient. *AAPS PharmSciTech, 6*, Article 67, E536–542.

Bala, I., Hariharan, S., & Kumar, M.N.V.R. (2004). PLGA nanoparticles in drug delivery: the state of the art. *Crit. Rev. Ther. Drug Carr. Syst.*, *21*, 387–422.

Bapat, N., & Boroujerdi, M. (1992). Uptake capacity and adsorption isotherms of doxorubicin on polymeric nanoparticles: effect of methods of preparation. *Drug Dev. Ind. Pharm.*, *18*, 65–77.

Beckstein, O., & Sansom, M.S.P. (2004a). The influence of geometry, surface character, and flexibility on the permeation of ions and water through biological pores. *Phys. Biol.*, *1*, 42–52.

Beckstein, O., Tai, K., & Sansom, M.S.P. (2004b). Not ions alone: barriers to ion permeation in nanopores and channels. *J. Am. Chem. Soc.*, *126*, 14694–14695.

Bhadra, D., Bhadra, S., & Jain, N.K. (2006). PEGylated peptide dendrimeric carriers for the delivery of antimalarial drug chloroquine phosphate. *Pharm. Res.*, *23*, 623–633.

Bhattarai, N., Ramay, H.R., Chou, S.H., & Zhang, M. (2006). Chitosan and lactic acid-grafted chitosan nanoparticles as carriers for prolonged drug delivery. *Int. J. Nanomed.*, *1*, 181–187.

Bilati, U., Allémann, E., & Doelker, E. (2005). Protein drugs entrapped within micro- & nanoparticles: an overview of therapeutic challenges & scientific issues. Drug *Deliver. Technol.*, *5*, 40–47.

Bisrat, M., & Nyström, C. (1988). Physicochemical aspects of drug release. VIII. The relation between particle size and surface specific dissolution rate in agitated suspensions. *Int. J. Pharm.*, *47*, 223–231.

Bisrat, M., Anderberg, E.K., Barnett, M.I., & Nyström, C. (1992). Physicochemical aspects of drug release. XV. Investigation of diffusional transport in dissolution of suspended, sparingly soluble drugs. *Int. J. Pharm.*, *80*, 191–201.

Boonsongrit, Y., Mitrevej, A., & Müller, B.W. (2006). Chitosan drug binding by ionic interaction. *Eur. J. Pharm. Biopharm.*, *62*, 267–274.

Borm, P., Klaessig, F.C., Landry, T.D., Moudgil, B., Pauluhn, J., Thomas, K., Trottier, R., & Wood, S. (2006). Research strategies for safety evaluation of nanomaterials, part V: role of dissolution in biological fate and effects of nanoscale particles. *Toxicol. Sci.*, *90*, 23–32.

Calvo, P., Vila-Jato, J.L., & Alonso, M.J. (1996). Comparative *in vitro* evaluation of several colloidal systems, nanoparticles, nanocapsules, and nanoemulsions, as ocular drug carriers. *J. Pharm. Sci.*, *85*, 530–536.

Chandrasekar, D., Sistla, R., Ahmad, F.J., Khar, R.K., & Diwan, P.V. (2007). The development of folate-PAMAM dendrimer conjugates for targeted delivery of anti-arthritic drugs and their pharmacokinetics and biodistribution in arthritic rats. *Biomaterials, 28*, 504–512.

Charalampopoulos, N., Avgoustakis, K., & Kontoyannis, C.G. (2003). Differential pulse polarography: a suitable technique for monitoring drug release from polymeric nanoparticle dispersions. *Anal. Chim. Acta,* 491, 57–62.

Chen, V.J., & Ma, P.X. (2006). The effect of surface area on the degradation rate of nano-fibrous poly(L-lactic acid) foams. *Biomaterials, 27*, 3708–3715.

Chorny, M., Fishbein, I., Danenberg, H.D., & Golomb, G. (2002). Study of the drug release mechanism from tyrphostin AG-1295-loaded nanospheres by in situ and external sink methods. *J. Control. Release, 83*, 401–414.

Couvreur, P., Barratt, G., Fattal, E., Legrand, P., & Vauthier, C. (2002). Nanocapsule technology: a review. *Crit. Rev. Ther. Drug Carr. Syst.*, *19*, 99–134.

Crisp, M.T., Tucker, C.J., Rogers, T.L., Williams, R.O., & Johnston, K.P. (2007). Turbidimetric measurement and prediction of dissolution rates of poorly soluble drug nanocrystals. *J. Control. Release*, *117*, 351–359.

Cruz, L., Soares, L.U., Costa, T.D., Mezzalira, G., da Silveira, N.P., Guterres, S.S., & Pohlmann, A.R. (2006). Diffusion and mathematical modeling of release profiles from nanocarriers. *Int. J. Pharm.*, *313*, 198–205.

De Geest, B.G., Sanders, N.N., Sukhorukov, G.B., Demeester, J., & De Smedt, S.C. (2007). Release mechanisms for polyelectrolyte capsules. *Chem. Soc. Rev.*, *36*, 636–649.

D'Emanuele, A., & Attwood, D. (2005). Dendrimer-drug interactions. *Adv. Drug Deliver. Rev.*, *57*, 2147–2162.

Dhanikula, R.S., & Hildgen, P. (2006). Synthesis and evaluation of novel dendrimers with a hydrophilic interior as nanocarriers for drug delivery. *Bioconjugate Chem.*, *17*, 29–41.

D'Souza, S.S., & DeLuca, P.P. (2006). Methods to assess in vitro drug release from injectable polymeric particulate systems. *Pharm. Res.*, *23*, 460–474.

Dutta, T., Agashe, H.B., Garg, M., Balasubramanium, P., Kabra, M., & Jain, N.K. (2007). Poly (propyleneimine) dendrimer based nanocontainers for targeting of efavirenz to human monocytes/macrophages *in vitro*. *J. Drug Target.*, *15*, 89–98.

Fontana, G., Pitarresi, G., Tomarchio, V., Carlisi, B., & San Biagio, P.L. (1998). Preparation, characterization and in vitro antimicrobial activity of ampicillin-loaded polyethylcyanoacrylate nanoparticles. *Biomaterials*, *19*, 1009–1017.

Gaber, N.N., Darwis, Y., Peh, K.-K., & Tan, Y.T.-F. (2006). Characterization of polymeric micelles for pulmonary delivery of beclomethasone dipropionate. *J. Nanosci. Nanotechnol.*, *6*, 3095–3101.

Galli, C. (2006). Experimental determination of the diffusion boundary layer width of micron and submicron particles. *Int. J. Pharm.*, *313*, 114–122.

Gaspar, M.M., Blanco, D., Cruz, M.E.M., & Alonso, M.J. (1998). Formulation of L-asparaginase-loaded poly(lactide-co-glycolide) nanoparticles: influence of polymer properties on enzyme loading, activity and in vitro release. *J. Control. Release*, *52*, 53–62.

Govender, T., Stolnik, S., Garnett, M.C., Illum, L., & Davis, S.S. (1999). PLGA nanoparticles prepared by nanoprecipitation: drug loading and release studies of a water soluble drug. *J. Control. Release*, *57,* 171–185.

Govender, T., Riley, T., Ehtezazi, T., Garnett, M.C., Stolnik, S., Illum, L., & Davis, S.S. (2000). Defining the drug incorporation properties of PLA-PEG nanoparticles. *Int. J. Pharm.*, *199*, 95–110.

Gref, R., Quellec, P., Sanchez, A., Calvo, P., Dellacherie, E., & Alonso, M.J. (2001). Development and characterization of CyA-loaded poly(lactic acid)-poly(ethylene glycol) PEG micro- and nanoparticles. Comparison with conventional PLA particulate carriers. *Eur. J. Pharm. Biopharm.*, *51*, 111–118.

Gupta, U., Agashe, H.B., Asthana, A., & Jain, N.K. (2006). Dendrimers: novel polymeric nanoarchitectures for solubility enhancement. *Biomacromolecules*, *7*, 649–658.

Guy, R.H., Hadgraft, J., Kellaway, I.W., & Taylor, M.J. (1982). Calculations of drug release rates from spherical particles. *Int. J. Pharm.*, *11*, 199–207.

Heiati, H., Tawashi, R., Shivers, R.R., & Phillips, N.C. (1997). Solid lipid nanoparticles as drug carriers I. Incorporation and retention of the lipophilic prodrug 3'-azido-3'-deoxythymidine palmitate. *Int. J. Pharm.*, *146*, 123–131.

Heywood, H. (1954). Particle shape coefficients. *J. Imp. Coll. Chem. Eng. Soc.*, *8*, 25–33.

Higuchi, T. (1963). Mechanism of sustained-action medication. Theoretical analysis of rate of release of solid drugs dispersed in solid matrices. *J. Pharm. Sci.*, *52*, 1145–1149.

Hixson, A.W., & Crowell, J.H. (1931). Dependence of reaction velocity upon surface and agitation. I. Theoretical considerations. *J. Ind. Eng. Chem.*, *23*, 923–931.

Hu, F.-Q., Jiang, S.-P., Du, Y.-Z., Yuan, H., Ye, Y.-Q., & Zeng, S. (2006). Preparation and characteristics of monostearin nanostructured lipid carriers. *Int. J. Pharm.*, *314*, 83–89.

Huo, Q., Liu, J., Wang, L.-Q., Jiang, Y., Lambert, T.N., & Fang, E. (2006). A new class of silica cross-linked micellar core-shell nanoparticles. *J. Am. Chem. Soc.*, *128*, 6447–6453.

Illum, L., Khan, M.A., Mak, E., & Davis, S.S. (1986). Evaluation of carrier capacity and release characteristics for poly(butyl 2-cyanoacrylate) nanoparticles. *Int. J. Pharm.*, *30*, 17–28.

Jenning, V., Thünemann, A.F., & Gohla, S.H. (2000). Characterisation of a novel solid lipid nanoparticle carrier system based on binary mixtures of liquid and solid lipids. *Int. J. Pharm.*, *199*, 167–177.

Jette, K.K., Law, D., Schmitt, E.A., & Kwon, G.S. (2004). Preparation and drug loading of poly(ethylene glycol)-*block*-poly(ε-caprolactone) micelles through the evaporation of a cosolvent azeotrope. *Pharm. Res.*, *21*, 1184–1191.

Jiang, B., Hu, L., Gao, C., & Shen, J. (2005). Ibuprofen-loaded nanoparticles prepared by a co-precipitation method and their release properties. *Int. J. Pharm.*, *304*, 220–230.

Jo, Y.S., Kim, M.-C., Kim, D.K, Kim, C.-J., Jeong, Y.-K., Kim, K.-J., & Muhammed, M. (2004). Mathematical modelling on the controlled-release of indomethacin-encapsulated poly(lactic acid-co-ethylene oxide) nanospheres. *Nanotechnology*, *15*, 1186–1194.

Johnston, A.P.R., Cortez, C., Angelatos, A.S., & Caruso, F. (2006). Layer-by-layer engineered capsules and their applications. *Curr. Opin. Colloid Interface Sci.*, *11*, 203–209.

Knapp, L.F. (1922). The solubility of small particles and the stability of colloids. *Trans. Faraday Soc.*, *17*, 457–465.

Kojima, C., Kono, K., Maruyama, K., & Takagishi, T. (2000). Synthesis of polyamidoamine dendrimers having poly(ethylene glycol) grafts and their ability to encapsulate anticancer drugs. *Bioconjugate Chem.*, *11*, 910–917.

Kolhe, P., Misra, E., Kannan, R.M., Kannan, S., & Lieh-Lai, M. (2003). Drug complexation, in vitro release and cellular entry of dendrimers and hyperbranched polymers. *Int. J. Pharm.*, *259*, 143–160.

Kolhe, P., Khandare, J., Pillai, O., Kannan, S., Lieh-Lai, M., Kannan, R.M. (2006). Preparation, cellular transport, and activity of polyamidoamine-based dendritic nanodevices with a high drug payload. *Biomaterials*, *27*, 660–669.

Kostanski, J.W., & DeLuca, P.P. (2000). A novel in vitro release technique for peptide-containing biodegradable microspheres. *AAPS PharmSciTech, 1*, http://www.pharmscitech.com.

Kumar, P.V., Asthana, A., Dutta, T., & Jain, N.K. (2006). Intracellular macrophage uptake of rifampicin loaded mannosylated dendrimers. *J. Drug Target.*, *14*, 546–556.

Landry, F.B., Bazile, D.V., Spenlehauer, G., Veillard, M., & Kreuter, J. (1997). Release of the fluorescent marker Prodan from poly(D,L-lactic acid) nanoparticles coated with albumin or polyvinyl alcohol in model digestive fluids (USP XXII). *J. Control. Release*, *44*, 227–236.

Lecaroz, C., Gamazo, C., Renedo, M.J., & Blanco-Prieto, M.J. (2006). Biodegradable micro- and nanoparticles as long-term delivery vehicles for gentamicin. *J. Microencapsul.*, *23*, 782–792.

Lee, E.S., Na, K., & Bae, Y.H. (2003). Polymeric micelle for tumor pH and folate-mediated targeting. *J. Control. Release*, *91*, 103–113.

Lee, J., Cho, E.C., & Cho, K. (2004). Incorporation and release behavior of hydrophobic drug in funtionalized poly(D,L-lactide)-block-poly(ethylene oxide) micelles. *J. Control. Release*, *94*, 323–335.

Lee, M.-K., Lim, S.-J., & Kim, C.-K. (2007). Preparation, characterization and in vitro cytotoxicity of paclitaxel-loaded sterically stabilized solid lipid nanoparticles. *Biomaterials*, *28*, 2137–2146.

Leo, E., Scatturin, A., Vighi, E., & Dalpiaz, A. (2006). Polymeric nanoparticles as drug controlled release systems: a new formulation strategy for drugs with small or large molecular weight. *J. Nanosci. Nanotechnol.*, *6*, 3070–3079.

Lin, W.-J., Juang, L.-W., & Lin, C.-C. (2003). Stability and release performance of a series of pegylated copolymeric micelles. *Pharm. Res.*, *20*, 668–673.

Liu, J., Lee, H., & Allen, C. (2006a). Formulation of drugs in block copolymer micelles: drug loading and release. *Curr. Pharm. Design*, *12*, 4685–4701.

Liu, H., Zhai, J., & Jiang, L. (2006b). Wetting and anti-wetting on aligned carbon nanotube films. *Soft Matter*, *2*, 811–821.

Liu, J., Hu, W., Chen, H., Ni, Q., Xu, H., & Yang, X. (2007). Isotretinoin-loaded solid lipid nanparticles with skin targeting for topical delivery. *Int. J. Pharm.*, *328*, 191–195.

Lo, C.-L., Lin, K.-M., & Hsiue, G.-H. (2005). Preparation and characterization of intelligent core-shell nanoparticles based on poly(D,L-lactide)-g-poly (N-isopropylacrylamide-co-methacrylic acid). *J. Control. Release*, *104*, 477–488.

Lopes, E., Pohlmann, A.R., Bassani, V., & Guterres, S.S. (2000). Polymeric colloidal systems containing ethionamide: preparation and physico-chemical characterization. *Pharmazie*, *55*, 527–530.

Losa, C., Marchal-Heussler, L., Orallo, F., Vila Jato, J.L., & Alonso, M.J. (1993). Design of new formulations for topical ocular administration: polymeric nanocapsules containing metipranolol. *Pharm. Res.*, *10*, 80–87.

Maestrelli, F., Mura, P., & Alonso, M.J. (2004). Formulation and characterization of triclosan sub-micron emulsions and nanocapsules. *J. Microencapsul.*, *21*, 857–864.

Manjunath, K., & Venkateswarlu, V. (2006). Pharmacokinetics, tissue distribution, and bioavailability of nitrendipine solid lipid nanoparticles after intravenous and intraduodenal administration. *J. Drug Target.*, *14*, 632–645.

Mayer, C. (2005). Nanocapsules as drug delivery systems. *Int. J. Artif. Organs*, *28*, 1163–1171.

Mihranyan, A., & Strømme, M. (2007). Solubility of fractal nanoparticles. *Surf. Sci.*, *601*, 315–319.

Montana, G., Bondi, M.L., Carrotta, R., Picone, P., Craparo, E.F., San Biagio, P.L., Giammona, G., & Di Carlo, M. (2007). Employment of cationic solid-lipid nanoparticles as RNA carriers. *Bioconjugate Chem.*, *18*, 302–308.

Mosharraf, M., & Nyström, C. (1995). The effect of particle size and shape on the surface specific dissolution rate of microsized practically insoluble drugs. *Int. J. Pharm.*, *122*, 35–47.

Müller, R.H., Mäder, K., & Gohla, S. (2000). Solid lipid nanoparticles (SLN) for controlled drug delivery – a review of the state of the art. *Eur. J. Pharm. Biopharm.*, *50*, 161–177.

Müller, R.H., Radtke, M., & Wissing, S.A. (2002). Nanostructured lipid matrices for improved microencapsulation of drugs. *Int. J. Pharm.*, *242*, 121–128.

Noyes, A.A., & Whitney, W.R. (1897). The rate of solution of solid substances in their own solutions. *J. Am. Chem. Soc.*, *19*, 930–934.

Opanasopit, P., Ngawhirunpat, T., Chaidedgumjorn, A., Rojanarata, T., Apirakaramwong, A., Phongying, S., Choochottiros, C., & Chirachanchai, S. (2006). Incorporation of camptothecin into *N*-phthaloyl chitosan-g-mPEG self-assembly micellar system. *Eur. J. Pharm. Biopharm.*, *64*, 269–276.

Pandey, R., Ahmad, Z., Sharma, S., & Khuller, G.K. (2005). Nano-encapsulation of azole antifungals: potential applications to improve oral drug delivery. *Int. J. Pharm.*, *301*, 268–276.

Panyam, J., Dali, M.M., Sahoo, S.K., Ma, W., Chakravarthi, S.S., Amidon, G.L., Levy, R.J., & Labhasetwar, V. (2003). Polymer degradation and in vitro release of a model protein from poly(D,L-lactide-co-glycolide) nano-and microparticles. *J. Control. Release*, *92*, 173–187.

Patri, A.K., Kukowska-Latallo, J.F., & Baker, J.R., Jr. (2005). Targeted drug delivery with dendrimers: comparison of the release kinetics of covalently conjugated drug and non-covalent drug inclusion complex. *Adv. Drug Deliver. Rev.*, *57*, 2203–2214.

Peppas, N.A., & Robinson, D.N. (2007). Nanospheres of intelligent networks for biomedical and drug delivery applications. In N.A. Peppas, J.Z. Hilt, & J.B. Thomas (Eds.), *Nanotechnology in Therapeutics* (pp. 361–379). Wymondham: Horizon Bioscience.

Pfeifer, B.A., Burdick, J.A., Little, S.R., & Langer, R. (2005). Poly(ester-anhydride):poly(β-amino ester) micro- and nanospheres: DNA encapsulation and cellular transfection. *Int. J. Pharm.*, *304*, 210–219.

Pohlmann, A.R., Soares, L.U., Cruz, L., Da Silveira, N.P., & Guterres, S.S. (2004). Alkaline hydrolysis as a tool to determine the association form of indomethacin in nanocapsules prepared with poly(ε-caprolactone). *Curr. Drug Deliv.*, *1*, 103–110.

Polakovič, M., Görner, T., Gref, R., & Dellacherie, E. (1999). Lidocaine loaded biodegradable nanospheres. II. Modelling of drug release. *J. Control. Release*, *60*, 169–177.

Powell, C., Fenwick, N., Bresme, F., & Quirke, N. (2002). Wetting of nanoparticles and nanoparticle arrays. *Colloid Surface A*, *206*, 241–251.

Qiu, X., Leporatti, S., Donath, E., & Möhwald, H. (2001). Studies on the drug release properties of polysaccharide multilayers encapsulated ibuprofen microparticles. *Langmuir*, *17*, 5375–5380.

Quaglia, F., Ostacolo, L., De Rosa, G., La Rotonda, M.I., Ammendola, M., Nese, G., Maglio, G., Palumbo, R., & Vauthier, C. (2006). Nanoscopic core-shell drug carriers made of amphiphilic triblock and star-diblock copolymers. *Int. J. Pharm.*, *324*, 56–66.

Redhead, H.M., Davis, S.S., & Illum, L. (2001). Drug delivery in poly(lactide-co-glycolide) nanoparticles surface modified with Poloxamer 407 and Poloxamine 908: in vitro characterization and in vivo evaluation. *J. Control. Release*, *70*, 353–363.

Reis, C.P., Neufeld, R.J., Ribeiro, A.J., & Veiga, F. (2006). Nanoencapsulation I. Methods for preparation of drug-loaded polymeric nanoparticles. *Nanomedicine*, *2*, 8–21.

Ritger, P.L., & Peppas, N.A. (1987a). A simple equation for description of solute release. I. Fickian and non-Fickian release from non-swellable devices in the form of slabs, spheres, cylinders or discs. *J. Control. Release*, *5*, 23–36.

Ritger, P.L., & Peppas, N.A. (1987b). A simple equation for description of solute release. II. Fickian and anomalous release from swellable devices. *J. Control. Release*, *5*, 37–42.

Ruckmani, K., Sivakumar, M., & Ganeshkumar, P.A. (2006). Methotrexate loaded solid lipid nanoparticles (SLN) for effective treatment of carcinoma. *J. Nanosci. Nanotechnol.*, *6*, 2991–2995.

Sdobnyakov, N.Y., & Samsonov, V.M. (2005). On the size dependence of surface tension in the temperature range from melting point to critical point. *Cent. Eur. J. Phys.*, *3*, 247–257.

Seijo, B., Fattal, E., Roblot-Treupel, L., & Couvreur, P. (1990). Design of nanoparticles of less than 50 nm diameter: preparation, characterization and drug loading. *Int. J. Pharm.*, *62*, 1–7.

Shekunov, B.Y., Chattopadhyay, P., Seitzinger, J., & Huff, R. (2006). Nanoparticles of poorly water-soluble drugs prepared by supercritical fluid extraction of emulsions. *Pharm. Res.*, *23*, 196–204.

Siepmann, J., & Göpferich, A. (2001). Mathematical modeling of bioerodible, polymeric drug delivery systems. *Adv. Drug Del. Rev.*, *48*, 229–247.

Siepmann, J., Faisant, N., & Benoit, J.-P. (2002). A new mathematical model quantifying drug release from bioerodible micrcoparticles using monte carlo simulations. *Pharm. Res.*, *19*, 1885–1893.

Solans, C., Izquierdo, P., Nolla, J., Azemar, N., & Garcia-Celma, M.J. (2005). Nano-emulsions. *Curr. Opin. Colloid Interface Sci.*, *10*, 102–110.

Soppimath, K.S., Aminabhavi, T.M., Kulkarni, A.R., & Rudzinski, W.E. (2001). Biodegradable polymeric nanoparticles as drug delivery devices. *J. Control. Release*, *70*, 1–20.

Sukhorukov, G.B., Fery, A., Brumen, M., & Möhwald, H. (2004). Physical chemistry of encapsulation and release. *Phys. Chem. Chem. Phys.*, *6*, 4078–4089.

Tang, R., Wang, L., Orme, C.A., Bonstein, T., Bush, P.J., & Nancollas, G.H. (2004). Dissolution at the nanoscale: self-preservation of biominerals. *Angew. Chem. Int. Ed.*, *43*, 2697–2701.

Tang, S., June, S.M., Howell, B.A., & Chai, M. (2006a). Synthesis of salicylate dendritic prodrugs. *Tetrahedron Lett*., *47*, 7671–7675.

Tang, S., Martinez, L.J., Sharma, A., & Chai, M. (2006b). Synthesis and characterization of water-soluble and photostable L-Dopa dendrimers. *Org. Lett*., *8*, 4421–4424.

Thote, A.J., & Gupta, R.B. (2005). Formation of nanoparticles of a hydrophilic drug using supercritical carbon dioxide and microencapsulation for sustained release. *Nanomedicine*, *1*, 85–90.

Tinke, A.P., Vanhoutte, K., De Maesschalck, R., Verheyen, S., & De Winter, H. (2005). A new approach in the prediction of the dissolution behavior of suspended particles by means of their particle size distribution. *J. Pharm. Biomed. Anal*., *39*, 900–907.

Tripathi, P.K., Khopade, A.J., Nagaich, S., Shrivastava, S., Jain, S., & Jain, N.K. (2002). Dendrimer grafts for delivery of 5-fluorouracil. *Pharmazie*, *57*, 261–264.

Üner, M. (2006). Preparation, characterization and physico-chemical properties of solid lipid nanoparticles (SLN) and nanostructured lipid carriers (NLC): their benefits as colloidal drug carrier systems. *Pharmazie*, *61*, 375–386.

Von Burkersroda, F., Schedl, L., & Göpferich, A. (2002). Why degradable polymers undergo surface erosion or bulk erosion. *Biomaterials*, *23*, 4221–4231.

Wang, J.-X., Sun, X., & Zhang, Z.-R. (2002). Enhanced brain targeting by synthesis of 3′,5′-dioctanoyl-5-fluoro-2′-deoxyuridine and incorporation into solid lipid nanoparticles. *Eur. J. Pharm. Biopharm*., *54*, 285–290.

Washington, C. (1990a). Drug release from microdisperse systems: a critical review. *Int. J. Pharm*., *58*, 1–12.

Washington, C., & Koosha, F. (1990b). Drug release from microparticulates; deconvolution of measurement errors. *Int. J. Pharm*., *59*, 79–82.

Wiwattanapatapee, R., Lomlim, L., & Saramunee, K. (2003). Dendrimers conjugates for colonic delivery of 5-aminosalicylic acid. *J. Control. Release*, *88*, 1–9.

Yang, H., & Kao, W.J. (2006) Dendrimers for pharmaceutical and biomedical applications. *J. Biomater. Sci., Polym. Ed*., *17*, 3–19.

Zhang, H., Gilbert, B., Huang, F., & Banfield, J.F. (2003). Water-driven structure transformation in nanoparticles at room temperature. *Nature*, *424*, 1025–1029.

Zhang, J.X., Li, X.J., Qiu, L.Y., Li, X.H., Yan, M.Q., Jin, Y., & Zhu, K.J. (2006a). Indomethacin-loaded polymeric nanocarriers based on amphiphilic polyphosphazenes with poly (N-isopropylacrylamide) and ethyl tryptophan as side groups: preparation, in vitro and in vivo evaluation. *J. Control. Release*, *116*, 322–329.

Zhang, N., Ping, Q., Huang, G., Xu, W., Cheng, Y., & Han, X. (2006b). Lectin-modified solid lipid nanoparticles as carriers for oral administration of insulin. *Int. J. Pharm*., *327*, 153–159.

Zhu, H., & McShane, M.J. (2005). Loading of hydrophobic materials into polymer particles: implications for fluorescent nanosensors and drug delivery. *J. Am. Chem. Soc*., *127*, 13448–13449.

Zur Mühlen, A., & Mehnert, W. (1998a). Drug release and release mechanism of prednisolone loaded solid lipid nanoparticles. *Pharmazie*, *53*, 552–555.

Zur Mühlen, A., Schwarz, C., & Mehnert, W. (1998b). Solid lipid nanoparticles (SLN) for controlled drug delivery. Drug release and release mechanism. *Eur. J. Pharm. Biopharm*., *45*, 149–155.

6

Nanotechnology-Based Biosensors in Drug Delivery

Guigen Zhang

Introduction

Traditional drug delivery vehicles are passive devices functioning mainly through a diffusion process in which the release of drugs is controlled either by the rate of diffusion through the pores of the drug carriers or by the rate of degradation of the carrier matrices. This passive process lacks the mechanism for a constant and on-demand means to administer drug delivery as needed. This has led to inability to deliver therapeutic moieties that can selectively reach the desired targets with marginal or no collateral damage to the normal organs and tissues (Ferrari, 2005).

Over the years, progresses have been made to improve the situation, specifically in ways to guide the accumulation of the drug delivery vehicles to desired sites and control the release mechanism (Barratt et al., 2002). For example, as a first generation of drug delivery systems, micro-capsules are often used for controlled release of proteins, peptides, or drugs within the body. Although they are capable of releasing the active substances at a somewhat desirable rate, they lack the ability to locate the specific site for action. The second-generation systems use environmental-sensitive (e.g., pH, temperature, or pressure sensitive) micro- or nanocapsules or magnetic spheres as delivery vehicles. With these added features, these drug delivery systems will release their payload upon receiving a specific signal such as a preset pH or temperature (Sawant et al., 2006). The third-generation systems are based on drug-carrying micro- or nano-shells or matrices that are functionalized with specific bioreceptors for specific target recognition. This feature adds the ability for these systems to self-recognize their target sites. Future drug delivery vehicles should be autonomous systems with both the diagnostic and therapeutic functionalities so that they will be able to constantly monitor the biological and physiological conditions, process the information, and administer the drug at a desired location, rate, and amount.

As drug delivery devices, these autonomous systems should ideally be small enough to be placed at, or be able to travel through, any desired location in the body. This has become increasingly feasible as the field of nanotechnology advances. Nanotechnology, by definition, deals with the observation, measurement, manipulation and fabrication of systems and

M.M. de Villiers et al. (eds.), *Nanotechnology in Drug Delivery*, DOI: 10.1007/978-0-387-77667-5_6,

constructs having dimensions themselves, or of their essential components, in the 1 nm–100 nm range at least in one dimension. Besides being small, nanotechnology offers materials and structures with unprecedented mechanical, physical, chemical, and biological properties and characteristics. In a sense, nanotechnology takes advantage of the analytical techniques and methodologies of multiple disciplines including mathematics, physics, chemistry, mechanical and electrical engineering, materials science, and molecular biology for the creation of new materials, constructs, devices, and systems.

For realizing such small autonomous systems for drug delivery, reliable nanotechnology-based biosensors are needed in the first place. This chapter will focus on some of the basic attributes of nanotechnology-based biosensors. The advantages of nanotechnology-based biosensors and the uniqueness of various common sensitive elements along with different underlying transducers will be discussed. Following that, some developments in nanostructure-based electrochemical biosensors will be discussed in detail. Finally, some future prospect for the development of nanotechnology-based biosensors will be presented.

The Advantages of Nanotechnology-Based Biosensors

Going nano means not only the size of a matter will be reduced but also the matter can be manipulated on the molecular and atomic levels. As a result, it will bring many benefits. In the case of a nanoparticle or a quantum dot, for example, reducing the size will increase the surface activity and induce unique quantum effects (e.g., confinement of electrons or photons by controlling the densities of electron states or photon states). This in turn will lead to unprecedented electronic, optical, and magnetic properties of the nanoparticle and quantum dot. Furthermore, the ability to arrange and rearrange atoms and molecules at will in a material will help render novel physical and chemical properties for the material.

In the case of biosensing, at the component level going nano means that the capability to sense and detect the state of biological systems and living organisms will be radically transformed by the emerging ability to control the patterns of matter on the nanometer scale (Alivisatos, 2004). Such a radical transformation is expected to enable sensing at the single-molecular level and with parallel detection of multiple signals in living cells. At the systems level, going nano will help decrease the size of the active sensing element to the scale of the target species (to increase the sensitivity and decrease the lower detection limit), reduce the required volumes of the analyte reagent, and minimize the detection time. Reducing the size of biosensors can also result in tiny devices which maybe deployable to any desired location in the body.

Sensors for Biosensors

In today's definition, biosensors are analytical devices that combine a biological-sensitive element with a physical transducer to selectively and quantitatively detect the presence of specific compounds in a given

biological environment. The biological-sensitive element consists of biological receptors (as probes) made of molecular species such as antibodies, enzymes, or nucleic acids for binding the target analytes, and the physical transducer is for converting the biological recognition or binding event into an electrical or optical signal. Thus, from a material's viewpoint, today's biosensors consist of two major components: an organic part as the sensitive element and an inorganic part as the transducer element.

In the future, the approach to biosensing may be drastically different. It is not inconceivable that future biosensors could be made of completely organic assemblies with the capability to communicate with external analytic and monitoring devices via a wireless means either electrically or optically. Currently, biosensors can be categorized mainly into two groups: in vivo and ex vivo biosensors according to their functions. In vivo biosensors are devices residing inside the body, either for a short or a prolonged period of time, for monitoring the biological target species, while ex vivo biosensors are devices for analyzing biological analyte species outside the body.

Basic Requirements for a Biosensor

A biosensor is, first of all, a sensor. This means that it needs to meet the basic requirements for any sensor: being sensitive, responsive, and reliable over a long period of time. Here reliability can be considered as being functioning well without producing false negative and/or false positive responses. But unlike a conventional sensor, a biosensor is often exposed to an environment containing many biological species that are similar in structures and binding behavior. Thus, in additional to meeting the above basic requirements, a biosensor needs to be specific, that is, be responsive only to a specifically targeted analyte species. With such specificity, the usefulness and reliability of a biosensor can be assured. Furthermore, because of the harsh and complex biological environment a biosensor often encounters, the loss of activity in the sensitive element is a major cause for the compromise of the reliability of a biosensor. This loss is mainly due to either the degradation of the molecular probes or their encapsulation (often termed fouling) by other microorganisms or large molecular weight proteins (Ratner et al., 2004). Thus, for a biosensor, the molecular probes to be used need to have long-lasting activity and antifouling behavior.

Due to the difference in their operational environments, in vivo and ex vivo biosensors often face different requirements for their fabrication. An in vivo biosensor has to be constructed using materials that are biocompatible with the body because of its implantation nature. Furthermore, the whole implanted in vivo device should not be encapsulated by the fibrous tissues in the body.

Various Sensitive Elements

Biosensors can be classified according to the type of their sensitive element. Currently, five types of sensitive elements are mainly being used, namely antibodies, nucleotides, enzymes, cells, and synthetic molecules (Kubik et al.,

2005). Biosensors using antibodies as the sensitive element operate based on the binding of an antigen to a specific antibody. Such biosensors are often used in conditions where nonspecific interactions are minimized. Biosensors with nucleotides as the sensitive element are usually used to target the genetic materials such as DNA. Because they rely on the complimentary binding of paired single strands of DNA, this class of biosensors often provides good specificity in detection. The challenge for nucleotide-based biosensors, however, is that the number of target nucleotides is usually very small, thus posing a need for making sufficient copies of the target nucleotides before an actual detection can take place. Biosensors using enzymes as the sensitive element operate based on catalytically induced chemical reactions. The use of enzymes in this class of biosensors adds certain degree of complexity. For instance, while some enzymes require no additional compounds for activity, many enzymes require a cofactor (i.e., either inorganic ions or complex organic or metalloorganic molecules) for their activity. Moreover, the catalytic activity of enzymes is governed by the integrity of their native protein conformation. When enzymes are denatured or dissociated, their catalytic activity will be destroyed, which in turn will compromise the reliability of the biosensors. Because of this, this class of biosensors often exhibits a degrading sensing performance over time.

Cell-based biosensors are another important class of sensors gaining more and more attention lately. The use of whole cells as the sensitive element is very attractive because cells can provide highly selective and sensitive receptors, channels, and enzymes. The main advantages of cell-based biosensors are that cells have built-in natural selectivity to biologically active chemicals and that cells can react to analytes in a physiologically relevant mode (Bousse, 1996; Stenger et al., 2001). With a cell-based biosensor, measurements of transmembrane potential, impedance, and metabolic activity can be made. Challenges abound, however, for long-term operations of this class of biosensors because the viability of the cells must be maintained under various harsh operating conditions. To date, cells such as neurons (Borkholder et al., 1997), cardiac myocytes (Pancrazio et al., 1998), liver cells (Powers et al., 2002), and genetically engineered B cells (Rider et al., 2003) have been used as the sensitive elements. Besides these cells, microorganisms and bacterial cells have also been used as the sensitive elements in biosensors for the detection and monitoring of environmental pollutants (D'Souza, 2001) and evaluation of the effectiveness of drugs (Reining-Mack et al., 2002; Thielecke et al., 2001). Whole cell-based biosensors can offer tremendous benefits for screening drugs and studying the effects of biochemicals on multi-cellular organisms.

Synthetic molecule-based biosensors often use synthetic polymers such as aptamers as the sensitive element (Cai et al., 2006). Aptamers are synthetic nucleic acids that can be synthesized to couple (or fit) with amino acids, drugs, proteins, and other non-nucleic molecules. Because of that, this class of biosensors can provide high affinity to a wide array of targets with excellent specificity. Furthermore, these biosensors can maintain prolonged reliability due to the synthetic nature of the polymeric-sensitive element which will not denature over time.

To be functional, these sensitive elements need to be immobilized onto the surface of an underlying transducer. The duty of such an underlying

transducer is to convert a biological recognition, binding, or reaction event into an electrical or optical signal. Many different detection methods and techniques have been used for fulfilling such a duty as the underlying signal transducer.

Various Underlying Detection Methods

For the underlying detection methods, various physical and chemical techniques are used for converting the biological recognition or binding events into electrical or optical signals. These methods can be generally categorized into mechanical, optical, electromagnetic, electrical, thermal, magnetic and electrochemical methods. The details of the operational principles for the mechanical, optical and electromagnetic, electrical and electrochemical methods are discussed here.

Mechanical Detection

In general, a mechanical-based transducer relies on either mechanical deformations or mechanical waves (or acoustic waves) as its sensing mechanism. To implement such a detection method, a mechanical structure in the form of a cantilever beam, a double-clamped beam, or a disc is often used as the underlying transducer, with the surface of the transducer functionalized by immobilizing a layer of a sensitive element (e.g., antibodies or enzymes) on it for target binding. Before further miniaturization is realized, this type of mechanical detection is better suited for ex vivo applications.

In the case of a cantilever beam, a common mode of detection is through the measurement of cantilever defection caused by the surface stresses generated as a result of molecular binding. Its working principle relies on the induced differential surface stress produced when molecules bind to one side of the cantilever surface (Berger et al, 1997; Sepaniak et al., 2002; Cherian et al., 2003). Surface stress mainly arises from intermolecular forces such as electrostatic interaction or van der Waals. Once generated, the differential stress will cause the cantilever to deflect. According to the classical work by Stoney (1909), for a fixed set of cantilever geometric and material properties, its deflection is linearly proportional to the differential surface stress which is related to the amount of molecular binding. The cantilever deflection is often measured by two common techniques. The first one is via an optical means in which a laser beam is focused on the free end of the cantilever and the cantilever deflection is measured with a four-segment photo detector. The second technique is through an electrical means in which a resistive or capacitive circuitry is used to measure the cantilever deflection (Porter et al., 2003). This mode of mechanical detection has its advantages. For example, when a flexible nanometer-scale cantilever is used, this class of mechanical biosensors is capable of detecting mismatches in oligonucleotide hybridization without labeling (Carrion-Vazquez et al., 1999) and of performing protein recognition with extremely high sensitivity. Moreover, this method is compatible with many analyte species in gaseous or aqueous forms (Wu et al., 2001). There are limitations as well. If the molecular binding events are exothermic, the heat generated may compromise the detection because a

differential thermal stress will also lead to deflection in the cantilever (Mertens et al., 2003). Another issue is with the nonlinear and viscoelastic nature of the molecular structures which may render it invalid to use Stoney's equations in interpreting the relationship between the measured cantilever deflection and the amount of molecular binding (Zhang & Gilbert, 2004; Zhang, 2005).

In the cases of a double-clamped beam or a disc structure, a common mode of detection is through the changes in the acoustic characteristics such as the resonant frequency, attenuation, and phase of wave propagation. In this mode of detection, the mechanical structures operate like oscillators, and a molecular binding event serves as mass loading which often leads to either a shift in the resonant frequency, an increase in amplitude attenuation, or a delay in the phase of wave propagation. Its basic operating principle relies on the fact that any mechanical structure possesses a unique resonate frequency (the lowest eigen frequency of the structure) along with a certain amount of attenuation and phase of propagation. When molecular binding occurs at the active surface of such a mechanical structure, the mass of the structure and damping to the wave propagation will increase (Headrick et al., 2003). Under this circumstance, the structure will exhibit certain changes in its wave characteristics when it is perturbed by an external acoustic wave. To increase the detection sensitivity, the mechanical structure (a beam or disc) should possess a high-quality factor (Davis et al., 2002). In general, the quality factor decreases when the size and damping of the mechanical structure increase. Bulk acoustic waves are more susceptible to liquid-damping-induced attenuation than surface acoustic waves; thus detections based on bulk acoustic waves (in the cases of a double-clamped beam or a quartz crystal microbalance) are preferably used in a dry environment and detections based on surface acoustic waves are often used in a liquid environment. A detailed discussion of the applications of bulk and surface acoustic wave devices can be found in a review by Rao and Zhang (2006). By detecting the frequency shift, the attenuation drop, and the phase shift, the amount of bound analyte can be determined. The advantage of this mode of detection is that a single frequency sweep can provide a quick measurement of the mass of the bound molecules at a resolution down to picogram level (Thundat et al., 1995). The challenge for this type of mechanical detection, however, lies in the difficulty in distinguishing the type and the uniformity of the bound species, thus rendering it less specific in biological sensing.

Optical and Electromagnetic Detection

Optical detection is one of the widely used mechanisms for biosensing because this method can be incorporated into many different types of spectroscopic techniques, including luminescence, absorption, polarization, and fluorescence (Wickline & Lanza, 2003). With this detection method, different spectrochemical properties such as amplitude, energy, polarization, decay time, and phase of a target analyte can be measured. These spectroscopic properties can be correlated to the concentration of the analyte of interest.

Of the many optical techniques, fluorescence-based detection is probably the most used method. In this method, fluorescent markers that emit

light at specific wavelengths are used as detecting labels for the target analytes, and measurements of fluorescent intensity are made for the presence of the targets or the binding of targets to the probes. Many micro-array gene chips use this technique for the detection of hybridization. Furthermore, fluorescence-based detection methods have been used to systematically analyze protein–protein and protein–DNA interactions. This technique has been proved capable of single molecule detection (Vo-Dinh & Cullum, 2000; Nie & Zare, 1997; Moerner & Orrit, 1999).

The sensing principle based on the evanescent wave is another common mode of optical detection. In this method, an optical waveguide is used to confine the light traveling through the waveguide by total internal reflection. With a majority part of the light confined inside the waveguide, a small part of it (i.e., the evanescent wave field) travels through a region that extends about several tens of nanometers into the surrounding medium. This evanescent wave can be used for sensing purposes. In a sensing application, the waveguide surface is functionalized with a biological-sensitive element, and the change in the optical properties of the evanescent wave is measured in response to the binding of the target and probe molecules. Evanescent wave-based sensors are very selective and sensitive for the detection of low levels of chemicals and biological species, and they are suited for the measurement of molecular interactions in situ and in real time (Liu & Tan, 1999). One of the most used evanescent wave biosensors is the surface plasmon resonance (SPR) sensor owing to its high sensitivity and simplicity. In a SPR sensor, the change in the refractive index of the evanescent wave, caused by the interaction between the target molecules and the sensitive probing molecules immobilized on the sensor surface in the evanescent field, is measured.

A well-known electromagnetic detection method is based on the theory of surface-enhanced Raman spectroscopy (SERS). Surface-enhanced Raman scattering is observed for molecules placed close to a rough metal surface featured with silver or gold nanostructures (e.g., nanoparticles or nanowires) because of surface plasmon resonance. This makes SERS a very sensitive detection technique. The working mechanism by which a SERS detection operates is still a debating issue. It is believed that it operates from a local electromagnetic field enhancement provided by an optically active nanoparticle. The electromagnetic effect alone, however, does not account for all that is observed through SERS. Molecular resonances, charge-transfer transitions, and other processes such as ballistic electrons transiently probing the region where the molecule resides and modulating electronic processes of the metal certainly contribute to the rich information that SERS measures (Moskovits, 2005). Nevertheless, ultrasensitive analytical strategies and bioassays based on SERS have been realized (Emery et al., 1998: Krug et al., 1999), in which an enhancement as large as 10^{14}, enough to allow routine detection of Raman from single molecules, is achieved.

Electrical Detection

Although it has not been as widely used as the mechanical or optical detection methods, electrical detection actually possesses some desirable features as an underlying transducer due to its ease of use, label-free

detection capability, portability, and miniaturization. Conductometric and potentiometric techniques are two common modes of electrical detection, and they mainly rely on the measurement of changes in conductance (or impedance) and potential in response to a biological binding event occurring at the electrode surfaces.

Conductometric sensors detect changes in the electrical resistance or impedance between two electrodes (Chen et al., 2003, 2004). In this case, the changes in resistance or impedance are due to either molecular interactions between nucleotides, proteins, and antigens and antibodies or excretion of metabolites near the electrode surfaces or in the surrounding media. This mode of detection is attractive because it does not require a specialized reference electrode as in the case of electrochemical detection. So far, this method has been used to detect a wide variety of chemical and biological target species, toxins, and nucleic acids, to measure the metabolic activity of microorganisms, and to monitor DNA hybridization (Sosnowski et al., 1997; Marrazza et al., 1999; Drummond et al., 2003). Currently, a practical challenge for a conductance base biosensing method is the understanding of the underlying mechanism for the changes in electrical properties of the electrode material caused by molecular adsorption and coupling.

Potentiometric sensors measure the potential changes between electrodes. The most common design of potentiometric sensors uses ion-sensitive field effect transistors or chemical field effect transistors (Bashir, 2004). A pH meter is such an example. Potentiometric sensors have been used to perform label-free detection of hybridization of DNA by measuring the field effect in silicon due to the intrinsic molecular charges on the DNA (Fritz et al., 2002). Recently, potentiometric sensors have been miniaturized to nanometer dimension through the use of silicon nanowires (Cui et al., 2001) and carbon nanotubes (Besteman et al., 2003) for enhanced sensitivity due to the increased surface to volume ratio for the electrodes.

Electrochemical Detection

Biosensors using an electrochemical method as the underlying transducer are often used to measure electrical responses resulted from the electrochemical reactions of the target redox species catalyzed by the enzymatic-sensitive element. These biosensors are usually configured in a three-electrode format: a working electrode, a counter electrode, and a reference electrode. The reference electrode needs to meet the special requirement of maintaining at a constant potential with respect to the electrolytic solution.

For biological detections, three modes of operations, namely amperometric, voltammetric, and impedimetric, are most commonly used. Amperometric biosensors measure the electrical current generated by the electron exchange between the electrodes and ionic species in response to electrode polarization at a constant potential. The measured steady-state limiting current (due to the encountered diffusion limit) is linearly proportional to the concentration of the electroactive analyte species. Voltammetric biosensors measure the current–potential relationships (i.e., voltammograms) induced by a redox process. The obtained peak currents and peak potentials (oxidation and reduction), or limiting currents in the

case of sigmoidal voltammograms for nanometer electrodes, are related to the transport phenomena and efficiency as well as the concentration of the redox species. Impedimetric biosensors measure the changes in the complex impedance of an electrochemical process upon cyclic excitations of the working electrode at a predetermined range of frequency. The measured results, often in Bode plots or Nyquist plots, are indicative of the electron transfer resistance which is related to the electrode/solution interfacial properties and the concentration of the analyte.

For the functionalization of these biosensors, enzymes are often used for catalytic-based sensing and other sensitive receptors (e.g., antibodies, nucleotides, cells, and proteins) are used for affinity-based sensing. In the case of a glucose sensor, the working electrode is usually functionalized with glucose oxidase for catalyzing glucose oxidation, and the current response is measured. Electrochemical-based biosensors have been used in the detection of glucose, lactose, urea, lactate, and DNA hybridization (Hintsche et al., 1991, 1995; Umek et al., 2001; Cia et al., 2002; Popovich & Thorp 2002; Zhu & Snyder, 2003).

Biosensors for Drug Delivery

Although future drug delivery devices may be autonomous systems with integrated capabilities of biosensing and drug delivery, the actual realization of such capabilities will rely on further advances in nanotechnology. Many progresses have been made in the development of lab-on-a-chip microscale devices (Bashir, 2004), and surely these devices will become more compact and more functional with higher sensitivity, specificity, and reliability in terms of sensing and with higher controllability in terms of drug delivery as the field of nanobiotechnology advances, but full-fledged autonomous systems of biosensors for drug delivery applications may still be years away. Currently, the development of biosensors for drug delivery takes a slightly different route. As discussed in the Introduction, drug delivery systems have been evolving from the totally passive drug-carrying vehicles of the first-generation systems, the environmental-sensitive drug-carrying vehicles of the second-generation system, to the target-specific and bioactive drug-carrying vehicles of the third-generation systems. Following this route, one can see that by adding sensitive components to the drug delivery systems, integrated capabilities of biosensing and drug delivery can be realized. Thus, it is conceivable that the next-generation drug delivery systems could be biologically sensitive drug-carrying vehicles incorporated with an underlying transducer (e.g., optical or image based) for signal detection and communication. This route may eventually converge with the lab-on-a-chip route, leading to an autonomous system with both the diagnostic and therapeutic functionalities.

But for now, one of the challenges in developing biosensitive drug delivery vehicles is to devise drug carriers that are biocompatible, resistive to biodegradation, resistive to host inflammatory and immunologic responses, and sensitive to specific targets, among other things. In addition, the drug carrier constructs should be highly effective in prolonged drug retention, especially for water-soluble drugs. Biological constructs such as liposomes are potentially good drug carrier materials due to their

abilities to protect drugs from degradation and to target the specific site for action (Knight, 1981). Because of their low encapsulation efficiency, rapid leakage of water-soluble drugs in the presence of blood elements, poor storage stability, and susceptibility to immunologic attacks, their application as drug carriers is severely hampered. To overcome this obstacle, a polymer coating that protects the liposomes from immunologic destruction and other degradation has been applied to form the so-called stealth-liposomes. In contrast, synthetic conjugated molecular assemblies and nanocapsules are more efficient drug carriers, and they have been used for many drugs including antibiotics, antiviral drugs, vitamins, proteins, peptides, enzymes, hormones, and oligonucleotides (Sun et al., 2006). Encapsulation is attractive because it can reduce systemic toxicity, protect vulnerable molecules from degradation in the digestive tract, and provide controlled release properties. Nanocapsules as drug carriers have been shown to protect insulin from degradation by digestive enzymes, to provide prolonged therapeutic effect, and to reduce drug-related immunologic responses (Aboubakar et al., 2000; Damage et al., 1997; Fernandez-Urrusuno et al., 1999).

For the nanocapsule-based biosensitive drug delivery systems, they should ideally be able to accumulate at specific sites of an organ or tissue, penetrate into target cells, and release the payload drug. The current systems rely on the immobilization of specific bioreceptors onto these drug carriers to perform site-specific targeting. To fulfill the cell-wall penetration function, it is necessary for these biosensitive drug carriers to have multiple active moieties for multiple functions including site-specific targeting and cell-wall penetration. These multiple moieties should be able to switch on and off upon certain environmental stimulations (e.g., pH, temperature, ion concentration, or partial pressure of oxygen and carbon dioxide).

Nanostructure-Based Electrochemical Biosensing

Electrochemical-based biosensing method is unique in many aspects including high sensitivity and specificity, low cost, ease of use, and ease of integration with micro-/nano-electronic and fluidic devices. To enhance the performances of such a sensing method, electrodes incorporated with arrays of nanostructures such as nanorods, nanowires, nanotubes, and nanopillars have been recently explored (Bharathi & Nogami, 2001; Koehne et al, 2004; Anandan et al, 2005, 2006). Because of the ultrasensitivity provided by these nanostructures having critical dimensions less than the lengths of the diffusion layer typically encountered on voltammetric time scales, investigation of electrochemical phenomena in fast-electron transfer reactions by steady-state experiments becomes possible (Arrigan, 2004). The use of these nanostructured electrodes in biosensors has extended electrochemical methodology into previously inaccessible domains of time, space, and medium. For example, electrodes incorporated with nanostructures are found to enhance significantly the electrochemical performances in DNA and glucose detections (Wang & Mustafa, 2004; Gasparac et al., 2004; Yemini et al., 2005; Anandan et al, 2006).

In an electrochemical biosensor, the dimension of its electrodes plays a significant role affecting the sensing performance. Electrodes with a smaller critical dimension can enable 3D radial nonlinear diffusion and provide steady-state voltammetric response. Because of the unique metal/solution interface in an electrochemical process, electrodes are often surrounded by an electrical double layer (EDL) structure. As the electrode size becomes equivalent to that of EDL (e.g., a fraction of a nanometer), the electrical field generated near the electrodes will influence the transfer of electrons and transport of ions, thus altering the electrode reaction and current response (Morris et al., 1987; Seibold et al., 1989; Mirkin et al., 1990; Chen & Kucernak, 2002). Thus, for nanoscale electrochemical electrodes, it is important to know how the EDL structure affects the electron transfer and current response. When used for biosensing, the electrochemical performances of nanostructured electrodes will also vary with functionalization methods and molecules as well as kinetics of mass transport, in addition to geometrical shapes and dimensions of the nanostructures. These aspects of nanostructure-based electrochemical electrodes are discussed here.

Nanopillar Array Electrodes

Slender nanostructures such as nanowires, nanotubes, and nanorods can now be routinely fabricated using chemical vapor deposition (CVD), physical vapor deposition (PVD), and template-based electrodeposition technique (Lau et al., 2003; Fan et al., 2004; Anandan et al., 2005, 2006). But not all these slender nanostructures are suitable for electrochemical applications. For example, vertically standing carbon nanotubes and silicon nanorods developed by CVD and PVD are not able to sustain the capillary forces generated by the nanostructure–liquid interaction (Lau et al., 2003; Fan et al., 2004). As shown in Figure 6.1A, standing silicon nanorod arrays fabricated by PVD technique deformed severely upon water contact due to the aqueous capillary interaction between the nanostructures and the liquid medium (Kralchevsky & Nagayama, 2000; Fan et al., 2004) as well as the amorphous nature of the silicone nanostructures.

This kind of deformation in the nanostructures upon liquid interaction poses a serious problem for their application in electrochemical biosensors. Although a much improved situation is achieved by annealing silver

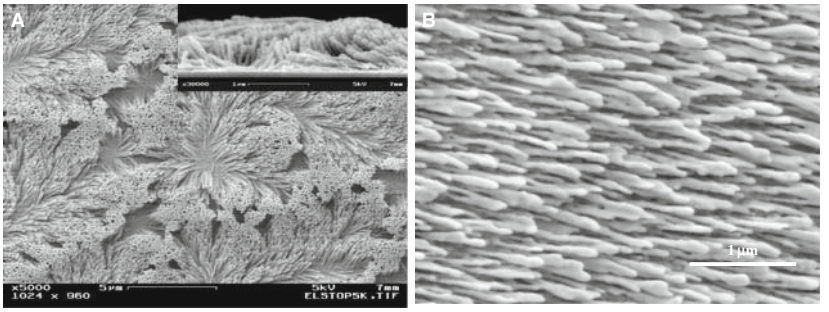

Figure 6.1 Nanorod arrays fabricated by a PVD technique: (**A**) silicon nanorods and (**B**) silver nanorods.

nanorods prior to electrochemical evaluations (see Figure 6.1B; Tang et al., 2006), a better alternative is to use nanostructures fabricated by a cost-effective aqueous-based electrodeposition technique (Anandan et al., 2005; Rao et al., 2005).

This electrodeposition technique takes a three-step fabrication process: (1) fabricating porous anodic alumina (PAA) templates by anodization, (2) depositing nanopillar arrays using the PAA templates, (3) removing the PAA templates. Some representative SEM images of PAA templates developed by the anodization technique are shown in Figure 6.2A (a top view) and Figure 6.2B (a side view), and SEM images of the electrodeposited nanopillar array structures are shown in Figure 6.2C (silver) and Figure 6.2D (gold).

In addition to producing strong vertically aligned nanopillar array structures, this electrodeposition method allows a control of the nanopillar diameter and spacing by simply adjusting the anodization potential (Figure 6.3A) based on the relationships of PD (nm) = 1.35 (nm/V) × AP (V) and PS (nm) = 2.58 (nm/V) × AP (V), where PD stands for the nanopillar diameter, PS the nanopillar spacing, and AP the anodization potential (Rao et al., 2005). When these nanopillar array structures are used as electrochemical electrodes, their active area will increase significantly, which in turn will lead to enhanced current responses. Figure 6.3B shows a series of cyclic voltammograms of a gold nanopillar array electrode in 0.3 M sulfuric acid solution where it is seen that both the oxidation and reduction current responses increase as the height (or the roughness factor) of the nanopillars increases.

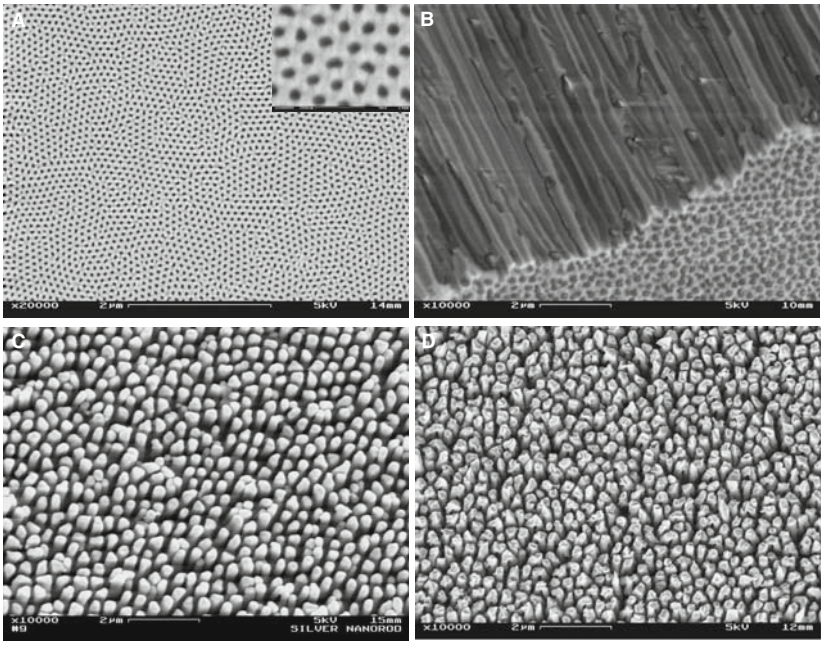

Figure 6.2 Scanning electron microscopic views of PAA templates and electrodeposited nanopillar array structures: (**A**) a top view of a PAA template, (**B**) a side view of a PAA template, (**C**) electrodeposited silver nanopillar array structures, and (**D**) electrodeposited gold nanopillar array structures.

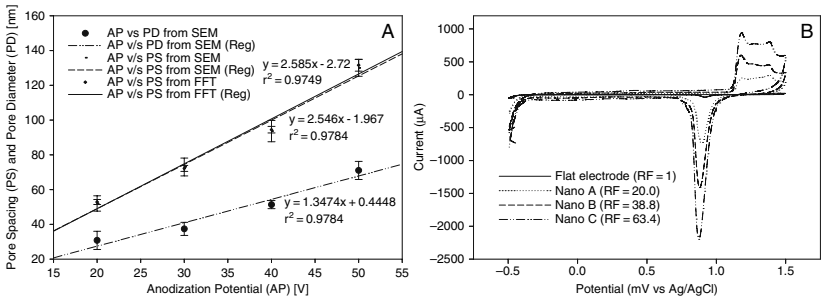

Figure 6.3 (**A**) Calibration curves for the anodization potential (AP) dependent pore spacing (PS) and pore diameter (PD). (**B**) Voltammograms of electrodes made of gold nanopillar array structures with different nanopillar heights and a flat surface (note that RF stands for the roughness factor determined by the ratio of the area under the reduction peak between a nanostructured surface and a flat surface).

Amperometric and Voltammetric Responses of Nanopillar Array Electrodes

With nanopillar array electrodes, much-enhanced electrical currents in both amperometric and voltammetric processes are observed. Figure 6.4A shows the amperometric current responses of bare (non-functionalized) nanopillar array electrodes at various concentrations of $K_4Fe(CN)_6$ under a constant potential of 350 mV (versus Ag/AgCl) in 0.5 M Na_2SO_4 solution. Figure 6.4B shows the amperometric current responses of functionalized

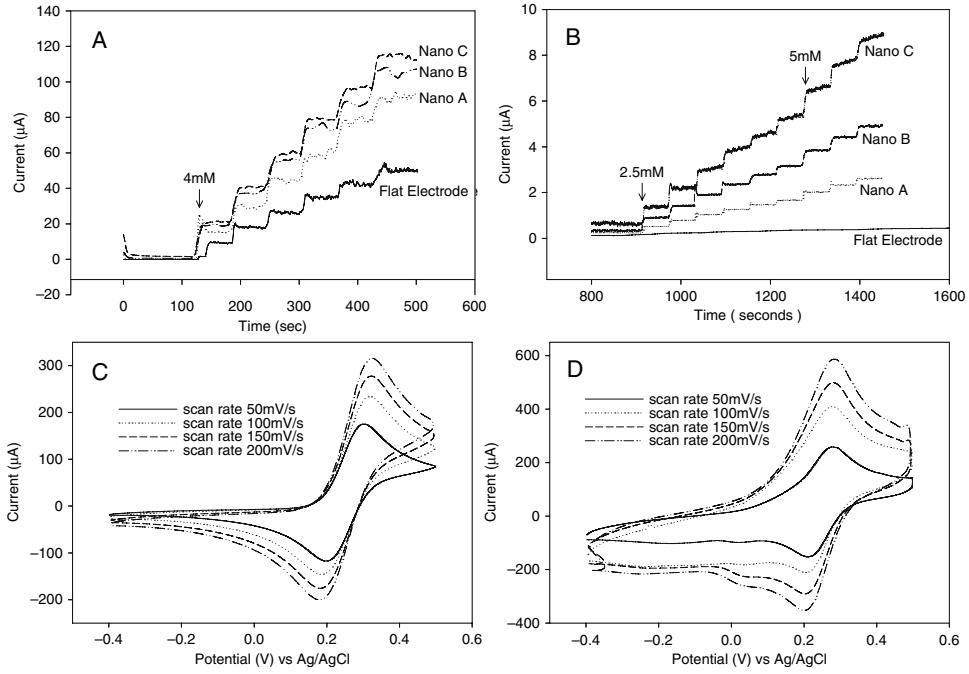

Figure 6.4 (**A**) Amperometric current responses of bare nanopillar array electrodes at various concentrations of $K_4Fe(CN)_6$. (**B**) Amperometric current responses of functionalized nanopillar array electrodes at different glucose concentrations. (**C**) Voltammetric current responses of a flat electrode at various sweep rates. (**D**) Voltammetric current responses of a nanopillar array electrode at various sweep rates.

(with glucose oxidase) nanopillar array electrodes at different glucose concentrations. In general, the nanopillar array electrodes exhibit higher currents than the flat electrode in bare condition for oxidizing $K_4Fe(CN)_6$ and in functionalized condition for oxidizing glucose.

Figure 6.4C and D shows the voltammetric current responses of a flat electrode and a nanopillar array electrode at various sweep rates (50 mV/s, 100 mV/s, 150 mV/s, and 200 mV/s) in a potential range of –0.4 V to +0.5 V against Ag/AgCl in 0.5 M Na_2SO_4 and 4 mM $K_4[Fe(CN)_6]$ (note that the electrodes have the same geometric area, about 16 mm^2). The redox peaks for the $[Fe(CN)_6]^{4-}/[Fe(CN)_6]^{3-}$ couple are higher for the nanopillar array electrodes (Figure 6.4D) than for the flat electrode (Figure 6.4C), and that the peak current increases with increasing scan rate. The oxidation–reduction peak separation (∇E_p) of the voltammograms for the nanopillar array electrode is measured to be about 70 mV, which is close to an ideal Nernstian behavior ($\nabla E_p = 56.4$ mV) (Bard & Faulkner, 2001). Comparing it with ∇E_p for the flat electrode (~110 mV), it is clear that the mass transport at the nanopillar array electrode is significantly enhanced.

Impedance Measurements of Nanopillar Array Electrodes

In an electrochemical process, the change in electrode impedance can be used to characterize the interfacial properties between the electrode and solution. This feature is often exploited in affinity-based electrochemical biosensors, in which changes in electrode impedance caused by molecular binding are measured (Laureyn et al., 2000; Ma et al., 2006). With an avidin–biotin couple, the change in the impedance of nanopillar array electrodes at various degrees of avidin–biotin binding has been characterized (Lee et al., 2008). To prepare the nanopillar array electrodes, avidin is first immobilized with the use of a self-assembled monolayer (SAM) of 11-mercapto- undecanoic acid (MUA) and the subsequent activation of the COOH-terminated group of MUA. Following that, the impedance of such avidin functionalized electrodes is measured in PBS (0.01 M, pH 7.4) with increasing biotin concentrations (from 1 ng/ml to 50 ng/ml).

To show the advantage or disadvantage of impedance measurements versus voltammetric measurements in detecting avidin–biotin binding, both the impedance and voltammetric responses are measured in PBS having 2.5 mM K_4[Fe(CN)6] and 2.5 mM K_3[Fe(CN)6]. The obtained Nyquist plots and voltammograms at various biotin concentrations are shown in Figure 6.5. From the voltammetric responses (Figure 6.5A), it is seen that the highest current level decreases with the increase of biotin concentration. Furthermore, as the biotin concentration increases, the voltammetric curve becomes less peak shaped and more sigmoid shaped. This can be attributed to the increased electron transfer resistance causing the slowdown of the redox activity such that the rate of diffusion becomes equivalent to the rate of oxidation. At a higher biotin concentration (>8 ng/ml), however, the voltammograms seem to stack on top of each other, making it difficult to distinguish the concentration-dependent current responses.

This is not the case with the impedance measurements. The impedance measurements show that the radius of these semicircular Nyquist plots (Figure 6.5B) increases as the biotin concentration increases (causing more

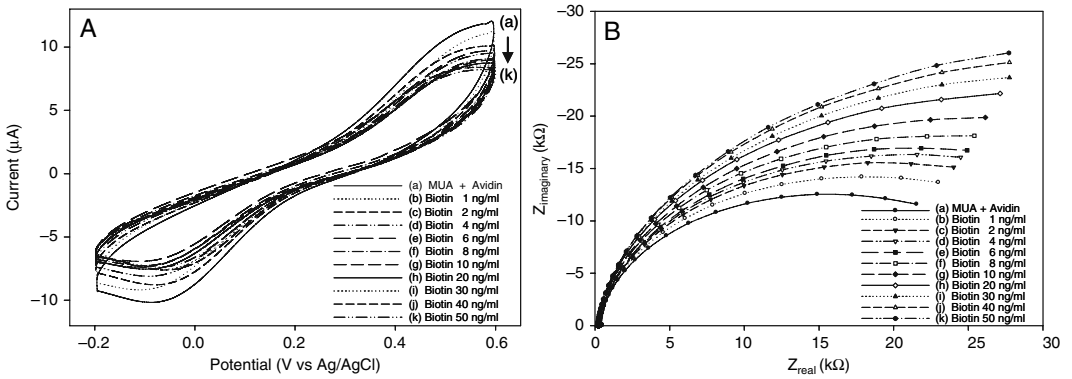

Figure 6.5 Voltammograms (**A**) and Nyquist plots (**B**) obtained for nanopillar array electrodes functionalized with avidin at various biotin concentrations.

biotin to bind to avidin). Therefore, the impedance-based sensing technique with nanopillar array electrodes can provide very good sensitivity and low detection limit (1 ng/ml) with distinct Nyquist plots at different biotin concentrations. By contrast, the voltammetric measurements are less sensitive to the change in biotin concentration, especially at a high concentration of biotin.

Interdigitated Electrodes

For affinity-based biosensing, impedance measurements surely have some advantages. But the drawback is that an impedance-based detection method is very time consuming (Yang et al., 2004): it may take hours to complete a test run during which the electrochemical environment may have changed. In contrast, voltammetric measurements are known for their fast response and ease of use, although they suffer from lack of sufficient sensitivity and lower detection limit. To alleviate this problem, integration of a voltammetric method with interdigitated electrodes (IDEs) has been explored recently (Yang & Zhang, 2005, 2006, 2007).

In IDEs, generator electrodes are placed side by side with collector electrodes in an interdigitated manner. With IDEs, an electroactive species gets oxidized at the generators, diffuses across the thin-layer gap due to a concentration gradient, and gets reduced at the collectors. The reduced species at the collectors then diffuses back to the generators following its concentration gradient. This redox cycling (or feedback) activity makes the measured currents at both the generators and collectors extremely high. Because of the proximity of the generators and collectors, a very high percentage of the oxidized species produced at the generators gets reduced at the collectors with a very low solution resistance (Aoki, 1990; Niwa et al., 1990; Paeschke et al., 1995; Phillips & Stone, 1997; Jeng, et al., 2001). Additionally, a steady-state current can be achieved at IDEs by holding the collectors at a fixed potential while sweeping the potential at the generators.

It has been shown that that the presence of the generators and collectors in nanometer proximity facilitated feedback cycling of oxidation and reduction with extremely high mass transport efficiency, thus leading to high current response and steady-state sigmoidal voltammogram.

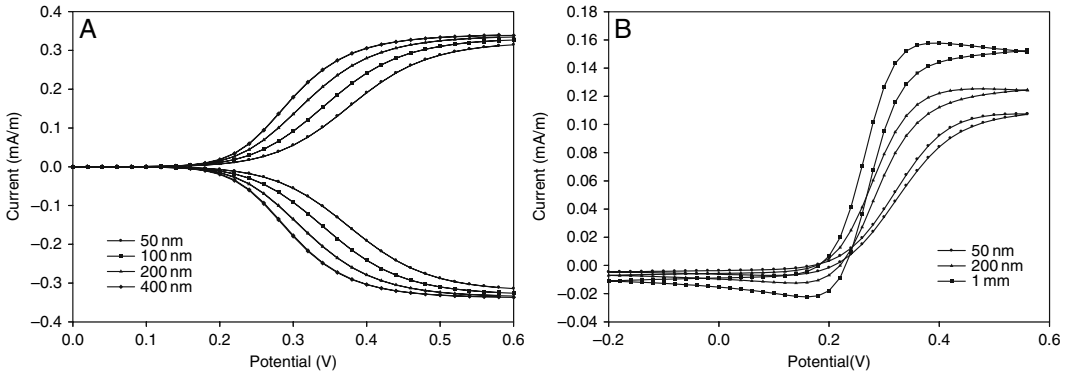

Figure 6.6 (**A**) Sigmoidal voltammograms obtained for IDEs electrodes. (**B**) Peak-shaped voltammograms obtained for single electrodes.

Figure 6.6A shows the voltammograms for IDEs with an electrode width less than 500 nm. Owing to the highly efficient redox cycling, the steady-state current levels at both the anode and cathode are very close despite the significant difference in their electrode widths. By contrast, single electrodes behave quite differently because of a lack of the redox cycling. As shown in Figure 6.6B, the voltammograms obtained for single electrodes are peak shaped with hysteresis, indicating a low efficiency in mass transport by diffusion. Furthermore, the current levels are much lower than those obtained for the IDEs.

When these IDEs are used in biosensors, their current response will rely on the redox cycling behavior and mass transport phenomena at and near the electrode/solution interface which will be altered by the electrode functionalization and further probe/target recognition or binding. Thus, the current response will depend on the electron transfer rate constant (i.e., the k_0 value) of the electrode reactions involved. A decreasing k_0 value represents a situation in which increasing molecular binding may occur at the electrode surface. Figure 6.7 shows the voltammograms at various

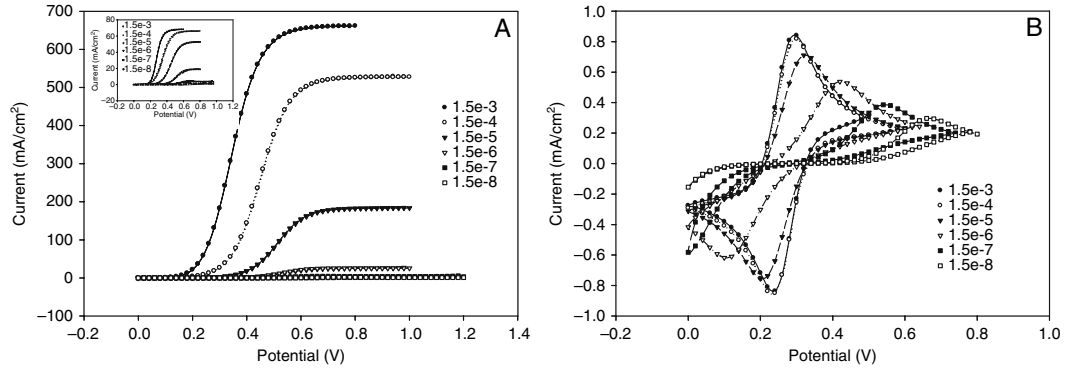

Figure 6.7 Voltammograms obtained for the IDEs with $w = 100$ nm (**A**) and for the single electrode (**B**) at various k_0 values (from 1.5×10^{-3} m/s to 1.5×10^{-9} m/s). The insert shows the voltammograms for the IDEs with $w = 1$ μm.

k_0 values for an IDEs electrode (with a critical dimension of 100 nm; Figure 6.7A) and a single electrode (Figure 6.7B).

For the single electrode, peak-shaped voltammograms are produced when the k_0 value is high. As the k_0 value decreases, the peak current of the voltammogram decreases. This suggests that the rate of diffusion and the rate of oxidation become equivalent, as is the case for the nanopillar array electrodes in avidin–biotin binding experiments (see Figure 6.5A). In comparison, steady-state voltammograms with sigmoidal shape are obtained for the IDEs. At a higher k_0 value, the limiting current obtained for the three IDEs is much higher (hundreds times higher) than the peak current for the single electrode. This increased current response is attributed to the enhanced mass transport near the IDEs. As k_0 decreases, a decrease in the limiting (or peak) current is observed in both cases, but a more drastic decrease is seen with the IDEs than with the single electrode. This fact suggests that the voltammetric performance of IDEs is more sensitive to the change of k_0 as compared with that of the single electrode.

From Figure 6.7A it is seen that the narrower the electrode gets, the more sensitive it becomes to the change of k_0, especially when k_0 is large ($>1.5\times10^{-6}$). For instance, a change in k_0 from 1.5×10^{-3} to 1.5×10^{-4} caused almost a 20% reduction in the limiting current for the IDEs with $w = 100$ nm (Figure 6.7A), whereas a mere 3% reduction was seen for the IDEs with $w = 1$ μm (Figure 6.7A insert). With each set of IDEs, as k_0 decreases, not only the limiting current decreases significantly but also the voltammogram shifts to the right. These facts indicate that the voltammetric current response of the IDEs is indeed sensitive to the change of k_0, and that a higher overpotential is needed to drive the electron transfer as k_0 decreases.

In a more recent study by Strutwolf and Williams (2005) and Yang and Zhang (2007), it is found that the sensing performance can be further enhanced by using 3D IDEs. As shown in Figure 6.8, the limiting current is the highest, intermediate, and the lowest for the nanorod-

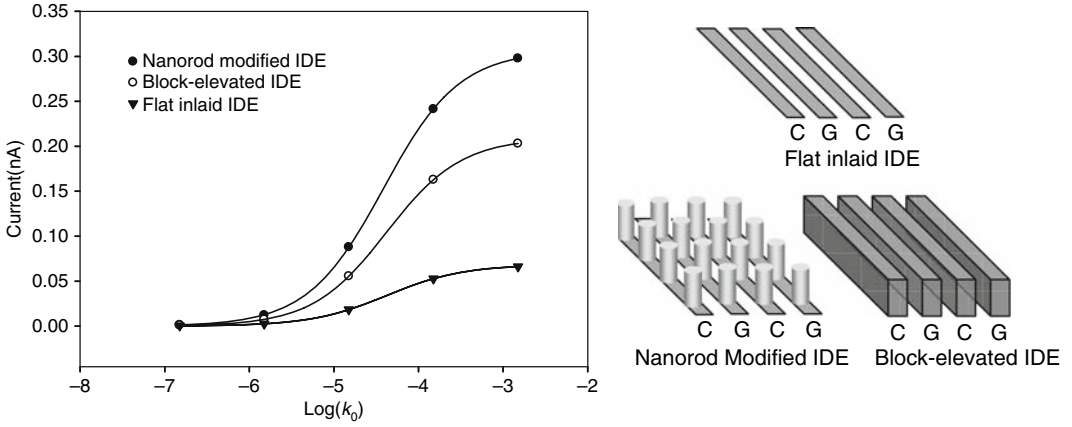

Figure 6.8 Variation of the voltammetric limiting current with $\log(k_0)$ for three 3D IDEs cases: nanorod modified IDE, block-elevated IDE, and flat inlaid IDE. Note that the width for the base collector (C) and generator (G) electrodes is 100 nm in all three cases.

modified, block-elevated, and inlaid IDEs, respectively, at any given k_0. This is attributed to the increased surface area of the electrodes caused by the larger height of the 3D electrodes, which enable a heightened redox cycling activity between the vertical walls of the neighboring generator and collector electrodes.

Effect of Functionalization Molecules and Kinetics of Mass Transport

For nanopillar array electrodes, their electrochemical-based biosensing performances are affected by the type of functionalization molecules used to immobilize the sensitive elements. In the case of self-assembled monolayer (SAM) molecules, their chain length and surface coverage will affect electron transfer. For example, when two SAMs with different chain lengths are used as the underlying molecules for immobilizing glucose oxidase onto the nanopillar array electrodes, they present different electron transfer resistances and detection sensitivities. As shown in Figure 6.9, significantly higher detection sensitivity is achieved for the case with a shorter SAM (i.e., 3-mercaptopropionic acid, or MPA) than for the case with a longer SAM (i.e., 11-mercaptoundecanoic acid, or MUA). This is true for the nanopillar array electrodes with three different nanopillar heights (1 μm, 2 μm, and 3 μm). This result can be attributed to the fact that a shorter SAM is likely to form highly ordered SAM coverage over a larger area and to hold the enzyme at a closer distance to the electrode surface, both of which are crucial for facilitating enhanced electron transfer. Furthermore, in each SAM case, the taller the nanopillars the higher the detection sensitivity. This is due to the increased surface area of the electrodes because of the increased nanopillar height.

The kinetics of mass transport near the electrode/solution interface also plays an important role influencing the current responses of electrochemical-based biosensors (Anandan et al., 2007). When bare nanopillar array electrodes are tested for the redox of $K_4Fe(CN)_6$ at various concentrations, electrodes with different nanopillar heights exhibit almost the same sensitivity response (see Table 6.1), although the sensitivity of nanopillar array

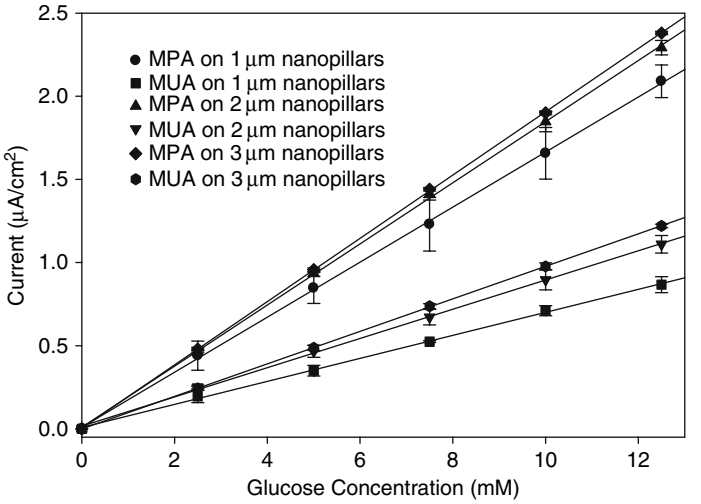

Figure 6.9 Calibration curves of the amperometric steady-state current versus glucose concentration. Cases considered here include nanopillar array electrodes of three different nanopillar heights and two different immobilization molecules.

Table 6.1 Measured values for the roughness ratio, detection sensitivity, and K_m for various nanopillar array electrodes and flat electrode.

Specimen	Roughness factor	Sensitivity of bare electrodes to $K_4Fe(CN)_6$ ($\mu A/mM \cdot cm^2$)	Sensitivity of functionalized electrodes to glucose ($\mu A/mM \cdot cm^2$)	K_m glucose (mM)
Flat	1.0	19.30	0.27	24.8
Nano A	20.0	41.40	0.91	29.3
Nano B	38.8	41.05	1.80	32.6
Nano C	63.4	41.70	3.13	52.0

electrodes is much higher than that of the flat electrode. It is speculated that the electroactive species $K_4Fe(CN)_6$ may encounter certain difficulties in its transport to the small spaces between the nanopillars as a result of either a low diffusivity or a fast-electron transfer rate constant. When the diffusivity is low, it will be difficult for $K_4Fe(CN)_6$ to diffuse deep into the small spaces between the nanopillars, and when the electron transfer rate constant is high, most of the species $K_4Fe(CN)_6$ will get oxidized near the top ends of the nanopillars before it gets diffused deep down the gaps. Under these circumstances, it is conceivable that only the top ends of the nanopillars are serving their active duty in transferring electrons to oxidize $K_4Fe(CN)_6$. The situation for functionalized nanopillar array electrodes (with glucose oxidase) is quite different. The sensitivity of these nanopillar array electrodes in glucose detection increases as the height of the nanopillars (or the roughness ratio) increases. An increase of about 12 times in sensitivity is observed for a nanostructured electrode having a roughness factor of 63.4 as compared with the flat electrode (see Table 6.1).

An enzymatic kinetics study using the Michaelis–Menten equation indicates that the apparent Michaelis–Menten constant (K_m) increases with the presence of nanopillars and increase of their height. As listed in Table 6.1, the K_m values for the nanostructured electrodes are higher than the intrinsic K_m value (25 mM) for dissolved glucose oxidase (Calvo & Wolosiuk, 2004). This implies that the activity of the enzyme immobilized onto these nanostructured electrodes has actually decreased as compared with the freely dissolved enzyme, suggesting that the increase in sensitivity in the functionalized nanopillar array electrodes is due to factors other than enzyme activity.

That the nanostructure-induced sensitivity enhancement for the functionalized electrodes (11.6 times) is higher than that for the bare electrodes (2 times) may be attributed to the difference in electrochemical reactions and kinetics of transport. But these two electroactive species (i.e., glucose and $K_4Fe(CN)_6$) have a similar value of diffusivity (8×10^{-10} m^2/s for $K_4Fe(CN)_6$ and $7.6\times10^{-10} m^2/s$ for glucose) (Winkler, 1995); it is thus possible that different electrode reactions involved in these two cases may play a more dominate role in affecting the current responses. This speculation is confirmed by a computer simulation of the situation.

Figure 6.10A shows the simulated amperometric current responses obtained for a functionalized nanopillar electrode and a flat electrode with the surface-reaction rate constants set at 5×10^{-4} m/s, 5×10^{-5} m/s,

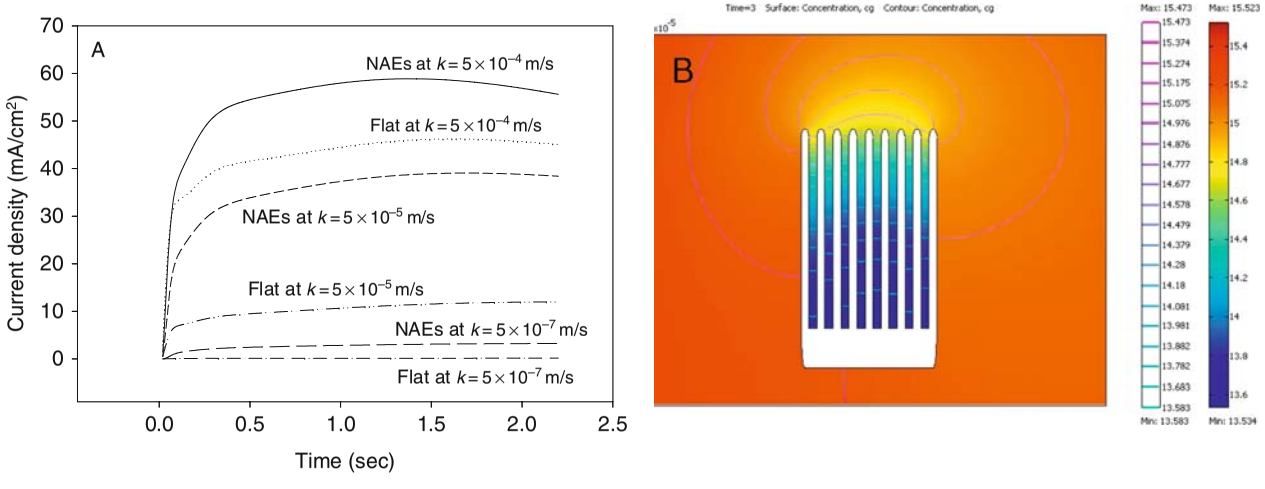

Figure 6.10 (**A**) Simulated current response for a functionalized nanopillar electrode and a flat electrode at various surface-reaction rate constants. (**B**) Contour plot of glucose concentration near the nanopillar electrode obtained at a reaction rate constant of 5×10^{-7} m/s. (*See* Color Plate 12)

Table 6.2 Simulated steady-state amperometric current obtained at various reaction rate constants.

	Current density (mA/cm^2)		
Reaction rate constant (m/s)	**Nano**	**Flat**	**Nano/flat**
5×10^{-4}	58.9	46.2	1.27
5×10^{-5}	39.1	12.0	3.26
5×10^{-7}	3.25	0.146	22.26

and 5×10^{-7} m/s. As expected, a higher current response is seen for the nanostructured electrode than for the flat electrode (see Table 6.2). But the increase in the current response due to the presence of nanopillars is significantly affected by the surface-reaction rate constant for glucose. At a rate constant of 5×10^{-4} m/s, the increase in current due to nanopillars is 1.27-fold, whereas at a rate constant of 5×10^{-7} m/s the increase is 22.26-fold (see Table 6.2).

At a higher surface-reaction rate constant, glucose gets easily oxidized at the top ends of the nanopillars before it can diffuse deep into the space between the nanopillars, while at a lower rate constant, more glucose will be able to diffuse into the deep space between the nanopillars to get oxidized, thus leading to a higher enhanced current response as compared with a flat electrode. These arguments are supported by the fact that a higher glucose concentration is found at the bottom of the spaces between nanopillars in the case with a lower reaction rate constant. The glucose concentration is found to be 0.285 mol/m^3, 0.497 mol/m^3, and 13.583 mol/m^3, respectively, at the bottom of the spaces between nanopillars for cases with the rate constant of 5×10^{-4} m/s, 5×10^{-5} m/s, and 5×10^{-7} m/s. Figure 6.10B shows a contour plot for glucose concentration at a rate constant of 5×10^{-7} m/s, where it is seen that a significant amount of glucose reached to the bottom of the spaces between nanopillars.

These results indicate that the enhanced current response in glucose sensing with functionalized nanostructured electrodes can be attributed to the effective mass transport facilitated by the relatively low reaction rate constant of glucose. Since in most experiments the reaction rate constant cannot be altered easily, it is thus necessary to optimize the dimensions and geometries of the nanopillars (in terms of their diameter, spacing, and height, etc.) in order to accommodate the specific analyte species for achieving the highest possible efficiency in mass transport and electron transfer.

Effect of Electrical Double Layer

The electrical double layer (EDL) structure surrounding the nanometer-scale electrodes will affect their electron transfer and current response (Martynov & Salem 1983; He at al., 2006; Yang & Zhang, 2007). Figure 6.11A shows the voltammograms (normalized to their corresponding limiting current obtained when the effect of EDL is not considered) for electrodes of various sizes when the charge valence (z) of the redox species

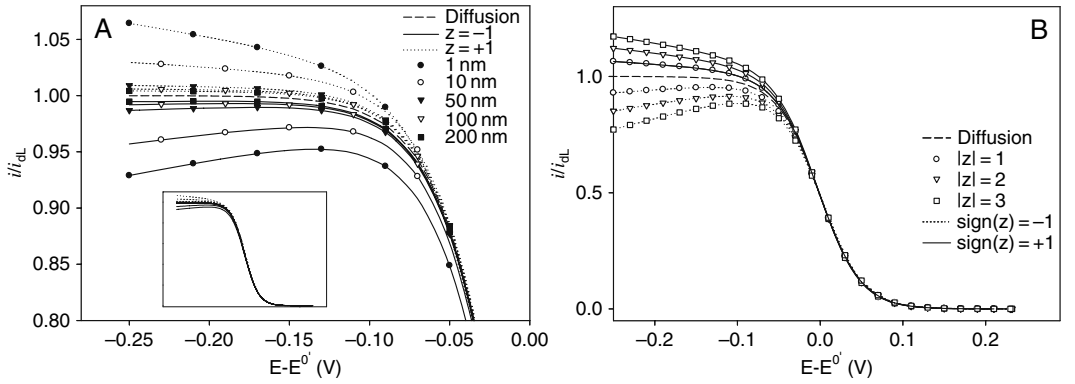

Figure 6.11 (**A**) The reduction end of the simulated voltammograms for single nanometer electrodes of various sizes (from 1 nm to 200 nm). The insert shows the entire voltammograms. (**B**) Simulated voltammograms for an electrode of $r_0 = 1$ nm when the reactant species has different charge valences.

is $z = \pm 1$. Clearly, all the voltammograms exhibit a sigmoidal shape and the curves with $z = 1$ have their normalized limiting current higher than unity while the curves with $z = -1$ have the normalized limiting current lower than unity. This is so because at a negative (reduction) electrode potential the positive-charged redox species would experience attraction and the negative-charged species repulsion, thus causing the current to be either enhanced or suppressed in the respective conditions. In view of the limiting current, the smaller the electrode becomes, the more the normalized limiting current deviates from unity. This EDL-induced current change becomes negligible when the size of the electrode is sufficiently large (>100 nm). In addition to the size effect, the charge valence of the redox species also affects the current response: the higher the charge valence (in its absolute value) is, the more the normalized current deviates from unity (see Figure 6.11B).

Future Perspective

The integration of nanotechnology and biotechnology holds great promises for the realization of autonomous systems for advanced diagnostics and therapies. These systems will perform both biosensing and drug delivery functions. They will make it possible to constantly monitor the biological conditions, process the information in real time, and administer the drug at a desired location, rate, and amount when necessary. These devices can be either micro- or nano-electromechanical systems equipped with biosensors, on-board drugs, and a computer or entirely organic molecular assemblies (e.g., molecular machines) conjugated with specific drug moieties as well as target and environmental-sensitive moieties for site recognition, cell-wall penetration, and drug releasing. These systems will bring benefits of reduced intrusiveness, increased patient comfort, greater fidelity of sensing results, and greater precision for site, amount, and rate controllable drug delivery.

In the coming years, it is anticipated that nanotechnology-based biosensors will continue to evolve and expand their use in many areas of life

sciences, particularly in biomedical diagnosis and drug delivery. For drug delivery applications, these biosensors are expected to possess some ideal features such as high sensitivity, high specificity, fast response and action, low detection limit (such that an early detection of clinically significant proteins and cancer markers is possible), continuous and long-term monitoring capability, carrier of personalized medicine for site-specific and rate-controlled delivery, passively operational (carries no battery, or turns the physiological metabolic events into fuel power), and wirelessly operational (be able to communicate with external monitoring devices wirelessly).

Acknowledgment. Many thanks to my students Y.L. Rao, V. Anandan, X. Yang, R. Cai, X. Tang and postdoctoral fellow S.J. Lee for their contributions to the work discussed here. The financial supports from the National Science Foundation, the University of Georgia Research Foundation, the Faculty of Engineering and the College of Agricultural and Environmental Science at The University of Georgia are acknowledged.

References

Aboubakar, M., Couvreur, P., Pinto-Alphandary, H. & Couritin, B. (2000). Drug Dev Res, 49, 109–117.

Alivisatos P. (2004). The use of nanocrystals in biological detection, Nature Technology, 22, 1, 47–52.

Anandan, A., Rao, Y. L. & Zhang, G. (2005). Nanopillar arrays with superior mechanical strength and optimal spacing for high sensitivity biosensors. Proceedings of Nanotech, 217–220.

Anandan, V., Rao, Y. L. & Zhang, G. (2006). Nanopillar Array Structures for Enhancing Biosensing Performance, Int J Nanomedicine 1(1), 73–79.

Anandan, V., Yang, X., Kim, E., Rao, Y.L. & Zhang, G. (2007). Role of reaction kinetics and mass transport in glucose sensing with nanopillar array electrodes, Journal of Biological Engineering, 1–5.

Aoki, K. (1990). Approximate Models of Interdigitated Array Electrodes for Evaluating Steady-State Currents. J Electroanal Chem, 284, 35–42.

Arrigan, D. W. M. (2004). Nanoelectrodes, nanoelectrode arrays and their applications, Analyst, 129, 1157–1165.

Bard, A. & Faulkner, L. (2001). Electrochemical Methods: Fundamentals and Applications, 2nd Edition, New York: John Wiley and Sons.

Barratt, G., Courraze, G., Couvreur, P. & Dubernet, C. (2002). Polymeric Materials, (Dumitriu, S., Ed). Dekker, New York, 753–782.

Bashir, R. (2004). BioMEMS: state-of-the-art in detection, opportunities and prospects, Adv Drug Deliv Rev 56, 1–22.

Berger, R., Delamarche, E., Lang, H. P., Gerber, C., Gimzewski, J. K., Meyer, E. & Guntherodt, H. J. (1997). Surface stress in the self-assembly of alkanethiols on gold, Science 276, 2021–2023.

Besteman, K., Lee, J. L., Wiertz, F. G. M., Heering, H. A. & Dekker, C. (2003). Nano Lett 3, 727.

Bharathi, S. & Nogami, M. (2001). A glucose biosensor based on electrodeposited biocomposites of gold nanoparticles and glucose oxidase enzyme. Analyst 126, 1919–1922.

Borkholder, D. A., Bao, J., Maluf, N. I., Perl., E. R. & Kovacs, G. T. A. (1997). Microelectrode arrays for stimulation of neural slice preparations, J Neurosci Methods 77(1), 61–66.

Bousse, L. (1996). Whole cell biosensors, Sensors and Actuators, B Chem B34, 1–3, 270–275.

Cai, H.L., Lee, H., Hsing, T. M., & Ming, I. (2006). Label-free protein recognition using an aptamer-based impedance measurement assay, Sens. Actuators, B, Chem 114, 433–437.

Calvo, E. J & Wolosiuk, A. (2004). Supramolecular Architectures of Electrostatic Self-Assembled Glucose Oxidase Enzyme Electrodes, Chem Phys Chem 5, 235–239.

Carrion-Vazquez, M., Oberhauser, A. F., Fowler, S. B., Marszalek, P. E., Broedel, S. E., Clarke, J. & Fernandez, M. J. (1999). Mechanical and chemical unfolding of a single protein: A comparison, Biophysics 96, 3694–3699.

Chen, R. J., Bangsaruntip, S. & Dai, H. (2003). Noncovalent functionalization of carbon nanotubes for highly specific electronic biosensors, PANS 100, 4984–4989.

Chen, R. J., Choi, H. C. & Dai, H. (2004) An investigation of the mechanism of electronic sensing of protein adsorption on carbon nanotube devices, JACS 126, 1563–1568.

Chen, S. & Kucernak, A. (2002). The Voltammetric Response of Nanometer-Sized Carbon Electrodes, J Phys Chem B 106, 9396–9404.

Cherian, S., Gupta, R. K., Mullin, B. C. & Thundat, T. (2003). Detection of heavy metal ions using protein-functionalized microcantilever sensors, Biosens Bioelectron 19, 41–46.

Cia, X., Klauke, N., Glidle, A.,Cobbold, P., Smith, G. L. & Cooper J. M. (2002). Ultra-low-volume, real-time measurements of lactate from the single heart cell using Microsystems technology, Anal Chem 74(4), 908–914.

Cui, Y., Wei, Q., Park, H., & Lieber, C. M. (2001). Nanowire nanosensors for highly sensitive and selective detection of biological and chemical species, Science 293, 1289–1292.

Damage, C., Vonderscher, J., Marbach, P. & Pinget, M. (1997). Pharm Res 18, 949–954.

Davis, Z. J., Abadal, G., Kuhn, O., Hansen, O., Grey, F. & Boisen, A. (2002). Fabrication and characterization of nanoresonating devices for mass detection, J Vac Sci Technol B 18(2), 612–616.

Drummond, T. G., Hill, M. G. & Barton, J. K. (2003). Nature Biotechnology 21, 1192–1199.

D'Souza, S. F. (2001). Biosens Bioelectron 16, 337–353.

Emery, S. R., Haskins, W. E. & Nie, S. (1998). J Am Chem Soc 120, 8009.

Fan, J. G., Dyer, D., Zhang, G. & Zhao, Y. P. (2004). Nanocarpet effect: pattern formation during wetting of vertically aligned nanorod arrays. Nanoletters 4, 2133–2138.

Fernandez-Urrusuno, R., Calvo, P, Remunan-Lopez, C. & Vila-Jato, J. L. (1999). Pharm Res 16, 1576–1581.

Ferrari, M. (2005). Cancer nanotechnology: opportunities and challenges, Nat Rev 5, 161–171.

Fritz, J., Cooper, E. B., Gaudet, S., Sorger, P. K., & Manalis, S. R. (2002). Electronic detection of DNA by its intrinsic molecular charge, PNAS 99, 14142–14146.

Gasparac, R., Taft, B.J., Lapierre-Devlin, M.A., Lazareck, A.D., Xu, J.M. & Kelley S.O. (2004). Ultrasensitive electrocatalytic DNA detection at two and three dimensional nanoelectrodes. J Am Chem Soc 126, 12270–12271.

He, R., Chen, S., Yang, F., & Wu, B. (2006). Dynamic Diffuse Double-Layer Model for the Electrochemistry of Nanometer-Sized Electrodes. J Phys Chem B 110, 3262–3270.

Headrick, J. J., Sepaniak, M. J., Lavrik, N. V. & Datskos, P. G. (2003). Enhancing chemi-mechanical transduction in microcantilever chemical sensing by surface modification, Ultramicroscopy 97, 417–424.

Hintsche, R., Moller, B., Dransfeld, I., Wollenberger, U., Scheller, F. & Hoffmann, B. (1991). Chip biosensors on thin-film metal electrodes, Sens Actuators, B Chem B4 (3–4), 287–291.

Hintsche, R., Kruse, Ch., Uhlig, A., Paeschke, M., Lisec, T., Schnakenberg, U. & Wager, B. (1995). Chemical microsensor systems for medical applications in catheters, Sens Actuators, B Chem B27 (1–3), 471–473.

Jeng, P., Yamaguchi, F., Oi, F. & Matsuo, F. (2001). Glucose Sensing Based Interdigitated Array Microelectrode. Anal Sci 17, 841–846.

Knight, C. G. (1981). Liposomes from physical structure to therapeutic applications, Elsevier, Amsterdam.

Koehne, J., Li, J., Cassel, A. M., Chen, H., Ye, Q., Ng, H. T., Han, J. & Meyyappan, M. (2004). The Fabrication and Electrochemical Characterization of Carbon nanotube Nanoelectrode Arrays. J Mater Chem 14, 676–684.

Kralchevsky, P. A. & Nagayama, K. (2000). Capillary interactions between particles bound to interfaces, liquid films and biomembranes. Adv colloid interface sci 85, 145–192.

Krug, J. T., Wang, G. D., Emory, S. R. & Nie, S. (1999), J Am Chem Soc 121, 9208.

Kubik, T., Bogunia-Kubik, K. & Sugisaka, M. (2005). Nanotechnology on duty in medical applications, Curr Pharm Biotechnol 6, 17–33.

Lau, K. K. S., Bico, J. & Teo, K. B. K. (2003). Superhydrophobic carbon nanotube forests. Nanoletters 3, 1701–1705.

Laureyn, W., Nelis, D., Gerwen, P., Baert, K., Hermans, L., Magnée, R., Pireaux, J., & Maes, G. (2000). Nanoscaled interdigitated titanium electrodes for impedimetric biosensing, Sens. Actuator, B, chem 68, 360–370.

Lee, S. J., Anandan, V. & Zhang, G. (2008). Electrochemical fabrication and evaluation of highly sensitive nanorod-modified electrodes for a biotin/avidin system, Biosensors and Bioelectronics, 1117–1124.

Liu, X. & Tan, W. (1999). A fiber-optic evanescent wave DNA biosensor based on novel molecular beacons, Anal Chem 71, 5054–5059.

Ma, K., Zhou, H., & Zoval, Z. (2006). DNA hybridization detection by label free versus impedance amplifying label with impedance spectroscopy, Sens. Actuators, B, Chem 114, 58–64.

Marrazza, G., Chianella, I. & Mascini, M. (1999). Biosens Bioelectron 14, 43–51.

Martynov, G. A. & Salem, R. R. (1983). Electrical double layer at a metal-dilute electrolyte solution interface, New York: Springer-Verlag Berlin Heidelberg.

Mertens, J., Finota, E., Thundat, T., Fabrea, A., Nadal, M. H., Eyraud, V. & Bourillota, E. (2003). Effects of temperature and pressure on microcantilever resonance response, Ultramicro 97, 119–126.

Mirkin, R. B., Fan, F. R. F. & Bard, A. J. (1990). Evaluation of the Tip Shapes of Nanometer Size Microelectrodes, J Electroanal Chem 328, 47–62.

Moerner, W. E. & Orrit, M. (1999). Illuminating single molecules in condensed matter, Science 283, 1670–1676.

Morris, R. B., Franta, D. J. & White, H. S. (1987). Electrochemistry at Pt Electrodes of Width Approaching Molecular Dimensions. Breakdown of Transport Equations at Very Small Electrodes, J Phys Chem 91, 3559–3564.

Moskovits, M. (2005). Surface-enhanced raman spectroscopy: a brief retrospective, J Raman Spectroscopy 36, 485–496.

Nie, S. & Zare, R. N. (1997). Optical detection of single molecules, Ann Rev Biophys Biomol Struct 26, 567–596.

Niwa, O., Morita, M. & Tabei, H. (1990). Electrochemical Behavior of Reversible Redox Species at Interdigitated Array Electrodes With Different Geometries Consideration of Redox Cycling and Collection Efficiency. Anal Chem 62 (5): 447–452.

Paeschke, M., Wollenberger, U., Kiihler, C., Lisec, T., Schnakenberg, U. & Hintsche, R. (1995). Properties of Interdigital Electrode Arrays With Different Geometries. Analytica Chimica Acta 305, 126–136.

Pancrazio, J. J., Bey, P. P., Cuttino, D. S., Kusel, J. K., Borkholder, D. A., Shaffer, K. M., Kovacs, G. T. A. & Stenger, D. A. (1998). Portable cell-based biosensor system for toxin detection, Sens Actuators, B. Chem 53(3), 179–185.

Phillips, C. & Stone, H. (1997). Theoretical Calculation of Collection Efficiencies for Collector-Generator Microelectrode Systems. J Electroanal Chem 437, 157–165.

Popovich, N. D. & Thorp, H. H. (2002). New Strategies for Electrochemical Nucleic Acid Detection, Interface 11(4), 30–34.

Porter, T. L., Eastman, M. P., Macomber, C., Delinger, W. G., & Zhine, R. (2003). An embedded polymer piezoresistive microcantilever sensor, Ultramicroscopy 97, 365–369.

Powers, M. J., Domansky, K. & Griffith, L. G. (2002). A microfabricated array bioreactor for perfused 3D liver culture, Biotechnol Bioeng 78, 3, 257–269.

Rao, L. R., Anandan, V. & Zhang, G. (2005). FFT Analysis of Pore Pattern in Anodized Alumina Formed at Various Conditions, Journal of Nanoscience and Nanotechnology, Vol. 2, No. 12, 2070–2075.

Rao, L. R. & Zhang, G. (2006). Enhancing the Sensitivity of SAW Sensors with Nanostructures, Current Nanoscience 2(4), 311–318.

Ratner, B. D., Hoffman, A. S., Schoen, F. J. & Lemons, J. E. (2004). Biomaterials Science, 2nd Edition, Academic Press.

Reining-Mack, A., Thielecke, H. & Robitzki, A. A. (2002). Trends Biotechol 20, 56–61.

Rider, T. H., Petrovick, M. S. & Hollis, M. A. (2003). A B-cell based sensor for rapid identification of pathogens, Science 301, 213–215.

Sawant, R. M., Hurly, J. P., Salmaso, S. & Torchilin, V. P. (2006). "Smart" drug delivery systems: double-targeted pH-responsive pharmaceutical nanocarriers, Bioconjugate Chem 17, 943–949.

Seibold, J. D., Scott, E. R. & White, H. S. (1989). Diffusion Transport to Nanoscopic Band Electrodes, J Electroanal Chem 264, 281–289.

Sepaniak, M., Datskos, P., Lavrik, N. & Tipple, C. (2002). Microcantilever Transducers: A New Approach in Sensor Technology, Anal Chem 1, 568A–575A.

Sosnowski, R. G., Tu, E., Butler, W. F., O'Connell, J. P. & Heller, M. J. (1997). Rapid Determination of Single Base Mismatch in DNA Hybrids by Direct Electrical Field Control. PNAS 94, 1119–1123.

Stenger, D. A., Gross, G. W., Keefer, E. W., Shaffer, K. M., Andreadis, J. D., Ma, W. & Pancrazio, J. J. (2001). Detection of physiologically active compounds using cell-based biosensors, Trends Biotech 19(8), 304–309.

Stoney, G. G. (1909). Proc R Soc London, serial A, 82, 172–277.

Strutwolf, J. & Willams, D. (2005). Electrochemical Sensor Design Using Coplanar and Elevated Interdigitated Array Electrodes. A computational Study. Electroanalysis 17 (2): 169–177.

Sun, E. Y., Josephson, L., Kelly, K. A. & Weissleder, R. (2006). Development of nanoparticle libraries for biosensing, Bioconjugate Chem 17, 109–113.

Tang, X. J, Zhang, G. & Zhao, Y. P. (2006). Electrochemical characterization of silver nanorod electrodes prepared by oblique angle deposition, Nanotechnology 17, 4439–4444.

Thielecke, H., Mack, A. & Robizki, A. (2001). Anal Bioanal Chem 369, 23–29.

Thundat, T., Wachter, E. A., Sharp, S.L. & Warmack, R. J. (1995). Appl Phys Let 66, 1695–1697.
Umek, R., Lin, M., Vielmetter, S. W. & Chen, D. H. (2001). Chem Mol Diagn 3, 74–84.
Vo-Dinh, T. & Cullum, B. (2000). Biosensors and biochips: advances in biological and medical diagnostics, J Anal Chem 366, 540–551.
Wang, J. & Mustafa, M. (2004). Carbon nanotube screen-printed electrochemical sensors. Analyst 129, 1–2.
Winkler, K. (1995). The kinetics of electron transfer in Fe (CN)6 4–/3– redox system on platinum standard-size and ultramicroelectrodes, J Electroanal Chem 388, 151–159.
Wickline, S. A. & Lanza, G. M. (2003). Nanotechnology for molecular imaging and target therapy, Circulation 107,1092–1095.
Wu, G. H., Datar, R. H., Hansen, K. M., Thundat, T., Cote, R. J. & Majumdar, A. (2001). Bioassay of prostate-specific antigen (PSA) using microcantilevers, Nat Biotechnol 19, 856–860.
Yang, L., Li, Y., & Erf, G. F. (2004). Interdigitated Array Microelectrode-Based Electrochemical Impedance Immunosensor for Detection of Escherichia coli O157:H7, Anal. Chem 76, 1107–1113.
Yang, X. & Zhang, G. (2005). Diffusion-Controlled Diffusion-Controlled Redox Cycling at Nanoscale Interdigitated Electrodes, Proceedings of the COMSOL Multiphysics Conference, 285–290.
Yang, X. & Zhang, G. (2006) Effect of Electron Transfer Rate on the Electrochemical Process of Interdigitated Electrodes, Proceedings of the COMSOL Conference, 233–238.
Yang, X. & Zhang, G. (2007) The Voltammetric Performance of Interdigitated Electrodes with Different Electron-Transfer-Rate Constants, Sens. Actuators, B 126, 624–631.
Yemini, M., Reches, M. & Rishpon, J. (2005). Novel electrochemical biosensing platform using self assembled peptide nanotube. Nanoletters 5, 183–186.
Zhang, G. & Gilbert, J. L, (2004). A New Method for Real-Time and In-Situ Characterization of the Mechanical and Material Properties of Biological Tissue Constructs, Tissue Engineered Medical Products (TEMPs), ASTM STP 1452, Picciolo and Schutte Eds., 120–133.
Zhang, G. (2005). Evaluating the Viscoelastic Properties of Biological Tissues in a New Way. Journal of Musculoskelet Neuronal Interact 5(1), 85–90.
Zhu, H. & Snyder, M. (2003). Curr Opin Chem Biol 7, 55–63.

Part II

Biopharmaceutical, Physiological, and Clinical Considerations for Nanotechnology in Drug Delivery

7

Nanomaterials and Biocompatibility: BioMEMS and Dendrimers

Sean T. Zuckerman and Weiyuan John Kao

Introduction

"Biocompatibility" is a term often used by researchers and laypersons. The website for the National Institutes of Health uses the word biocompatibility more than 300 times (www.nih.gov); yet a clear definition of biocompatibility is difficult to locate. What criteria define biocompatibility? Scientists have struggled to define the word biomaterial. Therefore it follows there has been much difficulty quantifying biocompatibility. The European Society for Biomaterials called a consensus conference in 1986 to define basic terms such as biomaterial, host response, and biocompatibility. The attending members agreed that biocompatibility is, "the ability of a material to perform with an appropriate host response in a specific application." The host response was subsequently defined as, "the reaction of a living system to the presence of a material" (Williams, 1987). This definition of biocompatibility begs the question, "What is an 'appropriate' host response?" To determine what is an "appropriate" host response requires measurement of a biological phenomenon. Both the extent and the duration of the host response are critical factors determining the appropriateness of the body's response. The difficulty therefore lies in quantifying a graded response. In vitro tests enable more comprehensive and invasive analysis but are limited in scope to simplified models. In vivo testing, on the other hand, offers more physiologically relevant data but is not always feasible or ethical to perform. In addition, in vivo testing is complicated by complex interactions between multiple systems. Therefore a combination of in vitro and in vivo testing must be performed to draw relevant and accurate conclusions.

In order to provide uniformity and guidance, the International Organization for Standardization (ISO) (www.iso.org, 2003) and the American Society for Testing Materials Standards have constructed guidelines to aid industry and academic researchers. Table 7.1 shows the breakdown of ISO 10993. Part 1 outlines the basis for evaluating medical devices including classifying the device based on the type and length of contact with the host. Part 1 then outlines the appropriate tests necessary to analyze interactions

M.M. de Villiers et al. (eds.), *Nanotechnology in Drug Delivery*, DOI: 10.1007/978-0-387-77667-5_7,

Table 7.1. International organization for standardization 10993 biological evaluation of medical devices (ISO, 2006).

Part	Title
1	Evaluation and testing within a risk management system
2	Animal welfare requirements
3	Tests for genotoxicity, carcinogenicity, and reproductive toxicity
4	Selection of tests for interactions with blood
5	Tests for in vitro cytotoxicity
6	Tests for local effects after implantation
7	Ethylene oxide sterilization residuals
9	Framework for identification and quantification of potential degradation products
10	Tests for irritation and delayed-type hypersensitivity
11	Tests for systemic toxicity
12	Sample preparation and reference materials
13	Identification and quantification of degradation products from polymeric medical devices
14	Identification and quantification of degradation products from ceramics
15	Identification and quantification of degradation products from metals and alloys
16	Toxicokinetic study design for degradation products and leachables
17	Establishment of allowable limits for leachable substances
18	Chemical characterization of materials
19	Physico-chemical, morphological, and topographical characterization of materials
20	Priniciples and methods for immunotoxicology testing of medical devices

with the body based on the class of material. The remaining 18 subsections to ISO 10993 cover a range of tests to determine blood compatibility (ISO 10993-4), in vitro cytotoxicity (ISO 10993-5), local (ISO 10993-6) and systemic (ISO 10993-11) effects post-implantation, identification of degradation products (ISO 10993-13, -14, and -15), as well as material characterization (ISO 10993-18 and -19). The American Society for Testing Materials Standards has similar protocols outlined under F748 Standard practice for selecting generic biological test methods for materials and devices. This F748 protocol also addresses pyrogen testing as well as batch testing for production lots (American Society for Testing Materials Standards, 2004). The Food and Drug Administration issued a blue book memorandum (G95-1) in May of 1995 based on the ISO 10993 Biological Evaluation of Medical Devices document governing approval of medical devices for commercial sale in the United States of America (United States Food and Drug Administration, 1995). This blue book document adopted the material categories from ISO 10993 and instituted additional testing requirements. The American Society for Testing Materials Standards F748, ISO 10993, and G95-1 therefore establish the minimum body of knowledge necessary for commercialization of medical devices.

The two chapters on "Biocompatibility of Nanotechnology" will focus on the biocompatibility of current and emerging nanomaterials such as bioMEMS, dendrimers, carbon nantotubes, and fullerenes from a

structure–function standpoint. Liposomes have been researched since the late 1970 s and their toxicity and compatibility are relatively well characterized. Hence liposomes will not be discussed. Several reviews have been published on the matter (Zhang, Liu & Huang, 2005; Vermette & Meagher, 2003; Lian & Ho, 2001; Woodle & Scaria, 2001; Kaneda, 2000; Nagayasu, Uchiyama, & Kiwada, 1999). We will present trends and data from current primary literature correlating the structure of a material with its observed effect on the body ranging from cytotoxicity to hypersensitivity. In addition, we will highlight the differences in the data obtained ranging from different material preparation methods to different animal models and how these upstream choices influence the comparison of conclusions drawn regarding each type of material. The subjective nature of assessing the extent of a biological phenomenon such as the host response to a given material for a species should become apparent.

Known Structure–Function Relationships

BioMEMS and Nanobiotechnology

The field of nanobiotechnology has been growing rapidly over the past decade. Advances in micro- and nanofabrication technologies have spurred much of the growth (Blattler, Huwiler, Ochsner, Stadler, Solak, Voros, & Grandin, 2006). Nanobiotechnology involves materials and molecules less than 100 nm in size while the microelectro-mechanical systems (MEMS) are designed to function on the micrometer scale. However, the two have become tightly entwined recently as research into biosensors and drug delivery vehicles increases (Gourley, 2005). Biological MEMS (bioMEMS) are designed to interact with a biological environment either as a sensor or directly through drug delivery or electrical stimulation (Meyer, 2002). The recent advances in nanofabrication technology have enabled increased potential for diagnostic capabilities through the ability to pattern biological molecules such as enzymes onto a given substrate. BioMEMS interface with nanobiotechnology by providing the substrate and microscale architecture to direct fluid to the biological molecules as shown in Figure 7.1. In addition, bioMEMS provide the ability to take mechanical or electrical action based on the output from the nanoscale analysis. This coupling has led to the development of glucose sensors using enzymatic detection of glucose levels that could be followed by insulin release stimulated by the bioMEMS (Figure 7.1) (Zimmerman, Fienbork, Flounders, & Liepmann, 2004).

Implantable microscale sensors have been identified as a market estimated to surpass $10 billion USD by 2008 (Gourley, 2005). BioMEMS are ideal candidates for these implantable sensors because they couple the ability to analyze complex solutions such as those found in vivo with actuating the appropriate response in an implantable format. In addition, nanoarrays of biological molecules such as enzymes on bioMEMS could perform diagnostic analysis in vivo aiding diagnosis of the patient's condition by medical staff. BioMEMS are also capable of recording force transduction in heart muscle (Lin, Pister, & Roos, 2000) and integrating

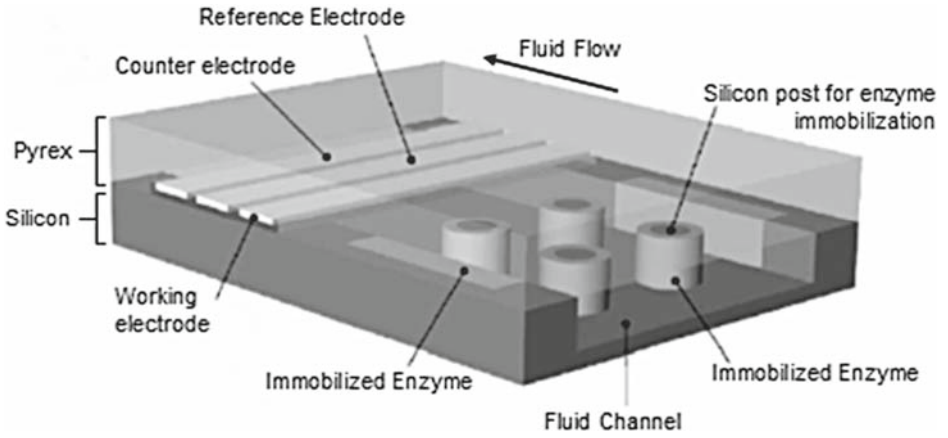

Figure 7.1 An example of a bioMEMS-based sensor. Adapted from Zimmerman et al. (2004).

neurological functions such as retinal implants to restore lost vision (Meyer, 2002). The ability to integrate molecular motors into bioMEMS also exists (Hiratsuka, Miyata, Tada, & Uyeda, 2006). Microfluidic bioMEMS offer researchers the ability to carefully manipulate cell conditions at the level of individual cells (Chin, Taupin, Sanga, Scheel, Gage, & Bhatia, 2004). Researchers have constructed microfluidic devices to control biochemical signals allowing a complex matrix of conditions to be analyzed on one device simultaneously (Ziaie, Baldi, Lei, Gu, & Siegel, 2004). This multitude of conditions enables researchers to determine the gradient effect of different growth factors or cytokines upon stem cell differentiation ex vivo, for instance.

The tremendous potential for bioMEMS to address many problems currently plaguing researchers has led the field to focus on functionality and manufacturing capabilities. However, an implantable device must be tolerated and integrated into the host for long-term efficacy. Little research has been done investigating the biocompatibility of bioMEMS. Even less research has been performed to determine the effect that sterilization and packaging have upon biocompatibility. Madou (1997) addressed the need for more attention to compatibility issues nearly 10 years ago. "Biocompatibility is the single most complex factor facing in vivo sensor development and it needs addressing up front in the sensor design." This information vacuum can be partly explained by previous medical applications of MEMS. Many devices such as pacemakers are entirely encapsulated within a sealed vessel such as a titanium (Ti) shell. Therefore only the compatibility of the Ti shell and the exposed lead insulator are required for implantation (Kotzar, Freas, Abel, Fleischman, Roy, Zorman, Moran, & Melzak, 2002). In the past researchers have relied on previous biocompatibility testing of similar materials. The difficulty in relying on these previous studies is that many of them investigated the compatibility of a particular material for applications experiencing different mechanical and cellular environments. For instance, data from silicon carbide (SiC)-coated stents (Amon, Bolz, & Schaldach, 1996) or orthopedic joints (Nordsletten, Hogasen, Konttinen, Santavirta, Aspenberg, &

Aasen, 1996) has been used to gauge the compatibility of SiC for bioMEMS applications. The ISO and FDA have standards for sterilization of medical devices for implantation (ISO 10993 and G95-1). Many of the previous studies either have not conformed to established sterilization procedures or did not specify how sterilization was achieved. The ISO 10993 guidelines represent the minimum knowledge needed to commercialize a given device or material. In many cases the tests recommended by ISO 10993 must be expanded in scope or depth or supplemented with additional testing to obtain a full characterization of compatibility. BioMEMS and nanobiotechnology are difficult to isolate and will thus be discussed herein simultaneously. The survey presented here focuses mainly on bioMEMS compatibility but applies to bioMEMS with nanopatterning and immobilized biological molecules as well.

Non-ISO 10993 Biocompatibility Testing

Silicon-Based Materials

Silicon is used extensively in integrated circuits and has been adopted as a substrate for many MEMS because the processing is well characterized and enables electrical conduction (Stoldt & Bright, 2006; Zhu, Zhang, & Zhu, 2005). Previously nanocrystals of silicon have been shown in a number of studies to exhibit no significant cytotoxicity (Bayliss & Buckberry, 1999; Bayliss, Heald, Fletcher, & Buckberry, 1999; Bayliss, Harris, Buckberry, & Rousseau, 1997; Bayliss, Buckberry, Harris, & Tobin, 2000). While Bayliss and Buckberry's research found no significant toxicity, Kubo and co-workers (1997) observed nodule formation by periodontal ligament fibroblasts in response to what they hypothesized was silicon leaching from glass. Ten nanometer pores were found to be the optimal substrate for B50 neuronal growth compared to bulk polished silicon or plasma-enhanced chemical vapor deposition. However, Chinese hamster ovary cells demonstrated affinity for the plasma-enhanced chemical vapor-deposited silicon over the polished or nanoporous silicon surfaces showing a cell-type-dependent relationship between cell viability and surface architecture (Bayliss & Buckberry 1999). Bayliss et al. (2000) also investigated sterilization procedures and determined that autoclaving was optimal.

Research on another silicon-based material, silicon carbide (SiC), found that the α form was marginally more cytotoxic than the β form at doses above 0.1 mg/ml to macrophages, osteoblast-like cells, and fibroblasts (Allen, Butter, Chandra, Lettington, & Rushton, 1995). Radiofrequency sputtering of SiC did not appear cytotoxic; however, attachment of fibroblasts and osteoblasts was lower than desired and proliferation of osteoblasts was inhibited (Naji & Harmand, 1991). Amon et al. (1996) followed ISO 10993-5 guidelines for cytotoxicity experiments testing L929 murine fibroblasts' response to SiC-coated tantalum stents. The SiC coating showed no cytotoxicity or mutagenicity in these experiments, but the applicability of SiC-coated stents to bioMEMS is limited. Stents need to withstand high shear stress induced from fluid flow and are in intimate contact with blood, which some bioMEMS may not experience, in vivo.

In addition to SiC, silicon nitride (Si_3N_4) nanopowder has also been investigated for compatibility in vitro and in vivo. Rabbit marrow stromal

cells were initially adhered to the upper surface of Si_3N_4 disks but spread to only the edges after 4 weeks (Wan, Williams, Doherty, & Williams,1994). Marrow stromal cells cultured with Si_3N_4 and implanted for 5 weeks showed differentiation around the Si_3N_4 but not on the surface or within the pores. Interestingly, porous bone was observed to integrate with the Si_3N_4 when the Si_3N_4 was directly implanted into the femoral marrow cavity. In other in vitro testing, the human osteosarcoma MG-63 cell line showed no decrease in DNA synthesis after incubation with 1, 10, or 100 μg/ml Si_3N_4 nanoparticles for 48 h compared to the polystyrene-negative control (Sohrabi, Holland, Kue, Nagle, Hungerford, & Frondoza, 2000). Reaction-bonded silicon nitride disks showed an increase in the pro-inflammatory cytokines interleukin 1β or tumor necrosis factor alpha and sintered-reaction-bonded silicon nitride showed no change in these cytokines compared to the negative control surface. Kue and colleagues (1999) came to a similar conclusion that the sintering process resulted in little change in MG-63 cell proliferation and metabolism. These experiments revealed that material processing can have a significant effect upon downstream cellular responses even though the mechanistic impact of sintering on MG-63 cells was not elucidated.

In addition to cell adhesion, the hemocompatibility is a critical factor determining the efficacy of blood-contacting devices. The hemocompatibility of various materials commonly used in MEMS was measured as a function of platelet adhesion (Weisenberg & Mooradian, 2002). Platelets were isolated from human donors and cultured statically for 5 min at which time the platelets were imaged and counted. Si, Si_3N_4, low-stress silicon nitride ($S_{1.0}N_{1.1}$), and SU-8 photoresist all exhibited higher platelet adhesion than the Chronoflex AR/LT polycarbonate (PC) -based polyurethane control. These materials are all common bioMEMS components and therefore relevant. Platelet adhesion to SiO_2 and thin parylene C films were not significantly different from the control surface. The PC-based polyurethane was chosen based on previous literature demonstrating its hemocompatibility (Elam & Nygren, 1992; Chen, Zhang, Kodama, & Nakaya, 1999); however, the data based on spreading and circularity obtained indicated the choice of reference material may not be appropriate (Weisenberg & Mooradian, 2002).

Many implantable bioMEMS will have intimate contact with blood such as biosensors for glucose. The hemocompatibility is critical to the efficacy of such blood-contacting devices as well as cellular compatibility since many types of cells circulate in the blood. Thus various SiN_x:H films created by plasma-enhanced chemical vapor deposition were tested for hemocompatibility with platelets (Wan, Yang, Shi, Wong, Zhou, Huang, & Chu, 2005). The number of N atoms was varied to change the degree of hydrophilicity. The samples were incubated with human platelets for 2 h and the results compared against low-temperature isotropic pyrolytic carbon, which is the most commonly used material in commercialized medical devices contacting blood (Wan et al., 2005). Platelets were chosen based on their role in coagulation and thrombus formation, which can have serious implications if a blood-contacting device tips the homeostatic equilibrium in the blood. Wan et al. (2005) found that platelets adhered less to the three forms of SiN_x:H than to the low-temperature

isotropic pyrolytic carbon. Scanning electron microscopy analysis showed less pseudopodia and spreading, which has been shown to be indicative of thrombus formation (Gibbins, 2004). Wan et al. (2005) hypothesized that the hydrophilic nature of the surface induced less conformational rearrangement in the proteins adsorbed to the surface resulting in lower protein adhesion and less platelet activation. Surprisingly no hemolysis of red blood cells was investigated. Little other hemocompatibility data is published for any material used in MEMS devices thus the applicability of this data is rather limited. In addition, most devices considered for implant will have much more complex architecture than simple plasma-enhanced chemical vapor deposition coatings limiting these findings further. More extensive characterization of commonly used MEMS materials following ISO 10993 needs to be published to help guide researchers in material selection during the design phase.

Implantation in sub-cutaneous cages was used to determine the inflammatory response of Sprague–Dawley rats to silicon-based microreservoir MEMS (Voskerician, Shive, Shawgo, von Recum, Anderson, Cima, & Langer, 2003). The components of the microreservoir drug delivery MEMS tested were: Si, Si_3N_4, SiO_2, gold, and Su-8. The leukocyte concentration in the exudate was determined as was the number of adherent macrophages and foreign body giant cells, which was used as a determinant of protein adsorption. With the exception of Si, all of the exudate from materials tested at 7 and 14 days showed similar leukocyte concentrations as the empty cage implant indicating minimal acute and chronic inflammation resulting from the material residing within the cage. The leukocyte concentration in the Si-containing cage tapered off after 21 days but was still higher than the negative control levels. SU-8 was found to exhibit delamination after 21 days; SiO_2 and Si_3N_4 showed similar biofouling levels inferred from macrophage and foreign body giant cell numbers leaving the choice for dielectric layer to be determined by mechanical demands and/or fabrication limitations (Voskerician et al., 2003). This data is an important step to characterizing the in vivo response to bio-MEMS components.

Nanostructured Titanium (Ti)

Nanostructured TiO_2 has been investigated for its role as a cellular adhesive substrate. Mouse fibroblasts showed enhanced adhesion to porous TiO_2 with 50–200 nm diameter pores that were 25–75 nm deep (Zuruzi, Butler, MacDonald, & Safinya, 2006). The fibroblasts adhered to the porous TiO_2 more rapidly than SiO_2 or Si_3N_4 up to 18 hr; after 24 h adhesion was not significantly different for the three materials. Scanning electron microscopy analysis of cell morphology revealed more spherical cells on SiO_2 than nanoporous TiO_2 indicating less adhesion and less interaction. Interestingly, the fibroblasts adhered to and adopted the shape of square micropatterned nanoporous TiO_2 structures 10 and 20 μm long. However, Webster and co-workers (2000) found that fibroblasts adhered less to nanoporous alumina (Al_2O_3), titania (TiO_2), and hydroxyapatite ($Ca_5(PO_4)_3(OH)$) than the traditional ceramics after 4 h. Endothelial cells exhibited similar behavior to fibroblasts. Osteoblasts conversely showed more adhesion to these nanoporous ceramics than the

conventional forms. This increased osteoblast adhesion was attributed to increased vitronectin adsorption on the nanoporous ceramics (Webster et al., 2000).

Surface Modification of Various Substrates:* In Vitro *Assessment

As Voskerician et al. (2003) noted biofouling is an important phenomenon for all implanted devices including bioMEMS. Cells interact with implanted materials through a layer of adsorbed proteins. Many researchers believe that eliminating protein adsorption will eliminate the current problems of fibrous capsule formation, sustained chronic inflammation, and material degradation. Surface modification is one popular technique to decrease protein adsorption and thus biofouling. In particular the use of polyethylene glycol (PEG) (Figure 7.2) has been adopted to minimize or direct protein adsorption depending upon the application. For bioMEMS applications the PEG film thickness varies between 2 and 20 nm and exhibits a hydrophilic character resulting from the PEG-modified surface and not the underlying substrate (Richards Grayson, Shawgo, Johnson, Flynn, Li, Cima, & Langer, 2004). Sharma and colleagues (2002) modified silicon surfaces with PEG using two different methods: solution phase PEG–silane coupling or vapor deposition of polyethylene oxide. The PEG–silane solution chemistry allowed for the addition of 2 nm of PEG. The low nanometer thickness of the PEG film is crucial for efficacy of biosensor MEMS that require diffusion to and from the material. Both vapor deposition and solution coupling yielded similar decreases in fibrinogen and bovine serum albumin adsorption, which represent a range of protein molecular weights that many bioMEMS will encounter in vivo. Lee, Bhushan, & Hansford (2005) found similar results using vapor deposition to deposit two fluoropolymers or fluorosilane on silicon wafers. This method yielded film thicknesses <10 nm for all three polymers with fluorosilane exhibiting characteristics of a monolayer. Thus vapor deposition is an attractive surface modification technique for multiple polymers allowing researchers to tailor hydrophobicity/hydrophilicity with surface thickness and roughness in order to optimize the coating for the various nanoscale architectures of the device such as fluid channels or micro/nanoreservoirs. Hanein, Pan, Ratner, Denton, & Bohringer (2001) achieved similar results using photolithography to produce PEG films. PEG modification via photolithography or vapor deposition allows for precise control of PEG modification and thus preserves the electrical conductivity compared to the solution phase chemistry, which offers no control over surface modification patterns. Thus solution phase PEG modification could modify electrical leads or plug channels within the device reducing or eliminating its function. Therefore as the complexity of bioMEMS increases, the use of solution phase surface modification will likely decrease significantly. PEG

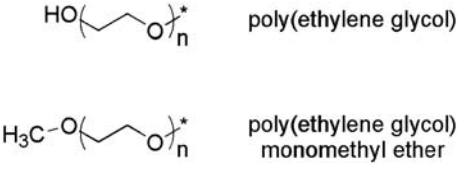

Figure 7.2 Poly(ethylene glycol) and monomethyl ether poly(ethylene glycol) are used for modification of various surfaces to minimize protein adsorption.

surface modification was used to create hydrophilic channels in a microfluidic network based on Si, gold, or polydimethylsiloxane (Papra, Bernard, Juncker, Larsen, Michel, & Delamarche, 2001). The PEG chains prevent protein adsorption to the fluidic channels while creating a hydrophilic environment that allows proteins to diffuse along the microfluidic channel and deposit into patterned microreservoirs. Si–PEG–Si was identified as the best choice for modification of polydimethylsiloxane leading to hydrophilic stability for up to 3 weeks (Papra et al., 2001). Gold MEMS surfaces are very flexible allowing researchers to selectively pattern one alkanethiol via microcontact printing and masking the remaining gold surface with a second alkanethiol in solution. Thus complex patterns can be created leading to selective protein adsorption or the creation of complex fluidic channels leading to microreservoirs.

Chemical vapor deposition of various forms of poly(*p*-xylenes) has also been shown to successfully modify enclosed, complex microchannels on silicon using polydimethylsiloxane molds (Chen, Elkasabi, & Lahann, 2005). The channels were open on both ends and ranged from 1600 μm for a straight channel to 2800 μm for an S-curved channel. This meandering channel formed a series of S-curves with an aspect ratio of 37; the straight channel had an aspect ratio of 21. The film thickness varied by xylene isoform deposited but was homogeneous throughout the film for each polymer, which is difficult to achieve through other surface modification methodologies for materials with high aspect ratios. Xylene also retained its functionality after chemical vapor deposition as evidenced by biotin conjugation and visualization via rhodamine (Chen et al., 2005). Thus chemical vapor deposition has shown uniform modification of simple and complex surfaces providing researchers a powerful tool to modify complex micro and nanoscale patterning on bioMEMS.

In addition to PEG, other polymers have been investigated for their non-fouling properties and cytotoxicity. Silica gels were investigated as a potential surface coating to prevent the undesired adsorption of proteins to glucose sensors (Kros, Gerritsen, Sprakel, Sommerdijk, Jansen, & Nolte, 2001). Tetraethylorthosilicate was mixed with PEG, heparin, dextran sulfate, Nafion, or polystyrene sulfonate to form sol gel, which is a soluble colloidal suspension that can be gelled into a workable solid. While the sol gel-based coatings showed similar hydrophilicity, human dermal fibroblasts adhered to and proliferated on sol gel, sol gel-heparin, sol gel-Nafion, and sol gel-PEG at the same level as the Thermanox coverslip used as a negative control (Kros et al., 2001). The level of fibroblast adhesion and proliferation on sol gel-polystyrene sulfonate and sol gel-dextran sulfate was much lower than the reference surface. However, the morphology of the fibroblasts on the sol gel-polystyrene sulfonate and sol gel-dextran sulfate surfaces was normal indicating that cell adhesion was lower rather than surface-mediated toxicity. Because both polystyrene sulfonate and dextran sulfate have a high number of sulfate groups available for cellular interactions, Kros et al. (2001) hypothesized that the sulfate groups mediate fibroblast adhesion and proliferation. In vitro testing of the coated glucose sensor also revealed that the sol gel-coated glucose sensors retained more activity than uncoated sensors in complete serum while maintaining the same level of activity in an albumin solution. Thus

various additives to silica gel are successful in mediating adsorption of serum proteins while retaining non-toxic properties toward human dermal fibroblasts. This coating could therefore be used to help increase the compatibility and function of an implanted bioMEMS into the host tissue while retaining activity.

Photolithography can also be used to create self-assembling monolayers on the MEMS surface maintaining any surface-dependent functionality (Richards Grayson et al., 2004). Monolayers have been created from oligomers of ethylene oxide and PEG terminated with various end groups such as alkoxysilyl or trichlorosilyl. Self-assembled monolayers enable researchers to finely control both thickness and density of the surface modification. Tokachichu and Bhushan (2006) modified polymethylmethacrylate and polydimethylsiloxane with a perfluorodecyltriethoxysilane self-assembling monolayer. Protein adsorption to both surfaces was not significantly different as measured by atomic force microscopy using a fetal bovine serum-coated needle in phosphate-buffered saline solution or in air. This low level of protein adhesion could allow flow through nanoscale channels on microfluidic devices. Monomethyl ether PEG (mPEG) (Figure 7.2) modified silicon surfaces exhibited decreased fibrinogen and immunoglobulin G adsorption compared to non-modified clean silicon (Lan, Veiseh, & Zhang, 2005). Murine fibroblasts and macrophages on the mPEG-modified Si surfaces demonstrated lower adhesion correlating to lower protein adsorption. Fibroblasts showed similar morphology on both clean Si and mPEG-modified Si while macrophages exhibited a more round morphology on the mPEG-modified Si surface. When gold ridges or squares were patterned on the surface more protein adhered to the patterned gold areas of the surface than the mPEG-modified areas. Because little to no protein adsorbed onto the mPEG-modified Si the fibrinogen and immunoglobulin G showed concentrated adsorption on the gold patterns. Finally, cells were cultured on gold-patterned Si surfaces where the non-patterned portions of the Si were modified with mPEG to resist protein adsorption (Lan et al., 2005). Fibronectin was allowed to adsorb on to the modified Si surface followed by culture with fibroblasts or macrophages for 24 h. Both the macrophages and fibroblasts adhered only to the gold patterns and aligned with the topographical features of squares or ridges. Thus mPEG was shown to be an effective surface modification to direct protein adsorption and consequently cell adhesion onto Si surfaces patterned with gold. Self-assembled monolayers on bioMEMS have also been successfully created from phospholipid-based Langmuir–Blodgett films (Kim, Kim, & Byun, 2001). Therefore researchers can use various methods such as solution phase chemistry, lithography, or chemical vapor deposition to selectively modify bioMEMS surfaces to enhance functionality and efficacy.

Surface Modification of Various Substrates: In Vivo *Assessment*

A limited number of in vivo studies have been performed with surface-modified bioMEMS sensors. Ishikawa and colleagues (1998) found that glucose sensors with PEG-modified sensor tips functioned for 3 days in 20 patients with a sensitivity range of 2–28 mmol/L and a 10 min response time, which compared favorably to other sensors that reported response

times of 20–45 min. Another group reported glucose sensing activity 14 days post-implantation using a needle sensor modified with the phospholipid-based copolymer 2-methacryloyloxyethylphosphorylcholine and *n*-butylmethacrylate (Ishihara, Nakabayashi, Nishida, Sakakida, & Shichiri, 1994). The phospholipid nature of this surface modification is theorized to elicit similar interactions with proteins as host cells in vivo (Wisniewski & Reichert, 2000). This type of phospholipid polymeric surface modification has many difficulties to commercialization. Most importantly the coating can limit diffusion to the sensor immediately decreasing its efficacy. In addition, delamination from the sensor due to poor adhesion or mechanical stress is difficult to quantify (Wisniewski & Reichert, 2000). These polymeric surface modifications may also be detrimental to any biological molecules such as enzymes contained in the sensor. Various types of fluid flow systems have been developed to prevent protein adsorption and hence cell adhesion but will not be addressed here since these systems require constant perfusion and do not directly address the issue of biocompatibility (Wisniewski & Reichert, 2000). Other surface treatments such as the perfluorosulfonic acid polymer known as Nafion have been investigated based on their ease of application. Nafion can be dip coated onto sensors; however, this method does not allow for control over the surface pattern meaning microfluidic channels and other reservoir-like features can become clogged. Although Nafion did improve the immunogenicity and increased sensor functioning to 10 days post-implantation (Moussy, Harrison, & Rajotte, 1994). The in vivo trials conducted thus far have focused more on sustaining sensor activity than on solving long-term implantation issues. Researchers have used various surface coatings to resist protein adsorption and cell adhesion. To varying degrees the studies have worked but have not correlated directly to the compatibility between implanted materials and the host.

ISO 10993 Biocompatibility Testing

While the previous studies made relevant observations and important conclusions regarding material compatibility, few published studies adhered to the guidelines outlined by ISO 10993 for characterization of a biomaterial. One of the first papers to apply the ISO standard tests also investigated sterilization effects (Kotzar et al., 2002). The materials were chosen to cover a wide array of materials used in bioMEMS including Si-based materials, Ti, and SU-8 photoresist epoxy. The negative surface control was polyethylene per the United States Pharmacopeia's standard for implantation experiments. Both autoclaving and γ-irradiation were used to sterilize materials. The materials were characterized under the guidelines of ISO 10993-14 including extractables, infrared analysis, and mechanical testing. Scanning electron microscopy was also performed pre- and post-sterilization to determine any sterilization-dependent surface changes in the material. The scanning electron microscopy micrographs revealed no apparent damage to the material surface. However, Kotzar did note that the SU-8 surface was difficult to image because the surface is very smooth. The material extracts were classified as less than Grade 2 toward the L929 murine fibroblast line meaning the material can officially be

classified as "mildly reactive." This label satisfies the ISO 10993 criteria that the material extracts be less than a Grade 2 response and the positive control be a Grade 3 or 4. To further verify their in vitro findings, Kotzar et al. (2002) implanted these materials into rabbits for 1 or 12 weeks analyzing the results via histological staining. The fibrous capsule observed around the test materials was nearly "indistinguishable from the [polyethylene] negative controls." The in vivo data was important because the ASTM standard F67 outlines standards for commonly used Ti alloy processing methods for implantable Ti but does not cover Ti sputtering. The sputtered Ti surfaces tested by Kotzar et al. (2002) exhibited similar results to those previously obtained for sputtered Ti (Johansson, Hansson, & Albrektsson, 1990). Similarly, no established standards existed for SiC or Si_3N_4. Thus the preliminary results based on ISO 10993 testing by Kotzar et al. (2002) showed that SiC and Si_3N_4 prepared via standard MEMS processing techniques elicit no significant biological response. This conclusion is among the first direct data using established guidelines that supports the compatibility of these materials in MEMS applications.

Summary

An increased demand for implantable bioMEMS has surfaced in the past 5–10 years. Therefore in depth in vitro and in vivo biocompatibility testing is not yet widely performed. The extent of biocompatibility testing published investigates the components of bioMEMS rather than entire devices and does not follow the guidelines established by ISO 10993 for characterization of implantable materials. Therefore compatibility testing adhering to ISO 10993 standards needs to be performed on all components of bioMEMS. This biocompatibility data would then aid researchers during sensor design as predicted by Madou nearly a decade ago.

Dendrimers

Dendrimers exhibit low polydispersity and a reproducible pharmacokinetic profile making them ideal candidates for drug delivery (Yang & Kao, 2006; Boas & Heegaard, 2004). The functional groups (Figure 7.3) present on the dendrimer surface provide an easy mechanism to conjugate drug to

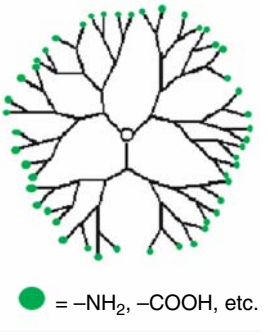

Figure 7.3 Dendrimer functional groups allow complexation or conjugation with various molecules such as DNA or pharmaceutical agents. (*See* Color Plate 13)

the surface in addition to physical encapsulation during dendrimer synthesis (Patri, Kukowska-Latallo, & Baker, Jr., 2005). However, their behavior in vivo is the most critical determinant of their efficacy. Myriad factors of dendrimer structure contribute to in vivo behavior including but not limited to: molecular weight, architecture, surface charge, and hydrophilicity/hydrophobicity. Therapeutic drug will be difficult to deliver to the desired target if the dendrimer is cleared rapidly from the bloodstream. Thus toxicity and blood clearance, or blood half-life, are potential roadblocks to the development of dendrimer-based drug delivery systems.

In vitro cytotoxicity is one of the first tests performed to characterize a potential candidate's in vivo toxicity. If the dendrimer proves to be excessively toxic to immortalized cell lines then the dendrimer will likely exhibit similar behavior in vivo. Additional testing such as hemolysis of red blood cells is performed to determine the effects of dendrimers in the bloodstream. Finally, radiolabeled dendrimer is used to determine in vivo distribution and blood clearance in animal models. Toxicity to vital organs such as the lungs, liver, or kidneys and ultimately morbidity may result if the dendrimer accumulates in these organs. Thus in vitro testing such as cytotoxicity and hemolysis combined with in vivo animal testing to determine preferential localization and excretion pathways of dendrimers provides a reasonable model to support or reject testing in humans. The structure–function relationship of dendrimer-induced biological response in different cell and animal models is highlighted. A brief summary of the experiments reviewed here is shown in Tables 7.2–7.5.

Polyamidoamine (PAMAM)

Since dendrimers are being investigated for potential drug delivery roles, cytotoxicity studies must investigate both the properties of the parent molecule and that of the drug- or gene-conjugated molecule. In this subsection several cationic PAMAM dendrimers conjugated with various therapeutics are surveyed.

Cationic PAMAM: Effect of Generation and Dosage

Haensler and Szoka (1993) investigated the effects of cationic PAMAM generation 2–10 (G2–10) (Figure 7.4) in the monkey fibroblast cell line CV-1. The dendrimer's diameter, dose, and the presence/absence of DNA were factors determining the toxicity of cationic PAMAM toward the adherent CV-1. Cells were incubated with 0–60 μg of poly-L-lysine (PLL) or PAMAM G6 for 5 h in serum-free media followed by culture in serum-containing media for 48 h without dendrimer. The effect upon CV-1 was quantified by measuring total cellular protein in addition to the MTT dye reduction assay, which measures mitochondrial activity through reduction of MTT into formazan. PAMAM G6 was significantly less toxic than the polycationic polymeric control PLL. The lethal dose for 50% of the cells (LD_{50}) was above 300 μg/ml for PAMAM G6 and was 25 μg/ml for PLL. When DNA was complexed with the PAMAM G6 dendrimer in a 10:1 ratio of primary amines:nucleotide, the LD_{50} of G6 increased nearly threefold to 100 μg/ml while that of PLL remained unchanged. Another

Table 7.2 Summary of in vitro studies on cationic polyamidoamine (PAMAM), polyethyleneimine-based diaminobutane (DAB) dendrimers.

Dendrimer	Generation Tested (G)	Species	Cells	Assay	Reference
	G2 - 10	monkey	fibroblast CV-1	Cytotoxicity	Haensler & Szoka, 1993
	G5	sheep	red blood cells	Hemolysis	Plank et al, 1996
	G3, 5 & 7	Chinese har	lung fibroblast V79	Cytotoxicity	Roberts et al., 1996
	G4	rat	Extensor digitorum longus myocytes	Cytotoxicity	Brazeau et al., 1997
	G2 - 4	murine	B16F10 melanoma	Cytotoxicity	Malik et al., 2000
	G5	human	HeLa cervical cancer	Cytotoxicity	Yoo & Juliano, 2000
	G5 Superfect	monkey	Cos-7 kidney fibroblasts	Cytotoxicity	Gebhart et al., 2001
PAMAM	G0 - 4	human	Caco-2 intestinal adenocarcinoma	Cytotoxicity	El Sayed et al., 2002
	G3	murine rat	L929 fibroblasts red blood cells	Cytotoxicity Hemolysis	Fischer et al., 2003
	G2 -4	human	Caco-2 intestinal adenocarcinoma	Cytotoxicity	Jevprasesphant et al., 2003
	G5-PEG triblock	human	293 kidney RAW 264.7 macrophage-like	Cytotoxicity	Kim et al., 2004
	G5	murine	NIH/3T3 fibroblasts BNL CL.2 hepatocytes	Cytotoxicity	Kuo et al., 2005
DAB	G2-4	murine	B16F10 melanoma	Cytotoxicity	Malik et al., 2000
	G1 - 5	human	A431 epidermoid cancer	Cytotoxicity	Zinselmeyer et al., 2002
	G5	murine	RAW 264.7 macrophage-like	Cytotoxicity	Kuo et al., 2005
	Q1 - 4	human	A431 epidermoid cancer	Cytotoxicity	Schatzlein et al., 2005
DAE	G1-3	murine	B16F10 melanoma	Cytotoxicity	Malik et al., 2000

Table 7.3 Summary of *in vitro* studies on anionic Polyamidoamine (PAMAM) & Polyethyleneimine-based diaminobutane (DAB) dendrimers.

Dendrimer	Generation Tested (G)	Species	Cells	Assay	Reference
PAMAM	G1.5 - 7.5	murine	B16F10 melanoma	Cytotoxicity Hemolysis	Malik et al., 2000
DAB	G1.5 - 3.5	murine	B16F10 melanoma	Cytotoxicity Hemolysis	

study investigated the effect of G3, G5, and G7 on V79 Chinese hamster lung fibroblasts at 4 and 24 h (Roberts, Bhalgat, & Zera, 1996). Three concentrations of dendrimer were used: 100 nM, 10 μM, or 1 mM. After treatment the adherent cells were harvested from the surface, counted, and re-plated for 6–7 days at which time the cells were stained with crystal

Table 7.4 Summary of *in vivo* studies on cationic Polyamidoamine (PAMAM) & Polyethyleneimine-based diaminobutane (DAB) dendrimers.

Dendrimer	Generation Tested (G)	Animal models	Assay	Reference
PAMAM	G3, 5 & 7	Swiss-Webster mice	Biodistribution & toxicity	Roberts et al., 1996
	G3	rats	Accumulation	Margerum et al., 1997
	G3 & 4	Wistar rats	Biodistribution & toxicity	Malik et al., 2000
	G4	nude mice	Blood half-life	Kobayashi et al., 2001
DAB	G1 - 4	BALB/c mice	Toxicity	Schatzlein et al., 2005

Table 7.5 Summary of *in vivo* studies on anionic Polyamidoamine (PAMAM) dendrimers.

Generation Tested (G)	Animal models	Assay	Reference
G2.5, 3.5 & 5.5	Wistar rats	Blood clearance & accumulation	Malik et al., 2000
G3.5	C57 mice	Toxicity	Matsumura & Maeda, (1986)

violet dye and colonies of $\geq$50 cells were counted. Not surprisingly a concentration- and generation-dependent toxicity was observed. PAMAM G3 was highly toxic (<10% survival) only at the 1 mM dosage while G5 was toxic at 10 μM. G7 was toxic at all concentrations tested. Increased culture time of 24 h vs 4 h did not significantly increase toxicity to V79 cells. These results coincide with observations by Tomalia and co-workers (1990) that below G3 PAMAM is more flexible and possesses a 3-D conformation similar to a starfish. The addition of two generations of linear branching restricts the conformation of PAMAM G5 and above into a rigid sphere. Haensler and Szoka (1993) theorized that the spherical PAMAM may be more efficient at destabilizing a cell's plasma membrane while Roberts and co-workers (1996) proposed the generation-dependent increase in toxicity was due primarily to the increasing cationic nature of the dendrimer surface.

PAMAM G2–4 was investigated for toxicity against B16F10 murine melanoma cells (Malik, Wiwattanapatapee, Klopsch, Lorenz, Frey, Weener, Meijer, Paulus, & Duncan, 2000). Dendrimers were cultured with cells in serum-containing media for 67 h before the addition of MTT dye for the last 5 h for a total of 72 h. PAMAM G2–4 showed lower toxicity to B16F10 than PLL at concentrations below 0.1 mg/ml. PAMAM G1 showed no concentration-dependent toxicity toward B16F10. PAMAM G3 and G4 showed similar IC_{50} values as the PLL-positive control from 0.1 to 5 mg/ml. In addition, there was a weak generation-dependent toxicity observed for PAMAM. Morphological changes determined by scanning electron microscopy were not present for B16F10 treated with PAMAM at 1 h but were apparent by 5 h. The generation of PAMAM was not noted. Thus the generation and concentration effects observed by Malik et al. (2000) are in support of previous conclusions.

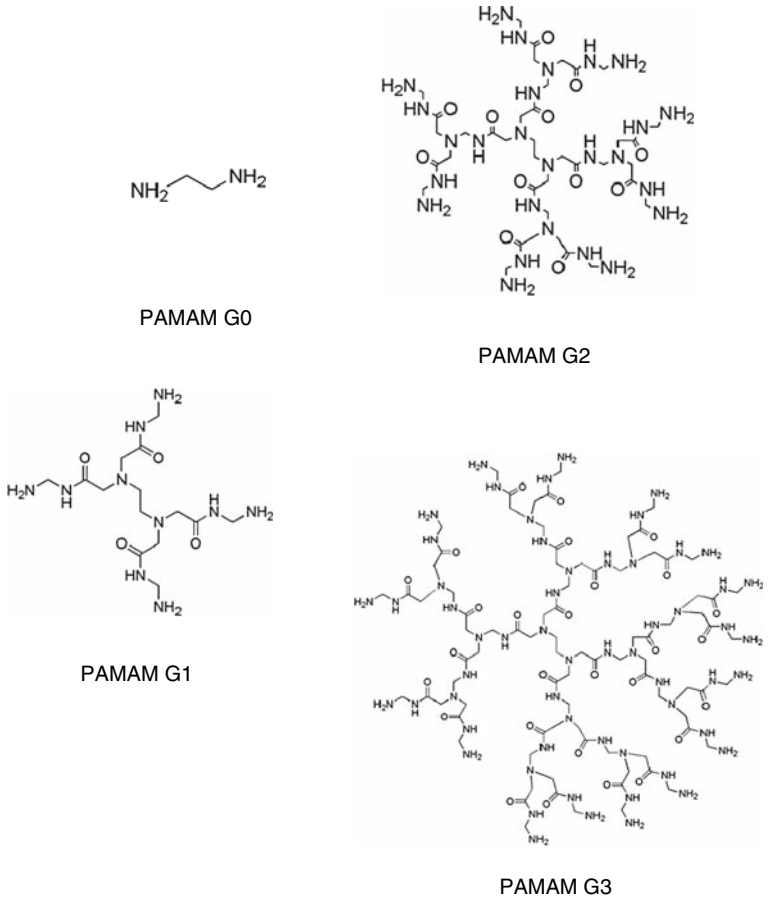

Figure 7.4 Cationic polyamidoamine (PAMAM) generation (G) 0–3 dendrimers.

MTT dye reduction was also used to assess the toxicity of PAMAM G3 dendrimers to L929 mouse fibroblastic cells (Fischer, Li, Ahlemeyer, Krieglstein, & Kissel, 2003). L929 were treated with PAMAM G3 for 3, 12, or 24 h at which time the cells were cultured with MTT for 4 h. PAMAM G3 showed no toxic effects at 0.01 or 0.1 mg/ml at 3, 12, or 24 h. PAMAM G3 showed >80% L929 viability at 3 and 12 h with a slight decrease at 24 h. PAMAM G3 showed significantly higher viability than PLL or linear polyethyleneimine (PEI) at 0.1 and 1 mg/ml and all time points. Both PLL and PEI at 0.1 and 1 mg/ml were highly toxic (Fischer et al., 2003). The extent of membrane damage caused by various polycationic polymers was also investigated at 0.01, 0.1, and 1 mg/ml via lactate dehydrogenase (LDH) release measured at 0, 30, and 60 min for each concentration. PAMAM G3 did not induce significant LDH levels whereas PLL significantly compromised the cellular membrane at 0.01 mg/ml after 30 min. PEI affected membrane integrity at 0.01 mg/ml after 60 min. Membrane destabilization was more pronounced at 0.1 and 1 mg/ml. It is important to note that the PLL and PEI tested here were the linear polymers and not dendrimer formulations. Thus the PAMAM G3

with tertiary amine groups on its surface showed less toxicity and membrane damage than PLL or PEI. However, this data is difficult to compare against other cytotoxicity studies because the pH and osmolarity of the cell culture medium was adjusted to pH 7.4 and 295 mosm/kg whereas none of the other studies mentioned any culture adjustments.

Caco-2 human intestinal adenocarcinoma cells were incubated with 0.1, 1, or 10 mM PAMAM G0–4 and LDH leakage assayed at 90, 150, and 210 min (El-Sayed, Ginski, Rhodes, & Ghandehari, 2002). LDH leakage of Caco-2 caused by PAMAM G0–4 was observed to increase with generation. G0 and G1 did not induce significant LDH leakage at any concentration tested up to 210 min. PAMAM G2 caused significant membrane damage only at 10 mM after 210 min. PAMAM G3 resulted in significant LDH levels at all concentrations only at 210 min while G4 caused extensive membrane destabilization at all concentrations and time points (El-Sayed et al., 2002). LDH measures damage to the plasma membrane, which allows the LDH to leak from the cell, in contrast to MTT, which measures metabolic activity in the mitochondria. Using parallel assays can confirm the true effect of a particular treatment or reveal potentially misleading interactions. As shown by El-Sayed et al. (2002) and Fischer et al. (2003), LDH confirmed the previous observations by MTT that PAMAM exhibits generation- and dose-dependent toxicity to cells in vitro.

While most research has focused solely on metabolic effects of the cationic dendrimers via MTT dye reduction, Kuo and co-workers (2005) investigated the mechanism of cell death in RAW 264.7 murine macrophage-like cells caused by PAMAM G5. Cytotoxicity was assayed by MTT dye assay and membrane damage measured by LDH release after exposure to the dendrimer for 24 h; 264.7 viability decreased significantly at 0.01 mg/ml with highly toxic effects at 0.1 and 0.2 mg/ml. A DNA fragmentation assay showed a DNA ladder consistent with DNA fragmentation during apoptosis in PAMAM G5-treated cells indicating the macrophages underwent programmed cell death rather than necrotic lysis (Kuo et al., 2005). Interestingly, NIH/3T3 and BNL CL.2 murine fibroblasts and liver cells, respectively, were not sensitive to cationic PAMAM dendrimer-induced apoptosis (Kuo et al., 2005). Previously murine macrophages were found to be significantly more sensitive to cationic polymer-induced toxicity than rat hepatocytes or bovine microvessel endothelial cells (Choksakulnimitr, Masuda, Tokuda, Takakura, & Hashida, 1995). Thus relative toxicity of the same polymer to different cell lines must be considered when comparing toxicity results and doses from different studies using various cells from different animal or human sources.

Initial toxicity screening allows researchers to predict the expected behavior of a given compound in vivo before proceeding with further testing. The interaction between cationic PAMAM dendrimers and blood cells is critical to their in vivo efficacy because dendrimers ultimately will circulate in the blood independent of the route of administration. Therefore the hemolytic properties of dendrimers are of particular interest. PAMAM G3 dendrimers at 0.01, 0.1, 5, and 10 mg/ml were incubated with red blood cells isolated from Wistar rats for 60 min (Fischer et al., 2003). The concentration of hemoglobin as detected by spectrophotometry was

less than 10% of the Triton X-100 positive control for all PAMAM concentrations tested and was therefore deemed non-toxic. While the data was obtained in triplicate no other time points or generations of PAMAM were tested. Malik and co-workers (2000) performed a more comprehensive study of the hemolytic properties of PAMAM G2–4, which showed both dose- and generation-dependent hemolysis after 1 h. Interestingly, PAMAM G1 showed no dose- or generation-dependent hemolysis, which may be due to its small molecular weight and low surface charge. This observation also eliminates the possibility of core-induced toxicity at low PAMAM generations. Scanning electron microscopy data obtained on these rat red blood cells showed significant morphological change at doses as low as 10 μg/ml for PAMAM contrasting the spectrophotometer data that showed hemolysis only at doses above 1 mg/ml. At 1 mg/ml red blood cells also showed more aggregation likely due to dendrimer cross-linking (Malik et al., 2000). Altered morphology can have significant impact upon red blood cell function in vivo as shown by the single amino acid mutation leading to sickle cell anemia. These hemolysis results highlight the importance of multiple assays to assess in vitro behavior. The spectrophotometer measurements did not indicate any cytotoxic effects; however, the scanning electron microscopy photos clearly showed a difference in morphology indicative of cell membrane damage and cell death (Malik et al., 2000).

Cationic PAMAM: Effect of Conjugated Molecules

The effect of PAMAM G4 with and without plasmid DNA (pDNA) upon extensor digitorum longus (EDL) muscles from Sprague–Dawley rats was calculated by total creatine kinase release determined at 30, 60, and 90 min by spectrophotometry (Brazeau, Attia, Poxon, & Hughes, 1998). At 1 mg/ml naked PAMAM G4 and G4-pDNA (3:1 w:w) showed similar toxicity to EDL muscle cells. However, naked G4 at 5 mg/ml was three times more myotoxic than G4-pDNA (3:1 w:w). A potential charge reducing complex might be formed upon addition of pDNA, or a change in particle size potentially leading to compaction similar to DNA on histones may lead to this decreased toxicity. pDNA is also a possible free radical scavenger thereby decreasing oxidative damage to the cells. Dendrimers stimulated the highest release of creatine kinase followed by PLL and liposomes. This decrease in toxicity of negatively charged pDNA complexed with the cationic PAMAM dendrimer supports Roberts et al. (1996) hypothesis that cytotoxicity is surface charge dependent.

Yoo and Juliano (2000) used PAMAM G5 conjugated to Oregon green 488 (G5-Org) fluorophore to study the cellular localization of dendrimers compared to their cargo. HeLa cells were incubated for 24 h with 30% fetal calf serum and without serum in the presence of G5-Org at which time the viability of the cells was determined via MTT dye reduction. Viability increased significantly for both the naked and oligonucleotide-conjugated G5-Org cultured with serum vs without. Interestingly, 30% serum decreased oligonucleotide delivery to the cells as determined by luciferase activity compared to the absence of serum but was similar to commercially available PAMAM dendrimer known as Superfect^{TM}. The hydrophobic Oregon green 488 fluorophore sufficiently shields the cationic charge on

the surface of Superfect™ to decrease its toxicity (Yoo & Juliano, 2000). The cytotoxicity of Superfect™ toward Cos-7 monkey kidney fibroblasts was investigated at different cell confluency and time points (Gebhart & Kabanov, 2001). Cos-7 at 40, 70, or 90% confluency were exposed to Superfect™ for 2 or 4 h after which the cells were grown in serum-containing media for 72 h before MTT analysis. Approximately 80% viability was observed for 40, 70, or 90% confluency Cos-7 at 2 and 4 h. This relatively low toxicity is beneficial because transfection increased significantly between 2 and 4 h. No other dendrimers or PAMAM generations were tested limiting the ability of these findings to support the generation- and concentration-dependent toxicity previously observed.

Cationic PAMAM: Effect of PEGylation or Other Surface Modification

The Caco-2 cell line was also used to investigate the toxicity of PEG or lauroyl fatty acid chain surface-modified PAMAM G2–4 dendrimers (Jevprasesphant, Penny, Jalal, Attwood, McKeown, & D'Emanuele, 2003). Consistent with previous findings, unmodified PAMAM dendrimers showed both a generation- and concentration-dependent cytotoxicity toward Caco-2. Viability was measured by MTT after 3 h of exposure to 90% confluent cells and 4 h of culture with both dendrimer and MTT. Surface modification of the tertiary amine groups on PAMAM G3 and G4 with six lauroyl chains reduced toxicity an order of magnitude compared to unmodified PAMAM G3 or G4. While six lauroyl chains showed marked reduction in PAMAM G3 and G4 toxicity, the addition of nine lauroyl chains to G2–4 resulted in similar toxicity as unmodified PAMAM G2–4. This difference in toxicity between six and nine lauroyl groups on the dendrimer surface is likely due to increased hydrophobic interaction with and destabilization of the plasma membrane. The addition of two PEG 2000 chains to PAMAM G4 had no effect on toxicity; however, four PEG 2000 chains resulted in a near sixfold reduction in toxicity. This PEG-dependent reduction in toxicity is consistent with previous findings that shielding the surface charge decreases toxicity. The two PEG chains likely did not sufficiently shield the charge amine groups on the PAMAM dendrimer. The reduction in toxicity shown by Jevprasesphant et al. (2003) reveals that shielding charge on the dendrimer surface via surface modification plays a significant role in toxicity but molecular weight and architecture are still important factors.

A PAMAM–PEG–PAMAM triblock copolymer dendrimer was synthesized to further investigate the impact of PEG modification on biocompatibility (Kim, Seo, Choi, Jang, Baek, Kim, & Park, 2004). Transformed human kidney 293 cells were exposed to PAMAM–PEG–PAMAM G5 dendrimer for 4 h at 70–80% confluency followed by 2 h incubation with MTT and cell lysis overnight in detergent. The copolymer G5 dendrimer showed no toxicity up to 0.15 mg/ml whereas PAMAM G4 showed slight toxicity (~80% viability) up to 0.15 mg/ml. Linear PEI (25 kDa) showed significant toxicity to 293 cells at 0.05 mg/ml. The PAMAM–PEG–PAMAM triblock dendrimer study did not investigate higher generation or higher concentrations to determine the role inserting PEG into the dendrimer architecture has upon biocompatibility compared to unmodified PEG. Thus the conclusions drawn by Kim et al. (2004) are

limited in their applicability to understanding the effect of molecular weight, surface functionality, and surface charge.

Cationic PAMAM: Immune Response and* In Vivo *Reaction

In addition to non-toxic and non-hemolytic, a dendrimer for drug delivery applications must not elicit an excessive immune response. A dendrimer with low toxicity and hemolysis but high immunogenicity could lead to death upon administration in the extreme case or rapid elimination in less severe cases. Thus immunogenicity is a critical determinant in the success of any drug delivery vehicle. Hemolysis of antibody-sensitized sheep red blood cells by complement proteins in serum was used to measure the complement activation induced by PAMAM G5 with and without complexation to DNA (Plank, Mechtler, Szoka, & Wagner, 1996). The complement system is part of the innate immune system capable of triggering non-specific cell lysis via formation of a membrane attack complex that forms a pore in plasma membranes. Complement proteins adsorb onto the surface of the dendrimer and are depleted from the serum. The lower concentration of complement proteins then induces less hemolysis in a dose-dependent manner allowing researchers to gauge the extent of complement activation. The hemoglobin released from red blood cell lysis via the membrane attack complex can be measured using a spectrophotometer to determine the extent of complement activation. No complement activation was detectable at a charge ratio of 1:1; however, complement activation increased with the charge ratio reaching a maximum with only PAMAM G5 present (Plank et al., 1996). The charge ratio of DNA to dendrimer thus determines complement activation supporting the previous data that charge is important in determining the host response.

In vitro assays such as cytotoxicity and hemolysis provide information to guide researchers toward the best application for a particular dendrimer formulation. The cytotoxicity data guides dosage selection while hemolysis data influences surface modification and dosage frequency among other factors. The in vivo biodistribution of dendrimers is critical to therapeutic efficacy, toxicity, and morbidity. If a particular dendrimer formulation stimulates red blood cell aggregation an embolism, or clot, can form leading to entrapment in the lungs or brain. Also, many polymer therapies fail in vivo testing because of excessive accumulation and toxicity in vital organs such as the kidneys and liver. Thus animal testing is required to obtain preliminary data about biodistribution, accumulation, and toxicity before pursuing further experiments focusing on therapeutic efficiency. The in vivo toxicity of intraperitoneal (ip) ^{14}C-labeled PAMAM G3, 5, or 7 dendrimers at 5×10^{-6}, 5×10^{-5}, or 5×10^{-4} mmol/kg after 7 or 30 days and 5×10^{-4} mmol/kg at 6 months was investigated in Swiss–Webster male mice (20 g) (Roberts et al., 1996). No change in body weight or behavior was observed; however, one mouse in the 7-day group died 24 h after injection with G7 at the highest dose of 45 mg/kg (5×10^{-4} mmol/kg). No further investigation into the specific cause of death was performed. Mice in the 6-month group were investigated for the long-term effects of weekly 5×10^{-4} mmol/kg ip injections of G3, G5, and G7; however, the G7 dendrimer dosage was lowered to 5×10^{-5} mmol/kg after one mouse died 24 h after the initial dose. As with the 7- and 30-day groups, there was no change

in weight compared to the control group after 6 months. Interestingly, all of the liver samples obtained from the 6-month group exhibited liver vacuolization but no further investigation was performed (Roberts et al., 1996). This vacuolization is indicative of lysosomal storage instead of degradation (Duncan & Izzo, 2005). In addition to the overall toxicity the biodistribution of these PAMAM dendrimers was investigated using ^{14}C-labeled PAMAM G3, 5, or 7 dendrimers at 0.05–0.25 μCi ^{14}C ($2–6\times10^{-4}$ mmol/kg). PAMAM G3 and G5 showed similar liver accumulation up to 48 h and were higher than G7, which remained relatively constant. No difference in kidney or spleen accumulation was found. G5 exhibited slightly higher pancreatic levels than G3 or G7 but were not significant. Interestingly, the G7 dendrimer was primarily excreted in urine at 2, 4, and 8 h. After 8 h urine excretion of G7 mimicked that of G3 and G5, which remained constant over 48 h. Significant differences in the amount of G3 pancreatic accumulation was observed between two independent trials. Roberts concluded that G3 and G5 appear to be suitable candidates for further in vivo therapies while G7 is not due to toxicity at high doses. This research supports previous findings that liposomes accumulate preferentially in the pancreas after ip but not iv injection (Goto & Ibuki, 1994). However, the number of surface-conjugated methyl groups required to gain a ^{14}C signal may influence the physicochemical properties of the dendrimer altering its biodistribution (Roberts et al., 1996). Therefore the distribution of ^{125}I core-labeled G3 and G4 PAMAM was observed at 1 h after ip or iv injection into male Wistar rats (250 g) (Malik et al., 2000). Blood levels were similar for both G3 and G4 after ip or iv injection. Ip injection resulted in similar liver accumulation for G3 and G4; PAMAM G4 showed significantly lower liver levels (~60% recovered dose) than G3 (~85%) after iv injection. The accumulation in other organs was not reported. It appears that surface charge and molecular weight have no role in liver accumulation after ip injection but do play a role after iv injection.

Conjugating PEG to PAMAM G3-gadolinium (Gd)-chelated dendrimers increased blood circulation significantly and decreased liver accumulation nearly fivefold at 7 days in rats (breed and weight were not reported) (Margerum, Campion, Koo, Shargill, Lai, Marumoto, & Sontum, 1997). The effects of PEG conjugation to ^{153}Gd-labeled PAMAM G4 were investigated as a potential means to increase blood half-life of the magnetic resonance imaging contrast agent 2-(*p*-isothiocyanatobenzl)-6-methyldiethylenetriaminepentaacetic acid (1B4M) conjugated to the dendrimer (Kobayashi, Kawamoto, Saga, Sato, Hiraga, Ishimori, Konishi, Togashi, & Brechbiel, 2001). Nude mice were injected with 1 μCi/200 μl for biodistribution studies and 3 μCi/200 μl for blood clearance. Conjugation of one or two 20,000 molecular weight PEG chains significantly increased blood circulation time compared to the non-PEGylated G4 dendrimer. Two PEG chains resulted in recovery of 20% of the initial dose/g in blood compared to 9% for one PEG chain and 2% for the non-PEGylated dendrimer. In addition, two PEG chains decreased liver accumulation compared to one PEG or non-PEGylated dendrimer, which showed similar levels. Two PEG chains did increase the accumulation in the lungs, which is likely due to increased molecular weight (96 kDa for two PEG chains vs 77 kDa for one PEG chain and 57 kDa for non-PEGylated

G4 PAMAM). PEGylating the G4-1B4M dendrimer also significantly increased blood clearance (Kobayashi et al., 2001). ^{153}Gd was continually excreted in the urine and feces of the mice with the PEGylated G4-1B4M showing higher excretion than the G4-1B4M parent molecule. Since the intent was to study blood retention of a contrasting agent no toxicity was obtained and only blood clearance investigated beyond 48 h. Nonetheless this data on PEG-modified PAMAM G4 is valuable for illustrating the in vivo effect of surface modification on blood clearance.

Anionic PAMAM: Effect of Generation, Dosage, and* In Vivo *Response

Much attention has focused on cationic PAMAM; however, anionic dendrimers can be synthesized that will not directly interact with the negatively charged plasma membrane (Figure 7.5). Malik et al. (2000) found that cationic PAMAM dendrimers showed toxicity to murine B16F10 melanoma cells above 100 μg/ml, but anionic PAMAM dendrimers G1.5–7.5 showed similar toxicity as the negative control dextran-treated cells up to 1 mg/ml. Anionic PAMAM dendrimers were not tested above 1 mg/ml. Similar results were found for anionic PAMAM G2.5 and G3.5 dendrimers in Caco-2 (Jevprasesphant et al., 2003). The cationic PAMAM G2–4 showed a concentration- and generation-dependent toxicity toward Caco-2 cells; however, G2.5 and G3.5 anionic PAMAM did not show significant toxicity even at

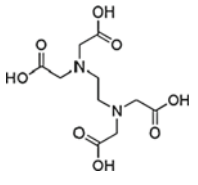

PAMAM G0.5

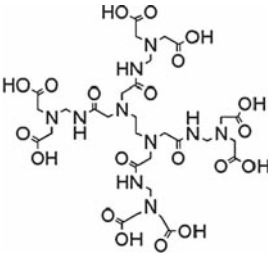

PAMAM G1.5

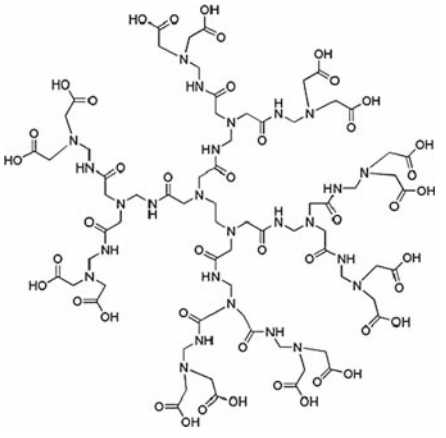

PAMAM G2.5

Figure 7.5 Anionic polyamidoamine (PAMAM) generation (G) 0.5–2.5 dendrimers.

1 mM. These findings are consistent with previous conclusions that surface charge plays an important role in the cytotoxicity of dendrimers. The cationic PAMAM can interact with a cell's negatively charged plasma membrane via electrostatic attraction and cause destabilization. The anionic PAMAM dendrimers are repulsed by the negatively charged plasma membrane preventing charge-dependent destabilization.

The negative surface charge on anionic PAMAM dendrimers showed similar results as the in vitro toxicity for decreasing hemolysis. Anionic PAMAM G1.5–3.5 showed no generation- or dose-dependent hemolysis up to 2 mg/ml after 1 h. However, PAMAM G7.5 and G9.5 were hemolytic at doses 2 mg/ml and above, which confirms the previously observed generational cytotoxicity likely due to the increase in molecular weight (212 and 852 kDa for G7.5 and G9.5, respectively vs <13 kDa for G1.5–3.5) and size. Anionic PAMAM G3.5 incubated with rat red blood cells for 24 h did not cause any dose-dependent increase in hemolysis (Malik et al., 2000). PAMAM G3.5–9.5 showed no morphological changes up to 2 mg/ml via scanning electron microscopy supporting the spectrophotometer measurements. Thus even at high concentrations anionic PAMAM showed little hemolytic properties. This lack of hemolysis further supports the theory that positively charged molecules destabilize the membrane leading to cell lysis since cationic and anionic PAMAM dendrimers share similar architecture but differing functional groups.

Based on the low in vitro toxicity and hemolytic properties of anionic PAMAM dendrimers, one would expect little to no in vivo toxicity even at high doses. Anionic PAMAM G2.5, 3.5, or 5.5 radiolabeled with ^{125}I were injected either ip or iv into Wistar rats (250 g) with blood clearance and liver accumulation assayed at 1 h (Malik et al., 2000). IV injection exhibited consistent blood levels recovered for G2.5, 3.5, and 5.5. G2.5 showed slightly higher blood levels than G3.5 or G5.5 at 1 h after ip administration. All three PAMAM dendrimers showed higher blood levels after ip injection than iv. Correspondingly liver levels for iv-administered PAMAM G2.5, 3.5, or 5.5 were higher than those for the respective ip-injected dendrimer indicating the liver may play a role in anionic PAMAM clearance. PAMAM G3.5 showed lower hepatic accumulation upon conjugation to platinum compared to the unconjugated PAMAM G3.5 dendrimer (Malik et al., 2000). Thus both positive and negative surface charge appears to play some role in localizing PAMAM dendrimers to the liver as evidenced by G3.5-platinate and cationic PAMAM findings and the PAMAM G3 and G4 results (Malik et al., 2000). The overall tolerability of PAMAM G3.5 was further illustrated by Matsumura and Maeda (1986). C57 mice with B16F10 tumors dosed with 95 mg/kg of PAMAM G3.5 via ip injection showed no weight change. This relatively high dose shows the comparatively low toxicity of anionic dendrimers compared to cationic, which showed lethality at 45 mg/kg with PAMAM G7. This difference appears to be driven largely by surface charge over molecular weight, size, and architecture.

PEI Dendrimers

In addition to PAMAM, PEI-based dendrimers have been investigated. These dendrimers differ in their core and dendrons from PAMAM.

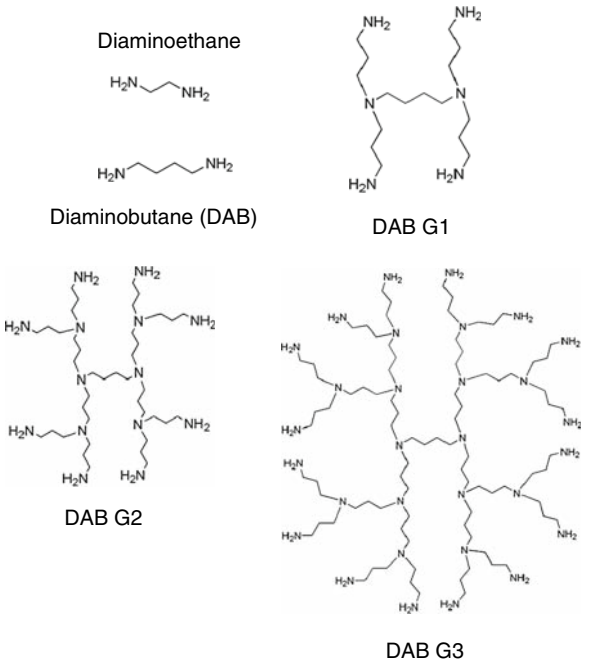

Figure 7.6 Cationic polyethyleneimine-based diaminobutane (DAB) generation (G) 0–3 dendrimers.

Diaminobutane (DAB) and diaminoethane (DAE) are the two most commonly used PEI-based dendrimer cores (Figure 7.6).

Cationic PEI: Effect of Generation, Dosage, and* In Vivo *Response

Malik and colleagues (2000) observed that DAB G2–4 or DAE core G1–3 showed lower toxicity to B16F10 than PLL at concentrations below 0.1 mg/ml. DAB G2–4 and DAE G3 showed similar inhibitory concentrations for half the cells (IC_{50}) as the PLL-positive control from 0.1 to 5 mg/ml. In addition, there was a weak generation-dependent toxicity observed for DAB and DAE dendrimers toward B16F10. Electron microscopy showed morphological changes in B16F10 after 1 h at concentrations as low as 0.001 mg/ml for DAB and DAE. However, significant morphological changes were seen at 1 mg/ml indicating toxicity for DAB and DAE. The generation of the dendrimers observed was not noted. PAMAM dendrimers did not show any morphological changes after 1 h demonstrating that architecture contributes to in vitro toxicity as PAMAM, DAB, and DAE have similar surface charge and functional groups but DAB and DAE are approximately half the molecular weight for a given generation.

In addition to PAMAM G5, Kuo et al. (2005) investigated the effect of PEI-based DAB G5 upon RAW 264.7. Viability decreased significantly at 0.01 mg/ml with highly toxic effects at 0.1 and 0.2 mg/ml. The results were nearly identical for PAMAM and DAB G5. LDH release corresponded to the increased toxicity with a significant LDH release increase at 0.1 mg/ml for both PAMAM G5 and DAB G5. A DNA fragmentation assay showed a DNA ladder consistent with DNA fragmentation during apoptosis in RAW 264.7 treated with DAB G5. These cells also exhibited a higher sub-G1 population than PAMAM G5 evidenced by higher propidium iodide

staining further supporting the apoptosis conclusion. While B16F10 appear sensitive to changes in architecture, 264.7 macrophages are more sensitive to surface charge, which may stem from their phagocytic role in the reticuloendothelial system (Kuo et al., 2005). In contrast to the dose- and generation-dependent hemolysis after 1 h caused by exposure to PAMAM G2–4, PEI-based dendrimers DAB G2–4 and DAE G1–3 exhibited only dose-dependent hemolysis up to 6 mg/ml at 1 h. This difference in hemolysis was attributed to a difference in molecular weight for a given number of surface groups (i.e., charge) and the presence of different interior functional groups such as secondary or tertiary amines (Kuo et al., 2005).

PEI-based DAB dendrimers showed increasing toxicity to A431 human epidermoid cancer cells with increasing generation from G1 to G5 with the exception of G1, which was more toxic than G2 but less toxic than G3 (G2 < G1 < G3 < G4 < G5) (Zinselmeyer, Mackay, Schatzlein, & Uchegbu, 2002). Therefore the previous observation by Roberts and co-workers (1996) that increasing generation show increasing toxicity is further supported and appears to be based primarily on surface charge and molecular weight. Complexing DAB G1 and G2 with DNA (5:1 DAB:DNA w:w) significantly reduced toxicity to A431 fourfold and twofold, respectively. There was little change in toxicity at higher generations (G3 and G4) complexed with DNA. Therefore with a 5:1 w:w ratio of DAB:DNA toxicity toward A431 is generation dependent. As a result of this lowered toxicity at lower generations, DAB G1–3 showed higher DNA transfection rates than G4 and G5 (Zinselmeyer et al., 2002). The reduction of toxicity resulting from complexing cationic dendrimer to anionic DNA also supports the theory that cationic dendrimers exhibit cytotoxicity through interaction with cellular anions critical for viability. This data was obtained by MTT after A431 were exposed to DAB and DAB–DNA for 4 h followed by fresh media for 72 h. MTT was incubated with the cells for 4 h before obtaining absorbance data.

The effect of tertiary amine groups on DAB G1–4 was compared against quaternized DAB dendrimers (Q1–4) at coinciding generations to better characterize the role surface charge plays in toxicity (Schatzlein, Zinselmeyer, Elouzi, Dufes, Chim, Roberts, Davies, Munro, Gray, & Uchegbu, 2005). DAB Q1 and Q2 increased cytotoxicity compared to G1 and G2; Q3 showed no change from G3 while Q4 showed a slight decrease in IC_{50} value compared to DAB G4. The effect on A431 cytotoxicity of complexing Q1–4 with DNA was also compared against G1–4. The IC_{50} value for Q1:DNA 5:1 w:w was higher than that for DAB G1:DNA 5:1 meaning the quaternized DAB was less toxic. DNA in a 5:1 w:w ratio decreased the IC_{50} value for Q2 to that of G2 without DNA but was still approximately half the value of G2:DNA 5:1. Toxicity data for Q3:DNA was only obtained at 3:1 ratio but was threefold lower than Q3 without DNA and G3. Thus the IC_{50} value for Q3:DNA may partially be the result of lower dendrimer concentration in the sample. The IC_{50} value for Q4:DNA 5:1 was 33 μg/ml compared to 11 μg/ml for Q4 and 5.7 μg/ml for DAB with or without DNA. These findings support the observation that shielding the surface of cationic dendrimers by complexation with anionic compounds such as DNA decreases their toxicity.

The effect of surface charge for cationic polymers was further investigated in vivo by testing the effect of quaternizing the terminal amine groups on the PEI-based dendrimer DAB G1–4 (Schatzlein et al., 2005); 100 μg DAB G2:DNA at a 5:1 dendrimer nitrogen:DNA phosphate (N:P) injected intravenously was lethal to female BALB/c mice resulting in what the authors described as "embolism-like (rapid) death" (Schatzlein et al., 2005). Interestingly, the quaternized Q2 dendrimer:DNA conjugate at the same dose was not lethal. This decreased lethality was attributed to the quaternized dendrimer's increased ability to complex with DNA. This fact was reinforced by IC_{50} values that showed a sevenfold decrease in toxicity when the Q2 dendrimer was complexed with DNA (49 μg/ml without DNA vs 350 μg/ml with DNA). The Q2 dendrimer with 16 external quaternary amine groups was ideal because 14 moles of DNA phosphate were associated with each mole of dendrimer. Increasing the dendrimer size to Q3 with 32 external quaternary amines only resulted in 15 moles of DNA phosphate associated per mole dendrimer. Thus Q2 with 16 surface quaternary amine groups maximized DNA conjugation and hence charge shielding while minimizing molecular weight and size. The amine groups on DAB were quaternized by methylation resulting in a dendrimer structure similar to that used by Roberts et al. (1996) potentially explaining why Q16:DNA accumulated to a significant extent in the liver (Schatzlein et al., 2005). As was shown with the in vitro cytotoxicity data, shielding of external surface charge on dendrimers through complexation with DNA or via surface modification such as PEG grafting decreases in vivo toxicity and in the case of quaternized DAB G2 also increases gene transfer (Schatzlein et al., 2005).

Anionic PEI: Effect of Generation and Dosage

Changing surface charge from cationic to anionic decreased in vitro toxicity in PAMAM dendrimers. Therefore a similar decrease would be expected from PEI-based dendrimers based on previous observations that charge plays a large role in toxicity. DAB G1.5–3.5 also showed similar toxicity as dextran up to 1 mg/ml but were toxic to B16F10 at high doses near 10 mg/ml (Malik et al., 2000). This finding was confirmed by scanning electron microscopy, which showed no significant morphological changes in B16F10 cells except at the highest dose of DAB. Even at doses above 1 mg/ml, DAB and DAE anionic dendrimers were less toxic than PLL or the corresponding generation cationic PEI dendrimer. Thus a dynamic relationship between surface charge, size, and concentration are critical factors determining dendrimer toxicity. Surprisingly little hemolytic data is published for anionic PEI dendrimers. Anionic DAB G1.5–3.5 showed no generation- or dose-dependent hemolysis up to 2 mg/ml after 1 h in contrast to cationic DAB G2–4 and DAE G1–3 that showed dose-dependent toxicity. Cationic PAMAM G2–4 exhibited both generation- and dose-dependent toxicity. Therefore surface charge eliminates the dose-dependent hemolytic property while architecture suppresses the generation-dependent effect. There is a small variation in molecular weight between PEI and PAMAM dendrimers. Cationic PEI dendrimers are approximately half the molecular weight of the corresponding generation PAMAM dendrimer; anionic PEI is approximately 30% smaller than PAMAM at the same generation and surface charge (Malik et al., 2000).

Despite significantly lower toxicity more research has been performed with cationic than anionic dendrimers. The ease of cargo loading such as DNA is a major factor in this focus on cationic dendrimers. Electrostatic attraction complexes negatively charged DNA with positively charged dendrimer. Anionic dendrimers are more difficult to conjugate to DNA. Since gene delivery is a major research focus for dendrimers the focus is obviously on cationic dendrimers. Even more surprising is that there currently are no published in vivo studies using anionic DAB or DAE dendrimers despite their low toxicity. With the current emphasis on developing more elegant drug delivery systems this lack of data using anionic PEI dendrimers will not likely last.

Other Dendrimer Core Structures

Carbosilane-Based Dendrimers

Most dendrimer research has focused on PAMAM based on an ethylene diamine core or PEI built around either a diaminobutane or diaminoethane core. However, dendrimers are not limited to just these core structures. Carbosilane can be grafted with poly(ethylene oxide) (CSi-PEO) to form a dendrimer with PEO arms (Figure 7.7). These CSi-PEO G1 dendrimers showed significantly higher toxicity at doses above 1 mg/ml than the G2 dendrimer to B16F10 but were less toxic than PLL at all doses (Malik et al., 2000). This decreased toxicity for CSi-PEO G2 can be explained by the greater degree of shielding from the toxic core. However, these CSi-PEO dendrimers were not toxic to CCRF and human HepG2 hepatoma cells at doses up to 2 mg/ml. These findings again highlight the observation by Choksakulnimitr et al. (1995) that different cell lines demonstrate different levels of sensitivity to insult with polymers.

Further research into these carbosilane dendrimers investigated the effect surface charge has upon toxicity to primary cells obtained from human donors (Ortega, Bermejo, Chonco, de Jesus, de la Mata, Fernandez, Flores, Gomez, Serramia, & Munoz-Fernandez, 2006). Carbosilane G2 dendrimers with surface amine groups (8 or 16) quaternized with methyl iodide showed similar toxicity to peripheral blood monoculear cells at 1, 5, 10, 20, or 100 μM after 48 h incubation. Mitochondrial activity and thus viability were determined by MTT dye reduction after 4 h incubation with the MTT dye. Carbosilane G2 dendrimer with 8 or 16 surface methyl groups decreased mitochondrial activity from 80% at 1 μM to 30% at 5 μM. A dose of 10 μM showed a reduction to ~10% activity while 20 and 100 μM showed similar activities ~5% of the control cells without dendrimer exposure. These observations coincided with phase contrast microscopy of the peripheral blood monoculear cells. No morphological difference was observable between cells treated with 1 or 5 μM carbosilane G2 and the untreated control cells. However, above 10 μM membrane birefringence was significantly reduced and cell debris from dead peripheral blood monoculear cells was observable (Ortega et al., 2006). Peripheral blood monoculear cells are more difficult to culture and are more sensitive to dendrimers than immortalized cell lines, but the data obtained from these experiments is more physiologically relevant to in vivo behavior. As with the findings of Roberts et al. (1996) the addition of the

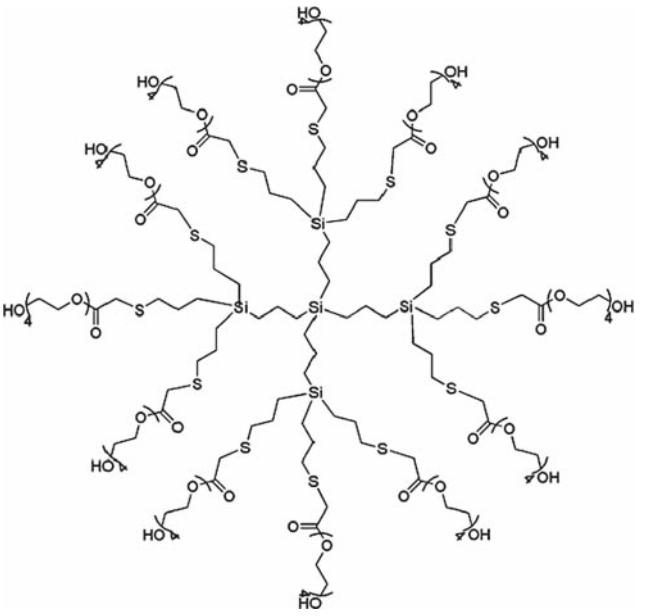

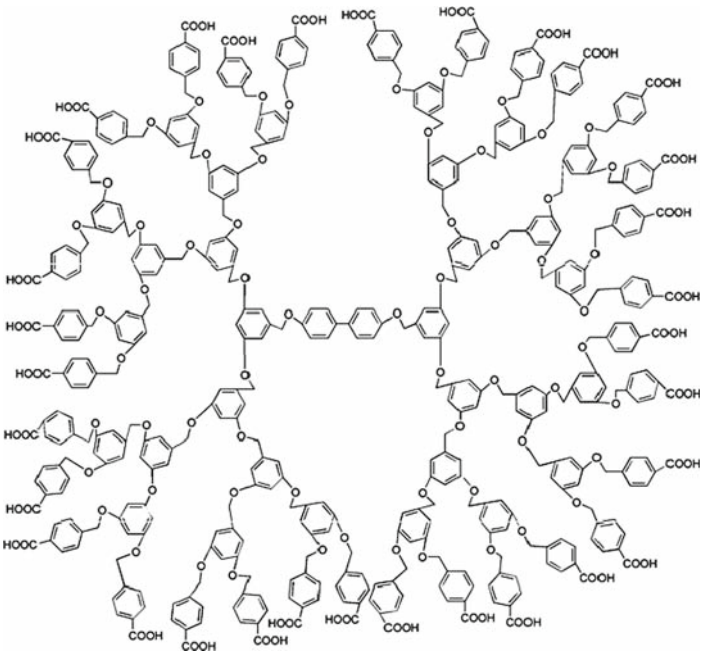

Figure 7.7 Carbosilane–polyethylene oxide and poly aryl ether dendrimers.

hydrophobic methyl group on the periphery of the dendrimer may affect the behavior of the quaternized carbosilane dendrimer. Despite promising in vitro toxicity data little in vitro hemolysis data is published for carbosilane dendrimers. These CSi dendrimers showed a similar hemolytic

behavior as the anionic dendrimers with $< 5\%$ hemolysis up to 2 mg/ml. More research into the effect of core toxicity, surface functional groups, and quaternization with hydrophobic methyl groups is needed prior to extensive in vivo testing.

Polyether-Based Dendrimers

De Jesus and co-workers (2002) conjugated methoxy-capped triethylene glycol to a propanoic acid-based polyester G4 dendrimer synthesized via the methodology of Inhre and co-workers (2002). The methoxy-capped triethylene glycol-modified polyester G4 dendrimer significantly increased toxicity of the dendrimers to B16F10 cells at doses higher than 5 mg/ml after 48 h. The toxicity of the modified dendrimer (11,500 Da) may be explained by the increase in molecular weight over the unmodified dendrimer (3790 Da). However, another dendrimer using three-armed PEO and G2 polyester dendrons (23,500 Da) showed similarity toxicity as the unmodified G4 polyester dendrimer (3790 Da) after 48 h at doses ranging up to 10 mg/ml. At 20 and 40 mg/ml this PEO-polyester G2 dendrimer showed significantly less toxicity toward B16F10 cells than the unmodified G4 polyester as determined by sulforhodamine B (SRB). De Jesus et al. (2002) theorized that PEO-polyester dendrimer appeared to inhibit growth of B16F10 resulting in the appearance of dendrimer-mediated toxicity as compared to the control. The ether and carbonyl nature of the backbone may also contribute to the cytotoxicity. Despite using the same cell line, the results found by De Jesus are difficult to compare to those by Malik because different cell viability assays were used (MTT vs sulforhodamine B assay), incubation time varied (48 h vs 72 h for Malik), and doses varied by nearly an order of magnitude. In addition, the doses used by De Jesus et al. (2002) are significantly higher than most experiments reviewed here with the exception of two in vivo tests discussed previously in this section.

A convergent poly aryl ether dendrimer was synthesized with either a carboxylate terminal group or malonate (Malik et al., 2000) (Figure 7.7). The poly aryl ether G2 dendrimers showed no dose- or concentration-dependent hemolysis after 1 h for either the carboxylate or malonate terminal groups, but both forms of G2 polyether dendrimer did cause complete hemolysis at $\geq$ 1 mg/ml after 24 h. The G0 dendrimer with carboxylate groups showed hemolysis at concentrations above 3 mg/ml at 1 h due to hydrophobic aromatic groups capable of interacting with the plasma membrane (Malik et al., 2000). As the generation increased to G2 these aromatic rings were buried more within the polyether dendrimer preventing interaction with cells making them less toxic. Thus even with anionic polyether dendrimers architecture plays an important role in toxicity and hemolysis (Malik et al., 2000).

Studies on the in vivo behavior of these higher generation anionic polyester and polyether dendrimers are limited. Polyester-based G4 dendrimers (MW 3790 Da) and three-armed PEG-G2 polyester dendrons (MW 23,500 Da) were iv injected into CD-1 nude mice at 1.3 g/kg (De Jesus et al., 2002). The unmodified polyester dendrimer showed immediate lethality in one mouse with no evidence indicating embolism. The second mouse was sacrificed at 24 h and showed no gross toxicity to its organs. The higher molecular weight dendrimer based on three-armed PEG was not lethal to either mouse, which may be due to its flexibility and low core toxicity. After

24 h neither mouse exhibited signs of gross toxicity to its organs. Based upon these results biodistribution studies were undertaken using ^{125}I-labeled dendrimer to determine localization. The polyester G4 dendrimer was excreted through the kidneys as expected for a small molecular weight compound and was completely eliminated by 4 h post-injection (De Jesus et al., 2002). The methoxy-capped triethylene glycol-modified version of the G4 polyester dendrimer was also renally excreted despite have a threefold higher molecular weight. After 30 min less than 5% of the methoxy-capped polyester dendrimer was detected in serum and was primarily excreted by 5 h post-injection. The three-armed PEG-based polyester dendrimer showed significant liver accumulation just 3 min post-injection. Liver levels remained high throughout the experiment with 53% of the injected dose still residing in the liver after 5 h. The three-armed PEG-based dendrimer could not be labeled using the same reaction mechanism as for G4 polyester dendrimer thus the ^{125}I was located on the surface of the dendrimer rather than on the core. Hydrolysis of the ^{125}I linkage was ruled out because liver accumulation was observed after just 3 min and radioactivity was detected in the high molecular weight fraction of G-50 spin columns (De Jesus et al., 2002). Further experiments were performed using this three-armed PEG-based polyester dendrimer conjugated to the potent chemotherapeutic drug doxorubicin. Polyester dendrimer–doxorubicin did not accumulate significantly in the lungs, heart, or liver in contrast to free doxorubicin, which is well known to accumulate in the heart and lungs. Thus this PEG-polyester-based dendrimer shows potential to increase therapeutic efficiency of doxorubicin without the toxicity and organ accumulation concomitant with administration of the free drug.

Melamine-Based Dendrimers

A triazine ring was used as the core for dendrimers based on melamine (Neerman, Zhang, Parrish, & Simanek, 2004). This core structure allows researchers to specifically tailor both the functional groups present on the dendrimer surface along with their spatial arrangement (Zhang, Jiang, Qin, Perez, Parrish, Safe, & Simanek, 2003). Neerman et al. used a G3 melamine dendrimer with amine functional groups and found that these dendrimers exhibited toxicity to Clone 9 rat liver cells at 0.1 mg/ml. This relatively high level of toxicity is likely due to a combination of the terminal amine groups and the architecture, which is rich in polyether bonds and triazole rings. The in vivo effects of these melamine dendrimers were also investigated (Neerman et al., 2004). Melamine G3 was found to be lethal at the extremely high dose of 160 mg/kg in male C3H mice at 6–12 h. Blood urea nitrogen was used to assess renal toxicity. No significant difference between the melamine G3 and the control group was found at 2.5, 10, or 40 mg/kg after 48 h or 6 weeks. The chronic time point taken at 6 weeks comprised three doses every 3 weeks for 6 weeks total. Alanine transaminase was used to assess liver function. Again no difference was found between G3 melamine treatment and the control at 2.5 and 10 mg/kg after 48 h or 6 weeks; however, there was a significant difference between both the 48 h and 6-week groups dosed at 40 mg/kg melamine G3 and PBS-treated mice. Thus melamine G3 is apparently not toxic to the kidney even at high doses and was confirmed through histological staining

with hemotoxylin and eosin (Neerman et al., 2004). However, liver toxicity is an issue at 40 mg/kg as evidenced by hepatocyte necrosis in histological slides. These findings are comparable to those by Roberts et al. (1996) who found that cationic PAMAM was relatively well tolerated even at high doses near 40 mg/kg except for G7.

Summary

Based on the studies presented, a complex combination of dendrimer architecture, molecular weight, and surface functionality/charge plays a role in toxicity in vitro. The effect on a specific cell model may be unique and cannot be extrapolated to other cell types. The behavior of dendrimers in vivo is less well defined and unified. In vitro and in vivo disconnect also exists. For example, cationic PAMAM dendrimers that show relatively high toxicity in vitro are reasonably tolerated in vivo even at high doses (Roberts et al., 1996; Malik et al., 2000; Neerman et al., 2004). Other groups have injected even higher doses of anionic dendrimer. PEG-G2 polyester dendrons (MW 23,500 Da) were iv injected into CD-1 nude mice at 1.3 g/kg with immediate lethality in one of two mice (De Jesus et al., 2002). In addition, the major focus of dendrimer research has focused on cationic PAMAM and PEI dendrimers with significantly fewer studies on anionic dendrimers or different architecture (Tables 7.2–7.5). The current body of work supports some generalized hypotheses. First, cationic surface charge increases toxicity through membrane destabilization. And second, the structure of the dendrons also plays a role in membrane destabilization as seen with the melamine dendrimer (Neerman et al., 2004) and polyether G0 dendrimer (Malik et al., 2000). However, more research is needed into the full mechanism underlying the complex interaction of dendrimer molecular weight, size, surface charge, and architecture.

Conclusions

More research has been performed on cationic dendrimer biocompatibility than bioMEMS or anionic dendrimer biocompatibility. A few general conclusions can be made regarding dendrimer structure, surface charge, and architecture, but more mechanistic research is needed to better understand the complex role these factors play. In addition, little standardized biocompatibility have been performed for bioMEMS and dendrimers. More conclusions regarding dendrimer biocompatibility could be drawn with more careful selection of cell model and culture conditions as evidenced previously and in Tables 7.2–7.5. Therefore more research adhering to the guidelines established by ISO 10993 and ASTM F748 will allow researchers to draw conclusions from similar experiments that are not currently available.

References

Allen, M., Butter, R., Chandra, L., Lettington, A., & Rushton, N. (1995). Toxicity of particulate silicon carbide for macrophage, fibroblasts and osteoblast-like cells *in vitro*. *Bio-medical Materials and Engineering,* 5, 151–9.

Amon, M., Bolz, A., & Schaldach, M. (1996). Improvement of stenting therapy with a silicon carbide coated tantalum stent. *Journal of Materials Science-Materials in Medicine,* 7, 273–8.

American Society for Testing Materials Standards International. (2004). ASTM F 748-04: Standard practice for selecting generic biological test methods for materials and devices. Retrieved October 20, 2006, from http://www.astm.org.

Bayliss, S.C. & Buckberry, L.D. (1999). A material for melding humans and machines. *Materials World,* 7, 213–5.

Bayliss, S.C., Heald, R., Fletcher, D.I., & Buckberry, L.D. (1999). The culture of mammalian cells on nanostructured silicon. *Advanced Materials,* 11, 318–21.

Bayliss, S.C., Buckberry, L.D., Harris, P.J., & Tobin, M. (2000). Nature of the silicon-animal cell interface. *Journal of Porous Materials,* 7, 191–5.

Bayliss, S.C., Harris, P.J., Buckberry, L., & Rousseau, C. (1997). Phosphate and cell growth on nanostructured semiconductors. *Journal of Materials Science Letters,* 16, 737–40.

Blattler, T., Huwiler, C., Ochsner, M., Stadler, B., Solak, H., Voros, J., & Grandin, H.M. (2006). Nanopatterns with biological functions. *Journal of Nanoscience and Nanotechnology,* 6, 2237–64.

Boas, U. & Heegaard, P.M.H. (2004). Dendrimers in drug research. *Chemical Society Reviews,* 33, 43–63.

Brazeau, G.A., Attia, S., Poxon, S., & Hughes, J.A. (1998). *In vitro* myotoxicity of selected cationic macromolecules used in non-viral gene delivery. *Pharmaceutical Research,* 15, 680–4.

Chen, H.Y., Elkasabi, Y., & Lahann, J. (2005). Surface modification of confined microgeometries via vapor-deposited polymer coatings. *Journal of the American Chemical Society,* 128, 374–80.

Chen, Z., Zhang, R.F., Kodama, M., & Nakaya, T. (1999). Preparations and properties of a novel grafted segmented polyurethane-bearing glucose groups. *Journal of Biomaterials Science-Polymer Edition,* 10, 901–16.

Chin, V.I., Taupin, P., Sanga, S., Scheel, J., Gage, F.H., & Bhatia, S.N. (2004). Microfabricated platform for studying stem cell fates. *Biotechnology and Bioengineering,* 88, 399–415.

Choksakulnimitr, S., Masuda, S., Tokuda, H., Takakura, Y., & Hashida, M. (1995). *In vitro* cytotoxicity of macromolecules in different cell culture systems. *Journal of Controlled Release,* 34, 233–41.

De Jesus, O.L.P, Ihre, H.R., Gagne, L., Frechet, J.M.J., & Szoka, F.C. (2002). Polyester dendritic systems for drug delivery applications: *in vitro* and *in vivo* evaluation. *Bioconjugate Chemistry,* 13, 453–61.

Duncan, R. & Izzo, L. (2005). Dendrimer biocompatibility and toxicity. *Advanced Drug Delivery Reviews,* 57, 2215–37.

Elam, J.H. & Nygren, H. (1992). Adsorption of coagulation proteins from whole blood on to polymer materials – relation to platelet activation. *Biomaterials,* 13, 3–8.

El-Sayed, M., Ginski, M., Rhodes, C., & Ghandehari, H. (2002). Transepithelial transport of poly(amidoamine) dendrimers across Caco-2 cell monolayers. *Journal of Controlled Release,* 81, 355–65.

Fischer, D., Li, Y., Ahlemeyer, B., Krieglstein, J., & Kissel, T. (2003). *In vitro* cytotoxicity testing of polycations: influence of polymer structure on cell viability and hemolysis. *Biomaterials,* 24, 1121–31.

Gebhart, C.L. & Kabanov, A.V. (2001). Evaluation of polyplexes as gene transfer agents. *Journal of Controlled Release,* 73, 401–16.

Gibbins, J.M. (2004). Platelet adhesion signaling and the regulation of thrombus formation. *Journal of Cell Science,* 117, 3415–25.

Goto, R. & Ibuki, Y.D. (1994). Tissue distribution of liposomes prepared from synthetic amphiphiles after intraperitoneal injection into mice. *Applied Radiation and Isotopes,* 45, 47–62.

Gourley, P.L. (2005). Brief overview of biomicronano technologies. *Biotechnology Progress,* 21, 2–10.

Haensler, J. & Szoka Jr., F.C. (1993). Polyamidoamine cascade polymers mediate efficient transfection of cells in culture. *Bioconjugate Chemistry,* 4, 372–9.

Hanein, Y., Pan, Y.V., Ratner, B.D., Denton, D.D., & Bohringer, K.F. (2001). Micromachining of non-fouling coatings for bio-MEMS applications. *Sensors and Actuators B-Chemical,* 81, 49–54.

Hiratsuka, Y., Miyata, M., Tada, T., & Uyeda, T.Q.P. (2006). A microrotary motor powered by bacteria. *Proceedings of the National Academy of Sciences of the United States of America,* 103, 13618–23.

Ihre, H.R., De Jesus, O.L.P., Szoka, F.C., & Frechet, J.M.J. (2002). Polyester dendritic systems for drug delivery applications: design, synthesis, and characterization. *Bioconjugate Chemistry,* 13, 443–52.

International Organization for Standards. (2003). Biological evaluation of medical devices. Retrieved October 20, 2006, from http://www.iso.org.

Ishikawa, M., Schmidtke, D.W., Raskin, P., & Quinn, C.A.P. (1998). Initial evaluation of a 290-μm diameter subcutaneous glucose sensor: glucose monitoring with a biocompatible, flexible-wire, enzyme-based amperometric microsensor in diabetic and nondiabetic humans. *Journal of Diabetes and Its Complications,* 12, 295–301.

Jevprasesphant, R., Penny, J., Jalal, R., Attwood, D., McKeown, N.B., D'Emanuele, A. (2003). The influence of surface modification on the cytotoxicity of PAMAM dendrimers. *International Journal of Pharmaceutics,* 252, 263–6.

Johansson, C.B., Hansson, H.A., & Albrektsson, T. (1990). Qualitative interfacial study between bone and tantalum, niobium or commercially pure titanium. *Biomaterials,* 11, 277–80.

Kaneda, Y. (2000). Virosomes: evolution of the liposome as a targeted drug delivery system. *Advanced Drug Delivery Reviews,* 43, 197–205.

Kim, K., Kim, C., & Byun, Y. (2001). Preparation of a dipalmitoylphosphatidylcholine/cholesterol Langmuir–Blodgett monolayer that suppresses protein adsorption. *Langmuir,* 17, 5066–70.

Kim, T.-I., Seo, H.J., Choi, J.S., Jang, H.-S., Baek, J.-U., Kim, K., & Park J.-S. (2004). PAMAM-PEG-PAMAM: novel triblock copolymer as a biocompatible and efficient gene delivery carrier. *Biomacromolecules,* 5, 2487–92.

Kobayashi, H., Kawamoto, S., Saga, T., Sato, N., Hiraga, A., Ishimori, T., Konishi, J., Togashi, K., & Brechbiel, M.W. (2001). Positive effects of polyethylene glycol conjugation to generation-4 polyamidoamine dendrimers as macromolecular MR contrast agents. *Magnetic Resonance in Medicine,* 46, 781–8.

Kotzar, G., Freas, M., Abel, P., Fleischman, A., Roy, S., Zorman, C., Moran, J.M., & Melzak, J. (2002). Evaluation of MEMS materials of construction for implantable medical devices. *Biomaterials,* 23, 2737–50.

Kros, A., Gerritsen, M., Sprakel, V.S.I., Sommerdijk, N.A.J.M., Jansen, J.A., & Nolte, R.J.M. (2001). Silica-based hybrid materials as biocompatible coatings for glucose sensors. *Sensors and Actuators B-Chemical,* 81, 68–75.

Kubo, K., Tsukasa, N., Uehara, M., Izumi, Y., Ogino, M., Kitano, M., & Sueda, T. (1997). Calcium and silicon from bioactive glass concerned with formation of nodules in periodontal ligament fibroblasts *in vitro*. *Journal of Oral Rehabilitation,* 24, 70–5.

Kue, R., Sohrabi, A., Nagle, D., Frondoza, C. & Hungerford, D. (1999). Enhanced proliferation and osteocalcin production by human osteoblast-like MG63 cells on silicon nitride ceramic discs. *Biomaterials,* 20, 1195–201.

Kuo, J.S., Jan, M.S., & Chiu, H.W. (2005). Mechanism of cell death induced by cationic dendrimers in RAW 264.7 murine macrophage-like cells. *Journal of Pharmacy and Pharmacology,* 47, 489–95.

Lan, S., Veiseh, M., & Zhang, M. (2005). Surface modification of silicon and gold-patterned silicon surfaces for improved biocompatibility and cell patterning selectivity. *Biosensors and Bioelectronics,* 20, 1697–708.

Lee, K.K., Bhushan, B., & Hansford, D. (2005). Nanotribological characterization of fluorpolymer thin films for biomedical micro/nanoelectromechanical system applications. *Journal of Vacuum Science & Technology: A,* 23, 804–10.

Lian, T. & Ho, R.J.Y. (2001). Trends and developments in liposome drug delivery systems. *Journal of Pharmaceutical Sciences,* 90, 667–80.

Lin, G., Pister, K.S.J., & Roos, K.P. (2000). Surface micromachined polysilicon heart cell force transducer. *Journal of Microelectromechanical Systems,* 9, 9–17.

Madou, M. (1997). Fundamentals of microfabrication (p. 471). Boca Raton, FL: CRC Press LLC.

Malik, N., Wiwattanapatapee, R., Klopsch, R., Lorenz, K., Frey, H., Weener, J.W., Meijer, E.W., Paulus, W., & Duncan, R. (2000). Dendrimers: relationship between structure and biocompatibility *in vitro*, and preliminary studies on the biodistribution of ^{125}I-labelled polyamidoamine dendrimers *in vivo*. *Journal of Controlled Release,* 65, 133–148.

Margerum, L.D., Campion, B.K., Koo, M., Shargill, N., Lai, J.-J., Marumoto, A., & Sontum, P.C. (1997). Gadolinium(III) DO3A macrocycles and polyethylene glycol coupled to dendrimers – effect of molecular weight on physical and biological properties of macromolecular magnetic resonance imaging contrast agents. *Journal of Alloys and Compounds,* 249, 185–90.

Matsumura, Y. & Maeda, H. (1986). A new concept for macromolecular therapeutics in cancer- chemotherapy – mechanism of tumoritropic accumulation of proteins and the antitumour agent SMANCS. *Cancer Research,* 46, 6387–92.

Meyer, J.U. (2002). Retina implant – a bioMEMS challenge. *Sensors and Actuators A – Physical,* 97–98, 1–9.

Moussy, F., Harrison, D.J., & Rajotte, R.V. (1994). A miniaturized Nafion-based glucose sensor – *in vitro* and *in vivo* evaluation in dogs. *International Journal of Artificial Organs,* 17, 88–94.

Nagayasu, A., Uchiyama, K., & Kiwada, H. (1999). The size of liposomes: a factor which affects their targeting efficiency to tumors and therapeutic activity of liposomal antitumor drugs. A*dvanced Drug Delivery Reviews,* 40, 75–87.

Naji, A. & Harmand, M.F. (1991). Cytocompatibility of two coating materials, amorphous alumina and silicon carbide, using human differentiated cell cultures. *Biomaterials,* 12, 690–4.

Neerman, M.F., Zhang, W., Parrish, A.R., & Simanek, E.E. (2004). *In vitro* and *in vivo* evaluation of a melamine dendrimer as a vehicle for drug delivery. *International Journal of Pharmaceutics,* 281, 129–32.

Nordsletten, L., Hogasen, A.K.M., Konttinen, Y.T., Santavirta, S., Aspenberg, P., & Aasen, A.O. (1996). Human monocytes stimulation by particles of hydroxyapatite, silicon carbide and diamond: *in vitro* studies of new prosthesis coatings. *Biomaterials,* 17, 1521–7.

Ortega, P., Bermejo, J.F., Chonco, L., de Jesus, E., de la Mata, F.J., Fernandez, G., Flores, J.C., Gomez, R., Serramia, M.J., & Munoz-Fernandez, M.A. (2006).

Novel water-soluble carbosilane dendrimers: synthesis and biocompatibility. *European Journal of Inorganic Chemistry,* 7, 1388–96.

Papra, A., Bernard, A., Juncker, D., Larsen, N.B., Michel, B., & Delamarche, E. (2001). Microfluidic networks made of poly(dimethylsiloxane), Si, and Au coated with polyethylene glycol for patterning proteins onto surfaces. *Langmuir,* 17, 4090–5.

Patri, A.K., Kukowska-Latallo, J.F., & Baker Jr., J.R. (2005). Targeted drug delivery with dendrimers: comparison of the release kinetics of covalently conjugated drug and non-covalent drug inclusion complex. *Advanced Drug Delivery Reviews,* 57, 2203–14.

Plank, C., Mechtler, K., Szoka, F.C., & Wagner, E. (1996). Activation of the complement system by synthetic DNA complexes: a potential barrier for intravenous gene delivery. *Human Gene Therapy,* 7, 1437–46.

Richards Grayson, A.C., Shawgo, R.S., Johnson, A.M., Flynn, N.T., Li, Y., Cima, M.J., & Langer, R. (2004). A bioMEMS review: MEMS technology for physiologically integrated devices. *Proceedings of the Institute of Electrical and Electronics Engineers,* 92, 6–21.

Roberts, J.C., Bhalgat, M.K., & Zera, R.T. (1996). Preliminary biological evaluation of polyamidoamine (PAMAM) Starburst™ dendrimers. *Journal of Biomedical Materials Research,* 30, 53–65.

Schatzlein, A.G., Zinselmeyer, B.H., Elouzi, A., Dufes, C., Chim, Y.T.A., Roberts, C.J., Davies, M.C., Munro, A., Gray, A.I., & Uchegbu, I.F. (2005). Preferential liver gene expression with polypropyleneimine dendrimers. *Journal of Controlled Release,* 101, 247–58.

Sharma, S., Popat, K.C., & Desai, T.A. (2002). Controlling nonspecific protein interactions in silicon biomicrosystems with nanostructured poly(ethylene glycol) films. *Langmuir,* 18, 8728–31.

Sohrabi, A., Holland, C., Kue, R., Nagle, D., Hungerford, D.S., & Frondoza, C.G. (2000). Proinflammatory cytokine expression of IL-1β and TNF-α by human osteoblast-like MG-63 cells upon exposure to silicon nitride *in vitro*. *Journal of Biomedical Materials Research,* 50, 43–9.

Stoldt, C.R. & Bright, V.M. (2006). Ultra-thin film encapsulation processes for micro-electro-mechanical devices and systems. *Journal of Applied Physics D: Applied Physics,* 39, R163–70.

Tokachichu, D.R. & Bhushan, B. (2006). Bioadhesion of polymers for bioMEMS. *Institute of Electrical and Electronics Engineers Transactions on Nanotechnology,* 5, 228–31.

Tomalia, D.A., Naylor, A.M., & Goddard, W.A. (1990). Starburst dendrimers – molecular-level control of size, shape, surface-chemistry, topology, and flexibility from atoms to macroscopic matter. *Angewandte Chemie International Edition-England,* 29, 138–175.

United States Food and Drug Administration. (1995). Required Biocompatibility Training and Toxicology Profiles for Evaluation of Medical Device. Retrieved October 20, 2006, from http://www.fda.gov/cdrh/g951.html.

Voskerician, G., Shive, M.S., Shawgo, R.S., von Recum, H., Anderson, J.M., Cima, M.J., & Langer R. Biocompatibility and biofouling of MEMS drug delivery devices. *Biomaterials,* 24, 1959–67.

Wan, H., Williams, R.L., Doherty, P.J., & Williams, D.F. (1994). Cytotoxicity evaluation of Kevlar and silicon carbide by MTT assay. *Journal of Materials Science-Materials in Medicine,* 5, 441–5.

Wan, G.J., Yang, P., Shi, X.J., Wong, M., Zhou, H.F., Huang, N., & Chu, P.K. (2005). *In vitro* investigation of hemocompatibility of hydrophilic SiN_x:H films fabricated by plasma-enhanced chemical vapor deposition. *Surface & Coatings Technology,* 200, 1945–9.

Webster, T.J., Ergun, C., Doremus, R.H., Siegel, R.W., & Bizios, R. (2000). Specific proteins mediate enhanced osteoblast adhesion on nanophase ceramics. *Journal of Biomedical Materials Research,* 51, 475–83.

Weisenberg, B.A. & Mooradian, D.L. (2002). Hemocompatibility of materials used in microelectromechanical systems: platelet adhesion and morphology *in vitro*. *Journal of Biomedical Materials Research,* 60, 283–91.

Wisniewski, N. & Reichert, M. (2000). Methods for reducing biosensor membrane biofouling. *Colloids and Surfaces B-Biointerfaces,* 18, 197–219.

Woodle, M.C. & Scaria, P. (2001). Cationic liposomes and nucleic acids. *Current Opinion in Colloid & Interface Science,* 6, 78–84.

Yang, H. & Kao, W.J. (2006). Dendrimers for pharmaceutical and biomedical applications. *Journal of Biomedical Materials Research-Polymer Edition,* 17, 3–19.

Yoo, H. & Juliano, R.L. (2000). Enhanced delivery of antisense oligonucleotides with fluorophore-conjugated PAMAM dendrimers. *Nucleic Acids Research,* 28, 4225–31.

Zhang, W., Jiang, J., Qin, C., Perez, L.M., Parrish, A.R., Safe, S.H., & Simanek, E.E. (2003). Triazine dendrimers for drug delivery: evaluation of solubilization properties, activity in cell culture, and *in vivo* toxicity of a candidate vehicle. *Supramolecular Chemistry,* 15, 607–16.

Zhu, Z., Zhang, J., & Zhu J. (2005). An overview of Si-based biosensors. *Sensor Letters,* 3, 71–88.

Ziaie, B., Baldi, A., Lei, M., Gu, Y., & Siegel, R.A. (2004). Hard and soft micromachining for bioMEMS: review of techniques and examples of applications in microfluidics and drug delivery. *Advanced Drug Delivery Reviews,* 56, 145–72.

Zimmerman, S., Fienbork, D., Flounders, A.W., & Liepmann, D. (2004). In-device enzyme immobilization: wafer-level fabrication of an integrated glucose sensor. *Sensors and Actuators B-Chemical,* 99, 163–73.

Zinselmeyer, B.H., Mackay, S.P., Schatzlein, A.G., & Uchegbu, I.F. (2002). The lower-generation polypropylenimine dendrimers are effective gene-transfer agents. *Pharmaceutical Research,* 19, 960–7.

Zuruzi, A.S., Butler, B.C., MacDonald, N.C., & Safinya, C.R. (2006). Nanostructured TiO_2 thin films as porous cellular interfaces. *Nanotechnology,* 17, 531–5.

8

Nanomaterials and Biocompatibility: Carbon Nanotubes and Fullerenes

Sean T. Zuckerman and Weiyuan John Kao

Introduction

The definition of "biocompatibility" and the related background material are detailed in the previous chapter covering the biocompatibility of biological microelectricalmechanical systems and dendrimers. This chapter will focus on the biocompatibility of current and emerging carbon-based nanomaterials such as carbon nanotubes and fullerenes from a structure–function standpoint. We will present trends and data from current primary literature correlating the structure of a material with its observed effect on the body ranging from cytotoxicity to hypersensitivity. In addition, we will highlight the differences in the data obtained ranging from different material preparation methods to different animal models and how these upstream choices influence the comparison of conclusions drawn regarding each type of material. The subjective nature of assessing the extent of a biological phenomenon such as the host response to a given material for a species should become apparent.

Known Structure–Function Relationships of Carbon Nanotubes (CNTs)

Carbon nanotubes (CNT) are a unique allotrope of carbon with a unique combination of properties that has attracted attention from researchers in the biomedical community, as well as electrical engineers and mechanical engineers, and among others. CNTs have two different structures – single walled and multiwalled. The single-walled CNT (SWCNT) is comprised of a hollow tube of graphite and it follows that the multiwalled CNT (MWCNT) is a series of concentric graphite tubes (Figure 8.1). SWCNTs typically are $\sim$1 nm in diameter and range in length up to several microns. MWCNTs are usually 40–50 nm in diameter but are shorter than SWCNTs. CNTs have attracted attention because they possess a high tensile strength, are excellent conductors of electricity, and are both chemically and thermally stable. Biomedical engineers and pharmaceutical scientists have found interest in CNTs based on their potential for drug delivery, biomaterials,

M.M. de Villiers et al. (eds.), *Nanotechnology in Drug Delivery*, DOI: 10.1007/978-0-387-77667-5_8,

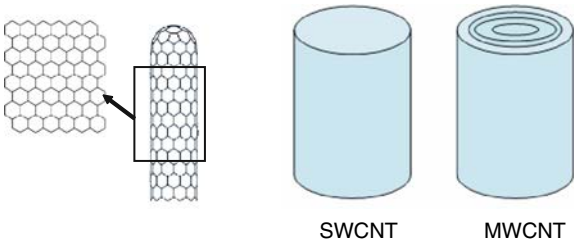

Figure 8.1 Single- and multiwalled carbon nanotubes (SWCNT and MWCNT, respectively). (*See* Color Plate 14)

and biosensor applications. The mechanical properties of CNTs can be used to reinforce current polymers or induce electrical conductivity by means of doping. CNTs are potentially a powerful drug delivery vehicle due to their high aspect ratio and high surface area.

The announcement of the National Nanotechnology Initiative by the Clinton administration in 2000 brought additional attention to nanoscale potential. The additional federal funding for research into nanomaterials, such as CNTs, has increased the demand for CNTs, necessitating large-scale manufacturing of CNTs. The national attention brought to nanomaterials by this initiative also brought extra scrutiny on the safety of nanomaterials. Every day millions of people are exposed to very low levels of CNTs resulting from the combustion of hydrocarbons such as natural gas and diesel fuel. This level of daily exposure is orders of magnitude less than that the laboratory and manufacturing personnel would be exposed to. The question of worker exposure was thus raised in addition to the questions surrounding the safety of using CNTs as pharmaceutical agents. The production, characterization, and properties of CNTs are discussed in depth elsewhere in this textbook. This chapter will focus on the health hazards posed by CNTs in addition to the current body of knowledge regarding CNT toxicity and biocompatibility.

Lung Toxicity and Inhalation Hazards

In order to commercially produce CNTs, manufacturers first had to classify the material for safety risks. Based on molecular similarities to carbon, CNTs were formally classified as synthetic graphite on the Material Safety Data Sheet submitted by Carbon Nanotechnologies, Inc. (Carbon Nanotechnologies International, 2003). This classification established known inhalation limits on workers exposed to CNTs in the work place. Specifically, the Occupational Safety and Health Administration sets the limits at 15 mg/m^3 of total dust, with 5 mg/m^3 allowable for the inhalable fraction of CNTs and graphite. However, unlike graphite, CNTs possess a fibrous nature and tend to agglomerate. Worker exposure to inhalable fibrous particles such as asbestos is well documented. Lung toxicity is based on the geometry and surface chemistry of inhaled particulates (Donaldson & Tran, 2002; Lippmann, 1994). The surface chemistry plays a role in the biopersistence of the particle. The longer a particle resides in the lungs, the higher the levels of accumulation from exposure ultimately leading to toxic effects (Hesterberg, Chase, Axten, Miller, Mussleman, Kamstrup, Hadley, Morscheidt, Bernstein, & Thevenaz, 1998). In addition, the surface area to

mass ratio is a critical determinant of the interaction between the particle and the cells in the alveoli. A large surface area also allows for a greater probability of a toxicant adsorbing to the particulate surface (Tran, Buchanan, Cullen, Searl, Jones & Donaldson, 2000). CNTs pose a unique perspective on previous lung toxicity data: CNTs posses an unusual surface area to weight ratio previously not encountered while combining the properties of nanoparticles with fibers.

Limited data is available regarding the lung exposure to materials with very high surface area to mass ratios. The potential for toxicity is inversely proportional to decreasing particle size and proportional to increasing surface area (Donaldson & Tran, 2004; Driscoll, Carter, Howard, Hassenbein, Pepelko, Baggs, & Oberdoerster, 1996). For instance, inhalation of microsized carbon black particles is less toxic than inhalation of nanosized carbon black (also called ultrafine) (Driscoll et al., 1996). In addition, 14 nm carbon black particles induced oxidative stress and stimulated migration of murine alveolar macrophages approximately twofold more than 260 nm carbon black particles (Barlow, Donaldson, MacCallum, Clouter, & Stone, 2005; Stone, Shaw, Brown, Macnee, Faux, & Donaldson, 1998). Thus, even a decrease from hundreds of nanometers to tens of nanometers can make a significant difference in the host response. As with previous observations of asbestos exposure, inhalation of carbon black for long periods at sub-toxic levels led to mutagenesis in rat lungs (Gallagher, Sams, Inmon, Gelein, Elder, Oberdorster, & Prahalad, 2003; Nikula, Snipes, Barr, Griffith, Henderson, & Mauderly, 1995). Fiber particle toxicity must also be considered. Similar to nanoparticles, the size and geometry of the fiber particle play a critical role in its potential toxicity. If the diameter of a fiber is too large, it will likely be trapped in the protective cilia of the upper respiratory tract (Donaldson & Tran, 2004). A relatively long fiber can be inhaled if its diameter is sufficiently small, but if that fiber is too long (> 20 μm), alveolar macrophages cannot phagocytose and destroy it (Ye, Shi, Jones, Rojanasakul, Cheng, Schwegler-Berry, Baron, Deye, Li, & Castranova, 1999). The fiber residence time is a critical determinant of toxicity. The longer a fiber is present in the lung, the more likely toxicity will result (Smart, Cassady, Lu, & Martin, 2006). Unlike nanosized particles no toxicological data is available for nanosized fibers.

In Vivo Studies: SWCNTs

The first group to investigate the effects of inhaled CNTs dosed Dunkin Hartley guinea pigs with unpurified CNTs and observed pulmonary function 4 weeks post-exposure (Huczko, Lange, Calko, Grubek-Jaworksa, & Droszcz, 2001). No specification was given whether the CNTs were single or multiwalled; however, the CNTs were produced via arc-discharge sublimation of a graphitic node doped with Co/Ni catalyst. Surfactant was used to disperse the aggregated CNTs, which were instilled in the trachea at a dose of 25 mg. Broncheal alveolar lavage (BAL) and other noninvasive techniques were used to assess pulmonary function. No difference was observed between the CNT group and the CNT-free soot control (Huczko et al., 2001). No further research on in vivo inhalation exposure was performed until 2004 when Lam et al. and Warheit et al. published

papers assessing the toxicity of SWCNT instilled intratracheally to mice and rats (Lam, James, McCluskey, & Hunter, 2004; Warheit, Laurence, Reed, Roach, Reynolds, & Webb, 2004).

Lam et al. (2004) investigated three different formulations of SWCNTs: raw and purified SWCNTs produced via high-pressure carbon monoxide conversion catalyzed with iron and CNTs from arc-discharge sublimation of a graphitic node doped with Ni catalyst compared against quartz or carbon black. These materials were exposed to B6C3F1 mice via intratracheal instillation, which is a commonly used screening method to model exposure to dust for toxicity (Lam et al., 2004). Mice were treated with 0, 0.1, or 0.5 mg of each material in 50 μl. After 7 or 90 days the mice were sacrificed and subjected to histology. SWCNTs were observed to cause dose-dependent lung lesions characterized by interstitial granulomas independent of production technique and metal content. The granulomas present at 7 days persisted and appeared worse at 90 days. Lam et al. (2004) point out that the unpurified SWCNT and arc-discharge SWCNT contained significant metal impurities such as nickel that are known to be highly toxic (Benson, Carpenter, Hahn, Haley, Hanson, Hobbs, Pickrell, & Dunnick, 1987). Quartz was observed to only elicit what was described as "mild to moderate inflammation"; therefore, Lam et al. (2004) concluded that SWCNTs are more toxic than quartz.

Warheit's group used the same exposure technique but SWCNTs isolated from laser ablation (2004). Male Crl:CD(SD)IGS BR rats (~8 weeks of age) were intratracheally instilled with 1 or 5 mg/kg and observed for 24 h, 1 week, 1 or 3 months. BAL, cell proliferation, and histology were used to assess the extent of pulmonary damage. Based on BAL and cell proliferation assays SWCNTs appeared to induce only transient inflammation while histology revealed a non-dose-dependent incidence of granulomas indicating a foreign body reaction. These granulomas were not uniformly dispersed throughout the lung and were also observed to resolve between 1 and 3 months (Warheit et al., 2004). Thus, the histology results appear to contradict the BAL and cell proliferation results indicating minimal inflammation and injury. This inconsistency is likely an artifact of dosage. CNTs aggregate extensively. A single bolus injected into the trachea of a mouse or rat effectively simulates inhalation of a dust, but CNTs do not behave solely like dust particles. This aggregation was apparent after injection of the 5 mg dosage when 15% of rats died due to mechanical blockage of the upper airways by CNT aggregation despite solubilization with surfactant (Warheit et al., 2004). Thus, the tracheal instillation is not ideal for modeling exposure to CNTs regardless of purity or source.

The previous studies used intratracheal injections, but the histological analysis showed that this method leads to CNT aggregation and in some cases death (Warheit et al., 2004). Therefore, pharyngeal aspiration of purified SWCNT (>99%) in C57BL/6 mice was used to model the effects of SWCNT inhalation (Shvedova, Kisin, Mercer, Murray, Johnson, Potapovich, Tyurina, Gorelik, Arepalli, Schwegler-Berry, Hubbs, Antonini, Evans, Ku, Ramsey, Maynard, Kagan, Castranova, & Baron, 2005). This technique involves the administration of a 50 μl drop of material on the back of the tongue of mouse allowing it to form an aerosol. The results of 0, 10,

20, or 40 μg/mouse were assessed by BAL, LDH, and histopathology. The BAL was assayed for tumor necrosis factor α, interleukin 1β, and transforming growth factor β1 inflammatory cytokines. In vitro experiments on RAW 264.7 macrophages were also performed investigating the effect of SWCNTs. Shvedova et al. (2005) found that the SWCNTs formed either compact aggregates or dispersed into the lungs. In addition, the inflammatory cytokine tumor necrosis factor α and interleukin 1β increased in a dose-dependent manner, with SWCNTs corresponding to neutrophil recruitment while transforming growth factor 1β increased at later time points (3–7 days) corresponding to macrophage recruitment. However, the acute inflammation resolved within 2 months. Dose-dependent granuloma formation was observed within 7 days of SWCNT treatment and was not resolved after 60 days. The SWCNTs were observed to elicit an acute inflammatory response while the dose-dependent granuloma formation occurred primarily in sites of dispersed SWCNT exposure (Shvedova et al., 2005). Interestingly, fibrosis was observed at sites distant from deposited aggregates that did not experience persistent inflammation typically consistent with fibrotic response. Ultrafine carbon black and silica did not induce alveolar wall thickening or granuloma formation and stimulated a much lower inflammatory response when administered via pharyngeal aspiration. Therefore, Shvedova et al. (2005) concluded that SWCNTs introduced to C57BL/6 mice via pharyngeal aspiration induced acute inflammation and elicited the early appearance of granulomas and fibrotic response. The doses chosen for this experiment were based on the Occupational Safety and Health Administration's permissible exposure limit to investigate the effects of occupational exposure and were equivalent to ~0.5 mg/mouse.

The work performed by Lam et al. (2004) was supported by Jia et al. (2005) who exposed alveolar macrophages to SWCNTs in vitro. These SWCNTs were made by electric arc discharge and purified to ~90% purity, with amorphous carbon the major impurity. The catalyst metals nickel, yttrium, and iron were also present in trace amounts. These SWCNTs showed approximately fourfold higher toxicity to alveolar macrophages than SiO_2 at 22.60 μg/cm^2 as determined by MTT dye reduction (Jia et al., 2005). In addition, SWCNTs decreased the ability of alveolar macrophages to phagocytose latex beads at 0.38 μg/cm^2, which is one full order of magnitude lower than other nanomaterials such as fullerenes also investigated. Alveolar macrophages treated with SWCNTs also demonstrated a dose-dependent shift from phagocytic to non-phagocytic cells (Jia et al., 2005). Evidence of apoptosis was seen at doses as low as 0.76 μg/cm^2 and became apparent at 3.06 μg/cm^2 when phagosomes and vacuoles were evident along with endoplasmic reticulum swelling. Therefore, Jia et al. (2005) concluded that SWCNTs were toxic toward alveolar macrophages and that individual toxicities of nanomaterials needed to be assessed.

Murine alveolar macrophages RAW 267.9 were exposed to SWCNTs in vitro (Soto, Carrasco, Powell, Garza, & Murr, 2005). These SWCNTs contained nickel catalyst and demonstrated bundle- or rope-like aggregates. The aggregate size varied from 2 to 20 μm for the bundles with 10–200 nm diameters. The toxicity of SWCNTs to RAW 267.9 paralleled

that of chrysotile asbestos in vitro, which forms bundles of 0.5–15 μm and has fiber diameters 15–40 nm. (Soto et al,. 2005). However, Soto et al. point out that fibrous asbestos can align with laminar air flow in the lungs but that SWCNTs would have to disperse from the aggregates to behave similarly. Also, nanoparticles have a high percentage of exhaled fractions ~80% (Lippmann, 1986) making further inferences from this in vitro data difficult. Thus, in vitro studies are limited in their application to inhaled SWCNT toxicity in vivo.

In Vivo Studies: MWCNTs

Despite the aggregation issues evident in the previous studies, intratracheal instillation was used to investigate the effects of MWCNTs solubilized with detergent on guinea pigs (Huzcko, Lange, Bystrzejewski, Baranowski, Grubek-Jaworska, Nejman, Przybylowski, Czuminska, Glapinski, Walton, & Kroto, 2005). This study used BAL, lung resistance, and histology to assess pulmonary damage at 90 days. Five different MWCNTs were instilled including commercially available CNT and CNT produced by arc discharge as well as CVD. Alveolar macrophages were identified in the BAL of guinea pigs exposed to MWCNTs (Huzcko et al, 2005). In addition, numerous lesions were identified by histology, and lung resistances were abnormal for all animals exposed to MWCNTs. These results are in contrast to Warheit et al. (2004) who found that BAL and cell proliferation contradicted histology. Drawing on conclusions from their previous study, Huzcko et al. (2005) concluded that exposure time is a critical determinant in pulmonary toxicity of MWCNTs. This conclusion supports previous theories that biopersistence is a major factor determining toxic effects of an inhaled particle.

Guinea pigs intratracheally instilled with 12.5 mg of commercially attained MWCNTs solubilized with detergent showed increased levels of interleukin 8 (Grubek-Jaworska, Nejman, Czuminska, Przybylowski, Huczko, Lange, Bystrzejewski, Baranowski, & Chazan, 2006). MWCNTs from NanoLab synthesized via chemical vapor deposition at 95% purity showed increased levels of neutrophils, macrophages, and lymphocytes in the BAL after 3 months; MWCNTs from NanoLab at 80% purity resulted in increased macrophages and eosinophils only. MWCNTs from Showa Denko did not show any difference in BAL cell population from control animals injected with phosphate buffer saline containing Tween detergent (Grubek-Jaworska et al., 2006). While all animals showed lung lesions regardless of MWCNT source, the MWCNTs obtained from Showa Denko elicited the most extensive pathology determined by histology. The NanoLab 95% purity and Showa Denko MWCNTs were reported as being iron free while the NanoLab 80% purity CNTs contained <0.01 parts per million iron (Grubek-Jaworska et al., 2006).

Muller et al. (2005) also investigated the effects of various doses of inhaled MWCNTs at 60 days. Female Sprague-Dawley rats were intratracheally instilled with 0.5, 2, or 5 mg of purified MWCNTs or ground MWCNTs, which were chosen to investigate the effects of aggregation versus dispersion in the rat lungs. Muller et al. (2005) used both carbon black and asbestos as controls allowing comparison between ultrafine particles and fibers. The effects of MWCNT exposure were assayed

using BAL, histology, and biopersistence. MWCNTs were found to be slowly cleared from rat lung, with 81% of the initial dose remaining at 60 days for intact MWCNT and 36% remaining for the ground MWCNTs. Grinding did not significantly reduce aggregation in vivo; however, the ground MWCNTs did demonstrate more uniform dispersion in the lung compared to intact MWCNTs and prevented intraluminal granulomas (Muller et al., 2005). As with previous studies, MWCNTs still exhibited aggregation despite use of surfactant (Muller et al., 2005; Huzcko et al., 2005; Huczko et al., 2001). Tumor necrosis factor α was found to be elevated in rats exposed to asbestos, carbon black, MWCNTs at 2 mg, and ground MWCNTs at 0.5 and 2 mg during acute inflammation. After 60 days, tumor necrosis factor α production, which is a known pro-inflammatory and pro-fibrosis cytokine, in the BAL was evident only in rats treated with asbestos or ground MWCNTs at 0.5 and 2 mg (Muller et al., 2005). In vitro peritoneal macrophages produced tumor necrosis factor α in response to asbestos, carbon black, and ground MWCNTs but not intact MWCNTs. This increase in tumor necrosis factor α production was paralleled by a dose-dependent increase in toxicity assessed by LDH release (Muller et al., 2005). MWCNT aggregates accumulated in the airways of Sprague-Dawley rats led to collagen-rich granulomas in the bronchial lumen. Ground MWCNTs were better dispersed throughout the rat lung eliciting an inflammatory and fibrotic response. Both ground and intact MWCNTs stimulated increased tumor necrosis factor α. Therefore, Muller et al. (2005) called for restrictive measures to reduce worker exposure during manufacturing and research.

These previous in vivo studies demonstrated that intratracheal instillation of CNTs can cause lethality due to mechanical blockage resulting from CNT aggregation in addition to granuloma formation and fibrosis. Nitrogen doped MWCNTs did not induce lethality in CD-1 nude mice after introduction at doses up to 5 mg/kg (Carrero-Sanchez, Elias, Mancilla, Arrellin, Terrones, Laclette, & Terrones, 2006). The MWCNTs were synthesized using chemical vapor deposition with ferrocene ($FeCp_2$) as a catalyst. Nitrogen doped MWCNTs were synthesized via a similar process resulting in 2–4 wt% nitrogen (Carrero-Sanchez et al., 2006). The iron content for both types of CNTs was 2–2.5 wt% and both CNTs were oxidized via acid treatment increasing surface hydrophilicity. A variety of administration routes were used including nasal, oral, intratracheal, and intraperitoneal. However, neither oral nor intraperitoneal injections resulted in significant host response up to 30 days (Carrero-Sanchez et al., 2006). In addition, the nasal injections at 1, 2.5, or 5 mg/kg either in a single bolus or dosed daily for 1 week did not result in nitrogen doped CNT deposition in the lungs or inflammation up to 30 days. Carrero-Sanchez et al. theorized that the lack of nitrogen doped CNTs and inflammation via nasal injections is likely due to entrapment in the mucosal linings of the nasal and upper respiratory tracts; however, no further investigation into the presence of nitrogen doped CNTs in these secretions was made (Carrero-Sanchez et al. 2006). Mice intstilled intratracheally with 1 mg/kg nitrogen doped CNTs showed no lung deposition, but the presence of nitrogen doped CNTs was detected at 2.5 and 5 mg/kg. However, no other gross toxicity was apparent in other organs (Carrero-Sanchez et al., 2006). The

lungs from mice with 2.5 mg/kg intratracheal instillation demonstrated aggregation of the nitrogen doped CNTs in bronchioles at 24 and 48 h as well as after 1 week. At 1 month, these mice demonstrated insignificant granuloma formation assessed by histology. The extremely high dose of 5 mg/kg led to time-dependent tissue infiltration and host inflammatory response (Carrero-Sanchez et al., 2006). Histology revealed that the inflammation was mediated primarily by lymphocytes, macrophages, and fibroblast proliferation. MWCNTs instilled intratracheally at 1, 2.5, and 5 mg/kg resulted in significant and immediate lethality of the mice (30, 60, and 90%, respectively) (Carrero-Sanchez et al., 2006). Dyspnea was the primary cause of death for these mice. Dose-dependent deposition was observed in the lung tissue via histology. In the mice that survived instillation, multiple granuloma formation was apparent in the lung interstitium at 15 days. Granuloma formation was also evident at early time points in mice dosed with 2.5 mg/kg (Carrero-Sanchez et al., 2006). Thus, both MWCNTs and nitrogen doped MWCNTs induced time- and dose-dependent pathological changes in the lung tissue of intratracheally instilled CD-1 nude mice. Carrero-Sanchez et al. (2006) theorized that this difference in pathology demonstrated by nitrogen doped MWCNTs and pristine MWCNTs was related to the ability to aggregate in solution with MWCNTs showing a higher propensity to form large aggregates. These aggregates likely resulted in the dyspnea-induced death of the mice instilled with MWCNTs. Carrero-Sanchez et al. (2006) claim that MWCNTs are more toxic than SWCNTs administered at higher doses in support of previous findings (Lam et al. 2004, Warheit et al. 2004) while nitrogen doped MWCNTs are less toxic. There was a significant length difference between the MWCNTs synthesized (450 μm long) and the nitrogen doped MWCNTs (300 μm long), which was not addressed in the experiment. Therefore, it appears that surface chemistry plays a significant role in the toxicity and pathology of MWCNTs, but the effect of CNT length on toxicity needs to be addressed.

In Vitro Studies: MWCNTs

The aspect ratio and surface area of MWCNTs were compared against carbon nanofibers and carbon black to determine their role in toxicity toward H596, H446, and Calu-1 human lung tumor cell lines in vitro (Magrez, Kasas, Salicio, Pasquier, Seo, Celio, Catsicas, Schwaller, & Forro, 2006). Cell viability for all lines decreased in a dose-dependent manner for the three carbon nanomaterials tested. H596 were the most sensitive to insult with MWCNTs up to 4 days while the H446 were the least sensitive. The nanofibers and MWCNTs were less toxic than carbon black at 0.002 and 0.02 μg/ml, with MWCNTs exhibiting the least toxicity toward H596 (Magrez et al., 2006). Therefore, Magrez et al. concluded that ultrafine carbon black particles are more toxic than nanofibers or MWCNTs. In addition, all three materials induced cell detachment and apoptosis evidenced by light microscopy and MTT dye reduction, respectively (Magrez et al., 2006). MWCNTs were acid treated to determine the effect of surface functionalization on lung cell toxicity. The acid treatment creates a more hydrophilic surface via the addition of carbonyl (–C = O), carboxylate (–COOH), or hydroxyl groups (–OH) (Magrez et al., 2006).

Toxicity toward H596 increased for both nanofibers and MWCNTs. This increase in toxicity is likely due to increased dispersion in aqueous media as a result of the acid treatment-dependent increase in hydrophilicity.

In contrast to the results observed by Carrero-Sanchez et al. (2006), Jia et al. (2005) observed that MWCNTs were less toxic than SWCNTs to alveolar macrophages at the same dose. The SWCNTs also exhibited a dose-dependent cytotoxicity compared to the relatively dose-independent cytotoxicity associated with the MWCNTs as shown by MTT. The MWCNTs were less toxic than SWCNTs but were still more toxic to alveolar macrophages than SiO_2 and fullerenes (Jia et al., 2005). In addition, MWCNTs impaired macrophage phagocytosis less than SWCNTs on a mass basis (Jia et al., 2005). However, MWCNTs induced similar apoptotic morphological changes as SWCNTs at 3.06 $\mu g/cm^2$ including condensed chromatin and organelles as well as cytoplasm vacuolization. Therefore, based on the experiment performed by Jia et al. (2005), MWCNTs appear less toxic than SWCNTs toward alveolar macrophages. It should be noted that the MWCNTs were >95% purity, with <3% amorphous carbon and ~0.6% nickel compared to the ~90% purity for SWCNTs. In addition, the MWCNTs were 10–20 nm in diameter and 0.5–40 μm long compared to 1.4 nm diameter and approximately 1 μm long (Jia et al., 2005). The effect these differences in size and aggregation states had on macrophage cytotoxicity was not addressed.

Soto et al. (2005) also investigated the effects of MWCNTs and ground MWCNTs on RAW 276.9 murine alveolar macrophages compared to chrysotile asbestos. The ground MWCNTs exhibited aggregations approximately 0.1–3 μm and 10–30 nm in diameter. Only about half of the ground MWCNT aggregates were CNTs. The other half was fullerenes (Soto et al., 2005). The aggregated MWCNTs were 1–3 μm long and 5–30 nm in diameter. As with carbon black and SWCNTs, both ground and aggregated MWCNTs demonstrated similar toxicity toward RAW 276.9 as chrysotile asbestos as determined by MTT (Soto, Carrasco, Powell, Murr, & Garza, 2006). Therefore Soto et al. recommended against inhaling MWCNTs (Soto et al., 2006, Soto et al., 2005).

Summary

Studies investigating the toxicity of inhaled CNTs have thus come to no consensus conclusions. Despite using various techniques such as surfactants (Huczko et al., 2001; Huczko et al., 2005; Muller et al., 2005; Warheit et al., 2004), sonication (Muller et al., 2005; Lam et al., 2004), or grinding (Muller et al., 2005), single and multiwalled CNTs aggregated in the lungs of guinea pigs, mice, and rats. The study by Shvedova et al. (2005) showed that even more physiologically relevant inhalation techniques such as pharyngeal aspiration lead to aggregation in vivo. In addition, intratracheal instillation and pharyngeal aspiration bypass the filtering effects of the nose and introduce the toxicant as one bolus. Physiologically relevant assays would instead expose animals to lower levels of CNTs in an inhalable formulation, which has not been feasible due to difficulty obtaining the large quantities of CNTs required for creating CNT-aerosol environments. Therefore, until these more relevant experiments are performed,

only specific conclusions relating to various exposure methods to either SWCNT or MWCNTs can be made. In addition, no long-term studies have been performed to determine the carcinogenic effect SWCNTs or MWCNTs may have on workers chronic exposed to these materials.

Skin Toxicity and Irritation

SWCNTs

CNTs used for drug delivery applications may come into contact with workers' or patients' skin in addition to the risk posed by inhalation. Proper precautions must be taken to prevent skin exposure if CNTs are highly toxic. Huczko and Lange also investigated the effects of CNTs on Draize albino rabbits (2001). Unrefined CNTs were injected into one eye of each rabbit and the irritation assessed at 72 h. The remaining eye served as the CNT control. No difference was found in the levels of irritation between SWCNTs and CNT-free soot. The effects of CNT skin exposure to humans were also investigated (Huczko & Lange, 2001). Filter paper was saturated with unrefined CNTs suspended in water and placed on the skin of 40 willing volunteers. After 96 h, no significant difference was observed between the CNT treatment and the CNT-free soot control. Based on the albino rabbit eye irritation results and the human skin contact results, Huczko and Lange (2001) concluded that CNTs do not require any special handling protocols to prevent skin contact and potential toxicity.

In vitro exposure of human HaCaT immortalized epidermal keratinocytes contradicted these initial findings by Huczko and Lange (2001). HaCaT cells were exposed to unrefined SWCNTs at doses ranging from 0.06 to 0.24 mg/ml for up to 18 h (Shvedova, Castranova, Kisin, Schwegler-Berry, Murray, Gandelsman, Maynard, & Baron, 2003). Oxidative stress was apparent at all time points after exposure to SWCNTs. Free radicals were observed by electron spin resonance 5 min after SWCNT addition (Shvedova et al., 2003). Other signs of oxidative stress included depleted levels of the antioxidant vitamin E, build-up of peroxidative byproducts, and the dose-dependent depletion of non-protein and protein thiol antioxidants such as glutathione. In addition to the oxidative markers, HaCaT morphology was significantly altered after 18 h exposure to even the lowest dose of SWCNTs at 0.06 mg/ml. This altered morphology was evident through cell toxicity. SWCNTs were not toxic up to 0.24 mg/ml at 4 h; however, viability decreased in a time-dependent manner after 4 h with a significant decrease in cell viability at 18 h (Shvedova et al., 2003). Therefore, these results indicate that exposure to SWCNTs may induce dermal toxicity and oxidative stress in exposed persons. However, Shvedova et al. (2003) reported the unrefined SWCNTs to contain 30% iron by mass. These iron atoms can catalyze a variety of reactive oxygen species via Fenton chemistry to produce superoxide or hydroxyl radicals (Valko, Morris, & Cronin, 2005). The oxygen-based radicals can then induce lipid oxidation resulting in lipid peroxide, which reacts with water to produce an alcohol group on the lipid and oxygen radical. Lipid peroxidation proceeds in this manner until an antioxidant scavenges a radical or two radicals meet. Cellular damage results when lipid oxidation creates a

sufficiently hydrophilic plasma membrane that eventually dissociates causing cell lysis. Thus, the oxidative stress and cellular toxicity observed by Shvedova et al. (2003) may have been induced by the iron impurities (~30% by mass).

Free radical production by SWCNTs was also observed by Manna et al. (2005). SWCNTs cultured with HaCaT human keratinocytes showed a dose-dependent increase in reactive oxygen species. The increase in free radical production was observed in conjunction with a dose-dependent decrease in cell viability via MTT dye reduction assay at SWCNT concentrations as low as 0.5 μg/ml. Activation of the nuclear factor kappa β signaling pathway was observed above 1 μg/ml. Time-dependent DNA binding and transcription initiation was dependent on IκBα degradation, which showed significant decreases after 6 h (Manna et al., 2005). Therefore, SWCNTs appeared to activate the nuclear factor kappa β via IKK phosphorylation and degradation followed by protein 65 translocation to the nucleus. Activation by nuclear factor kappa β has been observed in response to interleukin 8 (Manna et al., 2005). In addition, interleukin 8 release has been observed after incubation with MWCNTs (Monteiro-Riviere, Nemanich, Inman, Wang, & Riviere, 2005).

A549 human alveolar epithelial cells demonstrated a 50% reduction in cell viability after treatment with oxidized and sonicated SWCNTs via MTT dye reduction (Worle-Knirsch, Pulskamp, & Krug, 2006). However, reduction of a different tetrazolium salt (WST-1) by A549 showed no toxicity. The results of the WST-1 assay were confirmed by lactate dehydrogenase release, annexin-V/propidium iodide staining and analysis by flow cytometry as well as mitochondrial membrane potential measurements by fluorescence-activated cell sorting (Worle-Knirsch et al., 2006). The SWCNTs interact with MTT-formazan crystals that precipitate out of solution after reduction by mitochondrial dehydrogenases. No interaction is observed with water-soluble tetrazolium salts such as INT, WST-1, or XTT (Worle-Knirsch et al., 2006). The MTT-formazan crystals are either entrapped within SWCNT aggregates or bind to SWCNTs, but the precipitation of the crystals is critical for interference with the assay. Therefore, based on the multiple assays of cytotoxicity by Worle-Knirsch et al. (2006), SWCNTs are non-toxic to A549 alveolar epithelial cells. This discovery raises questions about other experimental observations where only MTT dye reduction is used to assess cytotoxicity. Therefore, at least two assays should be used to assess the cytotoxicity of CNTs toward cell lines to prevent false results such as those found by Worle-Knirsch et al. (2006).

Tian et al. (2006) investigated the structure–function effects of SWCNTs on human fibroblasts. In contrast to previous studies, only refined SWCNTs were tested and found to elicit the strongest response from fibroblasts of the five materials tested. A significantly lower concentration of refined SWCNTs (25 μg/ml) increased higher apoptosis and necrosis than 0.06 mg/ml of unrefined SWCNTs. Increasing cytotoxicity to human fibroblasts correlated with increasing surface area (Tian et al., 2006). In addition, surface chemistry was believed to play a key role in decreasing the toxicity of unrefined SWCNTs. These unrefined SWCNTs were able to aggregate decreasing surface area and size as well as decreasing cytotoxicity. The purified SWCNTs were observed to disperse with significantly less

aggregation. Tian et al. (2006) therefore theorized that the transition metal catalysts play opposing roles in cytotoxicity, allowing the generation of free radicals in unrefined SWCNTs increasing toxicity but also allowing aggregation decreasing surface area and toxicity. The expression of several proteins that are involved with adhesion was observed to decrease after treatment with SWCNTs, which may be a result of the hydrophobic interaction between the dispersed, purified SWCNTs and the fibroblasts. Focal adhesion kinase distributed around the nucleus after treatment with SWCNTs instead of dispersed throughout the cell at sites of focal adhesion (Tian et al., 2006). In addition, p-cadherin and f-actin distribution were altered in response to purified SWCNTs. P-cadherin links the actin cytoskeleton to the plasma membrane indicating that SWCNTs induce detachment of adherent cells as observed by Tian et al. (2006). Therefore, purified SWCNTs induced higher toxicity than unpurified SWCNTs, indicating both surface chemistry and surface area are important factors determining cytotoxicity of nanomaterials.

MWCNTs

Monteiro-Riviere et al. (2005) investigated the response of human epidermal keratinocytes exposed to various doses of purified MWCNTs synthesized via plasma-enhanced chemical vapor deposition using an iron catalyst. Human epidermal keratinocytes were observed to internalize MWCNTs in both free cytoplasm and vacuoles; however, the presence of MWCNTs in the free cytoplasm was rarer than in vacuoles. Internalization of MWCNTs was observed to be time- and dose dependent (Monteiro-Riviere et al., 2005). Keratinocyte viability was found to exhibit slight dose- and time dependence at 24 and 48 h by neutral red dye assay. Interleukin 8 release was significantly higher than controls after 8 h and was also higher in cells treated with the highest dose of MWCNTs (0.4 mg/ml). MWCNT internalization was lower and interleukin 8 release was not different from controls when a 0.2 μm filter was used to remove MWCNT aggregates. Therefore, the study by Monteiro-Riviere et al. (2005) revealed that epidermal keratinocytes can internalize MWCNTs without modifications or adjuvants and release interleukin 8 in response to treatment with MWCNTs, which is known to participate in dermal irritation. However, Moteiro-Riviere et al. point out this interleukin 8 release may be dependent on MWCNT association with the plasma membrane in addition to the internalized MWCNTs.

The phenotypic response of human skin fibroblasts to MWCNTs at 0.06 and 0.6 μg/ml was characterized by gene expression arrays (Ding, Stilwell, Zhang, Elboudwarej, Jiang, Selegue, Cooke, Gray, & Chen, 2005). MWCNTs induced cell cycle arrest, apoptosis, necrosis, and decreased proliferation. These changes in cell viability were observable through staining for necrosis/apoptosis, the stage of cell cycle, and live/dead staining in addition to changes in gene expression. Ding et al. (2005) theorized that the fibroblast response may be mediated by the type I interferon response, which is known to involve apoptosis, cell death, and decreased proliferation. Interestingly, different sets of genes were affected by the low or high dose of MWCNTs, but the genes induced by both MWCNTs and multiwalled carbon nanoonions were similar at each dose indicating that the cellular response was similar to

different materials at different doses. The low dose of MWCNTs altered metabolism-related genes such as Golgi transport pathways and cell cycle progression with the exception of protein ubiquitination (Ding et al., 2005). MWCNTs shifted the cellular response from metabolism-related genes to inflammation and immune-related genes at 0.6 μg/ml. The majority of genes upregulated by MWCNTs were involved in the innate immune pathway. Ding et al. (2005) also observed that the fibroblasts' response to insult with MWCNTs was similar to viral infection, which they theorized may be due in part to similar size. Tian et al. (2006) also investigated the effects of MWCNTs (5 nm × 5 μm) on human fibroblasts. Purified MWCNTs were significantly less toxic than purified SWCNTs and more toxic than only carbon graphite. Carbon black, activated carbon, and purified SWCNTs were more toxic than purified MWCNTs, respectively (Tian et al., 2006). These results reinforced their conclusion regarding increased surface area and decreased aggregation leading to higher toxicity to human fibroblasts.

Cytotoxicity

SWCNT Toxicity to Epithelial Cells and Keratinocytes

In addition to HaCaT human keratinocyte cells, Manna et al. (2005) also observed a dose-dependent decrease in cell viability in HeLa human tumor-derived cervix epithelial cells and A549 and H1299 human lung carcinoma in response to SWCNTs.

SWCNTs were observed to stimulate apoptosis, detachment, and decrease proliferation of human embryonic kidney (HEK) 293 cells (Cui, Tian, Ozkan, Wang, & Gao, 2005). These effects of SWCNTs on HEK 293 were dose- and time dependent. HEK 293 attempted to isolate the SWCNTs by secreting 20–30 kDa proteins that allowed the cells to attach to the aggregated SWCNTs and form nodules (Cui et al., 2005). SWCNTs also appeared to arrest cell cycle progression by upregulating protein 16, a known regulator of the cyclin-dependent kinase pathway, which regulates cell cycle. In addition, SWCNTs induced DNA fragmentation between 1 and 5 days, chromatin condensation, morphological changes, and apoptotic gene upregulation (Cui et al., 2005). Also several proteins involved in cellular adhesion showed downregulation by gene chip array similar to other work from Gao's group (Tian et al., 2006). SWCNT aggregation was observed; however, HEK 293 not interacting with SWCNTs appeared normal and exhibited behavior similar to negative controls (Cui et al., 2005). Therefore, SWCNTs appear to exhibit dose- and time-dependent toxicity toward human embryonic kidney 293 evidenced by apoptosis, increased detachment of adherent cells, and decreased proliferation (Cui et al., 2005). Cui et al. theorized that apoptosis was a protective measure after the embryonic kidney cells attempted to internalize and isolate the SWCNTs.

SWCNT Toxicity to Monocytes and Macrophages

Mouse peritoneal macrophage-like cells actively phagocytosed SWCNTs with and without surfactant to aid in CNT dispersion (Cherukuri, Bachilo, Litovsky, & Weisman, 2004). No visible changes in macrophage behavior or morphology were apparent; however, no specific viability assays such as MTT or live/dead staining were performed. Temperature-dependent

phagocytosis was observed supporting previous observations (Matsui, Ito, & Ohnishi, 1983) but contrasting with Pantarotto et al. (2004) who found that functionalized SWCNTs penetrated macrophages in a temperature-independent manner. Despite high levels of what appeared to be phagocytosis and fluorescence, no toxicity was apparent.

The effect of iron impurities in SWCNT on RAW 264.7 murine macrophages was also investigated (Kagan, Tyurina, Tyurin, Konduru, Potapovich, Osipov, Kisin, Schwegler-Berry, Mercer, Castranova, & Shvedova, 2006). The unpurified SWCNTs contained 26 wt% iron while the purified contained 100-fold less (0.26 wt%). As expected, the unpurified SWCNTs produced significantly higher levels of hydroxyl radicals in the presence of zymosan-activated RAW 264.7. High iron levels in SWCNTs were also responsible for converting superoxide generated by the xanthine/xanthine oxidase system into highly reactive hydroxyl radicals (Kagan et al., 2006). Interestingly, neither purified nor non-purified SWCNTs were capable of stimulating intracellular superoxide or nitric oxide production. Signs of oxidative stress were evident in the macrophages (Kagan et al., 2006). Glutathione levels were depleted after incubation with SWCNTs containing high levels of iron. In addition, the level of lipid peroxides, markers of lipid oxidation, was increased after treatment with unpurified SWCNTs. Based on these results, Kagan et al. (2006) concluded that toxicology studies utilizing non-purified SWCNTs should factor in the effect of radical-producing impurities such as iron. No intracellular radicals were produced in RAW 264.7, but extracellular radical generation and intracellular depletion of antioxidants coupled with increased signs of lipid peroxidation indicate that unpurified SWCNTs induce higher toxicity than purified SWCNTs. Kagan et al. (2006) theorized that this change in redox state may account for the fibrotic response observed after intratracheal instillation. This theory is supported by Shvedova et al. (2005) who observed that SWCNTs stimulated release of transforming growth factor β and interleukin 10 from RAW 264.7, which are both anti-inflammatory and pro-fibrogenic. This pro-fibrotic response is believed to stem from low levels of phagocytosis of SWCNTs. Typically, increased oxidative burst is observed after phagocytosis of foreign material such as bacteria that usually results in destruction of the foreign species (Forman & Torres, 2002). Increased apoptosis is usually concomitant with this increased oxidative burst (DeLeo, 2004); however, neither Shvedova nor Kagan observed increased RAW 264.7 apoptosis after stimulation with SWCNTs (Shvedova et al., 2005; Kagan et al., 2006), and Kagan et al. (2006) observed no increase in intracellular superoxide or nitric oxide production indicating little phagocytosis. Adsorption of phosphatidylserine to the surface of SWCNTs stimulated phagocytosis by RAW 264.7; however, phosphatidylserine is a known activator of intracellular free radicals, which may further increase toxicity and oxidative stress. Therefore, the fibrosis seen after instillation of SWCNTs may be reduced by increased phagocytosis (Kagan et al., 2006).

MWCNT Toxicity to Monocytes and Macrophages

The work by Muller et al. illustrated the difference CNT length can have on lung toxicity and inflammatory response. This length dependence was

further investigated by Sato et al. (2005). MWCNTs were synthesized via chemical vapor deposition at approximately 98% purity after purification. Concentrated acid and ultrasonication were used to cleave the MWCNTs. Two populations were generated at 220 and 825 nm. The two lengths stimulated the human monocytic THP-1 cell line to produce the inflammatory cytokine tumor necrosis alpha in similar levels, which were significantly lower than those induced by the FSL-1 lipopeptide (Sato et al., 2005). The 825 nm long MWCNTs showed significantly higher aggregation levels in phosphate buffered saline in vitro, so 5, 50, and 500 ng/ml concentrations were used. In vivo tests were also performed to determine the effects of CNT length on inflammatory response. Six-week-old Wistar rats were injected with 0.1 mg of 220 or 825 nm MWCNTs intraperitoneal (Sato et al., 2005). Granulation tissue containing macrophages, fibroblasts, and foreign body giant cells was observed around aggregates of both 220 and 825 nm MWCNTs. More 220 nm MWCNTs were observed phagocytosed by macrophages than 825 nm MWCNTs. The inflammatory response to the 220 nm MWCNTs was less for the shorter CNTs. This inflammatory response to the 220 nm long MWCNTs was almost completely resolved while no significant change was observed for 825 nm MWCNTs (Sato et al., 2005). Of the 825 nm CNTs visible within phagocytic cells the majority were not surrounded by membranes indicating cytoplasmic localization. Sato et al. theorized that the shorter 220 nm MWCNTs dispersed better due to Brownian motion and physicochemical properties. The 825 nm MWCNTs exhibit a bend in the middle that is thought to aid in aggregation making phagocytosis more difficult. Therefore, length and length-dependent physicochemical properties can play an important role in the host inflammatory response to MWCNTs in vitro and in vivo.

SWCNT Toxicity to T Cells and Lymphocytes

Promyelocytic HL60 and Jurkat T cells endocytosed purified, oxidized, and sonicated SWCNT conjugated to fluorescein isothiocyanate (Kam, Jessop, Wender, & Dai, 2004). SWCNTs conjugated to streptavidin were also endocytosed. Endocytosis was time dependent increasing up to 4 h for both SWCNT species. No toxicity to HL60 was observed after 24 or 48 h from oxidized, fluorescein-, or biotin-conjugated SWCNTs. The biotin-conjugated SWCNT complexed with streptavidin showed dose-dependent toxicity based on the amount of streptavidin loaded (Kam et al., 2004). These results were consistent throughout other non-lymphocyte cell lines such as 3T3 fibroblasts and Chinese hamster ovary cells (Kam et al., 2004). Kam et al. theorized that the uptake of SWCNT was via endocytosis since no fluorescence was observable at 4°C consistent with temperature-dependent endocytosis (Cherukuri et al., 2004; Matsui et al., 1983).

Koyama et al. (2006) investigated the effects purified SWCNTs have on $CD4^+$ and $CD8^+$ T lymphocytes in BALB/c mice up to 3 months. These SWCNTs were synthesized via chemical vapor deposition and were observed to aggregate into bundles. An increased $CD4^+/CD8^+$ T-cell population was evident 1 and 3 weeks after 2 mg was subcutaneously implanted with granulomas were evident after 3 weeks (Koyama et al., 2006). The major histocompatibility complex class I pathway was activated after 1 week and was followed by activation of the major histocompatibility class II pathway

after 2 weeks (Koyama et al., 2006). Thus, SWCNTs appear to elicit a foreign body reaction evidenced by increased levels of $CD4^+$, $CD8^+$, and $CD4^+/CD8^+$ (Rosenberg, Mizuochi, Sharrow, & Singer, 1987; Sprent, Schaefer, Lo, & Kormgold, 1986; Koyama et al., 2006). Koyama et al. theorized that as the granulomas formed around the SWCNTs the antigenic difference observed between the BALB/c mice and the SWCNT aggregates decreased due to isolation by the foreign body reaction. Koyama et al. (2006) used the findings from a previous study to infer that the biological response was less for CNTs than for asbestos (Koyama, Tanaka, Yamaguchi, Haniu, Takeichi, Konishi, & Koyama, 2002).

MWCNT Toxicity to T Cells and Lymphocytes

MWCNTs synthesized via chemical vapor deposition, obtained from NanoLab, induced time-dependent toxicity of Jurkat T leukemia cells (Bottini, Bruckner, Nika, Bottini, Bellucci, Magrini, Bergamaschi, & Mustelin, 2006). Oxidized MWCNTs with a highly hydrophilic surface were toxic to 80% of T cells at 400 μg/ml after 5 days. In contrast, pristine MWCNTs were toxic to less than half of Jukat T cells at the same time point (Bottini et al., 2006). A reduced dose of 40 μg/ml led to lower toxicity for both oxidized and pristine MWCNTs, but the trend of oxidized MWCNTs showing more toxicity was still evident. MWCNTs induced apoptosis in T cells in addition to morphological changes such as condensation of chromatin and membrane blebs (Bottini et al., 2006). Despite inducing toxicity, MWCNTs had no effect on T-cell receptor activation. Therefore, oxidized and pristine MWCNTs were toxic to Jurkat T cells in a dose- and time-dependent manner. In addition, both forms of MWCNTs were more toxic than carbon black. Bottini et al. (2006) theorized that the higher toxicity shown by oxidized MWCNTs is likely due to higher dispersion and higher concentration of free CNTs in solution. The pristine MWCNTs are highly hydrophobic and therefore aggregate extensively reducing their concentration in solution. Bottini et al. (2006) recommended using MWCNTs at concentrations lower than 40 μg/ml in addition to close monitoring of cell viability.

Koyama et al. (2006) used MWCNTs with different diameters (20–70 or 50–150 nm) to investigate the effect of size on biological response from BALB/c mice. $CD4^+$ and $CD8^+$ T cells decreased significantly 1 week after implantation with MWCNTs 20–70 nm in diameter, but after 2 weeks the $CD4^+$ and $CD4^+/CD8^+$ T cells increased significantly. Granuloma formation also increased with time after implantation (Koyama et al., 2006). The values for $CD4^+/CD8^+$ T cells were lower than controls 3 weeks after implantation with the 50–150 nm diameter MWCNTs. The smaller diameter MWCNTs inhibited major histocompatibility complex class I response. The 50–150 nm diameter MWCNTs inhibited both class I and class II type responses (Koyama et al., 2006). Therefore, Koyama et al. suggest using T-cell response as a measure of CNT-induced toxicity.

SWCNT Toxicity to Cardiac Myocytes, Chinese Hamster Ovary Cells, and Endothelial Cells

H9c2 (2-1) rat heart muscle cells showed no significant toxicity toward 0.2 mg/ml purified SWCNTs up to 3 days (Garibaldi, Brunelli, Bavastrello,

Ghigliotti & Nicolini, 2006). No visible morphological changes were evident up to 3 days via light microscopy. However, SWCNTs did bind to H9c2 and were not able to be washed off. After 3 days, the adherent H9c2 were trypsinized and re-seeded. H9c2 treated with SWCNTs exhibited irregular morphology, limited proliferative ability, and 25% higher cell death than negative control H9c2 not treated with SWCNTs (Garibaldi et al., 2006). Flow cytometry revealed a threefold increase in apoptotic cells after re-seeding and nearly a fourfold increase in late-apoptotic or necrotic cells. However, repeated re-seeding allowed the SWCNT-treated H9c2 to partially recover viability (Garibaldi et al., 2006). Therefore, highly purified SWCNTs appear to be non-toxic to rat cardiac myocytes at short time periods. In addition, CNTs are non-degradable leading to potential accumulation in the case of chronic administration. Garibaldi et al. theorized that the long-term toxicity observed for SWCNTs is induced by mechanical damage, which is supported by the flow cytometry data showing high numbers of necrotic or late apoptotic cells. Thus, the previously observed SWCNT toxicity is likely due to mechanical interactions rather than surface-mediated chemical interactions (Garibaldi et al., 2006).

SWCNTs are capable of blocking potassium channels in Chinese hamster ovary cells due to their fibrous nature (Park, Chhowalla, Iqbal, & Sesti, 2003). This blockage is believed to be actuated by stabilization of the inactive state evidenced by increased inactive potassium channels in Chinese hamster ovary cells treated with SWCNTs (Park et al., 2003). Size also played a role in the effectiveness at blocking potassium. SWCNTs that were 0.9 nm in diameter were more effective blocking ion channels than those with 1.3 nm diameter. Therefore, SWCNTs appear to block potassium ion channels due solely to their size (Park et al., 2003). This blockage could have significant consequences in systemic administration of SWCNTs for drug delivery purposes.

Three mixtures of MWCNTs showed no toxicity toward human umbilical vein endothelial cells (Flahaut, Durrieu, Remy-Zolghadri, Bareille, & Baquey, 2006). The MWCNTs were synthesized via catalytic chemical vapor deposition and consisted primarily of two- and three-walled CNTs, although two of the samples contained small populations of CNTs with as many as six walls. No cytotoxicity was reported by either MTT dye reduction or neutral red for the three MWCNT formulations at 0.5, 0.64, and 0.9 μg/ml, respectively. Human umbilical vein endothelial cells were chosen as a model because future pharmaceutical applications would likely include intravenous injections and also because these cells are particularly sensitive to environmental changes (Flahaut et al., 2006). No diameter-dependent trend in cytotoxicity or metabolic activity was apparent. Flahaut theorized that this lack of size dependence is due to cell size (30–50 μm) compared to MWCNT size (1–5 nm diameter). The length of the MWCNTs was reported between 5 and 100 μm (Flahaut et al., 2006). Therefore, MWCNTs appear to be non-toxic to endothelial cells based on Flahaut's work (2006).

SWCNT Biodistribution and Blood Clearance

The distribution of nanomaterials in vivo is critical to efficacy. Accumulation in vital organs such as the heart, lungs, liver, or kidneys can lead to

long-term toxicity especially for non-degradable CNTs. Furthermore, if CNTs do not distribute into the tissue or cells of interest then another choice of drug delivery vehicle is necessary. Circulation time in the bloodstream is also critical to the efficacy of CNT-based therapies. If CNTs are rapidly cleared from circulation in response to administration, the drug of interest will not reach its intended target and therapeutic concentrations of drug will not be achieved. Therefore, biodistribution and blood clearance are critical determinants to the success of CNT-based therapies.

SWCNTs functionalized with the metal chelator diethylenetriaminepentaacetic acid and chelated with indium (^{111}In) were rapidly cleared from the bloodstream of BALB/c mice preventing significant accumulation (Singh, Pantarotto, Lacerda, Pastorin, Klumpp, Prato, Bianco, & Kostarelos, 2006). The half-life of these functionalized SWCNTs was 3 h. Adding cationic charge to the ^{111}In-chelated SWCNTs had no significant affect on retention or accumulation (Singh et al., 2006). Therefore, excretion studies were performed with doses up to 400 μg using SWCNTs and MWCNTs with 60% of the diethylenetriaminepentaacetic acid chelated to ^{111}In. No acute toxicity was observed and analysis of the urine revealed that both the SWCNTs and MWCNTs were intact (Singh et al., 2006). Furthermore, no time-dependent organ accumulation was observed. Thus Singh et al. claimed this lack of tissue specificity was beneficial to further development of SWCNT-based therapies since no inherent tissue affinity needs to be addressed such as liver accumulation and toxicity. Compared to the currently used gene therapy vectors such as adenovirus (half-life = 2 min) (Alemany, Suzuki, & Curiel, 2000) or cationic liposplexes (half-life = 5–30 min) (Dash, Read, Barrett, Wolfert, & Seymour, 1999; Oupicky, Howard, Konak, Dash, Ulbrich, & Seymour, 2000), functionalized SWCNTs therefore represent a significant increase in circulation time (Singh et al., 2006).

MWCNT Free Radical Production or Scavenging in Cell Free Systems

Despite previous evidence showing free radical production in response to MWCNTs, purified MWCNTs containing 0.29% cobalt, 0.47% iron, and 0.05% aluminum did not generate any hydroxyl or carbon-based radicals in a cell free system (Fenoglio, Tomatis, Lison, Muller, Fonseca, Nagy, & Fubini, 2006). On the contrary, MWCNTs were found to be potent scavengers of hydroxyl radicals generated via iron-based Fenton chemistry rather than inactivating the iron particles (Fenoglio et al., 2006). MWCNTs also scavenged superoxide radicals generated by cytochrome. Fenoglio et al. (2006) believed that these scavenging properties of MWCNTs are similar to that shown by fullerenes whereby the radical is grafted onto the carbon tube structure. This theory is supported by an electron affinity similar to fullerenes (Fenoglio et al., 2006). Cell free systems are not complete models of oxidative stress or oxidative bursts in cell containing systems in vitro or in vivo; however, the scavenging properties of MWCNTs may reduce the presence of reactive oxygen species. Shvedova et al. (2005) observed that SWCNTs with similar metal impurities as those used by Fenoglio et al. did not generate superoxide radicals. This lack of oxygen

radicals may be due to scavenging ability or the absence of oxygen radicals generated by relatively pure CNTs (Fenoglio et al., 2006).

Summary

No clear consensus on structure–functional relationship regarding biocompatibility of SWCNTs or MWCNTs can be drawn from the present body of data. Different synthesis methods such as laser ablation, catalytic chemical vapor deposition, and arc discharge result in slightly different structures and different catalytic metals (Baddour & Briens, 2005; Dupuis, 2005). In addition, the different treatments post-synthesis such as oxidation with acid, sonication, or grinding have differing effects on both the individual CNTs and the aggregates. As shown by the previously discussed studies, both dispersed CNTs and aggregates contribute significantly to overall toxicity. Further research into the mechanism underlying free radical scavenging or production is needed before definite conclusions can be drawn regarding the effect CNTs have on cells. In addition, the response to dispersed CNTs needs more research. Finally, and perhaps most importantly, chronic exposure data is needed to determine potential carcinogenicity of CNTs. Since this nanomaterial does not appear to degrade, previous findings from asbestos and carbon black indicate that CNTs may be carcinogenic due to biopersistence. However, in the absence of definitive information, worker exposure to CNTs should be minimized through careful handling techniques and use of proper personal protective equipment.

Fullerenes (C_{60})

The discovery of a new carbon form called fullerenes in 1985 opened up a new field of research (Kroto, Heath, O'Brien, Curl, & Smalley, 1985). These new structures were comprised of carbon rings similar to graphite and containing odd-numbered rings such as pentagonal or heptagonal conferring a three-dimensional spherical shape. These structures have thus been called fullerenes or "Bucky Balls" (Figure 8.2) after Buckminster Fullerene, the designer of the geodesic dome. Fullerenes have remarkable mechanical properties such as high aspect ratio and modulus, but their physicochemical properties prevented their widespread application as pharmaceutical agents. Fullerenes are highly hydrophobic and thus are not soluble in aqueous solutions, which initially limited their application to biological systems. However, several solutions to this limited solubility have been derived. The use of surfactants or surface modifications has greatly increased the ability of fullerenes to solubilize in water (Cusan, Da Ros, Spalluto, Foley, Janot, Seta, Larroque, Tomasini, Antonelli, Ferraro, & Prato, 2002; Yamakoshi, Yagami, Fukuhara, Sueyoshi, & Miyata, 1994; Lin, Chyi, Wang, Yu, Kanakamma, Luh, Chou, & Ho, 1999) and brought more attention to their potential pharmaceutical uses. The focus of this chapter will be the observed properties of C_{60}-derived fullerenes in vivo and in vitro and the controversy regarding their behavior

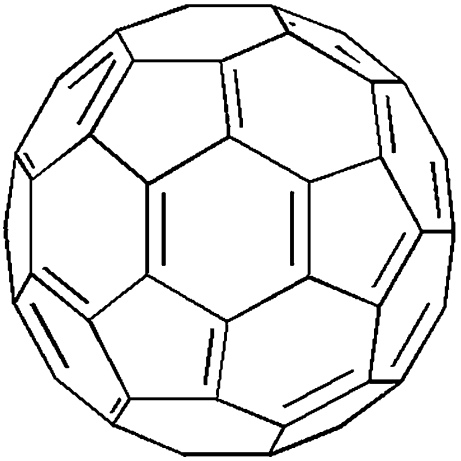

Figure 8.2 A C_{60} Buckminster fullerene.

as scavengers or producers of reactive oxygen species. The use of various cell and animal models is summarized in Table 8.1.

C_{60}

Nano-C_{60} Cytotoxicity – Effect of Reactive Oxygen Species and Lipid Oxidation

The addition of fullerenes to water forms marginally soluble nanoscale aggregates termed "nano-C_{60}." Sayes et al. (2004) found that nano-C_{60} was soluble at 50 mg/l (50 ppm). This formulation was then used to determine the toxicity against HepG2 human liver carcinoma and human dermal fibroblasts. The non-functionalized nano-C_{60} were found to be lethal to 50% of human dermal fibroblasts (LD_{50}) at 20 parts per billion (ppb). The aggregates were shown to be toxic by treatment of cells with the centrifuged pellet containing the fullerenes. The pellet had identical toxicity to cells as the original solution (Sayes et al., 2004). No change in mitochondrial activity was evident via MTT assay and no change in DNA concentration was apparent indicating that membrane damage was likely the cause of cytotoxicity. These experiments were repeated with the addition of neuronal human astrocytes (Sayes, Gobin, Ausman, Mendez, West, & Colvin, 2005). LDH measurements were obtained after 48 h; LD_{50} values were determined as 20 ppb for fibroblasts, 50 ppb for HepG2, and 2 ppb for astrocytes (Sayes et al., 2005). Since macrophages are the primary phagocytic population in the body and the cell type likely to be in intimate contact with fullerenes, Fiorito et al. (2006) investigated the response = of human monocyte-derived macrophages treated with an unspecified amount of C_{60}. The fullerenes partially activated the macrophages and stimulated a negligible amount of apoptosis as determined by propidium iodide staining. Interestingly, the graphite controls showed the highest level of macrophage activation and apoptosis (Fiorito et al., 2006). However, Fiorito et al. (2006) were cautious in their conclusions stating the toxicity of C_{60} is difficult to assess due to numerous issues such as aggregation, exposure to UV. C_{60} was found to localize to the nuclear membrane and nucleus in addition to the cytoplasm and secondary lysosomes (Porter,

Table 8.1 Summary of cell and animal models used for assessing fullerene (C_{60}) biocompatibility.

Fullerene	Species	Cell	Reference
C_{60}	human	HepG2 hepatoma	Sayes et al., 2004
		dermal fibroblasts	
		neuronal astrocytes	Sayes et al., 2005
		monocyte derived macrophages	Fiorito et al., 2006
C_{60} + surfactant	human	monocyte derived macrophages	Fiorito et al., 2006
	murine	SLC-ICR midbrain cells	Tsuchiya et al., 1996
		SLC-ICR embryos[a]	
	sheep	red blood cells	Yamakoshi et al., 1994
C_{60}-COOH	human	HeLa S3 cervic uteri tumor	Tokuyama et al., 1993
		Hela cervic uteri tumor	Yang et al., 2002
		Hep3B hepatoma	Huang et al., 1998
		peripheral blood mononuclear	Monti et al., 2000
		MCF7 breast cancer	Bosi et al., 2004
		HepG2 hepatoma	
		ddY mice[a]	Yamago et al., 1995
	murine	neocortical cells	Dugan et al., 1997
		L929 fibroblasts	Nakajima et al., 1996
	rat	Sprague-Dawley[a]	Rajagopalan et al., 1996
			Lin et al., 1999
	porcine	LLC-PK1 renal proximal tubular	Bosi et al., 2004
C_{60}-OH	human	umbilical vein endothelial	Yamawaki and Iwai, 2006
C_{60}-PEG[b]	murine	CDF1 mice[a]	Tabata et al., 1997
	rat	Sprague-Dawley cerebral cortical	Cusan et al., 2002

[a] *In vivo* study
[b] Poly(ethylene glycol)

Muller, Skepper, Midgley, & Welland, 2006). C_{60} also localized to the plasma membrane, which supports other observations that C_{60} toxicity is mediated by lipid oxidation. In addition, the presence of C_{60} in the secondary lysosome could lead to further oxidative damage to the cell if lipid oxidation results in the lysis of the lysosome causing highly reactive species to enter the intracellular milieu (Porter et al., 2006). The presence of C_{60} in the nucleus indicated there might be an alternative uptake pathway. Large C_{60} crystals were detected in the lysosome, which degraded into finer particles (Porter et al., 2006). This increase in C_{60} surface area could increase the production of ROS leading to lipid oxidation and ultimately

cell death. Fiorito et al. (2006) observed that murine macrophages showed no increase in nitric oxide release after stimulation with nano-C_{60}. These macrophages were previously treated with lipopolysaccharide, which is a potent activator of inflammation. Thus, no increase in nitric oxide production reveals that nano-C_{60} does not stimulate an inflammatory response. However, these macrophages did increase NO release in response to stimulation with graphite particles (Fiorito et al., 2006). This lack of inflammatory response was likely due to low levels of phagocytosis of the nano-C_{60}. More experiments investigating macrophage phagocytosis of C_{60} and potential reactive oxygen species generation or scavenging by fullerenes inside the cell are needed to better resolve the effect fullerenes have on the inflammatory response.

C_{60} can absorb up to 34 methyl radicals (Krusic, Wasserman, Keizer, Morton, & Preston, 1991). This ability to terminate free radical reactions is critical in vivo where lipid oxidation propagates nearly unchecked. Lipid oxidation is instigated by attack from an oxygen radical creating a lipid radical. This lipid radical reacts with oxygen to create lipid peroxide, which is hydrophilic. The accumulation of lipid peroxides eventually leads to dissociation of the lipid membrane resulting in cell death unless a scavenger intercedes or two peroxide radicals meet initiating termination (Wang, Tai, Lee, Kanakamma, Shen, Luh, Cheng, & Hwang, 1999). The role of C_{60} in lipid oxidation was investigated by Wang et al. (1999). Free radicals were created by the xanthine oxidase system that oxidizes xanthine into uric acid and superoxide radical (O_2^-) via the iron-based Fenton reactions. Lipid oxidation was measured by changes in absorbance of a liposome-encapsulated dye that leaked into the media as the liposome membrane was oxidized. Lipid oxidation increased with increasing iron concentration evidenced by higher absorbance readings (Wang et al., 1999). This membrane leakage was significantly reduced by 0.5 mol% C_{60}, which was more effective at preventing lipid oxidation than vitamin E (Wang et al., 1999). This observation is not surprising since C_{60} can potentially add up to 34 radicals *per molecule* (Krusic et al., 1991) versus just one radical per molecule of vitamin E.

Sayes et al. (2004) found that toxic concentrations of nano-C_{60} were indicative of membrane damage rather than mitochondrial dehydrogenase leakage protein or DNA oxidation in human HepG2, dermal fibroblasts, and astrocyte cells. Leaky plasma membranes were observed via LDH release and diffusion of various molecular weight fluorescent dyes into the cells. The production of superoxide radicals by nano-C_{60} was confirmed by the xanthine/xanthine oxidase assay as well as the iodophenol photometric assay. Nano-C_{60} was capable of superoxide radical production, but fully hydroxylated C_{60} was not indicating that the ability of radical production decreases with increasing functionality (Sayes et al., 2004). Therefore, the cytotoxicity of nano-C_{60} likely occurs through lipid oxidation and membrane dissociation. This theory was supported by the same group using two methods to analyze lipid oxidation (Sayes et al., 2005). Lipid oxidation was measured by tracking the production of free radicals resulting from malondialdehyde oxidation. There was a small increase in free radical production resulting from 0.24 to 4.8 ppb nano-C_{60} with a significant increase at 240 and 2,400 ppb. A similar trend

was observed for the naturally occurring antioxidant glutathione (Sayes et al., 2005). The lipid oxidation was also visualized through the use of C11-BODIPY$_{581/591}$dye. The dye turned from red to green at the plasma fs acid prevented this lipid oxidation. These findings contradict those by Wang et al. (1999) who found that 0.5 mol% C_{60} decreased lipid oxidation.

C_{60} + Surfactant Cytotoxicity – Effect of Reactive Oxygen Species and Lipid Oxidation

The addition of surfactants such as Triton X-100, cyclodextrin, or polyvinylpyrrolidone (PVP) is a method of preventing aggregation and formation of nano-C_{60} (Yamakoshi et al., 1994). Tsuchiya et al. (1996) found that treating mouse embryos with C_{60} solubilized with PVP increased the extent of midbrain cell differentiation but decreased the number of differentiated midbrain cells. C_{60} and PVP also showed significantly higher toxicity toward in vitro culture of midbrain cells dissociated from embryos removed from SLC-ICR mice at day 11 of development than PVP controls. Differentiation was also decreased in a dose-dependent manner in addition to the toxic effect. The antioxidant enzymes catalase and superoxide dismutase were added to in vitro cultures to determine if C_{60} was damaging cells through peroxide or superoxide radical production, respectively. No difference in cell differentiation was observed after enzyme addition; however, the cell proliferation previously observed to decrease was rescued (Tsuchiya et al., 1996). In vivo studies were also performed. Pregnant mice were injected with 137 mg/kg of C_{60} with PVP and embryos inspected after 18 h. All of the embryos injected with C_{60} were dead and showed signs of abnormal development (Tsuchiya et al., 1996). The lower dose of 50 mg/kg was found to distribute evenly throughout the embryo based on color and resulted in 50% of the embryos demonstrating head and tail developmental abnormalities. Upon inspection of the yolk sac, embryos treated with 50 mg/kg showed decreased vasculature and a "shrunken membrane" (Tsuchiya et al., 1996). Only one embryo injected with 25 mg/kg showed abnormal development. The control PVP or water injections resulted in no visible deformations (Tsuchiya et al., 1996). The proliferation and differentiation of midbrain cells were also found to be impaired by C_{60} injection at and above 25 mg/kg in vivo. Thus, C_{60} appears to damage cells via hydroxyl or superoxide radicals, but the effect on differentiation of midbrain cells remains unresolved.

A sodium salt of benzoic acid-derived C_{60} was solubilized in both water and the polar solvent dimethylsulfoxide with PVP or Triton X-100 to determine the effect of ultraviolet light (Orfanopoulos & Kambourakis, 1995). Oxygen was bubbled through the solution while a 300 W Xenon lamp irradiated the solution with ultraviolet light. Two photooxygenation products were obtained differing in stereochemistry. These two products were obtained in the same ratio given by reaction with Rose-Bengal, which is a known producer of singlet oxygen. Thus Orfanopoulos and Kambourakis (1995) showed that fullerenes have the potential to be a sensitizer given UV exposure. However, C_{60}'s mechanism of radical propagation in vitro and in vivo remains unknown.

Yamakoshi et al. (1994) challenged sheep red blood cells with C_{60} solubilized in 5% PVP for 30 min. C_{60} was not found to be hemolytic in the solubilized form compared to the positive control digitonin. The hemolytic dose for 50% of the red blood cells for digitonin was 4 μg/ml compared to >200 μg/ml for C_{60}. Given the data supporting reactive oxygen species production by C_{60} more research into the effect fullerenes may have on red blood cells is needed prior to assessing hemocompatibility.

DNA Cleavage

Fullerenes are hydrophobic and electron-poor. Previous observation of light-activated DNA cleavage by C_{60} (Tokuyama, Yamago, Nakamura, Shiraki, & Sugiura, 1993; Yamakoshi et al., 1996) prompted Bernstein et al. (1999) to investigate the mechanism of DNA cleavage by fullerenes. Two potential mechanisms can result in DNA cleavage: (1) direct electron transfer from guanosine residues to C_{60} or (2) energy transfer via singlet oxygen generated by C_{60} and light. The different mechanisms result in different cleavage patterns. Damage by mechanism (1) will result in preferential damage at the 5′ end of two adjacent guanosine residues while type (2) will randomly damage guanosine residues in either the 3′ or 5′ positions of adjacent guanosine residues, which are particularly susceptible to oxidation (Bernstein et al., 1999). An electron was observed transferring from guanosine to C_{60} creating the more reactive form 8-oxoguanosine than type II DNA cleavage (Bernstein et al., 1999). It should be noted that these experiments were done using dihydrofullerene, a C_{60} fullerene with two sp^3 hybridized C atoms, in benzonitrile instead of aqueous media. The presence of water may alter the mechanism observed by Bernstein et al. (1999).

Computational work has shown that the binding energy between C_{60} and DNA is between –27 and –42 kcal/mol (Zhao, Striolo, & Cummings, 2005). This interaction between C_{60} and DNA is much larger than the binding energy for two fullerenes (–7.5 kcal/mol). The calculations were limited to 20 ns; therefore only 12 nucleotides were used to simulate DNA strands. However, the sequence was carefully chosen to mimic actual DNA sequences while maintaining the 20 ns constraint for computation. C_{60} was observed to bind primarily to the free ends of double-stranded DNA but can also interact with the minor groove. This phenomenon may occur due to the hydrophobic nature of the DNA ends and the C_{60} molecule (Zhao et al., 2005). The binding of C_{60} to the B-form of DNA was found to confer significant deformation via 6.5 kcal/mol deformation energy. The docking of C_{60} with A-DNA results in –4.5 kcal/mol deformation energy caused by the conformational change from A- to B-DNA. This deformation resulting from C_{60} binding was more pronounced in single-stranded DNA where the end docked with C_{60} underwent extensive deformation. Zhao et al. (2005) theorized that single-stranded DNA would likely wrap around the fullerene given sufficient DNA length, but computational time limits prevented this analysis. The authors pointed out that the energies calculated were binding energy and not free energy. Thus, the results of entropic rearrangements were included in the numbers reported. In this case, entropic results are significant since water molecules are displaced from the C_{60}-DNA docking site (Zhao et al., 2005). Perhaps most interesting

was the response of C_{60} to DNA damage in the form of missing nucleotides. Based on the computational results, C_{60} appeared to fill in the gap left by missing nucleotides. Zhao and coworkers (2005) believe that the C_{60} would likely disrupt the DNA repair process by preventing the repair machinery from recognizing the nick.

C_{60}-COOH

Cytotoxicity – Effect of the Extent of Modification, Reactive Oxygen Species, and Lipid Oxidation

In an attempt to make fullerenes more water soluble, carboxylic acid moieties have been added to the surface of C_{60} particles. These –COOH chains can adopt a variety of spatial arrangement on the fullerene surface depending on addition chemistry leading to different physicochemical properties.

Tokuyama et al. (1993) observed that carboxylic acid derivatives of C_{60} with only one functionalized group (Figure 8.3) only inhibited growth of HeLa S3 cells in the presence of low-intensity fluorescent light. Both the C_{60}-RCOOH and the triethylamine salt of the carboxylic acid derivative showed similar decreases in the inhibitory concentration for 50% of cells (IC_{50}) from >100 μM in the dark to 6 μM with 6 W of fluorescent light. Another carboxylic acid derivative of C_{60} functionalized with one group was found to be tolerated at 200–500 mg/kg by ddY mice in a single iv injection (Yamago, Tokuyama, Nakamura, Kikuchi, Kananishi, Sueki, Nakahara, Enomoto, & Ambe, 1995) (Figure 8.4). The mice did demonstrate signs of acute toxicity including writhing, trunk stretching, and weight loss, but no mice died from the injection after 7 days. Oral absorption was poor with ~97% of ^{14}C found in the feces within 48 h (Yamago et al., 1995). However, there were traces of ^{14}C found in the liver at 3 and 6 h. After iv administration, excretion was slow with ^{14}C primarily found in the feces (Yamago et al., 1995). This retention is consistent with its highly hydrophobic nature evidenced by the octanol–water partition coefficient log P_{ow} = 4.8. This long residence time in vivo could lead to long-term toxicity resulting from chronic iv dosing. However, Rajagopalan

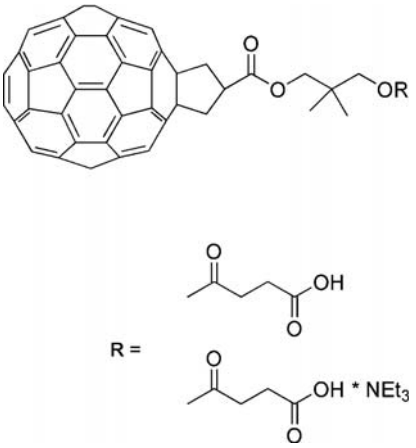

Figure 8.3 An example of C_{60}-COOH derivates adapted from Tokuyama et al., 1993.

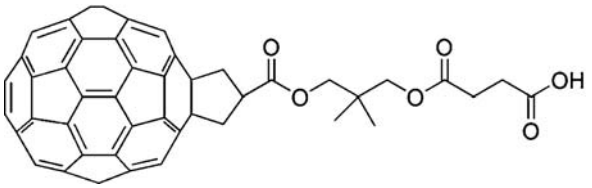

Figure 8.4 An example of C_{60}-COOH derivative adapted from Yamago et al., 1995.

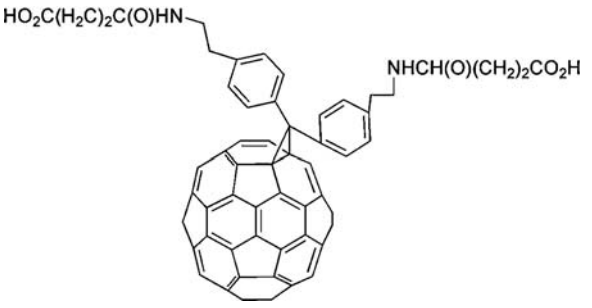

Figure 8.5 An example of C_{60}-COOH derivative adapted from Rajagopalan et al., 1996.

et al. (1996) found that 50 mg/kg of a bis(monosuccinimide) C_{60}-COOH derivative (Figure 8.5) exhibited no gross toxicity after daily iv administration to Sprague-Dawley rats for 6 days. Also no detectable urine levels were observed indicating no renal clearance. Bis(monosuccinimide) C_{60} was found to be extensively dispersed into peripheral tissue with a peripheral tissue residence time nearly 10 times higher than for the trunk (Rajagopalan et al., 1996).

Three malonic acid groups were conjugated to C_{60} in two different stereochemical patterns resulting in C_3 and D_3 isomers (Figure 8.6) (Dugan, Turetsky, Du, Lobner, Wheeler, Almli, Shen, Luh, Choi, & Lin, 1997). Both isomers showed scavenging activity for hydroxyl ($^{\cdot}OH$) and superoxide radicals ($O_2^{\cdot -}$). C_3 and D_3 were very potent hydroxyl radical scavengers requiring one to two orders of magnitude less concentration for elimination than other known scavengers. Mouse neocortical cells were exposed to excitotoxicants *N*-methyl-*d*-aspartate and α-amino-3-hydroxy-5-methyl-4-isoxazolepropionic acid, which can bind and activate glutamate receptors that are known to be upregulated during periods of cellular oxidative stress (Cerutti, 1985; Reynolds & Hastings, 1995). Both C_3 and D_3 showed dose-dependent neuronal protection (Dugan et al., 1997). However, C_3 was more potent and induced more complete protection from neuronal death indicating

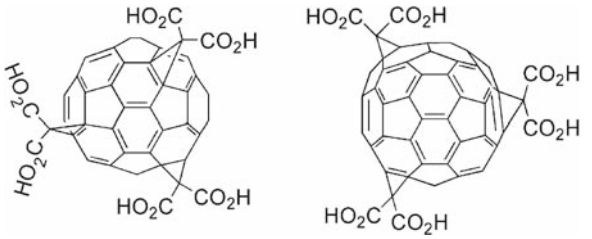

C_3 D_3

Figure 8.6 C_3 and D_3 isomers of C_{60}-malonic acid adapted from Dugan et al., 1997.

it may have a more favorable interaction with the plasma membrane than D_3. Electron spin resonance spectroscopy revealed that C_3 interacts with the interior of the plasma membrane more extensively than D_3, which is evidenced by C_3's partition coefficient (Dugan et al., 1997). Also, examination of the molecule reveals that C_3 is dipolar – one half of the fullerene has three malonic acid functional groups leaving the other half very hydrophobic. D_3 has an equatorial arrangement of its malonic acid derivatives limiting its ability to interact with hydrophobic regions (Figure 8.6) (Dugan et al., 1997). Thus C_3 and D_3 C_{60} derivatized with malonic acid showed the ability to decrease neuronal death caused by rapid and extensive stimulation of *N*-methyl-*d*-aspartate receptors, which few free radical scavengers are capable of doing (Dugan et al., 1997). C_3 was able to attenuate neuronal death caused by glucose starvation and *N*-methyl-*d*-aspartate receptor activation. Addition of C_3 or D_3 to neocortical culture during serum starvation also decreased the production of free radicals and apoptosis. Therefore, these C_3 and D_3 isomers of malonic acid-derived C_{60} show extensive free radical scavenger properties (Dugan et al., 1997). However, no direct cytotoxicity data was obtained.

The free radical scavenger properties of carboxy fullerenes were confirmed by Huang et al. (1998). Human Hep3B hepatoma cells were treated with transforming growth factor β for 48 h and reactive oxygen species measured by flow cytometry via oxidation of a fluorescent dye. Only C_3 carboxyfullerene was observed to quench all reactive oxygen species after transforming growth factor β treatment. Known antioxidants *N*-acetylcysteine and ascorbic acid also did not exhibit any scavenger properties in response to transforming growth factor β-induced reactive oxygen species in Hep3B (Huang et al., 1998). C_3 appears to have a much stronger interaction with the lipid membrane than D_3 as visualized via Stern–Volmer fluorescence quenching (Huang et al., 1998) supporting Dugan et al. observation (1997). No direct cytotoxicity was measured against Hep3B by Huang et al. (1998). Wang et al. (1999) found that C_3 resulted in significantly less membrane leakage from liposomes than D_3 implying less cytotoxicity. Thus, Wang et al. (1999) theorized that the number of sites for radical addition, the ability of the antioxidant to penetrate the lipid membrane, and consequently the strength of hydrophobic interaction between the antioxidant and lipids determined the differences in membrane leakage resulting from free radical lipid oxidation.

The functional consequence of additional malonic acid side chains to light-induced C_{60}cytotoxicity was investigated (Yang, Fan, & Zhu, 2002). C_{60} was conjugated with malonic acid generating di-, tri-, and quadricmalonic acid with carboxylate functional groups (Yang et al., 2002). Human cervix uteri tumor-derived HeLa cells were treated with various doses of dimalonic acid, trimalonic acid, or quadricmalonic acid and exposed to 300 W halogen lamp three times for 30 min with 24 h recovery between each exposure. MTT was then used to determine cell viability. The stage of the cell cycle was also determined via flow cytometry. Dimalonic acid was non-cytotoxic at concentrations below 64 μM; however, upon exposure to light dimalonic acid became significantly cytotoxic at 32 μM and showed dose-dependent toxicity at higher concentrations (Yang et al., 2002). This toxicity was also evident through morphological changes seen via light microscopy. Dimalonic acid, trimalonic acid, and quadricmalonic acid

were non-toxic in the absence of light at 40 μM but showed significant cytotoxicity at 40 μM in the presence of light. Interestingly, the toxicity of the carboxyfullerenes decreased with increasing number of malonic acid derivatives, which indicates the more highly substituted fullerenes may be more photostable (Yang et al., 2002). This cytotoxic activity was identical to the light-induced production of reactive oxygen species found previously (Hamano, Okuda, Mashino, Hirobe, Arakane, Ryu, Mashiko, & Nagano, 1997; Cheng, Yang, & Zhu, 2000), which potentially links the ability to produce reactive oxygen species with cytotoxicity. In addition, the hydroxyl radical scavenger mannitol was unable to decrease light-induced cytotoxicity of HeLa cells at 10 μM indicating that the mechanism of cell death might occur by another radical. However, Nakajima et al. (1996) found that superoxide dismutase, which converts superoxide into oxygen and hydrogen peroxide, was not effective at decreasing C_{60}-ethylene diamine-PEG-COOH toxicity to L929 murine fibroblasts. This lack of scavenger activity may be due to limited scavenger concentration or incompatible mechanism of action. Neither group investigated multiple scavenger concentrations (Nakajima et al., 1996; Yang et al., 2002).

C_{60}-COOH were also observed to decrease the amount of natural and iron-induced lipid oxidation in cortical brain homogenates from Sprague-Dawley rats in a dose-dependent manner in vitro (Lin et al., 1999). At high doses, these C_{60}-COOH returned lipid oxidation to basal or below basal levels (Lin et al., 1999). In vivo C_{60}-COOH also prevented lipid oxidation resulting from elevated iron levels in the nigrostriatal dopaminergic system of anesthetized Sprague-Dawley rats. These findings were further supported by suppression of hydroxyl radicals generated by iron in a cell free preparation (Lin et al., 1999). In addition, no difference was observed between C_3 and D_3 isomers related to lipid oxidation induced by iron. Furthermore, Lin et al. (1999) showed that vitamin E was more able to prevent lipid oxidation than carboxyfullerenes in contrast to Wang et al. (1999).

C_{60}-COOH derivatives have also been investigated to determine the free radical generation or scavenging properties. Peripheral blood mononuclear cells were challenged with 2-deoxy-*d*-ribose or tumor necrosis factor α and cycloheximide (Monti, Moretti, Salvioli, Straface, Malorni, Pellicciari, Schettini, Bisaglia, Pincelli, Fumelli, Bonafe, & Franceschi, 2000). Both 2-deoxy-*d*-ribose and tumor necrosis factor α interfere with cells' redox equilibrium. 2-Deoxy-*d*-ribose shifts the balance of glutathione-*S*-transferase to the oxidized form and inhibits proliferation while also inducing apoptosis. The antioxidant *N*-acetylcysteine prevents apoptosis caused by 2-deoxy-*d*-ribose (Kletas, Barbieri, Stathakos, Botti, Bergamini, Tomasi, Monti, Malorni, & Franceschi, 1998). In addition, tumor necrosis factor α is known to alter the redox equilibrium state of cells and induce apoptosis (Glosli, Tronstad, Wergedal, Muller, Svardal, Aukrust, Berge, & Prydz, 2002; Hansen, Zhang, & Jones, 2006). Therefore, Monti et al. (2000) investigated the effect C_{60}-COOH had on 2-deoxy-*d*-ribose- and tumor necrosis factor α-induced apoptosis. In both cases the C_{60}-COOH provided cytoprotective behavior preventing apoptosis from tumor necrosis factor α or 2-deoxy-*d*-ribose treatment. Because both tumor necrosis factor α and 2-deoxy-*d*-ribose are known to act via oxidative pathways,

the anti-apoptotic behavior of C_{60}-COOH is believed to occur through their scavenger properties (Monti et al., 2000). These C_{60}-COOH were also observed to prevent mitochondrial depolarization. This preference for tumor necrosis factor α can be explained by the proposed action of tumor necrosis factor α and cycloheximide, which are believed to act in concert to increase superoxide production at the mitochondrial surface. Thus, the theorized radical scavenging ability of C_{60}-COOH would act to decrease these superoxide radicals. It should be noted as well that the decrease in mitochondrial depolarization was less extensive than the anti-apoptotic nature of C_{60}-COOH on entire cells (Monti et al., 2000).

Sayes et al. (2004) found that the LD_{50} of C_3 C_{60}-COOH was 10,000 ppb, which is 500 times less toxic to dermal fibroblasts than nano-C_{60}. Also the sodium salt of carboxyfullerene, $Na^{+}{}_{2-3}[C_{60}O_{7-9}(OH)_{12-15}]$, was even less toxic than C_{60}-COOH with an LD_{50} of 40,000 ppb. Therefore, as hydrophilicity increases toxicity decreases. Bosi et al. (2004) analyzed cytotoxicity as a function of structure in a variety of functionalized C_{60}. Those fullerenes functionalized with carboxylate groups or carboxylate derivatives were not cytotoxic to human MCF7 breast cancer, rat Hep-G2 liver, or LLC-PK1 pig renal proximal tubular cells at concentrations up to 80 μM. The fullerenes with two cationic functional groups did show significant toxicity to all three cell lines. These cationic functionalized fullerenes demonstrated LD_{50} around 20 μM for Hep-G2 and MCF-7 but were highly toxic to the LLC-PK_1 cells with an LD_{50} <1 μM (Bosi et al., 2004). Comparing hemolytic and cytotoxic values reveals that cytotoxic concentrations are lower than hemolytic concentrations. Therefore, surface also appears to affect cytotoxicity similar to that seen for dendrimers.

Hemocompatibility

Bis(monosuccinimide) derivative of *p*,*p*′-bis(2-amino-ethyl)-diphenyl-C_{60} (15 mg/kg) was iv injected into Sprague-Dawley rats (Rajagopalan et al., 1996). The blood clearance was found to exhibit bi- or tri-exponential decay. Also >99% of the bis(monosuccinimide) derivative of *p*,*p*′-bis(2-amino-ethyl)-diphenyl-$C_{60}$was found to be bound to plasma proteins, which would increase its circulation time in blood. This observation is supported by computational modeling by Noon et al. (2002) who found that fullerenes are capable of binding antibody with high-affinity while leaving ~20% of the fullerene surface available for solvation. The protein bound to the fullerene typically exhibited a complementary conformation in addition to side chain moieties capable of pi-stacking interactions. Noon et al. (2002) theorized that these pi-stacking interactions could be a common biological recognition motif for carbon nanoparticles which are typically rich in pi-bond electrons.

Bosi et al. (2004) found that C_{60} functionalized with bis-carboxy chains were non-hemolytic to human red blood cells up to 80 μM regardless of the position of the functional group on the fullerene. One cationic chain showed similar properties to the carboxylated fullerene; however, those fullerenes with two cationic chains showed significant hemolysis from 20–60 μM (Bosi et al., 2004). Interestingly, the position of the two cationic chains appeared critical to hemolytic activity as C_{60} with equatorially positioned cationic chains demonstrated 50% hemolysis at 20 μM while

the other geometrical configurations only conferred 5–10% hemolysis. This observation supports previous findings regarding activity and hydrophobicity/hydrophilicity. For instance, the difference between C_3 and D_3 scavenger function is due to position of the side chains allowing C_3 to penetrate the lipid membrane more efficiently. For the cationic functionalized C_{60}, the position of the side chain appears to confer surfactant properties allowing these molecules to destabilize the membrane allowing cell death. The hemolytic activity of these compounds was supported by the calculation of the hydrophobic to hydrophilic surface area ratio. A linear correlation was obtained for hemolytic activity and hydrophobic to hydrophilic ratio. The correlation was only $r^2 = 0.779$ for 30 μM but increased to $r^2 = 0.944$ for 80 μM indicating that the hydrophobic nature of the molecule interacting with red blood cells is critical to hemolysis. This data also warrants more investigation into the cytotoxicity of C_3 and D_3 C_{60}-COOH to determine if their radical scavenging properties are offset with inherent toxicity.

DNA Cleavage

The triethylamine salt of C_{60}-COOH tested by Tokuyama et al. (1993) was found to be highly selective for guanine bases. The mechanism underlying this selective DNA cleavage was not probed; however, light-induced DNA cleavage by C_{60}-COOH was enhanced by treatment with base, which is consistent with DNA damage induced by singlet oxygen.

C_{60}-OH Cytotoxicity – Effect of Reactive Oxygen Species and Lipid Oxidation

Fullerene hydroxylation is one method of overcoming the very low solubility in aqueous media (Figure 8.7). The hydroxyl groups provide increased hydrophilicity allowing better dispersion in addition to providing potential sites for drug conjugation. Sayes et al. (2004) found that as the degree of functionalization increased, toxicity to HDF cells decreased. The $C_{60}(OH)_{24}$ molecule was the least toxic of all the compounds tested with an LC_{50} of > 5,000,000 ppb. In contrast to these findings, $C_{60}(OH)_{24}$was toxic to human umbilical vein endothelial cells at 100 μg/ml but altered cell morphology at 1 or 10 μg/ml (Yamawaki & Iwai, 2006). The dose-dependent morphological changes included cytosoloic vacuole formation and lower cell density. $C_{60}(OH)_{24}$ (100 μg/ml) significantly increased LDH release resulting in cytotoxic membrane damage. As a result of cytotoxicity, 100 μg/ml $C_{60}(OH)_{24}$ demonstrated growth inhibition to 30% confluent endothelial cells as shown by the reduction of MTT into formazan by mitochondrial

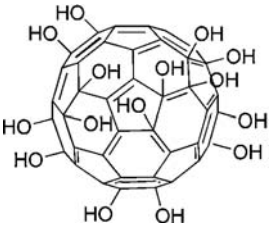

Figure 8.7 An example of C_{60}-OH derivative adapted from Sayes et al., 2004.

dehydrogenases (Yamawaki & Iwai, 2006). $C_{60}(OH)_{24}$ did not induce cleavage of caspase-3 or PARP, two common indicators of apoptosis; however, protein ubiquitination increased in a dose-dependent manner with $C_{60}(OH)_{24}$ (Yamawaki & Iwai, 2006). In addition, $C_{60}(OH)_{24}$ was internalized into autophagosomes. Chronic exposure of endothelial cells to 1 μg/ml $C_{60}(OH)_{24}$ resulted in no toxicity.

Fullerenes functionalized with 18–20 hydroxyl groups ($C_{60}(OH)_{18–20}$) were tested for their free radical properties in an in vitro system (Chiang, Lu, & Lin, 1995). Xanthine oxidase converts xanthine into uric acid, which absorbs at 290 nm allowing its generation to be tracked. No change in uric acid concentration was seen with increasing concentrations of $C_{60}(OH)_{18–20}$. This led Chiang et al. (1995) to determine the ability of the fullerenol to absorb superoxide radicals. The xanthine/xanthine oxidase system was used again, but the addition of the chemiluminescent lucigenin allowed easy detection of superoxide production. This experiment revealed a decrease in chemiluminescence dependent on $C_{60}(OH)_{18–20}$concentration. Thus, fullerenols were shown to act as a radical sponge for superoxide radicals (Chiang et al., 1995).

C_{60}-PEG Cytotoxicity

PEG 5460 was added to C_{60} to create a molecule with total molecular weight of 26,000 (Tabata, Maurakami, & Ikada, 1997). After iv injection into CDF-1 mice containing Meth A fibrosarcoma cell tumors, the radiolabeled C_{60}-PEG molecules preferentially located to the tumor with tissue ratios of 2.7 and 19 for tumor to skin and muscle, respectively. Upon exposure to visible light, tumor necrosis was present but host healthy tissue was not damaged (Tabata et al., 1997). A more pronounced effect was seen with the C_{60}-PEG conjugate than with the positive control Photofrin despite a 10-fold lower dose of C_{60}-PEG. Full excretion was observed after 7 days via renal clearance, and doses up to 1.8 g/kg of C_{60}-PEG were well tolerated with no excessive accumulation in host tissue or mouse lethality (Tabata et al., 1997). This dose is also reported to be 4,000 times higher than that needed for light-induced tumor necrosis.

Cusan et al. (2002) previously evaluated C_3 and D_3 C_{60}COOH. The carboxy chains overcame the solubility and aggregation issues; however, an increase in side chain groups has been shown to decrease the radical scavenger abilities of fullerenes (Krusic et al., 1991). Therefore, Cusan et al. designed and synthesized a C_{60} molecule with three ethylene glycol and ammonium groups contained in one side chain (Figure 8.8). However, this C_{60} molecule did not affect the concentration of superoxide radicals produced by the xanthine/xanthine oxidase cell free system (Cusan et al., 2002). Its neuroprotective activity was tested against cerebral cortical cells from Sprague-Dawley rats incubated with 100 μM glutamate. Surprisingly, ethylene glycol/ammonium functionalized C_{60} contributed to cortical cell toxicity in a dose-dependent manner. Cusan and coworkers (2002) theorized that this increased toxicity was likely due to the dipolar nature of the molecule whereby the intact fullerene was very hydrophobic and the functionalized side chain was highly hydrophilic conferring surfactant properties upon the functionalized C_{60} molecule allowing it to destabilize

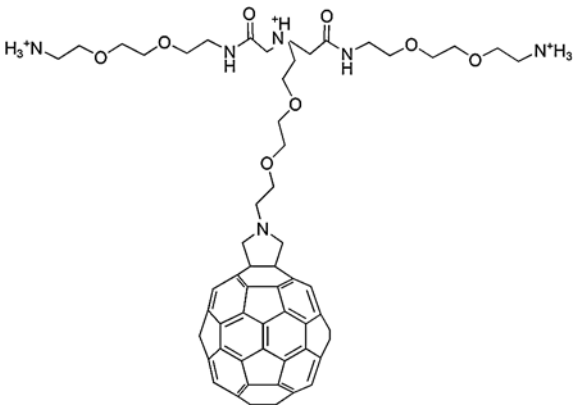

Figure 8.8 An example of C_{60} conjugated with triethylene glycol adapted from Bosi et al., 2004.

the cellular plasma membrane. Thus, the number and arrangement of functional groups added to a C_{60} fullerene appear more important for neuroprotective activity than the nature of the functional group.

Summary

Inconsistent data exists regarding fullerene biocompatibility. For example, C_{60} has been observed to generate free radicals and scavenge them under different experimental conditions such as cell type and fullerene derivative. In addition, C_{60} has demonstrated significant toxicity toward a variety of cells (Sayes et al., 2004); however, others claim that C_{60} is in fact not toxic (Andrievsky, Klochkov, & Derevyanchenko, 2005). Additional research into the effects of surface modification on a fullerene's electronegativity is needed. Also, resolution of the mechanism underlying fullerenes ability to scavenge free radicals is needed.

Conclusions

More research into the biocompatibility of SWCNTs has been performed than for MWCNTs. Aggregation poses significant toxicity for both SWCNTs and MWCNTs. Therefore, more research into the effect synthesis technique, length, metal content, and surface treatment have on biocompatibility and possible free radical generation or scavenging is needed. No consensus conclusions can be drawn regarding fullerene structure and biocompatibility. Conflicting data exists indicating that C_{60} may act as both a free radical generator and a scavenger under different conditions. Various surface modifications such as –COOH or –OH can improve the solubility of C_{60}. Based on the current experiments, it appears that the geometry of these surface modifications is critical to toxicity and biocompatibility. However, more research is needed to understand the mechanism related to fullerene-mediated toxicity. Guidelines such as the International Organization for Standards 10993 and the American Society for Testing Materials Standards F748 will decrease variability between exposure times, cell lines, and animal models for a given material. Therefore,

adherence to these standards will accelerate our understanding of the biocompatibility of SWCNTs, MWCNTs, and fullerenes.

References

Alemany, R., Suzuki, K., & Curiel D.T. (2000). Blood clearance rates of adenovirus type 5 in mice. *Journal of General Virology*, 81, 2605–9.

Andrievsky, G., Klochkov, V., & Derevyanchenko, L. (2005). Is the C_60 fullerene toxic?! *Fullerene, Nanotubes, and Carbon Nanostructures*, 13, 363–76.

Baddour, C.E. & Briens, C. (2005). Carbon nanotube synthesis: A review. *International Journal of Chemical Reactor Engineering*, 3, R3:1–20.

Barlow, P.G., Donaldson, K., MacCallum, J., Clouter, A., & Stone, V. (2005). Serum exposed to nanoparticle carbon black displays increased potential to induce macrophage migration. *Toxicology Letters*, 155, 397–401.

Benson, J.M., Carpenter, R.L., Hahn, F.F., Haley, P.J., Hanson, R.L., Hobbs, C.H., Pickrell, J.A., & Dunnick, J.K. (1987). Comparative inhalation toxicity of nickel subsulfide to F344/N rats and B6C3F1 mice exposed for 12 days. *Fundamental and Applied Toxicology,* 9, 251–65.

Bernstein, R., Prat, F., & Foote, C.S. (1999). On the mechanism of DNA cleavage by fullerenes investigated in model systems: electron transfer from guanosine and 8-oxo-guanosine derivatives to C_{60}. *Journal of the American Chemical Society*, 121, 464–5.

Bosi, S., Feruglio, L., Da Ros, T., Spalluto, G., Gregoretti, B., Terdoslavich, M., Decorti, G., Passamonti, S., Moro, S., & Prato, M. (2004). Hemolytic effects of water-soluble fullerene derivatives. *Journal of Medicinal Chemistry*, 47, 6711–5.

Bottini, M., Bruckner, S., Nika, K., Bottini, N., Bellucci, S., Magrini, A., Bergamaschi, A., & Mustelin, T. (2006) Multi-walled carbon nanotubes induce T lymphocyte apoptosis. *Toxicology Letters*, 160, 121–6.

Carbon Nanotechnologies Incorporated. (2003). Material Safety Data Sheet Product: Single Wall Carbon Nanotubes. Retrieved October 20, 2006, from http://www.cnanotech.com/download_files/MSDS%20for%20CNI%20SWNT.pdf.

Carrero-Sanchez, J.C., Elias, A.L., Mancilla, R., Arrelin, G., Terrones, H., Laclette, J.P., & Terrones, M. (2006). Biocompatibility and toxicological studies of carbon nanotubesdoped with nitrogen. *Nano Letters*, 6, 1609–16.

Cerutti, P.A. (1985). Prooxidant states and tumor promotion. *Science*, 227, 375–81.

Cheng, F.Y., Yang, X.L., & Zhu, H.S. (2000). Hydroxyl radical scavenging and producing activities of water-soluble malonic acid C-60. *Fullerene Science and Technology*, 8, 113–24.

Cherukuri, P., Bachilo, S.M., Litovsky, S.H., & Weisman, R.B. (2004) Near-infrared fluorescence miscroscopy of single-walled carbon nanotubes in phagocytic cells. *Journal of theAmerican Chemical Society*, 126, 15638–9.

Chiang, L.Y., Lu, F.-J., & Lin, J.-T. (1995). Free radical scavenging activity of water-soluble fullerenols. *Journal of the Chemical Society-Chemical Communications*, 12, 1283–4.

Cui, D., Tian, F., Ozkan, C.S., Wang, M., & Gao, H. (2005). Effect of single wall carbon nanotubes on human HEK293 cells. *Toxicology Letters*, 155, 73–85.

Cusan, C., Da Ros, T., Spalluto, G., Foley, S., Janot, J.-M., Seta, P., Larroque, C., Tomasini, M.C., Antonelli, T., Ferraro, L., & Prato, M. (2002). A new multicharged C_{60} derivative: synthesis and biological properties. *European Journal of Organic Chemistry*, 17, 2928–34.

Dash, P.R., Read, M.L., Barrett, L.B., Wolfert, M.A., & Seymour, L.W. (1999). Factors affecting blood clearance and *in vivo* distribution of polyelectrolyte complexes for gene delivery. *Gene Therapy*, 6, 643–50.

DeLeo, F.R. (2004). Modulation of phagocyte apoptosis by bacterial pathogens. *Apoptosis*, 9, 399–413.

Ding, L., Stilwell, J., Zhang, T., Elboudwarej, O., Jiang, H., Selegue, J.P., Cooke, P.A., Gray, J.W., & Chen, F.F. (2005). Molecular characterization of the cytotoxic mechanism of multiwall carbon nanotubes and nano-onions on human skin fibroblasts. *Nano Letters,* 5, 2448–64.

Donaldson, K. & Tran, C.L. (2002). Inflammation caused by particles and fibers. *Inhalation Toxicology,* 14, 5–27.

Donaldson, K. & Tran, C.L. (2004). An introduction to the short-term toxicology of respirable industrial fibres. *Mutation Research*, 553, 5–9.

Driscoll, K.E., Carter, J.M., Howard, B.W., Hassenbein, D.G., Pepelko, W., Baggs, R.B., & Oberdoerster, G. (1996). Pulmonary inflammatory, chemokine, and mutagenic responses in rats after subchronic inhalation of carbon black. *Toxicology and Applied Pharmacology*, 136, 372–80.

Dugan, L.L., Turetsky, D.M., Du, C., Lobner, D., Wheeler, M., Almli, C.R., Shen, C.K.-F., Luh, T.-Y, Choi, D.W., & Lin, T.-S. (1997). Carboxyfullerenes as neuroprotective agents. *Proceedings of the National Academy of Sciences of the United States of America*, 94, 9434–9.

Dupuis, A.C. (2005). The catalyst in the CCVD of carbon nanotubes – a review. *Progress in Materials Science*, 50, 929–61.

Fenoglio, I., Tomatis, M., Lison, D., Muller, J., Fonseca, A., Nagy, J.B., & Fubini, B. (2006). Reactivity of carbon nanotubes: free radical generation or scavenging activity? *Free Radical Biology & Medicine*, 40, 1227–33.

Fiorito, S., Serafino, A., Andreola, F., & Bernier, P. (2006). Effects of fullerenes and single-wall carbon nanotubes on murine and human macrophages. *Carbon*, 44, 1100–5.

Flahaut, E., Durrieu, M.C., Remy-Zolghadri, M., Bareille, R., & Baquey, C.H. (2006). Study of the cytotoxicity of CCVD carbon nanotubes. *Journal of Materials Science*, 41, 2411–6.

Forman, H.J. & Torres, M. (2002). Reactive oxygen species and cell signaling: respiratory burst in macrophage signaling. *American Journal of Respiratory and Critical Care Medicine*, 166, S4–S8.

Gallagher, J., Sams II, R., Inmon, J., Gelein, R., Elder, A., Oberdorster, G., & Prahalad, A.K. (2003). Formation of 8-oxo-7,8-dihydro-2'deoxyguanosine in rat lung DNA following subchronic inhalation of carbon black. *Toxicology and Applied Pharmacology,* 190, 224–31.

Garibaldi, S., Brunelli, C., Bavastrello, V., Ghigliotti, G., & Nicolini, C. (2006). Carbon nanotube biocompatibility with cardiac muscle cells. *Nanotechnology*, 17, 391–7.

Glosli, H., Tronstad, K.J., Wergedal, H., Muller, F., Svardal, A., Aukrust, P., Berge, R.K., & Prydz, H. (2002). Human TNF-α in transgenic mice induces differential changes in redox status and glutathione-regulating enzymes. *FASEB Journal*, 16, 1450–2.

Grubek-Jaworska, H., Nejman, P., Czuminska, K., Przybylowski, T., Huczko, A., Lange, H., Bystrzejewski, M., Baranowski, P., & Chazan, R. (2006). Preliminary results on the pathogenic effects of intratracheal exposure to one-dimensional nanocarbons. *Carbon*, 44, 1057–63.

Hamano, T., Okuda, K., Mashino, T., Hirobe, M., Arakane, K., Ryu, A., Mashiko, S., & Nagano, T. (1997). Singlet oxygen production from fullerene derivatives: effect of sequential functionalization of the fullerene core. *Journal of the Chemical Society-Chemical Communications*, 1, 21–2.

Hansen, J.M., Zhang, H., & Jones, D.P. (2006). Mitochondrial thioredoxin-2 has a key role in determining tumor necrosis factor-α-induced reactive oxygen species generation, NF-κB activation, and apoptosis. *Toxicological Sciences*, 91, 643–50.

Hesterberg, T.W., Chase, G., Axten, C., Miller, W.C., Musselman, R.P., Kamstrup, O., Hadley, J., Morscheidt, C., Bernstein, D.M., & Thevenaz, P. (1998). Biopersistence of synthetic vitreous fibers and amosite asbestos in the rat lung following inhalation. *Toxicology and Applied Pharmacology*, 151, 262–75.

Huang, Y.-L, Shen, C.K.-F., Luh, T.-Y., Yang, H.C., Hwang, K.C., & Chou, C.-K. (1998). Blockage of apoptotic signaling of transforming growth factor-β in human hepatoma cells by carboxyfullerene. *European Journal of Biochemistry*, 254, 38–43.

Huczko A. & Lange H. (2001). Carbon nanotubes: experimental evidence for a null risk of skin irritation and allergy. *Fullerene Science and Technology*, 9, 247–50.

Huczko, A., Lange, H., Calko, E., Grubek-Jaworksa, H., & Droszcz, P. (2001). Physiological testing of carbon nanotubes: Are they asbestos like? *Fullerene Science and Technology,* 9, 251–4.

Huzcko, A., Lange, H., Bystrzejewski, M, Baranowski, P, Grubek-Jaworska H, Nejman, P., Przybylowski, T., Czuminska, K., Glapinski, J., Walton, D.R.M., & Kroto, H.W. (2005). Pulmonary toxicity of 1-D nanocarbon materials. *Fullerenes, Nanotubes, and Carbon Nanostructures*, 13, 141–45.

Jia, G., Wang, H., Yan, L., Wang, X., Pei, R., Yan, T., Zhao, Y., & Guo X. (2005). Cytotoxicity of carbon nanomaterials: single-wall nanotube, multi-wall nanotube, and fullerene. *Environmental Science and Technology*, 39, 1378–83.

Kagan, V.E., Tyurina, Y.Y., Tyurin, V.A., Konduru, N.V., Potapovich, A.I., Osipov, A.N., Kisin, E.R., Schwegler-Berry, D., Mercer, R., Castranova, V., & Shvedova, A.A. (2006). Direct and indirect effects of single walled carbon nanotubes on RAW 264.7 macrophages: Role of iron. *Toxicology Letters*, 165, 88–100.

Kam, N.W.S., Jessop, T.C., Wender, P.A., & Dai, H. (2004). Nanotube molecular transporters: internalization of carbon nanotube-protein conjugates into mammalian cells. *Journal of American Chemical Society*, 126, 6850–1.

Kletsas, D., Barbieri, D., Stathakos, D., Botti, B., Bergamini, S., Tomasi, A., Monti, D., Malorni, W., & Franceschi, C. (1998). The highly reducing sugar 2-deoxy-D-ribose induces apoptosis in human fibroblasts by reduced glutathione depletion and cytoskeletal disruption. *Biochemical and Biophysical Research Communications*, 243, 416–25.

Koyama, S., Tanaka, S., Yamaguchi, Y., Haniu, H., Takeichi,T. Konishi, G., & Koyama, H. (2002). Different tissue reactions to activated carbon fibers – pathological and immunological findings after subcutaneous implantation. *Molecular Crystals and Liquid Crystals*, 388, 581–5.

Koyama, S., Endo, M., Kim, Y.A., Hayashi, T., Yanagisawa, T., Osaka, K., Koyama, H., Haniu, H., & Kuroiwa, N. (2006). Role of systemic T-cells and histopathological aspects after subcutaneous implantation of various carbon nanotubes in mice. *Carbon*, 44, 1079–92.

Kroto, H.W., Heath, J.R., O'Brien, S.C., Curl., R.F., & Smalley, R.E. (1985). C_{60}: Buckminsterfullerene. *Nature*, 318, 162–3.

Krusic, P.J., Wasserman, E., Keizer, P.N., Morton, J.R., & Preston, K.F. (1991). Radical reactions of C_{60}. *Science,* 254, 1183–5.

Lam, C.W., James, J.T., McCluskey, R., Hunter, R.L. (2004). Pulmonary toxicity of single-walled carbon nanotubes in mice 7 and 90 days after intratracheal instillation. *Toxicological Sciences*, 77, 126–34.

Lin, A.M.Y., Chyi, B.Y., Wang, S.D., Yu, H.-H., Kanakamma, P.P., Luh, T.-Y., Chou, C.K., & Ho, L.T. (1999). Carboxyfullerene prevents iron-induced oxidative stress in rat brain. *Journal of Neurochemistry*, 72, 1634–40.

Lippmann, M., (1986). Respiratory tract deposition and clearance of aerosols. In S.D. Lee, T. Schneider, L.D. Grant, & P.J. Verkerk (Eds.), *Aerosols* (pp.43–57). Chelsea, MI: Lewis Publishers.

Lippmann, M. (1994). Nature of exposure to chrysotile. *Annals of Occupational Hygiene,* 38, 459–67.

Magrez, A., Kasas, S., Salicio, V., Pasquier, N., Seo, J.W., Celio, M., Catsicas, S., Schwaller, B., & Forro, L. (2006). Cellular toxicity of carbon-based nanomaterials. *Nano Letters*, 6, 1121–25.

Manna, S.K., Sarkar, S., Barr, J., Wise, K., Barrera, E.V., Jejelowo, O., Rice-Ficht, A.C., &Ramesh G.T. (2005). Single-walled carbon nanotube induces oxidative stress and activates nuclear transcription factor-κB in human keratinocytes. *Nano Letters*, 5, 1676–84.

Matsui, H., Ito, T., & Ohnishi, S.I. (1983). Phagocytosis by macrophages: III. Effects of heat-labile opsonin and poly(L-lysine). *Journal of Cell Science*, 59, 133–43.

Monteiro-Riviere, N.A., Nemanich, R.J., Inman, A.O., Wang, Y.Y., Riviere, J.E. (2005). Multi-walled carbon nanotube interactions with human epidermal keratinocytes. *ToxicologyLetters*, 155, 377–84.

Monti, D., Moretti, L., Salvioli, S., Straface, E., Malorni, W., Pellicciari, R., Schettini, G., Bisaglia, M., Pincelli, C., Fumelli, C., Bonafe, M., & Franceschi, C. (2000). C60 carboxyfullerene exerts a protective activity against oxidative stress-induced apoptosis in human peripheral blood mononuclear cells. *Biochemical and Biophysical Research Communications*, 277, 711–7.

Muller, J., Huaux, F., Moreau, N., Misson, P., Heilier, J.-F., Delos, M., Arras, M., Fonseca, A., Nagy, J.B., Lison, D. (2005). Respiratory toxicity of multi-wall carbon nanotubes. *Toxicology and Applied Pharmacology*, 207, 221–31.

Nakajima, N., Nishi, C., Li, F.M., & Ikada, Y. (1996). Photo-induced cytotoxicity of water-soluble fullerene. *Fullerene Science and Technology*, 4, 1–19.

Nikula, K.J., Snipes, M.B., Barr, E.B., Griffith, W.C., Henderson, R.F., & Mauderly, J.L. (1995). Comparative pulmonary toxicities and carcinogenicities of chronically inhaled diesel exhaust and carbon-black in F344 rats. *Fundamental and Applied Toxicology*, 25, 80–94.

Noon, W.H., Kong, Y., & Ma, J. (2002). Molecular dynamics analysis of a buckyball-antibody complex. *Proceedings of the National Academy of Sciences of the United States of America*, 99, 6466–70.

Orfanopoulos, M. & Kambourakis, S. (1995). Chemical evidence of singlet oxygen production from C_{60} and C_{70} in aqueous and other polar media. *Tetrahedron Letters*, 36, 435–8.

Oupicky, D., Howard, K.A., Konak, C., Dash, P.R., Ulbrich, K., & Seymour, L.W. (2000). Steric stabilization of poly-L-lysine/DNA complexes by the covalent attachment of semitelechelic poly[N-(2-hydroxypropyl)methacrylamide]. *Bioconjugate Chemistry*, 11, 492–501.

Pantarotto, D., Briand, J.-P., Prato, M., & Bianco, A. (2004). Translocation of bioactive peptides across cell membranes by carbon nanotubes. *Chemical Communications*, 1, 16–17.

Park, K.H., Chhowalla, M., Iqbal, Z., & Sesti, F. (2003). Single-walled carbon nanotubes are a new class of ion channel blockers. *The Journal of Biological Chemistry*, 278, 50212–6.

Porter, A.E., Muller, K., Skepper, J., Midgley, P., & Welland, M. (2006). Uptake of C_{60} by human monocyte macrophages, its localization and implications for toxicity: studied by high resolution electron microscopy and electron tomography. *Acta Biomaterialia*, 2, 409–19.

Rajagopalan, P., Wudl, F., Schinazi, R.F., & Boudinot, F.D. (1996). Pharmacokinetics of a water-soluble fullerene in rats. *Antimicrobial Agents and Chemotherapy*, 40, 2262–5.

Reynolds, I.J. & Hastings, T.G. (1995). Glutamate induces the production of reactive oxygen species in cultured forebrain neurons following NMDA receptor activation. *The Journal of Neuroscience*, 15, 3318–27.

Rosenberg, A.S., Mizuochi, T., Sharrow, S.O., & Singer, A. (1987). Phenotype, specificity, and function of T cell subsets and T cell interactions involved in skin allograft rejection. *Journal of Experimental Medicine*, 165, 1296–315.

Sato, Y., Yokoyama, A., Shibata, K.-I., Akimoto, Y., Ogino, S.-I., Nodasaka, Y., Kohgo, T., Tamura, K., Akasaka, T., Uo, M., Motomiya, K., Jeyadevan, B., Ishiguro, M., Hatakeyama, R., Watari, F., & Tohji K. (2005). Influence of length on cytotoxicity of multi-walled carbon nanotubes against human acute monocytic leukemia cell line THP-1 in vitro and subcutaneous tissue of rats in vivo. *Molecular Biosystems,* 1, 176–82.

Sayes, C.M., Fortner, J.D., Guo, W., Lyon, D., Boyd, A.M., Ausman, K.D., Tao, Y.J., Sitharaman, B., Wilson, L.J., West, J.L., & Colvin, V.L. (2004). The differential cytotoxicity of water soluble fullerenes. *Nano Letters*, 4, 1881–7.

Sayes, C.M., Gobin, A.M., Ausman, K.D., Mendez, J., West, J.L., & Colvin, V.L. (2005). Nano-C_{60} cytotoxicity is due to lipid peroxidation. *Biomaterials*, 26, 7587–95.

Shvedova, A.A., Castranova, V., Kisin, E.R., Schwegler-Berry, D., Murray A.R., Gandelsman, V.Z., Maynard, A., & Baron, P. (2003). Exposure to carbon nanotube material: assessment of nanotube cytotoxicity using human keratinocyte cells. *Journal of Toxicology and Environmental Health, Part A*, 66, 1909–26.

Shvedova, A.A., Kisin, E.R., Mercer, R., Murray A.R., Johnson, V.J., Potapovich, A.I., Tyurina, Y.Y., Gorelik, O., Arepalli, S., Schwegler-Berry, D. Hubbs, A.F., Antonini, J., Evans, D.E., Ku, B.-K., Ramsey, D. Maynard, A., Kagan, V.E., Castranova, V., & Baron, P. (2005). Unusual inflammatory and fibrogenic pulmonary responses to single-walled carbon nanotubes in mice. *American Journal of Physiology – Lung Cellular and Molecular Physiology*, 289, L698–L708.

Singh, R., Pantarotto, D., Lacerda, L., Pastorin, G., Klumpp, C., Prato, M., Bianco, A., & Kostarelos, K. (2006). Tissue biodistribution and blood clearance rates of intravenously administered carbon nanotube radiotracers. *Proceedings of the National Academy of Sciences of the United States of America-Physical Sciences*, 103, 3357–62.

Smart, S.K, Cassady, A.I., Lu, G.Q., & Martin, D.J. (2006). The biocompatibility of carbon nanotubes. *Carbon*, 44, 1034–47.

Soto, K.F., Carrasco, A., Powell, T.G., Garza, K.M, & Murr, L.E. (2005). Comparative in vitro cytotoxicity assessment of some manufactured nanoparticulate materials characterized by transmission electron microscopy. *Journal of Nanoparticle Research*, 7, 145–69.

Soto, K.F., Carrasco, A., Powell, T.G., Murr, L.E., & Garza K.M. (2006). Biological effects of nanoparticulate materials. *Materials Science and Engineering C-Biomimetic and Supramolecular Systems*, 26, 1421–27.

Sprent, J., Schaefer, M., Lo, D., & Kormgold, R. (1986). Properties of purified T cell subsets: II. In vivo responses to class I vs. class II H-2 differences. *Journal of Experimental Medicine*, 163, 998–1011.

Stone, V., Shaw, J., Brown D.M., Macnee, W., Faux, S.P., & Donaldson, K. (1998). The role of oxidative stress in the prolonged inhibitory effect of ultrafine carbon black on epithelial cell function. *Toxicology In Vitro*, 12, 649–59.

Tabata, Y., Murakami, Y., Ikada, Y. (1997) Photodynamic effect of polyethylene glycol-modified fullerene on tumor. *Japanese Journal of Cancer Research*, 88, 1108–16.

Tian, F., Cui, D., Schwarz, H., Estrada, G.G., & Kobayashi H. (2006). Cytotoxicity of single-wall carbon nanotubes on human fibroblasts. *Toxicology In Vitro*, 20, 1202–12.

Tokuyama, H., Yamago, S., Nakamura, E., Shiraki, T., & Sugiura, Y. (1993). Photoinduced biochemical activity of fullerene carboxylic acid. *Journal of the American Chemical Society*, 115, 7918–9.

Tran, C.L., Buchanan, D., Cullen, R.T., Searl A., Jones, A.D., & Donaldson K. (2000). Inhalation of poorly soluble particles. II. Influence of particle surface area on inflammation and clearance. *Inhalation Toxicology*, 12, 1113–26.

Tsuchiya, T., Oguri, I., Yamakoshi, Y.N., & Miyata, N. (1996). Novel harmful effects of [60]fullerene on mouse embryos in vitro and in vivo. *FEBS Letters*, 393, 139–45.

Valko, M., Morris, H., & Cronin, M.T.D. (2005). Metals, toxicity and oxidative stress. *Current Medicinal Chemistry*, 12, 1161–1208.

Wang, I.C., Tai, L.A., Lee, D.D., Kanakamma, P.P., Shen, C.K.-F., Lauh, T.-Y., Cheng, C.H., & Hwang, K.C. (1999). C_{60} and water-soluble fullerene derivatives as antioxidants against radical-initiated lipid peroxidation. *Journal of Medicinal Chemistry*, 42, 4614–20.

Warheit, D.B., Laurence, B.R., Reed, K.L., Roach, D.H., Reynolds, G.A.M., & Webb, T.R. (2004). Comparative pulmonary toxicity assessment of single-walled carbon nanotubes in rats. *Toxicological Sciences*, 77, 117–25.

Worle-Knirsch, J.M., Pulskamp, K., & Krug, H.F. (2006). Oops they did it again! Carbon nanotubes hoax scientists in viability assays. *Nano Letters*, 6, 1261–68.

Yamago, S., Tokuyama, H., Nakamura, E., Kikuchi, K., Kananishi, S., Sueki, K., Nakahara, H., Enomoto, S., & Ambe, F. (1995). In vivo biological behavior of a water-miscible fullerene: ^{14}C labeling, absorption, distribution, excretion, and acute toxicity. *Chemistry and Biology*, 2, 385–9.

Yamakoshi, Y.N., Yagami, T., Fukuhara, K., Sueyoshi, S., & Miyata, N. (1994). Solubilizationof fullerenes into water with polyvinylpyrrolidone applicable to biological tests. *Journal of the Chemical Society-Chemical Communications*, 4, 517–8.

Yamakoshi, Y.N., Yagami, T., Sueyoshi, S., & Miyata, N. (1996). Acridine adduct of [60] fullerene with enhanced DNA-cleaving activity. *Journal of Organic Chemistry*, 61, 7236–7.

Yamawaki, H. & Iwai, N. (2006). Cytotoxicity of water-soluble fullerene in vascular endothelial cells. *American Journal of Physiology-Cell Physiology*, 290, C1495–C1502.

Yang, X.L., Fan, C.H., & Zhu, H.S. (2002). Photo-induced cytotoxicity of malonic acid [C_{60}]fullerene derivatives and its mechanism. *Toxicology In Vitro*, 16, 41–6.

Ye, J., Shi, X., Jones, W., Rojanasakul, Y., Cheng, N., Schwegler-Berry, D., Baron, P., Deye, G.J., Li, C. & Castranova, V. (1999). Critical role of glass fiber length in TNF-α production and transcription factor activation in macrophages. *American Journal of Physiology- Lung Cellular and Molecular Physiology,* 276, L426–L434.

Zhao, X., Striolo, A., & Cummings, P.T. (2005). C_{60} binds to and deforms nucleotides. *Biophysical Journal*, 89, 3856–62.

9

Factors Controlling Pharmacokinetics of Intravenously Injected Nanoparticulate Systems

S. Moein Moghimi and Islam Hamad

Introduction

Particulate nanosystems, such as liposomes, polymeric micelles, and nanospheres have long been used for site-specific delivery of therapeutic and diagnostic agents following intravenous injection (Moghimi et al., 2005a). Additionally, there is a catalogue of nanoparticulate entities exhibiting unique physical and chemical properties, such as high rigidity, high thermal and electrical conductivity, and superparamagnetism, which have applications in experimental imaging, cell ablation, and even drug delivery following introduction into the vasculature (Moghimi et al., 2005a; Moghimi & Kissel, 2006). Examples include semiconductive single- and multi-walled carbon nanotubes (SWNT and MWNT, respectively) and iron/iron oxide core–shell nanoclusters (Klumpp et al., 2006; Qiang et al., 2006).

The biological performance of intravenously injected nanoparticles is controlled by a complex array of physicochemical and physiopathological factors (Moghimi et al., 2001, 2005a, 2006c). Physicochemical considerations include nanoparticle size distribution, shape, density, rigidity or deformability, and surface characteristics (e.g. surface electric charge, surface density, and conformation of adsorbed or grafted synthetic polymers and biological ligands). These factors not only control the flow properties of nanoparticles within the blood vessels and at bifurcations in vascular and capillary systems, but also modulate nanoparticle circulation times, tissue deposition patterns, mode of entry into cells (as in *Rho*-dependent phagocytosis, clathrin-mediated endocytosis, internalization through membrane rafts, and uptake mechanisms independent of phagocytosis, clathrin, and caveolae), intracellular trafficking, contents release, and toxicity (Andresen et al., 2004; Bhatia et al., 2003; Decuzzi & Ferrari, 2006; Harush-Frenkel et al., 2007; Lovrić et al., 2005; Moghimi et al., 2001, 2004, 2005a, 2006c; Patil et al., 2001; Poznansky & Juliano, 1984). For instance, oblate ellipsoidal particles have been proposed to adhere more effectively to the biological substrates than their corresponding classical spherical particles of the same volume (Decuzzi & Ferrari, 2006). In addition, non-spherical nanoparticles can carry more drugs and

M.M. de Villiers et al. (eds.), *Nanotechnology in Drug Delivery*, DOI: 10.1007/978-0-387-77667-5_9,

contrast agents than their corresponding spherical particles of the same adhesive strength, which may improve therapeutic and diagnostic efficacy.

Biological considerations that control nanoparticle circulation times in the blood and tissue distribution include determinants of phagocytic/endocytic recognition and ingestion, the "state-of-responsiveness" of the host immune system, and escape routes from the vasculature (Moghimi, 2003; Moghimi et al., 2001, 2005a).

A clear understanding of the above-mentioned events is crucial for optimization and development of complex multi-functional nanoparticles for investigative, diagnostic, and therapeutic needs. This article briefly examines the interplay between physicochemical and biological factors that control nanoparticle pharmacokinetics following intravenous route of injection.

Protein Adsorption and Opsonization Events

Numerous studies have confirmed that, following contact with the blood, nanoparticles acquire a coating of plasma proteins (Chonn et al., 1992, 1995; and reviewed in Moghimi et al., 2001; Moghimi & Szebeni, 2003). This coating differs considerably in amount and in pattern depending on the dose, the physicochemical characteristics of the nanoparticles, and the exposure time. The protein coating has a number of important ramifications for pharmacokinetics and tissue distribution of nanoparticles. One aspect concerns the extent of nanoparticle aggregation and trapping in the first capillary bed encountered. Another consequence of nanoparticle–protein interaction is opsonization that is the adsorption of those plasma proteins subsequently capable of interacting with their receptors expressed by macrophages in contact with the blood (Moghimi et al., 2001; Moghimi & Szebeni, 2003). Examples of opsonic proteins include various subclasses of immunoglobulins, certain components of the complement system (e.g. C1q, C3b, iC3b), fibronectin, C-reactive protein, lipopolysaccharide-binding protein, and von Willebrand factor. Non-specific protein adsorption may also play an important role in particle clearance. Following adsorption, non-specific proteins could undergo conformational changes and expose chemical structures that could either be recognized directly by macrophage receptors or could act as a template for subsequent recognition by opsonic proteins.

The largest population of macrophages in contact with blood is located in the liver sinuses (Kupffer cells). Therefore, it is not surprising to see that after intravenous injection opsonized particles are rapidly, and predominantly, intercepted by Kupffer cells. In addition, nanoparticle clearance from the blood by splenic marginal zone and red-pulp macrophages, persinal phagocytes of the bone marrow, and blood monocytes also occurs to some extent. Thus, following intravenous injection of drug-encapsulated nanoparticles, drug exposure becomes limited to lysosomal and cytoplasmic compartments of macrophages, and is advantageous for treatment of disease and disorders of the reticuloendothelial system (Moghimi, 2003; Moghimi et al., 2005a). Macrophage recognition and clearance of nanoparticles from the blood can be further accelerated by surface attachment of substrates/ligands for macrophage scavenger, integrin, dectin,

galactose/fucose, mannose, and Toll-like receptors. Here, associated signalling events will be different, depending on the target receptor.

Blood monocytes can also migrate out of the circulation into various locations such as lungs and the brain, and differentiate into macrophages. The specific targeting of one or more immunomodulators to monocytes could, therefore, significantly enhance host resistance against cancer in specific locations; for instance, the lungs are a major site of disseminated metastatic disease, and an organ that is not rich in reticuloendothelial activity.

Differential Opsonization and Macrophage Heterogeneity

Of particular interest is the concept of "differential opsonization", which may account for the observed differences in clearance rates and phagocyte sequestration of nanoparticles and vesicles (Moghimi et al., 2001, 2005a; Moghimi & Hunter, 2001; Yan et al., 2004). For example, certain liposomes of 200–500 nm in size are more efficient in activating the complement system, and hence are cleared faster from the blood than their smaller counterparts (50 nm) (Devine et al., 1994). This is a reflection of the surface dynamic and geometric effects on the assembly of proteins and proteases involved in complement activation. The extent and the mode of complement activation by liposomes also depend on vesicular lipid composition, bilayer packing, and surface characteristics (Moghimi & Hunter, 2001). For instance, in the absence of anti-phospholipid and anti-cholesterol antibodies, liposomes containing anionic phospholipids (e.g. cardiolipin and phoshpatidylglycerol) in their bilayer interact with C1q, a process that leads to activation of the classical pathway of the complement system in rats and humans and fixation of complement opsonic C3 fragments (Marjan et al., 1994). On the other hand, cationic liposomes tend to activate the human complement system via the alternative pathway. In contrast to charged lipids, liposomes composed of zwitterionic egg phosphatidylcholine seem to activate complement only after prolonged exposure to serum, presumably via C-reactive protein-binding pathway (Volanakis & Wirtz, 1979). Elevated levels of plasma lipoproteins can also modulate the extent of complement activation. For example, we (Moghimi et al., 2006b) have shown that elevated levels of serum LDL and HDL can significantly suppress cholesterol-rich liposome-mediated complement activation, Figure 9.1.

Depending on surface characteristics of nanoparticles, non-specific adsorption of intact C3 may initiate complement activation in the presence of factors B and D (Moghimi & Szebeni, 2003). Activation of the alternative pathway may even involve antibodies via their F(ab) portion (Moore et al., 1982), the binding of which to C3b is most likely to depend on a two antigenic subsite-fixed orientation of IgG.

Hydrophobic entities such as carbon nanotubes also activate complement, but the activation process is dependent on nanotube morophology. Both hydrophobic SWNTs and MWNTs activate the human complement system via the classical pathway through surface adsorption of C1q, but DWNTs further activate complement through the alternative pathway (Salvador-Morales et al., 2006). In addition, binding of other plasma proteins to carbon nanotubes is a highly selective process; remarkably, there is no IgG, IgM, pentraxin, and fibronectin binding, but protein

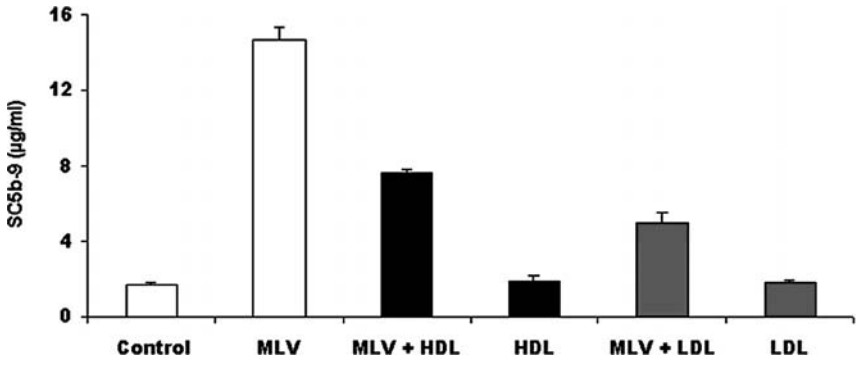

Figure 9.1 The effect of elevated levels of HDL and LDL in human serum on liposome-mediated complement activation. Multilamellar vesicles (MLV) were composed of dimyristoylphosphatidylcholine, dimyristoylphosphatidylglycerol, and cholesterol (50:5:45 mole ratios). The final concentration of liposomes in serum was 5 mg/mL. The cholesterol and triglyceride levels of the serum were normal, and approximately 180 and 200 mg/dL, respectively. The addition of purified HDL to serum increased cholesterol levels by 25–30%. The addition of purified LDL doubled serum cholesterol levels, a situation similar to that encountered in heterozygous familial hypercholesterolemia. Liposome-mediated complement activation, through both calcium-sensitive and alternative pathways, in undiluted human serum was monitored by measuring the production of the S-protein-bound form of the terminal complex, SC5b-9, using an enzyme-linked immunosorbent assay kit (Moghimi et al., 2006b).

adsorption is exclusive to apolipoprotein AI, AIV, C-III, albumin, and fibrinogen. These observations are also in line with rapid Kupffer cell deposition of intravenously injected carbon nanotubes of 1 nm diameter and 300 nm length (Cherukuri et al., 2006). Longer nanotubes (spanning from several to tens of micrometer in length), however, may be too large to be phagocytosed, and as a result of complement activation, inflammatory responses and granuloma formation may follow.

The concept of differential opsonization is also important as macrophages are heterogeneous with respect to physiological function and phenotype, even within the same organ (Moghimi, 2003; Moghimi et al., 2001). Therefore, some populations of macrophages may utilize one particular predominant recognition mechanism. In relation to this statement, a recent study has demonstrated the predominant localization of intravenously injected liposomes, which were surface modified with the anionic 1,5-dihexadecyl-L-glutamate-*N*-succinic acid, to persinal macrophages of the rabbit bone marrow (Sou et al., 2006). The dynamic and differential processes of protein/opsonin binding to nanoparticles could even indicate an arrangement based on a recognition hierarchy. Thus a specific macrophage receptor might recognize the earliest changes associated with a particle surface, whereas other receptors might recognize particles at a later stage, ensuring their complete removal from the systemic circulation.

The Role of Protein Adsorption on Particle Binding to Non-phagocytic Cells

Adsorption of blood proteins on to nanoparticles may even affect nanoparticle binding to and clearance by non-phagocytic cells. For instance,

following complement activation and binding of C3b, C4b, or C3b breakdown products iC3b and C3d, nanoparticles may further interact with platelets and erythrocytes. In rats, platelets express type I complement receptors (CR1) that bind C3b-opsonized liposomes (Loughrey et al., 1990), whereas in primates erythrocytes express CR1 (Cornacoff et al., 1983), which could play a critical role in pharmacokinetic of certain C3b-opsonized nanoparticles. Another example is surface enrichment of polysorbate-80-coated nanospheres within the blood by apolipoproteins-B and E, resulting in some nanoparticle recognition by the LDL receptors of the rat blood–brain barrier endothelial cells (Kreuter et al., 2003). Apolipoprotein-E was also shown to play an exclusive role in recognition of electrically neutral liposomes by murine hepatocytes (Scherphof & Kamps, 2001; Yan et al., 2005).

Suppression of Opsonization Events

The surface of nanoparticles, nanotubes, and even viruses can be manipulated with a wide range of polymeric materials that are capable of generating a hydrophilic steric barrier (Liu et al., 2006; reviewed in Moghimi, 2006; Moghimi et al., 2001, 2005a; Moghimi & Szebeni, 2003; Romberg et al., 2007). In principle, the engineered steric barrier should combat surface opsonization events, and hence minimize nanoparticle clearance by macrophages in contact with the blood (Moghimi et al., 1993b). As a result, the circulation time of nanoparticles in the blood is expected to be prolonged, and nanoparticles may be targeted "passively" or "actively" to accessible non-macrophage elements. The pharmacokinetics of such engineered entities, however, depends on density and conformation of surface-projected hydrophilic polymers, Figure 9.2 (Al-Hanbali et al., 2006; Gbadamosi et al., 2002). For example, the tetrafunctional polyethylene oxide/polypropylene oxide ethylenediamine block copolymer poloxamine 908 can adsorb on to the surface of hydrophobic nanoparticles via its central polypropylene oxide chains, which leaves the relatively hydrophilic polyethylene oxide segments to extend outwards from the nanoparticle surface (Moghimi et al., 1993b). We (Al-Hanbali et al., 2006) recently demonstrated that accommodation of at least 11,500 poloxamine molecules on the surface of a polystyrene nanoparticle of 230 nm diameter was necessary for suppressing nanoparticle-mediated complement consumption (but not totally inhibiting the process) and conferring longevity in the blood when compared with a naked nanoparticle. These conditions generated a sufficient density of polyethylene oxide on nanoparticle surface, where projected chains assumed a brush-like configuration to combat rapid complement activation and particle clearance by the hepatic macrophages. At a lower surface density, while maintaining the brush configuration of the projected polyethylene oxide chains, complement consumption was increased and nanoparticles were more prone to phagocytic clearance. At a critical surface density of 3,700 poloxamine 908 molecules per nanoparticle, polyethylene oxide chains assumed a mushroom-like configuration as supported by biophysical characterization. Here, complement consumption proceeded rapidly in a manner comparable to uncoated nanoparticles, and the engineered particles circulated in the blood for considerably shorter periods of time.

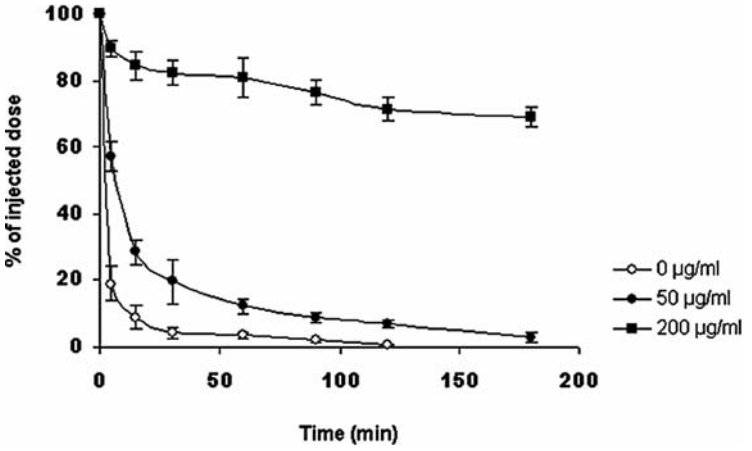

Figure 9.2 The effect of poloxamine 908 surface coverage on polystyrene nanoparticle circulation profile in rats. The core size of polystyrene nanoparticles was 60 nm in diameter. Particles were surface labelled with [^{125}I]Na prior to poloxamine coverage. Surface modification was achieved by incubating nanoparticles with poloxamine 908 at room temperature overnight. The equilibrium poloxamine concentration was either 50 or 200 μg/ml, respectively. At the lower equilibrium poloxamine concentration, the surface-projected poly(ethylene oxide) chains are spread laterally with portions in close contact with the surface of nanoparticles (mushroom configuration) and correspond to the first plateau region on the adsorption isotherm (Al-Hanbali et al., 2006). At an equilibrium poloxamine 908 concentration of 200 μg/ml, which corresponds to the top plateau region of the adsorption isotherm, poly(ethylene oxide) chains assume a laterally compressed elongated random coil conformation in a direction perpendicular to the plane of particle surface. Particles (3.5 mg polystyrene/kg body weight) were injected intravenously via tail vein and the blood concentration of nanoparticles was evaluated at various intervals.

Methoxy(polyethylene glycol)$_{2000}$-grafted liposomes (PEGylated liposomes) are also known to exhibit prolonged circulation time in the blood (reviewed in Moghimi et al., 2001; Moghimi & Szebeni, 2003). For example, a clinical formulation of PEGylated liposomes (Doxil®) shows a biphasic circulation half-life of 84 min and 46 h in humans. Contrary to the view that poly(ethylene glycol) grafting should suppress opsonization processes, we have (Moghimi et al., 2006a) shown that PEGylated liposomes can efficiently activate the human complement system via both classical and alternative pathways and fix complement proteins (Figure 9.3). Our studies indicated that complement activation was due to the expression of the net anionic charge on the oxygen phosphate moiety of phospholipid-methoxy (polyethylene glycol) conjugate; methylation of the phosphate oxygen, and hence the removal of the negative charge, totally prevented generation of complement activation products (e.g. SC5b-9 complexes), anaphylatoxins, and complement split products (e.g. Bb and C4d) in human serum (Moghimi et al., 2006a). Remarkably, complement fixation by PEGylated liposomes seemed to play a minor role in macrophage clearance via complement receptors; the surface-projected methoxy(polyethylene glycol) chains sterically interfered with the binding of surface-bound iC3b to the macrophage complement receptor. This process seems to explain the prolonged circulation times of "stealth" liposomes.

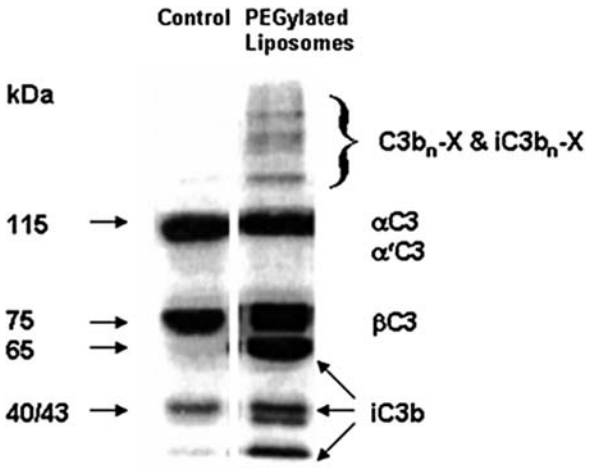

Figure 9.3 SDS-PAGE analysis of PEGylated liposome-mediated complement activation in 20% (v/v) human serum supplemented with [^{125}I]-labelled C3. Generation of the scission products of iC3b (40/43 kDa bands) together with the lack of α′C3 band implies efficient inactivation of C3b to iC3b by factors H and I (Moghimi et al., 2006b). The presence of C3b$_n$-X/iC3b$_n$-x complexes suggests that C3 processing has occurred in a similar fashion to immune aggregate-mediated complement activation.

Long-circulating entities are further amenable to surface modification with biological ligands for targeting to blood elements (e.g. lymphocytes or blood clots) and vascular endothelial cells (Moghimi, 2006; Moghimi et al., 2005a; Allen, 2002; Murray & Moghimi, 2003). Pharmacokinetics and biodistribution of these entities will be modulated by their size and stability in the blood as well as surface density, location (direct attachment to the particle surface, or to distal end of surface-projected polymer chains, or both), and conformation of the attached ligands (Bendas et al., 2003).

Nanoparticle Escape from the Vasculature

Splenic Red-Pulp

If confinement of long-circulating nanoparticles to the vascular system is necessary (e.g. for slow and controlled drug release), then splenic filtration processes in the red-pulp regions must be considered. In sinusoidal spleen (as in rat and human) blood flow is mainly through the open route of circulation (little or no endothelial continuity from arterial capillaries to venous vessels, resulting in direct blood contact with the reticular meshwork of marginal zone and the red-pulp), where particulate filtration at inter-endothelial cell slits of venous sinuses become predominant. Splenic filtration is frequently observed for non-deformable entities whose size exceeds the width of cell slits (200–250 nm) (Moghimi et al., 1991). Thus, long-circulating "rigid" nanoparticles will be cleared efficiently by the splenic filter, providing that their size exceeds 200 nm. Otherwise, opportunities are there for gaining access to the splenic red-pulp regions, which are rich in macrophages. Indeed, we (Moghimi et al., 1991, 1993a) have shown that within a few hours of intravenous injection, poloxamine 908-coated polystyrene nanoparticles of 230 nm size predominantly localize to the splenic red-pulp compartments. Remarkably, resident macrophages of the red-pulp phagocytosed filtered nanoparticles (Moghimi et al., 1993a). This was a surprising observation, since poloxamine-coated nanoparticles were expected to resist ingestion by quiescent macrophages. The phagocytic

process, presumably had occurred after intrasplenic loss of some surface-adsorbed poloxamine molecules (as a result of inter-endothelial cell slit resistance to blood flow through the reticular meshwork and altered dynamic flow properties of red blood cells and plasma), thus triggering local opsonization events at the nanoparticle surface. This notion is in agreement with significant levels of complement activation and fixation with nanoparticles bearing a critical number of poloxamine molecules (see above) (Al-Hanbali et al., 2006).

The meshwork of the red-pulp also expresses an enormous contact surface area for particulate matters; its large cross-sectional area for flow can slow down red blood cell and particle velocity and facilitate their trapping. Here, factors influencing particulate retention are principally physicochemical and are related to surface properties such as surface charge and adhesiveness.

Bone Marrow Sinuses

The medullary sinuses in the bone marrow are formed from an uninterrupted layer of spindle-shaped endothelial cells, an outer discontinuous layer of supporting adventitial cells, and a discontinuous basal lamina. Macrophages abound in the vicinity of marrow sinuses, and in some species they are considered as a component of the marrow–blood barrier. Systemic nanoparticles, however, may reach the bone marrow compartment through transport mechanisms across the blood–bone marrow barrier, which includes transcellular and intracellular routes. The former route is through diaphragmed fenestrae of endothelial walls, whereas the intracellular route is associated with the formation of bristle-coated pits on the luminal surface of the endothelium (Moghimi, 1995).

A remarkable case, however, was reported with poloxamer 407-coated polystyrene particles of 60 nm size after intravenous injection into rabbits (Porter et al., 1992). These particles were resistant to clearance by scavengers of the liver and the spleen, but within 12 h of injection predominant nanoparticle localization to sinus endothelial cells of the bone marrow was notable without evidence of transcytosis. Thus exquisite levels of recognition and specificity are achievable with surface modification, either directly or through a time-dependent differential protein-binding phenomenon.

Open Fenestrations in the Liver and Pathological Vessels

Nanoparticle escape from the circulation may further occur at sites where the blood capillaries have open fenestrations, or when the integrity of the endothelial barrier is perturbed by inflammatory processes, or dysregulated angiogenesis. For example, open fenestrations are found in the sinus endothelium of the liver, where the size of fenestrae can be as large as 150 nm. A significant fraction of some deformable particles and vesicles (even larger than 150 nm) may get access to the hepatic parenchyma through the space of Disse, between the lining cells and the hepatocyte surface, by “endothelial massaging” (Romero et al., 1999). Although this may provide an opportunity for targeting of particles to hepatocytes and

hepatic stellate cells, the number and frequency of endothelial fenestrae is significantly decreased in chronic liver diseases.

Hyper-permeability of tumour microvessels to macromolecules as well as to nanoparticles is long established (reviewed in Moghimi, 2007a; Munn, 2003). Detailed morphological investigations have demonstrated heterogeneity in pore sizes along a typical tumour blood vessel; tumours that were grown subcutaneously exhibited a characteristic pore cut-off size ranging from 200 to 1200 nm with the majority ranging between 380 and 780 nm (Hobbs et al., 1998). The pore cut-off size in tumours is also modulated by microenvironmental factors such as hormones and growth factors. For instance, the pore cut-off size is reduced when tumours are grown in the cranium (Hobbs et al., 1998). In androgen-dependent mouse mammary tumour, testosterone withdrawal also reduced the pore cut-off size from 200 nm to less than 7 nm within 48 h (Hobbs et al., 1998). Nevertheless, the idea of exploiting the vascular abnormalities of the tumours, restricting penetration into normal tissue interstitium while allowing better access to that of the tumour with long-circulatory and multi-functional nanoparticles and vesicles of different shape, size, and composition, is an attractive one, and has received considerable attention (reviewed in Moghimi et al., 2001, 2005a; Moghimi, 2006, 2007a). These approaches should, therefore, be used before hormone ablation therapies or other therapies that may reduce transvascular transport. In the case of macromolecules, transport across tumour blood vessels may further occur via caveolae and vesicular vacuolar organelles.

Following extravasation into tumour interstitium, nanoparticulate carrier systems must be able to release its cargo at a rate that maintains free drug levels in the therapeutic range; a process also amenable to modulation by nanoengineering (Andresen et al., 2004). While passively targeted long-circulating carriers can show anti-tumour activity, higher and more selective anticancer activity is achievable by surface decoration of long-circulating nanoparticles with a plethora of tumour-specific ligands, such as monoclonal antibodies (e.g. anti-HER2 antibodies), folate, transferrin, vasoactive intestinal peptide, and sigma-1 selective substrates (Allen, 2002; Sudimack & Lee, 2000).

Lymph Nodes

Small fractions of particles of 1–20 nm size range may slowly extravasate from the vasculature into the interstitial spaces, from which they are transported to the regional lymph nodes by way of patent junctions of the lymphatic vessels (Moghimi & Bonnemain, 1999). Also, depending on the species type, some nanoparticles may leave the vascular compartment through post-capillary venules and adjoining capillaries, where blood flow is sluggish and endothelial permeability is controlled by a number of mediators, and reach the lymph nodes. Indeed, these modes of particle extravasation from the vascular system have been exploited in medical imaging using dextran-coated superparamagnetic iron oxide nanocrystals. For instance, such nanocrystals have aided visualization of micrometastases in lymph nodes by magnetic resonance imaging (Harisinghani et al., 2003).

The Glomerular Filter

The capillary endothelium of glomerular filter contains large round fenestrations of 50–100 nm diameter, which occupies approximately 20% of the endothelial surface. These fenestrations do not exhibit diaphragms. However, nanoparticle passage across these fenestrations is hampered by the presence of a continuous and thick (240–340 nm) basement membrane as well as by the primary processes of podocytes, which embrace the capillaries, giving rise to pedicels, which interdigitate with those of the primary processes. The openings between the pedicels, or the filtration slits, are approximately 25 nm in width and bridged by a delicate electron-dense diaphragm of 4 nm thick. Podocytes also possess phagocytic function, that is to ensure the removal of large molecules and small particles that may have been trapped in the outer layers of the filter. Macromolecules and particles trapped on the endothelial side are cleared by mesangial cells.

In spite of these barriers, a recent study involving carbon nanotubes has claimed that following intravenous injection into mice, water-soluble functionalized SWNTs (20–40 nm in width and variable long lengths) are cleared rapidly intact from the systemic circulation through the renal excretion route (Singh et al., 2006). These observations presumably indicate that carbon nanotubes are capable of damaging the endothelial barrier of the glomerular capillaries (primarily the filtration slits) following insertion through their hydrophilic termini. The damage may even extend to fenestrated capillaries of proximal- and distal-convoluted tubule regions. Unfortunately, kidney function tests and morphological studies were not conducted to assess the integrity of glomerular filter following nanotube administration. In the absence of such studies, the proposed therapeutic applications of intravenously injected carbon nanotubes cannot be perceived safe.

The capillary endothelium of glomerular filter and the outer surface of the podocytes, including the filtration slits, exhibit a strong negative electric charge. These sites may play a role in binding to small entities that exhibit cationic charge in plasma. For example, efficient kidney accumulation of generation 3 poly(amidoamine) Starburst dendrimers was reported by Roberts et al. (1996).

Dosing Regimen

It is now apparent that particulate nanocarriers exert substantial effects on pharmacokinetics and body distribution of their entrapped cargo. However, limited information is available for differing dose schedules and dose intensities. This is of particular importance where patients are expected to receive multiple injections, as in delivery of anticancer agents with long-circulating nanoparticles. Here, one should ensure that the first dose has had time to clear before subsequent doses.

A recent study (Charrois & Allen, 2003) has evaluated the effect of dosing schedule on the pharmacokinetics of doxorubicin entrapped in long-circulating liposomes (Doxil®) following multiple intravenous injections into mice (four injections of liposomes at a dose of 9 mg/kg and dose intervals of either 1, 2, or 4 weeks). Interestingly, plasma pharmacokinetics

of doxorubicin in each injection cycle was independent of the next cycle. Initially, these observations, however, would appear to contradict those of Ishida et al. (2003, 2006b) who demonstrated that an injection of PEGylated liposomes in rats could elicit the production of a poly(ethylene glycol)-specific IgM in the spleen (independent of T-cells), resulting in opsonization (complement activation) and rapid hepatic elimination of a subsequent liposome dose given 5 days later. Increasing the time interval between the two injections, however, weakened the effect and by third dose, hardly any effect on pharmacokinetics relative to the first injection was seen. In addition, the altered pharmacokinetics was dose dependent (Ishida et al., 2006a). For instance, no rapid clearance of the second liposome dose occurred when the first liposome dose exceeded 5 μmol phospholipid/kg body weight. Further, it was shown that doxorubicin encapsulation could also control pharmacokinetics of subsequent liposome injections (Ishida et al., 2006a). The first dose of doxorubicin-encapsulated liposomes failed to dramatically increase plasma levels of poly(ethylene glycol)-specific IgM antibodies, presumably as a consequence of doxorubicin-mediated macrophage death and inhibition of B cell-proliferation and/or killing of proliferating B cells, resulting in prolonged circulation times of subsequent liposome doses. Altered pharmacokinetics of long-circulating liposomes following repeated administration has also been reported by other investigators (Dams et al., 2000; Romberg et al., 7007).

The most notable dose-limiting toxicity associated with continuous and repeated infusion of Doxil® is doxorubicin accumulation in the skin, resulting in palmar–plantar erythrodysesthesis (PPE) (Lyass et al., 2000). The incidence of PPE can be lowered substantially by reducing the dose intensity as well as the interval between subsequent dosing. For example, recent studies in mice have demonstrated that skin pharmacokinetics of one injection cycle of Doxil® was independent of the next injection cycle when the dose interval was 4 weeks, with little evidence of symptoms of PPE (Charrois & Allen, 2003).

In contrast to liposomes, repeated intravenous injection of long-circulating polymeric nanospheres generates different responses. For instance, a single intravenous dose of poloxamine 908-coated polystyrene nanospheres of 60 nm size dramatically affected the circulation half-life and body distribution of a second subsequent dose in a time-dependent, but opsonic-independent, manner (Moghimi & Gray, 1997). At 3 days after a single intravenous dose, Kupffer cells and splenic macrophages could clear a second dose of long-circulating nanospheres from the blood. When the interval between the two injections was increased to 14 days, the second dose behaved as long circulatory. Remarkably, the coating material (poloxamine 908) was shown to trigger nanosphere clearance by resident Kupffer cells and certain sub-populations of splenic macrophages, since a single intravenous injection of an endotoxin-free solution of poloxamine 3 days before the administration of long-circulating nanospheres induced similar effects (Moghimi & Gray, 1997). The observations may be due to altered macrophage functions through gene activation and signalling pathways, leading to increased mobility of some plasma membrane receptors or expression of new receptors capable of directly recognizing surface characteristics of long-circulating nanospheres.

The State of Macrophage Responsiveness

Macrophage priming and activation can be induced experimentally (e.g. by lipopolysaccharide or zymosan challenge), and is also known to occur in certain physiopathological conditions. Such macrophages can proceed with recognition and internalization of long-circulating nanoparticles via both opsonic-dependent and opsonic-independent modes (reviewed in Moghimi et al., 2001). These observations are of importance in therapeutic protocols that utilize long-circulating carriers for targeting to non-macrophage sites in clinical conditions associated with globally or regionally enhanced macrophage activity.

Conclusions

The biomedical applications of nanoparticle carriers for site-specific delivery of therapeutic and contrast agents are well established. This trend will surely continue with the advent of nanotechnology and parallel developments in design of functional entities (e.g. metal and rod nanoshells, porous silicon nanoparticles) as well as multi-functional nanomedicines for simultaneous sensing, signalling, and drug release. Such innovations and novel approaches are already the focus of the US National Institute of Health's Nanomedicine Roadmap Initiative as well as the European Science Foundation. Nanoparticles, however, do not behave similarly when injected intravenously. Their pharmacokinetics is controlled by complex and inter-related physicochemical, anatomical, pathophysiological, and immunobiological factors, as well as the dosing regimen. These parameters must be studied individually for each specific nanoparticle. In the case of intravenous gene therapy with polyplexes and cationic nanoparticles, issues such as poor transfection efficiency, polycation-mediated cell death, and insufficient distribution to target cells are substantial and need to be resolved (Moghimi, 2007b; Moghimi et al., 2005b). A clear understanding of these issues could lead to design and engineering of multi-functional nanomedicines with optimal biological performances in relation to specific clinical conditions.

References

Al-Hanbali, O., Rutt, K. J., Sarker, D. K., Hunter, A. C., & Moghimi, S. M. (2006). Concentration dependent structural ordering of poloxamine 908 on polystyrene nanoparticles and their modulatory role on complement consumption. *J. Nanosci. Nanotechnol.*, *6*, 3126–3133.

Andresen, T. L., Jensen, S. S., & Jørgensen, K. (2004). Advanced strategies in liposomal cancer therapy: problems and prospects of active tumor specific drug release. *Prog. Lipid Res., 44*, 68–97.

Allen, T. M. (2002). Ligand-targeted therapeutics in anticancer therapy. *Nat. Rev. Cancer, 2*, 750–763.

Bendas, G., Rothe, U., Scherphof, G. L., & Kamps, J. A. A. M. (2003). The influence of repeated injections on pharmacokinetics and biodistribution of

different types of sterically stabilized immunoliposomes. *Biochim. Biophys. Acta, 1609*, 63–70.

Bhatia, S. K., King, M. R., & Hammer, D. A. (2003). The state diagram for cell adhesion mediated by two receptors. *Biophys. J., 84*, 2671–2690.

Charrois, G. J. R., & Allen, T. M. (2003). Multiple injections of PEGylated liposomal doxorubicin: pharmacokinetics and therapeutic activity. *J. Pharmacol. Exp. Ther., 306*, 1058–1067.

Cherukuri, P., Gannon, C. J., Leeuw, T. K., Schmidt, H. K., Smalley, R. E., Curley, S. A., & Weisman, R. B. (2006). Mammalian pharmacokinetics of carbon nanotubes using intrinsic near-infrared fluorescence. *Proc. Natl. Acad. Sci. USA, 103*, 18882–18886.

Chonn, A., Semple, S. C., & Cullis, P. R. (1992). Association of blood proteins with large unilamellar liposomes in vivo. Relation to circulation lifetimes. *J. Biol. Chem., 267*, 18759–18765.

Chonn, A., Semple, S. C., & Cullis, P. R. (1995). β2-Glycoprotein I is a major protein associated with very rapidly cleared liposomes in vivo, suggesting a significant role in the immune clearance of 'non-self' particles. *J. Biol. Chem., 270*, 25845–25849.

Cornacoff, J. B., Hebert, L. A., Smead, W. L., & Van Aman, M. E. (1983). Primate erythrocyte-immune complex-clearing mechanism. *J. Clin. Invest., 71*, 236–247.

Dams, E. T. M., Laverman, P., Oyen, W. J. G., Storm, G., Scherphof, G. L., Van der Meer, J. W. M., Corstens, F. H., & Boerman, O. C. (2000). Accelerated blood clearance and altered biodistribution of repeated injections of sterically stabilized liposomes. *J. Pharmacol. Exp. Ther., 292*, 1071–1079.

Decuzzi, P., & Ferrari, M. (2006). The adhesive strength of non-spherical particles mediated by specific interactions. *Biomaterials, 27*, 5307–5314.

Devine, D. V., Wong, K., Serrano, K., Chonn, A., & Cullis, P. R. (1994). Liposome-complement interactions in rat serum: implications for liposome survival studies. *Biochim. Biophys. Acta, 1191*, 43–51.

Gbadamosi, J. K., Hunter, A. C., & Moghimi, S. M. (2002). PEGylation of microspheres generates a heterogeneous population of particles with differential surface characteristics and biological performance. *FEBS Lett., 532*, 338–344.

Harisinghani, M. G., Barentsz, J., Hahn, P. F., Deserno, W. M., Tabatabaei, S., Hulsbergen van de Kaa, C., de la Rosette, J., & Weissleder, R. (2003). Noninvasive detection of clinically occult lymph-node metastases in prostate cancer. *New Engl. J. Med., 348*, 2491–2499.

Harush-Frenkel, O., Debotton, N., Benita, S., & Altschuler, Y. (2007). Targeting of nanoparticles to the clathrin-mediated endocytic pathway. *Biochem. Biophys. Res. Commun., 353*, 26–32.

Hobbs, S. K., Monsky, W. L., Yuan, F., Roberts, W. G., Griffith, L., Torchilin, V. P., & Jain, R. K. (1998). Regulation of transport pathways in tumor vessels: Role of tumor type and microenvironment. *Proc. Natl. Acad. Sci. USA, 95*, 4607–4612.

Ishida, T., Atobe, K., Wang, X., & Kiwada, H. (2006a). Accelerated blood clearance of PEGylated liposomes upon repeated injections: effect of doxorubicin-encapsulation and high-dose first injection. *J. Control. Rel., 115*, 251–258.

Ishida, T., Ichihara, M., Wang, X., & Kiwada, H. (2006b). Spleen plays an important role in the induction of accelerated blood clearance of PEGylated liposomes. *J. Control. Rel., 115*, 243–250.

Ishida, T., Maeda, R., Ichihara, M., Irimura, K., & Kiwada, H. (2003). Accelerated clearance of PEGylated liposomes in rats after repeated injections. *J. Control. Rel., 88*, 35–42.

Klumpp, C., Kostarelos, K., Prato, M., & Bianco, A. (2006). Functionalized carbon nanotubes as emerging nanovectors for the delivery of therapeutics. *Biochim. Biophys. Acta, 1758*, 404–412.

Kreuter, J., Ramge, P., Petrov, V., Hamm, S., Gelperina, S. E., Engelhardt, B., Alyautdin, R., von Briesen, H., & Begley, D. J. (2003). Direct evidence that polysorbate-80-coated poly(butylcyanoacrylate) nanoparticles deliver drugs to the CNS via specific mechanisms requiring prior binding of drugs to the nanoparticles. *Pharm. Res., 20*, 409–416.

Liu, Z., Cai, W., He, L., Nakayama, N., Chen, K., Sun, X., Chen, X., & Dai, H. (2006). In vivo distribution and highly efficient tumour targeting of carbon nanotubes in mice. *Nat. Nanotechnol., 2*, 47–52.

Loughrey, H. C., Bally, M. B., Reinish, L. W., & Cullis, P. R. (1990). The binding of phosphatidylglycerol liposomes to rat platelets is mediated by complement. *Thromb. Haemost., 64*, 172–176.

Lovrić, J., Cho, S. J., Winnik, F. M., & Maysinger, D. (2005). Unmodified cadmium telluride quantum dots induce reactive oxygen species formation leading to multiple organelle damage and cell death. *Chem. Biol., 12*, 1227–1234.

Lyass, O., Uziely, B., Ben-Yosef, R., Tzemach, D., Heshing, N. I., Lotem, M., Brufman, G., & Gabizon, A. (2000). Correlation of toxicity with pharmacokinetics of PEGylated liposomal doxorubicin (Doxil) in metastatic breast carcinoma. *Cancer, 89*, 1037–1047.

Marjan, J., Xie, Z., & Devine, D. V. (1994). Liposome-induced activation of the classical complement pathway does not require immunoglobulin. *Biochim. Biophys. Acta, 1192*, 35–44.

Moghimi, S. M. (1995). Exploiting bone marrow microvascular structure for drug delivery and future therapies. *Adv. Drug Deliv. Rev., 17*, 61–73.

Moghimi, S. M. (2003). Exploitation of macrophage clearance functions. In S. Gordon (Ed.), *Hand-Book of Experimental Pharmacology: The macrophage as therapeutic target,* Volume 158 (pp. 41–54). Berlin: Springer-Verlag.

Moghimi, S. M. (2006). Recent development in polymeric nanoparticle engineering and their applications in experimental and clinical oncology. *Anti-cancer Agent. Med. Chem., 6*, 553–561.

Moghimi, S. M. (2007a). Passive targeting of solid tumors: pathophysiological principles and physicochemical aspects of delivery systems. In M. M. Amiji (Ed.), *Nanotechnology for cancer therapy* (p. 11–18). Boca Raton: CRC Press.

Moghimi, S. M. (2007b). Nanotoxicology of synthetic gene-transfer vectors: poly(ethylenimine)- and polyfectin-mediated membrane damage and apoptosis in human cell lines. In C. S. S. R. Kumar (Ed.), *Nanotechnologies for Life Sciences: Nanomaterials for medical diagnosis and therapy*, Volume 10 (pp. 629–643). Berlin: Wiley-VCH Verlag.

Moghimi, S. M., & Bonnemain, B. (1999). Subcutaneous and intravenous delivery of diagnostic agents to the lymphatic system: applications in lymphoscintigraphy and indirect lymphography. *Adv. Drug Deliv. Rev., 37*, 295–312.

Moghimi, S. M., & Gray, T. (1997). A single dose of intravenously injected poloxamine-coated long-circulating particles triggers macrophage clearance of subsequent doses in rats. *Clin. Sci. (Lond.) 93*, 371–379.

Moghimi, S. M., Hamad, I., Andresen, T. L., Jørgensen, K., & Szebeni, J. (2006a). Methylation of the phosphate oxygen moiety of phospholipids-methoxy(polyethylene glycol) conjugate prevents PEGylated liposome-mediated complement activation and anaphylatoxin production. *FASEB J., 20*, 2591–2593 (doi: 10.1096/fj.06-6186fje, electronic pages: E2057–E2067).

Moghimi, S. M., Hamad, I., Bünger, R., Andresen, T. L., Jørgensen, K., Hunter, A. C., Baranji, L., Rosivall, L., & Szebeni, J. (2006b). Activation of the human complement system by cholesterol-rich and PEGylated liposomes–Modulation of cholesterol-rich liposome-mediated complement activation by elevated serum LDL and HDL levels. *J. Liposome Res., 16*, 167–174.

Moghimi, S. M., Hedeman, H., Muir, I. S., Illum, L., & Davis, S. S. (1993a). An investigation of the filtration capacity and the fate of large filtered sterically-stabilized microspheres in rats. *Biochim. Biophys. Acta, 1157*, 233–240.

Moghimi, S. M., & Hunter, A. C. (2001). Recognition by macrophages and liver cells of opsonized phospholipids vesicles and phospholipids headgroups. *Pharm. Res., 18*, 1–8.

Moghimi, S. M., Hunter, A. C., & Murray, J. C. (2001). Long-circulating and target-specific nanoparticles: theory to practice. *Pharmacol. Rev., 53*, 283–318.

Moghimi, S. M., Hunter, A. C., & Murray, J. C. (2005a). Nanomedicine: current status and future prospects. *FASEB J., 19*, 311–330.

Moghimi, S. M., Hunter, A. C., Murray, J. C., & Szewczyk, A. (2004). Cellular distribution of non-ionic micelles. *Science, 303*, 626–627.

Moghimi, S. M., & Kissel, T. (2006). Particulate nanomedicines. *Adv. Drug Deliv. Rev., 58*, 1451–1455.

Moghimi, S. M., Muir, I. S., Illum, L., Davis, S. S., & Kolb-Bachofen, V. (1993b). Coating particles with a block copolymer (poloxamine-908) suppresses opsonization but permits the activity of dysopsonins in the serum. *Biochim. Biophys. Acta, 1179*, 157–165.

Moghimi, S. M., Porter, C. J. H., Muir, I. S., Illum, L., & Davis, S. S. (1991). Non-phagocytic uptake of intravenously injected microspheres in rat spleen: influence of particle size and hydrophilic coating. *Biochem. Biophys. Res. Commun., 177*, 861–866.

Moghimi, S. M., Symonds, P., Murray, J. C., Hunter, A. C., Debska, G., & Szewczyk, A. (2005b). A two-stage poly(ethylenimine)-mediated cytotoxicity: implications for gene-transfer/therapy. *Mol. Ther., 11*, 990–995.

Moghimi, S. M., & Szebeni, J. (2003). Stealth liposomes and long circulating nanoparticles: critical issues in pharmacokinetics, opsonization and protein-binding properties. *Prog. Lipid Res., 42*, 463–478.

Moghimi, S. M., Vegas, E., Garcia, M. L., Al-Hanbali, O. A. R., & Rutt, K. J. (2006c). Polymeric nanoparticles as drug carriers and controlled release implant devices. In V. P. Torchilin (Ed.), *Nanoparticles as drug carriers* (p. 29–42). London: Imperial College Press.

Moore, Jr. F. D., Austen, K. F., & Fearon, D. T. (1982). Antibody restores human alternative complement pathway activation by mouse erythrocytes rendered functionally deficient by pre-treatment with pronase. *J. Immunol., 128*, 1302–1306.

Munn, L. L. (2003). Aberrant vascular architecture in tumors and its importance in drug-based therapies. *Drug Discov. Today, 8*, 396–403.

Murray, J. C., & Moghimi, S. M. (2003). Endothelial cells as therapeutic targets in cancer: new biology and novel delivery systems. *Crit. Rev. Ther. Drug Carr. Syst., 20*, 139–152.

Patil, V. R. S., Campbell, C. J., Yun, Y. H., Slack, S. M., & Goettz, D. J. (2001). Particle diameter influences adhesion under flow. *Biophys. J., 80*, 1733–1743.

Porter, C. J. H., Moghimi, S. M., Illum, L., & Davis, S. S. (1992). The polyoxyethylene/polyoxypropylene block co-polymer poloxamer-407 selectively redirects intravenously injected microspheres to sinusoidal endothelial cells of rabbit bone marrow. *FEBS Lett., 305*, 62–66.

Poznansky, M., & Juliano, R. L. (1984). Biological approaches to controlled delivery of drugs: a critical review. *Pharmacol. Rev., 36*, 277–336.

Qiang, Y., Antony, J., Sharma, A., Nutting, J., Sikes, D., & Meyer, D. (2006). Iron/iron oxide core-shell nanoclusters for biomedical applications. *J. Nanoparticle Res., 8*, 489–496.

Roberts, J. C., Bhalgat, M. K., & Zera, R. T. (1996). Preliminary biological evaluation of polyamidoamine (PAMAM) Starburst dendrimers. *J. Biomed. Mat. Res., 30*, 53–65.

Romberg, B., Oussoren, C., Snel, C. J., Carstens, M. G., Hennink, W. E., & Storm, G. (2007). Pharmacokinetics of poly(hydroxyethyl-L-asparagine)-coated liposomes is superior over that of PEG-coated liposomes at low lipid dose and upon repeated administration. *Biochim. Biophys. Acta,* doi: 10.1016/j.bbamem.2006.12.005, *1768*, 2655–2666.

Romero, E. L., Morilla, M. J., Regts, J., Koning, G. A., & Scherphof, G. L. (1999). On the mechanism of hepatic transendothelial passage of large liposomes. *FEBS Lett., 448*, 193–196.

Salvador-Morales, C., Flahaut, E., Sim, E., Sloan, J., Green, M. L. H., & Sim, R. B. (2006). Complement activation and protein adsorption by carbon nanotubes. *Mol. Immunol*., *43*, 193–201.

Scherphof, G. L., & Kamps, J. A. A. M. (2001). The role of hepatocytes in the clearance of liposomes from the blood circulation. *Prog. Lipid Res., 40*, 149–166.

Singh, R., Pantarotto, D., lacerda, L., Pastorin, G., Klumpp, C., Prato, M., Bianco, A., & Kostarelos, K. (2006). Tissue distribution and blood clearance rates of intravenously administered carbon nanotube radiotracers. *Proc. Natl. Acad. Sci. USA, 103*, 3357–3362.

Sou, K., Goins, B., Takeoka, S., Tsuchida, E., & Phillips, W. T. (2006). Selective uptake of surface-modified vesicles by bone marrow macrophages in vivo. Biomaterials, *28*, 2655–2666.

Sudimack, J., & Lee, R. J. (2000). Targeted drug delivery via the folate receptor. *Adv. Drug Deliv. Rev., 41*, 147–162.

Volanakis, J. E., & Wirtz, K. W. A. (1979). Interaction of C-reactive protein with artificial phosphatidylcholine bilayers. *Nature, 281*, 155–157.

Yan, X., Kuipers, F., Havekes, L. M., Havinga, R., Dontje, B., Poelstra, K., Scherphof, G. L., & Kamps, J. A. A. M. (2005). The role of lipoprotein E in the elimination of liposomes from blood by hepatocytes in the mouse. *Biochem. Biophys. Res. Commun., 328*, 57–62.

Yan, X., Morselt, H. W. M., Scherphof, G. L., Poelstra, K., & Kamps, J. A. A. M. (2004). The role of beta(2)-glycoprotein I in liposome-hepatocyte interaction. *Biochim. Biophys. Acta, 1667*, 208–214.

10

Controlled Release and Nanotechnology

Tania Betancourt, Amber Doiron, Kimberly A. Homan,
and Lisa Brannon-Peppas

Introduction

Nanosized controlled release systems for drug delivery are segregated into several categories including polymeric nanoparticles, liposomes, solid lipid nanoparticles, polymeric micelles, and dendrimers. This topic is extensive and as such is only briefly reviewed here. More detailed information may be found in more focused chapters of this book. With this in mind, this chapter will provide an overview of nanoparticulate systems, followed by some of the more interesting opportunities and applications of nanotechnology in controlled release: metal–organic systems, nanotubes, responsive systems, and personal care products.

The use of a drug as a therapeutic agent is often a delicate balance between therapeutic efficacy and detrimental side effects including toxicity. The control of the amount of drug delivered over time and the spatial localization of that delivery are paramount in overcoming the challenges of providing optimal therapy. This challenge drives the design of various drug delivery strategies that strive to revolutionize the way drugs exert their actions. Much of this attention has focused on nanoparticles due to their small size, relatively high surface area, influence on biodistribution, ability to make drugs available for intravascular delivery, their stabilizing effect on therapeutic agents, and the capability of sustaining release of the agent (Mainardes and Silva 2004). All these elements ultimately lead to more effective delivery of the active agent to a desired physiological or pathophysiological location.

Modification of the nanocarrier composition largely controls the release of the active agent from the carrier. This can be accomplished by using various types of polymers or lipids, changing the molecular weight of those components, or changing the surface characteristics such as by crosslinking or adding a separate component like poly (ethylene glycol). In addition, more specific modifications can be made in order to achieve the optimal controlled drug release from the nanodevice. The following reviews the major classes of nanoscale drug delivery devices.

M.M. de Villiers et al. (eds.), *Nanotechnology in Drug Delivery*, DOI: 10.1007/978-0-387-77667-5_10,

Types of Nanoscale Drug Delivery Devices

Structure and Behavior of Polymeric Nanoparticles

Polymeric nanoparticles have been investigated as drug delivery devices for several decades due to their ability to carry a wide variety of drugs or genes and sustain delivery for an extended period of time. Nanoparticles are submicron-sized polymeric colloidal spheres that can entrap an active agent within the polymer matrix, or the active agent can be adsorbed or conjugated to the outside of the particle. The term nanoparticle encompasses both nanocapsules and nanospheres. Nanocapsules have a core–shell morphology with the active agent trapped within the core by the polymeric shell. The matrix structure of a nanosphere serves to entrap the drug molecules, or alternatively, the drug is conjugated at the surface of the particle (Brannon-Peppas 1995; Soppimath and Aminabhavi 2002; Mainardes and Silva 2004).

Many techniques have been used successfully to prepare nanoparticles and are generally stratified into (i) methods that use preformed polymer and (ii) methods involving the polymerization of monomers. These methods include but are not limited to the following: emulsion–solvent evaporation, salting out, production using supercritical fluid technology, phase separation, and in situ polymerization (Jain 2000; Soppimath, Aminabhavi et al. 2001).

Various classes of polymers have been used in drug delivery applications and are stratified into biodegradable polymers and non-biodegradable polymers. Biodegradable nanoparticles have received much attention because they do not require further intervention, i.e., removal, after being placed into the body. Depending on the formulation type, the drug is released by one or a combination of several mechanisms: desorption of adsorbed drug, diffusion through the polymer matrix, diffusion through the polymeric membrane shell in the case of nanocapsules, and polymer degradation and erosion (Uhrich et al. 1999; Jain 2000; Soppimath, Aminabhavi et al. 2001; Mainardes and Silva 2004). These mechanisms are influenced by the rate of degradation of the material, and the choice of polymer largely dictates the controlled release properties of the system (Uhrich Cannizzaro et al. 1999; Jain 2000; Soppimath, Aminabhavi et al. 2001). Many factors outside of the kinetics of degradation must be considered for a polymer used in a drug delivery device including the difficulty of preparation, biocompatibility, favorable interactions with the active agent, and mechanical properties (Uhrich, Cannizzaro et al. 1999; Jain 2000).

Nanocapsules and nanospheres differ in their release profiles due to the nature of the containment of the active agent. Nanospheres encapsulate the drug molecules within the matrix of polymer in a uniform distribution. The release of the drug from the matrix occurs through diffusion as well as erosion of the matrix itself. If diffusion occurs more quickly than degradation, then the process is diffusion dependent, otherwise the process of degradation is highly influential (Niwa, Takeuchi et al. 1993). An initial burst release is observed due to the presence of drug near or adsorbed to the large surface area of the nanoparticle. After the burst effect, diffusion

largely controls the release leading to an exponential delayed release rate. Matrix-type nanoparticles usually exhibit first-order kinetics (Fresta, Puglisi et al. 1995; Radwan 1995).

Conversely, nanocapsules have a reservoir-like morphology and exhibit release profiles as such. The drug is contained in the core and must diffuse through the polymer shell in order to be released. This morphology theoretically leads to zero-order kinetics of release. It has been shown experimentally that drug release from nanocapsules can occur by either partitioning of the drug or diffusion across the polymer coating (Calvo, VilaJato et al. 1996; Lu, Bei et al. 1999). Additionally, it has been shown that the method of drug incorporation, conjugation or adsorption, greatly affects the release profile with adsorption leading to higher burst release and a quicker overall release (Soppimath, Aminabhavi et al. 2001).

Polymers Used in Nanoscale Release Systems

Various synthetic polymers have been used in drug delivery devices including poly(esters), poly(ortho esters), poly(anhydrides), poly(amides), and phosphorus-containing polymers, and many naturally derived polymers such as chitosan, dextran, and gelatin have also been extensively researched. Several of the most common polymers used in nanoscale devices are reviewed here.

Poly(esters)

The most studied and best characterized class of polymers for controlled release is the poly(esters). One of the most common polymers used in nanoparticle drug delivery approaches is poly(lactic-*co*-glycolic acid) (PLGA) due to its degradation properties, biocompatibility, and the fact that it is very well characterized (Jain 2000). PLGA degrades in an aqueous environment through the hydrolysis of the backbone ester linkages (Brannon-Peppas 1995; Uhrich, Cannizzaro et al. 1999; Jain 2000). The polymeric device based on PLGA degrades through bulk erosion at a uniform rate throughout the matrix (Jain 2000). The degradation process is self-catalyzed as the number of terminal carboxylic acid groups rises with increasing chain scission, and the acids catalyze the hydrolysis. The degradation is highly dependent on the ratio of lactide to glycolide moieties as lactide is more hydrophobic and reduces the rate of degradation (Jain 2000; Mainardes and Silva 2004). Also, important factors in the degradation process are the degree of crystallinity, the molecular weight, and the glass transition temperature of the polymer (Jain 2000).

PLGA has been used to encapsulate a myriad of drugs and genes for controlled delivery applications for many diseases or other applications, and only a few are mentioned here. One popular area for the application of PLGA nanoparticles is in the treatment of cancer. Paclitaxel is a drug used in cancer treatment that causes cell death by inhibiting cell division (Brannon-Peppas and Blanchette 2004). Fonseca et al. loaded paclitaxel into nanoparticles (< 200 nm) with near 100% efficiency using an interfacial deposition method. The loaded PLGA nanoparticles released

approximately half of their payload within the first 24 hours and had a slowing release rate over the subsequent 4 days. Significant losses in viability were shown in the human small lung cancer cell line NCI-H69 with exposure to as little as 0.025 μg/ml paclitaxel-loaded nanoparticles (Fonseca, Simões et al. 2002). Doxorubicin is a widely used cancer drug that impedes nucleic acid synthesis, yet is also known to have various systemic side effects (Brannon-Peppas and Blanchette 2004). Nanoparticles prepared from PLGA–doxorubicin conjugates of about 200 nm in diameter suppressed tumor growth for 12 days after a single administration (Yoo, Lee et al. 2000). The hydrophilic cancer drug 5-fluorouracil has been encapsulated in PLGA/O-CMC (*O*-carboxmethyl-chitosan) nanoparticles along with antisense EGFR (epidermal growth factor receptor) plasmids by Hu and colleagues in a novel approach to combine chemotherapy and gene therapy for the treatment of cancer. Encapsulation efficiencies of both agents in the 90th percentile were achieved, and release of 5-fluorouracil was prolonged for up to 3 weeks. In glioma cells, the nanoparticles caused cytotoxicity upward of 90%, and decreased EGFR expression confirmed transfection of the cells (Hu, Chang et al. 2005).

Polymeric PLGA nanoparticles have also been used as a method to prolong release of and control distribution of antiproliferative drugs at the sight of balloon injury in a dog atherosclerosis model (Guzman, Labhasetwar et al. 1996; Labhasetwar, Song et al. 1998). Nanoparticles containing dexamethasone were delivered to the arterial wall and observed to penetrate the wall without additional modification. Within several days, systemic levels of the drug were undetectable, but nanoparticles were detected in the artery wall for up to 14 days. This is indicative of the ability of PLGA nanoparticles to control the release of drugs and be useful in sustaining release in a stent-like treatment without inducing systemic toxicity of these powerful drugs. Additional work has been accomplished in this area showing the promise of active targeting and the further utility of nanoparticles to prevent restenosis (Labhasetwar, Song et al. 1998; Lanza, Yu et al. 2002). These studies show the utility of nanoparticles to sustain and spatially concentrate the delivery of an active agent in treatment of restenosis (Caves and Chaikof 2006).

Poly(ortho esters)

Devices degrading through bulk erosion have an undesirable release profile for many applications, and the need for a device controlling release solely through hydrolysis of chains at the surface of the device effected the design of poly(ortho esters) (Uhrich, Cannizzaro et al. 1999). The release rates from devices composed of poly(ortho esters) can be controlled by including acidic or basic excipients into the matrix as its hydrolysis is acid catalyzed. This has been used in the release of 5-fluorouracil (Seymour, Duncan et al. 1994), tetracycline (Roskos, Fritzinger et al. 1995), and others (Uhrich, Cannizzaro et al. 1999). Additionally, the mechanical properties of these polymers can be tailored by choosing from the various diols available (Mainardes and Silva 2004).

Poly(anhydrides)

Poly(anhydrides) degrade by hydrolysis yet the polymer itself is hydrophobic in nature. These properties lead to surface erosion of the polymeric device and nearly zero-order release. The hydrolytic bond cleavage of poly(anhydrides) produces water-soluble products that in many cases are considered biocompatible. Poly(anhydrides) are most commonly produced through a melt-condensation polymerization. The most common polymers in this class are based on sebacic acid, *p*-(carboxyphenoxy)propane, and *p*–(carboxyphenoxy)hexane. Variations in monomer composition, such as hydrophobicity, influence the degradation rate of the polymeric device. The degradation can last from days to years depending on the composition (Uhrich, Cannizzaro et al. 1999).

The photosensitizer phthalocyanine was chemically incorporated into nanoparticles based on biodegradable poly(sebacic anhydride) by Fu and colleagues (Fu, Li et al. 2002) for cancer treatment through photodynamic therapy. The attachment of the phthalocyanines to the polymer in the nanoparticles impedes the tendency of the agent to aggregate and become less useful for photodynamic therapy. The average hydrodynamic radius of the nanoparticles was found to be 166 nm. The release of photosensitizer from the particles was degradation dependent, and the rate of degradation increased with pH and temperature. This colloidal system has the potential to be useful for the delivery and controlled release of photosensitizer for photodynamic therapy (Fu, Li et al. 2002). Many other types of poly(anhydrides) have been used in drug delivery applications in the nanoscale size range.

Chitosan

As opposed to the other materials mentioned above, chitosan is a naturally derived polysaccharide created by the deacetylation of chitin (Mainardes and Silva 2004). The advantageous properties of chitosan include its biocompatibility, positive charge, the abundance of amine groups available for crosslinking, ease of processing, mucoadhesiveness, and its degradation into amino sugars, which are all attractive for drug delivery applications (Agnihotri, Mallikarjuna et al. 2004; Mainardes and Silva 2004). Chitosan nanoparticles have been formulated by a variety of techniques including emulsion crosslinking, complex coacervation, emulsion droplet coalescence method, ionic gelation, ionotropic gelation, and the reverse micellar method. The molecular weight of the chitosan, its degree of deacetylation, the extent of crosslinking, and its interactions with the encapsulated molecule play a role in controlling the release of the therapeutic agent from the particle. Due to its charge, the pH of the release media also influences release from chitosan particles. Release from chitosan particles occurs through similar mechanisms as mentioned for other particles: desorption of surface-adhered drug, diffusion through a swollen rubbery polymer matrix, and release due to erosion. Release of drugs from surface layers of the matrix involves a large burst effect, but increasing the crosslinking density can reduce this effect (Agnihotri, Mallikarjuna et al. 2004). Diffusion out of the matrix occurs through a three-step process: diffusion of water into the matrix causing swelling, transition from glassy to rubbery polymer, and

diffusion of drug out of the matrix. The release follows a typical hydrogel release profile (Agnihotri, Mallikarjuna et al. 2004).

Chitosan nanoparticles of approximately 100 nm in diameter prepared by a microemulsion method have been used to encapsulate a doxorubicin–dextran conjugate. In a mouse model, tumor volume was reduced after four weekly injections of the nanoparticle formulation 40% more than in mice treated with the conjugate alone, and injection of drug alone had no effect over control conditions (Mitra, Gaur et al. 2001). As an adjuvant to another cancer therapy–neutron-capture therapy–gadopentetic acid (Gd-DTPA) has been loaded in chitosan nanoparticles formed by an emulsion droplet coalescence technique. Less than 2% of the Gd-DTPA was released over 7 days in PBS, but over 90% was released in plasma over 1 day. After an intratumoral injection in a mouse melanoma model, 92% of the Gd-DTPA was contained within the tumor site compared to only 1.2% of the Gd-DTPA injected in a non-nanoparticle formulation (Tokumitsu, Ichikawa et al. 1999). The Gd-DTPA chitosan nanoparticles have been shown to have a high affinity for uptake in several cell types, suggesting the mechanism for high retention in tumor (Shikata, Tokumitsu et al. 2002).

Gelatin

Gelatin is a naturally occurring biopolymer that is biocompatible and biodegradable. The polymer is obtained through heat-dissolution and partial hydrolysis of collagen obtained from animal connective tissues. It has been used for many years in pharmaceutical applications such as capsules and ointments as well as early nanoformulations (Zwiorek, Kloeckner et al. 2004; Verma, Sachin et al. 2005). Recently, gelatin nanoparticles made by a two-step desolvation process involving crosslinking of the polymer using gluteraldehyde have been used to entrap cycloheximide, a protein synthesis inhibitor used in cancer treatment. Cycloheximide was entrapped with 26% efficiency in nanoparticles of 168 nm diameter. The particles were stable in whole blood, and they showed anti-tumor activity in two breast cancer cell lines over a period of time. The release kinetics curve was interestingly biphasic, and release was relatively slow. The gelatin nanoparticles are reportedly a good candidate for biopharmaceutical delivery (Verma, Sachin et al. 2005). Zwiorek et al. produced gelatin nanoparticles by the same desolvation method as a carrier for plasmid DNA (Zwiorek, Kloeckner et al. 2004). The particles were cationized in order to have an electrostatic interaction with the DNA which bounds onto the surface of the particles. The nanoparticles showed little cytotoxic effect, and efficient gene transfection was exhibited by an exponential increase in gene expression in B16 F10 cells (Zwiorek, Kloeckner et al. 2004).

Other Structures for Nanoparticle Delivery Systems

Polymeric Micelles

Block copolymers have been used as the basis for drug delivery carriers due to their ampiphilic nature and ability to organize into concentric regions.

A polymeric micelle consists of a dense core region comprised of hydrophobic blocks and a region of more loosely packed hydrophilic blocks. Polymeric micelles are typically 20–100 nm in diameter, and polyethylene oxide (PEO) is often used as the hydrophilic block. Polymeric micelles have a low critical micelle concentration and as such have higher stability than low molecular weight surfactants and many liposome formulations. Micelles have a small size and small polydispersity due to their molecular organization. The hydrophilic shell has been shown to prevent immune recognition and increase circulation time in vivo, and many groups have investigated polymeric micelles for drug and gene delivery (Mainardes and Silva 2004). The stability has been increased even more by incorporating crosslinking into the preparation scheme. This additional step also affects the release of active agent from the carrier in a system-specific manner (O'Reilly, Hawker et al. 2006).

One polymer class popular for use as the dense core in polymer micelles is poly(ortho esters) due to their hydrophobic nature and favorable interactions with poorly soluble hydrophobic drugs. The value for the critical micelle concentration for these types of polymers is in the range of 10^{-4} g/l, which is low enough to insure stability upon injection in vivo. The entrapment efficiency of taxol has been shown to be approximately 40% using a PEG–poly(ortho ester)–PEG block copolymer micelle (Heller, Barr et al. 2002).

Liposomes and Lipid-Based Systems

Liposomes

Lipids are organic molecules that contain a hydrophilic head group and a hydrophobic chain region. Much like polymer micelles, lipids organize in water into aggregates called liposomes with the hydrophobic regions packed in a core and the hydrophilic heads freely interacting with the surrounding water. Although cationic lipids are the most predominant, anionic and neutral lipids are also investigated for use in drug and gene delivery. Lipid design is an increasingly important avenue of research as the controlled release applications of lipids grow (Bhattacharya and Bajaj 2005). Liposomes are classified on the basis of their size, which can range from several nanometers to microns, and the number of lipid bilayers. Both hydrophilic and hydrophobic drugs can be carried by liposomes depending on the lipid structure.

Liposomes have been under investigation for many decades and the number of drugs and genes investigated for controlled release with liposome formulations is very extensive. Liposomes have been investigated for use in cancer treatment (Brannon-Peppas and Blanchette 2004), have been shown to reduce systemic side effects (Mainardes and Silva 2004), and have been researched for the delivery of proteins and nucleic acids (Mainardes and Silva 2004; Bhattacharya and Bajaj 2005). Like all other colloidal systems, liposomes suffer from various shortcomings including interactions with lipoproteins, having a high critical micelle concentration that limits stability, and limited availability of inexpensive pharmaceutical grade lipid (Muller, Mader et al. 2000; Mainardes and Silva 2004; Bhattacharya and Bajaj 2005).

Solid Lipid Nanoparticles

Solid lipid nanoparticles are a matrix device composed of solid lipid in the size range of 50–1000 nm. They are prepared through a variety of techniques including hot or cold high-pressure homogenization, microemulsion, and precipitation. Drugs such as paclitaxel, gadolinium complexes, prednisone, and many others have been incorporated into solid lipid nanoparticles. The drug loading and subsequent release is dependent on the solubility of the drug in the melted lipid, the miscibility of drug melt with lipid melt, the structure of the solid lipid matrix, and the polymorphic state of lipid material. Solid lipid nanoparticles can be modified in order to provide either a large burst release or a slow uniform release rate for a period of several weeks. The production parameters are influential on the release profile but size is not a significant factor in release (Muller, Mader et al. 2000).

Dendrimers

Dendrimers are a newer class of polymeric drug delivery devices with a unique macromolecular structure. The three-dimensional complexes are produced in an iterative sequence of reaction steps leading to generations of branches organized around an inner core. The hierarchical synthesis of these complexes lends itself to finely controlled size, composition, and reactivity. Poly(amidoamine) dendrimers were the first constructed and characterized, but dozens of other dendrimer types have been investigated to date (Mainardes and Silva 2004). Dendrimers are formed either by divergent or convergent methods, each having its own advantages and disadvantages. The behavior and characteristics of dendrimers can differ greatly from their linear counterparts. Due to their step-wise synthesis, the polydispersity of dendrimers is quite low, contributing to their utility as drug delivery devices. The scaffold provides an ideal platform for drug molecules that does not depend on thermodynamics or physical factors. The choice of polymer used in the dendritic system plays heavily into its utility as a drug carrier owing to the association between the polymer and drug molecule.

The drug indomethacin was loaded (11 wt%) into dendritic micelles composed of a hydrophobic Fréchet-type dendrimer and a shell of hydrophilic poly(ethylene glycol) by Fréchet et al. The release of the drug from the complex was much slower than that of the same drug from a cellulose membrane: all drug was released over 25 hours as opposed to 4 hours with the cellulose (Liu, Kono et al. 2000). 5-Fluorouracil has been incorporated into poly(amidoamine) dendrimers augmented with mPEG-500. The complexation between the hydrophilic drug and dendrimer occurred with incubation. In vitro release from the PEGylated dendrimers occurred over 6 days, whereas the non-PEGylated formulations released all drug over 1 day. This same relationship was true in studies in albino rats with PEGylated formulations showing prolonged release, without producing any significant hematological instability (Bhadra, Bhadra et al. 2003). Instead of entrapment within the dendrimer, drugs may also be electrostatically or covalently bound to the surface of the dendrimer. Owing to the highly branched and functionalized structure of dendrimers,

oftentimes there are large numbers of ionizable groups at the surface that are available for complexation (D'Emanuele and Attwood 2005).

Viral Vectors

Viral vectors have been proposed as efficient gene delivery devices due to their evolutionary advantage over man-made colloidal systems for transfection of cells. Synthetic or modified viruses carry the therapeutic gene in their capsid, being able to protect it until it reaches its intended target. Many exciting strides have been made in this field, yet many hurdles remain to make the device safe and viable in vivo (Mainardes and Silva 2004).

In addition to the various examples listed above, other classes of nanoscale-controlled delivery devices exist including protein-based delivery devices, magnetic nanoparticles, inorganic nanoparticles, and others.

Controlled Release from Metal–Organic Nanoparticles and Complexes

Bioinorganic chemistry is an expanding field showing great promise for applications in medicine, both for novel drug formulations and drug delivery vehicles. As mentioned in the first section of this chapter, metallic and metal oxide nanostructures have gained significant attention in recent years. In fact, elucidating the mechanisms by which metals interact naturally in the body (Guo and Sadler 1999) has allowed researchers to devise new metallodrugs involving such metals as vanadium and zinc for insulin-mimetic solutions (Sakurai, Katoh et al. 2006), platinum for use in the very popular anti-tumor drug cisplatin (van Zutphen and Reedijk 2005; Bontha, Kabanov et al. 2006), and selenium for use in the anti-inflammatory and anti-viral drug ebselen and its derivatives (Wojtowicz, Kloc et al. 2004; Bhabak and Mugesh 2007), just to name a few.

Metallodrugs are clearly an area of growing research, but they are not the focus of our discussion here. Rather, this section reports on the budding field of metal–organic complexes as an alternative to strictly organic constructs used for controlled drug and gene delivery. The incorporation of metal nanoshells into organic frameworks to provide remote control release of drugs is also presented. Finally, where controlled discharge of metal ions is desired, their release through organic nanoconstructs is briefly considered.

Metal–Organic Hybrids in Controlled Release

Polymers represent the most extensively studied class of materials for controlled release. Since most of these organic systems operate to control drug release via diffusion, controlling pore size in these systems is critical and challenging (Horcajada, Serre et al. 2006). As a result of these challenges, many researchers searched for other materials with well-defined, tunable porous structures and found zeolites to be the answer. Zeolites are minerals consisting of metals or metalloid components in a crystalline

framework with nanopore sizes in the range of 2–20Å (Smaihi, Gavilan et al. 2004). When AlO_4 is part of the zeolite, it adds an ion-exchange component that can be used to increase the loading efficiency of charged compounds or drugs into the porous structure (Zhang, Kim et al. 2006). In a proof of concept study, Zhang et al. loaded zeolite Y with a common herbicide, paraquat, and then modified the pore size of the zeolite by functionalizing the surface with 1,1,3,3-tetramethyldisilazane (TMDS) (Zhang, Kim et al. 2006). Functionalizing the surface effectively reduced the pore size after paraquat loading, which allowed for maximum loading efficiencies to be conserved in conjunction with a subsequent controlled release of paraquat. Results proved that undamaged paraquat released in aqueous solution by Na^+ exchange from functionalized zeolite Y over a 7-day period, versus the 20-min release exhibited by the unfunctionalized zeolite Y (Zhang, Kim et al. 2006). Although this study used an herbicide, the concept of loading and exhibiting controlled release can be extrapolated to small, charged drugs and the use of zeolites for controlled release applications was clearly demonstrated.

Researchers have recently produced stable colloidal suspensions of zeolite nanoparticles. Functionalized nanocrystalline zeolite particles hold promise as future controlled release capsules or chemical sensors (MacLachlan, Manners et al. 2000). One group has developed a procedure for making template-free zeolite nanoparticles with the possibility of altering surface functional groups. Producing zeolites with different functionalities allows for a range of future interactions with targeting agents and other drugs (Smaihi, Gavilan et al. 2004).

A common zeolite used for controlled release applications is crystalline aluminosilicate. By changing the ratio of Si/Al in this zeolite framework, overall zeolite pore size and ion-exchange properties can be tuned (Horcajada, Marquez-Alvarez et al. 2006). Many claim that the uniform pore size and structure of zeolites lend to more even drug loading, and thus, more predictable controlled release behavior. A pictorial representation of a Y-type zeolite with cubo-octahedral sodalite cages is shown in Figure 10.1. One study proved using release of ibuprofen from an aluminosilicate Y-type zeolite, that after an initial period of diffusion-controlled release

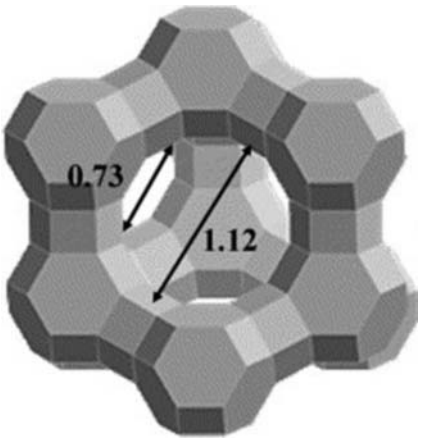

Figure 10.1 Building units of zeolite Y showing the dimensions of the supercage and windows (nm). Modified from Horcajada, Marquez-Alvarez et al. (2006).

which remained similar for all models, further discharge of ibuprofen from the zeolite could be controlled by varying the Al content in the zeolite framework (the hydrophobic nature of the zeolite increases as Al content decreases). They showed that dealuminating the zeolite structure increased the rate of hydrophobic drug release, like ibuprofen, but only up until a specified Si/Al ratio of 22. At higher ratios, van der Waals forces between the drug and the zeolite framework slowed release (Horcajada, Marquez-Alvarez et al. 2006). Controlled release through zeolite structures is gaining popularity for a host of applications in medical and agricultural sciences and is expected to continue populating the literature in coming years.

Metal Nanoshells for Remote Controlled Release

Metal nanoshells generally have dielectric core–shell morphologies where a silica core is surrounded by a thin layer of metal. The surrounding metal could be Ag, Au, Pt, or any other bulk metal, but the Au-layered shells are the most widely studied. The beauty of the core–shell design is that the plasmon optical resonance peak of elemental gold can be shifted from the visible to the near infrared region (NIR) by varying the core diameter and metal shell thickness (Lin, Lewinski et al. 2005). This shift to the NIR is critical considering that light in the NIR region can penetrate deep (2–3 cm) into biological tissue (Steinbrink, Wabnitz et al. 2001). Thus, metal nanoshells have the potential, once injected into the body, to respond thermally to light shone externally on the body. The numerous applications of these novel metal nanoshells in the realm of imaging are covered elsewhere in this book, so here we focus on the use of these nanoshells in triggering drug release.

One interesting method of effecting a pulsatile drug release involves incorporation of these metal nanoshells via entrapment into a temperature-sensitive polymer–drug matrix. One example includes the widely studied thermosensitive polymer *N*-isopropylacrylamide (NIPAAm). When NIPAAm is copolymerized with acrylamide and formed as a hydrogel, the hydrogel exhibits a lower critical solution temperature (LCST) slightly above body temperature (Hirsch, Gobin et al. 2006). Once this LCST is reached, the polymer matrix exhibits a drastic phase change and collapses, as shown in Figure 10.2. During the collapse, water and much of the encapsulated drug are expelled. Sershen et al. proved that these hydrogel systems with entrapped gold nanoshells can in fact be used for pulsatile protein release in response to a pulsed NIR laser light (Sershen, Westcott et al. 2000). Another example includes the work of Owens and Peppas who created temperature-sensitive inter-penetrating polymer networks (IPN) using acrylamides and acrylic acids formed as hydrogels which exhibited an upper critical solution temperature (UCST) (Owens III and Peppas 2006). In their case, the polymer remained compact under the UCST and exhibited a phase change by expanding above the UCST. Again, gold nanoshells were incorporated into these IPNs via entrapment, and pulsatile release of encapsulated drug was observed in correlation with pulsed external laser light excitation.

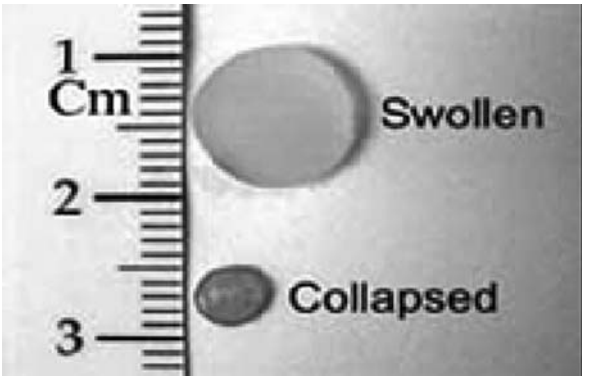

Figure 10.2 NIPAAm-co-acrylamide hydrogels shown in the swollen state (below LCST) and collapsed state (above LCST). Adopted from Hirsch, Gobin et al. (2006).

Remote control of drug release through polymeric systems can also be achieved using magnetically responsive metal particles. In the 1980s the first triggered release using magnetic particles was forged by Kost, Edelmen, and Langer at the Massachusetts Institute of Technology (Kost, Noecker et al. 1985; Edelman, Brown et al. 1987; Kost, Wolfrum et al. 1987). In these first works, cylindrical magnets (1.4 mm) were placed inside polymeric matrices with encapsulated bovine serum albumin (BSA). Upon induction of an oscillating magnetic field, the release rates of BSA significantly increased. Upon removal of the field, release rates returned to baseline (diffusion-controlled release). They later proved that externally triggered delivery of insulin to diabetic rats was possible using similar methods (Kost, Wolfrum et al. 1987). In these cases, the motion of the magnets induced a mechanical deformation of the matrix, which in turn allowed for the increased drug release (Edelman, Fiorino et al. 1992).

A more recent attempt to build a magnetically responsive construct was made by Gaponik et al. at the University of Munich. They created a multifunctional polymeric microcapsule which houses both CdTe semiconductor nanocrystals and magnetic Fe_3O_4 nanoparticles (Gaponik, Radtchenko et al. 2004). The CdTe nanocrystals are meant to serve as luminescent markers while the magnetic oxide nanoparticles aid in targeting of the microcapsule. The general nature of their method for building the construct allows for drug encapsulation in future studies. In that case, the role of magnetic oxide in the microcapsule could be used not just for targeting, but for triggered drug release by employing similar methods used by Langer and inducing oscillating magnetic fields to spark increased drug release.

Magnetic iron oxides nanoparticles are also being used to enhance gene delivery. Plank et al. from the Technical University Munich have coined the term magnetofection for their science of magnetically induced transfection (Plank, Schillinger et al. 2003). The general method is that superparamagnetic iron oxide particles are surface treated with polyelectrolytic coating. This coating allows for the nanoparticles' salt-induced colloidal aggregation with viral and non-viral gene vectors. Applied magnetic gradients during transfection experiments using these new constructs in vitro showed dramatically reduced transfection times (Plank, Scherer et al. 2003). Classical carriers act via diffusion to deliver genes and can take several hours to transfect what the magnetofection method attained in

10 min (Plank, Schillinger et al. 2003). Effectively, the use of these iron oxide nanoparticles and induced magnetic field is enhancing the interaction between target cells and gene vectors, effecting the delivery of the gene in a timely manner. In trying to elucidate the mechanism of magnetofection, some theorize that endocytic uptake of genes on the cell surface is not sped up by the magnetic forces, instead the magnetic forces simply serve to accelerate sedimentation of magnetofectins on the cell surface (Huth, Lausier et al. 2004).

Controlled Release of Metal Ions Through Organic Nanoconstructs

Some metals such as silver and copper have been known to exhibit antibacterial properties. Considering these biocidal properties, silver have been used in formulations to treat or prevent infection in postoperative scenarios or cases such as burn victims. In these instances, the mode of action for "drug" delivery is the controlled release of the silver ions into the wound which subsequently interacts with bacterial DNA, preventing replication. Several researchers have created intriguing conjugates of silver to polymeric materials and nanoconstructs (Balogh, Swanson et al. 2001; Bromberg, Buxton et al. 2001; Abo El Ola, Kotek et al. 2004; Kumar, Howdle et al. 2005; Isab and Wazeer 2006; Rhim, Hong et al. 2006). Others have validated the use of silver nanoparticle impregnation methods as a way to reduce postimplantation infection risk (Karlov, Khlusov et al. 2002; Sambhy, MacBride et al. 2006).

Dendrimer–silver complexes represent one example of these interesting silver–polymer conjugates produced on the nanoscale. In one study, poly (amidoamine) (PAMAM) dendrimers were surface-modified to contain immobilized silver ions in stabile, silver domains (Balogh, Swanson et al. 2001). Using standard agar overlay methods, Balogh and collaborator's silver–PAMAM dendrimers exhibited significant antimicrobial activity against three bacterial strains: *Staphylococcus aureus*, *Pseudomonas aeruginosa*, and *Escherichia coli*. Most studies of silver ion release in biological tissue show decreased antimicrobial efficacy of the silver in the presence of chloride or sulfate ions, mostly because their interaction with silver forms insoluble complexes (Schierholz, Lucas et al. 1998; Brett 2006). Silver–PAMAM complexes, however, maintain their antimicrobial activity in the presence of sulfate or chloride ions. Balogh et al. attributed this apparent continued silver activity to that fact that "macroscopically, the silver remained conjugated to the dendrimer in the form of ions, stabile metallic silver clusters or silver compounds." Since the dendrimer itself is soluble and the silver ions remain active while attached to the polymer complex, sulfate and chloride ions in the media are no longer a factor, and the movement of silver ions which impart antibacterial properties is only limited by the diffusion of the dendrimer itself.

Nanotubes

Carbon nanotubes can be thought of as tubular nanoscale particles that can potentially be used as delivery systems for imaging and therapeutic agents through conjugation or other techniques. Numerous studies have

shown that nanotubes can readily enter cells for intracellular delivery of active agents (Kam and Dai 2005; Wu, Wieckowski et al. 2005). Although studies of in vivo biodistribution of carbon nanotubes have not observed toxicity (Singh, Pantarotto et al. 2006), the actual properties of nanotubes are highly dependent on their functionalization, water solubility, size, etc., and need to be further studied for the numerous nanotube-based drug delivery systems that have been developed to date.

Functionalization of carbon nanotube surfaces is necessary to confer water solubility to these systems and for conjugation of therapeutic agents. Georgakilas et al. have reported on the orthogonal functionalization of carbon nanotubes via 1,3-dipolar cycloaddition reaction that allows selective conjugation of N-protected amino-terminated tether molecules to the walls of the tubes (Georgakilas, Kordatos et al. 2002; Georgakilas, Tagmatarchis et al. 2002). Further derivatization of surface carboxylic acid groups formed by acid-mediated oxidation of nanotubes permits simultaneous conjugation of two different therapeutic molecules.

Pastorin et al. have recently reported on the use of various protection methods for selective conjugation of therapeutic and imaging agents to multifunctional carbon nanotubes derivatized by the above-mentioned methods (Pastorin, Wu et al. 2006). One scheme utilizes *tert*-butyloxycarbonyl (Boc) and benzyloxycarbonyl as protecting groups of the conjugated amino-terminated tether groups. These protecting groups require treatment with strong acids for removal of the protecting groups, and are consequently not appropriate for conjugation of labile molecules. The second method is based on the protection of the amino groups by Boc and mono-phthalimide (Pht), respectively. While the Boc group is still removed by acid treatment, Pht is removed with hydrazine in alcohol at room temperature. Utilizing the second protection scheme, carbon nanotubes were successfully conjugated to fluorescein isothiocyanate and methotrexate for fluorescence detection and in vitro therapeutic evaluation, respectively (Pastorin, Wu et al. 2006). This group was able to show that the functionalized carbon nanotubes were readily internalized by human Jurtak T lymphocytes in a dose-dependent manner with confocal microscopy (Pastorin, Wu et al. 2006).

Similar techniques were utilized for conjugation of fluorescein and the antifungal antibiotic amphotericin B (AmB) to carbon nanotubes (Wu, Wieckowski et al. 2005). Conjugation of AmB to carbon nanotubes was found to significantly reduce toxicity of this drug to human Jurtak T lymphoma cells even after 16 hours or exposure (Wu, Wieckowski et al. 2005). On the other hand, AmB was found to be more effective against three fungi species when conjugated to carbon nanotubes than in the free form, possibly because of higher drug solubility, higher payload, and the prevention of AmB aggregation which commonly occurs in solution. Additionally, this group observed maximum nanotube uptake into the cells after just 1 hour of incubation. Further studies suggested that endocytosis was not involved in the rapid uptake of the nanotubes (Wu, Wieckowski et al. 2005).

Nanotubes have emerged as nanomaterials with high potential for application in drug delivery and biosensing. Further research is needed for gaining full understanding of the benefits and limitations of these

systems for biomedical applications. The combination of mechanical, electrical, and structural properties of carbon nanotubes will surely be exploited in the near future for the development of complex systems with very specific functionalities.

Responsive Drug Delivery Systems

Responsive drug delivery systems, as their name implies, are those that are able to act in response to a trigger, be it an external signal or changes in the surrounding environment (Tirelli 2006). The triggered response could include dissolution, precipitation, degradation, swelling, collapsing, change in hydrophilic/hydrophobic balance, phase separation, and shape alteration, among other conformational changes (Schmaljohann 2006). Systems that respond to external trigger commonly combine metals and polymers, as was discussed earlier in this chapter. In this section we focus on polymeric drug delivery systems able to recognize and modulate the delivery of a drug based on localized changes in temperature, pH, or concentration of oxidizing molecules.

Temperature-Sensitive Nanoparticles

Poly(*N*-isopropylacrylamide) (PNIPAAm) has been extensively used for the formulation of temperature-sensitive drug delivery systems because it exhibits a lower critical solution temperature (LCST) of about 30–34°C (Schmaljohann 2006). Below the LCST the polymer is soluble in water, while above this temperature the polymer becomes insoluble. This behavior can be utilized for controlling the delivery of active agents from temperature-sensitive drug delivery systems such as core–shell micelles of copolymers containing PNIPAAm and a hydrophobic polymer. Above the LCST, the micelles deform as the PNIPAAm, initially present in the nanoparticle shell in contact with the aqueous environment, becomes insoluble and disrupts the equilibrium of the core–shell configuration. If the LCST of a given temperature-sensitive polymer is higher than physiological temperature of 37°C, micelles of this polymer will remain stable until the local temperature of the target pathological tissue is raised above the LCST by external heating. For materials that have an LCST lower than normal body temperature, their thermoresponsive behavior can also be exploited for delivery of drugs to regions of low temperature such as hypoxic tissue (Patton and Palmer 2005). It is important to note that the LCST of polymers such as PNIMPAAm can be increased or decreased upon conjugation to a hydrophobic or hydrophilic copolymer, respectively (Schmaljohann 2006). For a more extensive review on temperature-sensitive systems readers are referred to a review by Dirk Schmaljohann (Schmaljohann 2006).

One example of temperature-responsive drug delivery systems based on PNIPAAm consists of self-assembled micelles of amphiphilic Y-shaped copolymers of poly(undecylenic acid) and PNIPAAm, or P(UA-Y-NIPAAm), as shown in Figure 10.3 (Li, Zhang et al. 2006). These micelles presented a very low critical micelle concentration of 20 μg/ml and a LCST

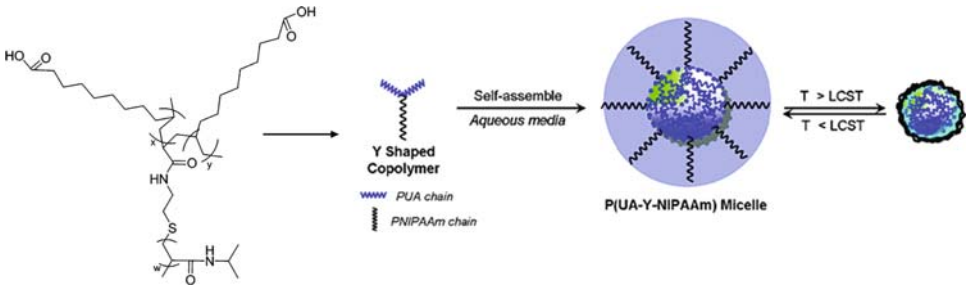

Figure 10.3 Schematic of temperature-sensitive micelles self-assembled in aqueous solutions from Y-shaped copolymers of poly(undecylenic acid) (PUA) and poly(*N*-isopropylacrylamide) (PNIPAAm). Reproduced with permission from Li, Zhang, et al. (2006). (*See* Color Plate 15)

of 31°C. Above this temperature the PNIPAAm shell of the micelles becomes hydrophobic and deforms, thus leading to the rapid release of encapsulated drugs, as shown for the anti-inflammatory drug prednisone acetate. In vitro tests revealed that this novel copolymer was biocompatible at concentrations as high as 1 mg/ml in 3T3 fibroblasts.

Another example of a thermoresponsive drug delivery system was reported by Nakayama et al. and consists of biodegradable polymeric micelles of the hydrophilic copolymer of PNIPAAm-poly(dimethylacrylamide) conjugated to the hydrophobic polymers poly(D,L-lactic acid) (PLA), poly(ε-caprolactone) (PCL), or PLA–PCL (Nakayama, Okano et al. 2006). These systems presented a LCST of about 40°C, which would enable external triggering of drug release. Interestingly, only micelles that had PLA–PCL copolymer in the hydrophobic core resulted in thermoresponsive character. Evaluation of this system with the drug doxorubicin proved a highly thermoresponsive release behavior, with the drug slowly diffusing out of the micelles at body temperature but exhibiting a high release rate 5°C above this temperature (Nakayama, Okano et al. 2006).

pH-Responsive Nanosystems

Polymers and drug delivery systems able to undergo conformation changes depending on the acidity of the surrounding environment have a number of important applications in nanomedicine. For example, these nanocarriers can selectively deliver chemotherapeutic agents at the site of a tumor as a result of the lower pH found in the tumor interstitium (Wike-Hooley, Haveman et al. 1984; Vaupel, Kallinowski et al. 1989), while sparing the rest of the body from the toxic drug (Schmaljohann 2006). Additionally, these systems can be designed to delay release of a specific drug until after the nanocarrier is endocytosed by a target cell and exposed to the lower pH of the endolysosomal compartments (Schmaljohann 2006). Some systems by means of their pH responsiveness are able to escape lysosomes upon configuration changes that allow them to interact with the organelle membrane (Panyam, Zhou et al. 2002). Finally, pH-responsive systems have also been extensively studied for applications in oral drug delivery (Schmaljohann 2006). Responsive nanocarriers can protect labile drugs

from the acid environment of the stomach while promoting their absorption in the more neutral small intestine. Examples of recently developed pH-responsive nanocarriers are reviewed here.

Nanoparticles of poly(beta-amino ester) (PbAE) modified with poloxamers, triblock copolymers of poly(ethylene oxide)–poly(propylene oxide)–poly(ethylene oxide), were designed for the delivery of hydrophobic drugs to the acidic environment of tumors and intracellular acidic organelles (Potineni, Lynn et al. 2003; Shenoy, Little et al. 2005). Studies demonstrated that the pH-responsive PbAE nanoparticles successfully delivered the chemotherapeutic drug paclitaxel to SKOV-3 ovarian cancer cells in vitro, and led to higher paclitaxel accumulation at the tumor than when administered as free drug in solution or in pH-insensitive pluronic-modified poly(ε-caprolactone) (PCL) nanoparticles in vivo (Shenoy, Little et al. 2005; Shenoy, Little et al. 2005). Further in vivo studies revealed that paclitaxel-loaded PbAE nanoparticles resulted in greater therapeutic efficacy than the free drug and paclitaxel PCL in mice xenografts of ovarian cancer, and did not result in systemic toxicity as judged from body weight losses or blood cell counts (Devalapally, Shenoy et al. 2007).

Another pH-responsive nanoparticle design is based on block copolymers of poly[2-(*N*,*N*-diethylamino)ethyl methacrylate] (PDEA) and poly (ethylene glycol) (PEG) (Xu, Van Kirk et al. 2006). This copolymer formed approximately 80 nm core–shell nanoparticles with a pH-responsive core and a PEG-dense shell. These pH-responsive nanoparticles were designed in such a way that they would release the drug in a very short period of time upon being endocytosed by target cancer cells and consequently being exposed to the acidic conditions of the lysosomal compartments. Such rapid release is achieved by the ability of the PDEA–PEG nanoparticles to become soluble in the aqueous biological environment when the pH drops below about 6. PDEA–PEG nanoparticles loaded with cisplatin were used to evaluate their potential to overcome multidrug resistance in SKOV-3 ovarian cancer cells in vitro and in vivo in nude mice xenografts (Xu, Van Kirk et al. 2006). Results showed that PDEA–PEG nanoparticles were in fact internalized by cells into lysosomes and caused significantly higher cellular growth inhibition than free cisplatin. In vivo, this system was observed to lower the number of blood vessels and increase the number of apoptotic cells in tumors.

Block ionic complexes (BIC) formed by ionic interactions between hydrophilic block copolymers containing ionic and nonionic regions with an oppositely charged molecule have been recently proposed as responsive drug delivery systems because of their ability to undergo changes in response to the environmental conditions (Oh, Bronich et al. 2006). The core of BIC is formed by electrostatically bound polyion–counterion complexes. Active agents can be encapsulated within these systems via hydrophobic or electrostatic interactions. The composition and structure of these systems can be customized by the choice of block copolymer and counterion. One specific BIC system recently reported consists of copolymers of Pluronic grafted with poly(acrylic acid) (PAA) complexed with the cationic surfactant hexadecyltrimethylamonium bromide (HTAB) (Oh, Bronich et al. 2006). Formation of the complexes occurs upon mixing aqueous solutions of the copolymer and of the surfactant, and results in

particles of about 50–100 nm depending on the relative amounts of copolymer and surfactant. Similar to the size, the surface charge of the particles is highly dependent on the ratio of the constituents. These BICs were observed to respond to changes in salt concentration, pH, and temperature (Oh, Bronich et al. 2006). Specifically, increased salt concentration resulted in up to an eightfold increase in particle size up to a ceiling salt concentration above which the complexes completely dissociated. Increased pH led to decreased zeta potential, with a charge inversion from positive to negative at pH 6.0. This pH sensitivity can be effectively exploited for intracellular drug delivery through the endocytic pathway since the acidification of the endosomes would reverse the charge of the BIC and permit its interaction with the endosomal membrane.

An interesting drug delivery platform that utilizes pH-cleavable bonds to modify the surface of micelles and liposomes was recently proposed by Sawant et al. (Sawant, Hurley et al. 2006). By blending copolymers containing and lacking pH-cleavable bonds, this system is able to control the presentation or masking of functional moieties, such as targeting agents, according to the environmental pH, as can be seen in Figure 10.4. pH-cleavable polymers were made by linking poly(ethylene glycol) and phosphatidylethanolamine via a hydrazone bond (PEG–Hz–PE) (Sawant, Hurley et al. 2006). Nanocarriers were formulated with blends of low molecular weight pH-insensitive PEG–PE polymers conjugated to cell-penetrating peptide (TATp), high molecular weight pH-insensitive PEG–PE polymer conjugated to antibodies, and high molecular weight pH-sensitive PEG–Hz–PE. In such systems, the targeting antibody would be freely accessible on the surface of the nanoparticle shell and actively participate in targeting the nanocarriers to the diseased tissue, while the TATp moiety would be shielded by longer pH-sensitive PEG–Hz–PE chains. Once localized in the more-acidic tumor or inflamed interstitium, the medium-sized PEG chains would be cleaved off as a result of destabilization of the hydrazone bond, thus exposing the cell-penetrating agents and promoting internalization of the nanocarriers into the target cells. In vitro results showed that nanocarriers functionalized with monoclonal antimyosin antibody 2G4 bound specifically to the antigen myosin at all pH tested as expected since the antibody was present at the surface and was conjugated to the nanocarriers via a non-pH-sensitive polymer. However, internalization of nanocarriers with the cell-penetrating peptide bound to hidden PEG–PE molecules was increased only after the carriers had been exposed to acidic conditions which could remove the shielding PEG coat from the PEG–Hz–PE polymer (Sawant, Hurley et al. 2006).

Sajeesh and Sharma recently reported on the preparation of pH-responsive nanoparticles for oral delivery of proteins (Sajeesh and Sharma 2005). The nanoparticles were created spontaneously by ionic complexation of poly(methacrylic acid)–chitosan–poly(ethylene glycol) prepared by free radical polymerization in an aqueous environment. Loading of active agents was achieved by a diffusion filling method in which the nanoparticles are equilibrated in solutions of the agent, thus allowing the agent to partition into the polymeric system. Despite their irregular morphology, these nanoparticles displayed properties potentially useful for oral delivery of labile molecules. Release of model protein bovine serum albumin and

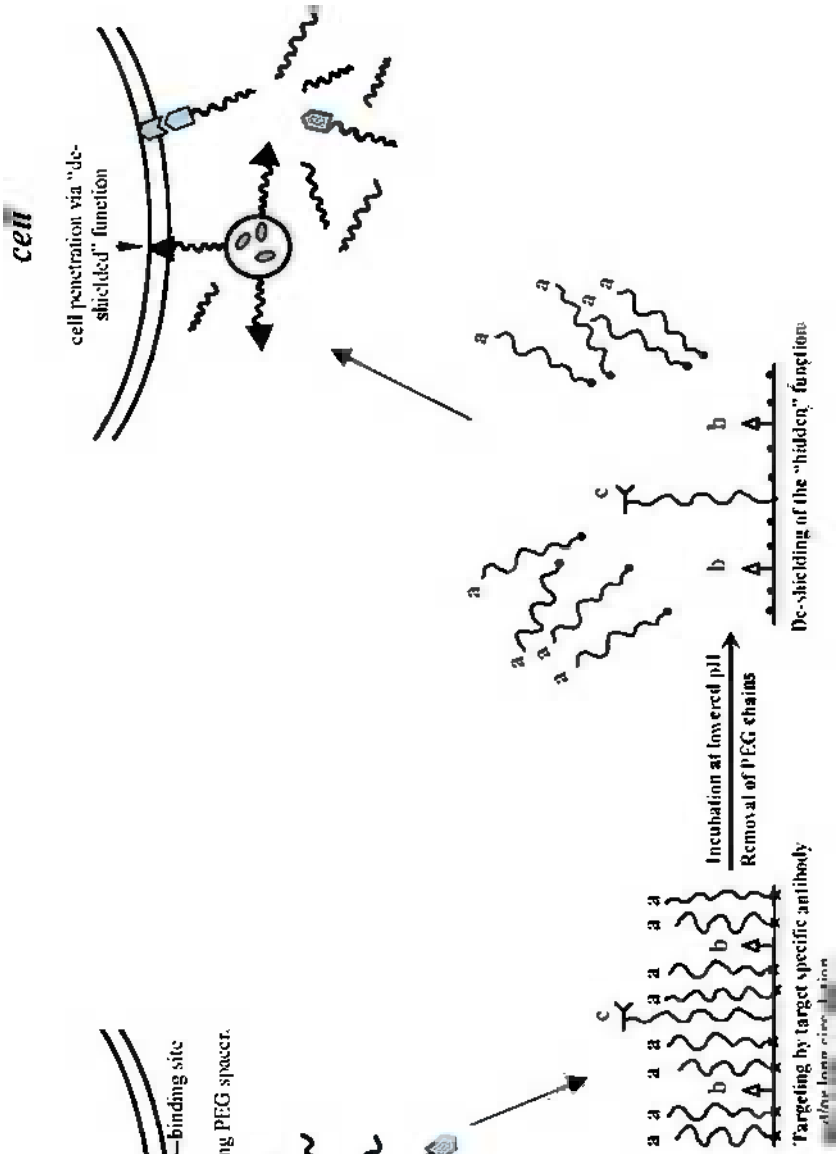

Figure 10.4 Diagram of pH-responsive nanocarriers that include permanent and cleavable surface polymeric chains that are used to modify the surface functionality at specific pathological conditions. Reproduced with permission from Sawant, Hurley, et al. (2006). (*See* Color Plate 16)

insulin was significantly delayed at a pH of 1.2, representative of the stomach, compared to a pH of 7.4. For example, only about 10% of loaded insulin was released from the nanoparticles at the acidic pH compared to about 90% at pH 7.4 (Sajeesh and Sharma 2005). The release of the protein at pH 7.4 was mostly complete by 4 hours, which is relevant to the residence time of the particles in the small intestine. The pH-dependent release behavior was attributed to the ability of the PMAA polymer to swell and shrink as the pH increases or decreases because of the protonation and deprotonation of carboxylic acid groups, respectively. When used for oral delivery, the nanoparticles would protect the active agent from degradation in the acidic environment of the stomach, but would release it at the small intestine as a result of nanoparticle swelling in the more neutral environment.

Nanocarriers with Combined Temperature- and pH-Responsive Properties

As described earlier, temperature-sensitive polymers such as PNIPAAm are most useful for drug delivery purposes if their LCST is higher than body temperature and their destabilization is triggered by artificially heating the target tissue to a temperature above the LCST with external sources. However, this limits their clinical applicability to the treatment of superficial malignancies due to low penetration of common heating sources. To overcome this problem, drug delivery systems incorporating both pH and temperature sensitivity have been investigated.

One such system consists of core–shell nanoparticles of poly(*N*-isopropylacrylamide-*co*-*N*,*N*-dimethylacrylamide-*co*-10-undecenoic acid) (PNIPAAm-co-DMAAm-co-UA) (Soppimath, Tan et al. 2005). In this system, UA makes up the hydrophobic and pH-sensitive core while PNIPAAm is present at the surface in contact with the aqueous environment. DMMAm, being a hydrophilic polymer, shifts the LCST of PNIPAAm to a higher temperature depending on the molar composition of the copolymers: the higher the molecular weight of the DMMAm section, the higher the LCST of the copolymer. This group was able to prepare a copolymer that had an LCST greater than body temperature (38.6°C) at physiological pH 7.4, and lower than body temperature (35.5°C) at a pH of 6.6 (Soppimath, Tan et al. 2005). Consequently, nanoparticles from this copolymer could easily deliver drugs selectively to the acidic interstitium of tumors while remaining stable and preventing toxicity to non-diseased tissue. The pH dependence of the LCST was attributed to the protonation and consequent decrease of hydrophobicity of the UA core with increasing pH, which resulted in increasing LCST for the copolymer. This system was evaluated with the chemotherapeutic drug doxorubicin and demonstrated significantly increased release rate, deformation, and precipitation at acidic pH and physiological temperature.

Wei et al reported on the preparation of temperature- and pH-responsive core–shell micelles that remain stable below the low critical solution temperature (LCST) of the polymer despite changes in pH, but become unstable and release the loaded drug in a pH-dependent manner above the LCST (Wei, Zhang et al. 2006). These micelles, which presented a critical micelle

concentration of 174 μg/ml, an LCST of 31°C, were prepared from the amphiphilic copolymer poly(10-undecenoic acid-*b*-*N*-isopropylacrylamide) (PUA-b-PNIPAAm), in which PUA represents the hydrophilic block while PNIPAAm represents the hydrophobic pH- and temperature-sensitive block (Wei, Zhang et al. 2006). Micelles loaded with the anti-inflammatory drug prednisone acetate displayed significantly increased release rates above the LCST due to deformation and precipitation at the higher temperature. In addition, lower environmental pH led to an initial faster release rate compared to that at normal physiological pH (7.4) when the temperature was maintained at 37°C which is above the LCST of the micelles. At 13°C, the drug release profile was not different at the two solution-pH tested.

Oxidation-Responsive Systems

Nanocarriers based on oxidation-sensitive materials have gained interest for application in drug delivery to inflamed tissue rich in oxidizing substances (Tirelli 2006). Polymeric vesicles of amphiphilic copolymer PEG–poly(propylene sulfide)–PEG (PEG–PPS–PEG) have been prepared for this application (Napoli, Valentini et al. 2005). PPS makes up the hydrophobic and oxidation-sensitive block. Upon exposure to an oxidative environment, PPS in the vesicles is transformed into hydrophilic poly (propylene sulfoxide) and poly(propylene sulfone), transforming the vesicles into worm-like and spherical micelles of progressively decreasing size that can ultimately be removed by glomerular filtration.

Another similar oxidation-responsive nanocarrier design consists of crosslinked poly(propylene sulfide) nanoparticles prepared by living emulsion polymerization of propylene sulfide in an aqueous phase containing Pluronic F-127 followed by curing by air exposure or by reaction with a bifunctional molecule (Rehor, Hubbell et al. 2005). Pluronic is presumed to cover the surface of the nanoparticles, thus imparting stability in aqueous environments. Nanoparticle size was easily controlled in the range of 25–250 nm by the ratio of Pluronic to PPS. As for the system previously described, exposure to oxidizing conditions leads to the transformation of the hydrophobic PPS onto hydrophilic poly(sulfoxides) and poly(sulfone), and in this case to the swelling and dissolution of the nanoparticles.

Personal Care Products

Although there is tremendous potential for nanotechnology in drug delivery, nanotechnology and nanoparticles, in particular, have already made a significant impact in consumer products. This mirrors the development of microparticle-based systems which appeared on supermarket shelves and cosmetic counters long before the pharmacy window.

In this section we will describe the use of nanotechnology in consumer products, primarily personal care products. Since these products are for external use and do not usually make substantiated medical claims, they are not often subject to FDA approval. Hence, the time from invention to market is much faster than for drug delivery systems. The research and development in the area is significant. For example, the company L'Oreal

ranks number six in their number of nanotechnology patents in the US with more than 190 patents using nanotechnology. For example, they hold patents on photoprotective and sunscreen products (Boutelet & Candau, 2006; Hansenne & Rick, 2002), nanocapsules based on poly(alkylene adipate) (Simonnet, Richart & Biatry, 2003), nanocapsules based on dendritic polymers (Simonnet & Richart, 2002), and nanoparticles containing oils for delivery to the upper layers of the epidermis based on poly(alkyl cyanoacrylates) (Handjani & Ribier, 2001).

Along with so many products containing nanoparticles, nanocapsules, fullerenes, nanosomes, and other nanoencapsulated ingredients comes public concern over the safety of such products. This concern rises primarily from the enhanced effectiveness which is often seen in nanosized formulations over conventional or even micron-sized formulations. In Table 1 there

Table 10.1 Examples of personal care products currently on the market containing nano-scale ingredients, nanoparticles, nanocapsules and nano-delivery systems.

Company	Product	Potentially nano-sized ingredient or relevant label term
Acne treatment		
Celazome	O-Plex Target Acne Spot Treatment	Lyphazome nanospheres
Wilma Schumann	Acne Kit	Vitamin E (nanoparticles)
DS Laboratories	Trioxil Anti-Acne Gel	Wheat-germ, barley and arnica nanosomes
After sun product		
L'Oreal , Lancome	Soleil Instant Cooling Sun Spritz	Vitamin nanocapsules
Anti-aging		
Sircuit Skin Cosmeceuticals Inc.	Skin Addict Firming Anti-Oxidant Serum	Fullerenes
Sircuit Skin Cosmeceuticals Inc.	Skin O.M.G. Anti-Aging Skin Resusc Serum	Fullerenes
Can Do Spirit, Inc., TYK	TYK Revelation	Nanodelivery system
Cosmetic Dermatology, Inc.	Dr. Brandt Laser Tight	Nanoencapsulated ingredients
ProCyte Corporation	Neova Therapy Dual Action Lotion	Nanoencapsulated retinol
emerginC	emerginC Hyper-Vitalizer	Nanoliposome delivery system
DS Laboratories, Inc.	Viterol.A (viatrozene gel) 29%	Nanosomes of sodium lactate, calendula, witch hazel, ginseng, urea, Vitamin A, Vitamin E, Pro-vitamin B5, alpha-bisabolol and germal II
DS Laboratories, Inc.	Viterol.A (viatrozene gel) 16%	Nanosomes of Vitamin A
L'Oreal, Lancome	Soleil Soft-Touch Anti-Wrinkle Sun Cream SPF 15	Vitamin nanocapsules
Anti-itch/rash cream		
Cosmetic Dermatology, Inc.	Dr. Brandt Laser Relief	Nanoencapsulated ingredients
Around-eye cream		
Sircuit Skin Cosmeceuticals Inc.	White Out Daily Under Eye Care	Fullerenes
Celazome New Zealand Limited	Eye Treat with Lyphazome Technology	Lyphazome nanospheres
PerfectRx	Eye Perfect Serum	Nanodelivery system

(*Continued*)

Table 10.1 (*Continued*).

Company	Product	Potentially nano-sized ingredient or relevant label term
Body firming lotion		
Nutra Luxé M.D.	Lipo Reduction Anti-Cellulite Creme	Nanodelivery system
DS Laboratories, Inc.	Oligo.DX Cellulite Reducing Gel	Nanosomes of centella asiatica
DS Laboratories, Inc.	Oligo DX Cellulite Treatment	Nanosomes of centella asiatica
Osmotics Corporation	Lipoduction Body Perfecting Complex	Nano-technology delivery system
Body wash/cleanser		
DS Laboratories, Inc.	Hydroviton.CR Liquid Normalizing Soap	Nanosomes of Vitamin A
Concealer		
DERMAdoctor	Faux Fillment	Nanospheres of hyaluronic acid and fulvic acid
Facial cleanser		
Fancl International, Inc.	Boscia MakeUp BreakUp Cool Cleansing Oil	Nanotechnology ingredients
Facial moisturizer/treatment		
Ferndale Laboratories, Inc.	Nouriva Repair Moisturizing Cream	Nanoparticle delivery system
Hair-loss treatment		
DS Laboratories, Inc.	Spectral DNC Hair Loss Treatment	Nanosomes
Mask		
Celazome New Zealand Limited	Spoil Me Body Lotion	Lyphazome nanospheres
Nail treatment		
Celazome New Zealand Limited	Tip Treat Cuticle Exfoliator	Lyphazome nanospheres
Pain/wound treatment		
Marlyn Nutraceuticals, Inc.	Naturally Vitamins Wobenzyme N Pain Relieving Creme	Nanosphere technology
Sunscreen/tanning oil		
Korres Natural Products Ltd.	Red Vine Year Round Hair Sun Protection	Nanoparticles
Korres Natural Products Ltd.	Red Vine Year Round Hair Sun Protection Spray	Nanoparticles
DERMAdoctor	Fun in the Sun Kit	Nanotechnology ingredients
L'Oreal, Lancome	Soleil Soft-Touch Moisturising Sun Lotion SPF 15	Vitamin nanocapsules

is a summary of some, but certainly not all, personal care products that contain nanoscale materials. Much of this information has been compiled by the Environmental Working Group who prepared an analysis of 25,000 personal care product labels and found that approximately 250 of them specifically mentioned containing nanoscale or micron-sized ingredients. Some examples are shown in Table 1 (Environmental Working Group, 2006). Not all of these certainly would have controlled-release-based nanoscale components, but a great many do. A large number of these products contain nanosomes, or nanoscale liposomes, which provide stability to the encapsulated product, better skin coverage of the product, and subsequent controlled release of the active agent. Although the term nanosome has been

trademarked by Elsom Research, it also appears in the research literature and product descriptions by DS Laboratories, Min New York, Lipoxidil, L'Oreal, and Cosmosome to name just a few. Enhanced penetration of these nansomes can also occur since the gaps between dead skin cells on the surface of the epidermis are approximately 100 nm wide. This allows products which can easily penetrate the lipid matrix between dead skin cells, such as nanosomes, to deliver not only cosmetics and personal care products but also therapeutic agents directly to the living cells of the epidermis.

These companies are not just utilizing nanotechnology, they are marketing it as well. A look at the website for Beyond Skin Science (Beyond Skin Science, 2007) reveals the logos of the National Nanotechnology Initiative and the Nano Science Technology Institute, although there are no links to their websites and it is confusing what this Institute actually is. Their own technology is called "Nanochem" and their products are labeled as "Nanochem certified." Duprey cosmetics is using NanoDulcine™, nanosized particles of a low glycemic, human grade edible fruit glycoside, to deliver L-arginine and vitamin C "deep within the cells" of the epidermis. Their website carries a logo stating "Certified Nano Technology" (Duprey Cosmetics, 2007).

The greatest challenge in determining what actually goes into nanoscale skin care products is that more are proprietary and may or may not actually be patented and very few are described in the scientific literature. Most work described in the scientific literature addresses solid lipid nanoparticles (SLN), a system which combines the solubility and stability-enhancing advantages of liposomes for many compounds with the additional stability of solid formulations (Müller, Radtke & Wissing, 2002; Wissing & Müller, 2003). This form is achieved by exchanging the liquid lipid (oil) in liposome formulations with a lipid which is solid at room and body temperatures. The structure of these SLNs can be a matrix, a compound-enriched shell, or a compound-enriched core. For epidermal delivery, these formulations may show improved skin penetration and targeting, but those results may be dependent on the interaction of the drug and particle (Borgia, Regehly, Sivaramakrishnan, Mehnert, Korting, Danker, Röder, Kramer & Schäfer-Korting, 2005; Chen, Chang, Du, Liu, Liu, Weng, Yang, Xu & X, 2006). The most commonly reported studies involve delivery of retinol-based active agents for cosmetic use and dermatological disease (Jee, Lim, Park & Kim, 2006; Liu, Hu, Chen, Ni, Xu & Yang, 2007; Taha, Samy, Kassem & Khan, 2005), sunblock formulations (Cengiz, Wissing, Müller & Yazan, 2006; Song & Liu, 2005), and vitamin A delivery (Jenning, Gysler, Schäfer-Korting & Gohla, 2000; Jenning, Schäfer-Korting & Gohla, 2000).

References

Abo El Ola, S. M., R. Kotek, et al. (2004). "Studies on poly(trimethylene terephthalate) filaments containing silver." *J Biomater Sci Polym Ed* **15**(12): 1545–59.

Agnihotri, S. A., N. N. Mallikarjuna, et al. (2004). "Recent advances on chitosan-based micro- and nanoparticles in drug delivery." *J Control Release* **100**(1): 5–28.

Balogh, L., D. R. Swanson, et al. (2001). "Dendrimer-silver complexes and nanocomposites as antimicrobial agents." *Nano Lett* **1**(1): 18–21.

Beyond Skin Science (2007). Corona, CA (March 20, 2007); http://www.beyondskinscience.com

Bhabak, K. P. and G. Mugesh (2007). "Synthesis, characterization, and antioxidant activity of some ebselen analogues." *Chem A Eur J* **13**(16): 4594–4601.

Bhadra, D., S. Bhadra, et al. (2003). "A PEGylated dendritic nanoparticulate carrier of fluorouracil." *Int J Pharm* **257**: 111–124.

Bhattacharya, S. and A. Bajaj (2005). "Recent advances in lipid molecular design." *Curr Opin Chem Biol* **9**(6): 647–655.

Bontha, S., A. V. Kabanov, et al. (2006). "Polymer micelles with cross-linked ionic cores for delivery of anticancer drugs." *J Control Release* **114**(2): 163–74.

Borgia, S. L., Regehly, M., Sivaramakrishnan, R., Mehnert, W., Korting, H. C., Danker, K., Röder, B., Kramer, K. D. and Schäfer-Korting, M. (2005). "Lipid nanoparticles for skin penetration enhancement-correlation to drug localization within the particle matrix as determined by fluorescence and parelectric spectroscopy." *J Control Release*, **110**: 151–163.

Brannon-Peppas, L. (1995). "Recent advances on the use of biodegradable microparticles and nanoparticles in controlled drug delivery." *Int J Pharm* **116**: 1–9.

Brannon-Peppas, L. and J. O. Blanchette (2004). "Nanoparticle and targeted systems for cancer therapy." *Adv Drug Del Rev* **56**: 1649–1659.

Brett, D. W. (2006). "A discussion of silver as an antimicrobial agent: alleviating the confusion." *Ostomy Wound Manage* **52**(1): 34–41.

Bromberg, L. E., D. K. Buxton, et al. (2001). "Novel periodontal drug delivery system for treatment of periodontitis." *J Control Release* **71**(3): 251–9.

Boutelet, K. and D. Candau (2006). Photoprotective/cosmetic compositions comprising sulfonic/hydrophobic amphiphilic polymers, USA, L' Oreal, Patent 7,045,120.

Calvo, P., J. L. VilaJato, et al. (1996). "Comparative in vitro evaluation of several colloidal systems, nanoparticles, nanocapsules, and nanoemulsions, as ocular drug carriers." *J Pharm Sci* **85**(5): 530–536.

Caves, J. M. and E. L. Chaikof (2006). "The evolving impact of microfabrication and nanotechnology on stent design." *J Vasc Surg* **44**(6): 1363–1368.

Cengiz, E., Wissing, S. A., Müller, R. H. and Yazan, Y. (2006). Sunblocking efficiency of various ti)2-loaded solid lipid nanoparticle formulations. *Int J Cosm Sci* **28**: 371–378.

Chen, H., Chang, X., Du, D., Liu, W., Liu, J., Weng, T., Yang, Y., Xu, H. and Yang, X. (2006). Podophyllotoxin-loaded solid lipid nanoparticles for epidermal targeting. *J Control Release*, **110**: 296–306.

D'Emanuele, A. and D. Attwood (2005). "Dendrimer-drug interactions." *Adv Drug Del Rev* **57**(15): 2147–2162.

Devalapally, H., D. Shenoy, et al. (2007). "Poly(ethylene oxide)-modified poly (beta-amino ester) nanoparticles as a pH-sensitive system for tumor-targeted delivery of hydrophobic drugs: part 3. Therapeutic efficacy and safety studies in ovarian cancer xenograft model." *Cancer Chemo Pharmacol* **59**(4): 477–484.

Duprey Cosmetics (2007). (March 10, 2007); St. Pete Beach, Fl.; http://www.dupreycosmetics.com/ nano_dulcine.html

Edelman, E. R., L. Brown, et al. (1987). "In vitro and in vivo kinetics of regulated drug release from polymer matrices by oscillating magnetic fields." *J Biomed Mater Res* **21**(3): 339–53.

Edelman, E. R., A. Fiorino, et al. (1992). "Mechanical deformation of polymer matrix controlled release devices modulates drug release." *J Biomed Mater Res* **26**(12): 1619–31.

Environmental Working Group (2006). Washington, DC (October 10, 2006); http://www.ewg.org/issues/cosmetics/20061010/table2.php

Fonseca, C., S. Simões, et al. (2002). "Paclitaxel-loaded PLGA nanoparticles: preparation, physiochemical characterization and in vitro anti-tumoral activity." *J Control Release* **83**: 273–286.

Fresta, M., G. Puglisi, et al. (1995). "Pefloxacine mesilate-loaded and ofloxacin-loaded polyethylcyanoacrylate nanoparticles- Characterization of the colloidal drug carrier formulations." *J Pharm Sci* **84**(7): 895–902.

Fu, J., X. Li, et al. (2002). "Encapsulation of phthalocyanines in biodegradable poly(sebacic anhydride) nanoparticles." *Langmuir* **18**(10): 3843–3847.

Gaponik, N., I. L. Radtchenko, et al. (2004). "Luminescent polymer microcapsules addressable by a magnetic field." *Langmuir* **20**(4): 1449–52.

Georgakilas, V., K. Kordatos, et al. (2002). "Organic functionalization of carbon nanotubes." *J Am Chem Soc* **124**(5): 760–761.

Georgakilas, V., N. Tagmatarchis, et al. (2002). "Amino acid functionalization of water soluble carbon nanotubes." *Chem Communs* **24**: 3050–4051.

Guo, Z. and P. Sadler (1999). "Metals in medicine." *Angewandte Chemie-International Edition* **38**(11): 1513–1531.

Guzman, L. A., V. Labhasetwar, et al. (1996). "Local intraluminal infusion of biodegradable polymeric nanoparticles – A novel approach for prolonged drug delivery after balloon angioplasty." *Circulation* **94**(6): 1441–1448.

Handjani, R.-M. and Ribier, A. (2001). Compositions for the cosmetic and/or pharmaceutical treatment of the epidermis by topical application to the skin, and corresponding preparation process, USA, L' Oreal, Patent 6,203,802.

Hansenne, I. and Rick, D. W. (2002). High SPF nontacky/nongreasy uv-photoprotecting compositions comprising particulates of MMA crosspolymers, USA, L' Oreal, Patent 6,432,389.

Heller, J., J. Barr, et al. (2002). "Poly(ortho esters): synthesis, characterization, properties and uses." *Adv Drug Del Rev* **54**(7): 1015–1039.

Hirsch, L. R., A. M. Gobin, et al. (2006). "Metal nanoshells." *Ann Biomed Eng* **34**(1): 15–22.

Horcajada, P., C. Marquez-Alvarez, et al. (2006). "Controlled release of ibuprofen from dealuminated faujasites " *Solid State Sciences* **8**(12): 1459–1465

Horcajada, P., C. Serre, et al. (2006). "Metal-organic frameworks as efficient materials for drug delivery." *Angew Chem Int Ed Engl* **45**(36): 5974–8.

Hu, Y. X., J. Chang, et al. (2005). Preparation and evaluation of 5-FU/PLGA/gene nanoparticles. *Asbm6: Advanced Biomaterials Vi*. Zurich-Uetikon, Trans Tech Publications Ltd: 147–150.

Huth, S., J. Lausier, et al. (2004). "Insights into the mechanism of magnetofection using PEI-based magnetofectins for gene transfer." *J Gene Med* **6**(8): 923–36.

Isab, A. A. and M. I. Wazeer (2007). "Synthesis and characterization of thiolate-Ag(I) complexes by solid-state and solution NMR and their antimicrobial activity." *Spectrochim Acta A Mol Biomol Spectrosc* **66**(2): 364–370.

Jain, R. A. (2000). "The manufacturing techniques of various drug loaded biodegradable poly(lactide-co-glycolide) (PLGA) devices." *Biomaterials* **21**(23): 2475–2490.

Jee, J.-P., Lim, S.-J., Park, J.-S. and Kim, C.-K. (2006). "Stabilization of all-trans retinol by loading lipophilic antioxidants in solid lipid nanoparticles." *Eur J Pharm Biopharm*, **63**: 134–139.

Jenning, V., Gysler, A., Schäfer-Korting, M. and Gohla, S. H. (2000). "Vitamin A loaded solid lipid nanoparticles for topical use: Occlusive properties and drug targeting in the upper skin." *Eur J Pharm Biopharm*, **49**: 211–218.

Kam, N. W. and H. Dai (2005). "Carbon nanotubes as intracellular protein transporters: generally and biological functionality." *J Am Chem Soc* **127**(16): 6021–6026.

Karlov, A. V., I. A. Khlusov, et al. (2002). "Adhesion of Staphylococcus aureus to implants with different physicochemical characteristics." *Bull Exp Biol Med* **134**(3): 277–80.

Kost, J., R. Noecker, et al. (1985). "Magnetically controlled release systems: effect of polymer composition." *J Biomed Mater Res* **19**(8): 935–40.

Kost, J., J. Wolfrum, et al. (1987). "Magnetically enhanced insulin release in diabetic rats." *J Biomed Mater Res* **21**(12): 1367–73.

Kumar, R., S. Howdle, et al. (2005). "Polyamide/silver antimicrobials: effect of filler types on the silver ion release." *J Biomed Mater Res B Appl Biomater* **75**(2): 311–9.

Labhasetwar, V., C. X. Song, et al. (1998). "Arterial uptake of biodegradable nanoparticles: Effect of surface modifications." *J Pharm Sci* **87**(10): 1229–1234.

Lanza, G. M., X. Yu, et al. (2002). "Targeted antiproliferative drug delivery to vascular smooth muscle cells with a magnetic resonance imaging nanoparticle contrast agent implications for rational therapy of restenosis." *Circulation* **106**(22): 2842–2847.

Li, Y.-Y., X.-Z. Zhang, et al. (2006). "Novel stimuli-responsive micelle self-assembled from Y-shaped P(UA-Y-NIPAAm) copolymer for drug delivery." *Biomacromolecules* **7**(11): 2956–2960.

Lin, A. W., N. A. Lewinski, et al. (2005). "Optically tunable nanoparticle contrast agents for early cancer detection: model-based analysis of gold nanoshells." *J Biomed Opt* **10**(6): 064035.

Liu, J., Hu, W., Chen, H., Ni, Q., Xu, H. and Yang, X. (2007). "Isotretinoin-loaded solid lipid nanoparticles with skin targeting for topical delivery." *Int J Pharm*, **328**: 191–195.

Liu, M. J., K. Kono, et al. (2000). "Water-soluble dendritic unimolecular micelles: Their potential as drug delivery agents." *J Control Release* **65**(1–2): 121–131.

Lu, Z., J. Z. Bei, et al. (1999). "A method for the preparation of polymeric nanocapsules without stabilizer." *J Control Release* **61**(1–2): 107–112.

MacLachlan, M., I. Manners, et al. (2000). "New (inter)faces: Polymers and inorganic materials " *Adv Materials* **12**(9): 675–681.

Mainardes, R. M. and L. P. Silva (2004). "Drug delivery systems: Past, present, and future." *Curr Drug Targets* **5**(5): 449–455.

Mitra, S., U. Gaur, et al. (2001). "Tumour targeted delivery of encapsulated dextran-doxorubicin conjugate using chitosan nanoparticles as carrier." *J Control Release* **74**: 317–323.

Muller, R. H., K. Mader, et al. (2000). "Solid lipid nanoparticles (SLN) for controlled drug delivery – a review of the state of the art." *Eur J Pharm Biopharm* **50**(1): 161–177.

Müller, R. H., Radtke, M. and Wissing, S. A. (2002). Solid lipid nanoparticles (SLN) and nanostructured lipid carriers (NLC) in cosmetic and dermatological preparations. *Adv Drug Del Rev*, **54**: S131–S155.

Nakayama, M., T. Okano, et al. (2006). "Molecular design of biodegradable polymeric micelles for temperature-responsive drug release." *J Control Release* **115**(1): 46–56.

Napoli, A., M. Valentini, et al. (2005). "Oxidation-responsive polymeric vesicles." *Nature Biomaterials* **3**(3): 183–189.

Niwa, T., H. Takeuchi, et al. (1993). "Preparation of biodegradable nanospheres of water-soluble and insoluble drugs with D,L-lactide/glycolide copolymer by a novel spontaneous emulsification solvent diffusion method, and the drug release behavior." *J Control Release* **25**: 89–93.

O'Reilly, R. K., C. J. Hawker, et al. (2006). "Cross-linked block copolymer micelles: functional nanostructures of great potential and versatility." *Chemical Society Reviews* **35**(11): 1068–1083.

Oh, K. T., T. K. Bronich, et al. (2006). "Block ionomer complexes as prospective nanocontainers for drug delivery." *J Control Release* **115**(1): 9–17.

Owens III, D. and N. Peppas (2006). "Integration of thermally responsive nanosphere hydrogels with gold nanoparticles for intelligent therapeutic applications." *Trans Soc Biomater* **31**: 150–151.

Panyam, J., W.-Z. Zhou, et al. (2002). "Rapid endo-lysosomal escape of poly (D,L-lactide-co-glycolide) nanoparticles: implications for drug and gene delivery." *FASEB* **16**(10): 1217–1226.

Pastorin, G., W. Wu, et al. (2006). "Double functionalization of carbon nanotubes for multimodal delivery." *Chem Commun* **11**: 1182–1184.

Patton, J. N. and A. F. Palmer (2005). "Engineering temperature-sensitive hydrogel nanoparticles entrapping hemoglobin as a novel type of oxygen carrier." *Biomacromolecules* **6**(4): 2204–2212.

Plank, C., F. Scherer, et al. (2003). "Magnetofection: enhancing and targeting gene delivery with superparamagnetic nanoparticles and magnetic fields." *J Liposome Res* **13**(1): 29–32.

Plank, C., U. Schillinger, et al. (2003). "The magnetofection method: using magnetic force to enhance gene delivery." *Biol Chem* **384**(5): 737–47.

Potineni, A., D. M. Lynn, et al. (2003). "Poly(ethylene oxide)-modified poly(beta-amino ester) nanoparticles as a pH-sensitive biodegradable system for paclitaxel delivery." *J Control Release* **86**(2–3): 223–234.

Radwan, M. A. (1995). "In-vitro evaluation of polyisobutylcyanoacrylate nanoparticles as a controlled drug carrier for theophylline." *Drug Dev Ind Pharm* **21**(20): 2371–2375.

Rehor, A., J. A. Hubbell, et al. (2005). "Oxidation-sensitive polymeric nanoparticles." *Langmuir* **21**(1): 411–417.

Rhim, J. W., S. I. Hong, et al. (2006). "Preparation and characterization of chitosan-based nanocomposite films with antimicrobial activity." *J Agric Food Chem* **54**(16): 5814–22.

Roskos, K. V., B. K. Fritzinger, et al. (1995). "Development of a drug-delivery system for the treatment of periodontal-disease based on bioerodible poly(ortho esters)." *Biomaterials* **16**(4): 313–317.

Sajeesh, S. and C. P. Sharma (2005). "Novel pH responsive polymethacrylic acid-chitosan-polyethylene glycol nanoparticles for oral peptide delivery." *J Biomat Mater Res B: Appl Biomat* **76B**(2): 298–305.

Sakurai, H., A. Katoh, et al. (2006). "Chemistry and biochemistry of insulin-mimetic vanadium and zinc complexes. Trial for treatment of diabetes mellitus." *Bull. Chem. Soc. Jpn.* **79**(11): 1645–1664

Sambhy, V., M. M. MacBride, et al. (2006). "Silver bromide nanoparticle/polymer composites: dual action tunable antimicrobial materials." *J Am Chem Soc* **128**(30): 9798–808.

Sawant, R. M., J. P. Hurley, et al. (2006). ""SMART" drug delivery systems: double-targeted pH-responsive pharmaceutical nanocarriers." Bioconjug Chem **17**(4): 943–949.

Schierholz, J. M., L. J. Lucas, et al. (1998). "Efficacy of silver-coated medical devices." *J Hosp Infect* **40**(4): 257–62.

Schmaljohann, D. (2006). "Thermo- and pH-responsive polymers in drug delivery." *Adv Drug Del Rev* **58**(15): 1655–1670.

Sershen, S. R., S. L. Westcott, et al. (2000). "Temperature-sensitive polymer-nanoshell composites for photothermally modulated drug delivery." *J Biomed Mater Res* **51**(3): 293–8.

Seymour, L. W., R. Duncan, et al. (1994). "Poly(ortho ester) matrices for controlled release of the antitumor agent 5-fluorouracil." *J Control Release* **31**: 201–206.

Shenoy, D., S. Little, et al. (2005). "Poly(ethylene oxide)-modified poly(beta-amino ester) nanoparticles as a pH-sensitive system for tumor-targeted delivery of hydrophobic drugs. Part 1 In vitro evaluations." *Mol Pharmacy* **2**(5): 357–366.

Shenoy, D., S. Little, et al. (2005). "Poly(ethylene oxide)-modified poly(beta-amino ester) nanoparticles as a pH-sensitive system for tumor-targeted delivery of hydrophobic drugs: Part 2. In vivo distribution and tumor localization studies." *Pharm Res* **22**(12): 2107–2114.

Shikata, F., H. Tokumitsu, et al. (2002). "In vitro cellular accumulation of gadolinium incorporated into chitosan nanoparticles designed for neutron-capture therapy of cancer." *Eur. J. Pharm Biopharm*. **53**: 57–63.

Simonnet, J.-T. and Richart, P. (2002). Nanocapsules based on dendritic polymers, USA, L' Oreal, Patent 6,379,683.

Simonnet, J.-T., Richart, P. and Biatry, B. (2003). Nanocapsules based on poly (alkylene adipate), process for their preparation and cosmetic or dermatological compositions containing them, USA, L' Oreal, Patent 6,565,886.

Singh, R., D. Pantarotto, et al. (2006). "Tissue biodistribution and blood clearance rates of intravenously administered carbon nanotube radiotracers." *PNAS* **103**(9): 3357–3362.

Smaihi, M., E. Gavilan, et al. (2004). "Colloidal functionalized calcined zeolite nanocrystals " *J Mater Chem* **14**(8): 1347–1351.

Song, C. and Liu, S. (2005). "A new healthy sunscreen system for humans: Solid lipid nanoparticles as carrier for 3,4,5-trimethoxybenzoylchitin and the improvement by adding vitamin E." *Int J Bio Macromol*, **36**: 116–119.

Soppimath, K. S. and T. M. Aminabhavi (2002). "Ethyl acetate as a dispersing solvent in the production of poly(DL-lactide-co-glycolide) microspheres: effect of process parameters and polymer type." *J Microencapsulation* **19**(3): 281–292.

Soppimath, K. S., T. M. Aminabhavi, et al. (2001). "Biodegradable polymeric nanoparticles as drug delivery devices." *J Controlled Release* **70**(1–2): 1–20.

Soppimath, K. S., D. C.-W. Tan, et al. (2005). "pH-Triggered thermally responsive polymer core-shell nanoparticles for drug delivery." *Adv Mater* **17**(3): 318–323.

Steinbrink, J., H. Wabnitz, et al. (2001). "Determining changes in NIR absorption using a layered model of the human head." *Phys Med Biol* **46**(3): 879–896.

Taha, E. I., Samy, A. M., Kassem, A. A. and Khan, M. A. (2005). Response surface methodology for the development of self-nanoemulsified drug delivery system (SNEDDS) of all-trans-retinol acetate. *Pharm Dev Tech*, **10**: 363–370.

Tirelli, N. (2006). "(Bio)responsive nanoparticles." *Curr Opin Colloidal & Interface Sci* **11**(4): 210–216.

Tokumitsu, H., H. Ichikawa, et al. (1999). "Chitosan-gadopentetic acid complex nanoparticles for gadolinium neutron-capture therapy of cancer: Preparation by novel emulsion-droplet coalescence technique and characterization." *Pharm Res* **16**(12): 1830–1835.

Uhrich, K. E., S. M. Cannizzaro, et al. (1999). "Polymeric systems for controlled drug release." *Chem Rev* **99**(11): 3181–3198.

van Zutphen, S. and J. Reedijk (2005). "Targeting platinum anti-tumour drugs: Overview of strategies employed to reduce systemic toxicity." *Coordination Chem Rev* **249**(24): 2845–2853.

Vaupel, P., F. Kallinowski, et al. (1989). "Blood flow, oxygen and nutrient supply and metabolic microenvironment of human tumors: a review." *Cancer Res* **49**(23): 6449–6465.

Verma, A. K., K. Sachin, et al. (2005). "Release kinetics from bio-polymeric nanoparticles encapsulating protein synthesis inhibitor - Cycloheximide, for possible therapeutic applications." *Curr Pharm Biotechnol* **6**(2): 121–130.

Wei, H., X.-Z. Zhang, et al. (2006). "Self-assembled thermo- and pH-responsive micelles of poly(10-undecenoic acid-b-N-isopropylacrylamide) for drug delivery." *J Control Release* **116**(3): 266–274.

Wike-Hooley, J. A., J. Haveman, et al. (1984). "The relevance of tumor pH to the treatment of malignant disease." *Radiother Oncol* **2**(4): 343–366.

Wissing, S. A. and Müller, R. H. (2003). "Cosmetic applications for solid lipid nanoparticles (SLN)." *Int J Pharm*, 254, 65–68.

Wojtowicz, H., K. Kloc, et al. (2004). "Azaanalogues of ebselen as antimicrobial and antiviral agents: synthesis and properties." *Farmaco* **59**(11): 863–8.

Wu, W., S. Wieckowski, et al. (2005). "Targeted delivery of amphotericin B to cells by using functionalized carbon nanotubes." *Angew. Chem. Int. Ed.* **44**(39): 6358–6362.

Xu, P., E. A. Van Kirk, et al. (2006). "Anticancer Efficacies of Cisplatin-Releasing pH-Responsive Nanoparticles." *Biomacromolecules* **7**(3): 829–835.

Yoo, H. S., K. H. Lee, et al. (2000). "In vitro and in vivo anti-tumor activities of nanoparticles based on doxorubicin-PLGA conjugates." *J Control Release* **68**(3): 419–431.

Zhang, H., Y. Kim, et al. (2006). "Controlled release of paraquat from surface-modified zeolite Y." *Microporous and Mesoporous Materials* **88**(1–3): 312–318

Zwiorek, K., J. Kloeckner, et al. (2004). "Gelatin nanoparticles as a new and simple gene delivery system." *J Pharm Pharmac Sci* **7**(4): 22–28.

11

Nanotechnology for Intracellular Delivery and Targeting

Vladimir P. Torchilin

Intracellular Drug Delivery and Pharmaceutical Nanocarriers

Intracellular transport of biologically active molecules with therapeutic properties is one of the key problems in drug delivery in general. Many pharmaceutical agents need to be delivered intracellularly to exert their therapeutic action inside cytoplasm or onto the nucleus or other individual organelles, such as lysosomes, mitochondria, or endoplasmic reticulum. Among such agents we can find preparations for gene and antisense therapy, which have to reach cell nuclei; pro-apoptotic drugs, which target mitochondria; lysosomal enzymes, which have to reach lysosomal compartment; and some others (see Figure 11.1). Namely intracellular drug delivery can overcome certain important limitations for drug action, such as multidrug resistance in cancer chemotherapy. However, the very nature of cell membranes prevents proteins, peptides, and nanoparticulate drug carriers from entering cells unless there is an active transport mechanism, which is usually the case for very short peptides (Egleton & Davis, 1997). So far, multiple and only partially successful attempts have been made to bring various low-molecular-weight and macromolecular drugs and drug-loaded pharmaceutical carriers directly into the cell cytoplasm bypassing the endocytic pathway to protect drugs and DNA from the lysosomal degradation, thus enhancing drug efficiency or DNA incorporation into the cell genome. And even being safely delivered into the cell cytoplasm drugs still have to find their way to specific organelles (nuclei, lysosomes, mitochondria), where they are expected to utilize their therapeutic potential. Various vector molecules promote the delivery of associated drugs and drug carriers inside the cells via receptor-mediated endocytosis (Park et al., 2001). This process involves attachment of the vector molecule and an associated drug carrier to specific ligands on target cell membranes, followed by the energy-dependent formation of endosomes. The problem, however, is that any molecule/particle entering cell via the endocytic pathway and becoming entrapped into endosome, eventually ends in lysosome, where active degradation processes take place under the action of numerous lysosomal enzymes. As a result, only a small fraction of unaffected substance appears in the cell cytoplasm. Thus, even if an efficient cellular

M.M. de Villiers et al. (eds.), *Nanotechnology in Drug Delivery*, DOI: 10.1007/978-0-387-77667-5_11,

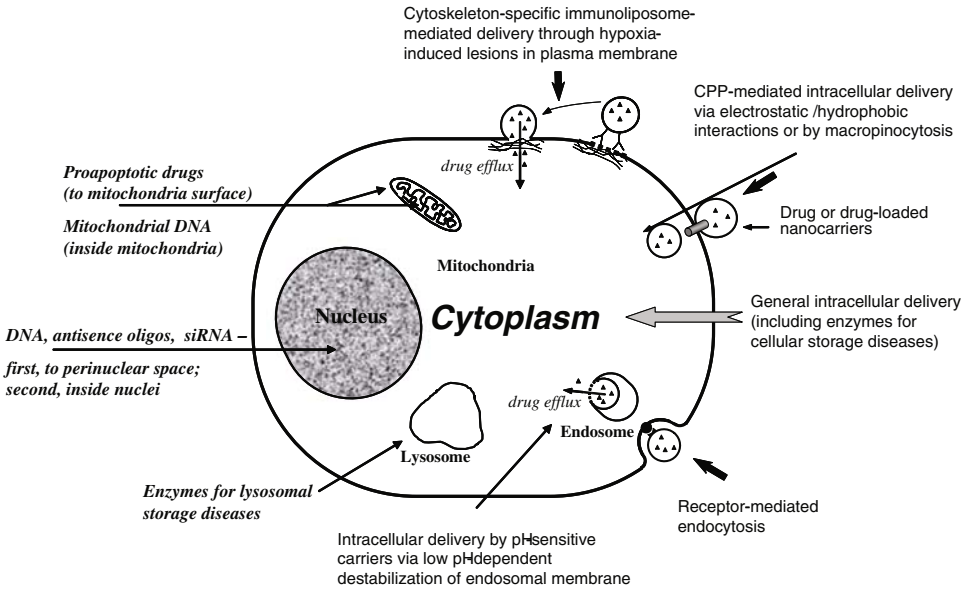

Figure 11.1 General scheme of intracellular drug delivery. Types of diseases, organelles involved, and required drugs are shown together with possible delivery routes and protocols.

uptake via endocytosis is observed, the delivery of intact peptides and proteins is compromised by an insufficient endosomal escape and subsequent lysosomal degradation. This results in the situation where many compounds showing a promising potential in vitro cannot be applied in vivo due to bioavailability problems.

The methods like microinjection or electroporation used for the delivery of membrane-impermeable molecules in cell experiments are invasive in nature and could damage cellular membrane (Arnheiter & Haller, 1988; Chakrabarti, Wylie, & Schuster, 1989). Much more efficient are the non-invasive methods, which allow for the endosomal escape of certain preparations. Enhanced endosomal escape can be achieved through the use of, for example, lytic peptides (Kamata, Yagisawa, Takahashi, & Hirata, 1994; Mastrobattista et al., 2002; Midoux, Kichler, Boutin, Maurizot, & Monsigny, 1998), pH-sensitive polymers (Lackey, Press, Hoffman, & Stayton, 2002), or swellable dendritic polymers (Lackey et al., 2002). These agents have provided encouraging results in overcoming limitations of endocytosis-based cytoplasmic delivery, but there is still a need for further improvement or consideration of alternative delivery strategies.

Among current "cutting-edge" treatment approaches, the problem of efficient intracellular delivery is especially important in case of gene delivery. Gene therapy is now considered by many as a major contender in the future treatment protocols for various diseases, including cancer (Roth et al., 1998) and AIDS (Lisziewicz, Sun, Lisziewicz, & Gallo, 1995). Though some early initial trails were encouraging, the latest results have raised certain concerns (Aalto-Setala & Vuorio, 1997). Viral vectors for DNA delivery suffer from non-specificity and inherent risks of virus-induced complications. Non-viral delivery systems, first of all, cationic lipids/liposomes (Farhood, Serbina, & Huang, 1995), also have certain

drawbacks, such as non-specificity and cytotoxic reactions (Filion & Phillips, 1997; Scheule et al., 1997); although, new cationic lipid derivatives with decreased toxicity are currently under development (Tang & Hughes, 1999). Still, the traditional routes of internalization of DNA carriers by endocytosis or pinocytosis with subsequent degradation of the delivered DNA by lysosomal nucleases strongly limit the efficacy of transfection (Xu & Szoka, 1996). From this point of view, the development of new methods that can deliver genetic constructs directly into the cytoplasm of the target cells would be highly desirable.

As of now, the only way to deliver drugs to individual cell organelles is to modify them with certain molecules demonstrating somewhat increased ability to associate with these organelles. Thus, for example, a large variety of small molecules have been identified to specifically target and accumulate in lysosomes (summarized in Horobin & Kiernan, 2002). Among them, rhodamine B is routinely used for the visualization of lysosomes and other acidic organelles in live cells (Horobin, 2002; Minier & Moore, 1996), and its hydrophobized derivative, octadecyl rhodamine B, allows to anchor rhodamine B in lipidic membranes. The latter has been widely used for monitoring membrane fusion (Daugelavicius et al., 2005; Hoekstra, de Boer, Klappe, & Wilschut, 1984; Hoekstra & Klappe, 1986; Pozzi et al., 1993) and for studying lysosomal metabolism (Kuwana, Mullock, & Luzio, 1995; Ohashi et al., 1999; Ohashi, Murata, & Ohnishi, 1992). Huth et al. (Huth, Wieschollek, Garini, Schubert, & Peschka-Suss, 2004) have demonstrated that rhodamine-B-phosphoethanolamine incorporated into the liposomal membrane results in increased accumulation of liposomes in lysosomes, i.e., influences the uptake of particles and their intracellular distribution. Lysosomotropic properties have also been shown for *N*-(3-((2,4-dinitrophenyl)-amino)propyl)-*N*-(3-aminopropyl)methylamine (Hirota et al., 2004; Inoue, Yoshida, & Akisaka, 1999; Larsson, Clapp, Park, Cannon, & Tisher, 1987; Verlander, Madsen, Larsson, Cannon, & Tisher, 1989) and for Neutral red (Horobin, 2002). Mitochondriotropic ligands include Rhodamine 123 (Chen et al., 1982b) and triphenylphosphonium cation which are already used to prepare mitochondria-specific conjugates of several drugs (Asin-Cayuela, Manas, James, Smith, & Murphy, 2004; Burns & Murphy, 1997; Burns, Smith, & Murphy, 1995; Coulter, Smith, & Murphy, 2001; James et al., 2003; Kelso et al., 2001; Kelso et al., 2002; Lin et al., 2002; Ross, Filipovska, Smith, Gait, & Murphy, 2004; Smith, Porteous, Coulter, & Murphy, 1999; Smith, Porteous, Gane, & Murphy, 2003). Nuclear-localized proteins, such as histones, transcription factors, viral proteins, and others bearing nuclear localization signal (NLS) peptides, have the ability to be transported into the nucleus by a receptor-mediated process (Csermely, Schnaider, & Szanto, 1995; Ragin, Morgan, & Chmielewski, 2002). Another approach to the nuclear-targeted delivery of biologically active molecules is based on proteins and peptides, which have been found to traverse through the cellular membranes delivering their cargo molecules into the cytoplasm and/or nucleus (cell-penetrating peptides, CPP) (Elliott & O'Hare, 1997; Frankel & Pabo, 1988; Green & Loewenstein, 1988; Joliot, Pernelle, Deagostini-Bazin, & Prochiantz, 1991).

Since in many cases, various pharmaceutical nanocarriers are used to increase the stability of administered drugs, improve their efficacy, and

decrease undesired side effects, numerous attempts have been made to engineer the set of nanoparticulate drug carrier systems [(*ligand:nanocarrier:drug*) complexes] capable of specific delivery of various pharmaceuticals including pro-apoptotic anticancer drugs and DNA to intracellular targets, such as nuclei, lysosomes, and mitochondria. Among the most popular and well-investigated drug carriers one can name liposomes (mainly, for the delivery of water-soluble drugs) and micelles (for the delivery of poorly soluble drugs). Liposomes are artificial phospholipid vesicles with the size varying from 50 to 1000 nm and even more, which can be loaded with a variety of water-soluble drugs (into their inner aqueous compartment) and sometimes even with water-insoluble drugs (into the hydrophobic compartment of the phospholipid bilayer). Liposomes are considered as promising drug carriers for well over two decades (Lasic, 1993; Torchilin, 2005). They are biologically inert and completely biocompatible; they cause practically no toxic or antigenic reactions; and drugs included into liposomes are protected from the destructive action of the external media. Association of drugs with carriers, such as liposomes, has pronounced effects on the pharmacokinetic profile of the drug resulting in delayed drug absorption, restricted drug biodistribution, decreased volume of drug biodistribution, delayed drug clearance, and retarded drug metabolism (Allen, Newman, Woodle, Mayhew, & Uster, 1995). Plain liposomes are rapidly eliminated from the blood and captured by the cells of the reticuloendothelial system (RES), primarily, in liver and spleen, as the result of rapid opsonization. Most liposomes are internalized by phagocytic cells via endocytosis and destined to lysosomes for degradation (Senior, 1987). The use of targeted liposomes, i.e., liposomes selectively accumulating inside the affected organ or tissue, may increase the efficacy of the liposomal drug and decrease the loss of liposomes and their contents in RES. To obtain targeted liposomes, many protocols have been developed to bind corresponding targeting moieties including antibodies to the liposome surface without affecting the liposome integrity and antibody properties (Lasic, 1993; Torchilin, 1985). However, the approach with immunoliposomes may, nevertheless, be limited because of a short life-time of liposomes and immunoliposomes in the circulation (Senior, 1987). The majority of antibody-modified liposomes still accumulate in the liver, which hinders their significant accumulation in target tissues, particularly those with a diminished blood supply (ischemic or necrotic areas) and/or those with a low concentration of a target antigen. Dramatically better accumulation can be achieved if the circulation time of liposomes could be extended leading to the increased total quantity of immunoliposomes passing through the target and increasing their interactions with target antigens. This is why long-circulated (usually, coated with polyethylene glycol, PEG, i.e., PEGylated) liposomes have attracted so much attention over the last decade (Lasic & Martin, 1995). It was demonstrated (Torchilin, Narula, Halpern, & Khaw, 1996) that unique properties of long-circulating and targeted liposomes could be combined in one preparation, where antibodies or other specific binding molecules have been attached to the water-exposed tips of PEG chains (Torchilin et al., 2001).

Micelles, including polymeric micelles (Torchilin & Weissig, 2000), represent another promising type of pharmaceutical carrier. Micelles are

colloidal dispersions and have the particle size within 5 to 50–100 nm range. An important property of micelles is their ability to increase the solubility and bioavailability of poorly soluble pharmaceuticals. The use of certain special amphiphilic molecules as micelle-building blocks can also introduce the property of micelle-extended blood half-life upon intravenous administration. Because of their small size (5–50 nm), micelles demonstrate a spontaneous penetration into the interstitium in the body compartments with the leaky vasculature (tumors and infarcts) by the enhanced permeability and retention (EPR) effect, a form of selective delivery termed as "passive targeting" (Maeda, Wu, Sawa, Matsumura, & Hori, 2000). It has been repeatedly shown that micelle-incorporated anticancer drugs, such as adriamycin (see, for example, Kwon & Kataoka, 1995), better accumulate in tumors than in non-target tissues, thus minimizing the undesired drug toxicity toward normal tissue. Diffusion and accumulation parameters for drug carriers in tumors have recently been shown to be strongly dependent on the cutoff size of the tumor blood vessel wall; and the cutoff size varies for different tumors (Yuan et al., 1995). Specific ligands (such as antibodies and/or certain sugar moieties) can be attached to the water-exposed termini of hydrophilic blocks (Torchilin et al., 2001). In case of targeted micelles, a local release of a free drug from micelles in the target organ should lead to the increased efficacy of the drug, while the stability of the micelles en route to the target organ or tissue should contribute better drug solubility and toxicity reduction due to less interaction with non-target organs.

Both liposomes and micelles could be modified in specific ways allowing for their intracellular delivery. One of the options for the intracellular delivery of drugs loaded into liposomes and micelles (as well as of macromolecular drugs) is the exploitations of intracellular pH gradients (Asokan & Cho, 2002). The fact that all intracellular organelles (cytoplasm, endosomes, lysosomes, endoplasmic reticulum, mitochondria, and nuclei) maintain their own characteristic pH value, which varies between 4.5 and 8 among different organelles, allows for the attachment of pH-sensitive units to macromolecular drugs and drug carriers in such a way that they can provide desired drug/drug carrier partition between individual organelles or cause a variety of membrane phenomena resulting in drug release within the required compartment.

pH-Sensitive Pharmaceutical Nanocarriers for Cytosolic Delivery

Quite a few approaches for cytosolic drug delivery with such pharmaceutical nanocarriers as liposomes and micelles have been developed. Historically, pH-sensitive liposomes were suggested earlier.

pH-Sensitive Liposomes

Among different methods of liposomal content delivery into the cytoplasm (Torchilin, 1991) it was proposed that the liposome is made of pH-sensitive components and, after being endocytosed in the intact form, it fuses with

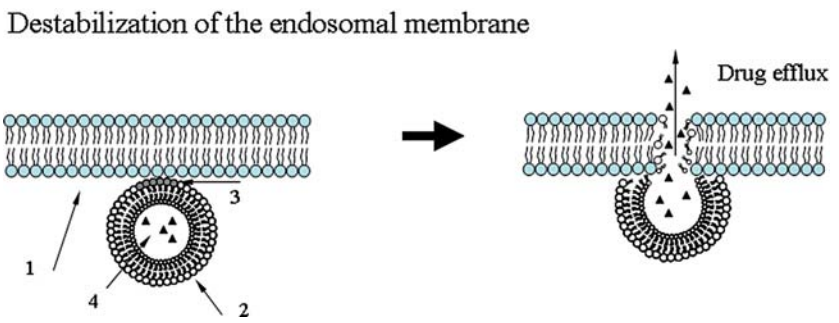

Figure 11.2 Schematics of endosomal drug escape with the use of pH-sensitive liposomes. (1) endosomal membrane; (2) endocytosed liposome; (3) pH-sensitive liposomal component interacting with the endosomal membrane and destabilizing it; (4) liposomal drug.

the endovacuolar membrane under the action of lowered pH inside the endosome (below 6) and destabilizes the latter, releasing its content directly into the cytoplasm (Torchilin, Zhou, & Huang, 1993); see the scheme on Figure 11.2. Thus, namely endosomes become the gates from the outside into the cell cytoplasm (Sheff, 2004). Since this approach was reviewed many times in various publications (in 2004, the endosomal escape by pH-sensitive drug delivery systems was discussed in a special issue of Advanced Drug Delivery Reviews #56, J.C. Leroux, ed.), here we will briefly consider only some recent examples of this approach. Cellular drug delivery mediated by pH-sensitive liposomes is not a simple intracellular leakage from the lipid vesicle since the drug has to cross also the endosomal membrane (Asokan & Cho, 2003). It is usually assumed that inside the endosome, the low pH and some other factors destabilize the liposomal membrane, which, in turn, interacts with the endosomal membrane provoking its secondary destabilization and drug release into the cytoplasm. The presence of fusogenic lipids in the liposome composition, such as unsaturated DOPE, with their ability to easily adopt inverted hexagonal phase, is usually required to make liposomes pH sensitive (Shalaev & Steponkus, 1999). Importantly (since many current liposomal-dosage forms are based on the use of long-circulating, PEGylated liposomes), long-circulating PEGylated DOPE-containing liposomes although demonstrate a decreased pH sensitivity compared to non-PEGylated liposomes, still effectively deliver their contents into cytoplasm (review in Gaspar, Perez-Soler, & Cruz, 1996). Antisense oligonucleotides are delivered into cells by anionic pH-sensitive PE-containing liposomes stable in the blood, however, undergoing phase transition at acidic endosomal pH and facilitating oligo release into cell cytoplasm (review in Stanimirovic, Markovic, Micic, Spatz, & Mrsulja, 1994). The study on the mechanism of endosomal delivery of genes by pH-sensitive liposomes revealed that lipids with histidine-containing head group show the involvement of imidazole ring protonation in the endosomal DNA escape (Lo, Tsai, & Kuo, 2004). New pH-sensitive liposomal additives were recently described including oleyl alcohol (Heeremans et al., 1995) and pH-sensitive morpholine lipids (mono-stearoyl derivatives of morpholine) (Rubas et al., 1986). The combination of liposome pH sensitivity and specific ligand targeting for

cytosolic drug delivery utilizing decreased endosomal pH values was described for both folate and Tf-targeted liposomes (Kisel et al., 2001). Additional modification of pH-sensitive liposomes with an antibody results in pH-sensitive immunoliposomes. The advantages of antibody-bearing pH-sensitive liposome include cytoplasmic delivery, targetability, and facilitated uptake (i.e., improved intracellular availability) via the receptor-mediated endocytosis. Successful application of pH-sensitive immunoliposomes has been demonstrated in delivery of a variety of molecules including fluorescent dyes, antitumor drugs, proteins, and DNA (Geisert, Del Mar, Owens, & Holmberg, 1995).

In addition to membrane-destabilizing lipid components, there exists a large number of membrane-destabilizing anionic polymers that also can enhance the endosomal escape of various drugs and biomacromolecules (Yessine & Leroux, 2004). This family includes various carboxylated polymers, copolymers of acrylic and methacrylic acids, copolymers of maleic acid, polymers and copolymers of *N*-isopropylacrylamide (NIPAM). Copolymers of NIPAM demonstrate lower critical solution (solubility/insolubility switch) at physiological temperatures and when precipitated, they destabilize biomembranes they are interacting with (Chen & Hoffman, 1995). Such polymers can be attached to the surface of drug/DNA-loaded liposomes or polymeric micelles allowing for endosomal destabilization and cytoplasmic escape. Thus, serum stable, long-circulating PEGylated pH-sensitive liposomes were prepared using, on the same liposome, the combination of PEG and pH-sensitive terminally alkylated copolymer of *N*-isopropylacrylamide and methacrylic acid (Fonseca, Jagtenberg, Haisma, & Storm, 2003).

pH-Sensitive Micelles

Since micelle-based preparations of various poorly water-soluble drugs are considered as promising dosage forms for such drugs, and many of those drugs (for example, paclitaxel) target intracellular organelles, various micelles (polymeric micelles) have been prepared that can also demonstrate pH sensitivity and ability to escape from endosomes. Thus, micelles prepared from PEG-poly(aspartate hydrazone adriamycin) easily release an active drug at lowered pH values typical for endosomes and facilitate its cytoplasmic delivery and toxicity against cancer cells (Bae et al., 2005). Alternatively, micelles for intracellular delivery of antisense oligonucleotides (ODN) were prepared from ODN-PEG conjugates complexed with a cationic fusogenic peptide, KALA, and provided much higher intracellular delivery of the ODN that could be achieved with free ODN (Jeong, Kim, & Park, 2003).

It is also possible to enhance an intracellular delivery of drug-loaded micelles by adding to their composition lipid components used in membrane-destabilizing Lipofectin®. Thus, PEG-lipid micelles, for example, carry a net negative charge (Lukyanov, Hartner, & Torchilin, 2004), which might hinder their internalization by cells. On the other hand, it is known that the net positive charge usually enhances the uptake of various nanoparticles by cells, and after the endocytosis the drug/DNA-loaded particles could escape from the endosomes and enter a cell's cytoplasm through

disruptive interaction of the cationic lipid with endosomal membranes (Hafez, Maurer, & Cullis, 2001). The compensation of the micelle negative charge by the addition of positively charged lipids to PEG-PE micelles could improve the uptake by cancer cells of drug-loaded mixed PEG-PE/positively charged lipid micelles. It is also possible that after the enhanced endocytosis, such micelles could escape from the endosomes and enter the cytoplasm of cancer cells. With this in mind, an attempt was made to increase an intracellular delivery and, thus, the anticancer activity of the micellar paclitaxel by preparing paclitaxel-containing micelles from the mixture of PEG-PE and Lipofectin® lipids (LL) (Wang, Mongayt, & Torchilin, 2005). When studying the cellular uptake of various fluorescently labeled micelles in adherent BT-20 cells, it was found that while both "plain" PEG-PE micelles and PEG-PE/LL micelles were endocytosed by BT-20 cells as confirmed by the presence of fluorescent endosomes in cells after 2 hours of co-incubation with fluorescently labeled micelles, however, in the case of PEG-PE/LL micelles, endosomes became partially disrupted and their content was released into the cell cytosol. The addition of LL facilitating the intracellular uptake and cytoplasmic release of paclitaxel-containing PEG-PE/LL micelles resulted in a substantially increased level of cell death compared to that under the action of free paclitaxel or paclitaxel delivered using non-cationic LL-free PEG-PE micelles. In BT-20 cancer cells, the IC_{50} values of free paclitaxel, paclitaxel in PEG-PE micelles, and paclitaxel in PEG-PE/LL micelles were 24.3, 9.5, and 6.4 μM, respectively. In A2780 cancer cells, the IC_{50} values for the same preparations were 22.5, 5.8, and 1.2 μM, respectively.

pH-Sensitive PEG Conjugates

The function of pH sensitivity can also be introduced into PEG-lipid conjugates used to make long-circulating pharmaceutical nanocarriers and build pharmaceutical micelles. In this case, the pH sensitivity is expected to allow for the detachment of protecting polymer (PEG) chains under the action of certain local stimuli characteristics, such as decreased pH value. The matter is that the stability of PEGylated nanocarriers may not always be favorable for drug delivery inside cells or for the endosomal escape. Thus, if the carrier has to be taken up by a cell via an endocytic pathway, the presence of the PEG coat on its surface may preclude the contents from escaping the endosome and being delivered in the cytoplasm. In order to solve these problems, for example, in the case of long-circulating liposomes, the chemistry was developed to detach PEG from the lipid anchor in the desired conditions. Labile linkage that would degrade only in the acidic conditions characteristic of the endocytic vacuole or the acidotic tumor mass can be based on the diorto esters (Guo & Szoka, 2001), vinyl esters (Boomer & Thompson, 1999), cysteine-cleavable lipopolymers (Zalipsky et al., 1999), double esters, and hydrazones that are quite stable at pH around 7.5 but hydrolyzed relatively fast at pH values of 6 and below (Guo & Szoka, 2001; Kratz, Beyer, & Schutte, 1999; Zhang, Zalipsky, Mullah, Pechar, & Allen, 2004). Polymeric components with pH-sensitive (pH-cleavable) bonds are used to produce stimuli-responsive drug delivery systems that are stable in the

circulation or in normal tissues, however, they acquire the ability to degrade and release the entrapped drugs in body areas or cell compartments with lowered pH, such as tumors, infarcts, inflammation zones, or cell cytoplasm or endosomes (Roux, Francis, Winnik, & Leroux, 2002; Roux, Passirani, Scheffold, Benoit, & Leroux, 2004; Simoes, Moreira, Fonseca, Duzgunes, & de Lima, 2004). A variety of liposomes (Leroux, Roux, Le Garrec, Hong, & Drummond, 2001; Roux et al., 2002) and polymeric micelles (Lee, Na, & Bae, 2003; Lee, Shin, Na, & Bae, 2003; Sudimack, Guo, Tjarks, & Lee, 2002) have been described that include the components with acid-labile bonds.

The stimuli sensitivity of PEG coats can also allow for the preparation of multifunctional drug delivery systems with temporarily "hidden" functions, which under normal circumstances are "shielded" by the protective PEG coat, however, they become exposed after PEG detaches. Nanoparticular drug delivery systems can be prepared that are capable of accumulating in the required organ or tissue, and then penetrate inside target cells delivering its load there (drug or DNA). The initial target accumulation could be achieved by the passive targeting via the EPR effect or by the specific ligand(antibody)-mediated active targeting, whereas the subsequent intracellular delivery could be mediated by certain internalizable ligands (folate, transferrin) or by cell-penetrating peptides (CPPs, such as TAT or polyArg). When in the blood, the cell-penetrating function should be temporarily inactivated (sterically shielded) to prevent a non-specific drug delivery into non-target cells, however, when inside the target, the nanocarrier loses its protective coat, exposes the cell-penetrating function, and provides intracellular drug delivery (Sawant et al., 2006). The systems as the one described above require that multiple functions attached to the surface of the nanocarrier should function in a certain orchestrated and coordinated way. For the above system, the following requirement have to be met: (a) the life of the carrier in the circulation should be long enough to fit EPR effect or targeted delivery requirements (i.e., PEG coat mediating the longevity function or specific ligand mediating the targeting function should not be lost by the nanocarrier when in the circulation) and (b) the internalization of the carrier within the target cells should proceed fast not to allow for the carrier degradation and drug loss in the interstitial space (i.e., local stimuli-dependent removal of the protective function and the exposure of the temporarily hidden second function should proceed fast).

Cytoskeletal Antigen-Specific Immunoliposomes for Intra-cytoplasmic Delivery

It is known that sarcolemmal lesions typical of hypoxic myocyte damage and associated with the exposure of intracellular cytoskeletal proteins, such as myosin, could be specifically identified with the use of the antimyosin antibody (Khaw, Fallon, Beller, & Haber, 1979). Moreover, cytoskeletal antigen (myosin)-specific immunoliposomes (CSIL) were shown to seal membrane lesions in hypoxic cardiocytes by anchoring CSIL to the exposed cytoskeletal antigen via the antimyosin antibody, which results in the prevention of the leakage of the intracellular contents, membrane

repair, and restoration of cell viability (Khaw, Torchilin, Vural, & Narula, 1995; Khaw, Vural, DaSilva, & Torchilin, 2000) as was clearly demonstrated with H9C2 rat embryonic cardiocytes, subjected to temporary artificial hypoxia and incubated with liposomal preparations. Using silver grain-loaded CSIL and electron microscopy, it was also shown that a significant part of cell-attached CSIL fuse with cell membranes delivering their load directly into the cell cytoplasm (Khaw et al., 1995). It was concluded from this data that artificially imposed hypoxia could be applied to facilitate intracellular delivery of various drugs including DNA constructs by CSIL. If the target cells for drug and/or gene delivery are subjected to artificially imposed hypoxic stress, stress-induced small membrane lesions will allow for the specific attachment to these lesions of loaded liposomes rendered specific for an intracellular antigen. As a result, such liposomes may simultaneously seal hypoxia-induced cell membrane lesions and provide intracellular drug (gene) release; see the schematics in Figure 11.3. For in vitro-targeted gene transfection, transient, reversible hypoxic injury may be induced in the target cells or tissue grafts, and DNA-bearing CSIL deliver the constructs directly into the cytoplasm with the restoration of the membrane integrity and cell viability (the method was termed as CSIL-fection) (Torchilin, Khaw, & Weissig, 2002).

The approach was verified in tissue cultures utilizing H9C2 rat embryonic cardiocytes as target cells and CSIL containing various reporter genes as carriers for targeted gene transfection. To prepare DNA-loaded immunoliposomes, corresponding plasmids together with hydrophobically modified antibody for liposome membrane incorporation were added to mild detergent (octylglucoside)-solubilized liposomal lipids prior to the detergent removal by dialysis (Khaw, daSilva, Vural, Narula, & Torchilin,

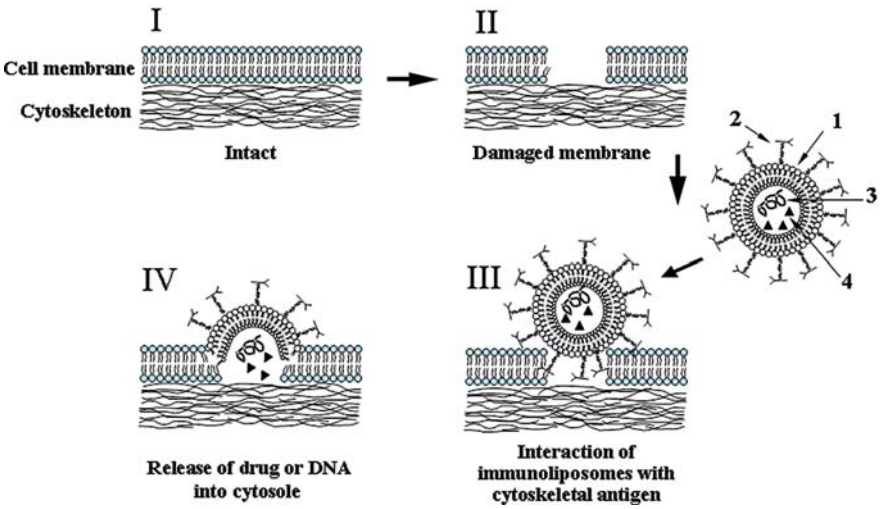

Figure 11.3 Schematics of intracellular drug or DNA delivery with the use of cytoskeleton-specific immunoliposomes. When normal cell membrane (I) becomes compromised and "perforated" under the action of ischemia (II), drug/DNA-loaded immunoliposome attaches to the appearing "holes" via exposed cytoskeletal antigens (III), and, when fusing with the cell membrane, releases its contents into the cell cytoplasm. (1) Liposome; (2) cytoskeleton-specific antibody; (3) drug; (4) DNA.

2001). The prepared assemblies were incubated with cardiocytes subjected to limited hypoxia for 24 hours. Using different plasmids, pEScFv – a eukaryotic expression vector containing the antimyosin single-chain Fv (ScFv) fragment linked with domain B of protein A of *Staphylococcus aureus*, pGL2 encoding for luciferase, and pSV-β-galactosidase vector, it was clearly demonstrated that the efficacy of the CSIL-fection process was 5-to-40 times higher than with control preparations (plasmid-loaded plain liposomes, cationic liposomes, and non-specific immunoliposomes) (Khaw et al., 2001; Torchilin et al., 2002). The CSIL-fection experiments with the three reporter genes, described above, clearly indicated that the method of direct intra-cytoplasmic delivery of drugs and DNA utilizing CSIL and transitional and reversible artificial hypoxia is highly effective and quite comparable with existing non-viral methods, such as transfection with the use of cationic lipids. By using a specific combination of other intracellular cytoskeletal antigens and the corresponding antibodies, this method of drug delivery/transfection should also be applicable to other cell types. Enhanced efficiency of transfection by this novel method could have practical therapeutic applications in ex vivo genetic modification of cells that could then be reimplanted into patients for gene therapy. Furthermore, in myocardial ischemia, toxic or inflammatory insult to the myocardium results in the loss of sarcolemmal integrity leading to the exposure of intracellular myosin to the extracellular milieu (Khaw et al., 1982). Earlier, targeting of the infarcted myocardium has been achieved with radiolabeled antimyosin immunoliposomes in rabbits and dogs (Torchilin et al., 1996, 1994). Therefore, one may hypothesize that if CSIL were loaded with an angiogenic vector, such as gene for VEGF, and were delivered to the compromised cardiocytes during the very acute phase of cell membrane lesion evolution, concurrent with thrombolytic therapy, CSIL might be able to seal the lesions and simultaneously induce neoangiogenesis for the enhanced blood supply to hypoxic areas.

Intracellular Delivery of Nanocarriers by Cell-Penetrating Peptides

A promising approach that seems to be the solution of overcoming the cellular barrier for intracellular drug delivery has emerged over the last decade. In this approach, certain proteins or peptides can be tethered to the hydrophilic drug of interest and together the construct possesses the ability to translocate across the plasma membrane and deliver the payload intracellularly. This process of translocation is called "protein transduction". Such proteins or peptides contain domains of less than 20 amino acids, termed as protein transduction domains (PTDs) or cell-penetrating peptides (CPPs) that are highly rich in basic residues. These peptides have been used for intracellular delivery of various cargoes with molecular weights several times greater than their own (Schwarze & Dowdy, 2000).

The property of translocation across the cell membrane was introduced in 1988 when two independent authors Green (Green & Loewenstein, 1988) and Frankel (Frankel & Pabo, 1988) demonstrated that the 86-mer trans-activating transcriptional activator, TAT, protein encoded by HIV-1

was efficiently internalized by cells in vitro when introduced in the surrounding media, and subsequently resulted in trans-activation of the viral promoter. Such trans-activation was observed at nano-molar concentrations in the presence of lysosomotrophic agents and TAT was eventually localized within the nucleus. Subsequently, a number of peptides, either derived from proteins or synthesized chemically, demonstrated the property of translocation. These peptides include Antennapedia (Antp) (Joliot et al., 1991), VP22 (Elliott & O'Hare, 1997), transportan (Pooga, Hallbrink, Zorko, & Langel, 1998), model amphipathic peptide MAP (Oehlke et al., 1998), signal sequence-based peptides (Rojas, Donahue, Tan, & Lin, 1998), and synthetic polyarginines (Futaki et al., 2001), such as R_9-TAT, HIV-1 Rev (34–50), flock house virus coat (35–49) peptide, and DNA-binding peptides as c-Fos (139–164), c-Jun (252–279), and yeast GCN4 (231–252).

CPPs can be divided into three classes: protein-derived peptides, model peptides, and designed peptides (Lindgren, Hallbrink, Prochiantz, & Langel, 2000; Zorko & Langel, 2005). Protein-derived peptides are the short stretches of the protein domain that are primarily responsible for the translocation ability, also called PTDs, examples are TAT peptide (48–60) derived from 86-mer TAT protein (Vives, Brodin, & Lebleu, 1997), penetratin (43–58) derived from homeodomain of *Drosophila* Antennapedia (Derossi, Joliot, Chassaing, & Prochiantz, 1994), pVEC derived from murine vascular endothelial cadherin (Elmquist, Lindgren, Bartfai, & Langel, 2001), and signal sequence-based peptides or membrane translocating sequences (MTSs) (Rojas et al., 1998). Model peptides are CPPs that mimic the translocation properties of known CPPs; example is the model amphipathic peptide (MAP) (Oehlke et al., 1998). Designed CPPs encompass the chimeric peptides that are produced by the fusion of hydrophilic and hydrophobic domains from different sources; examples are transportan, fusion of galanin and mastoparan (Pooga et al., 1998); and MPG, chimera of peptide from fusion sequence of HIV-1 gp41 protein and peptide from the nuclear localization sequence of SV40 T-antigen (Morris, Vidal, Chaloin, Heitz, & Divita, 1997). In addition, synthetic peptides such as polyarginines also show potential for translocation (Futaki et al., 2001). All the CPPs are highly positively charged, contributed by basic residues lysine or arginine; lysine is the primary contributor in transportan and model amphipathic peptide (MAP), while arginine contributes in TAT peptide, penetratin, and pVEC.

TAT peptide, the most frequently used CPP, is derived from the transcriptional activator protein encoded by human immunodeficiency virus type 1 (HIV-1) (Jeang, Xiao, & Rich, 1999). TAT protein plays an important role in the viral replication, primarily by regulating the transcription from the HIV-1 long terminal repeat. TAT protein-mediated transduction was first utilized in 1994 for the intracellular delivery of variety of cargoes such as β-galactosidase, horseradish peroxidase, RNase A, and domain III of *Pseudomonas* exotoxin A in vitro (Fawell et al., 1994). In vivo transduction using TAT peptide (37–72) conjugated to β-galactosidase resulted in protein delivery to different tissues such as heart, liver, spleen, lung, and skeletal muscle. Next, attempts were made to narrow down to the specific domain responsible for transduction. For this, synthetic peptides with

deletions in the α-helix domain and the basic cluster domain were prepared for investigating their translocation ability (Vives et al., 1997). The positive charge in the transduction domain is responsible for the transduction ability of TAT protein and the commonly used transduction domain of TAT (TAT peptide) extends from residues 47 to 57: Tyr-Gly-Arg-Lys-Lys-Arg-Arg-Gln-Arg-Arg-Arg, which contains six arginines (Arg) and two lysine residues (Schwarze, Hruska, & Dowdy, 2000). In terms of the cellular uptake and cargo delivery kinetics, MAP has the fastest uptake, followed by transportan, TATp (48–60), and penetratin. Similarly, MAP has the highest cargo delivery efficiency, followed by transportan, TATp (48–60), and penetratin.

Different studies have suggested diversity of mechanisms for the translocation of CPPs across the cellular membrane. Earlier studies suggested that the internalization of TAT peptide (48–60), penetratin (43–58), and transportan was independent of receptor and temperature (Derossi et al., 1996; Pooga et al., 1998; Vives et al., 1997), excluding the involvement of endocytosis. Recent studies, however, suggest the lipid raft-mediated uptake (Ferrari et al., 2003; Fittipaldi et al., 2003) and macropinocytosis as the key mechanisms of the uptake of CPP conjugated to large cargoes (Wadia, Stan, & Dowdy, 2004). A different mechanism has been presented for the transport of guanidinium-rich CPPs alone or conjugated to small molecules (MW $<$3000 Da) (Rothbard, Jessop, Lewis, Murray, & Wender, 2004; Rothbard, Jessop, & Wender, 2005). The guanidinium groups of the CPPs form bidentate hydrogen bonds with the negative residues on the cell surface; the resulting ion pairs then translocate across the cell membrane under the influence of the membrane potential. The ion pair dissociates on the inner side of the membrane, releasing the CPPs into the cytosol. However, the number of guanidinium groups is critical for translocation, around eight groups being the optimum number for efficient translocation. Thus, more than one mechanism works for CPP-mediated intracellular delivery of small and large molecules. Individual CPPs or CPP conjugated to small molecules are internalized into cells via electrostatic interactions and hydrogen bonding, while CPP conjugated to large molecules occur via the energy-dependent macropinocytosis. However, in both cases, the direct contact between the CPPs and negative residues on cell surface is a prerequisite for the successful transduction.

Over the last decade, CPPs have been widely exploited for the intracellular delivery of different size cargoes in a range of cell types both in vitro and in vivo. The cargoes delivered range from peptides, proteins, genetic material, antibodies, imaging agents, and toxins to nanoparticles and liposomes. A complete review of the different "large" cargoes delivered by CPPs can be found in Gupta, Levchenko, & Torchilin (2005). The concept of CPP-mediated nanoparticulate delivery was first realized in 1999 by Josephson, Tung, Moore, & Weissleder, where they showed that the dextran-coated superparamagnetic iron oxide particles (CLIO), when coupled to TAT peptide, provide efficient labeling of the cells, and thereby serve as a tool for magnetic resonance imaging (MRI) or magnetic separation of homed cells in vivo. The average size of the particles was 41 nm and the conjugate carried an average of 6.7 TAT moieties per particle. The cellular uptake studies of TAT-CLIO were performed on

mouse lymphocytes, human natural killer cells, and HeLa cells. In all the three cell lines tested, the uptake of TAT-CLIO nanoparticles was higher than the nonmodified iron oxide particle. The internalization of TAT-CLIO was about 100-fold higher than for the nonmodified iron oxide particles, within mouse lymphocytes. The intracellular distribution of TAT-CLIO was then followed by fluorescence microscopy in all the three cell lines. The fluorescence microscopy studies on the live cells revealed that the conjugate was first accumulated in lysosomes as evidenced by the punctuate staining, followed by intense localization within the nuclei. The experiments clearly suggested that TAT-modified-CLIO particles are better tools for intracellular labeling of the cells than TAT-free particles. The authors next explored the MRI potential of TAT-CLIO on mouse lymphocytes under in vitro conditions. When the cells were incubated with TAT-CLIO and nonmodified iron oxide particles, the cells incubated with TAT-CLIO were readily detected by MRI as compared to the cells incubated with nonmodified iron oxide particles. Furthermore, TAT-CLIO-labeled cells were retained on magnetic separation columns unlike iron oxide-labeled cells, suggesting that TAT-CLIO labeling also allows for magnetic separation of homed cells in vivo.

In an extension of this study, the same group studied TAT-CLIO nanoparticles for tracking progenitor cells under in vivo conditions (Lewin et al., 2000). The magnetic labeling of stem and progenitor cells allows for following their migration and imaging them by MRI in physiological settings, enhancing the knowledge for the application of stem cells in therapeutics. The authors showed that TAT-CLIO could label different types of cells such as human hematopoietic CD34+ cells, mouse neural progenitor cells C17.2, human CD4+ lymphocytes, and mouse splenocytes. The labeling with TAT-CLIO did not induce toxicity and did not alter the differentiation or proliferation pattern of CD34+ cells. Another illustration of MRI with the TAT-CLIO-labeled cells was presented in Dodd et al. (2001), where T cells were magnetically labeled without affecting their normal responses to stimulation. Upon intravenous injection, the homing of T cells to the spleen could be detected by MRI and their biodistribution profile could be followed with time by MRI in vivo. Other similar studies observed the uptake of TAT peptide-labeled iron oxide particles by T cells, B cells, and macrophages over 72 hours and found that the uptake was quick with no loss in the cell viability (Kaufman et al., 2003). However, the TAT peptide-iron oxide conjugates were accumulated primarily in the cytoplasm in contrast to nuclear localization as observed by other authors. In vivo studies on mice showed that the attachment of TAT to iron oxide nanoparticles reduced the half-life of the conjugate in the blood (Wunderbaldinger, Josephson, & Weissleder, 2002). Both the TAT-modified and nonmodified iron oxide nanoparticles were removed from the circulation by the reticuloendothelial system (RES). However, they differ in their distribution profile within the RES. The nonmodified iron oxide nanoparticles accumulated along the hepatic vessels in the endothelial and/or Kupffer cells, while TAT peptide-modified iron oxide nanoparticles were distributed intensely throughout the parenchyma. Subcellular analysis revealed the nuclear accumulation of TAT-iron oxide nanoparticles. The study suggested the possibility of exploiting

CPP-modified contrast agents for the intracellular imaging in vivo. Also, by modifying the surface of nanoparticles with CPPs, the cell permeability of nanoparticulate-based therapeutics can be enhanced (Koch, Reynolds, Merkle, Weissleder, & Josephson, 2005). When the surface of CLIO was modified with D-polyarginyl peptide or TAT peptide, the nanoparticles could traverse through the cell monolayers. Thus the permeability of the drugs in nanoparticulate carriers can be augmented by their surface modification with CPPs.

CPPs have also been used to enhance the delivery of genes via solid lipid nanoparticle (SLN) (Rudolph et al., 2004). SLN gene vector was modified with dimeric TAT peptide (TAT2) and compared with polyethylenimine (PEI) for gene expression in vitro and in vivo. Presence of TAT2 in SLN gene vector enhanced the gene transfection compared to PEI both in vitro and in vivo. In another study, TAT peptide (47–57) conjugated to nanocage structures showed binding and transduction of the cells in vitro (Liu, Zhang, Remsen, & Wooley, 2001). The shell cross-linked (SCK) nanoparticles were prepared by the micellization of amphiphilic block copolymers of poly(epsilon-caprolactone-b-acrylic acid) and conjugated to TAT peptide that was independently built on a solid support, resulting in TAT-modified nanocage conjugate. Such conjugate was analyzed by confocal microscopy with CHO and HeLa cells. The conjugated nanoparticles showed binding and transduction inside the cells. The authors then characterized the SCK nanoparticles for the optimum number of TAT peptide per particle required to enhance the transduction efficiency (Becker, Remsen, Pan, & Wooley, 2004). The authors prepared the conjugates with 52, 104, and 210 CPP peptides per particle, which were then evaluated for the biocompatibility in vitro and in vivo (Becker, Bailey, & Wooley, 2004). In vitro studies showed the inflammatory responses to the conjugates, but in vivo evaluation of the conjugates in mice did not result in major incompatible responses. Thus, TAT peptide-SCK conjugate can be used as scaffolds for preparing antigen for immunization.

A new area of interest with CPP-mediated delivery is the labeling of cells with quantum dots using CPP-modified quantum dot-loaded polymeric micelles (Stroh et al., 2005). Quantum dots are gaining popularity over standard fluorophores for studying tumor pathophysiology since they are photostable, very bright fluorophores, can be tuned to a narrow emission spectrum, and are relatively insensitive to the wavelength of the excitation light. Besides, quantum dots have the ability to distinguish tumor vessels from both the perivascular cells and the matrix, with concurrent imaging. Quantum dots were trapped within micelles prepared of polyethylene glycol-phosphatidyl ethanolamine (PEG-PE) conjugates bearing TAT-PEG-PE linker. TAT-quantum dot conjugate could label mice endothelial cells in vitro. For in vivo tracking, bone marrow-derived progenitor cells were labeled with TAT-bearing quantum dot-containing micelle *ex vivo*, and then injected in the mice bearing a tumor in a cranial window model. It was then possible to track the movement of labeled progenitor cell to tumor endothelium, introducing an attempt toward understanding fine details of tumor neovascularization.

Intracellular distribution studies conducted on TAT peptide-modified gold nanoparticles suggested that the conjugates were internalized by

endocytosis and did not localize into the nuclei of NIH 3T3 or HepG2 cells (Tkachenko et al., 2004). In contrast, the studies of de la Fuente & Berry (2005) showed that TAT peptide-modified gold nanoparticles traversed through the cell membrane of a human fibroblast cell and accumulated within the nuclei. The modified nanoparticles were biocompatible as no changes in the cell metabolism and proliferation were observed, and normal cell viability was retained.

CPPs have also augmented the intracellular delivery of liposomal drug carriers. TAT peptide (47–57)-modified liposomes could be delivered intracellularly in different cells, such as murine Lewis lung carcinoma (LLC) cells, human breast tumor BT20 cells, and rat cardiac myocyte H9C2 cells (Torchilin, Rammohan, Weissig, & Levchenko, 2001). The liposomes were tagged with TAT peptide via the spacer, *p*-nitrophenylcarbonyl-PEG-PE, at the density of a few hundreds of TAT peptide per single liposome vesicle. It was shown that the cells treated with liposomes, in which TAT peptide–cell interaction was hindered either by direct attachment of TAT peptide to the liposomes surface or by the long PEG grafts on the liposome surface shielding the TAT moiety did not show TAT-liposome internalization; however, the preparations of TAT-liposomes, which allowed for the direct contact of TAT peptide residues with cells, displayed an enhanced uptake by the cells. This suggested that the translocation of TAT peptide (TATp)-liposomes into cells require direct free interaction of TAT peptide with the cell surface. Further studies on the intracellular trafficking of rhodamine-labeled TATp-liposomes loaded with FITC-dextran revealed that TATp-liposomes remained intact inside the cell cytoplasm within 1 h of translocation, after 2 h they migrated into the perinuclear zone, and at 9 h the liposomes disintegrated there (Torchilin et al., 2003). The TATp-liposomes were also investigated for their gene delivering ability. For this, TATp-liposomes prepared with the addition of a small quantity of a cationic lipid (DOTAP) were incubated with DNA. The liposomes formed firm noncovalent complexes with DNA. Such TATp-liposome-DNA complexes when incubated with mice fibroblast NIH 3T3 and cardiac myocytes H9C2 showed substantially higher transfection in vitro, with lower cytotoxicity than the commonly used Lipofectin®. Under in vivo conditions, the intratumoral injection of TATp-liposome-DNA complexes into the Lewis lung carcinoma tumor in mice resulted in an efficient transfection of the tumor cells. The study thus implicated the usefulness of TATp-liposomes for in vitro and localized in vivo gene therapy.

Another study examined the kinetics of uptake of the TAT- and penetratin-modified liposomes (Tseng, Liu, & Hong, 2002). It was found that the translocation of liposomes by TAT peptide or penetratin was proportional to the number of peptide molecules attached to the liposomal surface. A peptide number of as few as five was already sufficient to enhance the intracellular delivery of liposomes. The kinetics of the uptake was peptide- and cell-type dependent. With TATp-liposomes, the intracellular accumulation was time dependent, and with penetratin-liposomes, the accumulation within the cells was quick reaching the peak within 1 h, after which it gradually declined. Study on the similar lines showed that Antp (43–58) and TAT (47–57) peptides coupled to small unilamellar liposomes were accumulated in higher proportions within tumor cells

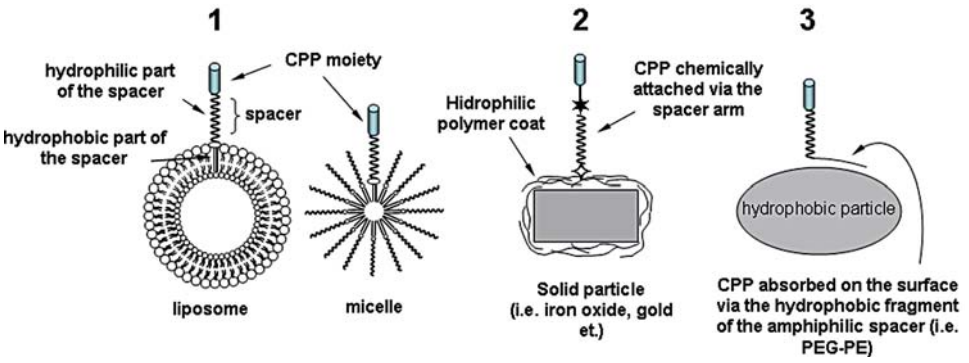

Figure 11.4 Different ways to attach CCPs to nanoparticulates. (1) CPP can be attached to nanoparticulates, such as liposomes or micelles, by the insertion into the hydrophobic phase of the carrier (liposome membrane or micelle inner core) via the spacer arm (linker) with hydrophobic terminus; (2) CPP can be chemically bound to the surface of the appropriately modified nanoparticle. (3) Hydrophobically modified CPP can be adsorbed onto the nanoparticle surface.

Table 11.1 Some examples of nanoparticles delivered inside cells by CPPs.

Particle and size	CPP	Cell	Purpose	Reference
Paramagnetic CLIO (MION) particles, 40 nm	TAT peptide	Mouse lymphocytes, human natural killer, HeLa, human hematopoietic CD34+, mouse neural progenitor C17.2, human lymphocytes CD4+, T cells, B cells, macrophages	Intracellular labeling, MRI, magnetic cell separation	Dodd et al., 2001; Josephson et al., 1999; Kaufman et al., 2003; Lewin et al., 2000
Sterically stabilized liposomes, 65–75 nm	Penetratin and TAT peptide coupled to the linker	Human bladder carcinoma HTB-9, murine colon carcinoma C26, human epidermoid carcinoma A431, human breast cancer SK-BR-3, MCF7/WT, MCF7/ADR, murine bladder cancer MBT2, dendritic cells	Studies on the internalization kinetics of CPP-liposomes	Marty et al., 2004; Tseng et al., 2002
Quantum dot-loaded polymeric micelles, 20 nm	TAT peptide coupled to the linker	Mouse endothelial cells, bone marrow-derived progenitor cells	Studies on tumor pathophysiology	Stroh et al., 2005
Sterically stabilized liposomes, 200 nm	TAT peptide coupled to the linker	Mouse LLC, human BT20, rat H9C2, LLC tumor in mice	Intracellular delivery of drugs and genes in vitro and in vivo.	Torchilin et al., 2003, 2001; Tseng et al., 2002
Gold particles, 20 nm	TAT peptide	NIH3T3, HepG2, HeLa, human fibroblasts	Intracellular localization studies	de la Fuente & Berry, 2005; Tkachenko et al., 2004

and dendritic cells than unmodified control liposomes (Marty, Meylan, Schott, Ballmer-Hofer, & Schwendener, 2004). The uptake was time and concentration dependent and at least 100 PTD molecules per small unilamellar liposomes were required for efficient translocation inside cells. The uptake of the modified liposomes was inhibited by the preincubation of liposomes with heparin, confirming the role of heparan sulfate proteoglycans in CPP-mediated uptake. Antp-liposomes were considered as a carrier system for an enhanced cell-specific delivery of liposome-entrapped molecules (Marty et al., 2004). Thus, the transduction function could carry a great potential to deliver a wide range of large molecules and small particles both in vitro and in vivo. Possible ways to attach CPPs to the surface of nanocarriers is shown in the Figure 11.4. The data on nanoparticle delivery into cells by CPPs are also summarized in Table 11.1.

Lipoplexes/Polyplexes for Cytosolic Delivery of DNA

The use of cationic lipids and cationic polymers as transfection vectors for efficient intracellular delivery of DNA was suggested in Felgner et al. (1987) and Wu & Wu (1987). Currently, this is a well-developed approach discussed in numerous reviews and monographs (see one of the recent reviews in Elouahabi & Ruysschaert, 2005). Nanosized complexes between cationic lipids (such as Lipofectin®, an equimolar mixture of *N*-[1-(2,3-dioleyloxy)propyl]-*N*,*N*,*N*-trimethylammonium chloride and dioleoyl phosphatidylethanolamine) and DNA (lipoplexes) and complexes between cationic polymers, such as polyethyleneimine (PEI) (Kunath et al., 2003), and DNA (polyplexes) are formed because of strong electrostatic interactions between the positively charged carrier and negatively charged DNA. Both carriers condense DNA (Kunath et al., 2003). A slight net positive charge of already formed lipoplexes and polyplexes is believed to facilitate their interaction with negatively charged cells and improve transfection efficiency (Sakurai et al., 2000). The data are available regarding the involvement of cell surface proteoglycans in lipoplex/polyplex interaction with cells (Labat-Moleur et al., 1996). Endocytosis (including the receptor-mediated endocytosis) was repeatedly confirmed as the main mechanism of lipoplex/polyplex internalization by cells (Ogris, Steinlein, Carotta, Brunner, & Wagner, 2001). Of special importance is the fact that despite endocytosis-mediated uptake of lipoplexes and polyplexes, DNA does not end in lysosomes but releases in the cytoplasm due to the destabilization of the endosomal membrane provoked by the lipid or polymeric component of the complexes. In particular, lipoplexes fuse with the endosomal membrane when they contain a fusogenic lipid (Felgner et al., 1994), which easily undergoes the transition from bilayer to hexagonal phase facilitating the fusion (Koltover, Salditt, Radler, & Safinya, 1998). In the case of polyplexes, which cannot directly destabilize the endosomal membrane, the mechanism of DNA escapes from endosomes is believed to be associated with the ability of polymers, such as PEI, to strongly protonate under the acidic pH inside endosomes and create a charge gradient eventually provoking a water influx and endosomal swelling and disintegration (Boussif et al., 1995). In both cases, however, DNA-containing complexes

when released into the cytosol dissociate allowing for nuclear entry of free DNA. Nuclear translocation of the plasmid DNA is relatively inefficient because of the barrier function of the nuclear membrane and small size of nuclear pores (ca. 25 nm), in addition, DNA degrades rather fast under the action of cytoplasmic nucleases (Pollard et al., 2001). It was estimated that only 0.1% of plasmids undergo nuclear translocation from the cytosol (Pollard et al., 1998). The attachment of nuclear localization sequences to plasmid DNA may significantly enhance its nuclear translocation and transfection efficiency (Branden, Mohamed, & Smith, 1999). In any case, the cytosolic delivery of DNA by lipoplexes and polyplexes is an interesting, important, and promising approach in intracellular delivery of drugs and DNA with a promising clinical potential, although still requiring more mechanistic and optimization studies (Zuhorn & Hoekstra, 2002). New approaches in using nanocarriers for DNA delivery include the application of bimetallic nanorods that can simultaneously bind compacted DNA plasmid and targeting ligands in a spatially defined manner (Salem, Searson, & Leong, 2003).

Nanocarriers for Targeting Lysosomes

The necessity of lysosomal targeting is determined by many unresolved issues with the enzyme therapy of lysosomal storage diseases. These diseases (usually inherited) are connected with the deficiency of some lysosomal enzymes (so-called storage diseases) and can be treated only by the administration of exogenous enzymes (Grabowsky & Desnick, 1981; Tager, Daems, & Hooghwinkel, 1974). Despite relative rarity of each of those diseases, being taken together they pose a serious medical problem (Desnick, Thorpe, & Fiddler, 1976; Grabowsky & Desnick, 1981). Storage diseases can be divided into two main groups (Desnick et al., 1976). In the first group, an abnormal (usually, deficient) enzyme is localized in the vacuolar apparatus of the cell. As a result, non-degraded substrates accumulate in the lysosomes of affected cells. Diseases such as Tay–Sachs', Gaucher's, peroxidase unsufficiency, and different mucopolysaccharidoses are typical examples. The second group includes cases where the activity of cytoplasmic enzymes is decreased; in this case, non-degraded substrates accumulate in the cell cytoplasm. Pathologies such as the Lesh–Nyhan syndrome or adenosine deaminidase insufficiency represent this group.

Enzymes for the therapy of lysosomal storage diseases include glucocerebrosidase, various glucosidases, phenylalanine ammonia lyase, and some others (Grabowsky & Desnick, 1981; Tager et al., 1974). For many storage pathologies, the treatment with purified exogenous enzymes shows very promising results. Unfortunately, therapy with native enzymes gives only a short-term relief because of their limited life in the circulation and relatively inefficient transport to lysosomes (Del Gaizo, MacKenzie, & Payne, 2003). In addition, it was found that endocytosis (the usual way of uptake of therapeutic enzyme by the cells) could not provide sufficient amounts of the "naked" therapeutic enzyme inside the cells. Thus, intravenous administration of purified hexoseaminidase has been tried in the

treatment of Tay–Sachs' disease (Johnson et al., 1973). The enzyme was thought to enter the affected cells of the central nervous system via endocytosis and destroy the ganglioside GM_2 accumulated in cell lysosomes. However, predominant accumulation of hexoseaminidase was discovered in the liver instead of target CNS cells. Similar problems are linked to unsuccessful attempts with purified glucocerebrosidase and ceramidetrihexosidase (Brady, Pentchev, Gal, Hibbert, & Dekaban, 1974; Brady et al., 1973).

Liposomes were suggested as pharmaceutical nanocarriers for replacement enzymes, which could protect them from the inactivation in vivo and enhance their intracellular delivery and, thus, transport into lysosomes. From the clinical point of view, the potential ability of liposome-encapsulated enzymes to enter the cytoplasm or lysosomes of live cells is of primary importance for the treatment of inherited diseases caused by the abnormal functioning of some intracellular enzymes. The use of liposome-immobilized enzymes instead of their native precursors opens new opportunities for enzyme therapy (Gregoriadis, 1978; Gregoriadis & Dean, 1979) especially in the treatment of diseases localized in liver cells that are natural targets for liposomes. Thus, the biodistribution of liposomes made of phosphatidylcholine, phosphatidic acid, and cholesterol (in 7:1:2 molar ratio) and containing β-fructofuranosidase has been studied (Gregoriadis & Ryman, 1972). It was shown that after 6 hours, 45% of the enzyme activity accumulated in the liver. The enzyme preserves its activity for a long time – 25% of the administered activity can be found in the liver after 48 hours. It is very important that up to 50% of the intracellular enzyme activity is localized in the lysosomal fraction. Similar data have been obtained for intravenously administered liposome-encapsulated α-mannosidase (Patel & Ryman, 1974) and neuraminidase (Gregoriadis, Putman, Louis, & Neerunjun, 1974). Liposomal β-glucuronidase also demonstrated fast accumulation in the liver of experimental mice. The enzyme remained active for more than a week, being associated with the lysosomes of liver cells (Steger & Desnick, 1977). In another experiment, rats treated with the liposomal dextranase (intravenous injection) demonstrated the decrease in the dextran content by 70% in 2 days (Colley & Ryman, 1976). The ability of the liposomal β-galactosidase to degrade GM_1-ganglioside in lysosomes of feline fibroblasts with pathological accumulation of this substrate has also been demonstrated (Reynolds, Baker, & Reynolds, 1978). The native enzyme was unable to penetrate cells and perform the therapeutic function. It was also shown that the incorporation of liposome-encapsulated therapeutic enzymes into appropriate cells could be enhanced by rather simple methods (Das, Murray, Zirzow, Brady, & Barranger, 1985). Thus, β-glucocerebrosidase included into liposomes was predominantly captured by Kupffer cells in the liver; the modification of liposomes with mannose residues increased the capture because of the presence of mannose-specific receptors on target cells. At the same time, liposome modification with galactose re-targeted them to hepatocytes. β-Galactosidase-containing liposomes obtained from a mixture of lecithine, cholesterol, and sulfatide (in 7:2:1 molar ratio) are readily incorporated into the liver and spleen of mice hosting the model of globoid cell leukodystrophy. The liposome-encapsulated therapeutic enzyme administered

as a single injection after preliminary injection of liposomes with galactocerebroside into experimental mice causes the breakdown of 70–80% of intracellular galactocerebroside (Umezawa, Eto, Tokoro, Ito, & Maekawa, 1985). The inherited abnormal metabolism of porphyrins results in porphyriasis. The molecular basis of the disease can be correlated with the increase in δ-aminolevulinate synthetase activity in conjunction with normal or even decreased activity of δ-aminolevulinate dehydratase. Espinola, Wider, Stella, & Batlle (1983) succeeded to incorporate purified δ-aminolevulinate dehydratase into liposomes. Under optimal conditions, the encapsulation efficiency can reach 40% and the enzyme completely preserves its activity.

The first clinical experiments utilizing liposome-encapsulated therapeutic enzymes have also been performed with preparations designed for the treatment of disease of the reticuloendothelial system. Impressive results have been achieved by treatment of a patient suffering from Gaucher's disease (inherited glucocerebrosidase insufficiency, causing excessive glucocerebroside accumulation in liver lysosomes), using liposomal glucocerebrosidase (Belchetz, Crawley, Braidman, & Gregoriadis, 1977). Therapy with the native enzyme gave no results because of its inability to penetrate cells. The administration of the enzyme encapsulated in liposomes, over a period of 13 months produced a pronounced effect, in particular, a decrease in liver size with a very small amount of the active enzyme used. Better understanding of fine mechanisms associated with the permeability of the lysosomal membrane will certainly contribute to the further progress in this area (Lloyd, 2000).

Drug and DNA Delivery to/into Mitochondria with Mitochondria-Specific Nanocarriers

Mitochondria represent another important intracellular target for drugs and DNA. The major function of mitochondria that are present in all eukaryotic cells is the production of ATP. Mitochondria are also involved in other metabolic pathways, such as the citrate cycle, the oxidation of fatty acids, and the synthesis of steroid hormones and gluconeogenesis. Mitochondrial dysfunction contributes to a variety of human disorders, ranging from neurodegenerative diseases, obesity, and diabetes to ischemia-reperfusion injury and cancer. Many clinically approved drugs, including paclitaxel, directly act on mitochondria triggering an apoptosis (Costantini, Jacotot, Decaudin, & Kroemer, 2000) since mitochondria play a key role in the complex apoptosis mechanism (Preston, Abadi, Wilson, & Singh, 2001; Zhao, Kircher, Josephson, & Weissleder, 2002). The number of diseases found to be associated with defects of the mitochondrial genome has grown significantly over the last decade (Wallace, 1999). Among the first mitochondrial diseases to be understood at the molecular level was a group of neuromuscular diseases resulting from mitochondrial DNA (mtDNA) deletions (Holt, Harding, & Morgan-Hughes, 1988). Large deletions as well as point mutations of mtDNA were found to lead to the whole variety of mitochondrial myopathies (Harding, 1991). However, mitochondrial

gene therapy is currently only at the very early stage of its development (Sperl, 1997).

Since one of the major roles of mitochondria in the metabolism of eukaryotic cells is the synthesis of ATP by oxidative phosphorylation via the respiratory chain, this process creates a transmembrane electrochemical gradient, which includes contributions from both a membrane potential (negative inside) and a pH difference (acidic outside). The membrane potential of mitochondria in vitro is between 180 and 200 mV, which is the maximum a lipid bilayer can sustain while maintaining its integrity (Murphy, 1989). Therefore, positively charged molecules are attracted by mitochondria in response to the highly negative membrane potential. Although most charged molecules could not enter the mitochondrial matrix because the inner mitochondrial membrane is impermeable to polar molecules, however, certain amphiphile compounds are able to cross both mitochondrial membranes and accumulate in the mitochondrial matrix in response to the negative membrane potential. It has long been known that amphiphile compounds with delocalized cationic charge accumulate in mitochondria (Weissig & Torchilin, 2001). Rhodamine 123 is the best known representative of this group used as a stain for mitochondria in living cells (Chen et al., 1982a). Mitochondrial accumulation of tetraphenylphosphonium chloride and other cationic aryl phosphonium salts was also demonstrated (Rideout, Bustamante, & Patel, 1994). The mitochondrial accumulation and retention of dequalinium (DQA), a single-chain bola amphiphile with two delocalized positive charge centers was also demonstrated (Weissig & Torchilin, 2001).

Earlier, it was found that upon sonication DQA forms spherical aggregates with diameters between about 70 and 700 nm (Weissig et al., 1998; Weissig & Torchilin, 2000). The hypothesis put forward was that because of their positive charge and mitochondria-tropic properties, DQAsomes could bind or entrap various drugs and DNA and transport it to the mitochondria. In particular, a strong interaction between DQAsomes and plasmid DNA (Weissig et al., 1998) was demonstrated as well as the fact that the complex formation effectively protects DNA from digestion by nucleases (Lasch et al., 1999). Moreover, it was clearly demonstrated that DQAsome complexes with DNA can enter cells, approach mitochondria, and release the bound DNA after interacting with the mitochondrial membrane (D'Souza, Rammohan, Cheng, Torchilin, & Weissig, 2003), which is crucial for the subsequent DNA transport into the mitochondrial matrix via the mitochondrial protein import machinery. Mitochondriotropic liposomes have also been described as prepared by adding to the liposomal lipid composition of amphiphilic tetraphenylphosphonium derivative (Boddapati et al., 2005).

Although drug delivery to other intracellular organelles/compartments as well as alternative ways of intracellular drug delivery are significantly less developed, still there exist quite a few potentially important publications considering such options. Thus, a growing interest toward caveolae, bottleshape invaginations of the plasma membrane, can be noticed over the last few years (Bathori, Cervenak, & Karadi, 2004). Their importance is in the fact that opposite to the classic clathrin-dependent endocytosis, the internalization via the caveolar pathway bypasses the lysosomes.

Taking into account that caveolae are involved in such key cellular processes as endocytosis and pinocytosis, the possibility of selective initiation of caveolae-mediated uptake might provide an interesting opportunity for the cytoplasmic drug/gene delivery. Importantly, even for cells which do not express caveolin I protein and, consequently, cannot develop caveolae, a similar mechanism exists, i.e., the formation of lipid rafts (Helms & Zurzolo, 2004) also allowing for non-lysosmal uptake.

Among novel intracellular targets one can name the endoplasmic reticulum (ER), which is responsible for the export of membrane-bound and soluble molecules, and is involved in signaling pathways regulating cell growth and differentiation (Moyer & Balch, 2001). Since misfolding and/or aggregation of proteins synthesized in ER as well as disregulation of normal processing inside the ER are causing a broad range of serious diseases, Alzheimer's disease and cystic fibrosis among them, the ER represents an interesting and promising target for therapeutical interventions. Thus, pH-sensitive liposomes have been used for the ER-specific delivery of imino-sugar *N*-butyldeoxynojiromycin, which effectively inhibits tyrosinase (i.e., N-glycosylation processing in the ER) in melanoma cells (Costin, Trif, Nichita, Dwek, & Petrescu, 2002).

With a better understanding of the molecular basis of various diseases, the number of intracellular therapeutic targets as well as the means to specifically reach them inside cells will grow, providing novel and more efficient therapeutic strategies. The role of nanomedicine in this process is hard to overestimate.

References

Aalto-Setala, K., & Vuorio, E. (1997). Gene Therapy of single-gene disorders: preface to the special section. *Ann Med*, *29*, 549–551.

Allen, T. M., Newman, M. S., Woodle, M. C., Mayhew, E., & Uster, P. S. (1995). Pharmacokinetics and anti-tumor activity of vincristine encapsulated in sterically stabilized liposomes. *Int J Cancer*, *62*(2), 199–204.

Arnheiter, H., & Haller, O. (1988). Antiviral sTATe against influenza virus neutralized by microinjection of antibodies to interferon-induced Mx proteins. *Embo J*, *7*(5), 1315–1320.

Asin-Cayuela, J., Manas, A. R., James, A. M., Smith, R. A., & Murphy, M. P. (2004). Fine-tuning the hydrophobicity of a mitochondria-targeted antioxidant. *FEBS Lett*, *571*(1–3), 9–16.

Asokan, A., & Cho, M. J. (2002). Exploitation of intracellular pH gradients in the cellular delivery of macromolecules. *J Pharm Sci*, *91*(4), 903–913.

Asokan, A., & Cho, M. J. (2003). Cytosolic delivery of macromolecules. II. Mechanistic studies with pH-sensitive morpholine lipids. *Biochim Biophys Acta*, *1611*(1–2), 151–160.

Bae, Y., Nishiyama, N., Fukushima, S., Koyama, H., Yasuhiro, M., & Kataoka, K. (2005). Preparation and biological characterization of polymeric micelle drug carriers with intracellular pH-triggered drug release property: tumor permeability, controlled subcellular drug distribution, and enhanced in vivo antitumor efficacy. *Bioconjug Chem*, *16*(1), 122–130.

Bathori, G., Cervenak, L., & Karadi, I. (2004). Caveolae – an alternative endocytotic pathway for targeted drug delivery. *Crit Rev Ther Drug Carrier Syst*, *21*(2), 67–95.

Becker, M. L., Bailey, L. O., & Wooley, K. L. (2004). Peptide-derivatized shell-cross-linked nanoparticles. 2. Biocompatibility evaluation. *Bioconjug Chem*, *15*(4), 710–717.

Becker, M. L., Remsen, E. E., Pan, D., & Wooley, K. L. (2004). Peptide-derivatized shell-cross-linked nanoparticles. 1. Synthesis and characterization. *Bioconjug Chem*, *15*(4), 699–709.

Belchetz, P. E., Crawley, J. C., Braidman, I. P., & Gregoriadis, G. (1977). Treatment of Gaucher's disease with liposome-entrapped glucocerebroside: beta-glucosidase. *Lancet*, *2*(8029), 116–117.

Boddapati, S. V., Tongcharoensirikul, P., Hanson, R. N., D'Souza, G. G., Torchilin, V. P., & Weissig, V. (2005). Mitochondriotropic liposomes. *J Liposome Res*, *15*(1–2), 49–58.

Boomer, J. A., & Thompson, D. H. (1999). Synthesis of acid-labile diplasmenyl lipids for drug and gene delivery applications. *Chem Phys Lipids*, *99*(2), 145–153.

Boussif, O., Lezoualc'h, F., Zanta, M. A., Mergny, M. D., Scherman, D., Demeneix, B., et al. (1995). A versatile vector for gene and oligonucleotide transfer into cells in culture and in vivo: polyethylenimine. *Proc Natl Acad Sci USA*, *92*(16), 7297–7301.

Brady, R. O., Pentchev, P. G., Gal, A. E., Hibbert, S. R., & Dekaban, A. S. (1974). Replacement therapy for inherited enzyme deficiency. Use of purified glucocerebrosidase in Gaucher's disease. *N Engl J Med*, *291*(19), 989–993.

Brady, R. O., Tallman, J. F., Johnson, W. G., Gal, A. E., Leahy, W. R., Quirk, J. M., et al. (1973). Replacement therapy for inherited enzyme deficiency. Use of purified ceramidetrihexosidase in Fabry's disease. *N Engl J Med*, *289*(1), 9–14.

Branden, L. J., Mohamed, A. J., & Smith, C. I. (1999). A peptide nucleic acid-nuclear localization signal fusion that mediates nuclear transport of DNA. *Nat Biotechnol*, *17*(8), 784–787.

Burns, R. J., & Murphy, M. P. (1997). Labeling of mitochondrial proteins in living cells by the thiol probe thiobutyltriphenylphosphonium bromide. *Arch Biochem Biophys*, *339*, 33–39.

Burns, R. J., Smith, R. A. J., & Murphy, M. P. (1995). Synthesis and characterization of thiobutyltriphenylphosphonium bromide, a novel thiol reagent targeted to the mitochondrial matrix. *Arch Biochem Biophys*, *322*, 60–68.

Chakrabarti, R., Wylie, D. E., & Schuster, S. M. (1989). Transfer of monoclonal antibodies into mammalian cells by electroporation. *J Biol Chem*, *264*(26), 15494–15500.

Chen, G., & Hoffman, A. S. (1995). Graft copolymers that exhibit temperature-induced phase transitions over a wide range of pH. *Nature*, *373*(6509), 49–52.

Chen, L. B., Summerhayes, I. C., Johnson, L. V., Walsh, M. L., Bernal, S. D., & Lampidis, T. J. (1982a). Probing mitochondria in living cells with rhodamine 123. *Cold Spring Harb Symp Quant Biol*, *46 Pt 1*, 141–155.

Chen, L. B., Summerhayes, I. C., Johnson, L. V., Walsh, M. L., Bernal, S. D., & Lampidis, T. J. (1982b). Probing mitochondria in living cells with rhodamine 123. *Cold Spring Harb Symp Quant Biol*, *46*, 141–155.

Colley, C. M., & Ryman, B. E. (1976). The use of a liposomally entrapped enzyme in the treatment of an artificial storage condition. *Biochim Biophys Acta*, *451*(2), 417–425.

Costantini, P., Jacotot, E., Decaudin, D., & Kroemer, G. (2000). Mitochondrion as a novel target of anticancer chemotherapy. *J Natl Cancer Inst*, *92*(13), 1042–1053.

Costin, G. E., Trif, M., Nichita, N., Dwek, R. A., & Petrescu, S. M. (2002). pH-sensitive liposomes are efficient carriers for endoplasmic reticulum-targeted drugs in mouse melanoma cells. *Biochem Biophys Res Commun*, *293*(3), 918–923.

Coulter, C. V., Smith, R. A. J., & Murphy, M. P. (2001). Synthesis, characterization, and biological properties of a fullerene triphenylphosphonium salt. *Fullerene Science and Technology*, *9*, 339–350.

Csermely, P., Schnaider, T., & Szanto, I. (1995). Signaling and transport through the nuclear membrane. *Biochim Biophys Acta*, *1241*, 425–452.

D'Souza, G. G., Rammohan, R., Cheng, S. M., Torchilin, V. P., & Weissig, V. (2003). DQAsome-mediated delivery of plasmid DNA toward mitochondria in living cells. *J Control Release*, *92*(1–2), 189–197.

Das, P. K., Murray, G. J., Zirzow, G. C., Brady, R. O., & Barranger, J. A. (1985). Lectin-specific targeting of beta-glucocerebrosidase to different liver cells via glycosylated liposomes. *Biochem Med*, *33*(1), 124–131.

Daugelavicius, R., Cvirkaite, V., Gaidelyte, A., Bakiene, E., Gabrenaite-Verkhovskaya, R., & Bamford, D. H. (2005). Penetration of enveloped double-stranded RNA bacteriophages phi13 and phi6 into Pseudomonas syringae cells. *J Virol*, *79*(8), 5017–5026.

de la Fuente, J. M., & Berry, C. C. (2005). Tat peptide as an efficient molecule to translocate gold nanoparticles into the cell nucleus. *Bioconjug Chem*, *16*(5), 1176–1180.

Del Gaizo, V., MacKenzie, J. A., & Payne, R. M. (2003). Targeting proteins to mitochondria using TAT. *Mol Genet Metab*, *80*(1–2), 170–180.

Derossi, D., Calvet, S., Trembleau, A., Brunissen, A., Chassaing, G., & Prochiantz, A. (1996). Cell internalization of the third helix of the Antennapedia homeodomain is receptor-independent. *J Biol Chem*, *271*(30), 18188–18193.

Derossi, D., Joliot, A. H., Chassaing, G., & Prochiantz, A. (1994). The third helix of the Antennapedia homeodomain translocates through biological membranes. *J Biol Chem*, *269*(14), 10444–10450.

Desnick, R. J., Thorpe, S. R., & Fiddler, M. B. (1976). Toward enzyme therapy for lysosomal storage diseases. *Physiol Rev*, *56*(1), 57–99.

Dodd, C. H., Hsu, H. C., Chu, W. J., Yang, P., Zhang, H. G., Mountz, J. D., Jr., et al. (2001). Normal T-cell response and in vivo magnetic resonance imaging of T cells loaded with HIV transactivator-peptide-derived superparamagnetic nanoparticles. *J Immunol Methods*, *256*(1–2), 89–105.

Egleton, R. D., & Davis, T. P. (1997). Bioavailability and transport of peptides and peptide drugs into the brain. *Peptides*, *18*(9), 1431–1439.

Elliott, G., & O'Hare, P. (1997). Intercellular trafficking and protein delivery by a herpesvirus structural protein. *Cell*, *88*(2), 223–233.

Elmquist, A., Lindgren, M., Bartfai, T., & Langel, U. (2001). VE-cadherin-derived cell-penetrating peptide, pVEC, with carrier functions. *Exp Cell Res*, *269*(2), 237–244.

Elouahabi, A., & Ruysschaert, J. M. (2005). Formation and intracellular trafficking of lipoplexes and polyplexes. *Mol Therv*, *11*(3), 336–347.

Espinola, L. G., Wider, E. A., Stella, A. M., & Batlle, A. M. D. C. (1983). Enzyme replacement therapy in porphyrias—II: Entrapment of δ-aminolaevulinate dehydratase in liposomes. *Int J Biochem*, *15*(3), 439–445.

Farhood, H., Serbina, N., & Huang, L. (1995). The role of dioleoyl phosphatidylethanolamine in cationic liposome mediated gene transfer. *Biochim Biophys Acta*, *1235*(2), 289–295.

Fawell, S., Seery, J., Daikh, Y., Moore, C., Chen, L. L., Pepinsky, B., et al. (1994). TAT-mediated delivery of heterologous proteins into cells. *Proc Natl Acad Sci USA*, *91*(2), 664–668.

Felgner, J. H., Kumar, R., Sridhar, C. N., Wheeler, C. J., Tsai, Y. J., Border, R., et al. (1994). Enhanced gene delivery and mechanism studies with a novel series of cationic lipid formulations. *J Biol Chem*, *269*(4), 2550–2561.

Felgner, P. L., Gadek, T. R., Holm, M., Roman, R., Chan, H. W., Wenz, M., et al. (1987). Lipofection: a highly efficient, lipid-mediated DNA-transfection procedure. *Proc Natl Acad Sci USA*, *84*(21), 7413–7417.

Ferrari, A., Pellegrini, V., Arcangeli, C., Fittipaldi, A., Giacca, M., & Beltram, F. (2003). Caveolae-mediated internalization of extracellular HIV-1 tat fusion proteins visualized in real time. *Mol Ther*, *8*(2), 284–294.

Filion, M. C., & Phillips, N. C. (1997). Toxicity and immunomodulatory activity of liposomal vectors formulated with cationic lipids toward immune effector cells. *Biochim Biophys Acta*, *1329*(2), 345–356.

Fittipaldi, A., Ferrari, A., Zoppe, M., Arcangeli, C., Pellegrini, V., Beltram, F., et al. (2003). Cell membrane lipid rafts mediate caveolar endocytosis of HIV-1 Tat fusion proteins. *J Biol Chem*, *278*(36), 34141–34149.

Fonseca, M. J., Jagtenberg, J. C., Haisma, H. J., & Storm, G. (2003). Liposome-mediated targeting of enzymes to cancer cells for site-specific activation of prodrugs: comparison with the corresponding antibody-enzyme conjugate. *Pharm Res*, *20*(3), 423–428.

Frankel, A. D., & Pabo, C. O. (1988). Cellular uptake of the tat protein from human immunodeficiency virus. *Cell*, *55*(6), 1189–1193.

Futaki, S., Suzuki, T., Ohashi, W., Yagami, T., Tanaka, S., Ueda, K., et al. (2001). Arginine-rich peptides. An abundant source of membrane-permeable peptides having potential as carriers for intracellular protein delivery. *J Biol Chem*, *276*(8), 5836–5840.

Gaspar, M. M., Perez-Soler, R., & Cruz, M. E. (1996). Biological characterization of L-asparaginase liposomal formulations. *Cancer Chemother Pharmacol*, *38*(4), 373–377.

Geisert, E. E., Jr., Del Mar, N. A., Owens, J. L., & Holmberg, E. G. (1995). Transfecting neurons and glia in the rat using pH-sensitive immunoliposomes. *Neurosci Lettv*, *184*(1), 40–43.

Grabowsky, G. A., & Desnick, R. J. (1981). Enzyme replacement in genetic diseases. In J. S. Holcenberg & J. Roberts (Eds.), *Enzymes as drugs* (pp. 167). New York: Wiley.

Green, M., & Loewenstein, P. M. (1988). Autonomous functional domains of chemically synthesized human immunodeficiency virus tat trans-activator protein. *Cell*, *55*(6), 1179–1188.

Gregoriadis, G. (1978). Liposomes in the therapy of lysosomal storage diseases. *Nature*, *275*(5682), 695–696.

Gregoriadis, G., & Dean, M. F. (1979). Enzyme therapy in genetic diseases. *Nature*, *278*(5705), 603–604.

Gregoriadis, G., Putman, D., Louis, L., & Neerunjun, D. (1974). Comparative effect and fate of non-entrapped and liposome-entrapped neuraminidase injected into rats. *Biochem J*, *140*(2), 323–330.

Gregoriadis, G., & Ryman, B. E. (1972). Lysosomal localization of -fructofuranosidase-containing liposomes injected into rats. *Biochem J*, *129*(1), 123–133.

Guo, X., & Szoka, F. C., Jr. (2001). Steric stabilization of fusogenic liposomes by a low-pH sensitive PEG-diortho ester-lipid conjugate. *Bioconjugate Chem*, *12*(2), 291–300.

Gupta, B., Levchenko, T. S., & Torchilin, V. P. (2005). Intracellular delivery of large molecules and small particles by cell-penetrating proteins and peptides. *Adv Drug Deliv Rev 57*(4), 637–651.

Hafez, I. M., Maurer, N., & Cullis, P. R. (2001). On the mechanism whereby cationic lipids promote intracellular delivery of polynucleic acids. *Gene Ther*, *8*(15), 1188–1196.

Harding, A. E. (1991). Neurological disease and mitochondrial genes. *Trends Neurosci*, *14*(4), 132–138.

Heeremans, J. L., Prevost, R., Bekkers, M. E., Los, P., Emeis, J. J., Kluft, C., et al. (1995). Thrombolytic treatment with tissue-type plasminogen activator (t-PA) containing liposomes in rabbits: a comparison with free t-PA. *Thromb Haemost*, *73*(3), 488–494.

Helms, J. B., & Zurzolo, C. (2004). Lipids as targeting signals: lipid rafts and intracellular trafficking. *Traffic*, *5*(4), 247–254.

Hirota, Y., Masuyama, N., Kuronita, T., Fujita, H., Himeno, M., & Tanaka, Y. (2004). Analysis of post-lysosomal compartments. *Biochem Biophys Res Commun*, *314*(2), 306–312.

Hoekstra, D., de Boer, T., Klappe, K., & Wilschut, J. (1984). Fluorescence method for measuring the kinetics of fusion between biological membranes. *Biochemistry*, *23*(24), 5675–5681.

Hoekstra, D., & Klappe, K. (1986). Use of a fluorescence assay to monitor the kinetics of fusion between erythrocyte ghosts, as induced by Sendai virus. *Biosci Rep*, *6*(11), 953–960.

Holt, I. J., Harding, A. E., & Morgan-Hughes, J. A. (1988). Deletions of muscle mitochondrial DNA in patients with mitochondrial myopathies. *Nature*, *331*(6158), 717–719.

Horobin, R. W. (2002). Xanthenes. In R. W. Horobin, Kiernan, J.A. (Ed.), *Conn's Biological Stains, 10th Edition* (pp. 237). Oxford, UK: BIOS Scientific Publishers.

Horobin, R. W., & Kiernan, J.A. (eds). (2002). *Conn's Biological Stains* (10th ed.). Oxford, UK: BIOS Scientific Publishers.

Huth, U., Wieschollek, A., Garini, Y., Schubert, R., & Peschka-Suss, R. (2004). Fourier transformed spectral bio-imaging for studying the intracellular fate of liposomes. *Cytometry A*, *57*(1), 10–21.

Inoue, M., Yoshida, H., & Akisaka, T. (1999). Visualization of acidic compartments in cultured osteoclasts by use of an acidotrophic amine as a marker for low pH. *Cell Tissue Res*, *298*(3), 527–537.

James, A. M., Blaikie, F. H., Smith, R. A., Lightowlers, R. N., Smith, P. M., & Murphy, M. P. (2003). Specific targeting of a DNA-alkylating reagent to mitochondria. Synthesis and characterization of [4-((11aS)-7-methoxy-1,2,3,11a-tetrahydro-5H-pyrrolo[2,1-c][1,4]benzodiaze pin-5-on-8-oxy)butyl]-triphenylphosphonium iodide. *Eur J Biochem*, *270*(13), 2827–2836.

Jeang, K. T., Xiao, H., & Rich, E. A. (1999). Multifaceted activities of the HIV-1 transactivator of transcription, Tat. *J Biol Chem*, *274*(41), 28837–28840.

Jeong, J. H., Kim, S. W., & Park, T. G. (2003). Novel intracellular delivery system of antisense oligonucleotide by self-assembled hybrid micelles composed of DNA/PEG conjugate and cationic fusogenic peptide. *Bioconjug Chem*, *14*(2), 473–479.

Johnson, W. G., Desnick, R. J., Long, D. M., Sharp, H. L., Krivit, W., Brady, B., et al. (1973). Intravenous injection of purified hexosaminidase A into a patient with Tay-Sachs disease. *Birth Defects Orig Artic Ser*, *9*(2), 120–124.

Joliot, A., Pernelle, C., Deagostini-Bazin, H., & Prochiantz, A. (1991). Antennapedia homeobox peptide regulates neural morphogenesis. *Proc Natl Acad Sci U S A*, *88*(5), 1864–1868.

Josephson, L., Tung, C. H., Moore, A., & Weissleder, R. (1999). High-efficiency intracellular magnetic labeling with novel superparamagnetic-Tat peptide conjugates. *Bioconjug Chem*, *10*(2), 186–191.

Kamata, H., Yagisawa, H., Takahashi, S., & Hirata, H. (1994). Amphiphilic peptides enhance the efficiency of liposome-mediated DNA transfection. *Nucleic Acids Res*, *22*(3), 536–537.

Kaufman, C. L., Williams, M., Ryle, L. M., Smith, T. L., Tanner, M., & Ho, C. (2003). Superparamagnetic iron oxide particles transactivator protein-fluorescein isothiocyanate particle labeling for in vivo magnetic resonance imaging detection of cell migration: uptake and durability. *Transplantation*, *76*(7), 1043–1046.

Kelso, G. F., Porteous, C. M., Coulter, C. V., Hughes, G., Porteous, W. K., Ledgerwood, E. C., et al. (2001). Selective targeting of a redox-active ubiquinone

to mitochondria within cells: antioxidant and antiapoptotic properties. *J Biol Chem*, *276*(7), 4588–4596.

Kelso, G. F., Porteous, C. M., Hughes, G., Ledgerwood, E. C., Gane, A. M., Smith, R. A., et al. (2002). Prevention of mitochondrial oxidative damage using targeted antioxidants. *Ann NY Acad Sci*, *959*, 263–274.

Khaw, B. A., daSilva, J., Vural, I., Narula, J., & Torchilin, V. P. (2001). Intracytoplasmic gene delivery for in vitro transfection with cytoskeleton-specific immunoliposomes. *J Control Release*, *75*(1–2), 199–210.

Khaw, B. A., Fallon, J. T., Beller, G. A., & Haber, E. (1979). Specificity of localization of myosin-specific antibody fragments in experimental myocardial infarction. Histologic, histochemical, autoradiographic and scintigraphic studies. *Circulation*, *60*(7), 1527–1531.

Khaw, B. A., Scott, J., Fallon, J. T., Cahill, S. L., Haber, E., & Homcy, C. (1982). Myocardial injury: quantitation by cell sorting initiated with antimyosin fluorescent spheres. *Science*, *217*(4564), 1050–1053.

Khaw, B. A., Torchilin, V. P., Vural, I., & Narula, J. (1995). Plug and seal: prevention of hypoxic cardiocyte death by sealing membrane lesions with antimyosin-liposomes. *Nat Med*, *1*(11), 1195–1198.

Khaw, B. A., Vural, I., DaSilva, J., & Torchilin, V. P. (2000). Use of cytoskeleton-specific immunoliposomes for preservation of cell viability and gene delivery. *S. T.P, Pharma Sci*, *10*, 279–283.

Kisel, M. A., Kulik, L. N., Tsybovsky, I. S., Vlasov, A. P., Vorob'yov, M. S., Kholodova, E. A., et al. (2001). Liposomes with phosphatidylethanol as a carrier for oral delivery of insulin: studies in the rat. *Int J Pharm*, *216*(1–2), 105–114.

Koch, A. M., Reynolds, F., Merkle, H. P., Weissleder, R., & Josephson, L. (2005). Transport of surface-modified nanoparticles through cell monolayers. *Chembiochem*, *6*(2), 337–345.

Koltover, I., Salditt, T., Radler, J. O., & Safinya, C. R. (1998). An inverted hexagonal phase of cationic liposome-DNA complexes related to DNA release and delivery. *Science*, *281*(5373), 78–81.

Kratz, F., Beyer, U., & Schutte, M. T. (1999). Drug-polymer conjugates containing acid-cleavable bonds. *Crit Rev Ther Drug Carrier Syst*, *16*(3), 245–288.

Kunath, K., von Harpe, A., Fischer, D., Petersen, H., Bickel, U., Voigt, K., et al. (2003). Low-molecular-weight polyethylenimine as a non-viral vector for DNA delivery: comparison of physicochemical properties, transfection efficiency and in vivo distribution with high-molecular-weight polyethylenimine. *J Control Release*, *89*(1), 113–125.

Kuwana, T., Mullock, B. M., & Luzio, J. P. (1995). Identification of a lysosomal protein causing lipid transfer, using a fluorescence assay designed to monitor membrane fusion between rat liver endosomes and lysosomes. *Biochem J*, *308 (Pt 3)*, 937–946.

Kwon, G. S., & Kataoka, K. (1995). Block copolymer micelles as long-circulating drug vehicles. *Adv Drug Deliv Rev*, *16*, 295–309.

Labat-Moleur, F., Steffan, A. M., Brisson, C., Perron, H., Feugeas, O., Furstenberger, P., et al. (1996). An electron microscopy study into the mechanism of gene transfer with lipopolyamines. *Gene Ther*, *3*(11), 1010–1017.

Lackey, C. A., Press, O. W., Hoffman, A. S., & Stayton, P. S. (2002). A biomimetic pH-responsive polymer directs endosomal release and intracellular delivery of an endocytosed antibody complex. *Bioconjug Chem*, *13*(5), 996–1001.

Larsson, L., Clapp, W. L., 3rd, Park, C. H., Cannon, J. K., & Tisher, C. C. (1987). Ultrastructural localization of acidic compartments in cells of isolated rabbit PCT. *Am J Physiol*, *253*(1 Pt 2), F95–F103.

Lasch, J., Meye, A., Taubert, H., Koelsch, R., Mansa-ard, J., & Weissig, V. (1999). Dequalinium vesicles form stable complexes with plasmid DNA which are protected from DNase attack. *Biol Chem*, *380*(6), 647–652.

Lasic, D. D. (1993). *Liposomes : from physics to applications*. Amsterdam ; New York: Elsevier.

Lasic, D. D., & Martin, F. J. (1995). *Stealth liposomes*. Boca Raton: CRC Press.

Lee, E. S., Na, K., & Bae, Y. H. (2003). Polymeric micelle for tumor pH and folate-mediated targeting. *J Control Release*, *91*(1–2), 103–113.

Lee, E. S., Shin, H. J., Na, K., & Bae, Y. H. (2003). Poly(L-histidine)-PEG block copolymer micelles and pH-induced destabilization. *J Control Release*, *90*(3), 363–374.

Leroux, J., Roux, E., Le Garrec, D., Hong, K., & Drummond, D. C. (2001). N-isopropylacrylamide copolymers for the preparation of pH-sensitive liposomes and polymeric micelles. *J Control Release*, *72*(1–3), 71–84.

Lewin, M., Carlesso, N., Tung, C. H., Tang, X. W., Cory, D., Scadden, D. T., et al. (2000). TAT peptide-derivatized magnetic nanoparticles allow in vivo tracking and recovery of progenitor cells. *Nat Biotechnol*, *18*(4), 410–414.

Lin, T. K., Hughes, G., Muratovska, A., Blaikie, F. H., Brookes, P. S., Darley-Usmar, V., et al. (2002). Specific modification of mitochondrial protein thiols in response to oxidative stress: a proteomics approach. *J Biol Chem*, *277*(19), 17048–17056.

Lindgren, M., Hallbrink, M., Prochiantz, A., & Langel, U. (2000). Cell-penetrating peptides. *Trends Pharmacol Sci*, *21*(3), 99–103.

Lisziewicz, J., Sun, D., Lisziewicz, A., & Gallo, R. C. (1995). Antitat gene therapy: a candidate for late-stage AIDS patients. *Gene Ther*, *2*(3), 218–222.

Liu, J., Zhang, Q., Remsen, E. E., & Wooley, K. L. (2001). Nanostructured materials designed for cell binding and transduction. *Biomacromolecules*, *2*(2), 362–368.

Lloyd, J. B. (2000). Lysosome membrane permeability: implications for drug delivery. *Adv Drug Deliv Rev*, *41*(2), 189–200.

Lo, Y. L., Tsai, J. C., & Kuo, J. H. (2004). Liposomes and disaccharides as carriers in spray-dried powder formulations of superoxide dismutase. *J Control Release*, *94*(2–3), 259–272.

Lukyanov, A. N., Hartner, W. C., & Torchilin, V. P. (2004). Increased accumulation of PEG-PE micelles in the area of experimental myocardial infarction in rabbits. *J Control Release*, *94*(1), 187–193.

Maeda, H., Wu, J., Sawa, T., Matsumura, Y., & Hori, K. (2000). Tumor vascular permeability and the EPR effect in macromolecular therapeutics: a review. *J Control Releasev*, *65*(1–2), 271–284.

Marty, C., Meylan, C., Schott, H., Ballmer-Hofer, K., & Schwendener, R. A. (2004). Enhanced heparan sulfate proteoglycan-mediated uptake of cell-penetrating peptide-modified liposomes. *Cell Mol Life Sci*, *61*(14), 1785–1794.

Mastrobattista, E., Koning, G. A., van Bloois, L., Filipe, A. C., Jiskoot, W., & Storm, G. (2002). Functional characterization of an endosome-disruptive peptide and its application in cytosolic delivery of immunoliposome-entrapped proteins. *J Biol Chem*, *277*(30), 27135–27143.

Midoux, P., Kichler, A., Boutin, V., Maurizot, J. C., & Monsigny, M. (1998). Membrane permeabilization and efficient gene transfer by a peptide containing several histidines. *Bioconjug Chem*, *9*(2), 260–267.

Minier, C., & Moore, M. N. (1996). Rhodamine B accumulation and MXR protein expression in mussel blood cells: effects of exposure to vincristine. *Marine Ecology – Progress Series*, *142*, 165–173.

Morris, M. C., Vidal, P., Chaloin, L., Heitz, F., & Divita, G. (1997). A new peptide vector for efficient delivery of oligonucleotides into mammalian cells. *Nucleic Acids Res*, *25*(14), 2730–2736.

Moyer, B. D., & Balch, W. E. (2001). A new frontier in pharmacology: the endoplasmic reticulum as a regulated export pathway in health and disease. *Expert Opin Ther Targets*, *5*(2), 165–176.

Murphy, M. P. (1989). Slip and leak in mitochondrial oxidative phosphorylation. *Biochim Biophys Acta*, *977*(2), 123–141.

Oehlke, J., Scheller, A., Wiesner, B., Krause, E., Beyermann, M., Klauschenz, E., et al. (1998). Cellular uptake of an alpha-helical amphipathic model peptide with the potential to deliver polar compounds into the cell interior non-endocytically. *Biochim Biophys Acta*, *1414*(1–2), 127–139.

Ogris, M., Steinlein, P., Carotta, S., Brunner, S., & Wagner, E. (2001). DNA/polyethylenimine transfection particles: influence of ligands, polymer size, and PEGylation on internalization and gene expression. *AAPS PharmSci*, *3*(3), E21.

Ohashi, M., Miwako, I., Nakamura, K., Yamamoto, A., Murata, M., Ohnishi, S., et al. (1999). An arrested late endosome-lysosome intermediate aggregate observed in a Chinese hamster ovary cell mutant isolated by novel three-step screening. *J Cell Sci*, *112*(Pt 8), 1125–1138.

Ohashi, M., Murata, M., & Ohnishi, S. (1992). A novel fluorescence method to monitor the lysosomal disintegration of low density lipoprotein. *Eur J Cell Biol*, *59*(1), 116–126.

Park, J. W., Kirpotin, D. B., Hong, K., Shalaby, R., Shao, Y., Nielsen, U. B., et al. (2001). Tumor targeting using anti-her2 immunoliposomes. *J Control Release*, *74*(1–3), 95–113.

Patel, H. M., & Ryman, B. E. (1974). α-Mannosidase in zinc-deficient rats. Possibility of liposomal therapy in mannosidosis. *Biochem Soc Transv*, *2*, 1014–1017.

Pollard, H., Remy, J. S., Loussouarn, G., Demolombe, S., Behr, J. P., & Escande, D. (1998). Polyethylenimine but not cationic lipids promotes transgene delivery to the nucleus in mammalian cells. *J Biol Chem*, *273*(13), 7507–7511.

Pollard, H., Toumaniantz, G., Amos, J. L., Avet-Loiseau, H., Guihard, G., Behr, J. P., et al. (2001). Ca2 + -sensitive cytosolic nucleases prevent efficient delivery to the nucleus of injected plasmids. *J Gene Med*, *3*(2), 153–164.

Pooga, M., Hallbrink, M., Zorko, M., & Langel, U. (1998). Cell penetration by transportan. *Faseb J*, *12*(1), 67–77.

Pozzi, D., Lisi, A., De Ros, I., Ferroni, L., Giuliani, A., Ravagnan, G., et al. (1993). Use of octadecylrhodamine fluorescence dequenching to study vesicular stomatitis virus fusion with human aged red blood cells. *Photochem Photobiol*, *57*(3), 426–430.

Preston, T. J., Abadi, A., Wilson, L., & Singh, G. (2001). Mitochondrial contributions to cancer cell physiology: potential for drug development. *Adv Drug Deliv Rev*, *49*(1–2), 45–61.

Ragin, A. D., Morgan, R.A., & Chmielewski, J. (2002). Cellular import mediated by nuclear localization signal Peptide sequences. *Chem Biol*, *9*(8), 943–948.

Reynolds, G. C., Baker, H. J., & Reynolds, R. H. (1978). Enzyme replacement using liposome carriers in feline Gm1 gangliosidosis fibroblasts. *Nature*, *275*(5682), 754–755.

Rideout, D., Bustamante, A., & Patel, J. (1994). Mechanism of inhibition of FaDu hypopharyngeal carcinoma cell growth by tetraphenylphosphonium chloride. *Int J Cancer*, *57*(2), 247–253.

Rojas, M., Donahue, J. P., Tan, Z., & Lin, Y. Z. (1998). Genetic engineering of proteins with cell membrane permeability. *Nat Biotechnol*, *16*(4), 370–375.

Ross, M. F., Filipovska, A., Smith, R. A., Gait, M. J., & Murphy, M. P. (2004). Cell-penetrating peptides do not cross mitochondrial membranes even when conjugated to a lipophilic cation: evidence against direct passage through phospholipid bilayers. *Biochem J*, *383*(pt 3), 457–458.

Roth, J. A., Swisher, S. G., Merritt, J. A., Lawrence, D. D., Kemp, B. L., Carrasco, C. H., et al. (1998). Gene therapy for non-small cell lung cancer: a preliminary report of a phase I trial of adenoviral p53 gene replacement. *Semin Oncol*, *25*(3 Suppl 8), 33–37.

Rothbard, J. B., Jessop, T. C., Lewis, R. S., Murray, B. A., & Wender, P. A. (2004). Role of membrane potential and hydrogen bonding in the mechanism of translocation of guanidinium-rich peptides into cells. *J Am Chem Soc*, *126*(31), 9506–9507.

Rothbard, J. B., Jessop, T. C., & Wender, P. A. (2005). Adaptive translocation: the role of hydrogen bonding and membrane potential in the uptake of guanidinium-rich transporters into cells. *Adv Drug Deliv Rev*, *57*(4), 495–504.

Roux, E., Francis, M., Winnik, F. M., & Leroux, J. C. (2002). Polymer based pH-sensitive carriers as a means to improve the cytoplasmic delivery of drugs. *Int J Pharm*, *242*(1–2), 25–36.

Roux, E., Passirani, C., Scheffold, S., Benoit, J. P., & Leroux, J. C. (2004). Serum-stable and long-circulating, PEGylated, pH-sensitive liposomes. *J Control Release*, *94*(2–3), 447–451.

Roux, E., Stomp, R., Giasson, S., Pezolet, M., Moreau, P., & Leroux, J. C. (2002). Steric stabilization of liposomes by pH-responsive N-isopropylacrylamide copolymer. *J Pharm Sci*, *91*(8), 1795–1802.

Rubas, W., Supersaxo, A., Weder, H. G., Hartmann, H. R., Hengartner, H., Schott, H., et al. (1986). Treatment of murine L1210 lymphoid leukemia and melanoma B16 with lipophilic cytosine arabinoside prodrugs incorporated into unilamellar liposomes. *Int J Cancer*, *37*(1), 149–154.

Rudolph, C., Schillinger, U., Ortiz, A., Tabatt, K., Plank, C., Muller, R. H., et al. (2004). Application of novel solid lipid nanoparticle (SLN)-gene vector formulations based on a dimeric HIV-1 TAT-peptide in vitro and in vivo. *Pharm Res*, *21*(9), 1662–1669.

Sakurai, F., Inoue, R., Nishino, Y., Okuda, A., Matsumoto, O., Taga, T., et al. (2000). Effect of DNA/liposome mixing ratio on the physicochemical characteristics, cellular uptake and intracellular trafficking of plasmid DNA/cationic liposome complexes and subsequent gene expression. *J Control Release*, *66*(2–3), 255–269.

Salem, A. K., Searson, P. C., & Leong, K. W. (2003). Multifunctional nanorods for gene delivery. *Nat Mater*, *2*(10), 668–671.

Sawant, R. M., Hurley, J. P., Salmaso, S., Kale, A., Tolcheva, E., Levchenko, T. S., et al. (2006). "SMART" drug delivery systems: double-targeted pH-responsive pharmaceutical nanocarriers. *Bioconjug Chem*, *17*(4), 943–949.

Scheule, R. K., St George, J. A., Bagley, R. G., Marshall, J., Kaplan, J. M., Akita, G. Y., et al. (1997). Basis of pulmonary toxicity associated with cationic lipid-mediated gene transfer to the mammalian lung. *Hum Gene Ther*, *8*(6), 689–707.

Schwarze, S. R., & Dowdy, S. F. (2000). In vivo protein transduction: intracellular delivery of biologically active proteins, compounds and DNA. *Trends Pharmacol Sci*, *21*(2), 45–48.

Schwarze, S. R., Hruska, K. A., & Dowdy, S. F. (2000). Protein transduction: unrestricted delivery into all cells? *Trends Cell Biol*, *10*(7), 290–295.

Senior, J. H. (1987). Fate and behavior of liposomes in vivo: a review of controlling factors. *Crit Rev Ther Drug Carrier Syst*, *3*(2), 123–193.

Shalaev, E. Y., & Steponkus, P. L. (1999). Phase diagram of 1,2-dioleoylphosphatidylethanolamine (DOPE):water system at subzero temperatures and at low water contents. *Biochim Biophys Acta*, *1419*(2), 229–247.

Sheff, D. (2004). Endosomes as a route for drug delivery in the real world. *Adv Drug Deliv Rev*, *56*(7), 927–930.

Simoes, S., Moreira, J. N., Fonseca, C., Duzgunes, N., & de Lima, M. C. (2004). On the formulation of pH-sensitive liposomes with long circulation times. *Adv Drug Deliv Rev*, *56*(7), 947–965.

Smith, R. A., Porteous, C. M., Coulter, C. V., & Murphy, M. P. (1999). Selective targeting of an antioxidant to mitochondria. *Eur J Biochem*, *263*(3), 709–716.

Smith, R. A., Porteous, C. M., Gane, A. M., & Murphy, M. P. (2003). Delivery of bioactive molecules to mitochondria in vivo. *Proc Natl Acad Sci USA*, *100*(9), 5407–5412.

Sperl, W. (1997). [Diagnosis and therapy of mitochondriopathies]. *Wien Klin Wochenschr*, *109*(3), 93–99.

Stanimirovic, D. B., Markovic, M., Micic, D. V., Spatz, M., & Mrsulja, B. B. (1994). Liposome-entrapped superoxide dismutase reduces ischemia/reperfusion 'oxidative stress' in gerbil brain. *Neurochem Res*, *19*(12), 1473–1478.

Steger, L. D., & Desnick, R. J. (1977). Enzyme therapy. VI: Comparative in vivo fates and effects on lysosomal integrity of enzyme entrapped in negatively and positively charged liposomes. *Biochim Biophys Acta*, *464*(3), 530–546.

Stroh, M., Zimmer, J. P., Duda, D. G., Levchenko, T. S., Cohen, K. S., Brown, E. B., et al. (2005). Quantum dots spectrally distinguish multiple species within the tumor milieu in vivo. *Nat Med*, *11*(6), 678–682.

Sudimack, J. J., Guo, W., Tjarks, W., & Lee, R. J. (2002). A novel pH-sensitive liposome formulation containing oleyl alcohol. *Biochim Biophys Acta*, *1564*(1), 31–37.

Tager, J. M., Daems, W. T., & Hooghwinkel, G. J. M. (1974). *Enzyme therapy in lysosomal storage diseases. Proceedings of the Workshop on Cell Biological and Enzymological Aspects of the Therapy of Lysosomal Storage Diseases, Leiden, The Netherlands, April 2–3, 1974 and Papers presented at a Boerhaave Advanced Course on Lysosomal Enzymopathies, Leiden, The Netherlands, April 4–5, 1974*. Amsterdam: North-Holland Pub. Co., New York American Elsevier Pub. CO.

Tang, F., & Hughes, J. A. (1999). Use of dithiodiglycolic acid as a tether for cationic lipids decreases the cytotoxicity and increases transgene expression of plasmid DNA in vitro. *Bioconjug Chem*, *10*(5), 791–796.

Tkachenko, A. G., Xie, H., Liu, Y., Coleman, D., Ryan, J., Glomm, W. R., et al. (2004). Cellular trajectories of peptide-modified gold particle complexes: comparison of nuclear localization signals and peptide transduction domains. *Bioconjug Chem*, *15*(3), 482–490.

Torchilin, V. P. (1985). Liposomes as targetable drug carriers. *Crit Rev Ther Drug Carrier Syst*, *2*(1), 65–115.

Torchilin, V. P. (2005). Recent advances with liposomes as pharmaceutical carriers. *Nat Rev Drug Discov*, *4*(2), 145–160.

Torchilin, V. P. (Ed.). (1991). *Immobilized enzymes in medicine*. Berlin, New York: Springer-Verlag.

Torchilin, V. P., Khaw, B. A., & Weissig, V. (2002). Intracellular targets for DNA delivery: nuclei and mitochondria. *Somat Cell Mol Genet*, *27*(1–6), 49–64.

Torchilin, V. P., Levchenko, T. S., Lukyanov, A. N., Khaw, B. A., Klibanov, A. L., Rammohan, R., et al. (2001). p-Nitrophenylcarbonyl-PEG-PE-liposomes: fast and simple attachment of specific ligands, including monoclonal antibodies, to distal ends of PEG chains via p-nitrophenylcarbonyl groups. *Biochim Biophys Acta*, *1511*(2), 397–411.

Torchilin, V. P., Levchenko, T. S., Rammohan, R., Volodina, N., Papahadjopoulos-Sternberg, B., & D'Souza, G. G. (2003). Cell transfection in vitro and in vivo with nontoxic TAT peptide-liposome-DNA complexes. *Proc Natl Acad Sci U S A*, *100*(4), 1972–1977.

Torchilin, V. P., Narula, J., Halpern, E., & Khaw, B. A. (1996). Poly(ethylene glycol)-coated anti-cardiac myosin immunoliposomes: factors influencing

targeted accumulation in the infarcted myocardium. *Biochim Biophys Acta*, *1279*(1), 75–83.

Torchilin, V. P., Rammohan, R., Weissig, V., & Levchenko, T. S. (2001). TAT peptide on the surface of liposomes affords their efficient intracellular delivery even at low temperature and in the presence of metabolic inhibitors. *Proc Natl Acad Sci USA*, *98*(15), 8786–8791.

Torchilin, V. P., Trubetskoy, V. S., Milshteyn, A. M., Canillo, J., Wolf, G. L., Papisov, M. I., et al. (1994). Targeted delivery of diagnostic agents by surface-modified liposomes. *J. Controlled Release*, *28*, 45–58.

Torchilin, V. P., & Weissig, V. (2000). Polymeric micelles for delivery of poorly soluble drugs. In K. Park & R. J. Mrsny (Eds.), *Controlled drug delivery : designing technologies for the future* (pp. 297–313). Washington, D.C: American Chemical Society.

Torchilin, V. P., Zhou, F., & Huang, L. (1993). pH-Sensitive liposomes. *J Liposome Res*, *3*, 201–255.

Tseng, Y. L., Liu, J. J., & Hong, R. L. (2002). Translocation of liposomes into cancer cells by cell-penetrating peptides penetratin and tat: a kinetic and efficacy study. *Mol Pharmacol*, *62*(4), 864–872.

Umezawa, F., Eto, Y., Tokoro, T., Ito, F., & Maekawa, K. (1985). Enzyme replacement with liposomes containing beta-galactosidase from Charonia lumpas in murine globoid cell leukodystrophy (twitcher). *Biochem Biophys Res Commun*, *127*(2), 663–667.

Verlander, J. W., Madsen, K. M., Larsson, L., Cannon, J. K., & Tisher, C. C. (1989). Immunocytochemical localization of intracellular acidic compartments: rat proximal nephron. *Am J Physiol*, *257*(3 Pt 2), F454–F462.

Vives, E., Brodin, P., & Lebleu, B. (1997). A truncated HIV-1 Tat protein basic domain rapidly translocates through the plasma membrane and accumulates in the cell nucleus. *J Biol Chem*, *272*(25), 16010–16017.

Wadia, J. S., Stan, R. V., & Dowdy, S. F. (2004). Transducible TAT-HA fusogenic peptide enhances escape of TAT-fusion proteins after lipid raft macropinocytosis. *Nat Med*, *10*(3), 310–315.

Wallace, D. C. (1999). Mitochondrial diseases in man and mouse. *Science*, *283*(5407), 1482–1488.

Wang, J., Mongayt, D., & Torchilin, V. P. (2005). Polymeric micelles for delivery of poorly soluble drugs: preparation and anticancer activity in vitro of paclitaxel incorporated into mixed micelles based on poly(ethylene glycol)-lipid conjugate and positively charged lipids. *J Drug Target*, *13*(1), 73–80.

Weissig, V., Lasch, J., Erdos, G., Meyer, H. W., Rowe, T. C., & Hughes, J. (1998). DQAsomes: a novel potential drug and gene delivery system made from Dequalinium. *Pharm Res*, *15*(2), 334–337.

Weissig, V., & Torchilin, V. P. (2000). Mitochondriotropic cationic vesicles: a strategy towards mitochondrial gene therapy. *Curr Pharm Biotechnol*, *1*(4), 325–346.

Weissig, V., & Torchilin, V. P. (2001). Cationic bolasomes with delocalized charge centers as mitochondria-specific DNA delivery systems. *Adv Drug Deliv Rev*, *49*(1–2), 127–149.

Wu, G. Y., & Wu, C. H. (1987). Receptor-mediated in vitro gene transformation by a soluble DNA carrier system. *J Biol Chem*, *262*(10), 4429–4432.

Wunderbaldinger, P., Josephson, L., & Weissleder, R. (2002). Tat peptide directs enhanced clearance and hepatic permeability of magnetic nanoparticles. *Bioconjug Chem*, *13*(2), 264–268.

Xu, Y., & Szoka, F. C., Jr. (1996). Mechanism of DNA release from cationic liposome/DNA complexes used in cell transfection. *Biochemistry*, *35*(18), 5616–5623.

Yessine, M. A., & Leroux, J. C. (2004). Membrane-destabilizing polyanions: interaction with lipid bilayers and endosomal escape of biomacromolecules. *Adv Drug Deliv Rev*, *56*(7), 999–1021.

Yuan, F., Dellian, M., Fukumura, D., Leunig, M., Berk, D. A., Torchilin, V. P., et al. (1995). Vascular permeability in a human tumor xenograft: molecular size dependence and cutoff size. *Cancer Res*, *55*(17), 3752–3756.

Zalipsky, S., Qazen, M., Walker, J. A., 2nd, Mullah, N., Quinn, Y. P., & Huang, S. K. (1999). New detachable poly(ethylene glycol) conjugates: cysteine-cleavable lipopolymers regenerating natural phospholipid, diacyl phosphatidylethanolamine. *Bioconjug Chem*, *10*(5), 703–707.

Zhang, J. X., Zalipsky, S., Mullah, N., Pechar, M., & Allen, T. M. (2004). Pharmaco attributes of dioleoylphosphatidylethanolamine/cholesterylhemisuccinate liposomes containing different types of cleavable lipopolymers. *Pharmacol Res*, *49*(2), 185–198.

Zhao, M., Kircher, M. F., Josephson, L., & Weissleder, R. (2002). Differential conjugation of tat peptide to superparamagnetic nanoparticles and its effect on cellular uptake. *Bioconjug Chem*, *13*(4), 840–844.

Zorko, M., & Langel, U. (2005). Cell-penetrating peptides: mechanism and kinetics of cargo delivery. *Adv Drug Deliv Rev*, *57*(4), 529–545.

Zuhorn, I. S., & Hoekstra, D. (2002). On the mechanism of cationic amphiphile-mediated transfection. To fuse or not to fuse: is that the question? *J Membr Biol*, *189*(3), 167–179.

Part III

Nanotechnology for the Delivery of Small Molecules, Proteins and Nucleic Acids

12

Nano-sized Advanced Delivery Systems as Parenteral Formulation Strategies for Hydrophobic Anti-cancer Drugs

Patrick Lim Soo, Michael Dunne, Jubo Liu, and Christine Allen

Introduction

An estimated 40% of the new drug candidates that are emerging through efforts in drug discovery are hydrophobic or lipophilic in nature (Hite et al., 2003). In addition to the low aqueous solubility of these compounds, many are plagued with unfavorable pharmacokinetics, poor biodistribution profiles and/or toxicity issues that prevent full exploitation of their therapeutic potential (Strickley, 2004; Danson et al., 2004). Conventional formulations and advanced delivery systems have been employed as strategies to move these molecules forward from bench to market.

There are several conventional excipients that are commonly used to prepare injectable formulations of hydrophobic drugs including non-ionic surfactants (e.g., polyethoxylated castor oil, polysorbate 80), water-soluble organic solvents (e.g., ethanol, polyethylene glycol 400, polypropylene glycol), cyclodextrins and phospholipids as outlined in Strickley's review (Strickley, 2004). These conventional formulations have successfully facilitated the clinical use of a large number of hydrophobic compounds including carmustine (BiCNU®), docetaxel (Taxotere®), etoposide (VePesidv®), fulvestrant (Faslodex®) and paclitaxel (PTX, Taxol®). Despite the success of conventional formulations, there are several limitations associated with their use including the inherent toxicity of many excipients, their limited solubilization capacity for hydrophobic drugs and/or rapid dissociation of the drug from the formulation components following administration. Specifically, the use of many conventional excipients has been reported to cause adverse effects such as inflammation and pain upon injection (Brazeau et al., 1998) as well as other side effects (e.g., nephrotoxicity, neurotoxicity) following administration. Therefore, there are dose limitations associated with most of the conventional excipients (Strickley, 2004; Reed et al., 1985; Fu et al., 1987; Bartsch, 1976; Montaguti, 1994). For example, polysorbate 80 and Cremophor EL® have been found clinically to be associated with significant side effects including peripheral nephrotoxicity and acute hypersensitivity reactions (van Zuylen, 2001; Sparreboom, 1999). Parenteral administration of cyclodextrins has also been reported to be associated with toxic effects

M.M. de Villiers et al. (eds.), *Nanotechnology in Drug Delivery*, DOI: 10.1007/978-0-387-77667-5_12,

including nephrotoxicity and loss of body, liver, as well as kidney weight (Frank et al., 1976). The solubilization capacity of these excipients for hydrophobic drugs can also be quite limited and result in precipitation of the drug upon the dilution that occurs following intravenous (i.v.) administration (Panchagnula, 1998). For example, the commercially available formulation of docetaxel, Taxotere®, must be diluted in 0.9% sodium chloride or 5% dextrose to obtain a concentration range of 0.3–0.8 mg/mL prior to administration (Sanofi-Aventis) (Thiesen and Kramer, 1999). Similarly, the PTX concentration in Taxol® (Bristol-Myers Squibb Company) is diluted with saline or 5% dextrose to obtain a final concentration of 0.3–1.2 mg/mL prior to use (Guchelaar et al., 1994). Consequently, in order to administer clinically relevant doses of drug, infusions are required over a 2- to 3-hour period which in turn necessitates hospitalization of the patient. Also, following i.v. administration, drugs tend to dissociate quite rapidly from the components of conventional formulations. For example, it has been found that 30 minutes following i.v. administration of Taxol® (i.e., 50% polyoxyethylated castor oil and 50% ethanol) more than 97% of the PTX is released from the vehicle and bound to plasma protein (Ramaswamy et al., 1997). Therefore, although conventional excipients provide a relatively simple, straightforward and economical means of formulating a drug, they primarily function to increase the apparent aqueous solubility of the drug and often only provide modest alterations in the pharmacokinetics and biodistribution profiles. Also, conventional formulations do not provide site-specific delivery of the drug to the diseased site.

Advanced drug delivery systems have been developed as strategies to overcome many of the obstacles that are associated with conventional formulations. In addition, these advanced systems have been designed with the objective of developing "magic bullets" that provide site-specific delivery of the drug to the target or diseased site (Ehlrich, 1906). A vast array of nano-sized delivery systems have been put forth and these are largely formed from polymer and lipid materials. The lipid-based systems include liposomes, poly(ethylene glycol) (PEG)–lipid micelles, lipid–drug complexes and lipid bilayer discs, while the polymer-based delivery vehicles comprise nanoparticles, nanospheres, polymer–drug conjugates, block copolymer micelles, block copolymer vesicles (Discher and Eisenberg, 2002; Lim Soo, Eisenberg, 2004) as well as others (Choucair and Eisenberg, 2003). In addition, various polymer–lipid hybrid systems have emerged including polymer–lipid micelles (Vakil and Kwon, 2006) and nanoparticles (Wong et al., 2006) In this way, the colloidal systems have been formed from various natural and synthetic lipids (e.g., 1,2-dipalmitoyl-*sn*-glycero-3-phosphocholine (DPPC), 1,2-distearoyl-*sn*-glycero-3-phosphoethanolamine (DSPE), egg phosphatidylcholine (ePC), PEG–lipid derivatives) as well as hydrophilic homopolymers (e.g., PEG, *N*-(2-hydroxypropyl) methacrylamide HPMA), hydrophobic homopolymers (e.g., poly(caprolactone) PCL, poly(lactide) PLA, poly(glycolic acid) PGA), random copolymers (e.g., poly(lactide)-*co*-(glycolide)) PLGA, graft copolymers, block copolymers, polyethylene glycol-*b*-poly(lactide) PEG-*b*-PLA, polyethylene glycol-*b*-poly(caprolactone) PEG-*b*-PCL) and copolymers of other architectures (e.g., star copolymer). Many of these materials have been demonstrated to be biocompatible with low toxicity profiles, in comparison to the

conventional excipients listed above (Kim et al., 2001; Le Garrec et al., 2004; Uchino et al. 2005). These materials also vary in terms of physical and chemical properties and thus they can be used to prepare colloidal systems that are suitable for delivery of a vast array of compounds. For example, optimization of the compatibility/miscibility between the drug and the delivery vehicle-forming material (Liu et al., 2004) has been shown to provide up to a 30,000-fold increase in the apparent aqueous solubility of the drug (Le Garrec et al., 2004; Liu et al., 2005; Liu et al. 2006).

Another important attribute of the colloidal systems is their hydrodynamic diameter, which is typically about 3–20 nm for polymer–drug conjugates (Duncan et al., 2006) and between 10 and 200 nm for colloidal particles such as micelles or liposomes. The colloidal nature or size of these vehicles can facilitate their retention within the circulation for prolonged periods, in comparison to low molecular weight small molecules. A prolonged retention time in the circulation may permit passive targeting to inflamed or leaky tissue, such as tumors, via the enhanced permeation and retention (EPR) effect (Matsumura and Maeda, 1986). The EPR effect may be described as the accumulation of macromolecules or particles at a tumor site due to both leaky vasculature and a reduction in the tendency for return to the circulation via the lymphatic system, in comparison to normal tissue. In this way, the EPR effect provides a means of enhancing accumulation of colloidal particles at solid tumors (Maeda and Matsumura, 1989). Therefore, if the drug can be retained with the vehicle, the colloidal system can specifically deliver the drug to tumors and thereby increase the efficacy of the drug and/or decrease systemic toxicity. Exploitation of the EPR effect has been shown to allow colloidal delivery systems to increase the tumor accumulation of drug (Kwon et al., 1994; Hamaguchi et al., 2005).

This chapter is focused on reviewing three of the advanced drug delivery strategies, shown in Scheme 12.1, that have resulted in the successful translation of active compounds into i.v. injectable drugs that are currently in clinical trial development or approved for treatment. Specifically, block copolymer micelles, polymer–drug conjugates and liposomes are reviewed in terms of their composition, relevant physico-chemical properties, biological performance and clinical success attained to date. A review of the patent and publication literature between 1970 and 2007, using the Scopus™ database (Elsevier B.V.), revealed that indeed liposomes have been the most well documented of these technologies with a total of 95,082 citations, while polymer–drug conjugate systems had a total of 30,979 citations and block copolymer micelles had 7453. This is in agreement with the fact that the first liposome-based therapy was approved for treatment of AIDS-related Kaposi's sarcoma in 1995; while the first polymer–drug conjugate systems only entered clinical trials in the early 1990s and the first drug relying on formulation in block copolymer micelles entered clinical evaluation in 2000 (Duncan, 2006). Therefore, liposomes are the most well established of the advanced drug delivery systems to be discussed in this chapter yet the polymer-based systems are well on their way to proving themselves as viable formulation strategies. This chapter provides an overview of these three systems while more

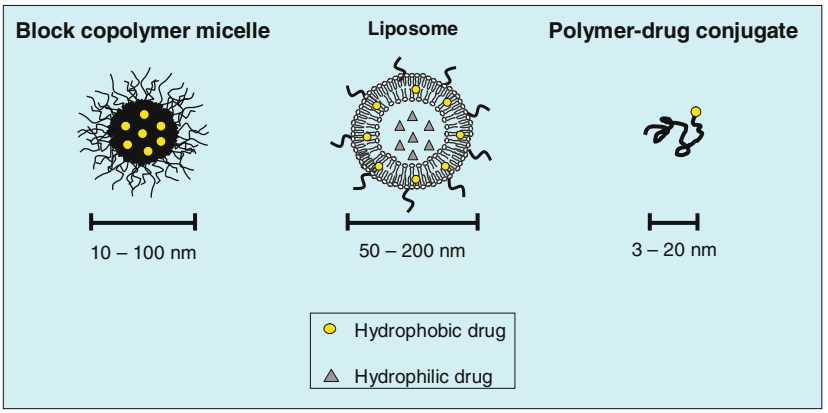

Scheme 12.1 Illustrations of the three advanced drug delivery technologies discussed in this chapter. (*See* Color Plate 17)

comprehensive reviews of each distinct system and various aspects of drug delivery are referred to throughout.

Block Copolymer Micelles

One of the first articles written about the use of block copolymers in drug delivery was by Ringsdorf and his group (Bader, 1984). Their initial work was on the use of micelle-forming block copolymer conjugates. Specifically, Ringsdorf proposed the covalent attachment of drug to the hydrophobic block of the amphiphilic copolymer (Kabanov and Alakhov, 2000). In the late 1980s, the first non-covalent incorporation of drugs into block copolymer micelles was reported by Kabanov and his group (Kabanov et al., 1989). This was also the first time that block copolymer micelles were used in vivo for drug delivery experiments (Kabanov and Alakhov, 2000).

Amphiphilic block copolymers, for drug delivery, are most commonly linear diblock and triblock copolymers. In aqueous media, the amphiphilic diblock copolymers self-assemble into nano-sized micelles with a hydrophobic core surrounded by a hydrophilic corona. The hydrophobic core of the micelle serves to solubilize or entrap hydrophobic drugs while the hydrophilic block forms a hydrated corona that stabilizes the micelle. The hydrophobic block of the diblock copolymers has most often been a poly(amino acid), poly(ester) or poly(ether). Recently, new hydrophobic blocks have been utilized such as modified poly(esters) (Trimaille et al., 2006), polycarbonates (Liu et al., 2005) and poly(allyl glycidyl ether) (Hruby et al., 2005). In terms of the hydrophilic component of the copolymers, it is usually PEG (Allen et al., 1999). Recently, other polymers have been used as the hydrophilic component, for example, poly(*N*-vinyl-2-pyrrolidone) was employed by both Leroux's group (Benahmed et al., 2001) and Cho's group (Chung et al., 2004), poly(2-ethyl-2 oxazoline) by Kim's group (Kim et al., 2002) and poly(vinyl alcohol) substituted with oleic acid was used by Zecchi's group (Luppi et al., 2002; Luppi et al., 2005). For triblock copolymer micelles, the poly(ethylene

oxide)-*b*-poly(propylene oxide)-*b*-poly(ethylene oxide) copolymers, known as Pluronics®, are used most extensively (Kabanov et al., 2002a).

Several different methods may be employed for micelle preparation depending on the solubility of the copolymer in aqueous media and the properties of the drug to be encapsulated. The method commonly employed for loading drugs into micelles that are formed from copolymers that are relatively soluble in water (e.g., Pluronics®) is termed the "direct dissolution method" (Kabanov et al., 2002b). In this method, the drug and the copolymers are directly dissolved in distilled water or buffer. The drug is then loaded into the micelles by stirring, heating and/or sonicating the mixture. Various drugs including doxorubicin (DOX), nystatin, etoposide and haloperidol have been successfully loaded into Pluronic® micelles using this method (Batrakova et al., 1999; Croy and Kwon, 2004). The dialysis method involves the dissolution of both the drug and the copolymers in a good solvent (e.g., organic), followed by dialysis against another solvent (e.g., water) (Allen et al., 1999). This process allows for the slow removal of the organic solvent and subsequent micelle formation. Indomethacin, clonazepam, amphotericin B, papaverine and DOX have been successfully incorporated into micelles using the dialysis method (La et al., 1996; Nah et al., 1998; Lavasanifar et al., 2001; Lee et al., 2004; Liu et al., 2005). The dry-down or evaporation method is most commonly employed for preparation of micelles from copolymers that have fairly low aqueous solubility (Lim Soo et al., 2002). In this method, a thin film of polymer and drug is produced by evaporation of an organic solvent that is suitable for both. An aqueous solution is then added while mixing to produce the micelles. Using this method, a number of different drugs have been successfully loaded including adriamycin, neurotrophic agents (FK506, L-685,818), dihydrotestosterone, indomethacin, amphotericin B, ellipticine, estradiol, cyclosporine A and fenofibrate (Liu et al., 2004; Lavasanifar et al., 2001; Yokoyama et al., 1998; Fukushima et al., 1999; Allen et al., 1998; Allen et al., 2000; Lin et al., 2003; Lim Soo et al., 2005; Aliabadi et al., 2005; Jette et al., 2004). In addition, Leroux's group recently reported a new method for drug encapsulation into micelle systems (Le Garrec et al., 2004; Fournier et al., 2004). Specifically, the drug and copolymers are first dissolved in a mixture of water and a solvent that is approved for use in parenteral formulations (e.g., *tert*-butanol, dimethyl acetamide). The solvent mixture is then freeze-dried and the dried powder is resuspended in water or buffer prior to use. Using this method, a variety of agents including PTX, docetaxel, teniposide and etoposide have been effectively encapsulated into micelles (Le Garrec et al., 2004; Fournier et al., 2004).

To further optimize micelle-based drug delivery systems, a thorough understanding of the relationship between the properties of the copolymers involved, characteristics of the micelle formulation and their biological performance is essential. Scheme 12.2 includes an illustration of the main properties of copolymers that have been found to control the physico-chemical characteristics of micelles and consequently play an important role in determining their biological performance.

Kataoka's research has demonstrated the importance of using well-characterized, pure copolymers that have a homogeneous composition and a low degree of polydispersity. In their study, a mono-modal sized

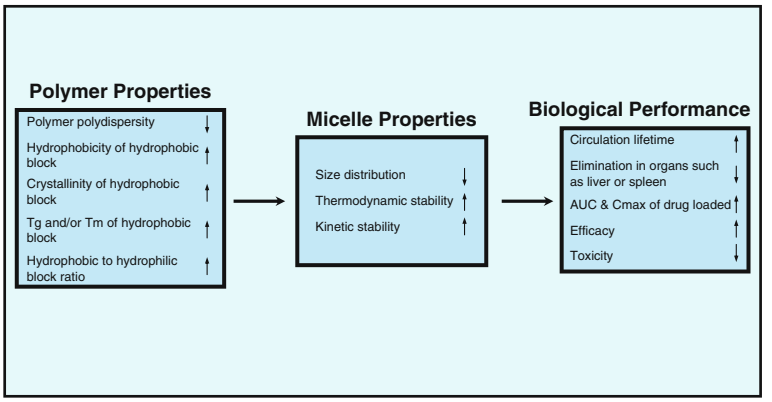

Scheme 12.2 Correlation between the properties of block copolymers, physico-chemical characteristics of micelles and their biological performance as drug delivery vehicles.

population of micelles (d = 30 nm) with a narrow size distribution was prepared from PLA-*b*-PEG synthesized by sequential anionic polymerization (Yasugi et al., 1999). The "living" polymerization synthetic technique has been employed to prepare various block copolymers with defined block lengths and a low polydispersity index (i.e., PI < 1.1) for each block (Hsieh and Quirk, 1996). The PLA-*b*-PEG micelles achieved a longer circulation half-life, with 25% of the total injected dose remaining in plasma for 24 hours post-administration, as well as limited accumulation of the micelles in the liver and spleen (Yamamoto et al., 2001). The half-life of this micelle system is equal to or greater than most of the well-established, long-circulating liposome systems. The narrow degree of polydispersity of the acetal-PEG-*b*-PLA copolymers employed in this study was considered to be one of the factors responsible for extending the circulation half-life for this micelle system (Yamamoto et al., 2001).

Another critical factor that determines the biological performance of block copolymer micelles as delivery systems is their stability, which has also been demonstrated to be highly dependent on the composition of the micelle-forming materials. In an aqueous environment, the stability of micelles can be considered to include a thermodynamic and a kinetic component (Allen et al., 1999). The thermodynamic stability of a micelle system is dictated by the critical micelle concentration (CMC) of the copolymer. The CMC is defined as the concentration below which the copolymer exists only as single chains and above which the copolymer is assembled as micelles that are in equilibrium with a small population of single chains (Allen et al., 1999). The CMC of copolymers is known to largely depend on the properties of the core-forming block such as degree of hydrophobicity and length. Typically, a decrease in the hydrophobicity and/or length of the core-forming block results in an increase in the CMC. By selecting copolymers that have the optimal composition (i.e., appropriate block length and degree of hydrophobicity for the core-forming block), block copolymer micelles can be designed to have a greater degree of thermodynamic stability than typical small molecule surfactant micelles (Allen et al., 1999; Liu and Allen, 2003; Adams et al., 2003).

The kinetic stability of the micelle refers to the rate at which the micelle disassembles into single chains once the copolymer concentration falls below the CMC (Kwon and Okano, 1996). The kinetic stability is largely influenced by the physical state of the core (i.e., amorphous or semi-crystalline), which is also dependent on the thermal properties of the core-forming block (i.e., glass transition temperature and melting temperature). Studies have shown that both thermodynamic and kinetic stability are very important in determining the in vivo fate of micelles. Specifically, Kabanov's group studied the distribution kinetics of a triblock copolymer, Pluronic® P85, following administration via the tail vein in female C57/Bl/6 mice as micellar aggregates or single chains (Batrakova et al., 2004). Similar clearance rates were obtained for the triblock copolymer irrespective of its micellar or unimer form (Batrakova et al., 2004). Liu et al. also studied the in vivo fate of PEG-*b*-PCL micelles administered as thermodynamically stable micelles (i.e., concentration above CMC prior to and after i.v. injection) and unstable micelles (i.e., concentration above CMC prior to injection, but below CMC following injection due to dilution) (Liu et al., 2007). The in vivo fate of both groups of micelles was compared with that of single copolymer chains. Interestingly, it was found that the formation of micelles effectively entraps the copolymer within the plasma compartment, as demonstrated by a significantly longer circulation half-life for the intact micelles in comparison to that for the copolymer single chains (Liu et al., 2007). In the same study, thermodynamically unstable micelles were found to have a relatively long circulation half-life in plasma, in comparison to single copolymer chains, pointing to the influence that the kinetic stability of micelle systems can have on their biological fate (Liu et al., 2007).

To this point, it has been well established that a prolonged circulation half-life for colloidal particles results in increased accumulation in tissues (e.g., tumors) that have a high degree of vascular permeability due to the EPR effect (Papahadjopoulos et al., 1991; Baban and Seymour, 1998; Maeda, 2001). However, even with long-circulating systems, the pharmacokinetics and biodistribution of the encapsulated drug are only improved if the drug is retained within the delivery system following administration. Under conditions of thermodynamic equilibrium, hydrophobic drugs that are physically encapsulated in block copolymer micelles partition between the micelles and the external medium (La et al., 1996; Allen et al., 2000; Kwon et al., 1994). Following i.v. administration, micelles introduced into the circulation are exposed to a vast array of proteins, blood cells and other blood components. These proteins and blood components can serve as a reservoir for hydrophobic drugs that are entrapped within micelles. The drug can be "extracted" from the micelles, due to a high affinity for blood components, resulting in rapid drug release in vivo. As a result, the protein-bound drug will be cleared more rapidly from the circulation in comparison to micelle-loaded drug (Matsumura et al., 2004). In this connection, it has been shown that despite the extended circulation half-lives that some colloidal delivery systems may have, a significant amount of the drug is extracted from the delivery system and eliminated from the plasma, resulting in only marginal improvements in the circulation half-life of the drug (Liu et al. 2006). In the case of copolymer micelles, the in vivo release

profile of the encapsulated drug is largely determined by the compatibility between the drug and the core-forming block and the affinity of the drug for plasma protein (Ramaswamy et al., 1997; Liu et al., 2004; Liu et al., 2005; Seki et al., 2004). As a result, the competition between the microenvironment within the delivery system and the plasma components largely determines the drug release profile in vivo.

Several new in vitro release methods have been established and validated in order to facilitate a more accurate prediction of in vivo drug release profiles (Liu et al., 2005; Cho et al., 2004, Shabbits et al., 2002). In addition, emphasis has been placed on improving drug retention in micelle systems by maximizing the degree of miscibility and interaction between the drug and the core-forming block. Several successful examples have clearly demonstrated that a high degree of interaction between the drug and the core-forming block leads to a higher drug-loading capacity and improved drug retention. For example, Kwon's group has examined the conjugation of methotrexate (MTX) to PEG-*block*-poly(2-hydroxyethyl-L-aspartamide) copolymers as a means to increase the suitability of this system for delivery of MTX (Li and Kwon, 2000). It was found that conjugation of MTX to the copolymer decreased the CMC and resulted in the formation of more stable micelles (Li and Kwon, 2000). Also, Kwon et al. prepared PEG-*block*-poly(*N*-hexyl-L-aspartamide)-acyl conjugate micelles that included various acyl esters (Adams and Kwon, 2003). The length of the acyl side chains was found to have an influence on the aggregation of the drug amphotericin B in the micelles, and resulted in a lower degree of hemolytic activity for this drug (Adams and Kwon, 2003). Shuai et al. examined different PCL-*b*-PEG micelles loaded with DOX and found that three factors influenced the drug-loading content, namely, the crystallinity of the core, hydrophobicity of the core and the degree of hydrogen bonding interactions between PCL and DOX (Shuai et al., 2004). Specifically, a lower degree of crystallinity within the core was found to result in a more favorable degree of compatibility between the core and the drug (Shuai et al., 2004). In this study, an increase in micelle core size was shown to result in an increase in the degree of crystallinity of the core and as a result a decrease in drug loading. Micelles having smaller PCL cores, with their lower degree of crystallinity, were found to enable favorable hydrogen bonding interactions between the amino and hydroxyl groups of deprotonated DOX and carbonyl groups of the amorphous (non-crystalline) PCL (Shuai et al., 2004). Furthermore, two micelle formulations that are currently in clinical trials, namely NK911 (i.e., micelle formulation for DOX) and NK105 (i.e., micelle formulation for PTX), have micelle cores that have been modified in order to maximize the degree of core–drug compatibility.

Four of the micelle formulations that are in clinical development, namely SP1049C (for DOX), NK911 (for DOX), Genexol-PM (for PTX) and NK105 (for PTX), have been summarized in Scheme 12.3. Also, included in Scheme 12.3 is NanoPlatin (NC-6004) (for cisplatin) (Uchino et al., 2005); however, this will not be discussed in detail, since it is a formulation for a hydrophilic anti-cancer agent. As described in detail in the following section, these formulations for hydrophobic anti-cancer agents have demonstrated that block copolymer micelles can increase the

	Drug	Polymer	Highlights
SP1049C	Doxorubicin	**Pluronic ®** 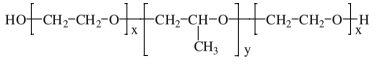 PEG PPO PEG **Pluronic L61:** X= 4.5 Y= 31 **Pluronic F127:** X= 200 Y= 65 1 : 8 (w/w)	▪ Presence of 0.01 % (w/v) Pluronic® L61 increases the cytotoxicity of DOX by 200 to 3500 fold in various multi-drug resistant cell lines compared to free DOX. ▪ 2.1 fold increase in AUC compared to free DOX at a dose of 10 mg/kg ▪ Potential indications include soft tissue sarcoma, acute leukemia, bone sarcoma, breast carcinoma, gynaecologic carcinoma, testicular carcinoma, Hodgkin's disease and gastric carcinoma. ▪ Clinical trial status: Phase II (Europe), Orphan drug status (US).
NK911	Doxorubicin & Polymer-DOX	**PEG-b-PAsp-Dox** 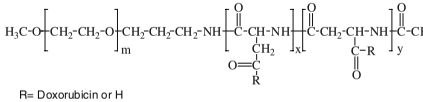 R= Doxorubicin or H	▪ Includes both PEG-b-PAsp-DOX and free DOX. ▪ $t_{1/2}$, AUC and plasma C_{max} were found to increase 2.5, 36.4 and 28.6 fold respectively compared to free DOX administered at the same dose. ▪ Improved efficacy and decreased toxicity of encapsulated DOX. ▪ Treatment for pancreatic cancer. ▪ Clinical trial status: Phase III (Japan)
Genexol-PM	Paclitaxel	**PEG-b-PLA** 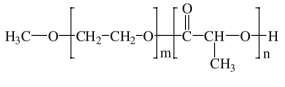	▪ Decreased AUC and $t_{1/2}$ for PTX in comparison to PTX administered as Taxol®. ▪ Good solubilizer. ▪ Increased the maximum tolerated dose of PTX to 390 mg/m^2 (135–200 mg/m^2 for Taxol®). ▪ Treatment against breast and non-small cell lung cancer. ▪ Clinical trial status: Phase II (US)/ Phase II (Korea)
NK105	Paclitaxel	**PEG-b-modified PAsp** 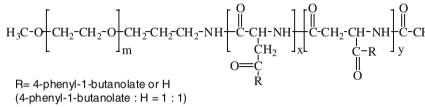 R= 4-phenyl-1-butanolate or H (4-phenyl-1-butanolate : H = 1 : 1)	▪ Increased AUC for PTX by 50-86 fold in comparison to PTX administered as Taxol®. ▪ Increased $t_{1/2}$ for PTX 4-6 fold in comparison to Taxol®. ▪ Treatment for gastrointestinal cancers. ▪ Clinical trial status: Phase II (Japan)
NanoPlatin (NC-6004)	Cisplatin	**PEG-b-PGlu** 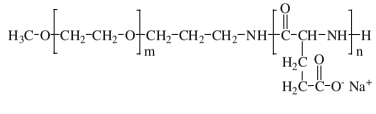	▪ *In vivo* efficacy of NC-6004 shown to be comparable to or greater than free cisplatin. ▪ Increased AUC for cisplatin by 65 fold in comparison to free cisplatin. ▪ Clinical trial status: Phase I (UK).

Scheme 12.3 Summary of block copolymer micelle formulations currently in clinical evaluation.

aqueous solubility, decrease the systemic toxicity and/or improve the therapeutic index of the encapsulated agents following i.v. administration (Hamaguchi et al., 2005; Matsumura et al., 2004; Nakanishi et al., 2001; Mizumura et al., 2001; Kim et al., 2004).

SP1049C is a micelle formulation of DOX that has been researched and developed by Kabanov's group and Supratek Pharma Inc. (Montreal, QC, Canada). It is composed of two copolymers, namely Pluronic® F127 and Pluronic® L61 in a ratio of 1:8 (wt/wt) (Alakhov et al., 1999). Each copolymer employed has a unique role in the formulation: F127 primarily serves to stabilize the formulation and L61 has a hypersensitization effect. Studies in nine animal models have shown that treatment with SP1049C has superior anti-tumor efficacy when compared to the conventional formulation of DOX (Alakhov et al., 1999). The ability of this formulation to hypersensitize multidrug-resistant tumor cells has also been demonstrated. Specifically, following treatment with DOX in the presence of 0.01% w/v copolymer (i.e., Pluronic® L61), a significant increase in sensitivity was observed in multidrug-resistant cell lines (i.e., MCF-7/ADR: 740-fold, SKOVLB: 1020-fold, B16F10: 2082-fold, SP2/ Dox: 203-fold, LoVo/ Dox: 3500-fold) (Alakhov et al., 1999). This is considered to be a significant advantage for this DOX formulation particularly for the treatment of resistant disease. In addition, SP1049C has been shown to modify the pharmacokinetics profile of DOX. Specifically, at a dose of 10 mg/kg, the area under the plasma concentration–time curve (AUC) in healthy C57BL/6 mice was found to be 14.6 μg·h/mL providing a 2.1-fold increase in the AUC compared to that for free DOX administered at a similar dose (Alakhov et al., 1999). Currently, SP1049C is completing Phase II clinical trials in Europe and clinical studies have shown that this formulation is effective for patients suffering from Stage IV non-resectable adenocarcinoma of the esophagus (Supratek Pharma Inc.). In 2005, the FDA granted orphan drug status (i.e., treatment for less than 200,000 people in the United States) to SP1049C for the treatment of carcinoma of the esophagus (Alakhov et al., 2006).

NK911 is another micelle formulation that is being developed for the delivery of DOX (Matsumura et al., 2004; Nakanishi et al., 2001). This formulation was first explored by Kataoka's group and is currently in Phase III clinical trial in Japan for the treatment of pancreatic cancer (Okusaka et al., 2004). NK911 includes both chemically conjugated and physically entrapped DOX within PEG-*block*-poly(aspartic acid) (PEG-*b*-PAsp) copolymer micelles ranging in size from 15 to 60 nm (Nishiyama and Kataoka, 2006). The conjugated drug does not contribute to the antitumor activity of the formulation, but rather acts to increase the hydrophobicity and maximize the core–drug compatibility which affords a higher drug-loading level and enhancement in formulation stability. DOX administered in the NK911 formulation in vivo in mice bearing colon 26 has been shown to have a prolonged circulation half-life (i.e., $t_{1/2} = 98$ hours) (Nakanishi et al., 2001). The change in the pharmacokinetic profile of the drug has been shown to translate into a significant increase in therapeutic efficacy, as evidenced in studies in mice bearing colon 26 and MX-1 tumors (Nakanishi et al., 2001). The NK911 system was able to increase accumulation of DOX at the tumor site due to the

EPR effect. In addition, even after administration of the highest dose of NK911 in all tumor models, the treatment resulted in less toxicity than with free drug. In Phase I clinical trials (2001), administration of the NK911 formulation at a dose of 50 mg/m^2 provided a significant increase in the half-life ($t_{1/2}$) and AUC as well as a decrease in the steady-state volume of distribution (V_{ss}) for this drug, in comparison to the conventional formulation. Specifically, in comparison to free DOX, the $t_{1/2}$, AUC and plasma C_{max} were found to increase 2.6-, 28.6- and 36.4-fold, respectively, after administration of the same dose (Nakanishi et al., 2001). This marked improvement in the biological performance has been attributed to the following micelle properties: small size, ability to retain the drug following administration and long circulation half-life.

Two additional successful examples of micelle formulations in clinical development are Genexol-PM and NK105. Genexol-PM is a PEG-*b*-poly(D,L-lactide) (PEG-*b*-PDLLA) micelle formulation for PTX that is devoid of the toxic excipient, Cremophor EL that is used in the commercially available formulation Taxol® (Kim et al., 2001). In nude mice, Genexol-PM was found to have a maximum tolerated dose (MTD) of 60 mg/kg compared to only 20 mg/kg for Taxol® (Kim et al., 2001). In SPF C57BL/6 mice, the biodistribution of PTX in the heart, liver, lungs, kidney, spleen and tumor were found to be 2- to 3-fold greater than that for Taxol® (Kim et al., 2001). When Genexol-PM was administered to patients at a dose of 135 mg/m^2, the AUC was 5473 ng·h/mL, this value is lower than the AUC (i.e., 9309 ng·h/mL) administered as Taxol® (Kim et al., 2004; Gianni et al., 1995). Therefore, the Genexol-PM formulation may be considered primarily as a solubilizer for PTX given that the drug appears to be released rapidly from the PEG-*b*-PDLLA micelles following administration. However, in humans, this micelle formulation significantly increased the MTD of PTX to 390 mg/m^2 compared to 135–200 mg/m^2 of PTX administered as Taxol® (Kim et al., 2004; Gianni et al., 1995). Samyang Corporation (Seoul, Korea) is developing Genexol-PM, which according to the company is undergoing Phase II trials in the United States for an unspecified cancer and currently completing three Phase II clinical trials for breast and non-small cell lung cancer in Korea (Samyang Corporation website).

NK105 was first developed by Kataoka and co-workers, in collaboration with NanoCarrier (Japan) and Nippon Kayaku (Japan) in 2005. It is a micelle formulation composed of PEG as the hydrophilic block and modified poly(aspartate) (PAsp) as the core-forming block for the delivery of PTX (Hamaguchi et al., 2005). The PAsp block was conjugated with 4-phenyl-1-butanol in order to increase interaction with PTX. As a result, the micelles have a drug-loading capacity of 23% (w/w) with a mean diameter of 85 nm. In preclinical studies, administration of the NK105 formulation resulted in significant improvements to the main pharmacokinetic parameters for PTX, in comparison to Taxol®. Specifically, the AUC of PTX in the NK105 formulation was increased by 50- to 86-fold and the $t_{1/2}$ was increased by 4- to 6-fold (Hamaguchi et al., 2005). The therapeutic efficacy of NK105 was investigated in a HT-29 colon cancer xenograft model. The results showed that the anti-tumor activity of NK105 administered at a PTX-equivalent dose of 25 mg/kg was

comparable to that obtained following treatment with Taxol® at a much higher PTX dose (i.e., 100 mg/kg). In addition, tumors were completely eliminated in all mice treated with 100 mg/kg of PTX in the NK105 dose group and all mice remained tumor-free for the duration of the study (Hamaguchi et al., 2005). This formulation was demonstrated to result in similar modifications to the pharmacokinetic profile of PTX in patients in the Phase I clinical trial and is now in Phase II evaluation (Jan 2007) (Kato et al., 2006).

Polymer–Drug Conjugates

Polymer–drug conjugates are a class of polymer therapeutics that consist of a water-soluble polymer that is chemically conjugated to a drug through a biodegradable linker. In 1975, Ringsdorf put forth the idea to use polymer–drug conjugates to deliver hydrophobic small molecules (Ringsdorf, 1975). The rationale for this strategy was primarily based upon the fact that small molecule drugs, especially hydrophobic compounds, commonly have a low aqueous solubility and a broad tissue distribution profile. Therefore, administration of the free drug can result in serious side effects. The conjugation of these compounds to hydrophilic, biocompatible polymers would significantly increase their aqueous solubility, modify their tissue distribution profile and enhance their plasma circulation half-life.

One of the significant differences between polymer–drug conjugates and delivery systems that contain physically entrapped drug (e.g., micelles and liposomes) is that the drug is chemically conjugated to the polymer and therefore these systems qualify as new chemical entities (NCE). Classification as an NCE is often accompanied by additional development and regulatory hurdles that must be met in order to receive approval.

Over the last 5 years, polymer-conjugate technology has seriously proven itself as a viable formulation strategy with the successful delivery of biomolecules. Specifically, the bioconjugation of protein and peptide to PEG has been shown to significantly improve the efficacy of these macromolecular drugs by increasing their stability in the presence of proteases and decreasing their immunogenicity (Harris and Chess, 2003; Veronese and Pasut, 2005; Parveen and Sahoo, 2006). Studies have also shown that by using PEG in a specific molecular weight range, the fast renal clearance and mononuclear phagocytic system (MPS) uptake of the drugs can be prevented or delayed leading to a prolonged plasma half-life for the conjugated molecules. Successful applications have led to several FDA-approved products (e.g., Zinostatin Stimalmer®, Oncaspar®, PEG-Intron™, PEGasys®, Neulasta™, etc.) with others in clinical trials (e.g., ADI-PEG20, PEG-PGA and DON, Prothecan™, etc.). The first practical use of polymer therapeutics that resulted in an FDA-approved anti-cancer treatment was the introduction of PEG-L-asparaginase (Oncaspar®) in 1994 (Graham, 2003). This conjugate is composed of PEG polymer (MW $\sim$ 5 kD) attached to the enzyme, L-asparaginase, and is used for the treatment of acute lymphoblastic leukemia (Graham, 2003). A significant increase in the plasma half-life of L-asparaginase has been observed using the PEGylation technique. Specifically, Oncaspar®

has a plasma half-life of 357 hours following i.v. administration (i.e., dose 500–8000 units/m^2 infused over 1 hour) compared to the unconjugated enzyme with a half-life of only about 20 hours (Ho et al., 1986). In addition, the conjugate required less frequent administration (i.e., once every 2 weeks versus 2–3 times per week for 4 weeks) and vastly reduced the degree of hypersensitivity reactions (Satchi-Fainaro et al., 2006). PEG has also been conjugated to biological response modifiers such as recombinant human granulocyte colony-stimulating factor (i.e., GCSF to produce Neulasta®) and interferon α (i.e., INFα to form PEG-Intron™ and PEGasys®) to improve their pharmacological effects. GCSF promotes the regeneration of white blood cells, which decrease dramatically after chemotherapy. Neulasta®, which includes GCSF conjugated to 20 kD PEG has a much longer plasma half-life than the native enzyme (i.e., median serum half-life of 42 hours compared to approximately 4 hours) (Molineux, 2004). As a supplementary treatment during chemotherapy, the PEGylated GCSF can be given as a single subcutaneous injection on the second day of each chemotherapy cycle, compared to the native GCSF that has to be administered daily for 2 weeks to obtain a similar effect (Duncan, 2003). In the case of INFα, this protein can be used for the treatment of hepatitis B and C, but can also be used for specific bladder cancers (Lam et al., 2003) and particular leukemias (Hauswirth et al., 2004). PEGasys® is composed of 40 kD branched PEG attached to INFα (Vicent, 2006). PEGasys® has been demonstrated to decrease the toxicity of INFα, while increasing the plasma half-life. Also, PEGasys® has been shown to be effective in the treatment of chronic hepatitis C (Fried et al., 2002). Other PEGylated protein systems such as PEGylated arginine deiminase (ADI-PEG20) and PEGylated glutaminase with 6-diazo-5-oxo-l-norleucine (PEG-PGA and DON) are currently in clinical trial development (Vicent, 2006; Shen and Shen, 2006).

There are several key criteria that should be considered when designing polymer-small molecule drug conjugates. Polymers that can be used for this purpose must be non-toxic and non-immunogenic in terms of both the intact polymers and their metabolites. The molecular weight of the polymer (typically 10–100 kD) needs to reach a specific cutoff if a prolonged circulation lifetime is required. If the polymer is non-biodegradable, then the molecular weight should be less than 40 kD in order to ensure elimination from the body by renal excretion (Duncan, 2006). In addition, these systems need a high enough drug to polymer ratio in order to deliver sufficient drug within the allowed total polymer dose. Finally, the linker that attaches the polymer to the drug must be designed such that it retains the drug prior to reaching the tumor site and releases the drug following arrival at this site. To date, there are four polymers that have been explored most extensively in the preparation of polymer–drug conjugates for anti-cancer therapy. These are *N*-(2-hydroxypropyl)methacrylamide (HPMA), PEG, poly(glutamic acid) (PGA) and dextran (Satchi-Fainaro et al., 2006). A summary of their drug conjugate development status is provided in Scheme 12.4.

HPMA has been explored since the 1980s for preparation of polymer–drug conjugates (Lammers et al., 2005). The optimal molecular weight for the HPMA copolymer has been determined to be 30,000 kD due to

Polymer	Drug	Name	Polymer MW (kD)	Cancer indication	Status
N-(2-hydroxypropyl) methacrylamide (HPMA)	Doxorubicin	PK1; FCE 28068	30	Non-small cell lung, breast	Phase III
	Doxorubicin-galactosamine	PK2; FCE 28069	25	Hepatocellular carcinoma	Phase I/II
	Paclitaxel	PNU 166945	30	Refractory solid tumors	Phase I
	Camptothecin	MAG-CPT; PNU 166148	30	Gastric and gastroesophageal tumors	Phase I
Poly-L-glutamic acid (PGA)	Paclitaxel	Xyotax®; CT-2103	49	Non-small cell lung, ovarian	Phase III
	Camptothecin	CT-2106	50	Various cancers	Phase I
Poly(ethylene glycol) (PEG)	Camptothecin	Prothecan™	40	Small cell lung Gastric and gastroesophageal tumors	Phase II
Dextran	Doxorubicin	AD-70; DOX-OXD	70	Refractory solid tumors	Phase I
Modified dextran	Camptothecin analog (DX8951)	DE-310	34	Refractory solid tumors, operable solid tumors	Phase I

Scheme 12.4 Summary of current polymer-small molecule drug conjugates in clinical evaluation.

its molecular weight-dependent circulation half-life in plasma and non-biodegradability (Duncan et al., 1981; Seymour et al., 1987). For most HPMA-based conjugates, an enzyme-degradable peptide linker (Gly-Phe-Leu-Gly) has been used due to its stability in plasma and susceptibility to cleavage by lysosomal proteases following internalization by endocytosis (Duncan et al., 1982). Due to the existence of multiple pendant groups on HPMA copolymers that may be used for drug conjugation, high drug to polymer ratios may be achieved with the optimal found to be 1:10 (w/w) (Duncan, 2006). This copolymer has been successfully conjugated to several drugs including doxorubicin (PK1, FCE28068 and PK2, FCE28069) (Vasey et al., 1999; Seymour et al., 2002), paclitaxel (PNU166945) (Meerum Terwogt et al., 2001) and camptothecin (MAG-CPT, PNU166148) (Wachters et al., 2004). Most of these polymer–drug conjugates are in various stages of clinical development (refer to Scheme 12.4). The use of this copolymer has effectively improved drug solubility, increased circulation times and resulted in enhanced tumor accumulation of the drug by taking advantage of the EPR effect.

Among HPMA-based polymer–drug conjugates, the most well studied is HPMA-Gly-Phe-Leu-Gly-DOX (PK1, FCE28068). In 1994, this polymer–drug conjugate (MW 30 kD) entered clinical trials and the results from the Phase I evaluation were very encouraging. The MTD was 4- to 5-fold greater than that for the conventional formulation of DOX, the circulation half-life of DOX was also prolonged significantly, and the liver accumulation was decreased (Vasey et al., 1999; Thomson et al., 1999). In addition, the polymer–drug conjugate was found to be eliminated mainly through the kidneys with 50–75% of the total injected dose cleared within 24 hours of administration (Vasey et al., 1999). Phase II evaluations revealed improved response from patients suffering from breast cancer and non-small cell lung cancer. Also, the HPMA-related toxicity or immunogenicity was

found to be quite negligible indicating that an even higher dose could be employed, if required. PK2 (galactosamine-HPMA-Gly-Phe-Leu-Gly-DOX) containing galactosamine as the targeting moiety to target the hepatocyte asialoglycoprotein receptor was primarily developed to treat liver cancer. It is an active targeting version of PK1 and is currently in Phase I/II clinical trials (Duncan et al., 2001). PK2 has been found to show efficacy against primary hepatocellular carcinoma (Seymour et al., 2002). Specifically, at least three patients are reported to have shown partial response to this treatment for periods of at least 26 months. The same study has also shown that 24 hours after administration, 16.9% ± 3.9% of the administered dose of DOX was targeted to the liver and 3.3% ± 5.6% of the dose was delivered to the tumor (Seymour et al., 2002). This specific accumulation was not observed with PK1, demonstrating tumor-specific delivery by the PK2 conjugate (Seymour et al., 2002).

PEG is another polymer that is utilized extensively to prepare polymer–drug conjugates. It is one of the most widely used hydrophilic polymers in protein delivery (Harris and Chess, 2003). PEG has been well characterized and shown to be non-toxic, non-immunogenic and approved by the FDA. The highly flexible and water-soluble PEG chains are capable of forming a "hydrophilic corona" to mask conjugated molecules (Veronese and Pasut, 2005). The current living polymerization techniques have enabled the synthesis of linear or branched PEG with molecular weights ranging from 5000 to 40,000 kD and narrow molecular weight distributions (PI $\sim$ 1.0). The narrow molecular weight distribution of the polymer ensures a uniform pharmacokinetic profile for all polymer–drug conjugates within a single sample. Due to the superior hydrophilicity and good biocompatibility of PEG as well as the success of PEG–protein conjugates, PEG conjugation has been explored as a delivery strategy for hydrophobic small molecules.

For example, Prothecan^{TM}, a PEGylated CPT has been evaluated in Phase II clinical trials for the treatment of various cancers (Greenwald et al., 2003). CPT is a prototypic DNA topoisomerase I inhibitor that has been screened by the National Cancer Institute. This drug has been shown to have significant cytotoxic activity against a wide range of murine and human leukemias and solid malignancies, as well as a lack of cross-resistance with available agents (Slichenmyer et al., 1993). The clinical potential of CPT has yet to be fully explored, due to its low aqueous solubility, adverse reactions and limited stability in the presence of human albumin. Specifically at physiological pH, in the absence of human albumin, 20% of CPT is present in the lactone form which is considered to be pharmacologically active. However, human serum albumin can rapidly shift the equilibrium to produce an inactive carboxylate form of the lactone ring, thus significantly decreasing the pharmacological activity of this compound. The toxicity of CPT has also been shown to be markedly schedule dependent, with a greater degree of cytotoxicity resulting from more frequent dosing schedules (Slichenmyer et al., 1993). Prothecan^{TM} was developed as a means to address many of these issues. Specifically, when PEG is chemically conjugated to the C-20-OH position of CPT, Prothecan^{TM} effectively creates an "inert" prodrug: CPT is locked in the active lactone configuration as a component of the acylated

PEG-CPT (Greenwald et al., 1996). In this way, by taking advantage of its high molecular weight and the EPR effect, the polymer–drug conjugate can improve active CPT accumulation at tumor sites and slowly release its drug payload in the pharmacologically active form, in an acidic environment. The plasma half-life of CPT was determined to be more than 72 hours, following conjugation, compared to the median half-life of only 22 hours for sodium CPT (Rowinsky et al., 2003). Also, a substantially lower and more biologically relevant C_{max} was achieved with Prothecan™ in comparison to that for sodium CPT, which results in a reduced overall toxicity profile for the drug and warrants future disease-directed clinical evaluation.

However, to date, even though some PEG–small molecule conjugates are currently in either preclinical or clinical evaluation, no PEG–small molecule conjugates have been FDA approved. The major shortcoming of PEG–small molecule systems is the limited polymer to drug ratio that may be achieved due to the lack of multiple drug conjugation sites on PEG and the high molecular weight that is required for this polymer in order to achieve an extended circulation lifetime. Specifically, Yamaoka et al. found that the renal clearance of PEG decreased when its molecular weight increased with the most dramatic change occurring at 30 kD (Yamaoka et al., 1994). Therefore, the molecular weight of PEG must be greater than or equal to 30 kD in order to obtain a significant improvement in the circulation half-life of the conjugated drug. In addition, in contrast to polymers such as HPMA and PGA that have multiple pendant functional groups for drug attachment, PEG contains a maximum of two terminal –OH groups suitable for conjugation. The drug to polymer ratio of Prothecan™ is reported to be 1–60 (w/w) resulting in a 1.7 wt% drug weight content in the final formulation. In this way, even though the half-life of the conjugated drug has been significantly improved (greater than 72 hours), the dose that can be administrated to patients is limited.

In order to improve these shortcomings, various strategies have been investigated. For example, Kataoka et al. have successfully developed a PEG-*b*-PAsp micelle system with DOX (DOX) conjugated to the PAsp block. Their studies demonstrated that the conjugation of DOX significantly improved the retention of free DOX that is physically entrapped within the micelles resulting in an improved circulation half-life of the drug following i.v. administration (Nakanishi et al., 2001). However, the DOX conjugated to the polymer has been found to be inactive (Nakanishi et al., 2001).

Poly-L-glutamic acid (PGA) has also been considered as a viable polymer candidate for polymer–small molecule drug conjugate development. Unlike PEG or HPMA, the PGA backbone is biodegradable (Shaffer et al., 2002). There are currently two PGA-related polymer–small molecule conjugates in clinical evaluation: a conjugate of PTX, namely CT-2103 (Xyotax®), in Phase III trials and a conjugate of CPT CT-2106 in Phase I trials. In comparison to the PEG or HPMA conjugates, the PGA products contain a much higher drug load. For example, CT-2103 has a 37% w/w PTX load achieved through chemical conjugation of PGA to PTX through its 2′ position with a total molecular weight of 49 kD for the polymer–drug conjugate. The non-enzymatic controlled release of PTX from the

CT-2103 system has been found to be limited with only 14% released in a 24-hour period. CT-2103 was reported to result in superior anti-cancer activity and a significant decrease in the systemic toxicity of PTX, in comparison to the drug administered as Taxol®, in various preclinical studies. Phase I clinical trial evaluation of this conjugate revealed a lower toxicity profile with an increase in the MTD to 233 mg/m^2 (PTX equivalent), in comparison to an MTD of 135–200 mg/m^2 for PTX administered as Taxol® . Also, a significant number of patients with non-small cell lung cancer, mesothelioma, renal cell carcinoma and PTX-resistant ovarian cancer demonstrated partial response or stabilized disease following treatment with CT-2103 (Langer, 2004). However, Phase III trials that evaluated CT-2103 for treatment of PS2 NSCLC failed to demonstrate significant improvements in survival in comparison to the first-line therapy for this indication which includes the combination of gemcitabine and vinorelbine. However, the conjugate was shown to reduce severe side effects and significantly improved survival rates in comparison to vinorelbine alone. The PGA-based conjugate of CPT, known as CT-2106, with a total molecular weight of 50 kD and a drug-loading level of 33–35 wt% is currently in Phase I clinical trials (Bhatt et al., 2003).

Dextran, a polysaccharide composed of α-1,6-polyglucose units has also been used in the preparation of polymer–drug conjugates. For example, dextran (MW ~70 kD) has been attached to DOX to form AD-70. Phase I clinical trial evaluation of AD-70 revealed significant toxicity for this conjugate at a starting dose of 40 mg/m^2 and as a result the dose range had to be reduced to 12.5–40 mg/m^2 (Danhauser-Riedl et al., 1993). The toxicity was attributed to the fact that macrophages of the MPS have a receptor for glucose . As a result, the MTD was found to be 40 mg/m^2 and the recommended dose for Phase II trials, which showed minimal toxicity, was 12.5 mg/m^2 (Danhauser-Riedl et al., 1993). A modified dextran–polyalcohol polymer (i.e., carboxymethyldextran polyalcohol) (MW = 34 kD) has also been employed to prepare a conjugate of a CPT analogue (DX-8951). This polymer–drug conjugate known as DE-310 is now in Phase I development (Soepenberg et al., 2005; Wente et al., 2005).

The success of polymer–drug conjugates and polymer-based delivery systems is evidenced by the number of drugs that have reached the stage of clinical trial development and rely on these technologies for formulation. The next section discusses lipid-based delivery systems with a major focus on liposomes which are the most established of the advanced delivery technologies.

Lipid-Based Colloidal Systems

Liposomes are spherical vesicles with an aqueous core surrounded by one or more concentric bilayers of lipid. These lipid vesicles can be prepared to vary widely in terms of size from 30 nm to several microns, but for intravenous delivery they are usually smaller than 200 nm in diameter (Gabizon, 2007).

Liposomes were first explored over 40 years ago by Bangham et al. as a means to study membrane dynamics and gain an improved understanding

of molecular flux in and out of cells (Bangham et al., 1965). The first liposomes were composed of phosphatidylcholine derived from egg, a material that is still commonly used to form liposomes today (Bangham et al., 1965). In subsequent years other groups continued to use liposomes to study membrane permeability (Scarpa and Degier, 1971; Sessa and Weissman, 1968). Since 1971 when Gregoriadis et al. first proposed liposomes as drug carriers (Gregoriadis and Ryman, 1971), an extensive amount of research has been performed on the use of liposomes for this and other biomedical applications. Material selection and preparation methods have been optimized to increase drug loading and retention, extend circulation lifetime in vivo and thus improve drug accumulation at diseased sites such as tumors. Liposomes have been shown to provide an attractive means to deliver drugs to tumors, in comparison to conventional methods, since they are relatively less toxic and can provide an improved biodistribution profile. The first liposome formulation was approved by the FDA in 1995 (Gabizon, 2001). This formulation known as Doxil® consists of DOX encapsulated in liposomes formed from fully hydrogenated soy phosphatidylcholine (HSPC), cholesterol (CH) and PEG-conjugated distearoylphosphatidylethanolamine (PEG-DSPE) (Allen and Martin, 2004; Simard et al., 2007). In the past decade two additional formulations that rely on liposome-based technologies have been FDA approved for anti-cancer treatment while countless others are in preclinical evaluation. Other lipid-based systems such as micelles (Lukyanov and Torchilin, 2004) and bilayer disks (Carmona-Ribeiro, 2006) have also been studied as potential drug delivery technologies, but they are beyond the scope of this chapter.

The composition and physical properties of liposomes largely dictates their fate in vivo. Liposomes are composed of three main types of materials: phospholipids, sphingolipids and sterols. Phospholipids being the most abundant component in mammalian cell membranes are also the most prevalent building block in liposomes (Simard et al., 2007). Phospholipids are amphiphilic molecules with a polar headgroup and two aliphatic carbon chains. The headgroup can be neutral or have a net positive or negative charge, while the hydrocarbon chains can vary in length and have different degrees of saturation. It is usually a phosphatidylcholine lipid such as dimyristoylphosphatidylcholine (DMPC), dipalmitoylphosphatidylcholine (DPPC) or distearoylphosphatidylcholine (DSPC) that comprises at least 40% of most liposome formulations. PC lipids are neutral and are the predominant phospholipid component of cell membranes. Sphingolipids are composed of a fatty acid, a sphingosine moiety, and a polar headgroup (Simard et al., 2007). The most commonly used type is sphingomyelin (SM), which is often combined with cholesterol (CH) in a molar ratio of 55:45 to produce liposomes with an extended circulation lifetime (Zhigaltsev et al., 2005). Sterols are steroid-based alcohols, the most commonly employed of which is cholesterol. Cholesterol is also common in human cells, especially plasma membranes, and is found in most liposomes used for i.v. administration (Simard et al., 2007). Cholesterol causes rigid liposome membranes to become more fluid and fluid membranes to be more rigid (Mayhew et al., 1979). Using cholesterol to increase the rigidity of the bilayer can result in slower drug release

and prevent various small-sized solutes from crossing the bilayer (Raffy and Teissie, 1999). Cholesterol also seems to reduce liposome interactions with plasma proteins, although the underlying mechanism associated with this effect has not been clearly elucidated (Drummond et al., 1999).

The physico-chemical properties of liposomes that have been shown to have the most significant influence on their performance as delivery systems include zeta potential, size, size distribution and stability. The overall charge of a liposome is referred to as the zeta potential and has an effect on the pharmacokinetics and biodistribution profile of the liposomes in vivo. As mentioned previously the PC lipids that are commonly used as the base component of most liposome formulations are neutral, yet positive (e.g., stearylamine) and/or negative (e.g., phosphatidylglycerol) lipids can also be incorporated into the bilayer in order to alter surface charge. Traditionally, a small amount of charged lipid has been incorporated into liposome formulations as a means to prevent aggregation (Papahadjopoulos, 1999). However, the presence of positive or negative charge at the surface of liposomes can result in increased opsonin binding which in turn may lead to a more rapid clearance of the vesicles by the MPS (Juliano and Stamp, 1975).

Various methods have been put forth for liposome preparation. Overall, the goal has been to prepare liposomes that are of a well-defined size with a narrow size distribution such that the entire population of vesicles behaves in the same manner. One of the most commonly employed methods known as the extrusion method involves the use of high pressure to force the suspension through polycarbonate membranes. Hope et al. have shown that five to ten extrusion cycles through a polycarbonate membrane with pores of a specific size is an effective method to produce liposomes with a relatively narrow size distribution (Hope et al., 1985). The circulation time of liposomes has been shown to be highly dependant on size – with vesicles smaller than 100 nm remaining in the circulation longer than larger 200 or 400 nm liposomes (Senior et al., 1985). As previously discussed, colloidal particles smaller than 400 nm are able to accumulate in tumor regions due to EPR effect (Yuan et al., 1995). Therefore, smaller liposomes will often have an increased circulation lifetime and greater degree of tumor accumulation due to the EPR effect.

Liposomes were not effective drug delivery vehicles during their early development due to their short circulation lifetime in the bloodstream. Even if parameters such as size, surface charge and lipid composition were optimized, significant accumulation in the liver and spleen still occurred within several hours of administration (Senior, 1987). For this reason, steric stabilization was explored in order to reduce interactions with both molecules such as opsonins in the blood and other liposomes. Monosialoganglioside (GM_1) phosphatidylinositol (PI) were first used to sterically stabilize liposomes (Allen and Chonn, 1987; Gabizon and Papahadjopoulos, 1988). They were successful in improving circulation time, but shortcomings associated with both GM_1 and PI made their widespread use unviable. PI has poor solubility in many solvents, possibly causing heterogeneity throughout the liposome population (Woodle and Lasic, 1992), while the high cost of GM_1 prohibits its commercial use (Allen, 1994).

At the beginning of the 1990 s, PEG was introduced as a steric stabilizing agent (Allen et al., 1991; Klibanov et al., 1990). PEG is usually conjugated to a lipid such as DSPE that serves to anchor the hydrophilic polymer to the bilayer surface. Liposomes sterically stabilized with PEG were found to have enhanced circulation lifetimes and reduced accumulation in the liver and spleen, in comparison to conventional liposomes (Allen et al., 1991). The in vivo pharmacokinetics of the PEG-stabilized vesicles have been found to have a log-linear dose dependence: meaning their clearance rate is not dependent on the dose that is administered (Allen et al., 1991). Drummond et al. have combined previous studies to show that the choice of lipid becomes less important when the liposomes are sterically stabilized with PEG. Liposomes formed from unsaturated lipids that had shorter circulation lifetimes without PEG remain in the circulation just as long as liposomes formed from saturated lipids when they are sterically stabilized (Drummond et al., 1999). Steric stabilization is an important strategy in the delivery of chemotherapeutic agents since the extended circulation lifetime it affords can lead to increased tumor accumulation due to the EPR effect. Typically, a range of 5–10 mol% of the PEGylated lipid is employed to stabilize the formulation (Simard et al., 2007). Yet, it should be noted that inclusion of PEG-DSPE in some liposome formulations has been shown to result in premature drug release so different lipid anchors may sometimes need to be employed (Webb et al., 1998).

Liposomes have been widely explored to solubilize and/or actually deliver hydrophilic (e.g., cytarabine) (Kim and Howell, 1987), hydrophobic (e.g., PTX, CPT) (Chow et al., 2000; Zhang et al., 2005) and amphiphilic compounds (e.g., DOX, vincristine) (Abraham et al., 2005; Waterhouse et al., 2005). Hydrophilic drugs can be passively encapsulated at high concentrations within the aqueous core of the liposome; however, release rates tend to be slow because the drug must pass through the hydrophobic region of the bilayer (Allen and Stuart, 1999). Drugs of intermediate solubility are usually poorly retained in the liposome, unless the physical conditions of the aqueous core are designed such that the drug will form complexes and thus become less susceptible to crossing the bilayer. Active loading is a technique that involves the creation of a gradient (e.g., pH, ionic) across the liposome membrane, which causes the drug to enter the aqueous core and form such complexes. Active loading techniques are particularly effective for amphiphilic molecules that are weak acids or weak bases (Haran et al., 1993).

Hydrophobic drugs have been found to intercalate within the hydrophobic region of the lipid bilayer (Defrise-Quertain et al., 1984). The bilayer can serve as a suitable microenvironment for effective solubilization of drugs, particularly if there is a high degree of miscibility between the drug and the bilayer-forming material. However, since the drug is stored in a location that is in close proximity to the external environment the bilayer must compete with components within the external medium, such as lipoproteins, in order to retain the drug. Therefore, the composition of the lipid bilayer plays a major role in influencing the loading efficiency, capacity and retention of hydrophobic drugs.

Amphotericin B (AmB) is a hydrophobic drug that has been incorporated successfully in a liposome formulation that is now in clinical use (i.e., Ambisome®, Gilead Pharmaceuticals Inc.). Liposome formulations of AmB have been studied quite extensively; thus, this literature provides significant information on the potential of liposomes as delivery systems for hydrophobic compounds. Studies on liposomal AmB have demonstrated that the incorporation of the drug does not alter the surface properties of the liposomes (Moribe et al., 1999). The localization of the drug in the hydrophobic region of the bilayer has also been confirmed by fluorescence quenching and potassium permeability measurements (Moribe et al., 1999). In addition, it has been shown that the lipid components must interact favorably with the drug in order to optimize drug loading and retention. Moribe et al. compared DPPC, DPPC/DSPE-PEG and DPPC/CH/DSPE-PEG formulations of AmB and demonstrated that the presence of DSPE-PEG increased the loading potential since the drug interacts favorably with DSPE (Moribe et al., 1999). As well, Matsuoka et al. reported on the preparation of AmB containing liposomes formed from ePC and PC (4:1 mol/mol) that varied in terms of acyl-chain length from C_{10} to C_{18} (Matsuoka and Murata, 2003). It was found that the addition of the shorter acyl-chain length lipids (i.e., C_{10} or C_{12}) resulted in a more permeable bilayer whereas medium chain length (i.e., C_{14} or C_{16}) lipids caused no change in membrane permeability. Also, it was found that the lipid membrane was more rigid with the addition of DSPC (C_{18}) than without. The increase in rigidity was suggested to be due to a strong interaction between DSPC and AmB.

The degree of saturation of the lipids that are used for formulation is also an important consideration. Chen et al. prepared liposomes using both unsaturated (SPC) and saturated (HSPC) phospholipids with 25 mol% cholesterol to solubilize 9-nitrocamptothecin (Chen et al., 2006). Using a 1:3 HSPC:SPC molar ratio allowed for a fourfold increase in drug loading compared to the SPC/CH formulation. The liposome bilayer that resulted was found to separate into two phases, a gel phase and a liquid-crystalline phase. The coexistence of these two immiscible phases in the membrane was said to create discontinuous regions in the bilayer, which reduced the movement and aggregation of the drug, resulting in increased stability of the formulation. Liu et al. were also able to use unsaturated lipids, in this case a mixture of ePC and PEG-DSPE, to achieve a high loading level of a novel, hydrophobic anti-cancer drug (i.e., 10 mg/mL drug concentration, 1:3.5 drug:lipid mol/mol) (Liu et al. 2006). The final formulation was found to be stable for up to 3 weeks at 37°C even in the presence of physiologically relevant concentrations of protein.

Cholesterol is commonly employed in liposome formulations because, as discussed previously, it can increase drug retention in the aqueous compartment, minimize the interaction of liposomes with serum proteins and increase the stability of the liposomes. However, for hydrophobic drugs, studies have shown that the inclusion of cholesterol in the formulation significantly decreases the solubilization of drug in the bilayer (Saetern et al., 2004). For example, Liu et al. attributed the low

drug-loading level achieved in the presence of cholesterol to the fact that the cholesterol itself is a bulky molecule that intercalates within the bilayer and reduces the cargo space available for hydrophobic drug (Liu et al. 2006). In fact, several studies have confirmed the negative impact that cholesterol can have on the loading capacity and efficiency of liposomes for hydrophobic drugs. For example, Zhang et al. reported that an increase in the cholesterol content from 5 to 37 mol% decreased the loading efficiency of liposomes for PTX from 99 to 6% (Zhang et al., 2005).

The FDA-approved formulations of anti-cancer agents that rely on liposomes are for cytarabine (i.e., DepoCyte®), (Jaeckle et al., 2001) which is hydrophilic or for the amphiphilic anthracyclines DOX (i.e., Doxil®) (Gabizon, 2001), and daunorubicin (i.e., DaunoXome®) (Forssen, 1997). Doxil® is composed of HSPC, cholesterol and PEG-DSPE in a 56.2:38.3:5.3 molar ratio (Allen and Martin, 2004). An active loading technique based on an ammonium sulfate gradient is used to encapsulate 2 mg/mL DOX inside the aqueous core of the liposomes in this formulation. In Europe and Canada another liposomal DOX formulation called Myocet® is approved for clinical use. It is composed of ePC and cholesterol in a 55:45 molar ratio (Swenson et al., 2001). The lack of steric stabilization of Myocet® compared to Doxil® results in a noticeably shorter circulation half-life (i.e., 2–3 versus 41–70 h) and lower AUC (46 versus 902 μg/mL·h) (Hofheinz et al., 2005) for this formulation. The differences in the pharmacokinetic and biodistribution profiles for these two DOX formulations makes them suited for treatment of different cancers: Doxil® is primarily used to treat ovarian cancer and AIDS-related Kaposi's sarcoma while the primary indication of Myocet® is breast cancer (Allen and Martin, 2004).

There are a wide range of liposome-based formulations of anti-cancer drugs that are in various stages of clinical development including a few for hydrophobic drugs. For example, LEP-ETU (NeoPharm Inc.) is a liposome formulation of PTX that has completed Phase II clinical trials (Scheme 12.5). LEP-ETU is composed of DOPC, cholesterol and cardiolipin (90:5:5 mol/mol) and contains 2 mg/mL PTX (Zhang et al., 2005). Cholesterol is included in the formulation as a means to improve the circulation lifetime in vivo, while cardiolipin, a negatively charged lipid, is added because it has been reported to alter the pharmacokinetics and biodistribution of the liposomes resulting in reduced cardiotoxicity (Cabanes et al., 1998). The amounts of both cholesterol and cardiolipin included in the formulation are limited due to their negative effect on the loading efficiency for PTX (Zhang et al., 2005). The highest drug-loading level achieved in the LEP-ETU formulation corresponds to a drug to lipid ratio of 1:33 (mol:-mol). MediGene Inc. is also developing a liposome-based formulation of PTX known as EndoTAG®-1 (MediGene, Inc.) Phase II clinical trials for pancreatic cancer are underway and effectiveness in treating various other solid tumors is also being examined (Medigene AG Website). The Endo-TAG®-1 formulation consists of DOTAP and DOPC in a 50:47 molar ratio and solubilizes 0.5 mg/mL PTX with a drug to lipid ratio of 1:33 (Strieth et al., 2004). The positively charged lipid DOTAP has been included in this formulation since studies have shown that the inclusion of DOTAP can result in a threefold increase in tumor accumulation, in comparison to

Drug	Name	Company	Lipid Composition	Lipid Ratio	Indication	Status	Reference
Anthracyclines							
doxorubicin	Doxil	Ortho Biotech	HSPC:CH:PEG-DSPE	56.2:38.3:5.3	ovarian cancer, Kaposi's sarcoma	Approved	Gabizon, 2007
doxorubicin	Myocet	Cephalon	ePC:CH	55:45	breast cancer	Approved (Europe)	Swenson et al. 2001
daunorubicin	DaunoXome	Gilead	DSPC:CH	2:1	Kaposi's sarcoma	Approved	Forssen, 1997
Camptothecins							
lurtotecan	OSI-211	OSI	HSPC:CH	2:1	ovarian, small cell lung cancer	Phase II	Emerson et al. 2000
SN-38	LE-SN38	NeoPharm	DOPC:CH:cardiolipin	50:40:10	colorectal cancer	Phase II	Zhang et al. 2004
Taxanes							
paclitaxel	LEP-ETU	NeoPharm	DOPC:CH:cardiolipin	90:5:5	breast cancer	Phase II completed	Zhang et al. 2005
paclitaxel	EndoTAG-1	MediGene	DOTAP:DOPC	50:47	pancreatic, breast cancer	Phase II	Strieth et al. 2004

Scheme 12.5 Summary of liposome formulations of hydrophobic anti-cancer agents that are currently approved or in clinical evaluation.

accumulation for either neutral or anionic liposomes (Krasnici et al., 2003). Interestingly, both the LEP-ETU and EndoTAG®-1 formulations of PTX include both unsaturated (i.e., DOTAP, DOPC) and charged (i.e., DOTAP, cardiolipin) lipids. Unsaturated lipids have proven to be effective for encapsulation of hydrophobic drugs, while charged lipids prevent liposome aggregation and alter the pharmacokinetics.

Liposome formulations have also been explored for the hydrophobic anti-cancer agent CPT. Clinical effectiveness of CPT has been limited by its poor water solubility and as mentioned previously in "Polymer–Drug Conjugates", the instability of its lactone ring. Analogues with increased aqueous solubility such as irinotecan (Campto®) and topotecan (Hycamtin®) have been approved for clinical use and other hydrophobic analogues with greater lactone stability are under development (e.g., 9-nitrocamptothecin). A liposome formulation of lurtotecan, OSI-211 (OSI Pharmaceuticals), which is another water-soluble CPT analogue is currently in Phase II clinical trials. Preclinical studies of this liposome formulation, which consists of HSPC and cholesterol in a 2:1 ratio and a 1:20 drug to lipid ratio, have demonstrated a 9–67 fold increase in the tumor accumulation of the drug, in comparison to drug administered in 5% dextrose (Emerson et al., 2000). NeoPharm Inc. has also developed a liposome formulation for SN-38 (LE-SN38), which is known to be a metabolite of irinotecan. The LE-SN38 formulation is comprised of DOPC, cholesterol and cardiolipin in a 50:40:10 molar ratio with a drug to lipid ratio of 1:18 and total drug concentration of 2 mg/mL (Zhang et al., 2004). Formulation preparation involves loading of the drug in its inactive, open lactone ring conformation in alkaline medium followed by lyophilization of the vesicles. The formulation is then hydrated in an acidic aqueous solution in order to convert the drug to its less soluble, more potent form which is said to cause the drug to intercalate into the lipid bilayer (Zhang et al., 2004). This formulation is now in Phase II clinical trial development.

Summary

In summary, liposomes have proven themselves as a viable formulation strategy for anti-cancer drugs with their success being most prevalent for delivery of hydrophilic compounds or drugs that are amenable to active loading techniques. The vast body of literature available on liposomes should serve as a guide to further the development of other colloidal systems such as block copolymer micelles and polymer–drug conjugates. In terms of delivery of hydrophobic drugs, both liposomes and micelles are versatile platforms yet as mentioned above the compositions of these systems must be tailored to suit the formulation of each specific drug. The advantage of the conjugate systems is that it appears that less drug-specific optimization is required for development. However, each new polymer–drug conjugate system is considered an NCE and thus associated with various additional regulatory hurdles. Overall, there are strengths and limitations associated with each technology platform, but together they form a "toolbox" that better serves the wide range of drugs that require formulation for treatment of a vast array of indications.

For those focused in the area of polymer-based drug delivery this is a particularly exciting time considering the large number of formulations based on block copolymer micelles and polymer–drug conjugates that are now in the late stages of clinical development. The success of formulations relying on these technologies is bringing increased interest to this area of research. Integration of the design of these delivery systems with our increased understanding of the molecular basis of many cancers will likely lead to further significant "milestone" developments in this field.

References

Abraham, S. A.; Waterhouse, D. N.; Mayer, L. D.; Cullis, P. R.; Madden, T. D.; Bally, M. B., The liposomal formulation of doxorubicin. *Liposomes, Pt E*, 2005; Vol. 391, pp 71–97.

Adams, M. L.; Kwon, G. S., Relative aggregation state and hemolytic activity of amphotericin B encapsulated by poly(ethylene oxide)-block-poly(N-hexyl-L-aspartamide)-acyl conjugate micelles: effects of acyl chain length. *Journal of Controlled Release* **2003,** 87, (1–3), 23–32.

Adams, M. L.; Lavasanifar, A.; Kwon, G. S., Amphiphilic block copolymers for drug delivery. *Journal of Pharmaceutical Sciences* **2003,** 92, (7), 1343–55.

Alakhov, V., Polymer-Based Nanomedicines for Oncology: From Preclinical Studies to the Clinical Proof of the Concept. In *4th International Nanomedicine and Drug Delivery Symposium*, Omaha, Nebraska, US, 2006.

Alakhov, V., Klinski, E., Li, S., Pietrzynski, G., Venne, A., Batrakova, E., Bronitch, T., and Kabanov, A., Block copolymer-based formulation of doxorubicin. From cell screen to clinical trials. *Colloids and Surfaces B: Biointerfaces* **1999,** 16, 113–134.

Aliabadi, H. M.; Mahmud, A.; Sharifabadi, A. D.; Lavasanifar, A., Micelles of methoxy poly(ethylene oxide)-b-poly(ε-caprolactone) as vehicles for the solubilization and controlled delivery of cyclosporine A. *Journal of Controlled Release* **2005,** 104, (2), 301–311.

Allen, C., Han, J., Yu, T., Maysinger, D., and Eisenberg, A., Polycaprolactone-b-poly(ethylene oxide) copolymer micelles as a delivery vehicle for dihydrotestosterone. *Journal of Controlled Release* **2000,** 63, 275–286.

Allen, C., Maysinger, D., and Eisenberg, A., Nano-engineering block copolymer aggregates for drug delivery. *Colloids and Surfaces B: Biointerfaces* **1999,** 16, 3–27.

Allen, C.; Yu, Y.; Maysinger, D.; Eisenberg, A., Polycaprolactone-b-poly(ethylene oxide) block copolymer micelles as a novel drug delivery vehicle for neurotrophic agents FK506 and L-685,818. *Bioconjugate Chemistry* **1998,** 9, (5), 564–72.

Allen, T. M., Long-Circulating (Sterically Stabilized) Liposomes for Targeted Drug-Delivery. *Trends in Pharmacological Sciences* **1994,** 15, (7), 215–220.

Allen, T. M.; Chonn, A., Large Unilamellar Liposomes with Low Uptake into the Reticuloendothelial System. *Febs Letters* **1987,** 223, (1), 42–46.

Allen, T. M.; Hansen, C.; Martin, F.; Redemann, C.; Yauyoung, A., Liposomes Containing Synthetic Lipid Derivatives of Poly(Ethylene Glycol) Show Prolonged Circulation Half-Lives Invivo. *Biochimica Et Biophysica Acta* **1991,** 1066, (1), 29–36.

Allen, T. M.; Martin, F. J., Advantages of liposomal delivery systems for anthracyclines. *Seminars in Oncology* **2004,** 31, (6), 5–15.

Allen, T. M.; Stuart, D. D., Liposome Pharmacokinetics. *Liposomes - Rational Design*, Janoff, A. S., Ed. Marcel Dekker, Inc.: New York, 1999; pp 63–87.

Baban, D. F.; Seymour, L. W., Control of tumour vascular permeability. *Advanced Drug Delivery Reviews* **1998,** 34, (1), 109–119.

Bader, H.; Ringsdorf, H.; Schmidt, B., Watersoluble Polymers in Medicine. *Die Angewandte Makromolekulare Chemie* **1984,** 123/124, 457–485.

Bangham, A. D.; Standish, M. M.; Watkins, J. C., Diffusion of Univalent Ions across Lamellae of Swollen Phospholipids. *Journal of Molecular Biology* **1965,** 13, (1), 238–252.

Bartsch, W.; Sponer, G.; Dietmann, K.; Fuchs, G., Acute toxicity of various solvents in the mouse and rat. LD50 of ethanol, diethylacetamide, dimethylformamide, dimethylsulfoxide, glycerine, N-methylpyrrolidone, polyethylene glycol 400, 1,2-propanediol and Tween 20. *Arzneimittelforschung* **1976,** 26, (8), 1581–3.

Batrakova, E. V., Li, S., Li, Y., Alakhov, V.Y., Elmquist, W.F., and Kabanov, A.V., Distribution kinetics of a micelle-forming block copolymer Pluronic P85. *Journal of Controlled Release* **2004,** 100, 389–397.

Batrakova, E. V., Li, S., Miller, D.W., and Kabanov, A.V., Pluronic P85 increases permeability of a broad spectrum of drugs in polarized BBMEC and caco-2 cell monolayers. *Pharmaceutical Research* **1999,** 16, (9), 1366–1372.

Benahmed, A.; Ranger, M.; Leroux, J. C., Novel polymeric micelles based on the amphiphilic diblock copolymer poly(N-vinyl-2-pyrrolidone)-block-poly(D,L-lactide). *Pharmaceutical Research* **2001,** 18, (3), 323–8.

Bhatt, R.; De Vries, P.; Tulinsky, J.; Bellamy, G.; Baker, B.; Singer, J. W.; Klein, P., Synthesis and in vivo antitumor activity of poly(L-glutamic acid) conjugates of 20(S)-camptothecin. *Journal of Medicinal Chemistry* **2003,** 46, (1), 190–193.

Brazeau, G. A.; Cooper, B.; Svetic, K. A.; Smith, C. L.; Gupta, P., Current perspectives on pain upon injection of drugs. *Journal of Pharmaceutical Sciences* **1998,** 87, (6), 667–77.

Cabanes, A.; Briggs, K. E.; Gokhale, P. C.; Treat, J. A.; Rahman, A., Comparative in vivo studies with paclitaxel and liposome-encapsulated paclitaxel. *International Journal of Oncology* **1998,** 12, (5), 1035–1040.

Carmona-Ribeiro, A. M., Lipid bilayer fragments and disks in drug delivery. *Current Medicinal Chemistry* **2006,** 13, (12), 1359–1370.

Chen, J.; Ping, Q. N.; Guo, J. X.; Chu, X. Z.; Song, M. M., Effect of phospholipid composition on characterization of liposomes containing 9-nitrocamptothecin. *Drug Development and Industrial Pharmacy* **2006,** 32, (6), 719–726.

Cho, Y. W.; Lee, J.; Lee, S. C.; Huh, K. M.; Park, K., Hydrotropic agents for study of in vitro paclitaxel release from polymeric micelles. *Journal of Controlled Release* **2004,** 97, (2), 249–57.

Choucair, A.; Eisenberg, A., Control of amphiphilic block copolymer morphologies using solution conditions. *The European Physical Journal E* **2003,** 10, 37–44.

Chow, D. S. L.; Gong, L.; Wolfe, M. D.; Giovanella, B. C., Modified lactone/carboxylate salt equilibria in vivo by liposomal delivery of 9-nitro-camptothecin. In *Camptothecins: Unfolding Their Anticaner Potential*, 2000; Vol. 922, pp 164–174.

Chung, T. W.; Cho, K. Y.; Lee, H.-C.; Nah, J. W.; Yeo, J. H.; Akaike, T.; Cho, C. S., Novel micelle-forming block copolymer composed of poly (ε- caprolactone) and poly(vinyl pyrrolidone). *Polymer* **2004,** 45, (5), 1591–1597.

Croy, S. R.; Kwon, G. S., The effects of Pluronic block copolymers on the aggregation state of nystatin. *Journal of Controlled Release* **2004,** 95, (2), 161–171.

Danhauser-Riedl, S.; Hausmann, E.; Schick, H.-D.; Bender, R.; Dietzfelbinger, H.; Rastetter, J.; Hanauske, A.-R., Phase I clinical and pharmacokinetic trial of dextran conjugated doxorubicin (AD-70, DOX-OXD). *Investigational New Drugs* **1993,** 11, (2–3), 187–195.

Danson, S.; Ferry, D.; Alakhov, V.; Margison, J.; Kerr, D.; Jowle, D.; Brampton, M.; Halbert, G.; Ranson, M., Phase I dose escalation and pharmacokinetic study of pluronic polymer-bound doxorubicin (SP1049C) in patients with advanced cancer. *British Journal of Cancer* **2004,** 90, (11), 2085–2091.

Defrise-Quertain, F.; Chatelain, P.; Delmelle, M.; Ruysschaert, J.-M., Model Studies for Drug Entrapment and Liposome Stability. In *Liposome Technology*, Gregoriadis, G., Ed. CRC Press, Inc: Boca Raton, 1984; Vol. II, pp 1–18.

Discher, D. E.; Eisenberg, A., Polymer vesicles. *Science* **2002,** 297, (5583), 967–73.

Drummond, D. C.; Meyer, O.; Hong, K. L.; Kirpotin, D. B.; Papahadjopoulos, D., Optimizing liposomes for delivery of chemotherapeutic agents to solid tumors. *Pharmacological Reviews* **1999,** 51, (4), 691–743.

Duncan, R., Polymer conjugates as anticancer nanomedicines. *Nature Reviews Cancer* **2006,** 6, (9), 688–701.

Duncan, R., The dawning era of polymer therapeutics. *Nature Reviews Drug Discovery* **2003,** 2, (5), 347–360.

Duncan, R.; Cable, H. C.; Lloyd, J. B.; Rejmanova, P.; Kopecek, J., Degradation of side-chains of N-(2-hydroxypropyl)methacrylamide copolymers by lysosomal thiol-proteinases. *Bioscience Reports* **1982,** 2, (12), 1041–6.

Duncan, R.; Gac-Breton, S.; Keane, R.; Musila, R.; Sat, Y. N.; Satchi, R.; Searle, F., Polymer-drug conjugates, PDEPT and PELT: Basic principles for design and transfer from the laboratory to clinic. *Journal of Controlled Release* **2001,** 74, (1–3), 135–146.

Duncan, R.; Pratten, M. K.; Cable, H. C.; Ringsdorf, H.; Lloyd, J. B., Effect of molecular size of 125I-labelled poly(vinylpyrrolidone) on its pinocytosis by rat visceral yolk sacs and rat peritoneal macrophages. *Biochemical Journal* **1981,** 196, (1), 49–55.

Duncan, R.; Ringsdorf, H.; Satchi-Fainaro, R., Polymer therapeutics: Polymers as drugs, drug and protein conjugates and gene delivery systems: Past, present and future opportunities. *Advances in Polymer Science* **2006,** 192, (1), 1–8.

Ehlrich, P., *Collected Studies on Immunity*. J. Wiley & Sons: New York, 1906; p 442.

Emerson, D. L.; Bendele, R.; Brown, E.; Chiang, S. M.; Desjardins, J. P.; Dihel, L. C.; Gill, S. C.; Hamilton, M.; LeRay, J. D.; Moon-McDermott, L.; Moynihan, K.; Richardson, F. C.; Tomkinson, B.; Luzzio, M. J.; Baccanari, D., Antitumor efficacy, pharmacokinetics, and biodistribution of NX 211: A low-clearance liposomal formulation of lurtotecan. *Clinical Cancer Research* **2000,** 6, (7), 2903–2912.

Forssen, E. A., The design and development of DaunoXome(R) for solid tumor targeting in vivo. *Advanced Drug Delivery Reviews* **1997,** 24, (2–3), 133–150.

Fournier, E.; Dufresne, M. H.; Smith, D. C.; Ranger, M.; Leroux, J. C., A novel one-step drug-loading procedure for water-soluble amphiphilic nanocarriers. *Pharmaceutical Research* **2004,** 21, (6), 962–968.

Frank, D. W.; Gray, J. E.; Weaver, R. N., Cyclodextrin nephrosis in the rat. *American Journal of Pathology* **1976,** 83, (2), 367–82.

Fried, M. W.; Shiffman, M. L.; Reddy, K. R.; Smith, C.; Marinos, G.; Goncales Jr., F. L.; Haussinger, D.; Diago, M.; Carosi, G.; Dhumeaux, D.; Craxi, A.; Lin, A.; Hoffman, J.; Yu, J., Peginterferon alfa-2a plus ribavirin for chronic hepatitis C virus infection. *New England Journal of Medicine* **2002,** 347, (13), 975–982.

Fu, R. C.; Lidgate, D. M.; Whatley, J. L.; McCullough, T., The biocompatibility of parenteral vehicles–in vitro/in vivo screening comparison and the effect of excipients on hemolysis. *Journal of Parenteral Science and Technology* **1987,** 41, (5), 164–8.

Fukushima, S., Machida, M., Akutsu, T., Shimizu, K., Tanaka, S., Okamoto, K., Mashiba, H., Yokoyama, M., Okano, T., Sakurai, Y., and Kataoka, K., Roles of adriamycin and adriamycin dimer in antitumor activity of the polymeric micelle carrier system. *Colloids and Surfaces B: Biointerfaces* **1999,** 16, 227–236.

Gabizon, A. A., Applications of Liposomal Drug Delivery Systems to Cancer Therapy. In *Nanotechnology for Cancer Therapy*, Amiji, M. M., Ed. CRC Press: Boca Raton, 2007; pp 595–611.

Gabizon, A. A., Pegylated liposomal doxorubicin: Metamorphosis of an old drug into a new form of chemotherapy. *Cancer Investigation* **2001,** 19, (4), 424–436.

Gabizon, A.; Papahadjopoulos, D., Liposome Formulations with Prolonged Circulation Time in Blood and Enhanced Uptake by Tumors. *Proceedings of the National Academy of Sciences of the United States of America* **1988,** 85, (18), 6949–6953.

Gianni, L.; Kearns, C. M.; Giani, A.; Capri, G.; Vigano, L.; Locatelli, A.; Bonadonna, G.; Egorin, M. J., Nonlinear Pharmacokinetics and Metabolism of Paclitaxel and Its Pharmacokinetic/Pharmacodynamic Relationships in Humans. *Journal of Clinical Oncology* **1995,** 13, (1), 180–190.

Graham, M. L., Pegaspargase: A review of clinical studies. *Advanced Drug Delivery Reviews* **2003,** 55, (10), 1293–1302.

Greenwald, R. B.; Choe, Y. H.; McGuire, J.; Conover, C. D., Effective drug delivery by PEGylated drug conjugates. *Advanced Drug Delivery Reviews* **2003,** 55, (2), 217–50.

Greenwald, R. B.; Gilbert, C. W.; Pendri, A.; Conover, C. D.; Xia, J.; Martinez, A., Drug delivery systems: water soluble taxol 2'-poly(ethylene glycol) ester prodrugs-design and in vivo effectiveness. *Journal of Medicinal Chemistry* **1996,** 39, (2), 424–31.

Gregoriadis, G.; Ryman, B. E., Liposomes as Carriers of Enzymes or Drugs - New Approach to Treatment of Storage Diseases. *Biochemical Journal* **1971,** 124, (5), 58P.

Guchelaar, H.-J.; Ten Napel, C. H. H.; De Vries, E. G. E.; Mulder, N. H., Clinical, toxicological and pharmaceutical aspects of the antineoplastic drug taxol: A review. *Clinical Oncology* **1994,** 6, (1), 40–48.

Hamaguchi, T.; Matsumura, Y.; Suzuki, M.; Shimizu, K.; Goda, R.; Nakamura, I.; Nakatomi, I.; Yokoyama, M.; Kataoka, K.; Kakizoe, T., NK105, a paclitaxel-incorporating micellar nanoparticle formulation, can extend in vivo antitumour activity and reduce the neurotoxicity of paclitaxel. *British Journal of Cancer* **2005,** 92, (7), 1240–6.

Haran, G.; Cohen, R.; Bar, L. K.; Barenholz, Y., Transmembrane Ammonium-Sulfate Gradients in Liposomes Produce Efficient and Stable Entrapment of Amphipathic Weak Bases. *Biochimica Et Biophysica Acta* **1993,** 1151, (2), 201–215.

Harris, J. M.; Chess, R. B., Effect of pegylation on pharmaceuticals. *Nature Reviews Drug Discovery* **2003,** 2, (3), 214–21.

Hauswirth, A. W.; Simonitsch-Klupp, I.; Uffmann, M.; Koller, E.; Sperr, W. R.; Lechner, K.; Valent, P., Response to therapy with interferon alpha-2b and prednisolone in aggressive systemic mastocytosis: Report of five cases and review of the literature. *Leukemia Research* **2004,** 28, (3), 249–257.

Hite, M.; Turner, S.; Federici, C., Part 1: Oral Delivery of Poorly Soluble Drugs. *Pharmaceutical Manufacturing and Packing Sourcer* **2003,** Summer '03.

Ho, D. H.; Brown, N. S.; Yen, A., Clinical pharmacology of polyethylene glycol-L-asparaginase. *Drug Metabolism and Disposition* **1986,** 14, (3), 349–352.

Hofheinz, R. D.; Gnad-Vogt, S. U.; Beyer, U.; Hochhaus, A., Liposomal encapsulated anti-cancer drugs. *Anti-Cancer Drugs* **2005,** 16, (7), 691–707.

Hope, M. J.; Bally, M. B.; Webb, G.; Cullis, P. R., Production of Large Unilamellar Vesicles by a Rapid Extrusion Procedure - Characterization of Size Distribution, Trapped Volume and Ability to Maintain a Membrane-Potential. *Biochimica Et Biophysica Acta* **1985,** 812, (1), 55–65.

Hruby, M.; Konak, C.; Ulbrich, K., Polymeric micellar pH-sensitive drug delivery system for doxorubicin. *Journal of Controlled Release* **2005,** 103, (1), 137–148.

Hsieh, H. L.; Quirk, R. P., *Anionic Polymerization : Principles and Practical Applications*. Marcel Dekker: New York, 1996; p 727.

Jaeckle, K. A.; Phuphanich, S.; van den Bent, M. J.; Aiken, R.; Batchelor, T.; Campbell, T.; Fulton, D.; Gilbert, M.; Heros, D.; Rogers, L.; O'Day, S. J.; Akerley, W.; Allen, J.; Baldas, S.; Gertler, S. Z.; Greenberg, H. S.; LaFollette, S.; Lesser, G.; Mason, W.; Recht, L.; Wong, E.; Chamberlain, M. C.; Cohn, A.; Glantz, M. J.; Guthell, J. C.; Maria, B.; Moots, P.; New, P.; Russell, C.; Shapiro, W.; Swinnen, L.; Howell, S. B., Intrathecal treatment of neoplastic meningitis due to breast cancer with a slow-release formulation of cytarabine. *British Journal of Cancer* **2001,** 84, (2), 157–163.

Jette, K. K.; Law, D.; Schmitt, E. A.; Kwon, G. S., Preparation and drug loading of poly(ethylene glycol)-block-poly(ε-caprolactone) micelles through the evaporation of a cosolvent azeotrope. *Pharmaceutical Research* **2004,** 21, (7), 1184–91.

Juliano, R. L.; Stamp, D., Effect of Particle-Size and Charge on Clearance Rates of Liposomes and Liposome Encapsulated Drugs. *Biochemical and Biophysical Research Communications* **1975,** 63, (3), 651–658.

Kabanov, A.; Alakhov, V. Y., Micelles of amphiphilic block copolymers as vehicles for drug delivery. In *Amphiphilic Block Copolymers: Self-Assembly and Applications*, Alexandridis, P.; Lindman, B., Eds. Elsevier Science B.V.: The Netherlands, 2000; pp 347–376.

Kabanov, A. V.; Alakhov, V. Y., Pluronic® block copolymers in drug delivery: From micellar nanocontainers to biological response modifiers. *Critical Reviews in Therapeutic Drug Carrier Systems* **2002,** 19, (1), 1–72.

Kabanov, A. V.; Batrakova, E. V.; Alakhov, V. Y., Pluronic (R) block copolymers as novel polymer therapeutics for drug and gene delivery. *Journal of Controlled Release* **2002,** 82, (2–3), 189–212.

Kabanov, A. V.; Chekhonin, V. P.; Alakhov, V. Y.; Batrakova, E. V.; Lebedev, A. S.; Melik-Nubarov, N. S.; Arzhakov, S. A.; Levashov, A. V.; Morozov, G. V.; et al., The neuroleptic activity of haloperidol increases after its solubilization in surfactant micelles. Micelles as microcontainers for drug targeting. *FEBS Letters* **1989,** 258, (2), 343–5.

Kato, K.; Hamaguchi, T.; Yasui, H.; Okusaka, T.; Ueno, H.; Ikeda, M.; Shirao, K.; Shimada, Y.; Nakahama, H.; Muro, K.; Matsumura, Y., Phase I study of NK105, a paclitaxel-incorporating micellar nanoparticle, in patients with advanced cancer. *Journal of Clinical Oncology* **2006,** 24, (18), 83 s–83 s.

Kim, C.; Lee, S. C.; Kwon, I. C.; Chung, H.; Jeong, S. Y., Complexation of poly(2-ethyl-2-oxazoline)-block-poly(ε-caprolactone) micelles with multifunctional carboxylic acids. *Macromolecules* **2002,** 35, (1), 193–200.

Kim, S.; Howell, S. B., Multivesicular Liposomes Containing Cytarabine Entrapped in the Presence of Hydrochloric-Acid for Intracavitary Chemotherapy. *Cancer Treatment Reports* **1987,** 71, (7–8), 705–711.

Kim, S. C., Kim, D.W., Shim, Y.H., Bang, J.S., Oh, H.S., Kim, S.W., and Seo, M.H., In vivo evaluation of polymeric micellar paclitaxel formulation: toxicity and efficacy. *Journal of Controlled Release* **2001,** 72, 191–202.

Kim, T. Y., Kim, D.W., Chung, J.Y., Shin, S.G., Kim, S.C., Heo, D.S., Kim, N.K., and Bang, Y.J., Phase I and pharmacokinetics study of Genexol-PM, a cremophor-free, polymeric micelle-formulated paclitaxel, in patients with advanced malignancies. *Clinical Cancer Research* **2004,** 10, 3708–3716.

Klibanov, A. L.; Maruyama, K.; Torchilin, V. P.; Huang, L., Amphipathic Polyethyleneglycols Effectively Prolong the Circulation Time of Liposomes. *Febs Letters* **1990,** 268, (1), 235–237.

Krasnici, S.; Werner, A.; Eichhorn, M. E.; Schmitt-Sody, M.; Pahernik, S. A.; Sauer, B.; Schulze, B.; Teifel, M.; Michaelis, U.; Naujoks, K.; Dellian, M., Effect

of the surface charge of liposomes on their uptake by angiogenic tumor vessels. *International Journal of Cancer* **2003,** 105, (4), 561–567.

Kwon, G., Suwa, S., Yokoyama, M., Okano, T., Sakurai, Y., and Kataoka, K., Enhanced tumor accumulation and prolonged circulation times of micelle-forming poly(ethylene oxide-aspartate) block copolymer-adriamycin conjugates. *Journal of Controlled Release* **1994,** 29, 17–23.

Kwon, G. S.; Naito, M.; Kataoka, K.; Yokoyama, M.; Sakurai, Y.; Okano, T., Block copolymer micelles as vehicles for hydrophobic drugs. *Colloids and Surfaces, B: Biointerfaces* **1994,** 2, (4), 429–34.

Kwon, G. S.; Okano, T., Polymeric micelles as new drug carriers. *Advanced Drug Delivery Reviews* **1996,** 21, (2), 107–116.

La, S. B., Okano, T., and Kataoka, K., Preparation and characterization of the micelle-forming polymeric drug indomethacin-incorporated poly(ethylene oxide)-poly(β-benzyl L-aspartate) block copolymer micelles. *Journal of Pharmaceutical Sciences* **1996,** 85, (1), 85–90.

Lam, J. S.; Benson, M. C.; O'Donnell, M. A.; Sawczuk, A.; Gavazzi, A.; Wechsler, M. H.; Sawczuk, I. S., Bacillus Calmete-Guerin plus interferon-α2B intravesical therapy maintains an extended treatment plan for superficial bladder cancer with minimal toxicity. *Urologic Oncology: Seminars and Original Investigations* **2003,** 21, (5), 354–360.

Lammers, T.; Kuhnlein, R.; Kissel, M.; Subr, V.; Etrych, T.; Pola, R.; Pechar, M.; Ulbrich, K.; Storm, G.; Huber, P.; Peschke, P., Effect of physicochemical modification on the biodistribution and tumor accumulation of HPMA copolymers. *Journal of Controlled Release* **2005,** 110, (1), 103–18.

Langer, C. J., CT-2103: a novel macromolecular taxane with potential advantages compared with conventional taxanes. *Clinical Lung Cancer* **2004,** 6 Suppl 2, S85–8.

Lavasanifar, A.; Samuel, J.; Kwon, G. S., Micelles self-assembled from poly(ethylene oxide)-block-poly(N-hexyl stearate L-aspartamide) by a solvent evaporation method: effect on the solubilization and haemolytic activity of amphotericin B. *Journal of Controlled Release* **2001,** 77, (1–2), 155–160.

Le Garrec, D.; Gori, S.; Luo, L.; Lessard, D.; Smith, D. C.; Yessine, M. A.; Ranger, M.; Leroux, J. C., Poly(N-vinylpyrrolidone)-block-poly(D,L-lactide) as a new polymeric solubilizer for hydrophobic anticancer drugs: in vitro and in vivo evaluation. *Journal of Controlled Release* **2004,** 99, (1), 83–101.

Lee, J.; Cho, E. C.; Cho, K., Incorporation and release behavior of hydrophobic drug in functionalized poly(D,L-lactide)-block-poly(ethylene oxide) micelles. *Journal of Controlled Release* **2004,** 94, (2–3), 323–35.

Li, Y.; Kwon, G. S., Methotrexate esters of poly(ethylene oxide)-block-poly(2-hydroxyethyl-L-aspartamide). Part I: Effects of the level of methotrexate conjugation on the stability of micelles and on drug release. *Pharmaceutical Research* **2000,** 17, (5), 607–11.

Lim Soo, P.; Eisenberg, A., Preparation of block copolymer vesicles in solution. *Journal of Polymer Science: Part B: Polymer Physics* **2004,** 42, (6), 923–938.

Lim Soo, P.; Lovric, J.; Davidson, P.; Maysinger, D.; Eisenberg, A., Polycaprolactone-block-poly(ethylene oxide) micelles: A nanodelivery system for 17B-estradiol. *Molecular Pharmaceutics* **2005,** 2, (6), 519–527.

Lim Soo, P.; Luo, L.; Maysinger, D.; Eisenberg, A., Incorporation and Release of Hydrophobic Probes in Biocompatible Polycaprolactone-block-poly(ethylene oxide) Micelles: Implications for Drug Delivery. *Langmuir* **2002,** 18, (25), 9996–10004.

Lin, W. J., Lee, W.J., and Lin, C.C., Stability and release performance of a series of pegylated copolymeric micelles. *Pharmaceutical Research* **2003,** 20, (4), 668–673.

Liu, J., Xiao, Y., and Allen, C., Polymer-drug compatibility: a guide to the development of delivery systems for the anticancer agent, ellipticine. *Journal of Pharmaceutical Sciences* **2004,** 93, (1), 132–143.

Liu, J.; Allen, C., Polymeric Nanocarriers: Delivery Technology for Therapies of the 21st Century. *The Drug Delivery Companies Report Autumn/Winter 2003* **2003**, 25–29.

Liu, J.; Lee, H.; Huesca, M.; Young, A.; Allen, C., Liposome formulation of a novel hydrophobic aryl-imidazole compound for anti-cancer therapy. *Cancer Chemotherapy and Pharmacology* **2006,** 58, (3), 306–318.

Liu, J.; Zeng, F.; Allen, C., In vivo fate of unimers and micelles of a poly(ethylene glycol)-block-poly(caprolactone) copolymer in mice following intravenous administration. *European Journal of Pharmaceutics and Biopharmaceutics* **2007,** 65, (3), 309–319.

Liu, J.; Zeng, F.; Allen, C., Influence of serum protein on polycarbonate-based copolymer micelles as a delivery system for a hydrophobic anti-cancer agent. *Journal of Controlled Release* **2005,** 103, (2), 481–97.

Liu, S. Q.; Tong, Y. W.; Yang, Y.-Y., Incorporation and in vitro release of doxorubicin in thermally sensitive micelles made from poly(N-isopropylacrylamide-co-N,N-dimethylacrylamide)-b- poly(D,L-lactide-co-glycolide) with varying compositions. *Biomaterials* **2005,** 26, (24), 5064–5074.

Lukyanov, A. N.; Torchilin, V. P., Micelles from lipid derivatives of water-soluble polymers as delivery systems for poorly soluble drugs. *Advanced Drug Delivery Reviews* **2004,** 56, (9), 1273–1289.

Luppi, B.; Bigucci, F.; Cerchiara, T.; Andrisano, V.; Pucci, V.; Mandrioli, R.; Zecchi, V., Micelles based on polyvinyl alcohol substituted with oleic acid for targeting of lipophilic drugs. *Drug Delivery: Journal of Delivery and Targeting of Therapeutic Agents* **2005,** 12, (1), 21–26.

Luppi, B.; Orienti, I.; Bigucci, F.; Cerchiara, T.; Zuccari, G.; Fazzi, S.; Zecchi, V., Poly(vinylalcohol-co-vinyloleate) for the preparation of micelles enhancing retinyl palmitate transcutaneous permeation. *Drug Delivery: Journal of Delivery and Targeting of Therapeutic Agents* **2002,** 9, (3), 147–152.

Maeda, H., The enhanced permeability and retention (EPR) effect in tumor vasculature: the key role of tumor-selective macromolecular drug targeting. *Advances in Enzyme Regulation* **2001,** 41, 189–207.

Maeda, H.; Matsumura, Y., Tumoritropic and lymphotropic principles of macromolecular drugs. *Critical Reviews in Therapeutic Drug Carrier Systems* **1989,** 6, (3), 193–210.

Matsumura, Y., Hamaguchi, T., Ura, T., Muro, K., Yamada, Y., Shimada, Y., Shitao, K., Okusaka, T., Ueno, H., Ikeda, M., and Watanabe, N., Phase I clinical trial and pharmacokinetic evaluation of NK911, a micelle-encapsulated doxorubicin. *British Journal of Cancer* **2004,** 91, 1775–1781.

Matsumura, Y.; Maeda, H., A new concept for macromolecular therapeutics in cancer chemotherapy: mechanism of tumoritropic accumulation of proteins and the antitumor agent smancs. *Cancer Research* **1986,** 46, 6387–92.

Matsuoka, S.; Murata, M., Membrane permeabilizing activity of amphotericin B is affected by chain length of phosphatidylcholine added as minor constituent. *Biochimica Et Biophysica Acta-Biomembranes* **2003,** 1617, (1–2), 109–115.

Mayhew, E.; Rustum, Y. M.; Szoka, F.; Papahadjopoulos, D., Role of Cholesterol in Enhancing the Anti-Tumor Activity of Cytosine-Arabinoside Entrapped in Liposomes. *Cancer Treatment Reports* **1979,** 63, (11–1), 1923–1928.

Medigene AG Website. www.medigene.com/englisch/projekte

Meerum Terwogt, J. M.; ten Bokkel Huinink, W. W.; Schellens, J. H.; Schot, M.; Mandjes, I. A.; Zurlo, M. G.; Rocchetti, M.; Rosing, H.; Koopman, F. J.;

Beijnen, J. H., Phase I clinical and pharmacokinetic study of PNU166945, a novel water-soluble polymer-conjugated prodrug of paclitaxel. *Anticancer Drugs* **2001,** 12, (4), 315–23.

Mizumura, Y.; Matsumura, Y.; Hamaguchi, T.; Nishiyama, N.; Kataoka, K.; Kawaguchi, T.; Hrushesky, W. J.; Moriyasu, F.; Kakizoe, T., Cisplatin-incorporated polymeric micelles eliminate nephrotoxicity, while maintaining antitumor activity. *Japanese Journal of Cancer Research* **2001,** 92, (3), 328–36.

Molineux, G., The design and development of pegfilgrastim (PEG-rmetHuG-CSF, Neulasta®). *Current Pharmaceutical Design* **2004,** 10, (11), 1235–1244.

Montaguti, P.; Melloni, E.; Cavalletti, E., Acute intravenous toxicity of dimethyl sulfoxide, polyethylene glycol 400, dimethylformamide, absolute ethanol, and benzyl alcohol in inbred mouse strains. *Arzneimittelforschung* **1994,** 44, (4), 566–70.

Moribe, K.; Maruyama, K.; Iwatsuru, M., Encapsulation characteristics of nystatin in liposomes: effects of cholesterol and polyethylene glycol derivatives. *International Journal of Pharmaceutics* **1999,** 188, (2), 193–202.

Nah, J.-W.; Jeong, Y.-I.; Cho, C.-S., Clonazepam release from core-shell type nanoparticles composed of poly(B-benzyl L-glutamate) as the hydrophobic part and poly(ethylene oxide) as the hydrophilic part. *Journal of Polymer Science, Part B: Polymer Physics* **1998,** 36, (3), 415–423.

Nakanishi, T.; Fukushima, S.; Okamoto, K.; Suzuki, M.; Matsumura, Y.; Yokoyama, M.; Okano, T.; Sakurai, Y.; Kataoka, K., Development of the polymer micelle carrier system for doxorubicin. *Journal of Controlled Release* **2001,** 74, (1–3), 295–302.

Nishiyama, N.; Kataoka, K., Current state, achievements, and future prospects of polymeric micelles as nanocarriers for drug and gene delivery. *Pharmacology and Therapeutics* **2006,** 112, (3), 630–648.

Okusaka, T.; Matsumura, Y.; Aoki, K., New approaches for pancreatic cancer in Japan. *Cancer Chemotherapy and Pharmacology* **2004,** 54, (SUPPL. 1).

Panchagnula, R., Pharmaceutical aspects of paclitaxel. *International Journal of Pharmaceutics* **1998,** 172, (1–2), 1–15.

Papahadjopoulos, D., Steric Stabilization. In *Liposomes – Rational Design*, Janoff, A. S., Ed. Marcel Dekker, Inc.: New York, 1999; pp 1–12.

Papahadjopoulos, D.; Allen, T. M.; Gabizon, A.; Mayhew, E.; Matthay, K.; Huang, S. K.; Lee, K. D.; Woodle, M. C.; Lasic, D. D.; Redemann, C.; et al., Sterically stabilized liposomes: improvements in pharmacokinetics and antitumor therapeutic efficacy. *Proceedings of the National Academy of Sciences of the United States of America* **1991,** 88, (24), 11460–4.

Parveen, S.; Sahoo, S. K., Nanomedicine: Clinical applications of polyethylene glycol conjugated proteins and drugs. *Clinical Pharmacokinetics* **2006,** 45, (10), 965–988.

Raffy, S.; Teissie, J., Control of lipid membrane stability by cholesterol content. *Biophysical Journal* **1999,** 76, (4), 2072–2080.

Ramaswamy, M.; Zhang, X.; Burt, H. M.; Wasan, K. M., Human plasma distribution of free paclitaxel and paclitaxel associated with diblock copolymers. *Journal of Pharmaceutical Sciences* **1997,** 86, (4), 460–4.

Reed, K. W.; Yalkowsky, S. H., Lysis of human red blood cells in the presence of various cosolvents. *Journal of Parenteral Science and Technology* **1985,** 39, (2), 64–9.

Ringsdorf, H., Structure and Properties of Pharmacologically Active Polymers. *Journal of Polymer Science, Polymer Symposia* **1975**, (51), 135–153.

Rowinsky, E. K.; Rizzo, J.; Ochoa, L.; Takimoto, C. H.; Forouzesh, B.; Schwartz, G.; Hammond, L. A.; Patnaik, A.; Kwiatek, J.; Goetz, A.; Denis, L.; McGuire, J.; Tolcher, A. W., A phase I and pharmacokinetic study of pegylated camptothecin as a 1-hour infusion every 3 weeks in patients with advanced solid malignancies. *Journal of Clinical Oncology* **2003,** 21, (1), 148–57.

Saetern, A. M.; Flaten, G. E.; Brandl, M., A method to determine the incorporation capacity of camptothecin in liposomes. *Aaps Pharmscitech* **2004,** 5, (3).

Samyang Corporation website. www.samyangpharm.com

Satchi-Fainaro, R.; Duncan, R.; Barnes, C. M., Polymer therapeutics for cancer: Current status and future challenges. *Advances in Polymer Science* **2006,** 193, (1), 1–65.

Scarpa, A.; Degier, J., Cation Permeability of Liposomes as a Function of Chemical Composition of Lipid Bilayers. *Biochimica Et Biophysica Acta* **1971,** 241, (3), 789–797.

Seki, J.; Sonoke, S.; Saheki, A.; Koike, T.; Fukui, H.; Doi, M.; Mayumi, T., Lipid transfer protein transports compounds from lipid nanoparticles to plasma lipoproteins. *International Journal of Pharmaceutics* **2004,** 275, (1–2), 239–48.

Senior, J. H., Fate and Behavior of Liposomes Invivo - a Review of Controlling Factors. *Crc Critical Reviews in Therapeutic Drug Carrier Systems* **1987,** 3, (2), 123–193.

Senior, J.; Crawley, J. C. W.; Gregoriadis, G., Tissue Distribution of Liposomes Exhibiting Long Half-Lives in the Circulation after Intravenous-Injection. *Biochimica Et Biophysica Acta* **1985,** 839, (1), 1–8.

Sessa, G.; Weissman, G., Phospholipid Spherules (Liposomes) as a Model for Biological Membranes. *Journal of Lipid Research* **1968,** 9, (3), 310–318.

Seymour, L. W.; Duncan, R.; Strohalm, J.; Kopecek, J., Effect of molecular weight (Mw) of N-(2-hydroxypropyl)methacrylamide copolymers on body distribution and rate of excretion after subcutaneous, intraperitoneal, and intravenous administration to rats. *Journal of Biomedical Materials Research* **1987,** 21, (11), 1341–58.

Seymour, L. W.; Ferry, D. R.; Anderson, D.; Hesslewood, S.; Julyan, P. J.; Poyner, R.; Doran, J.; Young, A. M.; Burtles, S.; Kerr, D. J., Hepatic drug targeting: phase I evaluation of polymer-bound doxorubicin. *Journal of Clinical Oncology* **2002,** 20, (6), 1668–76.

Shabbits, J. A.; Chiu, G. N.; Mayer, L. D., Development of an in vitro drug release assay that accurately predicts in vivo drug retention for liposome-based delivery systems. *Journal of Controlled Release* **2002,** 84, (3), 161–70.

Shaffer, S. A.; Baker Lee, C.; Kumar, A.; Singer, J. W., Proteolysis of xyotax by lysosomal cathepsin B; metabolic profiling in tumor cells using LC-MS. *European Journal of Cancer* **2002,** 38, S129–S129.

Shen, L.-J.; Shen, W.-C., Drug evaluation: ADI-PEG-20 - A PEGylated arginine deiminase for arginine-auxotrophic cancers. *Current Opinion in Molecular Therapeutics* **2006,** 8, (3), 240–248.

Shuai, X.; Ai, H.; Nasongkla, N.; Kim, S.; Gao, J., Micellar carriers based on block copolymers of poly(ε-caprolactone) and poly(ethylene glycol) for doxorubicin delivery. *Journal of Controlled Release* **2004,** 98, (3), 415–426.

Simard, P.; Leroux, J.-C.; Allen, C.; Meyer, O., Liposomes for Drug Delivery. In *Nanoparticles for Pharmaceutical Applications*, Domb, A. J.; Tabata, Y.; Ravi Kumar, M. N. V.; Farber, S., Eds. ASP: Stevenson Ranch, 2007; pp 1–62.

Slichenmyer, W. J.; Rowinsky, E. K.; Donehower, R. C.; Kaufmann, S. H., The current status of camptothecin analogues as antitumor agents. *Journal of National Cancer Institute* **1993,** 85, (4), 271–91.

Soepenberg, O.; De Jonge, M. J. A.; Sparreboom, A.; De Bruin, P.; Eskens, F. A. L. M.; De Heus, G.; Wanders, J.; Cheverton, P.; Ducharme, M. P.; Verweij, J., Phase I and pharmacokinetic study of DE-310 in patients with advanced solid tumors. *Clinical Cancer Research* **2005,** 11, (2 I), 703–711.

Sparreboom, A.; van Zuylen, L.; Brouwer, E.; Loos, W. J.; de Bruijn, P.; Gelderblom, H.; Pillay, M.; Nooter, K.; Stoter, G.; Verweij, J., Cremophor EL-mediated alteration of paclitaxel distribution in human blood: clinical pharmacokinetic implications. *Cancer Research* **1999,** 59, (7), 1454–7.

Strickley, R. G., Solubilizing excipients in oral and injectable formulations. *Pharmaceutical Research* **2004,** 21, (2), 201–30.

Strieth, S.; Eichhorn, M. E.; Sauer, B.; Schulze, B.; Teifel, M.; Michaelis, U.; Dellian, M., Neovascular targeting chemotherapy: Encapsulation of paclitaxel in cationic liposomes impairs functional tumor microvasculature. *International Journal of Cancer* **2004,** 110, (1), 117–124.

Supratek Pharma Inc. website. www.supratek.com

Swenson, C. E.; Perkins, W. R.; Roberts, P.; Janoff, A. S., Liposome technology and the development of Myocet (TM) (liposomal doxorubicin citrate). *Breast* **2001,** 10, 1–7.

Thiesen, J.; Kramer, I., Physico-chemical stability of docetaxel premix solution and docetaxel infusion solutions in PVC bags and polyolefine containers. *Pharmacy World and Science* **1999,** 21, (3), 137–141.

Thomson, A. H.; Vasey, P. A.; Murray, L. S.; Cassidy, J.; Fraier, D.; Frigerio, E.; Twelves, C., Population pharmacokinetics in phase I drug development: A phase I study of PK1 in patients with solid tumours. *British Journal of Cancer* **1999,** 81, (1), 99–107.

Trimaille, T.; Mondon, K.; Gurny, R.; Moller, M., Novel polymeric micelles for hydrophobic drug delivery based on biodegradable poly(hexyl-substituted lactides). *International Journal of Pharmaceutics* **2006,** 319, (1–2), 147–154.

Uchino, H.; Matsumura, Y.; Negishi, T.; Koizumi, F.; Hayashi, T.; Honda, T.; Nishiyama, N.; Kataoka, K.; Naito, S.; Kakizoe, T., Cisplatin-incorporating polymeric micelles (NC-6004) can reduce nephrotoxicity and neurotoxicity of cisplatin in rats. *British Journal of Cancer* **2005,** 93, (6), 678–687.

Vakil, R.; Kwon, G. S., Poly(ethylene glycol)-b-poly(ε-caprolactone) and PEG-phospholipid form stable mixed micelles in aqueous media. *Langmuir* **2006,** 22, (23), 9723–9729.

van Zuylen, L.; Verweij, J.; Sparreboom, A., Role of formulation vehicles in taxane pharmacology. *Investigational New Drugs* **2001,** 19, (2), 125–141.

Vasey, P. A.; Kaye, S. B.; Morrison, R.; Twelves, C.; Wilson, P.; Duncan, R.; Thomson, A. H.; Murray, L. S.; Hilditch, T. E.; Murray, T.; Burtles, S.; Fraier, D.; Frigerio, E.; Cassidy, J., Phase I clinical and pharmacokinetic study of PK1 [N-(2- hydroxypropyl)methacrylamide copolymer doxorubicin]: First member of a new class of chemotherapeutic agents - Drug-polymer conjugates. *Clinical Cancer Research* **1999,** 5, (1), 83–94.

Veronese, F. M.; Pasut, G., PEGylation, successful approach to drug delivery. *Nature Reviews Drug Discovery* **2005,** 10, (21), 1451–8.

Vicent, M. J.; Duncan, R., Polymer conjugates: Nanosized medicines for treating cancer. *Trends in Biotechnology* **2006,** 24, (1), 39–47.

Wachters, F. M.; Groen, H. J.; Maring, J. G.; Gietema, J. A.; Porro, M.; Dumez, H.; de Vries, E. G.; van Oosterom, A. T., A phase I study with MAG-camptothecin intravenously administered weekly for 3 weeks in a 4-week cycle in adult patients with solid tumours. *British Journal of Cancer* **2004,** 90, (12), 2261–7.

Waterhouse, D. N.; Madden, T. D.; Cullis, P. R.; Bally, M. B.; Mayer, L. D.; Webb, M. S., Preparation, characterization, and biological analysis of liposomal formulations of vincristine. *Liposomes, Pt E*, 2005; Vol. 391, pp 40–57.

Webb, M. S.; Saxon, D.; Wong, F. M. P.; Lim, H. J.; Wang, Z.; Bally, M. B.; Choi, L. S. L.; Cullis, P. R.; Mayer, L. D., Comparison of different hydrophobic anchors conjugated to poly(ethylene glycol): Effects on the pharmacokinetics of liposomal vincristine. *Biochimica Et Biophysica Acta-Biomembranes* **1998,** 1372, (2), 272–282.

Wente, M. N.; Kleeff, J.; Buchler, M. W.; Wanders, J.; Cheverton, P.; Langman, S.; Friess, H., DE-310, a macromolecular prodrug of the topoisomerase-I-inhibitor

exatecan (DX-8951), in patients with operable solid tumors. *Investigational New Drugs* **2005,** 23, (4), 339–347.

Wong, H. L.; Bendayan, R.; Rauth, A. M.; Wu, X. Y., Simultaneous delivery of doxorubicin and GG918 (Elacridar) by new Polymer-Lipid Hybrid Nanoparticles (PLN) for enhanced treatment of multidrug-resistant breast cancer. *Journal of Controlled Release* **2006,** 116, (3), 275–284.

Woodle, M. C.; Lasic, D. D., Sterically Stabilized Liposomes. *Biochimica Et Biophysica Acta* **1992,** 1113, (2), 171–199.

Yamamoto, Y.; Nagasaki, Y.; Kato, Y.; Sugiyama, Y.; Kataoka, K., Long-circulating poly(ethylene glycol)-poly(D,L-lactide) block copolymer micelles with modulated surface charge. *Journal of Controlled Release* **2001,** 77, (1–2), 27–38.

Yamaoka, T.; Tabata, Y.; Ikada, Y., Distribution and tissue uptake of poly(ethylene glycol) with different molecular weights after intravenous administration to mice. *Journal of Pharmaceutical Sciences* **1994,** 83, (4), 601–6.

Yasugi, K.; Nagasaki, Y.; Kato, M.; Kataoka, K., Preparation and characterization of polymer micelles from poly(ethylene glycol)-poly(D,L-lactide) block copolymers as potential drug carrier. *Journal of Controlled Release* **1999,** 62, (1–2), 89–100.

Yokoyama, M., Fukushima, S., Uehara, R., Okamoto, K., Kataoka, K., Sakurai, Y., and Okano, T., Characterization of physical entrapment and chemical conjugation of adriamycin in polymeric micelles and their design for in vivo delivery to a solid tumor. *Journal of Controlled Release* **1998,** 50, 79–92.

Yuan, F.; Dellian, M.; Fukumura, D.; Leunig, M.; Berk, D. A.; Torchilin, V. P.; Jain, R. K., Vascular-Permeability in a Human Tumor Xenograft - Molecular-Size Dependence and Cutoff Size. *Cancer Research* **1995,** 55, (17), 3752–3756.

Zhang, J. A.; Anyarambhatla, G.; Ma, L.; Ugwu, S.; Xuan, T.; Sardone, T.; Ahmad, I., Development and characterization of a novel Cremophor (R) EL free liposome-based paclitaxel (LEP-ETU) formulation. *European Journal of Pharmaceutics and Biopharmaceutics* **2005,** 59, (1), 177–187.

Zhang, J. A.; Xuan, T.; Parmar, M.; Ma, L.; Ugwu, S.; Ali, S.; Ahmad, I., Development and characterization of a novel liposome-based formulation of SN-38. *International Journal of Pharmaceutics* **2004,** 270, (1–2), 93–107.

Zhigaltsev, I. V.; Maurer, N.; Akhong, Q. F.; Leone, R.; Leng, E.; Wang, J.; Semple, S. C.; Cullis, P. R., Liposome-encapsulated vincristine, vinblastine and vinorelbine: A comparative study of drug loading and retention. *Journal of Controlled Release* **2005,** 104, (1), 103–111.

13

Engineering of Amphiphilic Block Copolymers for Drug and Gene Delivery

Xiao-Bing Xiong, Hasan Uludağ, and Afsaneh Lavasanifar

Introduction

Amphiphilic block copolymers have been used for diverse applications in pharmaceutical industry for decades (Croy and Kwon, 2006; Alexandridis and Lindman, 2000). They have been used as safer replacements for low molecular weight surfactants in the solubilization of poorly soluble drugs (Kwon, 2003), as stabilizing agents in the formulation of coarse and colloidal dispersions (Tadros, 2006; Shenoy and Amiji, 2005), as gels providing depot or formulations (Vinogradov et al., 2002), and, more recently, as core/shell self-assembled colloids for nanoscale drug and gene delivery (Nishiyama and Kataoka, 2006).

Modern pharmaceutics rely heavily on the design and development of nanoscale dosage forms that can incorporate therapeutic agents effectively, change the normal fate of drugs in a biological system, and direct them toward their cellular or sub-cellular targets. Polymeric micelles are important dosage forms in this regard, since segregation of core/shell structure along with versatility of block copolymer chemistry provides infinite opportunities for the manipulation of their structure. This can lead to the development of optimum delivery system for challenging therapeutic agents, e.g., poorly soluble drugs, proteins, and genes. Block copolymers and polymeric micelles have been the subject of several excellent and extensive review articles, book chapters, and books in recent years (Croy and Kwon, 2006; Alexandridis and Lindman, 2000; Xiong et al., 2006; Aliabadi and Lavasanifar, 2006; Osada and Kataoka, 2006; Lavasanifar et al., 2002a). To our knowledge, six polymeric micellar formulations, all developed for the solubilization and delivery of anticancer drugs, are currently in different stages of clinical trials in Japan, Canada, Europe, and South Korea.

Perhaps one of the most widely used types of block copolymers, especially in traditional pharmaceutics, are di- or triblocks of ethylene oxide (EO) and propylene oxide (PO), namely, Pluronics® or Polaxamers. The water-soluble EO-*b*-PO block copolymers are stable over a wide range of pH and compatible with biological tissue. It is possible to change the size of EO and PO blocks with or without change in the hydrophilic lipophilic

M.M. de Villiers et al. (eds.), *Nanotechnology in Drug Delivery*, DOI: 10.1007/978-0-387-77667-5_13,

balance (HLB) of amphiphile and vary the molecular weight of the whole polymer. As a result of such structural changes, different properties and functions may be achieved from the amphiphilic macromolecules at the interfaces (Newman et al., 1998a,b). Pluronics have also shown unique biological activities themselves, such as reducing the activity of membrane efflux pumps in drug-resistant tumor cells (Kabanov et al., 2002; Minko et al., 2005) and enhancing the transfection efficiency of viral vectors in gene delivery (Kabanov et al., 2005; Kabanov et al., 2002; Wang et al., 2005).

Amphiphilic block copolymers with poly(*l*-amino acid) (PLAA), poly(esters), and poly(amine) as their hydrophobic block are the most extensively researched micelle-forming polymers for nanoscale delivery (Aliabadi and Lavasanifar, 2006; Osada and Kataoka, 2006; Arnida et al., 2006). The aim of this chapter is to review the general synthesis of amphiphilic block copolymers and provide an overview of chemical modifications performed to enhance the biological performance of micelle-forming PLAA, poly(esters), and poly(amine) block copolymers in drug and gene delivery. Such polymers have been an integral part of first-generation polymeric micelles, whose function relies on prolonged residence of drugs in systemic circulation. For each category, development of second generation polymeric micelles, i.e., polymeric micelles that can specifically seek and actively deliver their therapeutic cargo to diseased cells, will be briefly discussed. A condensed overview on third-generation polymeric micelles, i.e., multifunctional carriers designed to respond to more than one internal/external stimulus at the same time, will be provided, as well. Most recent research in the field is highlighted, without an extensive overview on single polymeric micellar system. It is noteworthy to mention that this chapter does not provide a critical review, but rather a survey of different chemical strategies for generating polymeric micellar delivery systems.

PEO-*b*-poly(amino acid) Block Copolymers

General Synthesis

Synthesis of PLAAs is usually achieved though ring-opening polymerization (ROP) of α-amino acid-*N*-carboxyanhydrides (NCAs) (Figure 13.1) (Smeenk, 2005), using different nucleophiles or bases (e.g., primary amines and alkoxide anions) (Harwood, 1984; Kricheldorf and Mulhaupt, 1979; Kricheldorf et al., 2005; Sekiguchi, 1981). NCAs can be prepared from

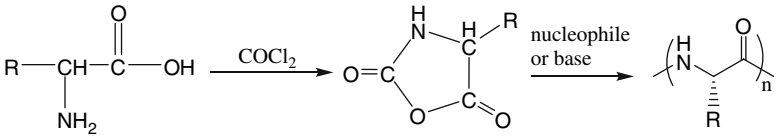

Figure 13.1 General scheme for the synthesis of PEO-*b*-PLAA-based block copolymers by ring-opening polymerization of α-amino acid-*N*-carboxyanhydrides (NCAs).

α-amino acids using a solution of phosgene in THF by the Fuchs–Farthing method (Fuller et al., 1976; Bikram et al., 2004).

PEO-*b*-PLAA block copolymers are synthesized using α-methoxy-ω-amino PEO as the initiator (Harada and Kataoka, 1995). When primary amines are used as initiators, the polymerization of NCAs may proceed by two mechanisms: amine mechanism and activated monomer (AM) mechanism (Figure 13.2) (Sekiguchi, 1981; Deming, 2002). The amine mechanism is a nucleophilic ring-opening chain-growth process in which the polymer grows linearly with monomer conversion (Figure 13.2A) and the initiator becomes ($R'NH_2$) part of the final product, leading to a copolymer. In AM mechanism, NCA will be deprotonated forming a nucleophile that initiates chain growth (Figure 13.2B). The initiator is not included in the final product and only homopolymer will be expected in this mechanism. In a given

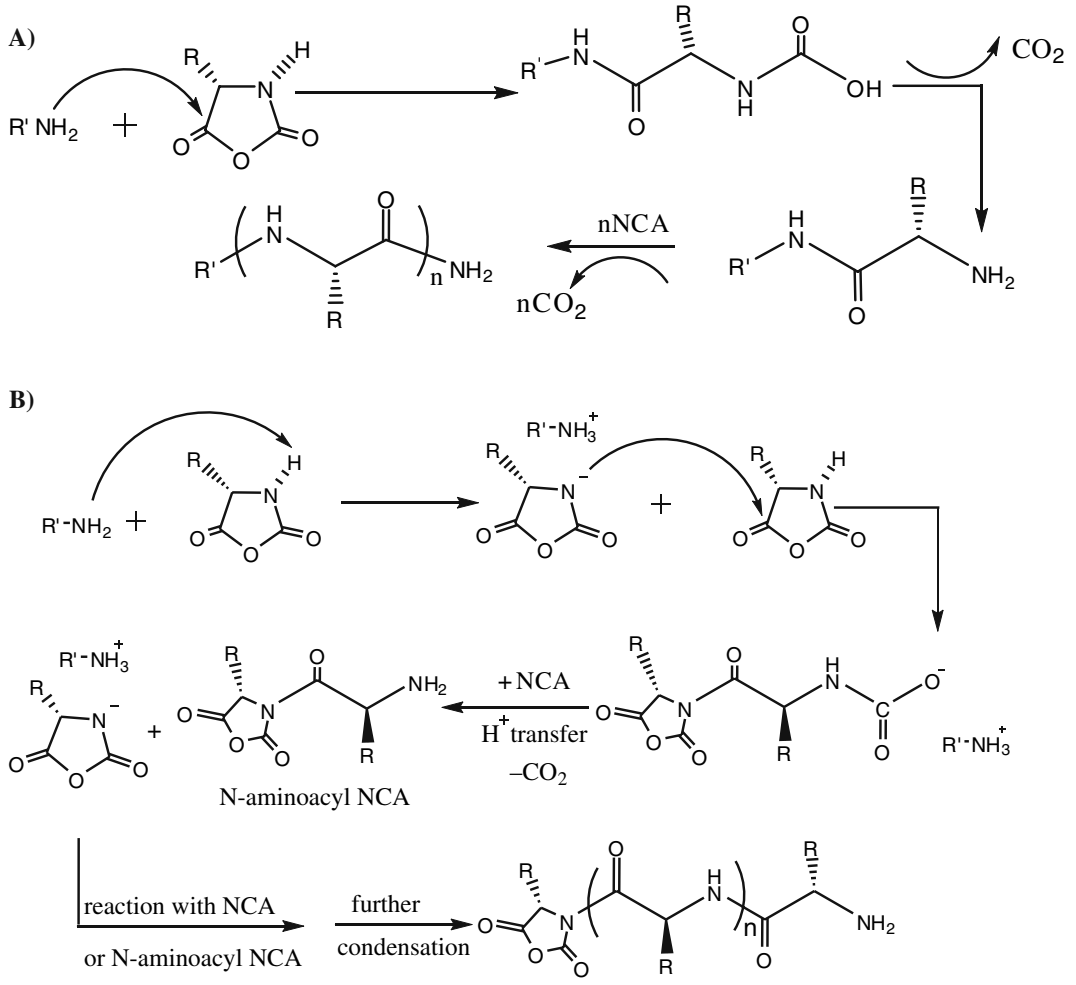

Figure 13.2 **(A)** Amine mechanism and **(B)** activated monomer (AM) mechanism of NCA polymerization (reproduced from Deming, 2002 with permission).

polymerization process, the system can switch back and forth between the amine and AM mechanisms. Since a propagation step for one mechanism is a side reaction for the other and vice versa, block polymers prepared from NCA method using amine initiators have structures different from those predicted by monomer feed compositions (Tsuruta et al., 1965) and most likely have considerable homopolymer contamination. Therefore, efforts to control the polymerization in the way of amine mechanism but to avoid the way of AM mechanism are expected to increase the product yield and efficiency to produce copolymers.

Transition metal initiators (Tsuruta et al., 1965; Deming, 1997; Freireic et al., 1974; Yamashit and Tani, 1974; Yamashit et al., 1974) have been developed to control the addition of each NCA monomer to the polymer chain-ends to reduce the side reactions in the NCA polymerization. However, this method is not suitable for the preparation of high molecular weight PLAAs due to the presence of chain-transfer reactions.

Living polymerization has been developed to overcome the limitations in the preparation of PLAAs (Brzezinska and Deming, 2004; Dvorak and Rypacek, 1995; Vayaboury et al., 2004). In this method, the transition metal initiator activates the monomers and forms covalent active species, which permit the formation of polypeptides via the living polymerization of NCAs (Figure 13.3). The metals react identically with NCA monomers to form metallacyclic complexes by oxidative addition across the anhydride bond of NCA (Deming, 2002; Brzezinska and Deming, 2004; Deming, 2000).

Alternatively, PEO-*b*-PLAA can be synthesized by coupling PEO to PLAA after the polymerization of PLAA. For instance, poly(L-Histidine) (p(L-His)) has been synthesized by base-initiated ring-opening polymerization of protected NCA of L-His and then coupled to carboxylated PEO to form PEO-*b*-p(L-His) via an amide linkage using dicyclohexyl carbodiimide (DCC) and *N*-hydroxysuccinimide (NHS) as catalysts (Lee et al., 2003b). Poly(L-aspartic acid-co-PEO) (p(L-Asp)-co-PEO) bearing amine side groups on the p(L-Asp) block has been synthesized by the melt polycondensation (post-polymerization) of the prepolymer prepared from *N*-CBz-L-aspartic acid anhydride and low molecular weight PEO using acid catalysts. The product was an alternating copolymer containing reactive amine groups on the p(L-Asp) residue (Won et al., 1998). Finally, solid and liquid phase peptide synthesis has also been used to prepare PEO-*b*-PLAAs (Van Domeselaar et al., 2003; Choi et al., 1999).

Chemical Modification of the Core in PEO-*b*-PLAA Micelles for Physical Drug Encapsulation

Existence of several functional side groups on a PLAA block is the primary advantage of the PEO-*b*-PLAAs over other micelle-forming block copolymers. Free functional side groups on the PLAA backbone provide several sites for the conjugation of different molecules. Besides, the systemic alterations in the chemical structure of the PLAA block and its side chains may lead to the customized optimization of polymeric micelles for the physical encapsulation and controlled delivery of individual therapeutic agents.

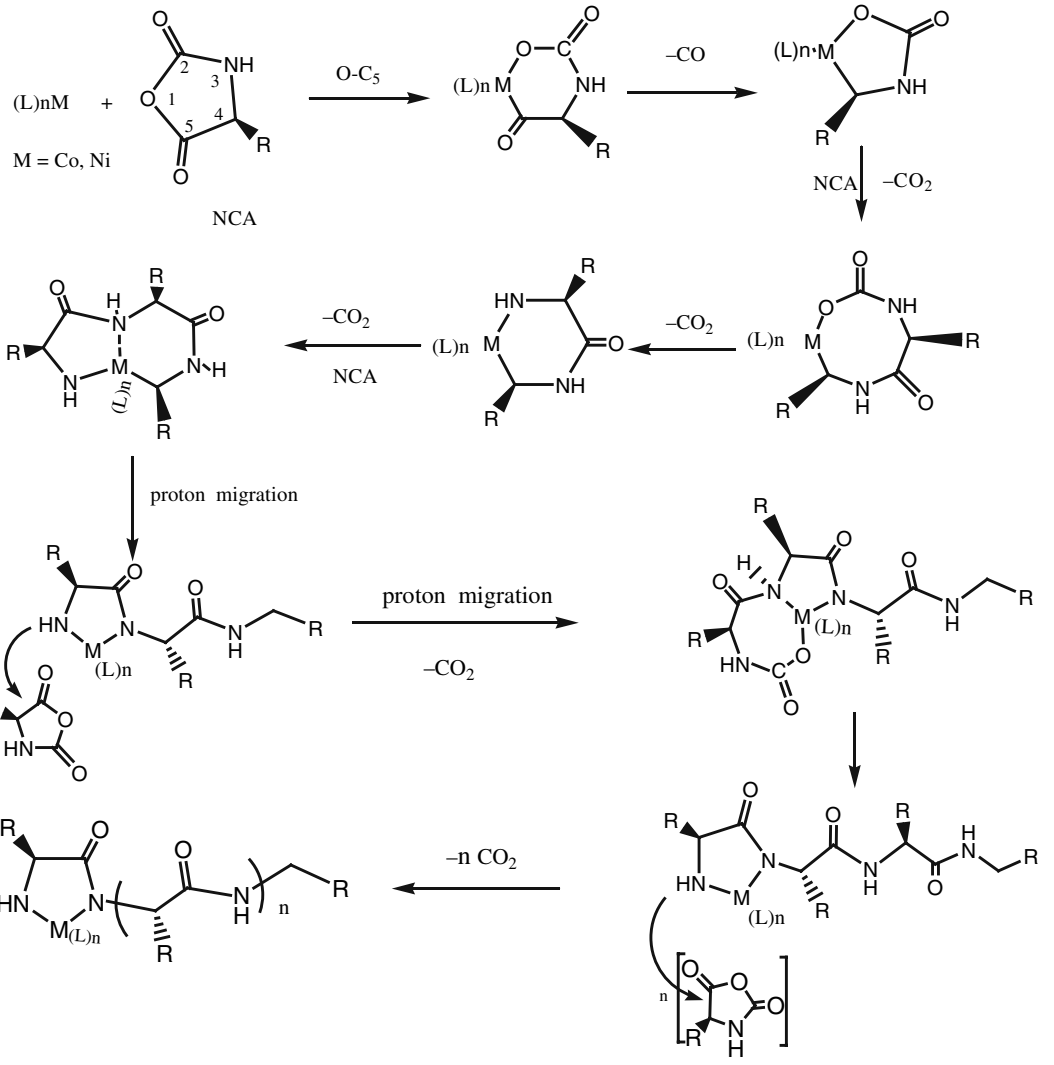

Figure 13.3 Living polymerization of NCA (reproduced from Xiong et al., 2006 with permission).

The most attention for the production of chemically modified cores in PEO-*b*-PLAA micelles for physical encapsulation of drugs has been focused on p(L-Asp) and poly(L-glutamic acid) (p(L-Glu)) (Osada and Kataoka, 2006; Lavasanifar et al., 2002a; Bae and Kataoka, 2006; Nishiyama and Kataoka, 2003; Kakizawa and Kataoka, 2002). Synthesis of PEO-*b*-poly(β-benzyl L-aspartate) (PEO-*b*-PBLA) and PEO-*b*-poly[ε-(benzyloxycarbonyl)-L-lysine] (PEO-*b*-PBLL) from polymerization of β-benzyl L-aspartate-*N*-carboxyanhydride (BLA-NCA) and *N*-carboxyanhydride of ε-(benzyloxycarbonyl)-L-lysine (BLL-NCA), respectively, using α-methoxy-ω-amino PEO as initiator has been reported (Harada and Kataoka, 1995). PEO-*b*-PBLA has shown extremely low critical micelle concentration (CMC) and such micelles were found to be highly rigid in core (Kwon et al., 1993). Micelles assembled from PEO-*b*-PBLA block

copolymers of different molecular weight and composition have been applied for the solubilization and delivery of DOX by Kataoka's group (Kataoka et al., 2000; Kwon et al., 1995). PEO-*b*-PBLA efficiently encapsulated DOX and sustained its release. The degree of polymerization of PBLA in the block copolymer seems to have little effect on the loading capacity of DOX in the micelles. Compared to free drug, the maximum tolerable dose (MTD) of DOX was raised 2.3-fold by PEO-*b*-PBLA in C26-bearing mice (Kataoka et al., 2000), which was possibly due to a change in the normal distribution of DOX by its polymeric micellar formulation away from heart (site of DOX toxicity).

PEO-*b*-PBLA micelles were also used to encapsulate Camptothecin (CPT) (Opanasopit et al., 2004; Yokoyama et al., 2004). The PBLA chain was modified by alkaline hydrolysis of its benzyl group followed by esterification with benzyl, *n*-butyl, or lauryl groups. Camptothecin has been physically encapsulated in micelles of PEO-*b*-p(L-Asp) having various side chains in the hydrophobic section. The presence of aromatic structures, e.g., benzyl or methylnaphthyl groups, was shown to be more efficient, resulting in the better stabilization of encapsulated CPT in the micellar structures. Release of CPT from the micelles was dependent on the benzyl contents and chain lengths. Sustained release, a property that relies on efficient drug diffusion from the core, was obtained when the benzyl content was high.

Micelles of PEO-*b*-PBLA have been used to solubilize indomethacin, resulting in a sustained release for the encapsulated drug. The release rate of the drug from PEO-*b*-PBLA micelles was found to be dependent on the ionization state of indomethacin, where maximum control on drug release was observed at pH values below the p*K*a of indomethacin (4.5). At this condition, indomethacin was unionized and favored the nonpolar environment of PBLA core in polymeric micelles (La et al., 1996a).

Star block copolymers and 'flower' micelles composed of PEO and poly (γ-benzyl-L-glutamate) (PBLG) have also been developed and used for DOX encapsulation (Jeong et al., 1999). Inhibition of DOX crystallization by the polymer was observed in micellar core. The PEO-*b*-PBLG-based micelles can remarkably sustain and prolong DOX release, resulting in threefold longer mean residence time for encapsulated versus free DOX in vivo.

Chemical conjugation of DOX to the p(L-Asp) block of PEO-*b*-p(L-Asp) was pursued to increase the physical entrapment of DOX inside the hydrophobic core of PEO-*b*-p(L-Asp)-DOX micelles (Nakanishi et al., 2001; Yokoyama et al., 1998; Yokoyama et al., 1994). In this system a 40–50% of DOX substitution on p(L-Asp) and a decrease in proportion of p(L-Asp)-DOX to PEO segment were necessary to achieve stable micelles. Polymeric micelles developed based on this design showed superior properties in terms of DOX release and targeting in animal models in comparison to PEO-*b*-PBLA micelles. This formulation is in clinical trials in Japan under the name of NK911.

By hydrolysis/ester exchange, or aminolysis of PBLA, benzyl ester has been replaced by various aliphatic chains to produce a variety of poly(aspartamide) derivatives that can potentially enhance the delivery of aliphatic drugs (Figure 13.4A). During the process of hydrolysis of PEO-*b*-PBLA under alkaline conditions, racemization of the aspartic acid units takes

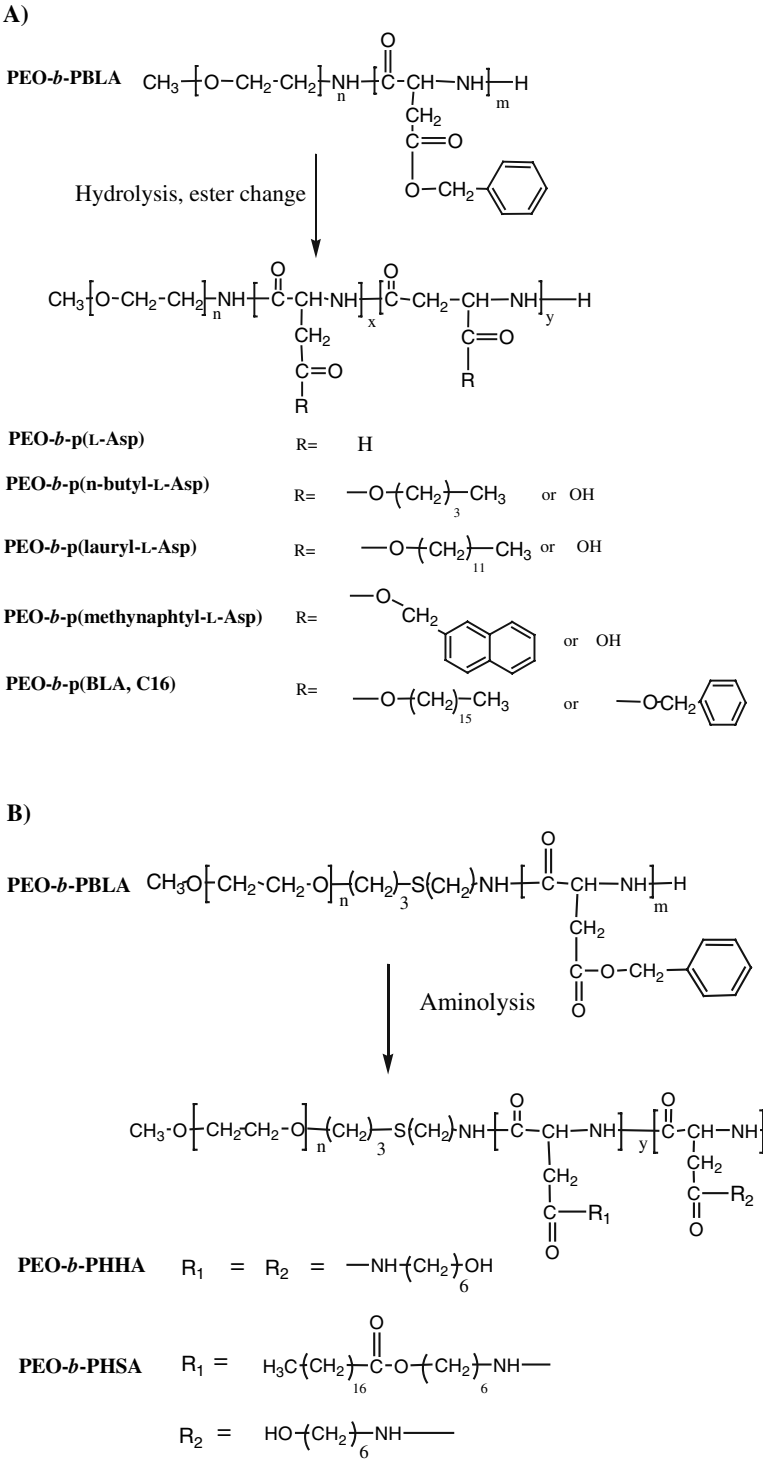

Figure 13.4 Chemical structure of PEO-*b*-PBLA bearing different substituted groups by (**A**) hydrolysis/ester change or (**B**) aminolysis.

place to form α- and β-aspartic units (Wolk et al., 1994). Notably, aminolysis reaction of PBLA with various amino compounds quantitatively proceeds even under mild conditions of room temperature (Figure 13.4B). This quantitative aminolysis reaction is quite unique for PBLA, and almost no reaction occurs for PBLG under the same conditions. Presumably, the ester group in the side chain of PBLA may be in the activated form due to the interaction with amide moieties in the main chain (Osada and Kataoka, 2006).

Block copolymers produced from hydrolysis/ester exchange (Figure 13.4A) were used to physically incorporate an aliphatic anticancer drug, KRN5500. Using DMSO as the solvent to prepare KRN5500-encapsulated micelles by the dialysis method, PEO-*b*-p(BLA, C16) (Figure 13.4A) micelles showed significantly higher KRN5500 encapsulation leading to a homogenous KRN5500 micellar solution, while precipitate was observed with KRN5500 in PEO-*b*-PBLA micelles (Yokoyama et al., 1998). Polymeric micellar KRN5500 and free drug were found to be similar in terms of anti-tumor activity against HT-29 (human colonic cancer) in vitro and MKN-45 xenografts in a mouse model, but polymeric micellar formulation was less toxic (Matsumura et al., 1999), possibly due to a reduction in non-specific interaction with healthy organs.

Micelles based on PEO-*b*-p(*l*-Asp)-bearing fatty acid esters as a side chain (Figure 13.4B) have been developed and used for the solubilization of amphotericin B (AmB) (Lavasanifar et al., 2002a; Adams et al., 2003; Adams and Kwon, 2003; Aramwit et al., 2000; Lavasanifar et al., 2001; Lavasanifar et al., 2002b). This system has shown clear advantage over PEO-*b*-PBLA in the solubilization of AmB due to the more lipophilic core. Besides, higher levels of fatty acid substitution on the p(L-Asp) backbone were shown to enhance AmB encapsulation and to lower the rate of drug release. As a result, hemolytic activity of AmB was reduced in its polymeric micellar formulation in comparison to free AmB or the common formulation Fungizone®. Polymeric micellar AmB has shown equal anti-fungal efficacy to that of Fungizone® both in vitro and in vivo (Adams et al., 2003).

Synthesis of Self-Associating PEO-b-PLAA-Drug Conjugates

PEO-*b*-PLAA-based block copolymers have also been extensively used for chemical conjugation of anticancer drugs to the core-forming block. Drugs were conjugated to the PLAA section via ester, amide, hydrazone, or disulfide bonds. The bond between the drug and polymeric carrier may be either hydrolyzable at acidic pH of the prelysosomal or lysosomal compartments, or cleaved by enzymatic hydrolysis in the lysosomal compartment (specific for amide or ester bonds).

The first example of this type of polymeric micelle has been developed by Ringsdorf et al. who reported on the preparation of micelle-forming conjugates of cyclophosphamide (CP) sulfide and PEO-*block*-poly(L-lysine) (PEO-*b*-PLL) (Hirano et al., 1979). Simultaneous conjugation of fatty acids to the polymeric backbone was used to reduce CMC and increase thermodynamic stability of this system. This formulation was found to be efficient in the stabilization of active CP metabolite in vivo, and caused a fivefold increase in the life span of L1210 tumor-bearing mice even at a reduced CP-equivalent dose.

Block copolymer drug conjugates of PEO-*b*-P(L-Asp)-DOX have been developed by Kataoka's group (Yokoyama et al., 1991; Kataoka et al., 1993). DOX was covalently conjugated to the side chain of the P(L-Asp) segment by an amide bond between the carboxylic group in P(L-Asp) and the primary amine group of the glycosidyl residue in DOX with a substitution ratio of 50% (Figure 13.5A). However, the amide bond was found to be too stable for efficient drug release in vivo. Therefore, in further studies, DOX was conjugated to p(L-Asp) through a hydrazone linker that is stable under physiological conditions but cleavable under the acidic intracellular environments of endosomes and lysosomes (Figure 13.5B) (Bae et al., 2003). When the micelles were incubated under various pH conditions from 7.4 to 3.0 in vitro, DOX was released in a time-dependent manner as external pH decreased, while no DOX release was observed under the physiological condition of pH 7.4 for over 48 h of incubation. The animal tests revealed that the pH-sensitive micelles showed an effective anti-tumor activity over a broad range of injection dose to suppress the tumor growth in mice, whereas the toxicity remained extremely low.

Development of Polyion Complex Micelles from PEO-b-PLAA for Drug Delivery

An electrostatic interaction between the ionizable groups on the PLAA block of PEO-*b*-PLAA block copolymers and charged drugs/genes has been used to produce polyion complex micelles. Incorporation of cisplatin (CDDP) into the PEO-*b*-p(L-Asp) and PEO-*b*-p(L-Glu) micelles uses this approach where an electrostatic complex between positively charged drugs/moieties and carboxyl ions on p(L-Asp) or p(L-Glu) block neutralized polymer and self-assembled it into micelles (Yokoyama et al., 1996; Nishiyama and Kataoka, 2001; Nishiyama et al., 2003). The PEO-*b*-PLAA-CDDP micelles showed an environment-responsive drug release behavior, long circulation, and passive tumor targeting (Figure 13.6) (Nishiyama et al., 2001; Nishiyama et al., 1999). The PEO-*b*-p(L-Glu) formulation of CDDP is currently in clinical trials in Japan under the name of NC-6004.

Development of Polyion Complex Micelles from PEO-b-PLAA for the Delivery of Nucleic Acid-Based Therapeutics

An exciting area of research involving micelles is the efforts to deliver nucleic acid-based therapeutics systemically. For a successful micelle-based gene delivery via systemic administration, four main concerns need to be addressed: (a) the core-forming block of the micelles should be able to combine and condense nucleic acid-based therapeutics in the core; (b) the micelles should maintain integrity under physiological conditions before they reaching the target cells; (c) the micelles should interact with the target cell specifically; and (d) the delivery system should dissociate in a predictable manner in the intracellular compartment of the target cell, facilitating the release of the entrapped nucleic acid-based moiety and making the therapeutic agent available for interaction with its intracellular targets. One can argue that the same properties are also required for an efficient

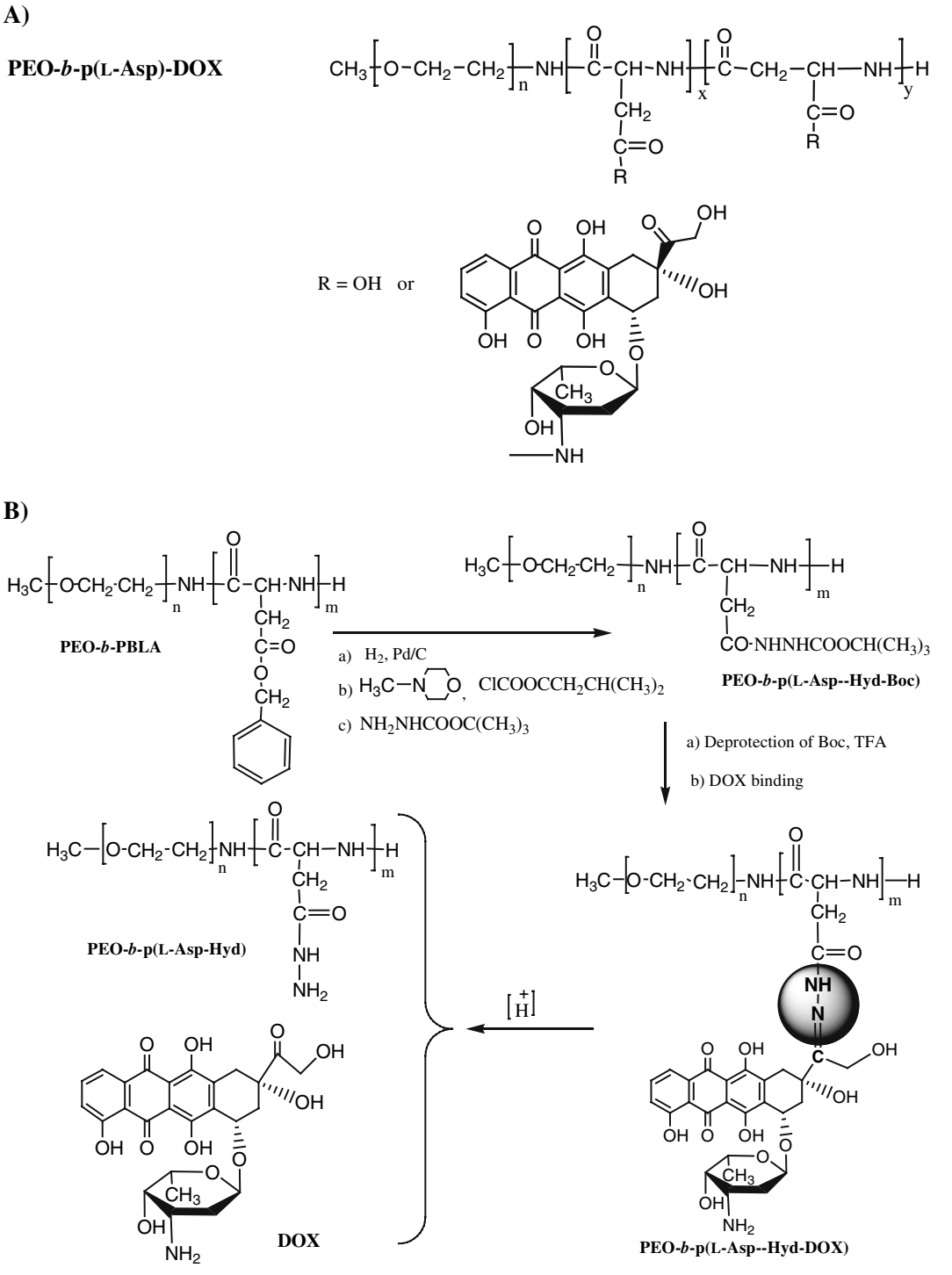

Figure 13.5 Chemical structure of PEO-*b*-PLAA-drug conjugate: (**A**) PEO-*b*-p(L-Asp-DOX) prepared by formation of amide bond, (**B**) PEO-*b*-p(L-Asp-DOX) prepared by the formation of hydrozone bound.

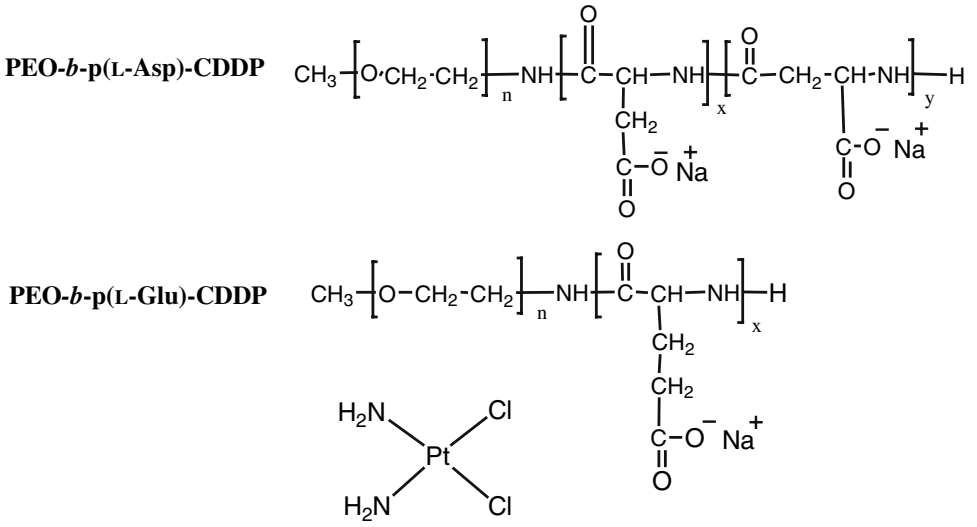

Figure 13.6 PEO-*b*-PLAA/CDDP complex (reproduced from Xiong et al., 2006 with permission).

polymeric micellar system when delivering small drugs. Given the larger molecular weight, higher charge density and toxicity of nucleic acid-based agents achieving success in targeted delivery for this new class of therapeutics is not only more crucial but rather challenging.

PEO-*b*-PLAA-based gene vectors can be engineered to meet these requirements for effective gene delivery. PEO-*b*-PLL have been used for application in gene delivery because the amine-contained core-forming block can form a stable polyion complex with macromolecular (plasmid) DNA through electrostatic interaction (Ward et al., 2002; Katayose and Kataoka, 1998; Katayose and Kataoka, 1997). PEO-*b*-PLL micelles were injected via supramesenteric vein and showed gene expression in the liver. The gene expression was sustained for 3 days. To increase the stability of PEO-*b*-PLL micelles against dissociation, a fraction of the lysine residues in the PLL core was substituted with thiol groups, that can readily form disulfide cross-links with other thiol groups on PEO-*b*-PLL and develop a network structure in the micelle core after DNA complexation (Figure 13.7, scheme 1) (Kakizawa et al., 1999; Kakizawa et al., 2001; Harada et al., 2001). The cross-linked core of the micelles were cleavable inside the cell due to the increased concentration of glutathione, which is a reducing agent abundant in the cytoplasm but not in blood compartment (Meister and Anderson, 1983). However, introduction of thiol groups was found to decrease the electrostatic association sites for the interaction of PLL and DNA. To deal with this problem, Traut's reagent was used to introduce the cross-linking thiol groups to the PLL and, meanwhile, avoid the loss of charge density of the block copolymer segment (Figure 13.7, scheme 2) (Miyata et al., 2004).

In most cases, gene/vector complexes entry into cells is dependent on endocytosis. For enhancing the transfection, the delivered gene needs to be

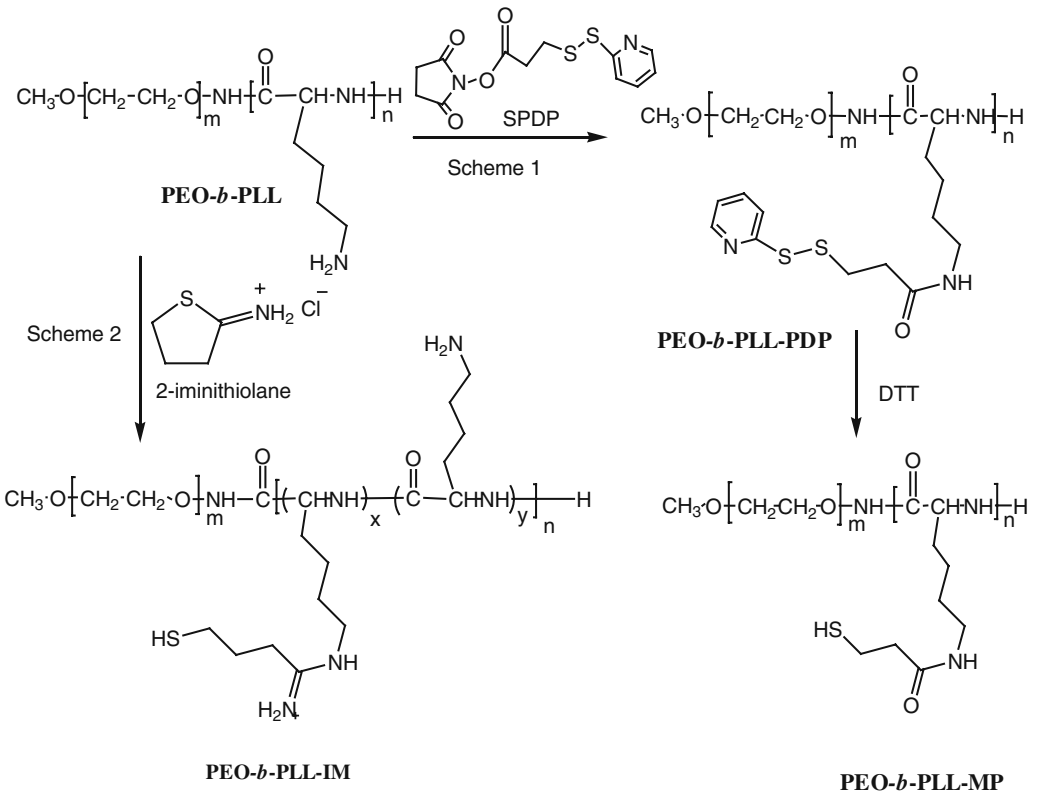

Figure 13.7 Synthesis of PEO-*b*-PLL copolymers with crosslinking and DNA binding groups in the core-forming block. Scheme 1: thiolation by *N*-succinimidyl 3-(2-pyridyldithio)propionate (SPDP) proceeds through the substitution reaction of the ε-amino groups, leading to decreased charge density (PEO-*b*-PLL-MP); Scheme 2: thiolation with 2-iminothiolane proceeds through the introduction of cationic imino groups so that the charge density of the PLL segments remained constant (PEO-*b*-PLL-IM).

released from the endosome into cytosol before endosomes fuse with lysosomes, where the vector and the encapsulated DNA will be destroyed (Erbacher et al., 1996). Certain polycations, such as polyethyleneimine (PEI), are believed to increase osmotic pressure in the endosome by the so-called 'proton sponge effect' resulting in endosomal disruption and DNA release (Behr, 1997; Boussif et al., 1995), although some studies debate the involvement of this mechanism as the main reason for endosomal escape for cationic polymers (Funhoff et al., 2004).

Triblock copolymer of PEO-*b*-PEI-*b*-PBLG has been synthesized where positively charged PEI and hydrophobic PBLG have been used to condense DNA and induce micellarization, respectively. The prepared micelle was shown to incorporate plasmid DNA effectively (Tian et al., 2005). High transfection efficiency and low cytotoxicity may be expected from this gene carrier because of the nature of micellarization and PEI-containing core.

Kataoka et al. designed new types of PEO-*b*-PLAA-based block copolymers that contain two or more amino groups in the side chain (Figure 13.8, scheme 1) (Kanayama et al., 2006; Itaka et al., 2004). The terminal primary amine group displayed a high p*K*a that was suitable for complexation with phosphate groups of siRNA or DNA. The secondary amine of the side

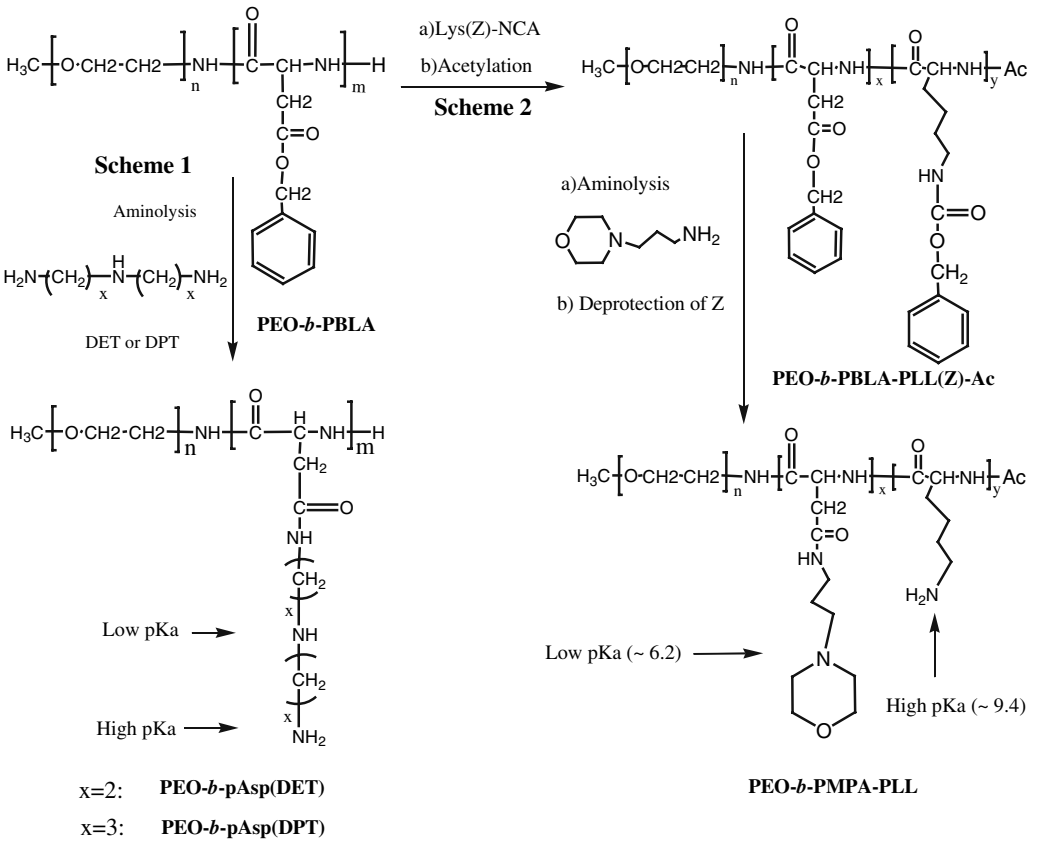

Figure 13.8 Synthesis of PEO-*b*-PLAA copolymers which possess the function of buffering capacity and high DNA affinity in the core-forming block. Scheme 1: synthesis of the diblock polymer PEO-PAsp(DPT) by aminolysis of PEO-*b*-PBLA with dipropylenetriamine; Scheme 2: synthesis of the triblock polymer PEO-*b*-PMPA-PLL by ring-opening polymerization of Lys(Z)-NCA using PEO-*b*-PBLA as the initiator followed by aminolysis and deprotection of benzyl group.

chain which was located closer to the polymeric backbone showed a lower p*K*a and was expected to provide buffering capacity for proton sponge effect. These block catiomers were prepared by the aminolysis of PEO-*b*-PBLA with either dipropylenetriamine (DPT), diethylenetriamine (DET), 4-methyldiethylenetriamine (MDET), or *N*,*N*-diethyldiethylenetriamine (DEDET). Both the PEO-*b*-p[Asp(MDET)] and PEO-*b*-p[Asp(DEDET)] polyplex micelles showed an appreciably lower transfection than the PEO-*b*-p[Asp(DET)] polyplex micelles (Kanayama et al., 2006). Especially, the polyion complex of PEO-*b*-p[Asp(DPT)] with siRNA has shown superior transfection efficiency over lipid-based commercial vector for siRNA delivery, i.e., RNAiFect (Itaka et al., 2004).

Free polycations substantially contribute to efficient transfection but mediate toxic effects as well. Hence, polyplex systems useful for in vivo gene delivery should achieve efficient transfection without free polycations. In order to achieve such delivery system, Kataoka et al. have designed a triblock copolymer consisting of PEO, as the hydrophilic segment, poly[(3-morpholinopropyl)aspartamide] (PMPA) as the low p*K*a

segment with buffering capacity, and PLL as the high p*K*a segment to condense DNA (Figure 13.8, scheme 2) (La et al., 1996b). Notably, when plasmid DNA was encapsulated in PEO-*b*-PMPA-*b*-PLL it revealed one order of magnitude higher transfection efficiency than PEO-*b*-PLL, which was comparable to the transfection efficiency of plasmid DNA-encapsulated PEI at the corresponding negative to positive (N/P) ratio, without showing appreciable cytotoxicity.

Synthesis of PEO-*b*-poly(ester) Block Copolymers

General Synthesis

Ring-opening polymerization of lactones or lactides was frequently used to synthesize poly(ester)s (Albertsson and Varma, 2003). Depending on the initiator, the polymerization can proceed by three different reaction mechanisms: cationic, anionic, or 'coordination-insertion' mechanisms (Stridsberg et al., 2002). The cationic ROP involves the formation of positively charged species which are subsequently attacked by a monomer (Figure 13.9A). Anionic ROP of cyclic ester monomers takes place by the nucleophilic attach of a negatively charged initiator on the carbonyl or on the carbon atom adjacent to the acyl oxygen, resulting in linear polyester (Figure 13.9B). Coordination-insertion ROP, also called pseudo-anionic ROP, is thought to proceed by coordination of the monomer to the active species, followed by insertion of the monomer into the metal–oxygen bond by rearrangement of the electrons (Figure 13.9C).

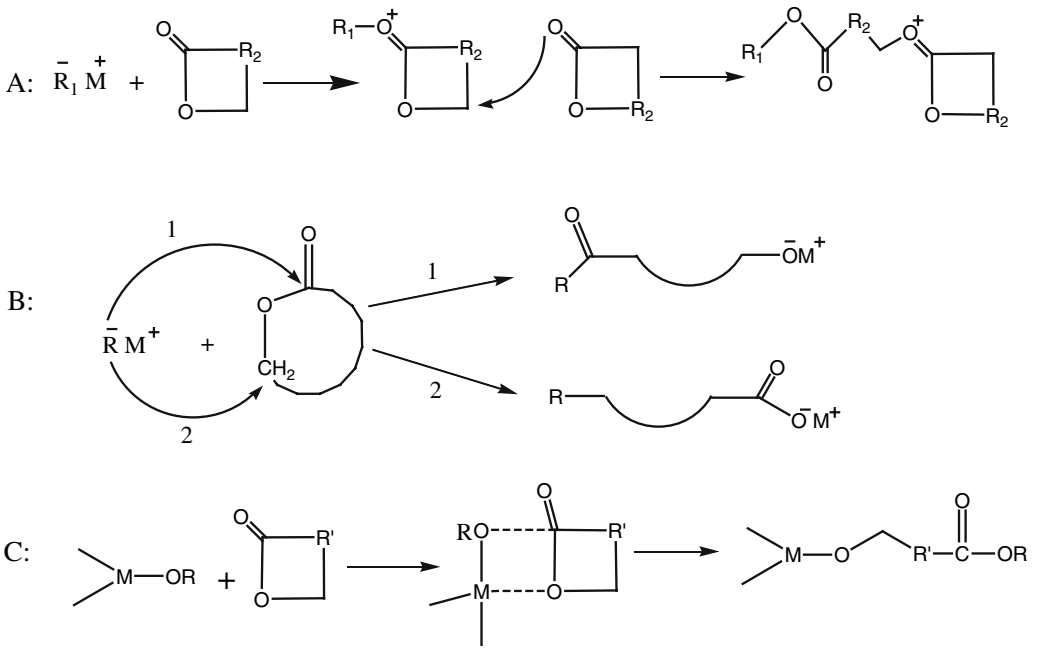

Figure 13.9 The ROP of a cyclic ester by **(A)** cationic, **(B)** anionic, and **(C)** coordination-insertion mechanism (reproduced from Stridsberg et al., 2002 with permission).

An extensive research effort has been made in the past few years to refine the technique of ring-opening polymerization so that polyesters with controlled architecture and properties could be prepared. Various monomers, such as glycolide (GA), lactide (LA), β-butyrolactone (β-BL), ε-caprolactone (ε-CL), 1,5-dioxepan-2-one (DXO), or their derivatives have been used to prepare poly(ester)s. The representative structures of these monomers and polymers are given in Figure 13.10. The polymerization is generally carried out in bulk or in solution (using THF, dioxane, toluene, etc.), emulsion, or dispersion (Scholz et al., 1995; Gadzinowski et al., 1996). The temperature of bulk polymerization is generally in the range of 100–150°C, whereas low temperature has been used (0–25°C) in solution polymerization. For example, PEO-*b*-PLA or PEO-*b*-PCL has been synthesized by solution polymerization using potassium naphthalene as the catalyst, or by bulk polymerization using stannous octoate as the catalyst (Iijima et al., 1999; Nguyen et al., 2003; Aliabadi et al., 2005; Deng et al., 2004). Studies by our research group and others have shown polymerization in solution generally leads to PLA or PCL chains with a lower molecular weight than expected values calculated from the initial monomer/initiator feeding ratios (Stridsberg et al., 2002; Ito et al., 1977; Xiong et al., 2007a). This observation can be explained by higher probability of inter- or intra-molecular transesterification in solution polymerization.

Chemical Modification of the Core in PEO-*b*-poly(ester) Micelles for Physical Drug Encapsulation

Synthesis of PEO-*b*-PLA block copolymers containing a small quantity of carboxylic acid side groups on the PLA block through ROP of 3(s)[(benzyloxycarbonyl)methyl]-1,4-dioxane-2,5-dione (BMD) monomer has been reported by Lee et al (Figure 13.11A) (Lee et al., 2004). The prepared block copolymer was observed to form micelles at a relatively low CMC. An increase in the drug loading was seen in polymeric micelles bearing higher carboxyl groups in their core structure. The observation was attributed to an increased interaction via hydrogen bonding between the micellar core and encapsulated drug.

Our research group has synthesized α-benzylcarboxylate-ε-caprolactone (BCL) (Mahmud et al., 2006) and α-cholesteryl carboxylate-ε-caprolactone (ChCL) (unpublished data). The functionalized monomers were then used in ROP reactions with methoxy PEO to produce poly(ethylene oxide)-*block*-poly(α-benzylcarboxylate-ε-caprolactone) (PEO-*b*-PBCL) and poly(ethylene oxide)-*block*-poly(α-cholesteryl carboxylate-ε-caprolactone) (PEO-*b*-PChCL) block copolymers (Figure 13.11B). PEO-*b*-PBCL was then reduced in the presence of H_2 to produce poly(ethylene oxide)-*block*-poly(α-carboxylic-ε-caprolactone) (PEO-*b*-PCCL). The average CMC for PEO-*b*-PBCL and PEO-*b*-PCCL block copolymers was estimated at 0.098 and 12.20 μM, respectively. By adjusting the molar ratio of unsubstituted and substituted monomers, e.g., ε-CL and BCL, block copolymers with a random copolymer structure in the core, e.g., PEO-*b*-poly(CL-co-BCL), can be obtained to meet different requirements for the delivery of individual drugs.

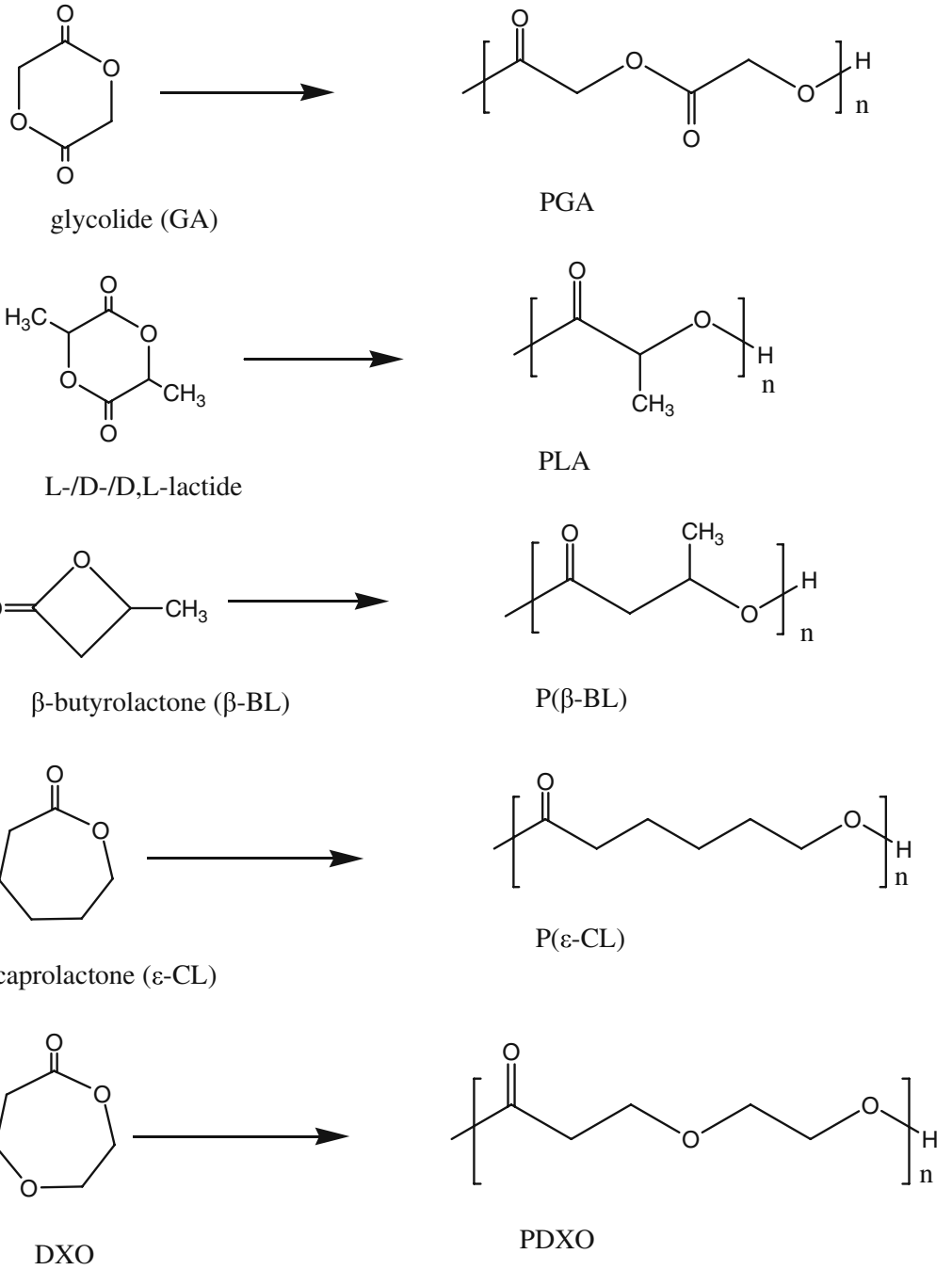

Figure 13.10 Chemical structure of common cyclic lactones used in the ROP reactions for the synthesis of poly(ester)s.

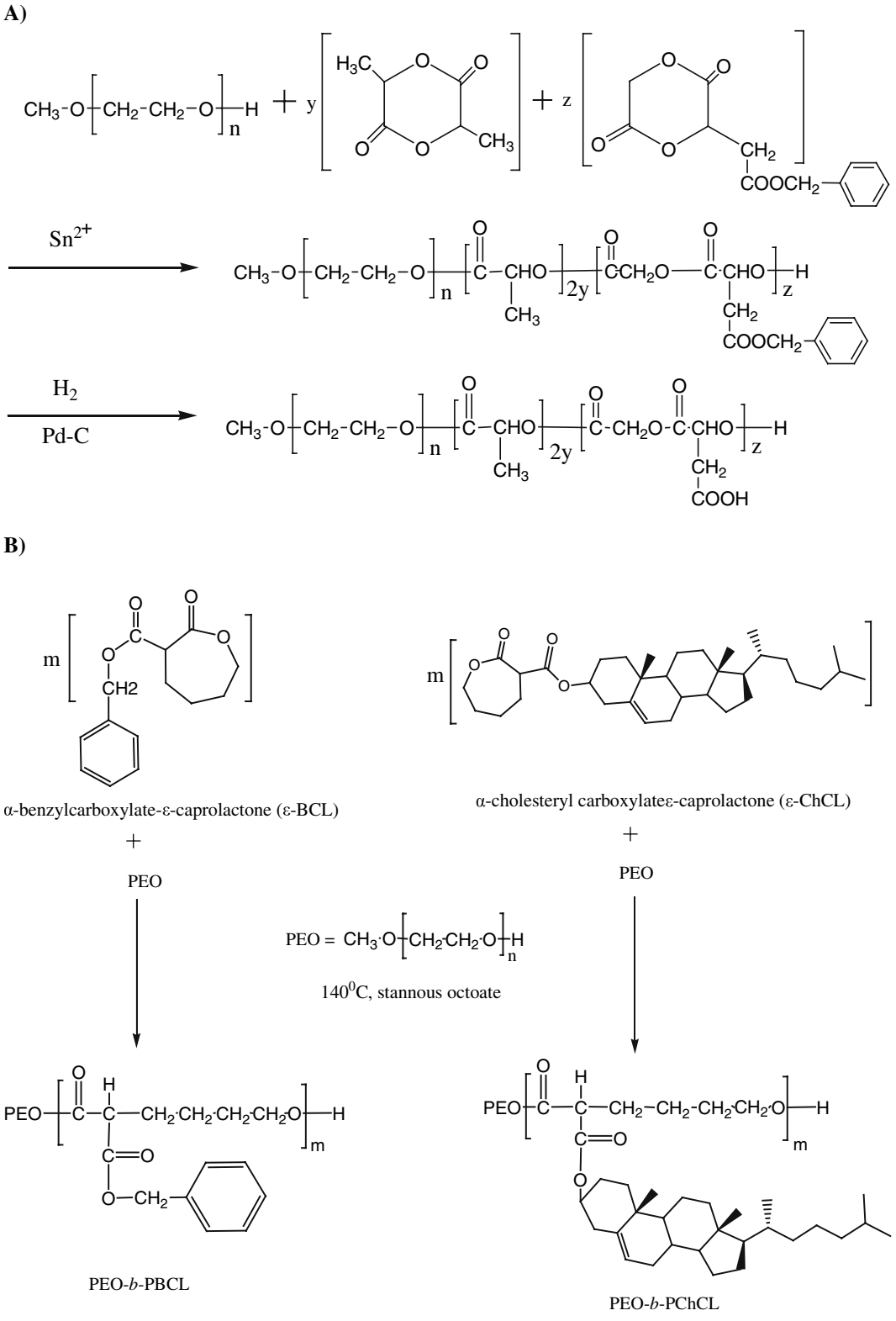

Figure 13.11 Synthetic scheme of polyester-substituted **(A)** PEO-*b*-PLA and **(B)** PEO-*b*-PCL block copolymers.

Synthesis of PEO-*b*-poly(ester)s-Drug Conjugates

Conjugation of drugs to PEO-*b*-poly(ester)s has usually been accomplished by functionalization of the terminal poly(ester) end which is followed by reaction with drugs. Zhang et al. have attached the water-insoluble anticancer drug, paclitaxel, to the PLA section of the PEO-*b*-PLA to increase its solubility (Figure 13.12A) (Zhang et al., 2005). Toward this goal, hydroxyl-terminated diblock copolymer of monomethoxy-poly(ethylene oxide)-*b*-poly(lactide) (MPEO-*b*-PLA) was first synthesized by ring-opening polymerization of L-lactide using MPEO as a macroinitiator. The terminal hydroxyl group of the PLA block was then converted to carboxyl group by reacting PEO-*b*-PLA with mono-*t*-butyl ester of diglycolic acid and subsequent deprotection of the *t*-butyl group with trifluoroacetic acid (TFA). Paclitaxel was then conjugated to the copolymer through formation of ester bonds between the terminal carboxylic groups of the copolymer and the hydroxyl group of paclitaxel in the presence of dicyclohexylcarbodiimide (DCC) and dimethylaminopyridine (DMAP). Because of the spatial hindrance in paclitaxel, 2′-hydroxyl is more active than the 7-hydroxyl for esterification and preferentially used for paclitaxel conjugation. Paclitaxel was released from the conjugate upon hydrolysis without loss of cytotoxicity.

Conjugation of DOX to the PEO-*b*-PLGA after activation of the PLGA terminus by *p*-nitrophenyl chloroformate has also been reported (Yoo and

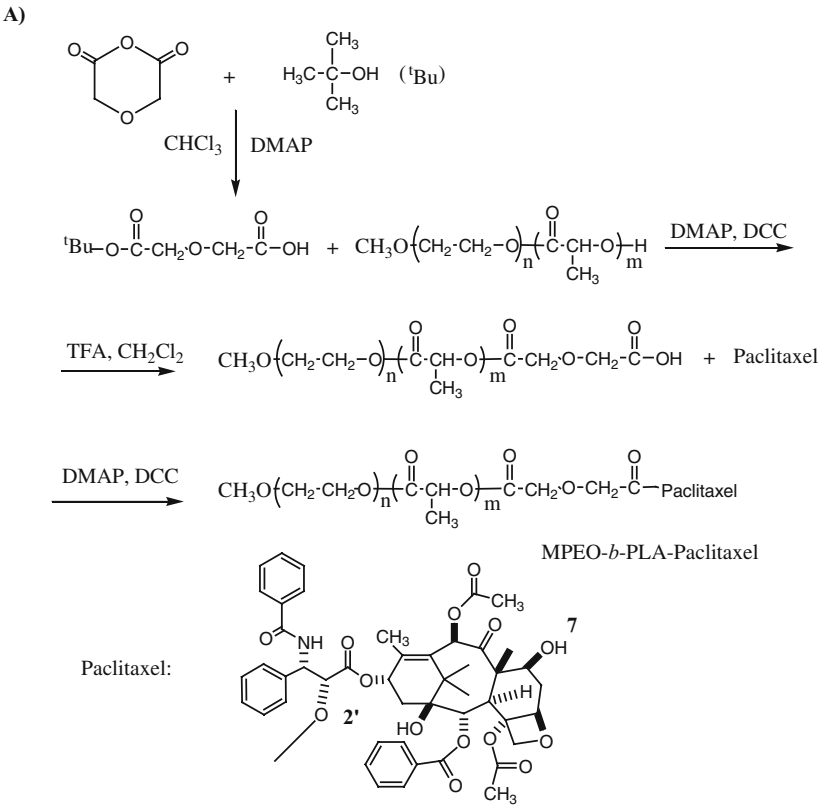

Figure 13.12 (*Continued*).

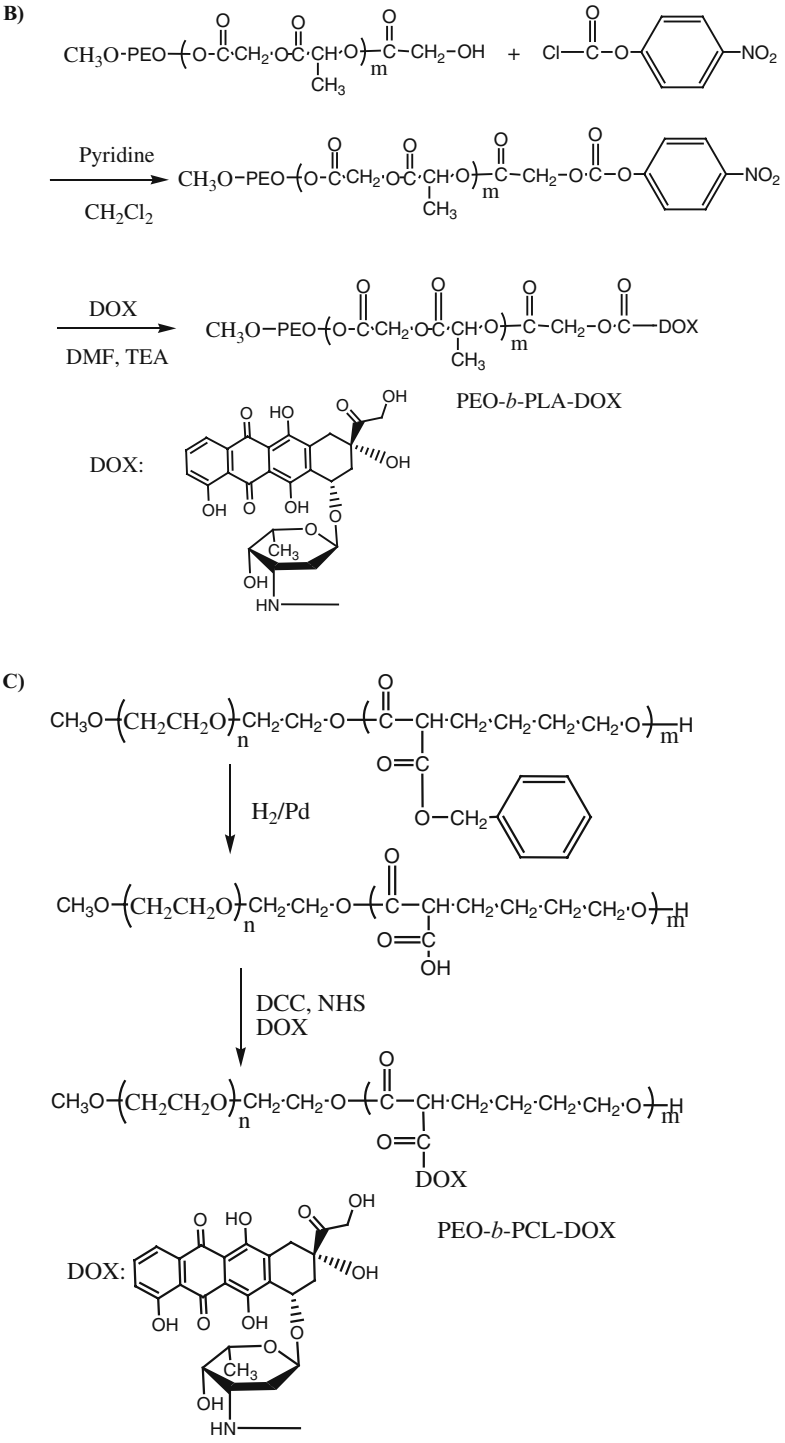

Figure 13.12 Synthesis of polymer-drug conjugates: (**A)** PEO-*b*-PLA-paclitaxel, (**B)** PEO-*b*-PLA-DOX, and (**C)** PEO-*b*-PCL-DOX.

Park, 2001) (Figure 13.12B). The micelles containing chemically conjugated DOX exhibited a more sustained release profile than PEG–*b*-PLGA micelles containing physically entrapped DOX. Interestingly, the cellular uptake of the DOX-conjugated micelles was more efficient than free DOX against HepG2 cells, leading to higher cytotoxic activity than free DOX.

By utilizing the single functional group at the end of the poly(ester) chain, the chemical drug-loading efficiency can only achieve 1:1 molar ratio (drug: polymer) at most. By attaching multiple functional side groups, however, one can achieve multiple copies of the drug per polymer chain and achieve higher drug:polymer molar ratios. In our group, DOX was conjugated to the PCL section of the PEO-*b*-PCCL copolymers by the reaction between the –COOH side group on the PCCL and amine group of DOX (Figure 13.12C). The degree of DOX conjugation to single polymer chains reached 2:1 molar ratio in our preliminary study (Mahmud et al., 2007).

Synthesis of PEO-*b*-poly(amine) Block Copolymers

The cationic polymer polyethylenimine (PEI), which is widely used for non-viral transfection, is advantageous over other polycations because it combines strong DNA compaction capacity with an intrinsic endosomolytic activity (Demeneix and Behr, 2005; Kircheis et al., 2001). PEI can be prepared in the form of branched or linear architectures.

Linear PEI has been synthesized via cationic ring-opening polymerization of either *N*(2-tetrahydropyranyl)azidirine or unsubstituted and two-substituted 2-oxazolines followed by acid- or base-catalyzed hydrolysis of the corresponding N-substituted polymer (Figure 13.13A) (Brissault et al., 2003). Branched PEI is synthesized by polymerization of aziridine either in aqueous or alcoholic solutions, where the reaction is controlled by adjusting the temperature and initiator concentration, or in a rather vigorous bulk polymerization of anhydrous aziridine at a lower temperature (Figure 13.13B) (von Harpe et al., 2000).

Incorporation of PEO into DNA complexes has been achieved either by condensing DNA with PEO-*b*-PEI copolymers (pre-PEGylation) or coupling a PEO layer onto the surface of preformed PEI/DNA polyplexes (post-PEGylation). Several strategies have been used to prepare PEO-*b*-PEI copolymers, most of them using homobifunctional or heterobifunctional PEO for conjugation onto branched or linear PEI (Figure 13.14) (Lungwitz et al., 2005). For post-PEGylation, the PEI/DNA polyplexes are usually formed in a solution with low ionic strength to generate small particles and the PEO chains are only allowed to react with the particle surface to create the protective PEO shield.

Although one may desire to utilize PEO-*b*-PEI conjugates for precise control over the complexation, since PEO-b-PEI can be separately prepared and characterized in a controlled fashion, attachment of PEO to PEI through pre-PEGylation approaches compromises the binding ability of PEI to the DNA, as well as the cells (Clements et al., 2006). Grafting PEO after the formation of nanoparticles may obviate this problem, at the expenses of a mere controlled chemistry. Post-PEGylation also places PEO molecules on the surface where they can exert a maximal impact on the micelle biodistribution.

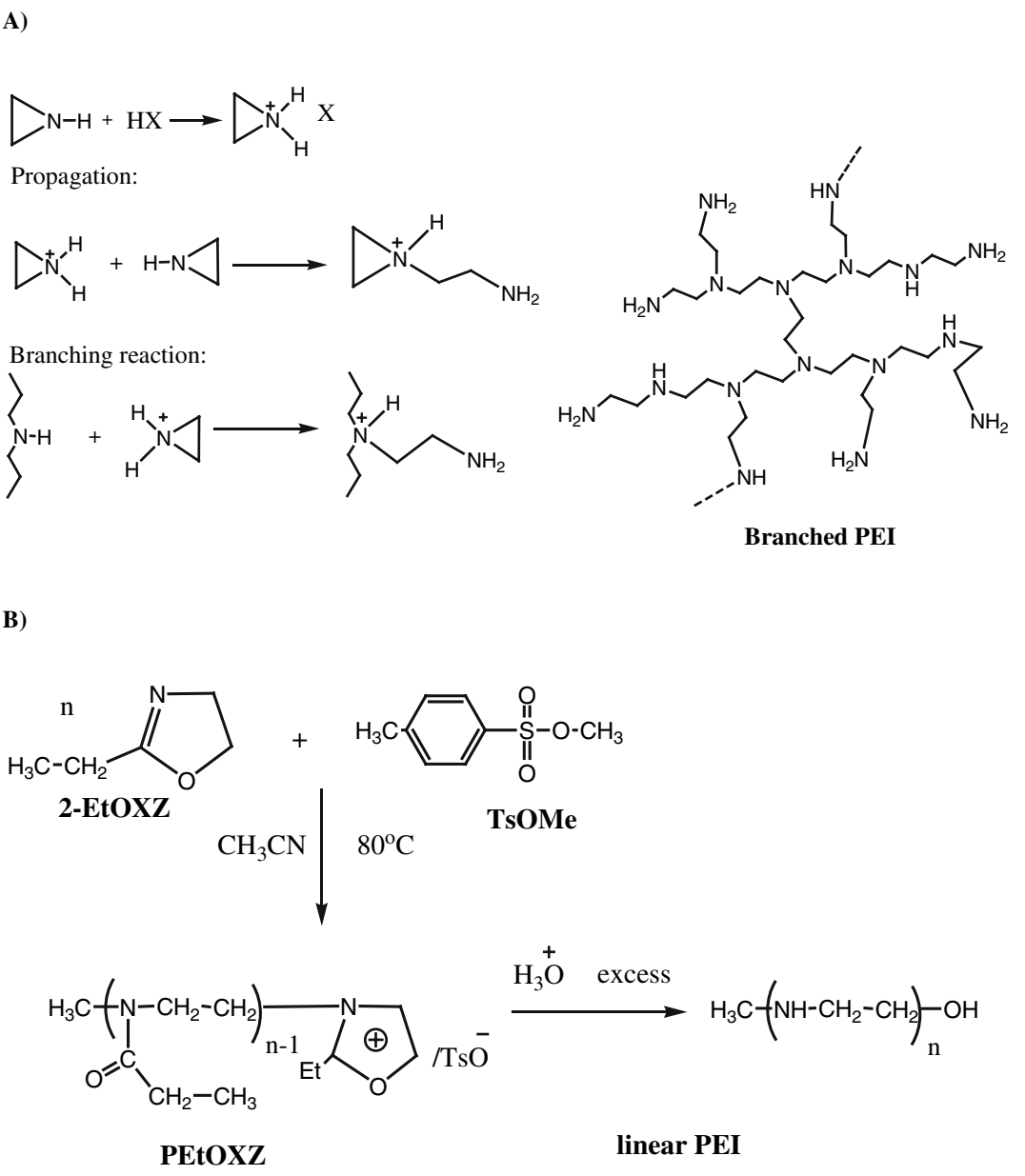

Figure 13.13 Synthesis scheme for **(A)** branched and **(B)** linear PEI (reproduced from Demeneix and Behr, 2005 with permission).

Chemical Modification of the Shell-Forming Block for Drug/Gene Targeting

Separation of the core and shell domains in polymeric micelles is a useful property. This architecture permits conjugation of ligands to the shell domain that can enhance tissue specificity and modify cellular, intracellular, or molecular interactions without affecting core-related properties,

Pre-PEGylation

Conjugation by homobifunctional linker

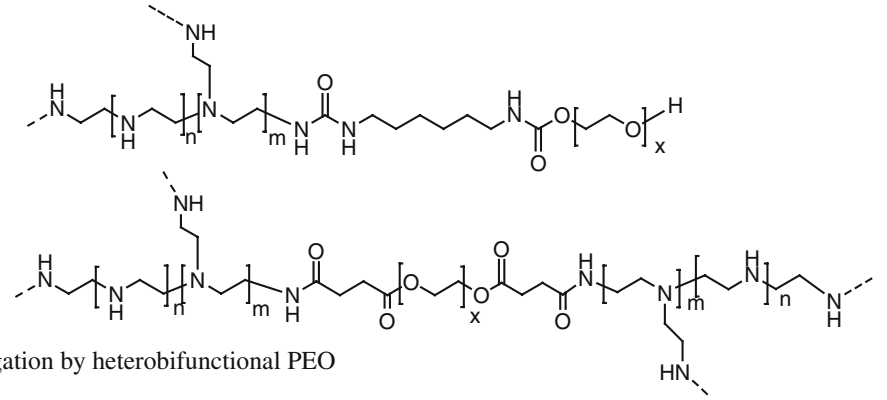

Conjugation by heterobifunctional PEO

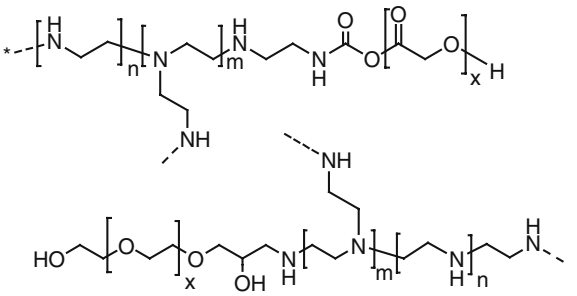

Copolymers cleavable by intracellular reduction

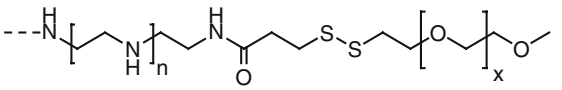

Post-PEGylation

Conjugation of monofunctional PEO

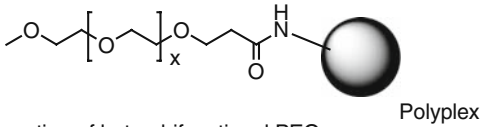

Conjugation of heterobifunctional PEO

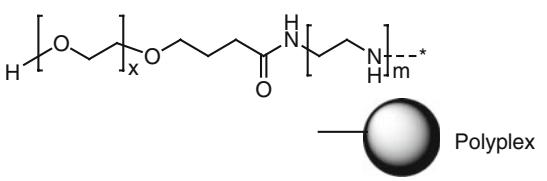

Figure 13.14 Various strategies for the production of PEO-*b*-PEI/DNA polyplexes (reproduced from Demeneix and Behr, 2005 with permission).

such as micellar stability and encapsulation efficiency. Various ligands including small organic molecules, carbohydrates, peptides, and antibodies (or their fragments) have been coupled to polymeric micelles to achieve active targeting. Ligands can be coupled to the shell-forming polymers before or after polymerization of the core-forming block. Conjugation of ligands to preformed polymers (or micelles) via ester, amide, disulfide, thioether, carbon-nitrogen bonds are more common. Otherwise, the ligands generally need to be derivatized to become suitable as initiator of the polymerization reaction.

Conjugation of folic acid to PEO-*b*-PLL, PEO-*b*-poly(*l*-Histidine) (Figure 13.15A) (Kim et al., 2005; Lee et al., 2005), and PEO-*b*-PLGA by amide bond (Figure 13.15B) (Lee et al., 2003a) has been pursued to enhance the interaction of polymeric micelles with cancer cells that overexpress folate receptor. In these studies, PEO with functional groups on both ends was used to couple folate and core-forming block at each end of the PEO. To synthesize the folate-PEO-*b*-PLL, the amine groups on the core-forming block have to be protected to avoid undesired side reactions.

Carbohydrate-mediated drug targeting via glycol receptors on hepatocytes have been pursued by several researchers (Goto et al., 1994; Omelyanenko et al., 1998; Wu et al., 2002; Murao et al., 2002; Opanasopit et al., 2002). Carbohydrate molecules such as galactose and mannose act as specific ligands for the glycol receptors. Kataoka et al. used both pre- and post-polymerization approaches to synthesize carbohydrate-decorated PEO-*b*-poly(D,L-lactide) (carbohydrate-PEO-*b*-PDLA) block copolymers (Nagasaki et al., 2001; Jule et al., 2003). In the pre-polymerization approach, the copolymers were synthesized through sequential anionic ROP of EO by chemically modified sugars like glucose and galactose. Four hydroxyl groups out of five were specifically protected by the acetal substituents in the glucose structure (Figure 13.16A). This step was followed by ROP of lactide and deprotection of initiator to achieve carbohydrate-PEO-*b*-PDLLA. In the post-polymerization method, PEO-*b*-PDLA micelles with aldehyde group at the distal end of the PEO chains, which is derived from the acetal-ended PEO-*b*-PLA block copolymers, were prepared. Carbohydrate conjugation was then accomplished by forming Schiff base between the amine group on the sugar and aldehyde group on the PEO chains (Figure 13.16B). Using the heterofunctional PEO (vinyl sulfone-PEO-hydroxysuccinimidyl, VS-PEO-NHS), galactose has also been conjugated to the PEO-*b*-PEI to form galactose-PEO-*b*-PEI for gene delivery to hepatocytes (Sagara and Kim, 2002).

Targeting tumor cells or tumor vasculature by small peptides is another promising strategy for delivering cytotoxic drugs for cancer therapy. Small size of the ligand, diversity of functional groups on the peptide (thiol, amine, and carboxyl groups) as well as possibility for engineering high-affinity peptides make them preferential ligands for active drug targeting.

Peptides containing the RGD sequence can recognize integrins that are overexpressed on the angiogenic endothelial cells of the tumor vasculature or on metastatic tumor cells. Gao et al. developed polymeric micelles that can selectively deliver hydrophobic drugs to angiogenic tumor endothelial cells that overexpressed $\alpha v\beta 3$ integrins (Figure 13.17A) (Nasongkla et al., 2004). To couple the cyclic pentapeptide C(Arg-Gly-Asp-d-Phe-Lys)

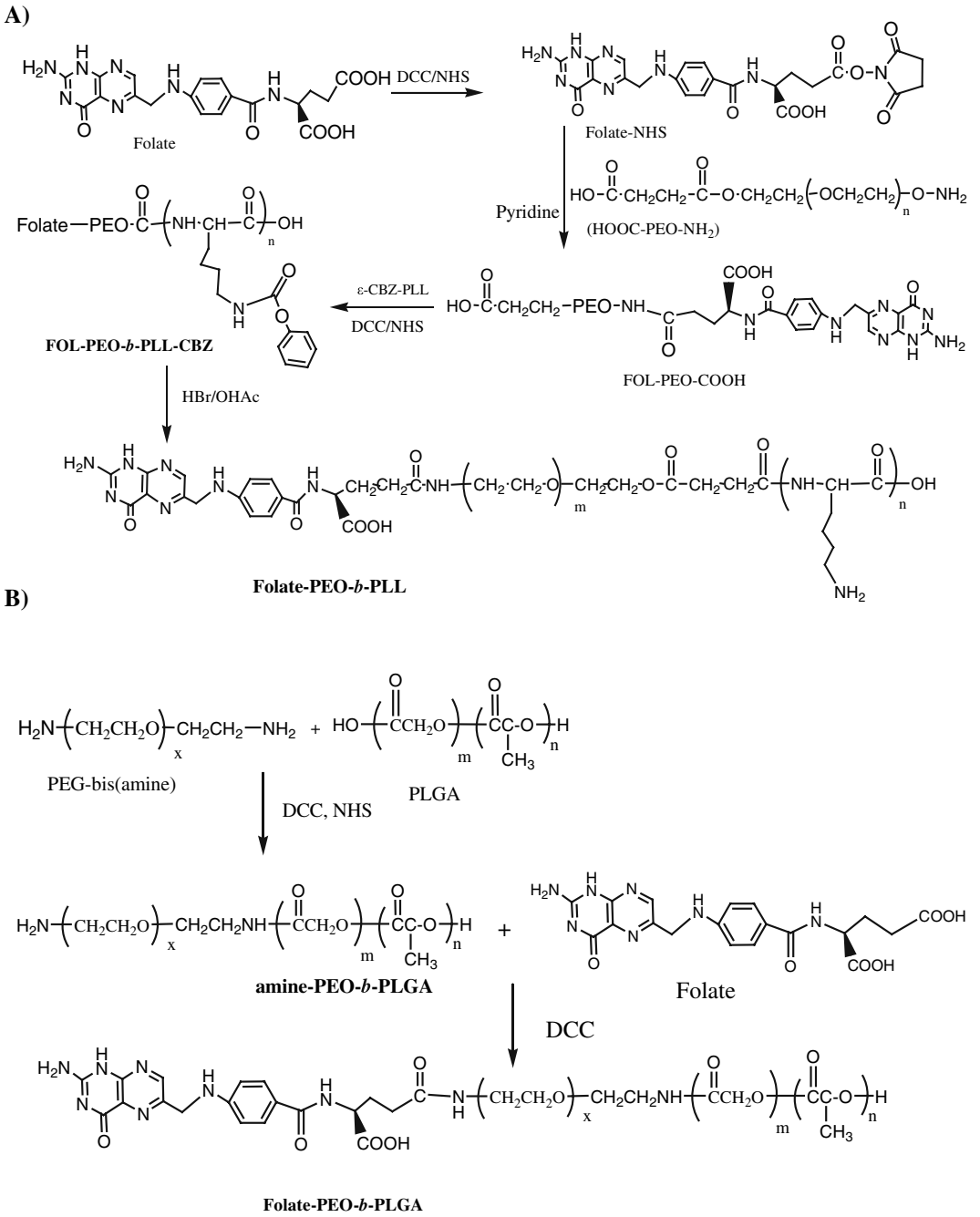

Figure 13.15 Synthesis of **(A)** folate-conjugated PEO-*b*-PLL and **(B)** folate-conjugated PEO-*b*-PLGA.

(cRGDfK) containing thiol in the structure, Gao et al. synthesized maleimide-terminated PEO-*b*-PCL (MAL-PEO-*b*-PCL). After micellarization, cRGDfK was coupled onto the micelle surface by electrophilic addition to form thioether bond between the thiol group on the peptide and ethylenic bond on the maleimide. Conjugation of epidermal growth

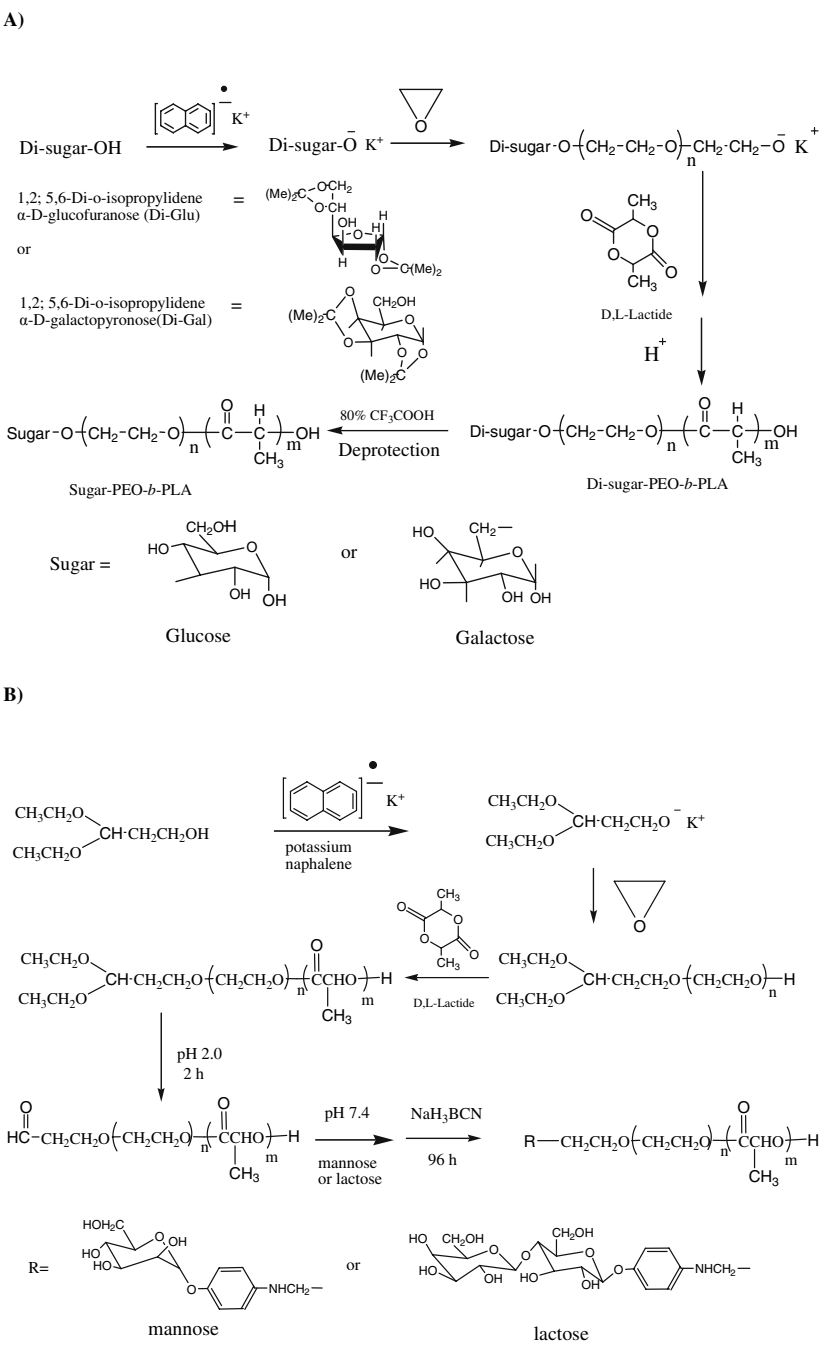

Figure 13.16 Synthesis of carbohydrate-conjugated PEO-*b*-PDLA through (**A**) pre- and (**B**) post-polymerization approaches.

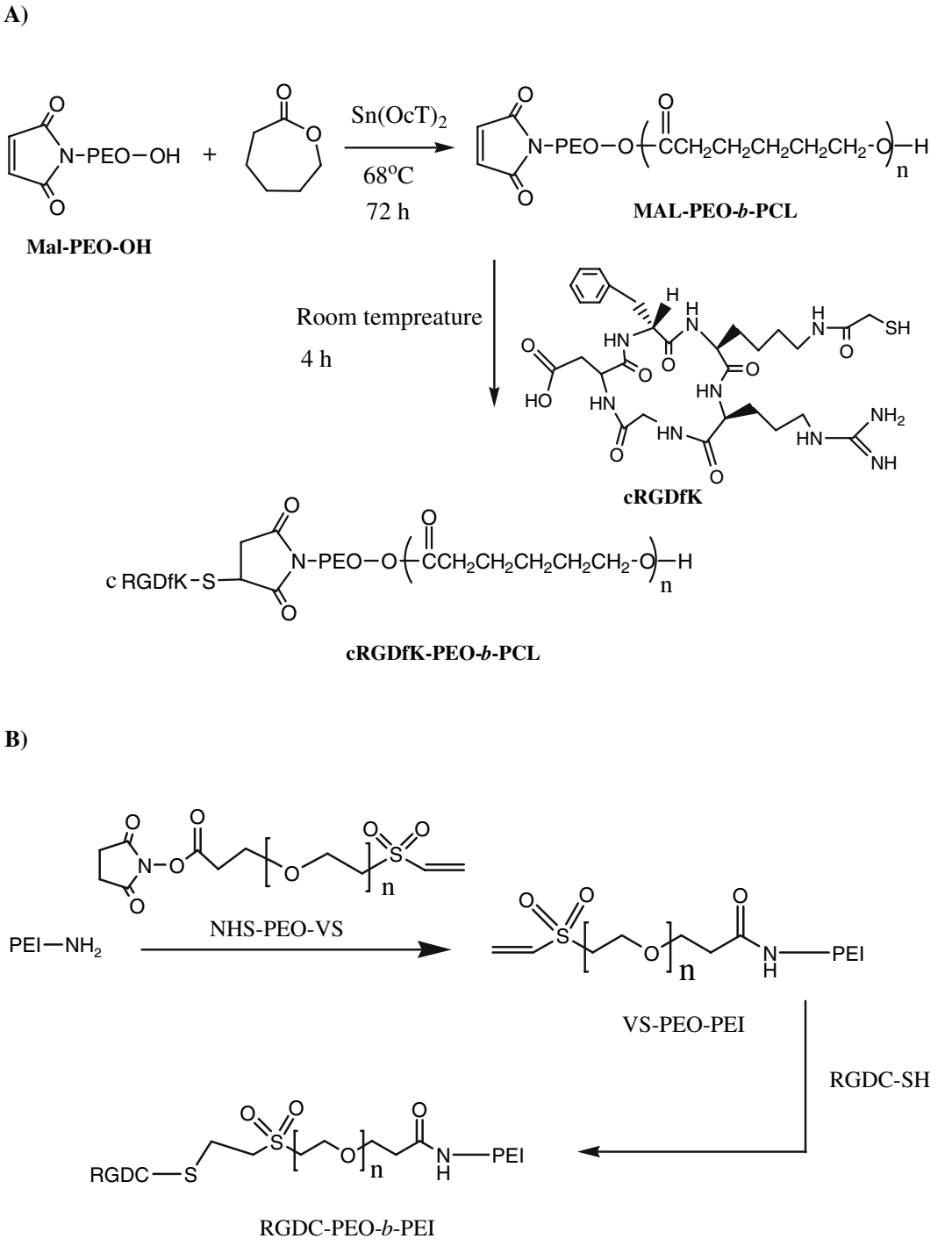

Figure 13.17 Synthesis of (**A**) cRGDfK-PEO-*b*-PCL and (**B**) RGDC-PEO-*b*-PEI copolymers.

factor (EGF) to the PEO end of PEO-*b*-PEI by the reaction of thiol group on the EGF and maleimide on the PEO section for targeted gene delivery has also been reported (Ogris et al., 2003). Using the heterofunctional PEO, i.e., VS-PEO-NHS, RGDC-conjugated PEO-*b*-PEI was synthesized for gene delivery (Figure 13.17B) (Kunath et al., 2003).

Amine group in the N-terminus of peptide has also been used for peptide conjugation to block copolymer micelles. Small peptides were coupled to acetal-terminated PEO-*b*-PDLA micelles to modify their surface charge by Kataoka et al. (Yamamoto et al., 1999). Our group has synthesized acetal-terminated PEO-*b*-PCL through anionic ROP of γ-caprolactone by acetal-PEO (Figure 13.18A) (Xiong et al., 2007a). After formation of micelles, the acetal group was converted to aldehyde at acidic pH and used for the conjugation of GRGDS to micellar surface by Schiff base reaction between the aldehyde group on the PEO chain and the amine group on the peptide. To extend the research, the more versatile polymer, acetal-PEO-*b*-PBCL block copolymer, was synthesized and then reduced in the presence of H_2 to produce acetal-PEO-*b*-PCCL. This novel polymer was aimed to covalently couple ligands to the shell-forming block and anticancer drugs to the core-forming block. The anticancer drug, DOX, was then covalently conjugated to the free-side COOH groups on the PCCL block by an amide bond to form acetal-PEO-*b*-PCL-DOX. After conversion of the acetal group into aldehyde, RGD-containing peptides such as GRGDS and ACDCRGDCFCG (RGD4C) (unpublished data) were attached to the surface of aldehyde-PEO-*b*-PCL-DOX micelles (Figure 13.18B). RGD peptide-modified micelles bearing conjugated DOX demonstrated higher cytotoxicity on B16-F10 cells than the control conjugate due to better uptake by the cells (Xiong et al., 2007b).

Preparation of shell-modified micelles for gene delivery has also been reported. For the conjugation of transferrin (Tf), a ligand that binds ubiquitously to a wide variety of cells, to PEO-*b*-PEI, the branched PEI was preactivated by succinimidyl 3-(2-pyridyldithio)propionate (SPDP) to introduce thiol groups. Amino groups of Tf was then reacted with heterobifunctional PEO (α-maleimide-ω-*N*-hydroxysuccinimide ester, MAL-PEO-NHS) to form Tf-PEO conjugate. The maleimide group at the distal end of the PEO chain in the Tf-PEO conjugate was then reacted with the thiol-functionalized PEI. The resulting Tf-PEO-*b*-PEI polymer after purification contained approximately one Tf ligand per two PEI molecules (Figure 13.19A). In the same study, a separate conjugation method was used to synthesize Tf-PEO-*b*-PEI polymers with linear PEI. In this method, both PEI and Tf were modified separately with iminothiolane. The modified transferrin was reacted with bifunctional PEO derivative PEO-bis-orthopyridyl-disulfide. The product was subsequently reacted with the sulfhydryl groups of the iminothiolane-modified PEI. The purified conjugate contained approximately one Tf ligand to one PEI molecule (Figure 13.19B) (Kursa et al., 2003).

Monoclonal antibodies are another promising class of tumor-targeting ligands. Similar to peptide conjugation, thiol, amine, or the carboxyl in the antibodies may be used for conjugation reaction. One typical example is the attachment of C225, i.e., the antibody against epidermal growth factor (EGF) receptors, to the PEO terminus of a PEO-*b*-p(L-Glu)-DOX using the reaction between thiol and vinylsulfone (Figure 13.20) (Vega et al., 2003).

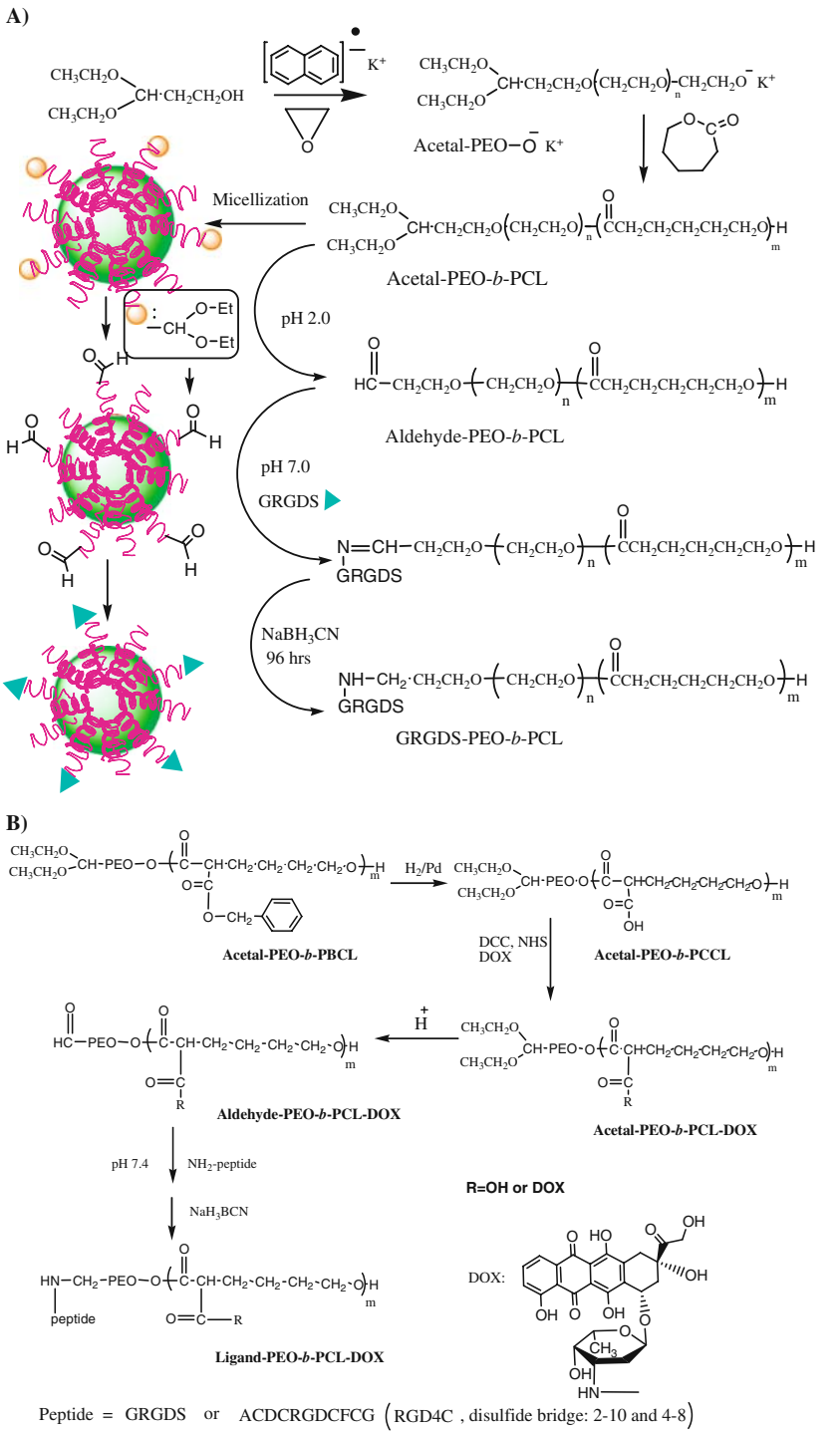

Figure 13.18 Preparation of (**A**) GRGDS-*b*-PEO-PCL (reproduced from Xiong et al., 2007 with permission) and (**B**) GRGDS-PEO-*b*-PCL-DOX block copolymers and micelles. (*See* Color Plate 18)

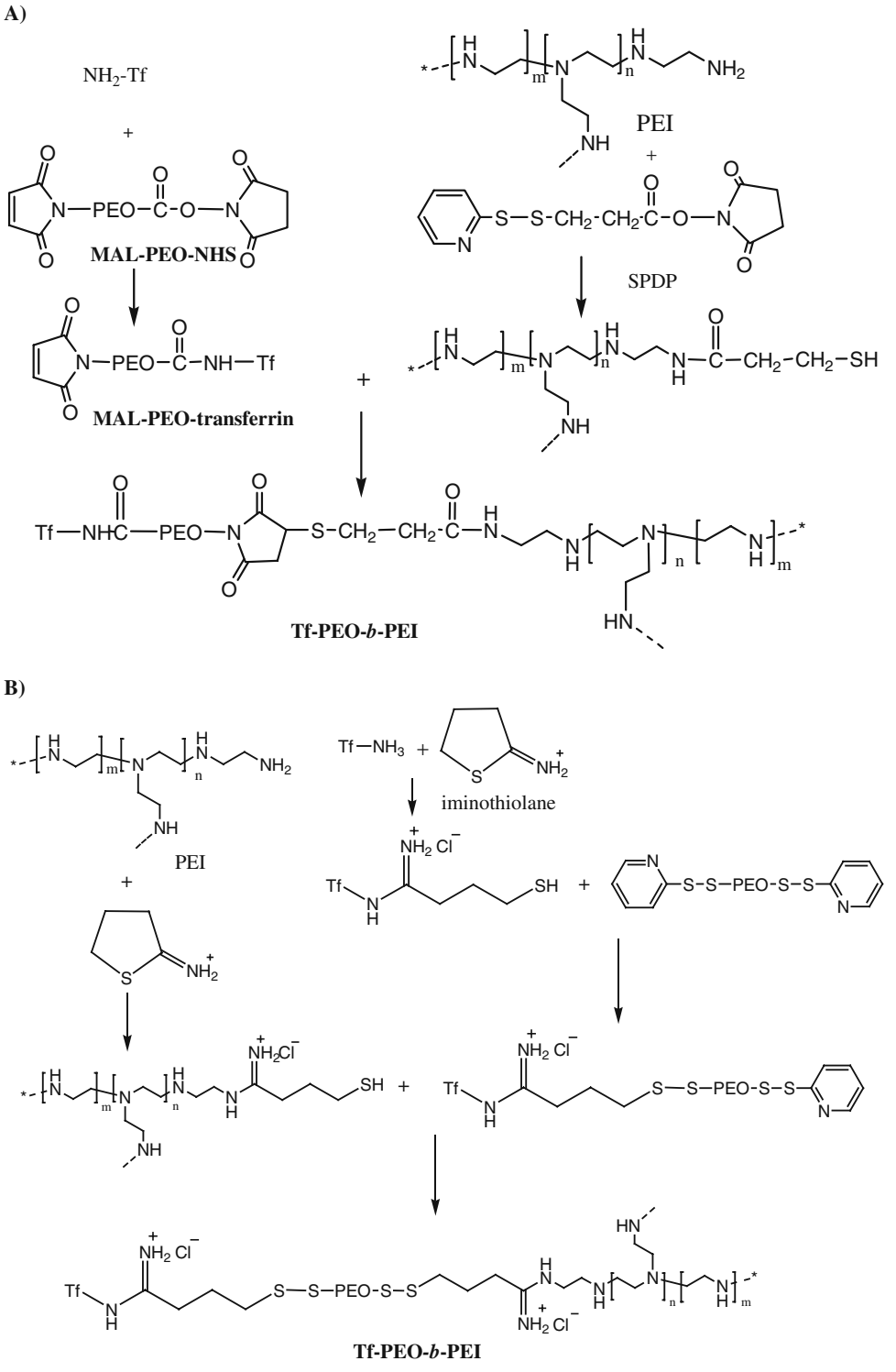

Figure 13.19 Conjugation of Tf to PEO-*b*-PEI.

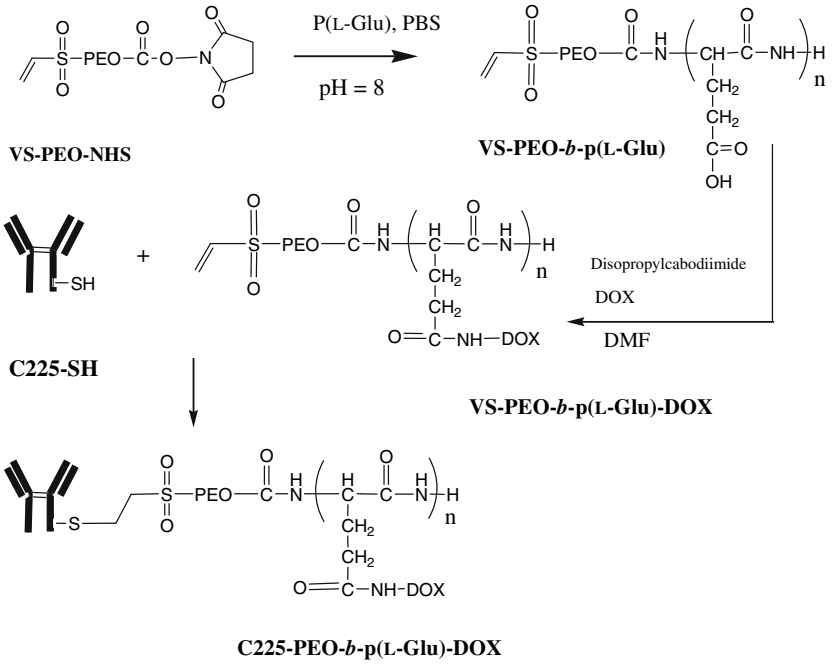

Figure 13.20 Synthesis of C225-PEO-*b*-p(L-Glu)-DOX and micelles with chemically loaded anticancer drugs (reproduced from Vega et al., 2003 with permission).

Conclusion

In this chapter, we provided an update on several chemical strategies used to enhance the properties of nanoscopic core/shell structures formed from self-assembly of amphiphilic block copolymers, namely polymeric micelles. Clearly, versatility of polymer chemistry in amphiphilic block copolymers provides unique opportunities for tailoring polymeric micelles for optimal properties in gene and drug delivery. Chemical modification of the polymer structure in the micellar core through introduction of hydrophobic or charged moieties, conjugation of drug compatible groups, core cross-linking has led to enhanced stability for the micellar structure and sustained or pH-sensitive drug release. The modification of polymeric micellar surface with specific ligands (carbohydrates, peptides, antibodies) has shown benefit in enhancing the recognition of carrier by selective cells leading to improved drug and gene delivery to the desired targets. Research in drug delivery by polymeric vesicles is still in its infancy, but a similar principle on the importance and benefit of chemical flexibility of block copolymers in improving the delivery properties of polymeric vesicles can also be envisioned. The demanding challenge of the future research in this field is to find the right carrier architecture and optimum polymer chemistry that can improve the delivery of sophisticated and complex therapeutic agents (e.g., poorly soluble drugs, proteins, and genes) to their cellular and intracellular targets.

Acknowledgments A. Lavasanifar would like to acknowledge support by the National Science and Engineering Research Council of Canada (NSERC) grant numbers G121210926 and G121220086. Uludağ acknowledges the financial support by the Canadian Institute of Health Research (CIHR).

References

Adams ML, Andes DR, Kwon GS. Amphotericin B encapsulated in micelles based on poly(ethylene oxide)-block-poly(L-amino acid) derivatives exerts reduced in vitro hemolysis but maintains potent in vivo antifungal activity. *Biomacromolecules* 2003, 4(3):750–7.

Adams ML, Kwon GS. Relative aggregation state and hemolytic activity of amphotericin B encapsulated by poly(ethylene oxide)-block-poly(N-hexyl-L-aspartamide)-acyl conjugate micelles: effects of acyl chain length. *J Control Release* 2003, 87(1–3):23–32.

Albertsson AC, Varma IK. Recent developments in ring opening polymerization of lactones for biomedical applications. *Biomacromolecules* 2003, 4(6):1466–86.

Alexandridis P, Lindman B. Amphiphilic Block Copolymers-Self Assembly and Applications. Elsevier 2000.

Aliabadi HM, Lavasanifar A. Polymeric micelles for drug delivery. *Expert Opin Drug Deliv* 2006, 3(1):139–62.

Aliabadi HM, Mahmud A, Sharifabadi AD, Lavasanifar A. Micelles of methoxy poly(ethylene oxide)-b-poly(epsilon-caprolactone) as vehicles for the solubilization and controlled delivery of cyclosporine A. *J Control Release* 2005, 104(2):301–11.

Aramwit P, Yu BG, Lavasanifar A, Samuel J, Kwon GS. The effect of serum albumin on the aggregation state and toxicity of amphotericin B. *J Pharm Sci* 2000, 89(12):1589–93.

Arnida, Nishiyama N, Kanayama N, Jang WD, Yamasaki Y, Kataoka K. PEGylated gene nanocarriers based on block catiomers bearing ethylenediamine repeating units directed to remarkable enhancement of photochemical transfection. *J Control Release* 2006, 115(2):208–15.

Bae Y, Fukushima S, Harada A, Kataoka K. Design of environment-sensitive supramolecular assemblies for intracellular drug delivery: Polymeric micelles that are responsive to intracellular pH change. *Angewandte Chemie-International Edition* 2003, 42(38):4640–43.

Bae Y, Kataoka K. Drug and gene delivery with nanotechnology. *Seikagaku* 2006, 78(9):882–87.

Behr JP. The proton sponge: A trick to enter cells the viruses did not exploit. *Chimia* 1997, 51(1–2):34–36.

Bikram M, Ahn CH, Chae SY, Lee MY, Yockman JW, Kim SW. Biodegradable poly(ethylene glycol)-co-poly(L-lysine)-g-histidine multiblock copolymers for nonviral gene delivery. *Macromolecules* 2004, 37(5):1903–16.

Brissault B, Kichler A, Guis C, Leborgne C, Danos O, Cheradame H. Synthesis of linear polyethylenimine derivatives for DNA transfection. *Bioconjug Chem* 2003, 14(3):581–87.

Brzezinska KR, Deming TJ. Synthesis of AB diblock copolymers by atom-transfer radical polymerization (ATRP) and living polymerization of alpha-amino acid-N-carboxyanhydrides. *Macromol Biosci* 2004, 4(6):566–69.

Boussif O, Lezoualch F, Zanta MA, Mergny MD, Scherman D, Demeneix B, et al. A Versatile Vector for Gene and Oligonucleotide Transfer into Cells in Culture

and in-Vivo – Polyethylenimine. *Proceedings of the National Academy of Sciences of the United States of America* 1995, 92(16):7297–301.

Choi JS, Lee EJ, Choi YH, Jeong YJ, Park JS. Poly(ethylene glycol)-block-poly (L-lysine) dendrimer: novel linear polymer/dendrimer block copolymer forming a spherical water-soluble polyionic complex with DNA. *Bioconjug Chem* 1999, 10(1):62–5.

Clements BA, Bai J, Kucharski C, Farrell LL, Lavasanifar A, Ritchie B, et al. RGD conjugation to polyethyleneimine does not improve DNA delivery to bone marrow stromal cells. *Biomacromolecules* 2006, 7(5):1481–8.

Croy SR, Kwon GS. Polymeric micelles for drug delivery. *Curr Pharm Des* 2006, 12(36):4669–84.

Deming TJ. Transition metal-amine initiators for preparation of well-defined poly(gamma-benzyl L-glutamate). *J Am Chem Soc* 1997, 119(11):2759–60.

Deming TJ. Living polymerization of alpha-amino acid-N-carboxyanhydrides. *J Polym Sci (A1)* 2000, 38(17):3011–18.

Deming TJ. Methodologies for preparation of synthetic block copolypeptides: materials with future promise in drug delivery. *Adv Drug Deliv Rev* 2002, 54(8):1145–55.

Demeneix B, Behr JP. Polyethylenimine (PEI). *Adv Genet* 2005, 53:217–30.

Deng M, Wang R, Rong G, Sun J, Zhang X, Chen X, et al. Synthesis of a novel structural triblock copolymer of poly(gamma -benzyl-l-glutamic acid)-b-poly(-ethylene oxide)-b-poly(epsilon-caprolactone). *Biomaterials* 2004, 25(17):3553–8.

Dvorak M, Rypacek F. Preparation and polymerization of N-carboxyanhydrides of alpha-amino-acids. *Chemicke Listy* 1995, 89(7):423–36.

Erbacher P, Roche AC, Monsigny M, Midoux P. Putative role of chloroquine in gene transfer into a human hepatoma cell line by DNA lactosylated polylysine complexes. *Exp Cell Res* 1996, 225(1):186–94.

Freireic S, Gertner D, Zilkha A. Polymerization of N-carboxy anhydrides by organotin catalysts. *Eur Polym J* 1974, 10(5):439–43.

Fuller WD, Verlander MS, Goodman M. A procedure for the facile synthesis of amino-acid N-carboxyanhydrides. *Biopolymers* 1976, 15(9):1869–71.

Funhoff AM, van Nostrum CF, Koning GA, Schuurmans-Nieuwenbroek NM, Crommelin DJ, Hennink WE. Endosomal escape of polymeric gene delivery complexes is not always enhanced by polymers buffering at low pH. *Biomacromolecules* 2004, 5(1):32–9.

Gadzinowski M, Sosnowski S, Slomkowski S. Kinetics of the dispersion ring-opening polymerization of epsilon-caprolactone initiated with diethylaluminum ethoxide. *Macromolecules* 1996, 29(20):6404–07.

Goto M, Yura H, Chang CW, Kobayashi A, Shinoda T, Maeda A, et al. Lactose-carrying polystyrene as a drug carrier – Investigation of body distributions to parenchymal liver-cells using I-125 labeled lactose-carrying polystyrene. *J Control Release* 1994, 28(1–3):223–33.

Harada A, Kataoka K. Formation of Polyion complex micelles in an aqueous milieu from a pair of oppositely-charged block-copolymers with poly(ethylene glycol) segments. Macromolecules 1995, 28(15):5294–99.

Harada A, Togawa H, Kataoka K. Physicochemical properties and nuclease resistance of antisense-oligodeoxynucleotides entrapped in the core of polyion complex micelles composed of poly(ethylene glycol)-poly(L-lysine) block copolymers. *Eur J Pharm Sci* 2001, 13(1):35–42.

Harwood HJ. Comments concerning the mechanism of strong base initiated NCA polymerization. *Abstracts of Papers of the American Chemical Society* 1984, 187(APR):72-Poly.

Hirano T, Klesse W, Ringsdorf H. Polymeric Derivatives of Activated Cyclophosphamide as drug delivery systems in anti-tumor

chemotherapy – Pharmacologically Active Polymers .20. *Makromolekulare Chemie-Macromolecular Chemistry and Physics* 1979, 180(4):1125–31.

Iijima M, Nagasaki Y, Okada T, Kato M, Kataoka K. Core-polymerized reactive micelles from heterotelechelic amphiphilic block copolymers. *Macromolecules* 1999, 32(4):1140–46.

Itaka K, Kanayama N, Nishiyama N, Jang WD, Yamasaki Y, Nakamura K, et al. Supramolecular nanocarrier of siRNA from PEG-based block catiomer carrying diamine side chain with distinctive pK(a) directed to enhance intracellular gene silencing. *J Am Chem Soc* 2004, 126(42):13612–13.

Ito K, Hashizuka Y, Yamashita Y. Equilibrium cyclic oligomer formation in anionic-polymerization of epsilon-caprolactone. *Macromolecules* 1977, 10(4):821–24.

Jeong YI, Nah JW, Lee HC, Kim SH, Cho CS. Adriamycin release from flower-type polymeric micelle based on star-block copolymer composed of poly (gamma-benzyl L-glutamate) as the hydrophobic part and poly(ethylene oxide) as the hydrophilic part. *Int J Pharm* 1999, 188(1):49–58.

Jule E, Nagasaki Y, Kataoka K. Lactose-installed poly(ethylene glycol)-poly(d,l-lactide) block copolymer micelles exhibit fast-rate binding and high affinity toward a protein bed simulating a cell surface. A surface plasmon resonance study. *Bioconjug Chem* 2003, 14(1):177–86.

Kabanov AV, Batrakova EV, Alakhov VY. Pluronic block copolymers for overcoming drug resistance in cancer. *Adv Drug Deliv Rev* 2002, 54(5):759–79.

Kabanov AV, Lemieux P, Vinogradov S, Alakhov V. Pluronic block copolymers: novel functional molecules for gene therapy. *Adv Drug Deliv Rev* 2002, 54(2):223–33.

Kabanov A, Zhu J, Alakhov V. Pluronic block copolymers for gene delivery. *Adv Genet* 2005, 53PA:231–61.

Kakizawa Y, Harada A, Kataoka K. Environment-sensitive stabilization of core-shell structured polyion complex micelle by reversible cross-linking of the core through disulfide bond. *J Am Chem Soc* 1999, 121(48):11247–48.

Kakizawa Y, Harada A, Kataoka K. Glutathione-sensitive stabilization of block copolymer micelles composed of antisense DNA and thiolated poly(ethylene glycol)-block-poly(L-lysine): A potential carrier for systemic delivery of antisense DNA. *Biomacromolecules* 2001, 2(2):491–97.

Kakizawa Y, Kataoka K. Block copolymer micelles for delivery of gene and related compounds. *Adv Drug Deliv Rev* 2002, 54(2):203–22.

Kanayama N, Fukushima S, Nishiyama N, Itaka K, Jang WD, Miyata K, et al. A PEG-based biocompatible block catiomer with high buffering capacity for the construction of polyplex micelles showing efficient gene transfer toward primary cells. *Chem Med Chem* 2006, 1(4):439–44.

Kataoka K, Matsumoto T, Yokoyama M, Okano T, Sakurai Y, Fukushima S, et al. Doxorubicin-loaded poly(ethylene glycol)-poly(beta-benzyl-L-aspartate) copolymer micelles: their pharmaceutical characteristics and biological significance. *J Control Release* 2000, 64(1–3):143–53.

Katayose S, Kataoka K. Water-soluble polyion complex associates of DNA and poly(ethylene glycol)-poly(L-lysine) block copolymer. *Bioconjug Chem* 1997, 8(5):702–7.

Katayose S, Kataoka K. Remarkable increase in nuclease resistance of plasmid DNA through supramolecular assembly with poly(ethylene glycol)-poly(L-lysine) block copolymer. *J Pharm Sci* 1998, 87(2):160–3.

Kataoka K, Kwon GS, Yokoyama M, Okano T, Sakurai Y. Block-Copolymer Micelles as Vehicles for Drug Delivery. *J Control Release* 1993, 24(1–3):119–32.

Kim SH, Jeong JH, Joe CO, Park TG. Folate receptor mediated intracellular protein delivery using PLL-PEG-FOL conjugate. *J Control Release* 2005, 103(3):625–34.

Kircheis R, Wightman L, Wagner E. Design and gene delivery activity of modified polyethylenimines. *Adv Drug Deliv Rev* 2001, 53(3):341–58.

Kricheldorf HR, Mulhaupt R. Mechanism of the NCA polymerization .7. primary and secondary amine-initiated polymerization of beta-amino acid NCAS. *Makromolekulare Chemie-Macromolecular Chemistry and Physics* 1979, 180(6):1419–33.

Kricheldorf HR, Von Lossow C, Schwarz G. Primary amine and solvent-induced polymerizations of L- or D,L-phenylalanine N-carboxyanhydride. *Macromol Chem Phys* 2005, 206(2):282–90.

Kwon GS. Polymeric micelles for delivery of poorly water-soluble compounds. *Crit Rev Ther Drug Carrier Syst* 2003, 20(5):357–403.

Kunath K, Merdan T, Hegener O, Haberlein H, Kissel T. Integrin targeting using RGD-PEI conjugates for in vitro gene transfer. *J Gene Med* 2003, 5(7):588–99.

Kursa M, Walker GF, Roessler V, Ogris M, Roedl W, Kircheis R, et al. Novel shielded transferrin-polyethylene glycol-polyethylenimine/DNA complexes for systemic tumor-targeted gene transfer. *Bioconjug Chem* 2003, 14(1):222–31.

Kwon G, Naito M, Yokoyama M, Okano T, Sakurai Y, Kataoka K. Micelles based on Ab block copolymers of poly(ethylene oxide) and poly(beta-benzyl L-aspartate). *Langmuir* 1993, 9(4):945–49.

Kwon GS, Naito M, Yokoyama M, Okano T, Sakurai Y, Kataoka K. Physical entrapment of adriamycin in AB block copolymer micelles. *Pharm Res* 1995, 12(2):192–5.

La SB, Okano T, Kataoka K. Preparation and characterization of the micelle-forming polymeric drug indomethacin-incorporated poly(ethylene oxide)-poly(beta-benzyl L-aspartate) block copolymer micelles. *J Pharm Sci* 1996a, 85(1):85–90.

La SB, Okano T, Kataoka K. Preparation and characterization of the micelle-forming polymeric drug indomethacin-incorporated poly(ethylene oxide)-poly(beta-benzyl L-aspartate) block copolymer micelles. *J Pharm Sci* 1996b, 85(1):85–90.

Lavasanifar A, Samuel J, Kwon GS. Micelles self-assembled from poly(ethylene oxide)-block-poly(N-hexyl stearate L-aspartamide) by a solvent evaporation method: effect on the solubilization and haemolytic activity of amphotericin B. *J Control Release* 2001, 77(1–2):155–60.

Lavasanifar A, Samuel J, Kwon GS. Poly(ethylene oxide)-block-poly(L-amino acid) micelles for drug delivery. *Adv Drug Deliv Rev* 2002a, 54(2):169–90.

Lavasanifar A, Samuel J, Sattari S, Kwon GS. Block copolymer micelles for the encapsulation and delivery of amphotericin B. *Pharm Res* 2002b, 19(4):418–22.

Lee ES, Na K, Bae YH. Polymeric micelle for tumor pH and folate-mediated targeting. *J Control Release* 2003a, 91(1–2):103–13.

Lee ES, Na K, Bae YH. Polymeric micelle for tumor pH and folate-mediated targeting. *J Control Release* 2003b, 91(1–2):103–13.

Lee J, Cho EC, Cho K. Incorporation and release behavior of hydrophobic drug in functionalized poly(D,L-lactide)-block-poly(ethylene oxide) micelles. *J Control Release* 2004, 94(2–3):323–35.

Lee ES, Na K, Bae YH. Doxorubicin loaded pH-sensitive polymeric micelles for reversal of resistant MCF-7 tumor. *J Control Release* 2005, 103(2):405–18.

Lungwitz U, Breunig M, Blunk T, Gopferich A. Polyethylenimine-based non-viral gene delivery systems. *Eur J Pharm Biopharm* 2005, 60(2):247–66.

Mahmud A, Xiong XB, Lavasanifar A. Novel self-associating poly(ethylene oxide)-block-poly(epsilon-caprolactone) block copolymers with functional side groups on the polyester block for drug delivery. *Macromolecules* 2006, 39(26):9419–28.

Mahmud A, Xiong XB, Lavasanifar A. Self-associating poly(ethylene oxide)-block-poly(e-caprolactone) copolymers with carboxyl, benzyl carboxylate and doxorubicin side group:Novel micellar nano-containers and drug conjugates.

Proceedings of the Annual Meeting of the Controlled Release Society, July 2007, US. 2007.

Matsumura Y, Yokoyama M, Kataoka K, Okano T, Sakurai Y, Kawaguchi T, et al. Reduction of the side effects of an antitumor agent, KRN5500, by incorporation of the drug into polymeric micelles. *Jpn J Cancer Res* 1999, 90(1):122–8.

Meister A, Anderson ME. Glutathione. *Annu Rev Biochem* 1983, 52:711–60.

Minko T, Batrakova EV, Li S, Li Y, Pakunlu RI, Alakhov VY, et al. Pluronic block copolymers alter apoptotic signal transduction of doxorubicin in drug-resistant cancer cells. *J Control Release* 2005, 105(3):269–78.

Murao A, Nishikawa M, Managit C, Wong J, Kawakami S, Yamashita F, et al. Targeting efficiency of galactosylated liposomes to hepatocytes in vivo: Effect of lipid composition. *Pharm Res* 2002, 19(12):1808–14.

Miyata K, Kakizawa Y, Nishiyama N, Harada A, Yamasaki Y, Koyama H, et al. Block catiomer polyplexes with regulated densities of charge and disulfide cross-linking directed to enhance gene expression. *J Am Chem Soc* 2004, 126(8):2355–61.

Nakanishi T, Fukushima S, Okamoto K, Suzuki M, Matsumura Y, Yokoyama M, et al. Development of the polymer micelle carrier system for doxorubicin. *J Control Release* 2001, 74(1–3):295–302.

Nasongkla N, Shuai X, Ai H, Weinberg BD, Pink J, Boothman DA, et al. cRGD-functionalized polymer micelles for targeted doxorubicin delivery. *Angew Chem Int Ed Engl* 2004, 43(46):6323–7.

Nagasaki Y, Yasugi K, Yamamoto Y, Harada A, Kataoka K. Sugar-installed polymeric micelle for a vehicle of an active targeting drug delivery system. *Abstracts of Papers of the American Chemical Society* 2001, 221:U434–U34.

Newman MJ, Actor JK, Balusubramanian M, Jagannath C. Use of nonionic block copolymers in vaccines and therapeutics. *Crit Rev Ther Drug Carrier Syst* 1998a, 15(2):89–142.

Newman MJ, Todd CW, Balusubramanian M. Design and development of adjuvant-active nonionic block copolymers. *J Pharm Sci* 1998b, 87(11):1357–62.

Nguyen CA, Allemann E, Schwach G, Doelker E, Gurny R. Cell interaction studies of PLA-MePEG nanoparticles. *Int J Pharm* 2003, 254(1):69–72.

Nishiyama N, Kataoka K. Preparation and characterization of size-controlled polymeric micelle containing cis-dichlorodiammineplatinum(II) in the core. *J Control Release* 2001, 74(1–3):83–94.

Nishiyama N, Kataoka K. Polymeric micelle drug carrier systems: PEG-PAsp(Dox) and second generation of micellar drugs Polymer Drugs in the Clinical Stage: Advantages and Prospects, 2003:155–77.

Nishiyama N, Kataoka K. Current state, achievements, and future prospects of polymeric micelles as nanocarriers for drug and gene delivery. *Pharmacol Ther* 2006, 112(3):630–48.

Nishiyama N, Kato Y, Sugiyama Y, Kataoka K. Cisplatin-loaded polymer-metal complex micelle with time-modulated decaying property as a novel drug delivery system. *Pharm Res* 2001, 18(7):1035–41.

Nishiyama N, Okazaki S, Cabral H, Miyamoto M, Kato Y, Sugiyama Y, et al. Novel cisplatin-incorporated polymeric micelles can eradicate solid tumors in mice. *Cancer Res* 2003, 63(24):8977–83.

Nishiyama N, Yokoyama M, Aoyagi T, Okano T, Sakurai Y, Kataoka K. Preparation and characterization of self-assembled polymer-metal complex micelle from cis-dichlorodiammineplatinum(II) and poly(ethylene glycol)-poly(alpha,-beta-aspartic acid) block copolymer in an aqueous medium. *Langmuir* 1999, 15(2):377–83.

Ogris M, Walker G, Blessing T, Kircheis R, Wolschek M, Wagner E. Tumor-targeted gene therapy: strategies for the preparation of ligand-polyethylene

glycol-polyethylenimine/DNA complexes. *J Control Release* 2003, 91(1–2):173–81.

Omelyanenko V, Kopeckova P, Gentry C, Kopecek J. Targetable HPMA copolymer-adriamycin conjugates. Recognition, internalization, and subcellular fate. *J Control Release* 1998, 53(1–3):25–37.

Opanasopit P, Sakai M, Nishikawa M, Kawakami S, Yamashita F, Hashida M. Inhibition of liver metastasis by targeting of immunomodulators using mannosylated liposome carriers. *J Control Release* 2002, 80(1–3):283–94.

Opanasopit P, Yokoyama M, Watanabe M, Kawano K, Maitani Y, Okano T. Block copolymer design for camptothecin incorporation into polymeric micelles for passive tumor targeting. *Pharm Res* 2004, 21(11):2001–08.

Osada K, Kataoka K. Drug and gene delivery based on supramolecular assembly of PEG-polypeptide hybrid block copolymers *Adv poly sci* 2006, 202:113–53.

Sagara K, Kim SW. A new synthesis of galactose-poly(ethylene glycol)-polyethylenimine for gene delivery to hepatocytes. *J Control Release* 2002, 79(1–3):271–81.

Scholz C, Iijima M, Nagasaki Y, Kataoka K. A Novel Reactive Polymeric Micelle with Aldehyde Groups on Its Surface. *Macromolecules* 1995, 28(21):7295–97.

Sekiguchi H. Mechanism of N-carboxy-alpha-amino acid anhydride (NCA) polymerization. *Pure Appl Chem* 1981, 53(9):1689–714.

Shenoy DB, Amiji MM. Poly(ethylene oxide)-modified poly(epsilon-caprolactone) nanoparticles for targeted delivery of tamoxifen in breast cancer. *Int J Pharm* 2005, 293(1–2):261–70.

Smeenk JM, Lowik DWPM, van Hest JCM. Peptide-containing block copolymers: Synthesis and potential applications of bio-mimetic materials. *Curr Org Chem* 2005, 9(12):1115–25.

Stridsberg KM, Ryner M, Albertsson AC. Controlled ring-opening polymerization: Polymers with designed macromolecular architecture. *Degradable Aliphatic Polyesters* 2002, 157:41–65.

Tadros T. Principles of emulsion stabilization with special reference to polymeric surfactants. *J Cosmet Sci* 2006, 57(2):153–69.

Tian HY, Deng C, Lin H, Sun JR, Deng MX, Chen XS, et al. Biodegradable cationic PEG-PEI-PBLG hyperbranched block copolymer: synthesis and micelle characterization. *Biomaterials* 2005, 26(20):4209–17.

Tsuruta T, Matsuura K, Inoue S. Copolymerization of Propylene Oxide with N-Carboxy-Dl-Alanine Anhydride by Organometallic Systems. *Makromolekulare Chemie* 1965, 83(APR):289-&.

Van Domeselaar GH, Kwon GS, Andrew LC, Wishart DS. Application of solid phase peptide synthesis to engineering PEO-peptide block copolymers for drug delivery. *Colloids Surf B-Biointerfaces* 2003, 30(4):323–34.

Vayaboury W, Giani O, Cottet H, Deratani A, Schue F. Living polymerization of alpha-amino acid N-carboxyanhydrides (NCA) upon decreasing the reaction temperature. *Macromol Rapid Commun* 2004, 25(13):1221–24.

Vega J, Ke S, Fan Z, Wallace S, Charsangavej C, Li C. Targeting doxorubicin to epidermal growth factor receptors by site-specific conjugation of C225 to poly(L-glutamic acid) through a polyethylene glycol Spacer. *Pharm Res* 2003, 20(5):826–32.

Vinogradov SV, Bronich TK, Kabanov AV. Nanosized cationic hydrogels for drug delivery: preparation, properties and interactions with cells. *Adv Drug Deliv Rev* 2002, 54(1):135–47.

von Harpe A, Petersen H, Li YX, Kissel T. Characterization of commercially available and synthesized polyethylenimines for gene delivery. *J Control Release* 2000, 69(2):309–22.

Wang Y, Liu S, Li CY, Yuan F. A novel method for viral gene delivery in solid tumors. *Cancer Res* 2005, 65(17):7541–5.

Ward CM, Pechar M, Oupicky D, Ulbrich K, Seymour LW. Modification of pLL/DNA complexes with a multivalent hydrophilic polymer permits folate-mediated targeting in vitro and prolonged plasma circulation in vivo. *J Gene Med* 2002, 4(5):536–47.

Wolk SK, Swift G, Paik YH, Yocom KM, Smith RL, Simon ES. One-Dimensional and 2-Dimensional Nuclear-Magnetic-Resonance Characterization of Poly(Aspartic Acid) Prepared by Thermal Polymerization of L-Aspartic Acid. *Macromolecules* 1994, 27(26):7613–20.

Won CY, Chu CC, Lee JD. Synthesis and characterization of biodegradable poly(L-aspartic acid-co-PEG). *J Polym Sci (A1)* 1998, 36(16):2949–59.

Wu J, Nantz MH, Zern MA. Targeting hepatocytes for drug and gene delivery: Emerging novel approaches and applications. *Frontiers in Bioscience* 2002, 7:D717–D25.

Xiong XB, Aliabadi HM, Lavasanifar A. PEO-modified Poly(L-amino acid) micelles for drug delivery. *Nanotechnology for Cancer Therapy* 2006. Editor, Mansoor M. Amiji, CRC 40(12):1085–90.

Xiong XB, Mahmud A, Uludag H, Lavasanifar A. Conjugation of arginine-glycine-aspartic acid peptides to poly(ethylene oxide)-b-poly(epsilon-caprolactone) micelles for enhanced intracellular drug delivery to metastatic tumor cells. *Biomacromolecules* 2007, 8:874–84a.

Xiong XB, Mahmud A, Uludag H, lavasanifar A. Novel RGD-functionalized polymer-drug conjugate for targeted drug delivery. *Proceedings of the Annual Meeting of the Controlled Release Society, July 2007, US*. 2007b.

Yamamoto Y, Nagasaki Y, Kato M, Kataoka K. Surface charge modulation of poly(ethylene glycol)-poly(D, L-lactide) block copolymer micelles: conjugation of charged peptides. *Colloids Surf B-Biointerfaces* 1999, 16(1–4):135–46.

Yamashit S, Tani H. Polymerization of gamma-benzyl L-glutamate N-carboxyanhydride with metal acetate-tri-normal-butylphosphine catalyst system. *Macromolecules* 1974, 7(4):406–09.

Yamashit S, Waki K, Yamawaki N, Tani H. Stereoselective polymerization of alpha-amino-acid N-carboxyanhydrides with nickel Dl-2-methylbutyrate-tri-normal-butylphosphine catalyst system. *Macromolecules* 1974, 7(4):410–15.

Yokoyama M, Fukushima S, Uehara R, Okamoto K, Kataoka K, Sakurai Y, et al. Characterization of physical entrapment and chemical conjugation of adriamycin in polymeric micelles and their design for in vivo delivery to a solid tumor. *J Control Release* 1998, 50(1–3):79–92.

Yokoyama M, Okano T, Sakurai Y, Kataoka K. Improved synthesis of adriamycin-conjugated poly(ethylene oxide) poly(aspartic acid) block-copolymer and formation of unimodal micellar structure with controlled amount of physically entrapped adriamycin. *J Control Release* 1994, 32(3):269–77.

Yokoyama M, Opanasopit P, Okano T, Kawano K, Maitani Y. Polymer design and incorporation methods for polymeric micelle carrier system containing water-insoluble anti-cancer agent camptothecin. *J Drug Target* 2004, 12(6):373–84.

Yokoyama M, Okano T, Sakurai Y, Ekimoto H, Shibazaki C, Kataoka K. Toxicity and antitumor activity against solid tumors of micelle-forming polymeric anticancer drug and its extremely long circulation in blood. *Cancer Res* 1991, 51(12):3229–36.

Yokoyama M, Okano T, Sakurai Y, Suwa S, Kataoka K. Introduction of cisplatin into polymeric micelle. *J Control Release* 1996, 39(2–3):351–56.

Yoo HS, Park TG. Biodegradable polymeric micelles composed of doxorubicin conjugated PLGA-PEG block copolymer. *J Control Release* 2001, 70(1–2):63–70.

Yokoyama M, Satoh A, Sakurai Y, Okano T, Matsumura Y, Kakizoe T, et al. Incorporation of water-insoluble anticancer drug into polymeric micelles and control of their particle size. *J Control Release* 1998, 55(2–3):219–29.

Zhang X, Li Y, Chen X, Wang X, Xu X, Liang Q, et al. Synthesis and characterization of the paclitaxel/MPEG-PLA block copolymer conjugate. *Biomaterials* 2005, 26(14):2121–8.

14

PAMAM Dendrimers as Nanoscale Oral Drug Delivery Systems

Kelly M. Kitchens and Hamidreza Ghandehari

Introduction

The application of nanotechnology to the diagnosis and treatment of diseases has coined the term *nanomedicine*. Nanometer-scale biomaterials have their role in nanomedicine since their nanoscopic size allows interaction with cellular membranes, subcellular organelles, passage through the microvasculature, and may reduce immunogenicity by avoiding reticuloendothelial uptake. Such features are desirable for nanomaterials to enhance the residence of poorly bioavailable drugs in the systemic circulation. Nanomaterials used as drug delivery systems, also termed nanocarriers, should be freely permeable to tumor vasculature since the endothelial pores range from 100 to 1000 nm (Hobbs et al., 1998). On the other hand, several moieties can be incorporated in these nanocarriers to enhance the delivery of bioactive and diagnostic agents. These include imaging agents for detection of the nanocarriers in the body, targeting ligands to direct the carrier to the site of action, enhanced cell permeation and intracellular trafficking with cell-penetrating moieties, as well as biodegradable linkers for drug release (Torchilin, 2006). Some examples of nanocarriers used for drug delivery applications include liposomes, micelles, polymers, and nanoemulsions, which have demonstrated the ability to serve as "multifunctional nanocarriers" (Torchilin, 2006). Water-soluble polymers have been used as targeted drug delivery systems since they can be designed to conjugate multiple drug compounds as well as targeting moieties. This results in alteration of a drug's pharmacokinetic profile and therapeutic index by changing drug solubility, toxicity, biodistribution, and intracellular trafficking compared to free drug (Duncan & Spreafico, 1994; Luo & Prestwich, 2002; Tomlinson et al., 2003). The major drawback of such systems is their large size, which limits their administration primarily to parenteral routes that are invasive and require frequent physician visits.

Oral drug administration offers high patient compliance due to the ease of administration, lack of discomfort and pain associated with injections, and lower cost. Yet a major limitation of polymers in oral drug delivery is their limited transport across the intestinal epithelium due to their large size relative to the tight, epithelial barrier of the gastrointestinal (GI) tract.

M.M. de Villiers et al. (eds.), *Nanotechnology in Drug Delivery*, DOI: 10.1007/978-0-387-77667-5_14,

Furthermore, the acidic environment of the stomach along with various enzymes of the GI tract can affect the stability of polymeric drug delivery systems. In order to develop orally bioavailable polymers, it is essential to investigate their stability in the GI tract, interaction with the epithelial barrier of the gut, transepithelial transport and subcellular trafficking, systemic distribution, extravasation into the target tissue(s), and elimination from the body.

One class of polymers that have demonstrated potential use as oral drug delivery carriers are poly(amidoamine) (PAMAM) dendrimers (D'Emanuele & Attwood, 2005; Duncan & Izzo, 2005; Kitchens et al., 2005; Svenson & Tomalia, 2005). Recent studies have demonstrated that PAMAM dendrimers of certain generations and surface charge can permeate the epithelial barrier of the gut, suggesting their potential as oral drug delivery carriers (Jevprasesphant et al., 2003a; Kitchens et al., 2005, 2006; Wiwattanapatapee et al., 2000). PAMAM-drug conjugates have also shown the potential to bypass intestinal epithelial efflux pumps (D'Emanuele et al., 2004). The toxicity and biocompatibility of these systems is dependent on size, surface charge, and concentration (Duncan & Izzo, 2005; El-Sayed et al., 2002, 2003b; Jevprasesphant et al., 2003b; Kitchens et al., 2006), which can be modulated by surface modification, particularly of the positively charged primary amine groups (Jevprasesphant et al., 2003a,b; Kolhatkar et al., 2007; Roberts, 1996). Initial studies indirectly suggested that the transepithelial transport of PAMAM dendrimers is due to a combination of para- and transcellular pathways (El-Sayed et al., 2003b; Jevprasesphant et al., 2004). More recent studies have provided visual evidence that indeed PAMAM dendrimers open tight junctions, and endocytosis mechanisms contribute to their internalization and intracellular trafficking (Kitchens et al., 2007). These studies have set the stage for the use of PAMAM dendrimers as orally bioavailable nanocarriers. In this chapter a brief overview of the synthesis and characterization of dendrimers will be described, followed by a general account of their biocompatibility and applications in the delivery of bioactive and diagnostic agents. The main focus will be on the use of PAMAM dendrimers as oral drug carriers.

Synthesis

Dendrimers involve the assembly of *dendrons* (Greek for "tree") to form a *dendrimer* (Tomalia, 1993). Dendrimer synthesis involves the use of typical organic monomers to produce macromolecules with polydispersities of around ~1.0005–1.10 (Esfand & Tomalia, 2001; Tomalia, 2004). Two general synthetic methods have been used to produce dendrimers: the *divergent* and *convergent* methods (Scheme 14.1). The *divergent* method was pioneered by Tomalia and involves outward branching from an initiator core around which the branches of the dendrimer originates (Tomalia, 2004). The *convergent* method was introduced by Hawker and Fréchet, and involves inward growth from what will become the dendrimer surface to the inner core by the formation of individual dendrons (Hawker & Fréchet, 1990). Although these two strategies are traditionally used and have resulted in the production of several hundred dendrimer families (Svenson & Tomalia,

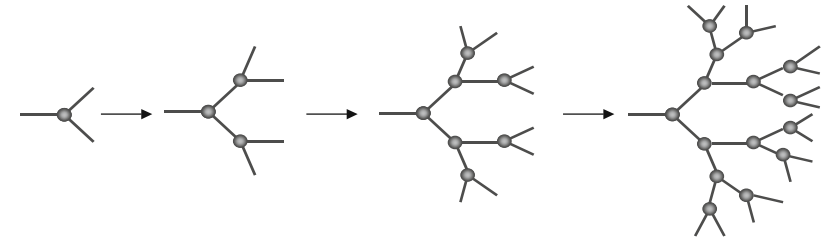

Divergent Synthesis

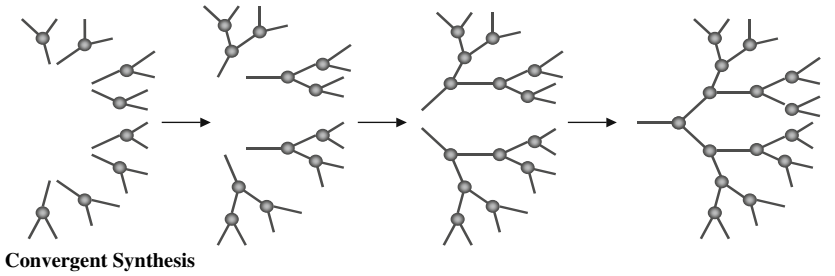

Convergent Synthesis

Scheme 14.1 Convergent and divergent synthesis of dendrimers.

2005), the synthetic approaches pose some challenges toward the commercialization of large quantities of dendrimer structures. Excess monomers and extensive purification techniques are required for the *divergent* process, while the *convergent* method is limited to the synthesis of lower generation (G) dendrimers due to steric hindrance that occurs from attaching outer dendrons toward the inner core (Svenson & Tomalia, 2005). To address these challenges, two alternative synthetic strategies have recently been introduced. One such method termed *lego chemistry* involves the synthesis of phosphorous-based dendrimers using functionalized cores and branched monomers, in which each generation is produced in a single-step reaction based on two types of alternating "layer blocks" ($P(S)\text{-}OC_6H_4PPh_2 = NP(S)$ or $P(S)NMeN = CHC_6H_4OP(S)$) and the only byproducts are nitrogen and water (Brauge et al., 2001; Maraval et al., 2003). *Lego chemistry* produces phosphines, hydrazides, and aldehydes as end groups, which allow for further reactions to produce additional generations. For instance, this chemistry allows the number of surface groups to multiply from 48 phosphines of G4 to 250 aldehydes of G5 in one step (Maraval et al., 2003). *Click chemistry* is another alternative synthetic method that has been exploited for defined locations of dendritic block copolymers (Wu et al., 2004a, 2005). This chemistry involves Cu(I)-catalyzed formation of 1,2,3-triazole linkage to prepare azide-acetylene diblock dendrimers. The addition of mannose and coumarin units to the functional end groups of these dendrimers facilitates the dual function of biorecognition and detection, respectively (Wu et al., 2004a).

The selection of the initiator core, branching cells, and exterior functional groups can offer a countless variety of dendritic structures.

Poly(propyleneimine) (PPI) dendrimers are also commercially available with a diaminobutane (DAB) core. PPI dendrimers are synthesized using the divergent method via Michael addition of acrylonitrile to the primary amine groups, followed by hydrogenation of the nitrile groups to result in primary amine groups (Loup et al., 1999). Poly(ethyleneimine) (PEI) dendrimers are synthesized with an initiator core of ammonia, and alkylation of diethylenetriamine with aziridine produces the core shell tris-(2-aminoethyl)amine (Tomalia et al., 1990). Protected, first-generation PEI dendrimers are obtained through alkylation of the terminal amine groups with activated aziridines, followed by deprotection with acid hydrolysis (Tomalia et al., 1990). As the generation of PEI dendrimers increases, branching ideality decreases and branch defects are more likely due to de Gennes packing. PEI dendrimers have greater chemical and physical stability than poly(amidoamine) (PAMAM) dendrimers due to their shorter branch lengths (0.5 nm compared to 1 nm) (Tomalia et al., 1990). Starburst® dendrimers are commercially available as PAMAM or PPI with ethylenediamine or DAB cores, respectively, and are also available with cores diaminohexane, diaminododecane, and cystamine. The surface groups of Starburst® dendrimers include amino, sodium carboxylate, succinamic acid, tris-(hydroxymethyl) amidomethane, and poly(ethylene glycol) (PEG). Dendrimers typically used in biological applications include polyesters (Grinstaff, 2002), polypeptides (Sadler & Tam, 2002), and glycodendrimers (Turnbull & Stoddart, 2002). Table 14.1 gives an

Table 14.1 Examples of types of dendrimers used for biomedical applications.

Dendrimer structure	Applications	References
PAMAM	Targeted delivery of paclitaxel in KB epidermoid carcinoma	Majoros et al., 2006
	Carrier for cisplatin in solid tumors	Malik et al., 1999
	Dendrimer-based Gd(III) chelates for MRI	Kobayashi and Brechbiel, 2005
	Cardiac diagnostic marker, e.g., Stratus® CS manufactured by Dade Behring	Halford, 2005
	Permeation enhancer for propanolol in Caco-2 epithelial cells	D'Emanuele et al., 2004
	Carrier for ibuprofen in A549 lung epithelial cells	Kolhe et al., 2006
	Gene transfection agent for nucleic acids, e.g., Superfect® manufactured by Qiagen	Dufes et al., 2005b
	Preventing scar tissue formation	Shaunak et al., 2004
PPI	Vector for TNF-α gene therapy of A431 epidermoid carcinoma, C33a cervix carcinoma, and LS174T colorectal adenocarcinoma	Dufes et al., 2005a
	Dendrimer-based Gd (III) chelates for MRI	Kobayashi and Brechbiel, 2005
	Gene transfection agent for nucleic acids	Dufes et al., 2005b
Polypeptide	Carrier of ara-C prodrugs for tumor inhibition	Choe et al., 2002
	Potential targeted drug delivery carrier to tumor cells	Tansey et al., 2004
Polyester	Carrier for anti-cancer agent doxorubicin in murine melanoma cell line; improved doxorubicin biodistribution in vivo	Padilla De Jesus et al., 2002
	Adhesive to repair corneal lacerations	Velazquez et al., 2004

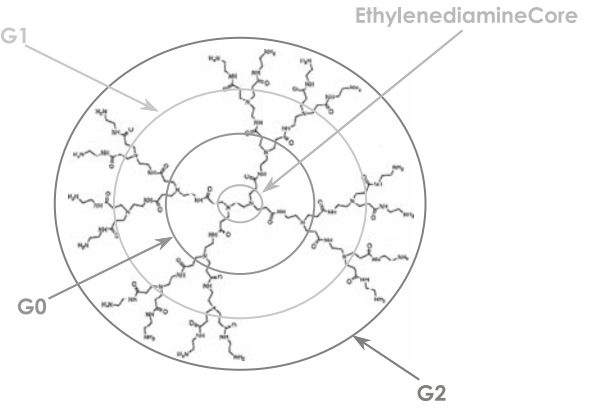

Scheme 14.2 Schematics of amine terminated PAMAM dendrimers: G denotes generation. Adapted from Tajarobi et al. (2001) (with permission from Elsevier).

overview of some dendrimer structures that have been employed in biomedical applications.

The focus of this article is on PAMAM dendrimers, which are the first dendrimer family to be completely synthesized, characterized, and commercialized (Tomalia, 2004). PAMAM dendrimers are synthesized using the *divergent* method, and dendrimer growth occurs in a radial fashion around a nucleophilic core (Scheme 14.2). The surface groups increase exponentially and the molecular mass of dendrimers increases almost twofold due to the inner core (N_c) and branch cell (N_b) multiplicity (Tomalia, 2004). PAMAM dendrimers are generally constructed with an initiator core (e.g., ethylene diamine or ammonia) where branching occurs via Michael addition of the amines with methyl acrylate to produce a half-generation (e.g., G0.5). This is followed by amidation of the ester groups with excess ethylene diamine to result in a full generation dendrimer with primary amine surface groups (e.g., G1) (Tomalia, 1993, 2004).

The molecular size of PAMAM dendrimers increases by approximately 1 nm with each generation, with sizes ranging from 1 to 15 nm (Esfand & Tomalia, 2001; Tomalia, 2004). The polydispersity values of PAMAM dendrimers range from ~1.000002 to 1.005 verified by gel electrophoresis and matrix-assisted laser desorption ionization time of flight (MALDI-TOF) mass spectrometry (Brothers II et al., 1998; Esfand & Tomalia, 2001).

Characterization

A major advantage of dendrimers over traditional polymers is the precise control over their architecture that results in monodispersed structures. This is a significant feature when considering the transport and biodistribution of nanostructures for drug delivery applications. Thus, it is crucial to employ analytical techniques to characterize and verify the structure of dendrimers. The monodispersity of dendrimers has typically been verified using size-exclusion chromatography, gel electrophoresis, mass spectrometry, and transmission electron microscopy (TEM) (Tomalia, 2004). Size-exclusion chromatography separates molecules on the basis of

molecular size, where large molecular weight molecules elute from a chromatography column earlier than small molecular weight molecules, and this technique is typically used to monitor dendrimer size, molecular mass, and polydispersity (Caminade et al., 2005). Polydispersities of 1.01–1.08 for G0–G9 have been obtained by size-exclusion chromatography (Tomalia et al., 1990), and when coupled with laser light scattering techniques it is used to determine the hydrodynamic radii of dendrimers (Caminade et al., 2005; Tomalia et al., 1990). Polyacrylamide gel electrophoresis (PAGE) analyses have shown that the mobility of PAMAM-succinamic dendrimers slows as the generation increases from 2 to 7, while capillary zone electrophoresis separated dendrimers based on their charge/mass ratio (Sedlakova et al., 2006; Shi et al., 2005). Comparative studies using native PAGE and sodium dodecyl sulfate (SDS)-PAGE analyses of PAMAM dendrimers revealed smaller G2 dendrimer migrated further than the larger G4 dendrimer (Kolhatkar et al., submitted). Dendrimer migration retarded with a decrease in the number of positively charged groups in PAGE analysis but dendrimers migrated further when the surface groups were completely acetylated and subjected to SDS-PAGE analysis (Kolhatkar et al., 2007). The difference in observations occurred because native PAGE separates compounds on the basis of charge and molecular weight, whereas SDS-PAGE separation is achieved on the basis of molecular weight only.

Mass spectrometry has revealed that convergent dendrimer synthesis produces the most monodisperse dendrimers since each growth step involves purification, which eliminates dendrimer imperfections such as branch defects and failed amidoamine couplings (Tomalia, 2004). Lower generation dendrimers (G0–G5) that are synthesized via the divergent method are also quite monodisperse as evidenced by mass spectrometry measurements that are consistent with the predicted mass values. The predicted mass values of higher generation dendrimers tend to deviate from theoretical values due to de Gennes packing, although their polydispersity remains very narrow (i.e., 1.05) (Tomalia, 2004; Tomalia et al., 1990). The characterization of dendrimers with mass of less than 3000 Da is limited to chemical ionization and fast atom bombardment mass spectrometry techniques. Higher generation dendrimers have been characterized with electro-spray ionization (ESI) and Fourier transform ion cyclotron resonance (FT-ICR) (Felder et al., 2005; Hummelen et al., 1997) as well as MALDI-TOF (Caminade et al., 2005). TEM has allowed the visualization of PAMAM dendrimer molecules (G5–G10) to compare their molecular sizes (Jackson et al., 1998). Intrinsic viscosity measurements also offer insight into the dimensional properties of dendrimers (Tomalia et al., 1990). Dendrimer volume grows faster than molecular weight with an increase in earlier generations, and vice versa for generations beyond the intrinsic viscosity maxima (Caminade et al., 2005).

Nuclear magnetic resonance (NMR) spectroscopy has been employed to verify the structure of dendrimers. ^{13}C-NMR has proven an effective method for confirming branching ideality, due to distinct resonances for ideal dendrimer branching versus incomplete acrylate alkylations (Tomalia et al., 1990). ^{1}H-, ^{13}C-, and ^{15}N-NMR are often used to

characterize the interior and end groups of organic dendrimers due to the chemical changes that occur with each branching step (Caminade et al., 2005; Tomalia et al., 1990), and particularly to confirm the functionalization of dendrimer surface groups (Hong et al., 2004a; Jevprasesphant et al., 2003a; Kolhatkar et al., 2007; Sanchez-Sancho et al., 2002), the conjugation of therapeutically active molecules (Khandare et al., 2005; Kolhe et al., 2004; Tang et al., 2006), imaging agents (Fu et al., 2006), and targeting moieties (Majoros et al., 2006). Two- and three-dimensional NMR techniques (^{1}H-, ^{13}C-) have also been used to characterize dendritic structures such as polyaryl (Rajca, 1991) and poly(propyleneimine) (PPI) dendrimers (Boas et al., 2001; Chai et al., 2001) when complex pulse sequences are required for appropriate signal assignment (Caminade et al., 2005). For "inorganic" dendrimers, additional NMR techniques such as ^{31}P-NMR for phosphorous dendrimers (Launay et al., 1995), ^{29}Si-NMR for silicon-based dendrimers (Chai et al., 1999), and ^{19}F-NMR for fluorinated end groups (Sakamoto et al., 2000) are used. Infra-red (IR) spectroscopy is also used to analyze chemical transformations during dendrimer synthesis and modifications (Tomalia et al., 1990), such as the synthesis of poly(aromatic amide) dendrimers using coupling steps via the convergent process (Aulenta et al., 2005), formation of cross-linked hydrogels composed of poly(vinyl alcohol) (PVA) and G6 PAMAM-NH_2 dendrimers through hydrogen bonding (Wu et al., 2004b), and the complexation of ibuprofen to PAMAM-NH_2 dendrimers (Kolhe et al., 2003).

Small-angle X-ray scattering (SAXS) techniques can be used to determine the size, shape, and internal structure of monodispersed polymers based on the intensity distribution of scattered particles as a function of scattering angles from an irradiated X-ray beam (Trewhella et al., 1998). The internal structure of PAMAM dendrimers, G0–G8, has been determined using SAXS measurements (Rathgeber et al., 2004). SAXS measurements of G3 PAMAM dendrimers have revealed structures that resemble star-like molecules, whereas larger generations, 9 and 10, had scattering features that were consistent with hard, sphere-like molecules (Prosa et al., 2001). Small-angle neutron scattering (SANS) techniques also give insight into the molecular structure of dendrimers, as well as inter- and intra-molecular associations. SANS measurements are based on the difference in scattering lengths between hydrogenous monomer units of structures in deuterated solvent (Wignall & Melnichenko, 2005). For instance, the scattering profiles of carboxyl-terminated dendrimers in solution was concentration dependent as indicated by interdendrimer interactions (Huang et al., 2005). Furthermore, SANS measurements have demonstrated silbenoid dendrimers exist as thick (1.8 nm), circular disks in deuterated toluene, whereas SAXS measurements only provided insight that these dendrimers exist as circular disks (Rosenfeldt et al., 2006). The molecular weight of G5 dendrimers in deuterated dimethylacetamide has been measured using SANS techniques (Potschke et al., 1999). In these studies, SANS measurements yield the contrast $\rho - \rho_m$, where ρ is the average scattering length density of the dissolved dendrimer and ρ_m is the scattering length density of the solvent, which allows molecular weight determination of the dendrimer.

Biocompatibility

The toxicity and biocompatibility of dendrimers must be considered for biomedical applications. One of the earlier accounts of testing dendrimer biocompatibility demonstrated a generation-dependent toxicity of PAMAM-NH_2 dendrimers (G3, G5, and G7) in vitro and in vivo (Roberts et al., 1996). Immunogenicity was not observed with these dendrimers. G3 dendrimers had the greatest accumulation in the kidneys of Swiss–Webster mice (15% ID/g after 48 hours), while G5 and G7 dendrimers had peak levels in the pancreas (32% ID/g at 24 hours, 20% ID/g at 2 hours, respectively) (Roberts et al., 1996). Additional studies investigated the toxicity and biodistribution of ^{125}I-labeled PAMAM dendrimers administered intravenously (i.v.) and intraperitoneally (i.p.) in male Wistar rats (Malik et al., 2000). Dendrimers with cationic amino groups (G1–G4) were generally hemolytic and displayed generation-dependent effect on cytotoxicity, whereas anionic carboxylate-terminated and carbosilane dendrimers were neither hemolytic nor cytotoxic after 1 hour. Yet the hemolytic activity of anionic and carbosilane dendrimers increased after 24 hours, and it was proposed the hemolytic behavior was caused by hydrophobic membrane interaction with the aromatic core of carbosilane dendrimers. Additionally, cationic dendrimers (G3, G4) were rapidly cleared from the circulation after i.v. and i.p. administration. In contrast anionic dendrimers had greater circulation times (15–40% recovered in blood after 1 hour) in a generation-dependent manner with appreciable liver accumulation (25–70% of recovered dose). To investigate the potential of PAMAM dendrimers as oral delivery systems, the glucose active transport assay was used to assess dendrimer toxicity, in which anionic dendrimers were able to transport glucose up to 100 μg/ml, while cationic G4 caused cytotoxicity at this concentration (Wiwattanapatapee et al., 2000). These initial studies suggested dendrimer architecture can be tailored based on size and surface chemistry to avoid toxicity, enhance transport across epithelial barriers, and/or prolong systemic circulation.

Cationic macromolecules have a favorable interaction with negatively charged cell membranes which leads to their enhanced uptake and increased toxicity caused by an osmotic imbalance (Karoonuthaisiri et al., 2003). Several studies have reported hole formation and lipid bilayer disruption caused by cationic dendrimers (Hong et al., 2004b, 2006; Mecke et al., 2005, 2004). Atomic force and fluorescence microscopy studies demonstrated cationic G7 dendrimers (10–100 nM) formed holes in 1,2-dimyristoyl-*sn*-glycero-3-phosphocholine (DMPC) lipid bilayers of 15–40 nm in size. G3 and G5 dendrimers did not form holes in these studies although G5 expanded holes at existing defects and were nontoxic up to 500 nM (Hong et al., 2004b, 2006; Mecke et al., 2005, 2004). Studies demonstrated that electrostatic interaction between the positively charged dendrimers and negatively charged lipid bilayers causes internalization of molecules (Hong et al., 2004b), and the lack of electrostatic interactions reduces the ability of dendrimers to disrupt the cell membranes (Mecke et al., 2004). These studies further suggest cytotoxicity is more likely to occur with cationic dendrimers of higher generations and

donor concentration. This is also demonstrated by TEM observations, which show that the application of large, cationic dendrimers to Caco-2 cells resulted in the loss of microvilli unlike anionic dendrimers (Figure 14.1A) (Kitchens et al., 2007). Further loss of microvilli occurred with an increase in G4NH2 concentration (Figure 14.1B). Among a series of dendrimers with surface groups of amine, guanidine, carboxylate, sulfonate, phosphonate, and PEGylated, the cationic dendrimers were more cytotoxic based on the 3-(4,5-dimethythiazole-2-yl)-2,5-diphenyltetrazolium bromide (MTT) assay compared with anionic and PEGylated dendrimers (Chen et al., 2004). Several studies have demonstrated the reduction of cationic dendrimer cytotoxicity when the surface groups were modified with hydrophobic moieties or PEG chains (Jevprasesphant et al., 2003a,b; Kitchens et al., 2006; Kolhatkar et al., 2007). It should be noted that dendrimer toxicity is not solely based on its surface chemistry. As previously mentioned, poly(-ethylene oxide) (PEO)-modified carbosilane dendrimers did cause

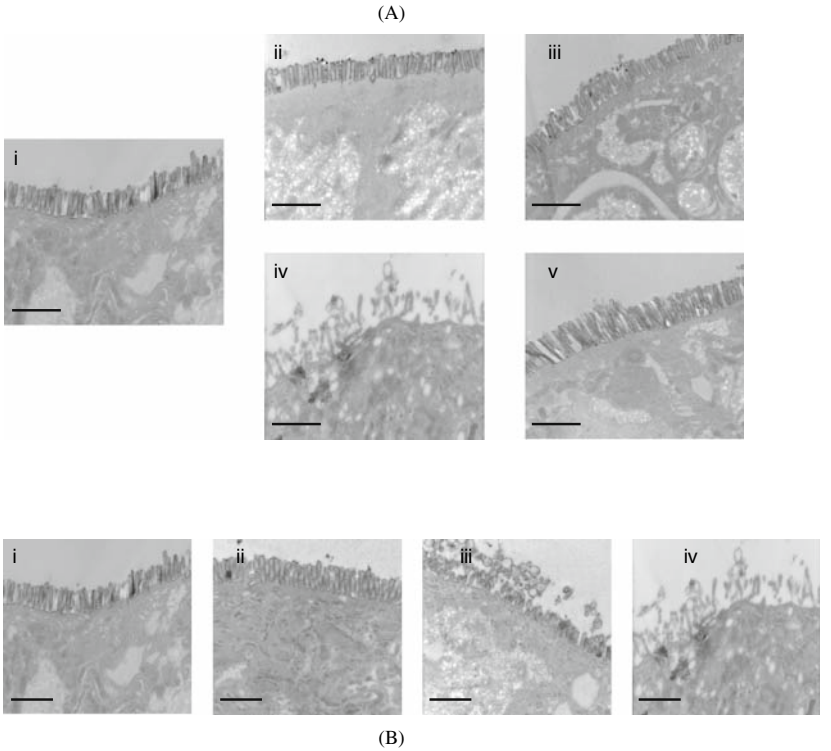

Figure 14.1 (**A**) Transmission electron microscopy (TEM) images of Caco-2 cell monolayers after treatment with PAMAM dendrimers (1 mM) for 2 hours: (i) control cells; (ii) $G2NH_2$; (iii) G1.5COOH; (iv) $G4NH_2$; (v) G3.5COOH. The images display a generation-dependent effect of PAMAM dendrimers on Caco-2 microvilli (magnification = 12,500×). (**B**) TEM images of Caco-2 cell monolayers after treatment with $G4NH_2$ dendrimers for 2 hours: (i) control cells; (ii) 0.01 mM $G4NH_2$; (iii) 0.1 mM $G4NH_2$; (iv) 1.0 mM $G4NH_2$. The images display a concentration-dependent effect of $G4NH_2$ on Caco-2 microvilli (magnification = 12,500×). Scale bars = 1 μm. Adapted from Kitchens et al. (2007) (with permission from ACS Publications).

hemolysis in vivo due to interactions between the aromatic core and the hydrophobic cell membranes (Malik et al., 2000). Furthermore, low generation dendrimers possess a more open molecular structure, which makes a possibly toxic core and surface groups more accessible to interact with the cell membranes (Duncan & Izzo, 2005). Along with molecular weight and surface charge density, the extent of polycation cytotoxicity can also depend on molecular conformation. For instance, PAMAM dendrimers have a compact, spherical structure in solution and were found to be less cytotoxic than linear polycations (Fischer et al., 2003).

Several studies have been conducted on the toxicity of dendrimers in vivo to date. For instance, the deaths of three mice were reported after administration of G7 dendrimers over a 2-hour period (Roberts et al., 1996). No toxicity or mortality was observed among C3H mice when single doses of PEGylated melamine were administered as 2.56 g/kg i.p. or 1.28 g/kg i.v. over 24 and 48 hours, respectively (Chen et al., 2004). Polyester-based dendrimers with hydroxyl or methoxy surface groups caused some inhibition of cell growth in vitro, but did not induce cell death up to 40 mg/ml (Padilla De Jesus et al., 2002). Mortality was only observed in one animal after 24 hours when these dendrimers were administered as a single dose (1.3 g/kg) (Padilla De Jesus et al., 2002). Additionally, the efficacy of dendrimer-based antiviral topical microbicides was demonstrated against herpes simplex virus type 2 (HSV-2) in female Swiss–Webster mice. Bourne et al. (2000) have reported the synthesis of PAMAM (BRI-6039) and polylysine dendrimers (BRI-2999 and BRI-6741) by the Biomolecular Research Institute (BRI, Parkville, Victoria, Australia) by the addition of polylysine repeat units to a benzhydrylamine core, with capping layers of naphthyl disodium disulfonate (BRI-2999) and phenyl disodium dicarboxylate (BRI-6741). Intravaginal application of BRI-6039, BRI-2999, and BRI-6741 significantly reduced the incidence of HSV-2 compared to control treatments, but only BRI-2999 dendrimers prevented infection when administered immediately and 30 minutes before intravaginal challenge. This research has led to the development of VivaGel^{TM}, a topical microbicide for the prevention of HIV and other sexually transmitted diseases (Jiang et al., 2005) by Starpharma Ltd. (Melbourne, Victoria, Australia). Phase I clinical studies investigated the safety of VivaGel^{TM} in a double-blinded study, and no irritation or inflammation was observed for the healthy women that received intravaginal doses of the gel (Svenson & Tomalia, 2005).

Dendrimers for Delivery of Bioactive Agents

Bioactive agents can be complexed with dendrimers by electrostatic interactions, chemically conjugated to the surface terminal groups, or incorporated within the dendritic box. Numerous groups have studied the use of dendrimers for the delivery of therapeutic and diagnostic agents. Comprehensive review of these reports are beyond the scope of this chapter and the reader is referred elsewhere (Cloninger, 2002; D'Emanuele & Attwood, 2005; Dufes et al., 2005b; Duncan & Izzo, 2005; Kobayashi & Brechbiel, 2005; Lee et al., 2005; Liu & Frechet, 1999; Patri et al., 2005; Svenson &

Tomalia, 2005). A few examples for delivery of nucleic acids, imaging agents, and small molecular weight drugs are discussed below.

Amine-terminated dendrimers such as PAMAM or PPI have been used as gene transfection agents (Dufes et al., 2005b). Haensler and Szoka (1993) were the first to demonstrate that PAMAM dendrimers efficiently express reporter genes in a suspension of mammalian cells. Maximal luciferase expression was achieved with G6 and a dendrimer to DNA charge ratio of 6:1. PAMAM dendrimer/DNA complexes showed lower toxicities than polylysine and greater transfection efficiency (Behr, 1994; Haensler & Szoka, 1993). It was thought that the enhanced efficiency of dendrimers occurred since they did not require lysosomotropic agents to escape the endosomes, but dendrimers have the ability to escape endosomes via the proposed "proton sponge" effect (Behr, 1994; Haensler & Szoka, 1993). This theory postulates that lysosomotropic activity occurs through protonation of the tertiary amine groups in PAMAM dendrimers, resulting in osmotic swelling of the endosomal compartments, thus leading to enhanced DNA delivery to the cytoplasm (Haensler & Szoka, 1993). In general, dendrimers enhance DNA expression by condensing the nucleic acids and acting as an endosomal pH buffer (Hughes et al., 1996). Interestingly "fractured" dendrimers were more effective transfection agents possibly due to their increased flexibility allowing nucleic acid release (Tang et al., 1996).

To increase circulation time and decrease toxicity, PAMAM-PEG-PAMAM triblock copolymers were synthesized which formed stable water-soluble complexes with high transfection efficiency in 293 cells (Kim et al., 2004). Although dendrimers promise to be effective delivery systems for gene therapy, issues such as toxicity and efficacy remain a concern for in vivo and clinical applications. Recent reports have demonstrated PPI dendrimers (G2, G4 and G5) display low cytotoxicity in several human cell lines when interior and exterior amines were modified with methyl iodide/chloride and carboxylic acid derivatives, respectively (Tack et al., 2006). These modified PPI dendrimers also enhanced the transfection efficiency of DNAzyme in ovarian cells, while dendrimer-DNAzyme complexes were localized in tumor nuclei following intravenous injection in Nude mice (Tack et al., 2006). These findings suggest the efficiency and safety of PPI dendrimers for gene therapy. Additionally, lipidic poly (lysine) dendrimers enhanced the intracellular delivery of recombinant firefly luciferase and a c-myc monoclonal antibody compared in various cell lines, which demonstrates the potential application of these peptidic dendrimers in protein therapeutics (Bayele et al., 2006).

Additional studies have investigated dendrimers for delivery of oligonucleotides. PAMAM dendrimer G5 was used to deliver antisense oligodeoxynucleotides and reduce chloramphenicol acetyl-transferase (CAT) expression in CHO cell lines by approximately 38% (Hughes et al., 1996). PAMAM:oligonucleotide complexes increased the intracellular uptake of oligonucleotides in astrocytoma cells 3- to 4-fold with 1:1 dendrimer:oligonucleotides and 50-fold for 20:1 complexes, as well as increased delivery to the nucleus (Bielinska et al., 1996; DeLong et al., 1997). Confocal microscopy and cell fractionation studies revealed oligonucleotide-dendrimer complexes are localized in the nucleus of HeLa cells, which suggests

dendrimers are capable of delivering oligonucleotides to nuclei where they exert their pharmacological actions and the complex remains intact unlike other cationic delivery agents that are typically degraded in the endosomes (Yoo & Juliano, 2000). Further studies revealed that while PAMAM dendrimers are effective in antisense oligonucleotide delivery, they are less effective in siRNA oligonucleotide delivery most likely due to incomplete release of siRNA from dendrimer (Kang et al., 2005). Furthermore, antisense and siRNA oligonucleotides delivered by PAMAM and TAT-PAMAM conjugates partially inhibited P-glycoprotein (P-gp) expression in NIH 3T3 multi-drug resistant cells at low concentrations, and greater inhibition was observed with higher dendrimer concentrations, yet greater toxicity was observed at these concentration levels (Kang et al., 2005). Although these studies demonstrate dendrimers are less effective than cationic lipid delivery agents, they are probably more suitable carriers for oligonucleotides since they are smaller than cationic lipid particles and would be less susceptible to rapid clearance (DeLong et al., 1997; Juliano, 2006).

Dendrimer-based contrast agents for magnetic resonance imaging (MRI) have allowed for enhanced MR images in vivo attributed to longer blood circulation, greater extravasation, and improved excretion compared to other macromolecular contrast agents (Kobayashi & Brechbiel, 2005). The free amines of PAMAM dendrimers have been conjugated to gadolinium (Gd) chelates, which exhibited greater molecular relaxivities than metal-chelate conjugates of other macromolecules including serum albumin, poly(lysine), and dextran. These dendrimer-based agents displayed longer enhancement half-lives than Gd(III)-diethylenetriaminepentaacetic acid (Gd(III)-DTPA) (Wiener et al., 1994). These earlier studies demonstrated the potential use of dendrimers as MRI contrast agents. PAMAM dendrimers (G6) with either ammonia (G6A) or ethylene diamine cores (G6E) were compared in terms of their blood retention, biodistribution, and renal excretion. ^{153}Gd-labeled G6E2-(*p*-isothiocyanatobenzyl)-6-methyl-diethylenetriaminepentaacetic acid (1B4M) conjugates had longer retention in the circulation due to more exterior amine groups available in G6E (256 amine groups) than G6A (192 amine groups) to react with Gd atoms. G6A-1B4M-Gd(III) had brighter kidney images, as well as faster clearance and higher renal accumulation, than G6E-1B4M-Gd(III) due to enhanced glomerular filtration (Kobayashi et al., 2001b). The conjugation of two PEG molecules to G4-1B4M-Gd resulted in prolonged retention in the circulation, increased excretion, and decreased accumulation in the liver and kidneys, compared to PEG(1)-G4-1B4M-Gd and G4-1B4M-Gd (Kobayashi et al., 2001a). DAB-based contrast agents displayed greater relaxivity than ammonia core PAMAM-based agents of similar size (G2) (Wang et al., 2003). Higher generation PPI contrast agents (G3 and G5) had prolonged blood signal enhancement than smaller (G0 and G1) dendritic agents (Langereis et al., 2006) suggesting higher generation PPI-based contrast agents may be more suitable for MRI than PAMAM-based agents.

Previous reports demonstrated PAMAM G4-Gd complexes conjugated to folic acid were capable of imaging tumors that expressed the folate receptor (Konda et al., 2000) and that dendrimer-folate conjugates do target and internalize within folate-expressing cells (Quintana et al.,

2002). Other applications of dendrimer-based diagnostics have included DNA-assembled dendrimers to target cancer cells (Choi et al., 2005). In these systems, oligonucleotides were used to self-assemble to PAMAM dendrimers (G5 or G7), one conjugated to folic acid to target KB cancer cells that over-express the folate receptor, while the other dendrimer was conjugated to fluorescein isothiocyanate (FITC) as an imaging agent (Choi et al., 2005). Dendritic contrast agents were prepared by the synthesis of dendrimers with PEG cores and *tert*-butyloxycarbonyl-L-lysine-generated branching architecture to generate G3–G5, followed by the conjugation of a clinically used computed tomography (CT) contrast agent, iobitridol, to their lysine amino groups (Fu et al., 2006). These dendritic contrast agents are being explored for potential use in CT imaging due to their prolonged circulatory retention, and potential toxicity reduction of iodinated small molecules (Yordanov et al., 2002). Dendrimers have also been used in oxygen imaging diagnostics, in which metalloporphryins were encapsulated in the cores of poly(glutamic acid), poly(aryl ether), and poly(ether amide) dendrimers to create water-soluble oxygen sensors (Dunphy et al., 2002). In these applications, the phosphorescence lifetime of the dendrimers is inversely proportional to oxygen concentration in tumors, which indicates if the tumor would respond to treatment (Ziemer et al., 2005).

Dendrimers have also been used for the delivery of small molecular weight drugs. When the anti-cancer drug cisplatin was encapsulated in PAMAM dendrimers with a payload of ~25%, lower toxicity, slower release, and increased accumulation in solid tumors were achieved compared to cisplatin alone (Malik et al., 1999). Other chemotherapeutic agents including doxorubicin and 5-flurouracil have been conjugated to dendrimers, which allowed the release of these drugs in vitro (Ihre et al., 2002; Padilla De Jesus et al., 2002; Zhuo et al., 1999). Similarly, dendrimer-propanolol conjugates increased the permeability of propanolol, a P-gp substrate, through bypassing the P-gp system (D'Emanuele et al., 2004). Another group has investigated the effect of PAMAM dendrimers and Perstrop Polyol, a fifth generation hyperbranched poly ester with hydroxyl surface groups, on the cellular entry of ibuprofen (Kannan et al., 2004; Kolhe et al., 2004, 2003). Ibuprofen was successfully complexed to all the surface groups of PAMAM dendrimers G3 and G4, and some ibuprofen was encapsulated in PAMAM G4, while the hyperbranched polyol was able to incorporate some ibuprofen without complexation due to the lack of electrostatic interactions between hydroxyl surface groups and carboxyl groups of ibuprofen (Kolhe et al., 2003). The ibuprofen-PAMAM complexes maintained the anti-inflammatory effect of ibuprofen, and ibuprofen displayed greater suppression of COX-2 in the complexed form compared to pure ibuprofen. Additionally, hyperbranched polyol- and polyglycerol-ibuprofen conjugates showed increased inhibition of prostaglandin synthesis compared to ibuprofen (Kolhe et al., 2004), as did methylprednisolone conjugated to G4OH via a glutaric acid spacer (Khandare et al., 2005). These studies demonstrate that dendrimers can carry a high therapeutic payload, are capable of maintaining the pharmacological activity of drugs, and can improve drug release to the site of action compared to free drug. Dendrimers have also been applied as solubility enhancers for poorly soluble, hydrophobic drugs (Milhem

et al., 2000), and dendrimer solubility enhancement has proven to be a function of surface chemistry (Chauhan et al., 2003), generation where solubility increased with generation number (Namazi & Adeli, 2005), and core chemistry which affects dendrimer flexibility (Liu et al., 2000).

In summary, dendrimers clearly offer many advantages in the delivery of bioactive and diagnostic agents. Their potential as drug carriers arises from the large number of surface groups to immobilize drugs, enzymes, targeting moieties, or other bioactive and imaging agents. These macromolecules are capable of enhancing drug solubility, increasing drug circulation due to their nanoscopic size, and targeted delivery with the incorporation of specific ligands to the surface groups. Due to the need to develop orally bioavailable polymeric drug delivery systems and the potential use of dendrimers in drug delivery applications, it is highly desirable to develop dendrimer-based drug delivery systems that are orally bioavailable.

PAMAM Dendrimers as Potential Oral Drug Delivery Carriers

Oral Absorption of Dendrimers

The first reports to demonstrate the oral administration of a dendrimer structure involved a lipidic polylysine dendrimer in Sprague–Dawley rats (Florence et al., 2000; Sakthivel et al., 1999). A dendrimer molecule of mean diameter 2.5 nm was synthesized and radiolabeled with tritium. A rapid uptake of the dendrimer within the GI tract was observed since 2% of administered dose was recovered from the stomach after 3 hours and less than 1% after longer times. The amount of dendrimer recovered in additional GI organs increased from 3 to 6 hours (Sakthivel et al., 1999). For instance, rapid absorption of the dendrimer was observed as indicated by 15 and 5% recovery of administered dendrimer in the small and large intestines after 6 hours, respectively. Overall, at least 20% of administered dendrimer was recovered in the stomach, small and large intestines after 6 hours, yet only 1% was recovered in these organs after 24 hours (Florence et al., 2000; Sakthivel et al., 1999). Furthermore, the amount of administered dendrimer recovered in the liver, kidneys, spleen, and blood increased from 3 to 6 hours, and approximately 1.2 and 3% of administered dose was recovered in the liver and blood, respectively, after 6 hours, while less than 1% was recovered in the spleen and kidneys as well as in all organs after 24 hours. These studies demonstrated the rapid absorption of the dendrimer after 24 hours in the GI tract.

Additional studies focused on comparing the uptake and transport rates of the dendrimer (2.5 nm) and polystyrene latex nanoparticles ranging from 50 to 3000 nm in diameter (Florence et al., 2000). After 10 days 15% of dendrimer and 12% of 50-nm polystyrene particles were recovered from the small intestine, although the dendrimer had less cumulative uptake in the liver and spleen than 50-nm polystyrene particles. The cumulative uptake of dendrimers in the liver, spleen, kidneys, and blood was less than that of the 50-nm polystyrene particles, which could be

explained by the greater amount of dendrimers detected in the blood due to slower rates of perfusion. It was anticipated that the smaller dendrimer would have greater uptake than the 50-nm latex nanoparticles, since previous studies suggested gut-associated lymphoid tissue uptake is size dependent over a range of 50–3000 nm nanoparticles (Florence, 1997). Further studies investigated how dendrimer generation and GI fluid influence the formation of aggregates (Singh & Florence, 2005). These studies suggested increase in generation number results in an increase in the number of lipid chain groups, which led to dendrimer aggregation.

Variations in dendrimer concentration affected aggregate formation, in which increased concentration for lower generation dendrimers (C_4 surface lipid chains) resulted in increased mean number diameter, whereas larger dendrimers (C_{10} and C_{12} surface lipid chain) had smaller diameters with an increase in dendrimer concentration. These observations indicated the dendrimers with shorter alkyl-chain surface groups had greater surface hydrophobic interactions that resulted in dendrimer aggregation. Finally, the stability of polylysine dendrimers was studied in GI fluid for 3 hours. The dendrimers were stable in intestinal fluid, however, the acidic environment of the stomach led to self-association of the dendrimer particles, which was evidenced by the increase in their hydrodynamic diameter (Singh & Florence, 2005). The smaller nanoparticles and lower generation dendrimers were more susceptible to aggregate formation due to their increased flexibility and thus accessibility to self-associate, and to possibly adsorb to the cell membrane. This may explain the lower uptake observed for 2.5-nm dendrimers compared to 50-nm polystyrene nanoparticles in the GI tract.

Transepithelial Transport of Poly(amidoamine) Dendrimers

One of the first studies to demonstrate the ability of PAMAM dendrimers to cross the GI tract investigated their rate of uptake and transport using everted rat intestinal sacs as an in vitro model of the intestinal epithelial barrier (Wiwattanapatapee et al., 2000). Cationic (G3 and G4) and anionic PAMAM dendrimers (G2.5, G3.5, and G5.5) were ^{125}I-labeled, and the amounts recovered in the tissue and serosal fluid were measured as a function of time. A major finding from this study was that cationic PAMAM dendrimers showed greater tissue uptake (3.3–4.8 μL/mg protein/h) than their serosal transfer rates (2.3–2.7 μL/mg protein/h) at each time point, whereas anionic G2.5 and G3.5 showed greater serosal transfer rates (3.4–4.4 μL/mg protein/h) than their tissue uptake (0.6–0.7 μL/mg protein/h). Anionic G5.5 had greater tissue uptake (2.48 μL/mg protein/h) than that of G2.5 and G3.5. The amount of G5.5 recovered in serosal fluid (65–70%) was less than that of G2.5 and G3.5 (80–85%). In summary, this study showed that cationic dendrimers had greater tissue association than anionic dendrimers of similar size, while anionic G5.5 had greater tissue accumulation than smaller G2.5 and G3.5.

The permeability of a series of cationic PAMAM-NH_2 dendrimers, G0–G4, was measured as a function of dendrimer generation and concentration across Madin–Darby Canine Kidney (MDCK) cells as model monolayers to assess their transepithelial transport (Tajarobi et al., 2001).

MDCK cells were used as a preliminary screening tool since drug permeability rates across MDCK cells is similar to Caco-2 cell permeability (Irvine et al., 1999). PAMAM dendrimers were fluorescently labeled with FITC, and the fluorescently labeled dendrimers were fractionated by size-exclusion chromatography techniques to ensure the permeability values were not attributed to small molecular weight fragments. The rank order of PAMAM permeability was G4 $\gg$ G0 $\approx$ G1 $>$ G3 $>$ G2, with apparent permeability (P_{app}) values ranging from 0.076 to 16.1 $\times$ 10^6 cm/s. These results demonstrated a clear relationship between dendrimer size and their transport. PAMAM permeability increased with size possibly due to increased interaction between the positively charged surface groups with the anionic cell surface. G2 permeability increased with an increase in dendrimer concentration in the range of 50–300 μg/ml. In this study, cytotoxicity assays were not performed to clarify whether the rank order of permeability was attributed to toxicity or not. Thus, the next logical step was to systematically evaluate the influence of size, charge, incubation time, and dendrimer concentration on their cytotoxicity and transepithelial transport across Caco-2 cell monolayers as a widely used in vitro model to assess the oral bioavailability of potential therapeutic agents (Artursson, 1990; Hilgers et al., 1990).

The influence of the physicochemical properties of PAMAM dendrimers (Table 14.2) on cytotoxicity and permeability across Caco-2 cells has been investigated (El-Sayed et al., 2002, 2003a; Kitchens et al., 2006; Kolhatkar et al., 2007). The permeability of the fluorescently labeled cationic PAMAM-NH_2 dendrimers changed as a function of incubation time, generation number, and concentration. Smaller dendrimers (G0–G2) had similar apical-to-basolateral (AB) permeability despite their different molecular weights. PAMAM permeability increased with time from 90

Table 14.2 Structural features of selected PAMAM dendrimers studied for oral drug delivery.*

Generation	Surface group	Molecular weight (Da)	Number of surface groups
G0	-NH_2	517	4
G1	-NH_2	1,430	8
G2	-NH_2	3,256	16
G3	-NH_2	6,909	32
G4	-NH_2	14,215	64
G2	-OH	3,272	16
G3	-OH	6,909	32
G4	-OH	14,215	64
G-0.5	-COOH	436	4
G0.5	-COOH	1,269	8
G1.5	-COOH	2,935	16
G2.5	-COOH	6,267	32
G3.5	-COOH	12,931	64
G4.5	-COOH	26,258	128

* Reported by the manufacturer, Dendritech, Inc., Midland, MI.

to 150 minutes (Figure 14.2A-B) and concentration from 1.0 to 10.0 mM (El-Sayed et al., 2002). Additionally, these smaller dendrimers exhibited higher permeability than G3 while exerting no toxicity at 1.0 mM toward Caco-2 cell monolayers. Lactate dehydrogenase (LDH) assay demonstrated that an increase in generation number, concentration, or incubation time

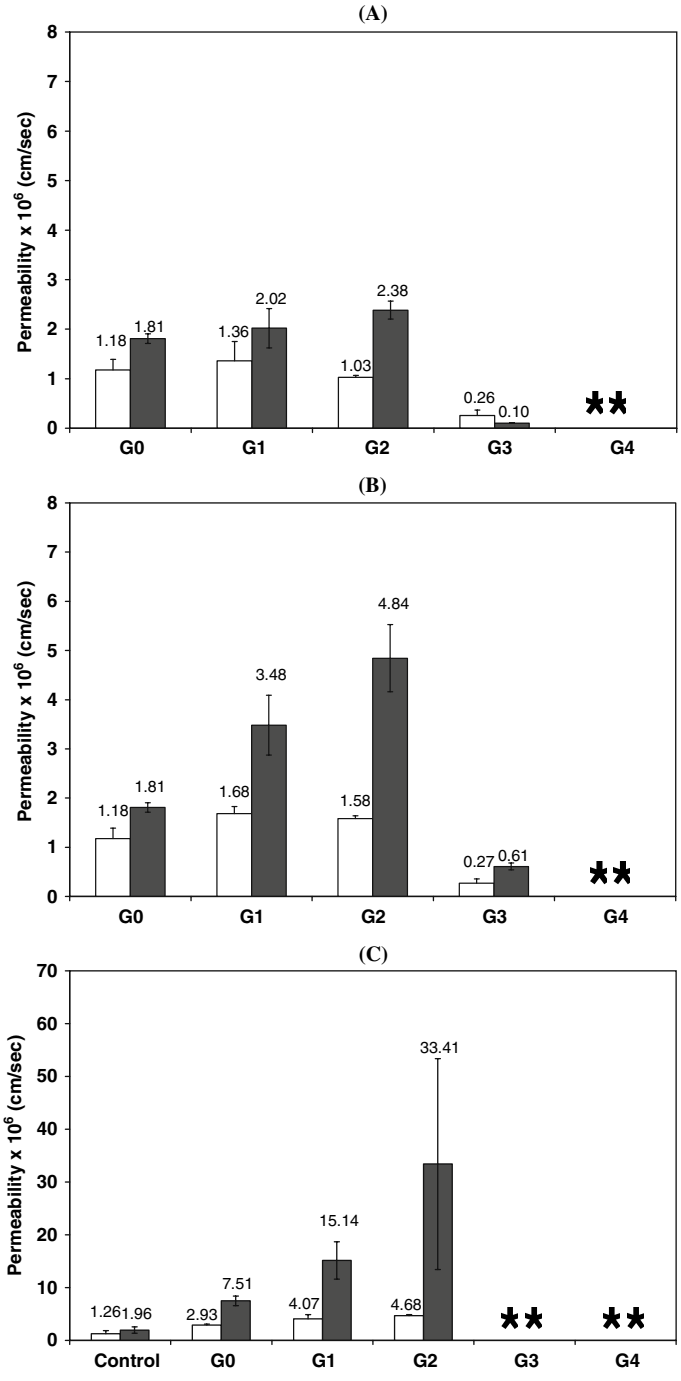

Figure 14.2 AB (□) and BA (■) Caco-2 permeability of PAMAM dendrimers (G0–G4) at a donor concentration of 1.0 mM and incubation times of: (**A**) 90 minutes and (**B**) 150 minutes; and (**C**) ^{14}C-mannitol at an incubation time of 210 minutes in the presence of 1.0 mM solution of PAMAM dendrimers (G0–G4). AB and BA permeability values are not reported (**) at toxic incubation time points. Results are reported as mean ± SEM ($n = 9$). Adapted from El-Sayed et al. (2002) with permission from Elsevier.

resulted in an increase in cytotoxicity. The increase in cytotoxicity and permeability may be facilitated by the interaction between cationic amine groups of PAMAM dendrimers and negatively charged Caco-2 cell epithelia. This interaction is prolonged with an increase in time, and by increased surface charge density with an increase in concentration and generation number. This enhanced interaction may result in cell membrane perturbation by the cationic PAMAM dendrimers or tight junction modulation.

The influence of PAMAM dendrimers on the integrity and paracellular permeability of Caco-2 cell monolayers was investigated through transepithelial electrical resistance (TEER) measurements and the permeability of a known paracellular permeability marker, ^{14}C-mannitol (El-Sayed et al., 2002, 2003a). TEER values decreased with an increase in cationic PAMAM-NH_2 generation number, donor concentration, and incubation time. ^{14}C-mannitol permeability in the presence of dendrimers increased with PAMAM-NH_2 generation and concentration (Figure 14.2C) (El-Sayed et al., 2002). Neutral PAMAM-OH dendrimers did not significantly influence TEER compared to control conditions, nor significantly enhance ^{14}C-mannitol permeability, whereas anionic PAMAM-COOH dendrimers had a generation-dependent effect on TEER and ^{14}C-mannitol permeability (El-Sayed et al., 2003a). G–0.5, G0.5, G1.5, and G4.5 caused no significant decline in TEER values nor significantly enhanced ^{14}C-mannitol permeability (at non-toxic conditions), whereas G2.5 and G3.5 caused a significant decline in TEER and significantly increased ^{14}C-mannitol permeability compared to control values. The observed decrease in TEER values and increased mannitol permeability suggest PAMAM dendrimers enhance paracellular transport via tight junction modulation.

These initial studies demonstrated a size and charge window of PAMAM dendrimers that can traverse the epithelial barrier of the gut, as well as enhance drug transport. Recent studies focused on a systematic correlation between the effect of size and charge on PAMAM permeability across the intestinal barrier. It was demonstrated that PAMAM permeability is affected by dendrimer size among anionic dendrimers (G1.5–G3.5) and charge among dendrimers of similar size and different surface functionality (G2NH_2, G2OH, G1.5COOH) (Kitchens et al., 2006). Permeability increased with an increase in generation among the PAMAM-COOH series without causing cytotoxicity (Figure 14.3). This data coupled with previous findings (Wiwattanapatapee et al., 2000) further confirm the potential of anionic PAMAM dendrimers as oral drug carriers. The influence of dendrimer surface charge on epithelial permeability was investigated while monitoring the ^{14}C-mannitol flux. The rank order of dendrimer (Figure 14.3) and ^{14}C-mannitol permeability (Figure 14.4), as well as their reduction in TEER (Figure 14.5), was G2NH_2 > G1.5COOH > G2OH. The effect of all tested PAMAM dendrimers on TEER, except G2NH_2, was reversible after 24 hours. Other studies demonstrating the reversible effect of cationic and anionic dendrimers on Caco-2 cells (Jevprasesphant et al., 2003a) coupled with their non-toxic effects based on the WST-1 cytotoxicity assay (Kitchens et al., 2006) suggest the feasibility of the design and development of safe and effective oral drug carriers.

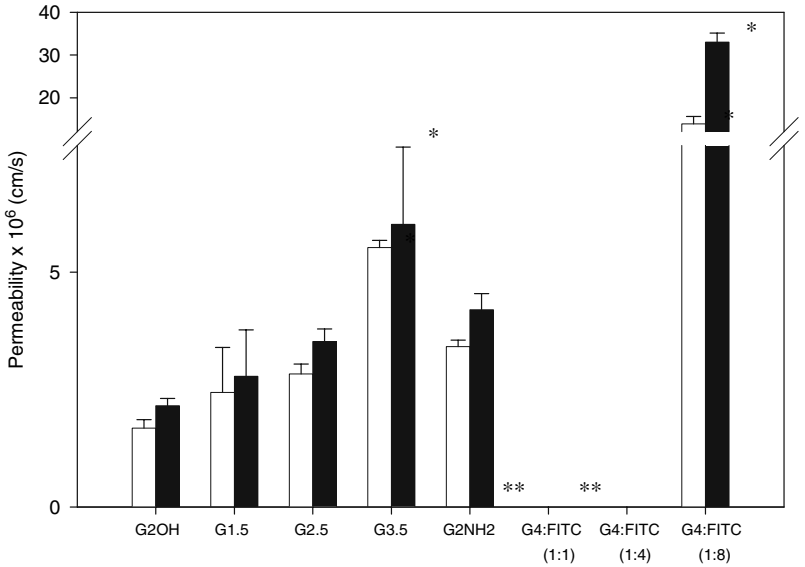

Figure 14.3 The permeability of fluorescently labeled PAMAM dendrimers of donor concentration 1.0 mM across Caco-2 cell monolayers at incubation times of (□) 60 minutes and (■) 120 minutes. Permeability values are not reported (**) for dendrimers that cause toxicity. Results are reported as mean ± SEM ($n = 9$). (*) Denotes a significant difference in permeability compared to permeability of $G2NH_2$, G2OH, G1.5COOH, and G2.5COOH dendrimers (G3.5COOH $P < 0.05$, $G4NH_2$:FITC (1:8) $P < 0.01$). Reprinted from Kitchens et al. (2006) (with permission from Springer).

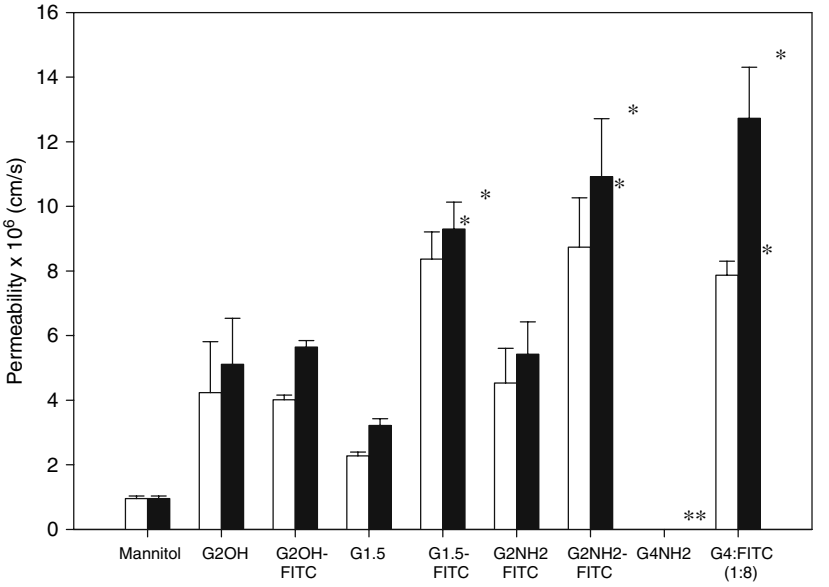

Figure 14.4 The permeability of ^{14}C-mannitol (3.3 μM) in the presence of fluorescently labeled and unlabeled PAMAM dendrimers of donor concentration 1.0 mM across Caco-2 cell monolayers at incubation times of (□) 60 minutes and (■) 120 minutes. Permeability values are not reported (**) for dendrimers that cause toxicity. Results are reported as mean ± SEM ($n = 9$). (*) Denotes a significant increase in permeability compared to control ($P < 0.001$). Reprinted from Kitchens et al. (2006) (with permission from Springer).

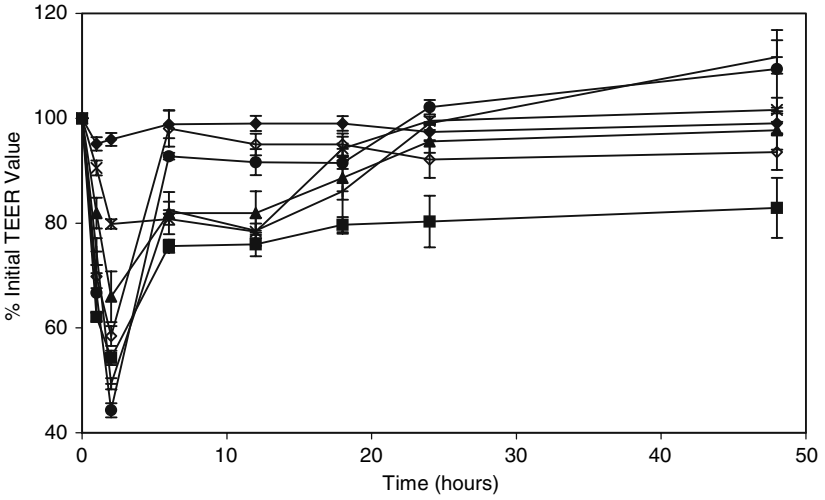

Figure 14.5 Transepithelial electrical resistance of Caco-2 cells in the presence of fluorescently labeled PAMAM dendrimers as a function of time: (♦) HBSS transport medium, (■) $G2NH_2$, (▲) G2OH, (×) G1.5COOH, (+) G2.5COOH, (●) G3.5COOH, (◇) $G4NH_2$-FITC (1:8). Results are reported as mean ± SEM ($n = 9$). Reprinted from Kitchens et al. (2006) (with permission from Springer).

Influence of Surface Modification on Poly(amidoamine) Cytotoxicity and Permeability

An interesting finding was ^{14}C-mannitol flux significantly increased in the presence of fluorescently labeled $G2NH_2$ and G1.5COOH dendrimers, where they caused a greater decline in TEER, relative to their unlabeled counterparts (Kitchens et al., 2006). $G4NH_2$ dendrimers were conjugated with FITC (as a model drug) at feed molar ratios of 1:1, 1:4, and 1:8 ($G4NH_2$:FITC) to investigate how an incremental increase in conjugation would modify the toxicity and permeability of the dendrimers. The toxicity of $G4NH_2$ dendrimers reduced with an increase in FITC content (Table 14.3). $G4NH_2$-FITC (1:8) displayed the highest relative permeability (Figure 14.3) with an increase in mannitol flux (Figure 14.4), most likely due to a higher degree of tight junctional modulation.

Other studies demonstrated surface modification of cationic PAMAM dendrimers with longer molecules such as lauroyl chains or PEG reduced their cytotoxicity in Caco-2 cells (Jevprasesphant et al., 2003b). Cell viability was based on the MTT assay, and the cytotoxicity of PAMAM dendrimers was a function of size, concentration, and surface charge (Jevprasesphant et al., 2003b). Anionic G2.5 and G3.5 dendrimers did not significantly reduce cell viability up to 1000 μM donor concentration and cationic G2 reduced cell viability at concentrations above 700 μM. G3 toxicity occurred when concentrations exceeded 10 μM, and G4 reduced cell viability at all donor concentrations tested. The cytotoxicity of PAMAM dendrimers decreased when they were modified with C_{12} lauroyl chains or PEG molecules, which was indicated by increased IC_{50} values when cationic dendrimers were modified with six lauroyl chains or four PEG molecules. The reduction in cytotoxicity can be explained by shielding of the positively

Table 14.3. Viability of Caco-2 cells measured with WST-1 assay reagent.*

Concentration	0.01 mM	0.1 mM	1.0 mM
HBSS		100.0%	
$G2NH_2$	80.3% ± 10.8%	78.0% ± 6.6%	*77.3% ± 1.9%*
$G2NH_2$-FITC	88.5 ± 7.5%	92.5 ± 4.9%	86.8 ± 5.5%
G2OH	103.7 ± 10.1%	103.6 ± 7.9%	96.7 ± 3.3%
G2OH-FITC	104.1 ± 6.5%	97.8 ± 13.8%	98.8 ± 4.2%
G1.5COOH	100.5 ± 17.1%	110.3 ± 3.4%	105.4 ± 7.4%
G1.5COOH-FITC	107.2 ± 6.8%	99.5 ± 5.8%	111.8 ± 6.6%
G2.5COOH	109.1 ± 3.1%	91.6 ± 13.5%	108.3 ± 3.7%
G2.5COOH-FITC	104.3 ± 11.2%	99.7 ± 16.5%	106.7 ± 10.0%
G3.5COOH	90.7 ± 1.5%	88.6 ± 2.6%	86.8 ± 4.9%
G3.5COOH-FITC	108.1 ± 3.1%	107.0 ± 9.4%	101.7 ± 11.7%
$G4NH_2$	*66.7 ± 28.8%*	*60.2 ± 6.2%*	*38.1 ± 7.1%*
$G4NH_2$-FITC (1:1)	*58.9 ± 4.3%*	*53.8 ± 9.8%*	*53.8 ± 10.4%*
$G4NH_2$-FITC (1:4)	85.1 ± 9.4%	*76.8 ± 13.5%*	*56.3 ± 3.8%*
$G4NH_2$-FITC (1:8)	97.7 ± 4.8%	76.5 ± 3.6%	74.3 ± 4.3%
FITC	107.3 ± 35.7%	108.5 ± 40.0%	98.1 ± 38.5%
Triton X-100		*30.4 ± 18.1%*	

*Results are reported as mean percentage ± standard deviation of the negative control, HBSS ($n = 3$). Italicized cells indicate a significant reduction in cell viability compared to the negative control, HBSS, based upon a p-value < 0.05 using Student's t-test. Reprinted from Kitchens et al. (2006) (with permission from Springer).

charged amine groups to interact with negatively charged cell surface proteins (Jevprasesphant et al., 2003b). The permeabilities of surface-modified dendrimers with unmodified counterparts were compared (Jevprasesphant et al., 2003a). PAMAM permeability generally increased with an increase in the number of lipid chains and concentration. The only exception was observed for G2 dendrimers when the number of lauroyl chains increased from six to nine, where the permeability of G2L9 was lower than G2L6. This was explained by the self-association of this conjugate, since aggregation was facilitated by the small size of G2 and the increased number of hydrophobic chains. Furthermore, lauroyl-modified dendrimers did not reduce TEER values as much as unmodified dendrimers. These results correspond with the observations that PAMAM cytotoxicity reduced with the conjugation of lipid chains by reducing the interaction between the cationic surface groups and the cell membrane. It is well established that fatty acids enhance membrane permeability, possibly by opening tight junctions (Aungst, 2000), and increased hydrophobicity generally enhances uptake and transport through the gut (Florence, 1997). Together, the studies described above (Jevprasesphant et al., 2003a,b; Kitchens et al., 2006) clearly demonstrate that surface modification reduces the toxicity of cationic PAMAM dendrimers and enhances their permeability across Caco-2 cells (Jevprasesphant et al., 2003a,b; Kitchens et al., 2006).

Recently Kolhatkar et al. (2007) modified the surface of G2 and G4 dendrimers with acetic anhydride (Figure 14.6A) to determine if an optimal surface charge density can be achieved where PAMAM dendrimers posses minimal cytotoxicity without compromising their permeability. Cell

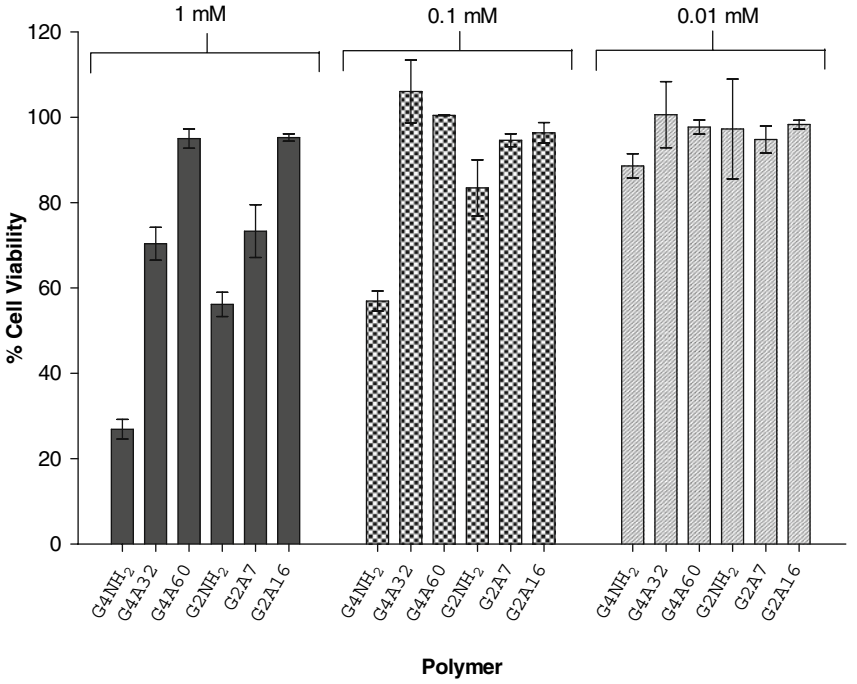

(A)

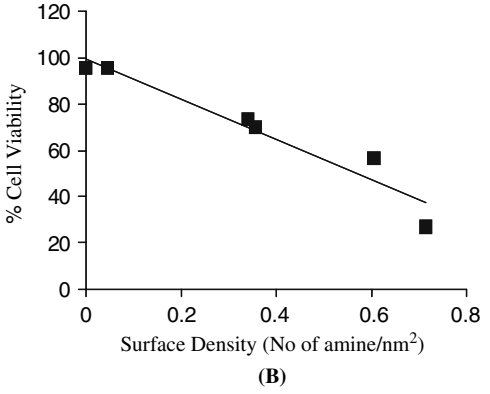

(B)

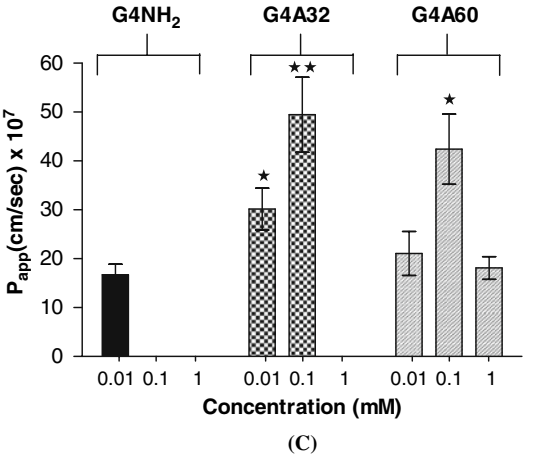

(C)

Figure 14.6 (**A**) In vitro cell viability of Caco-2 cells after incubation with dendrimers for 3 hours. Results are reported as mean ± SEM (n = 9). (**B**) Relationship between cell viability and surface density. (**C**) Permeability of (■) $G4NH_2$, (▨) G4A32, and (▨) G4A60 across Caco-2 cell monolayers after 120 min (G4Ax denotes generation 4 PAMAM-NH_2 dendrimers with x number of acetylated surface amine groups). Results are reported as mean ± SEM (n = 6). (*) ($p < 0.05$) and ($p < 0.01$); (**) denotes significant difference in permeability when compared to permeability of unmodified PAMAM dendrimer at 0.01 mM. (×) Permeability is not evaluated due to cytotoxicity. Adapted from Kolhatkar et al. (2007) (with permission from ACS Publications).

viability was at least 90% when cells were treated with partially and fully functionalized PAMAM dendrimers (0.1 mM) for 3 hours, suggesting partial modification is sufficient to reduce cytotoxicity (Figure 14.6A). At 1.0 mM, the toxic effects of PAMAM dendrimers decreased with an increase in surface acetylation, and a linear relationship was established between the surface density of amine groups and cytotoxicity (Figure 14.6B). A multi-regressional analysis (significant $F < 0.001$; $R^2 = 0.7$) was performed with the percentage cell viability as the dependant variable and surface density and concentration the independent variables, to give the following equation where C is concentration in mmol and SD_a is the surface density of amine groups (number of amine groups/nm^2):

$$\% \text{ Cell Viability} = 15.5\text{Log}(1/C) - 50.9\text{SD}_\text{a} + 87.6 \quad (1)$$

This equation describes cell viability as dependent on a combination of surface amine groups, dendrimer size, and concentration, and can be useful in predicting optimal surface modification to reduce PAMAM dendrimer toxicity (Kolhatkar et al., 2007). The AB permeability of non-toxic acetylated dendrimers was evaluated across Caco-2 cells. The permeability of both G4A32 and G4A60 at 0.01 mM was greater than that of unmodified G4, and a 1.5- and 2-fold enhancement of cellular permeability was achieved by increasing the G4A32 and G4A60 from 0.01 to 0.1 mM, respectively (Figure 14.6C).

Surface modification of PAMAM dendrimers also enhanced ^{14}C-mannitol permeability as a function of concentration and had a less drastic effect on TEER reduction compared to unmodified PAMAM dendrimers (Kolhatkar et al., 2007). TEER was reversible within 24 hours after dendrimer removal. The permeability enhancement of acetylated dendrimers could possibly be ascribed to a reduction of repulsive forces between surface amine groups, which would render the dendrimer structure more compact and result in increased permeability. Another possibility is that non-specific binding between dendrimers and the cell membrane may result in a relatively higher concentration of free dendrimer at the apical side of the membrane contributing to increased permeability (Kolhatkar et al., 2007). Further investigation revealed that surface modification of cationic PAMAM dendrimers leads to only modest decreases in cellular uptake compared to native dendrimer (Kolhatkar et al., 2007). Overall, these studies demonstrated acetylated PAMAM dendrimers had reduced cytotoxicity compared to unmodified dendrimers while maintaining appreciable permeability, therefore providing a window of opportunity for utilization of cationic PAMAM dendrimers in oral drug delivery.

Transport Mechanisms and Intracellular Fate of PAMAM Dendrimers

Several studies have attempted to elucidate the transport mechanisms of PAMAM dendrimers (Duncan & Izzo, 2005; Kitchens et al., 2005). Temperature-dependent studies demonstrated the permeability of cationic, anionic (Figure 14.7), and lipid-modified dendrimers was lower at 4°C

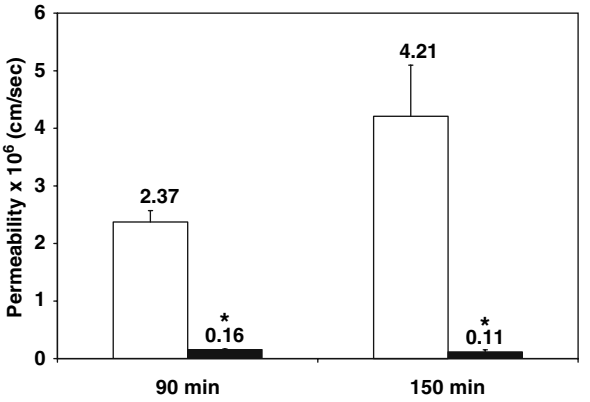

Figure 14.7 AB permeability of G2 across Caco-2 cell monolayers at incubation times of 90 and 150 minutes at 37°C (□) and 4°C (■). Statistical difference at $P < 0.05$ is denoted by (*). Results are reported as mean ± SEM. Reprinted from El-Sayed et al. (2003b) (with permission from Elsevier).

than observed at 37°C, suggesting the contribution of an energy-dependent process (El-Sayed et al., 2003b). Basolateral-to-apical (BA) permeability of PAMAM dendrimers was consistently greater than the corresponding AB permeability (El-Sayed et al., 2002, 2003a; Jevprasesphant et al., 2003a), thus the contribution of the P-gp efflux system to PAMAM transport was studied by measuring the permeability of ^{14}C-paclitaxel, a known P-gp substrate, in the absence and presence of $G2NH_2$ (El-Sayed et al., 2003b). There were no significant differences in the permeability of ^{14}C-paclitaxel in the presence of $G2NH_2$, nor did the permeability of $G2NH_2$ change in the presence of ^{14}C-paclitaxel, which suggested $G2NH_2$ is not a P-gp substrate (Figure 14.8). Additionally, the AB transport of propanolol, a poorly soluble P-gp substrate, increased while the BA transport decreased when propanolol was conjugated to $G3NH_2$ (D'Emanuele et al., 2004). This observation further demonstrates cationic dendrimers cannot be substrates for the P-gp efflux system since $G3NH_2$ enhanced the AB transport of propanolol. Finally, the application of palmitoyl carnitine, a typical absorption enhancer (Aungst, 2000), resulted in similar increases in the AB permeability of $G2NH_2$ and mannitol across Caco-2 cell monolayers (El-Sayed et al., 2003b). This observation, along with the observations that PAMAM dendrimers enhance mannitol permeability and decrease Caco-2 TEER through interaction with cellular tight junctions, suggest dendrimer transport is in part due to the paracellular route (El-Sayed et al., 2003b). Confocal laser scanning microscopy was used to visually confirm that PAMAM dendrimers open tight junctions (Kitchens et al., 2006). Caco-2 cells treated with PAMAM dendrimers for 2 hours displayed increased accumulation of the tight junctional protein occludin as evidenced by the disruptive staining pattern compared to control cells (Figure 14.9). Similar results were observed when cells were treated with rhodamine phalloidin to identify the actin protein. These data correspond to the observations that PAMAM dendrimers reduce TEER and increase ^{14}C-mannitol permeability, and directly confirm that they contribute to the opening of tight junctions. Together these studies clearly suggested $G2NH_2$ is transported across Caco-2 cell monolayers by a combination of the paracellular pathway and an energy-dependent process, such as endocytosis, and that $G2NH_2$ is not a substrate for the P-gp efflux system.

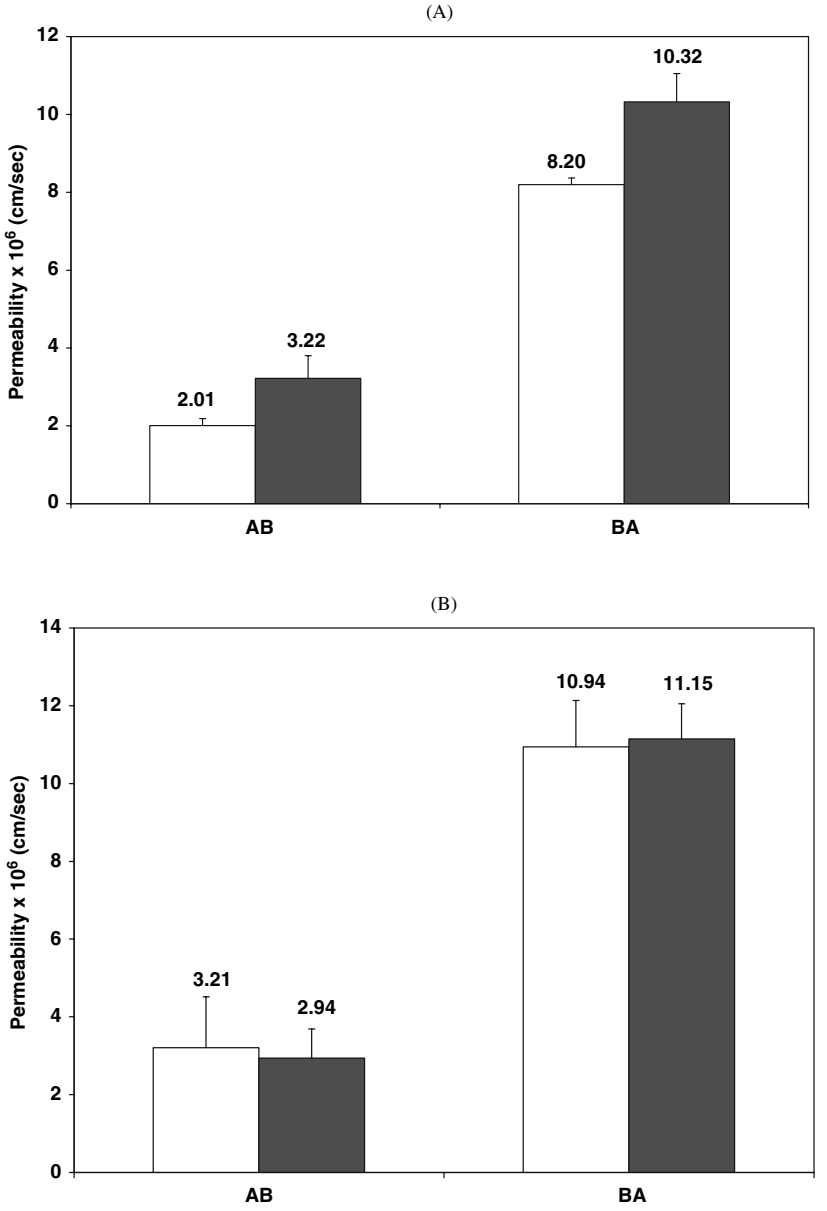

Figure 14.8 (**A**) AB and BA permeability of ^{14}C-paclitaxel across Caco-2 cell monolayers in absence (□) and presence (■) of G2 (10.0 mM) at incubation time of 150 minutes. (**B**) AB and BA permeability of G2 (10.0 mM) across Caco-2 cell monolayers in absence (□) and presence (■) of paclitaxel (200 nM) at incubation time of 150 minutes. Results are reported as mean ± SEM. Reprinted from El-Sayed et al. (2003b) (with permission from Elsevier).

To further investigate the endocytosis of PAMAM dendrimers, their intracellular location was explored using various microscopy techniques. First, significant levels of FITC-labeled dendrimers were measured in Caco-2 cells after 3 hours treatment using flow cytometry and confocal

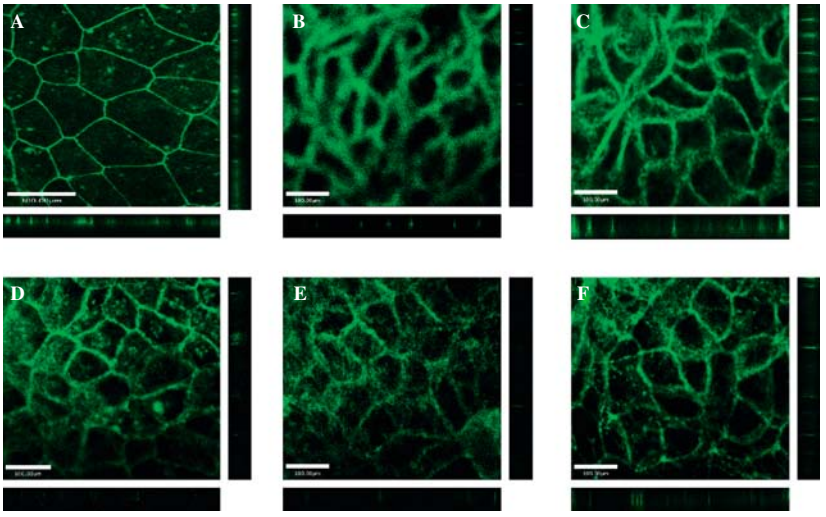

Figure 14.9 Staining of the tight junction protein occludin. (**A**) Caco-2 cells with no polymer treatment. Caco-2 cells incubated for 120 minutes with 1.0 mM: (**B**) $G2NH_2$; (**C**) G2OH, (**D**) G1.5COOH; (**E**) G2.5COOH; (**F**) G3.5COOH. Main panels illustrate the *xy* plane; horizontal bars illustrate the *xz* plane; vertical bars illustrate the *yz* plane. Scale bars equal 100.00 μm. Reprinted from Kitchens et al. (2006) (with permission from Springer). (*See* Color Plate 19)

laser scanning microscopy indicating that the polymers were internalized within the cells and not adsorbed to the cell surface (Jevprasesphant et al., 2004). TEM was used to track the internalization process of dendrimer-gold nanocomplexes in Caco-2 cells. The nanocomposites were localized in vesicular compartments located below the apical membrane, presumably endosomes, and in multivesicular compartments throughout the cells. These observations suggested an endocytosis process contributes to dendrimer transport. To confirm these indirect observations, confocal laser scanning microscopy techniques were used to visualize the intracellular localization of dendrimers in Caco-2 cells, and quantify the extent of colocalization between PAMAM dendrimers and established endocytosis markers (Kitchens et al., 2007). Both cationic and anionic PAMAM dendrimers internalized within 20 minutes and colocalized with endocytosis markers clathrin, EEA-1, and LAMP-1 (Figure 14.10). Fluorescently labeled dendrimers colocalized with the early endosomal markers, anti-clathrin and anti-EEA1, greater than 70% after 20 and 60 minutes (Table 14.4), and colocalized to a lesser extent with the lysosomal marker, LAMP-1, which suggests PAMAM dendrimers are primarily localized in endosomal compartments. Interestingly, colocalization of $G2NH_2$ with LAMP-1 increased proportionally with time, suggesting lysosomal trafficking of cationic dendrimers is incubation time dependent. Similarly, colocalization of PAMAM dendrimers with EEA-1, specific to early endosomes, was high after 20 minutes, and reduced with time (Table 14.4). The confocal data confirmed that PAMAM dendrimers are localized in endosomal compartments, and dendrimer trafficking to secondary endosomes and lysosomes is time and surface charge dependent.

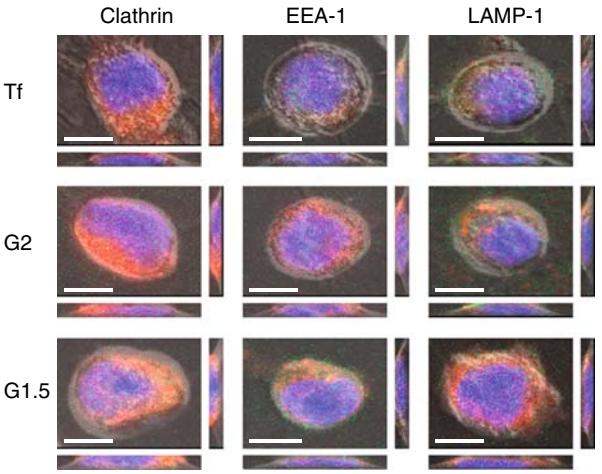

Figure 14.10 Internalization of fluorescently labeled transferrin (250 μg/ml) and PAMAM dendrimers (100 nM) in Caco-2 cells after 20 minutes. The orange color in merged panels indicates colocalization with clathrin heavy chain, early endosomal antigen-1 (EEA-1), and lysosome-associated membrane protein-1 (LAMP-1). Main panels illustrate the *xy* plane; vertical panels illustrate the *yz* plane; horizontal panels illustrate the *xz* plane. Scale bars = 5 μm. Adapted from Kitchens et al. (2007) (with permission from ACS Publications). (*See* Color Plate 20)

Table 14.4 Extent of colocalization between transferrin and PAMAM dendrimers with endocytosis markers.*

	Incubation time (min)	Clathrin	EEA-1	LAMP-1
Transferrin	20	80.3 ± 3.1%	70.4 ± 7.0%	63.9 ± 7.3%
	60	83.4 ± 0.2%	79.6 ± 0.4%	57.0 ± 8.6%
$G2NH_2$	20	74.3 ± 5.2%	76.7 ± 3.4%	37.4 ± 5.9%
	60	73.7 ± 3.8%	72.1 ± 0.4%	59.0 ± 5.2%
G1.5COOH	20	70.8 ± 3.9%	60.1 ± 6.8%	58.7 ± 2.0%
	60	75.3 ± 1.2%	53.8 ± 9.7%	48.9 ± 1.3%

*Colocalization coefficients (M_x) were calculated using the following equation:

$$M_X = \frac{\sum_i x_i \text{coloc}}{\sum_i x_i}$$

where $x_i$coloc is the value of voxel i of the overlapped FITC and Alexa Fluor 568® components, and x_i is the value of voxel i of the FITC component. M_x values are reported as mean ± standard error of the mean ($n = 6$). Reprinted from Kitchens et al. (2007) (with permission from ACS Publications).

Microvascular Extravasation of Poly(amidoamine) Dendrimers

Once drugs and macromolecules are absorbed orally, they are distributed throughout the circulatory system and must extravasate across the microvascular endothelium of capillary walls to reach the site of therapeutic action in neighboring interstitial tissues (El-Sayed et al., 2001; Takakura et al., 1998). Previous studies investigated the influence of dendrimer size and molecular weight on their microvascular extravasation (El-Sayed et al., 2001). The extravasation time of a series of fluorescently labeled PAMAM-NH_2 dendrimers and PEG (MW = 6000 Da) was investigated across the microvascular endothelium in the cremaster muscle of male Syrian hamsters using intravital microscopy techniques. The extravasation time was measured as the time required for fluorescence intensity in interstitial tissue to reach 90% the fluorescence intensity in the neighboring

microvasculature. Extravasation time increased exponentially with the increase in PAMAM dendrimer molecular weight and size, and the rank order of extravasation time was G0 < G1 < G2 < G3 < G4 < PEG, ranging from 143.9 to 453.9 seconds. This size-dependent selectivity is in part due to the increased exclusion of PAMAM-NH_2 dendrimers from the endothelial pores, 4-5 nm in radius, as dendrimer size (1.5–4.5 nm) and hydrodynamic volume increased (El-Sayed et al., 2001).

PEG had the earliest size-exclusion elution volume compared to the dendrimers, which indicates PEG had a greater hydrodynamic volume and consequently longer extravasation time than PAMAM dendrimers. The microvascular endothelium is lined with the glycocalyx layer, which is composed of negatively charged sulfated glycosaminoglycan (Adamson & Clough, 1992). The observed extravasation of PAMAM-NH_2 dendrimers and PEG molecules may also be a function of the electrostatic interactions between the polymers and the negatively charged endothelium. PAMAM-NH_2 dendrimers are positively charged at physiological pH, whereas PEG molecules are neutral. As a result, the electrostatic interaction between PAMAM-NH_2 dendrimers and the negatively charged glycocalyx lining was more favorable compared to the neutral PEG molecules, which led to the faster extravasation time observed for PAMAM-NH_2 dendrimers compared to PEG. Overall, this study demonstrated that an increase in molecular weight and size of polymers results in increased extravasation time across the microvascular endothelium. Molecular geometry and surface charge also influence the microvascular extravasation of water-soluble polymers across the endothelial barrier, in which compact, spherical, positively charged PAMAM dendrimers have shorter extravasation times than random-coiled, neutral PEG chains. It must be noted that in this study the uptake of polymers by tissues is a function of size and charge and its influence over extravasation time indeed warrants further consideration.

Conclusions and Future Directions

The potential of PAMAM dendrimers as oral drug delivery carriers has been demonstrated by their appreciable permeability and uptake across the intestinal epithelial barrier, given their macromolecular nature. Earlier studies demonstrated that dendrimers could be administered as oral formulations since they are rapidly absorbed in the GI tract and perfuse to the circulatory system. Further studies demonstrated cationic PAMAM dendrimers extravasate across the microvascular endothelium. The biocompatibility and transport of PAMAM dendrimers across the epithelial barrier demonstrate a size and charge window where PAMAM dendrimers can have utility in drug delivery applications. To lessen the toxic effects of cationic PAMAM dendrimers, it is possible to modify the surface amine groups with inert, hydrophobic moieties that do not compromise, and in some cases enhance, dendrimer permeability. Mechanistic studies suggested PAMAM dendrimers open the tight junctions and are endocytosed leading to their own enhanced permeability. Together these studies demonstrate the potential of PAMAM dendrimers in the oral delivery of bioactive agents for systemic absorption. The next logical step in these

studies is to conjugate specific potent drugs for translocation across the GI tract and absorption to the blood circulation for targeted delivery to distant sites. The challenges remaining are appropriate conjugation (or complexation) strategies to facilitate delivery to the target sites. Further mechanistic studies can delineate the kinetics of subcellular localization and transcytosis. Such delineation can open new avenues for sub- or transcellular delivery of bioactive agents. The mechanisms by which PAMAM dendrimers open the tight junctions are not well understood. Finally, pre-clinical and clinical development of orally bioavailable dendrimers require a battery of biocompatibility, stability, transport, biodistribution, and efficacy studies depending on the type of carrier, cargo, and targeting strategies.

Acknowledgments. Financial support was in part provided by the National Institute of General Medical Sciences National Research Service Award predoctoral fellowship to Kelly Kitchens (F31-GM67278) and a grant from the National Institutes of Health (RO1EB007470).

Abbreviations

Abbreviations:	Full name:
1B4M	*p*-Isothiocyanatobenzyl)-6-methyl-diethylenetriamine pentaacetic acid
AB	Apical-to-basolateral
BA	Basolateral-to-apical
BRI	Biomolecular Research Institute
CAT	Chloramphenicol acetyl-transferase
CT	Computed topography
Da	Daltons
DAB	Diaminobutane
DMPC	1,2-Dimyristoyl-*sn*-glycero-3-phosphocholine
DNA	Deoxyribonucleic acid
DTPA	Diethylenetriaminepentaacetic acid
EEA-1	Early endosomal antigen 1
FITC	Fluorescein isothiocyanate
G	Generation
Gd	Gadolinium
GI	Gastrointestinal
HSV-2	Herpes simplex virus type 2
ID/g	Injected dose per gram
IR	Infra-red
LAMP-1	Lysosome-associated membrane protein 1
LDH	Lactate dehydrogenase
MALDI-TOF	Matrix-assisted laser desorption ionization time of flight
MDCK	Madin–Darby canine kidney
MRI	Magnetic resonance imaging
MTT	3-(4,5-Dimethylthiazole-2-yl)-2,5-diphenyltetrazolium bromide
NMR	Nuclear magnetic resonance

P_{app}	Apparent permeability
PAGE	Polyacrylamide gel electrophoresis
PAMAM	Poly(amidoamine)
PEG	Poly(ethylene glycol)
PEI	Poly(ethyleneimine)
PEO	Poly(ethylene oxide)
P-gp	P-glycoprotein
PPI	Poly(propyleneimine)
PVA	Poly(vinyl alcohol)
SANS	Small-angle neutron scattering
SAXS	Small-angle X-ray scattering
SDS	Sodium dodecyl sulfate
TEER	Transepithelial electrical resistance
TEM	Transmission electron microscopy
TNF-α	Tumor necrosis factor

References

Adamson, R. H., & Clough, G. (1992). Plasma proteins modify the endothelial cell glycocalyx of frog mesenteric microvessels. *J Physiol*, *445*, 473–486.

Artursson, P. (1990). Epithelial transport of drugs in cell culture. I: A model for studying the passive diffusion of drugs over intestinal absorptive (Caco-2) cells. *J Pharm Sci*, *79*(6), 476–482.

Aulenta, F., Drew, M. G., Foster, A., Hayes, W., Rannard, S., Thornthwaite. D. W., Worrall, D. R., Youngs, T. G. (2005). Synthesis and characterization of fluorescent poly (aromatic amide) dendrimers. *J Org Chem*, *70*(1), 63–78.

Aungst, B. J. (2000). Intestinal permeation enhancers. *J Pharm Sci*, *89*(4), 429–442.

Bayele, H. K., Ramaswamy, C., Wilderspin, A. F., Srai, K. S., Toth, I., & Florence, A. T. (2006). Protein transduction by lipidic peptide dendrimers. *J Pharm Sci*, *95*(6), 1227–1237.

Behr, J. P. (1994). Gene transfer with synthetic cationic amphiphiles: Prospects for gene therapy. *Bionconjug Chem*, *5*(5), 382–389.

Bielinska, A., Kukowska-Latallo, J. F., Johnson, J., Tomalia, D. A., & Baker, J. R., Jr. (1996). Regulation of in vitro gene expression using antisense oligonucleotides or antisense expression plasmids transfected using starburst PAMAM dendrimers. *Nucleic Acids Res*, *24*(11), 2176–2182.

Boas, U, Karlsson, A. J., de Waal, B. F., Meijer, E. W. (2001). Synthesis and properties of new thiourea-functionalized poly (propylene imine) dendrimers and their role as hosts for urea functionalized guests. *J Org Chem*, *66*(6), 2136–2145.

Bourne, N. (2000). Dendrimers, a new class of candidate topical microbicides with activity against herpes simplex virus infection. *Antimicrob Agents Chemother*, *44*(9), 2471–2474.

Brauge, L., Magro, G., Caminade, A. M., & Majoral, J. P. (2001). First divergent strategy using two AB(2) unprotected monomers for the rapid synthesis of dendrimers. *J Am Chem Soc*, *123*(27), 6698–6699.

Brothers II, H. M., Piehler, I. T., & Tomalia, D. A. (1998). Slab-gel and capillary electrophoretic characterization of polyamidoamine dendrimers. *J Chromatogr A*, *814*(1–2), 233–246.

Caminade, A. M., Laurent, R., & Majoral, J. P. (2005). Characterization of dendrimers. *Adv Drug Del Rev*, *57*(15), 2130–2146.

Chai, M., Niu, Y., Youngs, W. J., Rinaldi, P.L. (2001). Structure and conformation of DAB dendrimers in solution via multidimensional NMR techniques. *J Am Chem Soc*, *123*(20), 4670–4678.

Chai, M., Pi, Z., Tessier, C., & Rinaldi, P. L. (1999). Preparation of carbosilane dendrimers and their characterization using $^{1}H/^{13}C/^{29}Si$ triple resonance 3D NMR methods. *J Am Chem Soc*, *121*(2), 273–279.

Chauhan, A. S., Sridevi, S., Chalasani, K. B., Jain, A. K., Jain, S. K., & Jain, N. K. (2003). Dendrimer-mediated transdermal delivery: Enhanced bioavailability of indomethacin. *J Control Release*, *90*(3), 335–343.

Chen, H. T., Neerman, M. F., Parrish, A. R., & Simanek, E. E. (2004). Cytotoxicity, hemolysis, and acute in vivo toxicity of dendrimers based on melamine, candidate vehicles for drug delivery. *J Am Chem Soc*, *126*, 10044–10048.

Choe, Y. H., Conover, C. D., Wu, D., Royzen, M., Gervacio, Y., & Borowski, V. (2002). Anticancer drug delivery systems: Multi-loaded N4-acyl poly(ethylene glycol) prodrugs of ara-C. II. Efficacy in ascites and solid tumors. *J Control Release*, *79*(1–3), 55–70.

Choi, Y. S., Thomas, T., Kotlayr, A., Islam, M. T., & Baker, J. R. (2005). Synthesis and functional evaluation of DNA-assembled polyamidoamine dendrimer clusters for cancer cell-specific targeting. *Chem Biol*, *12*(1), 35–43.

Cloninger, M. J. (2002). Biological applications of dendrimers. *Curr Opin Chem Biol*, *6*(6), 742–748.

D'Emanuele, A., & Attwood, D. (2005). Dendrimer-drug interactions. *Adv Drug Deliv Rev*, *57*(15), 2147–2162.

D'Emanuele, A., Jevprasesphant, R., Penny, J., & Attwood, D. (2004). The use of a dendrimer-propranolol prodrug to bypass efflux transporters and enhance oral bioavailability. *J Control Release*, *95*(3), 447–453.

DeLong, R., Stephenson, K., Loftus, T., Fisher, M., Alahari, S., Nolting, A., & Juliano, R. L. (1997). Characterization of complexes of oligonucleotides with polyamidoamine starburst dendrimers and effects on intracellular delivery. *J Pharm Sci*, *86*(6), 762–764.

Dufes, C., Keith, W. N., Bilsland, A., Proutski, I., Uchegbu, I. F., & Schatzlein, A. G. (2005a). Synthetic anticancer gene medicine exploits intrinsic antitumor activity of cationic vector to cure established tumors. *Cancer Res*, *65*(18), 8079–8084.

Dufes, C., Uchegbu, I. F., & Schatzlein, A. G. (2005b). Dendrimers in gene delivery. *Adv Drug Deliv Rev*, *57*(15), 2177–2202.

Duncan, R., & Izzo, L. (2005). Dendrimer biocompatibility and toxicity. *Adv Drug Deliv Rev*, *57*(15), 2215–2237.

Duncan, R., & Spreafico, F. (1994). Polymer conjugates. Pharmacokinetic considerations for design and development. *Clin Pharmacokinet*, *27*(4), 290–306.

Dunphy, I., Vinogradov, S. A., & Wilson, D. F. (2002). Oxyphor R2 and G2: Phosphors for measuring oxygen by oxygen-dependent quenching of phosphorescence. *Anal Biochem*, *310*(2), 191–198.

El-Sayed, M., Ginski, M., Rhodes, C., & Ghandehari, H. (2002). Transepithelial transport of poly(amidoamine) dendrimers across Caco–2 cell monolayers. *J Control Release*, *81*(3), 355–365.

El-Sayed, M., Ginski, M., Rhodes, C., & Ghandehari, H. (2003a). Influence of surface chemistry of poly (amidoamine) dendrimers on Caco-2 cell monolayers. *J Bioactive Compat Poly*, *18*, 7–22.

El-Sayed, M., Rhodes, C. A., Ginski, M., & Ghandehari, H. (2003b). Transport mechanism(s) of poly (amidoamine) dendrimers across Caco-2 cell monolayers. *Int J Pharm*, *265*(1–2), 151–157.

El-Sayed, M., Kiani, M. F., Naimark, M. D., Hikal, A. H., & Ghandehari, H. (2001). Extravasation of poly(amidoamine) (PAMAM) dendrimers across microvascular network endothelium. *Pharm Res*, *18*(1), 23–28.

Esfand, R., & Tomalia, D. A. (2001). Poly (amidoamine) (PAMAM) dendrimers: From biomimicry to drug delivery and biomedical applications. *Drug Discov Today*, *6*(8), 427–436.

Felder, T., Schalley, C. A., Fakhrnabavi, H., & Lukin, O. (2005). A combined ESI- and MALDI-MS(/MS) study of peripherally persulfonylated dendrimers: False negative results by MALDI-MS and analysis of defects. *Chemistry*, *11*(19), 5625–5636.

Fischer, D., Li, Y., Ahlemeyer, B., Krieglstein, J., & Kissel, T. (2003). In vitro cytotoxicity testing of polycations: Influence of polymer structure on cell viability and hemolysis. *Biomaterials*, *24*(7), 1121–1131.

Florence, A. T. (1997). The oral absorption of micro- and nanoparticles: Neither exceptional nor unusual. *Pharm Res*, *14*, 259–266.

Florence, A. T., Sakthivel, T., & Toth, I. (2000). Oral uptake and translocation of a polylysine dendrimer with a lipid surface. *J Control Release*, *65*(1–2), 253–259.

Fu, Y., Nitecki, D. E., Maltby, D., Simon, G. H., Berejnoi, K., Raatschen, H. J., Yeh, B. M., Shames, D. M., & Brasch, R. C. (2006). Dendritic iodinated contrast agents with PEG-cores for CT imaging: Synthesis and preliminary characterization. *Bioconjug Chem*, *17*(4), 1043–1056.

Grinstaff, M. W. (2002). Biodendrimers: New polymeric biomaterials for tissue engineering. *Chemistry*, *8*(13), 2838–2846.

Haensler, J., & Szoka, F.C., Jr. (1993). Polyamidoamine cascade polymers mediate efficient transfection of cells in culture. *Bionconjug Chem*, *4*(5), 372–379.

Halford, B. (2005). Dendrimers branch out. *Chem Eng News*, *83,* 30–36.

Hawker, C. J., & Frechet, J. M. J. (1990). Preparation of polymers with controlled molecular architecture. A new convergent approach to dendritic macromolecules. *J Am Chem Soc*, *112*(21), 7638–7647.

Hilgers, A. R., Conradi, R. A., & Burton, P. S. (1990). Caco-2 cell monolayers as a model for drug transport across the intestinal mucosa. *Pharm Res*, *7*(9), 902–910.

Hobbs, S. K., Monsky, W. L., Yuan, F., Roberts, W. G., Griffith, L., Torchilin, V. P., Jain, & R. K. (1998). Regulation of transport pathways in tumor vessels: Role of tumor type and microenvironment. *Proc Natl Acad Sci USA*, *95*(8), 4607–4612.

Hong, M. Y., Kim, Y. J., Lee, J. W., Kim, K., Lee, J. H., Yoo, J. S., Bae, S. H., Choi, B. S., & Kim, H. S. (2004a). Synthesis and characterization of tri(ethylene oxide)-attached poly(amidoamine) dendrimer layers on gold. *J Colloid Interface Sci*, *274*(1), 41–48.

Hong, S., Leroueil, P. R., Janus, E. K., Peters, J. L., Kober, M. M., Islam, M. T., Orr, B. G. Baker, J. R., Jr., & Banaszak Holl, M. M. (2006). Interaction of polycationic polymers with supported lipid bilayers and cells: Nanoscale hole formation and enhanced membrane permeability. *Bioconjug Chem*, *17*(3), 728–734.

Hong, S., Bielinska, A. U., Mecke, A., Keszler, B., Beals, J. L., Shi, X., Balogh, L., Orr, B. G., Baker, J. R., Jr., & Banaszak Holl, M. M (2004b). Interaction of poly(amidoamine) dendrimers with supported lipid bilayers and cells: Hole formation and the relation to transport. *Bioconjug Chem*, *15*(4), 774–782.

Huang, Q. R., Dubin, P. L., Lal, J., Moorefield, C. N., & Newkome, G. R. (2005). Small-angle neutron scattering studies of charged carboxyl-terminated dendrimers in solutions. *Langmuir*, *21*(7), 2737–2742.

Hughes, J. A., Aronsohn, A. I., Avrutskaya, A. V., & Juliano, R. L. (1996). Evaluation of adjuvants that enhance the effectiveness of antisense oligodeoxynucleotides. *Pharm Res*, *13*(3), 404–410.

Hummelen, J. C., Van Dongen, J. L. J., & Meijer, E. W. (1997). Electrospray mass spectrometry of poly(propylene imine) dendrimers – the issue of dendritic purity or polydispersity. *Chem Eur J*, *3*(9), 1489–1493.

Ihre, H. R., Padilla De Jesus, O. L., Szoka, F. C., Jr., & Frechet, J. M. (2002). Polyester dendritic systems for drug delivery applications: Design, synthesis, and characterization. *Bioconjug Chem*, *13*(3), 443–452.

Irvine, J. D., Takahashi, L., Lockhart, K., Cheong, J., Tolan, J. W., Selick, H. E., & Grove, J. R. (1999). MDCK (Madin-Darby Canine Kidney) cells: A tool for membrane permeability screening. *J Pharm Sci*, *88*(1), 28–33.

Jackson, C. L., Chanzy, H. D., Booy, F. P., Drake, B. J., Tomalia, D. A., Bauer, B. J., & Amis, E. J. (1998). Visualization of dendrimer molecules by transmission electron microscopy (TEM): Staining methods and cryo-TEM of vitrified solutions. *Macromolecules*, *31*(18), 6259–6265.

Jevprasesphant, R., Penny, J., Attwood, D., & D'Emanuele, A. (2004). Transport of dendrimer nanocarriers through epithelial cells via the transcellular route. *J Control Release*, *97*(2), 259–267.

Jevprasesphant, R., Penny, J., Attwood, D., McKeown, N. B., & D'Emanuele, A. (2003a). Engineering of dendrimer surfaces to enhance transepithelial transport and reduce cytotoxicity. *Pharm Res*, *20*(10), 1543–1550.

Jevprasesphant, R., Penny, J., Jalal, R., Attwood, D., McKeown, N. B., & D'Emanuele, A. (2003b). The influence of surface modification on the cytotoxicity of PAMAM dendrimers. *Int J Pharm*, *252*(1–2), 263–266.

Jiang, Y. H., Emau, P., Cairns, J. S., Flanary, L., Morton, W. R., McCarthy, T. D., & Tsai, C.C. (2005). SPL7013 gel as a topical microbicide for prevention of vaginal transmission of SHIV89.6p in macaques. *AIDS Res Hum Retroviruses*, *21*(3), 207–213.

Juliano, R. L. (2006). Intracellular delivery of oligonucleotide conjugates and dendrimer complexes. *Ann NY Acad Sci*, *1082*, 18–26.

Kang, H., DeLong, R., Fisher, M. H., & Juliano, R. L. (2005). Tat-conjugated PAMAM dendrimers as delivery agents for antisense and siRNA oligonucleotides. *Pharm Res*(12), *22*, 2099–2106.

Kannan, S., Kolhe, P., Raykova, V., Glibatec, M., Kannan, R. M., Lieh-Lai, M., & Bassett, D. (2004). Dynamics of cellular entry and drug delivery by dendritic polymers into human lung epithelial carcinoma cells. *J Biomater Sci Polym Ed*, *15*(3), 311–330.

Karoonuthaisiri, N., Titiyevskiy, K., & Thomas, J. L. (2003). Destabilization of fatty acid-containing liposomes by polyamidoamine dendrimers. *Colloids Surf B Biointerfaces*, *27*(24), 365–375.

Khandare, J., Kolhe, P., Pillai, O., Kannan, S., Lieh-Lai, M., & Kannan, R. M. (2005). Synthesis, cellular transport, and activity of polyamidoamine dendrimer-methylprednisolone conjugates. *Bioconjug Chem*, *16*(2), 330–337.

Kim, T. I., Seo, H. J., Choi, J. S., Jang, H. S., Baek, J. U., Kim, K., & Park, J. S. (2004). PAMAM-PEG-PAMAM: Novel triblock copolymer as a biocompatible and efficient gene delivery carrier. *Biomacromolecules*, *5*(6), 2487–2492.

Kitchens, K. M., El-Sayed, M. E., & Ghandehari, H. (2005). Transepithelial and endothelial transport of poly (amidoamine) dendrimers. *Adv Drug Deliv Rev*, *57*(15), 2163–2176.

Kitchens, K. M., Foraker, A. B., Kolhatkar, R. B., Swaan, P. W., & Ghandehari, H. (2007). Endocytosis and interaction of poly (amidoamine) dendrimers with Caco-2 cells. *Pharamaceutical Research*, 24:2138–2145.

Kitchens, K. M., Kolhatkar, R. B., Swaan, P. W., Eddington, N. D., & Ghandehari, H. (2006). Transport of poly(amidoamine) dendrimers across Caco-2 cell monolayers: Influence of size, charge and fluorescent labeling. *Pharm Res*, *23*(12), 2818–2826.

Kobayashi, H., & Brechbiel, M. W. (2005). Nano-sized MRI contrast agents with dendrimer cores. *Adv Drug Deliv Rev*, *57*(15), 2271–2286.

Kobayashi, H., Kawamoto, S., Saga, T., Sato, N., Hiraga, A., Ishimori, T., Konishi, J., Togashi, K., & Brechbiel, M. W. (2001a). Positive effects of polyethylene glycol conjugation to generation-4 polyamidoamine dendrimers as macromolecular MR contrast agents. *Magn Reson Med*, *46*(4), 781–788.

Kobayashi, H., Sato, N., Kawamoto, S., Saga, T., Hiraga, A., Haque, T. L., Ishimori, T., Konishi, J., Togashi, K., & Brechbiel, M. W. (2001b). Comparison of the macromolecular MR contrast agents with ethylenediamine-core versus ammonia-core generation-6 polyamidoamine dendrimer. *Bioconjug Chem*, *12*(1), 100–107.

Kolhatkar, K., Kitchens, K. M., Swaan, P. & Ghandehari, H. (2007), Surface acetylation of poly(amidoamine) (PAMAM) dendrimers decreases cytotoxicity while maintaining membrane permeability, *Bioconjugate Chemistry*, 18, 2054–2060.

Kolhe, P., Khandare, J., Pillai, O., Kannan, S., Lieh-Lai, M., & Kannan, R. M. (2006). Preparation, cellular transport, and activity of polyamidoamine-based dendritic nanodevices with a high drug payload. *Biomaterials*, *27*(4), 660–669.

Kolhe, P., Khandare, J., Pillai, O., Kannan, S., Lieh-Lai, M., & Kannan, R. (2004). Hyperbranched polymer-drug conjugates with high drug payload for enhanced cellular delivery. *Pharm Res*, *21*(12), 2185–2195.

Kolhe, P., Misra, E., Kannan, R. M., Kannan, S., & Lieh-Lai, M. (2003). Drug complexation, in vitro release and cellular entry of dendrimers and hyperbranched polymers. *Int J Pharm*, *259*(1–2), 143–160.

Konda, S. D., Aref, M., Brechbiel, M., & Wiener, E. C. (2000). Development of a tumor-targeting MR contrast agent using the high-affinity folate receptor: Work in progress. *Invest Radiol*, *35*(1), 50–57.

Langereis, S., de Lussanet, Q. G., van Genderen, M. H., Meijer, E. W., Beets-Tan, R. G., Griffioen, A. W., van Engelshoven, J. M., & Backes, W. H. (2006). Evaluation of Gd(III)DTPA-terminated poly(propylene imine) dendrimers as contrast agents for MR imaging. *NMR Biomed*, *19*(1), 133–141.

Launay, N., Caminade, A. M., & Majoral, J. P. (1995). Synthesis and reactivity of unusual phosphorus dendrimers. A useful divergent growth approach up to the seventh generation. *J Am Chem Soc*, *117*(11), 3282–3283.

Lee, C. C., MacKay, J. A., Frechet, J. M., & Szoka, F. C. (2005). Designing dendrimers for biological applications. *Nat Biotechnol*, *23*(12), 1517–1526.

Liu, M., & Frechet, J. M. (1999). Designing dendrimers for drug delivery. *Pharm Sci Technol Today*, *2*(10), 393–401.

Liu, M., Kono, K., & Frechet, J. M. (2000). Water-soluble dendritic unimolecular micelles: Their potential as drug delivery agents. *J Control Release*, *65*(1–2), 121–131.

Loup, C., Zanta, M. A., Caminade, A. M., Majoral, J. P., & Meunier, B. (1999). Preparation of water soluble cationic phosphorous containing dendrimers as DNA transfecting agents. *Chem Eur J*, *5*(12), 3644–3650.

Luo, Y., & Prestwich, G. D. (2002). Cancer-targeted polymeric drugs. *Curr Cancer Drug Targets*, *2*(3), 209–226.

Majoros, I. J., Myc, A., Thomas, T., Mehta, C. B., & Baker, J. R., Jr. (2006). PAMAM dendrimer-based multifunctional conjugate for cancer therapy: Synthesis, characterization, and functionality. *Biomacromolecules*, *7*(2), 572–579.

Malik, N., Evagorou, E. G., & Duncan, R. (2000). Dendrimers: Relationship between structure and biocompatibility in vitro, and preliminary studies on the biodistribution of ^{125}I-labelled polyamidoamine dendrimers in vivo. *J Control Release*, *65*(1–2), 133–148.

Malik, N., Evagorou, E. G., & Duncan, R. (1999). Dendrimer-platinate: A novel approach to cancer chemotherapy. *Anticancer Drugs*, *10*(8), 767–776.

Maraval, V., Pyzowski, J., Caminade, A. M., & Majoral, J. P. (2003). "Lego" chemistry for the straightforward synthesis of dendrimers. *J Org Chem*, *68*, 6043–6046.

Mecke, A., Majoros, I. J., Patri, A. K., Baker, J. R., Jr., Holl, M. M., & Orr, B. G. (2005). Lipid bilayer disruption by polycationic polymers: The roles of size and chemical functional group. *Langmuir*, *21*(23), 10348–10354.

Mecke, A., Uppuluri, S., Sassanella, T. M., Lee, D. K., Ramamoorthy, A., Baker, J. R., Jr., Orr, B. G., & Banaszak Holl, M. M. (2004). Direct observation of lipid bilayer disruption by poly (amidoamine) dendrimers. *Chem Phys Lipids*, *132*(1), 3–14.

Milhem, O. M., Myles, C., McKeown, N. B., Attwood, D., & D'Emanuele, A. (2000). Polyamidoamine starburst dendrimers as solubility enhancers. *Int J Pharm*, *197*(1–2), 239–241.

Namazi, H., & Adeli, M. (2005). Dendrimers of citric acid and poly (ethylene glycol) as the new drug-delivery agents. *Biomaterials*, *26*(10), 1175–1183.

Padilla De Jesus, O. L., Ihre, H. R., Gagne, L., Frechet, J. M., & Szoka, F. C., Jr. (2002). Polyester dendritic systems for drug delivery applications: In vitro and in vivo evaluation. *Bioconjug Chem*, *13*(3), 453–461.

Patri, A. K., Kukowska-Latallo, J. F., & Baker, J. R., Jr. (2005). Targeted drug delivery with dendrimers: Comparison of the release kinetics of covalently conjugated drug and non-covalent drug inclusion complex. *Adv Drug Deliv Rev*, *57*(15), 2203–2214.

Potschke, D., Ballauff, M., Lindner, P., Fischer, M., & Vogtle, F. (1999). Analysis of the structure of dendrimers in solution by small-angle neutron scattering including contrast variation. *Macromolecules*, *32*(12), 4079–4087.

Prosa, T. J., Bauer, B. J., & Amis, E. J. (2001). From stars to spheres: A SAXS analysis of dilute dendrimer solutions. *Macromolecules*, *34*(14), 4897–4906.

Quintana, A., Raczka, E., Piehler, L., Lee, I., Myc, A., Majoros, I., Patri, A. K., Thomas, T., Mule, J., & Baker, J. R., Jr. (2002). Design and function of a dendrimer-based therapeutic nanodevice targeted to tumor cells through the folate receptor. *Pharm Res*, *19*(9), 1310–1316.

Rajca, A. (1991). Synthesis of 1,3-connected polyarylmethanes. *J Org Chem*, *56*(7), 2557–2563.

Rathgeber, S., Pakula, T., & Urban, V. (2004). Structure of star-burst dendrimers: A comparison between small angle x-ray scattering and computer simulation results. *J Chem Phys*, *121*(8), 3840–3853.

Roberts, J. C., Bhalgat, M. K., & Zera, R. T. (1996). Preliminary biological evaluation of polyamidoamine (PAMAM) Starburst dendrimers. *J Biomed Mater Res*, *30*(1), 53–65.

Rosenfeldt, S., Karpuk, E., Lehmann, M., Meier, H., Lindner, P., Harnau, L., & Ballauff, M. (2006). The solution structure of stilbenoid dendrimers: A small-angle scattering study. *Chemphyschem*, *7*(10), 2097–2104.

Sadler, K., & Tam, J.P. (2002). Peptide dendrimers: Applications and synthesis. *J Biotechnol*, *90*(3–4), 195–229.

Sakamoto, Y., Suzuki, T., Miura, A., Fujikawa, H., Tokito, S., & Taga, Y. (2000). Synthesis, characterization, and electron-transport property of perfluorinated phenylene dendrimers. *J Am Chem Soc*, *122*(8), 1832–1833.

Sakthivel, T., Toth, I., & Florence, A. T. (1999). Distribution of a lipidic 2.5 nm diameter dendrimer carrier after oral administration. *Int J Pharm*, *183*(1), 51–55.

Sanchez-Sancho, F., Perez-Inestrosa, E., Suau, R., Mayorga, C., Torres, M. J., & Blanca, M. (2002). Dendrimers as carrier protein mimetics for Ige antibody recognition. Synthesis and characterization of densely penicilloylated dendrimers. *Bioconjug Chem*, *13*(3), 647–653.

Sedlakova, P., Svobodova, J., Miksik, I., & Tomas, H. (2006). Separation of poly(amidoamine) (PAMAM) dendrimer generations by dynamic coating capillary electrophoresis. *J Chromatogr B Analyt Technol Biomed Life Sci*, *841*(1–2), 135–139.

Shaunak, S., Thomas, S., Gianasi, E., Godwin, A., Jones, E., Teo, I., Mireskandari, K., Luthert, P., Duncan, R., Patterson, S., Khaw, P., & Brocchini, S. (2004). Polyvalent dendrimer glucosamine conjugates prevent scar tissue formation. *Nat Biotechnol*, *22*(8), 977–984.

Shi, X., Patri, A. K., Lesniak, W., Islam, M. T., Zhang, C., Baker, J. R., Jr., & Balogh, L. P. (2005). Analysis of poly(amidoamine)-succinamic acid dendrimers by slab-gel electrophoresis and capillary zone electrophoresis. *Electrophoresis*, *26*(15), 2960–2967.

Singh, B., & Florence, A. T. (2005). Hydrophobic dendrimer-derived nanoparticles. *Int J Pharm*, *298*(2), 348–353.

Svenson, S., & Tomalia, D. A. (2005). Dendrimers in biomedical applications – reflections on the field. *Adv Drug Deliv Rev*, *57*(15), 2106–2129.

Tack, F., Bakker, A., Maes, S., Dekeyser, N., Bruining, M., Elissen-Roman, C., Janicot, M., Brewster, M., Janssen, H. M., de Waal, B. F., Fransen, P. M., Lou, X., & Meijer, E. W. (2006). Modified poly(propylene imine) dendrimers as effective transfection agents for catalytic DNA enzymes (DNAzymes). *J Drug Target*, *14*(2), 69–86.

Tajarobi, F., El-Sayed, M., Rege, B. D., Polli, J. E., & Ghandehari, H. (2001). Transport of poly amidoamine dendrimers across Madin-Darby canine kidney cells. *Int J Pharm*, *215*(1–2), 263–267.

Takakura, Y., Mahato, R. I., & Hashida, M. (1998). Extravasation of macromolecules. *Adv Drug Deliv Rev*, *34*(1), 93–108.

Tang, M. X., Redemann, C. T., & Szoka, F. C., Jr. (1996). In vitro gene delivery by degraded polyamidoamine dendrimers. *Bioconjug Chem*, *7*(6), 703–714.

Tang, S., Martinez, L. J., Sharma, A., & Chai, M. (2006). Synthesis and characterization of water-soluble and photostable L-DOPA dendrimers. *Org Lett*, *8*, 4421–4424.

Tansey, W., Ke, S., Cao, X. Y., Pasuelo, M. J., Wallace, S., & Li, C. (2004). Synthesis and characterization of branched poly(L-glutamic acid) as a biodegradable drug carrier. *J Control Release*, *94*(1), 39–51.

Tomalia, D. A. (1993). Starburst^{TM}/cascade dendrimers: Fundamental building bocks for new nanoscopic chemistry set. *Aldrichimica Acta*, *26*(4), 91–101.

Tomalia, D. A. (2004). Birth of a new macromolecular architecture: Dendrimers as quantized building blocks for nanoscale synthetic organic chemistry. *Aldrichimica Acta*, *37*(2), 39–57.

Tomalia, D. A., Naylor, A. M., & Goddard III, W. A. (1990). Starburst dendrimers. Molecular-level control of size, shape, surface chemistry, topology, and flexibility from atoms to macroscopic matter. *Angew Chem Int Ed Engl*, *29*(2), 138–175.

Tomlinson, R., Heller, J., Brocchini, S., & Duncan, R. (2003). Polyacetal-doxorubicin conjugates designed for pH-dependent degradation. *Bioconjug Chem*, *14*(6), 1096–1106.

Torchilin, V. P. (2006). Multifunctional nanocarriers. *Adv Drug Deliv Rev*, *58*(14), 1532–1555.

Trewhella, J., Gallagher, S. C., Krueger, J. K., & Zhao, J. (1998). Neutron and x-ray solution scattering provide insights into biomolecular structure and function. *Sci Prog*, *81*(Pt 2), 101–122.

Turnbull, W. B., & Stoddart, J. F. (2002). Design and synthesis of glycodendrimers. *J Biotechnol*, *90*(3–4), 231–255.

Velazquez, A. J., Carnahan, M. A., Kristinsson, J., Stinnett, S., Grinstaff, M. W., & Kim, T. (2004). New dendritic adhesives for sutureless ophthalmic surgical procedures: In vitro studies of corneal laceration repair. *Arch Ophthalmol*, *122*(6), 867–870.

Wang, S. J., Brechbiel, M., & Wiener, E. C. (2003). Characteristics of a new MRI contrast agent prepared from polypropyleneimine dendrimers, generation 2. *Invest Radiol*, *38*(10), 662–668.

Wiener, E. C., Brechbiel, M. W., Brothers, H., Magin, R. L., Gansow, O. A., Tomalia, D. A., & Laterbur, P. C. (1994). Dendrimer-based metal chelates: A new class of magnetic resonance imaging contrast agents. *Magn Reson Med*, *31*(1), 1–8.

Wignall, G. D., & Melnichenko, Y. B. (2005). Recent applications of small-angle neutron scattering in strongly interacting soft condensed matter. *Rep Prog Phys*, *68*(8), 1761–1810.

Wiwattanapatapee, R., Carreno-Gomez, B., Malik, N., & Duncan, R. (2000). Anionic PAMAM dendrimers rapidly cross adult rat intestine in vitro: A potential oral delivery system? *Pharm Res*, *17*(8), 991–998.

Wu, P., Malkoch, M., Hunt, J. N., Vestberg, R., Kaltgrad, E., Finn, M. G., Fokin, V. V., Sharpless, K. B., & Hawker, C. J. (2005). Multivalent, bifunctional dendrimers prepared by click chemistry. *Chem Commun (Camb)* (46), 5775–5777.

Wu, P., Feldman, A. K., Nugent, A. K., Hawker, C. J., Scheel, A., Voit, B., Pyun, J., Frechet, J. M., Sharpless, K. B., & Fokin, V. V. (2004a). Efficiency and fidelity in a click-chemistry route to triazole dendrimers by the copper(I)-catalyzed ligation of azides and alkynes. *Angew Chem Int Ed Engl*, *43*(30), 3928–3932.

Wu, X. Y., Huang, S. W., Zhang, J. T., & Zhuo, R. X. (2004b). Preparation and characterization of novel physically cross-linked hydrogels composed of poly(vinyl alcohol) and amine-terminated polyamidoamine dendrimer. *Macromol Biosci*, *4*(2), 71–75.

Yoo, H., & Juliano, R. L. (2000). Enhanced delivery of antisense oligonucleotides with fluorophore-conjugated PAMAM dendrimers. *Nucleic Acids Res*, *28*(21), 4225–4231.

Yordanov, A. T., Lodder, A. L., Woller, E. K., Cloninger, M. J., Patronas, N., Milenic, D., & Brechbiel, M. W. (2002). Novel iodinated dendritic nanoparticles for computed tomography (CT) imaging. *Nano Lett*, *2*(6), 595–599.

Zhuo, R. X., Du, B., & Lu, Z. R. (1999). In vitro release of 5-fluorouracil with cyclic core dendritic polymer. *J Control Release*, *57*(3), 249–257.

Ziemer, L. S., Lee, W. M., Vinogradov, S. A., Sehgal, C., & Wilson, D. F. (2005). Oxygen distribution in murine tumors: Characterization using oxygen-dependent quenching of phosphorescence. *J Appl Physiol*, *98*(4), 1503–1510.

15

Nanoemulsions for Intravenous Drug Delivery

Jonathan P. Fast and Sandro Mecozzi

Introduction

Nanoemulsions are composed of nanoscale droplets of one immiscible liquid dispersed within another. Many drugs are hydrophobic, which leads to limited water solubility, causing the delivery of water-insoluble drugs to be a primary focus of drug delivery research. Emulsions provide a central oil core, stably dispersed in water, that can act as reservoir for hydrophobic drugs. While emulsions have long been used for topical administration, the small size of nanoemulsions makes them attractive for parenteral delivery. In addition to solubilization of hydrophobic drugs, emulsions can reduce pain or irritation upon injection, improve pharmacokinetics, allow for new forms of administration, and can provide for sustained or targeted release.

Emulsion Definitions

Emulsions have been broadly defined as two immiscible phases dispersed within another (Becher, 2001). In principle, this definition could apply to a number of systems including, but not limited to, gas-in-liquid, solid-in-liquid, or gas-in-solid. In conventional usage, however, the term solely refers to a liquid-in-liquid dispersion, The definition supplied by the United States Pharmacopeia is that emulsions are two-phase systems in which one liquid is dispersed throughout another liquid in the form of small droplets (*The United States Pharmacopeia*, 2006). Emulsions are not thermodynamically stable, but the stability can be improved by additives such as surfactants and finely divided solids. Within that definition there is no defined size boundary, either inherent or implied.

The two phases are referred to as the continuous and the dispersed phase, with the dispersed phase typically present as a smaller volume percentage. Highly concentrated emulsions, where the dispersed phase is more than 50 vol%, have been studied, but the high viscosity makes them unsuitable for intravenous drug delivery applications. A dispersion of oil in water, of most interest for pharmaceutical applications, is referred to as

M.M. de Villiers et al. (eds.), *Nanotechnology in Drug Delivery*, DOI: 10.1007/978-0-387-77667-5_15,

an oil-in-water (o/w) emulsion. For o/w emulsions the emulsifying agent is typically more soluble in the aqueous phase. The reverse emulsion, water-in-oil, is abbreviated w/o and is stabilized by surfactants that are more stable in the oil phase. Multiple phase emulsions such as w/o/w have been increasingly investigated for drug delivery use in recent years, but will not be addressed further here (Khan, Talegaonkar, Iqbal, Ahmed, & Khar, 2006).

Microemulsions

Microemulsions are isotropic, thermodynamically stable systems composed of oil, water, and surfactant. First reported by Schulman in 1943, the term microemulsion was coined by the same author in 1959 (Hoar & Schulman, 1943; Schulman, Stoeckenius, & Prince, 1959). The choice of nomenclature has been lamented by multiple authors as "confusing an emulsion phase with a thermodynamic phase" (Becher, 2001; Mason, Wilking, Meleson, Chang, & Graves, 2006), but it is still the historic and traditional usage. While thermodynamic stability, and not size, is the defining hallmark of a microemulsion, the droplet sizes are below 100 nm (and many times much smaller) (Jadhav, Shaikh, Ambade, & Kadam, 2006).

Nanoparticles

Nanoparticles are considered submicron colloidal systems, generally composed of polymers (Hillaireau & Couvreur, 2006). This general category can be divided into nanospheres, which consist of a polymeric matrix with drugs dispersed throughout, and nanocapsules, which have a polymeric wall enveloping a liquid core. In principle, the nature of the stabilizer should not alter the type or classification of the aggregate. Therefore, liquid containing nanocapsules should be considered as a subset of emulsions, not a fundamentally different vehicle. For that reason, this review will consider all systems with a dispersed oil core that is liquid at room temperatures (and in vivo), whether stabilized by polymers or not. One type of nanoparticle, which is differentiated from any of the above terms, is a solid lipid nanoparticle (SLN) with a lipid core that is solid at room temperature. During formation of SLNs the solid lipid is first melted, then emulsified as a liquid to form an o/w emulsion, and cooled to allow the lipid to solidify. Due to the similarity in formation and content, these particles have been referred to as "emulsions with solid fat globules" (Siekmann & Westesen, 1998). Though inclusion of these systems would not be inappropriate within this chapter, as stated previously only emulsions that have a liquid core at room temperature will be considered.

Nanoemulsion Definitions

As mentioned previously, the term emulsion carries with it no size connotation. Historically there have been efforts to delineate the smallest end of the size range, generally below 1 μm, with unique nomenclature such as miniemulsions (El-Aasser & Sudol, 2004) ultrafine emulsions (Nakajima,

1997) and submicron emulsions (Amselem & Friedman, 1998). Recently, the term nanoemulsion has come into more widespread usage, but it has not been used with consistent meaning. There have been three ways the term has been used. The first is as a replacement for the term microemulsion, to refer to systems that are defined by thermodynamic stability but have a small size (Sarker, 2005). The second is a more precise incarnation of the terms listed above, such as miniemulsion, to refer to emulsions that are smaller in size than 1 μm, i.e., in the nanometer range (Solans, Izquierdo, Nolla, Azemar, & Garcia-Celma, 2005). The third usage parallels the term nanotechnology in referring to emulsions that have a size near 100 nm (Mason et al., 2006). Though the prefix micro might give a misleading size connotation considering the low nanometer size range of microemulsions, the longstanding historical precedence of the term microemulsion should prevent change to the nomenclature. Furthermore, if the term was changed, it would be best to remove the word emulsion from the name completely so that there is no confusion over the level of thermodynamic stability. Microemulsions are thermodynamically stable, whereas emulsions, regardless of the size, are not. For these reasons, the term nanoemulsion should not be used as a substitute for the term microemulsion to refer to a thermodynamically stable system.

The lack of thermodynamic stability is a trait of all emulsions, so size is the only remaining distinguishing criteria. The US government's National Nanotechnology Initiative has defined nanotechnology as "the understanding and control of matter at dimensions of roughly 1–100 nm," which has become the conventional usage of the word. In correlation with the term nanotechnology, some have sought to define nanoemulsions as emulsions with droplet sizes below 100 nm. Even within that definition, there have been divided opinions as to whether the size should refer to the radius or the diameter (Mason et al., 2006). Though this usage might match current language trends, it establishes an arbitrary size boundary because emulsion properties do not instantly change upon crossing the 100 nm threshold.

Nanomemulsions are often mentioned as being translucent or transparent, rather than the characteristic opaque, milky white of traditional emulsions (Mason et al., 2006; Solans et al., 2005). While emulsion droplets do become translucent or transparent at sizes smaller than the optical wavelengths of visible light, the transition does not happen precisely at 100 nm. Furthermore, optical properties of an emulsion are also dependent on the volume fraction of the dispersed phase. A milky-white emulsion can become translucent upon dilution, though there is no reduction in the particle size. Since the properties of the droplet do not change upon dilution, neither should the nomenclature be changed.

It has also been stated that nanoemulsions are stable to creaming or sedimentation (Solans et al., 2005). The stated justification is that at smaller particle sizes the Brownian motion of the droplets is great enough to overcome the effects of gravity (Mason et al., 2006). However, creaming is dependent not only on size but also on the relative densities of the two phases. An o/w emulsion with an oil density of 0.97 g/mL will be much more resistant to creaming than an o/w emulsion with an oil density of 1.8, even if both emulsions have droplets of the same size. Though it is possible

to have nanoemulsions in which creaming does not occur, as with optical properties there is no specific cutoff at 100 nm.

Others have used the term nanoemulsion to mean emulsions that have a diameter in the nanometer range, i.e., below 1000 nm (Solans et al., 2005). This definition offers the most clarity and precision of meaning, by clearly stating that nanoemulsions are emulsions of a certain size, which is indicated by the prefix. A nanoemulsion should then be defined as a heterogeneous system composed of one immiscible liquid dispersed as droplets within another liquid, where the average droplet diameter is below 1000 nm.

However, size is one of the most important variables that can define an emulsion. The name nanoemulsion alone does not eliminate the necessity of using size as a primary defining characteristic. There will be more difference between a nanoemulsion with diameter of 50 nm and one with a diameter of 500 nm, than between a nanoemulsion with diameter of 900 nm and an emulsion with diameter of 1100 nm, even if the names are the same in the former comparison and different in the latter.

Formation of Nanoemulsions

As non-equilibrium systems, the formation of nanoemulsions requires an input of energy. This energy can be supplied by either mechanical equipment or the chemical potential inherent within the components (Solans et al., 2003). Systems that form spontaneously by self-assembly are thermodynamically stable and hence not emulsions.

Though energy is required for formation, the necessary amount varies. An active area of research involves low-energy emulsion formation, so-called spontaneous emulsification or self-emulsification (Gupta & Cannon, 2000; Miller, 2006). In this situation, an emulsion will form spontaneously upon addition of oil and surfactants to water due to the low interfacial tension from high surfactant levels. These systems are envisioned as a technique for oral drug delivery where gentle agitation provided by the gastrointestinal (GI) tract supplies any necessary energy (Gupta & Cannon, 2000).

Phase-Inversion Temperature

Nonionic surfactants containing a polyoxyethylene polar group become more lipophilic with increasing temperatures as the polyoxyethylene chains become dehydrated (Solans et al., 2003). A surfactant that is more soluble in the aqueous phase will favor the formation of o/w emulsions at low temperatures, but at high temperatures w/o emulsions will be more favored. The temperature at which the phase transition occurs has been called the phase-inversion temperature (PIT) (Shinoda & Saito, 1968). Emulsification at the PIT temperature is favorable and requires a minimal energy input, but the droplets formed are unstable (Salager, Loaiza-Maldonado, Miñana-Pérez, & Silva, 1982). Rapid cooling (or heating) can produce kinetically stable emulsions with small droplet sizes and narrow size distributions (Friberg & Solans, 1978). This method is widely

utilized in industrial emulsion formation (Forster & Von Rybinski, 1998). As might be expected, the PIT can be varied by altering the length of either the hydrophobic chain or the polyoxyethylene chain to make the molecule more hydrophobic or hydrophilic.

High-Energy Emulsification

High-energy emulsification methods involve the introduction of mechanical shear through such equipment as high-shear stirrers, high-pressure homogenizers, microfluidizers, or ultrasound generators. A microfluidizer is the piece of equipment most used in the pharmaceutical industry for the production of emulsions (Jafari, He, & Bhandari, 2006). It works by dividing a stream of liquid into two parts, passing each through a narrow opening and then colliding the streams under high pressure. The high-shear forces created by the collision provide very fine emulsions with generally narrow particle size distributions. In typical usage, a coarse emulsion (diameter > 1 μm) is first formed by some other method, and the size of that larger emulsion is reduced in the microfluidizer. The final droplet size and distribution shape will be dependent on both the emulsion components (surfactant amount, oil volume percent, etc.) and the processing parameters (time, temperature, pressure, etc.). As the desired droplet size decreases, the energy required for formation increases. Ultrasonic emulsification is also effective to reduce the size of emulsion droplets into the nanoscale. However, it is only appropriate for a smaller laboratory scale, and not for production level (Walstra & Smulders, 1998).

Emulsion Physical Properties

Though not thermodynamically stable systems, long-term kinetic stability is of paramount importance for nanoemulsions intended for commercial use, especially for drug delivery. Some of the necessary variables to monitor are particle (droplet) size, viscosity, osmolarity, zeta potential, pH, and conductivity for physical and chemical stabilities of the constituent parts (Gupta & Cannon, 2000). Nanoemulsions often contain unsaturated lipids, which can be susceptible to oxidation or hydrolysis.

Emulsion Destabilization

Emulsions in general, nanoemulsions included, can be destabilized by the following mechanisms: creaming (Becher, 2001) (or sedimentation), flocculation (Petsev, Denkov, & Kralchevsky, 1995; Verwey & Overbeek, 1948), coalescence (Kabalnov & Wennerstrom, 1996), or Ostwald ripening (Taylor, 1998). All of these mechanisms have been extensively reviewed elsewhere and therefore the specific relation to nanoemulsions will be emphasized.

Creaming is the separation of emulsion components based on the density of the droplets. The name is derived from the separation of the cream in unhomogenized milk (Becher, 2001). While creaming is usually

considered to be undesirable, the process does not result in irreversible breaking of the droplets. Oil that is less dense than water will rise while oil that is more dense (such as with perfluorocarbon liquids) will settle to the bottom (sediment). It is routinely stated that the small size of nanoemulsions prevents creaming. While this is true in some instances, a more thorough explanation is necessary.

Creaming is driven by gravitational forces. A theoretical treatment called the colloidal law of atmospheres (Russel, Saville, & Schowalter, 1989) has been developed to relate the gravitational potential energy of a droplet at height h above a surface with thermal energy:

$$mgh = k_B T \tag{1}$$

where m is the buoyant mass of a droplet, g is the acceleration of gravity, h is the height, k_B is Boltzmann's constant, and T is the absolute temperature. The mass of a droplet, m, is defined by

$$\frac{4}{3}\pi r^3 \Delta\rho \tag{2}$$

where r is the droplet radius and $\Delta\rho$ is the difference in density between the two phases. If $\Delta\rho$ is 0.1 g/cm^3, a particle with radius of 500 nm will have a gravitational height $\approx$ 0.01 mm, which means that creaming will occur. At the same density a particle with radius of 10 nm will have a gravitational height $\approx$100 cm, well above the height of most containers, and thus creaming will be prevented. However, with that same density difference, a particle with radius of 50 nm will have a gravitational height $\approx$ 0.8 cm so creaming will occur. Furthermore, this analysis only considers a situation where droplets repulse each other and there is no interaction with the solvent. If there is attraction between droplets, creaming can occur regardless of the size. Favorable electrostatic interactions between the droplets and the solvent, which are unaccounted for in this equation, also affect the rate of creaming. The end result is that the smallest nanoemulsions are stabilized against creaming, a significant advantage over macroemulsions, but only if densities of the dispersed phase and the continuous phase are fairly even.

Flocculation refers to a process in which clusters of two or more droplets behave kinetically as a unit, but individual droplets still maintain their identity (Becher, 2001). It is reversible, but may lead to coalescence, which is irreversible. In systems stabilized by nonionic surfactants, the droplets are attracted by van der Waals forces, but repulsed by steric interactions (Solans et al., 2003). The steric repulsion between emulsion droplets, W_s, can be represented by the following equation:

$$W_s \infty k_B T e^{-\pi D/L} \tag{3}$$

where k_B is the Boltzmann constant, T is the absolute temperature, D is the separation distance between droplet surfaces, and L is the film thickness of the adsorbed polymer. If the total interaction energy is smaller than the

energy imparted from Brownian motion, $\sim k_B T$, the particles will remain unflocculated. An increase in the film thickness, L, will increase W_s and thus lead to more stable emulsions. The van der Waals attractive potential between two spherical droplets (with identical radius) is linearly dependent on the radius, with the following relationship (Israelachvili, 1991):

$$W_{vdw} = \frac{-Ar}{12D} \tag{4}$$

where A is the Hamaker constant, r is the radius of the droplets, and D is the distance of separation between droplets. As the radius of the particles decreases, the attractive potential decreases. Therefore, in nanoemulsions with a small radius and large enough film thickness, flocculation can be prevented, another advantage over macroemulsions.

Coalescence is the collision, and subsequent irreversible fusion, of two droplets. The ultimate end of coalescence is complete phase separation. Flocculation precedes coalescence, so the same methods that are appropriate for prevention of flocculation also prevent coalescence. A thick, surfactant film adsorbed at the interface is often sufficient to prevent coalescence, whether in nano- or macroemulsions. However, with the same polymeric thickness, the stabilization will be greater for a nanoemulsion because the polymer layer will be a greater percentage of the total diameter.

Ostwald ripening is the growth in the size of emulsion droplets as the contents of one drop diffuse into another. The driving force for this growth is the difference in chemical potential between droplets, which is generally not substantial for droplets larger than 1 μm. Therefore, Ostwald ripening primarily affects nanoemulsions and is the most serious instability concern for nanoemulsions (Tadros, Izquierdo, Esquena, & Solans, 2004). This effect is related to the Laplace equation for spheres:

$$\Delta p = 2\gamma / r \tag{5}$$

where p is the pressure across an interface, γ is the interfacial tension, and r is the radius of the sphere.

Kelvin adjusted this equation to describe the difference in vapor pressure between a small droplet of a liquid and the bulk liquid, the situation found in an emulsion:

$$RT \ln \frac{p}{p^0} = \frac{2\gamma[V]}{r} \tag{6}$$

where R is the gas constant, T is the absolute temperature, p is the vapor pressure of the bulk, p^0 is the vapor pressure of the droplet with radius r, γ is the interfacial tension, and $[V]$ is the molar volume of the liquid.

As the radius increases, the pressure difference is reduced and the dispersed droplets become more soluble in the continuous phase. If there is any diffusion of the contents of the dispersed phase, large droplets will grow larger at the expense of smaller droplets and the average size of the particle distribution will continually increase. This effect

has been described by Lifshitz and Slyozov (Lifshitz & Slyozov, 1961) and independently by Wagner (Wagner, 1961). According to Lifshitz–Slyozov–Wagner (LSW) theory, the rate of Ostwald ripening, ω, can be expressed by the following equation:

$$\omega = \frac{\mathrm{d}r^3}{\mathrm{d}t} = \frac{8DC_\infty \gamma M}{9\rho^2 RT} \tag{7}$$

where r is the radius of the droplets, t is the time of storage, D is the diffusion coefficient of the molecules of the dispersed phase in the continuous phase, C_∞ is the bulk solubility of the dispersed phase in the continuous phase, γ is the interfacial tension between phases, M is the molar mass of the dispersed phase, ρ is the density of the dispersed phase, R is the gas constant, and T is the absolute temperature. However, the overall diffusion of the dispersed phase is affected by the diffusion across the interfacial layer in addition to the diffusion in the continuous medium, D. If the diffusion across the interface is slower than diffusion through the medium, then the overall rate of ripening will be slower than predicted. As can be seen, the cube of the particle radius varies linearly with time. For an o/w emulsion, the rate of ripening is directly related to the water solubility of the oil and ripening can even be seen in systems where the solubility is in the low nM range.

It should be noted that in the ideal situation of a perfectly monodispersed distribution there would be no ripening because there would be no differences in solubility of droplets based on size. Thus, narrow distributions will be more resistant to Ostwald ripening than broader distributions.

Higuchi and Misra suggested that the addition of a secondary, less water-soluble, component, could slow ripening (Higuchi & Misra, 1962). The slower diffusion of the secondary component will lead to a heterogeneous distribution with smaller droplets enriched in the less soluble component and larger droplets enriched in the more soluble component. However, this internal segregation will be thermodynamically opposed as osmotic pressure will act to limit differences between droplets and equilibrium will eventually be reached. This principle has been successfully applied with hydrocarbon (Taylor, 1998) and fluorocarbon emulsions (Sharma, Lowe, & Davis, 1988; Weers, Ni, Tarara, Pelura, & Arlauskas, 1994).

The rate of ripening of a two-component disperse phase system is represented by the following equation (Kabalnov & Shchukin, 1992):

$$\omega_{mix} = (\phi_1/\omega_1 + \phi_2/\omega_2)^{-1} \tag{8}$$

where ϕ represents the volume fraction and the subscripts 1 and 2 refer to the more and less water-soluble components, respectively. As ϕ_2 becomes larger, it becomes the dominant term until it solely controls the ripening rate. With a properly chosen additive, Ostwald ripening can be effectively eliminated.

There have been contradictory reports within the literature regarding the effect of excess surfactant upon emulsion stability (Taylor, 1998). In some instances, the rate of ripening has increased as the amount of surfactant has increased, whether the excess surfactant is present in the form of vesicles (Krafft, Rolland, & Riess, 1991) or micelles (Capek, 2004; Izquierdo et al., 2002; Taylor, 2003). One of the justifications cited for such an effect is that the supramolecular aggregate (micelle or vesicle) provides a reservoir to solubilize excess oil, thus increasing the effective solubility of the oil in water. As can be seen in Eq. (7), as the solubility, C_∞, increases, so too does the rate of ripening. However, a decrease in the ripening rate as the amount of surfactant increases has also been reported (De Smet, Deriemaeker, & Finsy, 1999; Liu, Sun, Li, Liu, & Xu, 2006). In these cases, it has been proposed that the oil solubilized in the micelles is not dispersed in the continuous phase, and therefore is not subject to the same mass transfer between droplets. In this argument, C_∞ is lowered as oil is withdrawn from the continuous phase into micelles, thus causing the ripening rate to decrease. An additional study showed that alkane emulsions stabilized by hexaethylene glycol dodecyl ether were unaffected by surfactant concentration (Hoang, La, Deriemaeker, & Finsy, 2003).

Though Ostwald ripening can be present in nanoemulsions, it has some advantages for pharmaceutical development. The ripening rate provides clear criteria for determining the acceptability of formulations. Commercialization of an emulsion mandates stability for at least 18 months (Gupta & Cannon, 2000). The rate of ripening allows the estimation of long-term stability, which in turn suggests guidelines for specifications and expiration dates. If the ripening rate is too rapid, then the nanoemulsion will be unacceptable for pharmaceutical use.

The instability of emulsions can also have some drawbacks. For emulsions intended for parenteral injection the FDA requires sterilization (*The United States Pharmacopeia*, 2006). The most commonly employed form, terminal heat sterilization such as with an autoclave, can often affect the physical stability of the emulsion droplets. Additionally, emulsions are often stored at 5°C for greater stability, which places limits on the product use and storage (Gupta & Cannon, 2000).

Emulsions for Intravenous Drug Delivery

Historical

Though not traditionally labeled as nanoemulsions, phospholipid-stabilized soybean oil emulsions were the first approved intravenous emulsion (Benita, 1998) and have been used clinically as i.v. nutritional supplements for over 40 years (Driscoll, 2006). With an average particle diameter around 300 nm these systems fall in the nano range, which makes them the first therapeutic nanoemulsion. Either egg or soy lecithin is used to emulsify an oil from a natural vegetable source (e.g., soybean). Because of the stabilizer, these emulsions are sometimes called lipid microspheres. Phosphatidylcholine (PC) is the primary component of lecithin, but the amount varies depending

on the degree of purification. Lipoid E80, a commonly used surfactant mixture, contains 80% PC. Phosphatidylethanolamine is the secondary component, followed by phosphatidylserine and phosphatidylinositol present in smaller amounts (*The United States Pharmacopeia*, 2006). As they are not intended for drug delivery per se, the history and development of these emulsions for nutritional purposes will not be discussed further (Figure 15.1).

Intravenous emulsions, like all parenteral products, are required to meet pharmacopeial requirements to be sterile, isotonic, nonpyrogenic, nontoxic, biodegradable, and stable, both physically and chemically (Benita & Levy, 1993). The biocompatibility of emulsions for parenteral nutrition, and concomitant FDA approval, has led them to be a template for future nanoemulsion development. The initial examples of nanoemulsions for drug delivery were all conceptually similar to nutritional emulsions. This similarity could take two forms: either extemporaneous development, where a drug is added to a pre-made commercially available emulsion, or de novo emulsification where an emulsion is made "from scratch" using the same components found in nutritional emulsions (Klang & Benita, 1998). In recent years, development has continued into more innovative emulsion formulations, such as varying the emulsified oil and/or including polymeric emulsifiers.

A number of excellent reviews concerning nanoemulsions for drug delivery appeared in the late 1990 s to 2000 (Buszello & Müller, 2000;

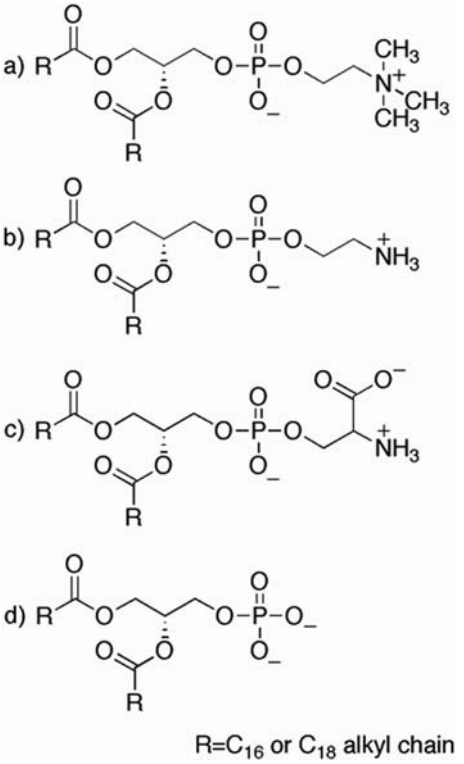

Figure 15.1 Structure of phospholipids present in lecithin, often used as an emulsifier for nanoemulsions: (**a**) phosphatidylcholine (**b**) phosphatidylethanolamine, (**c**) phosphatidylserine, and (**d**) phosphatidylinositol.

Table 15.1 Nanoemulsions that have been marketed for intravenous delivery. Emulsions for parenteral nutrition are not included in the list. Companies listed are those that originally developed the emulsion. In subsequent years, corporate mergers may have led to name changes, e.g., Zeneca has now become AstraZeneca.

Trade name	Drug	Company	Use	Market
Diprivan®	Propofol	Zeneca Pharmaceuticals, UK	General anesthesia	Worldwide
Limethason®	Dexamethasone palmitate	Green Cross, Japan	Chronic rheumatoid arthritis	Japan and Germany
Lipo-NSAID® Ropion®	Flurbiprofen axetil	Kaken Pharmaceutical Co., Japan	Post-operative and cancer pain	Japan
Liple®	Alprostadil (PGE1)	Green Cross, Japan	Peripheral vascular disorders and maintenance and patent ductus arteriosus	Japan
Diazemuls®	Diazepam	Kabi-Pharmacia, Sweden	Treatments for excitation, anxiety, tension, sedation, muscle spasm, convulsions, tetanus, delirium	Europe, Canada, Australia
Diazepam-Lipuro®		Braun, Germany		
Dizac®		Ohmeda Pharmaceuticals		
Etomidat Lipuro®	Etomidate	Braun, Germany	General anesthesia	Germany
Fluosol-DA®	Perfluorodecalin, Perfluoro-tripropylamine	Green Cross, Japan	Artificial blood substitutes	Worldwide

Gupta & Cannon, 2000; Klang & Benita, 1998). For that reason, specific examples in the following section will exclusively focus on the time period since 2000. Furthermore, though nanoemulsions have also been widely studied for oral and topical delivery, intravenous delivery will be the sole focus of this review. A comprehensive list of all marketed nanoemulsions for intravenous delivery (nutritional emulsions excluded) can be found in Table 15.1. Extended discussions for each example can be found elsewhere (Klang & Benita, 1998).

Marketed

[Table 15.1] presents nanoemulsions that have been marketing for intravenous delivery.

Current Research

While it is apparent that nanoemulsions (as with any drug delivery vehicle) will only be investigated if it is believed that an emulsion formulation can improve drug performance in some way, the nature of that enhancement can take many forms. Perhaps the most obvious improvement is for the solubilization of drugs with a low aqueous solubility.

Other areas of study include the reduction of pain/irritation upon injection, reduced toxicity of the drug in vivo, improved pharmacokinetics of the drug, or the possibility of a new method of delivery (e.g., intravenous versus oral administration). Nanoemulsion formulations can also provide drug targeting or multiple functionalities with imaging coupled to therapy. Finally, nanoemulsions can create a new therapeutic area that would not be present without emulsions, such as with fluorocarbon emulsions intended for blood substitutes. The following paragraphs will discuss examples for each of the above categories. Of course, some examples of nanoemulsion formulation will encompass more than one of the above categories, so there will be some unavoidable overlap. Table 15.2 shows a representative list of drugs that have been investigated for intravenous delivery via nanoemulsions since 2000.

Table 15.2 A representative list of drugs investigated for intravenous delivery via nanoemulsions since 2000.

Drug	Reference
All-*trans* retinoic acid	Chansri, Kawakami, Yamashita, and Hashida, 2006
Amphotericin B	Müller et al., 2004
BCH	Shawer, Greenspan, Oie, and Lu, 2002
Carbamazepine	Akkar & Müller, 2003a
Clomethiazole	Nordén, Siekmann, Lundquist, and Malmsten, 2001
Cyclosporin A	Kim, Choi, and Lee, 2002
Dexamethasone palmitate	Seki et al., 2004
Flunarizone	Wang, Wang, Zhang, He, and Tang, 2007
Halofantrine	Mosqueira, Legrand, and Barratt, 2006
Indomethacin	Cruz et al., 2006; Palakurthi, Vyas, and Diwan, 2005; Pohlmann, Weiss, Mertins, da Silveira, and Guterres, 2002
Itraconazole	Akkar and Müller, 2003b
Lorazepam	Medina, Salvadó, and del Pozo, 2001
Menatetrenone	Ueda et al., 2004
mTHPC	Bourdon, Mosqueira, Legrand, and Blais, 2000
Nalbuphine	Wang, Sung, Hu, Yeh, and Fang, 2006
Nimodipine	Yu, He, and Tang, 2006
Norcantharidin	Lixin, Haibing, Xing, Ruiying, and Dawei, 2006
Paclitaxel	Constantinides et al., 2000; Dias, Carvalho, Rodrigues, Graziani, and Maranhão, 2007; Tiwari, Tan, and Amiji, 2006
Pazufloxacin Mesylate	Liu, Huang, Peng, Liu, and Wu, 2007
Probucol	Ishida et al., 2004
Prostaglandin E1	Komori, Aiba, Kushima, Kawasaki, and Kurosaki, 2007
Resveratrol	Hung, Chen, Liao, Lo, and Fang, 2006
Silymarin	Abrol, Trehan, and Katare, 2004
SPK-843	Mozzi, Benelli, Bruzzese, Galmozzi, and Bonabello, 2002
Xanthone	Teixeira, Alonso, Pinto, and Barbosa, 2005
Zinc phthalocyanine	Primo et al., 2007

Solubilization of Poorly Soluble Drugs

As solubilization of poorly soluble drugs is the most apparent application for nanoemulsions, many examples can be found in prior reviews (Gupta & Cannon, 2000; Klang & Benita, 1998). Therefore, only a single representative example will be discussed here. Lorazepam is injected intravenously for premedication and sedation before an operation. It is usually administered as a solution in organic solvents such as propylene glycol. The highest concentration that can be achieved in an aqueous diluent (5% dextrose in water) is 0.05 mg/mL. A phospholipid-stabilized soybean oil emulsion was able to stably emulsify lorazepam at 1 mg/mL, a 20-fold increase, which could significantly reduce the volume needed for injection (Medina et al., 2001).

While emulsion solubilization has been applied to a host of lipophilic drugs, it traditionally cannot be employed if the drug has limited solubility in oils that have regulatory acceptance. One way to counter that deficiency is to position the drug directly in the interfacial lecithin layer. This has previously been achieved by dissolving the drug together with lecithin in an organic solvent, evaporating the solvent, and then using that mixture for de novo emulsification (Lance, Washington, & Davis, 1995). Unfortunately, this method is impractical on an industrial scale. Müller and coworkers devised a method to make the solubilization of drugs at the interfacial layer more feasible on a large scale. With this methodology, termed SolEmuls®, solid nanocrystals of the drug are homogenized with commercially available lipid emulsions, without the need of any organic solvents. In this way, they were able to stably emulsify carbamazepine (Akkar & Müller, 2003a), itraconazole (Akkar & Müller, 2003b), ketoconazole (Akkar, Namsolleck, Blaut, & Müller, 2004), and amphotericin B (Müller et al., 2004).

Reduced Pain/Irritation

At the direct site of intravenous injection, some drugs can cause local irritation. These drugs, as well as certain cosolvents in aqueous solutions, can also cause phlebitis, an inflammation of a vein that can lead to pain or redness. Nanoemulsions eliminate the need for cosolvents, as well as encapsulating drugs that might otherwise be irritants, and in both cases can reduce local irritation upon injection.

Polyene antifungal agents, like amphotericin B, contain a large macrocycle with a series of conjugated double bonds and are typically insoluble in water. Recent efforts have focused on synthesizing new agents that retain the strong antifungal activity while improving the water solubility (Strippoli, D'Auria, Simonetti, Bruzzese, & Simonetti, 2000). One candidate, SPK-843, showed promising antifungal activity but gave mild phlebitis upon repeated intravenous injections. Therefore, it was proposed to study the intravenous injection of SPK-843 in an emulsified form (Mozzi et al., 2002). The drug was extemporaneously added to commercial Intralipid emulsions. After formation, the venous toxicity of the nanoemulsion was tested in the ear vein of rabbits and compared to a 5% glucose solution

of SPK-843. A solution of 5% glucose alone (w/o drug) was tolerated for 17 infusions before vein occlusion due to phlebitis, but when the drug was added only three infusions could be tolerated. With the Intralipid alone, 13 infusions were tolerated, and when the drug was introduced the number remained at 13. Therefore, an emulsified form of the drug reduced the chance of phlebitis compared to an aqueous solution.

In patients with ruptured aneurysms, vasospasm of the cerebral arteries can lead to delayed ischemic deficits, which are responsible for morbidity and mortality. To reduce morbidity and mortality caused by these reasons, nimodipine (NM) is the only available therapy. It is given orally, but its bioavailability is limited. Intravenous injection, as an ethanol solution, has been studied, but leads to irritation. A soybean oil nanoemulsion with lecithin and Tween-80 as the emulsifiers was proposed as a method to reduce irritation (Yu et al., 2006). The irritation was measured both by the rabbit ear vein test, as in the prior example, and by the rat paw lick test. Upon injection of the NM-ethanol solution 100% of the rats licked their paws and the average number of licks was 12, suggesting both a high frequency and a high intensity of pain. With the NM-nanoemulsion formulations, only 60% of the rats licked their paws, and the average number of licks decreased to five, indicating that the both occurrence and intensity of irritation decreased. Furthermore, the nanoemulsions did not alter the pharmacokinetic parameters, as compared to the ethanol solution. Therefore, the in vivo performance was maintained as the pain was reduced.

In another study (Lixin et al., 2006), an anti-cancer drug, norcantharidin, was also formulated in lecithin/Tween-80-stabilized nanoemulsions and the irritation was studied using the rat paw lick test. In this instance, the frequency of rats that licked their paws remained the same at 100% between a solution formulation and a nanoemulsion formulation, but the average number of licks decreased from 18.2 to 8.7, indicating that the intensity of pain was diminished.

Reduced Toxicity of Drug

Beyond the site of injection, drugs or their delivery vehicles can also cause irritation or toxicity once in the body. Paclitaxel is an important chemotherapeutic agent used in the treatment of breast, ovarian, colon, and non-small cell lung carcinomas. The commercially available product Taxol® (Bristol-Myers Squibb) is formulated in a 1:1 v/v mixture of ethanol and polyoxyethylated castor oil (Cremophor EL). Cremophor EL has been associated with bronchospasms, hypotension, and other hypersensitive reactions. To reduce the toxicity associated with Cremophor EL, incorporation of paclitaxel into a wide variety of drug delivery vehicles, including liposomes, micelles, emulsions, and cyclodextrins, has been investigated. A representative nanoemulsion example will be described. Constantinides and coworkers created a nanoemulsion that did not employ any lecithin but used Vitamin E-TPGS (α-tocopherylpolyethyleneglycol-1000 succinate) and Poloxamer 407 to emulsify Vitamin E (DL-α-tocopheryl) as the oil phase (Constantinides et al., 2000). The nanoemulsion droplets had a mean diameter of 67 nm, with 99% below

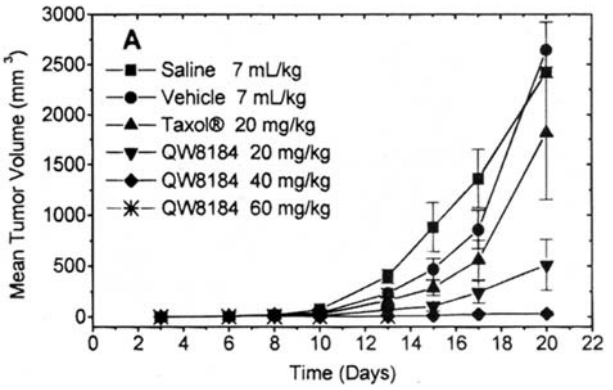

Figure 15.2 Mean tumor regression of B16 melanoma cells in response to QW8184, a paclitaxel nanoemulsion, and Taxol® as a function of time on q3d × 5 schedule. Error bars represent SEM ($n = 8$). Reproduced with permission from Springer.

150 nm, meaning that the emulsions could be filter sterilized with a 0.22 μm filter, an objective of the study. The maximum tolerated dose (MTD) was determined in mice using a tail vein injection. For the commercially available Taxol® formulation the MTD was approximately 20 mg/kg whereas for the nanoemulsion formulation it was approximately 70 mg/kg, over three times greater. The efficacy of the nanoemulsion formulation was assessed with B16 melanoma, a fast-growing solid murine tumor. Nanoemulsions showed increasing efficacy at increasing dosage amounts and were better than the commercial formulation in all cases (Figure 15.2).

Improved Pharmacokinetics

Pharmacokinetics is concerned with the fate of external substances introduced to the body, specifically the extent and rate of absorption, distribution, metabolism, and excretion of compounds. Improving these parameters for more favorable drug performance is a primary objective of drug delivery research in general and for nanoemulsions specifically. One specific parameter that will be mentioned multiple times is the area under the concentration–time curve, abbreviated AUC.

Nalbuphine is a morphine-like drug and one of its advantages over morphine is that it lacks significant withdrawal symptoms. However, due to its short elimination half-life and poor oral bioavailability it needs to be injected every 3–6 h (Lo, Schary, & Whitney, 1987). Prodrugs of nalbuphine have been investigated for parenteral administration, and Fang and coworkers sought to use nanoemulsions for both nalbuphine and its prodrugs (Wang et al., 2006). Egg phospholipid was used as the main emulsifier, along with cosurfactants Brij 30, Brij 98, and stearylamine. Depending on the emulsifier composition the average size ranged from 167 to 314 nm. It was found that the stearylamine-containing emulsions had the highest prodrug encapsulation, while the incorporation of Brij 98 reduced prodrug entrapment, suggesting that the nature of the oil/water interface and the co-emulsifier may affect drug loading. In vivo pharmacokinetic profiles indicate that the plasma concentration of nalbuphine and its prodrugs was enhanced by incorporation into nanoemulsions (Figure 15.3).

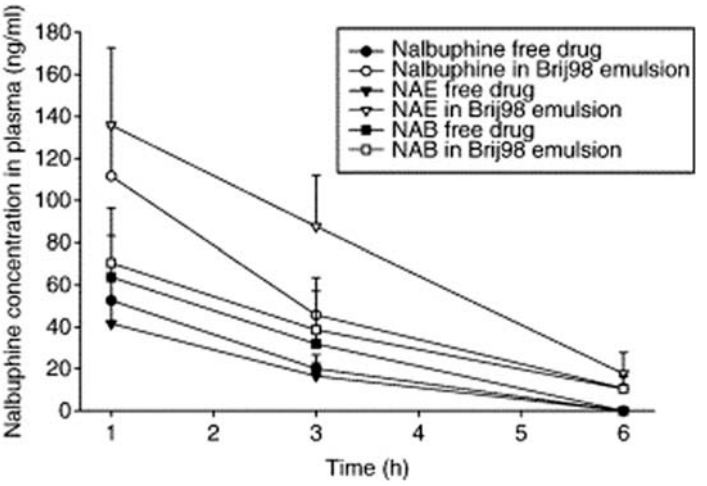

Figure 15.3 In vivo nalbuphine concentration in plasma versus time profiles after intravenous injection of nalbuphine and prodrugs nalbuphine enanthate (NAE) and nalbuphine benzoate (NAB). The free drugs were injected in pH 4 buffer and the emulsions were stabilized by lecithin and Brij 98. Each value represents the mean and SD ($n = 4$). Reproduced with permission from Elsevier.

Tang and coworkers studied the nanoemulsion delivery of flunarizine, a drug used for migraine prophylaxis in which oral administration is marked by low bioavailability and slow absorption (Y. J. Wang et al., 2007). A flunarizine solution (with 5% PEG 400 and 0.2% Tween-80 as stabilizers) and flunarizine-loaded nanoemulsions (both at 1 mg/mL) were compared. While all of the other pharmacokinetic parameters showed no significant difference, the AUC was 1.68 times greater for the nanoemulsion, demonstrating a prolonged circulation time in rats.

Cerebral malaria is a medical emergency that requires treatment that can rapidly reach effective active drug concentrations in vivo (Watkins, Woodrow, & Marsh, 1993). Halofantrine is a well-tolerated and effective antimalarial drug that acts more rapidly than quinine or mefloquine. However, it is given orally and its slow dissolution prevents the rapid therapeutic impact needed to treat cerebral malaria. An intravenous formulation could provide rapid delivery of the drug. A previously investigated parenteral formulation (Krishna et al., 1993) showed local irritation and toxicity. To improve upon those characteristics Barratt and coworkers investigated o/w water nanoemulsions. They demonstrated (Mosqueira et al., 2004) that an emulsion stabilized by poly-D,L-lactide (PLA) and its copolymer methoxy-polyethylene glycol-*co*-poly-D,L-lactide (PLA-PEG) increased the AUC more than sixfold compared to the previous intravenous formulation. In a later work (Mosqueira et al., 2006) poloxamer 188 and lecithin were used in different surfactant combinations with the PLA and PLA-PEG. In all examples, Miglyol® 810 N, a medium chain triglyceride, was used as the oil phase and lecithin as one of the surfactants. Overall, particle diameters of the drug-loaded emulsion ranged from 200 to 350 nm. It was found that the addition of PEG-PLA copolymers increased the emulsion stability compared to those prepared with lecithin alone as well as providing a more consistent, sustained release, which may have application in the treatment of cerebral malaria cases.

Other studies have also shown how PEG coating can affect nanoemulsion circulation and performance in vivo. Palakurthi and coworkers studied the biodisposition of nanoemulsions containing indomethacin, a

non-steroidal anti-inflammatory drug (NSAID) (Palakurthi et al., 2005). Encapsulation in nanoemulsions stabilized by phosphatidylcholine and cholesterol reduced the clearance of the drug by 1.4 compared to the free drug. When the nanoemulsion also contained a DSPE-PEG (1,2-distearoyl-*sn*-glycero-3-phosphoethanolamine-*N*-polyethylene glycol 2000) conjugate in the stabilizing layer, the drug clearance was reduced by a factor of 3. Because of the reduced uptake into tissues such as the liver and spleen, 7.5 times more of the PEG-coated nanoemulsions ended up at the site of inflammation compared to the uncoated nanoemulsion.

Circulation times were also studied by Ueda and coworkers with nanoemulsions containing menatetrenone and stabilized by polyoxyethylated-hydrogenated castor oils (HCOs) (Ueda et al., 2004). They found that plasma half-lives and liver uptake of nanoemulsions stabilized by HCOs with 10 PEG units were similar to and larger than, respectively, emulsions stabilized by egg yolk phospholipids. However, when the length of the PEG chain was increased to 20 and 60 units there was a marked increase in the circulation time and decrease in the liver uptake, suggesting that there is minimum length of PEG necessary to see improved pharmacokinetic parameters.

In another example, an o/w nanoemulsion of cyclosporin A was compared to commercially available formulations for both oral and intravenous delivery (Kim et al., 2002). When the nanoemulsion was delivered intravenously there was little difference with the commercial i.v. formulation (CIPOL Inj.®) and when delivered orally the AUC was actually less than the commercial oral formulation (Sandimmun Neoral®). However, with both routes of administration the pharmacodynamic efficiency was greater and pharmacodynamic availability was improved twofold versus the commercial formulations.

New Method of Delivery

There are many examples where a drug that is normally delivered orally can be incorporated into a nanoemulsion and injected intravenously, some of which are discussed in the pharmacokinetics section. Another instance where nanoemulsions can open up a new method of delivery is the case of volatile anesthetics for general anesthesia. Volatile anesthetics are low-boiling liquids that are given as gases by inhalation. However, if injected directly into the bloodstream, the time for the anesthetic to equilibrate with the lungs is eliminated, which leads to a more rapid onset of anesthesia. Because direct i.v. delivery of the neat anesthetic causes pulmonary damage and death (Kawamoto, Suzuki, & Takasaki, 1992; Kopriva & Lowenstein, 1969; Sandison, Sivapragasam, Hayes, & Woo-Ming, 1970), fat emulsions have been successfully utilized as a means of delivery for halothane, isoflurane, and sevoflurane (Chiari et al., 2004; Eger & MacLeod, 1995; Musser, Fontana, & Mongan, 1999; Zhou, Luo, Liang, & Liu, 2006). However, the modern volatile anesthetics (except for nitrous oxide) are all highly fluorinated, which reduces their solubility in classic hydrogenated oils and makes them more soluble in fluorinated oils. The solubility of sevoflurane in Intralipid (30%) is limited to a mere 3.5%

(Zhou et al., 2006). Cuignet et al. have demonstrated that the presence of Oxygent (a perfluorocarbon emulsion) greatly increases the blood:gas partition coefficient of isoflurane, sevoflurane, and desflurane compared to Intralipid (Cuignet, Baele, & Van Obbergh, 2002). Building upon this information, it was found that a nanoemulsion stabilized by a fluorinated surfactant, with a fluorinated secondary additive to slow the Ostwald ripening, was capable of stably emulsifying up to 25% sevoflurane, a sevenfold increase over Intralipid. The efficacy and safety of this formulation for intravenous delivery was tested in rats with bolus dosing and found to safely induce anesthesia, from which recovery was smooth and rapid (Fast, Perkins, Pearce, & Mecozzi, 2008).

Drug Targeting

As with other drug delivery vehicles, targeted emulsions are of interest. Targeting can either be active, such as the inclusion of a secondary component in the stabilizing monolayer that has a recognition or functional element for a specific site, or passive, where the final destination is dependent on the size or surface characteristics of the particles.

Active Targeting

Rapidly dividing cells, such as cancer cells, require higher amounts of cholesterol to build cell membranes. Low-density lipoprotein (LDL) is the natural carrier of cholesteryl esters in the body and therefore certain tumors have elevated LDL-receptor activity. Lu and coworkers (Shawer et al., 2002) developed a phospholipid-stabilized nanoemulsion to solubilize a cholesteryl ester of carborane, cholesteryl 1,12-dicarba-closo-dodecaborane-1-carboxylate (BCH), which mimics the natural core of LDL and can be used for boron neutron capture therapy (BNCT). The mean emulsion particle size was 155 nm. If preincubated together, human LDL particles and the nanoemulsions only gave one band in agarose electrophoresis, demonstrating particle interaction and ability of BCH to transfer to the human LDL. Cell culture data showed sufficient uptake of BCH in rat 9L glioma cells for the levels necessary for BNCT.

Cholesterol-rich nanoemulsions that mimic LDL have also been studied over the years by Maranhão and coworkers. In a recent example (Dias et al., 2007), paclitaxel was solubilized in cholesteryl oleate nanoemulsions stabilized by egg phosphatidylcholine. The pharmokinetics of the nanoemulsion and its ability to concentrate the drug in tumors was studied in patients with gynecologic cancers (ovarian, cervix, endometrium). It was shown that paclitaxel in nanoemulsions was stable in the bloodstream and the pharmacokinetic profile was improved compared to the commercial formulation (Figure 15.4). Furthermore, on average 3.5 times more paclitaxel was concentrated in malignant tissues versus normal tissues. Together, these results pave the way for future clinical trials of paclitaxel nanoemulsions.

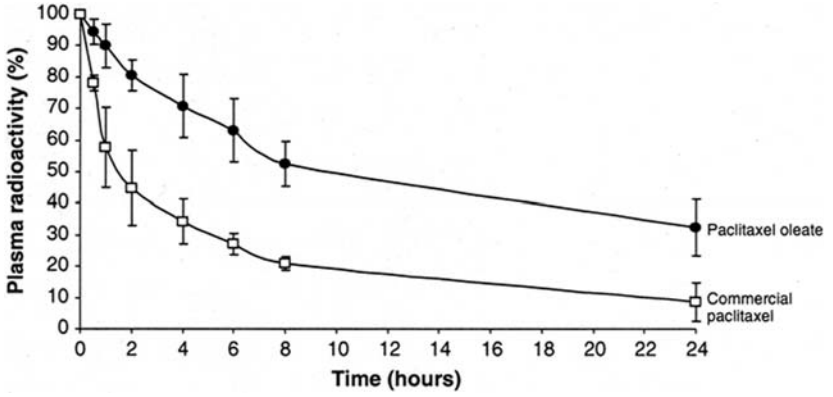

Figure 15.4 Plasma decay curve of nanoemulsion-associated paclitaxel oleate labeled with [^{3}H]-paclitaxel oleate (*filled circle*) and commercial labeled [^{3}H]-paclitaxel (*open square*). Plasma samples were taken over 24 h for radioactive counting in scintillation vials. Results are presented as mean ± SD (*bars*). Reproduced with permission from Springer.

Nanoemulsions have also been used for cell targeting by surface modification with carbohydrates. Hashida and coworkers tested a series of glycosylated emulsions, including galactosylated, mannosylated, and fucosylated. In the first example, a galactose-cholesterol conjugate (Gal-C4-Chol) was inserted into the phosphatidylcholine monolayer of a soybean oil emulsion for hepatocyte-selective targeting in a weight ratio of 70:25:5 soybean oil:PC:Gal-C4-Chol (Ishida et al., 2004). Nanoemulsions containing the Gal-C4-Chol had a higher rate of liver uptake than both emulsions without the Gal-C4-Chol and liposomes with it. Furthermore, a model lipophilic drug, probucol, showed efficient delivery to the liver as compared to Gal-liposomes (Figure 15.5).

A subsequent study showed that the same effect could be achieved with both mannosylated and fucosylated cholesterol conjugates (Yeeprae, Kawakami, Higuchi, Yamashita, & Hashida, 2005). Later work showed

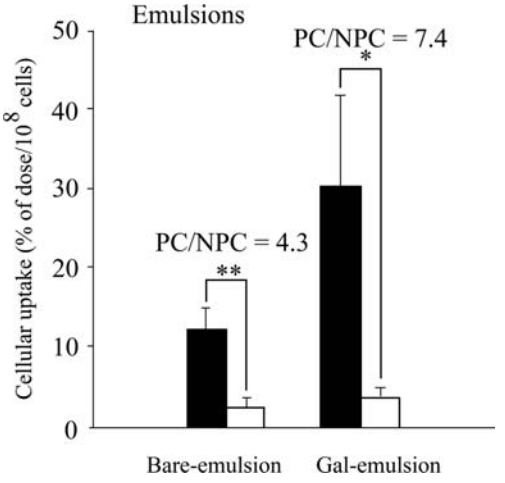

Figure 15.5 Hepatic cellular localization of [^{3}H]-labeled nanoemulsions after intravenous administration into mice. Radioactivity was determined 30 min post-injection in parenchymal cells (PC, filled bar) and non-parenchymal cells (NPC, unfilled bar). Each value represents the mean + SD of three experiments. Statistically significant differences from the control group are shown by *$p<0.05$, **$p<0.01$. Reproduced with permission from Springer.

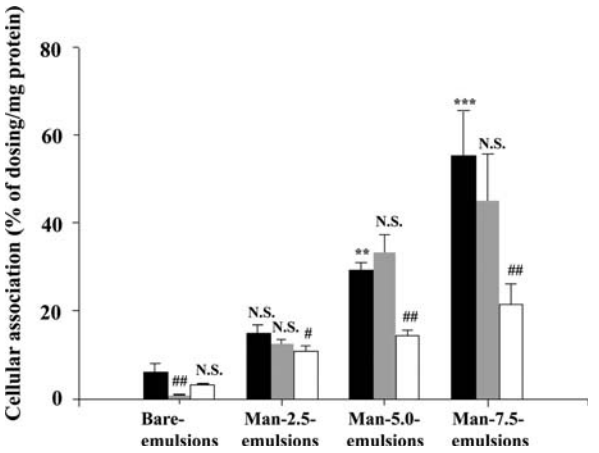

Figure 15.6 Hepatic cellular localization of emulsions after intravenous injection in mice. Radioactivity was determined 30 min post-injection in parenchymal cells (PC, unfilled bar) and non-parenchymal cells (NPC, filled bar). Each value represents the mean ± SD of three experiments. Statistically significant differences between PC and NPC in each group are shown by $*p<0.05$, $***p<0.001$; N.S., not significant. Reproduced with permission from Elsevier.

that the density of mannose on the surface plays a key role in the rate of uptake (Yeeprae, Kawakami, Yamashita, & Hashida, 2006). Nanoemulsions which contained only 2.5% mannose showed no difference in liver accumulation versus the control emulsions, but 5.0 and 7.5% mannose showed an increasingly greater amount of uptake (Figure 15.6).

Some amphiphiles, such as 1-*O*-alkylglycerols, can transiently open the blood brain barrier (BBB) to improve the brain delivery of some anticancer agents (Erdlenbruch, Jendrossek, Eibl, & Lakomek, 2000). Rambhau and coworkers used a variety of 1-*O*-alkylglycerols as cosurfactants along with lecithin to stabilize a soybean oil emulsion for the solubilization of carbamazepine (CBZ), used in the treatment of seizures (Madhusudhan, Rambhau, Apte, & Gopinath, 2007). CBZ is available for oral and chewable tablets, but intravenous delivery could allow for more rapid treatment in acute seizures. The nanoemulsions were around 200 nm in diameter. In emulsions containing 1-*O*-decylglycerol, the brain/serum concentration ratio was 3.0 after 30 min, suggesting the potential for brain targeting.

Passive Targeting

Passive targeting is mainly accomplished by altering the size of injected particles and is a justification for many drug delivery vehicles in place of a free drug. With a particle diameter of 200–300 nm, traditional emulsions for parenteral nutrition rapidly enter the liver and are removed from circulation. Using the same ingredients found in nutritional emulsions (soybean oil and purified egg lecithin), Seki and coworkers created nanoemulsions with a diameter between 25 and 50 nm and larger ones with a 200–300 nm diameter (Seki et al., 2004). It was found that there was a lower liver uptake of the smaller particles, which enabled a longer plasma half-life. The incorporated drug, dexamethasone palmitate (DMP), is an anti-inflammatory agent. It is well known that inflammation sites have leaky capillary walls, which allow smaller particles to passively diffuse across. With a greater plasma half-life, the smaller nanoemulsions passed

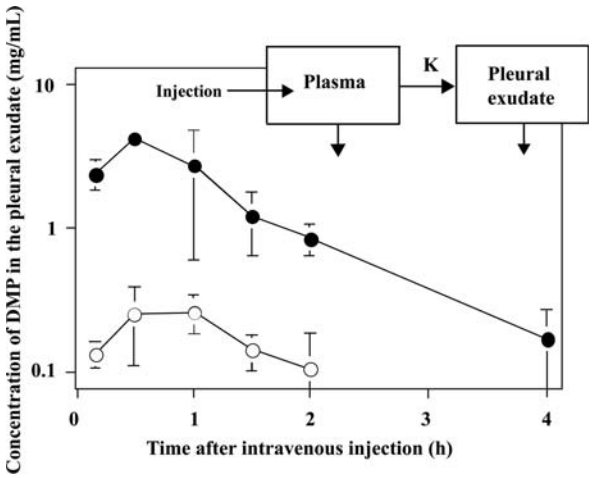

Figure 15.7 Concentration of dexamethasone palmitate (DMP) in the pleural exudate after the intravenous administration of nanoemulsions, incorporating DMP, to rats with experimental pleuritis (dose, 2.5 mg/kg). Each point represents the mean ± SD of five rats. *Closed circles* are nanoemulsions with average diameter 25–50 nm; *open circles* have average diameter 200–300 nm. Reproduced with permission from Elsevier.

into the inflammation sites with greater efficiency, delivering more than three times greater the amount of DMP than with the larger particles (Figure 15.7).

In the prior example, small size was desired so that the nanoemulsion particles could avoid liver uptake. However, in some situations the liver is the target destination of the drug, which makes a larger droplet size more desirable. All-*trans* retinoic acid (ATRA) is an anti-cancer agent that has been studied for the treatment of liver cancer metastasis. Oral administration has been studied, but bioavailability was highly variable, suggesting a possible improvement with intravenous delivery (Ozpolat, Lopez-Berestein, Adamson, Fu, & Williams, 2003). Hashida and coworkers formulated a soybean oil nanoemulsion that was stabilized by either egg phosphatidylcholine (PC)/cholesterol or egg PC/DSPE-PEG and cholesterol to incorporate ATRA (Chansri et al., 2006). The average particle diameter was

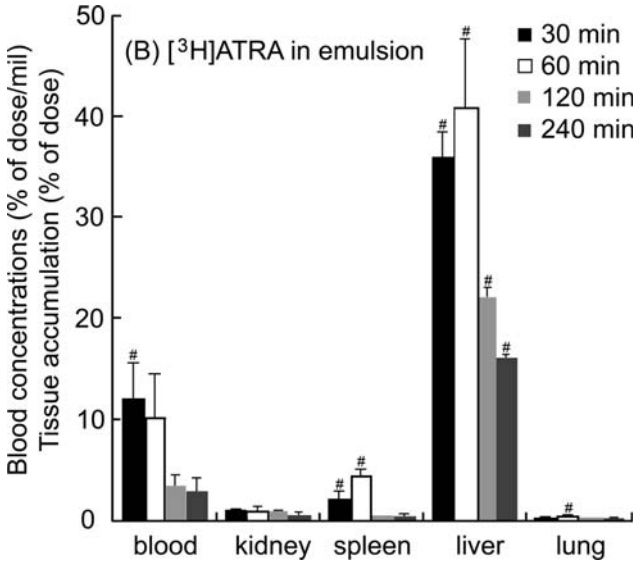

Figure 15.8 Distribution profiles of [^{3}H]all-trans retinoic acid (ATRA) incorporated nanoemulsions after intravenous injection in mice. Results are expressed as the mean + SD of three mice. Statistically significant differences for the emulsified form of [^{3}H]ATRA compared to the non-emulsified form are shown by #$p<0.01$. Reproduced with permission from Elsevier.

133 nm. The nanoemulsions were stable in the presence of albumin in the blood and showed a statistically greater accumulation in the liver, compared to the free drug (Figure 15.8). In CT26 tumor cells, it was shown that emulsified ATRA reduced the number of metastatic nodules and liver weight, compared to a saline solution, as well as ATRA loaded in hydrogenated castor oil (HCO-60) micelles.

Silymarin is a hepatoprotective agent that has a positive effect on metabolism and physiology of liver cells. Abrol and coworkers sought to use nanoemulsions for the delivery of silymarin, which could be passively targeted at the liver (Abrol et al., 2004). Physical characterization studies showed enhanced release of the silymarin from the nanoemulsions, but no in vivo work has been performed yet.

Multiple Functionality

A recent development in nanoemulsions, as with other delivery systems, is the combination of therapeutic and imaging capabilities together in one system. This approach couples drug delivery with tissue imaging to allow simultaneous delivery of the drug and visualization of the physiological effects. Amiji and coworkers devised a 20% pine nut oil emulsion stabilized by egg phosphatidylcholine for the simultaneous solubilization of paclitaxel and gadolinium ions (Gd^{3+}), for enhanced tissue contrast for magnetic resonance imaging (MRI) (Tiwari et al., 2006). The standard nanoemulsions had an average particle diameter of 90.4 nm. In addition to the phosphatidylcholine, a diethylenetriaminepentaacetic acid (DPTA)-phosphatidylethanolamine (PE) complex was added. The PE positions itself at the oil–water interface leaving the DPTA solvent exposed. DPTA is a known chelator for Gd^{3+}, and the high affinity provides for tight binding in an aqueous environment. MRI T_1 relaxation measurements showed similarity between the nanoemulsion and reported literature values for the commercial imaging agent Magnevist®, suggesting the appropriateness of the nanoemulsion as an imaging agent. The nanoemulsions also successfully delivered the paclitaxel to MCF-7 carcinoma cells in vitro, demonstrating the dual functionality, but the drug delivery performance was not superior to an aqueous paclitaxel solution.

New Therapies

Perhaps the most widely studied example of emulsions opening up a new therapeutic area, which would not be available otherwise, is the case of fluorocarbon emulsions for use as artificial blood substitutes. This topic has been extensively reviewed (Krafft, Riess, & Weers, 1998; Riess, 2001, 2005), and so will not be discussed in great detail here. Briefly, though, fully fluorinated molecules (perfluorocarbons, PFCs) have extremely low polarizability, which leads to low van der Waals interactions between molecules. The limited intermolecular forces in PFCs cause them to behave as nearly ideal, gas-like fluids, which allows them to dissolve significant amounts of gas such as O_2. If injected directly, these liquids could form an

oil embolism that could ultimately lead to death, but as an emulsified form, these liquids show no adverse effects in vivo and are able to transport and deliver tremendous amounts of oxygen. Fluosol-DA is an example of a fluorocarbon emulsion that garnered FDA approval, though it was not a commercial success because of practical limitations (the emulsion had to be stored frozen because of stability concerns, thawed and mixed with two annex solutions prior to use, and discarded no more than 8 h after mixing).

Conclusion

The development of new methodologies for the emulsification of o/w biphasic systems has allowed for the formation of nanoemulsions, which possess a stability and particle size that make them particularly suitable for the intravenous delivery of hydrophobic drugs. The combination of different surfactants, additives, and lipids has extended the utility of nanoemulsions to a wide array of drugs. Furthermore, the application of nanoemulsions in drug delivery has made possible the development of new therapies. The safety and efficacy of the use of nanosized emulsions in human patients has been demonstrated with a number of approved products, and current research is continually expanding the usefulness and applicability of nanoemulsion formulations for intravenous delivery. Specifically, the possibility of using nanoemulsions for both imaging and drug delivery has the potential of having a profound impact on the next generation of drug delivery systems.

References

Abrol, S., Trehan, A., & Katare, O. P. (2004). Formulation, characterization and in vitro evaluation of silymarin-loaded lipid microspheres. *Drug Delivery, 11*, 185–191.

Akkar, A., & Müller, R. H. (2003a). Formulation of intravenous Carbamazepine emulsions by SolEmuls Technology. *European Journal of Pharmaceutics and Biopharmaceutics, 55*, 305–312.

Akkar, A., & Müller, R. H. (2003b). Intravenous itraconazole emulsions produced by SolEmuls technology. *European Journal of Pharmaceutics and Biopharmaceutics, 56*, 29–36.

Akkar, A., Namsolleck, P., Blaut, M., & Müller, R. H. (2004). Solubilizing poorly soluble antimycotic agents by emulsification via a solvent-free process. *AAPS Pharmaceutical Science and Technology, 5*(1).

Amselem, S., & Friedman, D. (1998). Submicron emulsions as drug carriers for topical administration. In S. Benita (Ed.), *Submicron emulsions in drug targeting and delivery* (pp. 153–173). Amsterdam: Harwood Academic Publishers.

Becher, P. (2001). *Emulsions: Theory and Practice* (3rd ed.). New York: Oxford University Press.

Benita, S. (Ed.). (1998). *Submicron emulsions in drug targeting and delivery* (Vol. 9). Amsterdam: Harwod Academic Publishers.

Benita, S., & Levy, M. Y. (1993). Submicron emulsions as colloidal drug carriers for intravenous administration: comprehensive physicochemical characterization. *Journal of Pharmaceutical Sciences, 82*(11), 1069–1079.

Bourdon, O., Mosqueira, V., Legrand, P., & Blais, J. (2000). A comparative study of the cellular uptake, localization and phototoxicity of *meta*-tetra (hydroxyphenyl) chlorin encapsulated in surface-modified submicronic oil/water carriers in HT29 tumor cells. *Journal of Photochemistry and Photobiology B: Biology, 55*, 164–171.

Buszello, K., & Müller, B. W. (2000). Emulsions as drug delivery systems. In F. Nielloud & G. Marti-Mestres (Eds.), *Pharmaceutical emulsions and suspensions* (Vol. 105, pp. 191–228). New York: Marcel Dekker.

Capek, I. (2004). Degradation of kinetically-stable o/w emulsions. *Advances in Colloid and Interface Science, 107*, 125–155.

Chansri, N., Kawakami, S., Yamashita, F., & Hashida, M. (2006). Inhibition of liver metastasis by all-*trans* retinoic acid incorporated into O/W emulsions in mice. *International Journal of Pharmaceutics, 321*(1–2), 42–49.

Chiari, P. C., Pagel, P. S., Tanaka, K., Krolikowski, J. G., M., L. L., Trillo, R. A., et al. (2004). Intravenous Emulsified Halogenated Anesthetics Produce Acute and Delayed Preconditioning against Myocardial Infarction in Rabbits. *Anesthesiology, 101*, 1160–1166.

Constantinides, P. P., Lambert, K. J., Tustian, A. K., Schneider, B., Lalji, S., Ma, W., et al. (2000). Formulation development and antitumor activity of a filter-sterilizable emulsion of paclitaxel. *Pharmaceutical Research, 17*(2), 175–182.

Cruz, L., Schaffazick, S. R., Costa, T. D., Soares, L. U., Mezzalira, G., da Silveira, N. P., et al. (2006). Physico-Chemical characterization and *in vivo* evaluation of indomethacin ethyl-ester-loaded nanocapsules by PCS, TEM, SAXS, interfacial alkaline hydrolysis and antiedematogenic activity. *Journal of Nanoscience and Nanotechnology, 6*, 3154–3162.

Cuignet, O. Y., Baele, P. M., & Van Obbergh, L. J. (2002). A second-generation blood substitute (Perflubron Emulsion) increases the blood solubility of modern volatile anesthetics *in vitro*. *Anesthesia and Analgesia, 95*, 368–372.

De Smet, Y., Deriemaeker, L., & Finsy, R. (1999). Ostwald ripening of alkane emulsions in the presence of surfactant micelles. *Langmuir, 15*, 6745–6754.

Dias, M. L. N., Carvalho, J. P., Rodrigues, D. G., Graziani, S. R., & Maranhão, R. C. (2007). Pharmacokinetics and tumor uptake of a derivatized form of paclitaxel associated to a cholesterol-rich nanoemulsion (LDE) in patients in gynecologic cancers. *Cancer Chemotherapy and Pharmacology, 59*, 105–111.

Driscoll, D. F. (2006). Lipid injectable emulsions: pharmacopeial and safety issues. *Pharmaceutical Research, 23*(9), 1959–1969.

Eger, R. P., & MacLeod, B. A. (1995). Anaesthesia by intravenous emulsified isoflurane in mice. *Canadian Journal of Anesthesia, 42*(2), 173–176.

El-Aasser, M. S., & Sudol, E. D. (2004). Miniemulsions: overview of research and applications. *Journal of Coatings Technology and Research, 1*(1), 20–31.

Erdlenbruch, B., Jendrossek, V., Eibl, H., & Lakomek, M. (2000). Transient and controllable opening of the blood-brain barrier to cytostatic and antibiotic agents by alkylglycerols in rats. *Experimental Brain Research, 135*, 417–422.

Fast, J. P., Perkins, M. G., Pearce, R. A., & Mecozzi, S. (2008). Fluoropolymer-based emulsions for the intravenous delivery of sevoflurane. *Anesthesiology, 109*, October issue.

Forster, T., & Von Rybinski, W. (1998). Applications of emulsions. In B. Binks (Ed.), *Modern aspects of emulsion science* (pp. 395–426). Cambridge: The Royal Society of Chemistry.

Friberg, S., & Solans, C. (1978). Emulsification and the HLB-temperature. *Journal of Colloid and Interface Science, 66*, 367–368.

Gupta, P. K., & Cannon, J. B. (2000). Emulsions and microemulsions for drug solubilization and delivery. In R. Liu (Ed.), *Water-insoluble drug formulation* (pp. 169–211). Denver: Interpharm Press.

Higuchi, W. I., & Misra, J. (1962). Physical degradation of emulsions Via the molecular diffusion route and the possible prevention thereof. *Journal of Pharmaceutical Sciences, 51*(5), 459–466.

Hillaireau, H., & Couvreur, P. (2006). Polymeric nanoparticles as drug carriers. In I. F. Uchegbu & A. G. Schätzlein (Eds.), *Polymers in drug delivery*. Boca Raton: CRC.

Hoang, T. K. N., La, V. B., Deriemaeker, L., & Finsy, R. (2003). Ostwald ripening of alkane in water emulsions stabilized by hexaethylene glycol dodecyl ether. *Langmuir, 19*, 6019–6025.

Hoar, T., & Schulman, J. (1943). Transparent water-in-oil dispersions: The oleopathic hydro-micelle. *Nature, 152*, 102–103.

Hung, C.-F., Chen, J.-K., Liao, M.-H., Lo, H.-M., & Fang, J.-Y. (2006). Development and evaluation of emulsion-liposome blends for resveratrol delivery. *Journal of Nanoscience and Nanotechnology, 6*, 2950–2958.

Ishida, E., Managit, C., Kawakami, S., Nishikawa, M., Yamashita, F., & Hashida, M. (2004). Biodistribution characteristics of galactosylated emulsions and incorporated probucol for hepatocyte-selective targeting of lipophilic drugs in mice. *Pharmaceutical Research, 21*(6), 932–939.

Israelachvili, J. (1991). *Intermolecular and surface forces*. San Diego: Academic Press.

Izquierdo, P., Esquena, J., Tadros, T. F., Dederen, C., Garcia, M. J., Azemar, N., et al. (2002). Formation and stability of nano-emulsions prepared using the phase inversion temperature method. *Langmuir, 18*, 26–30.

Jadhav, K. R., Shaikh, I. M., Ambade, K. W., & Kadam, V. J. (2006). Applications of microemulsion based drug delivery system. *Current Drug Delivery, 3*, 267–273.

Jafari, S. M., He, Y., & Bhandari, B. (2006). Nano-emulsion production by sonication and microfluidization – A comparison. *International Journal of Food Properties, 9*, 475–485.

Kabalnov, A. S., & Shchukin, E. D. (1992). Ostwald ripening theory: Applications to fluorocarbon emulsion stability. *Advances in Colloid and Interface Science, 38*, 69–97.

Kabalnov, A. S., & Wennerstrom, H. (1996). Macroemulsion stability: The oriented wedge theory revisited. *Langmuir, 12*, 276–292.

Kawamoto, M., Suzuki, N., & Takasaki, M. (1992). Acute pulmonary edema after intravenous liquid halothane in dogs. *Anesthesia and Analgesia, 74*, 747–752.

Khan, A. Y., Talegaonkar, S., Iqbal, Z., Ahmed, F. J., & Khar, R. K. (2006). Multiple emulsions: An overview. *Current Drug Delivery, 3*, 429–443.

Kim, S.-J., Choi, H.-K., & Lee, Y.-B. (2002). Pharmacokinetic and pharmacodynamic evaluation of cyclosporin A O/W-emulsion in rats. *International Journal of Pharmaceutics, 249*(1–2), 149–156.

Klang, S., & Benita, S. (1998). Design and evaluation of submicron emulsions as colloidal drug carriers for intravenous administration. In S. Benita (Ed.), *Submicron emulsions in drug targeting and delivery* (Vol. 9, pp. 119–152). Amsterdam: Harwood Academic Publishers.

Komori, Y., Aiba, T., Kushima, M., Kawasaki, H., & Kurosaki, Y. (2007). Alteration of therapeutic efficacy of lipid microspheres incorporating prostaglandin E1 by mixing with aqueous solution. *Journal of Pharmaceutical Sciences, 96*(4), 935–943.

Kopriva, C. J., & Lowenstein, E. (1969). An anesthetic accident: cardiovascular collapse from liquid halothane delivery. *Anesthesiology, 30*, 246–247.

Krafft, M. P., Riess, J. G., & Weers, J. G. (1998). The design and engineering of oxygen-delivering fluorocarbon emulsions. In S. Benita (Ed.), *Submicron emulsions in drug targeting and delivery* (pp. 235–333). Amsterdam: Harwood Academic Publishers.

Krafft, M. P., Rolland, J.-P., & Riess, J. G. (1991). Detrimental effect of excess lecithin on the stability of fluorocarbon/lecithin emulsions. *Journal of Physical Chemistry, 95*, 5673–5676.

Krishna, S., ter Kuile, F., Supanaranond, W., Pukrittayakamee, S., Teja-Isavadharm, P., Kyle, D., et al. (1993). Pharmacokinetics, efficacy and toxicity of parenteral halofantrine in uncomplicated malaria. *British journal of clinical pharmacology, 36*, 585–591.

Lance, M. R., Washington, C., & Davis, S. S. (1995). Structure and toxicity of amphotericin B/triglyceride emulsion formulations. *Journal of Antimicrobial Chemotherapy, 36*(1), 119–128.

Lifshitz, I. M., & Slyozov, V. V. (1961). The kinetics of precipitation from supersaturated solid solutions. *Journal of Physics and Chemistry of Solids, 19*(1–2), 35–50.

Liu, W., Sun, D., Li, C., Liu, Q., & Xu, J. (2006). Formation and stability of paraffin oil-in-water nano-emulsions prepared by the emulsion inversion point method. *Journal of Colloid and Interface Science, 303*, 557–563.

Liu, Y., Huang, K., Peng, D., Liu, S., & Wu, H. (2007). Preparation of poly (butylene-co-ϵ-caprolactone carbonate) and their use as drug carriers for a controlled delivery system. *Journal of Polymer Science Part A: Polymer Chemistry, 45*(11), 2152–2160.

Lixin, W., Haibing, H., Xing, T., Ruiying, S., & Dawei, C. (2006). A less irritant norcantharidin lipid microspheres: Formulation and drug distribution. *International Journal of Pharmaceutics, 323*(1–2), 161–167.

Lo, M. W., Schary, W. L., & Whitney, C. C. (1987). The disposition and bioavailability of intravenous and oral nalbuphine in healthy volunteers. *Journal of Clinical Pharmacology, 27*, 866–873.

Madhusudhan, B., Rambhau, D., Apte, S. S., & Gopinath, D. (2007). 1-*O*-alkylglycerol stabilized carbamazepine intravenous o/w nanoemulsions for drug targeting in mice. *Journal of Drug Targeting, 15*(2), 154–161.

Mason, T., Wilking, J., Meleson, K., Chang, C., & Graves, S. (2006). Nanoemulsions: formation, structure and physical properties. *Journal of Physics: Condensed Matter, 18*, R635–R666.

Medina, J., Salvadó, A., & del Pozo, A. (2001). Use of ultrasound to prepare lipid emulsions of lorazepam for intravenous injection. *International Journal of Pharmaceutics, 216*(1–2), 1–8.

Miller, C. A. (2006). Spontaneous emulsification recent developments with emphasis on self-emulsification. In J. Sjoblom (Ed.), *Emulsions and emulsion stability* (2nd ed., Vol. 132, pp. 107–126). New York: Marcel Dekker.

Mosqueira, V., Legrand, P., & Barratt, G. (2006). Surface-modified and conventional nanocapsules as novel formulations for parenteral delivery of halofantrine. *Journal of Nanoscience and Nanotechnology, 6*, 3193–3202.

Mosqueira, V., Loiseau, P. M., Bories, C., Legrand, P., Devissaguet, J.-P., & Barratt, G. (2004). Efficacy and pharmacokinetics of intravenous nanocapsule formulations of halofantrine in Plasmodium berghei-infected mice. *Antimicrobial Agents and Chemotherapy, 48*, 1222.

Mozzi, G., Benelli, P., Bruzzese, T., Galmozzi, M. R., & Bonabello, A. (2002). The use of lipid emulsions for the iv administration of a new water soluble polyene antibiotic, SPK-843. *Journal of Antimicrobial Chemotherapy, 49*(2), 321–325.

Müller, R. H., Schmidt, S., Buttle, I., Akkar, A., Schmitt, J., & Bromer, S. (2004). SolEmuls – novel technology for the formulation of i.v. emulsions with poorly soluble drugs. *International Journal of Pharmaceutics, 269*(2), 293–302.

Musser, J. B., Fontana, J. L., & Mongan, P. D. (1999). The Anesthetic and Physiologic Effects of an Intravenous Administration of a Halothane Lipid Emulsion (5% vol/vol). *Anesthesia and Analgesia, 88*, 671–675.

Nakajima, H. (1997). Microemulsions in cosmetics. In C. Solans & H. Kunieda (Eds.), *Industrial applications of microemulsions* (pp. 175–197). New York: Marcel Dekker.

Nordén, T. P., Siekmann, B., Lundquist, S., & Malmsten, M. (2001). Physicochemical characterisation of a drug-containing phospholipid-stabilised o/w emulsion for intravenous administration. *European Journal of Pharmaceutical Sciences, 13*(4), 393–401.

Ozpolat, B., Lopez-Berestein, G., Adamson, P., Fu, C. J., & Williams, A. H. (2003). Pharmacokinetics of intravenously administered liposomal all-trans-retinoic acid (ATRA) and orally administered ATRA in healthy volunteers. *Journal of Pharmacy & Pharmaceutical Sciences, 6*, 292–301.

Palakurthi, S., Vyas, S. P., & Diwan, P. V. (2005). Biodisposition of PEG-coated lipid microspheres of indomethacin in arthritic rats. *International Journal of Pharmaceutics, 290*(1–2), 55–62.

Petsev, D., Denkov, N., & Kralchevsky, P. (1995). Flocculation of deformable emulsion droplets. II. Interaction energy. *Journal of Colloid and Interface Science, 176*, 201–213.

Pohlmann, A. R., Weiss, V., Mertins, O., da Silveira, N. P., & Guterres, S. S. (2002). Spray-dried indomethacin-loaded polyester nanocapsules and nanospheres: development, stability evaluation and nanostructure models. *European Journal of Pharmaceutical Sciences, 16*(4–5), 305–312.

Primo, F. L., Macaroff, P. P., Lacava, Z. G. M., Azevedo, R. B., Morais, P. C., & Tedesco, A. C. (2007). Binding of photophysical studies of biocompatible magnetic fluid in biological medium and development of magnetic nanoemulsion: a new candidate for cancer treatment. *Journal of Magnetism and Magnetic Materials, 310*, 2838–2840.

Riess, J. G. (2001). Oxygen Carriers ("Blood Substitutes";)-Raison d'Etre, Chemistry, and Some Physiology. *Chemical Reviews, 101*(9), 2797–2920.

Riess, J. G. (2005). Understanding the fundamentals of perfluorocarbons and perfluorocarbon emulsions relevant to in vivo oxygen delivery. *Artificial Cells, Blood Substitutes and Biotechnology, 33*, 47–63.

Russel, W., Saville, D., & Schowalter, W. (1989). *Colloidal dispersions*. Cambridge: Cambridge University Press.

Salager, J. L., Loaiza-Maldonado, I., Miñana-Pérez, M., & Silva, F. (1982). Surfactant-oil-water systems near the affinity inversion. Part I: Relationship between equilibrium phase behavior and emulsion type and stability. *Journal of Dispersion Science and Technology, 3*, 279–292.

Sandison, J. W., Sivapragasam, S., Hayes, J. A., & Woo-Ming, M. O. (1970). An experimental study of pulmonary damage associated with intravenous injection of halothane in dogs. *British Journal of Anaesthesia, 42*, 419–423.

Sarker, D. K. (2005). Engineering of nanoemulsions for drug delivery. *Current Drug Delivery, 2*, 297–310.

Schulman, J., Stoeckenius, W., & Prince, L. (1959). Mechanism of formation and structure of micro emulsions by electron microscopy. *Journal of Physical Chemistry, 63*, 1677–1680.

Seki, J., Sonoke, S., Saheki, A., Fukui, H., Sasaki, H., & Mayumi, T. (2004). A nanometer lipid emulsion, lipid nano-sphere (LNS), as a parenteral drug carrier for passive drug targeting. *International Journal of Pharmaceutics, 273*(1–2), 75–83.

Sharma, S. K., Lowe, K. C., & Davis, S. S. (1988). Novel Compositions of Emulsified Perfluorochemicals for Biological Uses. *Biomaterials, Artificial Cells, and Artificial Organs, 16*, 447–450.

Shawer, M., Greenspan, P., Oie, S., & Lu, D. R. (2002). VLDL-resembling phospholipid-submicron emulsion for cholesterol-based drug targeting. *Journal of Pharmaceutical Sciences, 91*(6), 1405–1413.

Shinoda, K., & Saito, H. (1968). Effect of temperature on the phase equilibria and the types of dispersions of the ternary system composed of water, cyclohexane, and nonionic surfactant. *Journal of Colloid and Interface Science, 26*, 70–74.

Siekmann, B., & Westesen, K. (1998). Submicron lipid suspensions (Solid Lipid Nanoparticles) versus lipid nanoemulsions: Similarities and differences. In S. Benita (Ed.), *Submicron emulsions in drug targeting and delivery* (pp. 205–218). Amsterdam: Harwood Academic Publishers.

Solans, C., Esquena, J., Forgiarini, A. M., Uson, N., Morales, D., Izquierdo, P., et al. (2003). Nano-emulsions: formation, properties, and applications. In *Adsorption and Aggregation of Surfactants in Solution* (Vol. 109, pp. 524–554). New York: Marcel Dekker, Inc.

Solans, C., Izquierdo, P., Nolla, J., Azemar, N., & Garcia-Celma, M. J. (2005). Nano-emulsions. *Current Opinion in Colloid & Interface Science, 10*, 102–110.

Strippoli, V., D'Auria, F. D., Simonetti, G., Bruzzese, T., & Simonetti, N. (2000). Anticandidal activity of SPA-S-843, a new polyenic drug. *Journal of Antimicrobial Chemotherapy, 45*, 235–237.

Tadros, T., Izquierdo, P., Esquena, J., & Solans, C. (2004). Formation and stability of nano-emulsions. *Advances in Colloid and Interface Science, 108–109*, 303–318.

Taylor, P. (1998). Ostwald ripening in emulsions. *Advances in Colloid and Interface Science, 75*, 107–163.

Taylor, P. (2003). Ostwald ripening in emulsions. Estimation of solution thermodynamics of the disperse phase. *Advances in Colloid and Interface Science, 106*, 261–285.

Teixeira, M., Alonso, M. J., Pinto, M. M. M., & Barbosa, C. M. (2005). Development and characterization of PLGA nanospheres and nanocapsules containing xanthone and 3-methoxyxanthone. *European Journal of Pharmaceutics and Biopharmaceutics, 59*, 491–500.

The United States Pharmacopeia. (2006). Vol. 29. Rockville: The United States Pharmacopeial Convention.

Tiwari, S., Tan, Y.-M., & Amiji, M. (2006). Preparation and *in vitro* characterization of multifunctional nanoemulsions for simultaneous MR imaging and targeted drug delivery. *Journal of Biomedical Nanotechnology, 2*, 217–224.

Ueda, K., Furukawa, T., Kawaguchi, Y., Miki, Y., Sakaeda, T., & Iwakawa, S. (2004). Prolonged circulation of menatetrenone by emulsions with hydrogenated castor oils in rats. *Journal of Controlled Release, 95*(1), 93–100.

Verwey, E., & Overbeek, J. (1948). *Theory of the stability of lyophobic colloids*. Amsterdam: Elsevier.

Wagner, C. (1961). *Z. Elektrochem., 65*, 581–591.

Walstra, P., & Smulders, P. (1998). Emulsion formation. In B. Binks (Ed.), *Modern aspects of emulsion science* (pp. 56–99). Cambridge: The Royal Society of Chemistry.

Wang, J.-J., Sung, K. C., Hu, O. Y.-P., Yeh, C.-H., & Fang, J.-Y. (2006). Submicron lipid emulsion as a drug delivery system for nalbuphine and its prodrugs. *Journal of Controlled Release, 115*(2), 140–149.

Wang, Y. J., Wang, J., Zhang, H. Y., He, H. B., & Tang, X. (2007). Formulation, preparation and evaluation of flunarizine-loaded lipid microspheres. *Journal of Pharmacy and Pharmacology, 59*, 351–357.

Watkins, W. M., Woodrow, C., & Marsh, K. (1993). Falciparum malaria: differential effects of antimalarial drugs on ex vivo parasite viability during the critical early phase of therapy. *American Journal of Tropical Medicine and Hygiene, 49*, 106.

Weers, J. G., Ni, Y., Tarara, T. E., Pelura, T. J., & Arlauskas, R. A. (1994). The effect of molecular diffusion on initial particle size distributions in phospholipid-stabilized fluorocarbon emulsions. *Colloids and Surfaces A: Physicochemical and Engineering Aspects, 84*, 81–87.

Yeeprae, W., Kawakami, S., Higuchi, Y., Yamashita, F., & Hashida, M. (2005). Biodistribution characteristics of mannosylated and fucosylated O/W emulsions in mice. *Journal of Drug Targeting, 13*(8), 479–487.

Yeeprae, W., Kawakami, S., Yamashita, F., & Hashida, M. (2006). Effect of mannose density on mannose receptor-mediated cellular uptake of mannosylated O/W emulsions by macrophages. *Journal of Controlled Release, 114*(2), 193–201.

Yu, J., He, H. B., & Tang, X. (2006). Formulation and evaluation of nimodipine-loaded lipid microspheres. *Journal of Pharmacy and Pharmacology, 58*, 1429–1435.

Zhou, J.-X., Luo, N.-F., Liang, X.-M., & Liu, J. (2006). The Efficacy and Safety of Intravenous Emulsified Isoflurane in Rats. *Anesthesia and Analgesia, 102*, 129–134.

16

Nanotechnology for Cancer Chemotherapy

Alisar S. Zahr and Michael V. Pishko

Abstract This chapter will provide an in-depth discussion on the development of nanometer-sized carriers for the treatment of cancer. Anti-cancer drugs given systemically remain problematic due to their non-specificity. These cytotoxic drugs destroy both cancerous and normal cells of the body, thus leading to potentially fatal side effects. In recent developments, new cytotoxic drugs have yielded compounds with poor physiochemical properties which require alternate routes in their delivery to the diseased tissue. The use of nanoparticles for the delivery of chemotherapeutics to cancer lesions and their microenvironment has offered solutions to the problems associated with conventional administration, delivery, and formulation of chemotherapeutics. Nanoparticles, submicron-sized colloidal structures, have shown to extravasate across tumor vascular walls, penetrate into the tumor interstitium, target surface receptors on cancer cells, and control the release of the anti-cancer drug locally. The design in the surface of the colloidal carrier is important in achieving a biocompatible, long circulating, and targeted drug delivery particulate system. The rational approach in engineering colloidal carriers with the potential to treat cancer is discussed and examples of drug delivery systems which have demonstrated therapeutic efficacy are provided.

Introduction

Cancer is the second leading cause of death in the United States and in many industrialized countries (Jain, 2001; Jemal, Murray, Ward, Samuels, Tiwari, Ghafoor, Feuer, and Thun, 2005; Vasir, and Labhasetwar, 2005). Cancer is recognized as a genetic disease in which cells display a diverse array of genetic alterations including gene rearrangements, point mutations, and gene amplification (K. R. Loeb, and Loeb, 2000; L. A. Loeb, 1991; Merlo, Pepper, Reid, and Maley, 2006). With regular screening, patients at high risk have improved patient prognosis and survival. However, earlier detection of the disease is necessary but is currently limited by poor resolution and high equipment cost for most imaging technologies (Kingsley, Dou, Morehead, Rabinow, Gendelman, and Destache, 2006;

M.M. de Villiers et al. (eds.), *Nanotechnology in Drug Delivery*, DOI: 10.1007/978-0-387-77667-5_16,

Weissleder, 2002). Approximately 85% of human cancers are solid tumors and can be surgically removed as a first method in anti-cancer therapy (Jang, Wientjes, Lu, and Au, 2003; Vasir, and Labhasetwar, 2005). After surgical removal, the remaining cancer cells and tissue are treated with radiotherapy, chemotherapy, immunotherapy, gene therapy, and hyperthermia. The most effective treatment for cancer is cytotoxic chemotherapy. The objective of chemotherapy is *total cell kill* resulting in a *total cure* (Gringauz, 1997; Minchinton, and Tannock, 2006). However, achieving total cell kill is a difficult task especially once the cancer has metastasized. Reasons for anti-cancer therapy failure have been attributed to poor drug selectivity to the diseased tissue, acquired multi-drug resistance, heterogeneous biology of growing tumors, low solubility of drug at physiological pH, and suppressed host immune system.

Current treatment regimes require high doses of the anti-cancer drug to be delivered systemically by intravenous injection or infusion. The larger the dose of the drug that can be administered, the greater the potential for cell death (Gringauz, 1997). Achieving a dose that would completely eradicate malignant cells is problematic because such a dose would result in elevated toxic levels contributing to patient mortality (Gringauz, 1997; Torchilin, 2004). Another dilemma encountered in chemotherapy is most anti-cancer drugs are water insoluble and require pharmaceutical solvents to be used for their clinical administration, and these solvents may cause life-threatening effects (Feng, and Chien, 2003; Torchilin, 2004). In addition, patient discomfort is caused by severe side effects associated with drug dosage form, scheduling, and patient condition (Brannon-Peppas, and Blanchette, 2004). Consequently, conventional systemic delivery of chemotherapeutics has a major impact on reducing the quality of life and survival time of cancer patients (Table 16.1).

The unmet medical need for the treatment of cancer is the design of drug delivery systems that can selectively deliver anti-cancer agents to the diseased tissue with high local drug concentrations thereby achieving therapeutic

Table 16.1 Chemotherapeutic agents.

Disadvantages of current anticancer therapy
* Non-selective with high toxicity against normal tissues
* Rapid elimination from the systemic circulation (e.g., renal filtration)
* Uptake by the immune system, mononuclear phagocyte system (MPS)
* Accumulation in non-targeted organs and tissues
* Enzymatic and hydrolytic degradation
* Inefficient cell entry
Advantages of nanotechnology and nanocarriers
* Nanovehicles provide a container that can hold agents within
* Nanometer size provides improved cell entry and extravasation
* Protection of the therapeutic agent from the biological milieu
* Decreased renal elimination
* Large surface are to a volume ratio provides a surface for chemical modification
* Improved bioavailability of the anticancer agent
* Increased solubility of water-insoluble anticancer agents

efficacy while minimizing toxic side effects. Drug delivery systems, such as nanometer-sized carriers that entrap the chemotherapeutic have shown to improve the treatment of cancer (Allen, 2002; Feng, and Chien, 2003; Kim, and Lim, 2002; Kingsley, Dou, Morehead, Rabinow, Gendelman, and Destache, 2006). The development of these drug delivery systems has been influenced by nanotechnology (Ferrari, 2005; Kingsley, Dou, Morehead, Rabinow, Gendelman, and Destache, 2006; Kipp, 2004; LaVan, McGuire, and Langer, 2003; Moghimi, Hunter, and Murray, 2005; Sanjeeb K. Sahoo, 2003), leading to the use of diverse number of colloidal carriers and nanoparticles for the treatment of cancer.

Nanoparticles for drug delivery may be defined as submicron colloidal particles (10–1000 nm) that contain a therapeutic agent either dispersed in a polymer carrier matrix, encapsulated within a polymer shell, covalently attached or adsorbed to the particle surface, or encapsulated within a structure such as a liposome (Brigger, Morizet, Aubert, Chacun, Terrier-Lacombe, Couvreur, and Vassal, 2002; Kingsley, Dou, Morehead, Rabinow, Gendelman, and Destache, 2006; Sanjeeb K. Sahoo, 2003). Nanotechnology-based drug delivery systems have included biodegradable nanoparticles (Brannon-Peppas, and Blanchette, 2004; Gref, Couvreur, Barratt, and Mysiakine, 2003; H. Liu, S. Farrell, and K. Uhrich, 2000; Sanjeeb K. Sahoo, 2003), dendrimers (Esfand, and Tomalia, 2001; Quintana, Raczka, Piehler, Lee, Mye, Majoros, Patri, Thomas, Mule, and Baker, 2002; Tomalia, and Frechet, 2002), polymeric micelles (H. Liu, S. Farrell, and K. Uhrich, 2000; Sanjeeb K. Sahoo, 2003; Torchilin, 2004), ferrofluids (Sanjeeb K. Sahoo, 2003), liposomes (Aplin, Howe, Alahari, and Juliano, 1998; Torchilin, 2006), hollow microcapsules (Liu, Gao, Shen, and Mohwald, 2005), solid lipid nanoparticles (Muller, Mader, and Gohla, 2000), and solid core–shell nanoparticles (Zahr, de Villiers, and Pishko, 2005; Lasic, Vallner, and Working, 1999; Lewanski, and Stewart, 1999; Yuan, Dellian, Fukumura, Leunig, Berk, Torchilin, and Jain, 1995). Association of the chemotherapeutic with the mentioned nanocarriers can provide sustained release, help circumvent biological barriers imposed by the tumor physiology, and protect the drug from the surrounding biological milieu (Table 16.1). There are numerous methods used to prepare particulate systems; unfortunately, there are disadvantages associated with each (Brigger, Morizet, Aubert, Chacun, Terrier-Lacombe, Couvreur, and Vassal, 2002; O'Donnell, and McGinity, 1997; Ruan, Feng, and Li, 2002). First, many of the methods use harsh chlorinated organic solvents and surfactants for their production. Secondly, unstable emulsions result in low encapsulation efficiencies, aggregation, and uncontrolled burst release (Thote, Chappell, Gupta, and Kumar, 2005), which is toxic to the body when released in healthy tissue. However, the fabrication of nanoparticles for drug delivery applications has alleviated the problems associated with conventional chemotherapy and offers promise in cancer patient treatment where efficacy could be improved dramatically by effective time-release at selective locations while simultaneously decreasing the occurrence of harmful side effects.

This chapter explores the development of nanoparticles for cancer treatment by addressing tumor growth and criteria for delivery, fabrication and characterization of colloidal carriers, surface engineering

techniques, current examples of drug delivery systems, and future explorations in the development of multifunctional colloidal carriers.

Design of a Drug Delivery System

In the rational design of an efficacious drug delivery system for cancer treatment certain functional and structural properties are required to be integrated within the final carrier. The fabrication must produce a drug delivery system that is biodegradable, injectable, biocompatible, targetable, and one which can control the release of the chemotherapeutic over a sustained period of time. These functional properties can be realized in the design of the drug delivery system and are dependent on drug properties and the type of cancer being targeted. The control of the physicochemical properties such as particle composition, size, surface characteristics, and mechanical properties can guarantee that the functional properties are met. Also, the fabrication method should achieve high drug recovery, in vivo stability, and storage stability conducive for a hospital environment. Advantages for associating the chemotherapeutic with nanoparticles arise from two controllable structural properties, which are their size and surface characteristics. These parameters will assist in avoiding the cellular and physical barriers imposed on the colloidal carrier after intravenous administration (Table 16.2).

Nanoparticles for anti-cancer therapy should have similar sizes to biological entities such as cellular organelles. The size of the nanocarrier is constrained by upper and lower limits. In the upper size limit, the nanocarrier should be equal to or smaller than the size of human red blood cells, which is approximately between 6 and 8 μm in diameter. The lower size limit is dependent on the goal of the delivery system. For example, gene

Table 16.2 Barriers to effective drug delivery to cancer lesions and their microenvironment.

By the Host
* Innate immunity
* Mononuclear phagocyte system (bone marrow progenitors, blood monocytes, and tissue macrophages)
* Opsonization by serum proteins (immunoglobulins, fibronectin, albumin, and complement proteins)
* Acquired immunity
* Antibodies
By Physical Barriers
* Tumor microenvironment
* High tumor intersitial pressure (outward convective flow)
* Endothelium (pore size and fenestrations)
* Dense extracellular matrix (diffusional limitations)
By Cellular Barriers
* Lipophilic cellular membrane
* Receptor specificity for targeted delivery
* Intracellular trafficking (endosomal compartment, lysomal compartment, and exocytosis and receptor recycling)
* Nuclear delivery

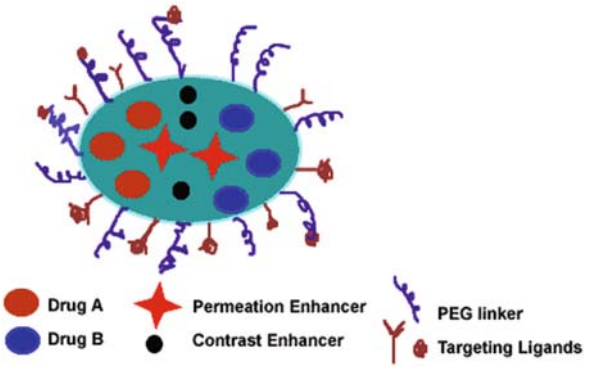

Figure 16.1 Schematic of a particulate drug delivery carrier. The carrier matrix can contain one or more therapeutic compounds, contrast enhancers, such as MRI agents, and permeation enhancers. The surface of the carrier is modified with ligands for selective targeting to diseased tissues and poly(ethylene glycol) (PEG) to achieve a stealth delivery (adapted from reference Ferrari, 2005). (*See* Color Plate 21)

therapy would require the carrier to be sequestered inside the cellular nucleus and this can be achieved with carriers of approximate size of 39 nm or smaller (Pante, and Kann, 2002). Within the range of 8 μm to 39 nm it has been found that colloidal carriers with nanometer size (10–1000 nm) have access to cell populations and body compartments upon intravenous injection (Moghimi, Hunter, and Murray, 2005). Nanoparticles delivered intravasculary can bypass the innate immune system by preventing uptake by the mononuclear phagocyte system (MPS), when compared to microparticles (> 1000 nm) (Hansen, Kao, Moase, Zalipsky, and Allen, 1995; Sahoo, and Labhasetwar, 2003). Their size also allows for penetration through the smallest pores of capillaries in the human vasculature (200–1000 nm) (Duncan, 2003; Hansen, Kao, Moase, Zalipsky, and Allen, 1995; Hobbs, Monsky, Yuan, Roberts, Griffith, Torchilin, and Jain, 1998; Kingsley, Dou, Morehead, Rabinow, Gendelman, and Destache, 2006; Sahoo, and Labhasetwar, 2003). Additionally, the characteristically high curvature of the surface of spherical nanoparticles promotes better surface coverage by hydrophilic polymers and targeting ligands, which is important to the success of a drug delivery system (S. I. Stolnik, L. Davis, S.S., 1995b; Storm, Belliot, Daemen, and Lasic, 1995a).

The ideal particulate carrier would have the capability to do the following: to carry one or more therapeutic agents, to target through one or more conjugated antibodies or other recognition moieties (Allen, 2002; Neri, and Bicknell, 2005), to image diseased tissue, and to avoid biological barriers that can promote clearance from the systemic circulation (Ferrari, 2005; S. Stolnik, Illum, and Davis, 1995) (Figure 16.1). Increasing the efficacy and reducing deleterious side effects associated with traditional chemotherapy may be realized with such a multifunctional drug delivery carrier for cancer treatment.

Tumor Growth and Angiogenesis

Cancer is the result of cell growth regulation gone awry (Leach, 1999). Any cell in the body has the potential to become cancerous if it receives a series of genetic mutations that result in growth deregulation (Leach, 1999). A single cancerous cell surrounded by healthy tissue replicates at a higher rate and places strain on nutrient supply. Once a small tumor mass has

formed, healthy cells are ultimately displaced. Also, tumor cells require new blood vessel growth in order to grow in size, and this growth process known as angiogenesis is initiated when the tumor diameter is greater than 2 mm (Brannon-Peppas, and Blanchette, 2004; Dua, Gui, and Isacke, 2005; Jang, Wientjes, Lu, and Au, 2003). Tumor vasculature originates from the host vasculature, and the mechanisms of angiogenesis for both are similar, but the organization of vessels, capillary beds, and blood flow rates significantly differ and are abnormal in the diseased tissue (Figure 16.2) (di Tomaso, Capen, Haskell, Hart, Logie, Jain, McDonald, Jones, and Munn, 2005). Normal healthy tissue contain blood vessels lined by a smooth layer of endothelial cells with pericytes that maintain integrity of the vessel on its outside (Heldin, Rubin, Pietras, and Ostman, 2004). In tumor vasculature, there is a defective endothelial cell barrier with loose attachment of pericytes which results in a leaky vasculature with fenestrations, irregular vessel diameters, high tortuosity, and random branching (di Tomaso, Capen, Haskell, Hart, Logie, Jain, McDonald, Jones, and Munn, 2005). Furthermore, many tumors lack lymphatic vessels, and tumors with lymphatic vessels have characteristically wider lumen, an increased number of intracellular spaces, and sprouting endothelial cells, which results in an increased interstitial fluid pressure (Dua, Gui, and Isacke, 2005; Heldin, Rubin, Pietras, and Ostman, 2004; Minchinton, and Tannock, 2006)

Tumor microvasculature has a characteristic pore cutoff size. The cutoff size is a functional description of the size of transvascular gaps based on the diameter by which particles extravasate and the upper limit of the particle diameter at which no extravasation occurs (Hobbs, Monsky, Yuan, Roberts, Griffith, Torchilin, and Jain, 1998; Yuan, Dellian, Fukumura, Leunig, Berk, Torchilin, and Jain, 1995). This pore cutoff size is important for the design of

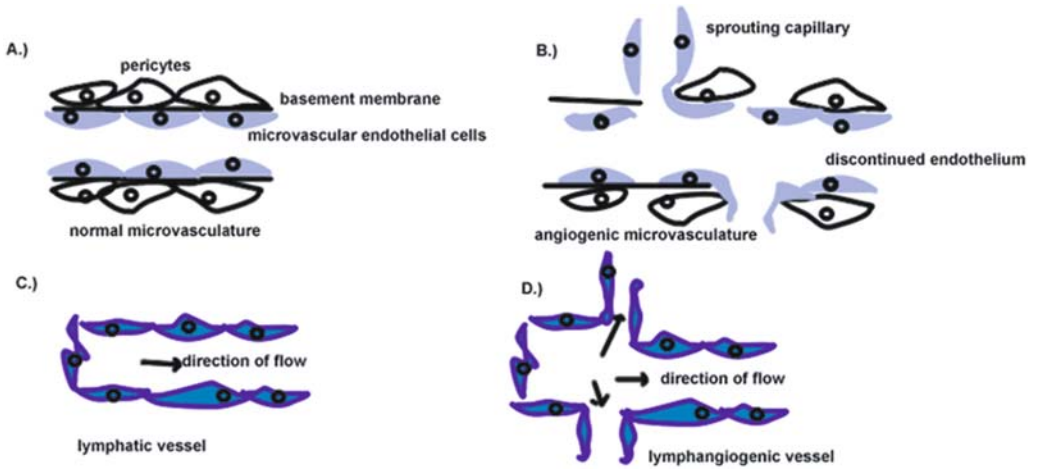

Figure 16.2 Structure of normal and tumor microvascular and lymphatic systems: (**a**) normal microvasculature with characteristically tight endothelium supported by a basement membrane and pericytes; (**b**) angiogenic microvasculature with characteristically discontinued endothelium, highly branched vasculature, and fragmented basement membrane; (**c**) normal lymphatic vessel which is blind ended with a lack of endothelial cell-to-cell junctions; (**d**) lymphangiogenic vessel with a characteristically wider lumen, sprouting endothelial cells, and increased intracellular spaces (redrawn from reference Dua, Gui, and Isacke, 2005). (*See* Color Plate 22)

a selective colloidal carrier. Transport across tumor microvasculature has been shown to occur via interendothelial junctions, fenestrations, and phagocytosis (di Tomaso, Capen, Haskell, Hart, Logie, Jain, McDonald, Jones, and Munn, 2005; Hobbs, Monsky, Yuan, Roberts, Griffith, Torchilin, and Jain, 1998). In normal vessels, interendothelial junctions have an effective size of 6–7 nm, which provide resistance to particulate drug delivery (Hobbs, Monsky, Yuan, Roberts, Griffith, Torchilin, and Jain, 1998; Saltzman, 2001). Hobbs and co-workers demonstrated that tumors grown subcutaneously have a tumor-dependent pore cutoff size ranging from 200 nm to 1.2 μm (Hobbs, Monsky, Yuan, Roberts, Griffith, Torchilin, and Jain, 1998). Tumor microvessels have been shown to be hyperpermeable to long-circulating PEG liposomes and polystyrene latex particles of up to 600 nm in diameter (Yuan, Dellian, Fukumura, Leunig, Berk, Torchilin, and Jain, 1995). Collectively, the results gathered by Hobbs, Yuan, and Dreher demonstrated that the size of the nanoparticle should be within a range of 100–780 nm to effectively transport across the microvascular wall into the tumor interstitium (Dreher, Liu, Michelich, Dewhirst, Yuan, and Chilkoti, 2006; Hobbs, Monsky, Yuan, Roberts, Griffith, Torchilin, and Jain, 1998; Yuan, Dellian, Fukumura, Leunig, Berk, Torchilin, and Jain, 1995).

Passive Targeting of Nanovectors

The delivery of nanovectors and macromolecules to the tumor interstitium is mediated by the concept of the enhanced permeability and retention (EPR) effect, first coined in 1989 (Maeda, Wu, Sawa, Matsumura, and Hori, 2000). The EPR effect has become the gold standard in anti-cancer drug delivery in the last decade (Maeda, Wu, Sawa, Matsumura, and Hori, 2000) and describes the process by which leaky tumor vessels allow macromolecular extravasation into the tumor interstitium by extravasation via diffusion and or convection through the discontinuous endothelium. The lack of an effective tumor lymphatic drainage system further prevents the clearance of macromolecules and promotes the accumulation of drug delivery carriers in the tumor interstitium (Maeda, Wu, Sawa, Matsumura, and Hori, 2000; Torchilin, 2004). The EPR effect has been observed in many mouse models and in human solid tumors. Reports from in vivo experimental work indicate that elevated levels of vascular permeability factors such as bradykinin, nitric oxide and vascular endothelial growth factor mediate vascular hyperpermeability and retention supporting the EPR effect (Heldin, Rubin, Pietras, and Ostman, 2004; Maeda, Wu, Sawa, Matsumura, and Hori, 2000).

Nanoparticles delivered by intravenous administration can also passively accumulate in the tumor interstitium as described by the EPR effect. The passive accumulation of macromolecular drug carriers undergoing the EPR effect has been observed in macromolecules with molecular weight ranging between 45 and 75 kDa (Dreher, Liu, Michelich, Dewhirst, Yuan, and Chilkoti, 2006; Maeda, Fang, Inutsuka, and Kitamoto, 2003). Although high molecular weight carriers accumulate in tumors, their tumor penetration from the microvasculature is significantly reduced (Dreher, Liu, Michelich, Dewhirst, Yuan, and Chilkoti, 2006). The reduced transport of nanovectors into the tumor tissue can lead the cancer

cells in the core to receive lower doses of drug compared to those cells at the periphery and close to the vascular surface. Despite this conclusion, cancer cells located close to the vascular surface proliferate more rapidly and are more sensitive to anti-cancer drug than cells found within the core regions of the tumor (Dreher, Liu, Michelich, Dewhirst, Yuan, and Chilkoti, 2006).

Although the EPR effect has its advantages for intravenous delivery, the accumulation of drug delivery particles within the capillaries not near the tumor is a severe problem. Accumulation can lead to recognition by the mononuclear phagocyte system, which rapidly removes foreign particles from systemic circulation (S. I. Stolnik, L. Davis, S.S., 1995b). The EPR effect can be combined with active targeting drug delivery systems to achieve high payload of drug within the tumor tissue.

Active Targeting of Nanovectors

While in vitro and in vivo studies for anti-tumor activity have demonstrated passive targeting using the EPR effect, further tumor accumulation and intracellular uptake is possible by active or selective targeting (Luo, and Prestwich, 2002; Vasir, and Labhasetwar, 2005). The principle to selective drug delivery is to exploit the biological differences between normal cells and malignant cells. It is well known that cancer cells express or overexpress specific surface receptors which can be targeted (Herbst, 2004). Drug delivery of the particulate system to cancer cells can be achieved with molecules that are specific to antigens or receptors expressed on the surface of cancer cells (Allen, 2002; Neri, and Bicknell, 2005). These molecules or ligands (antibodies, lectins, saccharides, hormones, small molecular weight compounds) bind to their cellular epitopes to trigger internalization via receptor-mediated endocytosis (RME) (Allen, 2002; Kingsley, Dou, Morehead, Rabinow, Gendelman, and Destache, 2006). This internalization process is the route for effective drug delivery; to exert their cytotoxic effect, anti-cancer drugs act on intracellular targets (e.g., mitochondria, microtubules, and nucleus). The endocytic process may hinder effective transport of the drug carrier to the cell cytosol due to recycling of the endosomes back to the plasma membrane. To escape this process, drug delivery systems take advantage of the acidified environment within the endosome by destabilizing the vesicular body and inducing release of the carrier into the cytosol (Sheff, 2004; Torchilin, 2006; Watson, Jones, and Stephens, 2005). This strategy has been accomplished with cationic polymer polyethyleneimine, amphipathic peptides, and phosphatidylethanolamine (Torchilin, 2006). The ultimate goal of active targeting is to increase the intracellular concentration of the chemotherapeutic at the diseased site while limiting systemic exposure, thus reducing toxic side effects for cancer patients.

With recent developments in antibody engineering, monoclonal antibodies or antibody fragments are slowly gaining clinical approval for the selective delivery of chemotherapeutics to cancer cells. Antibodies such as Herceptin target the HER2/neu receptor, which is overexpressed in 25–30% of breast cancer cells and can provide selective drug delivery (Kirpotin, Park, Hong, Zalipsky, Li, Carter, Benz, and Papahadjopoulous,

1997). However, in spite of recent advances in antibody engineering, antibodies remain expensive, require the need to be humanized to avoid rapid clearance, are time-consuming to produce, and present problems associated with storage stability and in vivo stability (Farokhzad, Cheng, Teply, Sherifi, Jon, Kantoff, Richie, and Langer, 2006). Other alternatives for drug targeting can be achieved with small molecules such as folic acid, which can target overexpressed folate receptors on 95% of ovarian carcinomas (Kirpotin, Park, Hong, Zalipsky, Li, Carter, Benz, and Papahadjopoulous, 1997; Leamon, Cooper, and Hardee, 2003). A relatively new class of ligands for drug targeting is aptamers, which are DNA or RNA oligonucleotides that through intramolecular interactions fold into three-dimensional conformations (Farokhzad, Cheng, Teply, Sherifi, Jon, Kantoff, Richie, and Langer, 2006). Aptamers as targeting molecules exhibit stability in a range of pH (4–9), temperatures, and organic solvents without loss of activity and are important especially when targeting to the tumor microenvironment which has a characteristically low pH (Farokhzad, Cheng, Teply, Sherifi, Jon, Kantoff, Richie, and Langer, 2006; Minchinton, and Tannock, 2006). Also, methods for attaching targeting ligands to the surface of nanocarriers include covalent and noncovalent linkages (Brannon-Peppas, and Blanchette, 2004; Farokhzad, Cheng, Teply, Sherifi, Jon, Kantoff, Richie, and Langer, 2006; Gref, Couvreur, Barratt, and Mysiakine, 2003; Nobs, Buchegger, Gurny, and Allemann, 2004; Torchilin, 2004). Therefore, in designing nanoparticles with targeting moieties, it is important to consider the stability of the ligand in vivo, and its ability to achieve high efficacy must be considered.

External Activation

Drug delivery carriers can be externally guided to cancer lesions and activated upon reaching the targeted tissue. External guidance via an applied magnetic field is one example by which colloidal carriers bypass physical and cellular barriers. Strategies which incorporate iron oxide nanoparticles and gold nanoparticles within the nanocarrier structure are beneficial for applications in magnetic resonance imaging (MRI), triggered drug release, and localized thermal therapy (Oliver, Ahmad, Kamaly, Perouzel, Caussin, Keller, Herlihy, Bell, Miller, and Jorgensen, 2006; Perez, Josephson, and Weissleder, 2004; Sukhishvili, 2005; Sunderland, Steiert, Talmadge, Derfus, and Barry, 2006). The concept of a magnetically targeted delivery system emerged in the 1970s (de Jaeghere, Doelker, and Gurny, 1999) and since then extensive research has been performed to illustrate the utility of these ferrofluids in cancer treatment (Kingsley, Dou, Morehead, Rabinow, Gendelman, and Destache, 2006). For example, superparamagnetic nanoparticles and magnetic liposomes have been used for tumor imaging to help provide information on the grade of the cancer and the leakiness of the tumor vasculature (Daldrup, Shames, Wendland, Okuhata, Link, Rosenan, Lu, and Brasch, 1998; Jaffer, and Weissleder, 2004).

Once the particulate drug delivery has collected in the tumor vasculature, external activation by focused ultrasound, radiofrequency, laser light (photodynamic therapy), or an applied magnetic field can help trigger drug release and cell death (thermal ablation therapy) (Hirsch, Halas, and

West, 2003; May, Allen, and Ferrara, 2002; Roy, Ohulchanskyy, Pudavar, Bergey, Oseroff, Morgan, Dougherty, and Parasad, 2003; Unger, Porter, Culp, Labell, Matsunaga, and Zutshi, 2004). Drug delivery carriers such as liposomes (MAGfect) (Oliver, Ahmad, Kamaly, Perouzel, Caussin, Keller, Herlihy, Bell, Miller, and Jorgensen, 2006), amine-functionalized magnetite nanoparticles (Wang, Bao, Wang, Zhang, and Li, 2005), and hollow microcapsule-loaded magnetite particles (Lu, Prouty, Guo, Golub, Kumar, and Lvov, 2005) have demonstrated MRI imaging and triggered release for anti-cancer applications. The combination of the EPR effect with external activation via a magnetic field has been investigated with animal models and in vitro models (Ferrari, 2005). This synergistic combination of active and passive targeting with externally activated drug delivery is expected to increase the selectivity of anti-cancer drugs in the diseased tissue.

Fabrication of Drug Delivery Carriers

The encapsulation of chemotherapeutic drugs within nanocarriers can be accomplished using liposomes (Scherphof, and Kamps, 1998), polymeric micelles (H. Liu, S. Farrell, and K. Uhrich, 2000; Torchilin, 2004), biodegradable polymer nanoparticles (Brannon-Peppas, and Blanchette, 2004; Feng, and Chien, 2003), dendrimers (Quintana, Raczka, Piehler, Lee, Mye, Majoros, Patri, Thomas, Mule, and Baker, 2002), and hollow microcapsules (Liu, Gao, Shen, and Mohwald, 2005) (Figure 16.3). The variety

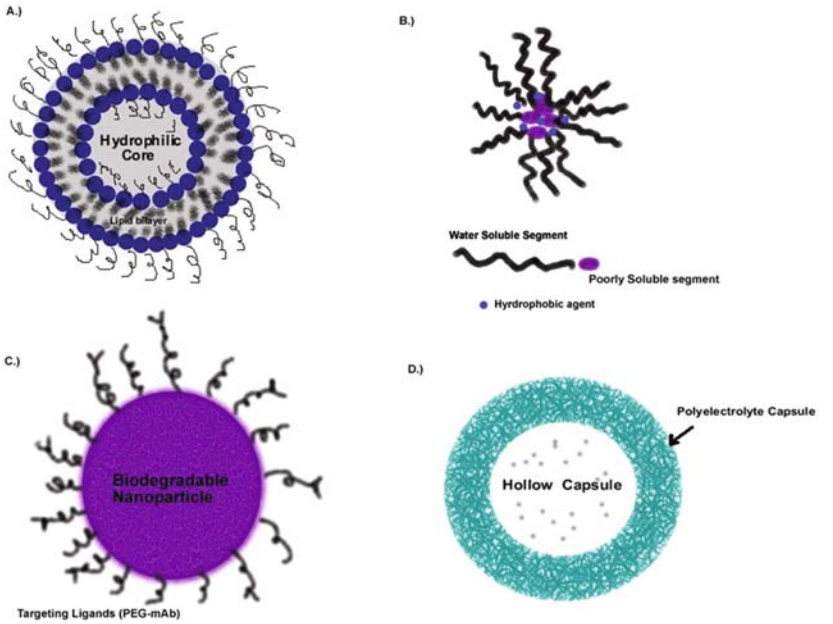

Figure 16.3 Current drug delivery nanoparticulate systems for anti-cancer therapy: (**a**) PEGylated liposome; (**b**) micelle; (**c**) biodegradable nanoparticles with targeted ligand attached to the distal end of poly(ethylene glycol) (PEG) chains; (d) hollow microcapsule assembled via the layer-by-layer assembly technique. (*See* Color Plate 23)

of delivering strategies is either being currently used or is in testing stages for cancer treatment (Moses, Brem, and Langer, 2003). Each delivering strategy has its own challenges to face, but recent advances have illustrated the therapeutic efficacy of each delivery mode using in vitro and in vivo models. This section summarizes the nanoparticles that have had the highest impact in the field of drug delivery.

Liposomes

Liposomes are spherical phospholipid bilayers, with sizes varying from 50 to 1000 nm, that spontaneously form in aqueous media to sequester either water-soluble or water-insoluble anti-cancer drugs and proteins within their hydrophilic interior or within their phospholipid bilayer (Aplin, Howe, Alahari, and Juliano, 1998; Jamil, Shiekh, and Ahmad, 2004). Their aqueous interior can be used to entrap peptides, proteins, and hydrophilic anti-cancer drugs such as 5-fluorouracil and doxorubicin. The size and shape of liposomes can be varied by controlling the mixture of phospholipids, the degree of saturation of fatty acid side chains, and the conditions of formation (Saltzman, 2001). After intravenous injection, traditional liposomes exhibit short circulating lifetimes, which can be attributed to their phospholipid surface that is recognized by the human immune system (Scherphof, and Kamps, 1998). Improvements in the in vivo stability of the carrier have been made after the development of poly(ethylene glycol) (PEG) modified liposomes (Harrington, Rowlinson-Busza, Syrigos, Uster, Vile, and Stewart, 2000; Lewanski, and Stewart, 1999). The circulation half-life of PEGylated liposomes has increased due to changes in the rate of uptake by phagocytic cells. Doxil® (ALZA Corporation), a PEGylated liposomal drug delivery system (5 mol% PEG 2000 Da, ~200 nm), is FDA approved for the delivery of anti-tumor drug doxorubicin for the treatment of ovarian cancer and AIDS-related Kaposi's sarcoma (Moses, Brem, and Langer, 2003). Although liposomes have been approved by the FDA for human use, many problems are associated with them due to their low encapsulation efficiency, their poor in vivo stability, deficient tumor penetration, and lack of storage stability (Aplin, Howe, Alahari, and Juliano, 1998; Gref, Couvreur, Barratt, and Mysiakine, 2003).

Polymeric Micelles

Polymeric micelles represent another class of pharmaceutical carriers which can entrap water-insoluble anti-cancer drugs, such as paclitaxel, camptothecin, and tamoxifen. Polymeric micelles are colloidal dispersions with particles size between 5 and 100 nm. These colloidal dispersions are spontaneously formed under certain concentrations and temperatures by surfactants or block copolymers consisting of hydrophilic and hydrophobic monomer units (Torchilin, 2004). The hydrophobic drug can be incorporated into the micelle either by covalent attachment to the hydrophobic segment or by non-covalent incorporation into the hydrophobic core; and loading capacities between 5 and 25% wt of drug can be achieved. The conventional polymeric micelle consists of a PEG block (MW between 1 and 15 kDa) covalently linked to a variety of hydrophobic polymers such as L-lysine, aspartic acid, caprolactone, phosphatidyl ethanolamine,

poly(propylene oxide), and D,L-lactic acid (Gao, Lukyanov, Singhal, and Torchilin, 2002; Torchilin, 2004). The surface of the micelle can be chemically modified with antibodies to create a polymeric immunomicelle which has cancer-targeting capabilities. Torchilin and co-workers demonstrated targeted delivery with PEG/phosphatidyl ethanolamine (PE) paclitaxel-loaded micelles conjugated with monoclonal antibody 2C5 (2004). In vivo instability of polymeric micelles is a major limitation of using this type of carrier system for anti-cancer therapy. Upon dilution into the systemic circulation these micelles dissociate into unimers and this takes place at concentrations below the critical micelle concentration (CMC). To prevent micelle degradation approaches have been taken to stabilize these structures in the biological milieu. One method utilizes phospholipids to increase the hydrophobicity of the core which reduces micelle dissociation upon dilution (Gao, Fain, and Rapoport, 2004).

Biodegradable Nanoparticles

Polymer particulate carriers are attractive because polymers can be chemically modified in any number of ways to improve drug delivery and targeting. By adjusting the chemical structure of the monomer unit, it may be possible to achieve a delivery system that produces an attractive therapeutic release profile, while also providing the means of escaping the body's various filtering and defense mechanisms (Langer, 2000; Peracchia, 1997). Synthetic biodegradable polymers including polylactide, polyglycolide, and copolymer poly(D,L-lactide-co-glycolic acid) (PLGA) are the most commonly used biomaterials for drug delivery. These biomaterials are FDA approved for human use because of their unique properties which include the ability to break down into naturally occurring metabolites, lactic and glycolic acids; degradation only requires water; and varying properties can be engineered via copolymerization of the monomer units. In the last 25 years many groups have evaluated the use of copolymers of lactide and gylcolide for the release of small and large molecules (Brannon-Peppas, and Blanchette, 2004; Saltzman, 2001). Other than synthetic biomaterials, natural polymers such as polypeptides and polysaccharides can be used to fabricate nanoparticles (Zhang, Mardyani, Chan, and Kumacheva, 2006). Recently, the first therapeutic nanoparticle drug delivery system, Abraxane^{TM}, was approved as a treatment for metastatic breast cancer (Duncan, 2006). This particulate carrier is composed of human serum albumin nanoparticles ($\sim$130 nm) bound with chemotherapeutic paclitaxel for intravenous delivery to target albumin receptors expressed on endothelial cells and in the tumor interstitium (Sparreboom, Baker, and Verweij, 2005).

The most common method for the production of biodegradable nanoparticles involves the use of liquid emulsions (Birnbaum, and Brannon-Peppas, ; Desgouilles, Vauthier, Bazile, Vacus, Grossiord, Veillard, and Couvreur, 2003; O'Donnell, and McGinity, 1997). The spontaneous emulsification–solvent evaporation (or diffusion) technique has been extensively used to prepare drug, lipophilic compounds, loaded PLGA micro- and nanoparticles (O'Donnell, and McGinity, 1997). Different emulsification-based methods have been described in literature and

depend on the polymer, drug, and organic solvents that are used (de Jaeghere, Doelker, and Gurny, 1999). The goal of the emulsification/evaporation technique is to prepare polymeric nanoparticles loaded with therapeutic agent by the use of immiscible liquids to form droplets of polymer solution in a continuous (*aqueous*) phase which subsequently hardens to form particles by polymer precipitation and organic solvent removal at the air/water interphase (Yeh, Coombes, Jenkins, and Davis, 1995). During the emulsification step, high shear imparted by a homogenizer, sonicator, or magnetic stir bar disrupt microdroplets to form stable polymeric nanoparticles. The aqueous phase usually consists of surfactants such as polysorbate, poloxamer, sodium dodecyl sulfate or stabilizer poly(vinyl alcohol) to minimize coalescence of the microdroplets (de Jaeghere, Doelker, and Gurny, 1999).

Variables that influence physiochemical properties such as size, size distribution, encapsulation efficiency, and internal morphology of the nanoparticles include polymer to drug ratio, emulsification speed, organic volume to aqueous volume ratio, viscosity of continuous and organic phase, temperature, and surfactant concentration (Desgouilles, Vauthier, Bazile, Vacus, Grossiord, Veillard, and Couvreur, 2003; O'Donnell, and McGinity, 1997). Although these parameters can be controlled, problems such as the use of toxic chlorinated solvents and non-biodegradable surfactants remain for the application of the emulsion techniques.

Characterization of Drug Carriers

The physicochemical properties which includes size, size distribution, surface and bulk morphology, surface chemistry, surface charge, drug encapsulation efficiency, and physical and chemical status of the drug encapsulated determine the therapeutic efficacy of the nanoparticle (Feng, and Chien, 2003). Various techniques are used to analyze the physicochemical properties of nanovectors. These techniques serve to evaluate the relationship between physicochemical properties of nanovectors and their interaction with blood components in the systemic circulation (de Jaeghere, Doelker, and Gurny, 1999).

Size and Size Distribution

The size of the nanoparticle and the distribution of size in a colloidal suspension are important design parameters for any drug delivery system. The nanometer size of a carrier provides a larger surface area to volume ratio, which facilitates drug release and surface chemical modification (Feng, and Chien, 2003). Size is important in preventing uptake by the mononuclear phagocyte system (MPS), penetrating the smallest capillaries of the human vasculature (< 5 μm), and transporting across fenestrated endothelium in diseased tissue (Gref, Couvreur, Barratt, and Mysiakine, 2003; Hansen, Kao, Moase, Zalipsky, and Allen, 1995; Hobbs, Monsky, Yuan, Roberts, Griffith, Torchilin, and Jain, 1998; Sanjeeb K. Sahoo, 2003). Also, a monodisperse size distribution is important in providing programmed drug release at the disease site. Nanoscale particle size may

pose problems in stability and is prone to aggregate in the biological environment (Moghimi, Hunter, and Murray, 2005). One way to circumvent this problem is utilizing non-ionic surfactants and stabilizers to sterically stabilize the particles in the biological media. Therefore, minimizing aggregation is an important criterion for stabilizing the colloidal carrier and producing an efficacious drug delivery system. The size and size distribution can be measured by dynamic laser light scattering (DLS) instruments such as the ZetaSizer NanoS. The uniformity of the nanoparticles is quantified by the polydispersity index (PI), where a PI of less than 0.2 indicates a monodisperse particulate system.

Surface and Bulk Morphology

Characterizing the surface and bulk morphology of the nanoparticle can be accomplished using high-resolution microscopy such as scanning electron microscopy (SEM) and transmission electron microscopy (TEM). These instruments may also be utilized to determine size and size distribution of the colloidal carrier. Depending on the magnification and the settings used, both techniques offer reliable results regarding both surface and bulk information.

In SEM an image is created after an incident electron beam strikes the sample surface and produces secondary electrons that provide topographic information. High sample resolution can be achieved by adjusting the working distance and accelerating voltage. Due to the nanometer size of the particles, surface features are better resolved when the working distance is close to the surface of the sample. The resolution may also be improved by decreasing the rate at which electrons bombard the sample. At 5.0 kV, the electrons are able to penetrate the surface of the sample, and the resolution of 3.5 nm can be achieved by the scatter of secondary electrons. At this lower limit, the nanometer size and surface features of the drug particles are visualized. Higher magnification ($\times$ 300 k) and antistigmatism becomes more difficult to achieve at this lower range because electron charging in the sample is prominent. The most severe drawback in using SEM is charging. Although the sample is coated with gold, after viewing the particles under these process conditions, charging can limit the resolution of the nanoparticles.

TEM uses a high-energy electron beam transmitted through a thin sample ($<$1000 Å) to analyze the sample with atomic scale resolution (Marshall, 2006). The electrons are accelerated at several hundred kV, such that 200 kV electrons have a wavelength of 0.025 Å. The resolution of TEM is limited by aberrations in electromagnetic lenses to give resolutions between 1 and 2Å (Marshall, 2006). The information gathered by TEM allows the user to study the topography, morphology, and composition of the sample. A criterion for TEM is that the sample must be thin enough to be electron transparent. There is a potential that the sample might be damaged from the high-energy electron beam. TEM has been used prominently by researchers to demonstrate the fabrication of thin polyelectrolyte films formed after electrostatic adsorption (Zahr, de Villiers, and Pishko, 2005).

The disadvantages or limitations in using SEM and TEM are due to the sample preparation which requires time and dry samples that must

withstand a high vacuum (Ratner, Johnston, and Lenk, 1987). The dry nature of the sample does not mimic the hydrated environment of the drug particles in aqueous solution. Also, since most polymeric nanoparticles are non-conductive, they are sputtered with gold to provide a conductive film for imaging in SEM making the image less realistic (Feng, and Chien, 2003). One limitation with TEM that is not shared with SEM is images are only in two dimensions and are viewed in transmission; therefore, TEM does not have a depth sensitivity that is obtained with SEM (Williams, and Carter).

Surface Composition

The surface characteristics of the nanoparticle play an important role in determining their in vitro and in vivo interactions with the biological milieu (Gbadamosi, Hunter, and Moghimi, 2002; Luck, Paulke, Schroder, Blunk, and Muller, 1998; Moghimi, and Szebeni, 2003). The design of a surface that can prevent protein adsorption and uptake by the immune system is a criterion for any drug delivery carrier (S. Stolnik, Daudali, Arien, Whetstone, Heald, Garnett, Davis, and Illum, 2001; S. Stolnik, Illum, and Davis, 1995; Torchilin, 2004). For example, it has been shown that methods such as emulsion–solvent evaporation produce particles with surfaces that may influence protein adsorption (Luck, Paulke, Schroder, Blunk, and Muller, 1998). Surface chemical analysis can be used to determine the concentration of an emulsifier or surfactant at the surface of a nanoparticle. X-ray photoelectron spectroscopy (XPS), a technique that probes the surface of a material with nano-sampling depth, can be used to characterize the surface chemistry.

XPS utilizes the photoelectron effect, which occurs when an incident beam of light interacts with matter (surface) that in turn causes emission of electrons (Moulder, Stickle, Sobol, and Bomben, 1992). High-energy x-ray photons, $h\nu$, bombard the sample and colloid with electrons present at the surface, causing photoelectrons to be emitted into a vacuum with kinetic energy, K_E. Next, the binding energy is calculated from the known kinetic energy of the photoelectron and energy of the x-ray photon. The result is a survey scan of all the atoms present at the surface (Zahr, de Villiers, and Pishko, 2005). The survey scan is a plot of counts per second (CPS) versus binding energy (BE). The data from the survey scan can be analyzed and atomic percents can be calculated via software program. Also, high-resolution scans taken at lower pass energies of 20 eV and longer acquisition times provide information regarding the oxidation species of the atoms present at the surface. The data collected from XPS can help confirm the presence of certain functional groups and ligands at the nanoparticle surface.

There are four advantages in using XPS for surface chemical analysis: (1) it is an analytical technique that can detect all elements with the high probability to capture core electrons; (2) it can be used to determine functional groups at the interface and the associated oxidation states of the atoms present; (3) it is surface sensitive with a penetration depth between 1 and 10 nm; (4) it is quantitative without the requirement for standards. Although this technique is surface sensitive, it does not probe the interface between drug particles and solution. Also, the nanoparticles

must be dried in order to be placed in a high-vacuum chamber (10^{-6} Pa). Due to the high-energy x-ray photons, the sample will be structurally modified. Also, this technique cannot detect hydrogen, has a poor lateral resolution (>5 μm), and large sample size is required especially for powders and may be difficult to attain.

Surface Charge

The surface charge density of the particulate carrier has been found to play an important role in uptake by phagocytic cells (Moghimi, Hunter, and Murray, 2005; Zahr, Davis, and Pishko, 2006). The surface charge can be determined by the measured zeta potential (ζ-potential). The ζ-potential is not a direct measure of the surface potential, which is more difficult to calculate. The ζ-potential is responsible for inter-particle forces that can dictate aggregation and this is affected by the pH, viscosity, and the ionic strength of the solution. Also, in general a highly charged particulate system will remain stabilized as described by the DLVO theory of colloidal thermodynamics. In physiological conditions the Debye length ~1–3 nm can induce aggregation, therefore carriers with high surface charge densities remain stable via charge repulsion forces.

Surface Engineering of Nanoparticles

A major challenge in drug delivery is the development of long-circulating carriers, which have a decreased rate of elimination from the systemic circulation, thus allowing for successful delivery to the diseased site. This challenge is due to the immediate interaction between the surface of the carrier with serum proteins and cells of MPS (Fernandez-Urrusuno, Fattal, Porquet, Feger, and Couvreur, 1995; Gref, Couvreur, Barratt, and Mysiakine, 2003; S. I. Stolnik, L. Davis, S.S., 1995a). Recent progress has been achieved in reducing the clearance of drug carriers after intravenous injection. A number of authors have illustrated that the surface of the colloidal carrier can be chemically or physically modified with non-ionic polymers and surfactants to increase in vivo circulation times (Duncan, 2003; Gbadamosi, Hunter, and Moghimi, 2002; Mosqueira, Legrand, Gref, Heuratault, Appel, and Barratt, 1999; S. Stolnik, Illum, and Davis, 1995). Therefore, surface modification of the nanoparticle can help achieve a more robust long-circulating drug delivery carrier.

Long-Circulating Drug Carriers

The efficient delivery of therapeutic agents to the diseased tissue requires long-circulating drug carriers. To reduce protein adsorption, and opsonization, by blood serum proteins (fibronectin, albumin, fibrinogen, IgG) (Papisov, 1998) the drug delivery carrier must have high curvature, nanometer size, a neutral surface charge, and a hydrophilic surface (Brigger, Morizet, Aubert, Chacun, Terrier-Lacombe, Couvreur, and Vassal, 2002; S. I. Stolnik, L. Davis, S.S., 1995a; Zeta-Meter, 2006). The carrier size, charge, and shape (Champion, and Mitragotri, 2006) greatly influence the

circulation time of the drug delivery system. Although the shape and size of the drug delivery system are important in prolonging circulation times, hydrophilic, thus water-soluble, nanoparticles are more desired. Nanoparticle surfaces grafted with hydrophilic polymers play an important role in a type of colloidal stability known as steric stabilization (Storm, Belliot, Daemen, and Lasic, 1995b). Particle stability is important in the biological milieu because it directly increases circulation half-life and thereby reduces uptake by the MPS.

A non-ionic polymer that has demonstrated biocompatibility in various medical applications and is FDA approved for in vivo use is poly(ethylene glycol) (PEG) (Bailon, 1998; Brigger, Morizet, Aubert, Chacun, Terrier-Lacombe, Couvreur, and Vassal, 2002; Gong, Dai, Griesser, and Mau, 2000; Gref, Couvreur, Barratt, and Mysiakine, 2003; Lasic, Vallner, and Working, 1999; Lewanski, and Stewart, 1999). Long-circulating PEG-coated carriers exhibit reduced adsorption of blood proteins and increased circulation half-life. The effect of PEG on protein adsorption can be attributed to PEG's unique solution properties and molecular conformation (S. I. Stolnik, L. Davis, S.S., 1995a). Protein adsorption can be explained in terms of interfacial energetics (Norde, 1996; Tripp, Magda, and Andrade, 1995). The steric repulsion resulting from a loss of conformational entropy upon protein adsorption contributes to the physiological properties of nanoparticles covered with PEG. Also, PEG chains attached to the nanoparticle surface minimally perturb the structure of water minimizing the tendency for hydrophobic interactions with proteins. Furthermore, PEG's interaction with water decreases interfacial energy at the water–PEG interface. With a low interfacial energy it is energetically unfavorable for blood proteins to adsorb to the nanoparticle surface. Consequently, hydration by water molecules helps prevent protein adsorption and creates a hydrophilic surface needed for long circulation of nanoparticles (Gref, Couvreur, Barratt, and Mysiakine, 2003; S. I. Stolnik, L. Davis, S.S., 1995a; Storm, Belliot, Daemen, and Lasic, 1995b). The ideal particulate carrier would have a uniform molecular cloud of hydrophilic PEG molecules over the surface which can protect the drug-loaded particles from protein adsorption and internalization by the MPS.

Coating Surfaces with Poly(ethylene glycol)

Modification of the nanoparticle surface with PEG can be attained by physical adsorption, chemical adsorption, or during nanoparticle fabrication using copolymers such as PLGA–PEG (Faraasen, Voros, Csucs, Textor, Merkle, and Walter, 2003). Coating nanoparticles with PEG-based surfactants, such as poloxamer 188 and pluronic F68, are current methods utilized for physical surface adsorption (Santander-Ortega, Jodar-Reyes, Csaba, Bastos-Gonzalez, and Ortega-Vinuesa, 2006). A major problem associated with these coatings is desorption of the surfactant from the nanoparticle surface upon intravenous administration. It has been suggested by Napper (Napper, 1983) that the stability of the polymer coverage determines the biodistribution of the particulate system. The stability of grafted PEG chains can be enhanced through covalent attachment. Covalent attachment of PEG 2, 5, and 20 kDa to the surface of

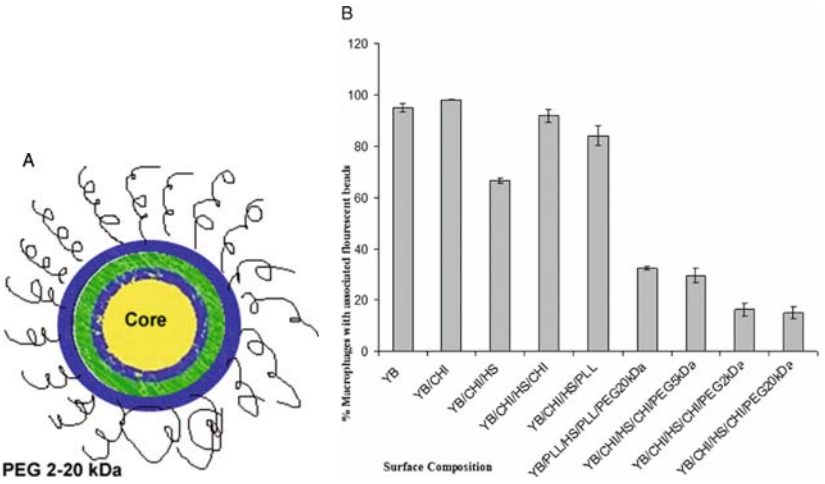

Figure 16.4 (**a**) Schematic of a core–shell nanoparticle assembled step-wise using the layer-by-layer self-assembly technique to create thin multilayered polyelectrolyte layers. The surface of the nanoshell is chemically modified with PEG molecules to produce a long-circulating drug delivery carrier. (**b**) Percent of (live) macrophages with associated fluorescent core–shell nanoparticles versus surface composition of the nanoshell introduced at time = 0 and incubated for 24 hours. (*See* Color Plate 24)

amine-terminated core–shell nanoparticles was demonstrated by Zahr and co-workers, Figure 16.4a (Zahr, Davis, and Pishko, 2006). Core fluorescent nanoparticles approximately 200 nm in diameter were encapsulated within a multilayered polyelectrolyte nanoshell assembled step-wise utilizing a layer-by-layer self-assembly technique. Surface chemical analysis was performed with XPS to confirm the successful medication of the nanoshell. Covalent attachment of PEG to the nanoshell resulted in an increase in atomic percent of oxygen and an increase in the peak area percent of $(C\text{-}C\text{-}O)_n$, which represents the repeat unit in the backbone of a PEG molecule. Also, a neutral ζ-potential re-confirmed the presence of non-ionic PEG grafted at the surface of the nanoshell. In vitro studies were performed to study the phagocytic uptake of core–shell fluorescent nanoparticles (200 nm) using a flow cytometric assay. Results showed that a neutral and hydrophilic nanoshell can reduce the uptake of core–shell nanoparticles after 24 hours of incubation with suspension macrophages (Figure 16.4b). The results to date hold promise in using the LbL technique to control the surface chemistry when fabricating a nanoshell for drug delivery applications.

Current Colloidal Drug Carriers

In the last decade nanometer size particles for tumor targeting have made an important contribution to cancer therapy. The turn-of-the-century insight made by Paul Ehrlich in the early 1900s described the concept of a "magic bullet," molecules that target a pathological disease with precision and reduce stimulation of the autoimmune system (S. I. Stolnik, L.

Davis, S.S., 1995a). Nanoparticles, which can target and localize the chemotherapeutic within the tumor tissue, are a medical necessity. The following section describes current colloidal carriers with targeting capabilities that authenticate Ehrlich's concept of the magic bullet.

Targeting with HER2/neu

The expression of HER2/neu provides an antibody-based targeting scheme for breast and ovarian cancer treatment (Kirpotin, Park, Hong, Zalipsky, Li, Carter, Benz, and Papahadjopoulous, 1997; Park, Barrett, Rubner, and Mayes, 2001). Anti-HER2, a monoclonal antibody, was covalently attached to PEG-modified liposomes for the delivery of adriamycin, a chemotherapeutic drug for breast cancer. In vitro studies performed with Anti-HER2-modified liposome by Kirpotin and colleagues demonstrate that uptake by SK-BR-3-cells at 37°C was slightly hindered if Anti-HER2 was directly attached to the PEGylated liposome surface (Kirpotin, Park, Hong, Zalipsky, Li, Carter, Benz, and Papahadjopoulous, 1997). The researchers hypothesized that PEG reduces the lateral mobility of the liposome-conjugated antigen fragment, which in turn reduces the number of antigen fragments that may be exposed to the cell surface (Kirpotin, Park, Hong, Zalipsky, Li, Carter, Benz, and Papahadjopoulous, 1997). To circumvent this problem, Anti-HER2 was covalently attached to the distal terminus of PEG 19 kDa and as a result the formation of multiple interactions between liposome and HER2 receptors was permitted. This multivalent interaction exhibits a higher affinity to the HER2 receptors and smaller dissociation constants. This study illustrates an apparent trade-off between a targeted and stealth delivery system.

Targeting with Folic Acid

Elevated expression of the folate receptor (FR) has been found in various types of human cancers and is weakly expressed in normal tissues including the lung, thyroid, and kidney (Sudimack, and Lee, 2000). There are three isoforms of FR found in the blood: α, β, and γ (Lu, Prouty, Guo, Golub, Kumar, and Lvov, 2005). FR-α is present at high levels in malignant tissues of epithelial cells, especially in the ovaries. The FR α-isoform, a glycosylphoshatidylinositol-linked membrane glycoprotein, has a dissociation constant (K_D) of $\sim$0.1 nM for folic acid, which is internalized into cells via a high-affinity receptor-mediated process (Quintana, Raczka, Piehler, Lee, Mye, Majoros, Patri, Thomas, Mule, and Baker, 2002). Folic acid is a popular targeting molecule because of its low immunogenicity, small molecular weight (Mw $\sim$ 441.4), compatibility with the use of organic solvents during preparation, and operational stability (Vandervoort, and Ludwig, 2002). Folic acid-conjugated proteins, chemotherapeutic drugs, virus vectors, dendrimers, and nanoparticles have been fabricated to achieve high tumor-selective targeting (Quintana, Raczka, Piehler, Lee, Mye, Majoros, Patri, Thomas, Mule, and Baker, 2002).

Covalent conjugation of folic acid to the nanovector surface may alter its function and targeting capabilities. Stella and co-workers demonstrated

that the covalent attachment of folic acid to ~15% of the total PEG chains improved targeting of the particulate drug delivery carrier (Waugh, Trissel, and Stella, 1991). Leamon and colleagues investigated the targeting activity of folic acid liposomes by modifying the length of the PEG linker. The length of the linker was important for the folate to enter the binding pocket of the cell surface receptor (Lee, and Low, 1994). Their results demonstrated that a molecular weight of PEG as low as 1000 was sufficient for efficient in vitro targeting to KB cells (Leamon, Cooper, and Hardee, 2003). Thus, a PEG-folate-modified drug delivery system enhances the targeted delivery of chemotherapeutic drugs to the cancer cells in vivo.

Targeting with Aptamers

Recent published results by Farokhzad and co-workers (Farokhzad, Cheng, Teply, Sherifi, Jon, Kantoff, Richie, and Langer, 2006) demonstrated the in vitro and in vivo efficacy of PEGylated PLGA nanoparticles (153 ± 13.9 nm, ζ-potential -42 ± 1 mV) bioconjugated with an aptamer that binds to prostate-specific membrane antigen (PSMA) on the surface of prostate cancer cells (Pca). The encapsulated chemotherapeutic agent Docetaxel (Dtxl) retained therapeutic activity within the nanoparticle, and in vitro results demonstrated a reduction in cell viability of $42 \pm 2\%$ after 30 minutes and $30 \pm 1\%$ after 2 hours of incubation with Pca cells. Efficacy and toxicity studies were performed for 109 days with seven mice, bearing tumors with size ~300 mm^3. Mice treated with Dtxl-Np-Apt demonstrated the best efficacy; tumor size was reduced to 119 ± 84 mm^3 and all mice in this group survived the 109-day study (Farokhzad, Cheng, Teply, Sherifi, Jon, Kantoff, Richie, and Langer, 2006). For toxicity studies, the researchers analyzed the effect of dose on white blood cell count (WBC) and found no evidence of toxicities with Dtxl-Np-Apt compared to Dtxl-Np. The authors suggested that toxicity associated with non-targeted nanoparticles was a result of Dtxl release in the extracellular space opposed to intracellular release with targeted nanoparticles (Farokhzad, Cheng, Teply, Sherifi, Jon, Kantoff, Richie, and Langer, 2006).

Conclusions

The impact of nanotechnology for cancer therapy is evident. The advantages of nanocarriers over current treatment regimes for cancer therapy include lower toxicity due entrapment of the cytotoxic drug, selectivity to the diseased tissue, and improved bioavailability of the anti-cancer drug.

Engineering nanoparticles with the appropriate surface chemistry to achieve a long-circulating and targeted delivery system is a challenging task. Challenges lie in maintaining particle stability upon surface chemical modification. Targeted delivery to the cancer lesion can increase selectivity there by minimizing the potential of adverse side effects. The surfaces of liposomes, biodegradable nanoparticles, and polymeric micelles have been successfully modified with targeting ligands specific to an overexpressed receptor on the surface of cancer cells. Combination of targeting

approaches such as utilizing the passive or active targeting with an externally applied magnetic field holds promise in cancer therapy. As new tumor-specific targets are identified the development of drug delivery systems which can avoid anatomical and physiological barriers is needed. Advances have been made in using nanoparticles for cancer therapy but there still remains an unmet medical need. Strategies for engineering surfaces with multifunctionality can perhaps enhance the therapeutic efficacy of anti-cancer drugs and provide new treatment strategies for patients.

Future Directions: Multifunctional Carriers

Multifunctional drug delivery systems which have the ability to target two or more cellular receptors, deliver a payload of two or more cytotoxic agents, and image the cancer lesion and microenvironment are becoming the new paradigm for anti-cancer drug delivery. This new paradigm supports an integrative approach to anti-cancer therapy and may offer a solution to current unmet medical needs in oncology (Moghimi, Hunter, and Murray, 2005; Sawant, Hurley, Salmaso, Kale, Tolcheva, Levchenko, and Torchilin, 2006; Sengupta, Eavarone, Capila, Zhao, Watson, Kiziltepe, and Sasisekharan, 2005). Currently, this integrative approach has yielded three sets of drug delivery carrier systems; the first uses a two-ligand-targeted approach, the second uses a nanocarrier that delivers two cytotoxic agents, and the third combines imaging contrast agents, therapeutics, and targeting into a nanocarrier.

The selectivity of the targeted carrier can be further enhanced by a dual-ligand approach. In such a double-targeted system, the nanocarrier can target two receptors expressed on one cell phenotype or receptors expressed on cells with different phenotypes (e.g., inflamed endothelium and cancer cells). In recent work, Sawant and co-workers developed a stimuli-responsive dual-targeted PEGylated liposome and PEG-phosphatidylethanolamine-micelle drug delivery system (Sawant, Hurley, Salmaso, Kale, Tolcheva, Levchenko, and Torchilin, 2006). The surface of these nanocarriers were modified with low-pH cleavable PEG chains covalently attached at the terminus with monoclonal antimyosin antibody 2G4 and shorter non-cleavable PEG chains covalently bound to TATp peptides. The monoclonal antibody targets to a specific organ or tissue while the TATp peptide allows for the delivery into the cellular membrane. Another group investigated the in vitro cytotoxicity of dual-ligand-targeted PEGylated liposome carriers (115–120 nm) in delivering anti-cancer drug doxorubicin to KB cells which express both the FR and the epidermal growth factor receptor (EGFR) (Saul, Annapragada, and Bellamkonda, 2006). In this work, Saul and co-workers (2006) modified the surface of the liposome with folic acid (200 ligands per liposome) and monoclonal antibody 225 (3 mAb225 per liposome) specific to EGFR to create a dual-targeted nanocarrier. Their work demonstrated that by modulating ligand numbers, a dual-targeted liposome carrier with optimized selectivity to KB cells can be fabricated when compared to single-ligand-targeted liposomes. It was concluded that dual-targeted nanocarriers can further reduce the toxicity to normal cells which

express low concentration of receptors identical to cancer cells and enhance the selective uptake by providing more ligand–receptor interactions.

The synergistic combination of two or more cytotoxic agents was recently illustrated by Sengupta and co-workers (2005). In this work an anti-angiogenic drug combrestatin A4 was combined with anti-cancer drug doxorubicin in a nanocarrier composed of a PLGA core entrapped within a phospholipid-PEG envelope (180–200 nm). The nanocarrier termed the "nanocell" enables the release of the anti-angiogenic drug, causing shutdown of the tumor vasculature; followed by the focal release of the anti-cancer drug extending over 15 days. In vivo results demonstrated the accumulation of these carriers after 24 hours of circulation, reduction in hydrostatic pressure, and inhibition of cancer growth.

This integrative approach combines anti-angiogenic and anti-cancer drugs to produce an improved therapeutic effect. The combination of imaging agent, therapeutic drug, and targeted drug delivery system is yet another approach to the new paradigm in anti-cancer drug delivery therapy. Reddy and co-workers fabricated a nanoparticle carrier (~40 nm) composed of polyacrylamide with encapsulated superparamagnetic nanoparticles and photodynamic agent, Photofrin, within its matrix (Reddy, Bhojani, McConville, Moody, Moffat, Hall, Kim, Koo, Woolliscroft, Sugai, Johnson, Philbert, Kopelman, Rehemtulla, and Ross, 2006). The surface of the nanoparticle was modified with PEG 2000 Da conjugated to tumor vascular targeting F3 peptide. In vitro results revealed that after encapsulation of Photofrin within the nanoparticle matrix, the agent retained its cytotoxic effect to yield singlet oxygen species. In vivo studies revealed that vascular targeting improved nanoparticle accumulation within the brain tumor environment providing an approximately twofold increase in contrast enhancement. Also, upon treatment with photodynamic therapy, the survival rate of the glioma-bearing rates was significantly improved. Since most anti-cancer drugs including photosensitizers are limited by systemic toxicity, entrapment of the cytotoxic drug within a targeted nanoparticle matrix hides the drug from the physiological milieu to prevent systemic exposure.

References

Allen, T. M. (2002). Ligand-Targeted Therapeutics in Anticancer Therapy. *Nature, 2*, 750–763.

Aplin, A. E., Howe, A., Alahari, S. K., and Juliano, R. L. (1998). Signal Transduction and Signal Modulation by Cell Adhesion Receptors: The Role of Integrins, Cadherins, Immunoglobulin-Cell Adhesion Molecules, and Selectins. *Phamacological Reviews, 50*(2), 199–252.

Bailon, P. B., W. (1998). Polyethylene glycol-conjugated pharmaceutical proteins. *Pharmaceutical Science and Technology Today, 1*(8), 352–356.

Birnbaum, D. T., and Brannon-Peppas, L. Microparticle Drug Delivery Systems. In D. M. Brown (Ed.), *Drug Delivery Systems in Cancer Therapy*. Totowa: Humana Press Inc.

Brannon-Peppas, L., and Blanchette, J. O. (2004). Nanoparticle and targeted systems for cancer therapy. *Advanced Drug Delivery Reviews, 56*, 1649–1659.

Brigger, I., Morizet, J., Aubert, G., Chacun, H., Terrier-Lacombe, M.-J., Couvreur, P., and Vassal, G. (2002). Poly(ethylene glycol)-Coated Hexadecylcyanoacrylate Nanospheres Display a Combined Effect for Brain Tumor Targeting. *The Journal of Pharmacology and Experimental Therapeutics, 303*(3), 928–936.

Champion, J. A., and Mitragotri, S. A. (2006). Role of target geometry in phagocytosis. *PNAS, 103*(13), 4030–4033.

Daldrup, H., Shames, D. M., Wendland, M., Okuhata, Y., Link, T. M., Rosenan, W., Lu, Y., and Brasch, R. C. (1998). Correlation of dynamic contrast-enhanced magnetic resonance imaging with histologic tumor grade: comparison of macromolecular and small-molecular contrast media. *Pediatric Radiology, 28*, 67–78.

de Jaeghere, F., Doelker, E., and Gurny, R. (1999). Nanoparticles. In E. Mathiowitz (Ed.), *Encyclopedia of Controlled Drug Delivery* (Vol. 2, pp. 641–664). New York: John Wiley & Sons, Inc.

Desgouilles, S., Vauthier, C., Bazile, D., Vacus, J., Grossiord, J.-L., Veillard, M., and Couvreur, P. (2003). The Design of Nanoparticles Obtained by Solvent Evaporation: A Comprehensive Study. *Langmuir, 19*, 9504–9510.

di Tomaso, E., Capen, D., Haskell, A., Hart, J., Logie, J. J., Jain, R. K., McDonald, D. M., Jones, R., and Munn, L. L. (2005). Mosaic Tumor Vessels: Cellular Basis and Ultrastructure of Focal Regions Lacking Endothelial Cell Markers. *Cancer Research, 65*(13), 5740–5749.

Dreher, M. R., Liu, W., Michelich, C. R., Dewhirst, M. W., Yuan, F., and Chilkoti, A. (2006). Tumor Vascular Permeability, Accumulation, and Penetration of Macromolecular Drug Carriers. *Journal of the National Cancer Institute, 98*(5), 335–344.

Dua, R. S., Gui, G. P. H., and Isacke, C. M. (2005). Endothelial adhesion molecules in breast cancer invasion into the vascular and lymphatic systems. *Journal of Cancer Surgery, 31*, 824–832.

Duncan, R. (2003). The Drawing Era of Polymer Therapeutics. *Nature Reviews, 2*, 247–359.

Duncan, R. (2006). Polymer conjugates as anticancer nanomedicines. *Nature 6*, 688–701.

Esfand, R., and Tomalia, D. A. (2001). Poly(amidoamine) (PAMAM) dendrimers: from biomimicry to drug delivery and biomedical applications. *Drug Discovery Today, 6*(8), 427–436.

Faraasen, S., Voros, J., Csucs, G., Textor, M., Merkle, H. P., and Walter, E. (2003). Ligand-specific targeting of microspheres to phagocytes by surface modification with poly(L-lysine)-grafted poly(ethylene glycol) conjugate. *Pharmaceutical Research, 20*(2), 237–246.

Farokhzad, O. C., Cheng, J., Teply, B. A., Sherifi, I., Jon, S., Kantoff, P. W., Richie, J. P., and Langer, R. (2006). Targeted nanoparticle-aptamer bioconjugates for cancer chemotherapy in vivo. *PNAS, 103*(16), 6315–6320.

Feng, S.-S., and Chien, S. (2003). Chemotherapeutic engineering: Application and further development of chemical engineering principles for chemotherapy of cancer and other diseases. *Chemical Engineering Science, 58*, 4087–4114.

Fernandez-Urrusuno, R., Fattal, E., Porquet, D., Feger, J., and Couvreur, P. (1995). Influence of Surface Properties on the Inflammatory Response to Polymeric Nanoparticles. *Pharmaceutical Research, 12*(9), 1995.

Ferrari, M. (2005). Cancer Nanotechnology: Opportunities and Challenges. *Nature Reviews, 5*, 161–172.

Gao, Z., Fain, H. D., and Rapoport, N. (2004). Ultrasound-enhanced tumor targeting of polymeric micellar drug carriers. *Molecular Pharmaceutics, 1*(4), 317–330.

Gao, Z., Lukyanov, A. N., Singhal, A., and Torchilin, V. P. (2002). Diacyllipid-Polymer Micelles as Nanocarriers for Poorly Soluble Anticancer Drugs. *Nano Letters, 2*(9), 979–982.

Gbadamosi, J. K., Hunter, A. C., and Moghimi, S. M. (2002). PEGylation of microspheres generates a heterogenous population of particles with different surface characteristics and biological performances. *FEBS Letters, 532*, 338–344.

Gong, X., Dai, L., Griesser, H. J., and Mau, A. W. H. (2000). Surface Immobilization of Poly(ethylene oxide) Structure and Properties. *Journal of Polymer Science: Part B: Polymer Physics, 38*, 2323–2332.

Gref, R., Couvreur, P., Barratt, G., and Mysiakine, E. (2003). Surface-engineered nanoparticles for multiple ligand coupling. *Biomaterials, 24*, 4529–4537.

Gringauz, A. (1997). *How Drugs Act and Why*. New York: Wiley-VCH.

Hansen, C. B., Kao, G. Y., Moase, E. H., Zalipsky, S., and Allen, T. M. (1995). Attachment of antibodies to sterically stabilized liposomes: Evaluation, comparison and optimization of coupling procedures. *Biochimica et Biophysica Acta, 1239*, 133–144.

Harrington, K. J., Rowlinson-Busza, G., Syrigos, K. N., Uster, P. S., Vile, R. G., and Stewart, J. S. W. (2000). Pegylated Liposomes Have the Potential as Vehicles for Intratumoral and Subcutaneous Drug Delivery *Clinical Cancer Research, 6*, 2528–2537.

Heldin, C.-H., Rubin, K., Pietras, K., and Ostman, A. (2004). High Interstitial Fluid Pressure- An Obstacle in Cancer Therapy. *Nature Reviews: Cancer, 4*, 806–813.

Herbst, R. S. (2004). Review of Epidermal Growth Factor Receptor Biology. *International Journal of. Radiation Oncology, Biology, Physics, 59*(2), 21–26.

Hirsch, L. R., Halas, N. J., and West, J. L. (2003). Nanoshell-mediated near-infrared thermal therapy of tumors under magnetic resonance guidance. *Proceeding of the National Academy of Sciences of the United States of America., 100*, 13549–13554.

Hobbs, S. K., Monsky, W. L., Yuan, F., Roberts, W. G., Griffith, L., Torchilin, V. P., and Jain, R. K. (1998). Regulation of transport pathways in tumor vessels: Role of tumor type and microenvironment *Proceeding of the National Academy of Sciences of the United States of America, 95*, 4607–4612.

Jaffer, F. A., and Weissleder, R. (2004). Seeing within: Molecular Imaging of the Cardiovascular System. *Circulation Research, 94*, 433–445.

Jain, R. K. (2001). Delivery of molecular and cellular medicine to solid tumors. *Advanced Drug Delivery Reviews, 46*, 149–168.

Jamil, H., Shiekh, S., and Ahmad, I. (2004). Liposomes: The Next Generation. *Modern Drug Discovery*, 37–39.

Jang, S. H., Wientjes, M. G., Lu, D., and Au, J. L.-S. (2003). Drug Delivery and Transport to Solid Tumors *Pharmaceutical Research, 20*(9), 1337–1350.

Jemal, A., Murray, T., Ward, E., Samuels, A., Tiwari, R. C., Ghafoor, A., Feuer, E. J., and Thun, M. J. (2005). Cancer Statistics, 2005. *CA: A Cancer Journal for Clinicians, 55*(1), 10–30.

Kim, C. K., and Lim, S. J. (2002). Recent progress in drug delivery systems for anticancer agents. *Archives of Pharmacal Research, 25*, 229–239.

Kingsley, J. D., Dou, H., Morehead, J., Rabinow, B., Gendelman, H. E., and Destache, C. J. (2006). Nanotechnology: A Focus on Nanoparticles as a Drug Delivery System. *Journal of Neuroimmunology and. Pharmacology, 1*, 340–350.

Kipp, J. E. (2004). The role of solid nanoparticle technology in the parenteral delivery of poorly water-soluble drugs. *International Journal of Pharmaceutics, 284*(284), 109–122.

Kirpotin, D., Park, J. W., Hong, K., Zalipsky, S., Li, W., Carter, P., Benz, C. C., and Papahadjopoulous, D. (1997). Sterically stabilized Anti-HER2 Immunoliposomes: Design and Targeting to Human Breast Cancer cells in vitro. *Biochemistry, 36*, 66–75.

Langer, R. (2000). Biomaterials in Drug Delivery and Tissue Engineering: One Laboratory's Experience. *Accounts of Chemical Research, 33*, 94–101.

Lasic, D. D., Vallner, J. J., and Working, P. K. (1999). Sterically stabilized liposomes in cancer therapy and gene delivery. *Current Opinion in Molecular Therapeutics, 1*(2), 177–185.

LaVan, D. A., McGuire, T., and Langer, R. (2003). Small-scale systems for in vivo drug delivery *Nature Biotechnology, 21*, 1184–1191.

Leach, K. J. (1999). *Cancer, Drug Delivery to Treat Local and Systemic* (Vol. 1). New York: John Wiley & Sons Inc.

Leamon, C. P., Cooper, S. R., and Hardee, G. E. (2003). Folate-Liposome-Mediated Antisense Oligodeoxynucleotide Targeting to Cancer Cells: Evaluation in Vitro and in Vivo. *Bioconjugate Chemistry, 14*, 738–747.

Lee, R. J., and Low, P. S. (1994). Delivery of Liposomes into Cultured KB Cells via Folate Receptor-mediated Endocytosis. *The Journal of Biological Chemistry, 269*, 3198–3204.

Lewanski, C. R., and Stewart, S. (1999). Pegylated liposomal adriamycin: a review of current and future applications. *Pharmaceutical Science and Technology Today, 2*(12), 473–477.

Liu, H., Farrell, S., and Uhrich, K. (2000). Drug release characteristics of unimolecular polymeric micelles. *Journal of Controlled Release, 68*, 167–174.

Liu, H., Farrell, S., and Uhrich, K. (2000). Drug release characteristics of unimolecular polymeric micelles. *Journal of Controlled Release, 68*(2), 167–174.

Liu, X., Gao, C., Shen, J., and Mohwald, H. (2005). Multilayer Microcapsules as Anti-Cancer Drug Delivery Vehicle: Deposition, Sustained Release and in vitro Bioactivity. *Macromolecular Bioscience, 5*, 1209–1219.

Loeb, K. R., and Loeb, L. A. (2000). Significance of multiple mutations in cancer. *Genes Chromosomes Cancer, 38*, 302–306.

Loeb, L. A. (1991). Mutator phenotype may be required for multistage carcinogenesis. *Cancer Research, 51*, 3075–3079.

Lu, Z., Prouty, M. D., Guo, Z., Golub, V. O., Kumar, C. S. S. R., and Lvov, Y. M. (2005). Magnetic Switch of Permeability for Polyelectrolyte Microcapsules Embedded with Co@Aug Nanoparticles. *Langmuir, 21*, 2042–2050.

Luck, M., Paulke, B. R., Schroder, W., Blunk, T., and Muller, R. H. (1998). Analysis of plasma protein adsorption on polymeric nanoparticles with different surface characteristics. *Journal of Biomedical Materials Research, 39*, 478–485.

Luo, Y., and Prestwich, G. D. (2002). Cancer-targeted polymeric drugs. *Current Cancer Drug Targets, 2*(3), 209–226.

Maeda, H., Fang, J., Inutsuka, T., and Kitamoto, Y. (2003). Vascular permeability enhancement in solid tumor: various factors, mechanisms involved and its implications. *International Immunopharmocology, 3*, 319–328.

Maeda, H., Wu, J., Sawa, T., Matsumura, Y., and Hori, K. (2000). Tumor vascular permeability and the EPR effect in macromolecular therapeutics: a review. *Journal of Controlled Release, 65*, 271–284.

Marshall, A. (2006). Transmission Electron Microscope (TEM) Facility.

May, D. J., Allen, J. S., and Ferrara, K. W. (2002). Dynamics and fragmentation of thick-shelled microbubbles. *IEEE Trans., 49*, 1400–1410.

Merlo, L. M. F., Pepper, J. W., Reid, B. J., and Maley, C. C. (2006). Cancer as an evolutionary and ecological process. *Nature Reviews: Cancer, advanced online publication*, 1–12.

Minchinton, A. I., and Tannock, I. F. (2006). Drug penetration in solid tumors. *Nature Reviews, 6*, 583–592.

Moghimi, S. M., Hunter, A. C., and Murray, J. C. (2005). Nanomedicine: current status and future prospects. *FASEB J., 19*, 311–330.

Moghimi, S. M., and Szebeni, J. (2003). Stealth liposomes and long circulating nanoparticles: Critical issues in pharmacokinetics, opsonization, and protein-binding properties. *Progress in Lipid Research, 42*, 463–478.

Moses, M. A., Brem, H., and Langer, R. (2003). Advancing the field of drug delivery: Taking aim at cancer. *Cancer Cell, 4*, 337–340.

Mosqueira, V. C. F., Legrand, P., Gref, R., Heuratault, B., Appel, M., and Barratt, G. (1999). Interactions between a Macrophage Cell line (J774A1) and surface-modified Poly(D,L-lactide) Nanocapsules Bearing Poly(ethylene glycol). *Journal of Drug Targeting, 7*(1), 65–78.

Moulder, J. F., Stickle, W. F., Sobol, P. E., and Bomben, K. D. (1992). *Handbook of X-ray Photoelectron Spectroscopy*. Eden Praire, MN: Perken-Elmer Corp.

Muller, R. H., Mader, K., and Gohla, S. (2000). Solid lipid nanoparticles (SLN) for controlled drug delivery – a review of the state of the art. *European Journal of Pharmaceutics and Biopharmaceutics, 50*, 161–177.

Napper, D. H. (1983). *Polymeric Stabilization of Colloidal Dispersion*. London: Academic Press.

Neri, D., and Bicknell, R. (2005). Tumor Vascular Targeting. *Nature Reviews, 5*, 436–447.

Nobs, L., Buchegger, F., Gurny, R., and Allemann, E. (2004). Current methods for attaching ligands to liposomes and nanoparticles. *Journal of Pharmaceutical Sciences, 93*, 1980–1992.

Norde, W. (1996). Driving Forces for Protein Adsorption at Solid Surfaces. *Macromol. Symp., 103*, 5–18.

O'Donnell, P. B., and McGinity, J. W. (1997). Preparation of microspheres by the solvent evaporation technique. *Advanced Drug Delivery Reviews, 28*, 25–42.

Oliver, M., Ahmad, A., Kamaly, N., Perouzel, E., Caussin, A., Keller, M., Herlihy, A., Bell, J., Miller, A. D., and Jorgensen, M. R. (2006). MAGfect: a novel liposome formulation for MRI labelling and visualization of cells. *Organic & Biomolecular Chemistry, 4*(18), 3489–3497.

Pante, N., and Kann, M. (2002). Nuclear Pore Complex is Able to Transport Macromolecules with Diameters $\sim$ 39 nm. *Molecular Biology of the Cell, 13*, 425–434.

Papisov, M. I. (1998). Theoretical considerations of RES-avoiding liposomes: Molecular mechanics and chemistry of liposome interactions. *Advanced Drug Delivery Reviews, 32*, 119–138.

Park, S. Y., Barrett, C. J., Rubner, M. F., and Mayes, A. M. (2001). Anomalous Adsorption of Polyelectrolyte Layers. *Macromolecules, 34*, 3384–3388.

Peracchia, M. T. (1997). PEG-coated nanospheres from amphiphilic diblock and multiblock copolymers: Investigation of their drug encapsulation and release characteristics. *Journal of Controlled Release, 46*, 223–231.

Perez, J. M., Josephson, L., and Weissleder, R. (2004). Use of magnetic nanoparticles to probe for molecular interactions. *ChemBioChem., 5*, 261–264.

Quintana, A., Raczka, E., Piehler, L., Lee, I., Mye, A., Majoros, I., Patri, A. K., Thomas, T., Mule, J., and Baker, J. R. (2002). Design and Function of a Dendrimer-Based Therapeutic Nanodeviced Targeted to Tumor Cells Through the Folate Receptor. *Pharmaceutical Research, 19*(9), 1310–1316.

Ratner, B. D., Johnston, A. B., and Lenk, T. J. (1987). Biomaterial Surfaces. *Journal of Biomedical Materials Research: Applied Biomaterials, 21*(A1), 59–90.

Reddy, G. R., Bhojani, M. S., McConville, P., Moody, J., Moffat, B. A., Hall, D. E., Kim, G., Koo, Y.-E. L., Woolliscroft, M. J., Sugai, J. V., Johnson, T., D., Philbert, M. A., Kopelman, R., Rehemtulla, A., and Ross, B. D. (2006). Vascular Targeted Nanoparticles for Imaging and Treatment of Brain Tumors. *Clin 12*(22), 6677–6686.

Roy, L., Ohulchanskyy, T. Y., Pudavar, H. E., Bergey, E. J., Oseroff, A. R., Morgan, J., Dougherty, T. J., and Parasad, P. N. (2003). Ceramic-based

nanoparticles entrapping water-insoluble photosensitizing anticancer drugs: a novel drug-carrier system for photodynamic therapy. *Journal of the American Chemical Society, 125*, 7860–7865.

Ruan, G., Feng, S.-S., and Li, Q.-T. (2002). Effects of material hydrophobicity on physical properties of polymeric microspheres formed by double emulsion process. *Journal of Controlled Release, 84*, 151–160.

Sahoo, S. K., and Labhasetwar, V. (2003). Nanotech approaches to drug delivery and imaging. *Drug Discovery Today, 8*, 1112–1120.

Saltzman, W. M. (2001). *Controlled Drug Delivery Systems* (Vol. 1). Oxford: Oxford University Press, Inc.

Sanjeeb K. Sahoo, V. L. (2003). Nanotech approaches to drug delivery and imaging. *DDT, 8*(24), 1112–1120.

Santander-Ortega, M. J., Jodar-Reyes, A. B., Csaba, N., Bastos-Gonzalez, D., and Ortega-Vinuesa, J. L. (2006). Colloidal stability of Pluronic F68-coated PLGA nanoparticles: A variety of stabilization mechanisms. *Journal of Colloid and Interface Science, 302*, 522–529.

Saul, J. M., Annapragada, A. V., and Bellamkonda, R. V. (2006). A dual-ligand approach for enhancing targeting selectivity of therapeutic nanocarriers. *Journal of Controlled Release, 114*, 277–287.

Sawant, R. M., Hurley, J. P., Salmaso, S., Kale, A., Tolcheva, E., Levchenko, S., and Torchilin, V. P. (2006). "SMART" Drug Delivery systems: Double-Targeted pH-Responsive Pharmaceutical Nanocarriers. *Bioconjugate Chemistry, 17*, 943–949.

Scherphof, G. L., and Kamps, J. A. A. M. (1998). Receptor versus non-receptor mediated clearance of liposomes. *Advanced Drug Delivery Reviews, 32*, 81–97.

Sengupta, S., Eavarone, D., Capila, I., Zhao, G., Watson, N., Kiziltepe, T., and Sasisekharan, R. (2005). Temporal targeting of tumour cells and neovasculature with a nanoscale delivery system. *Nature, 436*, 568–572.

Sheff, D. (2004). Endosomes as a route for drug delivery in the real world. *Advanced Drug Delivery Reviews, 56*, 927–930.

Sparreboom, A., Baker, S. D., and Verweij, J. (2005). Paclitaxel Repackaged in an Albumin-Stabilized Nanoparticle: Handy or Just a Dandy? *Journal of Clinical Oncology, 23*(31), 7765–7767.

Stolnik, S., Daudali, B., Arien, A., Whetstone, J., Heald, C. R., Garnett, M. C., Davis, S. S., and Illum, L. (2001). The effect of surface coverage and conformation of poly(ethylene oxide) (PEO) chains of poloxamer 407 on the biological fate of model colloidal drug carriers. *Biochimica et Biophysica Acta, 1514*(2), 261–279.

Stolnik, S., Illum, L., and Davis, S. S. (1995). Long circulating microparticulate drug carriers. *Advanced Drug Delivery Reviews, 16*(2–3), 195–214.

Stolnik, S. I., L. Davis, S.S. (1995a). Long circulating microparticulate drug carriers. *Advanced Drug Delivery Reviews, 16*(2–3), 195–214.

Stolnik, S. I., L. Davis, S.S. (1995b). Long circulating microparticulate drug carriers. *Advanced Drug Delivery Reviews, 16*(2–3), 195–214.

Storm, G., Belliot, S. H., Daemen, T., and Lasic, D. D. (1995a). Surface modification of nanoparticles to oppose uptake by the mononuclear phagocyte system. *Advanced Drug Delivery Reviews, 17*, 31–48.

Storm, G., Belliot, S. H., Daemen, T., and Lasic, D. D. (1995b). Surface modification of nanoparticles to oppose uptake by the mononuclear phagocyte system. *Advanced Drug Delivery Reviews, 17*, 31–48.

Sudimack, J., and Lee, R. J. (2000). Targeted drug delivery via the folate receptor. *Advanced Drug Delivery Reviews, 41*, 147–162.

Sukhishvili, S. A. (2005). Responsive polymer films and capsules via layer-by-layer assembly. *Current Opinion in Colloid & Interface Science, 10*, 37–44.

Sunderland, C. J., Steiert, M., Talmadge, J. E., Derfus, A. M., and Barry, S. E. (2006). Targeted nanoparticles for detecting and treating cancer. *Drug Development Research, 67*(1), 70–93.

Thote, A. J., Chappell, J. T., Gupta, R. B., and Kumar, R. (2005). *Drug Development and Industrial Pharmacy 31*(1), 43–57.

Tomalia, D. A., and Frechet, J. M. J. (2002). Discovery of dendrimers and dendritic polymers: a brief historical perspective. *Journal of Polymer Sciences Part A: PolymerChemistry., 40*, 2719–2728.

Torchilin, V. P. (2004). Targeted polymeric micelles for delivery of poorly soluble drugs. *Cellular and Molecular Life Sciences, 61*, 2549–2559.

Torchilin, V. P. (2006). Recent Approaches to Intracellular Delivery of Drugs and DNA and Organelle Targeting. *Annual Review in Biomedical Engineering, 8*, 343–375.

Tripp, B. C., Magda, J. J., and Andrade, J. D. (1995). *Journal of Colloid and Interface Science, 173*, 16–27.

Unger, E. C., Porter, T., Culp, W., Labell, R., Matsunaga, T., and Zutshi, R. (2004). Therapeutic applications of lipid-coated microbubbles. *Advanced Drug Delivery Reviews, 56*, 1291–1314.

Vandervoort, J., and Ludwig, A. (2002). Biocompatible stabilizers in the preparation of PLGA nanoparticles: a factorial design study. *International Journal of Pharmaceutics, 238*(1–2), 77–92.

Vasir, J. K., and Labhasetwar, V. (2005). Targeted Drug Delivery in Cancer Therapy. *Technology in Cancer Research & Treatment, 4*(4), 363–374.

Wang, L., Bao, J., Wang, L., Zhang, F., and Li, Y.-P. (2005). One-pot Synthesis and Bioapplication of Amine-Functionalized Magnetite Nanoparticles and Hollow Nanospheres. *European Journal of Medicinal Chemistry, 12*, 6341–6347.

Watson, P., Jones, A. T., and Stephens, D. J. (2005). Intracellular trafficking pathways and drug delivery: fluorescence imaging of living cells and fixed cells. *Advanced Drug Delivery Reviews, 57*, 43–61.

Waugh, W. N., Trissel, L. A., and Stella, V. J. (1991). Stability, compatibility, and plasticizer extraction of taxol injection diluted in infusion solutions and stored in various containers. *American. Journal of Hospital Pharmacist, 48*, 1520–1524.

Weissleder, R. (2002). Scaling down Imaging: Molecular Mapping of Cancer in Mice. *Nature Reviews Cancer, 2*, 1–8.

Williams, D. B., and Carter, C. B. *Basic* (Vol. 1). New York: Plenum Press.

Yeh, M.-K., Coombes, A. G. A., Jenkins, P. G., and Davis, S. S. (1995). A novel emulsification-solvent extraction technique for production of protein loaded biodegradable microparticles for vaccine and drug delivery. *Journal of Controlled Release, 33*, 437–445.

Yuan, F., Dellian, M., Fukumura, D., Leunig, M., Berk, D. A., Torchilin, V. P., and Jain, R. K. (1995). Vascular Permeability in Human Tumor Xenograft: Molecular Size Dependence and Cutoff Size. *Cancer Research, 55*(17), 3752–3756.

Zahr, A. S., Davis, C. A., and Pishko, M. V. (2006). Macrophage Uptake of Core-Shell Nanoparticles Surface Modified with Poly(ethylene glycol). *Langmuir, 22*, 8178–8185.

Zahr, A. S., de Villiers, M., and Pishko, M. V. (2005). Encapsulation of Drug Nanoparticles in Self-Assembled Macromolecular Nanoshells. *Langmuir, 21*(1), 403–410.

Zeta-Meter, I. (2006). *Zeta Potential: A complete Course in 5 minutes* (Catalog Information). Staunton, VA.

Zhang, H., Mardyani, S., Chan, W. C., and Kumacheva, E. (2006). Design of Biocompatible Chitosan Microgels for Targeted pH-Mediated Intracellular Release of Cancer Therapeutics. *Biomacromolecules, 7*, 1568–1572.

17

Nanotechnology for Cancer Vaccine Delivery

Samar Hamdy, Aws Alshamsan, and John Samuel

Introduction

In spite of all the efforts of the biomedical community, cancer still represents one of the leading causes of death, suffering, and disability. Worldwide, one of eight deaths is ascribed to cancer. Consequently, cancer is responsible for one-third of the lost years of life and is second to cardiovascular diseases as a major killer (World Health Organization 2005). Most cancer patients are treated by a combination of surgery, radiotherapy, and/or chemotherapy. Whereas the primary tumor can, in most cases, be efficiently treated by a combination of these standard therapies, preventing the metastatic spread of the disease through disseminated tumor cells is often not effective. Besides, lack of specificity by those standard therapies leads to debilitating and distressing side effects, destroying healthy tissues along with cancer cells. To overcome these obstacles, there has been a growing focus on immunotherapy as a means to combat this disease (Schuster, Nechansky, & Kircheis, 2006). Immunotherapy primarily aims to prevent the metastatic spread of the disease and to improve quality of life of the affected individuals. It refers to therapies that utilize the immune system to fight cancer. Approaches that are applied in immunotherapy are based on complementation (passive immunotherapy) or stimulation (active immunotherapy) of the immune system. Passive immunotherapy provides a tumor antigen-specific immune response by supplying high amounts of effector molecules, i.e., tumor-specific antibodies. Antibody-based therapies have both significant advantages and disadvantages relative to conventional cancer therapy. Advantages include versatility and specificity. Disadvantages include high cost and small markets that hinder commercial development. It is also short-lived and dependant on repeated applications (Casadevall, 1999). The logical next step is therefore to develop strategies that trigger a patient's immune system to target and destroy cancer cells, "active immunotherapy". One advantage of the active forms of immunotherapy is that they have the potential to elicit a multifaceted polyclonal immune response. This enables them to maintain control over a wider range of tumor cell phenotypes compared to passive therapy (Neeson & Paterson, 2006). Active immunotherapies are often

M.M. de Villiers et al. (eds.), *Nanotechnology in Drug Delivery*, DOI: 10.1007/978-0-387-77667-5_17,

referred to as cancer vaccines because they use the same vaccine strategies that successfully eradicated infectious diseases, such as measles and polio, to fight cancer. Cancer vaccines offer distinct advantages over conventional approaches: specificity, minimal toxicity, circumvention of drug resistance, and potential for durable therapeutic effects via immunologic memory.

There are four main categories of cancer vaccines. First is cell-based vaccine such as manipulated tumor cells, activated peripheral blood or bone marrow-derived lymphocyte, dendritic cells (DCs), and gene-modified tumor cells, or other cells engineered to express cytokines, growth factor, or tumor antigens (Gong, Chen, Kashiwaba, & Kufe, 1997; Kowalczyk, Wysocki, & Mackiewicz, 2003; Tuting, Storkus, & Lotze, 1997). While these strategies show promise, they can be cumbersome and expensive to perform in a clinical situation. The second category employs the use of subunit features, such as synthetic peptides, purified antigens, and tumor cell lysates (Albert, Sauter, & Bhardwaj, 1998; Nestle et al., 1998; Tamura, Peng, Liu, Daou, & Srivastava, 1997). These alternate approaches, however, often result in a vaccine that exhibits poor immunogenicity and efficacy. The third category is viral and plasmid vectors expressing therapeutic genes (Bernards et al., 1987; Lathe et al., 1987). Most of these are potent initiators of immune activation. However, safety concerns have limited their human application. They are also limited in terms of the type of immunomodulatory molecules that can be incorporated in them. Further, repeated use of most viral-vector systems (including replication-deficient vectors) results in the generation of neutralizing anti-vector antibodies, which can inhibit effective $CD8^+$ T-cell stimulation by subsequent vaccinations (Mack et al., 1997; Razzaque, Dye, & Puri, 2000). The fourth category of anti-cancer vaccines being developed and not yet extensively studied in humans includes synthetic non-living nano-sized vaccine delivery systems. Nano-sized vaccine delivery systems represent an integrated area that combines lipid/polymer technology with molecular immunology providing specific delivery of vaccine components to specialized antigen-presenting cells (APCs), including macrophages and DCs, in a targeted and prolonged manner. Nano-sized vaccine delivery systems include colloidal lipid-based particulate delivery system (e.g., nano-emulsion and liposomes), as well as polymeric nanoparticles. Such delivery systems offer greater flexibility with respect to the manipulation of physicochemical properties of the vehicle and the range of antigens that can be incorporated in them (O'Hagan & Valiante, 2003). Accumulating research on the immunological milieu of DC–T cell conjugation that favor the desired anti-cancer immune responses have provided us with additional clues to the design of appropriate delivery system for cancer vaccines. With better understanding of the "immune activating" signaling pathways of DCs and the "immune suppressing signaling" by tumor, such delivery systems may be used to deliver molecules that could "turn on" the molecular switches most relevant to potent and lasting anti-cancer immunity and "turn off" the molecular switches associated with the tumor-induced immunosuppression. In this regard, it is important that cancer vaccine delivery systems have sufficient flexibility for incorporation of a broad number of such immunomodulatory molecules varying in physicochemical

properties. This strategy allows delivering the correct amount of antigen and/or immunomodulatory molecules to the optimal location, i.e., DCs at the correct rate and timing, and leads to maximize the immunological response and minimize undesired effects.

Together with the increasing knowledge about how to optimize the elements of anti-tumor immunity in order to generate clinically relevant responses, there is an ever-increasing list of immune evasion mechanisms frustrating the efforts of cancer vaccines. A recent review on cancer vaccines including 1306 patients (Rosenberg, Yang, & Restifo, 2004) has shown that the overall objective response rate was only 3.3%. Among the various reasons for this, two important issues stand out: (1) T-cell responses induced by current cancer vaccines may be "weak", both qualitatively and quantitatively; (2) the immunosuppressive tumor microenvironment inhibits anti-tumor T-cell activity at the effector phase. Activation of robust and lasting immune responses against cancer antigens and the reversal of the "immunosuppressive milieu" of the tumor microenvironment are major challenges (Kaufman & Disis, 2004; Zou, 2005). The objective of this chapter is to highlight the potential of nano-sized delivery systems for meeting those challenges. The rationale and expected outcomes following co-delivery of antigens and variety of immunomodulatory molecules to DCs *in vivo* are further discussed.

Nano-sized Delivery Systems for Targeting Vaccine Components to Dendritic Cells

Targeted Delivery of Antigens to Dendritic Cells

Rationale

DCs exhibit several features which are necessary for the generation of T-cell-mediated anti-tumor immunity. They efficiently capture and take up antigens in peripheral tissues and transport these antigens to the secondary lymphoid organs where they express high levels of MHC class I and II molecules that present the processed peptide to T cells for the priming of antigen-specific $CD4^+$ and $CD8^+$ T-cell responses. In addition, DCs express high levels of co-stimulatory molecules (CD80, CD86, and CD40) and secrete high amounts of interleukine-12 (IL-12), additional signals required to optimally activate antigen-specific immune responses (Banchereau & Palucka, 2005; Banchereau & Steinman, 1998; Dermime, Armstrong, Hawkins, & Stern, 2002; Nestle, Banchereau, & Hart, 2001). A recent study exploring the migratory capacity of genetically marked DCs in situ showed that each draining lymph node contained approximately 5×10^3 antigen-bearing DCs, and these cells persisted for 2 weeks. Moreover, it has been shown that even in the absence of antigen, DCs contact 500 different T cells in an hour. In the presence of antigen, DCs are highly efficient in recruiting antigen-specific T cells; approximately 44% of adoptively transferred T cells specific for lymphocytic choriomeningitis virus glycoprotein interacted with DCs pulsed with this glycoprotein *in vivo* (Bousso & Robey, 2003). This substantial frequency and longevity of DCs, combined with the high efficiency with which these cells seek out

and activate naïve T cells in situ, ensure that ample antigen presentation and stimulation is available for the rare (1 in 10^5–10^6) antigen-specific T cells in the draining lymph nodes (Garg et al., 2003).

Strategies

In light of the described functional characteristics of DCs, an obvious strategy for designing new or better vaccine formulations is a more defined targeting of antigens to this cell type thereby exploiting the unique abilities of DCs for antigen acquisition and display. *Ex vivo* peptide/protein-pulsed or gene-modified DCs have been used in experimental model systems of cancer and are shown to induce strong $CD8^+$ cytotoxic T lymphocyte (CTL) mediated anti-tumor immune responses. These tailor-made vaccines are costly and labor intensive and are not suited for larger human immunization programs, but illustrate well the pronounced effect of targeted antigen delivery into DCs (Foged, Sundblad, & Hovgaard, 2002). As a next step in the development of DC vaccines, it is proposed to load DCs with antigens *in vivo*. Delivery systems that can selectively target cancer antigens to DCs *in vivo* would be of major significance to cancer vaccines. Optimizing delivery system with this in mind is expected to improve efficacy, reduce doses and the risks of side effects, and improve control of immunologic outcome. Several strategies can be followed to incorporate a targeting antigen into vaccine formulations: (1) at protein/peptide level, (2) at DNA level (DNA vaccine) with endogenous synthesis of antigen or synthesis of chimeric protein targeted to DC, or (3) at the level of the drug delivery system. Peptides/proteins and DNA molecules exert the same weaknesses as other proteins and macromolecular drug candidates in terms of stability and bioavailability. Particulate delivery of macromolecules seems to overcome these weaknesses and many different systems are tested. These include polymeric materials ranging from polylactic-co-glycolic acid, starch, and a large number of other natural and synthetic polymers, and also lipid systems such as nano-emulsions and liposomes (Foged et al., 2002).

Benefits

Enhanced Internalization by DCs. Several studies have verified that DCs can internalize polymeric nanoparticles and liposomes, and that the internalization mechanism used can be partially controlled by altering properties of the biomaterial vehicle, including size and surface characteristics (Copland et al., 2003; Elamanchili, Diwan, Cao, & Samuel, 2004; O'Hagan & Valiante, 2003; Reddy, Swartz, & Hubbell, 2006c; Walter et al., 2001). Biodegradable nanoparticles made of the polymer poly(D,L-lactic-co-glycolic acid) (PLGA) can bind to or encapsulate proteins and peptides, in addition to DNA (Newman, Samuel, & Kwon, 1998; Wang, Robinson, Kwon, & Samuel, 1999). These particles are naturally targeted to DCs through phagocytosis since their dimensions are comparable to those of microorganisms. Particles can, through phagocytosis, deliver antigens to DCs 1000- to 10,000-fold more efficiently than soluble antigens. Particles are thus multifunctional in that they deliver antigens to DCs in a form where antigen is concentrated in spherical structures and protected against enzymatic degradation in the tissues (Foged et al., 2002). In addition, DCs

also use lectin-like surface receptors including the mannose receptor, DC-205, and DC-SIGN, which are thought to be involved in the phagocytosis of pathogens. These receptors can facilitate binding and endocytosis of ligands that have a terminal sugar such as mannose, fucose, and *N*-acetyl glucosamine. With this in mind, nanoparticles and/or liposomes can be functionalized with ligands that bind to these receptors that then trigger internalization through endocytosis (Reddy et al., 2006a).

Enhanced Antigen Presentation. A cancer vaccine delivery system should have appropriate antigen retention/release characteristics. Since cancer antigens released into the systemic circulation can cause immune tolerance instead of immune activation, it is important that the delivery system retain the antigen until the particles are taken up by the DCs. However, once internalized by the DCs, the particles should release the antigen intracellularly in a manner that will enable processing by MHC class I, class II, or both (cross-presentation) pathways. Vaccine delivery systems that promote escapes of the antigens from endosomes to cytoplasm would be beneficial in facilitating cross-presentation of exogenous antigens by MHC class I pathway and therefore induction of CTL responses. In primary mouse bone marrow-derived DCs (BMDCs), the MHC class I presentation of PLGA-encapsulated ovalbumin (OVA) stimulated T-cell IL-2 secretion at 1000-fold lower concentration than soluble antigen. The nanoparticles also served as an intracellular antigen reservoir, leading to sustained MHC class I presentation of OVA for 72 h, decreasing by only 20% after 96 h, a time at which the presentation of soluble antigens was undetectable. Cytosol extraction demonstrated that antigen delivery via PLGA nanoparticles increased the amount of protein that escaped from endosomes into the cytoplasm, thereby increasing the access of exogenous antigen to the classic MHC class I loading pathway (Shen et al., 2006). To deliver exogenous antigen for inducing cellular immunity through the MHC class I pathway can be a challenging problem, as internalized nanoparticles are initially within endosomes but are trafficked rapidly to lysosomes, where they are then degraded enzymatically, preventing the antigen from being processed and presented intracellularly (Reddy et al., 2006b). To avoid lysosomal trafficking, pH-sensitive polymers have been recently designed (Murthy N, 2003). These polymers release oligonucleotides and peptides into the cytoplasm as the endosome is acidified before lysosomal fusion. These strategies demonstrate how polymeric materials can be designed to respond specifically to the intracellular environment for efficient antigen release and specific processing. In conclusion, these recent studies have established the potential for nano-sized delivery systems to function as antigen delivery vehicles. Furthermore, these delivery systems have dramatically enhanced DC internalization, antigen processing and presentation. Such unique properties potentially facilitate the clinical use of these systems in the delivery of cancer vaccines.

Targeted Delivery of Toll-Like Receptor (TLR) Ligands to Dendritic Cells

Rationale

An ideal delivery system for cancer vaccines could, in addition to just active targeting the antigens to DCs, possess additional features that

activate or modulate DC functions. With this in mind, it is now possible to design nano-sized vaccines that provide both the proper antigenic and accessory signals for induction of full scale anti-tumor T-cell responses. These signals employ molecularly defined innate immunity receptors such as those belonging to the toll-like receptor (TLR) family. In cancer, it is precisely the triggering of these receptors that is lacking. Therefore, despite abundant evidence of extensive natural processing of tumor antigens, and even of a considerable level of natural cross-priming, the resulting CTL effector cell responses are anemic and ineffective. Provision of proper TLR ligands from the microbial realm will drastically enhance these abortive responses and turn them into strong tumoricidal effector responses capable of eradicating established cancers. Rather than relying on poorly defined immune system triggers, such as recombinant vectors or adjuvants without molecularly defined function, the novel generation of TLR ligand-mimicking adjuvants induces very precise signal transduction pathways in DCs that, moreover, can be further manipulated for desired effect by very precise changes in the ligands (Melief, Van Der Burg, Toes, Ossendorp, & Offringa, 2002).

Inadequate function of DCs in cancer is one of the major elements of compromised anti-tumor immune response. Despite substantial progress in recent years, the mechanism of inadequate DC function in cancer still remains unclear. The tumor microenvironment has emerged as an important component contributing to DC malfunction. Several lines of evidence indicated that tumors affecting DC maturation, differentiation, and migration may induce the generalized failure of the host to mount an effective anti-tumor response. Immature DCs fail to provide an appropriate co-stimulatory signal to T cells, and tolerance or anergy may develop. Indeed, antigen presentation by immature DC has been reported to result in induction of tolerance through abortive proliferation or anergy of antigen-specific T cells *in vivo* (Probst, Lagnel, Kollias, & van den Broek, 2003). Also, immature DCs can induce tolerance through the generation of regulatory T cells (Treg) that suppress immune responses by producing IL-10 and transforming growth factor (TGF)-β (Dhodapkar, Steinman, Krasovsky, Munz, & Bhardwaj, 2001). The significance of TLRs in activating adaptive immunity is well established; TLR-mediated activation of DCs is a crucial step in this process (Akira, Takeda, & Kaisho, 2001; Beutler, 2004; Iwasaki & Medzhitov, 2004; Takeda, Kaisho, & Akira, 2003). The control exerted by TLRs in linking innate and adaptive immunity is instrumental in the efficacy of vaccines containing TLR ligands. When antigen is co-delivered with TLR ligands to the same population of DCs, antigenic peptide presentation on MHC is augmented. Upregulation of co-stimulatory and MHC molecules, expression of chemokine receptors, secretion of cytokines and chemokines are further accelerated in TLR-activated DCs (discussed below). In this respect, timing of antigen and adjuvant (TLR ligands) delivery is crucial: Administrating the maturation stimulus too late after an antigen reaches the DCs might induce tolerance, while antigens targeted to DCs that are already mature are not efficiently cross-presented. Therefore, vaccine strategies that aim at co-delivery of both antigen and adjuvant simultaneously to DCs could provide immune system activation and also rescue impaired DCs from tumor-induced

immunosuppression. The use of nano-sized particulate delivery system enables the delivery of both antigens and adjuvants to DCs. Focusing the effect of adjuvants on the key cells responsible for priming immune responses will limit the potential for adverse events by restricting their systemic distribution to the injection site (O'Hagan D, 2003). In this review, we will examine recent findings on TLR-mediated DC maturation and activation and emphasize the advantage of nano-sized particulate delivery of TLR ligands in cancer vaccine formulations. We will further discuss the potential role of TLR ligands to reverse tumor-induced DC impairment, overcome Treg-mediated suppression, and break tolerance against self-cancer antigens. In addition, the effect of particulate delivery of TLR ligands on influencing type and magnitude of T cell and natural killer (NK) responses is highlighted.

Potential of TLR Delivery to Induce DC Maturation/Activation

Upregulation of MHC and Co-stimulatory Molecules. Immature DCs with deficient expression of co-stimulatory molecules and poor capacity to stimulate T-cell responses have been reported in patients with basal cell, colorectal, and breast cancer (Chaux, Moutet, Faivre, Martin, & Martin, 1996; Gabrilovich, Corak, Ciernik, Kavanaugh, & Carbone, 1997). Similarly, DCs derived from melanoma patients have an immature phenotype, reduced T-cell stimulatory capacity, and induce anergy in syngeneic $CD4^+$ T cells *in vitro* (Enk, Jonuleit, Saloga, & Knop, 1997; Pinzon-Charry, Maxwell, & Lopez, 2005). The co-stimulatory proteins CD40, CD80, CD86, and CD70 are upregulated on DCs after TLR activation (Iwasaki & Medzhitov, 2004). Several experimental approaches have illustrated how co-stimulatory molecule-mediated signaling improves vaccine efficacy, including the use of agonist anti-CD40 antibodies (Diehl et al., 1999) and the co-delivery of co-stimulatory molecules with antigens (Yamaguchi et al., 2004). CD40 on DCs binds to CD40 ligand T cells. This binding transmits activating signals to the T cells and also activates the DCs to express B7 molecules (CD80 and CD86), thus stimulating further T-cell proliferation. In addition, CD70 was shown to increase CTL responses significantly after antigen exposure, even in the absence of $CD4^+$ T cells (Borst, Hendriks, & Xiao, 2005). Furthermore, TLR stimulation results in a decrease in the recycling pool of MHC class II molecules between lysosomes and the cell membrane. This leads to the accumulation of antigen–MHC II complexes on the DC surface, thus facilitating antigen presentation (Cella, Engering, Pinet, Pieters, & Lanzavecchia, 1997; Hertz et al., 2001). Therefore, by increasing the numbers of MHC and co-stimulatory molecules, TLR stimulation contributes to vaccine responses (van Duin, Medzhitov, & Shaw, 2006).

Enhanced DC Migration. Multiple studies have demonstrated that the density of DCs within tumors of a variety of histological types are correlated with prognosis (Tsujitani et al., 1987; Zeid & Muller, 1993) and it is important for induction of immune responses to emigrate and accumulate DCs into draining lymph nodes from tumor site (Cumberbatch & Kimber, 1995). Migratory capability of DCs is dictated by the change of responsiveness of DCs to various chemokines during their development and maturation. Immature DCs respond to inflammatory cytokines (MIP-3α,

RANTES, and MIP-1α) via chemokine receptors CCR1, 5, and 6, whereas mature DCs respond to chemokines that are expressed in secondary lymphoid organs (MIP-3β/ELC and SLC) via CCR7 instead (Hirao et al., 2000). *Ex vivo* generated cancer vaccines based on DCs are currently applied in the clinic; however, many questions still remain. One of the concerns is how to ensure effective migration of DCs to the T-cell areas in the lymph node. Recently completed patient trials applying 111-indium labeled monocyte-derived DCs (moDCs) as cancer vaccines revealed that less than 5% of intradermally administrated mature moDCs reach draining lymph nodes (De Vries et al., 2003). Moreover, data from mouse models employing *ex vivo* generated BMDCs revealed that DCs migration from the intradermal injection site is in the same efficacy range. These results showed that migration of ex vivo generated DCs is inefficient; however, this can be improved by preconditioning of the vaccine injection site with either inflammatory cytokines or TLR ligands. An alternative approach is to target tumor antigens as well as TLR ligands selectively to DCs in situ using nano-sized vaccine delivery system. This will not only enable usage of the intricate migratory capacity of DCs *in vivo* but also circumvent the huge amount of work to generate DCs *in vitro* for each individual patient.

TLR-stimulated DCs downregulate CCR5 and upregulate CCR7, facilitating DCs migration to regional lymph nodes and the induction of antitumor immune responses (Means, Hayashi, Smith, Aderem, & Luster, 2003). It has been shown that tumor necrosis factor (TNF)-α is required for accumulation of DCs in draining lymph node and optimal contact sensitization (Cumberbatch & Kimber, 1995). Particulate delivery of TLR ligands can dramatically enhance DC maturation, leading to significant increase in the amount of pro-inflammatory cytokines produced by DCs. We have recently shown that delivery of TLR4 ligand (monophosphoryl lipid A; MPLA) in PLGA nanoparticles (NP) induced about a 1000-fold greater amount of secreted IL-12, TNF-α, and IL-6 by the DCs as compared to the soluble formulations containing the same dose of MPLA (Elamanchili & Diwan, 2007). Particulate delivery of MPLA in PLGA-NP was also superior to soluble MPLA in the induction of CCR7 expression (our unpublished data). These findings highlight the importance of such delivery system in the development of vaccine formulation that could target DCs *in vivo* and circumvent the complex migration cascade required for efficient homing of *ex vivo* manipulated DCs.

Enhanced Cross-Priming: Cross-priming is an essential functional feature for vaccines to induce CTL from $CD8^+$ T cells in response to exogenously added antigens. Stimulation of $CD8^+$ T cells by class I MHC-associated peptides from exogenous antigen requires transport of the antigen to the cytosol of the DCs prior to its translocation to the endoplasmic reticulum for association with nascent MHC class I molecules. Consequently, agents which augment delivery of exogenous antigens into the cytoplasm of DCs and thereby into the classical MHC class I route could be effective in induction of CTL responses. Compared to free soluble antigen, inclusion of antigen into PLGA-NP increased the amount of protein that escaped from endosomes into cytoplasm, thereby increasing the access of exogenous antigen to the classic MHC class I loading pathway (Shen et al., 2006). Similarly, we have also shown that delivery of OVA protein encapsulated

in PLGA-NP (OVA NP) to BMDCs efficiently cross-primed naïve $CD8^+$ T cells as evidenced by stimulation index (SI) > 600. However, co-delivery of MPLA along with OVA protein in the same nanoparticle formulation (OVA/MPLA NP) dramatically increased the extent of antigen-specific $CD8^+$ T-cell stimulation, as evidenced by SI >3000. The activated $CD8^+$ T cells were capable of interferon (IFN)-γ secretion and also exhibited the typical effector cytotoxic T-cell phenotype: $CD11a^{hi}CD25^+$ $CD69^+CD62L^{lo}CD44^{hi}$(Hamdy S, 2007). Tumor-eradicating therapy in murine models suggests that a frequency of antigen-specific T cells of at least 1–10% of $CD8^+$T cells is required for eradication of established tumors (Yee, 2005). In patients, this translates to a dose of 2–20 $\times$ 10^9 cells. The non-specific expansion methods (cytokines, T-cell receptor (TCR), and co-stimulatory molecule triggering) have been used to successfully expand unselected peripheral blood mononuclear cells (PBMCs) to > 10^{10} cells *in vitro* over a period of 2–4 weeks. These methods are time and labor intensive, require infrastructure support to cultivate and qualify T-cell products, and can be prohibitively expensive in its current experimental phase (Yee, 2005). Particulate delivery of antigen plus MPLA to DCs could be an optimum strategy to generate a population of T cells of desired magnitude with defined phenotypic and functional properties in much shorter time. Such approach could reduce many of these cost-related and logistical issues (Hamdy S, in press).

Cross-priming has also been demonstrated in the context of stimulation of TLR3 and TLR9 (Schroder & Bowie, 2005). TLR3 stimulation resulted in cross-priming in two vaccine models: vaccination with either virally infected cells or isolated OVA protein (Schulz et al., 2005). Furthermore, CpG oligodeoxynucleotides (ODNs) induced cross-priming by both B cells and DCs in a TLR9-dependent manner (Datta et al., 2003; Heit et al., 2004; van Duin et al., 2006). The exact mechanisms that lead to TLR-induced cross-priming are yet to be delineated. TLR activation likely leads to multiple effects in DCs that promote cross-priming. TLR ligands upregulate co-stimulatory molecules and induce cytokine secretion, both of which play a role in T-cell activation (Datta et al., 2003). It is worth noting that TLR9 is predominantly localized in the endosomes of DCs rather than their cell surface, and its optimal signaling is dependant on acidic pH. With this in mind, PLGA-NP might be the optimal vehicle for intracellular delivery of CpG ODN, since the nanoparticles are internalized into endosome where CpG ODN will be released in an acidic environment. In addition, lactic and glycolic acids, the degradation products of PLGA, will also contribute toward further acidification of endosomes, providing the most favored microenvironment of TLR9 signaling. Further investigation of the ability of TLR ligands to induce cross-priming will lead to better understanding and uncover vaccination strategies that elicit improved anti-tumor cell-mediated immunity.

Potential of TLR Delivery to Activate Natural Killer (NK) Cells

The involvement of NK cells in anti-tumor responses has been observed in different experimental systems. However, in patients with cancer, NK-cell activities have been shown to be impaired as assessed by the reduced

functionality of NK cells from patients *ex vivo*. Anti-tumor NK-cell functionality is strongly increased after activation (Albertsson et al., 2003). Recently, a number of papers have reported that TLR-dependent, fully activated DCs can stimulate NK-cell activation (Kamath, Sheasby, & Tough, 2005; Walzer, Dalod, Robbins, Zitvogel, & Vivier, 2005; Zanoni, Foti, Ricciardi-Castagnoli, & Granucci, 2005). Upon stimulation of DCs through TLRs, DCs constitute a source of several cytokines known to trigger NK-cell functions. In particular, DCs-derived IL-15, IL-12/IL-18, and IFN-α/β could specifically enhance NK-cell proliferation, IFN-γ secretion, and cytotoxic function, respectively. In light of this, therapeutic approaches indicated that NK cells might be harnessed to reject mouse and human tumors, particularly when cytokines (for example, IL-2, IL-12, IL-15, IL-18, IL-21, and type I IFNs) are used to induce NK-cell differentiation and activation. However, the systemic administration of cytokines has been associated with considerable toxicity, particularly for cytokines (such as IL-2 and IFN-α) that non-specifically activate a broad range of immune effectors. Cancer vaccines that selectively activate DCs to produce NK-cell-activating cytokines might provide a precise route of NK-cell activation, minimizing the toxic side effects of systemic cytokine administration, with the added advantage that combined activation of NK cells and DCs can augment adaptive immune responses. NK cells can facilitate adaptive anti-tumor immunity by producing IFN-γ and other cytokines that recruit and activate DCs, T cells, and B cells (Degli-Esposti & Smyth, 2005; Smyth, Hayakawa, Takeda, & Yagita, 2002; Yuan, Koh, & Wilder, 1994; Yuan, Wilder, Dang, Bennett, & Kumar, 1992). Activated NK cells can also stimulate the maturation of DCs, "licensing" DCs to present antigen to CTLs in lymph nodes (Cooper, Fehniger, Fuchs, Colonna, & Caligiuri, 2004; Gerosa et al., 2002). It is worth noting that NK cells might enhance adaptive immunity to tumors in a more indirect way. The killing of tumor targets by NK cells could provide DCs with increased access to tumor antigens. Immature DCs efficiently phagocytose apoptotic and necrotic cells, process antigens for presentation to T cells, and mature after exposure to necrotic cells, most probably through the release of heat-shock proteins (Degli-Esposti & Smyth, 2005; Nicchitta, 2003; Wan et al., 2004).

It was recently shown that only TLR-dependent stimuli that confer to DCs NK-cell stimulatory capacity were typically associated *in vivo* with T helper (Th)-1 responses. In particular, lipopolysaccharide (LPS) and CpG ODN were able to induce DC-mediated NK-cell activation (IFN-γ production) and recruitment *in vitro* and *in vivo*, whereas the Th2 stimulus Pam3Cys, although it could stimulate DCs to elicit IFN-γ production from NK cells *in vitro*, was not able to promote *in vivo* DC-mediated NK-cell recruitment/proliferation at the draining lymph nodes (Zanoni et al., 2005). Th1 rather than Th2 type of immune responses are considered to be mediators of cancer rejection. Activation of Th1 responses would also be expected to augment CTL responses, antibody responses that can mediate cytotoxicity against tumor, and provide stimulus to the natural immune mechanisms involving NK cells and macrophage. If one can supplement the vaccine with appropriate TLR ligands that provide Th1 cytokine milieu, activation of both CTL and NK will be achieved. NK cells

are unique in their ability to independently survey the expression of almost every MHC molecule, a feature that enables them to limit the spread of pathogens and tumors that subvert innate and adaptive immune defenses by selectively downregulating certain MHC class I molecules (Degli-Esposti & Smyth, 2005). With cancer vaccine strategies that activate both CTL and NK, it would be possible to eliminate both MHC-positive and -negative target cells. The effect of particulate delivery of TLR ligands on inducing Th1-biased immune responses is further discussed in the next section.

Potential of TLR Delivery to Bias Th Immune Responses to the Th1 Type

An important question in the context of cancer vaccines is whether the delivery system can be used to manipulate the type of immune responses. Of particular interest are the effects of delivery systems on the Th1/Th2 balance. The microenvironment of antigen capture by DCs, processing and presentation to T cells has a major influence on Th1/Th2 balance of the $CD4^+$ T-cell responses. For example, the presence of IL-12 in the microenvironment of DC–T cell conjugation will favor Th1 response. Interestingly, we have shown that delivery of MPLA to DCs in PLGA-NP dramatically increased the amount of IL-12 secreted by DCs by greater than 1000-fold (relative to soluble form of MPLA) (Elamanchili & Diwan, in press). Consequently, co-delivery of peptide antigens and appropriate TLR ligands using PLGA-NP can be used to bias the immune responses toward a Th1 type. Even when a particular peptide has a tendency to elicit a Th2 type of immune response, nanoparticle delivery may be used to elicit a Th1 response (Lutsiak, Kwon, & Samuel, 2006). Therapeutic vaccines for cancer and chronic viral diseases are often administered to patients who already may have ongoing Th2 responses against the vaccine antigen. It is often difficult to elicit a Th1 immune response specific for a peptide epitope, when there is an already established ongoing Th2 response. Using a hepatitis core peptide (HBcAg129-140) which typically induces a Th2 response in C57BL/6 strain, we have demonstrated that delivery systems such as liposomes and PLGA-NP can switch the response from a Th2 to a Th1 mode (Lutsiak, Sosnowski, Wishart, Kwon, & Samuel, 1998). Whether such effects can be achieved in the context of an ongoing disease such as cancer or chronic hepatitis B infection remains to be seen.

Potential of TLR Delivery to Break Self-Tolerance Against Cancer Antigens

Tolerance against self-antigens is an important barrier against anti-cancer T-cell immunity. Cancer vaccine strategies should be able to overcome the "self-tolerance" against cancer antigens and activate antigen-specific T-cell responses. MUC1 lipopeptide (BLP25®) is a significant cancer vaccine candidate in the immunotherapy of $MUC1^+$ tumors (Palmer et al., 2001). MUC1-specific humoral immune responses and CTLs have been detected in cancer patients without any prior therapy. However, these existing responses do not translate into therapeutic benefit as tumors devise a variety of mechanisms to escape these responses. We have recently shown that human DCs derived from PBMCs and loaded with BLP25® in solution form are inefficient in priming MUC1-specific T cells. Delivery

of BLP25® and MPLA in PLGA nanoparticles broke the self-tolerance against MUC1 and induced the proliferation of MUC1-specific T cells in vitro with one cycle of stimulation. Co-delivery of MPLA with the antigen in the same nanoparticle formulation was essential to achieve this (Elamanchili & Diwan, in press). This is consistent with our results from MUC1 transgenic mice, in which BLP25/MPLA-NP could generate superior cellular and humoral immune responses in MUC1 transgenic mice and prolong survival period in mice challenged with $MUC1^+$ tumors without inducing autoimmunity (manuscript in preparation). These results are also in accordance with our earlier observation of induction of MUC1-specific T-cell responses following delivery of BLP25® along with MPLA in PLGA-NP to cord blood-derived DCs (Diwan, Elamanchili, Lane, Gainer, & Samuel, 2003). Some of the likely reasons for the success of particulate formulation in breaking self-tolerance are efficient uptake of nanoparticles by DCs, superior delivery of antigen and MPLA to the same DC leading to enhanced maturation and efficient antigen processing, and enhanced cross-presentation of the processed antigen. In addition to those mechanisms, there is now accumulating evidence suggesting that appropriate engagement of TLR may offer an avenue for breaking tolerance through reversal of Treg-suppressive effects (discussed below).

Potential of TLR Delivery to Reverse T Regulatory (Treg) Suppression

The immunosuppressive environment around the tumor may lend itself to the activation of Treg cells, perhaps through preventing activation of DCs and, therefore, favoring activation of the regulatory cells over conventional effector cells. Indeed the results of several *in vitro* studies imply that immature but not mature DCs promote Treg cell activation (Jonuleit, Schmitt, Schuler, Knop, & Enk, 2000; Mesa & Fernandez, 2004). TLR-induced activation of DCs can rescue the patient's immune system from the suppression induced by tumor, which will prevent the activation of new Treg cells. Furthermore, it has been recently shown that DCs that have been appropriately stimulated (by TLR4 or TLR9) secrete IL-6, which renders antigen-specific T cells refractory to the suppressive activity of Treg cells (Pasare & Medzhitov, 2003). Other studies have shown that stimulation of DCs with TLR ligands enhances the proliferation of naïve and effector T cells, making it harder for Treg cells to inhibit them (Fehervari & Sakaguchi, 2004; Kubo et al., 2004). We have recently shown that particulate delivery of TLR4 ligand (MPLA) leads to 1000-fold increase in the amount of IL-6 secreted by DCs (relative to soluble form) (Elamanchili & Diwan, in press). In addition, using OVA transgenic mice models (DO11.10 and OT-1), we have also shown that co-delivery of OVA and MPLA in PLGA-NP to DCs have dramatically enhanced the extent of in vitro primary $CD4^+$ and $CD8^+$ T-cell activation, as evidenced by more than 1000 and 3000 SI, respectively (Elamanchili & Diwan, in press; Hamdy S, in press). Such a vaccine delivery system with this capacity to induce IL-6 production by DCs and to activate primary $CD4^+$ and $CD8^+$ T-cell responses to this extent might help to guarantee that cancer vaccine-induced T cells would be refractory to suppression by Treg cells.

Particulate delivery can also facilitate simultaneous delivery of more than TLR ligands in the same formulations. Warger et al. have recently

shown that the synergistic effect of combined-TLR triggering on BMDCs included a faster and more sustained secretion of pro-inflammatory cytokines (IL-6 and IL-12) (Warger et al., 2006). More importantly, it also made both $CD4^+$ and $CD8^+$ T cells less sensitive toward inhibition by Treg cells. Unstimulated or single TLR-activated (with either TLR3 or TLR7 ligands) BMDCs were unable to break Treg-mediated suppression of $CD4^+$ and $CD8^+$ T-cell proliferation. However, $CD4^+$ and $CD8^+$ T cells activated by DCs treated with both TLR3 and TLR7 ligands were completely refractory to Treg-mediated suppression (Warger et al., 2006). These results imply that Treg-mediated suppression can be overcome by properly activated DCs.

Persistent signaling through TLR was required for overcoming tumor-induced immunosuppression mediated by Treg cells (Yang, Huang, Huang, & Pardoll, 2004). Particulate delivery systems could facilitate a sustained TLR signaling in DCs, consequently avoiding the need of repeated administration or high dosages of TLR ligands. In fact, most of these compounds may show serious undesired side effects when administered in high dose. It has been reported that repeated daily injections of modest doses of 60 μg of CpG ODN in mice caused splenomegaly within 7 days and drastic damages to lymphoid tissues and hepatic toxicity by day 14 of treatment (Heikenwalder et al., 2004). Particulate delivery of TLR ligand would permit use of very small doses and limit the non-specific effects of CpG ODN on a broad number of cells leading to toxicity. We have recently shown that the effective dose of CpG ODN needed for antigen-specific T-cell activation in mice could be reduced by 10- to 100-fold by its delivery in PLGA-NP (Diwan, Elamanchili, Cao, & Samuel, 2004) The significance of nanoparticle-mediated delivery for immunopotentiation is probably not limited to CpG ODN adjuvants only, but it can also be extended to other adjuvants and immunomodulatory molecules, where restricting the bioactive compounds from general circulation and dose sparing are the foremost concerns.

Targeted Delivery of Immunomodulatory Molecules to Dendritic Cells

a-Galactosyl-Ceramide: A Strategy for NKT Cell Activation

Natural killer T (NKT) cells are a subset of T cells that share properties of NK cells and conventional T cells (Mercer, Ragin, & August, 2005). In contrast to conventional $CD4^+/CD8^+$ T cells that recognize peptide antigens, NKT cells respond to glycolipid ligands in the context of CD1d (Brigl & Brenner, 2004). a-Galactosyl-ceramide (a-GalCer) is a synthetic ligand that is presented effectively on CD1d molecules to human and murine NKT cells (Kawano et al., 1997). Activation of NKT cells in mice by injection of a-GalCer is associated with a rapid release of cytokines within hours. Activated NKT cells do not need to directly kill the tumor cells, and they do not act primarily as effectors, but instead they recruit and promote a response by downstream effectors in an IFN-γ-dependent manner. a-GalCer-stimulated NKT cells may enhance both NK and CTL activities, and both effector cell types have been implicated in the a-GalCer-induced anti-tumor response (Smyth et al., 2002). NKT cell stimulation may also enhance tumor immunity by promoting DCs activation

and IL-12 production via CD40 ligand upregulation (Fujii, Shimizu, Smith, Bonifaz, & Steinman, 2003; Godfrey & Kronenberg, 2004; Kitamura et al., 1999).

A recent study had evaluated intravenous injection of monocyte-derived mature DCs that were loaded with a-GalCer in five patients who had advanced cancer. Injection of GalCer-pulsed, but not unpulsed, DCs led to 100-fold expansion of several subsets of NKT cells in all patients; these could be detected for up to 6 months after vaccination. NKT activation was associated with an increase in serum levels of interleukin-12 p40 and IFN-γ-inducible protein-10 (Chang et al., 2005). These observations can open a new avenue for targeted delivery of a-GalCer to DCs *in vivo* using nano-sized particulate delivery systems. Particulate delivery of a-GalCer to DCs will lead to reliable and sustained expansion of glycolipid-reactive NKT cells *in vivo* with the downstream activation of both innate and adoptive anti-tumor immune responses. This strategy can overcome the potential cost, time, and difficulties associated with *ex vivo* manipulations in DC-based vaccines.

STAT3 Inhibitors

By the time of clinical detection, cancer cells have escaped from immune responses due to establishment of immunosuppressive network. Although the underlying mechanisms have not been fully characterized, these include loss of some MHC class I molecules, production of immunosuppressive factors (e.g., such as vascular endothelial growth factor (VEGF), TGF-β, prostaglandin E2, and IL-10). Many studies have shown that different amounts of various soluble factors are produced by different types of tumor. However, all of these factors have similar effect in inducing DC impairment. This could indicate that there is a common molecular mechanism mediating the effect of all of these factors. Recent studies have identified one possible pathway involving signal transducer and activator of transcription 3 (STAT3). STAT3 has been implicated in manipulation of the immune system at two levels. First, increased STAT3 activity in DCs induces a tolerogenic phenotype (Cheng et al., 2003) and impairs antigen-specific T-cell responses. Second, STAT3 is persistently activated in surprisingly numerous human cancers. Cancer cells that constitutively express STAT3 mediate tumor immune evasion by downregulation of proinflammatory cytokines/chemokines and upregulation of factors such as VEGF and IL-10 that inhibit DC maturation and activation. It was evident that disrupting STAT3 signaling in APCs abrogates the negative effects of tumor-derived factors (TDF) on the differentiation of myeloid cells and results in priming antigen-specific $CD4^+$ T cells in response to an otherwise tolerogenic stimulus *in vivo* (Cheng et al., 2003; Nefedova et al., 2004). Consistently, the ability of tumor to inhibit DC function was remarkably reduced in DCs derived from STAT3-deficient bone marrow progenitor cells (Niu et al., 1999). Furthermore, a recent study indicated that STAT3 is constitutively activated in diverse tumor-infiltrating immune cells and ablating STAT3 in hematopoietic cells *in vivo* triggers an intrinsic immune-surveillance system that inhibits tumor growth and metastasis. Markedly enhanced function of DCs, T cells, NK cells, and neutrophils was observed in tumor-bearing mice with $STAT3^{-/-}$ hematopoietic cells (Kortylewski

et al., 2005). Altogether, these findings strongly support considering abnormally active STAT3 in DCs as a conceivable molecular target for cancer immunotherapy.

Several avenues to inhibit STAT3 hyperactivation, especially in the tumor side, have been followed. Peptidomimetics have been raised as a promising strategy for STAT3 signaling pathway inhibition. PY*LKTK was introduced as a prototype (Turkson et al., 2001). These molecules disrupt STAT3 activity by interacting with the SH2 domain in STAT3 molecule preventing STAT3 homo- or heterodimerization, which is an important conformatory modification for STATs to function on the target gene (Turkson et al., 2001). Inhibition of JAK/STAT pathway has also been proposed as another approach to disrupt STAT3 signal. Piceatannol (JAK1 inhibitor) and tyrphostin AG490 (JAK1/2 inhibitor) have been reported to inhibit the constitutive activity of STAT3 in 2F7 and U266, respectively. Upon treatment, cells became sensitive to apoptosis by a range of chemotherapeutic agents (Alas & Bonavida, 2003). Moreover, the recently discovered inhibitor of STAT3 phosphorylation, cucurbitacin I, was shown to be a rapid, potent, and specific inhibitor of Jak2/STAT3 pathway (Blaskovich et al., 2003). Blocking constitutively active STAT3– DNA binding activity *in vitro* reduced STAT3-mediated gene transcription. It inhibited tumor growth *in vivo* and significantly increased the survival of immunologically competent mice with melanoma (Blaskovich et al., 2003). Recently, cucurbitacin I was found to overcome the differentiation block on DCs induced by TDF and promote the differentiation of mature DCs (Nefedova et al., 2005a). Surprisingly, cucurbitacin I was remarkably able to activate immature DCs cultured in tumor-conditioned media as well as in control media (Nefedova et al., 2005b). *In vivo* administration of cucurbitacin I to tumor-bearing mice reduced the presence of immature myeloid cells and promoted accumulation of mature DCs. However, a significant reduction in T-cell proliferation was noticed after cucurbitacin I administration (Nefedova et al., 2005a). These findings were very tempting to include cucurbitacin I in cancer vaccine schedule. Besides pharmacological inhibition, attempts have been made to inhibit STAT3 expression by RNA interference (RNAi) technology. Targeting STAT3 expression in human astrocytes by small interfering RNA (siRNA) induced apoptosis in astrocytoma cell lines but not primary astrocytes (Konnikova, Kotecki, Kruger, & Cochran, 2003). In another study, STAT3 siRNA inhibits the levels of androgen-regulated prostate-specific antigen (PSA) expression in prostate cancer cells but does not inhibit the proliferation nor induces apoptosis of STAT3-inactive human prostate cancer cells (Lee et al., 2004). Moreover, siRNA-targeting STAT3 was able to downregulate the expression of Bcl-2, cyclin D1, and c-Myc in prostate cancer cells. The inhibition of STAT3 and its related genes was accompanied by growth suppression and induction of apoptosis in cancer cells *in vitro* and in tumors implanted in nude mice (Gao et al., 2005a). It has also been demonstrated that STAT3 siRNA had an effect on induction of either early or late stage apoptosis in laryngeal cancer cells (Gao et al., 2005b). Growth of laryngeal cancer has been inhibited *in vivo* as well when STAT3 was targeted by siRNA (Gao et al., 2006). Despite the currently ongoing studies to inhibit STAT3 activity in tumor by RNAi technology, none of these, so far, has ever been studied targeting tumor-induced

STAT3 in DCs by siRNA. Manipulation of DCs using siRNA has been experimented to inhibit the expression of several other proteins affecting many DC responses. These include IL-12, nuclear factor (NF)-κB, IL-10, suppressor of cytokine signaling-3 (SOCS-3), and granulocyte colony-stimulating factor receptor (G-CSFR) (Geng, Joshi, Podolsky, & She, 2007; Hill et al., 2003; Laderach, Compagno, Danos, Vainchenker, & Galy, 2003; Liu et al., 2004; Orabona et al., 2005; Xu et al., 2006). However, all of these studies used mean of delivery like viral vectors, commercially available cationic lipids or physical means to transfect DCs. Although they may provide efficient transfection, their impracticality is still considered an obstacle that pushes siRNA strategy to the bedside. Moreover, viral vectors and cationic lipids were associated with triggering immune response in target cell, a main drawback of siRNA itself that should be avoided (Richards Grayson, Doody, & Putnam, 2006). Therefore, it will be of great advantage to develop an siRNA formulation to safely and efficiently target DCs at two levels of specificity: specific delivery to DCs and specificity of siRNA for the target gene. Many non-viral polymer-based delivery systems were proposed to deliver siRNA to target cells other than DCs. These delivery systems include peptide-conjugated siRNA, polyethylene glycol (PEG)-based formulations, PLGA-based nanoparticles, receptor-binding RNA aptamer, chitosan/siRNA nanoparticles, fusogenic liposomes, and nanoplexes of polyethyleneimine (PEI) which is the most extensively studied (Chiu, Ali, Chu, Cao, & Rana, 2004; Howard et al., 2006; Itaka et al., 2004; Kakizawa, Furukawa, & Kataoka, 2004; Khaled, Guo, Li, & Guo, 2005; Khan et al., 2004; Kunisawa et al., 2005; Richards Grayson et al., 2006; Werth et al., 2006).

1-Methyl-tryptophan: A Strategy for IDO Inhibition

Vast amount of evidence currently points at the immunosuppressive enzyme, indoleamine-2,3-dioxygenase (IDO), as a key molecule in tumor-mediated immune tolerance (Muller & Prendergast, 2005). Encoded by the *INDO* gene, this enzyme is known to suppress effector T cells by enhancing tryptophan catabolism. Increased IDO activity in DCs is a proposed mechanism to mediate this effect (Hwu et al., 2000). Many factors may contribute to the high expression of IDO in DCs. Treg cells, for instance, induce IDO production in DCs as a mechanism for alloregulation. Such DCs may further induce IDO expression in T cells to regulate allo- and autoreactivity (Terness, Chuang, Bauer, Jiga, & Opelz, 2005). Moreover, IDO has been found to be expressed in tumors and in the surrounding APCs (Munn & Mellor, 2004). This is thought to play a role in the long-term insufficiency of immunosurveillance in cancer patients (Brandacher, Winkler, Schroecksnadel, Margreiter, & Fuchs, 2006). Besides tumoral vicinity, high expression of IDO has been noticed in APCs of tumor-draining lymph nodes (TDLN) (Lee et al., 2003). The increased IDO levels in such APCs might contribute, in part, to the extended antagonizing effects on anti-tumoral immune response of the host. DCs localized in such areas are currently getting massive focus of attention since they may provide a potential target for future research. It also ought to be mentioned that a recent study demonstrates the induction of IDO in DCs by activated STAT3 (Orabona et al., 2005). Although no

direct evidence, so far, has linked IDO-mediated escape of immunosurveillance to STAT3 activation, both IDO and STAT3 provide tempting targets for cancer immunotherapy.

Many indole-containing compounds were evaluated for their ability to inhibit IDO (Cady & Sono, 1991). Among them, 1-methyl-tryptophan (1-MT) was extensively used in experimental settings. In the presence of 1-MT, Lewis-lung carcinoma (LLC) cells stimulated more robust allogeneic T-cell response *in vitro* (Friberg et al., 2002). Furthermore, 1-MT resulted in delayed growth of the tumor when administered *in vivo* (Friberg et al., 2002). In another study, adoptively transferred DCs from TDLN into naïve hosts caused local T-cell anergy except in mice pre-treated with 1-MT (Munn et al., 2004). Along with the pharmacodynamic effects of 1-MT, the molecule provides favorable pharmacokinetics like oral bioavailability, low protein binding, and low clearance (Muller, DuHadaway, Donover, Sutanto-Ward, & Prendergast, 2005; Uyttenhove et al., 2003). Besides, no significant toxicity was reported about this compound. Recently, Gaspari and colleagues introduced novel derivatives of brassinin as more potent inhibitors than 1-MT (Gaspari et al., 2006). Therefore, it seems to be of great advantage to successfully formulate and deliver such compounds in the context of cancer vaccines.

Because of their ability to induce tumor immune tolerance, TDLN DCs are of great importance to be targeted with IDO inhibitors. For this purpose, different strategies should be attained other than what have been discussed earlier. Here the aim of the delivery will be the DCs residing in TDLN rather than conventionally targeted Langerhans cells in the skin. One of the most crucial factors that direct particulate formulations in the interstitial space to the lymphatic vessels is the particle size (Nishioka & Yoshino, 2001; Oussoren & Storm, 2001; Reddy, Berk, Jain, & Swartz, 2006a). It was shown that liposomes of particle size <40 nm are significantly taken up into the lymphatic vessels (Oussoren & Storm, 1997; Reddy et al., 2006c). Moreover, ultrasmall nanoparticles ($\sim$20 nm) designed of cross-linked poly(propylene sulfide) with PEG surface showed rapid and efficient uptake in lymphatic vessels and retain in lymph nodes for up to 120 h post-injection. Within the lymph node, it was shown that the nanoparticles are internalized exclusively by resident APCs (MHCII+ cells which include DCs and some macrophages) and other non-antigen-presenting macrophages (MHCII−) without a targeting ligand. A large fraction (up to 50%) of lymph node resident DCs internalized the 20 nm particles, with the number increasing over time (Reddy, Rehor, Schmoekel, Hubbell, & Swartz, 2006b; Reddy et al., 2006a; Rehor, Hubbell, & Tirelli, 2005). PPS nanoparticles thus offer the potential for a novel strategy to deliver immunomodulatory molecules, e.g., 1-MT or brassinin to DCs and other APCs in lymph nodes.

Conclusion

DC functions seem to be determined by many different factors that govern the final outcome of immune responses, for example, immunity vs tolerance and Th1 vs Th2. In other words, the function of the DCs is not fixed

but is adaptable in response to signals from the surrounding microenvironment. We anticipate that optimal exploitation of the various immunomodulatory molecules discussed in this review, coupled with the use of nano-sized delivery systems for vaccine purposes, will allow major strides forward to therapeutic vaccination of established cancer. The intrinsic design of such markedly improved vaccines will also obviate the need for *ex vivo* DC activation and antigen loading, because such vaccines equipped with proper DC-activating ligand(s) will achieve directly *in vivo* what therapeutic *ex vivo* prepared DC vaccines accomplish in a far more laborious way.

References

Akira, S., Takeda, K., & Kaisho, T. (2001). Toll-like receptors: Critical proteins linking innate and acquired immunity. *Nat Immunol*, 2(8), 675–680.

Alas, S., & Bonavida, B. (2003). Inhibition of constitutive stat3 activity sensitizes resistant non-Hodgkin's lymphoma and multiple myeloma to chemotherapeutic drug-mediated apoptosis. *Clin Cancer Res*, 9(1), 316–326.

Albert, M. L., Sauter, B., & Bhardwaj, N. (1998). Dendritic cells acquire antigen from apoptotic cells and induce class i-restricted ctls. *Nature*, 392(6671), 86–89.

Albertsson, P. A., Basse, P. H., Hokland, M., Goldfarb, R. H., Nagelkerke, J. F., Nannmark, U., et al. (2003). Nk cells and the tumour microenvironment: Implications for nk-cell function and anti-tumour activity. *Trends Immunol*, 24(11), 603–609.

Banchereau, J., & Palucka, A. K. (2005). Dendritic cells as therapeutic vaccines against cancer. *Nat Rev Immunol*, 5(4), 296–306.

Banchereau, J., & Steinman, R. M. (1998). Dendritic cells and the control of immunity. *Nature*, 392(6673), 245–252.

Bernards, R., Destree, A., McKenzie, S., Gordon, E., Weinberg, R. A., & Panicali, D. (1987). Effective tumor immunotherapy directed against an oncogene-encoded product using a vaccinia virus vector. *Proc Natl Acad Sci USA*, 84(19), 6854–6858.

Beutler, B. (2004). Inferences, questions and possibilities in toll-like receptor signalling. *Nature*, 430(6996), 257–263.

Blaskovich, M. A., Sun, J., Cantor, A., Turkson, J., Jove, R., & Sebti, S. M. (2003). Discovery of jsi-124 (cucurbitacin i), a selective janus kinase/signal transducer and activator of transcription 3 signaling pathway inhibitor with potent antitumor activity against human and murine cancer cells in mice. *Cancer Res*, 63, 1270–1279.

Borst, J., Hendriks, J., & Xiao, Y. (2005). Cd27 and cd70 in t cell and b cell activation. *Curr Opin Immunol*, 17(3), 275–281.

Bousso, P., & Robey, E. (2003). Dynamics of cd8 + t cell priming by dendritic cells in intact lymph nodes. *Nat Immunol*, 4(6), 579–585.

Brandacher, G., Winkler, C., Schroecksnadel, K., Margreiter, R., & Fuchs, D. (2006). Antitumoral activity of interferon-gamma involved in impaired immune function in cancer patients. *Curr Drug Metab*, 7(6), 599–612.

Brigl, M., & Brenner, M. B. (2004). Cd1: Antigen presentation and t cell function. *Annu Rev Immunol*, 22, 817–890.

Cady, S. G., & Sono, M. (1991). 1-methyl-dl-tryptophan, beta-(3-benzofuranyl)-dl-alanine (the oxygen analog of tryptophan), and beta-[3-benzo(b)thienyl]-dl-alanine (the sulfur analog of tryptophan) are competitive inhibitors for indoleamine 2,3-dioxygenase. *Arch Biochem Biophys*, 291(2), 326–333.

Casadevall, A. (1999). Passive antibody therapies: Progress and continuing challenges. *Clin Immunol*, 93(1), 5–15.

Cella, M., Engering, A., Pinet, V., Pieters, J., & Lanzavecchia, A. (1997). Inflammatory stimuli induce accumulation of mhc class ii complexes on dendritic cells. *Nature*, 388(6644), 782–787.

Chang, D. H., Osman, K., Connolly, J., Kukreja, A., Krasovsky, J., Pack, M., et al. (2005). Sustained expansion of nkt cells and antigen-specific t cells after injection of alpha-galactosyl-ceramide loaded mature dendritic cells in cancer patients. *J Exp Med*, 201(9), 1503–1517.

Chaux, P., Moutet, M., Faivre, J., Martin, F., & Martin, M. (1996). Inflammatory cells infiltrating human colorectal carcinomas express hla class ii but not b7-1 and b7-2 costimulatory molecules of the t-cell activation. *Lab Invest*, 74(5), 975–983.

Cheng, F., Wang, H. W., Cuenca, A., Huang, M., Ghansah, T., Brayer, J., et al. (2003). A critical role for stat3 signaling in immune tolerance. *Immunity*, 19(3), 425–436.

Chiu, Y. L., Ali, A., Chu, C. Y., Cao, H., & Rana, T. M. (2004). Visualizing a correlation between sirna localization, cellular uptake, and rnai in living cells. *Chem Biol*, 11(8), 1165–1175.

Cooper, M. A., Fehniger, T. A., Fuchs, A., Colonna, M., & Caligiuri, M. A. (2004). Nk cell and dc interactions. *Trends Immunol*, 25(1), 47–52.

Copland, M. J., Baird, M. A., Rades, T., McKenzie, J. L., Becker, B., Reck, F., et al. (2003). Liposomal delivery of antigen to human dendritic cells. *Vaccine*, 21(9–10), 883–890.

Cumberbatch, M., & Kimber, I. (1995). Tumour necrosis factor-alpha is required for accumulation of dendritic cells in draining lymph nodes and for optimal contact sensitization. *Immunology*, 84(1), 31–35.

Datta, S. K., Redecke, V., Prilliman, K. R., Takabayashi, K., Corr, M., Tallant, T., et al. (2003). A subset of toll-like receptor ligands induces cross-presentation by bone marrow-derived dendritic cells. *J Immunol*, 170(8), 4102–4110.

De Vries, I. J., Krooshoop, D. J., Scharenborg, N. M., Lesterhuis, W. J., Diepstra, J. H., Van Muijen, G. N., et al. (2003). Effective migration of antigen-pulsed dendritic cells to lymph nodes in melanoma patients is determined by their maturation state. *Cancer Res*, 63(1), 12–17.

Degli-Esposti, M. A., & Smyth, M. J. (2005). Close encounters of different kinds: Dendritic cells and nk cells take centre stage. *Nat Rev Immunol*, 5(2), 112–124.

Dermime, S., Armstrong, A., Hawkins, R. E., & Stern, P. L. (2002). Cancer vaccines and immunotherapy. *Br Med Bull*, 62, 149–162.

Dhodapkar, M. V., Steinman, R. M., Krasovsky, J., Munz, C., & Bhardwaj, N. (2001). Antigen-specific inhibition of effector t cell function in humans after injection of immature dendritic cells. *J Exp Med*, 193(2), 233–238.

Diehl, L., den Boer, A. T., Schoenberger, S. P., van der Voort, E. I., Schumacher, T. N., Melief, C. J., et al. (1999). Cd40 activation in vivo overcomes peptide-induced peripheral cytotoxic t-lymphocyte tolerance and augments anti-tumor vaccine efficacy. *Nat Med*, 5(7), 774–779.

Diwan, M., Elamanchili, P., Cao, M., & Samuel, J. (2004). Dose sparing of cpg oligodeoxynucleotide vaccine adjuvants by nanoparticle delivery. *Curr Drug Deliv*, 1(4), 405–412.

Diwan, M., Elamanchili, P., Lane, H., Gainer, A., & Samuel, J. (2003). Biodegradable nanoparticle mediated antigen delivery to human cord blood derived dendritic cells for induction of primary t cell responses. *J Drug Target*, 11(8–10), 495–507.

Elamanchili, P., Lutsiak, C., Hamdy, S., Diwan, M., & Samuel, J. (2007). Pathogen-mimicking' nanoparticles for vaccine delivery to dendritic cells. *J Immunother,* 30(4), 378–395.

Elamanchili, P., Diwan, M., Cao, M., & Samuel, J. (2004). Characterization of poly(d,l-lactic-co-glycolic acid) based nanoparticulate system for enhanced delivery of antigens to dendritic cells. *Vaccine*, 22(19), 2406–2412.

Enk, A. H., Jonuleit, H., Saloga, J., & Knop, J. (1997). Dendritic cells as mediators of tumor-induced tolerance in metastatic melanoma. *Int J Cancer*, 73(3), 309–316.

Fehervari, Z., & Sakaguchi, S. (2004). Control of foxp3 + cd25 + cd4 + regulatory cell activation and function by dendritic cells. *Int Immunol*, 16(12), 1769–1780.

Foged, C., Sundblad, A., & Hovgaard, L. (2002). Targeting vaccines to dendritic cells. *Pharm Res*, 19(3), 229–238.

Friberg, M., Jennings, R., Alsarraj, M., Dessureault, S., Cantor, A., Extermann, M., et al. (2002). Indoleamine 2,3-dioxygenase contributes to tumor cell evasion of t cell-mediated rejection. *Int J Cancer*, 101(2), 151–155.

Fujii, S., Shimizu, K., Smith, C., Bonifaz, L., & Steinman, R. M. (2003). Activation of natural killer t cells by alpha-galactosylceramide rapidly induces the full maturation of dendritic cells in vivo and thereby acts as an adjuvant for combined cd4 and cd8 t cell immunity to a coadministered protein. *J Exp Med*, 198(2), 267–279.

Gabrilovich, D. I., Corak, J., Ciernik, I. F., Kavanaugh, D., & Carbone, D. P. (1997). Decreased antigen presentation by dendritic cells in patients with breast cancer. *Clin Cancer Res*, 3(3), 483–490.

Gao, L., Zhang, L., Hu, J., Li, F., Shao, Y., Zhao, D., et al. (2005a). Down-regulation of signal transducer and activator of transcription 3 expression using vector-based small interfering rnas suppresses growth of human prostate tumor in vivo. *Clin Cancer Res*, 11(17), 6333–6341.

Gao, L. F., Xu, D. Q., Wen, L. J., Zhang, X. Y., Shao, Y. T., & Zhao, X. J. (2005b). Inhibition of stat3 expression by sirna suppresses growth and induces apoptosis in laryngeal cancer cells. *Acta Pharmacol Sin*, 26(3), 377–383.

Gao, L. F., Wen, L. J., Yu, H., Zhang, L., Meng, Y., Shao, Y. T., et al. (2006). Knockdown of stat3 expression using rnai inhibits growth of laryngeal tumors in vivo. *Acta Pharmacol Sin*, 27(3), 347–352.

Garg, S., Oran, A., Wajchman, J., Sasaki, S., Maris, C. H., Kapp, J. A., et al. (2003). Genetic tagging shows increased frequency and longevity of antigen-presenting, skin-derived dendritic cells in vivo. *Nat Immunol*, 4(9), 907–912.

Gaspari, P., Banerjee, T., Malachowski, W. P., Muller, A. J., Prendergast, G. C., DuHadaway, J., et al. (2006). Structure-activity study of brassinin derivatives as indoleamine 2,3-dioxygenase inhibitors. *J Med Chem*, 49(2), 684–692.

Geng, D., Joshi, S. K., Podolsky, R., & She, J. X. (2007). Gcsf receptor regulates antigen uptake and expression of cytokines and costimulatory molecules in dendritic cells. *Mol Immunol*, 44(4), 521–529.

Gerosa, F., Baldani-Guerra, B., Nisii, C., Marchesini, V., Carra, G., & Trinchieri, G. (2002). Reciprocal activating interaction between natural killer cells and dendritic cells. *J Exp Med*, 195(3), 327–333.

Godfrey, D. I., & Kronenberg, M. (2004). Going both ways: Immune regulation via cd1d-dependent nkt cells. *J Clin Invest*, 114(10), 1379–1388.

Gong, J., Chen, D., Kashiwaba, M., & Kufe, D. (1997). Induction of antitumor activity by immunization with fusions of dendritic and carcinoma cells. *Nat Med*, 3(5), 558–561.

Hamdy, S., Elamanchili, P., Alshamsan, A., Molavi, O., Satou, T., & Samuel, J. (2007). Enhanced antigen-specific primary cd4 + and cd8 + responses by co-delivery of ovalbumin and toll-like receptor ligand monophosphoryl lipid a in poly(d,l-lactic-co-glycolic acid) nanoparticles. *J Biomed Mater Res A*, 81(3), 652–662.

Heikenwalder, M., Polymenidou, M., Junt, T., Sigurdson, C., Wagner, H., Akira, S., et al. (2004). Lymphoid follicle destruction and immunosuppression after repeated cpg oligodeoxynucleotide administration. *Nat Med*, 10(2), 187–192.

Heit, A., Huster, K. M., Schmitz, F., Schiemann, M., Busch, D. H., & Wagner, H. (2004). Cpg-DNA aided cross-priming by cross-presenting b cells. *J Immunol*, 172(3), 1501–1507.

Hertz, C. J., Kiertscher, S. M., Godowski, P. J., Bouis, D. A., Norgard, M. V., Roth, M. D., et al. (2001). Microbial lipopeptides stimulate dendritic cell maturation via toll-like receptor 2. *J Immunol*, 166(4), 2444–2450.

Hill, J. A., Ichim, T. E., Kusznieruk, K. P., Li, M., Huang, X., Yan, X., et al. (2003). Immune modulation by silencing il-12 production in dendritic cells using small interfering rna. *J Immunol*, 171(2), 691–696.

Hirao, M., Onai, N., Hiroishi, K., Watkins, S. C., Matsushima, K., Robbins, P. D., et al. (2000). Cc chemokine receptor-7 on dendritic cells is induced after interaction with apoptotic tumor cells: Critical role in migration from the tumor site to draining lymph nodes. *Cancer Res*, 60(8), 2209–2217.

Howard, K. A., Rahbek, U. L., Liu, X., Damgaard, C. K., Glud, S. Z., Andersen, M. O., et al. (2006). Rna interference in vitro and in vivo using a novel chitosan/sirna nanoparticle system. *Mol Ther*, 14(4), 476–484.

Hwu, P., Du, M. X., Lapointe, R., Do, M., Taylor, M. W., & Young, H. A. (2000). Indoleamine 2,3-dioxygenase production by human dendritic cells results in the inhibition of t cell proliferation. *J Immunol*, 164(7), 3596–3599.

Itaka, K., Kanayama, N., Nishiyama, N., Jang, W. D., Yamasaki, Y., Nakamura, K., et al. (2004). Supramolecular nanocarrier of sirna from peg-based block catiomer carrying diamine side chain with distinctive pka directed to enhance intracellular gene silencing. *J Am Chem Soc*, 126(42), 13612–13613.

Iwasaki, A., & Medzhitov, R. (2004). Toll-like receptor control of the adaptive immune responses. *Nat Immunol*, 5(10), 987–995.

Jonuleit, H., Schmitt, E., Schuler, G., Knop, J., & Enk, A. H. (2000). Induction of interleukin 10-producing, nonproliferating cd4(+) t cells with regulatory properties by repetitive stimulation with allogeneic immature human dendritic cells. *J Exp Med*, 192(9), 1213–1222.

Kakizawa, Y., Furukawa, S., & Kataoka, K. (2004). Block copolymer-coated calcium phosphate nanoparticles sensing intracellular environment for oligodeoxynucleotide and sirna delivery. *J Control Release*, 97(2), 345–356.

Kamath, A. T., Sheasby, C. E., & Tough, D. F. (2005). Dendritic cells and nk cells stimulate bystander t cell activation in response to tlr agonists through secretion of ifn-alpha beta and ifn-gamma. *J Immunol*, 174(2), 767–776.

Kaufman, H. L., & Disis, M. L. (2004). Immune system versus tumor: Shifting the balance in favor of dcs and effective immunity. *J Clin Invest*, 113(5), 664–667.

Kawano, T., Cui, J., Koezuka, Y., Toura, I., Kaneko, Y., Motoki, K., et al. (1997). Cd1d-restricted and tcr-mediated activation of valpha14 nkt cells by glycosylceramides. *Science*, 278(5343), 1626–1629.

Khaled, A., Guo, S., Li, F., & Guo, P. (2005). Controllable self-assembly of nanoparticles for specific delivery of multiple therapeutic molecules to cancer cells using rna nanotechnology. *Nano Lett*, 5(9), 1797–1808.

Khan, A., Benboubetra, M., Sayyed, P. Z., Ng, K. W., Fox, S., Beck, G., et al. (2004). Sustained polymeric delivery of gene silencing antisense odns, sirna, dnazymes and ribozymes: In vitro and in vivo studies. *J Drug Target*, 12(6), 393–404.

Kitamura, H., Iwakabe, K., Yahata, T., Nishimura, S., Ohta, A., Ohmi, Y., et al. (1999). The natural killer t (nkt) cell ligand alpha-galactosylceramide demonstrates its immunopotentiating effect by inducing interleukin (il)-12 production by dendritic cells and il-12 receptor expression on nkt cells. *J Exp Med*, 189(7), 1121–1128.

Konnikova, L., Kotecki, M., Kruger, M. M., & Cochran, B. H. (2003). Knockdown of stat3 expression by rnai induces apoptosis in astrocytoma cells. *BMC Cancer*, 3, 23.

Kortylewski, M., Kujawski, M., Wang, T., Wei, S., Zhang, S., Pilon-Thomas, S., et al. (2005). Inhibiting stat3 signaling in the hematopoietic system elicits multicomponent antitumor immunity. *Nat Med*, 11(12), 1314–1321.

Kowalczyk, D. W., Wysocki, P. J., & Mackiewicz, A. (2003). Cancer immunotherapy using cells modified with cytokine genes. *Acta Biochim Pol*, 50(3), 613–624.

Kubo, T., Hatton, R. D., Oliver, J., Liu, X., Elson, C. O., & Weaver, C. T. (2004). Regulatory t cell suppression and anergy are differentially regulated by proinflammatory cytokines produced by tlr-activated dendritic cells. *J Immunol*, 173(12), 7249–7258.

Kunisawa, J., Masuda, T., Katayama, K., Yoshikawa, T., Tsutsumi, Y., Akashi, M., et al. (2005). Fusogenic liposome delivers encapsulated nanoparticles for cytosolic controlled gene release. *J Control Release*, 105(3), 344–353.

Laderach, D., Compagno, D., Danos, O., Vainchenker, W., & Galy, A. (2003). Rna interference shows critical requirement for nf-kappa b p50 in the production of il-12 by human dendritic cells. *J Immunol*, 171(4), 1750–1757.

Lathe, R., Kieny, M. P., Gerlinger, P., Clertant, P., Guizani, I., Cuzin, F., et al. (1987). Tumour prevention and rejection with recombinant vaccinia. *Nature*, 326(6116), 878–880.

Lee, J. R., Dalton, R. R., Messina, J. L., Sharma, M. D., Smith, D. M., Burgess, R. E., et al. (2003). Pattern of recruitment of immunoregulatory antigen-presenting cells in malignant melanoma. *Lab Invest*, 83(10), 1457–1466.

Lee, S. O., Lou, W., Qureshi, K. M., Mehraein-Ghomi, F., Trump, D. L., & Gao, A. C. (2004). Rna interference targeting stat3 inhibits growth and induces apoptosis of human prostate cancer cells. *Prostate*, 60(4), 303–309.

Liu, G., Ng, H., Akasaki, Y., Yuan, X., Ehtesham, M., Yin, D., et al. (2004). Small interference rna modulation of il-10 in human monocyte-derived dendritic cells enhances the th1 response. *Eur J Immunol*, 34(6), 1680–1687.

Lutsiak, C. M., Sosnowski, D. L., Wishart, D. S., Kwon, G. S., & Samuel, J. (1998). Use of a liposome antigen delivery system to alter immune responses in vivo. *J Pharm Sci*, 87(11), 1428–1432.

Lutsiak, M. E., Kwon, G. S., & Samuel, J. (2006). Biodegradable nanoparticle delivery of a th2-biased peptide for induction of th1 immune responses. *J Pharm Pharmacol*, 58(6), 739–747.

Mack, C. A., Song, W. R., Carpenter, H., Wickham, T. J., Kovesdi, I., Harvey, B. G., et al. (1997). Circumvention of anti-adenovirus neutralizing immunity by administration of an adenoviral vector of an alternate serotype. *Hum Gene Ther*, 8(1), 99–109.

Means, T. K., Hayashi, F., Smith, K. D., Aderem, A., & Luster, A. D. (2003). The toll-like receptor 5 stimulus bacterial flagellin induces maturation and chemokine production in human dendritic cells. *J Immunol*, 170(10), 5165–5175.

Melief, C. J., Van Der Burg, S. H., Toes, R. E., Ossendorp, F., & Offringa, R. (2002). Effective therapeutic anticancer vaccines based on precision guiding of cytolytic t lymphocytes. *Immunol Rev*, 188, 177–182.

Mercer, J. C., Ragin, M. J., & August, A. (2005). Natural killer t cells: Rapid responders controlling immunity and disease. *Int J Biochem Cell Biol*, 37(7), 1337–1343.

Mesa, C., & Fernandez, L. E. (2004). Challenges facing adjuvants for cancer immunotherapy. *Immunol Cell Biol*, 82(6), 644–650.

Muller, A. J., DuHadaway, J. B., Donover, P. S., Sutanto-Ward, E., & Prendergast, G. C. (2005). Inhibition of indoleamine 2,3-dioxygenase, an immunoregulatory target of the cancer suppression gene bin1, potentiates cancer chemotherapy. *Nat Med*, 11(3), 312–319.

Muller, A. J., & Prendergast, G. C. (2005). Marrying immunotherapy with chemotherapy: Why say ido? *Cancer Res*, 65(18), 8065–8068.

Munn, D. H., & Mellor, A. L. (2004). Ido and tolerance to tumors. *Trends Mol Med*, 10(1), 15–18.

Munn, D. H., Sharma, M. D., Hou, D., Baban, B., Lee, J. R., Antonia, S. J., et al. (2004). Expression of indoleamine 2,3-dioxygenase by plasmacytoid dendritic cells in tumor-draining lymph nodes. *J Clin Invest*, 114(2), 280–290.

Murthy N, C. J., Fausto N, Hoffman AS, Stayton PS. (2003). Bioinspired ph-responsive polymers for the intracellular delivery of biomolecular drugs. *Bioconjug Chem*, 14(2), 412–419.

Neeson, P., & Paterson, Y. (2006). Effects of the tumor microenvironment on the efficacy of tumor immunotherapy. *Immunol Invest*, 35(3–4), 359–394.

Nefedova, Y., Cheng, P., Gilkes, D., Blaskovich, M., Beg, A. A., Sebti, S. M., et al. (2005a). Activation of dendritic cells via inhibition of jak2/stat3 signaling. *J Immunol*, 175(7), 4338–4346.

Nefedova, Y., Nagaraj, S., Rosenbauer, A., Muro-Cacho, C., Sebti, S. M., & Gabrilovich, D. I. (2005b). Regulation of dendritic cell differentiation and antitumor immune response in cancer by pharmacologic-selective inhibition of the janus-activated kinase 2/signal transducers and activators of transcription 3 pathway. *Cancer Res*, 65(20), 9525–9535.

Nefedova, Y., Huang, M., Kusmartsev, S., Bhattacharya, R., Cheng, P., Salup, R., et al. (2004). Hyperactivation of stat3 is involved in abnormal differentiation of dendritic cells in cancer. *J Immunol*, 172(1), 464–474.

Nestle, F. O., Alijagic, S., Gilliet, M., Sun, Y., Grabbe, S., Dummer, R., et al. (1998). Vaccination of melanoma patients with peptide- or tumor lysate-pulsed dendritic cells. *Nat Med*, 4(3), 328–332.

Nestle, F. O., Banchereau, J., & Hart, D. (2001). Dendritic cells: On the move from bench to bedside. *Nat Med*, 7(7), 761–765.

Newman, K. D., Samuel, J., & Kwon, G. (1998). Ovalbumin peptide encapsulated in poly(d,l lactic-co-glycolic acid) microspheres is capable of inducing a t helper type 1 immune response. *J Control Release*, 54(1), 49–59.

Nicchitta, C. V. (2003). Re-evaluating the role of heat-shock protein-peptide interactions in tumour immunity. *Nat Rev Immunol*, 3(5), 427–432.

Nishioka, Y., & Yoshino, H. (2001). Lymphatic targeting with nanoparticulate system. *Adv Drug Deliv Rev*, 47(1), 55–64.

Niu, G., Heller, R., Catlett-Falcone, R., Coppola, D., Jaroszeski, M., Dalton, W., et al. (1999). Gene therapy with dominant-negative stat3 suppresses growth of the murine melanoma b16 tumor in vivo. *Cancer Res*, 59, 5059–5063.

O'Hagan D, S. M. (2003). Microparticles as vaccine adjuvants and delivery systems. *Expert Rev Vaccines*, 2, 269–283.

O'Hagan, D. T., & Valiante, N. M. (2003). Recent advances in the discovery and delivery of vaccine adjuvants. *Nat Rev Drug Discov*, 2(9), 727–735.

Orabona, C., Belladonna, M. L., Vacca, C., Bianchi, R., Fallarino, F., Volpi, C., et al. (2005). Cutting edge: Silencing suppressor of cytokine signaling 3 expression in dendritic cells turns cd28-ig from immune adjuvant to suppressant. *J Immunol*, 174(11), 6582–6586.

Oussoren, C., & Storm, G. (1997). Lymphatic uptake and biodistribution of liposomes after subcutaneous injection: Iii. Influence of surface modification with poly(ethyleneglycol). *Pharm Res*, 14(10), 1479–1484.

Oussoren, C., & Storm, G. (2001). Liposomes to target the lymphatics by subcutaneous administration. *Adv Drug Deliv Rev*, 50(1–2), 143–156.

Palmer, M., Parker, J., Modi, S., Butts, C., Smylie, M., Meikle, A., et al. (2001). Phase i study of the blp25 (muc1 peptide) liposomal vaccine for active specific immunotherapy in stage iiib/iv non-small-cell lung cancer. *Clin Lung Cancer*, 3(1), 49–57; discussion 58.

Pasare, C., & Medzhitov, R. (2003). Toll pathway-dependent blockade of cd4 + cd25 + t cell-mediated suppression by dendritic cells. *Science*, 299(5609), 1033–1036.

Pinzon-Charry, A., Maxwell, T., & Lopez, J. A. (2005). Dendritic cell dysfunction in cancer: A mechanism for immunosuppression. *Immunol Cell Biol*, 83(5), 451–461.

Probst, H. C., Lagnel, J., Kollias, G., & van den Broek, M. (2003). Inducible transgenic mice reveal resting dendritic cells as potent inducers of cd8+ t cell tolerance. *Immunity*, 18(5), 713–720.

Razzaque, A., Dye, E., & Puri, R. K. (2000). Characterization of tumor vaccines during product development. *Vaccine*, 19(6), 644–647.

Reddy, S. T., Berk, D. A., Jain, R. K., & Swartz, M. A. (2006a). A sensitive in vivo model for quantifying interstitial convective transport of injected macromolecules and nanoparticles. *J Appl Physiol*, 101(4), 1162–1169.

Reddy, S. T., Rehor, A., Schmoekel, H. G., Hubbell, J. A., & Swartz, M. A. (2006b). In vivo targeting of dendritic cells in lymph nodes with poly(propylene sulfide) nanoparticles. *J Control Release*, 112(1), 26–34.

Reddy, S. T., Swartz, M. A., & Hubbell, J. A. (2006c). Targeting dendritic cells with biomaterials: Developing the next generation of vaccines. *Trends Immunol*, 27(12), 573–579.

Rehor, A., Hubbell, J. A., & Tirelli, N. (2005). Oxidation-sensitive polymeric nanoparticles. *Langmuir*, 21(1), 411–417.

Richards Grayson, A. C., Doody, A. M., & Putnam, D. (2006). Biophysical and structural characterization of polyethylenimine-mediated sirna delivery in vitro. *Pharm Res*, 23(8), 1868–1876.

Rosenberg, S. A., Yang, J. C., & Restifo, N. P. (2004). Cancer immunotherapy: Moving beyond current vaccines. *Nat Med*, 10(9), 909–915.

Schroder, M., & Bowie, A. G. (2005). Tlr3 in antiviral immunity: Key player or bystander? *Trends Immunol*, 26(9), 462–468.

Schulz, O., Diebold, S. S., Chen, M., Naslund, T. I., Nolte, M. A., Alexopoulou, L., et al. (2005). Toll-like receptor 3 promotes cross-priming to virus-infected cells. *Nature*, 433(7028), 887–892.

Schuster, M., Nechansky, A., & Kircheis, R. (2006). Cancer immunotherapy. *Biotechnol J*, 1(2), 138–147.

Shen, H., Ackerman, A. L., Cody, V., Giodini, A., Hinson, E. R., Cresswell, P., et al. (2006). Enhanced and prolonged cross-presentation following endosomal escape of exogenous antigens encapsulated in biodegradable nanoparticles. *Immunology*, 117(1), 78–88.

Smyth, M. J., Crowe, N. Y., Hayakawa, Y., Takeda, K., Yagita, H., & Godfrey, D. I. (2002). Nkt cells – conductors of tumor immunity? *Curr Opin Immunol*, 14(2), 165–171.

Smyth, M. J., Hayakawa, Y., Takeda, K., & Yagita, H. (2002). New aspects of natural-killer-cell surveillance and therapy of cancer. *Nat Rev Cancer*, 2(11), 850–861.

Takeda, K., Kaisho, T., & Akira, S. (2003). Toll-like receptors. *Annu Rev Immunol*, 21, 335–376.

Tamura, Y., Peng, P., Liu, K., Daou, M., & Srivastava, P. K. (1997). Immunotherapy of tumors with autologous tumor-derived heat shock protein preparations. *Science*, 278(5335), 117–120.

Terness, P., Chuang, J. J., Bauer, T., Jiga, L., & Opelz, G. (2005). Regulation of human auto- and alloreactive t cells by indoleamine 2,3-dioxygenase (ido)-producing dendritic cells: Too much ado about ido? *Blood*, 105(6), 2480–2486.

Tsujitani, S., Furukawa, T., Tamada, R., Okamura, T., Yasumoto, K., & Sugimachi, K. (1987). Langerhans cells and prognosis in patients with gastric carcinoma. *Cancer*, 59(3), 501–505.

Turkson, J., Ryan, D., Kim, J. S., Zhang, Y., Chen, Z., Haura, E., et al. (2001). Phosphotyrosyl peptides block stat3-mediated dna binding activity, gene regulation, and cell transformation. *J Biol Chem*, 276(48), 45443–45455.

Tuting, T., Storkus, W. J., & Lotze, M. T. (1997). Gene-based strategies for the immunotherapy of cancer. *J Mol Med*, 75(7), 478–491.

Uyttenhove, C., Pilotte, L., Theate, I., Stroobant, V., Colau, D., Parmentier, N., et al. (2003). Evidence for a tumoral immune resistance mechanism based on tryptophan degradation by indoleamine 2,3-dioxygenase. *Nat Med*, 9(10), 1269–1274.

van Duin, D., Medzhitov, R., & Shaw, A. C. (2006). Triggering tlr signaling in vaccination. *Trends Immunol*, 27(1), 49–55.

Walter, E., Dreher, D., Kok, M., Thiele, L., Kiama, S. G., Gehr, P., et al. (2001). Hydrophilic poly(dl-lactide-co-glycolide) microspheres for the delivery of dna to human-derived macrophages and dendritic cells. *J Control Release*, 76(1–2), 149–168.

Walzer, T., Dalod, M., Robbins, S. H., Zitvogel, L., & Vivier, E. (2005). Natural-killer cells and dendritic cells: "l'union fait la force". *Blood*, 106(7), 2252–2258.

Wan, T., Zhou, X., Chen, G., An, H., Chen, T., Zhang, W., et al. (2004). Novel heat shock protein hsp70l1 activates dendritic cells and acts as a th1 polarizing adjuvant. *Blood*, 103(5), 1747–1754.

Wang, D., Robinson, D. R., Kwon, G. S., & Samuel, J. (1999). Encapsulation of plasmid dna in biodegradable poly(d, l-lactic-co-glycolic acid) microspheres as a novel approach for immunogene delivery. *J Control Release*, 57(1), 9–18.

Warger, T., Osterloh, P., Rechtsteiner, G., Fassbender, M., Heib, V., Schmid, B., et al. (2006). Synergistic activation of dendritic cells by combined toll-like receptor ligation induces superior ctl responses in vivo. *Blood*, 108(2), 544–550.

Werth, S., Urban-Klein, B., Dai, L., Hobel, S., Grzelinski, M., Bakowsky, U., et al. (2006). A low molecular weight fraction of polyethylenimine (pei) displays increased transfection efficiency of dna and sirna in fresh or lyophilized complexes. *J Control Release*, 112(2), 257–270.

World Health Organization. (2005). http://www.who.int/mediacentre/factsheet/fs297/en/index.html.

Xu, H., Chen, T., Wang, H. Q., Ji, M. J., Zhu, X., & Wu, W. X. (2006). Prolongation of rat intestinal allograft survival by administration of donor interleukin-12 p35-silenced bone marrow-derived dendritic cells. *Transplant Proc*, 38(5), 1561–1563.

Yamaguchi, N., Hiraoka, S., Mukai, T., Takeuchi, N., Zhou, X. Y., Ono, S., et al. (2004). Induction of tumor regression by administration of b7-ig fusion proteins: Mediation by type 2 cd8 + t cells and dependence on il-4 production. *J Immunol*, 172(3), 1347–1354.

Yang, Y., Huang, C. T., Huang, X., & Pardoll, D. M. (2004). Persistent toll-like receptor signals are required for reversal of regulatory t cell-mediated cd8 tolerance. *Nat Immunol*, 5(5), 508–515.

Yee, C. (2005). Adoptive t cell therapy: Addressing challenges in cancer immunotherapy. *J Transl Med*, 3(1), 17.

Yuan, D., Koh, C. Y., & Wilder, J. A. (1994). Interactions between b lymphocytes and nk cells. *Faseb J*, 8(13), 1012–1018.

Yuan, D., Wilder, J., Dang, T., Bennett, M., & Kumar, V. (1992). Activation of b lymphocytes by nk cells. *Int Immunol*, 4(12), 1373–1380.

Zanoni, I., Foti, M., Ricciardi-Castagnoli, P., & Granucci, F. (2005). Tlr-dependent activation stimuli associated with th1 responses confer nk cell stimulatory capacity to mouse dendritic cells. *J Immunol*, 175(1), 286–292.

Zeid, N. A., & Muller, H. K. (1993). S100 positive dendritic cells in human lung tumors associated with cell differentiation and enhanced survival. *Pathology*, 25(4), 338–343.

Zou, W. (2005). Immunosuppressive networks in the tumour environment and their therapeutic relevance. *Nat Rev Cancer*, 5(4), 263–274.

18

Stimuli-Sensitive Nanotechnology for Drug Delivery

Andre G. Skirtach and Oliver Kreft

Introduction

The challenges faced in drug delivery are to develop means for administering drugs with release rates that vary according to therapeutic needs of a patient. One of the most desirable features is to develop materials, structures and perhaps even devices which respond to external signals or trigger in a pre-determined mode. Such an undertaking is feasible for a platform that responds to external stimuli. An ideal stimuli-sensitive delivery platform would (1) monitor the related pharmacokinetic parameters of a patient; (2) produce a continuous feedback signal to the device; and (3) administer pre-determined doses of a drug upon request. Ultimately, the advantages of such a system would be (a) increase of therapeutic efficacy, (b) reduction of side effects and (c) circumvention of drug tolerance. All these functionalities can be implemented in a system responding to external stimuli such as pH, temperature, light, electric or magnetic fields. In fact, recent efforts by researchers have led to development of functional materials and structures that respond to such external stimuli. And although originally called "stimuli sensitive", these systems can be also referred to as "biologically smart" because their functions often mimic those of biological organisms. There are clear advantages of such smart systems in drug delivery due to possibilities to regulate on-and-off response and thus modulate drug release in response to an external stimulus. The size of such systems increasingly undergoes a careful scrutiny.

Nanotechnology is an emerging field which is envisioned to play a pivotal role not only in bio-medicine, in general, but also in the drug delivery area in particular, owing to the continuing trend in miniaturization of both structures and devices. Indeed, with recent advents in nano-engineered materials and investigative tools, new breakthrough nanomaterials, nano-structures and eventually nanotechnologies appear on the horizon. Furthermore, even micro-range-sized structures are now more often designed at the nano-level. Developing applications in such a way not only enhances existing properties but also introduces new functionalities and capabilities – a property that is relevant as ever before in drug delivery.

M.M. de Villiers et al. (eds.), *Nanotechnology in Drug Delivery*, DOI: 10.1007/978-0-387-77667-5_18,

Stimuli-Responsive Drug Delivery Systems: Introduction and Overview

Various drug delivery systems (DDS) have been actively pursued including micelles, liposomes, polymers, hydrogels and nano-/microparticles. It is almost impossible to present a comprehensive overview of the current status of all drug delivery systems (DDS) within the framework of this chapter, so only a brief overview of these DDS is given. Omitting the important field of surfactant-based micelle and liposome DDS, we rather devote a large part of coverage to the emerging area of nano-engineered polyelectrolyte multilayer (PEM) microcapsules. They offer a unique opportunity to combine surface multifunctionality with design flexibility – a necessary condition for delivery of encapsulated materials into designated biological compartments and cells. The main advantage of such systems is precise surface chemistry control, again, due to their design at the nano-level.

Overall, this chapter aims at providing information from the very basic textbook level to the latest developments. This introduction continues further with a brief overview of available platforms for drug delivery including materials and polymers from which these systems can be built. Subsequently, this chapter covers PEM microcapsules including detailed characterization of templates and wall/shell materials. Later on it presents an overview of nanotechnology and nano-level characterization methods widely used during the design of microcapsules. A significant part of this chapter is devoted to various encapsulation and release methods. Last but not least, it is important to note that exciting intracellular applications of microcapsules and other micro- and nano-containers necessitate considering the subject of biocompatibility of microcapsules and materials comprising them – raising this topic is one of the goals of this chapter.

Stimuli-Responsive Polymers

Polymers are the fundamental building blocks which enable the stimuli-sensitive functions of various structures. A classical example of a polymer responding to an external stimulus is poly(*N*-isopropylacrylamide) (PNIPAm) – presumably one of the most studied synthetic, temperature-responsive polymers. In aqueous solution, PNIPAm exhibits a sharp temperature-induced coil-globule transition. The phase transition temperature, referred to as the lower critical solution temperature (LCST) and situated around body temperature ($\sim 32^{\circ}$C) (Schild, 1992), characterizes a transition between hydrophilic ($T<$LCST) and hydrophobic states ($T>$LCST) of the polymer in water. The LCST phenomenon is quite common for polymers with H-bonding sites available for water molecules. The driving force of the phase transition from hydrophilic (solubilized) to hydrophobic (collapsed) state is entropic because water molecules associated with the side-chain moieties are expelled from the polymer. The LCST is located in the phase diagram region where the enthalpic contribution of water hydrogen bonded to the polymer chain becomes overcompensated by the entropic gain due to the release of water

molecules into the bulk solution (Schild, 1992). The LCST of a given polymer is largely determined by the capabilities of its monomer units to provide hydrogen bonding. In general, the LCST can be modified by the ratio of hydrophilic and hydrophobic segments of the polymer – the more hydrophobic monomers are incorporated into the polymer, the more the LCST decreases. For example, copolymerization with hydrophobic butylmethacrylate reduces the LCST of the polymer solution, while copolymerization with hydrophilic copolymers, namely acrylic acid or hydroxy ethyl methacrylate, leads to an increase of the LCST (Saunders, Crowther, Morris, Mears, Cosgrove, & Vincent, 1999). Other copolymers of this class are poly(*N*-vinylcaprolactam) (PVCL), poly(ethylene glycol) (PEG) or poly(ethylene oxide) (PEO) and poly(propylene oxide) (PPO). It is known that the continuous phase transition of PNIPAAm changes into a discontinuous phase if either a small amount of ionizable groups is introduced into the gel-like network (Yu & Grainger, 1993) or solvent composition is changed (Suzuki, Tomonaga, Kumazaki, & Nishio, 1996).

Another interesting class of temperature-sensitive polymers is represented by the pluronic polyols and their derivatives. Pluronic polyols are linear ABA tri-block copolymers composed of poly(ethylene oxide) (PEO) and poly(propylene oxide) (PPO). The PPO central block can be designed in a way that it undergoes a temperature-induced phase transition around body temperature. Pluronic F-127(Poloxamer 407, PF-127) is liquid at 4–5°C but exhibits reversible gelation upon warming to ambient temperatures. Early works on PF-127 for temperature-dependent drug delivery were already done in the 1980 s by Gilbert, Richardson, Davies, Pallin & Hadgraft (1987), and in the meantime, PF-127 has been employed as a carrier for various routes of drug administration (Escobar-Chávez, López-Cervantes, Naïk, Kalia, Quintanar-Guerrero, & Ganem-Quintanar, 2006). Recently, a new family of branched PEO–PPO block copolymers designed as tetronic polyols have been introduced by Mansur, Barboza, González & Lucas (2004).

Future trends in this growing scientific field concern the development of responsive biopolymers and polymer–biopolymer conjugates. Again, PNIPAm has been employed for the development of various temperature- and photo-switchable oligomer/polymer conjugates used to control the binding properties of functional biopolymers, such as enzymes, IgGs (Stayton, Shimoboji, Long, Chilkoti, Chen, Harris, & Hoffman, 1995) and antisense-RNA (Murata, Kaku, Anada, Sato, Kano, Maeda, & Katayama, 2003). Moreover, switchable peptide-based biomaterials, which respond to environmental changes, could already be synthesized by using molecular biology strategies. Current approaches on this topic have been carefully reviewed by de las Heras Alarcón, Pennadam & Alexander (2004) and Mart, Osborne, Stevens & Ulijn (2006).

In the area of non-viral gene delivery systems, intensive research has been done on polycation-based vectors (polyplexes). Typically, high-molecular-weight polycations, such as polyethyleneimine (PEI) (Boussif, Lezoualc'h, Zanta, , Mergny, Scherman, Demeneix, & Behr, 1995) or poly-L-lysine (PLL) (Kwoh, Coffin, Lollo, Jovenal, Banaszczyk, Mullen, Phillips, Amini, Fabrycki, Bartholomew, Brostoff, & Carlo, 1999), are employed as a non-viral vector system that effectively condenses plasmid

DNA (pDNA) and forms stable polyplexes (Wolff, 2002; Nori & Kopecek, 2005). New generations of drug and gene delivery systems (DGDS) should help to enhance gene transfection efficiencies by using different stimuli, both internal and external, and are expected to lead to the design of new generations of therapeutics. For example, the group of Oupicky synthesized a reducible poly-Lysine (rPLL) containing disulfide bonds in the backbone for the preparation of polyplexes. These polycations were capable of reductive degradation into low-molecular-weight species in the reducing intracellular environment, and facilitate the release of DNA. The authors report a more than 60-fold increased transfection activity when compared with control polyplexes based on PLL (Oupicky, Bisht, Manickam, Zhou, 2005). A similar system, based on a biocleavable polyrotaxane-pDNA polyplex, has been investigated by the group of Harashima (Ooya, Choi, Yamashita, Yui, Sugaya, Kano, Maruyama, Akita, Ito, Kogure, & Harashima, 2005).

Polymer Micelles

Polymeric micelles represent a class of micelles composed of block copolymers with hydrophilic and hydrophobic polymer domains. In aqueous solutions, amphiphilic block and graft copolymers can form micelles of mesoscopic size with considerably narrow size distribution consisting of a hydrophobic core stabilized by a surrounding hydrophilic corona (Tuzar & Kratochvil, 1976; Moffitt, Khougaz & Eisenberg, 1996). The major driving force for the copolymer self-assembly is the core segregation. That requires intermolecular forces: hydrophobic interactions (Kabanov, Chekhonln, Alakhov, Batrakova, Lebedev, Melik- Nubarov, Arzhakov, Levashov, Morozov, Severin, & Kabanov, 1989), electrostatic interactions (Harada & Kataoka, 1999), metal complexation (Nishiyama, Yokoyama, Aoyagi, Okano, Sakurai, & Kataoka, 1999) and hydrogen bonding (Kataoka, Ishihara, Harada, & Miyazaki, 1998) of the block copolymer units, along with sterical stabilization of the hydrophilic palisades. Core-forming hydrophobic blocks have been prepared of a broad variety of polymers (Torchilin, 2004). In comparison to surfactant micelles, polymeric micelles exhibit higher mechanical stability and slower dissociation rates leading to longer circulation times and higher accumulation of drug at designated sites. Moreover, further stabilization of polymeric micelles can be achieved by cross-linking of both the core (Guo, Liu & Tao, 1996) and the corona (Thurmond, Kowalewski & Wooley, 1996).

Important requirements for using polymer micelles as DDS are that the core provides high loading capacity, drug delivery at controlled release rates and finally compatibility between the hydrophobic components of the polymer and loaded drugs. So far, a large variety of chemically diverse drug molecules could be incorporated into the core by selectively tuning its properties for achieving strong enough interaction with the drug molecules (Yokoyama, Okano, & Kataoka, 1994). Poly (ethylene glycol) (PEG) blocks (molecular weight ranging from 1 to 15 kDa) are typical corona-forming blocks, although other hydrophilic polymers have been employed as well (Torchilin, Trubetskoy, Whiteman, Caliceti, Ferruti, & Veronese, 1995). The length of a hydrophobic core-forming block is usually not

greater than that of a hydrophilic block (Cammas, Suzuki, Sone, Sakurai, Kataoka, & Okano, 1997).

Stimuli response can be implemented into such systems by changing the intrinsic hydrophilic and hydrophobic properties via temperature or pH switching. Arotçaréna, Heise, Ishaya & Laschewsky (2002) reported a double thermoresponsive block copolymer consisting of two blocks with both lower critical solution temperature (LCST) and upper critical solution temperature (UCST). Such a design results in a thermally triggered exchange of the polymer segments forming the inner core and the hydrophilic "corona" around it. Therefore, without any additive but just depending on temperature, polymeric micelles can switch their structure from "inside" to "outside" and vice versa. Similar, pH-dependent systems have been reported by Liu & Armes (2002).

An alternative concept utilizes the formation of polyion complex (PIC) micelles through the electrostatically driven assembly of oppositely charged block copolymers. The first PIC micelles have been fabricated from a pair of poly(ethylene glycol)-grafted poly(L-lysin) and poly(α,β-aspartic acid), respectively, by Harada & Kataoka (1995). Due to their size (between 20 and 100 nm diameter) and their chemical properties, polymeric micelles can effectively circumvent the body defense system (reticuloendothelial system, RES). Thus, passive targeting into pathological sites with impeded vasculature (such as tumors, inflammations and infected areas) can be achieved via the enhanced permeability and retention effect (EPR) leading to an improved drug delivery in this area (Gref, Minaniitake, Peracchia, Trubetskoy, Torchilin, & Langer, 1994; Maeda, Wu, Sawa, Matsumura, & Hori, 2000). Stimuli-responsive polymer micelles for drug delivery have been thoroughly reviewed by Kataoka, Harada & Nagasaki (2001), by Kikuchi & Okano (2002) and Torchilin (2004).

Hydrogels

Hydrogels are cross-linked networks of hydrophilic polymers that can absorb and retain more than 20% of their weight of water, while maintaining the distinct three-dimensional structure of the polymer network. Hydrogel swelling in aqueous solutions is a consequence of water affinity of the hydrophilic hydrogel matrix. During de-swelling, compression of the matrix is accompanied by the loss of water and co-solutes, i.e., therapeutic agents. Most of the polymer matrices exhibit excellent elastic properties and, as a consequence, tolerate a large number of swelling/de-swelling cycles without impairment in structural or functional integrity. The main route for the preparation of hydrogel-based DDS employs cross-linking of linear polymer chains via the introduction of covalent- or hydrogen bonds, van der Waals interactions or even physical entanglements (Kamath & Park, 1993). Another route described in literature uses copolymerization of mono- and poly-functional monomer units (Hennink & van Nostrum, 2002). A large number of natural and synthetic polymers in use for the synthesis of hydrogels have been described, and the resulting structural and chemical variety of known hydrogels provides insight into the broad versatility of this system. Swelling properties, network structure, permeability or mechanical stability of hydrogels can be controlled by

external stimuli or physiological parameters (Lowman & Peppas, 1999). Stimuli such as pH, temperature, magnetic and electric fields, ionic strength and chemical agents have been explored (Gupta, Vermani & Garg, 2002 and Das, Zhang & Kumacheva, 2006).

Temperature-sensitive hydrogels are composed of polymers bearing hydrophobic groups, for example methyl, ethyl and propyl groups. Among other polymers of this class, PNIPAAm and poly(*N*,*N*-diethylacrylamide) (PDEAAm) are widely studied compounds used for drug delivery. Copolymerization of NIPAAm in the presence of other types of monomers can be applied for fabrication of hydrogels with such properties as altered LCST or swelling/de-swelling kinetics (Dong & Hoffman, 1990). Temperature-sensitive hydrogels have been extensively reviewed by Pelton (2000). In comparison, pH-sensitive hydrogels comprise polymers possessing either acidic or basic functional groups; therefore, they are capable of accepting or releasing protons in response to pH changes. Swelling of hydrogels with ionizable groups is much more efficient than that achievable with non-ionizable ones. The most common class of polymers containing ionizable groups is known as polyelectrolytes. Cross-linked cationic polyelectrolytes undergo swelling at pH values below the pKa of the polymer due to the ionization of the pendant groups. The other way around, hydrogels from polyanions get un-ionized below and ionized above the pKa of the polymer network and, therefore, swell at high pH values. The swelling is affected by both the conditions reducing electrostatic repulsion (pH, ionic strength) and the type of counterions (Firestone & Siegel, 1991). Comprehensive reviews on polymer hydrogels have been published by Qiu and Park (2001), Gupta, Vermani & Garg (2002) and by Kikuchi & Okano (2002).

The development of multi-stimuli-responsive hydrogels could be advantageous for in vivo applications, where drug release is dependent on the presence of more than one stimulus. A major disadvantage of most of the hydrogel systems is that the hydration response to changes in stimuli is too slow for therapeutic applications. To overcome this problem, further development of hydrogel structures at the micro- and nano-scale is necessary (Graham & Cameron, 1998). Recent reports showed progress in micro- and nano-gels of PNIPAm with ultrafast responses and attractive rheological properties (Gan & Lyon, 2001; Wu, Zhou, & Hu, 2003). However, these systems are only at their initial stage (de las Heras Alarcón, Pennadam & Alexander, 2005; Yoo and Seok & Sung, 2004).

Dendrimers and Cyclodextrins

Dendrimers are another type of polymers that could be used for drug delivery. Primarily, their studies concentrated on their use as uni-molecular micelles and "dendritic boxes" for the non-covalent encapsulation of drug molecules. For instance, DNA was shown to get complexed with polyamidoamine cascade polymers for gene delivery (Haensler & Szoka, 1993); hydrophobic drugs and dye molecules were introduced into a number of dendrimer cores (Jansen, Meijer, & Debraban der Vandenberg, 1994). A clear advantage of using dendritic uni-molecular micelles (compared with conventional polymeric micelles) is that covalent links allow to

maintain their micellar structure. This approach is, however, not free of drawbacks, for instance difficulty to control the release of molecules from the dendrimer core. (Jansen et al., 1995). The introduction of stabilizing PEO chains gave rise to the development of dendritic uni-molecular micelles for the incorporation of anticancer drugs (Bhadra, Bhadra, Jain, & Jain, 2003). And although that can slow down drug release rates, this method has yet to gain acceptance. Hybrids of PEO and dendrimers with pH-sensitive hydrophobic acetal groups on the dendrimer periphery (Gillies, Jonsson & Fréchet, 2004) offer a promising route. Here, the mechanism for release relies on the loss of the hydrophobic groups on acetal hydrolysis at mildly acidic pH (Gillies & Fréchet, 2005).

Because of their widely tuneable functionalities, cyclodextrins (CDs) are regarded as potential drug carriers in the development of advanced DDS. Hydrophilic and ionizable CDs have been reported to be suitable drug carriers for both immediate and delayed release drug delivery systems, whereas long-termed retardation of water-soluble drugs can be achieved by using hydrophobic CDs. Although cyclodextrins are expected to become important drug delivery vehicles, most of them are only at the beginning of safety evaluations (Hirayama & Uekama, 1999).

Nano- and Microspheres

Numerous examples of functional nanoparticle applications in the area of drug delivery prompt to provide a brief outline and highlight just some of them. Nano- and microspheres are a class of small objects that is more frequently used in various fields of drug delivery. Their most important properties are small size, high surface to volume ratio, precise control over physical and chemical surface properties, robustness and high specificity in target binding. They can be used as delivery agents alone or introduced into other structures like micro- and nano-capsules to stimulate magnetic, fluorescent or catalytic properties. Polymeric nanospheres are probably the most relevant type of small particles in the drug delivery area. They can be applied for delivery of drugs, genes and vaccines. In the latter case, nanospheres with entrapped antigens can be used for delivery of vaccines and adjuvants (Akagi, Ueno, Hiraishi, Baba, & Akashi, 2005). A novel concept of controlled release of anticancer drugs with magnetic nanoparticles incorporated within the polymeric shells has been reported. Nano- and microparticles embedded in alginate or liposome matrixes were also studied for controllable drug release by low-frequency magnetic fields, while DNA hybridization is possible by using radio-frequency magnetic field with nanoparticles bound to DNA strands.

Hydrocolloids, among them especially alginates, are widely employed for the development of controlled-release systems. Dependent on pH, alginates have the ability to form two types of gels, i.e., an acid gel and an ionotropic gel, thus giving the alginate polymer superior properties in comparison to neutral gel-forming compounds. Alginates gelify as well in the presence of divalent cations, like the calcium ion. Alginates can be tailored on demand for specific applications and up to now a broad variety of different alginate formulations have been described (Kikuchi & Okano, 2002; Tonnesen & Karlsen, 2002). Another example of application of microparticles in drug

delivery is targeting of phagocytes by functionalizing the surface of miroparticles (Faraassen, Vörös, Csucs, Textor, Merkle, & Walter, 2003).

Nano- and Microcapsules

To date, several techniques have been investigated and applied to encapsulate a substance of interest into different micro- and nano-capsules. Polymeric micro- and nano-capsules can be prepared by four principally different strategies: interfacial polymerization, interfacial precipitation, interfacial deposition and self-assembly processes. The reader can deal with these technologies in fine details in the comprehensive series of books edited by Arshady (1999). Capsule formation by self-assembly results in the formation of polymer micelles or vesicles, which have already been introduced in the preceding chapters. The preparation of nanocapsules by interfacial polymerization requires fast polymerization of a monomer at the interface between the organic and the aqueous phase of an emulsion. This type of capsule is mainly preferred for the encapsulation of lipophilic drugs. Encapsulation strategies for various oil-soluble compounds are given by the reviews from Mayer (2005) and Couvreur, Barrat, Fattal, Legrand & Vauthier (2002). The interfacial deposition route can be utilized for the fabrication of polyelectrolyte capsules. In the following chapters, we intend to concentrate on development, characterization and applications of stimuli-responsive microcapsules fabricated by layer-by-layer deposition of ultrathin polymeric films on sacrificial colloidal particles. In addition, overview of microcapsules and multilayers was presented by Sukhishvili (2005), while encapsulation into nano-organized microshells was given by Lvov, Antipov, Mamedov, Möhwald, & Sukhorukov (2001).

Polyelectrolyte Capsules

Coating Colloidal Particles with Polyelectrolytes

The fabrication of polyelectrolyte capsules is based on the layer-by-layer (LbL) self-assembly of polyelectrolyte thin films, originally revealed by research on ultrathin films on macroscopically flat surfaces by Decher (1997 and Decher & Hong, 1991). The technique is based on sequential physisorption of oppositely charged polyelectrolytes and yields polyelectrolyte multilayer (PEM) thin films of defined thickness and architecture. This highly versatile method facilitates the fabrication of custom-made polymer thin films with an infinitely large number of functional groups incorporated in its structure. Even freestanding nano-structures have been reported by Jiang & Tsukruk (2006). This flexibility is achieved using a relatively simple and inexpensive adsorption process. Multilayer growth is driven by electrostatic interactions between polyions and an oppositely charged interface (Figure 18.1, inset). During the self-assembly, polymer adsorption continues until the surface charge is reversed allowing the adsorption of a counterpolyion. The number of alternating adsorbed polycations and polyanions is optional.

In 1998, the technology was successfully transferred to the surfaces of sub-micron core particles or colloids (Sukhorukov, Donath, Davis,

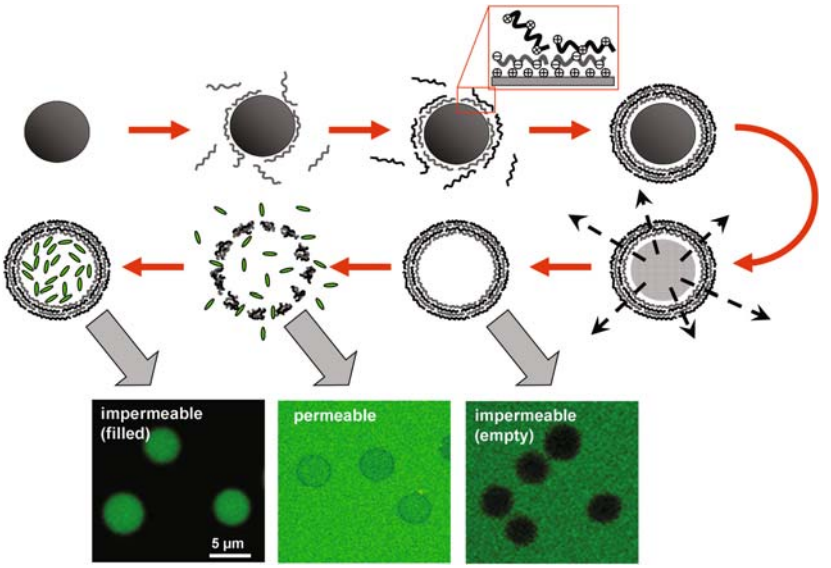

Figure 18.1 Schematic illustration of the polyelectrolyte multilayer build-up on colloidal templates and subsequent template removal. Initial steps involve the stepwise deposition of oppositely charged polyelectrolytes from aqueous solutions on a spherical, colloidal template (inset). After accomplishing the desired number of polyelectrolyte layers the template core is dissolved. Macromolecular species can be incorporated into the capsule interior by selectively and reversibly changing the permeability of the polyelectrolyte shell. CLSM images illustrate the encapsulation of high MW FITC-labeled dextran following this strategy. (*See* Color Plate 25)

Lichtenfeld, v, Popov, & Möhwald, 1998). Furthermore, the colloidal cores were removed (by dissolution or decomposition) preserving the assembled polyelectrolyte multilayers. This led to the formation of hollow structures resembling the original size and shape of the templating particles. Fabrication and properties of hollow polyelectrolyte shells were described in several reviews (Möhwald, Donath & Sukhorukov, 2003; Peyratout & Dähne, 2004), so we will only briefly summarize main aspects of the manufacturing procedure. Generally, polyelectrolytes are allowed to adsorb onto particles from aqueous solutions. The main strategy for the LbL assembly involves the addition of an excess of polyelectrolyte to the particles. After each adsorption step, the excess of polyelectrolyte molecules has to be removed from the particle suspension before adding the next, oppositely charged polyelectrolyte layer to the particles. The process is finished by applying at least three washing cycles. The separation of particles from bulk solutions requires a centrifugation or filtration step (Voigt, Lichtenfeld, Sukhorukov, Zastrow, Donath, Pumler, & Möhwald, 1999). Currently, the filtration method is the only viable option for scale-up production and automation. The layer growth can be monitored by measuring the zeta potential, using either single particle light scattering (SPLS) or neutron scattering. With the latter technique a mean thickness of 16.6 Å per layer was determined for a specific film (Estrela-Lopis, Leporatti, Moya, Brandt, Donath, & Möhwald, 2002), but the film thickness can be varied via pH, salt or the type of polyelectrolyte.

Templates

Template cores act as sacrificial supports, which are eliminated by dissolution or decomposition during capsule manufacturing. Therefore, potential template materials have to fulfill certain requirements: (1) stability during LbL growth, (2) stability of the multilayers upon dissolution of the template and (3) completeness of core removal. Other desirable parameters include monodispersity and spherical shape. A multitude of template cores ranging in size from about 30 nm (Schneider & Decher, 2004) to tens of microns have been applied for capsule fabrication: microbeads from synthetic resins, organic and inorganic microcrystals, metal nanoparticles, emulsion droplets (Donath, Sukhorukov, Caruso, Davies, & Möhwald, 1998; Peyratout & Dähne, 2004) and even biological materials. The most frequently used templates and their properties are listed in Table 18.1.

Weakly cross-linked, monodisperse melamine formaldehyde (MF) templates (size range = 0.5–12 μm) were originally used and most extensively studied for fabrication of hollow polyelectrolyte microcapsules. MF particles can be rapidly dissolved in organic solvents such as DMSO or via acid-catalyzed decomposition of the polymer network. The major drawbacks of this system are incomplete elimination of MF-oligomers (during the core dissolution) and their bioincompatibility (Gao, Moya, Lichtenfeld, Casoli, Fiedler, Donath, & Möhwald, 2001). Polystyrene (PS), another resin-based template, can be easily dissolved in organic solvents like THF or DMF (Park, Xia, Advincula, Schotz, & Caruso, 2001), but problems often arise with aggregation during core dissolution. Within the class of

Table 18.1 Selection of commonly used templates.

Types of properties	MF	PS	SiO_2	Erythrocytes	Carbonates	PLA/ PLGA
Size (μm)	0.5–12	0.1–1000	0.15–8	5.5–7.5	1–8	0.2–20
Shape	Spherical	Spherical	Spherical	Discoidal	Spherical	Spherical
Monodispersity	Very good	Very good	Very good	Good	Medium	Low
Template solvents	HCl, DMSO	THF	HF	NaOCl	EDTA	NMP/ acetone
Template dissolution	Incomplete	Incomplete	Complete	Complete	Complete	Incomplete
Drawbacks	Toxic residues	Toxic residues, aggregation	No problems	Cross-linking of PEM	Aggregation	Residues
Encapsulation strategy	Indirect loading	Indirect loading	Indirect loading	Indirect loading	Direct loading	Direct loading
Biocompatibility of encapsulation	Low/ medium	Low/medium	Medium	Medium	Very good	Very good
Efficiency of encapsulation	Medium	Medium	Good	Good	Good	Medium

MF = melamine formaldehyde; PS = polystyrene; PLA = polylactic acid; PLGA = poly(lactic-*co*-glycolic acid); DMSO = dimethylsulfoxide; THF = tetrahydrofurane; HF = hydrofluoric acid; NaOCl = sodium hypochloride; EDTA = ethylenediaminetetraacetic acid; NMP = 1-methyl-2-pyrrolidinone; perm. = permeability; PEM = polyelectrolyte multilayer. Direct and indirect encapsulation techniques are handled in detail in Chapter 4.

inorganic templates, silicium dioxide particles are promising, because they are available in a broad size range, display high monodispersity and can be entirely dissolved in hydrofluoric acid (Köhler, Shchukin, Möhwald, & Sukhorukov, 2005). Nevertheless, handling HF is hazardous and necessitates specialized laboratory equipment. A current development is the use of spherical carbonate crystals, such as $MnCO_3$ or $CaCO_3$, as templates. They can be prepared in the range of 1–8 μm in a relatively simple and inexpensive way (Sukhorukov, Volodkin, Günther, Petrov, Shenoy, & Möhwald, 2004). Biodegradable poly(lactic-*co*-glycolic acid) (PLGA) and polylactic acid (PLA) microspheres are also "biofriendly", but their limitations include polydispersity and aggregation tendency (Shenoy, Antipov Sukhorukov, & Möhwald, 2003). Yeast and HeLa cells showed maintained viability upon LbL coating (Diaspro, Silvano Krol, Cavalleri, & Gliozzi, 2002; Germain, Balaguer, Nicolas, Lopez, Esteve, Sukhorukov, Winterhalter, Richard-Foy, & Fournier, 2006), although it can be noted that limited membrane stability is one of the drawbacks of using biological cells as templates. To prevent membrane rupture, erythrocytes have been stabilized by glutaraldehyde prior to LbL coating (Moya, Dähne, Voigt, Leporatti, Donath, & Möhwald, 2001; Kreft, Georgieva, Bäumler , Steup , Müller-Röber, Sukhorukov, & Möhwald, 2006); the core removal was facilitated by strong oxidizing agents. Erythrocytes possess a few advantages over the "conventional" templates because they are available in non-spherical shapes, quasi-monodisperse and inexpensive. Apparently, each of these decomposable templates has its advantages and poses some drawbacks. Therefore, state-of-the-art microcapsules are designed using customized templates tailored for a specific application rather than seeking the universal template for the LbL technology. Knowing these properties is important and therefore they are outlined in Table 18.1.

Wall Materials

A large variety of charged polymers (polyelectrolytes) have been employed for the layer-by-layer build-up of PEM films. Different polyelectrolytes have different characteristics, such as structure (linear or branched), charge density or electrolyte type (strong/weak). For example, "strong" polyelectrolytes dissociate completely in solution at intermediate pH values (pH 2–10); thus, their charge is largely pH independent. By contrast, "weak" polyelectrolytes will only partially dissociate at intermediate pH values. Accordingly, their net charge can be altered by changing the pH of the solution. Although extensive investigations focussed on synthetic polyelectrolytes (Table 18.2), natural polyelectrolytes like nucleic acids, proteins and polysaccharides, as well as charged supramolecular biological assemblies, such as viruses or membrane fragments (Fischlechner, Zschörnig, Hofmann, & Donath, 2005), are gaining an increasing momentum for the fabrication of biodegradable and bio-functionalized capsule shells. Moreover, a number of standard polyelectrolytes have been modified to achieve anti-adhesive surface coatings protecting biomaterials against bacterial infection, or, by contrast, allow ligand-specific cell interactions via molecular recognition (Boulmedais, Frisch, Etienne, Lavalle, Picart, Ogier, Voegel, Schaaf, & Egles, 2004).

Table 18.2 Selection of commonly used polyelectrolytes.

	From synthetic monomers	From natural monomers
Polycations		
	Poly(allylamine hydrochloride); PAH (w)	Poly-L-ornithine (w)
	Poly(diallylmethyl ammonium chloride);PDADMAC (s)	Poly-L-arginine (w)
	Poly(ethylene imine); PEI (w)	Protamines (w)
	Polyvinylpyrrolidone; PVP (w)	Chitosan (w)
Polyanions		
	Poly(styrene sulfonate; PSS (s)	Poly-L-glutamic acid (w)
	Poly(acrylic acid); PAA (w)	Alginates (w)
	Polymethacrylic acid; PMA (w)	Dextran sulfate; DEXS (w)
	Poly(vinylsulfonate); PVS (w)	Carrageenan (w)
	polyphosphoric acid; PPA (s)	Nucleic acids (s)

(s) = strong polyeletrolyte; (w) = weak polyelectrolyte

Biocompatibility Considerations

Generally, bio-medical materials are to be subjected to *biocompatibility* assessments which have been generally drafted for the evaluation of implanted devices (Williams, 1999). In contrast to such mandatory *biocompatibility* assessments in medicine, "bio-friendliness" also has to be implemented for all processing techniques – a necessary requirement for maintaining functionality of encapsulated materials. Numerous applications of microcapsules and other DDS have been recently pursued both in vivo and in vitro. Since the ultimate goal of all DDS is to achieve high efficacy but minimum side effects, the aspects of *biocompatibility* are gaining particular relevance and should have a major impact on future research. To date, main efforts in the area of microcapsules have focussed on proof of principles for achieving efficient methods for encapsulation and release, and biocompatibility aspects are only starting to come to attention. In this regard, in the field of polymeric microencapsulation materials can be logically categorized due to their monomer constituents, which are of either synthetic (acrylic acid, styrene and allylamine – just to mention a few) or natural (amino acids, nucleic acids, sugars) origin. The latter ones are generally ascribed to the class of biodegradable polymers (de Geest, Vandenbroucke, Guenther, Sukhorukov, Hennink, Sanders, Demeester & De Smedt 2006 and Itoh, Matsusaki, Kida, & Akashi, 2006). Both types of polymers are listed separately in Table 18.2.

Nanotechnology in Microcapsule Design – Engineering the Surface on the Nano-level

Nanotechnology is distinct from any other field, in that it encompasses a wide range of disciplines and subjects. Indeed, all aspects of engineering, physics, chemistry and biology are part of this increasingly growing field.

That is due to the fact that nano-scale sizes on the one hand allow for tailoring molecular properties and on the other hand permit to construct devices whose small sizes are ideally suited for miniature applications in medicine, drug delivery, chemical reactions, computer memories, photonics and optoelectronic circuits, etc. All these factors make nanotechnology the future emerging discipline. In the bio-medical area nanoparticles have primarily stimulated the area of bio-diagnostics.

Up to date, several nanoparticle-based bio-diagnostic methods have been reported. In the area of DNA detection, these assays have been assessed to compete with PCR (polymerase chain reaction), and the easiest and the quickest approach monitors aggregation of nanoparticles upon addition of an analyte (Elghanian, Storhoff, Mucic, Letsinger, & Mirkin, 1997). The advantages of this method are simplicity, quickness, high degree of discrimination and often sensitivity. Surface plasmon resonance (Shipway, Katz, & Wilner, 2000) could be used for real-time detection of DNA hybridization with detection limits in the nM range (Kai, Sawata, Ikebukuro, Iida, Honda, & Karube, 1999). Fluorescence-doped silica nanoparticles can be used as labels in chip-based sandwich DNA assays (Hirsch, Jackson, Lee, Halas, & West, 2003). The drawbacks of these technologies, however, could be an uncontrolled aggregation. Quantum dots (QDs) are yet another type of nanoparticles used as fluorescence markers in bio-detection assays (Bruchez, Moronne, Gin, Weiss, & Alivisatos, 1998). In the protein bio-diagnostics area, the current standard is the enzyme-linked immunosorbent assay (ELISA), which relies on fluorophore labeling and is quite general. Other heterogeneous chip-based systems have been used for protein detection (Niemeyer & Ceyhan, 2001).

In addition to X-ray diffraction tools, the most commonly used methods for investigating of structures at the nano-level are atomic force microscopy (AFM), scanning electron microscopy (SEM) and transmission electron microscopy (TEM). The application of all these methods allows researching and developing nano-engineered objects. One example of such a structure is nano-engineered microcapsules Figure 18.2.

Metal Nanoparticles as Microcapsule Constituents: Brining Additional Functionality

Targeted for a wide range of applications in chemistry, physics and biomedicine, microcapsules are envisaged to play a major role in the area of drug delivery and delivery of encapsulated materials into biological cells. The possibility to custom-design the shell allows bringing multifunctionality to the shell of microcapsules. In drug delivery, microcapsules with nanoparticles can be used for remotely activating the microcapsules and releasing the encapsulated materials.

Two types of nanoparticles with regard to their surface stabilization can be generally used for functionalizing the microcapsules' shells. Stabilized are nanoparticles containing stabilizing ligands on their surface. For example, gold nanoparticles can be stabilized by 4-(dimethylamino)pyridine (DMAP) (Au_{DMAP}) (Gittins & Caruso, 2001). Au_{DMAP} nanoparticles are relatively monodisperse with a mean diameter of 5–10 nm, and aqueous

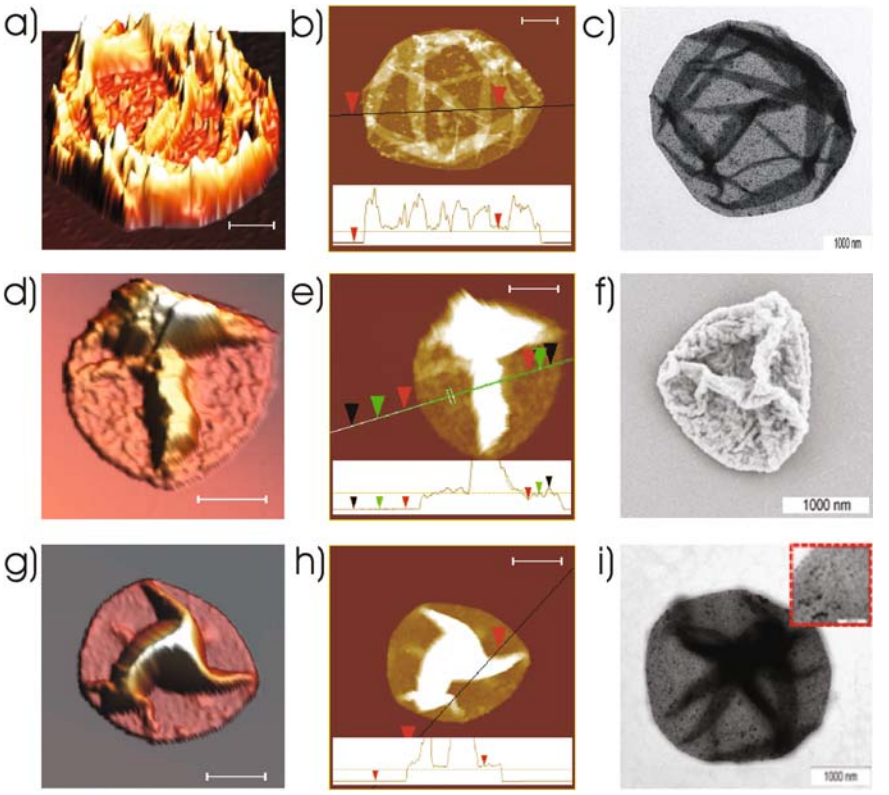

Figure 18.2 AFM (**a**,**b**,**d**,**e**,**g**,**h**), TEM (**c**,**i**) and SEM (**f**) images of a capsule with metal nanoparticles. The first row shows a microcapsule before, the other two rows another after thermal treatment. Capsules shown in the second row had no encapsulated polymers, while those in the third row had encapsulated polymers. (Reprinted with permission from *Angew. Chem. Int. Ed.* 2006, *42*, 4215. Copyright 2006 Wiley-VCH.) (*See* Color Plate 26)

suspensions can be obtained at high concentrations, on the order of 10^{14} nanoparticles/mL. Another way of stabilizing Au nanoparticles is by using thiol groups (Corbierre, Cameron, Sutton, Mochrie, Lurio, Ruhm, & Lennox, 2001). Non-stabilized are nanoparticles which do not, at least initially, contain any stabilizing ligands. One example of such nanoparticles is that referred to as gold sulfide. Gold nanoparticles were prepared by a two-step reaction of Na_2S with $HAuCl_4$ (Zhou, Honma, Komiyama, & Haus, 1994). The aggregation condition of these nanoparticles is the subject of continuing research (Halas et al., 1998, Norman, Grant, Magana, Zhang, Liu, Cao, Bridges, & van Buuren, 2002, Skirtach, Déjugnat, Braun, Susha, Rogach, & Sukhorukov, 2007a). The tools of nanotechnology took a prominent role not only in trying to answer questions of fundamental science but also in developing practical applications. For example, controlling the distribution of nanoparticles is important for developing novel nano-devices, nano- and bio-sensors and microelectronic devices. In drug delivery using PEM capsules, the degree of non-uniformity of the nanoparticle distribution allows for optimization and increase of efficiency of release. An easy way to control the aggregation condition

of nanoparticles with different surface functionalization on either microcapsules or planar films has been recently proposed by using polymers (Skirtach et al., 2007a).

Encapsulation and Release Techniques

Generally, polyelectrolyte capsules can be loaded with materials by two different strategies: In using the "direct loading" technique (also referred to as "active loading", Sukhorukov et al., 2004), materials are entrapped within or adsorbed onto template particles prior to LbL coating. After accomplishing the PEM build-up, template particles are dissolved and adherent materials are released into the interior of the emerging polyelectrolyte capsules. By contrast, "indirect loading" (or "passive loading") can be achieved by using prefabricated, hollow microcapsules. Here, materials of interest are driven into the capsules by using physicochemical forces that influence the permeability of the PEM. In this section, we provide a brief summary of such physicochemical forces, i.e., pH, temperature, ionic strength as well as external stimuli, such as light, ultrasound, magnetic fields, that can be used for both encapsulation and release.

External Stimuli for Reversible Permeability Changes

The multilayer structure of PEM microcapsules is determined by the interaction of their constituent layers. Therefore, understanding the details of this interaction and factors affecting it allows for control of the diffusion of molecules through the layers and, thus, leads to the development of versatile encapsulation procedures based on various external stimuli. Different stimuli such as pH, ionic strength and temperature can lead to a number of effects from controllable permeability change to morphological alterations (Decher et al., 1992). Such stimuli can be referred to as reversible because they alter the permeability in a reversible fashion and therefore can be used for both encapsulation and release of encapsulated materials.

pH Response: Hydrophobic and Electrostatic Forces

pH-responsive systems are obtained by introducing polyelectrolytes with weak acid and base functionalities into the capsule shells. In general, polyelectrolyte multilayers with pH-sensitive characteristics have drawn attention due to the possibility to control the average charge over the repeat unit and interaction between the charged polymers by adjusting the acidity of the surrounding solution (Sui & Schlenoff, 2004). Also, multilayers composed of weak polyelectrolytes can be affected and eventually destroyed at extreme pH conditions. This phenomenon is due to the pH-induced imbalance of charges, and they ultimately lead to the permeability change of the capsule walls.

Poly(allylamine hydrochloride) (PAH), PAA and poly(methacrylic acid) (PMA) are some representative and widely studied weak polyelectrolytes (Burke & Barrett, 2003). Polyelectrolyte multilayers and

microcapsules composed of such weak polyelectrolytes are stable depending on the pH range. Besides electrostatic stabilization, hydrogen bonding between uncharged carboxylic acids, amino functions and hydroxyl groups could also contribute to the stability of microcapsules (Stockton & Rubner, 1997). Other studies include structures made of weakly charged polyacids poly(acrylic acid) (PAA) and PMA, with uncharged polymers capable of undergoing hydrogen bond interactions like poly(ethylenoxide) (PEO) and poly(*N*-vinylpyrrolidone) (PVP) (Sukhishvili & Granick, 2000). Stable polyelectrolyte multilayers can be obtained using these polymers in the acidic pH range. The resulting structures, however, are sensitive to pH changes due to electrostatic repulsion between the layers.

Effects of Temperature

Temperature has been identified as one of such external post-treatment parameters affecting material properties and PEM formation (Izumrudov, Ortiz, Zezin, & Kabanov, 1998, Buscher, Graf, Ahrens, & Helm, 2002). Previous studies concentrated on the response of multilayers to the degree of humidity (Kügler, Schmitt, & Knoll, 2002), and response of films containing a thermo-sensitive polymer (Steitz, Leiner, Tauer, Khrenov, & von Klitzing, 2002). Notwithstanding, shrinking, in response to thermal treatment of PEM capsules, has been employed only recently for encapsulation by Köhler et al. (2005). Polyelectrolyte multilayers are kinetically stable structures, so it is logical to expect that a temperature increase can provide enough thermal energy to surpass the energy barrier necessary for polymeric film rearrangements. Also, PEM films deposited on flat substrates exhibit only negligible changes in thickness upon heating (Steitz et al., 2002). However, they shrink noticeably if heated at 100% humidity indicating that water desorption took place (Ahrens, Büscher, Eck, Förster, Luap, Papastavrou, Schmitt, Steitz, & Helm, 2004).

Initial research has shown that five bi-layer capsules made of poly(styrenesulfonate) (PSS) and poly(allylamine hydrochloride) (PAH) shrink to less than one-third of their initial size and exhibit increased wall thickness when incubated at elevated temperatures (Leporatti, Gao, Voigt, Donath, & Möhwald, 2001). In addition to size decrease, a significant reduction of the permeability for low-molecular-weight compounds accompanies heat treatment (Ibarz, Dähne, Donath, & Möhwald, 2002). On the other hand, the microcapsules composed of five bi-layers of PSS and poly(diallylmethyl ammonium chloride) (PDADMAC) swell at elevated temperatures (Gao, Leporatti, Moya, Donath, & Möhwald, 2003). At a first glance, such a discrepancy could be assigned to different charge distances in these systems: non-matching charge distance in the case of the PSS/PDADMAC pair versus matching charge distance in the case of the PSS/PAH pair. However, it was later established that the shrinking is due to reduction of the water/polyelectrolyte interface. Microcapsules shrunk at different temperatures are shown in Figure 18.3. One realizes that whereas the non-heated capsules on drying collapse into a folded structure, this effect does not take place at the highest temperature due to enforcement of the wall. The images at intermediate annealing temperatures show also less or no folding indicating that stiffness increases continuously with increase in temperature. The thermal method can be used for encapsulation of

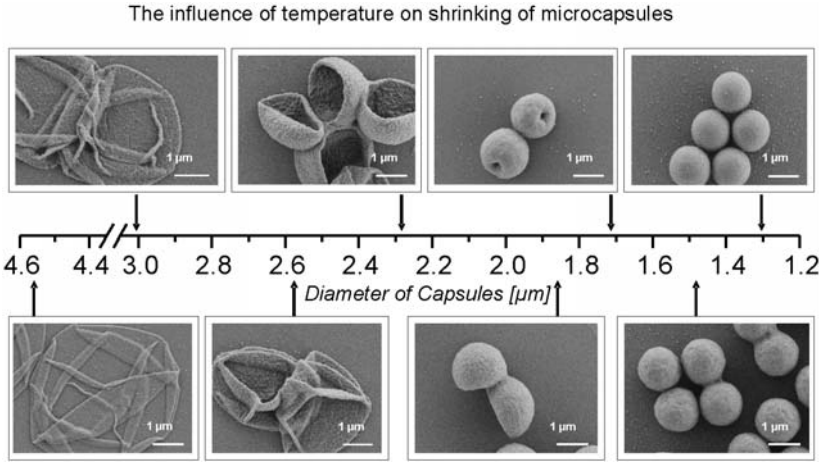

Figure 18.3 SEM images of initial capsules 4.55 μm (*left image*) and those thermally shrunk to various diameters (*right images*): 3 μm at 50°C, 2.5 μm at 52°C, 2.28 μm at 54°C, 1.5 μm at at 65°C.

polymers inside microcapsules; the electron microscopy images of a capsule with encapsulated polymers is shown in Figure 18.3 (bottom row).

Influence of Ionic Strength

PEM capsules are also responsive to ionic strength changes because of screening of electrostatic interaction between the oppositely charged polyelectrolyte polymers by salt ions. Ionic strength has been shown to affect multilayer film growth (Buscher et al., 2002). Even the finally prepared multilayer films show structural surface changes of polyelectrolyte films upon changing the ionic strength (Fery, Scholer, Cassagneau, & Caruso, 2001). Diffusion of charged ions may be described as hopping from one location to another, suggesting that the permeability of polyelectrolyte multilayers for ions depends on their charges (Farhat et al., 2000) and also on cavities within polyelectrolyte multilayers (Antipov, Sukhorukov, & Möhwald, 2003). This dependence is proportional to the salt concentration to the power of n, where n is the ion charge. It can be noted that pH is an important parameter and should be monitored. The ionic strength influences both the range of electrostatic interactions and their magnitude; therefore, high enough salt concentration can lead to complete destruction of multilayers.

Compared to planar films, microcapsules are an ideal system because in this case the polyelectrolyte multilayers are surrounded by liquid from both sides. The influence of ionic strength on PEM capsules can be traced by measuring dye molecule diffusion through or release from polyelectrolyte multilayers as a function of variable salt concentration (Antipov et al., 2003). The permeability coefficient was found to have a very strong nonlinear character and that the diffusion occurs through cavities in the multilayers. Increase in ionic strength decreases the free energy of polyelectrolyte interactions; pH affects the character of the interaction. Special attention has to be paid to the latter parameter because it also affects the microcapsule stability. Increasing ionic strength was found to change the

pH-dependent stability and swelling of microcapsules: the increased ionic strength leads to less stable microcapsules in pH regions from 2 to 3 and from 7 to 8 (Mauser, Dejugnat, & Sukhorukov, 2006). Also, the pH stability range decreases at higher salt concentrations: at low pH the swelling of microcapsules starts at higher pH values while at basic pH the swelling starts at lower pH values.

Other Encapsulation Techniques

The aforementioned external stimuli can be used for controlling diffusion of molecules through polyelectrolyte multilayers and therefore can be used for encapsulation (the so-called indirect loading). Here we describe other methods, i.e., those that are not based on external stimuli, and that can be also used for encapsulation and are generally denominated as "direct loading" techniques. Such techniques are particularly relevant for drug delivery and therefore are placed in this separate section. The simplest encapsulation strategy utilizes the compound to be encapsulated itself as a template for polyelectrolyte coating. So far, this strategy has been successfully applied on the encapsulation of protein aggregates, drug- and dye crystals. The problem is to obtain colloidal crystals of low dispersity and in the desired size range. Moreover, the materials should have a low solubility under the polyelectrolyte assembling conditions.

Recently, inorganic calcium carbonate microparticles have been utilized as a novel category of template particles having excellent loading capacity for biological materials (Sukhorukov et al., 2004; Petrov, Volodkin, & Sukhorukov, 2005; Volodkin, Larionova, & Sukhorukov, 2004). These spherical, 2–8 μm-sized $CaCO_3$, microcrystals can be loaded with biopolymers by either (1) electrostatic absorption of biopolymers onto the highly porous surface of prefabricated particles prior to polyelectrolyte coating ("adsorption method") or (2) incorporation of biocompounds into $CaCO_3$ spheres right from their synthesis ("coprecipitation method"). The latter case leads to a higher loading efficiency. Calcium carbonate is a non-toxic template and can be easily and gently removed by complexation with ethylenediaminetetraacetic acid (EDTA) making it suitable for the encapsulation of delicate biocompounds like enzymes or vaccines.

External Stimuli for Irreversible Permeability Changes: Remote Release Techniques

All aforementioned external stimuli such as pH, temperature and ionic strength affect the permeability of the shells of microcapsules in a reversible way by creating tiny pores in the polymeric structure and allowing or preventing the diffusion of molecules. They are useful for encapsulation under in vitro conditions, but they possess a severe limitation for the release of drugs in vivo. Therefore, in drug delivery and controllable release other, external remote triggers become particularly relevant.

Remote release techniques are referred to as irreversible because they lead to irreversible permeability changes. These remote methods are particularly useful in the case of drug delivery because they do not alter

chemical composition of environment and therefore could be conducted under physiological conditions where changing pH, ionic strength or oxidation is not a viable option. They can be classified into several groups.

Magnetic Activation of Microcontainers

Magnetic fields find increasing application in bio-medicine and drug delivery. In this regard, superparamagnetic properties of iron oxide particles can be used to guide microcapsules in place for delivery by external magnetic fields. For example, superparamagnetic magnetite (Fe_3O_4) could be introduced into the microcapsule's shell or in its interior. Magnetic particles can be produced by calcination of the core–shell magnetite particles at elevated temperatures. Not all materials are compatible with magnetic particles: the solubility of magnetic particles at pH 1 makes melamine formaldehyde (MF) unsuitable, thus leaving, for example, PS, silica or carbonates as a material of choice.

Besides utilizing magnetic particles for targeting techniques, they can as well be used to affect the permeability of microcapsules by applying external oscillating magnetic fields and release encapsulated materials upon request. For example, ferromagnetic cobalt nanoparticles containing a layer of gold (Co/Au) were incorporated into the assembly of PSS and PAH polyelectrolyte multilayer PEM shells of microcapsules. Subsequently, application of alternating magnetic fields with frequencies of 100–300 Hz and 1200 Oe strength results in increased permeability. It has been shown by Prouty, Guo, Golub, Kumar, & Lvov (2005) that magnetic fields affect the permeability of microcapsules by acting on aggregates of nanoparticles. In this regard, control of the aggregation state of nanoparticles by an easy method of mixing with polymers was recently reported (Skirtach et al., 2007a).

Ultrasound Activation of Microcapsules

Ultrasound is a method that was widely used for the synthesis of various nanomaterials, for example coating carbon nanotubes and noble metals. In the bio-medical field, ultrasound has been used in various applications: destruction and fragmentation of contrast agents, gas release, destruction of polymers, albumin or lipid shells of microbubbles and in drug delivery (Unger, 1997). Recent studies showed that ultrasound can be used for the destruction of PEM capsules (Shchukin, Gorin, & Möhwald, 2006, Skirtach, De Geest, Mamedov, Antipov, Kotov, & Sukhorukov, 2007b). Here, nanoparticles were used to increase the density of the shells of microcapsules. Affecting the denser shell of microcapsules, the ultrasound serves as a trigger to release encapsulated materials. It is worthwhile to notice that upon propagation an ultrasound wave experiences viscous and thermal absorption, and scattering in the medium. However, it is the cavitation microbubbles which occur as a result of the collapse of the generated microbubbles and the shear forces which cause the destruction of the polyelectrolyte capsules. Powers in the range of 100–500 W at frequencies of 20 kHz were applied for destruction of the capsules. It was found that nanoparticles adsorbed on microcapsules affect the action of ultrasound on their shells.

Organic Materials for Permeability Control of Microcapsules

Microcapsules containing the organic, infrared adsorbing dye IR-806 were studied in response to laser activation (Skirtach, Antipov, Shchukin, & Sukhorukov, 2004). The dye was incorporated as a layer in the polyelectrolyte multilayers. The capsules were deformed under the influence of a near-infrared laser beam affecting the shell's permeability. The location of the absorption peak of IR-806 in the near-infrared part of the spectrum makes this dye an interesting candidate for bio-medical applications.

The permeability of capsules can be also altered electrochemically by immersing the solution with capsules in a polypyrrole polymer film fabricated on electrodes (Shchukin, Köhler, & Möhwald, 2006). Then by applying voltage on the electrodes, the PSS/PDADMAC capsules changed their permeability allowing fluorescently labeled dextran to penetrate inside the microcapsules. Also, a permeability change of the microcapsules can be induced via redox-controlled reactions. For example, redox-active organometallic poly(ferrocenylsilane) (PFS) polyanion-based microcapsules were shown to change permeability (Ma, Dong, Hempenius, Möhwald, & Vancso, 2006). Incorporating PFS into the walls of the capsules allows one to use the effects of changing the redox chemical oxidation state on the walls permeability. In that process, fast capsule expansion accompanied by drastic permeability increases in response. This technique is less related to drug delivery because it requires chemical agents.

Enzyme-Mediated Drug Delivery

Enzyme-mediated drug delivery offers another route for releasing encapsulated materials inside the cells. Biodegradable polyelectrolyte multilayers from polysaccharides have been shown previously by Picart, Schneider, Etienne, Mutterer, Schaaf, Egles, Jessen, & Voegel (2005). In the drug delivery area, cellular uptake of polyelectrolyte capsules and intracellulary degradable polyelectrolyte capsules is particularly interesting. Such microcapsules could be attractive for the delivery of drugs with an intracellular target, for example nucleic acids and various proteins. Destroying the capsules with enzymes would be of high practical importance, and microcapsules were shown to disintegrate under the action of enzymes (Berth, Voigt, Dautzenberg, Donath, & Möhwald, 2002). De Geest et al. were the first to demonstrate capsule degradation by enzymes in 2006. Here, two types of degradable capsules based on $CaCO_3$ microparticles as a template were reported in that study. The first type of microcapsules responding to enzymatic degradation was composed of poly-L-arginine (PArg) as the polycation and dextran sulfate (DEXS) as the polyanion. For the second type, the authors utilized poly(hydroxypropylmethacrylamide dimethylaminoethyl) P(HPMA-DMAE) and PSS, respectively. Initially, the degradation of DEXS/PArg microcapsules was investigated by using Pronase®, a mixture of endo- and exo-proteases that cleaves proteins/peptides unspecifically down to single amino acids, and it turned out that DEXS/PArg microcapsules disintegrated completely within a few hours of incubation in a Pronase solution. Even more interesting, experiments carried out with African green monkey kidney cells (VERO-1 cells) revealed that both capsule types are subject to intracellular degradation. Figure 18.4 illustrates the Pronase-mediated degradation of a

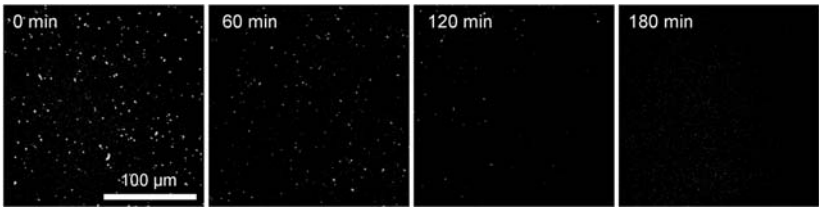

Figure 18.4 Confocal microscopy images of the enzymatic degradation of polyelectrolyte capsules consisting of three alternating layers of poly-L-arginine and poly-L-aspartic acid incubated in a Pronase solution (1 mg/ml) at 37°C.

similar type of polyelectrolyte capsules fabricated from PArg as the polycation and poly-L-aspartic acid (PAsp) as the polyanion (O. Kreft, unpublished results). The time-dependent microcapsule degradation is illustrated by a time series of CLSM micrographs. Even remnants of capsules could not be found after 2 h of incubation. Except laser activation of microcapsules inside living cells, this is the only other strategy that has been tested to date for drug delivery and intracellular release. Recently, Itoh et al. (2006) introduced another type of biodegradable polyelectrolyte capsules fabricated from DEXS and chitosan. Here, sustained release of encapsulated materials could be achieved via enzymatic capsule shell degradation by chitosanase. However, this specific system seems to be limited to in vitro applications, as chitosanase is not existent in mammalian cells. Self-disintegrating microcapsules were prepared by encapsulating Pronase into biodegradable polyelectrolyte shells by Borodina, Markvicheva, Kunizhev, Möhwald, Sukhorukov & Kreft, 2007. Here, Pronase was captured by micron-sized calcium carbonate particles that were subsequently embedded into onion-like shells of poly-L-arginine and poly-L-aspartic acid. EDTA treatment was used to extract calcium carbonate constituents from resulting core-shell particles. As a consequence, Pronase was released into the emerging capsule interior and started to digest the surrounding polyelectrolyte shell. Lifetimes of such self-disintegrating capsules could be successfully adjusted to seconds, hours or days by varying the amount of encapsulated Pronase. The enzyme-mediated, sustained release of encapsulated DNA was investigated as a prospective application in drug delivery.

Remote Activation and Release by Laser Light

Among other technologies, laser light has taken a prominent place as an external stimulus for remote release of encapsulated materials (Skirtach et al., 2004, Radt, Smith, & Caruso, 2004, Angelatos, Radt, & Caruso, 2005, Skirtach, Dejugnat, Braun, Susha, Rogach, Parak, Möhwald, & Sukhorukov, 2005). First and foremost, laser light can be coupled with microscopy providing visualization – an indispensable tool at the beginning of any study. Second, laser technology is sufficiently mature, so it is possible to choose a source with desired wavelength of emission, mode of operation, power, pulse duration, etc. These factors positioned laser as an indispensable method for investigation of chemical reactions, ablative decomposition of solid materials and polymers, study of the reaction kinetics, optical trapping and manipulation of microparticles, PDT

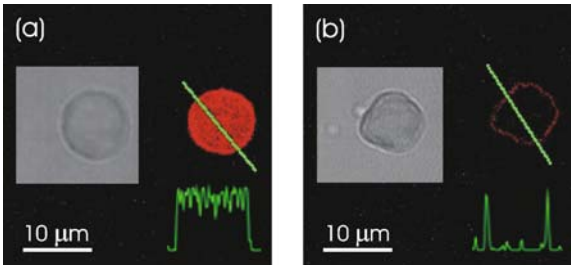

Figure 18.5 Release of encapsulated polymers from a microcapsule. The confocal microscope images are shown before (**a**) and after (**b**) laser illumination. (Reprinted with permission from *Nano. Lett.* 2005, *5*, 1371. Copyright 2005 American Chemical Society.) (*See* Color Plate 27)

(photo-dynamic therapy) for stimulation of apoptosis in the targeted cells by a laser. In the content of drug delivery, lasers can be used as a method for remote activation and release of encapsulated materials. An example of release of encapsulated materials is shown in Figure 18.5. Release can also be thought of in terms of releasing other substances, for example nanoparticles (Verberg, Alexeev, & Balazs, 2006).

These factors positioned laser as an indispensable method for investigation of chemical reactions, ablative decomposition of solid materials and polymers, study of the reaction kinetics, optical trapping and manipulation of microparticles, PDT (photo-dynamic therapy) for stimulation of apoptosis in the targeted cells by a laser. In the content of drug delivery, lasers can be used as a method for remote activation and release of encapsulated materials.

Remote Activation

Remote activation of microcapsules is defined as the action leading to a change of the permeability of microcapsules in response to an external field. Activation can be conducted with hollow, empty capsules. In the case of laser light illumination, the mechanism presented below is based on thermal excitation of nanoparticles by laser light (Skirtach et al., 2005), and the temperature increase around a heating sphere could be written as follows:

$$\frac{\mathrm{d}T(r_i)}{\mathrm{d}E} = \frac{r_0^3}{r_i} \tag{1}$$

where $E{=}A/(3K)$, A is the heating rate per unit volume per unit time and K is the thermal conductivity of the surrounding medium. The values for E can be calculated knowing that the rate A is proportional to the incident power density and absorption. It should be noted that such an analysis can be applied to interactions of metal nanoparticles with any external field. The temperature increase during laser light illumination indicates that metal nanoparticles can be efficiently excited by laser light (Skirtach et al., 2005). The increase was found to depend on nanoparticles' size, concentration and energy of the incident laser beam. A distinct feature of this newly developed method is that it is conducted in situ, i.e., in aqueous solution, whereas all previously existing optical probes of temperature were applicable only for non-aqueous solutions. The method uses the fluorescence intensity change of a temperature- and pH-sensitive dye in a TRIS solution upon varying the temperature. Calibration was performed in a temperature-controlled fluorimeter taking into consideration

thermophoresis of the dye with a Soret coefficient of 0.015/K (half of the decrease of the dye's intensity is due to the pH drop and half due to thermophoresis, resulting in a sensitivity of the dye of 1.85% fluorescence change per degree C at 20°C).

Remote Release

Release experiments were made using photostable materials. For example, AF-488 dextran conjugate was chosen because it is significantly brighter and more photostable than other green fluorophores (Skirtach, Munoz Javier, Kreft, Karen Köhler, Piera Alberola, Möhwald, Parak, & Sukhorukov, 2006). Excitation from the ground state to the first singlet state S1 dominates the absorption of the fluorescent dyes at low flux energy. The laser wavelength (830 nm) is located outside the 450–510 nm absorption band of AF-488 dextran, so a control experiment made with microcapsules without embedded nanoparticles showed no changes of their structure.

Applications in Drug Delivery

In order to successfully accomplish delivery of encapsulated materials into cells, the following properties have to be met: sufficient mechanical stability of capsules, pH and other chemical stability of microcapsules and encapsulated materials and successful uptake by cells.

Delivery into and Uptake by Cells

Mechanical Properties

Mechanical stability of the capsules – a subject of extensive research (Dubreuil, Elsner & Fery, 2003; Lulevich, Nordschild, & Vinogradova, 2004; Müller, Köhler, Weinkamer, Sukhorukov, & Fery, 2005) – is among the most important prerequisites for successful delivery of encapsulated materials into cells. Two strategies could be pursued: The first comprises elastic microcapsules (for example, resembling red blood cells), whereas the other utilizes stiff capsules. To date, there are no easy means to control the elasticity of the capsules, while hardness can be increased by thermally treating the microcapsules. For example, it was demonstrated (Müller et al., 2005) that after heating for 20 min at 50°C the stiffness increases by 4 times (from $\sim$ 220 to 870 pN/nm), and, even more amazingly, by more than 10 times (from $\sim$ 220 to 2600 pN/nm) upon heat treatment to 55°C. This is attributed to an increase of the wall thickness produced upon heat shrinking. Earlier experiments of uptake of microcapsules by cells also confirm such conclusions because the thickness of the walls influenced the percentage of intact capsules upon uptake. Therefore, thermally shrunk microcapsules with thicker walls, higher stiffness and mechanical stability are less likely to be deformed, so they are more suited for delivery of encapsulated materials.

Uptake of Capsules by Cells – Laser as a Tool for Uptake Studies

If the laser beam is directed from the bottom, an interesting phenomenon was observed: microcapsules not uptaken by cells were pushed up by the

laser beam away from the field of view due to the radiation pressure of light (Skirtach et al., 2006). The cell itself did not undergo changes, but microcapsules located on top of a cell were pushed out of the field of view by the laser. On one hand, these so-called flying capsules show that the release of encapsulated materials can be carried out only from capsules internalized by the cells, because microcapsules only adherent to the outer membrane are lifted up and moved away from the imaging plane. On the other hand, this observation provides an additional criterion to evaluate the internalization (uptake) of microcapsules or other small objects by cells. It is fairly simple and could be an efficient tool in the area of drug delivery into cells. The phenomenon of lifting microcapsules is based on pressure of light experiments carried out by Lebedew in 1901.

Microencapsulated Sensors as Cell-Residing Reporters

In cellular and clinical research, accurate quantification of analytes inside living cells and tissues with both high spatial and temporal resolution but negligible cell perturbation is an extremely challenging drug delivery task. Commonly used techniques are based on either visualization (using microscopy) or optical/electrochemical sensors. Their potential hindrances include chemical interactions or resolution in visualization or undesirable cell damage.

Our objective is to create micrometer-scale functionalized polymer capsules filled or assembled with dye sensors to simultaneously explore various cell functions on the single cell level. Such capsules should combine the advantages of multifunctionality of sensor tips and dye probes and, moreover, overcome physical and chemical drawbacks associated with these methods. pH is one parameter that is important for bio-medicine in general and drug delivery in particular. In recent and encouraging studies, we demonstrated that pH-induced spectral shift of a fluorescent pH indicator (SNARF®, Molecular Probes) is not affected by microencapsulation (Figure 18.6 and Kreft, Muñoz Javier, Sukhorukov & Parak, 2007).

In consequence of this proof of concept of a capsule-based ion sensor, experiments are devoted to the development of a capsule-based "sensor-tool-box" consisting of a modular assembly system that can be individually self-tailored to create complex sensing schemes for advanced and comprehensive applications in cell biology (i.e., flow cytometry), clinical chemistry and analytical chemistry. Parts of the tool-box are sensors for ionic analytes, such as Na^+, K^+, Ca^{2+}, Cl^-, PO_4^{3-},but also for compounds like oxygen and nitric oxide. Further research is focussed on in vivo applications and optimizations of detection including specificity and sensitivity.

Release into Cells

Laser Bio-Friendliness

In ideal experiments using laser–nanoparticle interaction, the laser should have minimum absorption by cells and tissue and maximum absorption by nanoparticles. In the former case, one can tune the wavelength of the laser to a desired region in the biologically "friendly" window (Roggan, Friebel,

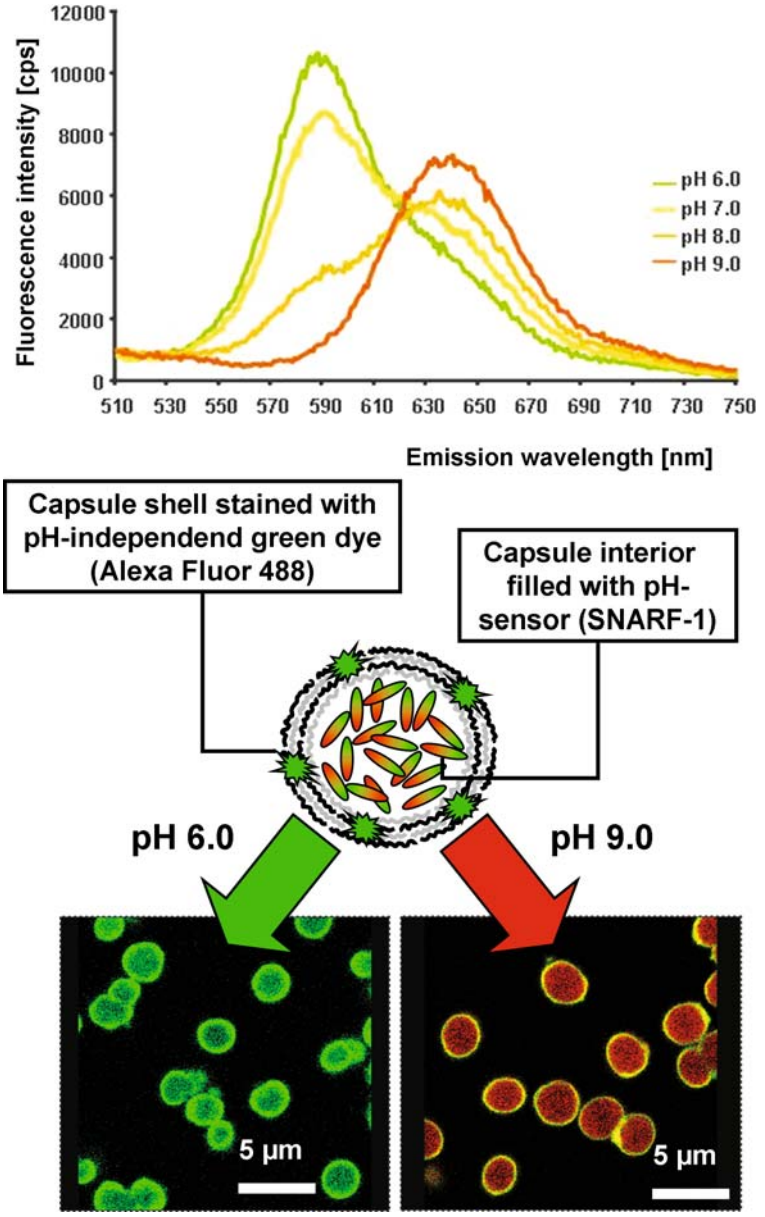

Figure 18.6 *Above*: Fluorescence emission spectra of SNARF-1-dextran (MW = 70,000) in aqueous solution. SNARF-1 exhibits a significant pH-dependent emission shift from *green* to *red* fluorescence under acidic and basic conditions, respectively. The ratio of the fluorescence intensities at 580 and 650 nm can be used for quantitative determinations of pH values. *Below*: Fluorescence properties of encapsulated SNARF-1-dextran. The inner void of the capsules is loaded with SNARF-1-dextran molecules (drawn in *red*/*green*), whereas the capsule shell is labeled with the *green* Alexa Fluor 488 dye, which is not sensitive to pH changes. Depending on pH, the fluorescence of the SNARF-1-dextran molecules and thus the inside of the capsules changes from *green* (acidic pH) to *red* (alkaline pH). In comparison, the *green* fluorescence of the capsule shell is maintained under alkaline conditions. The images show an overlay of CLSM images taken at 580 and 650 nm. The average diameter of the capsules is 5 µm. (*See* Color Plate 28)

Dorschel, Hahn, & Muller, 1999) – the near-infrared part of the spectrum. Nanoparticles have to be designed with maximum absorption. For example, silver nanoparticles larger than 20 nm were deposited in high concentration and cluster-like arrangement. These features lead to non-zero absorption in the near-infrared part of the spectrum due to dipole and higher order multipolar contributions as well as interaction between the nanoparticles (Kreibig, Schmitz, & Breuer, 1987). Furthermore, the concentration of metal nanoparticles is important for two reasons: First, when the distance between the two adjacent nanoparticles is of the order of their size, the thermal effects produced by adjacent nanoparticles add up, and second, the interaction of nanoparticles located in proximity to each other results in increase of absorption at the lower energies or higher wavelengths (causing the so-called red shift) compared to the surface plasmon resonance band of stand-alone nanoparticles (Kreibig et al., 1987). For these reasons, spatial distribution of nanoparticles is important and control of their distribution is vital.

Remote Release Inside Living Cells

Both remote activation and release of encapsulated materials inside living cells were recently reported (Skirtach et al., 2006). Remote activation experiments were conducted using microcapsules containing silver nanoparticles in their walls, whereas remote release experiments were reported for capsules containing gold–gold sulfide nanoparticles in their walls.

The release of encapsulated AF-488 labeled dextran inside a living cell upon laser illumination is shown in Figure 18.7. Figure 18.7(a) shows the fluorescence image of capsules, and Figure 18.7(b) shows the fluorescence and transmission signals from the same cell and the same capsules before laser light illumination. Before illumination the capsule is filled, Figure 18.7(c). The corresponding images of the same capsule after laser light illumination, Figure 18.7(d)–(f), demonstrate that most polymers left the

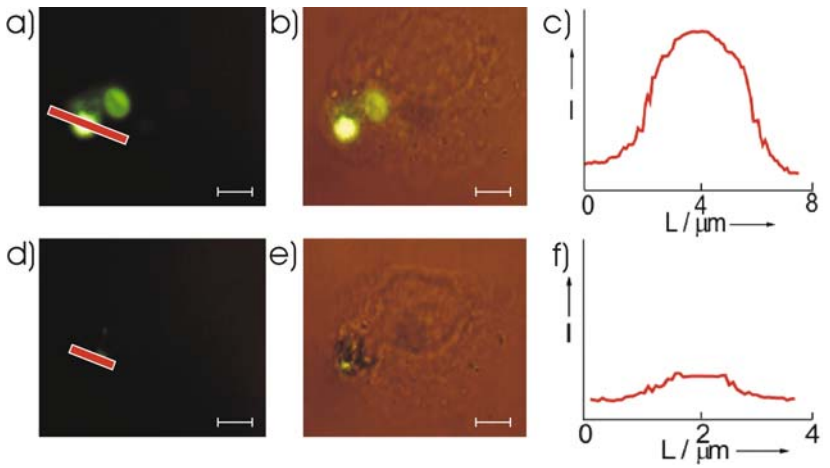

Figure 18.7 Remote release of encapsulated materials inside living cells: (**a**)–(**c**) before and (**d**)–(**f**) after laser illumination. (Reprinted with permission from *Angew. Chem. Int. Ed.* 2006, *42*, 4215. Copyright 2006 Wiley-VCH.) (*See* Color Plate 29)

interior of the capsule. The presence of some traces of the fluorescence signal in the microcapsule's shell after the release is consistent with the earlier reported experiments (Skirtach et al., 2005). The temperature rise during remote release experiments could be several degrees (Skirtach et al., 2005). The cells were found to adhere to the substrate both before and after the release of encapsulated polymers showing that this method is feasible for delivery of encapsulated materials into cells.

Acknowledgments. We are indebted to Prof. Helmuth Möhwald for critical reading of the manuscript and support during research; we also thank Dr. D. G. Shchukin and Prof. G. B. Sukhorukov for helpful discussions. We thank Dr. B. G. De Geest and K. Köhler for assistance in text and illustration preparations. The support by EU FP-6 programs ("SELECT-NANO" and "NANOCAPS") as well as Volkswagen-Foundation is kindly acknowledged.

References

Akagi, T., Ueno, M., Hiraishi, K., Baba, M., & Akashi, M. (2005) AIDS vaccine: Intranasal immunization using inactivated HIV-1-capturing core–corona type polymeric nanospheres. *J. Controlled Release*, *109*, 49–61.

Ahrens, H., Büscher, K., Eck, D., Förster, S., Luap, C., Papastavrou, G., Schmitt, J., Steitz, R., & Helm, C. A. (2004). Poly(styrene sulfonate) self-organization: Electrostatic and secondary interactions. *Macromol. Symp.*, *211*, 93–105.

Angelatos, A. S., Radt, B., & Caruso, F. (2005). Light-responsive polyelectrolyte / gold nanoparticle microcapsules. *J. Phys. Chem. B*, *109*, 3071–3076.

Antipov, A. A., Sukhorukov, G. B., & Möhwald, H. (2003). Influence of the ionic strength on the polyelectrolyte multilayers' permeability. *Langmuir*, *19,* 2444–2448.

Arotçaréna, M., Heise, B., Ishaya, S., & Laschewsky. A. (2002). Switching the inside and the outside of aggregates of water-soluble block copolymers with double thermoresponsitivity, *J. Am. Chem. Soc.*, *124*, 3787–3793.

Averitt, R. D., Sarkar, D., & Halas, N. J. (1997). Plasmon resonance shifts of Au-coated Au_2S nanoshells: Insight into multicomponent nanoparticle growth. *Phys. Rev. Lett.*, *78*, 4217–4220.

Berth, G., Voigt, A., Dautzenberg, H., Donath, E., & Möhwald, H. (2002). Polyelectrolyte complexes and layer-by-layer capsules from chitosan/chitosan sulfate. *Biomacromol.*, *3*, 579–590.

Bhadra, D., Bhadra, S., Jain, S., & Jain, N. K. (2003). A PEGylated dendritic nanoparticle carrier of fluorouracil. *Int. J. Pharm.*, 257, 111–124.

Bruchez, M., Jr., Moronne, M., Gin, P., Weiss S., & Alivisatos, A. P. (1998). Semiconductor nanocrystals as fluorescent biological labels. *Science*, *281*, 2013–2016.

Borodina, T., Markvicheva, E., Kunizhev, S., Möhwald, H., Sukhorukov, G. B. & Kreft, O. (2007). Controlled Release of DNA from Self-Degrading Microcapsules. Macromol. Rapid Commun. *28*, 1894–1899.

Boulmedais, F., Frisch, B., Etienne, O., Lavalle, Ph., Picart, C., Ogier, J., Voegel, J.-C., Schaaf, P.,& Egles, C. (2004). Polyelectrolyte multilayer films with PEGylated polypeptides as a new type of anti-microbial protection for biomaterials. *Biomaterials*, *25*, 2003–2011.

Boussif, O., Lezoualc'h, F., Zanta, M. A., Mergny, M. D., Scherman, D., Demeneix, B., & Behr, J. P. (1995) A versatile vector for gene and oligonucleotide transfer into cells in culture and *in vivo*: polyethyleneimine. *Proc. Natl. Acad. Sci. USA,* 92, 7297–7301.

Burke, S. E., & Barrett, C. J. (2003). pH-responsive properties of multilayered poly(L-lysine)/hyaluronic acid surfaces. *Biomacromol*., *4*, 1773–1783.

Buscher, K., Graf, K., Ahrens, H., & Helm, C. A. (2002). Influence of adsorption conditions on the structure of polyelectrolyte multilayers. *Langmuir*, *18*, 3585–3591.

Cammas, S., Suzuki, K., Sone, C., Sakurai, Y., Kataoka, K., & Okano, T. (1997). Thermo-responsive polymer nanoparticles with a core-shell micelle structure as site specific drug carriers. *J. Controlled Release* , *48*, 157–164.

Corbierre, M. K., Cameron, N. S., Sutton, M., Mochrie, S. G. J., Lurio, L. B., Ruhm, A., & Lennox,R. B. (2001). Polymer-stabilized gold nanoparticles and their incorporation into polymer matrices *J. Am. Chem. Soc*., *126*, 2867–2873.

Couvreur, P., Barratt, G., Fattal, E., Legrand, P., & Vauthier, C. (2002). Nanocapsule technology: A review. *Crit. Rev. Ther. Drug Carrier Syst*., *19*, 99–134.

Das, M., Zhang, H., & Kumacheva, E. (2006). Microgels: Old materials with new applications. *Ann. Rev. Mat. Res*., 36, 117–142.

Decher, G. (1997). Fuzzy nanoassemblies: Toward layered polymeric multicomposites, *Science*, *277*, 1232–1237.

Decher, G., & Hong, G. D. (1991). Buildup of ultrathin multilayer films by a self-assembly process: I. consecutive adsorption of anionic and cationic bipolar amphiphiles. *Macromol. Chem. Macromol. Symp*., *46*, 321–327.

Decher, G., Schaaf, P., Voegel, J.-C., & Picart, C. (2004). Improvement of stability and cell adhesion properties of polyelectrolyte multilayer films by chemical cross-linking. *Biomacromol*., *5*, 284–294.

De Geest, B. G., Dégunat, C., Sukhorukov, G. B., Braeckmans, K., De Smedt, S. C., & Demeester. J. (2005). Self-rupturing microcapsules. *Adv. Mater*., *17*, 2357–2361.

De Geest, B. G., Vandenbroucke, R. E., Guenther, A. M., Sukhorukov, G. B., Hennink, W. E., Sanders, N. N., Demeester, J., & De Smedt, S. C. (2006). Intracellularly degradable polyelectrolyte microcapsules. *Adv. Mater*., *18*, 1005–1009.

Diaspro, A., Silvano, D. Krol, S., Cavalleri, O., & Gliozzi, A. (2002). Single living cell encapsulation in nano-organized polyelectrolyte shells. *Langmuir,* 18, 5047–5050.

Donath, E., Sukhorukov, G. B., Caruso, F., Davies, S. A., & Möhwald, H. (1998). Novel hollow polymer shells by colloid-templated assembly of polyelectrolytes. *Angew. Chem. Int. Ed*., *37*, 2202–2205.

Dong, L. C., & Hoffman, A. S. (1990). Synthesis and application of thermally reversible heterogels for drug delivery, *J. Controlled Release*, *13*, 21–31.

Dubreuil, F., Elsner N., & Fery, A. (2003). Elastic properties of polyelectrolyte capsules studied by atomic-force microscopy and RICM. *Eur. Phys. J*., *12*, 215–221.

Elghanian, R., Storhoff, J. J., Mucic, R. C., Letsinger, R. L., & Mirkin, C. A. (1997). Optical properties of gold nanoparticles. *Science*, *277*, 1078–1081.

Escobar-Chávez, J. J., López-Cervantes, M., Naïk, A. Kalia, Y. N., Quintanar-Guerrero, D., & Ganem-Quintanar, A. (2006). Applications of thermoreversible pluronic F-127 gels in pharmaceutical formulations. *J. Pharm. Pharmaceut. Sci*., *9*, 339–358.

Estrela-Lopis, I., Leporatti, S., Moya, S., Brandt, A., Donath, E., & Möhwald, H. (2002). SANS studies of polyelectrolyte multilayers on colloidal templates. *Langmuir*, *18*, 7861– 7866.

Faraassen, S., Vörös, J., Csucs, G., Textor, M., Merkle, H. P., & Walter, E. (2003). Ligand-specific targeting of microspheres to phagocytes by surface modification with poly(L-lysine)-grafted poly(ethylene glycol) conjugate. *Pharm. Res*., *20*, 237–246.

Farhat T. R., & Schlenoff J. B. (2001). Ion transport and equilibria in polyelectrolyte multilayers. *Langmuir*, *17*, 1184–1192.

Fery, A., Scholer, B., Cassagneau, T., & Caruso, F. (2001). Nanoporous thin films formed by salt-induced structural changes in multilayers of poly(acrylic acid) and poly(allylamine). *Langmuir*, *17*, 3779–3783.

Fischlechner, M., Zschörnig, O., Hofmann, J., & Donath, E. (2005). Engineering virus functionalities on colloidal polyelectrolyte lipid composites. *Angew. Chem. Int. Ed.,* 44, 2892–2895.

Firestone, B. A., & Siegel, R. A. (1991). Kinetics and mechanisms of water sorption in hydrophobic, ionizable copolymer gels. *J. Appl. Polym. Sci.*, *43*, 901–914.

Haensler, J., & Szoka, F. C. (1993). Polyamidoamine cascade polymers mediate efficient transfection of cells in culture. *Bioconjug. Chem.,* 4, 372–379.

De las Heras Alarcón, C., Pennadam, S., & Alexander, C. (2005). Stimuli responsive polymers for biomedical applications. *Chem. Soc. Rev.*, *34*, 276–285.

Gan, D. J., & Lyon, L. A. (2001). Tunable swelling kinetics in core-shell hydrogel nanoparticles. *J. Am. Chem. Soc.*, *123*, 7511–7517.

Gao, C. Y., Moya, S., Lichtenfeld, H., Casoli, A., Fiedler, H., Donath, E., & Möhwald, H. (2001). The decomposition process of melamine formaldehyde cores: The key step in the fabrication of ultrathin polyelectrolyte multilayer capsules. *Macromol. Mater. Eng.*, *286*, 355–361.

Gao, C., Leporatti, S., Moya, S., Donath, E., & Möhwald, H. (2003). Swelling and shrinking of polyelectrolyte microcapsules in response to changes in temperature and ionic strength. *Chem.-Eur. J*, *9*, 915–920.

Germain, M., Balaguer, P., Nicolas, J.-C., Lopez, F., Esteve, J.-P., Sukhorukov, G. B., Winterhalter, M., Richard-Foy, H., & Fournier, D. (2006). Protection of mammalian cell used in biosensors by coating with a polyelectrolyte shell. *Biosens. and Bioelectron.*, *21*, 1566–1573.

Gilbert, J., Richardson, J. L. Davies, M. C., Pallin, K. J., & Hadgraft, J. (1987). The effect of solutes and polymers on the gelation properties of Pluronic F-127 solution for controlled drug delivery. *J. Controlled Release,* 5, 113–118.

Gillies, E. R., Jonsson, T. B., & Fréchet, J. M. J. (2004). Stimuli-responsive supramolecular assemblies of linear-dendritic copolymers. *J. Am. Chem. Soc.* 126, 11936–11943.

Gillies, E. R., & Fréchet, J. M. J. (2005). Dendrimers and dendritic polymers in drug delivery, *Drug Delivery Today*, *10*, 35–43.

Gittins, D., & Caruso, F. (2001). Spontaneous phase transfer of nanoparticulate metals from organic to aqueous media. *Angew. Chem. Int. Ed.*, *40*, 3001–3004.

Graham, N. B., & Cameron, A. (1998). Nanogels and microgels: The new polymeric materials playground. *Pure Appl. Chem.*, *70*, 1271–1275.

Gref, R., Minaniitake, Y., Peracchia, M. T., Trubetskoy, V., Torchilin, V., & Langer, R. (1994). Biodegradable long-circulating polymeric nanosphere. *Science*, *263*, 1600–1603.

Guo, A., Liu, G., & Tao, J. (1996). Star polymers and nanospheres from crosslinkable diblock copolymers, *Macromolecules*, *29*, 2487–2493.

Gupta, P., Vermani, K., & Garg, S. (2002). Hydrogels: from controlled release to pH-responsive drug delivery. *Drug Disc. Today*, *7*, 569–579.

Harada, A., & Kataoka, K. (1995). Formation of polyion complex micelles in aqueous milieu from a pair of oppositely-charged block copolymers with poly (ethylene glycol) segments, *Macromolecules*, *28*, 5294–5299.

Harada, A., & Kataoka, K. (1999). Chain length recognition: core–shell supramolecular assembly from oppositely charged block copolymers. *Science*, *283*, 65–67.

Hennink, W. E., & van Nostrum, C. F. (2002). Novel crosslinking methods to design hydrogels. *Adv. Drug Deliv. Rev.*, *54*, 13–36.

Hirayama, F., & Uekama, K. (1999). Cyclodextrin-based controlled drug release system. *Adv. Drug Del. Rev.*, *36*, 125–141.

Hirsch, L. R., Jackson, J. B., Lee, A., Halas, N. J., & West, J. L. (2003). A whole blood immunoassay using gold nanoshells. *Anal. Chem*, 75, 2377– 2381.

Ibarz, G., Dähne, L., Donath, E., & Möhwald, H. (2002). Controlled permeability of polyelectrolyte capsules via defined annealing. *Chem. Mater.*, *14*, 4059–4062.

Itoh, Y., Matsusaki, M., Kida, T., & Akashi, M. (2006). Enzyme-responsive release of encapsulated proteins from biodegradable hollow capsules. *Biomacromol.,* 7, 2715–2718.

Izumrudov, V. A., Ortiz, H. O., Zezin, A. B., & Kabanov, V. A. (1998). Temperature controllable interpolyelectrolyte substitution reactions. *Macromol. Chem. Phys.*, *199*, 1057– 1062.

Jansen, J. F. G. A., Debraban der Vandenberg, E. M. M., & Meijer, E. W. (1994). Encapsulation of guest molecules into a dendritic box. *Science*, *266*, 1226–1229.

Jansen, J. F. G. A., Meijer, E. W., & Debraban der Vandenberg, E. M. M. (1995). The dendritic box: shape-selective liberation of encapsulated guests. *J. Am. Chem. Soc.*, *117*, 4417–4418.

Jiang, C. Y., & Tsukruk, V. V. (2006). Freestanding nanostructures via layer-by-layer assembly. *Adv. Mater.*, *18*, 829–840.

Kabanov, A. V., Chekhonln, V. P., Alakhov, V. Y., Batrakova, E. V., Lebedev, A. S., Melik- Nubarov, N. S., Arzhakov S. A., Levashov, A. V., Morozov, G. V., Severin, E. S., & Kabanov, V. A. (1989). The neuroleptic activity of haloperidol increases after its solubilization in surfactant micelles Micelles as microcontainers for drug targeting, *FEBS Lett.,* 258, 343–345.

Kai, E., Sawata, S., Ikebukuro, K., Iida, T., Honda, T., & Karube, I. (1999). Detection of PCR products in solution using surface plasmon resonance. *Anal. Chem.*, *71*, 796–800.

Kamath, K., & Park, K. (1993). Biodegradable hydrogels in drug delivery, *Adv. Drug Del. Rev.*, *11*, 59–84.

Kataoka, K., Ishihara, A., Harada, A., & Miyazaki, H. (1998). Effect of secondary structure of poly(L-lysine) segments on the micellization of poly(ethylene glycol)–poly(L-lysine) block copolymer partially substituted with hydrocinnamoyl-group at the N -position in aqueous milieu. *Macromolecules*, *31*, 6071–6076.

Kataoka, K., Harada, A., & Nagasaki, Y. (2001). Block copolymer micelles for drug delivery: design, characterization and biological significance. *Adv. Drug Del. Rev.,* 47, 113–131.

Kikuchi, A., & Okano, T. (2002). Pulsatile drug release control using hydrogels, *Adv. Drug Del. Rev.*, *54*, 53–77.

Köhler, K., Shchukin, D. G., Möhwald, H., & Sukhorukov, G. B. (2005). Thermal behaviour of polyelectrolyte multilayer microcapsules. 1. The effect of odd and even layer number. *J. Phys. Chem. B*, *109,* 18250–18259.

Kreft, O., Georgieva, R., Bäumler, H., Steup, M., Müller-Röber, B., Sukhorukov, G. B., & Möhwald, H. (2006) Red blood cell templated polyelectrolyte capsules: A novel vehicle for the stable encapsulation of DNA and proteins. *Macromol. Rapid Commun.*, *27*, 435–440.

Kreft, O., Muñoz Javier, A., Sukhorukov, G. B. & Parak, W. J. (2007). Polymer Microcapsules as Mobile Local pH-sensors. *J. Materials Chemistry*. *17,* 4471–4476.

Kreibig, U., Schmitz, B., & Breuer, H. D. (1987). Separation of plasmon-polariton modes of small metal particles. *Phys. Rev. B*, *36*, 5027–5030.

Kügler, R., Schmitt, J., & Knoll, W. (2002). The swelling behavior of polyelectrolyte multilayers in air of different relative humidity and in water. *Macromol. Chem. Phys.,* 203, 413–419.

Kwoh, D. Y., Coffin, C. C., Lollo, C. P., Jovenal, J., Banaszczyk, M. G., Mullen, P., Phillips, A., Amini, A., Fabrycki, J., Bartholomew, R. M., Brostoff, S. W., & Carlo, D. J. (1999) Stabilization of poly-L-lysine/DNA polyplexes for *in vivo* gene delivery to the liver. *Biochim. Biophys. Acta,* 1444, 171–190.

Lebedew, P. (1901) Testings on the compressive force of light. *Ann. der Phys.,* 6, 433–458.

Leporatti, S., Gao, C., Voigt, A., Donath, E., & Möhwald, H. (2001). Shrinking of ultrathin polyelectrolyte multilayer capsules upon annealing: A confocal laser scanning microscopy and scanning force microscopy study. *Eur.Phys. J. E*, *5*, 13–20.

Liu, S. Y., & Armes, S. P. (2002). Polymeric surfactants for the new millennium: A pH-responsive, zwitterionic, schizophrenic diblock copolymer. *Angew. Chem. Int. Ed.*, *41*, 1413–1416.

Lowman, A. M., & Peppas, N. A. (1999). Hydrogels. In *Encyclopaedia of Controlled Drug Delivery* (Mathiowitz, E., ed.), pp. 397–418, John Wiley & Sons.

Lvov, Y., Antipov, A. A., Mamedov, A., Möhwald, H., & Sukhorukov, G. B. (2001). Urease encapsulation in nanoorganized microshells. *Nano Lett.*, *1*, 125–128.

Lu, Z., Prouty, M. D., Guo, Z., Golub, V. O., Kumar, C. S. S. R., & Lvov, Y. M. (2005). Magnetic switch of permeability for polyelectrolyte microcapsules embedded with Co@Au nanoparticles. *Langmuir*, *21*, 2042–2050.

Lulevich, V. V., Nordschild, S., & Vinogradova, O. I. (2004). Investigation of molecular weight and aging effect on the stiffness of polyelectrolyte multilayer microcapsules. *Macromolecules*, *37*, 7736–7741.

Ma, Y., Dong, W.-F., Hempenius, M. A., Möhwald, H., & Vancso, G. J. (2006). Redox-controlled molecular permeability of composite-wall microcapsules. *Nat. Mater.*, *5*, 724–729.

Maeda, H., Wu, J., Sawa, T., Matsumura, Y., & Hori, K. (2000). Tumor vascular permeability and the EPR effect in macromolecular therapeutics: a review. *J. Controlled Release*, *65*, 271–284.

Mansur, C. R. E., Barboza, S. P., González, G., & Lucas, E. F. (2004). Pluronic×tetronic polyols: Study of their properties and performance in the destabilization of emulsions formed in the petroleum industry, *J. Col. Int. Sci.*, *271*, 232–240.

Mart, R. J., Osborne, R. D., Stevens, M. M., & Ulijn, R. V. Peptide-based stimuli-responsive biomaterials (2006). *Soft Matter*, 2, 822–835.

Mayer, C. (2005). Nanocapsules as drug delivery systems. *Int. J. Artif Organs.*, 28, 1163–1171.

Mauser, T., Dejugnat, C., & Sukhorukov, G. B. (2006). Balance of hydrophobic and electrostatic forces in the pH response of weak polyelectrolyte capsules. *J. Phys. Chem. B*, *110*, 20246–20253.

Moffitt, M., Khougaz, K., & Eisenberg, A. (1996). Micellization of ionic block copolymers. *Acc. Chem. Res.*, *29*, 95–102.

Möhwald, H., Donath. E., & Sukhorukov, G. B. in Multilayer Thin Films, Wiley-VCH, New York, 2003, pp 363–392.

Moya, S., Dähne, L., Voigt, A., Leporatti, S., Donath, E., & Möhwald, H. (2001). Polyelectrolyte multilayer capsules templated on biological cells: core oxidation influences layer chemistry. *Colloids Surf. A*, *183*, 27– 40.

Müller, R., Köhler, K., Weinkamer, R., Sukhorukov, G., & Fery, A. (2005). Melting of PDADMAC/PSS capsules investigated with AFM force spectroscopy. *Macromol.*, *38*, 9766–9771.

Murata, M., Kaku, W., Anada, T., Sato, Y., Kano, T., Maeda, M., & Katayama, Y. (2003) Novel DNA/polymer conjugate for intelligent antisense reagent with improved nuclease resistance. *Bioorg. Med. Chem. Lett.*, 13, 3967–3970.

Niemeyer, C. M., & Ceyhan, B. (2001). DNA-directed functionalization of colloidal Gold with proteins. *Angew. Chem, Int. Ed.*, *40*, 3685–3688.

Nishiyama, N., Yokoyama, M., Aoyagi, T., Okano, T., Sakurai, Y., & Kataoka K. (1999). Preparation and characterization of self-assembled polymer–metal complex micelle from cis-dichlorodiamine platinum (II) and poly(ethylene glycol)–poly(a,b-aspartic acid) block copolymer in an aqueous medium. *Langmuir*, *15*, 377–383.

Nori, A., & Kopecek, J. (2005). Intracellular targeting of polymer-bound drugs for cancer chemotherapy. *Adv. Drug Delivery Rev.*, *57*, 609–639.

Norman, T., Jr., Grant, C. D., Magana, D., Zhang, J. Z., Liu, J., Cao, D., Bridges, F., & van Buuren, A. (2002). Near infrared optical absorption of gold nanoparticle aggregates. *J. Phys. Chem. B*, *106*, 7005–7012.

Ooya, T., Choi, H. S., Yamashita, A., Yui, N., Sugaya, Y., Kano, A., Maruyama, A., Akita, H., Ito, R., Kogure, K., & Harashima, H. (2005). Biocleavable polyrotaxane-plasmid DNA polyplex for enhanced gene delivery, *J. Am. Chem. Soc.,* 128, 3852–3853.

Oupicky, D., Bisht, H. S., Manickam, D. S., & Zhou, Q. (2005). Stimulus-controlled delivery of drugs and genes, *Expert Opin Drug Delivery*, *2*, 1–13.

Park, M. K., Xia, C. J., Advincula, R. C., Schotz, P., & Caruso, F. (2001). Cross-linked, luminescent spherical colloidal and hollow-shell particles. *Langmuir*, *17*, 7670–7674.

Pelton, R. (2000) Temperature-sensitive aqueous hydrogels. *Adv. Col. Int. Sci. 85*(1), 1–33.

Petrov, A. I., Volodkin, D. V., & Sukhorukov, G. B. (2005). Protein-calcium carbonate coprecipitation: A tool for protein encapsulation. *Biotechnol. Prog.,* 21, 918–925.

Peyratout, C. S., & Dähne, L. (2004). Tailor-made polyelectrolyte microcapsules: From multilayers to smart containers. *Angew. Chem. Int. Ed.*, *43*, 3762–3783.

Picart, C., Schneider, A., Etienne, O., Mutterer, J., Schaaf, P., Egles, C., Jessen, N., & Voegel, J.-C. (2005). Controlled degradability of polysaccharide multilayer films *in vitro* and *in vivo*. *Adv. Funct. Mat.*, *15*, 1771–1780.

Qiu, Y., & Park, K. (2001). Environment-sensitive hydrogels for drug delivery. *Advanced Drug Delivery Reviews,* 53, 321–339.

Radt, B., Smith, T. A., & Caruso, F. (2004). Optically addressable nanostructured capsules. *Adv. Mater.*, *16*, 2184–2189.

Roggan, A., Friebel, M., Dorschel, K., Hahn, A., & Muller, G. (1999). Optical properties of circulating human blood in the wavelength range 400–2500 NM. *J. Biomed. Opt.*, *4*, 36–46.

Saunders, B. R., Crowther, H. M., Morris, G. E., Mears, S. J., Cosgrove, T., & Vincent, B. (1999) Factors affecting the swelling of poly(N-isopropylacrylamide) microgel particles. *Coll. Surf. A* 149 (1–3), 57–64.

Schild, H. G. (1992). Poly(*N*-isopropylacrylamide): Experiment, theory and application. *Prog. Polym. Sci.*, *17*, 163–249.

Schneider, G., & Decher, G. (2004) From functional core/shell nanoparticles prepared via layer-by-layer deposition to empty nanospheres, *Nano Lett.,* 4, 1833

Shchukin, D. G., Gorin, D. A., & Möhwald, H. (2006). Ultrasonically induced opening of polyelectrolyte microcontainers. *Langmuir*, *22,* 7400–7404.

Shchukin, D. G., Köhler, K., & Möhwald, H. (2006). Microcontainers with electrochemically reversible permeability. *J. Am. Chem. Soc.*, *128*, 4560–4461.

Shenoy, D. B., Antipov, A. A., Sukhorukov, G. B., & Möhwald, H. (2003). Layer-by-layer engineering of biocompatible, decomposable core-shell structures. *Biomacromol.*, *4*, 265–272.

Shipway, A., Katz, E., & Wilner I. (2000). Nanoparticle arrays on surface for electronic, optical and sensor applications. *Chemphyschem*, *1*, 18–52.

Skirtach ,A. G., Antipov, A. A., Shchukin, D. G., & Sukhorukov, G. B.(2004). Remote activation of capsules containing Ag nanoparticles and IR dye by laser light. *Langmuir*, *20*, 6988–6992.

Skirtach, A. G., Dejugnat, C., Braun, D., Susha, A. S., Rogach, A. L., Parak, W. J., Möhwald, H., & Sukhorukov, G. B. (2005). The role of metal nanoparticles in remote release of encapsulated materials. *Nano. Lett.*, *5*, 1371–1377.

Skirtach, A. G. , Munoz Javier, A., Kreft, O., Karen Köhler, Piera Alberola, A., Möhwald, H., Parak, W. J., & Sukhorukov, G. B. (2006). Laser-induced release of encapsulated materials inside living cells. *Angew. Chem. Int. Ed.*, *45*, 4612–4617.

Skirtach, A. G., Déjugnat, C., Braun, D., Susha, A. S., Rogach, A. L., & Sukhorukov G. B. (2007a). Nanoparticles distribution control by polymers: Aggregates versus non-aggregates. *J. Phys. Chem. C*, *111*, 555–564.

Skirtach, A. G., De Geest, B. G., Mamedov, A., Antipov, A. A., Kotov, N. A., & Sukhorukov, G. B. (2007b). Ultrasound stimulated release and catalysis using polyelectrolyte multilayer capsules. *J. Mat. Chem., 17,* (1050–1054).

Stayton, P. S., Shimoboji, T., Long, C., Chilkoti, A., Chen, G. H., Harris, J. M., & Hoffman, A. S. (1995) Control of protein-ligand recognition using a stimuli-responsive polymer. *Nature,* 378, 472–474.

Steitz, R., Leiner, V., Tauer, K., Khrenov, V., & von Klitzing, R. (2002). Temperature-induced changes in polyelectrolyte films at the solid-liquid interface. *Appl. Phys. A: Mater. Sci. Process.*, *74*, S519–S521.

Stockton, W. B., & Rubner, M. F. (1997). Molecular-level processing of conjugated polymers .4. Layer-by-layer manipulation of polyaniline via hydrogen-bonding interactions. *Macromolecules*, *30*, 2717–2725.

Sui, Z. J., & Schlenoff, J. B. (2004). Phase separations in pH-responsive polyelectrolyte multilayers: Charge extrusion versus charge expulsion. *Langmuir*, 20, 6026–6031.

Sukhishvili, S. A. (2005). Responsive polymer films and capsules via layer-by-layer assembly. *Curr. Opin. Coll. Int. Sci*, *10*, 37–44.

Sukhishvili, S. A., & Granick, S. (2000). Layered, erasable, ultrathin polymer films. *J. Am. Chem. Soc.*, *122*, 9550–9551.

Sukhorukov, G. B., Donath, E., Davis, S., Lichtenfeld, H., Caruso, F., Popov, V. I., & Möhwald, H. (1998). Stepwise polyelectrolyte assembly on particle surfaces: a novel approach to colloid design. *Polym. Adv. Technol.*, *9*, 759–767.

Sukhorukov, G. B., Volodkin,D. V., Günther, A., Petrov, A. I., Shenoy, D. B., & Möhwald, H. (2004). Porous calcium carbonate microparticles as templates for encapsulation of bioactive compounds, *J. Mater. Chem., 14*, 2073–2081.

Suzuki, Y., Tomonaga, K., Kumazaki, M., & Nishio, I. (1996). Change in phase transition behavior of an NIPA gel induced by solvent composition: hydrophobic effect, *Polym. Gels Netw.*, *4*, 129–142.

Thies, C. A. (1999) A short history of microencapsulation technology. In R. Arshady (Ed.), *Microspheres, microcapsules and liposomes. Vol. I: Preparation and chemical application*, London: Citus Books.

Thurmond, K. B., Kowalewski, T., & Wooley, K. L. (1996). Water-soluble knedel-like structures: the preparation of shell-cross-linked small particles, *J. Am. Chem. Soc.*, *118*, 7239–7240.

Tonnesen, H. H., & Karlsen J. (2002). Alginate in drug delivery systems. *Drug Dev Ind Pharm.*, *28*, 621–630.

Torchilin, V. P. (2004). Targeted polymeric micelles for delivery of poorly soluble drugs. *Cell. Mol. Life Sci.*, *61*, 2549–2559.

Torchilin, V. P., Trubetskoy, V. S., Whiteman, K. R., Caliceti, P., Ferruti, P., & Veronese F. M. (1995). New synthetic amphiphilic polymers for steric protection of liposomes *in vivo*. *J. Pharm. Sci.*, *84*, 1049–1053.

Tuzar, Z., & Kratochvil, P. (1976). Block and graft copolymer micelles in solution. *Adv. Col. Int. Sci.,* 6, 201–232.

Unger, E. "Drug and gene delivery with ultrasound contrast agents", in The Leading Edge in Diagnostic Ultrasound, Atlantic City, NJ: May 13–16, 1997.

Verberg, R., Alexeev, A., & Balazs, A. C. (2006). Modeling the release of nanoparticles from mobile microcapsules. *J. Chem. Phys.*, *125*, 224712–224722.

Voigt, A., Lichtenfeld, H., Sukhorukov, G. B., Zastrow, H., Donath, E., Pumler, H. B., & Möhwald, H. (1999). Membrane filtration for microencapsulation and microcapsules fabrication by layer-by-layer polyelectrolyte adsorption. *Ind. Eng. Chem. Res.*, *38*, 4037–4043.

Volodkin, D. V., Larionova, N. I., & Sukhorukov, G. B. (2004). Protein encapsulation via porous $CaCO_3$ microparticles templating, *Biomacromol.* 5, 1962–1972.

Williams, D. F. (1999). *The Williams Dictionary of Biomaterials*. Liverpool: Liverpool University Press.

Wolff, J. A. (2002). The 'grand' problem of synthetic delivery, *Nat. Biotechnol., 20*, 768–769.

Wu, J. Z., Zhou, B., & Hu, Z. B. (2003). Phase behavior of thermally responsive microgel colloids. *Phys. Rev. Lett.*, *90*, 48304.

Yokoyama, M., Okano, T., & Kataoka, K. (1994). Improved synthesis of adriamycin-conjugated poly(ethylene oxide)-poly(aspartic acid) block copolymer and formation of unimodal micellar structure with controlled amount of physically entrapped adriamycin. *J. Controlled Release*, *32*, 269–277.

Yoo, M. K., Seok, W. K., & Sung, Y. K. (2004). Characterisation of stimuli-sensitive polymers for biomedical applications, *Macromol. Symp.*, *207*, 173–186.

Yu, H., & Grainger, D. W. (1993). Thermo-sensitive swelling behavior in cross-linked *N*-isopropylacrylamide networks: cationic, anionic, and ampholytic hydrogels, *J. Appl. Polym. Sci.*, *49*, 1553–1563.

Zhou, H. S., Honma, I., Komiyama, H., & Haus, J. W. (1994). Controlled synthesis and quantum-size effect in gold-coated nanoparticles. *Phys. Rev. B*, *50*, 12052–12056.

Part IV

A Look to the Future of Nanotechnology in Drug Delivery

19

Nanotechnology in Drug Delivery: Past, Present, and Future

Sungwon Kim, Il Keun Kwon, Ick Chan Kwon, and Kinam Park

Introduction

The word "nanotechnology" began as a technical term, but recently it became a popular term representing the current state-of-the-art technology. On the website of US National Science Foundation (NSF), nanotechnology is defined as research and technology development at the atomic, molecular, or macromolecular level, in the length scale of approximately 1–100 nm range, to provide a fundamental understanding of phenomena and materials at the nanoscale and to create and use structures, devices, and systems that have novel properties and functions because of their small and/or intermediate size (N.S.F., February 2000). The earliest definition concerned only the size of materials (1–100 nm) (Franks, 1987). The current term nanotechnology, however, covers almost all fields of science and engineering (Salamanca-Buentello, Persad, Court, Martin, Daar, & Singer, 2005), and the size of materials of interest can be much larger than 100 nm. The biomedical and pharmaceutical fields have been utilizing nanomaterials for various applications, such as tissue engineering, gene therapy, chemotherapy, peptide/protein delivery, molecular imaging, and high-throughput screening/assay, so the exact definition of nanotechnology is difficult to make solely based on size. As the concept and applications of nanotechnology are evolving, we are left with a question: "What does nanotechnology really mean and what can it do for the drug delivery area? " Finding answers to this question will be benefited from a brief review of the past and current drug delivery technologies.

The two fabrication methods in nanotechnology are "bottom-up" and "top-down." The former builds nanomaterials from the atomic and molecular levels, whereas the latter generates nanostructures out of macro-sized materials. Fabricated nano-sized devices or drug carriers, often called nanocarriers or nanovehicles, provide various advantages for effective drug delivery. Nanocarriers can carry poorly soluble, unstable, or systemically toxic drugs with extended blood half-lives and reduced side effects.

M.M. de Villiers et al. (eds.), *Nanotechnology in Drug Delivery*, DOI: 10.1007/978-0-387-77667-5_19,

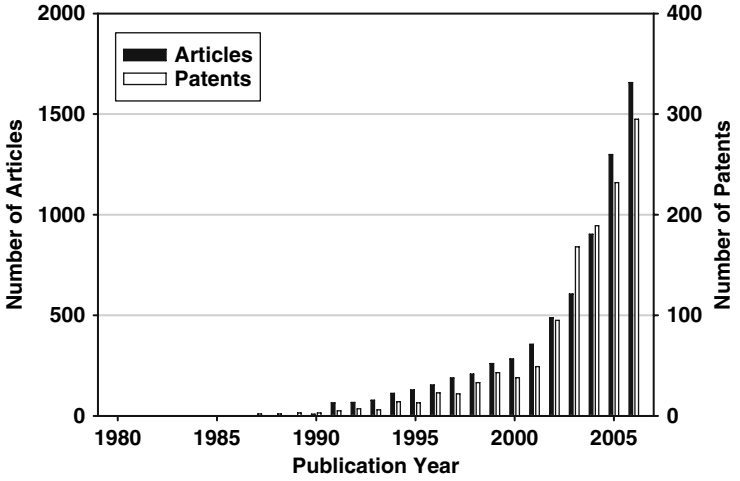

Figure 19.1 The number of research articles (■) and patents (□) on nanotechnology in drug delivery as a function of the year. A total of 6,091 articles during 1980–2006 were retrieved from ISI Web of Knowledge, while a total of 1,295 patents during 1980–2006 were retrieved from the Aureka searching engine.

In addition, intravenously injected nanovehicles travel along the blood stream without blocking vessels. Floating nanoparticles are accumulated at the inflamed site having leaky blood vessels by the enhanced permeability and retention (EPR) effect. The presence of targeting molecules at the surface of nanocarriers increases the targeting ability, resulting in higher accumulation at the target site (Kwon, Jeong, Kang, & Park, 2006; Orive, Hernandez, Rodriguez Gascon, Dominguez-Gil, & Pedraz, 2003).

As shown in Figure 19.1, the number of articles on nanotechnology in drug delivery was not noticeable in the 1980 s; however, it increased gradually in 1990 s and exponentially since 2000. A similar trend is also found in the number of patents filed worldwide. More than 35 countries throughout the world have developed various R&D programs since 2000 (Roco, 2003), and this must have contributed to the expansion of the worldwide phenomena in nanotechnology. For example, US National Nanotechnology Initiative (NNI) was founded in 2000 with $464 million budget for the fiscal year 2001. The current NNI budget is $1.3 billion for the fiscal year 2007 (T.N.N.I., July 2006). We are in the middle of the nanotechnology revolution; we are already witnessing the new drug delivery technologies developed from nanotechnology. To appreciate such advances in the drug delivery field, a few advanced drug delivery technologies (e.g., smart and multifunctional drug delivery systems, polymer–drug conjugates, and organic/inorganic composites) are described.

Advances in Drug Delivery Systems Based on Nanotechnology

Smart Drug Delivery Systems

Nanotechnology has had a great impact on the development of polymeric drug delivery systems. One of the most outstanding achievements in the

drug delivery field is the development of smart drug delivery systems (SDDSs), also called stimuli-sensitive delivery systems. The concept of SDDS is based on rapid transitions of a physicochemical property of polymer systems upon an environmental stimulus, which includes physical (temperature, mechanical stress, ultrasound, electricity, light), chemical (pH, ionic strength), or biological (enzymes, biomolecules) signals. Such stimuli can be either "internal" signals, resulting from changes in the physiological condition of a living subject, or "external" signals, artificially induced to provoke desired events. As illustrated in Figure 19.2, SDDS provides a programmable and predictable drug release profile in response to various stimulation sources. Depending on the applications, one can design on–off system, pulsatile/sustained drug release, and closed-loop drug delivery systems, for enhanced therapeutic efficiency with low systemic toxicity and side effects. SDDS provides various advantages over conventional drug delivery systems. The conventional controlled release systems are based on the predetermined drug release rate irrespective of the environmental condition at the time of application. On the other hand, SDDS is based on the release-on-demand strategy, allowing a drug carrier to liberate a therapeutic drug only when it is required in response to a specific stimulation. The best example of SDDS has been self-regulated insulin delivery systems that can respond to changes in the environmental glucose level (Chu, Liang, Chen, Ju, & Wang, 2004; Kim, & Park, 2001).

One of the most widely used SDDSs has been polymeric micelles. Many polymeric micelles consisting of hydrophobic and hydrophilic polymer blocks have been developed. They can dissolve water-insoluble drugs, such as doxorubicin or paclitaxel, at high concentrations. When polymeric micelles are administered to the body, usually into the blood stream, drug release from polymeric micelles depends on simple diffusion, degradation of the micelle blocks, or disruption of the micelles by body components. Although release kinetics of the loaded drug can be modulated by varying the degradation rate of hydrophobic polymer blocks, the degradation rate is usually very slow, and thus, the loaded drug is released by diffusion from polymeric micelles. This slow release by passive diffusion may not be

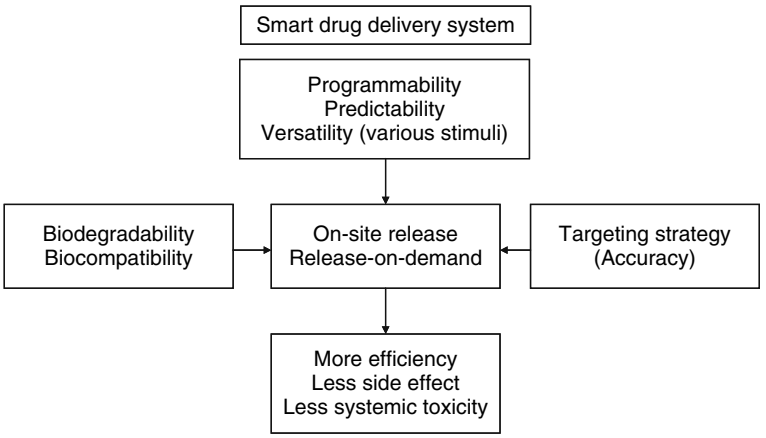

Figure 19.2 Advantages of the smart drug delivery systems (SDDSs).

desirable, as the polymeric micelles reaching the target site need to release their contents fast. To alleviate this problem, smart polymeric micelles have been designed to liberate the loaded therapeutic agent at the targeted site fast. Poly(ethylene glycol)-*b*-polyhistidine (PEG-*b*-PHis), for instance, forms micelles only over the pK_b of the PHis block (pH 6.5–7.0) (Lee, Shin, Na, & Bae, 2003). The pK_b can be adjusted by varying the molecular weight of PHis. Since solid tumors have a slightly acidic environment, a small reduction in pH to less than 7 at the tumor site triggers dissociation of the polymeric micelle to dump its contents. PEG-*b*-PHis micelles containing doxorubicin effectively killed multi-drug resistant (MDR) MCF-7 cells at pH 6.8 (Lee, Na, & Bae, 2005a). The SDDS can achieve a highly localized drug accumulation at the target site (Hruby, Konak, & Ulbrich, 2005), even though it is administered by systemic injection. The SDDS with enhanced targeting capability is highly promising in increasing the efficiency and efficacy of therapy with minimal side effects.

Polymer–Drug Conjugates

The polymer–drug conjugate itself can be considered as a nanovehicle. Various conjugates have been developed and clinically tested since the first drug conjugate for cancer therapy was proposed in the middle of 1970 s (Ringsdorf, 1975). Recent advances in polymer–drug conjugates are well described in excellent reviews (Duncan, 2006; Duncan, Vicent, Greco, & Nicholson, 2005). One of the major advantages of polymer–drug conjugates is prolonged circulation in the blood stream by retarding degradation/metabolism/excretion rates of the conjugated drugs. Many peptide and protein drugs cannot be delivered by oral administration because of their large molecular weights. Even when administered directly into the blood stream, they do not remain in the blood for a long time due to fast degradation and metabolism, limiting the clinical applications. The circulation times of these drugs have increased substantially by conjugation with polymers, such as PEG. For example, PEGylated form of L-asparaginase increased the plasma half-life up to 357 h, which was about 15 times longer than the natural form of L-asparaginase (half-life 20 h) (Ho, Brown, Yen, Holmes, Keating, Abuchowski, Newman, & Krakoff, 1986). The PEG-L-asparaginase received an FDA approval for clinical use. Another example is glucagon-like peptide-1 (GLP-1), which regulates food uptake and insulin release. GLP-1 is a very useful therapeutic agent for diabetic patients, but it is liable to degradation by a plasma enzyme, dipeptidyl dipeptidase IV. By introducing one PEG chain, its half-life was increased up to 40 folds over a natural form (Lee, Youn, Lee, Byun, & Lee, 2006). The polymer conjugation, especially PEGylation (Davis, 2002), appears to be a useful technology for developing new polymer–drug conjugates.

Another attractive feature of polymer–drug conjugates is the biodegradable linkage between the polymer backbone and the conjugated drug molecules. One well-known example is based on *N*-(2-hydroxypropyl)-methacrylamide (HPMA) (Chytil, Etrych, Konak, Sirova, Mrkvan, Rihova, & Ulbrich, 2006; Gao, Lu, Petri, Kopeckova, & Kopecek, 2006; Greco, Vicent, Gee, Jones, Gee, Nicholson, & Duncan, 2007). Although

the backbone polymer is not degradable, therapeutic drugs are suspended to the backbone via a degradable linkage. Once the conjugate enters into cells, the linkage is readily hydrolyzed by lysosomal enzymes (Duncan, Lloyd, & Kopecek, 1980). Usually, drugs with low molecular weight and high hydrophobicity have been used for conjugation. The degradation/clearance rate and toxicity of a conjugated drug, i.e., prodrug, are greatly reduced, and the therapeutic effect is achieved only by hydrolysis inside the target cells to release the original drug.

The polymers used in conjugation can have stimuli-responsiveness, providing a unique property to the conjugated drug. The activity of a conjugated drug can be turned on or off by external signals. For example, endoglucanase 12A (EG 12A), which had one site mutation (N55C) near the active site, was conjugated with either photo-sensitive (Shimoboji, Larenas, Fowler, Kulkarni, Hoffman, & Stayton, 2002) or thermo-sensitive polymers (Shimoboji, Larenas, Fowler, Hoffman, & Stayton, 2003). As a result, the catalytic activity of EG 12A could be turned on by application of UV light or high temperature. The active site of the enzyme was exposed by collapsing the conjugated long polymer chain by external stimuli. Once visible light was turned on or the temperature was lowered, the enzyme activity vanished due to the blocking of the active site by the extended polymer chain.

Multifunctional Drug Carriers

A multifunctional drug delivery system (MDDS) has two or more functions. SDDS and polymer–drug conjugates can be considered MDDS, because, in addition to delivering drugs, they can carry out the second function, such as stimuli-responsiveness or hydrolysis inside cells. Delivering drugs, however, should be considered as the inherent property for drug delivery systems, and thus, the MDDS is limited to the drug carrier that has multiple properties of prolonged blood circulation, passive or active localization at specific disease site, stimuli-sensitivity, ability to deliver drug into intracellular target organelles, and/or imaging ability (Torchilin, 2006). The goal of MDDS is to maximize the therapeutic efficiency of a drug loaded in nanocarriers as well as to minimize undesirable side effects of the drug. A good example of MDDS is biotin-tagged pH-sensitive polymeric micelles based on a mixture of PLA-*b*-PEG-*b*-PHis-biotin (PLA = poly(L-lactic acid)) and PEG-*b*-PHis block copolymers (Lee, Na, & Bae, 2005b). In that system, even the targeting moiety, biotin, was masked until the carrier was exposed to an expected environment of pH 7.0. Once the nanocarrier was internalized to cancer cells by ligand–receptor interactions, lowered pH (< 6.5) destabilized the carrier resulting in a burst release of the loaded drug. A more complicated example is a pH-degradable PEG-*b*-phosphatidylethanolamine (PE) liposome with attached anti-myosin monoclonal antibody as well as TAT or biotin on its surface (Lukyanov, Elbayoumi, Chakilam, & Torchilin, 2004; Sawant, Hurley, Salmaso, Kale, Tolcheva, Levchenko, & Torchilin, 2006). The liposome integrated pH sensitivity and double-targeting moieties in a single particle.

Organic/Inorganic Composites

Recently, a series of review papers on the lab-on-a-chip (LOC) approach was published (Craighead, 2006; DeMello, 2006; El-Ali, Sorger, & Jensen, 2006; Janasek, Franzke, & Manz, 2006; Psaltis, Quake, & Yang, 2006; Whitesides, 2006; Yager, Edwards, Fu, Helton, Nelson, Tam, & Weigl, 2006). The LOC is a micro/nano-electro-mechanical system (MEMS/NEMS) which embodies micron- or nano-sized machines composed of sophisticated circuits. Such microfluidic systems can miniaturize huge instruments, e.g., GPC, HPLC, and electrophoresis systems, into a single chip. Small devices provide many advantages including portability/disposability, low cost, high reproducibility, high-throughput screening, and multiple functionalities in a single device. In addition, combined with other technologies such as optics, single molecular imaging, or cell/protein-based assay systems, the BioMEMS or BioNEMS of biomedical LOC devices become an important part of drug discovery and diagnosis.

Drug delivery systems based on MEMS/NEMS are just beginning to appear (Li, Ho Duc, Tyler, Williams, Tupper, Langer, Brem, & Cima, 2005; Li, Shawgo, Tyler, Henderson, Vogel, Rosenberg, Storm, Langer, Brem, & Cima, 2004; Maloney, Uhland, Polito, Sheppard, Pelta, & Santini, 2005; Tao, & Desai, 2005). To release a drug from a nanodevice is more complicated than to perform assay or screening drug candidates. Successful drug delivery requires at least four components: drug reservoir, pump, valve, and sensor (Richards Grayson, Scheidt Shawgo, Li, & Cima, 2004). Drugs can be placed either in a fabricated reservoir of a MEMS/NEMS device or in conventional micro-/nanoparticles. Depending on the characteristics of a drug or a disease, different kinds of pumps (e.g., pulsatile, osmotic, or actuating) can be used. Since the valve and sensor directly contact biological constituents, good biocompatibility is essential. By adopting smart polymers as valves and sensors, versatility in drug release control can be obtained (Baldi, Gu, Loftness, Siegel, & Ziaie, 2003). One of the problems with MEMS/NEMS-based drug delivery systems is that the operating protocol is not user-friendly. Due to the complicated and highly integrated structure, operation is limited to highly trained people, although such devices have been originally designed for general users without professional skills. BioMEMS/BioNEMS systems still remain in the research domain, and more improvement is necessary for developing clinically useful systems.

Other important organic/inorganic composites are metal nanoparticles, such as quantum dot, iron oxide, or gold nanoparticles, coated with hydrophilic polymers. Their major application has been in diagnostic applications. Semi-conductive quantum dots emit sharp visible/near infrared lights with a wide range of wavelength by tuning the particle size (5–20 nm). Due to their high photostability, many quantum dots have been studied for optical diagnostic imaging of diseases as well as for labeling biomolecules (Ho, Chen, Leong, & Wang, 2006; Michalet, Pinaud, Bentolila, Tsay, Doose, Li, Sundaresan, Wu, Gambhir, & Weiss, 2005). The critical problem with quantum dot applications is their inherent toxicity, because quantum dots are composed of heavy metals. Gold nanoparticles that emit red light around 520 nm have also been used for drug delivery and bioimaging (Goldstein, Nassar, Lambert, Kadouche, & Benita, 2005; Lu, Zhang,

Tan, Hu, Jiang, & Fu, 2005; Maloney et al., 2005; Niidome, Yamagata, Okamoto, Akiyama, Takahashi, Kawano, Katayama, & Niidome, 2006). Recently, gold nanoshell was developed, which provided tunable emission light for bioimaging (Hirsch, Gobin, Lowery, Tam, Drezek, Halas, & West, 2006). In addition, gold nanoparticles can be detected by X-ray and emit thermal energy by excitation. For this reason, nano-sized gold particles are useful for medical imaging and thermal therapy. Super paramagnetic iron oxide (SPIO) nanoparticles have been developed for magnetic resonance imaging (MRI) of the whole body (Corot, Robert, Idee, & Port, 2006). These nanoparticles are primarily engulfed by monocyte or macrophage after intravenous administration. However, uptake of SPIO by macrophage does not induce activation of nearby cells. This is why SPIO nanoparticles can be used for diagnosis of inflammatory or degenerative diseases. By introducing homing markers, spatial resolution of MRI can be improved significantly.

Problems with Current Technology

Drug Loading Efficiency in Nanovehicles

The loading efficiency of a drug is one of the most important parameters in developing many drug delivery systems, especially the systems based on nanotechnology. The volume of a drug reservoir in a nano-sized drug carrier is extremely limited in comparison to macro drug delivery systems. For example, conventional micellar nanoparticles (e.g., PEG-*b*-PLG micelles) composed of diblock copolymers can hold a maximum of only 20–30% (weight of drug/total weight of carrier) of a hydrophobic drug. The drug loading into polymeric micelles is simply based on hydrophobic interactions between a hydrophobic drug and a hydrophobic polymer block forming the micelle core, and thus the drug loading is limited. The loss of a drug during the loading process is also not negligible. Although the limited drug reservoir is an inherent problem of polymeric nanoparticles, only a few studies have been done to improve the drug loading efficiency. One approach utilized the concept of hydrotropic polymers. Hydrotropic polymers are prepared from monomers that have hydrotropic properties for a selected therapeutic agent. If a drug is poorly soluble in water, then hydrotropic polymers drastically increase aqueous solubility of the drug (Cho, Lee, Lee, Huh, & Park, 2004). For example, the water solubility of paclitaxel (PTX), a highly potent anti-cancer drug, is less than 0.3 μg/mL (Lee, Lee, Acharya, Chang, & Park, 2003). While the maximum PTX loading content in a conventional micelle composed of PEG-*b*-PLA was reported to be 27.6%, a hydrotropic polymer, PEG-*b*-poly(2-(4-(vinylbenzyloxy)-*N,N*-diethyl-nicotinamide)) (PEG-*b*-PDENA), increased the drug content up to 37.4% (Huh, Lee, Cho, Lee, Jeong, & Park, 2005). Moreover, the stability of PTX-loaded hydrotropic micelles in aqueous solution was extended to months instead of days with conventional micelles, such as PEG-*b*-PLA micelles. In a different approach, polymeric micelles were crosslinked to retain the loaded drug with high stability (Miyata, Kakizawa, Nishiyama,

Harada, Yamasaki, Koyama, & Kataoka, 2004; Shuai, Merdan, Schaper, Xi, & Kissel, 2004).

Complexity of Nanocarriers

Efforts to develop more efficient and more intelligent drug carriers have caused more complicated drug carriers. For example, as described above, MDDS is promising for improving the therapeutic efficiency. Integrating multiple components in a single nano-sized carrier, however, requires multiple chemical synthetic steps and multiple formulation processes. Such multiple procedures inevitably lower the yield and increase the cost of production. Furthermore, complications in manufacturing procedures make the scale-up of production difficult. Complex systems also have more variables in their physicochemical properties, which make it more difficult to predict the fate and action mechanism of the systems after they are administrated into the human body. A combination of various materials as well as complicated structures of nanodevices also results in sterilization problems, which must involve a series of different protocols.

Interface Between Synthetic Materials and Biological Tissues/Components

It has been well recognized that biocompatibility is one of the most important issues in developing nanodevices. While researchers in the drug delivery field are developing new materials for more effective drug delivery, these new materials have not been used in clinical applications, mainly due to the lack of proper testing on biocompatibility. Without clear demonstration of the biocompatibility, there is little chance that the new materials, no matter how good they may be, are used in developing products for clinical applications. As clinical application of the new drug delivery systems is the ultimate goal, it is important to carefully examine interactions between engineered materials and biological components including cells, tissues, or biological molecules.

One of the definitions of "biocompatibility" is "the ability of a material to perform with an appropriate host response in a specific application (Ratner, Hoffman, Schoen, & Lemons, 2004)." The appropriate host response depends on the device and the mode of application. There are currently numerous materials and systems which are programmed or designed for appropriate interactions with biological components. To date, fast advances in biomaterials and drug delivery systems have not been accompanied with proper testing of their biocompatibility. In 1986, the International Standards Organization (ISO) began to develop harmonized standards for biocompatibility tests (ISO 10993). And up to now, twenty parts of ISO 10993 have been established and are under the harmonization process (I.S.O., 2007). A FDA blue book memorandum, #G95-1, "Required biocompatibility training and toxicology profiles for evaluation of medical devices," lists a guideline for biocompatibility test in the proper use of ISO 10993, which includes cytotoxicity, sensitization, irritation or intracutaneous reactivity, acute system toxicity, sub-chronic toxicity, genotoxicity, implantation, and hemocompatibility (Alpert, 1995). Despite these efforts, however, fast developing technologies and

unforeseen applications are making the FDA guidelines difficult to follow. ISO 10993 has been so ramified that it is not easy to choose the right protocol among the vast number of protocols. It is urgently required to develop reasonable guidelines which researchers can rely on before designing new drug delivery systems and performing biocompatibility tests. This will allow researchers to consider the biocompatibility issue from the beginning of the design of drug delivery systems.

Safety and Ethical Issues

The term "nanotoxicology" first showed up in 2004 (Service, 2004), which is defined as "science of engineered nanodevices and nanostructures that deals with their effects in living organisms" (Oberdorster, Oberdorster, & Oberdorster, 2005). The details about possible risks of the "ultrafine particle (UFP)" have been described and considered from various angles. Currently, a major route for nano-sized material to enter into the human body from air pollution is known to be the respiratory tract. However, the gastrointestinal tract and skin are now considered to be other major routes. For example, a recent report showed that even a commercially available nanomaterial, quantum dot, could be highly permeable to pig skin (Ryman-Rasmussen, Riviere, & Monteiro-Riviere, 2006). Experimentally proven pathophysiology and toxicity of nanomaterials include reactive oxygen species (ROS) generation, oxidative stress, mitochondrial perturbation, inflammation, uptake by reticuloendothelial system (RES), protein denaturation or degradation, nuclear uptake, and blood clotting (Nel, Xia, Madler, & Li, 2006). Although many individual researches have warned that nanomaterials can cause damage to the human body, the exact mechanisms of toxicity are unknown and conclusive data are yet to be established. Moreover, reports on nanotoxicity mostly focus on inorganic nanomaterials consisting of heavy metals. Investigation about the toxic effect of polymeric nanomaterials on living subjects is also urgently required.

In 2005, the International Risk Governance Council (IRGC) made a series of surveys about the current situation of the nanotechnology governance (I.R.G.C., 2006). The report consists of 4 parts, which summarized representative opinions of governments of 11 countries, 11 industrial organizations, 5 research organizations, and 9 non-government organizations (NGOs). Most of the participants in the report recognized the risk of nanotechnology, although the major focus of governments and industrial organizations was on the research and development (R&D) activity as well as potential benefits resulting from nanotechnology. However, most of the respondents could not identify any specified national or international regulations for nanotechnology. It is surprising that, except in USA (21st Century Nanotechnology Research and Development Act, Public Law 108–153, 2003), there is no government with nanotechnology-specific legislation or regulation, although the risk of the environment, health, and safety issue (EHS) is well accepted. Moreover, it was reported that governments and industrial organizations did not recognize any ethical, legal, and social issues (ELSI) of nanotechnology. It is very important to establish appropriate national regulatory programs and self-regulatory/training

programs in each organization. In addition, ethical issues including equality of benefit, individual privacy and security, environmental protection as well as complication between human and machine should be considered in detail, if nanotechnology is to be developed for the welfare of human beings (Jotterand, 2006; Mnyusiwalla, S., & Singer, 2003; Sandler, & Kay, 2006).

Nanotechnology for Future Drug Delivery Systems

Predicting the future of nanotechnology in drug delivery systems is not simple because the technology is moving forward fast and dynamically changing, and we are in the middle of such changes. One could, however, find possible clues from the efforts to overcome the problems facing the research community today. One of the first things that can be predicted is the minimalistic design of drug delivery systems. Multifunctional drug delivery systems have been reported, but only few of them were used successfully in small animal models (Lanza, Yu, Winter, Abendschein, Karukstis, Scott, Chinen, Fuhrhop, Scherrer, & Wickline, 2002; Reddy, Bhojani, McConville, Moody, Moffat, Hall, Kim, Koo, Woolliscroft, Sugai, Johnson, Philbert, Kopelman, Rehemtulla, & Ross, 2006). As our understanding on nano drug delivery vehicles improves, the system will become simpler and simpler, as that is probably the only way to bring the nanovehicles into clinical applications.

Nano/micro- or organic/inorganic composites also have great potential. Combination of different properties using different materials has been successfully used, and this effort will only be expanded in the future. For a representative example, metallic stents have poor biocompatibility resulting in multiple hazardous symptoms after implantation, such as inflammation and restenosis. Coating the stents with biocompatible polymers with loaded drugs improved the biocompatibility significantly (Acharya, & Park, 2006; Levin, Jonas, Hwang, & Edelman, 2005). Recently, the layer-by-layer (LBL) coating technique was introduced to generate multifunctional polymer coating layers, and this LBL technique is expected to find many applications in developing various composites (De Geest, Dejugnat, Verhoeven, Sukhorukov, Jonas, Plain, Demeester, & De Smedt, 2006; Huang, & Yang, 2006; Thierry, Winnik, Merhi, Silver, & Tabrizian, 2003; Ye, Wang, Liu, & Tong, 2005). In developing BioNEMS or BioMEMS, a combination with smart polymers can also result in interesting properties, such as microvalves actuated by environment-sensitive hydrogels (Baldi et al., 2003).

While nanotechnology is expected to produce new nano/micro devices, it is also expected to revolutionize the way the current drug delivery systems are produced. For example, nano/micro particles are currently made by solvent evaporation/extraction (Freitas, Merkle, & Gander, 2005) or solvent exchange (Yeo, & Park, 2004) methods. These approaches have been successfully used in producing a variety of nano/micro particles containing pharmaceutically active ingredients, but the processing methods require significant improvements. Current methods based on double emulsion and ultrasonic atomization need significant improvement in

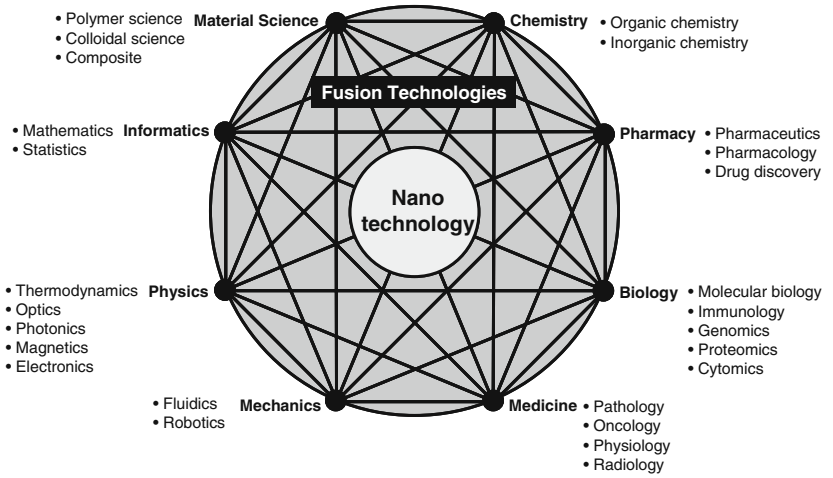

Figure 19.3 Interdisciplinary fusion technologies based on nanotechnology.

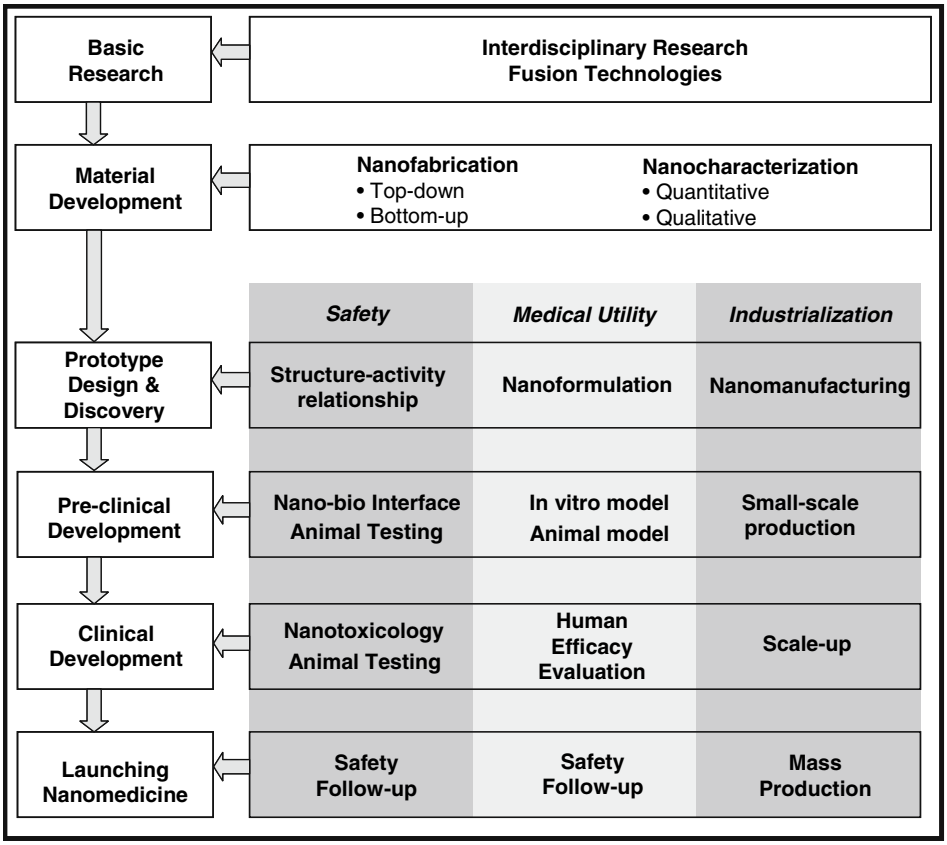

Figure 19.4 Critical path to new medical products (modified from FDA, Mar 2005).

the loading efficiency and production scale-up. Nanotechnology-based approaches, which is often called "nano/micro fabrication" or "nano/micro manufacturing," can provide powerful new ways for mass production of nano/micro particles with high drug loading efficiencies. As nanotechnology becomes mature, nano/micro devices are expected to become as practical as macro devices are today. We can be very optimistic to expect that the current macro devices will be shrunk into the nano/micro scale to manufacture nanovehicles reliably for mass production in the very near future.

The future of nanotechnology is expected to bring multitude of fusion technologies. As illustrated in Figure 19.3, different research fields and/or technologies are intimately connected to each other. Different technologies can be fused together to develop better, more useful technologies, and nanotechnology will play a central role in all fusion technologies. Drug delivery, although it sounds simple, requires complicated adaptation of various fusion technologies to be clinically useful. For example, drug delivery systems with targeting ability require material science for making the right polymers, biology for finding the right ligands able to interact with targets, physics to monitor the location of delivery systems, and chemistry for releasing the active at the right time and place. Utilization of fusion technologies and sequence of development of drug delivery systems are described in Figure 19.4, which is modified from a FDA report (FDA, Mar 2005). The critical path consists of basic research, material development, prototype design and discovery, pre-clinical development, clinical development, and final launching. Producing clinically useful nanomedicine requires consideration of the three factors of assessing safety, demonstrating medical utility, and industrialization for mass production. During development, efforts to improve the existing drug delivery systems, feedback control between each step, ethical/environmental regulation and standardization in protocol will have to be considered in parallel. The future of nanotechnology in drug delivery is very bright, as combined efforts of scientists in different disciplines are bound to make nanotechnology practical.

References

Acharya, G., & Park, K. (2006). Mechanisms of controlled drug release from drug-eluting stents. *Adv. Drug Deliv. Rev., 58*, 387–401.

Alpert, S. (1995). Required biocompatibility training and toxicology profiles for evaluation of medical devices. CDRH, U.S. Food and Drug Administration.

Baldi, A., Gu, Y., Loftness, P., Siegel, R. A., & Ziaie, B. (2003). A hydrogel-actuated environmentally-sensitive microvalve for active flow control. *J. Microelectromechanical Syst., 12*, 613–621.

Cho, Y. W., Lee, J., Lee, S. C., Huh, K. M., & Park, K. (2004). Hydrotropic agents for study of in vitro paclitaxel release from polymeric micelles. *J. Control. Release, 97*, 249–57.

Chu, L. Y., Liang, Y. J., Chen, W. M., Ju, X. J., & Wang, H. D. (2004). Preparation of glucose-sensitive microcapsules with a porous membrane and functional gates. *Colloids Surf. B: Biointerfaces, 37*, 9–14.

Chytil, P., Etrych, T., Konak, C., Sirova, M., Mrkvan, T., Rihova, B., & Ulbrich, K. (2006). Properties of HPMA copolymer-doxorubicin conjugates with pH-controlled activation: effect of polymer chain modification. *J. Control. Release, 115*, 26–36.

Corot, C., Robert, P., Idee, J. M., & Port, M. (2006). Recent advances in iron oxide nanocrystal technology for medical imaging. *Adv. Drug Deliv. Rev., 58*, 1471–504.

Craighead, H. (2006). Future lab-on-a-chip technologies for interrogating individual molecules. *Nature, 442*, 387–93.

Davis, F. F. (2002). The origin of pegnology. *Adv. Drug Deliv. Rev., 54*, 457–8.

De Geest, B. G., Dejugnat, C., Verhoeven, E., Sukhorukov, G. B., Jonas, A. M., Plain, J., Demeester, J., & De Smedt, S. C. (2006). Layer-by-layer coating of degradable microgels for pulsed drug delivery. *J. Control. Release, 116*, 159–69.

Demello, A. J. (2006). Control and detection of chemical reactions in microfluidic systems. *Nature, 442*, 394–402.

Duncan, R. (2006). Polymer conjugates as anticancer nanomedicines. *Nat. Rev. Cancer, 6*, 688–701.

Duncan, R., Lloyd, J. B., & Kopecek, J. (1980). Degradation of side chains of N-(2-hydroxypropyl) methacrylamide copolymers by lysosomal enzymes. *Biochem. Biophys. Res. Commun., 94*, 284–90.

Duncan, R., Vicent, M. J., Greco, F., & Nicholson, R. I. (2005). Polymer-drug conjugates: towards a novel approach for the treatment of endocrine-related cancer. *Endocr. Relat. Cancer, 12 Suppl 1*, S189–99.

El-Ali, J., Sorger, P. K., & Jensen, K. F. (2006). Cells on chips. *Nature, 442*, 403–11.

FDA. (Mar 2005). "Challenge and Opportunity on the Critical Path to New Medical Products."

Franks, A. (1987). Nanotechnology. *J. Phys. E: Sci. Instrum., 20*, 1442–1451.

Freitas, S., Merkle, H. P., & Gander, B. (2005). Microencapsulation by solvent extraction/evaporation: reviewing the state of the art of microsphere preparation process technology. *J. Control. Release, 102*, 313–32.

Gao, S. Q., Lu, Z. R., Petri, B., Kopeckova, P., & Kopecek, J. (2006). Colon-specific 9-aminocamptothecin-HPMA copolymer conjugates containing a 1,6-elimination spacer. *J. Control. Release, 110*, 323–31.

Goldstein, D., Nassar, T., Lambert, G., Kadouche, J., & Benita, S. (2005). The design and evaluation of a novel targeted drug delivery system using cationic emulsion-antibody conjugates. *J. Control. Release, 108*, 418–32.

Greco, F., Vicent, M. J., Gee, S., Jones, A. T., Gee, J., Nicholson, R. I., & Duncan, R. (2007). Investigating the mechanism of enhanced cytotoxicity of HPMA copolymer-Dox-AGM in breast cancer cells. *J. Control. Release, 117*, 28–39.

Hirsch, L. R., Gobin, A. M., Lowery, A. R., Tam, F., Drezek, R. A., Halas, N. J., & West, J. L. (2006). Metal nanoshells. *Ann. Biomed. Eng., 34*, 15–22.

Ho, D. H., Brown, N. S., Yen, A., Holmes, R., Keating, M., Abuchowski, A., Newman, R. A., & Krakoff, I. H. (1986). Clinical pharmacology of polyethylene glycol-L-asparaginase. *Drug Metab. Dispos., 14*, 349–52.

Ho, Y. P., Chen, H. H., Leong, K. W., & Wang, T. H. (2006). Evaluating the intracellular stability and unpacking of DNA nanocomplexes by quantum dots-FRET. *J. Control. Release, 116*, 83–9.

Hruby, M., Konak, C., & Ulbrich, K. (2005). Polymeric micellar pH-sensitive drug delivery system for doxorubicin. *J. Control. Release, 103*, 137–48.

Huang, L. Y., & Yang, M. C. (2006). Hemocompatibility of layer-by-layer hyaluronic acid/heparin nanostructure coating on stainless steel for cardiovascular stents and its use for drug delivery. *J. Nanosci. Nanotechnol., 6*, 3163–70.

Huh, K. M., Lee, S. C., Cho, Y. W., Lee, J., Jeong, J. H., & Park, K. (2005). Hydrotropic polymer micelle system for delivery of paclitaxel. *J. Control. Release, 101*, 59–68.

International Risk Governance Council, Switzerland. (2006, April). "Survey on nanotechnology governance." *Survey on nanotechnology governance*.

International Organization for Standardization, Switzerland. (2007). "Biological evaluation of medical devices." *ISO 10993 Standard Series*.

Janasek, D., Franzke, J., & Manz, A. (2006). Scaling and the design of miniaturized chemical-analysis systems. *Nature, 442*, 374–80.

Jotterand, F. (2006). The politicization of science and technology: its implications for nanotechnology. *J. Law Med. Ethics, 34*, 658–66.

Kim, J. J., & Park, K. (2001). Modulated insulin delivery from glucose-sensitive hydrogel dosage forms. *J. Control. Release, 77*, 39–47.

Kwon, I. K., Jeong, S. H., Kang, E., & Park, K. (2006). *Chapter 13: Nanoparticulate drug delivery systems for cancer therapy*. New York, American Scientific Publishers.

Lanza, G. M., Yu, X., Winter, P. M., Abendschein, D. R., Karukstis, K. K., Scott, M. J., Chinen, L. K., Fuhrhop, R. W., Scherrer, D. E., & Wickline, S. A. (2002). Targeted antiproliferative drug delivery to vascular smooth muscle cells with a magnetic resonance imaging nanoparticle contrast agent: implications for rational therapy of restenosis. *Circulation, 106*, 2842–7.

Lee, E. S., Na, K., & Bae, Y. H. (2005a). Doxorubicin loaded pH-sensitive polymeric micelles for reversal of resistant MCF-7 tumor. *J. Control. Release, 103*, 405–18.

Lee, E. S., Na, K., & Bae, Y. H. (2005b). Super pH-sensitive multifunctional polymeric micelle. *Nano. Lett., 5*, 325–9.

Lee, E. S., Shin, H. J., Na, K., & Bae, Y. H. (2003). Poly(L-histidine)-PEG block copolymer micelles and pH-induced destabilization. *J. Control. Release, 90*, 363–74.

Lee, J., Lee, S. C., Acharya, G., Chang, C. J., & Park, K. (2003). Hydrotropic solubilization of paclitaxel: analysis of chemical structures for hydrotropic property. *Pharm. Res., 20*, 1022–30.

Lee, S., Youn, Y. S., Lee, S. H., Byun, Y., & Lee, K. C. (2006). PEGylated glucagon-like peptide-1 displays preserved effects on insulin release in isolated pancreatic islets and improved biological activity in db/db mice. *Diabetologia, 49*, 1608–11.

Levin, A. D., Jonas, M., Hwang, C. W., & Edelman, E. R. (2005). Local and systemic drug competition in drug-eluting stent tissue deposition properties. *J. Control. Release, 109*, 236–43.

Li, Y., Ho Duc, H. L., Tyler, B., Williams, T., Tupper, M., Langer, R., Brem, H., & Cima, M. J. (2005). In vivo delivery of BCNU from a MEMS device to a tumor model. *J. Control. Release, 106*, 138–45.

Li, Y., Shawgo, R. S., Tyler, B., Henderson, P. T., Vogel, J. S., Rosenberg, A., Storm, P. B., Langer, R., Brem, H., & Cima, M. J. (2004). In vivo release from a drug delivery MEMS device. *J. Control. Release, 100*, 211–9.

Lu, W., Zhang, Y., Tan, Y. Z., Hu, K. L., Jiang, X. G., & Fu, S. K. (2005). Cationic albumin-conjugated pegylated nanoparticles as novel drug carrier for brain delivery. *J. Control. Release, 107*, 428–48.

Lukyanov, A. N., Elbayoumi, T. A., Chakilam, A. R., & Torchilin, V. P. (2004). Tumor-targeted liposomes: doxorubicin-loaded long-circulating liposomes modified with anti-cancer antibody. *J. Control. Release, 100*, 135–44.

Maloney, J. M., Uhland, S. A., Polito, B. F., Sheppard, N. F., Jr., Pelta, C. M., & Santini, J. T., Jr. (2005). Electrothermally activated microchips for implantable drug delivery and biosensing. *J. Control. Release, 109*, 244–55.

Michalet, X., Pinaud, F. F., Bentolila, L. A., Tsay, J. M., Doose, S., Li, J. J., Sundaresan, G., Wu, A. M., Gambhir, S. S., & Weiss, S. (2005). Quantum dots for live cells, in vivo imaging, and diagnostics. *Science, 307*, 538–44.

Miyata, K., Kakizawa, Y., Nishiyama, N., Harada, A., Yamasaki, Y., Koyama, H., & Kataoka, K. (2004). Block catiomer polyplexes with regulated densities of charge and disulfide cross-linking directed to enhance gene expression. *J. Am. Chem. Soc., 126*, 2355–61.

Mnyusiwalla, A., S., D. A., & Singer, P. A. (2003). 'Mind the gap': science and ethics in nanotechnology. *Nanotechnology, 14*, R9–R13.

National Science Foundation, USA. (February 2000). "Nanotechnology definition." from http://www.nsf.gov/crssprgm/nano/reports/omb_nifty50.jsp.

Nel, A., Xia, T., Madler, L., & Li, N. (2006). Toxic potential of materials at the nanolevel. *Science, 311*, 622–7.

Niidome, T., Yamagata, M., Okamoto, Y., Akiyama, Y., Takahashi, H., Kawano, T., Katayama, Y., & Niidome, Y. (2006). PEG-modified gold nanorods with a stealth character for in vivo applications. *J. Control. Release, 114*, 343–7.

Oberdorster, G., Oberdorster, E., & Oberdorster, J. (2005). Nanotoxicology: an emerging discipline evolving from studies of ultrafine particles. *Environ. Health Perspect., 113*, 823–39.

Orive, G., Hernandez, R. M., Rodriguez Gascon, A., Dominguez-Gil, A., & Pedraz, J. L. (2003). Drug delivery in biotechnology: present and future. *Curr. Opin. Biotechnol., 14*, 659–64.

Psaltis, D., Quake, S. R., & Yang, C. (2006). Developing optofluidic technology through the fusion of microfluidics and optics. *Nature, 442*, 381–6.

Ratner, B. D., Hoffman, A., Schoen, F., & Lemons, J. (2004). *Biomaterials Science: An Introduction to Materials in Medicine*. New York, Academic Press.

Reddy, G. R., Bhojani, M. S., Mcconville, P., Moody, J., Moffat, B. A., Hall, D. E., Kim, G., Koo, Y. E., Woolliscroft, M. J., Sugai, J. V., Johnson, T. D., Philbert, M. A., Kopelman, R., Rehemtulla, A., & Ross, B. D. (2006). Vascular targeted nanoparticles for imaging and treatment of brain tumors. *Clin. Cancer. Res., 12*, 6677–86.

Richards Grayson, A. C., Scheidt Shawgo, R., Li, Y., & Cima, M. J. (2004). Electronic MEMS for triggered delivery. *Adv. Drug Deliv. Rev., 56*, 173–84.

Ringsdorf, H. (1975). Structure and properties of pharmacologically active polymers. *J. Polym. Sci. Polym. Sympo., 51*, 135–153.

Roco, M. C. (2003). Nanotechnology: convergence with modern biology and medicine. *Curr. Opin. Biotechnol., 14*, 337–46.

Ryman-Rasmussen, J. P., Riviere, J. E., & Monteiro-Riviere, N. A. (2006). Penetration of intact skin by quantum dots with diverse physicochemical properties. *Toxicol. Sci., 91*, 159–65.

Salamanca-Buentello, F., Persad, D. L., Court, E. B., Martin, D. K., Daar, A. S., & Singer, P. A. (2005). Nanotechnology and the developing world. *PLoS Med., 2*, e97.

Sandler, R., & Kay, W. D. (2006). The national nanotechnology initiative and the social good. *J. Law Med. Ethics, 34*, 675–81.

Sawant, R. M., Hurley, J. P., Salmaso, S., Kale, A., Tolcheva, E., Levchenko, T. S., & Torchilin, V. P. (2006). "SMART" drug delivery systems: double-targeted pH-responsive pharmaceutical nanocarriers. *Bioconjug. Chem., 17*, 943–9.

Service, R. F. (2004). Nanotoxicology. Nanotechnology grows up. *Science, 304*, 1732–4.

Shimoboji, T., Larenas, E., Fowler, T., Hoffman, A. S., & Stayton, P. S. (2003). Temperature-induced switching of enzyme activity with smart polymer-enzyme conjugates. *Bioconjug. Chem., 14*, 517–25.

Shimoboji, T., Larenas, E., Fowler, T., Kulkarni, S., Hoffman, A. S., & Stayton, P. S. (2002). Photoresponsive polymer-enzyme switches. *Proc. Natl. Acad. Sci. U S A, 99*, 16592–6.

Shuai, X., Merdan, T., Schaper, A. K., Xi, F., & Kissel, T. (2004). Core-cross-linked polymeric micelles as paclitaxel carriers. *Bioconjug. Chem., 15*, 441–8.

The National Nanotechnology Initiative, USA. (July 2006). "Supplement to the President's 2007 budget."

Tao, S. L., & Desai, T. A. (2005). Micromachined devices: the impact of controlled geometry from cell-targeting to bioavailability. *J. Control. Release, 109*, 127–38.

Thierry, B., Winnik, F. M., Merhi, Y., Silver, J., & Tabrizian, M. (2003). Bioactive coatings of endovascular stents based on polyelectrolyte multilayers. *Biomacromolecules, 4*, 1564–71.

Torchilin, V. P. (2006). Multifunctional nanocarriers. *Adv. Drug Deliv. Rev., 58*, 1532–55.

Whitesides, G. M. (2006). The origins and the future of microfluidics. *Nature, 442*, 368–73.

Yager, P., Edwards, T., Fu, E., Helton, K., Nelson, K., Tam, M. R., & Weigl, B. H. (2006). Microfluidic diagnostic technologies for global public health. *Nature, 442*, 412–8.

Ye, S., Wang, C., Liu, X., & Tong, Z. (2005). Deposition temperature effect on release rate of indomethacin microcrystals from microcapsules of layer-by-layer assembled chitosan and alginate multilayer films. *J. Control. Release, 106*, 319–28.

Yeo, Y., & Park, K. (2004). A new microencapsulation method using an ultrasonic atomizer based on interfacial solvent exchange. *J. Control. Release, 100*, 379–88.

20

Nanotechnology in Drug Development and Life Cycle Management

Shingai Majuru and Moses O. Oyewumi

Introduction

Nanotechnology deals with the design, production, characterization and application of sub-micron-sized particles. The popularity and effectiveness of small-sized particles can be extended to broad areas in pharmaceutical, medical, chemical and engineering applications mainly due to their unique properties. The recognition for nanotechnology is well expressed by a great funding of US$1.28 billion to the US National Nanotechnology Initiative (NNI) for the fiscal year 2007.[1] Also, it is estimated that the drug market for nanotechnology could be worth as much as US$200 billion by 2015 (Breen, 2006). Examples of nanoparticulate drug carriers are liposomes, microemulsions, nanosuspensions and nanoparticles (Mumper, Cui & Oyewumi, 2003). These systems can be formulated into a variety of dosage forms including parenteral, tablets, hard gelatin capsules, soft gelatin capsules and oral liquid dosage forms. In many studies, nanoparticulate carriers have been demonstrated as effective delivery systems for a wide range of small molecular drugs as well as macromolecules (such as proteins, peptides or genes) (Mehnert & Mader, 2001; Brigger, Dubert & Couvreur, 2002). Nanotechnology drug delivery systems have been reported in literature to offer useful strategies to overcome some of the problems associated with drug therapy such as (Mehnert & Mader, 2001) (a) insufficient drug concentration in the blood due to poor absorption, rapid metabolism and elimination; (b) poor drug solubility and bioavailability; (c) high fluctuation of plasma levels due to erratic bioavailability from oral administration. It has been mentioned that one in ten marketed drugs has solubility problems and close to a third fail to reach profitability due to poor bioavailability or pharmacokinetics (Knight, 2006).

In drug delivery, small particles can aid in the direct entry of entrapped molecules into cells either passively (non-specifically) or actively via cell-targeting ligands placed directly on the particle surface. The diameter of human cells is about 10–20 μm while the size of cell organelles ranges from

[1] National NanoTechnology Initiative, http://www.nano.gov/, September 2006

M.M. de Villiers et al. (eds.), *Nanotechnology in Drug Delivery*, DOI: 10.1007/978-0-387-77667-5_20,

a few nanometers to a few hundred nanometers (Kim & Nie, 2005). Therefore, drug delivery systems having sizes in the few nanometer range will be able to directly interact with bio-molecules on the cell surface and within the cells in a non-invasive manner. A notable area of application of nanoparticulate carriers is in tumor-targeted delivery of drugs, where the ultimate goal of therapy is to ensure selective destruction of tumor cells while sparing normal tissues (Brigger et al., 2002). The difficulty in achieving antitumor specificity from cytotoxic agents may be due to a number of factors like low level of biochemical differentiation between normal and tumor tissues and heterogeneous nature of tumor cell populations. As such, site-specific delivery systems play a crucial role in cancer therapies not only to achieve substantial tumoricidal effect due to the anticancer agents but also to minimize systemic side effects (Brigger et al., 2002). Reduction of side effects is achieved by targeting the drug only to the tumor cells, leading to reduced exposure of normal cells to the drug and an overall reduction in the drug dose. The unique feature of nanoparticulate carriers is the small size that facilitates passage through biological barriers. Small particles are able to extravasate through blood vessels and tissues. This is especially important for tumor vessels, which are often dilated and fenestrated with an average pore size of less than a micron (Brigger et al., 2002). It has been demonstrated that the typical pore size of vascularized tumors is about 200–500 nm with fenestrations as small as 50–60 nm (Wu, Da, Rudoll, Needham, Whorton, & Dewhirst, 1993). As such, small particles are able to cross biological barriers and passively accumulate in cells with or without the aid of cell-targeted ligands.

Nanovectors, in development today, are multi-functional organic and inorganic nanoparticles, nanowires and nanotubes and have the potential to be a generic platform for different types of cancer treatments (Panchapakesan, 2005). They offer drug delivery with targeted localized killing of cancerous and precancerous cells through thermal ablation. Additionally, there is the potential to integrate nano-surgical tools with micro- and macro-surgical tools for treatment of cancer (Panchapakesan, 2005). The targeting of specific receptors in cancer cells can be achieved by using nanovectors for drug delivery where the surface has been modified with biological material such as antibodies to facilitate the targeting of specific receptors in cancer cells. These nanovectors can be heated in a localized way in vivo to kill cancer cells in parts of the body that are not accessible through traditional surgical techniques while hollow nanovectors can be filled with drugs that are released when they reach the target cancer cells. After drug release the nanovectors can be destroyed using external energy sources such as optics or magnets. Nanovectors for cancer treatment can be formulated as parenterals for injection directly into the cancer cells or into the blood stream to travel to the target site. To be highly effective they should be selectively directed against cancer clusters and should be able to kill both malignant cancer cells and cells in early stages of transformation without affecting the patients' quality of life (Panchapakesan, 2005). For successful development it is essential that the nanoparticles in the dosage form maintain their particle size throughout the shelf life of the product and that the stability of the drug is maintained.

Over the past years, a good number of studies have been carried out on tumor-specific systems involving liposomes and nanoparticles conjugated to transferrin fibroblast growth factor monoclonal antibodies, vitamin B12 and folic acid. A suitable summary on tumor-targeting ligands have been reviewed by Brigger et al. (2002) and Kim and Nie (2005). Other benefits from the application of small particles in cancer therapy as reviewed by Fahmy and colleagues in 2005 (Fahmy, Fong, Goyal, & Saltzman, 2005) are (i) achievement and maintenance of sustained intracellular drug delivery, (ii) bypassing multidrug resistance in drug and (iii) reduction of drug toxicity and side effects. Nanoparticles for cancer chemotherapy have been extensively investigated for drugs like paclitaxel (Feng, 2004); doxorubicin (Caelyx^{R}) (Yoo, Lee, Oh, & Park, 2000); and 5-FU (Yi, Yang, & Pan, 1999). Also, macromolecules such as proteins and peptides are increasingly important as therapeutic agents; however, their delivery is often a challenge because their transport through compartmental barriers in the body is inefficient and they are readily metabolized. Irrespective of the mode of delivery, small particles are increasingly more important in site-specific delivery of drugs, genes, diagnostics and vaccines. Examples of commercial application of nanotechnology in cancer therapy are (i) polyfunctional nanoparticles for tumor-targeted drug delivery commercially developed by Alnis BioSciences (NC, USA) and (ii) nanotechnology for drug delivery across the blood–brain barrier for treatment of brain tumors and Alzheimer disease (Advectus Life Sciences, Vancouver, CA).

Another application of small particles is to increase solubility of drugs. This is particularly important since a large number of new drug candidates emerging from high-throughput screening are water insoluble. The relevance in life cycle management is also crucial since existing drug products can be reformulated and reintroduced into the market. In reformulation, nanotechnology can offer the advantage of increasing drug solubility and bioavailability leading to decreased drug dose, cost and side effects. The increased solubility and bioavailability can offer the added advantage of decreased variability in plasma levels achieved following oral dosing. Additionally, its novelty allows for the development of new patentable formulations that extend the life cycle of the drug and increase profitability. Nanoparticles exhibit a very high surface area to volume ratio due to their small size, and as a result of this their dissolution rate is increased according to the Noyes Whitney and Kelvin equations. The utility of nanotechnology for the improvement of the solubility and bioavailability of poorly soluble drugs has been demonstrated for drugs such as paclitaxel, cyclosporine or amphotericin B (Kayser, Lemke, & Hernandez-Trejo, 2005). One approach for using nanoparticles to increase solubility and bioavailability involves milling of a high-density drug into nanoparticles. Using this approach Rapammune® used for the prevention of organ rejection following transplant surgery is made from rapamycin (Fahmy et al., 2005). The challenges of using milling drugs include possible polymorphic changes that can occur as well as drug degradation due to associated high energy. The generation of the amorphous form of the drug can cause problems because these forms can recrystallize during the shelf life of the drug product leading to changes in both solubility and bioavailability.

The small size of nanovehicles can result in the limitation of their utility in drug solubilization. One example of the limitation caused by the small size is seen with dendrimers whose size range of 5–20 nm results in a poor capacity to incorporate drugs. Solubilization can also be achieved by milling the drug and then stabilizing the resulting small particles with a coat to form nanocrystals suitably sized for oral delivery as well as for intravenous injection (Rabinow, 2004). Another approach for using nanotechnology to improve the solubility of poorly soluble drugs involves using phospholipids to aid the delivery of water-insoluble drugs. In this approach the drugs are in contact with the hydrophobic region of the phospholipids while the hydrophilic portion of the phospholipids is in contact with the water-rich fluids. The lipid matrix may be filled into soft gelatin capsules, dried and then filled into hard gelatin capsule or compressed into tablets. It is important that following administration and disintegration of the dosage form the nanoparticles are regenerated, otherwise the advantage of the nanoparticulate form will be lost. The drug also needs to be stable in the nanoparticulate formulation throughout the shelf life of the drug.

The effectiveness of small particles in all the areas of application is ascribed to improvement of bioavailability, prolongation of drug or gene effects in target tissue, improved solubilization of drugs for intravascular delivery and improvement in the stability of therapeutic agents against enzymatic degradation (Liversidge & Cundy, 1995; Hu, Johnston, & Williams, 2004; Kim & Nie, 2005).

Nanoparticulate Drug Delivery Systems

There are various nanoparticulate drug delivery systems such as liposomes, microemulsions, micellar systems and nanoparticles.

Liposomes

Liposomes are spherical vesicles that are prepared using one or more amphiphilic phospholipids (such as phosphatidylcholine) and cholesterol that self-associate into bilayers that have aqueous interior. Liposomes may be formulated into small structures (80–100 nm) that encapsulate either hydrophilic drug in the aqueous interior or lipophilic within the lipid bilayers. Drug release, in vivo stability and biodistribution are determined by the size, surface charge, surface hydrophobicity and membrane fluidity (Mehnert & Mader, 2001). Liposomes have low toxicity based on selection of components that are safe and application of processes that are not damaging to the drug. Some of the other benefits for liposomes in drug delivery are as follows: (i) they are versatile in size, (ii) composition and (iii) bilayer fluidity and (iv) they are capable of displaying drugs on their surface or encapsulating drugs within the bilayer. Cationic liposomes have been employed in non-viral gene delivery to condense DNA. Examples of lipids that are used to prepare cationic lipososmes are dioleylpropyl trimethylammonium chloride (DOTMA); dioleoyl trimethylammonium propane (DOTAP) and dimethylaminoethane carbamoyl cholestrerol

(DC-Chol). Application of liposomes has been imparted by factors such as low encapsulation efficiency, rapid leakage (premature release) of incorporated drug into the blood, poor stability and high cost of production at an industrial scale. In order to delay or prevent interactions with reticuloendothelial systems (RES) liposome formulations have been modified by inclusion of polyethylene glycol (PEG) that serves as a barrier preventing interaction with plasma proteins.

Microemulsion

A simplified definition for microemulsions is that they contain two phases consisting of two immiscible liquids that are mixed together and stabilized with the aid of a surfactant with or without a co-surfactant. Microemulsions are thermodynamically stable, fluid, isotropically clear and may have droplets in the range of 5–100 nm. They are quite different from emulsions in that emulsions are opaque mixtures of two immiscible liquids, thermodynamically unstable and usually require the application of high torque mechanical mixing or homogenization to produce dispersed droplets in the range of 0.2–25 μm (Mumper et al., 2003). Both microemulsions and emulsions can be made as water-in-oil (w/o) or oil-in-water (o/w) depending on the properties of the surfactant. The choice of the dispersed and continuous phases for microemulsion formulations is based on the hydrophilicity of the drug in consideration. Also, surfactants that have hydrophilic–lipophilic balances (HLB) of 3–6 tend to promote the formation of w/o microemulsions while those with HLB values of 8–10 tend to promote the formation of o/w microemulsions. It has been demonstrated that the formation and stability of microemulsions are dependent on the achievement of a very low interfacial tension between the dispersed and continuous phases. It is important that the droplets be stabilized against Ostwald ripening (Landfester, 2001), a phenomenon that leads to dissolution of the small droplets with a resulting increase in the size of the large droplets. Oswald ripening can occur by diffusion processes and/or coalescence due to microemulsion instability. The resulting change in the size of the droplets leads to changes in the desired advantages of the formulation upon storage and represents a loss of physical stability of the dosage form. To achieve the desired microemulsion stability, the components (surfactants, co-surfactants, oil phase and water phase) of microemulsions must be carefully chosen (Langevin, 1991). Another important consideration in component selection is safety. It has been observed that inclusion of short or medium chain length alcohols (such as 1-butanol, 2-butanol and ter-butanol) as co-surfactants could limit the potential use due to their irritant and toxic properties (Attwood, 1994). Microemulsions have been proposed as drug delivery systems to enhance the absorption of drug across biological membranes (Fendler, 1994). The application of microemulsions may offer many advantages for marketed pharmaceutical products, such as (i) increased solubility and stability of drugs incorporated in the dispersed phase and (ii) ease and economy of scale-up (since expensive mixing equipment is often not needed). Some of the major drawbacks are (a) premature leakage/release of incorporated drug since drugs are entrapped in droplets; (b) phase inversion which can occur from instability

in biological fluids; (c) many effective surfactants and or co-surfactants do not have a pharmaceutically acceptable toxicity profile; and (d) microemulsion systems often require development of complex systems that may be time consuming leading to significantly long product development time lines. Additionally, microemulsions have been used as templates to prepare solid nanoparticles. Solid nanoparticles were cured from microemulsion systems by use of photochemistry (Agostiano, Catalano, Curri, Della, Monica, Manna, & Vasanelli, 2000), polymerization (Fang, Stokes, Wiemann, & Zhou, 2000), or a sequence of heating and cooling (Gasco, 1997; Oyewumi & Mumper, 2002).

Nanoparticles

Nanoparticles are solid colloidal particles, ranging in size from 1 to 1000 nm, consisting of various macromolecules in which the therapeutic drugs can be adsorbed, entrapped or covalently attached. Solid nanoparticles offer distinct advantages in drug development which can be ascribed to their physical stability and the possibility of modifying the formulating materials in order to achieve controlled release characteristics. The ability to formulate nanoparticles to achieve sustained release offers an opportunity for product life cycle management by developing formulations with decreased dosing frequency for drugs that are going off patent. There has been a variety of materials used to engineer solid nanoparticles both with and without surface functionality. Perhaps the most widely used are the aliphatic polyesters such as poly(lactic acid) (PLA), the more hydrophilic poly(glycolic acid) (PGA) and their copolymers poly(lactide-coglycolide) (PLGA). The degradation rate of these polymers and often the corresponding drug release rate can vary from days (PGA) to months (PLA). The effectiveness of nanoparticles in drug delivery can be attributed to many factors such as physical and biological stability, good tolerability of the components, simplicity of the manufacturing process, possibility of facile scale-up of the manufacturing process, amenability to freeze drying and sterilization. In this chapter, particular attention will be placed on nanoparticles.

Ideal Properties of Nanoparticle Delivery Systems

Some of the properties of nanoparticles that are important for application in drug delivery are listed:

- The manufacturing process should be simple, affordable and easy to scale up. For consideration in drug product development, it is preferred that the manufacturing process excludes organic solvents or potentially toxic ingredients. All the components of the formulation should be commercially available, safe, affordable, non-toxic and biodegradable.
- The nanoparticles should be stable with respect to size, surface morphology, size distribution and other important physical and chemical properties. The formulation should be biocompatible and non-immunogenic. Nanoparticle formulation should be stable on storage and be able to regenerate the nanoparticles after administration.

- Nanoparticle formulation should ensure high loading of drugs (good drug payload) and exhibit very low possibility of premature release/leakage of the drug. Additionally, the manufacturing process should accommodate the inclusion of cell-targeting ligands if necessary.
- Depending on the drug development process, nanoparticle manufacturing process and formulation should be amenable to various secondary processes such as lyophilization, sterilization, drying, blending, granulation, compression, capsule filling and packaging.
- The resulting product from nanoparticle formulation should be stable, safe, non-toxic, easy to administer, bioavailable and achieve desirable bioavailability and blood circulation.
- Nanoparticle formulations should protect the incorporated drug from degradation and prevent premature release of its payload.
- Nanoparticle formulation should release the drug(s) completely in an active form at an optimal rate that is based on the formulation design.

Nanoparticle Preparation Methods

Nanoparticles can be categorized based on the types of polymers, formulation materials and manufacturing methods.

Nanosuspensions

Nanosuspension refers to production of sub-micron-sized particles by subjecting the combination of drug and a suitable emulsifier to the process of milling or high-pressure homogenization. Conventional milling and precipitation processes generally result in particles with sizes that are much greater than 1 μm. As such, a critical step in the nanosuspension preparation is the choice of the manufacturing procedure to ensure production of sub-micron particles. Particle size reduction to sizes below 1 μm is usually difficult due to possible particle aggregation and generation of high surface area materials. Milling techniques that have been used to generate nano-sized particles are ball milling or pearl milling that applies milling beads of sizes ranging from 0.4 to 3 mm (Kipp, 2004). These beads may be composed of glass, ceramics or plastics (Kipp, 2004). The time required for milling depends on the hardness and brittleness of the drug material in comparison to milling material and inertial forces set up within the mill. Some of the challenges that milling processes can pose in drug development are (i) undesirable erosion of the milling equipment components into the drug product; (ii) the process is usually time consuming, thereby prolonging drug development time; (iii) milling over a few days may bring the risk of microbiological problems or increases in the cost of production; also (iv) prolonged milling may induce the formation of amorphous domains in crystalline starting materials or may lead to changes in the polymorphic form of the drug. The generation of amorphous form of the drug is problematic because these forms may crystallize during the shelf life of the drug leading to changes in solubility and

bioavailability of the drug. An example of the conversion of crystalline to amorphous form of the drug was observed in jet milling of albuterol sulfate (Ward & Schultz, 1995). Also, the generation of high-energy surfaces that affected wettability was observed with acetylsalicylic acid (Huettenrauch, 1984). Some examples of nano-sized particles produced by milling are (i) naproxen nanoparticles approximately 200 nm in diameter (Setler, 1999) and (ii) danazol particles of a mean size of 169 nm (Liversidge & Cundy, 1995). An example of a commercialized mechanical process for nanoparticle preparation is NanoCrystal® technology that was developed and patented in 1992 which is now a platform technology of Elan Drug Technologies. There are four approved drug products in the USA that are based on NanoCrystal technology: (a) Rapamune (sirolimus) tablets by Wyeth; (b) Tricor (fenofibrate) tablets by Abbott; (c) Emend (aprepitant) capsules by Merck; and (d) Megace ES (megestrol) oral suspension by Par Pharmaceuticals (Knight, 2006).

Additionally, production of sub-micron-sized drug particles by high-pressure homogenization has been well reported (Kipp, 2004; Hu et al., 2004). An example of commercialized high-pressure homogenization process, Dissocubes® was developed and patented in 1994. The process has been applied in SkyePharma's insoluble drug delivery (IDD) and Baxter NanoEdge platforms (Knight, 2006). These have resulted in some drug products, namely: (i) Triglide (fenofibrate) by SkyePharma based on the IDD technology; (ii) Abrane, an albumin-stabilized nanoparticle formulation of paclitaxel by Abraxis BioScience. Abraxane is approved in the USA as a second-line therapy for breast cancer and in Canada for metastatic breast cancer. The formation of nanosuspensions is based on the cavitation forces created in high-pressure homogenizers such as piston-gap homogenizers. In the process, an aqueous suspension of the drug in surfactant solution is made which is subsequently passed through a high pressure of typically 1500 bar at 3–20 homogenization cycles (Muller, Jacobs, & Kayser, 2001). The suspension is then passed through a small gap in the homogenizer of typical width 25 μm at 1500 bar. The cavitation forces are built up due to a number of factors such as (i) narrowness of the gap resulting from streaming velocity of the suspension and dynamic fluid pressure increase and (ii) a decrease in static pressure of the fluid and resultant production of water vapor that escapes the homogenization gap. The cavitation forces that are created are strong enough to break drug microparticles to nanoparticles. An example is in the microfluidization of atovaquone to obtain particles in the 100–300 nm size range (Dearn, 1995). In most cases, nanosuspension particles have an average size ranging from 40 to 500 nm with a small (0.1%) proportion of particles larger than 5 μm (Hu, Johnson, & Williams, 2004). For the purpose of large-scale production of drug delivery systems, high-pressure homogenizers are available with different capacities that are suitable for drug development and large-scale manufacturing. A major challenge in the use of high-pressure homogenization is the possible changes in drug crystal structure that can cause batch-to-batch variation in crystallinity level. Therefore application in drug delivery should include the desired specification by which the quality of each batch will be evaluated. It is also likely to obtain amorphous form of the drug which might affect drug stability either immediately after production or on storage.

Polymeric nanoparticles

Polymeric nanoparticles made with biodegradable polymers have been widely applied in drug delivery. Many FDA-approved biodegradable and biocompatible polymers have been used in nanoparticle preparation. These include polylactide-polyglycolide copolymers, polyacrylates and polycaprolactones. Examples of natural polymers are albumin, gelatin, alginate, collagen and chitosan. Nanoparticles can be prepared from polymerization of monomers or from preformed polymer with the possibility of performing many chemical modifications. According to the technologies used, nanospheres or nanocapsules can be obtained. Nanospheres consist of a dense polymeric matrix, in which the drug can be dispersed, whereas nanocapsules present a liquid core surrounded by a polymeric shell.

Nanoparticle preparation methods based on the polymerization of monomers generally involve introducing the monomer to an aqueous phase or dissolving the monomer in a non-solvent of the polymer (Lockman et al., 2002). The polymerization reaction in these systems generally occurs in two steps: a nucleation phase followed by a growth phase. The process can be carried out in two ways either as emulsion polymerization or as interfacial polymerization. In emulsion polymerization, triggers for polymer growth are used such as high-energy radiation, UV light or hydroxyl ions. Emulsion polymerization offers many advantages: it is a fast process when compared to other processes; the process does not require stabilizers and surfactants; and the process can easily be scaled up. However, there are many challenges to the application of emulsion polymerization. These include (i) the requirement of organic solvents; (ii) the requirement for free-radical radiation or UV light used to trigger polymerization; this need for the triggers prevents the addition of proteins or peptides during polymerization. When nanoparticle preparation involves polymerization, it is undesirable to have residual monomers and initiators in the final nanoparticle formulation. A critical step of the process is the purification and removal of residual monomers. It is also very important to separate free (un-incorporated) drugs from the drug-loaded nanoparticle suspension. Some of the methods of nanoparticle purification involving dialysis and centrifugation may be difficult to scale up in large manufacturing. The interfacial polymerization is similar to emulsion polymerization except that polymerization occurs when an aqueous and an organic phase are brought together by homogenization, emulsification or microfluidization under high-torque mechanical stirring (Lockman et al., 2002). Drug incorporation is carried out by adding the drug with the monomer in the organic phase so as to ensure stability. A potential challenge for polymeric nanoparticles is associated with residues from organic solvents and polymer toxicity.

In the polymer dispersion method, the polymer is dissolved in an organic solvent such as dichloromethane, chloroform or ethyl acetate. If the drug to be incorporated in nanoparticles is hydrophobic, the drug is dissolved or dispersed into the polymer solution. The polymer solution is then added to an aqueous solution, followed by high-speed homogenization or sonication to form an oil-in-water emulsion. Nanoparticle preparation is usually facilitated and stabilized with the aid of an emulsifier or

stabilizer. If the drug to be incorporated in nanoparticles is hydrophilic, the drug is added to the aqueous phase and entrapped into nanoparticles through a double emulsification method to form water-in-oil-in-water emulsion (double emulsification) (Feng, 2004). Due to the implication on safety, it is important to remove organic solvent from the emulsion. Organic solvent can be removed by evaporation or a decreased pressure or under a vacuum environment with or without the aid of inert gas flow. Solid nanoparticles are cured from the suspension by centrifugation, filtration or freeze drying. Another method is based on particle precipitation upon addition of a non-solvent to polymer solution under mechanical stirring. This method allows the formation of nanoparticles without prior emulsification. Nanoparticle formation and characteristics are dependent on the choice of the polymer/solvent/non-solvent system that will ensure mutual miscibility of the solvent and non-solvent of the polymer. The method has been applied for many polymers like polylactide, polylactide-co-glycolide, polycaprolactone, ethycellulose, polyalkylcyanoacrylate and polystyrene. Nanoparticles can also be prepared from natural macromolecules using methods such as thermal denaturation of proteins (such as albumin) or gelification process such as in alginates.

In general, the controlling factors in the nanoparticle formulation process, which are adjustable for an ideal design, are the polymer type and its molecular weight, the copolymer blend ratio, the type of organic solvent, the drug loading level, the emulsifier/stabilizer and oil–water phase ratio, the mechanical strength of mixing, the temperature and the pH. In the production of a drug product it is important to set a limit for residual solvent in the formulation that is based on the acceptable daily intake and to develop analytical methods for testing of the solvent levels in the nanoparticles.

Polymers for Gene Delivery

A separate category of application of polymers is in DNA condensation for gene delivery. The success of gene therapy is based on the transport of DNA through the cell membrane for subsequent transfection that involves the cell's transcriptional and translational machinery. In non-viral gene therapy it is required that plasmid DNA be specifically delivered into desired cells of the body to produce therapeutic proteins. Since the transport of "naked" plasmid DNA is greatly limited, one of the attractive strategies for delivery is plasmid DNA/polyelectrolyte complexes that apply condensing agents like cationic polymers. At physiological pH, addition of cationic polymers to plasmid DNA will result in production of sub-micron-sized particles. At the research level, many synthetic DNA particles have been prepared for transfection in cell cultures and in animal studies. However, there are many issues that must be addressed in the development of DNA particles with cationic polymers. These are (i) potential toxicity of cationic polymers especially when administered at high concentrations; (ii) instability of particles on storage; (iii) instability of DNA particle size and particle size distribution leading to undesirable particle aggregation; (iv) poor transfection efficiency; (v) poor stability in blood circulation; and (vi) high cost of scaling up the process to achieve reproducible product quality.

Solid Lipid Nanoparticles

Another category of nanoparticles is solid lipid nanoparticles that are made from solid lipids using homogenization techniques and microemulsion methods (Mehnert & Mader, 2001). Examples of lipids that are used include triglycerides (e.g., tristearin), partial glycerides (e.g., Imwitor), fatty acids (e.g., stearic acid), steroids (e.g., cholesterol) and waxes (e.g., cetyl palmitate). To prepare particles using the homogenization method, the drug is dissolved or solubilized in the lipid that has been melted and heated to a temperature approximately 5–10°C above its melting point. For the hot homogenization technique, the drug dissolved in the lipid melt is dispersed under stirring in a hot aqueous surfactant solution of identical temperature. The obtained pre-emulsion is homogenized to produce nanoemulsions that are subsequently cooled to room temperature. Solid lipid nanoparticles are obtained upon lipid recrystallization at room temperature. Some of the process variables that will affect the particle size of nanoparticles as well as drug loading are (i) the type of homogenization technique; (ii) speed of homogenization; and (iii) rate of cooling in hot homogenization.

Cold homogenization is applied for highly temperature-sensitive drugs and hydrophilic drugs. For the cold homogenization technique the drug containing lipid melt is cooled and ground to obtain lipid particles. The lipid particles are dispersed in a cold surfactant solution that is homogenized at or below room temperature. The process avoids or minimizes the melting of lipids and therefore minimizing the loss of hydrophilic drugs to the water surface.

As mentioned previously, solid lipid nanoparticles can also be prepared by using microemulsions as precursors. Microemulsions are transparent, thermodynamically stable and easily manufactured systems. Essentially, microemulsions can be defined as small droplets (5–100 nm) of one liquid dispersed throughout another by virtue of the presence of fairly large concentrations of surfactants. Gasco reported SLN preparation techniques which are based on the dilution of microemulsions (Gasco, 1997). In this approach microemulsions are made by stirring an optically transparent mixture at 65–70°C, which is composed of low-melting fatty acid (e.g., stearic acid), an emulsifier (e.g., polysorbate 20, polysorbate 60, soy phosphatidylcholine, taurodeoxycholic acid sodium salt), co-emulsifiers (e.g., butanol, sodium monooctylphosphate) and water. The hot microemulsion is dispersed in cold water (2–3°C) under stirring using a typical volume ratio of the hot microemulsion to cold water in the range of 1:25–1:50. The dilution step is critically determined by the composition of the microemulsion. Other studies have investigated production of nanoparticles from warm microemulsions that required simple cooling of warm microemulsions at room temperature (Mumper et al., 2003). Microemulsions were prepared using materials such as waxes (e.g., emulsifying wax), polymeric surfactants such as Brij type, polyethylene glycol derivatives of fatty acids such as PEG-400 monostearate and phospholipids (Oyewumi & Mumper, 2002). The preparation of nanoparticles from microemulsion precursors is the platform technology that is being commercially applied to engineer drug and vaccine delivery systems (NaNoMed Pharmaceuticals;

Kalamazoo, MI, USA). Important process factors in the application of microemulsions to prepare nanoparticles include (a) preparing a homogeneous mixture of lipids (or waxes) and drug; (b) achievement of substantial drug loading within microemulsion window; (c) cooling of the warm microemulsion to obtain nanoparticles; and (d) a purification process to remove excess surfactants and unincorprorated drug from the nanoparticle suspension.

A commercial product that applies lipids in a nanoparticulate product is Doxil® doxorubicin liposome (ALZA, Mountain View, CA, USA). Also, the lead product of Starpharma (Melbourne, Australia) is VivaGel™ which is a based on development of an anti-HIV drug through dendrimer nanotechnology. Using micellar nanoparticle technology, Novavax has developed an estrogen-containing product, Estrasorb (estradiol) that is approved by the US FDA.

Characterization of Nanoparticles

The effectiveness of nanoparticles in drug delivery can be ascribed to the sub-micron size. From a study on Caco-2 cell line, it was demonstrated that the uptake of nanoparticles having sizes of about 100 nm was about 2.5-fold higher than particles with sizes of about 1 μm. Also, the uptake of particles of about 10 μm was nearly 6-fold lower than particles of 100 nm sizes (Desai, Labhasetwar, Walter, Levy, & Amidon, 1997). In comparison to larger particles, nanoparticles have greater ratio of surface area to weight or volume and this facilitates drug release (Feng, 2004). Measurement of sub-micron sizes can be carried out by photon correlation spectroscopy or dynamic light scattering. Photon correlation spectroscopy (PCS) determines the hydrodynamic diameter of the nanoparticles by Brownian motion which necessitates the need for specifications for these measurements in drug development. Examples of specifications that must be established in sample preparation for particle size measurement by PCS and at different stages of product development are the type of dispersing liquid, removal of dust from dispersing liquid prior to measurement, viscosity of the dispersing liquid, refractive index of the particles and the temperature of particle size measurement. In addition to the size, there are other properties that are very important to nanoparticle stability and performance as drug delivery systems including the following: (i) density, molecular weight and crystallinity can affect drug release and degradation; (ii) surface charge and hydrophobicity can significantly influence nanoparticle interaction and biological environment and biodistribution after systemic administration (Jung, Kamm, Bretenbach, Kaiserling, Xiao, & Kissel, 2000; Mehnert & Mader, 2001). The zeta potential can be employed to measure the cell-surface charge density. The surface and bulk morphology are also important in determining the drug release kinetics of nanoparticles. Nanoparticles can be visualized by scanning electron microscope (SEM) and atomic force microscopy (AFM). Particle imaging by AFM utilizes the force acting between a surface and a probing tip to achieve a spatial resolution of up to 0.01 nm (Mehnert & Mader, 2001). The performance of the drug-loaded nanoparticles can be evaluated by comparing

the therapeutic effects of the drug released from nanoparticles versus free drug under the same conditions. Examples of tests that are conducted are differential scanning calorimetry (DSC) analysis to evaluate thermal transitions of free drug and encapsulated drug. Changes in crystallinity of drug pre- and post-loading in nanoparticles can be monitored by x-ray crystallography. Other methods that are employed to characterize drug-loaded nanoparticles are drug encapsulation efficiency; physical properties such as size, shape, stability of size; and drug loading. Depending on the method of nanoparticle manufacture, various purification processes can be employed to (i) remove potentially toxic residues; (ii) separate unincorporated drug; and (iii) concentrate nanoparticle suspensions. Examples of nanoparticle purification processes are filtration, gel permeation or dialysis.

Nanoparticle Application in Non-parenteral Applications

Oral Administration

The oral route of administration is the most convenient method for drug products and is the most preferred in clinical cases that require frequent drug administration. However, the oral route is not suitable for drugs that are poorly permeable or easily degradable in the gastrointestinal tracts (GIT). For instance, delivery of proteins and peptides via the oral route will be greatly impacted by barriers such as (i) epithelial cell lining; (ii) the mucus layer; (iii) proteolytic enzymes in the gut lumen (such as pepsin, trypsin and chymotrypsin); and (iv) proteolytic enzymes (endopeptidases), at the brush border membrane. Drug loaded in nanoparticles will be protected from the enzymatic degradation along the GIT providing the potential benefit of enhanced absorption. Information available from various literatures indicates that particulate absorption takes place mainly at the intestinal lymphatic tissues (the Peyer's patches) (Jung et al., 2000). The epithelial cell layer overlying the Peyer's patches contains M cells. The differences between absorptive enterocytes and M cells are expressed in that M cells have (a) underdeveloped microvillous and glycocalyx structures, (b) apical microfolds, (c) increased intracellular vacuolization and (d) absence of mucus. The follicle-associated epithelia (FAE) are made up of the M cells and absorptive enterocytes (Jung et al., 2000). It has been demonstrated that the FAE and M cells are predominantly responsible for particle uptake along the GIT (Jung et al., 2000; Delie & Blanco-Prieto, 2005). Additional reports have indicated that particulate uptake along the GIT is not exclusive to the Peyer's patches (Delie & Blanco-Prieto, 2005). In this regard, nanotechnology is gaining a lot of attention in the development of proteins, peptides and DNA delivery systems.

In many applications, in order to improve nanoparticle absorption, targeting strategies have been investigated that will improve the interaction of nanoparticles with the absorptive enterocytes and M cells of Peyer's patches such as use of receptor-specific ligands (e.g., lectins, vitamin B-12) or non-specific interactions of nanoparticle with the intestinal epithelia (Jung et al., 2000).

Pulmonary Administration

Nanoparticles can be incorporated in aerosol formulations to deliver therapeutic agents to the respiratory tract. The final nanoparticulate formulation may be administered either as a nebulizer (metered dose inhalers) or dry powder inhalers. Local delivery of drugs to the lung is desirable for many clinical conditions such as asthma; chronic pulmonary infections, lung cancer and cystic fibrosis (Sham, Zhang, Finlay, Roa, & Lobenberg, 2004). For both local and/or systemic delivery, the effectiveness of drug delivery by inhalation may be greatly imparted by mucociliary clearance (Sham et al., 2004). Studies have shown that nanoparticles may facilitate transport of drugs to the epithelium while avoiding undesirable mucociliary clearance (Sham et al., 2004). Other benefits of nanoparticule-based formulations are in the suitability for (i) sustained drug effect due to possible prolonged residence of drug at the site of action or absorption; (ii) controlled or targeted drug delivery. The small size of nanoparticles makes them highly suitable for pulmonary delivery because they can easily be air borne and delivered to the alveolus. It is important that the components of the nanoparticle formulation are biodegradable to avoid accumulation in the lungs and that they do not cause irritation of the air ways and lung tissue. The control of the particle size of the formulation during manufacture and the entire shelf life of the drug product is also very important for an acceptable product.

Topical

The feasibility of applying nanoparticles in topical/cosmetic preparations has been recently reviewed (Wissing & Muller, 2003). This application employed such features of nanoparticles as (a) protection of labile compounds; (b) controlled release of incorporated drugs; (c) ability of solid lipid nanoparticles to act as occlusives to increase the water content of the skin; and (d) ability of nanoparticles to serve as physical barriers on the skin for blocking UV light and, as such, for use in sunscreen formulations. One example is the application of titanium nanoparticles in sunscreen produced by Procter & Gamble (Cincinnati, OH, USA).

Application of Nanotechnology in Drug Product Life Cycle Management

All drug and drug products have certain life cycles. A drug is the active ingredient that can elicit the desired therapeutic effect when administered. A drug product therefore contains both the drug (active) that has been formulated using special processes and materials (excipients) to ensure that the drug is stable and effective for easy administration to achieve the desired therapeutic benefit. The life cycle of any product can be viewed in five stages: (a) product development stage; (b) market introduction stage; (c) growth stage; (d) mature stage; and (e) decline stage. Patent protection of the drug substance and/or formulation allows the innovator company to have a limited monopoly of the market that allows the recovery of the cost of

development as well as to make profits. It is important to note that profits from products do decline as the patents expire (at the decline stage). Also, associated generic competition results in a decrease in the revenue that is generated from the drug. Life cycle management involves coming up with new formulations that have improved performance and are novel enough to obtain patent protection and extend the life time of the drug. Therefore, management of the life cycle of a drug and drug products is very important to the success of any pharmaceutical company. In general, life cycle management can offer many benefits for various pharmaceuticals such as (i) meeting the consumer and/or patent needs; (ii) provision of improved product to the market; (iii) increased recovery of research and development costs; and (iv) extending the life of the patent. In order to overcome many market-related challenges, drug delivery systems based on nanotechnology have sufficient novelty to be effective and valuable tools in the development of unique drug products and extension of product life cycles. The ability of nanoparticle delivery systems to target the drug to the intended site offers the benefit of formulations with a reduced side-effect profile and this can be used as a life cycle management approach. The other nanotechnology property that can be used in life cycle management is the development of sustained release formulations for drugs that are at the end of their life to produce formulations that are novel and require less frequent dosing. For dugs that have low bioavailability because of poor solubility drug life cycle managers can use nanotechnology to develop formulations that have significantly increased bioavailability and thus require less drug per dose. It has been estimated that about US$65 billion in annual revenues are accounted for by pharmaceuticals with poor bioavailability which may be attributed to poor water solubility (Breen, 2006). In these cases, reducing drugs to nanoscale is a promising strategy to improve water solubility and bioavailability.

Advantages of Nanotechnology in Life Cycle Management

(a) *To revive a product's competitive edge*: Improving therapeutic benefits with reduced side effects. Patients' compliance can be improved by changing the route of administration to non-parenteral. The market response is expected to increase with presentation of a drug product for non-parenteral administration (like oral; buccal; nasal and pulmonary routes).
(b) *To shorten market entry*: The development time of a new active can be reduced considerably with advanced drug delivery systems. Nanotechnology can be applied to improve properties of a drug associated with stability, solubility and bioavailability. Application of advanced drug delivery systems can ensure that effective drugs are not discarded during the early development stages.
(c) *To extend a patent's life*: A drug can be reformulated using delivery systems that are derived from nanotechnology thereby protecting or extending a product's patent exclusivity. After patent expiration, development of a generic product of the drug will be more challenging if novel delivery systems (from nanotechnology) are used in the original formulation. Drug delivery systems can be applied to formulate a new drug product with optimal dosing or to expand the overall market

for the original patented product such as application in children or elderly.

(d) *To improve convenience*: Immediate release formulations can be reformulated into sustained release formulations that require less frequent dosing and are patentable. Drug products that are convenient to administer are more preferred and will improve patients' compliance.

Application of Nanoparticle-Based Drug Product Development

The subsection highlights various factors that will influence the performance of nanoparticle-based formulations (in vitro and in vivo). These factors should also be considered for scale up as well as during drug product development for nanotechnology-based systems.

The Importance of Size

The effectiveness of nanoparticles is greatly dependent on size, size distribution, surface properties, polydispersity index and morphology. Nanoparticle size will affect the passage through the biological barriers and the in vivo fate in the blood circulation. Large particles may pass through biological barriers with difficulties. Cell targeting may be impacted if large particles are present in blood circulation; particles may be predominantly deposited in the lungs or captured by the RES. The process of drug product development should ensure that properties, especially size, are characterized at various stages such as formulation development, storage and drug product manufacturing. It is important to evaluate the stability of nanoparticle size in blood circulation. Jung et al. (2000) reviewed various factors that influence the absorption of poly(styrene) nanoparticles from the gastrointestinal tract. The review highlighted that (i) nanoparticles with sizes less than 100 nm showed higher uptake by absorptive enterocytes than nanoparticles with sizes greater than 300 nm; (ii) the uptake of nanoparticles with sizes less than 100 nm by follicle-associated epithelia is more efficient than uptake via absorptive enterocytes; (iii) uptake of nanoparticles with sizes greater than 500 nm by absorptive enterocytes is very unlikely; and (iv) only nanoparticles with sizes less than 500 nm can reach the general circulation.

Surface Characteristics

The surfaces of the nanoparticles will be dictated by the nature, type and amounts of the components in the formulations. For instance, positively charged nanoparticles or liposomes are obtained using various cationic lipids and polymers such as dioleoyl trimethylammonium propane (DOTAP), chitosan and poly-L-lysine (PLL). Immediately upon injection into the blood stream, colloidal particles may become coated with various blood components (opsonization). The rate and extent of particle coating by blood components is connected to RES-mediated clearance. In many therapeutic applications, rapid and extensive uptake of nanoparticles into the RES system is a significant disadvantage since nanoparticles will be withdrawn from blood circulation into the liver and spleen. Based on studies

using liposomes and nanoparticles, the blood circulation times of nanoparticles can be increased by modification of nanoparticle size, modification of nanoparticle composition and rigidity and modification of nanoparticle hydrophilicity. For instance, long circulating nanoparticles have been prepared with a layer of amphiphilic polymer chains such as coating nanoparticle surface with materials like polyethylene glycol (PEG), polyoxyethylene, poloxamers and poloxamines (Brigger et al., 2002; Kim & Nie, 2005). The modification of particle surface by polymers can be performed by polymer adsorption, incorporation during production of nanoparticles, covalent attachments to nanoparticle surface. It is important to use a method that will ensure that the adsorbed polymer is not easily displaced from the nanoparticle surface under in vivo blood shear flow. Also, the density of the steric barrier imposed by the adsorbed polymer must be sufficient to suppress the endogenous opsonization process or to directly prevent particle–macrophage interactions (Moghimi & Hunter, 2001).

Development of nanoparticles for the oral route of administration will pose a different requirement for surface characteristics. Studies on nanoparticles' affinity to the M cells have shown that a combination of nanoparticle hydrophilicity and surface charge can influence nanoparticle uptake along the GIT (Jung et al., 2000).

Formulating Materials

It is very important to choose formulating materials that are commercially available and safe. Drug loading efficiency and nanoparticle performance in drug delivery will be dependent on the formulating materials. For instance, for solid lipid nanoparticles, it has been reported that the average particle size increases when lipids with higher melting points are used (Mehnert & Mader, 2001). Other critical factors that will affect nanoparticle size and size distribution are the velocity of lipid crystallization, the lipid hydrophilicity (influence on self-emulsifying properties) and the shape of the lipid crystals. Compositions of lipids from different suppliers should be evaluated. Small changes in lipid composition may affect nanoparticle dispersion and retard the crystallization process. The amount of the formulating materials must be optimized. In cases where surfactants are required to prepare nanoparticles, the type and concentration of surfactant will determine the final nanoparticle properties and drug loading. Increasing the amounts may result in particles of large sizes and high polydispersity. In the development of nanoparticles for oral administration, polymers such as chitosan, polyacrylate and starch are known to facilitate paracellular transport (Jung et al., 2000).

Development of Nanoparticles into Dosage Forms

Nanoparticulate drug delivery systems can be developed for parenteral, oral or local administrations. The type of nanoparticles must be selected based on the drug and the intended mode of administration. Nanoparticules for parenteral delivery have to be biodegradable such as are polyacrylates or polyesters. The colloidal particles may be administered as aqueous

suspension or converted into powder by lyophilization. The lyophilized powder will then be reconstituted before administration.

For oral drug delivery, non-degradable polymers (such as cellulose or acrylate derivatives) can be used. The nanoparticles could be administered in the form of aqueous dispersion as the final dosage form. In most cases for oral application it will be desired to incorporate nanoparticle suspensions in solid dosage forms such as granules, spheres, pellets, capsules and tablets.

Secondary Production Steps

Sterilization: Nanoparticles for parenteral administration require sterile formulation which can be accomplished by aseptic process, filtration, gamma irradiation and heating. The filtration process is only suitable for formulations with particles below 200 nm. It is expected that filtration should not alter the properties of the nanoparticles with respect to size, size distribution, drug loading and drug release. The choice of gamma irradiation should be based on the chemical stability of the drug. Free radicals that are formed during gamma sterilization can initiate chemical modification of drugs. Sterilization by heat has been used for liposomes (Zuidam, Lee, & Cromelin, 1992). A major concern in the application of heat to sterilize nanoparticles is temperature-related changes of the physical properties. It is possible that sterilization might result in the formation of toxic degradation products even when the nanoparticle size is maintained (Mehnert & Mader, 2001). In general, it is important to conduct post-sterilization testing to ascertain the physical and chemical stability of the drug as well as nanoparticles.

Lyophilization: An important quality of nanoparticulate delivery systems is storage stability. This involves physical and chemical stability, preservation of particle size and prevention of degradation reactions such as hydrolysis. Storage stability also covers (i) stability of particle size distribution and prevention of crystal growth by Oswald ripening and (ii) stability of nanoparticle formulations during shipping. In large-scale manufacturing, it is important to convert the nanoparticle suspensions to powders so as to reduce the bulk volume and to improve the storage stability. Lyophilization is a promising way to improve chemical and physical stability over a long period of time. The resultant lyophilized powder of the nanoparticles can be reconstituted to achieve the nanoparticle suspensions or the lyophilized powder may be converted into other dosage forms. In the case of products for reconstitution the development process must determine that the particle size of the product after reconstitution does not change throughout the shelf life of the product. Essentially, lyophilization is achieved in two major steps of freezing the sample and evaporation of water under vacuum. It is important to state that freezing nanoparticle suspensions might bring about instability relating to changes in physical characteristics, particle aggregation, drug loading, osmolarity and pH. The quality of the lyophilized powder can be improved by using diluted nanoparticle suspensions since diluted suspensions will have higher sublimation velocities and a higher specific surface area (Pikal, Shah, Roy, & Putman, 1990). The process of drug development should establish the type, amount and nature of cryoprotectors. Cryoprotectors

function in many ways: (a) they decrease the osmotic activity of water and favor the glassy state of the frozen sample; (b) they prevent the contact between discrete nanoparticles; and (c) they interact with the polar head groups of surfactants to maintain a hydration shell. Examples of cryoprotectors that have been included in nanoparticulate formulations are sorbitol, mannose, trehalose, glucose and polyvinylpyrrolidone.

Spray-Drying: Spray-drying of nanoparticle suspensions could be applied as a less expensive alternative to lyophilization. The application of spray-drying for developing nanoparticles into dosage forms is expected to require little modifications since the process has been routinely applied in the food and pharmaceutical industries. Spray-drying consists of four steps: (a) atomization of the feed into spray; (b) spray–air contact; (c) drying of the spray; and (d) collection of the dried powder from the drying air. The main drawback for spray-drying application in converting nanoparticle suspension to powder is the application of temperature which can cause drug instability, particle aggregation and possible interference with drug entrapment in nanoparticles. Freitas and co-workers obtained a redispersible powder by spray-drying solid lipid nanoparticles. The resultant powder complied with the general requirements of intravenous injections (Freitas & Muller, 1988; Mehnert & Mader, 2001).

Dosage Form Characterization: Nanotechnology-based drug delivery systems can be formulated as parenteral dosage forms, oral solid dosage forms (e.g., granules, pellets or tablets) or oral liquid dosage forms for systemic uptake or local residence within the gastrointestinal tract. For peroral administration, the nanoparticles could be administered in the form of an aqueous dispersion; however this may have poor stability of the drug or polymer in the aqueous environment and it is also difficult to mask poor taste and so a solid dosage form may be required. To make a solid dosage form requires spray-drying or lyophilization of the dispersion together with suitable excipients followed by incorporation of the dry powder into capsules, tablets or pellets (Allènmann, Gurny, & Doelker, 1993). The nanoparticles could also be converted into a solid dosage form by granulation with suitable excipients followed by drying or through layering of the dispersion onto pellets in a fluidized bed followed by coating with a polymer if necessary (Schmidt & Bodmeier, 1999). For thermally unstable drugs this approach has limited utility. Typically in granulation, the drug and the excipients are granulated with a binder solution; however, in the case of nanoparticle suspensions the binder may be dissolved directly into the nanoparticle suspension. Alternatively, the suspension can be combined with an aqueous binder solution followed by granulation of the solid excipients. The advantage of this approach is that once the nanoparticles are formed the dosage form can be developed using equipment and expertise already available in a typical pharmaceutical company that manufactures solid dosage forms such as tablets and capsules. The challenges for formulation of nanoparticles into solid dosage forms include excipient compatibility and redispersibility of the nanoparticles after contact of the solid dosage form with aqueous media. Incompatibility between the nanoparticles and the binder molecules could be caused by electrostatic interactions of oppositely charged polymer particles and binder molecules, by bridging flocculation of the polymeric particles through

adsorbed binder or by osmotic effects. Additionally, for a successful product, the nanoparticles need to be released from the dosage form with their original particle size distribution and other properties in order to maintain the advantages of a nanoparticulate dosage form such as oral absorption and enhanced dissolution of lipophilic drugs (Schmidt & Bodmeier, 1999). During the preparation of the nanoparticles and their conversion into solid dosage forms flocculation or coalescence of the particles during the preparation step and incompatibilities with excipients can present challenges that need to be avoided. The reproducibility of the process used to convert the nanoparticles into solid dosage forms is also a critical part of developing a commercial product. In order to develop commercially viable nanotechnology-based drug products the processes for manufacturing the nanoparticles need to be scalable and amenable to validation. The particle size distribution and the physical characteristics of the nanoparticles need to be maintained throughout the manufacturing process and during the shelf life of the product.

The scale-up issues can be overcome as demonstrated by Yamanouchi's nanotechnology-based drug product Nanobase® that is in the market. The product is based on solid lipid nanoparticles (SLN) that were developed as an alternative carrier system to emulsions, liposomes and polymeric nanoparticles as a colloidal carrier system for controlled drug delivery. Solid lipid nanoparticles consist of a solid lipid matrix, normally containing the drug, with an average diameter of less than 1 μm (Kayser, Lemke, & Hernandez-Trejo, 2005). The system contains surfactant to prevent aggregation and to stabilize the dispersion. Another drug that has been formulated using nanotechnology-based approaches is paclitaxel, a microtubule-stabilizing agent that promotes tubulin polymerization, disrupting cell division and causing cell death (Kim & Nie, 2005). The drug displays neoplastic activity against primary epithelial ovarian carcinoma, breast, colon and lung cancers. It exhibits poor aqueous solubility and the drug product Taxol™ is formulated with Cremophor and ethanol. In a new nanotechnology-based formulation, Abraxane, for treatment of metastatic breast cancer, paclitaxel is conjugated to albumin nanoparticles. One advantage of the new formulation is that it takes advantage of albumin receptors to improve drug delivery to the cancer cells (Kim & Nie, 2005). This targeting of the drug to the cancer cells using nanotechnology may have the added benefit of reducing exposure of non-cancerous cells to the drug, thereby reducing side effects.

Drug Product Development

Nanotechnology-based product development begins with the selection of the colloidal system, i.e., liposome based, microemulsion based, nanocrystal based or nanoparticle based. Irrespective of the system, the next steps should include selection of the components used to make the systems. In order to facilitate product development within an acceptable time frame the components selected must have an adequate safety profile to be in a product approvable by the regulatory authorities. If components that do not have any or adequate safety data are chosen then the development

process must include the generation of toxicological data to support product development and approval. The required safety studies are outlined in the FDA May 2005 guidance document titled "Guidance for Industry Nonclinical Studies for the Safety Evaluation of Pharmaceutical Excipients". The full set of studies required depends on the route of administration of the products for which the excipients will be used and on the duration of treatment.

During development the compatibility of the excipients with the drug needs to be evaluated in order to avoid stability issues later on in the development process. Also, the optimum particle size distribution of the nanoparticles needs to be determined early on in the development process. Another critical consideration is the selection of nanoparticle formulations that will achieve optimal drug loading efficiency without interfering with drug release and therapeutic potency. The manufacturing process will then need to be optimized so that the particle size distribution is reproducible from batch to batch and that the reproducibility is maintained throughout the scale-up process. For successful commercialization of a nanotechnology-based formulation drug loading needs to be reproducible throughout the scale-up process. Additionally, drug release from the nanoparticle formulation needs to be reproducible and a specification for this needs to be set. Sufficient controls with supporting specifications and analytical methods need to be established so that batch-to-batch variability can be kept within an acceptable range throughout the development and commercial lifetime of the formulation.

For processes where the process of making the nanoparticles involves using organic solvent it is essential that acceptable limits for residual solvents are established. Residual solvents are organic volatile chemicals that are used or produced in the manufacturing of drug substances or excipients or in the preparation of drug products.[2] According to the guidance, all residual solvents should be removed to the extent possible to meet specifications, good manufacturing practices or other quality-based requirements. The amount of any residual solvent that is present in the drug product must be safe, based on available safety data. If safety data are not available or are inadequate it is the responsibility of the manufacturer to provide a justification for residual levels in the drug product. Once residual solvent methods are established analytical methods for determining these in the drug product need to be developed.

In order to commercialize a nanotechnology-based formulation the manufacturing processes for the nanoparticles and the final dosage form will need to be validated according to the principals of process validation for drug products. Validation refers to the establishment of documented evidence which provides a high degree of assurance that the process will consistently produce a product meeting its predetermined specifications and quality attributes.[3] Stability data on the drug product will also need to be generated as per industry practice and following applicable regulatory guidance.

---

[2] ICH Harmonized Tripartite Guideline, Impurities: Guideline for Residual Solvents Q3C (R3)

[3] FDA Guideline of General Principles of Process Validation, May 1987

Some examples of commercially available nanotechnology platforms for drug delivery are (i) BioOral nanocochleates that are comprised of lipid bilayers (BioDelivery Sciences, Newark, NJ, USA); (ii) NanoCap micellar nanoparticle for water-insoluble drugs (NaNoCarrier, Chiba, Japan); (iii) injectable nanospheres for therapeutic or diagnostic agents (Targetsome, Palo Alto, CA); (iv) Nanoshells for optical therapies developed by NanoSpectra Biosciences (Houston, TX); and (v) Nanoemulsions for antimicrobial drugs developed by NanoBio (Ann Arbor, MI).

References

Agostiano, A., Catalano, M., Curri, M.L. Della, Monica, M., Manna L., Vasanelli, L. (2000) Synthesis and structural characterization of CDs nanoparticles prepared in four-components "water-in-oil". microemulsion. Micron. 31, 253–258

Allènmann, E., Gurny, R., Doelker, E. (1993) Drug-loaded nanoparticles-preparation methods and drug targeting issues. Eur. J. Biopharm. 39, 173–191.

Attwood, D. (1994) Microemulsions. In: J Kreuter (eds) Colloidal drug delivery. New York Marcel Dekker

Breen, P.V. (2006) Small-tech big potential. Drug Deliv, November 2006, 30–31

Brigger, I., Dubernet, C., Couvreur, P. (2002) Nanoparticles in cancer therapy and diagnosis. Adv. Drug Deliv. Rev. 54, 631–651

Dearn, A.R. (1995) Atovaquone pharmaceutical compositions. European patent EU 0/075711, August 5

Delie, F., Blanco-Prieto, M.J. (2005) Polymeric particulates to improve oral bioavailability of peptide drugs. Molecules 10, 65–80.

Desai, M.P., Labhasetwar, V., Walter, E., Levy, R.J., Amidon, G.L. (1997) The mechanism of uptake of biodegradable microparticles in Caco-2 cells is size dependent. Pharm. Res. 14, 1568–1573

Fang, J., Stokes, K.L., Wiemann, J., Zhou, W. (2000) Nanocrystalline bismuth synthesized via an in situ polymerization microemulsion process. Mater. Lett. 42, 113–120

Fahmy, T. M. Fong, P.M. Goyal, A., Saltzman, W.M. (2005) Targeted for drug delivery. Nanotoday, August, 18–26

Fendler, J.H. (1994) Membrane-mimetic approach to advanced materials. In Advances in Polymer Science 113, Springer Berlin

Feng, S. (2004) Nanoparticles of biodegradable polymers for new-concept chemotherapy. Expert Rev. Med Devices 1, 115–125

Freitas, C., Muller, R.H. (1998) Spray-drying of solid lipid nanoparticles. Eur. J. Pharm and Biopharm. 46, 145–151

Gasco, M.R. (1997) Solid lipid nanospheres from warm microemulsions. Pharm. Tech. Eur. 9, 52–58

Huettenrauch, R. (1984) Molecular pharmaceutics. Part 86. Stability of activated states in solid drug forms. Pharmazie 39, 272

Hu, J., Johnston, K.P., Williams, R.O. (2004) Nanoparticle engineering process for enhancing the dissolution rates of poorly water soluble drugs. Drug Dev Ind. Pharm. 30, 233–245

Jung, T., Kamm, W., Bretenbach, A., Kaiserling, E., Xiao, J.X., Kissel, T. (2000) Biodegradable nanoparticles for oral delivery of peptides: is there a role for polymers to affect mucosal uptake? Eur. J. Pharma. Biopharm. 50, 147–160

Kayser, O., Lemke, A., Hernandez-Trejo, N. (2005) The impact of nanobiotechnology on the development of new drug delivery systems. Curr. Pharm. Biotech. 6, 3–5

Kim, G., Nie, S. (2005) Targeted cancer nanotherapy. Nanotoday 28–33
Kipp, J.E. (2004) The role of solid nanoparticle technology in the parenteral delivery of poorly water-soluble drugs. Int. J. Pharm. 284, 109–122
Knight, P. (2006) Transforming potential for difficult drugs. Drug Delivery, November 2006, 6–8
Landfester, K. (2001) Polyreactions in miniemulsions Macromol. Rapid Commun. 22, 896–936
Langevin, D. (1991) Microemulsions-interfacial aspects Adv Colloid Interface Sci. 34: 583
Liversidge, G.G., Cundy, K.C. (1995) Particle size reduction for improvement of oral bioavailability of hydrophobic drugs. Int. J. Pharm. 125, 91–97
Lockman, P.R., Mumper, R.J., Khan, M.A., Allen, D.D. (2002) Nanoparticle technology for drug delivery across the blood-brain barrier. Drug Dev. Ind. Pharm. 28.
Mehnert, W., Mader, K. (2001) Solid lipid nanoparticles: production, characterization and applications. Adv. Drug Del. Rev 47, 165–196
Muller, R.H. Jacobs, C., Kayser, O. (2001) Nanosuspension as particulate drug formulations in therapy rationale for development and what we can expect for the future. Adv. Drug Deliv. Rev. 47, 3–19
Mumper, R.J. Cui, Z., Oyewumi, M.O. (2003) Nanotemplate engineering of cell-specific nanoparticles. J. Disp. Sci. Tech. 24, 569–588
Moghimi, S.M., Hunter, A.C. (2001) Capture of stealth nanoparticles by body defences. Crit. Rev. Ther. Drug Carrier Sys. 6, 527–550
Oyewumi, M.O., Mumper, R.J. (2002) Gadolinium loaded nanoparticles engineered from microemulsion templates. Drug Dev. Ind. Pharm. 28, 317–328
Panchapakesan, B. (2005) Nanotechnology: Part 2 Tiny Technology-tremendous therapeutic potential. Oncology Issues Nov/Dec 2005
Pikal, M.J. Shah, S., Roy, M.L., Putman, R. (1990) The secondary drying stage of freeze drying: drying kinetics as a function of temperature and chamber pressure. Int. J. Pharm. 60, 203–217
Rabinow, B.E. (2004) Nanosuspensions in drug delivery. Nat. Rev Drug Discov. 3, 785–796.
Schmidt, C., Bodmeier, R. (1999) Incorporation of polymeric nanoparticles into solid dosage forms. J. Control. Rel. 57, 115–125
Setler, 1995, P. (1999) Identifying new oral technologies to meet your drug delivery needs for the delivery of peptides and proteins and poorly soluble molecules. IIR Limited Drug Delivery Systems, London, March 1999
Sham, J.O., Zhang, Y., Finlay, W.H., Roa, W.H., Lobenberg, R. (2004) Formulation and characterization for aerosol delivery to the lung. Int. J. Pharm. 269, 457–567
Ward, G.H., Schultz, R.K. (1995) Process-induced crystallinity changes in albuterol sulfate and its effect on powder physical stability. Pharm. Res. Pharm. Res. 12, 773–779
Wissing, S.A., Muller, R.H. (2003) Cosmetic applications for solid lipids nanoparticles (SLN). Int. J. Pharm. 254, 65–68
Wu, N.Z. Da, D., Rudoll, T.L., Needham, D. Whorton, A.R. Dewhirst, M.W. (1993) Increased microvascular permeability contributes to preferential accumulation of stealth liposomes in tumor tissue. Cancer Res. 53, 3765–3770
Yi, Y.M., Yang, T.Y., Pan W.M. (1999) Preparation and distribution of 5-fluorouracil I-125 sodium alginate-bovine serum albumin nanoparticles. World J. Gastroenterol. 5, 57–60
Yoo, H.S. Lee, K.H. Oh, J.E., Park, T.G. (2000) In vitro and in vivo antitumor activities of nanoparticles based on doxorubicin-PLGA conjugates. J. Control. Rel. 68, 419–431
Zuidam, N.J., Lee, S.S.L., Crommelin, D.J.A. (1992) Sterilization of liposomes by heat treatment. Pharm. Res. 10, 1591–1596

21

Nanopharmaceuticals: Challenges and Regulatory Perspective

Rakhi B. Shah and Mansoor A. Khan

Introduction

Products in nanometer size range offer "uniqueness" because of their altered properties as compared to their macro-counterparts. Improved solubility, permeability, or targetability of nanoparticles seems to be beneficial in the drug delivery area. As an example, "nano" paclitaxel molecules may reach a tumor cell line sooner than the "bulk" paclitaxel. Similarly, if a nanodrug is unable to reach a particular receptor, specialized nanoparticles have been proven to have the ability to reach that receptor (Dubey, 2006). Therefore, there is a lot of interest in using a nanotechnology platform to deliver drugs, and it explains the spurt in funding for nanotechnology research.

The research and development funding for nanotechnology from government and industry is estimated at nearly US$10 billion globally for 2005 (Lux research, 2006). By 2014, it is estimated that the global value of nanotechnology products will exceed US$2.5 trillion (Lux research, 2004). After formation of National Nanotechnology Initiative by the US government ("NNI", 2004), most developed countries have also focused their activities in the nanotechnology area. Japan and Europe have programs supported by their government. Other countries are also moving toward nanotechnology research. For example, Canadian National Research Council created the National Institute of Nanotechnology with substantial funding. Other countries including Korea, Australia Russia, Ukraine, and Mexico, as well as some Eastern European countries and many of the Asian countries, have invested substantially in nanotechnological research and development activities supported by either government or other organizations (Roco, 2003). International activities and agreements and

Disclaimer: The opinions expressed in this chapter are only of authors and do not necessarily reflect the policy and statements of the FDA.

M.M. de Villiers et al. (eds.), *Nanotechnology in Drug Delivery*, DOI: 10.1007/978-0-387-77667-5_21,

periodic workshops are some of the efforts showing a growing interest in nanotechnology globally.

Technology has always been a two-edged sword, offering both benefits and risks. There are increasing concerns that new nanotechnologies might bring risks to human health and environment (Maynard, 2006a). Due to their small size, there is fear that they might unintentionally penetrate the normal biological barriers that protect human health. Research has demonstrated that exposure to nanoparticulates might be associated with inhalation toxicity including pulmonary edema (Donaldson et al., 2002), immune adjuvant effects (Granum & Lovik, 2002), and systemic effects including blood coagulation and cardiovascular effects (Oberdoster, 2001; Borm & Kreyling, 2004). Also there is growing public fear due to possible "nanotoxicity" and its impact on socio-economic growth (Saxton, 2007). Some researchers have called for increasing the government's power to regulate nanoproducts (Davies, 2006; Kimbrell, 2006). However, others including the UK's Council for Science and Technology (CST) have a different position on this. "Existing preclinical trials for medicines and medical devises are very extensive, requiring manufacturers of medical devices to carry out extensive risk analysis" (UK, 2007). MHRA (Medicines and Healthcare Products Regulatory Agency of UK) has concluded that "the existing trials procedures are sufficiently rigorous to safely include medicines and medical devices that incorporate nanotechnologies. CST would thus agree that no additional legislation for nanomedicines or new medical devices is required at the current time" (UK, 2007). Attempts to expedite nanotechnology in drug delivery should include hastening the benefits while minimizing any potential downside.

Depending upon the preparation method and choice of excipients, the nanoparticles obtained can be of several different types. Published literature indicates that the type of nanoparticles includes nanocrystals, nanosuspensions, Dissocubes, liposomes, self-emulsifying drug delivery systems (SEDDS), nanoemulsion, dendrimers, fullerenes, nanotube, quantum dots, nanoshells, and a few others. The question most commonly asked is whether Food and Drug Administration (FDA) has the capability to approve all these types of products, if submitted. FDA is a science-based agency and has approved several complex products in the past. If appropriate science and technology demonstrates that a product can be consistently and reproducibly prepared with a desired quality and is safe and effective to the patients/public that it is intended for, such products can be approved. The next logical question would be whether one has the science and technology needed and what the challenges are.

Some of the nanoproducts have demonstrated safety to the point that their benefits to patients have been shown to outweigh the risks associated with them. Products such as Doxil®, Myocet®, Ambisome®, and Depocyt® have been approved which are nanometer in size range ("FDA"). However, some of the newer ones that are multifunctional are still evolving in terms of product development, safety, and efficacy for therapeutic use. The present chapter provides a brief overview of the methods and the type of nanoproducts, manufacturing, characterization and safety challenges, and finally the regulatory perspectives with respect to the state of science in these areas.

Manufacturing Challenges for Nanopharmaceuticals

Although historically nanoparticles were prepared to enhance the solubility of poorly soluble drugs, the technology has been applied to highly water-soluble drugs such as peptide and protein therapeutics as well (Lamprecht et al., 2000; Kramer et al., 2004) and for targeted drug delivery to organs such as brain (Lockman et al., 2002) and in the treatment of cancer (Brannon & Blanchette, 2004). Conventionally, nanoparticles have been prepared mainly by (i) size reduction, (ii) precipitation or emulsification, (iii) supercritical fluid technology, (iv) spray-drying, and (iv) polymerization. The first three methods may also be considered as top-down methods where the particle size is decreasing from coarser to finer particles. In the last method of polymerization, the growth from an atomic to molecular level takes place with particles ranging from nanometer to micrometer size range and is considered as bottom-up method. Table 21.1 lists some of the commercial nanotechnologies useful in drug delivery. A prime challenge for manufacturers is ensuring reproducibility and quality of nanotechnology products.

Size Reduction

Reduction in particle size and hence increasing the surface area might lead to a higher dissolution rate expressed by an equation leading to subsequent increase in the bioavailability for poorly soluble drugs (Liversidge & Cundy, 1995; Thanos et al., 2003; Waterman & Sutton, 2003; Garner et al., 2002; Nakada et al., 1996). According to Noyes–Whitney equation, dissolution rate linearly depends on surface area which can be depicted as

$$\frac{\mathrm{d}c}{\mathrm{d}t} = kA(C_\mathrm{s} - C) \tag{1}$$

where dc/dt is the rate of dissolution; C_s and C are solute's saturation solubility and concentration in the bulk phase, respectively; k is a dissolution

Table 21.1 Nanotechnologies in drug delivery and primary principle used to create nanoparticles or prevent aggregation (Muller et al., 1998; Liversidge, 1996; Liversidge & Cundy, 1995; Kipp, 2004; Muller et al., 2002; "Soliqs"; "Biodelivery science"; "Nucryst"; "Crititech"; "Fivestar tech").

Nanotechnologies in drug delivery	Principle
Dissocubes™, SkyePharma, London, UK	Piston-gap homogenization
NanoCrystal™, Elan, Prussia, PA	Wet-milling and stabilizer adsorption
Nanomorph™, Soliqs Abbott, Ludwigshafen, Germany	Conversion from crystalline to amorphous nanoparticles
Nanoedge™, Baxter, Round Lake, IL	Homogenization, microprecipitation, emulsification
Nanopure™, Pharmasol, Berlin, Germany	High-pressure homogenization
Nanocochelate (Bioral)™, BioDelivery, Morrisville, NC	Phospholipid cation precipitate as delivery vehicle
Silcryst™, Nucryst, Wakefield, MA	Nanocrystalline silver coating
CritiTech™, CritiTech, Lawrence, KS	Precipitation with compressed antisolvent
CFC Technology™, Five star tech, Cleveland, OH	Controlled flow cavitation

rate constant, and A is the surface area of the solute. Since reduction in particle size results in the increase in the surface area, rate of dissolution can be achieved by decreasing the particle size (Martin et al., 1983).

Comminution of poorly soluble drugs by conventional techniques produces overall particle size distribution in micrometer size range. The process of micronization increases the dissolution velocity of the drug due to the increase in surface area but does not change the saturation solubility. At very low saturation solubility, the achieved increase in dissolution velocity does not lead to a sufficiently high bioavailability. Therefore, drug companies are utilizing "nanoscience" to produce drug particles in nanometer range (Liversidge et al., 1991). Enhancing solubility is highly desirable in discovery of drugs where the molecules with poor solubility (BCS II and IV) pose a significant challenge to the formulation scientist at the preclinical as well as clinical development stage. Size reduction techniques include milling, microfluidization, or piston-gap homogenization.

Milling: Conventional milling with modifications can be used for producing nanoparticles which is usually operated below a critical speed above which no size reduction takes place. Also, size of the balls is an important criterion for obtaining the particles of desired size. This patented Nano-Crystal® technology was developed by NanoSystems (Liversidge et al., 1991) now acquired by Elan (Table 21.1). Rapamune® (sirolimus, Wyeth) and Emend® (Merck) use this technology. Challenges in this type of technique include erosion of the milling material (Redzisqewski, 1997; Joost & Schwedes, 1996; Chandrasekaran, 1993; Kerr & Reed, 1992) and generation of very high surface free energy. To reduce this energy, the nanoparticles will either have to reagglomerate to decrease the surface area or a formulation has to have a surfactant, polymer, or other stabilizers to keep them from agglomerating. Therefore, one has to balance out the toxicity associated with the amount and type of these additives with the stability of these systems. Also, cleaning is an issue as fine particles potentially remain even after removal of the grinding medium from the suspension. Moreover, the time required to achieve a desired size range might vary from hours up to several days (Liversidge, 1996).

Microfluidization or piston-gap homogenizer: This is a size reduction technique in which nanoparticles or nanosuspensions (DissoCubes®) are produced by high-pressure homogenization. The nanosuspensions were developed at Drug Delivery Services GmbH in Germany (Muller et al., 1998), now acquired by SkyePharma PLC. The feed particles play a vital role in the process performance (Kipp, 2004). The main factors contributing to size reduction include process parameters such as pressure, number of cycles applied, and material properties (Muller et al., 1996, 2001; Jacobs et al., 2000, 2001). Liposomes are also produced by this mechanical method in which the prepared liposomes by film method are size reduced (Lichetnberg & Barenholz, 1988). Manufacturing challenges include progressively larger amounts of energy input to sustain further size reduction. Also, clogging of the piston is a serious problem and scale-up is generally very difficult for this type of operation. Heavy metal contamination might also pose a serious problem in high-pressure homogenization (Krause et al., 2000). For liposomal drug products, low efficiency of encapsulation has usually been cited in literature (Crommelin, 1994).

Precipitation or Emulsification

This technique is alternatively called coacervation in which the drug is first dissolved and mixed with a miscible organic antisolvent. After the formation of a stable emulsion, the organic solvent is evaporated, e.g., Neoral® (microemulsion of cyclosporine) by Novartis. Alternatively, oil-based systems are also used to produce nanopharmaceuticals (Nazzal et al., 2002; Palamakula et al., 2004). Manufacturing challenges include variability of mixing processes which give rise to different particle size distribution. Also spontaneity of crystal growth once the nucleation occurs poses problems for controlling the particle size distribution within a narrow range. Furthermore, non-aqueous solvents utilized in the precipitation process must be reduced to toxicologically acceptable levels in the end product. A Quality by Design approach with control by PAT sensors has recently been reported (Zidan et al., 2007). Precipitation can be coupled with high-shear processing as in the case of Nanoedge® process (Baxter Healthcare Corporation). Because of their small size and shape, particles produced by rapid precipitation are often more friable than the starting material and hence more susceptible to fragmentation. Further, there is a need to remove solvent after homogenization. If solvent impurities remain in the drug-loaded NPs, then these become toxic and may degrade the pharmaceuticals within the polymer matrix.

Supercritical Fluid Technology

Supercritical fluids produce solvent-free particles and have become an environmentally friendly alternative to produce microparticles (Tom & Debenedetti, 1991a,1991b; Randolph et al., 1993; Mishima et al., 2000; Mawson et al., 1994) and more recently nanoparticulates (Chattopadhyay & Gupta, 2001a,b; Gupta & Chattopadhyay, 2000; Reverchon, 1999; Reverchon et al., 1998). In this method, the solute of interest is solubilized in a supercritical fluid and the solution is expanded through a nozzle. A development challenge includes the selection of a polymer as most polymers exhibit little or no solubility in supercritical fluids, thus making the technique less of practical interest (Mishima et al., 2000; Tom et al., 1994).

Spray-Drying

In this method, nanoparticle suspensions are first prepared by wet comminution in the presence of stabilizers followed by spray-drying. This process was used to prepare nanoparticles of an API (active pharmaceutical ingredient) in a Buchi mini spray dryer (Lee, 2003). A thorough understanding of the processing variables and their effect on the type of nanoparticles should be very helpful in product development.

Polymerization

Nanoparticles can also be prepared by polymerization of monomers. A review for this technique is presented elsewhere (Soppimath et al., 2001). The particle size is a function of the type and concentration of the

stabilizer and/or surfactant used, pH of the medium, concentration of monomer, speed of stirring. For example, emulsion polymerization provides particles of about 50–200 nm in diameter, emulsifier-free emulsion polymerization produces particles of about 100–1000 nm (0.1–1.0 μm), dispersion polymerization gives particles in the region of 0.3–10 μm, and suspension polymerization leads to the formation of particles of about 20 μm–2 mm (Arshdy, 1988). Fullerenes and dendrimers are some of the examples of nanopharmaceuticals in development (Tomalia et al., 2007; Jensen et al., 2005). Major drawbacks such as use of low pH (around 2) and cytotoxicity (Lherm et al., 1992) have presented serious issues to be addressed for use of this technique. Residual solvents and toxicity of monomers might present a challenge to manufacturers as well as regulators while dealing with such type of preparations. Safer monomers are being developed in order to overcome this drawback (DeKeyser et al., 1989, 1991; Mabela et al., 1993).

Characterization Challenges for Nanopharmaceuticals

Nanomaterials might have chemical, physical, or biological properties different from their large counterparts. Due to extremely small size and high ratio of surface area to volume, they might also have differing magnetic, electric, or optical activity. The characterization of nanoparticles poses a challenge to developers as well as regulators in terms of these properties. Two similar materials may have subtle but significant differences that determine their behavior and in such instances, they become extremely difficult to characterize. Validated assays are important for detecting and quantifying nanoparticles in tissues and medical products and how physical characteristics may impact product quality and performance. All the issues are critical for demonstrating control of a production process and for justifying drug release parameters and bioequivalence testing approaches. Additional standard test methods might ensure appropriate consistency and safety of nanoparticles for drugs and biologics. Nanoparticles might not necessarily be unsafe but some are new for safety evaluation (Taylor, 2006). Table 21.2 lists some of the physicochemical parameters for nanopharmaceuticals and measurement methods. There are additional methods available in literature which are compiled elsewhere (Kreuter, 1994). The following are some of the characteristics which are thought to be important.

Particle Size Distribution and Morphology

Particles and particle size distribution (PSD) significantly contribute to the mechanical strength as well as thermal and electrical properties of the final material (Wong et al., 2007). The term size is subject to controversy regarding size range as the length scale may be a hydrodynamic diameter or geometric length appropriate to the intended use of the nanoparticle. Also polydispersity and heterogeneity of samples become an issue. The particle size standards and validation of such methods remain to be addressed. The default shape for nanodrugs is thought to be spherical, but cylinders, disks, cubes, needles, and random shapes do exist (Vinee et al., 2006). Monitoring the presence of particles, powder size, and distribution

Table 21.2 Physicochemical characterization of nanopharmaceuticals (Kreuter, 1994; Haskell, 2006).

Parameter	Conventional methods
Particle size, distribution, and particle morphology*	Dynamic light scattering Photon correlation spectroscopy Scanning electron microscopy* Transmission electron microscopy* Atomic force microscopy*
Surface area, porosity	Gas adsorption
Surface charge, hydrophilicity	Electrophoresis Zeta potential Laser Doppler anemometry
Surface property	Static secondary ion mass spectroscopy Mössbauer spectroscopy
Surface element analysis	X-ray photoelectron spectroscopy
Density	Pycnometer
Molecular weight	Gel or size-exclusion chromatography
Purity	Spectroscopy, FTIR, NMR
Polymorphism, crystalline form	X-ray diffraction Differential scanning calorimetry
Residual solvents	Gas chromatography
Drug release	Release testing Turbidity

* Particle morphology can be characterized with microscopic methods only

data is an important aspect of process control. Mechanisms of agglomeration, adhesion, and particle–particle interaction in particulate materials need to be understood to solve current challenges in the pharmaceutical industry. A workshop was organized at the National Institute of Standards and Technology (NIST) to identify particle size measurement challenge which identified need for standards and potential technologies for adequate size distribution measurements (Jillavenkatesa et al., 2002). Dynamic light scattering and gravitational sedimentation techniques, atomic force microscopy (AFM), scanning and transmission electron microscopy are some of the measurement techniques currently used (Haskell, 2006). As light scattering methods do not give an idea of particle morphology, microscopic methods become an attractive alternative. Particles can be measured at ambient condition in AFM, while electron microscopy requires vacuum chambers and conductivity of the specimen. Precision and accuracy of such measurements is a main consideration when it is important to ensure that PSD lies within certain limits. National Characterization Laboratory (NCL, an alliance of NCI) is also developing nanopharmaceutical-specific assay methods which include particle size, shape among others ("NCL"). It is important to consider the fact that the particle sizes can be very different depending upon the method selected.

Complexity and Heterodispersity

Complexity and heterodispersity of nanopharmaceuticals are very difficult to address with current technologies. Lebovitz (2006) recommended

classification of nanomaterials by structural complexity and inherent heterogeneity rather than by size: low complexity (similar to small-molecule drugs); intermediate complexity (similar to biologicals); high complexity (new category). It was also recommended that regulation of low and intermediate complexity products should closely follow guidelines already set for small molecules and biologicals, respectively. Regulation of high-complexity products will require considerable modification to preclinical data requirements (CMC, PK, metabolism, PD) to ensure consistency and reproducibility of product and to understand how minor changes in supramolecular structure effect clinical parameters (efficacy toxicity, PK, PD) (Lebovitz, 2006). Isomeric and orientation heterogeneity are specifically important if nanoparticles are used as targeting delivery systems. Complexity issues for nanopharmaceuticals as compared to macro- or micropharmaceuticals are listed in Table 21.3.

Purity

Purification and size-based separation of nanoparticles are some of the challenges in the preparation of well-defined materials. Diafiltration shows considerable potential for the efficient and convenient purification and size separation of water-soluble nanoparticles, allowing for the removal of small-molecule impurities and for the isolation of small nanoparticles from larger nanostructures in a single process (Sweeney et al., 2006). However, for insoluble nanopharmaceuticals, purification by filtration is quite challenging. Filters of 0.22 μm size cut-off let the nanopharmaceuticals to pass through and therefore do not allow purification or sterilization of such preparations. Consideration of crystallinity and polymorphism needs attention for nanopharmaceutical purity and stability. Residual organic solvents should be below the acceptable limits for nanopreparations utilizing organic solvents during manufacturing. This is outlined in ICH Q3C (ICHQ3C, 1998).

Surface Structure and Aggregation

Surface reactivity, surface groups, coatings, and charge play a major role in nanoparticle aggregation. Introducing a small percentage of impurities to the surface of nano-TiO_2 particles may fundamentally alter their propensity to generate free radicals under UV radiation (Wakefiled et al., 2004). Changes over time such as coagulation, sintering, and chemical transformation might occur. Nanomaterials in the life-sciences area are

Table 21.3 Comparison of complexity issues for nanodrug delivery with respect to micro or macrodrug delivery.

Micro or macrodrug delivery	Nanodrug delivery
Purity	Polydispersity
Uniformity	Isomeric heterogeneity
Regularity of structure	Orientation heterogeneity
	Surface charge and aggregation

most likely to represent supramolecular aggregates of active and non-active atoms/molecules. Huang et al. observed reversible, surface-controlled structure transformation in nanoparticles induced by an aggregation state (Huang et al., 2004). It was found in the study that reversible switching between distorted and crystalline structures can be induced by changing the aggregation state via slow drying and ultrasonic agitation. The reversible nature also implies low activation energy of nanoparticle transformation and indicates that distorted nanoparticles are not trapped in a metastable state. X-ray diffraction and X-ray crystallography have been used to determine the transformations. Aggregated nanoparticles might prove to be toxic in some cases. Surface charges might be responsible for their reactivity as well as aggregation potential (Hollister et al., 1994). Therefore, surface charges seem to be an important characteristic. Surface properties of γ-Fe_2O_3 nanoparticles were shown to play an important role in interparticle interaction in another study (Tronc et al., 2000). Mössbauer spectroscopy can be used to measure the surface properties. Also the zeta potential measurements are performed for the determination of surface charge of nanopharmaceuticals (Nazzal et al., 2002, Palamakula et al., 2006, Zidan et al., 2007). Certain surface modifiers such as surfactants can be used to prevent aggregation (Kenneth et al., 1994). Analyte-directed aggregation of gold nanoparticles, a consequence of interacting particle surface plasmons and aggregate scattering properties, and DNA-induced aggregation of nanoparticles are well documented in the literature (Elghanian, 1997; Isabelle et al., 2003).

Stability

Nanoparticles can either increase stability (Wechsler, 2006) or decrease due to exposure of very high surface area. In the case of liposomes, size and surface components determine both stability and ability to elude reticuloendothelial sequestration. Nanosuspensions were shown to have greater stability as compared to micro or macrosuspensions in one of the studies (Jacobs et al., 2000). However, in this case, a sufficiently high concentration was needed to stabilize the formulation; and for particulate systems, it might degrade easily if the drug is prone to oxidation, hydrolysis, or photolysis. Nanosystems can be thermodynamically unstable. Moreover, they can easily have a mixture of amorphous and crystalline APIs. In such systems, long-term appropriate storage conditions need to be established. Therefore the stability of nanoparticles needs to be studied systematically.

Toxicity Screening

There is a growing concern that current toxicological screening methods might not be adequate to assess nanopharmaceuticals. Pharmacokinetic effects as well as pharmacodynamic effects of nanoproducts might be very different and if inadequately addressed, might carry unidentified risks. Also, the current toxicity screening methods are of short term and hence chronic effects due to nanoparticle exposure might not be accounted for. Toxicity screening when done on single cell types might not address the issue

of exposure to various tissues. Without rigorous nanomaterial-specific characterization, it will be extremely challenging to interpret toxicity studies, compare similar studies, and develop predictive models of nanopharmaceutical toxicity. Newer tests might be required as new toxicological risks are identified. This topic is further covered in the next section on safety consideration.

Safety Consideration of Nanopharmaceuticals

Both chemistry and structure are very important in determining health risk and safety of a drug product. Lung disease resulting from aerosol exposure is associated with particle size and composition (Maynard & Baron, 2004). Health hazard with asbestos can be minimized by altering the composition and morphology (Maynard, 2006b). Therefore impact of size or morphology along with chemistry needs to be assessed together to determine safety of nanopharmaceuticals. Inhaled insoluble particles in micrometer size range depositing within the alveolar region of the lungs are cleared with phagocytosis. However, due to extremely small size, the clearance path for nanoparticles might change and they might be translocated from one organ to another.

In one study, Kreyling et al. (2002) showed that by introducing 80 nm insoluble particles in animals' lungs, a significant mass translocated to liver at a low rate. However, at 15 nm, the translocation was significantly higher. Research also suggests that nanoparticles are able to cross the blood–brain barrier (Oberdorster et al., 2004; Elder et al., 2006). They might also be able to cross blood–placenta barrier and mutagenic or teratogenic depending upon the active ingredient. Also, there is evidence that submicron particles can penetrate the outer layers of mechanically flexed skin (Tinkle et al., 2003). In another study, it was demonstrated that cadmium selenium quantum dots having 4.6 nm particle sizes were able to penetrate through the dermis in skin samples (Ryman et al., 2006). Comparison of micro- and nano-sized TiO_2 particles showed that the latter was more potent (Oberdorster et al., 1994). In another study Umbreit et al. (2006) demonstrated that TiO_2 nanoparticles biodistribution was different when injected intravenously versus subcutaneously. For IV injected, the particles accumulated in liver, lung, and spleen, whereas, for SC injected, most of the dose remained at the injection site indicating their aggregation. Nanostructure was shown to be more important in exhibiting tissue thickening due to SWCNT aggregates at a specific site in lungs (Shvedova et al., 2005).

Thus determination of safety for nanopharmaceuticals becomes particularly important when the material interacts with the body in a way that nanostructure becomes biologically available and it elicits a biological response which is also associated with nanostructure (Maynard, 2006a). It is also believed that low concentrations of manufactured nanoparticles of titanium dioxide can produce harmful free radicals in brain cells and the potential for brain cell damage (ICTA, 2006). Engineered nanoparticles of aluminum oxide may bioaccumulate and stunt the growth of roots in at least five species of plants: corn, cucumber, cabbage, carrot, and

soybeans (ICTA, 2006). Fullerenes or buckyballs—a type of manufactured nanoparticle used in some cosmetics—cause rapid brain damage in fish and are toxic to small crustaceans (ICTA, 2006). Also cadmium selenide nanoparticles (quantum dots) can break down in the human body, potentially causing cadmium poisoning. Effects of nanotubes on the lungs of rats produced more toxic response than quartz dust (ICTA, 2006). Engineered nanoparticles of zinc oxide and titanium dioxide used in nanosunscreens can induce free radicals in skin cells and cause DNA damage (ICTA, 2006). Also environmental impact due to the release of nanomaterials from the manufacturing processes and exposure of humans working with it remain a potential concern (Beaver, 2004). To address some of these issues, EPA is conducting studies on TiO_2 nanoparticles and has issued a nanotechnology white paper (EPA, 2007). Friends of Earth (FoE) also believe that the nanoparticles marketed as sunscreens, cosmetics, and personal care products pose significant risk to consumers (Miller et al., 2006). They believe that many types of nanoparticles can be toxic to human tissue and cell cultures, resulting in increased oxidative stress, inflammatory cytokine production, DNA mutation, and even cell death. However, it is unclear how the standards advocated by FoE (Friends of Earth) could be met as few products come with absolute guarantee of safety of all portions of the population (Saxton, 2007).

Marketed and Pipeline Nanopharmaceuticals

Nanopharmaceuticals span a variety of structures including nanocrystals, nanosuspensions, nanoemulsions, dissocubes, SNEDDS, liposomes; micelles; prototypical nanostructures such as fullerenes, quantum dots, nanoshells, dendrimers; nanocrystals, cyclodextrins, and many more. FDA has already approved some of the products; examples include liposomal drug products, certain imaging agents including gadolinium MRI contrast agents, iron oxide contrast agent; reformulated drugs using nanocrystal technology to enhance bioavailability properties of previously approved drugs (immunosuppressants, antiemetic); as well as nanoparticle-based formulation of previously approved anti-tumor drugs.

A treatment for prostate and metastatic breast cancer using albumin to create nanoparticles of taxol is entering phase I/II clinical trials (Abraxis, 2007). Another potential nanotherapy is targeted delivery to lungs for lung cancer and is being developed by Cell Therapeutics (Cell Therapeutics, 2007). Doxorubicin, a treatment for cancer, has been reported to have advantages in the treatment of Kaposi's sarcoma when enclosed in a nanosized liposome (Doxil®) (Nei et al., 2006; Science policy, 2004; Hett, 2004). Increase in half-life of Doxil® has been achieved by surface modification with polyethylene glycol to avoid engulfing by the reticuloendothelial system. Liposomes are among the first nanodrugs approved by FDA. Other approved liposomal drugs include Ambisome® which contains liposomal amphotericin B (Gilead, Fujisawa), Myocet® (liposomal doxorubicin, Elan), and Depocyt® (liposomal cytosine arabinoside, SkyePharma) with more drugs currently in clinical trials ("FDA", Davidson et al., 1991; Waterhouse et al., 2005).

There are other nanopharmaceuticals in development (Gao et al., 2004; Loo et al., 2004). Doxorubicin attached to copolymers in nano-form is also in clinical trials (Vasey et al., 1999; Seymour et al., 2002). Rapamune® (sirolimus, Wyeth) uses NanoCrystal™ technology ("Elan", 2007) and received FDA approval in August 2002. Trivcor® (fenofibrate, Abbott), Emend® (aprepitant, Merck), and Megace® ES (Par Pharmaceutical) are some examples of reformulated drug products with NanoCrystal™ technology which received FDA approval. SILCRYST™ (nanocrystalline silver, Nucryst Pharmaceuticals) is used in Acticoat™, an antimicrobial barrier dressing. Polymeric micelles are being investigated for DNA delivery (Olivier, 2005; Roney et al., 2005; Otuska et al., 2003; Xu et al., 2006; Panyam et al., 2003). Basulin, an insulin formulation in nanoparticles, is in phase II trials (Constancis et al., 1999; "Flamel"). Dendrimers are synthetic polymeric structures with a central core, internal branches, and terminal groups symmetrically distributed (Svenson & Tomalia, 2005; Patri et al., 2002). Vivagel® dendrimer binds to HIV gp 120 proteins and is in phase II evaluation ("Dendrimer"). NB001 (an antiherpes drug), NB002 (targets nail fungus), and NB003 (targets vaginal infection) are on various stages of development which use dendrimer platforms (NanoBio Corps, 2007). Quantum dots and nanoshells which target, image, and treat various diseases like cancer are in various preclinical testing stages (Bakalova et al., 2004; Loo et al., 2005). They can act either as carriers for drugs or as drugs. Examples of carriers include calcium phosphate as a carrier for insulin, immunological adjuvants, or genes (Morcol et al., 2004; Biosante, 2007; He et al., 2000), colloidal gold for cancer chemotherapy or DNA (Paciotti et al., 2004; "CytImmune"; Thomas & Klibanov, 2003) or phosphate binder for renal disease by nanospheres (Roy et al., 2003; Altair, 2007). Those that act as drugs include tumor-specific ligands or antibodies (Gao et al., 2004; Akerman et al., 2002) or iron oxide nanoparticle for iron delivery ("Advanced magnetic"). In addition, some cosmetics and devices which make use of nanotechnology are in the "nano" size range and have also been approved by FDA.

Regulatory Perspectives

Nanotechnology is of interest to regulatory bodies because the physical, chemical, and biological properties of materials at this scale might differ in fundamental ways from the properties of individual atoms and molecules or bulk matter. Nanotechnology is considered an emerging technology in the field of medicine and currently its application is geared toward drug discovery and drug delivery. A federal R&D program was established to coordinate the multi-agency efforts in nanoscale science, engineering, and technology, in which FDA and 22 other federal agencies participated. It is called the National Nanotechnology Initiative (NNI). It defined "nanotechnology" as a technology that involves all of the following elements: (i) research and technology development at the atomic, molecular, or macromolecular levels, in length scale of approximately 1–100 nm range; (ii) creating and using structures, devices, and systems that have novel properties and functions because of their small

and/or intermediate size; and (iii) ability to control or manipulate on the atomic scale ("NNI", 2004).

American Standards for Testing and Materials (ASTM) defines nanotechnology as "a term referring to a wide range of technologies that measure, manipulate or incorporate materials and/or features with at least one dimension between approximately 1 and 100 nanometers. Such applications exploit the properties, distinct from bulk/macroscopic systems, of nanoscale components" (ASTM, 2006). It also defines nanoparticle which includes "in nanotechnology, a sub-classification of ultrafine particle with lengths in two or three dimensions greater than 0.001 micrometer (1 nm) and smaller than about 0.1 micrometer (100 nm) and which may or may not exhibit a size-related property". However, ASTM concerns that the term size and size range are subject to controversy as current usage emphasizes on size and not size-related property. Also, the length scale may be a hydrodynamic diameter or geometric length appropriate to the intended use of the nanoparticle.

A joint report by the British Royal Society and the Royal Academy of Engineering similarly defined nanotechnology as "the design, characterization, production, and application of structures, devices and systems by controlling shape and size at nanometer scale" ("UK", 2004). A recent report from US Congress defines nanotechnology as "In a more general context, nanotechnology can be seen as just the current stage of a long-term ability to understand and manipulate matter at ever smaller scales as time goes by" (Saxton, 2007). The report identified nanotechnology as basic building blocks of matter and life including molecular chemistry, genetic reproduction, cellular processes, and the current frontier of electronics, all occurring on the nanolevel. It is an overlap between traditional physics and quantum mechanics.

National Strategy for Combating Terrorism (NSCT)'s definition is "Nanotechnology involves research and technology development at the atomic, molecular, or macromolecular levels in the dimension range of approximately 1–100 nanometers to provide fundamental understanding of phenomena and materials at the nanoscale and to create and use structures, devices, and systems that have novel properties and functions because of their small and/or intermediate size. The novel and differentiating properties and functions are developed at a critical length scale of matter typically under 100 nm. Nanotechnology research and development includes control at the nanoscale and integration of nanoscale structures into larger material components, systems, and architectures. Within these larger scale assemblies, the control and construction of their structures and components remains at the nanometer scale" (NSCT, 2000).

A consensus definition among the tripatriate nation of United States, European Union, and Japan may need to emerge specifically for pharmaceuticals. Some interesting definitions are as follows: "In the context of nanomedicine, nanoscale should be taken to include active components or objects in the size range from 1–100s of nm" by European Science Foundation in 2003 (Swiss Re, 2004). Another definition by Duncan (Duncan, 2003) includes "drug delivery and related pharmaceutical development in the context of nanomedicine should be viewed as science and technology of nanometer-size scale, complex systems (10–1000 nm) consisting of at least

two components, one of which is an active ingredient. The whole system leads to a special function related to treating, preventing or diagnosing diseases which is sometimes referred to as smart drugs or theragnostics". Lux Research (Lux Research, 2004) defines nanotechnology as "the purposeful engineering of matter at scales of less than 100 nanometers to achieve size-dependent properties and functions". Another definition is "Nanotechnology is the engineering of functional systems at the molecular scale. This covers both current work and concepts that are more advanced. In its original sense, 'nanotechnology' refers to the projected ability to construct items from the bottom up, using techniques and tools being developed today to make complete, high performance products" (CRN, 2007).

National Nanotechnology Initiative in the United States ("NNI", 2004), consideration of nanotechnology as one of the fourth prioritized research area by Japanese government, a move toward better regulation for nanotechnology by United Kingdom, launching communication "Towards a European strategy for nanotechnology" by Europe ("How big", 2004), formation of Asian Nanotechnology Forum by Asian countries ("ANF", 2004), formation of International Council on Nanotechnology ("ICON", 2004) are some of the examples showing global interest in nanotech research.

Nanoproducts are not just for the therapeutic use of a new drug with a New Drug Application (NDA), Abbreviated New Drug Application (ANDA), or Biological Licensing Application (BLA). It is expected that FDA, a regulatory agency for drugs, medical devices, biotechnology products, vaccines, tissue-engineered products, cosmetics, food, animal drugs, combination products, radiation-emitting devices, among others ("FDA"), will receive a wide range of products utilizing nanotechnology or nanomaterials. Depending upon the nature of products developed the nanoproducts are overseen by the Center for Drug Evaluation and Research (CDER), Center for Biological Evaluations and Research (CBER), Center for Veterinary Medicine (CVM), Center for Device and Radiological Health (CDRH), and Office of Commissioner (a component of which is the Office of Combination Products). The compliance and inspection issues are handled by the Office of Regulatory Affairs (ORA). The developments in nanopharmaceuticals are expected to yield more combination products with multiple components, including delivery systems, therapy, and/or imaging agents. Such complex therapies will challenge FDA's Office of Combination Products in determining the primary mode of action as it determines which FDA Center will have primary regulatory oversight. FDA's Office of Science and Health Coordination (OSHC) oversees nanotechnology activities throughout the agency, including its participation on government-wide nanotechnology committees.

The current paradigm of drug approval regulations is applied for nanopharmaceuticals as there are no nanoparticles-specific guidance documents at this time. Center for Technology Assessment (CTA, a coalition of environmental and health organizations) (Kimbrell, 2006) considers nanoproducts to be dangerous. It is recognized by regulatory bodies that nanoparticles in drugs and cosmetics may gain access to tissues and cells more easily and there is little information on how long they remain in the

body, how they are cleared from tissues and blood, and whether they have additional effects on cellular functions or on different cell types. To address some of these issues, in-house as well as collaborative research is underway at various government organizations. It should be pointed out here that any new product or excipient goes through a battery of toxicity tests to ensure its short- and long-term safety. An ICH Guidance for preclinical toxicity screening can be a helpful guide to determine safety (ICH S6, 1997). It summarizes various tests to be considered depending upon the drug substance in use. The toxicity tests might include but are not limited to genotoxicity, immunotoxicity, carcinogenicity, considerations to ADME, pharmacology, etc. The guidance calls for relevant animal species for preclinical toxicity and evaluation of toxicity in two different animal species along with correlation to toxicity in humans whenever possible. Similarly new excipients are screened, and the guidance from FDA can be obtained from its website. The type and amounts of excipient used with previous history are provided in the inactive ingredient guide (IIG) which can be obtained from the FDA website. However, this list is for excipients when they are mostly in the macrosize range. What happens when they are in the nano size range still needs to be understood. The same comment applies to the generally regarded as safe (GRAS) compounds as listed in the Handbook of Pharmaceutical Excipients.

For the chemistry and manufacturing controls, the development scientists are encouraged to look at the new ICH guidances on product development (ICH Q8, 2004) and quality risk management (ICH Q9, 2005). These guidances address various Quality by Design (QbD) elements of product development including an understanding of all the variability and their interactions that are likely to affect the product quality. The ICH Q9 addresses the risk-based strategies to determine the likely failures and their consequences on product development and manufacturing.

In a report, the United Kingdom's Royal Society recommended that ingredients in the form of nanoparticles should undergo a full safety assessment by the relevant scientific advisory body before they are permitted for use in products (UK, 2004). Characterization of nanopharmaceuticals is an important consideration to ensure safety aspects. The National Academy of Sciences concluded that techniques and instrumentation for characterization and measurement be developed that will enable determination of the exact composition of a nanomaterial in a substance or product, as well as the physicochemical properties of specific nanomaterials. However, equipment to accurately measure and observe events at the nanoscale is still relatively primitive (Saxton, 2007).

Products Subject to Premarket Review

As FDA is charged with regulating drugs, medical devices, cosmetics, sunscreens, food packaging which directly affect consumers, the agency reviews products prior to marketing. The manufacturers generally provide the necessary scientific information to support the regulatory decisions prior to approval of their products for marketing. For nanopharmaceuticals, there are no specific regulatory requirements. Particle size related questions can be asked to manufacturers when it can be inferred that

information is relevant to determine safety, efficacy, and quality of the drug product. For inhalation and injectable drug products, sponsors submit the data for NDAs, ANDAs, or their supplements. The Secretary of Health and Human Services has the authority to "Promulgate regulations for the efficient enforcement" of the Federal Food, Drug, and Cosmetic Act (the "Act") (21 USC § 371). The secretary has re-delegated to the Commissioner of Food and Drug Administration (FDA) all the authority vested to the secretary under the act (21CFR 5). Thus FDA derives its regulations under FD&C act and utilizes it effectively to fulfill its mission of ensuring the safety and efficacy of the regulated products available to the American public ("FDA"). Under section 505(*k*) of the FD&C act, FDA has statutory and regulatory authority for regulated products. However, for certain over-the-counter products which have monograph as opposed to NDA application, such premarketing inspection does not normally occur. Also biological interaction of nanoparticles has been questionable. When such information becomes necessary for regulators to make necessary approval decision, it is sought from the sponsors. Labeling of the drug products containing nanopharmaceuticals also gets special considerations only if risks are identified that could be mitigated by appropriate labeling.

In a recent report, Taylor advised that (i) FDA should obtain early and adequate information on nanotechnology products in the development pipeline, (ii) it should define and enforce safety standards for nanomaterials, including the nature and extent of the testing required to satisfy them, (iii) place the initial and continuing burden to demonstrate safety on the nanotechnology products' sponsors, and (iv) review the nanotechnology products' safety prior to marketing and impose conditions as needed to ensure safety (Taylor, 2006). The debate on safety of using nanotechnology would be improved if three changes were made governing the use of nanotechnology in products according to a recent report from US Congress. (i) The use of nanotechnology should be clearly labeled on products so that consumers can make an informed choice about whether to use a particular product. (ii) Private companies should be required to disclose to the FDA the results of any safety testing that they conduct and the FDA should immediately publicize any results that show a clear negative health effect. And (iii) additional efforts to identify the environmental, health, and safety risks of nanoparticles will bring clear benefits. But the need to conduct these studies should not be used to prevent the introduction of new products (Saxton, 2007). Thus, fear associated with "nanotoxicity" can be minimized by educating the public about the benefits and risks associated with nanopharmaceuticals.

Products Subject to Postmarket Review

The FDA has authority to review postmarket safety of products under 21CFR *211.65* and has adequate adverse events reporting authority for approved drugs under 21CFR *314.80*, investigational new drugs under 21CFR *312.32*, and inspection authority under Section *704* of the FD&C Act. In Taylor's report (Taylor, 2006), he recommended that FDA should (i) require postmarket monitoring and testing of nanotechnology products

as needed to ensure safety, (ii) require timely adverse event reporting, (iii) inspect manufacturing establishments and examine records to nanotechnology product safety, and (iv) remove from the market nanotechnology products that appear to pose a significant safety hazard or no longer meet the applicable safety standard.

Products Not Subject to Premarket Review

Concerns for unapproved drug products, cosmetics, or dietary supplements containing nanoparticles remain to be addressed. Since the products are not subject to premarket approval, it becomes very challenging to regulators to become aware of such issues. However, FDA has the authority of adverse events reporting requirements from manufacturers marketing unapproved products under 21CFR *310.305*.

Conclusions

Nanopharmaceuticals are emerging complex drug delivery systems that are being shown to be beneficial for therapeutic use with their targetability and improved bioavailability. However, they might present new and unusual risks, and there is very little information from sponsors about how the risks can be identified, assessed, and controlled. Safe nanopharmaceuticals will not become a reality unless proper risk management and mitigation tools are utilized. The tendency of regulators is to adopt a precautionary approach to regulate for the highest risk case, undertake, and motivate research to fill critical knowledge gaps as identified in Critical Path Initiative 2004 and make science-based decisions when research and experience prove it to be of less risk. Priorities should be given to toxicity screening, characterization methods, and product and process understanding. Characterization of nanopharmaceuticals may also raise unique considerations. New tools and understanding are needed to assess the critical physical and chemical properties of these products, including residual solvents, processing variables, impurities, and excipients in addition to size and surface characteristics. A review of the FDA guidance on preclinical toxicity screening and the ICH guidances Q8 and Q9 should be very helpful for the development of nanopharmaceuticals as well other complex products.

Acronyms

ADME	Absorption, distribution, metabolism, and elimination
AFM	Atomic force microscopy
ANDA	Abbreviated New Drug Application
ANF	Asia Nano Forum
ASTM	American Standards for Testing and Materials
API	Active pharmaceutical ingredient
BCS	Biopharmaceutical Classification System
BLA	Biological Licensing Application
CBER	Center for Biological Evaluations and Research
CDER	Center for Drug Evaluation and Research

CDRH	Center for Device and Radiological Health
CFR	Code of Federal Registrar
CMC	Chemistry, manufacturing, and control
CRN	Center for Responsible Nanotechnology
CST	Council for Science and Technology (United Kingdom)
CTA	Center for Technology Assessment
CVM	Center for Veterinary Medicine
DNA	Deoxyribonucleic acid
EPA	Environmental Protection Agency
FDA	Food and Drug Administration
FD&C act	Food, Drug and Cosmetic Act
FoE	Friends of Earth
GRAS	Generally regarded as safe
ICH	International Conference on Harmonization
ICON	International Council on Nanotechnology
ICTA	International Center for Technology Assessment
IIG	Inactive Ingredient Guide
IV	Intravenous
MHRA	Medicines and Healthcare Products Regulatory Agency (United Kingdom)
MRI	Magnetic resonance imaging
NCL	National Characterization Laboratory
NCI	National Cancer Institute
NDA	New Drug Application
NIST	National Institute of Standards and Technology
NNI	National Nanotechnology Initiative
NSCT	National Strategy for Combating Terrorism
ORA	Office of Regulatory Affairs
OSHC	Office of Science and Health Coordination
PD	Pharmacodynamics
PK	Pharmacokinetics
PAT	Process analytical technology
PSD	Particle size distributionh
QbD	Quality by Design
R&D	Research and Development
SC	Subcutaneous
SEDDS	Self-emulsifying drug delivery systems
SNEDDS	Self-nano-emulsifying drug delivery systems
USC	United States Code
UV	Ultraviolet

References

21 CFR, 5. FDA organization. *Code of Federal Registrar*.

21CFR *211.65*. Equipment construction. *Code of Federal Registrar*.

21CFR *310.305*. Records and reports concerning adverse drug experiences on marketed prescription drugs for human use without approved new drug applications. *Code of Federal Registrar*.

21CFR *312.32*. IND safety reports. *Code of Federal Registrar*.

21CFR *314.80*. Post marketing reporting of adverse drug experiences. *Code of Federal Registrar*.

21 USC, § 371. Federal Food, Drug and Cosmetics Act.

Abraxis (2007). Abraxis BioScience to initiate two phase I/II clinical trials with nab-docetaxel in hormone refractory prostate and metastatic breast cancer. *Business wire;* http://www.abraxisbio.com.

Advanced Magnetic Inc Website (2007). http://www.advancedmagnetics.com.

Akerman, M. E., Chan, W. C. W., Laakkonen, P., Bhatia, S. N., & Ruoslahti, E. (2002). Nanocrystal targeting in vivo. *Proceedings of the National Academy of Sciences*, 99, 12617–12621.

Altair Nanotechnologies Website (2007). www.altairnano.com.

ANF. (2004). *Asia Nano Forum;* http://www.asia-nano.org.

Arshady, R. (1988). Preparation of polymer nano- and microspheres by vinyl polymerization techniques. *Journal of Microencapsulation*, 5, 101–114.

ASTM. (2006). Terminology for nanotechnology. *American Standards for Testing and Materials*, E2456-06.

Bakalova, R., Ohba, H., Zhelev, Z., Ishikawa, M., & Baba, Y. (2004). Quantum dots as photosensitizers? *Nature Biotechnology*, 22, 1360–1362.

Beaver, E. R. (2004). Implications of nanomaterials manufacture and use. *USEPA Nanotechnology STAR Review;* http://es.epa.gov/ncer/publications/workshop/8–18–04/ppt/beaver–2.ppt

Biodelivery sciences. http://www.biosantepharma.com/Products.php

Biosante Pharmaceuticals Website. www.biosantepharma.com

Borm, P. J. A., & Kreyling, W. (2004). Toxicological hazards of inhaled nanoparticles-potential implications for drug delivery. *Journal of Nanoscience & Nanotechnology*, 4, 521–531.

Brannon-Peppas, L., & Blanchette, J. O. (2004). Nanoparticle and targeted systems for cancer therapy. *Advanced Drug Delivery Reviews*, 56, 1649–1659.

Cell Therapeutics Inc. (2007). CTI files for special protocol assessment (SPA) for XYOTAX(TM) PGT307 lung cancer trial in women. *PR Newswire-FirstCall*, March 20; www.celltherapeutics.com

Chandrasekaran, T. (1993). Effect of microstructure and hardness on the grinding abrasive wear-resistance of a ball-bearing steel. *Wear*, 161, 105–109.

Chattopadhyay, P., & Gupta, R. B. (2001a). Production of griseofulvin nanoparticles using supercritical CO_2 antisolvent with enhanced mass transfer. *International Journal of Pharmaceutics*, 228, 9–31.

Chattopadhyay, P., & Gupta, R. B. (2001b). Production of antibiotic nanoparticles using supercritical CO2 as antisolvent with enhanced mass transfer. *Industrial Engineering & Chemical Research*, 40, 3530–3539.

Constancis, A., Meyrueix, R., Bryson, N., Huille, S., Grosselin, J. M., Gulik-Krzywicki, T., & Soula, G. (1999). Macromolecular colloids of diblock poly (amino acids) that bind insulin. *Journal of Colloid and Interface Science*, 217, 357–368

Crititech. http://www.crititech.com/currentRD.html

CRN. (2007). What is nanotechnology. *Center for Responsible Nanotechnology*; http://www.crnano.org/whatis.htm

Crommelin, D. J. A. (1994). Liposomes. In J. Kreuter (Ed.) *Colloidal Drug Delivery Systems*, (pp. 219–342) New York: Marcel Dekker.

CytImmune Sciences, Inc. http://www.cytimmune.com/go.cfm?do = Page.View&pid = 14

Davidson, R. N., Croft, S. L., Scott, A., Maini, M., Moody, A. H., & Bryceson, A. D. (1991). Liposomal amphotericin B in drug-resistant visceral leishmaniasis. *Lancet*, 337, 1061–1062.

Davies, J. C. (2006). Managing the effects of nanotechnology. *Woodrow Wilson International Center for Scholar: Project on emerging nanotechnology*, Washington D. C.; http://nanotechproject.org/index.php?s = reports

De Keyser, J., De Cock, C., Poupaert, J. H., & Dumont, P. (1989). Synthesis of ^{14}C labeled acrylic derivatives: diethyl [3-^{14}C] methylidenemalonate and isobutyl [3-^{14}C] cyanoacrylate. *Journal of labeled compounds & radiopharmaceuticals*, 27, 909–916.

De Keyser, J., Poupaert, J. H., & Dumont, P. (1991). Poly (diethyl methylidenemalonate) nanoparticles as a potential drug carrier: preparation, distribution and elimination after intravenous and peroral administration to mice. *Journal of Pharmaceutical Sciences*, 80, 67–70.

Dendrimer resource page. *Starpharma Holdings Ltd*; http://www.starpharma.com/dendrimers.asp

Donaldson, K., Brown, M. D., Cloucer, A., Duffin, R., MacNee, W., Renwick, I., & Stone, V. (2002). The pulmonary toxicology of ultrafine particles. *Journal of Aerosol Medicine*, 15, 213–220.

Dubey, R. (2006). Pure drug nanosuspension: Impact of nanosuspension technology on drug discovery and development. *Drug Delivery Technology*, 6, 65–71.

Duncan, R. (2003). The growing era of polymer therapeutics, *Nature Reviews*, 2, 347–360.

Elan Drug Technologies. http://www.elan.com/edt/drug_optimization/nanocrystal_technology.asp

Elder, A., Gelein, R., Silva, V., Feikert, T., Opanashuk, L., Carter, J., Potter, R., Maynard, A., Ito, Y., Finkelstein, J., & Oberdorster, G. (2006). Translocation of inhaled ultrafine manganese oxide particles to the central nervous system. *Environmental Health Perspectives*, 114, 1172–1178.

Elghanian, R., Storhoff, J. J., Mucic, R. C., Letsinger, R. L., & Mirkin, C. A. (1997). Selective Colorimetric Detection of Polynucleotides Based on the Distance-Dependent Optical Properties of Gold Nanoparticles. *Science,* 277, 1078–1081.

EPA Science Policy Council – Nanotechnology Workgroup. (2007). U.S. Environmental Protection Agency Nanotechnology: White Paper, February. *US Environmental Protection Agency;* http://es.epa.gov/ncer/nano/publications/whitepaper12022005.pdf

FDA. Food and Drug Administration; http://www.fda.gov.

Flamel Technologies. http://www.flamel.com/techAndProd/index.shtml

Fivestar tech. http://www.fivestartech.com/technology/

Gao, X., Cui, Y., Levenson, R. M., Chung, L. W. K., & Nie, S. (2004). In vivo cancer targeting and imaging with semiconductor quantum dots. *Nature Biotechnology*, 22, 969–976.

Garner, R. C., Garner, J. V., Gregory, S., Whattam, M., Calam, A., & Leong, D. (2002). Comparison of the absorption of micronized (Daflon 500 mg) and nonmicronized 14C-diosmin tablets after oral administration to healthy volunteers by accelerator mass spectrometry and liquid scintillation counting. *Journal of Pharmaceutical Sciences*, 91, 32–40.

Granum, B., & Lovik, M. (2002). The effect of particles on allergic immune response. *Toxicological Sciences*, 65, 7–17.

Gupta, R. B., & Chattopadhyay, P. (2000). Method of forming nanoparticles and microparticles of controllable size using supercritical fluids and ultrasound. *US Provisional Patent*, 60/206,644.

Haskell, R. (2006). Physical characterization of nanoparticles. In R. Gupta, & U. Kompella (Eds.) *Nanoparticle Technology for Drug Delivery* (pp103–138) NY: Taylor & Francis.

He, Q., Mitchell, A. R., Johnson, S. L., Wagner-Bartak, C., Morcol, T., & Bell, S. (2000). Calcium phosphate nanoparticle adjuvant. *Clinical and Diagnostic Laboratory Immunology*, 7, 899–903.

Hett, A. (2004). Nanotechnology: small matter, many unknowns. Zurich, Switzerland, *Swiss Re*.

Hollister, K. R., Ladd, D., McIntire, G., Na, G., Rajagopalan, N., & Yuan, B. (1994). Use of purified surface modifiers to prevent particle aggregation during sterilization, *US Patent number: 5352459, 1994*

How big is nanotechnology for Europe? The Commission launches an open consultation, Brussels, 30 (July 2004); http://ec.europa.eu/research/press/2004/pr3007en.cfm

Huang, F., Gilbert, B., Zhang, H., & Banfield, J. F. (2004). Reversible, surface-controlled structure transformation in nanoparticles induced by an aggregation state. *Physical Review Letters*, 92, 155501.

ICHQ3C (R3). (1988). Impurities: Residual solvents. *International Conference on Harmonization*.

ICHQ8. (2004). Pharmaceutical Development. *International Conference on Harmonization*.

ICHQ9. (2005). Quality risk management. *International Conference on Harmonization*.

ICH S6. (1997). Preclinical safety evaluation of biotechnology derived pharmaceuticals. ICH harmonized tripartite guideline, *International Conference on Harmonization*.

ICON. (2004). International Conference on Nanotechnology. In Nanotechnology, Small size, large impact? Swiss Re. Risk dialogue series, Center for global dialogue, December.

ICTA. (2006). CTA and Friends of the Earth Challenge FDA to Regulate Nanoparticles at FDA Hearing, *International Center for Technology Assessment*; http://www.icta.org/press/release.cfm?news_id = 21

Isabelle, P., Jean-Philippe, B., Jacques, P., & Alain, F. (2003). Surface charge, effective charge and dispersion/ aggregation properties of nanoparticles. *Polymer International*, 52, 619–624.

Jacobs, C., Kayser, O., & Muller, R. H. (2000). Nanosuspensions as a new approach for the formulation for the poorly soluble drug tarazepide. *International Journal of Pharmaceutics*, 196, 161–164.

Jacobs, C., Kayser, O., & Muller, R. H. (2001). Production and characterization of mucoadhesive nanosuspensions for the formulation of bupravaquone. *International Journal of Pharmaceutics*, 214, 3–7.

Jensen, A. W., Maru, B. S., Zhang, X., Mohanty, D. K., Fahlman, B. D., Swanson, D. R., & Tomalia, D. A. (2005). Preparation of fullerene-shell dendrimer-core nanoconjugates. *Nano Letters*, 5, 1171–1173.

Jillavenkatesa, A., & Kelly, J. F. (2002). Nanopowder Characterization: Challenges and Future Directions. *Journal of Nanoparticle Research*, 4, 463–468.

Joost, B., & Schwedes, J. (1996). Wear of grinding component on size reduction in stirred ball mills. *Chemical Engineering & Technology*, 68, 713–717.

Kerr, M. C., & Reed, J. S. (1992). Comparative grinding kinetics and grinding energy during ball milling and attrition milling. *American Ceramic Society Bulletin*, 71, 1809–1816.

Kimbrell, G. A. (2006). CTA Files Legal Action to Force FDA to Regulate Health Threats from Nanomaterials, International center for technology assessment. *International Center for Technology Assessment news*; http://www.icta.org/press/release.cfm?news_id = 19

Kipp, J. E. (2004). The role of solid nanoparticle technology in the parenteral delivery of poorly water-soluble drugs. *International Journal of Pharmaceutics*, 284, 109–122.

Kramer, S., Xie, H., Gaff, J., Williamson, J. R., Tkachenko, A. G., Nouri, N., Feldheim, D. A., & Feldheim, D. L. (2004). Preparation of protein gradients through the controlled deposition of protein-nanoparticle conjugates onto functionalized surfaces. *Journal of American Chemical Society*, 126, 5388–5395.

Krause, K. P., Kayser, O., Mader, K., Gust, R. & Muller, R. H. (2000). Heavy metal contamination of nanosuspensions produced by high-pressure homogenization. *International Journal of Pharmaceutics*, 196, 169–173.

Kreuter, J. (1994). Nanoparticles. In J. Kreuter (Ed.) *Colloidal Drug Delivery Systems*, (pp. 219–342) New York: Marcel Dekker.

Kreyling, W. G., Semmler, M., Erbe, F., Mayer, P., Takenaka, S., Schulz, H., Oberdörster, G., & Ziesenis, A. (2002). Translocation of ultrafine insoluble iridium particles from lung epithelium to extrapulmonary organs is size dependent but very low. *Journal of Toxicology and Environmental Health Part A*, 65, 1513–30.

Lamprecht, A., Ubrich, N., Hombreiro, P. M., Lehr, C., Hoffman, M., & Maincent, P. (2000). Influences of process parameters on nanoparticle preparation performed by a double emulsion pressure homogenization technique. *International Journal of Pharmaceutics*, 196, 177–182.

Lebovitz, R. (2006). Regulatory approaches to novel nanomaterials: Unique benefits versus unique risks. http://www.fda.gov/ohrms/dockets/ac/06/slides/2006-4241s2_9.ppt

Lee, J. (2003). Drug nano- and microparticles processed into solid dosage forms: Physical properties. *Journal of Pharmaceutical Sciences*, 92, 2057–2068.

Lherm, C., Muller, R. H., Puiseux, F., & Couvreur, P. (1992). Alkylcynoacrylate drug carriers: II. Cytotoxicity of cyanoacrylate nanoparticles with different alkyl chain length. *International Journal of Pharmaceutics*, 84, 13–22.

Lichetnberg, D., & Barenholz, Y. (1988). Liposomes: Preparation, characterization, and preservation. In D. Glick (Eds.), *Methods of Biological Analysis* (pp. 337–461) New York: John Wiley.

Liversidge, G. G. (1996). Drug nanocrystals for improved drug delivery. In: *Proceedings of the CRS Workshop on Particulate Drug Delivery Systems*, Kyoto, Japan.

Liversidge, G. G., & Cundy, K. C. (1995) Particle size reduction for improvement of oral bioavailability of hydrophobic drugs: I. Absolute oral bioavailability of nanocrystalline danazol in beagle dogs. *International Journal of Pharmaceutics*, 125, 91–97.

Liversidge, G. G., Cundy, K. C., Bishop, J., & Czekai, D. (1991). Surface modified drug nanoparticles. *US Patent No*, 5145684.

Lockman, P. R., Mumper, R. J., Khan, M. A., & Allen, D. D. (2002). Nanoparticle technology for drug delivery across the blood-brain barrier. *Drug Development Industrial Pharmacy*, 28, 1–13.

Loo, C., Lin, A., Hirsch L., Lee, M., Barton, J., Halas, N., West, J., & Drezek, R. (2004). Nanoshell-enabled photonics-based imaging and therapy of cancer. *Technology in Cancer Research and Treatment*, 3, 33–40.

Loo, C., Lowery, A., Halas, N., West, J., & Drezek, R. (2005). Immunotargeted nanoshells for integrated cancer imaging and therapy. *Nano Letters*, 5, 709–711.

Lux Research. (2004). Sizing nanotechnology's value chain. New York: Lux Research Inc.

Lux Research. (2006). The nanotech report. 4th edn. New York: Lux Research Inc.

Mabela, T. K. M., Poupaert, J. H., Dumont, P., & Haemers, A. (1993). Development of poly(dialkyl methylidenemalonate) nanoparticles as drug carriers. *International Journal of Pharmaceutics*, 92, 71–79.

Martin, A., Swarbrick, J., & Cammarata, A. (1983). Diffusion and Dissolution. In A. Martin, A., J. Swarbrick & A. Cammarata (Eds.) *Physical Pharmacy* (pp 399–444). 3rd edition, Philadelphia: Lea & Febiger publishers.

Mawson, S., Johnston, K. P., Combes, J. R., & DeSimone, J. M. (1994). Formation of poly(1,1,2,2-tetrahydroperfluorodecyl acrylate) submicron fibers and particles from supercritical carbon dioxide solutions. *Macromolecules*, 28, 3182–3191.

Maynard, A. D. (2006a). Nanotechnology: The next big thing, or much ado about nothing? *Annals of Occupational Hygiene*, 10, 1–12.

Maynard, A .D. (2006b). Nanotechnology: Managing the risks. *Nano Today*, 1, 22–33.

Maynard A. D., & Baron P. A. (2004). Aerosols in the industrial environment: Aerosols handbook. In L. S. Ruzer, & N. H. Harley, (Eds.) *Measurement, Dosimetry and Health Effects* (pp. 225–64) Boca Raton: CRC Press.

Miller, G., Archer, L., Pica, E., Bell, D., Senjen, R., & Kimbrell, G. (2006). Nanomaterials, sunscreens and cosmetics: Small ingredients, big risk. *Friends of Earth Report*, May 2006.

Mishima, K., Matsuyama, K., Tanabe, D., &Yamauchi, S. (2000). Microencapsulation of proteins by rapid expansion of supercritical solution with a nonsolvent. *American Institute of Chemical Engineering Journal*, 46, 857–865.

Morcol, T., Nagappan, P., Nerenbaum, L., Mitchell, A., & Bell, S. J. (2004). Calcium phosphate-PEG-insulin- casein (CAPIC) particles as oral delivery systems of insulin. *International Journal of Pharmaceutics*, 277, 91–97.

Muller, R. H., Becker, R., Kruss, B., & Peters, K. (1998). Pharmaceutical nanosuspensions for medicament administration as system of increased saturation solubility and rate of solution, *US Patent No,* 5858410.

Muller, R. H., Jacobs, C., & Kayser, O. (2001). Nanosuspensions as particulate drug formulations in therapy. Rationale for development and what we can expect for the future. *Advanced Drug Delivery Reviews*, 47, 3–19.

Muller, R. H., Mader, K., & Krause, K. (2002). Pharmasol GMbH dispersion for formulation of slightly or poorly soluble active ingredients. *US Patent No*, CA002388550A1.

Muller, R. H., Peters, K., Becker, R. & Kruss, B. (1996). Nanosuspensions for the i. v. administration of poorly soluble drugs-stability during sterilization and long-term storage. Proceedings of International Symposium on Controlled Release of Bioactive Material, 22, 574–575.

Nakada, Y., Fattal, E., Foulquier, M., & Couvreur, P. (1996). Pharmacokinetics and biodistribution of oligonucleotide adsorbed onto poly(isobutylcyanoacrylate) nanoparticles after intravenous administration in mice. *Pharmaceutical Research*, 13, 38–43.

NanoBio Corporations. http://www.nanobio.com/Platform-Technology/Nano-Stat-Platform.html.

Nazzal, S., Nutan, M., Palamakula, A., Shah, R., Zaghloul, A. A., & Khan, M., A. (2002). Optimization of a self-nanoemulsified tablet dosage form of Ubiquinone using response surface methodology: effect of formulation ingredients. *International Journal of Pharmaceutics*, 240, 103–114.

NCL (National Characterization Laboratory). Moving nanotechnology concepts to the clinic. *NCL news*, 1, 2-6; http://ncl.cancer.gov/newsletter_vol_001.asp.

Nei, A., Xia, T., Madler, L., & Li, N. (2006). Toxic potential of materials at nanolevel. *Science*, 311, 622–627.

NNI, National Nanotechnology Initiative (2004). Nanotechnology resources page; http://www.nano.gov/html/facts/whatIsNano.html

NSCT (2000). NSTC definition of nanotechnology. National strategy for combating terrorism, June 12; http://www.becon.nih.gov/nstc_def_nano.htm

Nucryst. http://www.nucryst.com/nanotech.htm

Oberdoster, G. (2001). Pulmonary effects of ultrafine particles. *Archives of Occupational & Environmental Health*, 74, 1–8.

Oberdorster, G., Ferin, J., & Lehnert, B. E. (1994). Correlation between particle-size, in-vivo particle persistence, and lung injury. *Environmental Health Perspectives*, 102, 173–179.

Oberdorster, G., Sharp, Z., Atudorei, V., Elder, A., Gelein, R., Kreyling, W., & Cox., C. (2004). Translocation of inhaled ultrafine particles to the brain. *Inhalation Toxicology*, 16, 437–45.

Olivier, J. (2005). Drug Transport to brain with targeted nanoparticles. *NeuroRx*, 2, 108–119.

Otuska, H., Nagasaki, Y., & Kataoka, K. (2003). PEGylated nanoparticles for biological and pharmaceutical applications. *Advanced Drug Delivery Reviews*, 55, 403–419.

Paciotti, G., Myer, L., Weinreich, D., Goia, D., Pavel, N., McLaughlin, R., & Tamarkin, L. (2004). Colloidal gold: A novel nanoparticle vector for tumor directed drug delivery. *Drug Delivery*, 11, 169–183.

Palamakula, A., Nutan, M., & Khan, M. A. (2004). Response Surface Methodology for Optimization and Characterization of Limonene-based Coenzyme Q10 Self-Nanoemulsified Capsule Dosage Form. *AAPS Pharmaceutical Science and Technology*, 5: article 66.

Panyam, J., & Labhasetwar, V. (2003). Biodegradable nanoparticles for drug and gene delivery to cells and tissue. *Advanced Drug Delivery Reviews*, 55, 329–347.

Patri, A. K., Majoros, J. I., & Baker, J. R., Jr. (2002). Dendritic polymer macromolecular carriers for drug delivery. *Current Opinion in Chemical Biology*, 6, 466–471.

Randolph, T. W., Randolph, A. D., Mebes, M., & Yeung, S. (1993). Sub-micron-sized biodegradable particles of poly(L-lactic acid) via the gas antisolvent spray precipitation process. *Biotechnology Progress*, 9, 429–435.

Redzisqewski, P. (1997). Predictive model for ball mill wear, *Canadian Metallurgical Quarterly*, 36, 87–93.

Reverchon, E. (1999). Supercritical antisolvent precipitation of micro- and nanoparticles. *Journal of Supercritical Fluids*, 15, 1–21.

Reverchon, E., DellaPorta, G., Trolio, A. D., & Pace, S. (1998). Supercritical antisolvent precipitation of nanoparticles of superconductor precursors. *Industrial Engineering & Chemical Research*, 37, 952–958.

Roco, M. C. (2003). Government nanotechnology funding: An international outlook. *National Science Foundation*, June 30.

Roney, C., Kulkarni, P., Arora, V., Antich, P., Bonte, F., Wu, A., Mallikarjuana N. N., Manohar, S., Liang, H. F., Kulkarni, A. R., Sung, H. W., Sairam, M., & Aminabhavi, T. M. (2005). Targeted nanoparticles for drug delivery through the blood-brain-barrier for Alzheimer's disease. *Journal of Controlled Release*, 108, 193–214.

Roy, I., Mitra, S., Maitra, A., & Mozumdar, S. (2003). Calcium phosphate nanoparticles as novel non-viral vectors for targeted gene delivery. *International Journal of Pharmaceutics*, 250, 25–33.

Ryman-Rasmussen, J. P., Riviere, J. E., & Monteiro-Riviere, N. A., (2006). Penetration of intact skin by quantum dots with diverse physicochemical properties. *Toxicological sciences*, 91, 159–165.

Saxton, J. (2007). Nanotechnology: The future is coming sooner than you think. *United States Congress Joint Economic Committee*, March, 1–20.

Science Policy Section. (2004). Nanosciences and nanotechnologies: Opportunities and uncertainties. *Royal Society and Royal Academy of Engineering*. July. www.nanotec.org.uk/finalReport.htm

Seymour, L. W., Ferry, D. R., Anderson, D., Hesselwood, S., Julyan, P., Poyner, R., Doran, J., Young, A., Burtles, S., & Kerr, D. (2002). Hepatic drug targeting: phase I evaluation of polymer-bound doxorubicin. *Journal of Clinical Oncology*, 20, 1668–1676.

Shvedova, A. A., Kisin, E. R., Mercer, R., Murray, A., Johnson, V., Potapovich, A., Tyurina, Y., Gorelik, O., Arepalli, S., Schwegler-Berry, D., Hubbs, A., Antonini, J., Evans, D., Ku, B., Ramsey, D., Maynard, A., Kagan, V., Castranova, V., & Baron, P. (2005). Unusual inflammatory and fibrogenic pulmonary responses to single-walled carbon nanotubes in mice. *American Journal of Physiology -Lung Cellular and Molecular Physiology*, 289, 698–708.

Soppimath, K. S., Aminabhavi, T. M., Kulkarni A. R., & Rudzinskib, W. E. (2001). Biodegradable polymeric nanoparticles as drug delivery devices. *Journal of Controlled Release*, 70, 1–20.

Soliqs. http://www.soliqs.com/NanoMorph-R.20.0.html

Svenson, S., & Tomalia, D. A. (2005). Dendrimers in biomedical applications-reflections on the field. *Advanced Drug Delivery Reviews*, 57, 2106–2129.

Sweeney, S., Woehrle, G., & Hutchison, J. (2006). Rapid purification and size Separation of gold nanoparticles via diafiltration. *Journal of the American Chemical Society,* 128(10), 3190–3197.

Swiss Re. (2004). Nanotechnology, Small size, large impact? *Risk dialogue series, Center for global dialogue,* December.

Taylor, M. (2006). Regulating the products of nanotechnology, does FDA have the tools it needs? *PEN 5*, October.

Thanos, C. G., Liu, Z., Reineke, J., Edwards, E., & Mathiowitz, E. (2003). Improving relative bioavailability of dicumarol by reducing particle size and adding the adhesive poly(fumaric-co-sebacic) anhydride. *Pharmaceutical Research*, 20, 1093–1100.

Thomas, M., & Klibanov, A. M. (2003). Conjugation to gold nanoparticles enhances polyethylenimine's transfer of plasmid DNA into mammalian cells. *Proceedings of the National Academy of Sciences*, 100, 9138–9143.

Tinkle, S. S., Antonini, J. M., Rich, B. A., Rich, B., Roberts, J., Salmen, R., DePree, K., & Adkins, E. (2003). Skin as a route of exposure and sensitization in chronic beryllium disease. *Environmental Health Perspectives*, 111, 1202–1208.

Tom, J. W., & Debenedetti, P. G. (1991a). Particle formation with supercritical fluids - a review. *Journal of Aerosol Science*, 22, 555–584.

Tom, J. W., & Debenedetti, P. G. (1991b). Formation of bioerodable polymeric microspheres and microparticles by rapid expansion of supercritical solution. *Biotechnology Progress*, 7, 403–411.

Tom, J. W., Debenedetti, P. G., & Jerome, R. (1994). Preparation of poly(L-lactic acid) and composite poly(L-lactic acid)-pyrene by rapid expansion of supercritical solution. *Journal of Supercritical Fluids*, 7, 9–29.

Tomalia, D. A., Reyna, L. A., & Svenson, S. (2007). Dendrimers as multi-purpose nanodevices for oncology drug delivery and diagnostic imaging. *Biochem Society Transaction*, 35, 61–67.

Tronc, E., Ezzirb, A., Cherkaouib, R., Chanéaca, C, Noguèsb, M., Kachkachib, H., Fioranid, D., Testa, A. M., Grenèchec, J. M., & Joliveta, J. P. (2000). Surface-related properties of γ-Fe2O3 nanoparticles. *Journal of Magnetism and Magnetic Materials*, 221, 63–79.

UK Council for Science and Technology report (2007). Nanoscience and nanotechnologies: A review of Government's progress on its policy commitments. *UK Council for Science and Technology*, March, 1–45.

UK Royal Society and the Royal Academy of Engineering report. (2004). Nanoscience and nanotechnologies: Opportunities and uncertainties. *Royal Society and the Royal Academy of Engineering*, July, pp. 5.

Umbreit, T. H., Weaver, J. L., Miller, T. J., Zhang, J., Shah, R. B., Khan, M.A., Stratmeyer, M. E., & Tomazic-Jezic V. J. (2007). Toxicology of titanium dioxide (TiO2) nanoparticles: 1. Characterization and tissue distribution in subcutaneously and intravenously injected mice. *Society of Toxicology Annual Meeting*, Charlotte, NC.

Vasey, P.A., Kaye, S.B., Morrison, R., Twelves, C., Wilson, P., Duncan, R., Thomson, A., Murray, L., Hilditch, T., Murray, T., Burtles, S., Fraier, D., Frigerio, E., Cassidy J., & on behalf of the Cancer Research Campaign Phase I/II Committee. (1999). Phase I clinical and pharmacokinetic study of PK of [N-(2-hydroxypropyl)methacrylamide copolymer doxorubicin]. *Clinical Cancer Research*, 5, 83–94.

Vinee, W., Guo, K., Zegelman, J., & Helsel, S. (2006). Nanotechnology: Nanodrugs, fact, fiction and fantasy, *Drug Delivery Technology*, 6, 34–39.

Wakefield, G., Green, M., Lipscomb, S., & Flutter, B. (2004). Modified titania nanomaterials for sunscreen applications—reducing free radical generation and DNA damage. *Materials Science and Technology*, 20, 985–988.

Waterhouse, D. N., Madden T. D., Cullis P. R., Bally, M. B., Mayer, L. D., & Webb, M. S. (2005). Preparation, characterization, and biological analysis of liposomal formulations of vincristine. *Methods in Enzymology*, 391, 40–57.

Waterman, K. C., & Sutton, S. C. (2003). A computational model for particle size influence on drug absorption during controlled-release colonic delivery. *Journal of Controlled Release*, 86, 293–304.

Wechsler, J. (2006). Regulatory beat: Nanotechnology presents opportunities and challenges for FDA and manufacturers. *Biopharmaceutics International*, Jul 1.

Wong, C., West, P. E., Olson, K. S., Mecartney, M. L., & Starostina, N. (2007). Tip dilation and AFM capabilities in the characterization of nanoparticles. *Journal of Metals*, 59, 12–16.

Xu, P., Van Kirk, E. A., Li, S., Murdoch, W. J., Ren, J., Hussain, M. D., Radosz, M., & Shen, Y. (2006). Highly stable core-surface-crosslinked nanoparticles as cisplatin carriers for cancer chemotherapy. *Colloids and Surfaces B*, 48, 50–57.

Zidan, A. S., Sammour, O. A., Hammad, M. A., Megrab, N. A., Habib, M. J., & Khan, M. A. (2007). Quality by design: understanding the formulation variables of a self-nanoemulsified drug delivery systems of cyclosporine A by Box-Behnken design and desirability function. *International Journal of Pharmaceutics*, 332, 55–63.

Index

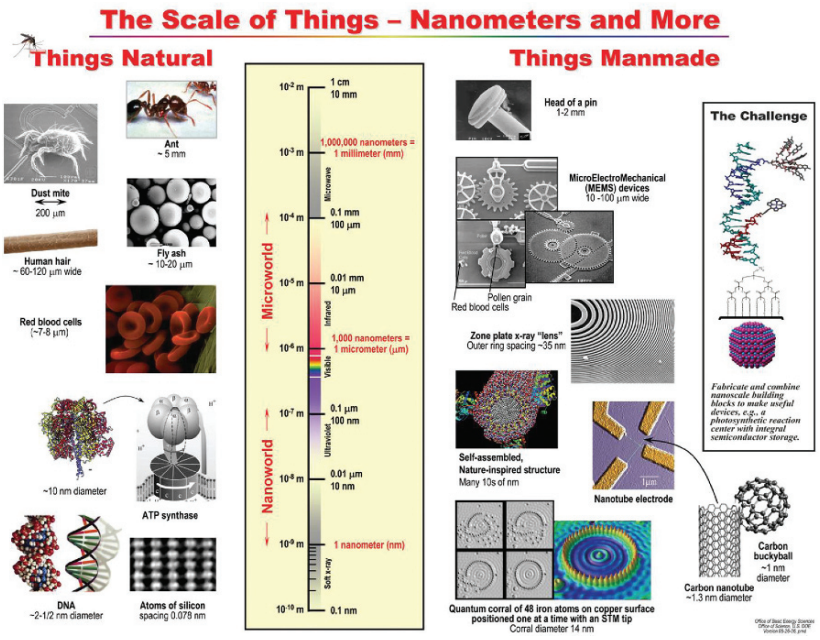

Color Plate 1 Relative size of nanoparticles compared to familiar items (McNeil, 2005).

Color Plate 2 A list of silver and gold nanoparticles having various morphologies, compositions and structures, together with their typical locations of surface plasmon resonance bands in the visible regime (Sun & Xia, 2003). (Reprinted with permission from The Royal Society of Chemistry.)

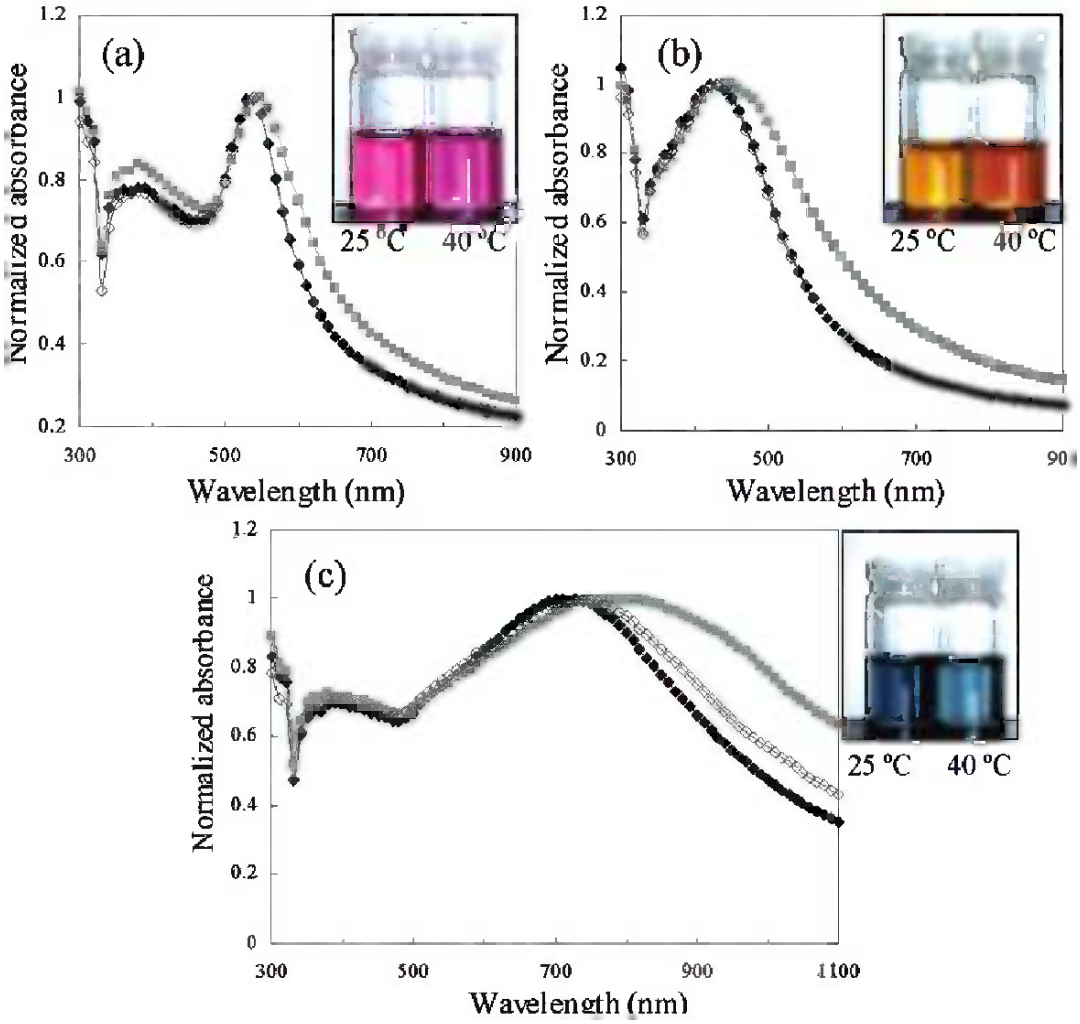

Color Plate 3 (**a**) UV–visible spectra of NG-NH_2-Au/Au2, (**b**) NG-NH_2-Au/Ag/Au microgels (NG is the copolymer gel), (**c**) measured at 25°C (*black diamonds*), 40°C (*gray squares*) and 25°C after 10 heating–cooling cycles (*open diamonds*). All spectra presented here were normalized by taking the temperature effects into account (Suzuki & Kawaguchi, 2006). (Reprinted with permission from ACS publications.)

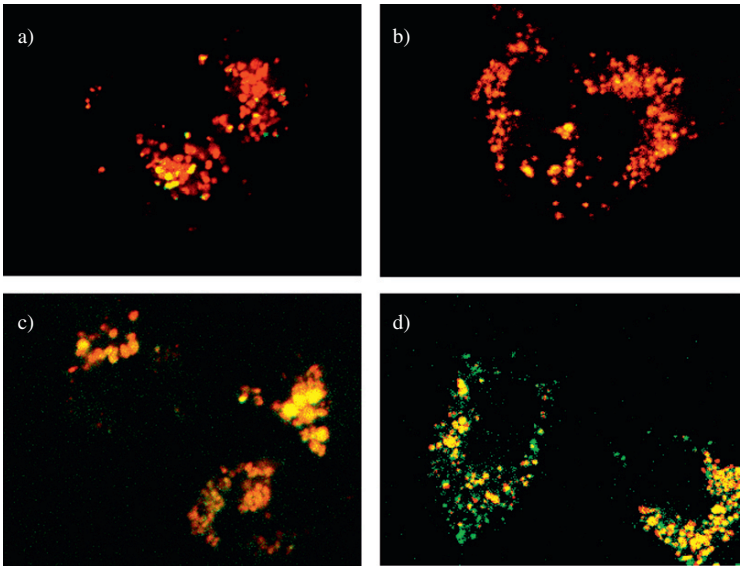

Color Plate 4 Confocal fluorescent microscope images of the HuH-7 cells in the presence of LysoTracker Red DND-99 and PIC micelles prepared at N/P = 3 with FITC-labeled pDNA. (**a**) lac-PEG-PDMAMA/pDNA PIC micelles (incubation time: 30 min), (**b**) lac-PEG-PDMAMA/pDNA PIC micelles (incubation time: 120 min), (**c**) lac-PEG-PSAO-PDMAMA/pDNA PIC micelles, (incubation time: 30 min), (**d**) lac-PEG-PSAO-PDMAMA/pDNA PIC micelles (incubation time: 120 min). These images are the typical image of triplicate experiments.

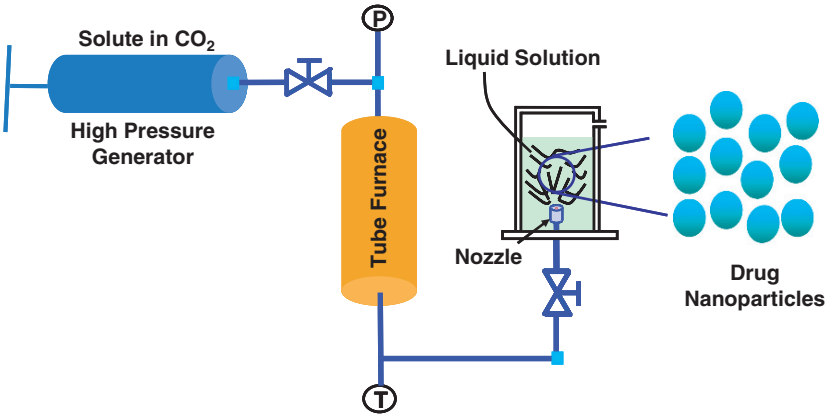

RESOLV for processing drug nanoparticles

Color Plate 5 RESOLV for processing drug nanoparticles.

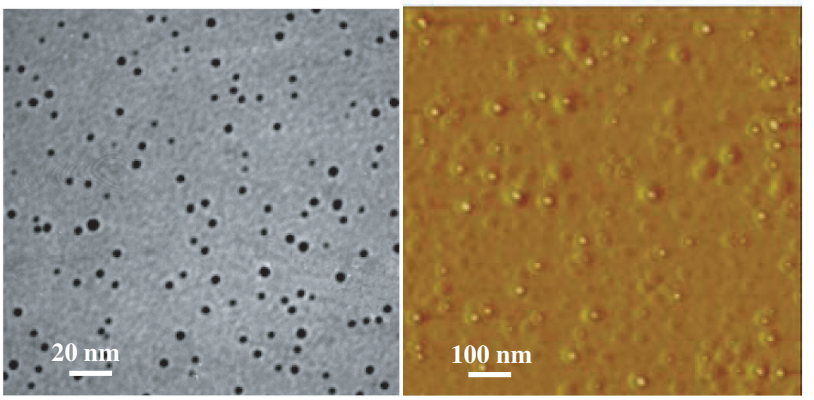

Color Plate 6 TEM (*left*) and AFM (*right*) images of BSA-conjugated Ag_2S nanoparticles prepared via RESOLV. (From Meziani and Sun, 2003.)

Color Plate 7 AmB nanoparticles from RESOLV in a stable and optically transparent aqueous suspension. (From Pathak et al., 2007a.)

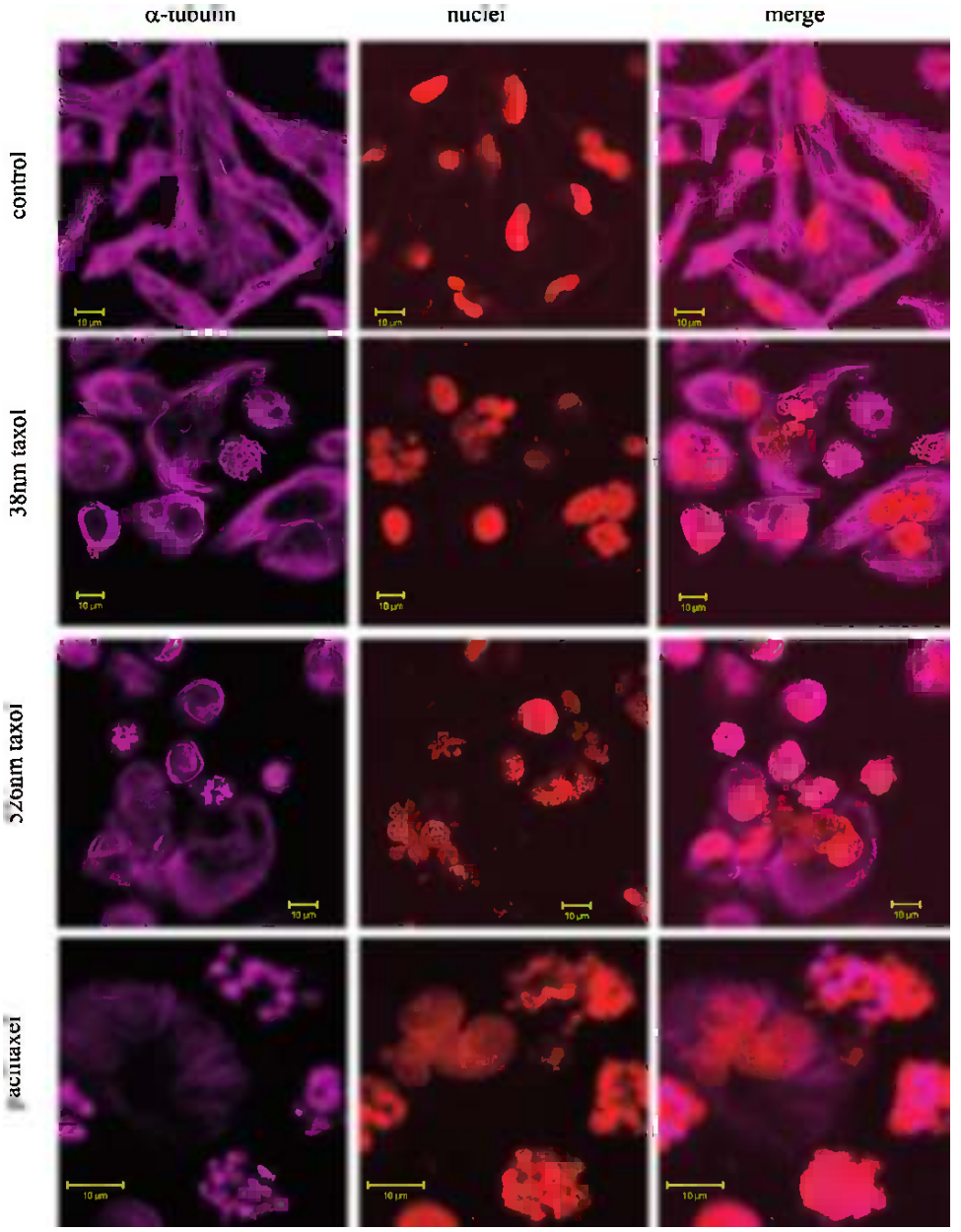

Color Plate 8 The cellular organization of microtubule network in MDA-MB-231 cells with and without paclitaxel treatment (10 μm for all scale bars). Experimentally, the cells were plated in Nunc chamber slides and allowed to attach overnight. After the treatment with the drug (10 μM concentration for all) in the different forms for 6–24 h, or no treatment as control, the cells were fixed with paraformaldehyde and stained for microfilaments with anti-actin antibody followed by rhodamine-conjugated antibody, and then reacted with DAPI to stain nuclei (DNA). Samples were mounted using Prolong Antifade kit (Molecular Probes) for imaging on a Zeiss LSM 510 confocal microscope. (From Pathak et al., 2007b.)

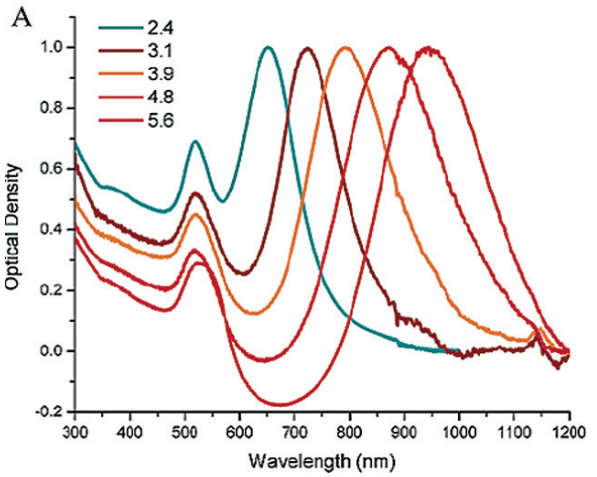

Color Plate 9 Surface plasmon absorption spectra of gold nanorods with varying aspect ratios; this demonstrates the sensitivity of the strong longitudinal band to the aspect ratios of the nanorods (Huang 2006).

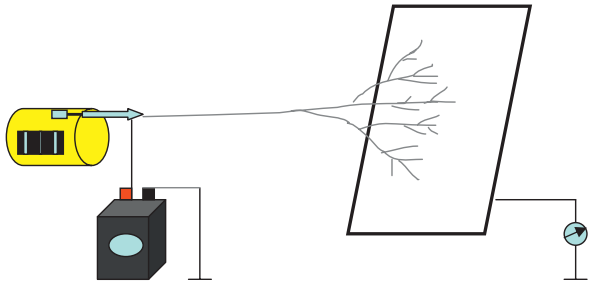

Color Plate 10 Diagram of the electrospinning process (Adapted from Thandavamoorthy et al. 2006).

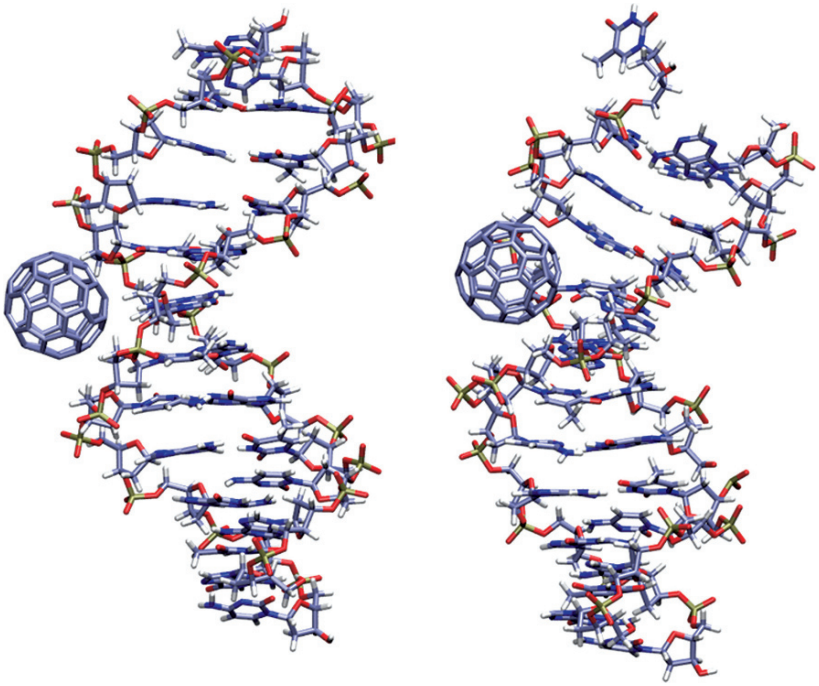

Color Plate 11 Complexes of C_{60} in the minor groove, starting from the B-DNA (***a***) and A-DNA (***b***) conformations. C_{60} has more contact with DNA starting from A-form than that from B-form, resulting in a slightly greater (more negative) binding energy (Zhao 2005).

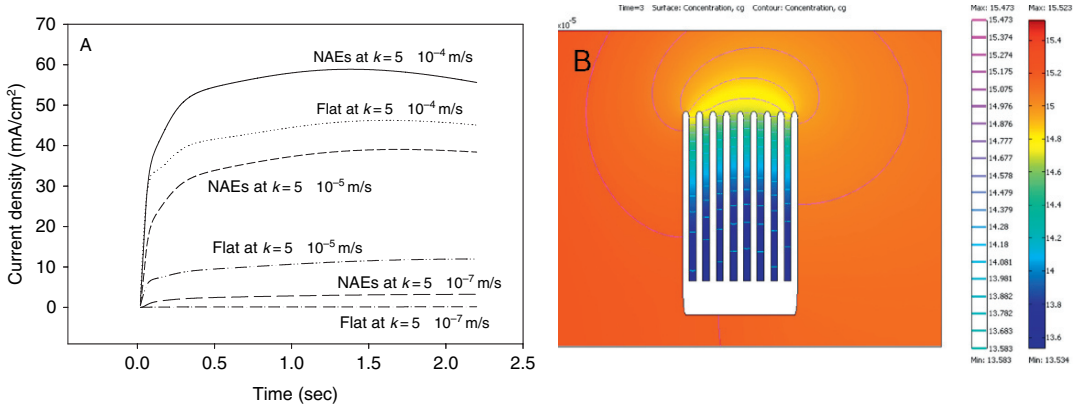

Color Plate 12 (**A**) Simulated current response for a functionalized nanopillar electrode and a flat electrode at various surface-reaction rate constants. (**B**) Contour plot of glucose concentration near the nanopillar electrode obtained at a reaction rate constant of 5×10^{-7} m/s.

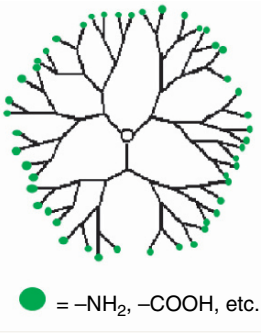

Color Plate 13 Dendrimer functional groups allow complexation or conjugation with various molecules such as DNA or pharmaceutical agents.

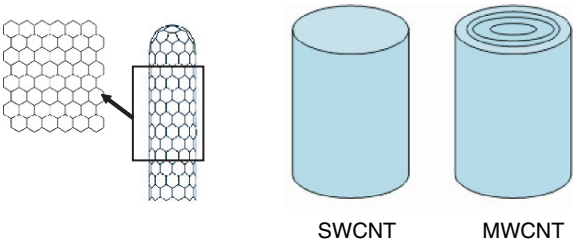

Color Plate 14 Single- and multiwalled carbon nanotubes (SWCNT and MWCNT, respectively).

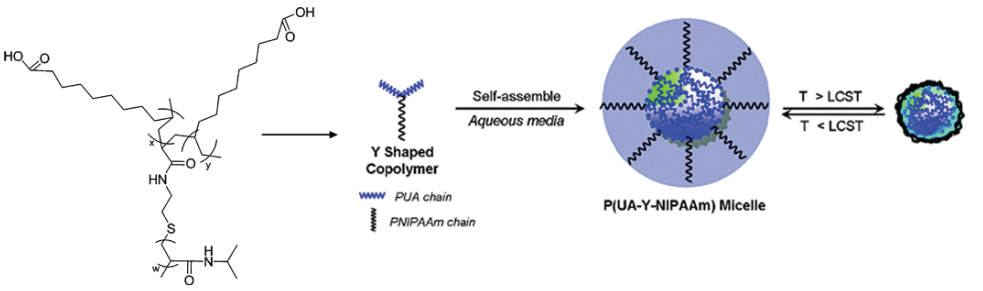

Color Plate 15 Schematic of temperature-sensitive micelles self-assembled in aqueous solutions from Y-shaped copolymers of poly(undecylenic acid) (PUA) and poly(*N*-isopropylacrylamide) (PNIPAAm). Reproduced with permission from Li, Zhang, et al. (2006).

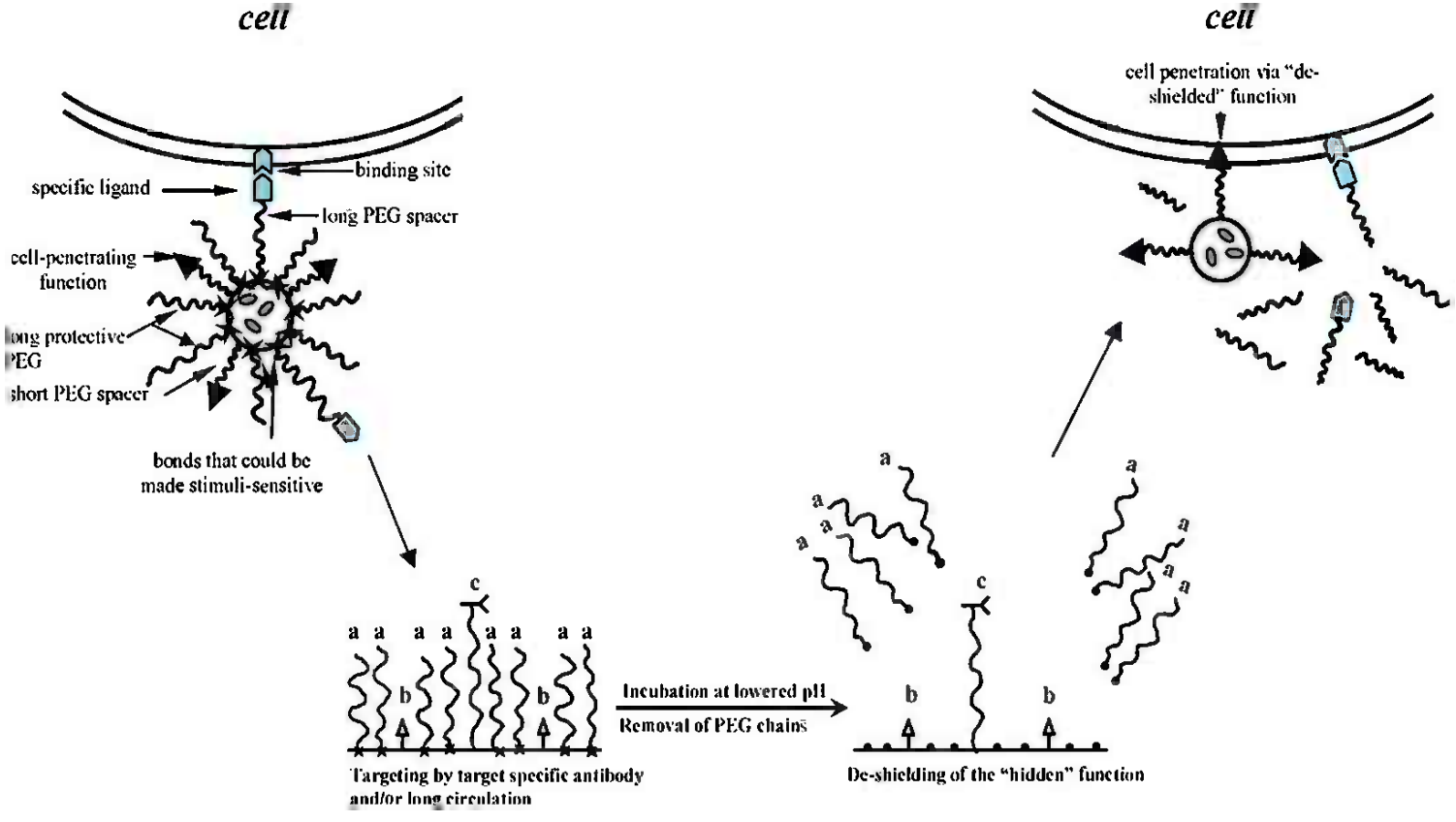

Color Plate 16 Diagram of pH-responsive nanocarriers that include permanent and cleavable surface polymeric chains that are used to modify the surface functionality at specific pathological conditions. Reproduced with permission from Sawant, Hurley, et al. (2006).

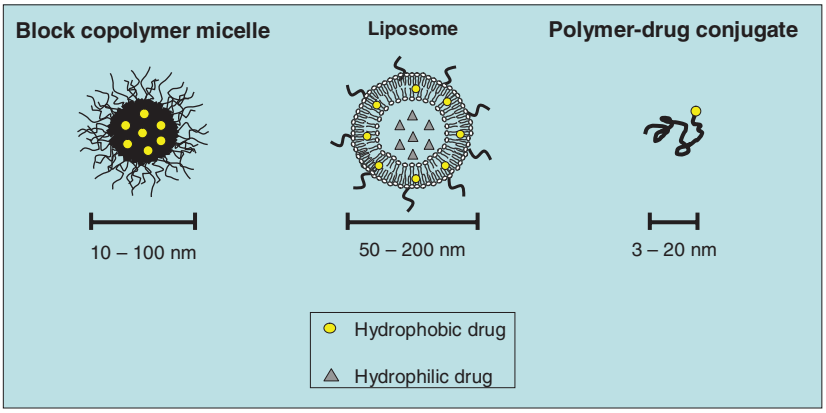

Color Plate 17 Illustrations of the three advanced drug delivery technologies discussed in this chapter.

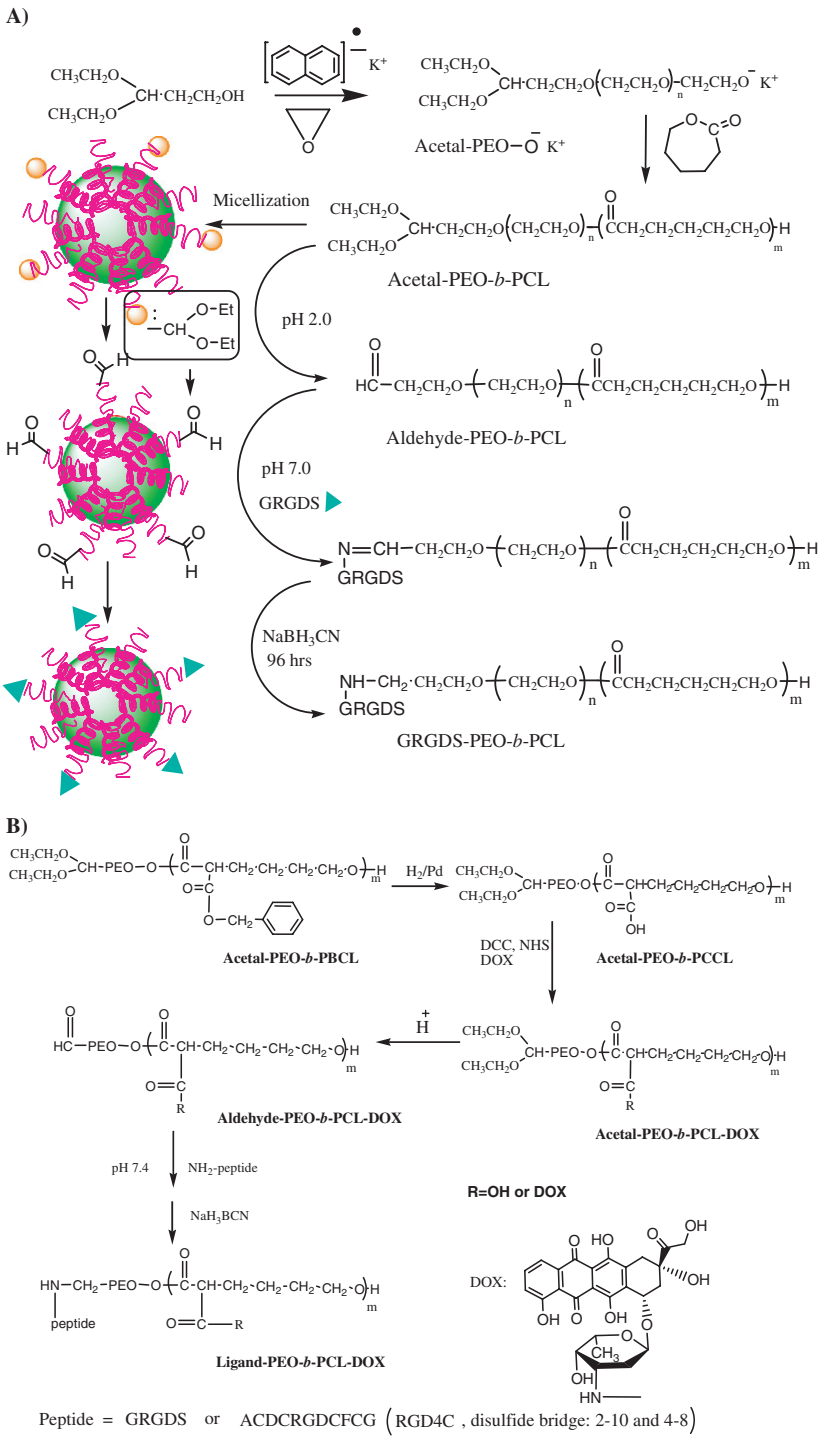

Color Plate 18 Preparation of (**A**) GRGDS-*b*-PEO-PCL (reproduced from Xiong et al., 2007 with permission) and (**B**) GRGDS-PEO-*b*-PCL-DOX block copolymers and micelles.

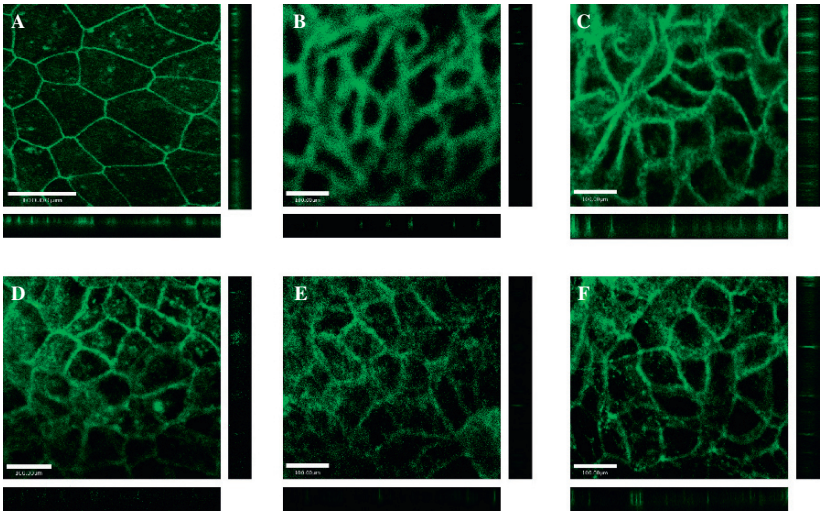

Color Plate 19 Staining of the tight junction protein occludin. (**A**) Caco-2 cells with no polymer treatment. Caco-2 cells incubated for 120 minutes with 1.0 mM: (**B**) $G2NH_2$; (**C**) G2OH, (**D**) G1.5COOH; (**E**) G2.5COOH; (**F**) G3.5COOH. Main panels illustrate the *xy* plane; horizontal bars illustrate the *xz* plane; vertical bars illustrate the *yz* plane. Scale bars equal 100.00 μm. Reprinted from Kitchens et al. (2006) (with permission from Springer).

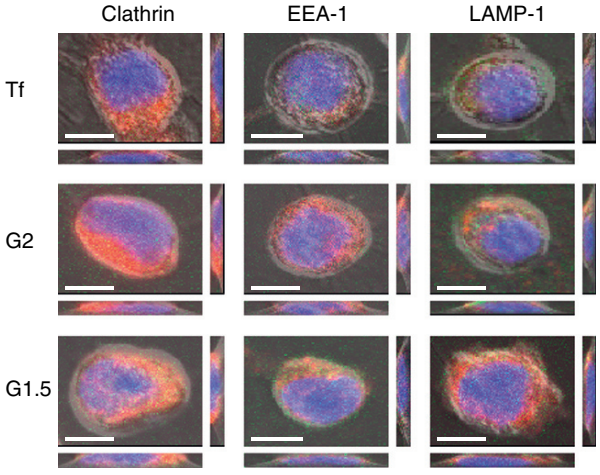

Color Plate 20 Internalization of fluorescently labeled transferrin (250 μg/ml) and PAMAM dendrimers (100 nM) in Caco-2 cells after 20 minutes. The orange color in merged panels indicates colocalization with clathrin heavy chain, early endosomal antigen-1 (EEA-1), and lysosome-associated membrane protein-1 (LAMP-1). Main panels illustrate the *xy* plane; vertical panels illustrate the *yz* plane; horizontal panels illustrate the *xz* plane. Scale bars = 5 μm. Adapted from Kitchens et al. (submitted) (with permission from ACS Publications).

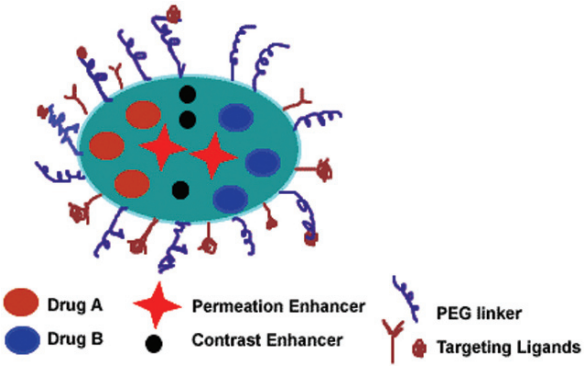

Color Plate 21 Schematic of a particulate drug delivery carrier. The carrier matrix can contain one or more therapeutic compounds, contrast enhancers, such as MRI agents, and permeation enhancers. The surface of the carrier is modified with ligands for selective targeting to diseased tissues and poly(ethylene glycol) (PEG) to achieve a stealth delivery (adapted from reference Ferrari, 2005).

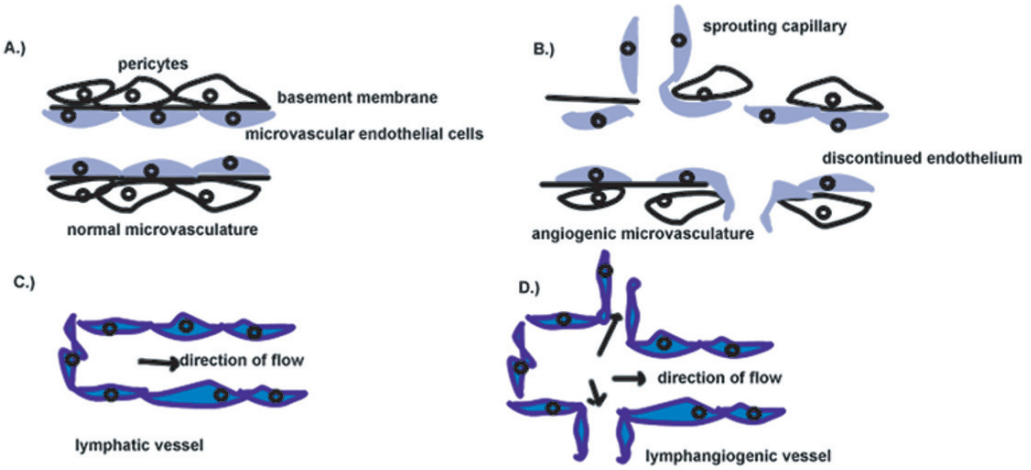

Color Plate 22 Structure of normal and tumor microvascular and lymphatic systems: (**a**) normal microvasculature with characteristically tight endothelium supported by a basement membrane and pericytes; (**b**) angiogenic microvasculature with characteristically discontinued endothelium, highly branched vasculature, and fragmented basement membrane; (**c**) normal lymphatic vessel which is blind ended with a lack of endothelial cell-to-cell junctions; (**d**) lymphangiogenic vessel with a characteristically wider lumen, sprouting endothelial cells, and increased intracellular spaces (redrawn from reference Dua, Gui, and Isacke, 2005).

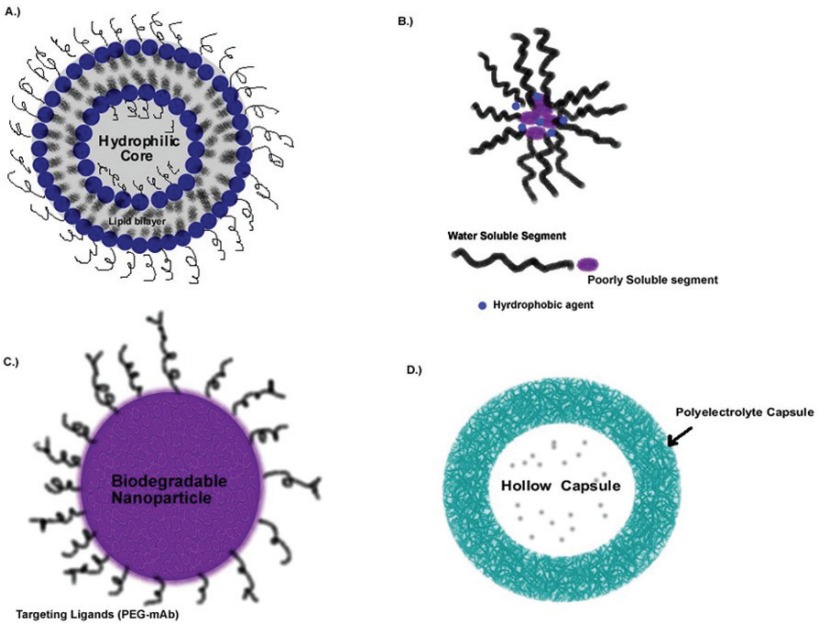

Color Plate 23 Current drug delivery nanoparticulate systems for anti-cancer therapy: (**a**) PEGylated liposome; (**b**) micelle; (**c**) biodegradable nanoparticles with targeted ligand attached to the distal end of poly(ethylene glycol) (PEG) chains; (d) hollow microcapsule assembled via the layer-by-layer assembly technique.

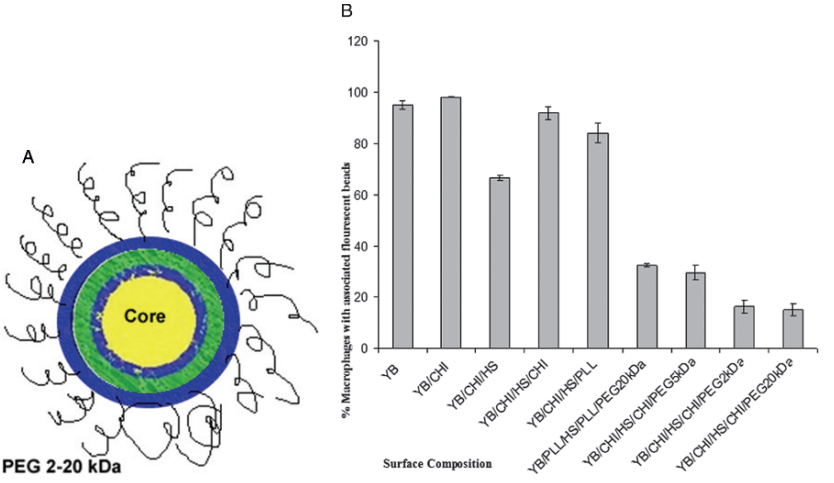

Color Plate 24 (**a**) Schematic of a core–shell nanoparticle assembled step-wise using the layer-by-layer self-assembly technique to create thin multilayered polyelectrolyte layers. The surface of the nanoshell is chemically modified with PEG molecules to produce a long-circulating drug delivery carrier. (**b**) Percent of (live) macrophages with associated fluorescent core–shell nanoparticles versus surface composition of the nanoshell introduced at time = 0 and incubated for 24 hours.

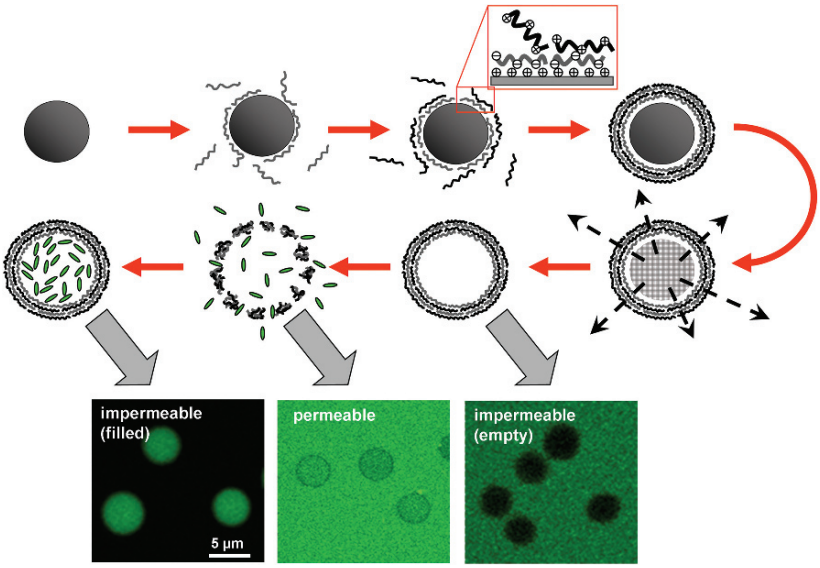

Color Plate 25 Schematic illustration of the polyelectrolyte multilayer build-up on colloidal templates and subsequent template removal. Initial steps involve the stepwise deposition of oppositely charged polyelectrolytes from aqueous solutions on a spherical, colloidal template (inset). After accomplishing the desired number of polyelectrolyte layers the template core is dissolved. Macromolecular species can be incorporated into the capsule interior by selectively and reversibly changing the permeability of the polyelectrolyte shell. CLSM images illustrate the encapsulation of high MW FITC-labeled dextran following this strategy.

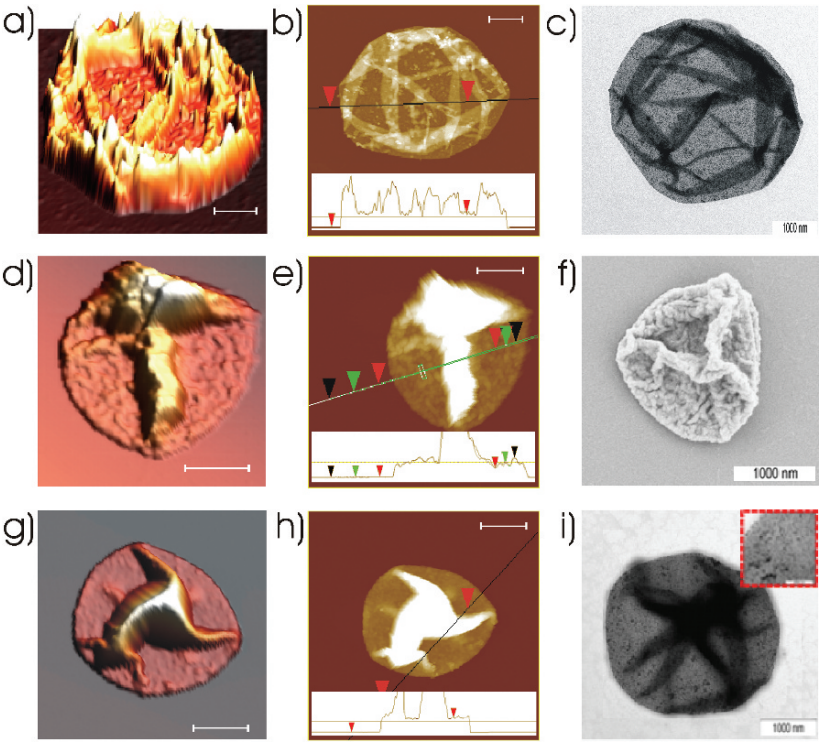

Color Plate 26 AFM (**a**,**b**,**d**,**e**,**g**,**h**), TEM (**c**,**i**) and SEM (**f**) images of a capsule with metal nanoparticles. The first row shows a microcapsule before, the other two rows another after thermal treatment. Capsules shown in the second row had no encapsulated polymers, while those in the third row had encapsulated polymers. (Reprinted with permission from *Angew. Chem. Int. Ed.* 2006, *42*, 4215. Copyright 2006 Wiley-VCH.)

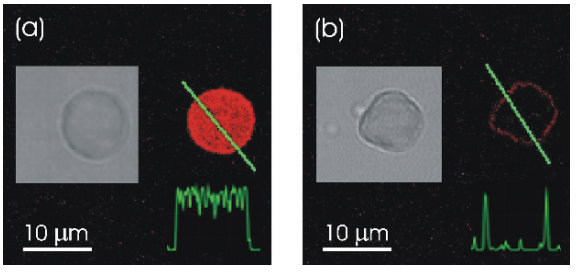

Color Plate 27 Release of encapsulated polymers from a microcapsule. The confocal microscope images are shown before (**a**) and after (**b**) laser illumination. (Reprinted with permission from *Nano. Lett.* 2005, *5*, 1371. Copyright 2005 American Chemical Society.)

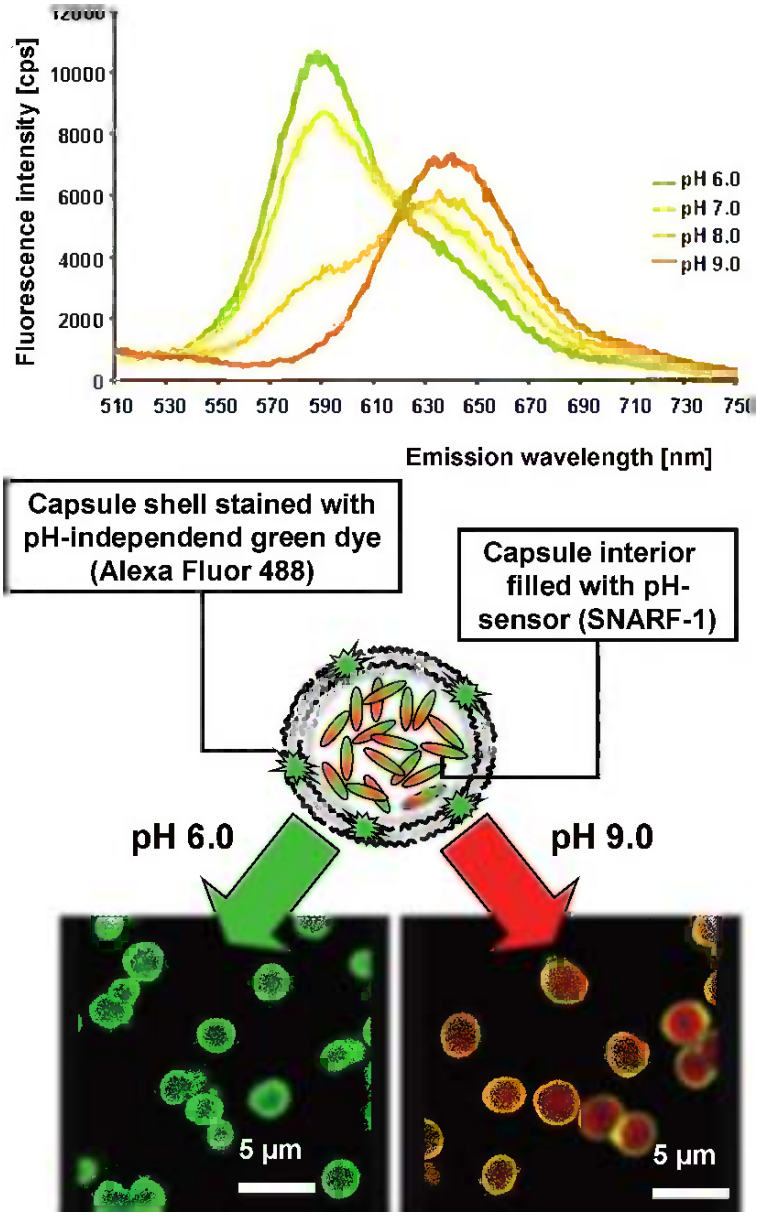

Color Plate 28 *Above*: Fluorescence emission spectra of SNARF-1-dextran (MW = 70,000) in aqueous solution. SNARF-1 exhibits a significant pH-dependent emission shift from *green* to *red* fluorescence under acidic and basic conditions, respectively. The ratio of the fluorescence intensities at 580 and 650 nm can be used for quantitative determinations of pH values. *Below*: Fluorescence properties of encapsulated SNARF-1-dextran. The inner void of the capsules is loaded with SNARF-1-dextran molecules (drawn in *red*/*green*), whereas the capsule shell is labeled with the *green* Alexa Fluor 488 dye, which is not sensitive to pH changes. Depending on pH, the fluorescence of the SNARF-1-dextran molecules and thus the inside of the capsules changes from *green* (acidic pH) to *red* (alkaline pH). In comparison, the *green* fluorescence of the capsule shell is maintained under alkaline conditions. The images show an overlay of CLSM images taken at 580 and 650 nm. The average diameter of the capsules is 5 µm.

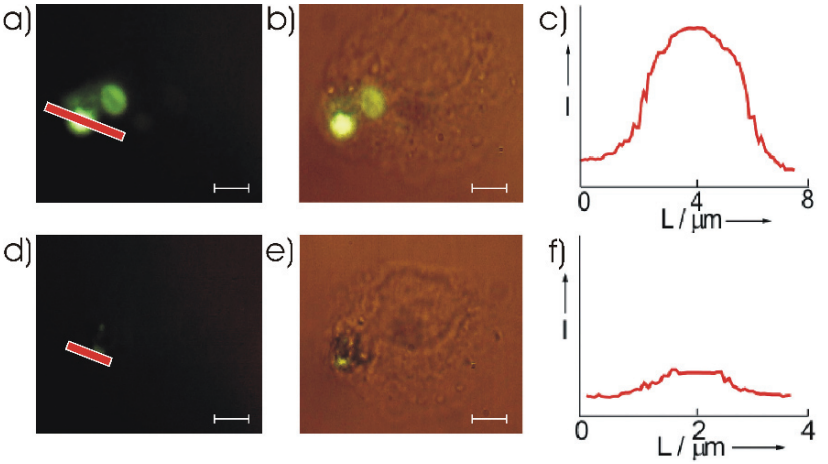

Color Plate 29 Remote release of encapsulated materials inside living cells: (**a**)–(**c**) before and (**d**)–(**f**) after laser illumination. (Reprinted with permission from *Angew. Chem. Int. Ed.* 2006, *42*, 4215. Copyright 2006 Wiley-VCH.)